NASA SP-351

THIRD EARTH RESOURCES TECHNOLOGY SATELLITE–1 SYMPOSIUM

57

Volume I: Technical Presentations

Section B

A symposium held by
GODDARD SPACE FLIGHT CENTER
Washington, D.C.
December 10–14, 1973

NATIONAL AERONAUTICS AND SPACE ADMINISTRATION

NASA SP-351

THIRD EARTH RESOURCES TECHNOLOGY SATELLITE-1 SYMPOSIUM

Volume I: Technical Presentations

Section B

The proceedings of a symposium held by
Goddard Space Flight Center
at Washington, D.C.
on December 10-14, 1973

Compiled and Edited by

Stanley C. Freden
Enrico P. Mercanti
Missions Utilization Office

and

Margaret A. Becker
Technical Information Division
Goddard Space Flight Center

Prepared at Goddard Space Flight Center

Scientific and Technical Information Office 1974
NATIONAL AERONAUTICS AND SPACE ADMINISTRATION
Washington, D.C.

PREFACE

The Third Symposium on Significant Results Obtained from the first Earth Resources Technology Satellite (ERTS-1) was held from December 10-14, 1973 at the Statler Hilton Hotel in Washington, D. C. The Symposium was sponsored by the National Aeronautics and Space Administration, Goddard Space Flight Center. The structure of this Symposium was similar to the one held from March 5-9, 1973. The Opening Plenary Session on Monday morning contained two papers of general interest to the entire audience, one on the status of the ERTS-1 system and a report on the Canadian ERTS program. The next two and one-half days were devoted to contributed papers in the various disciplines presented during three parallel sessions. These papers are contained in Volume I of the Proceedings.

The Thursday Summary Session, as before, was designed to highlight and summarize the significant results from the first three days and also to present some typical examples of the applications of ERTS data for solving resources management problems at the national, state and local levels. This Session was highlighted by an introductory address by Dr. James C. Fletcher, NASA Administrator, and by a keynote address by Dr. John C. Whitaker, Under Secretary of the Interior, U.S. Department of the Interior. The presentations from this session are contained in Volume II of the Proceedings.

Volume III contains the Discipline Summary Reports. These are based on a report produced from a two-week long series of intensive interviews with the individual ERTS-1 Principal Investigators and then updated and extended from the material presented at the Third ERTS Symposium. The interviews were organized and directed by Dr. O. Glenn Smith of the Earth Resources Program Office at the Johnson Space Center and were held at the Goddard Space Flight Center from October 22 to November 2, 1973. The Discipline Summary Reports were written by Working Groups in each of the disciplines which were convened on Friday, December 14. These Working Groups were chaired by the respective discipline session chairmen and were composed of selected specialists in the various disciplines. Opinions and recommendations expressed in these reports are those of the panel members and do not necessarily reflect an official position of NASA.

Stanley C. Freden
Symposium Chairman

TABLE OF CONTENTS

TABLE OF CONTENTS (Continued)

TABLE OF CONTENTS (Continued)

TABLE OF CONTENTS (Continued)

TABLE OF CONTENTS (Continued)

TABLE OF CONTENTS (Continued)

TABLE OF CONTENTS (Continued)

TABLE OF CONTENTS (Continued)

TABLE OF CONTENTS (Continued)

TABLE OF CONTENTS (Continued)

TABLE OF CONTENTS

VOLUME II

SUMMARY SESSION

SELECTED SIGNIFICANT ACCOMPLISHMENTS

APPLICATIONS AND KEY FINDINGS

SUMMARIES IN SELECTED DISCIPLINES

TABLE OF CONTENTS

VOLUME III

DISCIPLINE SUMMARY REPORTS

WATER RESOURCES

Paper W 1

MAPPING SNOW EXTENT IN THE SALT-VERDE WATERSHED AND THE SOUTHERN SIERRA NEVADA USING ERTS IMAGERY

James C. Barnes, Clinton J. Bowley and David A. Simmes, *Environmental Research & Technology, Inc., Lexington, Massachusetts 02173*

ABSTRACT

In much of the western United States a large part of the utilized water comes from accumulated mountain snowpacks; thus, accurate measurements of snow distributions are required for input to streamflow prediction models. The application of ERTS imagery for mapping snow has been evaluated for two geographic areas, the Salt-Verde Watershed in central Arizona and the southern Sierra Nevada in California. Techniques have been developed to identify snow and to differentiate between snow and cloud. The snow extent for these two drainage areas has been mapped from the MSS-5 (0.6-0.7 μm) imagery and compared with aerial survey snow charts, aircraft photography, and ground-based snow measurements.

INTRODUCTION

Snow cover greatly affects the large-scale geophysical environment of the earth, influencing both the heat balance at the surface and the world-wide water balance. Moreover, in many parts of the world, including the western United States, snow has a direct economic impact. In the West, much of the utilized water comes from accumulated mountain snowpacks. The snowmelt runoff is used for irrigation, industrial production, power generation, public consumption, and recreation. Too much runoff may have strong adverse effects in the form of destructive flooding. One only has to look at the 1972-73 winter season to gain an understanding of the impact of snow on the economy of the western part of the country; in central Arizona exceptional winter snowfall resulted in replenished groundwater and a summer of abundant water supplies, whereas in the Pacific Northwest a winter of well-below normal snowfall produced a power-generation crisis later in the year.

Because of the hydrologic importance of snow accumulation, accurate monitoring of the snowpack distribution is required. Remote sensing from earth-orbiting satellites now provides observations of snow that have not previously been available and offers promise for eventually providing a more cost-effective means for snowpack monitoring. In fact, as long ago as 1960, snow could be detected in eastern Canada in the initial pictures taken by the first weather satellite, TIROS-1. Snow, therefore, can perhaps be considered as the very first water resource to be observed from space.

APPLICATION OF SATELLITE OBSERVATIONS TO SNOW HYDROLOGY

Studies such as those by Leaf (1969) and Leaf and Haeffner (1971) have shown that in mountain snowpacks, a functional characteristic exists between extent of snow cover during the melt season and accumulated runoff. These snow-cover depletion relationships are useful for determining both the approximate timing and the magnitude of seasonal snowmelt peaks. Thus, snow extent, which can be readily observed from space, is in itself a significant hydrologic parameter.

Since the time of the first TIROS pictures, an increasing use has been made of remote sensing from satellites to map snow extent. Studies have demonstrated that valuable information on snow distributions could be derived even from the relatively poor resolution data of the earlier meteorological satellites (Barnes and Bowley, 1968; McClain, 1970, 1973). Now, the NOAA and ERTS spacecraft systems are providing data with greatly improved sensor resolutions. The hydrologic applications of the NOAA-2 VHRR (Very High Resolution Radiometer) are discussed by Wiesnet and McGinnis (1973); the preliminary results of snow-mapping studies using ERTS-1 were presented at the Second ERTS Symposium by Barnes and Bowley (1973a) and by Meier (1973).

This paper presents further results of the investigation to evaluate the application of ERTS data for mapping snow cover, primarily in the mountainous areas of the western United States. The specific objectives of the study were to determine the spectral interval most suitable for snow detection, to determine the accuracy with which snow lines can be mapped in comparison with the accuracies attainable from other types of measurements, and to develop techniques to differentiate reliably between snow and clouds and to understand the effects of terrain and forest cover on snow detection. The snow extent mapped from the ERTS imagery has been correlated with standard snow measurements, aerial survey snow charts, and aircraft photography.

LOCATIONS OF TEST SITES

The investigation of the ERTS data has been concentrated in two geographic areas in which snow hydrology is of great importance: the southern Sierra Nevada in California and the Salt-Verde Watershed in central Arizona. The area of interest in the southern Sierras, shown in Figure 1, comprises four river basins, which eventually drain into the San Joaquin Valley. The four basins with their approximate areas are the Kings (4000 km^2), the Kaweah (1450 km^2), the Tule (1013 km^2), and the Kern (5372 km^2). As pointed out by Anderson (1963), the annual stream flow in the areas adjacent to the southern San Joaquin Valley is the most variable of any California watershed, due mainly to a large variability in the number and intensity of the winter storms crossing the region.

The Salt and Verde river basins are considerably larger in area, being approximately 15,128 km^2 and 14,646 km^2, respectively. In his paper on the use of

remote sensing as a water management tool on the Salt-Verde Watershed, Warskow (1971) points out that although the water content of the Salt-Verde snowpack is diminutive in comparison with that of areas such as the Sierras and Cascades, it is still the major source of surface runoff in the state of Arizona. Moreover, the Arizona snowpack is extremely variable from year to year because of its location at the southern edge of the continental snowpack.

In both of the geographic areas of the investigation, the snowpack was above normal for the sample period, the 1972-1973 snow season. In the southern Sierra Nevada, the California Department of Water Resources reports that early in the winter the snowpack that had accumulated by late December was depleted at lower elevations and reduced at higher elevations by warm storms during early January, but subsequent storms and colder weather brought the snowpack to above normal by the first of February. A relatively wet February raised the water content of the snowpack, and the continuation through March of cool, wet weather boosted the snow water content to greater amounts in most watersheds. On the first of April, the snow water content at mid-elevations of the Kern, Kaweah, Tule, and Kings River Basins was greater in percentage of normal than at the higher elevations. In fact, two snow courses in this area had water contents that exceeded the maximum water content ever recorded. Although precipitation was below normal during April, the snowpack water content was still well above normal in early May. Snow course measurements made about the first of May indicated a snowpack water content as high as 315 percent of average in the Tule River Basin. On this date the water-year streamflow for the San Joaquin drainage area was forecast to be 100 to 150 percent of average.

The 1972-73 season produced a record snowpack accumulation in the Salt-Verde Watershed. Precipitation for the October through April period was much above normal, and the snowpack at its maximum in early April was estimated to be as much as 500 percent of normal in the Verde River Watershed and 300 percent in the Salt. In April the runoff forecast for the Verde was nearly 400 percent of the 1953-1967 average and for the Salt more than 350 percent. Obviously, throughout the 1972-1973 winter and spring seasons, snow hydrology was a vital concern in Arizona water management programs.

PROCEDURES FOR IDENTIFYING AND MAPPING SNOW

Examination of the ERTS data has shown that contrast between snow covered and snow free terrain is greatest in the MSS-4 (0.5 to 0.6 μm) and MSS-5 (0.6 to 0.7 μm) spectral bands. The MSS-5 data appear to be the more useful of the two bands for snow mapping, because in some of the MSS-4 images snow covered areas are near saturation, causing a loss of detail in the snow pattern. In the longer wavelengths, especially the MSS-7 near-IR band (0.8 to 1.1 μm), snow cover is more difficult to detect. A limited sample of color composite data has also been examined.

Snow cover can be identified in the MSS-5 data because of its greater reflectance than the surrounding snow free terrain. Although snow and clouds have similar reflectances, mountain snow cover can be differentiated from cloud primarily because the configuration of the snow patterns is very different from cloud fields and can be instantly recognized. The snow boundaries are also sharper than typical cloud edges, and snow fields usually appear with a more uniform reflectance than do clouds, which have considerable variation in texture. Furthermore, cloud shadows are usually visible, especially with cumuliform clouds, and various terrestrial features can be recognized in cloud-free areas. Because of the high-resolution of the ERTS data, numerous terrestrial features that are not visible in lower-resolution meteorological satellite photographs can be recognized. In addition to natural features, such man-made features as roads, power line swaths, and cultivated fields are detectable. In the heavily forested areas of the Cascades, timber cuts are clearly visible.

In the analysis procedure the snow line was mapped at the edge of the brighter tone without regard to changes in brightness within the overall area deduced to be snow covered. Although snow covered areas often exhibit fairly uniform reflectance, variations due primarily to forest effects are observed. For the specified test sites the snow limit was mapped from the 9.5 inch ERTS prints supplied by NASA (scale 1:1 million) and, in some instances, from reprocessed enlarged prints (scale 1:500,000). In the central Arizona test site no significant differences have been found between the original and reprocessed prints. In the Sierra Nevada test site, however, the effects of mountain shadows, which are a problem in the low-sun angle winter data, are somewhat reduced through the reprocessing; certain snow - no snow boundaries that are obscured in the original prints can be detected in the reprocessed prints. For the Arizona test sites, the scale of the 9.5 inch ERTS prints is the same as the scale of aerial survey snow charts, used as one source of correlative information; therefore, transfer of the snow extent mapped from the ERTS image to the aerial survey base map could be easily accomplished.

RESULTS OF DATA ANALYSIS FOR SOUTHERN SIERRA NEVADA

In the ERTS orbital configuration the Kern Basin is covered on one day and the Kings, Kaweah, and Tule (and part of the Kern) on the following day. Because of cloud obscuration, the entire four-basin area was not mapped in each case; however, during the period from early December through late May, a major part of the area was sufficiently cloud free to be mapped on seven of the ten ERTS cycles. In Figures 3 and 4, ERTS MSS-5 images covering the Kings River Basin on 20 April and 26 May are displayed. The decrease in snow extent during the 36 day interval is evident.

For each river basin of the southern Sierra Nevada the snow line elevation was determined directly by comparing the snow map derived from the ERTS MSS-5 image with superimposed elevation contours. In addition, the snow line elevation was determined by measuring with a planimeter the percentage of the basin snow covered and referring to the area - altitude curve for the particular

basin. In an earlier study using meteorological satellite photography, the snow line elevation for the Kings Basin was determined in this way (Barnes and Bowley, 1970). Recently, the snow line determined from areal snow extent, or the equivalent snow line altitude (ESA), has been discussed further with regard to ERTS data (Meier, 1973).

The snow line elevation determined from a direct comparison with a contour chart varies considerably within each river basin. The Kings River Basin in the southern Sierras, for example, was divided into three sections, and the mean elevation for each section was determined from a large number of data points. For three cases during the spring season, the mean difference between the section with the highest snow line elevation and that with the lowest is of the order of 400m. Because of the observed variation in the snow line elevation measured directly, which can be influenced significantly by small mapping errors, it is believed that the equivalent snow line altitude (ESA) is a more meaningful measurement with regard to the application of satellite data to snow mapping.

COMPARISON BETWEEN ERTS DATA AND AERIAL SURVEY SNOW CHARTS

Aerial survey snow charts depicting snow extent in the four-basins area were prepared by the Corps of Engineers on five dates between 27 April and 11 June. The percentages of basin snow covered as measured from the ERTS imagery (by transferring the snow line to a base map and planimetering the area) and as measured from the aerial survey snow charts, are shown for each river basin in Figure 5. In addition, for the instances where an ERTS observation was available near the date of an aerial survey, the percentages measured from each were compared directly. The comparative values are shown below in Table 1.

TABLE 1

SNOW EXTENT IN SOUTHERN SIERRA NEVADA MEASURED FROM ERTS AND FROM AERIAL SURVEY SNOW CHARTS

Data Sample		% Snow Cover		ESA*	
River Basin	Number of Cases	Mean Difference	Maximum Difference	Mean Difference	Maximum Difference
Kings	4	4.5%	5%	137m	152m
Kaweah	3	9.0	14	264	426
Tule	3	4.3	6	203	244
Kern	2	3.5	6	92	122

*ESA is Equivalent Snowline Altitude

The results of the comparison indicate overall close agreement between the ERTS and aerial survey data. For each case tested the percentage of the basin snow-covered measured from ERTS is somewhat greater than that measured from the aerial survey. Thus, the ESA determined from ERTS is lower than the ESA determined from the aerial survey chart. The maximum difference in percentage snow-cover is 6% for every basin tested except one; the one value greater than 6% is 14% for the Kaweah Basin in the comparison between the 26 May ERTS and 22 May aerial survey observations. From an examination of the comparative snow extent maps, it appears that more detail can be mapped from the ERTS imagery than is mapped by the aerial observer.

The slightly greater percentage snow-cover measured from the ERTS data may be the result of spring storms that deposit snow below the elevation of the substantial snowpack. Personnel at the Corps of Engineers report that in the late spring light snowfalls (a few inches) are not mapped as snowpack by the aerial observer. In the ERTS imagery, the areas covered by only a few inches of snow may still appear very bright and be mapped as the snowpack. In the case with the greatest discrepancy, however, the value derived from the aerial survey chart for the Kaweah Basin on 22 May seems to be out of line with the other values and with the values measured on that date for the other river basins (Figure 5). It may be, therefore, that in the Kaweah Basin the aerial survey snow line for that date is questionable rather than the ERTS analysis being in error.

<u>Comparison Between ERTS Imagery and Aircraft Photography</u>

In support of the ERTS investigation, high-altitude aircraft photography were collected by the NASA/ARC Earth Research Aircraft Project (ERAP) over the southern Sierra Nevada on 20 February. Three segments of the flight cross areas covered in the ERTS imagery of 25 February. Parts of two of the segments are within the four-basin area, whereas the third is just northeast of that area. The segment northeast of the Kings River Basin crosses Mono Lake and the Owens River in the vicinity of Bishop. A portion of the ERTS image covering the area near Bishop is shown in Figure 6; the corresponding aircraft photography in approximately the same spectral band (0.58 - 0.68 μm) is shown in Figure 7.

In both the aircraft and ERTS data, the snow line can be identified in the area north of Bishop indicated on the topographic chart to be an area of volcanic tableland essentially unvegetated. The snow line appears to be at about the 1500 m level, with little change having occurred during the five-day interval between 20 and 25 February. More detail in the snow line and same patchy snow south of the edge of the solid snow cover can be mapped from the aircraft data. However, the edge of the area of significant snow cover can be mapped as precisely from ERTS as from the aircraft photography.

In another segment of the overflight, the area of the Courtright and Wishon

Reservoirs in the northern Kings Basin can be identified in both the ERTS and aircraft data. The two reservoirs, which are frozen and snow covered, and the Lost Peak area in between appear very bright. The surrounding area consists of a mixture of open and forested terrain, appearing alternately bright and very dark in the aircraft photography. In the ERTS image, the larger bright areas can be identified whereas the smaller areas are integrated with the forested areas to produce a gray tone. It appears, therefore, that even though more detailed patterns can be identified in the aircraft data, the information content of the ERTS image with regard to mapping snow cover is equal to that of the higher resolution photography.

DATA ANALYSIS FOR SALT-VERDE WATERSHED

Snow extent for at least a portion of the Salt-Verde Watershed could be mapped from imagery for seven of the ten ERTS cycles between mid-November 1972 and early May 1973. For each cycle the eastern third of the watershed is covered on one day and most of the remaining part on the following day. On one occasion (26 December) most of the area was cloud-free, but the imagery was not of useable quality. Thus, even in a year with much above average precipitation, the central Arizona area was sufficiently cloud-free that useful snow information could be derived on most of the potential ERTS passes.

Because of the transient characteristics of the snowpack in the Salt-Verde Watershed, aerial surveys are flown at approximately two-week intervals throughout the winter season, and more often during periods of rapid melt. For each flight, the observer makes an ocular estimate of the snow depth using the logs left from timber operations in the mountain areas, ground and vegetation textural characteristics, and cultural features (such as fences, road cuts) as indicators of the snow depth; both the areal outline of the snowpack and the observed depths are recorded on a map overlay (Warskow, 1971). With these charts available throughout the winter, it was possible to prepare a comparative map for each ERTS observation. ERTS images covering central Arizona, including a part of the Salt-Verde Watershed, are shown in Figures 8 and 9; the map comparing the snow extent derived from the 18 and 19 February ERTS images with the 15 February aerial survey is shown in Figure 10.

Comparison Between ERTS Data and Aerial Survey Snow Charts

As was true for the Sierra Nevada, the comparative map shown in Figure 10 indicates that more detail in the snow line can apparently be mapped from the ERTS data than can be mapped by the aerial observer. In general for all cases analyzed, the locations of the snow lines are in good agreement, particularly in the Verde Watershed west of about 111°W. In nearly all areas in which a discrepancy occurs, the aerial survey chart depicts a greater snow extent than is mapped from the ERTS imagery. In some cases this difference can be explained by melting that occurred during the interval

between the observations; in a November case, for example, much of the light snow cover very likely melted during the seven-day period between the two observations. It may also be that in Arizona much smaller snow amounts are mapped by the aerial observer than in the Sierras; this can explain in part why the snow extents mapped from ERTS appear to be slightly less than the aerial surveys in the Salt-Verde Watershed, but generally greater than the aerial surveys in the river basins of the southern Sierras.

Comparison Between ERTS Imagery and Aircraft Photography

On 16 March aircraft data for the central Arizona mountains were collected by the NASA/ARC Earth Resources Aircraft Project. The aircraft photography is similar to that collected over the southern Sierras. Two segments of the flight path were over or near the Salt-Verde Watershed, one crossing the Flagstaff area in the Verde Basin and the other crossing the Mt. Baldy area in the eastern Salt Basin.

The ERTS data nearest the time of the aircraft flight are for 26 March, ten days later. During the intervening period, substantial snowfall did occur (about 20 inches at Flagstaff and 13 inches at McNary); however, the snow on the ground at both stations was less on the 26th (25 and 4 inches, respectively) than on the 16th (30 and 18 inches, respectively). The most recent previous snowfalls at both stations were on 14 March, two days before the aircraft flight, and on 23 March, three days before the ERTS passage. The results of the comparative analysis of these data indicate that that detailed snow features that cannot be detected in the ERTS imagery can be seen in the aircraft photography. However, it appears that all significant snow cover (i.e., substantial snow cover, not small amounts such as might be found along small topographic features) can be detected in the ERTS imagery.

MULTISPECTRAL DATA ANALYSIS

In an investigation of the application of ERTS data for mapping sea ice (Barnes and Bowley, 1973b), the combined use of the visible (MSS-5) and near-IR (MSS-7) spectral bands has been found to be extremely useful for distinguishing ice types. Similarly, snow lines on arctic glaciers can be detected by comparing the visible and near-IR bands. In the California and Arizona test sites, contrast between snow and bare ground is considerably lower in the MSS-7 than in the MSS-5 imagery. Despite the lower contrast, however, the snow line in the wintertime images can be mapped from the MSS-7, and the snow extent appears to be about the same as determined from the MSS-5.

In some late spring cases, the areas appearing very bright in MSS-7 are smaller than those appearing bright in MSS-5. For example, in the Kern

Basin on 30 June, the brightest tones in MSS-7 are limited to the highest ridges, whereas in MSS-5 a distinctly larger area is mapped as being snow covered. There is evidence, therefore, that the combined use of the visible and near-IR may have application for distinguishing areas of melting snow.

Color composite transparencies have also been examined for the two test sites. In the color composites, certain features can be identified more readily than in the black and white products. The features include lakes, rivers, and vegetation areas. Color composite data may also have some advantages for distinguishing snow in shadow areas and for distinguishing areas that consist of patchy snow surrounded by highly reflective rock surfaces as opposed to continuous snow cover. An example of the latter is the 16 September 1972 data for the southern Sierras; areas that could be mapped as snow based on the black and white imagery alone are seen in the color product to consist mostly of bare ground.

CONCLUSIONS

Based on the results of the completed data analyses, it is concluded that the amount of information in ERTS imagery with practical application to snow mapping is substantial. Moreover, for two mountain areas in which snow hydrology is a major concern, the Salt-Verde Watershed in Arizona and the southern Sierra Nevada in California, useful snow cover information could be derived from ERTS data on 70 to 80 percent of the cycles during the past winter and spring seasons. Thus, in these two areas, cloud obscuration does not appear to be a serious deterrent to the use of satellite data for snow survey.

The results of the analysis of ERTS imagery for the Arizona and California test sites indicate that the extent of the mountain snowpacks can be mapped from ERTS data in more detail than is depicted in aerial survey snow charts. In four river basins of the southern Sierra Nevada, the agreement between the percentage of the basin snow covered as measured from ERTS and from the aerial survey charts is of the order of 5 percent for all cases except one. Moreover, in both test sites, significant discrepancies between the ERTS and aerial survey data can usually be explained by changes in snow cover during the interval between the two observations. In the southern Sierras the snow extent mapped from ERTS is consistently somewhat greater than that depicted on aerial survey snow charts; in central Arizona the opposite is generally true. This difference may in part be the result of differing observing techniques used by the aerial oberver in the two areas.

In addition to comparative analysis with aerial snow charts, the ERTS data have also been compared with high-altitude aircraft photography. The results of the comparative analysis indicate that although small details in the snow line that cannot be detected in the ERTS data can be mapped from the higher-resolution aircraft data, the boundaries of the areas of significant snow cover can be mapped as accurately from the ERTS imagery

as from the aircraft photography. There is also evidence that the combined use of visible and near-IR imagry may have application for distinguishing areas of melting snow. Color composite data also appear to have advantages for detecting snow in certain conditions; however, the information content of the more readily available black and white imagery is sufficient for most snow-mapping purposes.

The costs involved in deriving snow extent maps from ERTS imagery appear to be very reasonable in comparison with current data collection methods. For example, the flight time to survey the Salt-Verde Watershed is approximately five hours, with another hour or so needed to compile the snow chart. On the other hand, the snow extent can be mapped from an ERTS image covering nearly the entire watershed area by an experienced analyst in about two hours. Eventual machine processing can be expected to reduce this time considerably.

The major drawbacks to the use of ERTS data as input to an operational system are the availability of the data and the rate of repetitive coverage. To be useful operationally the data would have to be made available to the user within twenty-four hours. The rate of repetitive coverage in the central Arizona area, where snowmelt can occur rapidly, would ideally have to be of the order of less than one week. In the southern Sierras, aerial surveys are normally conducted bi-weekly; thus, in that area a repetitive rate of coverage of the order of one week appears to be sufficient, allowing for the possibility of some data being cloud obscured.

REFERENCES

Anderson, H. W., 1963: Managing California's Snow Zone Lands for Water, U.S. Forest Service Research Paper PSW-6, Pacific SW Forest and Range Experiment Station, Berkeley, California.

Barnes, J. C., and C. J. Bowley, 1968: Snow Cover Distribution as Mapped from Satellite Photography. Water Resources Research, 4(2). pp. 257-272.

Barnes, J. C., and C. J. Bowley, 1970: "Measurement of Mountain Snow Extent Using Satellite Data," paper presented at National Fall Meeting of AGU, San Francisco, California, December 1970.

Barnes, J. C., and C. J. Bowley, 1973a: Use of ERTS Data for Mapping Snow Cover in the Western United States. Proceedings of Symposium on Significant Results Obtained from ERTS-1, NASA-Goddard Space Flight Center, NASA SP-327, pp. 855-862.

Barnes, J. C., and C. J. Bowley, 1973b: Use of ERTS data for Mapping Arctic Sea Ice. Proceedings of symposium on significant results obtained from ERTS-1, NASA-Goddard Space Flight Center, NASA SP-327, pp. 1377-1384.

Leaf, C. F., 1969: "Aerial Photographs for Operational Streamflow Forecasting in the Colorado Rockies," Proc. 37th Western Snow Conference, Salt Lake City, Utah.

Leaf, C. F. and A. D. Haeffner, 1971: "A Model for Updating Streamflow Forecasts Based on Areal Snow Cover and a Precipitation Index." Western Snow Conference, Thirty-ninth Annual Meeting, pp. 9-16.

McClain, E. P., 1970: Applications of Environmental Satellite Data to Oceanography and Hydrology, ESSA Tech. Memo. NESCTM-19, Environmental Science Services Administration.

McClain, E. P., 1973: Snow Survey from Earth Satellites, World Meteorological Organization, WMO Pub. No. 353, Geneva.

Meier, M. F., 1973: "Evaluation of ERTS Imagery for Mapping Snowcover," paper presented at Symposium on Significant Results Obtained from ERTS-1, NASA-Goddard Space Flight Center, NASA SP-327, pp 863-878.

Warskow, W. L., 1971: "Remote Sensing as a Watershed Management Tool on the Salt-Verde Watershed," paper presented at the ARETS Seminar on Applied Remote Sensing of Earth Resources in Arizona, Tuscon, Arizona.

Wiesnet, D. R., and D. F. McGinnis, 1973: "Hydrologic Applications of the NOAA-2 Very High Resolution Radiometer," Symposium on Remote Sensing and Water Management, Burlington, Ontario, Canada (June).

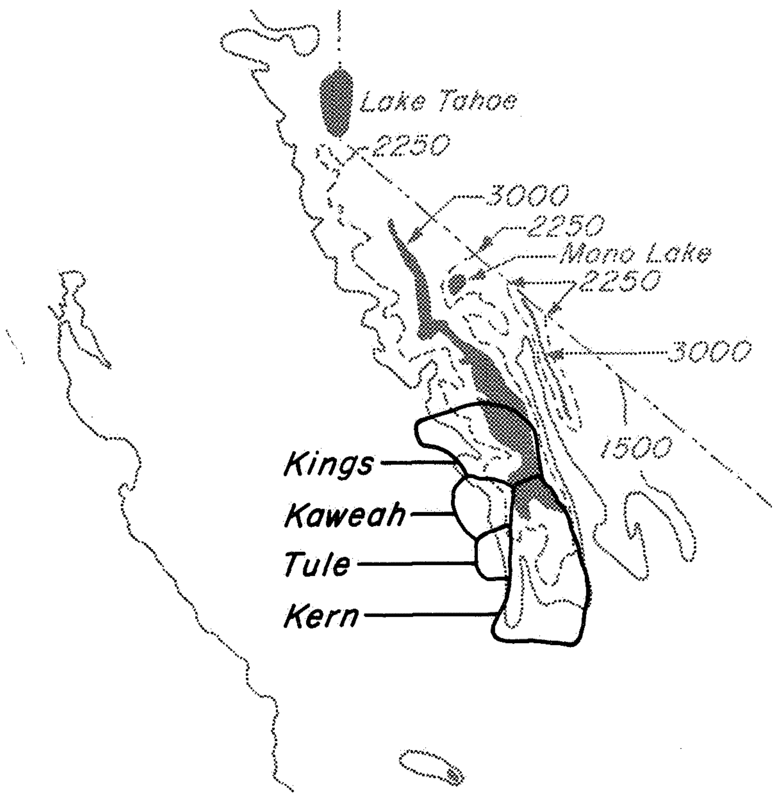

Figure 1 Map showing river basins in southern Sierra Nevada. Elevation contours are in meters.

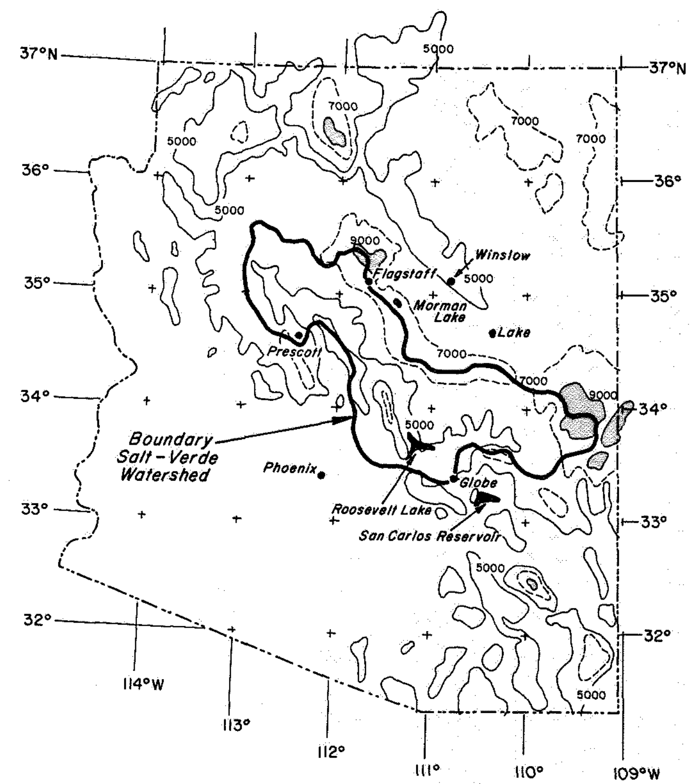

Figure 2 Map showing Salt-Verde Watershed. Contours for 1500m(5000ft.), 2100m(7000ft.), and 2700m(9000ft.) are indicated.

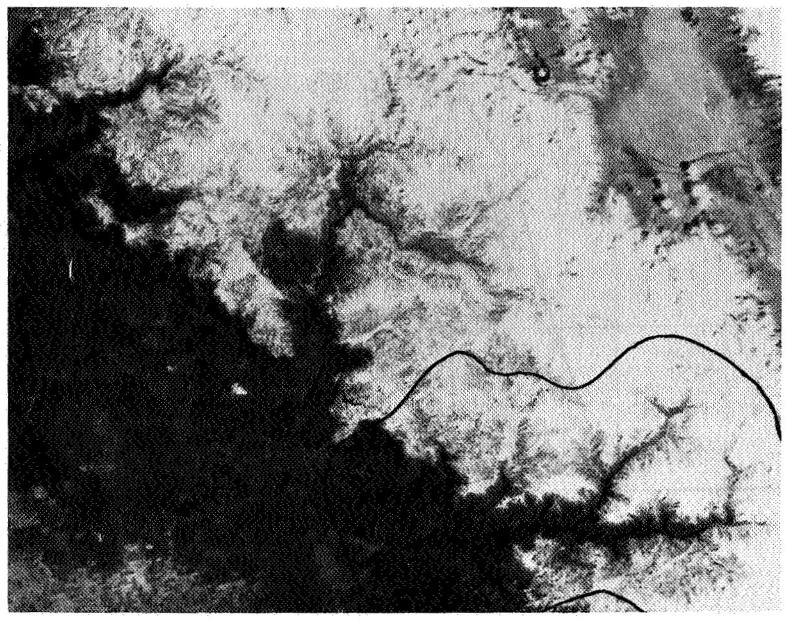

Figure 3 ERTS MSS-5 image showing Kings River Basin, 20 April 1973 (ID No. 1271-18070). Boundary of river basin is indicated.

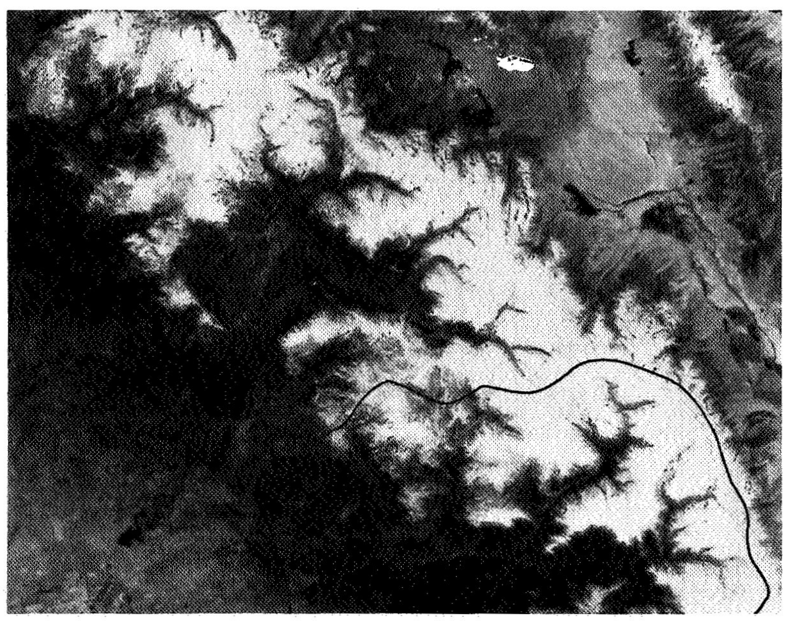

Figure 4 ERTS MSS-5 image showing same area as in Figure 3, 26 May 1973 (ID No. 1307-18064). Note decreased snow extent.

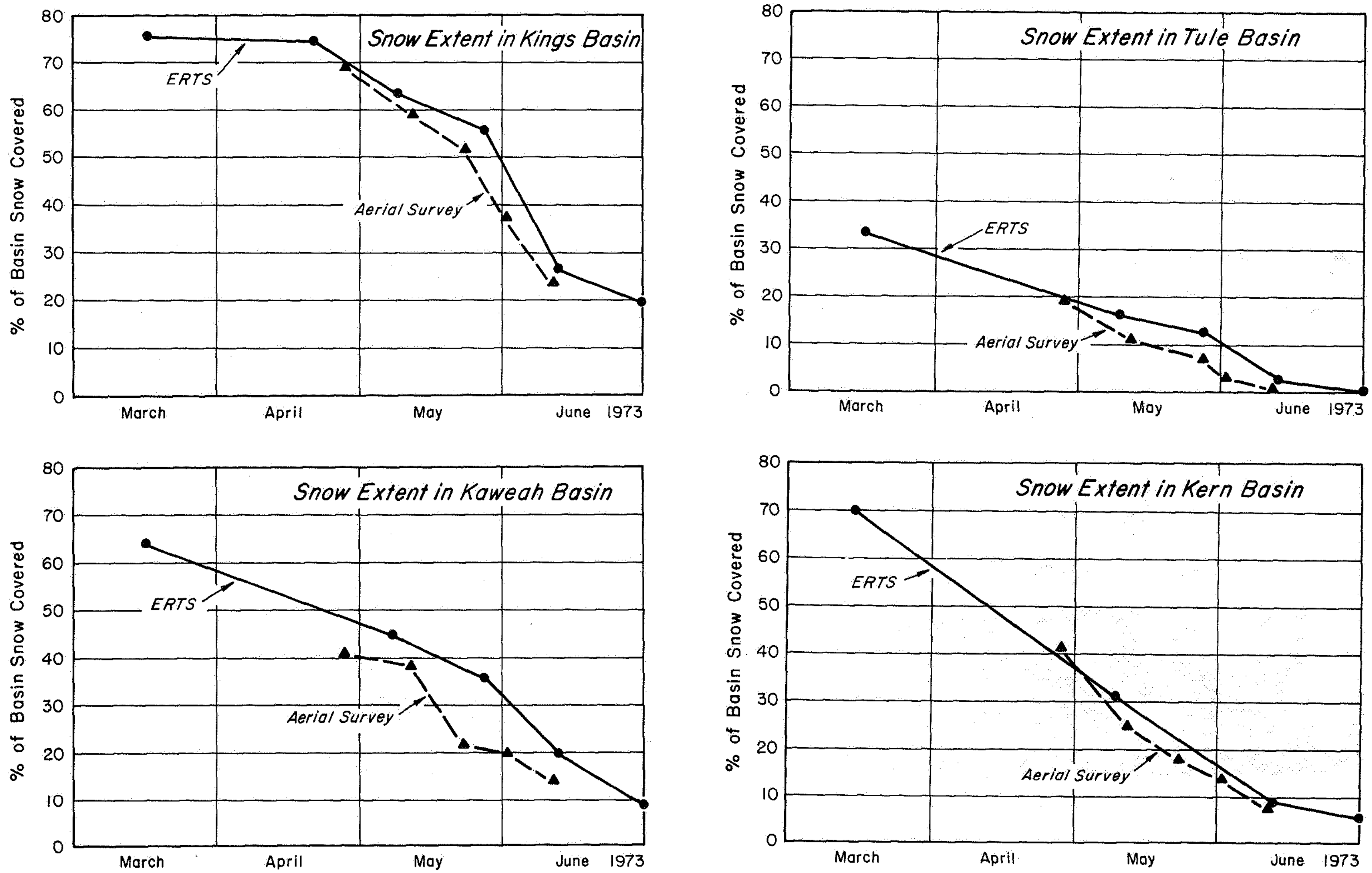

Figure 5 Snow extent in southern Sierra Nevada mapped from ERTS and from aerial survey snow charts. Values are in percentage of basin snow covered; dates of observations are indicated.

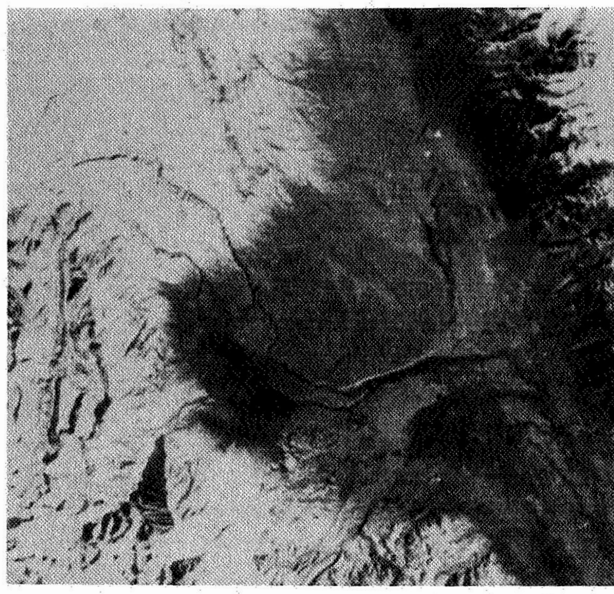

Figure 6 ERTS MSS-5 image showing Owens River Valley near Bishop, California, 25 February 1973 (ID No. 1217-18065).

Figure 7 High-altitude aerial photograph showing a part of the area covered in the ERTS image (Figure 6). Photograph was taken 20 February 1973.

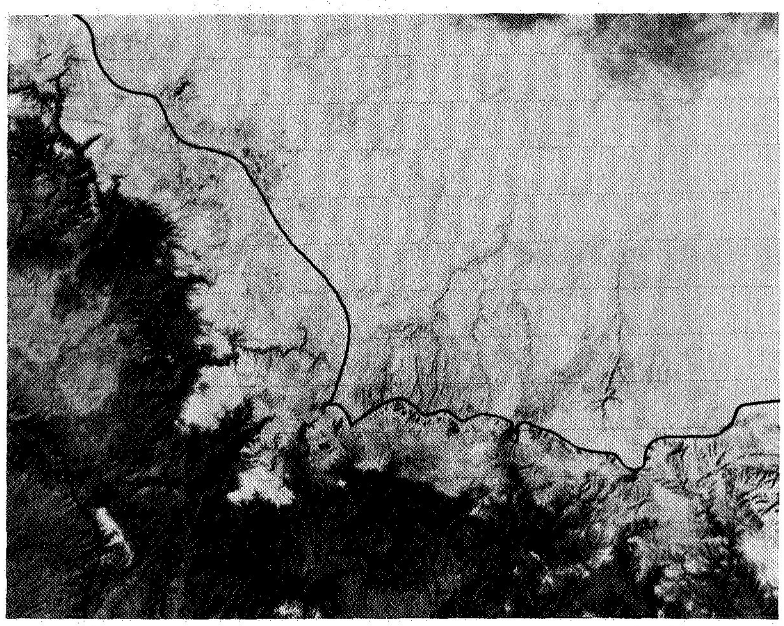

Figure 8 ERTS MSS-5 image showing portion of Salt-Verde Watershed, 19 February 1973 (ID No. 1211-17332). Watershed is within boundaries indicated.

Figure 9 ERTS MSS-5 image showing portion of Salt-Verde Watershed, 2 May 1973 (ID No. 1283-17332). Note decreased snow extent and unfrozen lakes.

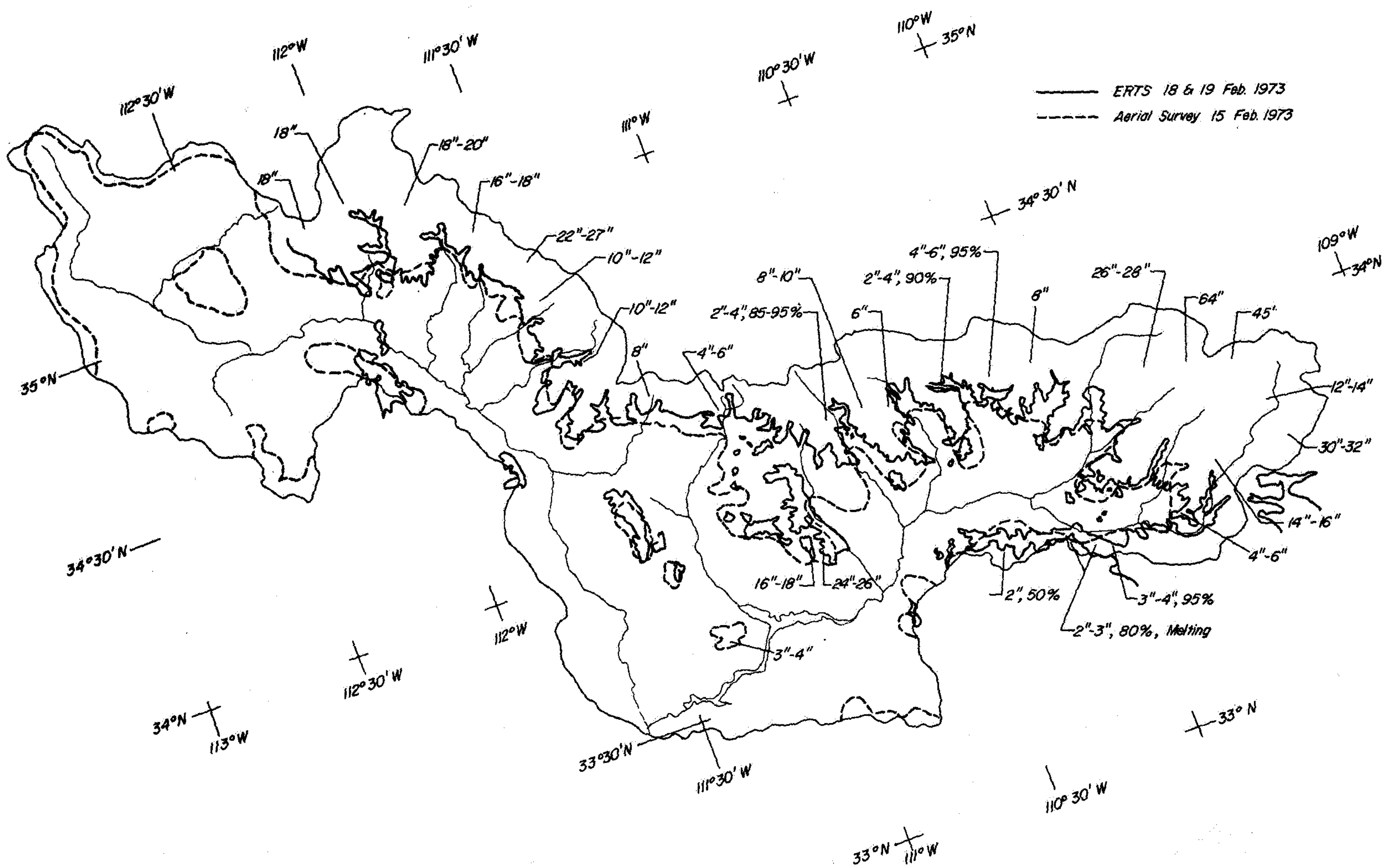

Figure 10 Comparison between snowlines mapped from ERTS imagery and by aerial survey, Salt-Verde Watershed. The eastern third of the area was covered by ERTS on 18 February, and the rest on 19 February (Figure 8); the aerial survey was flown on 15 February.

Paper W 2

SNOW-EXTENT MAPPING AND LAKE ICE STUDIES USING ERTS-1 MSS TOGETHER WITH NOAA-2 VHRR

D. R. Wiesnet and D. F. McGinnis, Jr. *(U.S. Dept. of Commerce, NOAA/NESS)*

ABSTRACT

Five snow extent maps of the 5,601 km^2 American River Basin were prepared using a Zoom Transfer Scope from ERTS-1 MSS band 4 imagery. The maps were generally completed within one hour. A snowmelt curve based on ERTS-1 imagery was used as a "calibration" standard or comparison for maps prepared from NOAA-2 VHRR imagery in the same manner. Cost comparisons with U-2 derived imagery indicate that ERTS-1 snow mapping of the basins is six times faster. Conservative estimates of comparable aircraft snow survey flights yields a cost figure 200 times that of the ERTS-1 snow map. Snow mapping attempts in the Lake Ontario Basin demonstrated that ERTS-1 is not well suited to large basins. Optimum size of basins for ERTS studies is believed to range from about 250 km^2 to 30,000 km^2. The value of the ERTS-1 MSS for Great Lake ice evaluation was proved during the past winter on Lake Erie. Not only were ice features and types of ice identified, but melting ice was detected through the combined use of band 5 (0.6-0.7μm) and band 7 (0.8-1.1μm). Ice movement (direction and speed) was mapped by examining imagery from two successive days. The resolution of NOAA-2's VHRR was checked by comparison of ice leads as seen in the MSS band 5.

INTRODUCTION

Two geographic areas have been chosen for hydrologic assessment by the application of ERTS-1 imagery. One is the Sierra Nevada region, specifically, the American and Feather River Basins. Both basins are part of the Sacramento River drainage system in California. The other geographic area is the Lake Ontario-Lake Erie Basins, particularly Lake Ontario, presently under intensive study by the International Field Year on the Great Lakes (IFYGL) program.

The American River is fed by the melting Sierra snowpack, a highly managed and rather important water resource. Except for occasional aircraft photoreconnaissance surveys, snow measurements within the rugged highland areas of this basin are sparse. Nevertheless, eight remote readout stations for

measuring snow can be monitored during satellite transits. The objective in the Sierra Nevada area is to evaluate the capability of ERTS-1 sensors to monitor snowmelt on an 18-day cycle basis.

Lake Ontario and Lake Erie are large temperate-region lakes. The objective here is to assess, as quantitatively as possible, the hydrologic information that can be extracted from ERTS-1 sensors. Imagery of ERTS-1 is also examined to assess ice features, types of ice and possible melting ice and ice movement, especially in Lake Erie.

SIERRA NEVADA STUDIES

U-2 Photography

All available U-2 color-IR (0.51-0.90μm) photography of the Feather River Basin was examined to determine which contained the best variety of snow, ice and no-snow areas. The overall clarity of the film (i.e. exposure, image contrast, absence of scratches, etc.) was also an important factor considered. Imagery from flight number 72-036 (accession number 00221) taken on 6 March 1972 was ultimately selected. Color-IR offered the best contrast between snow and no-snow areas when compared with the other spectral bands. The photographs (1:445,000) were projected individually onto a topographical map of the basin (1:250,000) by use of the Zoom Transfer Scope (ZTS). This photo-optical device allowed each image to be enlarged, rotated and stretched until the image registered at the 1:250,000 scale. Edge distortion of the photographs was evident, and whenever possible only the central portion of the photograph was used for mapping. Twenty-three photographs were required to map the basin. It should be noted that "data holidays" in the coverage at the edges of the basin precluded 100 percent coverage of the basin.

Comparison of the snow map on the basis of the U-2 photography with limited ground truth showed one discrepancy. French Hill had 35.4 inches of water content in existing snow, yet the aerial photograph indicated no snow. The discrepancy has been attributed to the fact that this area was found close to the edge of two aerial photographs, hence positional error of the snowline may be likely. Unless photogrammetric techniques are used, this type of error is inherent in mapping from air photographs.

The mean elevation of the snowline on south-facing slopes was determined to be 100 feet lower than that on north-facing slopes. This is contrary to expectation and could be the result of the deep shadow effect in steep-walled canyons and cliffs as well as the previously described positional problems.

Production of this snow map required a total of 22 man-hours of labor, four of which were used to prepare and mount frames prior to the actual mapping operation.

ERTS-1 Imagery

ERTS-1 imagery of the Feather River Basin for 29 November 1972, 4 January

1973, and 22 January 1973 was utilized for snow-extent mapping. The 1:3,369,000-scale 70-mm ERTS chip (MSS band 4) was enlarged to 1:500,000 in the ZTS and mapped directly onto the base map in the same manner as described in the section U-2 Photography. The ERTS-1 data was much easier to handle, mount and register onto the base map. It was much quicker as well--half an hour for setup and three hours for mapping produced a finished map. This represents a 6:1 ratio in favor of the ERTS-1 snow mapping over the use of high-altitude aerial photographs in terms of man-hours saved. Furthermore, the shadow problem is greatly reduced, the positional accuracy of the snow-line is much more consistent and the light forest cover tends to be less of a problem with reduced ground resolution. Six ERTS-1 images were similarly used to provide snow maps for the American River Basin. The retreat (21 April 1973, 9 May 1973, and 27 May 1973) of the snowline in the 5,601 km^2 basin is observed in Figure 1.

NOAA-2 Imagery

NOAA-2 Very High Resolution Radiometer (VHRR) visible band imagery has been acquired over the Sierra Nevada daily. Thirteen cloudfree images over the American River Basin were selected for analysis, using the ZTS as described previously. Figure 2 shows the portion of the VHRR visible image used to map the snow cover on 2 March 1973. The resulting snow map of the basin is seen in Figure 3. Rectification in this case was much more difficult, owing to the large distortion found in the imagery, especially at the extreme edge of the image. The images were enlarged, usually about seven times, and stretched to make the drainage pattern of the image fit the drainage pattern of the map. The results, as well as those obtained using the ERTS-1 imagery, are shown as a snowmelt plot in Figure 4. These data will be compared with discharge data, which have not yet been secured. As of 15 July 1973, a trace of snow is still visible on Pyramid Peak (3043 m) in this basin.

Cost/Comparison Estimate of Satellite Snow Mapping

At the request of the Director of the National Environmental Satellite Service, a cost/comparison figure was calculated for satellite (NOAA-2) measurement of Sierra Nevada snow cover and for conventional aircraft measurements. Assuming that 20 basins were of interest and that a simple altimeter survey by a light plane is possible, at least 40 hours would be required at a total cost of at least $20,000. Using satellite data, the entire Sierra block could be mapped in two man-days for a direct cost of about $100. This is a comparative cost ratio of 200:1 in favor of the satellite.

Discussion

In terms of man-hours, ERTS-1 is six times faster than U-2 snow cover mapping, however, NOAA-2 VHRR snow cover mapping is almost as fast as ERTS-1, but the NOAA-2 VHRR data is more frequently available. With systematic scheduled coverage (and with no clouds) daily mapping of snow cover could be accomplished. The results of repeated trials of both ERTS-1 and VHRR snow mapping attempts are given in Table 1. The greater ground resolution of ERTS-1 and its cartographic fidelity make it outstanding as a snow mapping satellite. It has no peer in this respect. Yet to be of operational service, NOAA/NWS requires data at least weekly, and preferably semi-weekly. For operational

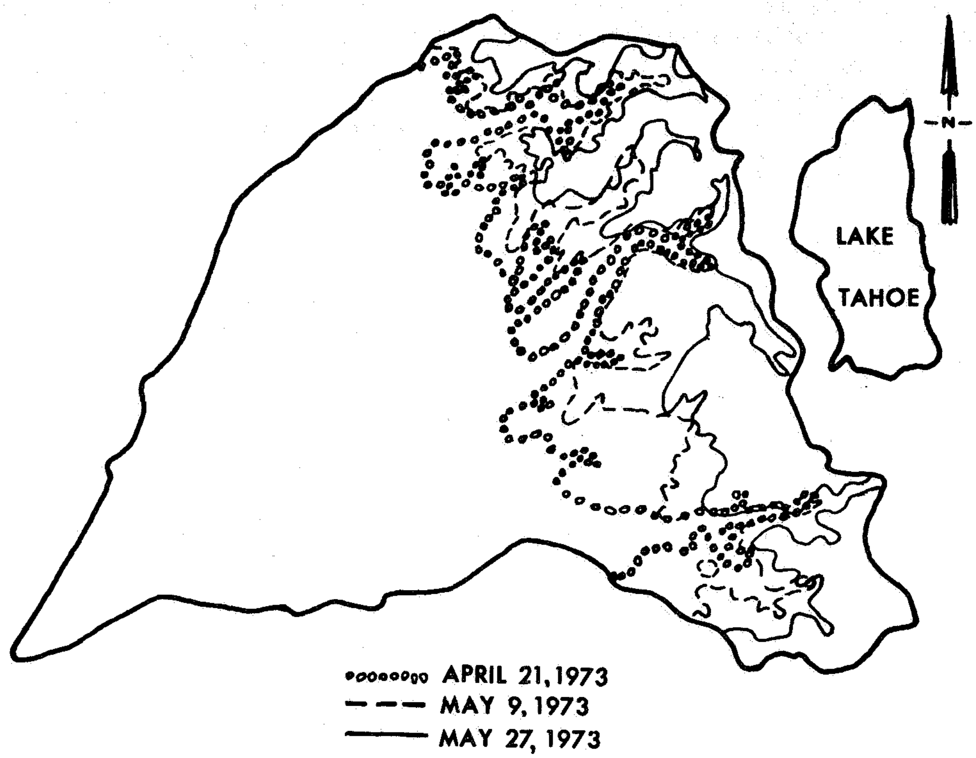

Figure 1. Composite snow extent map for the American River Basin, California, prepared from ERTS-1 MSS 4 imagery of 21 April, 9 May and 27 May 1973.

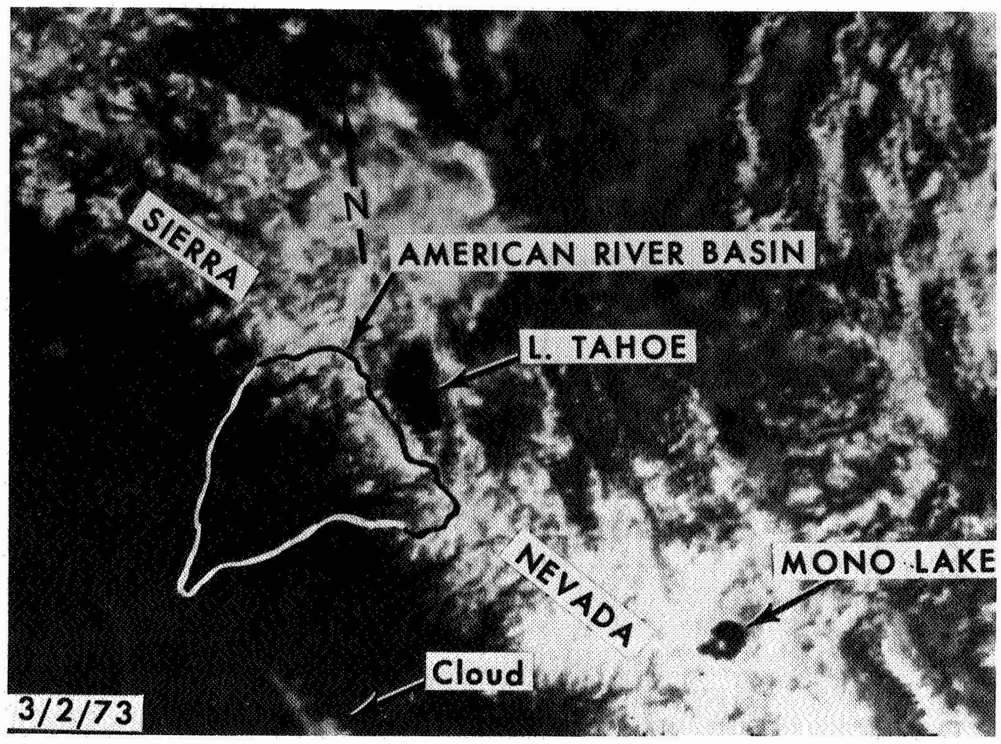

Figure 2. Enlarged VHRR-VIS image of the central Sierra Nevada 1713 GMT, orbit 1728 (recorded data). Figure 3 was prepared from this distorted image. Scale is about 1:4,000,000 and ground resolution is about one kilometer.

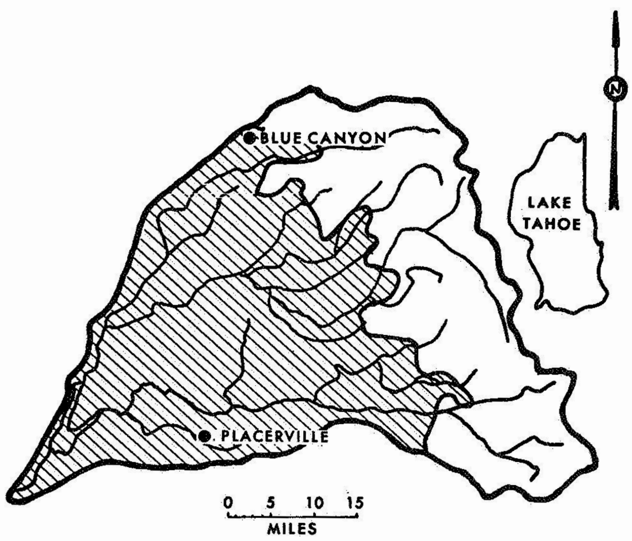

Figure 3. Snow-extent map for the American River Basin, Calif., prepared from NOAA-2 VHRR imagery shown in figure 2. Patterned area is snowfree.

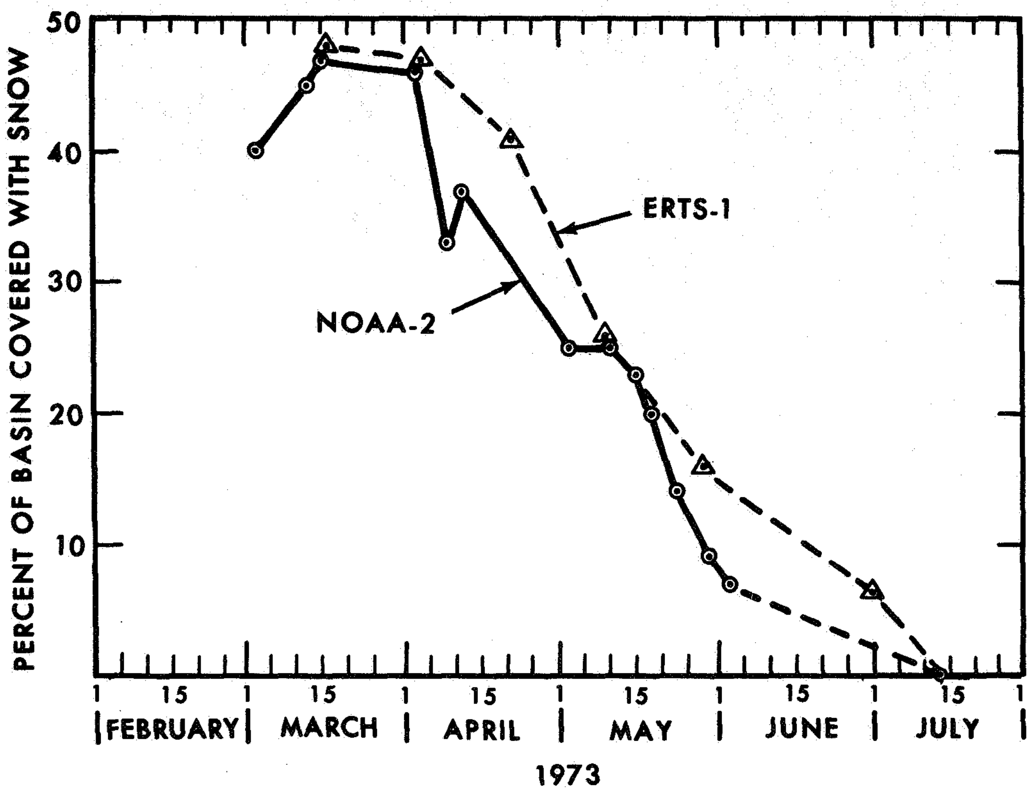

Figure 4. Comparison of snow-extent mapping of the American River Basin, California, by NOAA-2 and ERTS-1 satellites.

purposes, NOAA-2's daily visible and twice daily thermal IR coverage appears to be more useful for operational snow mapping and water-level forcasting. value of the ERTS-1 is its ability to provide a reliable check, or "calibration standard", with which the NOAA-2 satellite sensors can be compared and corrected. Another obvious drawback to the use of ERTS-1 data for forcasting purposes is the lag time between receipt of the data and its arrival in the hands of the concerned principal investigator.

AMERICAN RIVER BASIN, CALIFORNIA

Date	ERTS-1	NOAA-2
3/15/73	46%	46%
4/2/73	48%*	45%*

*Average of 4 trials, 2 operators. Each trial consists of 3 areal measurements.

Table 1. Preliminary comparison of snow extent (in percent of basin covered) by ERTS-1 and NOAA-2.

GREAT LAKES STUDIES

Lake Ice Dynamics

As shallowest of the Great Lakes, Lake Erie is subject to more extensive freezing and ice formation than any other of the Great Lakes. Freeze-up tends to be much more sudden than break-up and melting, which however can also be rather dynamic. For monitoring changing ice conditions, ERTS-1's 18-day revisit cycle again presents problems, as ice formation, movement and break-up may all occur within a very short time span and be unrecorded by the ERTS-1 satellite sensors.

Despite this possibility, excellent images of Lake Erie ice were recorded on 17-18 February 1973 and again on 8 March 1973. Strong, 1973, has already reported on an analysis of ice movement from changes noted on the sidelap portions of the images on the 17th and 18th. The two-day ERTS-1 sequence is shown in Figure 5.

Weather conditions may preclude this type of sidelap analysis of movement in many cases, but by analysis of the fracture patterns, it is believed that reasonably good estimates of ice movement may be made. Antecedent meteorological conditions are vital to such an analysis, as they are an overriding factor in determining the physical conditions and movement of the ice. As an example, imagery of the Cleveland area was analyzed by measuring the displacement of a series of characteristic ice edges which had broken from shorefast ice within the preceding 24 hours.

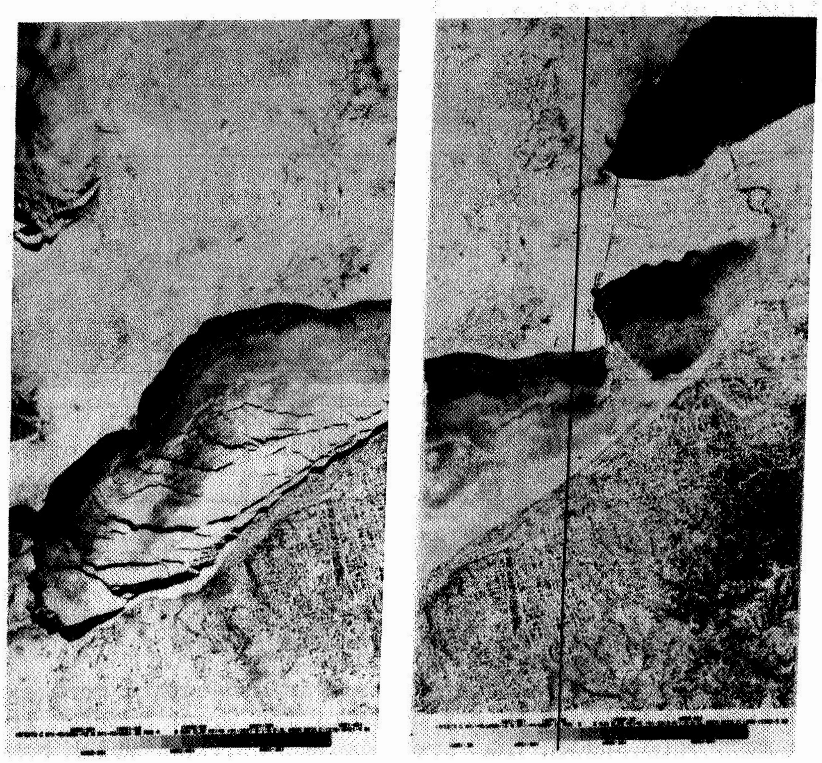

18 FEB. 1973   17 FEB. 1973

Figure 5. ERTS-1 sequel imagery of Lake Erie showing ice coverage on 17 and 18 February 1973. Air temperatures were below freezing at all stations for both days. Ice cracks seen in 18 February image had occurred during past 24 hours.

Preliminary estimates of ice movement range from 0.3 km/hr to 0.8 km/hr (0.2-0.4 knots) to the west. Strong's sidelap analysis of motion gave figures ranging from 0.5 km/hr to 1.5 km/hr (0.3-0.8 knots). Considering the fact that the onset of motion is not precisely known, the figures are in rather good agreement. The 100-m resolution of ERTS-1 provides outstanding data for synoptic ice pack studies, but it is severely constrained by the low frequency of coverage.

Snow and Ice Melt Detection

The near-IR (0.7-1.3μm), in combination with the visible band data (from Nimbus-3), can be used to detect melting snow (Strong, McClain and McGinnis, 1971). An early investigation (Mantis, 1951) showed that a large drop in the reflectance of melting snow occurs in the near-IR range of the spectrum (Figure 6). A recent, and soon to be published, work by the Cold Regions Research and Engineering Laboratories (CRREL) produced similar results (Figure 7). As these bands are present on the ERTS-1 MSS, attempts have been made to identify melting snow in mountainous areas (Wiesnet, 1973; Meier, 1973; and Barnes, 1973 using ERTS-1 MSS bands 5 (0.6-0.7μm) and 7 (0.8-1.1μm). However, the effectiveness of ERTS-1 in identifying areas of melting snow and ice is somewhat inhibited by the fact that MSS band 7 observes energy only to 1.1μm rather than to 1.3μm (as the High Resolution Infrared Radiometer [HRIR] did on Nimbus). It is between 1.1 and 1.3μm where reflectance of melting snow shows the greatest decrease.

ERTS-1 MSS imagery over Lake Erie (8 March 1973) has been examined (images #1228-15422-5 and -7, Figures 8a and 8b, respectively) for melting ice. The ice field in band 5 has high reflectance but the ice field has a "lacy" appearance resulting from many thaw holes, characteristic of "rotten" ice (i.e. ice deteriorating under warm temperatures). Table 2 shows the air temperatures and wind data for stations near Lake Erie before and after the ERTS-1 pass (1542 GMT). Note that no station reported below freezing temperatures.

STATION	TEMP (°F)			WIND (KNOTS)		
	1200Z	1500Z	1800Z	1200Z	1500Z	1800Z
Erie	45	54	56	SW 10	SW 10	NW 20
Cleveland	43	55	61	SW 5	SW 5	W 10
Toledo	39	52	61	S 10	W 5	W 10
Detroit	38	50	57	SW 5	SW 5	SW 20
London, Ont.	38	47	52	SW 5	W 15	W 20
Buffalo	42	49	54	SW 5	SW 15	W 20

Table 2. Meteorological data before and after the ERTS-1 pass on 8 March 1973.

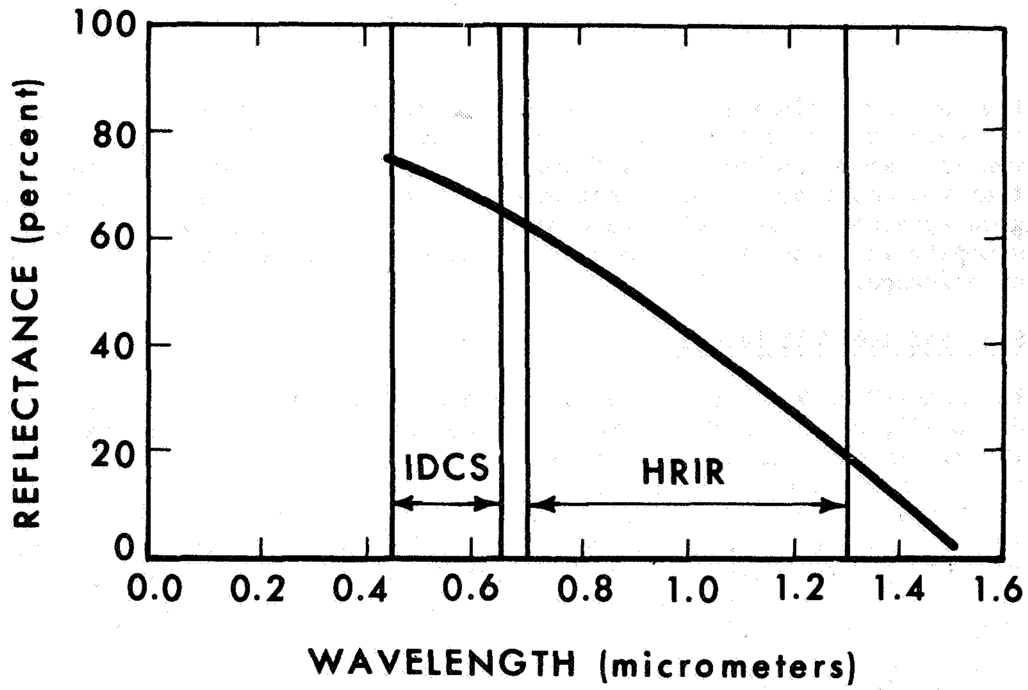

Figure 6. Spectral reflectance of melting snow (Mantis, 1951).

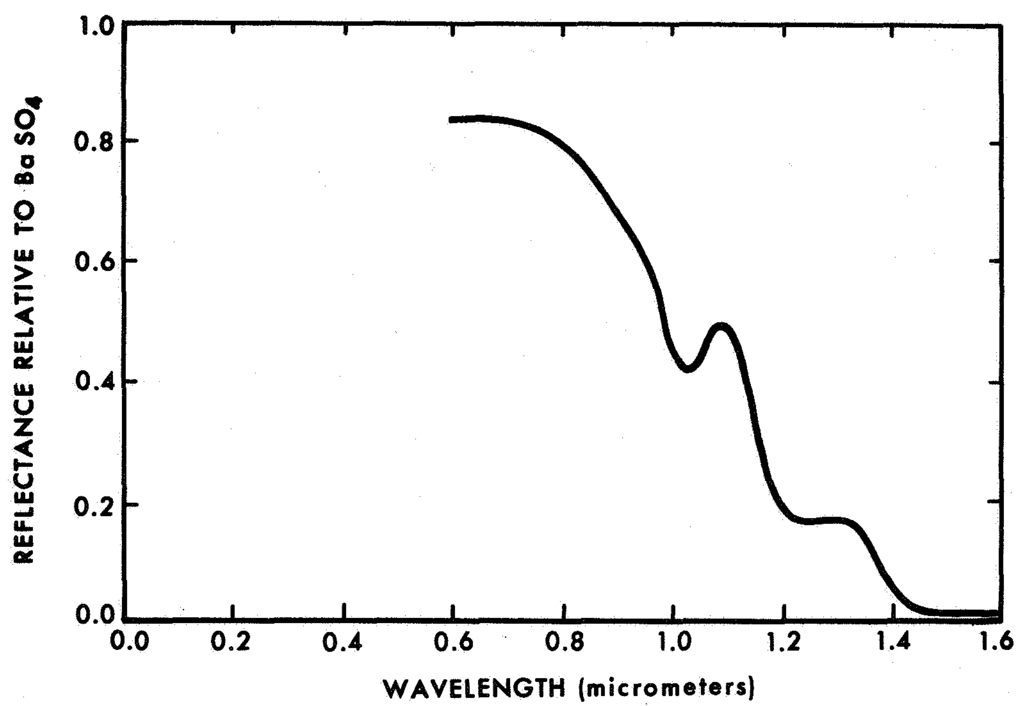

Figure 7. Spectral reflectance of melting snow at 0°C in cold room at CRREL, Hanover, New Hampshire, 1973.

Figure 8a. ERTS-1 image of Lake Erie in MSS band 5, 8 March 1973.

Figure 8b. ERTS-1 image of Lake Erie in MSS band 7, 8 March 1973.

The decreased reflectance in the near-IR (band 7) is rather pronounced, particularly in the central region of the ice where many thaw holes exist. Here the southerly winds have not compacted the ice, as is evident along portions of the southern ice edge and along the northern lake shore. However, it is apparent that the two images were developed and processed differently. To eliminate this photographic shortcoming, computer printouts of these images are presently being examined to compare quantitatively the spectral differences.

Other ice features tentatively identified on these images are: grounded ice west of Pt. Aux Pins, Ontario; an icefoot near Marblehead, Ohio and along the east edge of Pt. Pelee, Ontario; the compacted ice edge of the southern edge of the icefield northwest of Cleveland, Ohio; the young ice-snow sheet broken up by wave action east of Pt. Aux Pins; and brash belts oriented almost N-S between Painesville and Astabula, Ohio.

Snow Mapping of the Lake Ontario Basin

Difficulty was encountered in attempting to snowmap the Lake Ontario Basin. The 70,000 km^2 basin requires two ERTS-1 frames from four orbits, each a day apart. The changing winter weather patterns, as well as the cloud-inducing open water on Lake Ontario, prevent a four-day cloudfree period from occurring. The best period for snow mapping was 9-12 January 1973. Even so, cloudiness in the eight frames of ERTS-1 imagery ranged from 10 to 80 percent. The problem of cloud contamination, however, should be greatly alleviated for basins less than 30,000 km^2 in area.

SUMMARY AND CONCLUSIONS

Snow mapping studies of the Sierra Nevada have shown that maps can be produced six times as fast by the use of ERTS-1 imagery than from high altitude (64,000 feet) aerial photographic surveys. ERTS-1 70-mm images are most effectively used for snow mapping in moderately-sized (250 - 30,000 km^2) basins, such as the American and Feather River Basins in California. The images are especially useful in checking the accuracy of the daily VHRR data from NOAA-2, which are not as precise cartographically as the ERTS-1 data. Preliminary estimates are that VHRR maps are usually within five percent of the ERTS-1 estimate. The cost of Sierra Nevada snow maps produced from imagery of either satellite are estimated to be one-two hundredths of the cost of maps made from aerial surveys.

Ice conditions in the Great Lakes can be readily determined by ERTS-1. Ice features characteristic of thawing conditions, such as rotten ice, brash belts and compacted ice edges, can be identified. A great decrease in apparent reflectivity in band 7 compared with band 5 also indicates melting conditions.

The ERTS-1 satellite has proved itself capable of providing data for assessing various hydrologic characteristics, especially as regards ice and snow. The 100-meter ground resolution of the Multispectral Scanner (MSS) produces unsurpassed images to measure snow extent or to assess ice conditions on large lakes. ERTS-1 is hampered by the 18-day revisit time and by the 30- to 60-day wait from the collection of data to receipt by the investigator. Drainage

basins greater in area than 34,000 km^2 exceed the size of one ERTS-1 frame and present snow mapping problems when two or more successive day's passes are needed. However, the ERTS-1 truly presents a great opportunity to the hydrologic community to plan and carry out an improved program of satellite snow and ice observations.

REFERENCES

Barnes, J.C., 1973, Use of ERTS Data for Mapping Snow Cover in the Western United States, Symposium on Significant Results Obtained from ERTS-1, March 5-9, 1973, New Carrollton, Maryland.

Mantis, H.T., 1951, Review of the Properties of Snow and Ice, available from U.S. Cold Regions Research and Engineering Laboratory, Hanover, N.H., p. 62.

Meier, M.F., 1973, New Ways to Monitor the Mass and Areal Extent of Snow-cover, Symposium on Approaches to Earth Survey Problems through the use of Space Techniques, COSPAR, Konstanz, West Germany.

Strong, A.E., McClain, E.P. and McGinnis, D.F., 1971, Detection of Thawing Snow and Ice Packs through the Combined use of Visible and Near-Infrared Measurements from Earth Satellites, Monthly Weather Review, Vol. 99, No. 11, pp. 828-830.

Strong, A.E., 1973, New Sensor on NOAA-2 Satellite Monitors the 1972-73 Great Lakes Ice Season, Proc. Amer. Water Resources Assoc. Symposium on Remote Sensing and Water Management, Burlington, Ontario, Canada.

Wiesnet, D.R., 1973, Detection of Snow Conditions in Mountainous Terrain, Earth Resources Technology Satellite-1, Symposium Proceedings, September 29, 1972, pp. 131-132.

Paper W 3

NEW SPACE TECHNOLOGY ADVANCES KNOWLEDGE OF THE REMOTE POLAR REGIONS

William R. MacDonald, *Chief, Branch of International Activities Topographic Division, U.S. Geological Survey National Center, Reston, Virginia 22092*

ABSTRACT

The application of ERTS-1 imagery is rapidly increasing man's knowledge of polar regions. Products compiled from this imagery relating to the experiments being conducted under proposal SR-149 at scales of 1:250,000, 1:500,000 and 1:1,000,000 are already providing valuable information to earth scientists working in Antarctica. Significant finds detected by these "bench mark" products were glaciological changes, advancement in ice fronts, discovery of new geographic features, and the repositioning of nunataks, islands, and ice tongues. In cooperation with the American Geographical Society and funded by the National Science Foundation, ERTS imagery has been used for the compilation of a 1:5,000,000-scale map of the Arctic.

Products such as single-scene pictorial images and photoimagery mosaics have been compiled that often exceed the accuracy of existing cartographic products in Antarctica. A graticule has been fitted to the imagery based on a least-squares adjustment of identifiable control points which were established by standard surveying techniques as well as by satellite geodesy.

Tests conducted under proposal SR-149 in Antarctica have proven the feasibility of tracking Navy navigation satellites to establish ground control for positioning ERTS-1 imagery in remote areas. ERTS imagery coupled with satellite geodesy shows great promise and may prove to be the most practical and cost effective way to meet the small-scale cartographic requirements of the polar science community.

Prepared for presentation at the Third ERTS-1 Principal Investigator's Symposium - December 10-13, 1973, Washington, D.C.

INTRODUCTION

ERTS imagery perhaps has its most immediate application and benefit to the scientific community in the Antarctic region. Although millions of dollars have been expended over more than 25 years toward obtaining aerial photo coverage for small-scale mapping in the Antarctic, only about one third of the continent has been photographed or adequately mapped. In this regard ERTS offers the most practical means of obtaining cloud-free imagery over the millions of square miles yet to be mapped. ERTS appears to be the only way that the cartographic community has of meeting, in a relatively short period, the demands for small-scale imagery products by national and international polar scientists.

ERTS-1 MSS IMAGERY REQUIREMENTS

The nine experimental areas listed in proposal SR-149 aggregate areas from 60° to 82° latitude in both polar regions and add up to millions of square miles. The number of ERTS images of the areas of interest received from NASA on automatic distribution increased so rapidly that a system of indexing became necessary. To date about 500 scenes over Antarctica and about 3,500 scenes over the Arctic region have been received, amounting to 16,000 individual negatives (4 MSS bands) with cloud cover less than 14%.

Storage and retrieval of each ERTS-1 70-mm image and each 1:1,000,000-scale contact print were done manually, but it was too time consuming to search the files for the best imagery, and the cartographer could never be sure that all the available imagery had been reviewed. What was needed was an efficient system that would tell the cartographer the cloud-cover percentage of any particular ERTS image.

IMAGERY INDEXES

To meet these needs indexes were designed in graphic form (fig. 1). They have proved convenient to prepare and practical to use. A CalComp drum plotter was used to plot the individual scenes with identifying scene numbers. The original index plots were prepared on a stable transparent base and keyed to a 1:10,000,000-scale base map. Each 18-day cycle is depicted on two index sheets--odd days on one sheet and even days on another. Data used to plot these indexes were obtained from punched cards from the U.S. Geological Survey's EROS Data Center, Sioux Falls, S. Dak.

Separate indexes show imagery with percentages of cloud cover: 0 to 14, 15 to 34, and 35 to 54. A composite index showing all available imagery, with cloud cover from 0 to 100 percent, was prepared for each 18-day cycle.

ARCTIC **ANTARCTICA**

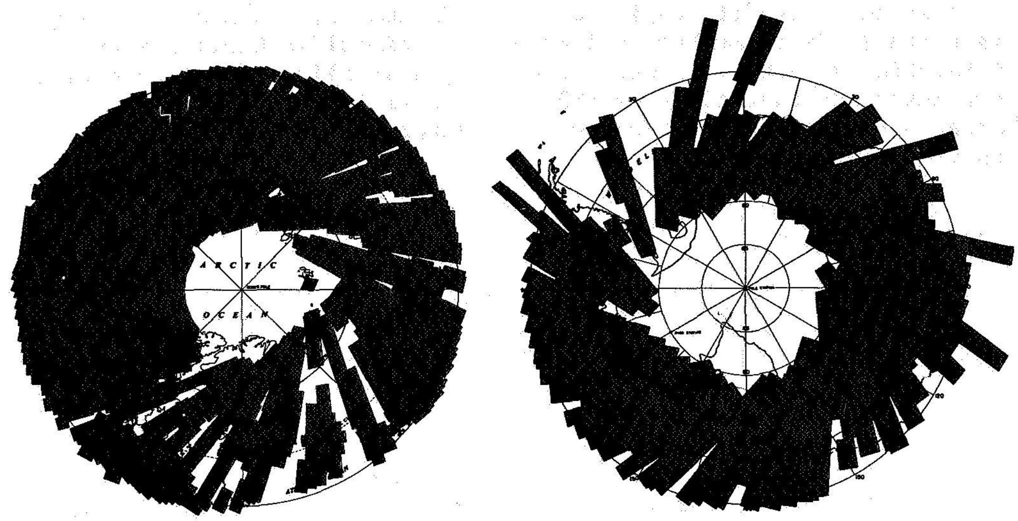

ERTS-1 Imagery Diagrams
Coverage, 0% - 100% cloud cover

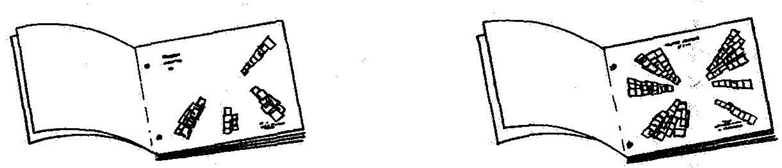

Coverage: 18 day cycles

Cloud Cover : 0 - 100% 15 - 34%
0 - 14% 35 - 54%

Figure 1.--ERTS-1 Imagery Index Binders. The Arctic and Antarctic binders are prepared at 1:10,000,000 scale for each 18-day cycle and depict percentages of cloud cover.

Transparent or paper copies can be produced by the diazo process. Copies of the indexes of the polar regions can be purchased from the USGS, Map Information Office, National Center, 12201 Sunrise Valley Drive, Reston, Va. 22092. Transparent copies cost $3.50 each, and paper copies cost 75 cents each.

As a spinoff benefit, copies of all ERTS Imagery Indexes are being made available to member nations of the Scientific Committee on Antarctica Research. Japan, Argentina, Australia, and South Africa are currently investigating the use of ERTS imagery over their areas of interest in Antarctica as a direct result of investigations carried out under this proposal.

IMAGERY PRODUCTS

Although we have a long way to go, ERTS has already disclosed a few of Antarctica's secrets. Products compiled in accordance with the objectives outlined under proposal SR-149 have demonstrated their value to the polar research community. Orthoimage products compiled include 1:1,000,000-scale imagery mosaics and single-scene 1:250,000- and 1:500,000-scale gridded images. Imagery has also been used as a source for recompilation of small-scale maps in the Antarctic and Arctic regions. Significant finds resulting from analysis of these products include discovery of new geographic features, advances in the world's largest ice fronts, coastal glaciological changes, and repositioning of nunataks, islands, and ice tongues. Figures 2, 3, and 4 are examples of imagery application.

Our preliminary results, which have been published[1], indicate that ERTS imagery has the potential for rapid compilation of orthoimage products that meet the small-scale map requirements of the cartographic and scientific communities. However, the usefulness of any ERTS imagery product is extremely limited unless the image data can be related to an Earth reference system. Therefore, ground control points must be used to maintain the relative and absolute relationship between image points and their earth positions. Thus, if ERTS imagery is to be fully utilized as a cartographic and scientific tool, a framework of geodetic control must be available to relate the image data to an Earth reference system.

MEETING ERTS POLAR REGIONS CONTROL REQUIREMENTS

Since control in the polar regions is very sparse and extremely expensive and difficult to establish, it was necessary to find an economical means of acquiring the amount of control needed to maintain the integrity of ERTS cartographic products.

[1] R. B. Southard and W. R. MacDonald, The Cartographic and Scientific Application of ERTS-1 Imagery in Polar Regions (A.6.4.), presented at the Symposium on Approaches to Earth Survey Problems, Konstanz, FRG, May 1973.

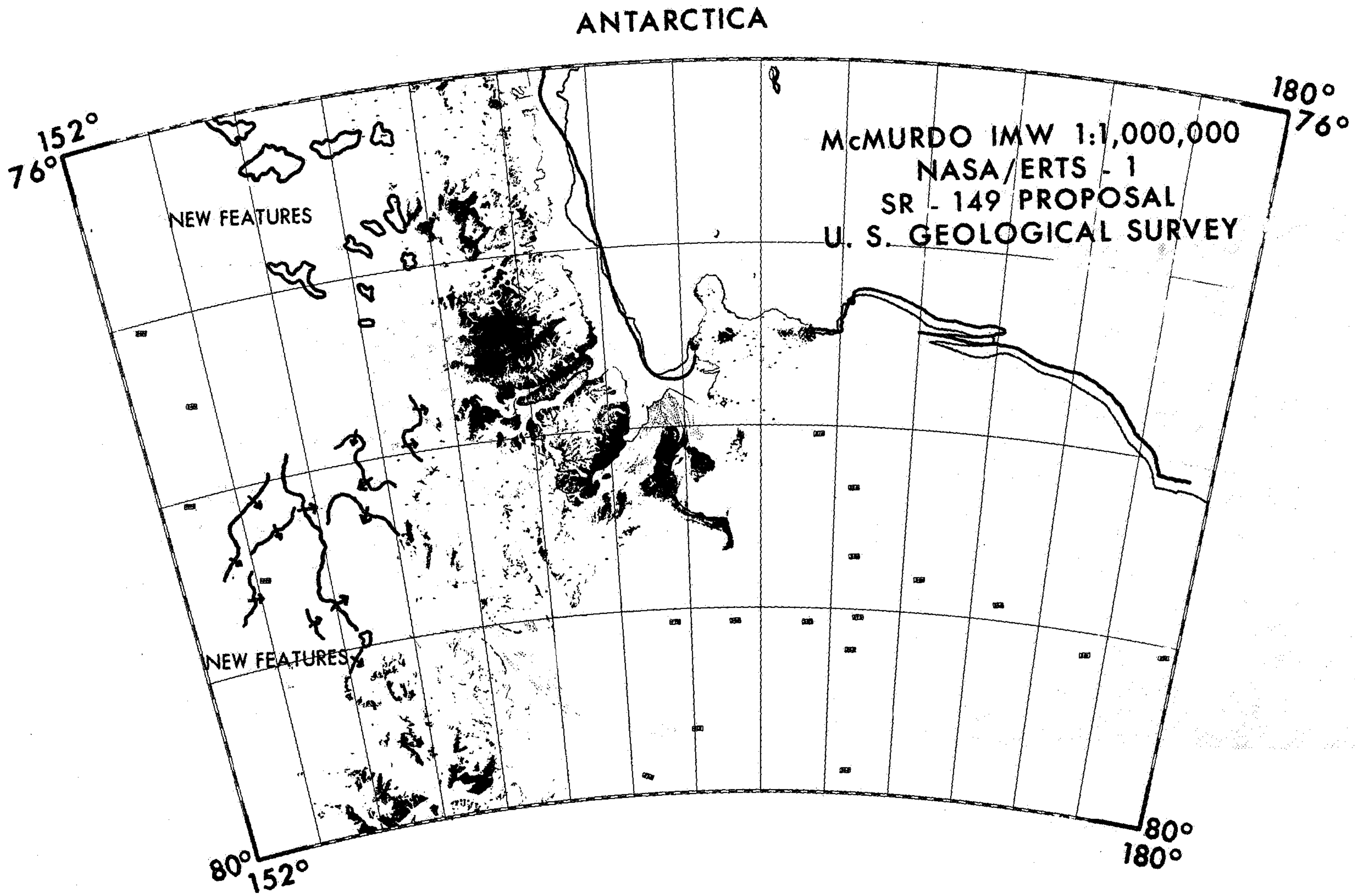

Figure 2.--McMurdo IMW Manuscript. Annotations indicate additions and changes determined from ERTS imagery to coastlines, advancement of the Ross Ice Shelf front by about 4 miles, and the repositioning of Franklin Island by about 4.5 miles.

Figure 3.--Drygalski Ice Tongue, Victoria Land Coast, Antarctica. From ERTS imagery, the 1:250,000-scale U.S. Geological Survey topographic maps will be revised during compilation of the next editions. Annotations depict changes to glaciers, ice tongues, and coastlines:

A Harbord Glacier

B Drygalski Ice Tongue

C Fast ice

Figure 4.--Arctic Region, Alaskan-Western Canadian Quadrant. ERTS-1 imagery was used as latest data source in compiling 1:5,000,000-scale American Geographical Society (AGS) Arctic Region map scheduled for publication in 1974. Blocked areas indicate sections where ERTS-1 imagery was used to revise the manuscript. The three additional quadrants were treated in the same manner.

Investigations jointly funded by NASA and the National Science Foundation were conducted by the USGS in Antarctica to determine the practicality of using recently developed Doppler positioning and navigation systems for establishing the much-needed control. The mode tested was the single-point positioning method, which consists of a receiver tracking a satellite pass and computing the position from the Doppler shift and the satellite ephemeris. The experiments proved that Doppler-equipped polar-orbiting satellites can be used as a surveying tool and that mapping control can be obtained under Antarctic field conditions.

As a result of the Doppler positioning experiments, it is now possible to make maximum cartographic use of ERTS imagery in polar regions by deploying specially equipped rover teams of topographic engineers to establish ERTS ground control. In the Antarctic, plans are to deploy teams by aircraft to preselected ERTS image points, which they will occupy with Geoceiver equipment for a predetermined period depending on the image accuracy requirements (a one-pass real-time solution will give an accuracy of 100 to 200 meters) and the geometry of the Navy Navigational Satellite's orbit. An attempt will be made to establish ERTS imagery control in the Thwaites Iceberg Tongue area during an expedition into Pine Island Bay in February 1974.

GRIDDED ERTS IMAGERY

Positions obtained during the Doppler positioning experiments were used along with existing control to fit a grid to a single-scene image (1174-19433-7, January 1973) of the McMurdo Sound Region, Antarctica (fig. 5).

The technique of converting an ERTS scene into a cartographic product by manipulating the grid rather than the image (rectification) appears to be the most practical and cost-effective way of relating polar ERTS image data to the Earth's surface. Normally the procedure is to manipulate the photoimage through tilt analysis and rectification to fit a grid. However, when applying these procedures to ERTS imagery, geometry is improved but too much detail (resolution) is lost during the photographic processes. Four steps are required to fit a grid to an ERTS image:

1. Identification of discrete image points whose coordinates are known.

2. Accurate measurement of the x and y values of these control points on the image scene.

3. Determination of the transformation parameters to relate one system to the other and computation of the intersection of the grid lines in an image coordinate system, warping the grid to fit the image.

4. Plotting the grid on an overlay keyed to the image.

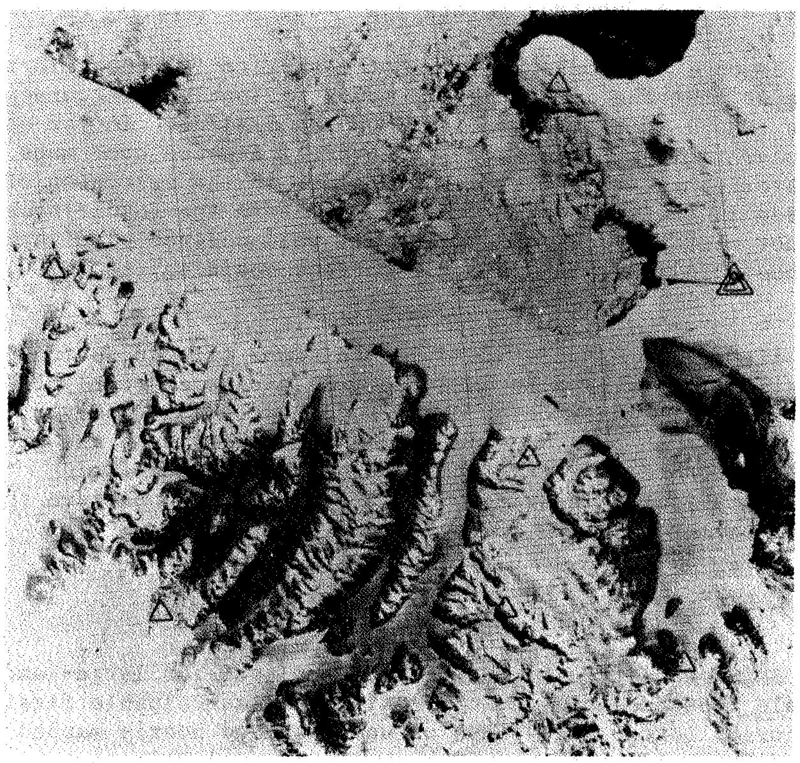

Legend

△ Geodetic Control
(Standard Surveying Methods)

△ Geodetic Control
(Derived from Doppler Satellite Data)

Figure 5.--Ross Island Dry Valley Area, Antarctica. Annotations indicate distribution of geodetic control stations used to construct the fitted grid for the single ERTS-1 scene (1174-19433-7, January 1973). Produced at scales of 1:500,000 and 1:250,000.

The accuracy of photoidentification of the control points is the primary element that determines the accuracy of the grid fit. In the mid-latitudes, where large-scale accurate maps are available, good results can be obtained by using images of timber corners, fence lines, centers of bridges over streams, pipe and power line crossings, etc., as control points.

In these areas it is possible, in most cases, to fit the grid to the image so that the image product meets National Map Accuracy Standards (NMAS) at scales of 1:500,000 and smaller. In the poorly mapped polar regions, especially in Antarctica where good maps and control are scarce, there is less certainty in the selection of points used in the gridding process. Therefore the resulting grid fit may not meet NMAS (90 percent of all well-defined planimetric detail should fall within 0.5 mm of correct position) at 1:500,000 scale.

The grid fit to the McMurdo Sound Region scene (fig. 6) using 13 triangulation points gave an RMSE (root-mean-square error) of 183 meters or about 10 meters over what would meet NMAS. However, if discrete points had been preselected on the imagery and the ground positions for these points established by the Doppler field techniques previously described, it is reasonable to believe that NMAS could be met at 1:500,000 scale and smaller.

SUMMARY

Although ERTS products will not replace the need for large- and small-scale topographic maps, they will serve as valuable first-look pictorial (orthoimage) maps of unmapped and poorly mapped regions of the world. They will be extremely valuable as scientific and logistic planning documents, for identifying new geographic features, and for assessing the areal cartographic needs of the polar regions. If we are to have a better understanding of the way the polar regions affect man, especially in Antarctica with its potential resources, there is an immediate need to know what's there and where. ERTS with the aid of the Navy Navigational Satellites appears to be the tool to satisfy these most pressing needs. Space technology offers a new concept for producing small-scale imagery products of remote regions that is substantially cheaper and quicker than production by conventional means.

CONCLUSIONS

Conclusions as to the use of ERTS MSS imagery in polar regions are summarized as follows:

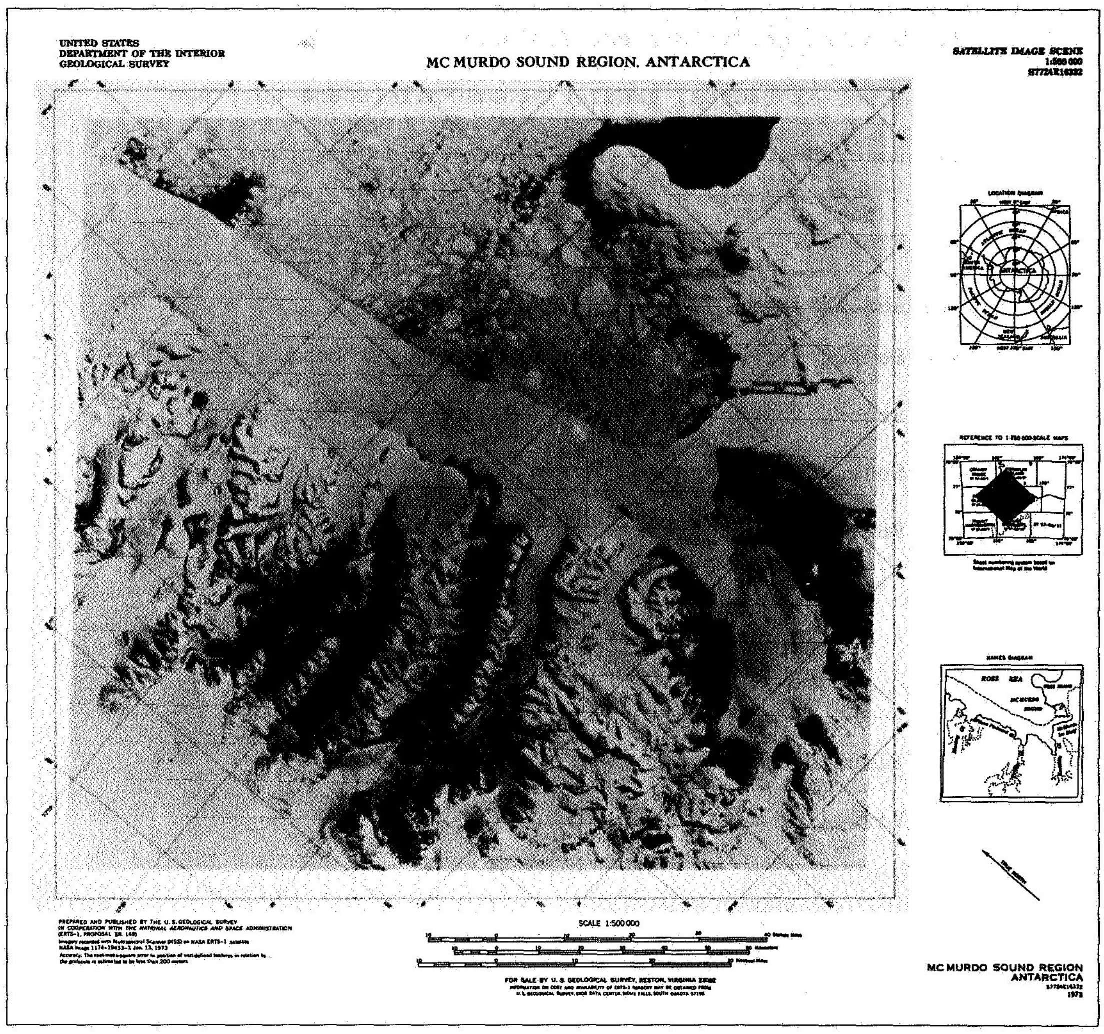

Figure 6.--McMurdo Sound Region, Antarctica. A single ERTS-1 image scene, 1174-19433-7, January 1973, was enlarged to 1:500,000 scale. A fitted grid was prepared from existing geodetic control and superimposed on the image.

Advantages - ERTS Synoptic Coverage

1. Current, complete, and repetitive coverage

2. First-look imagery of unmapped areas

3. Weather conditions not dominant

4. Fewer exposures; greater square-mile scene coverage

5. Reduced compilation cost for small-scale products (ie: 1:1,000,000)

6. Single scene; broad overview

Special Uses and Benefits

1. Source for medium- and small-scale orthoimage products

2. Source for medium- and small-scale map revision

3. Source for image mosaics

4. Real-time bench mark for thematic mapping:

   Coastal change detection

   Sea ice studies

   Ice movement studies

5. Planning document

6. Visual navigational aides

Paper W 4

ERTS-1 DATA IN SUPPORT OF THE NATIONAL PROGRAM OF INSPECTION OF DAMS

G. E. Graybeal and F. G. Hall, *NASA, Johnson Space Center, Houston, Texas,* B. H. Moore and E. H. Schlosser, *Lockheed Electronics Co., Inc., Houston, Texas*

ABSTRACT

The National Aeronautics and Space Administration's role in the national Earth Resources Survey Program emphasizes the development and transfer of remote sensing technology to operational organizations such as federal agencies, or state and local governments. Within the scope of this effort a computer-aided procedure, for use in the detection and location of areas of surface water, has been developed by the Earth Observations Division in the Science and Applications Directorate at the Lyndon B. Johnson Space Center, Houston, Texas.

The procedure was developed in support of the National Program of Inspection of Dams established by Public Law 92-367. The procedure utilizes data acquired by the unmanned Earth Resources Technology Satellite (ERTS-1) in conjunction with ancillary data in the form of topographic and highway maps, and meteorological data summaries.

The procedure is divided into several distinct phases. A five-volume manual has been prepared to instruct potential users of the procedure.

INTRODUCTION

The overall goals of the national Earth Resources Program are to provide a data acquisition capability to collect remotely sensed information on the conditions of the land, the oceans, and the atmosphere; to provide a data handling and processing capability for translating the data into an analyzable form and insure effective distribution; to provide interpretative techniques and methods of analysis for converting data into earth resources information; and to provide the means for applications analysis and technological transfer permitting the effective application of information to management of the earth's resources. The goals and objectives of the National Aeronautics and Space Administration in the Earth Resources Program are based on the above, with emphasis on the development and transfer of remote sensing technology to operational organizations, such as federal agencies, states, and local governments. This paper illustrates a remote sensing technological application which is available for transfer to the user community.

In August 1972, the President signed Public Law 92-367 authorizing the Secretary of the Army to undertake a National Program of Inspection of Dams. A report by the Secretary of the Army to Congress is due on or before July 1, 1974. The report is to include (1) an inventory of all dams located in the United States, (2) a review of each inspection made, and recommendations furnished to the governor of the state in which such dam is located and information as to the implementation of such recommendations, and (3) recommendations for a comprehensive national program for the inspection and regulation for safety purposes of dams of the nation and the respective responsibilities which should be assumed by the federal, state and local governments and by public and private interests.

To facilitate completion of a nationwide inventory of all impoundments, deemed to be within the Scope of the National Program of Inspection of Dams, the U.S. Army Corps of Engineers (COE) designed an information form which basically divides the information required into two general categories. The first category is related to the identification and location of each impoundment while the second category is related to physical parameters, design information, and previous inspection information related to each impoundment.

An up-to-date inventory of all water impoundments in the United States is a prerequisite for satisfying the first requirement of the National Program of Inspection of Dams, and a partial basis for selection of those impoundments to be included in the comprehensive national program. The computer-aided procedure described in this paper will provide a methodology for use in the completion of the initial inventory and for use as a method of updating this inventory as part of the comprehensive national program.

In December 1972, the Texas Water Rights Commission (TWRC) submitted, through the Office of the Governor of Texas, a request for assistance by the Earth Observations Division, Science and Applications Directorate, Johnson Space Center, in the development of an operational prodedure for utilizing data acquired by the Earth Resources Technology Satellite (ERTS-1) in detecting and locating surface water.

PROCEDURE DEVELOPMENT

Pursuant to the Texas Water Rights Commission's request, the Earth Observations Division undertook design of a controlled investigation in which the feasibility of developing a procedure or procedures for using ERTS-1 data to detect and locate surface water would be evaluated quantitatively.

Operational Constraints

The first step in the design of the controlled investigation was to define the major operational constraints, the Texas Water Rights Commission would be required to apply to a developed procedure. The constraints and the technical implications related to each constraint are

a. The only digital data display device available was a standard line printer operating at six lines per inch. Asymmetrical aspects of the ERTS-1 digital data along with the use of the line printer display required registration of the ERTS-1 data prior to generation of a digital display. The selected registration process combined with a digital display at a scale of 1:24,000 resulted in approximately 28% of the original digital data being discarded. As a result of the uncertainty of this data loss on classification accuracy, a technical constraint was adopted which precluded registration prior to classification processing.

b. The technical analysts anticipated to use the developed procedure in an operational climate would be relatively unfamiliar with computer-aided processing of remotely sensed data. This required the development of highly proceduralized techniques to maintain the reliability of the classifier by minimizing the effects of human subjectivity.

c. The transferred procedure must be cost effective in comparison to other techniques being evaluated by the State. From this constraint, it was determined that acquisition of ground truth for classifier training by either field visits or collection of aircraft imagery would not be cost effective. Therefore, it was determined that the analyst would only have access to existing maps and conventional records for supporting the selection of training data and that the analyst would be required to select training data, using only the information contained on the ERTS-1 system corrected computer compatible tapes, and prior knowledge of the spectral appearance of water as recorded by the ERTS-1 multispectral scanner.

Performance Criteria

The second step in the investigation design was the establishment of performance criteria for use in quantitatively evaluating the developed computer-aided procedure(s). The Public Law addresses the physical dimensions of impounding dams together with the volume of water capable of being impounded by the dams. Ground resolved distances within ERTS-1 MSS data precludes the determination of physical dimensions of dams but is compatible with the resolution of surface water 4.04 hectares (10 acres) or greater in areal extent.

Discussions were held between NASA and the TWRC, together with the COE, to arrive at a surface area threshold which could reasonably be correlated with minimum volumes of impounded water as addressed in the Public Law. TWRC decided that water bodies in Texas with a surface areal extent of 4.04 hectares (10 acres) or greater would be a reasonable approximation to the requirements defined in the Public Law. Onsite investigations by personnel of the TWRC of those water bodies detected and located would yield additional data required pursuant to the Public Law.

The discussions culminated in an agreement by the NASA, the TWRC, and the COE on the following evaluation criteria to be applied to each procedure tested. This criteria is as follows:

A procedure is acceptable if all areas of surface water 4.04 hectares (10 acres) or greater in areal extent are correctly detected and identified with an accuracy of 90% or greater with a frequency of false detection of 10% or less. In addition, the information to be extracted is to be registrable to a scale of 1:24,000 with the geographic location of each resolution element (pixel) classified as water determined to a positional accuracy of 300 meters (1,000 feet) or closer.

Performance Evaluation Procedure

The third step in the design was the development of a performance evaluation procedure to facilitate a decision related to the acceptability of the developed computer-aided procedure(s). The computer-aided procedures for the detection and location of surface water each produce results in the form of alphanumeric symbols on computer line printer output. Each symbol corresponds to the ADP classification of an ERTS-1 MSS pixel as water. The line printer output is defined as a classification map.

Initial experience gained in the conduct of this investigation indicated a correlation between actual water surface area and the number of line printer symbols classified by the ADP technique to be water.

To analyze the results, it was decided to define three surface water area classes based on the number of contiguous ADP identifications of water on the classification map:

a. Class 1 area - A classification map area containing one ADP symbol is defined as the ADP identification of areas of surface water of 0.8 to 2.79 hectares (2 to 6.9 acres).

b. Class I area - A classification map area containing two contiguous ADP symbols is defined as the ADP identification of areas of surface water of 2.53 to 4.01 hectares (7.0 to 9.9 acres).

c. Class III area - A classification map area containing three or more contiguous ADP symbols is defined as the ADP identification of areas of surface water of 4.04 hectares (10 acres) or more.

The evaluation procedure was based on the defined classes. Table 1 gives a set of equations which were utilized to evaluate the various ADP techniques employed.

Selection of Study Area

The fourth step in the design was the selection of a geographic study area which supported the controlled aspects of the evaluation of

TABLE 1:

	Class I	Class II	Class III
Percent of each class identified as Class I	F_{11}	F_{12}	F_{13}
Percent of each class identified as Class II	F_{21}	F_{22}	F_{23}
Percent of each class identified as Class III	F_{31}	F_{32}	F_{33}
Percent of each class falsely identified	F_{01}	F_{02}	F_{03}

F_{ij} = frequency with which ADP identification of class j areas were actually class i areas (i.e. class j areas mis-identified as class i areas).

F_{oj} = frequency with which ADP identification of class j areas were actually not an area of any class. (Frequency of False Detection)

$$F_{ii} = \frac{L_i}{M_i} \qquad\qquad F_{ij} = \frac{K_{ij}}{N_j}$$

L_i = the total number of correct ADP identifications of class i areas.

M_i = the total number of class i areas in study area.

N_j = the total number class j areas.

K_{ij} = number of ADP identifications of class j areas which were actually class i areas.

K_{oj} = number of ADP identifications of Class j areas which were actually not an area of any class.

candidate computer-aided procedures.

To evaluate the ADP techniques, it was necessary to select a study area for which an inventory of surface water 4.04 hectares (10 acres) or greater, together with an intensive study area with 0.80 hectares to 4.04 hectares (2 - 10 acres) surface water could be generated. Such information could be generated by selecting an area for which there existed nearly concurrent overpasses of ERTS-1 and aircraft photographic missions. The inventory of surface water in the selected study area determined from aircraft imagery would constitute the "ground truth" for evaluation.

A survey was therefore made of available in-house ERTS-1 tapes being used within the Earth Observations Division ERTS-1 Project. The corresponding 1:24,000 United States Geological Survey (USGS) topographic sheets were reviewed to identify geographic areas with lakes of various sizes. The review indicated that the Lake Somerville area of East-Central Texas was desirable for selection as a study area. An area was found which had both ERTS-1 coverage and relatively concurrent aircraft imagery, both cloud-free. The imagery from Mission 220, flown November 8, 1972, is a subportion (approximately 1/4) of the area covered by the October 23, 1972, ERTS-1 computer compatible tape (CCT), number 3 of 4 (ERTS-1 scene E1092-16305). The area extends from the Colorado River north to the Bryan-College Station area. Therefore, the geographic area covered by Mission 220 imagery was selected as the study area. The ERTS-1 CCT, Mission 220 imagery, and the corresponding 1:24,000 topographic sheets were acquired as tools for this investigation. Figure 1 shows the complete ERTS-1 frame and the third strip containing the study area.

Generation of Ground Truth Overlay

The fifth step was the generation of a ground truth overlay for the geographic study area detailing the location and sizes of surface water areas. This overlay was compiled at a scale of 1:24,000 to correspond to existing USGS, 7 1/2 minute quadrangle maps, using the Mission 220 color infrared imagery.

The study area imagery was analyzed to provide the surface water inventory. Information was compiled at a scale of 1:24,000 for the total number of water bodies above about 3.24 hectares (8 acres), and for the location of each water body. To facilitate the use of the ground truth information a clear acetate overlay was produced containing the derived information.

The following is a description of the steps employed in generating the ground truth overlay:

a. The 21 frames of Mission 220 imagery, roll number 3, frames 45 through 66, relating to the study area were acquired together with 1:24,000 topographic maps for the same area.

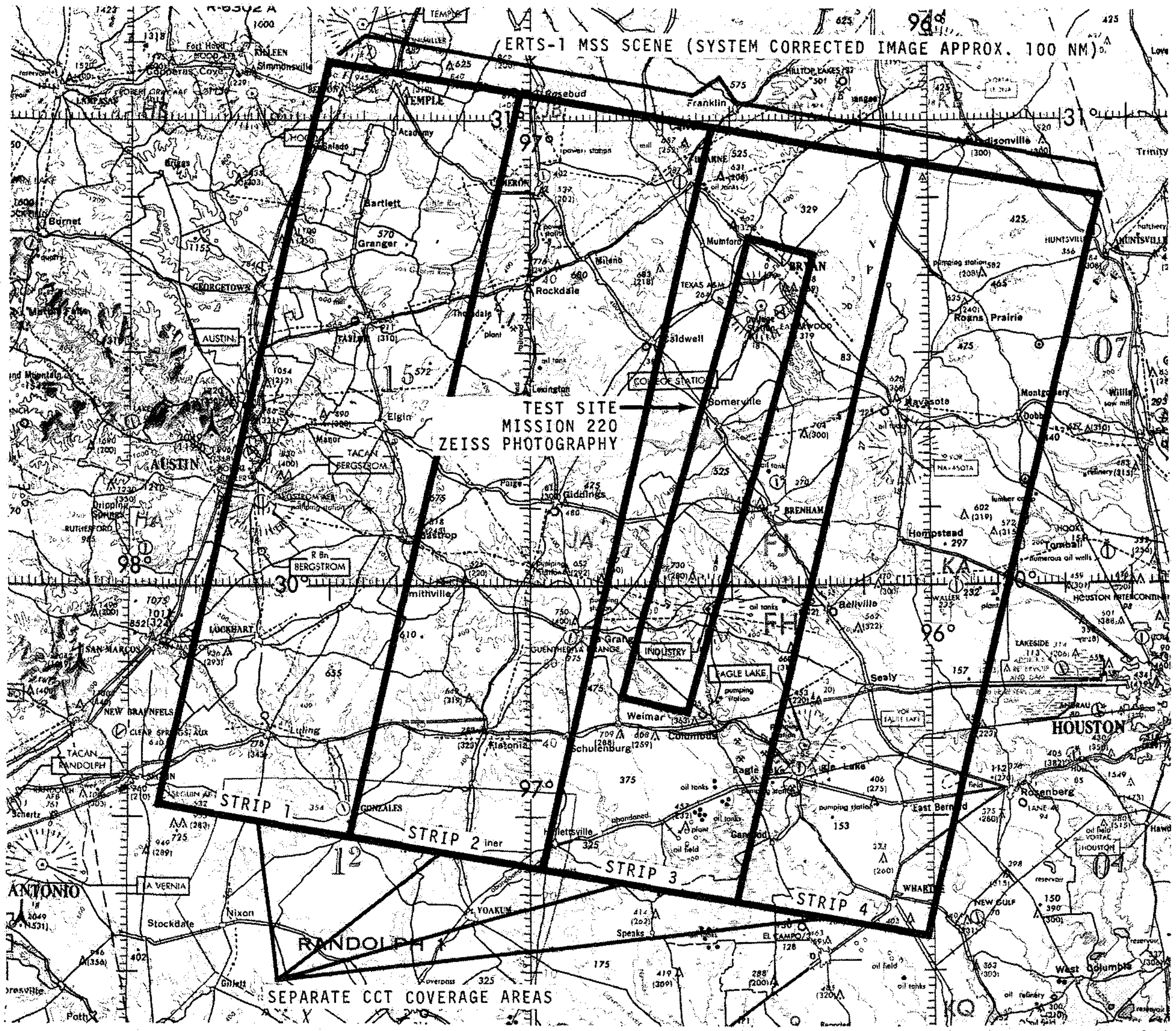

FIGURE. - An illustration of the ERTS-1 frame coverage on 1:1,000,000 scale ONC chart with strip 3 and the study area covered by Mission 220 aircraft photography.

b. With the topographic maps as a base, the imagery was used with an Analytical Stereo-Plotter to produce vellum overlays with all water bodies of approximately 3.24 hectares (8 acres) surface area and larger compiled at a 1:24,000 scale. The 21 frames of imagery yielded 20 vellum overlays at 1:24,000 scale.

c. Frame number 53, of the study area imagery, was analyzed in complete detail to determine the size and location of all distinguishable water bodies. The area covered by this frame was designated as the intensive study area.

d. The vellum overlays on which the water body boundaries were indicated were planimetered using a digital planimetric device to obtain surface areal measurements.

e. The 20 vellum overlays were mosaicked, a single sheet of clear acetate overlaid onto the mosaic and the data on the vellums transferred to the acetate overlay.

The clear acetate overlay of water bodies at 1:24,000 scale together with the tabular data of surface area of the water bodies constituted the ground truth for evaluation of the automatic data processing technique.

Figure 2 shows a portion of the clear acetate overlay and shows the overlay position on a corresponding 1:24,000 topographic sheet as well as a 1:24,000 scale computer line-printer output depicting water classification symbols.

Computer-Aided Data Processing

Given the operational constraints, evaluation criteria, evaluation procedures and the selected study area and its related ground truth overlay, five computer-aided procedures were defined and evaluated.

Three of the procedures utilized variations in training field selection for developing training statistics for use with a maximum likelihood classification algorithm along with data from all four ERTS-1 multispectral scanner channels. Two of these procedures differed only in the method of selection training data and required the analyst to train the classifier using classes related only to water. The first of these two methods of selecting training data required the analyst to locate water in the ERTS-1 scene using only the line printer digital display, along with existing conventional maps. The second of these two methods required the analyst to select training data from the line printer digital display based solely on prior knowledge of the spectral appearance of water as recorded by the ERTS-1 multispectral scanner and the analyst was provided no information as to actual location of water in the ERTS-1 scene. The third procedure required the analyst to select training data for water classes and a spectrally similar non-water class. Again, the analyst was not required to know the location of either the

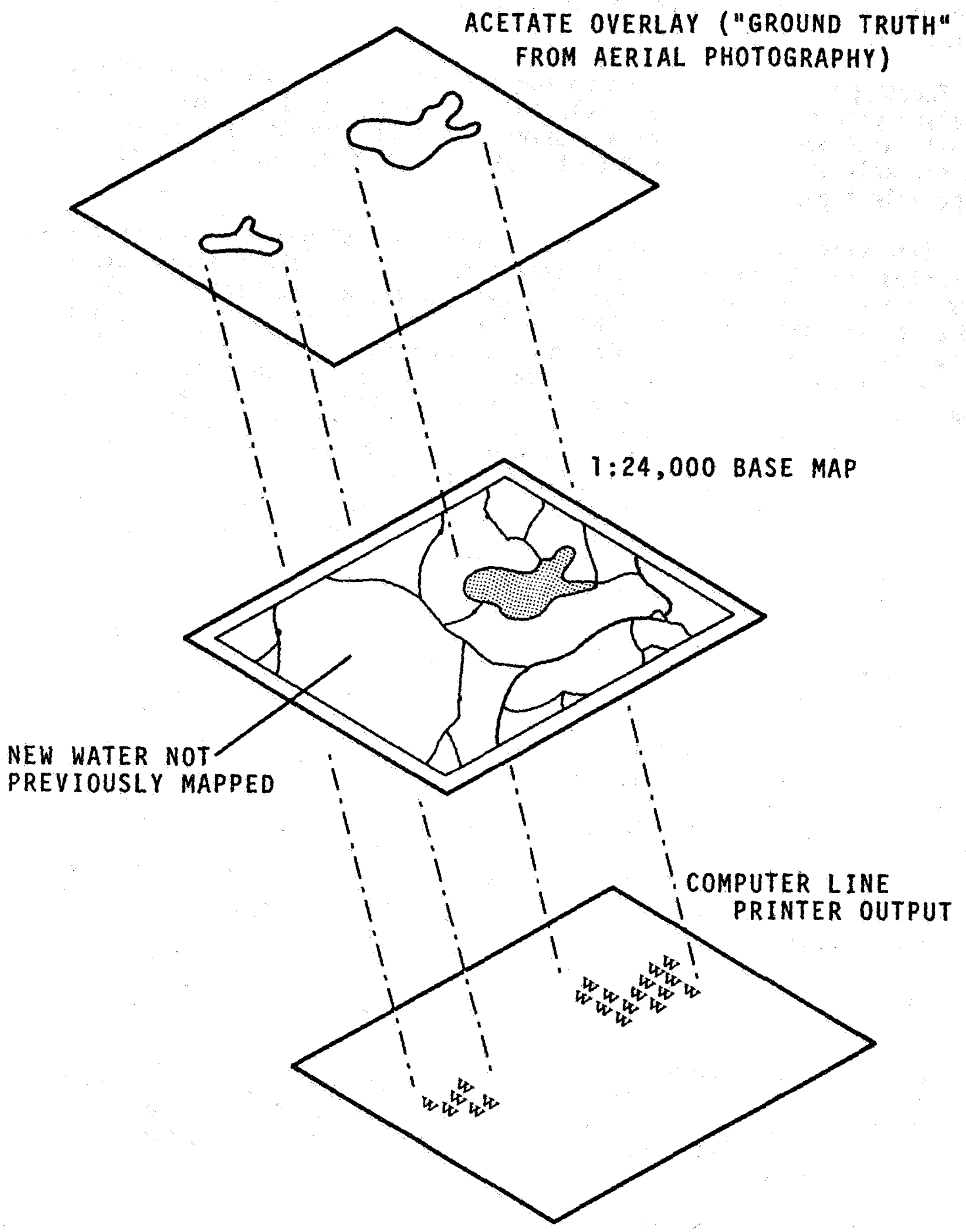

FIGURE 2. - Interrelationship of Evaluation Materials

water or similar classes in the ERTS-1 scene prior to selection of the training data.

The fourth procedure was based on the premise that an acceptable classification procedure could be developed using only data from band 7 of the ERTS-1 multispectral scanner and using a line printer to display the lowest six data values contained on the ERTS-1 system corrected computer compatible tape.

The fifth procedure was developed by using the RB57 ground truth overlays, a spectral clustering program to obtain the means of the spectral clusters related to bodies of water of varying sizes and turbidity levels and other terrain features. The cluster means were plotted on a family of two-dimensional spectral diagrams (e.g., band 4 vs. band 7, band 5 vs. band 7, and band 6 vs. band 7). From this family of diagrams, the two-dimensional diagram which showed the greatest separation between the water classes and all other features was selected. Using this diagram, a linear discriminant boundary was empirically selected for use in separating water from all other classes of features. This empirical linear discriminant boundary was empirically moved within the band 4 vs. band 7 diagram until an acceptable performance was obtained. It was assumed that this fixed linear discriminant boundary procedure would be evaluated over the entire State of Texas.

Of the five procedures evaluated, only the fifth procedure produced a result which met the established performance criteria. The procedure which used only band 7 data and the lowest six data values resulted in an unacceptable level of correct identification in addition to an unacceptable frequency of false identification (misclassification of non-water areas as water). The other three procedures which required the selection of training data for use with a maximum likelihood algorithm all resulted in unacceptable performance. In all three cases, which used a maximum likelihood algorithm, the frequency of false identification was excessive. The resulting unacceptable performance related to these three procedures was a result of incorrect training statistics. These incorrect statistics resulted from either the inclusion of non-water training samples in the water training statistics, or from the selection of water training samples which were not statistically representative of the classes of water which existed in the ERTS-1 scene.

The acceptable performance obtained using the two-channel linear discriminant technique using data acquired over the study area resulted in a recommendation that it be the classification algorithm for the operational procedure. The results of the performance evaluation are shown in Table 2.

Finally, it was determined, from previous work by personnel in the Earth Observations Division, that it was feasible to incorporate a registration technique into the computer software which classifies the data as either water or other, retains the elements classified as water, then registers the data retaining those classified elements previously dropped during registration. For these reasons, it was recommended that

the two-channel linear discriminant algorithm along with a registration technique be packaged into an operational program.

OPERATIONAL PROCEDURE DESCRIPTION

The procedure is structured around a set of computer programs for Detection And Mapping, known as the DAM package, which are presently implemented on Univac 1100 series computers at the Johnson Space Center. However, the computer programs can be repackaged for operation on most standard computers that range from the mini-computer classification to large scale data processing systems. The procedure has been divided into four distinct phases:

- Data Acquisition
- Control Network Establishment
- Classification and Mapping
- Information Correlation and Interpretation

The sequence of operations involved in using the procedure is graphically illustrated in Figure 3 and briefly described below.

Data Acquisition

The purpose of the data acquisition phase is to assemble the ERTS-1 imagery and data tapes, maps, meteorological data, and ERTS-1 data catalogs required for implementation of the procedure.

After data acquisition, the next phase of this computer-aided procedure is control network establishment.

Control Network Establishment

The purpose of this phase is to select a network of ground control points identifiable on both the ERTS-1 data and corresponding maps. These will be used to tie the two data types together to ensure a computer-generated map, which is accurately scaled and registered (located with respect to the earth's surface) for correlation with a conventional map. ERTS-1 system-corrected computer-compatible tapes have not been corrected to achieve precise geometric correction and registration; consequently, corrections for the geometric distortions are required to ensure an acceptable computer-generated cartographic product.

Control network establishment is accomplished by a series of steps performed on each set of four ERTS-1 digital tapes, corresponding to a 100 by 100 n.mi. scene for the area to be analyzed.

Classification and Mapping

Classification and mapping is the last phase of computer-processing in the detection and mapping of surface water using ERTS-1 data. It results

TABLE 2

Performance Evaluation Results
Two-Channel Ratio Technique

Channels 1 and 4

	Class I	Class II	Class III
Percent of each class identified as Class I	F_{11} = 8%	F_{12} = 29%	F_{13} = 0%
Percent of each class identified as Class II	F_{21} = 0%	F_{22} = 43%	F_{23} = 0%
Percent of each class identified as Class III	F_{31} = 0%	F_{32} = 14%	F_{33} = 100%
Percent of each class falsely identified	F_{01} = 0%	F_{02} = 0%	F_{03} = 0%

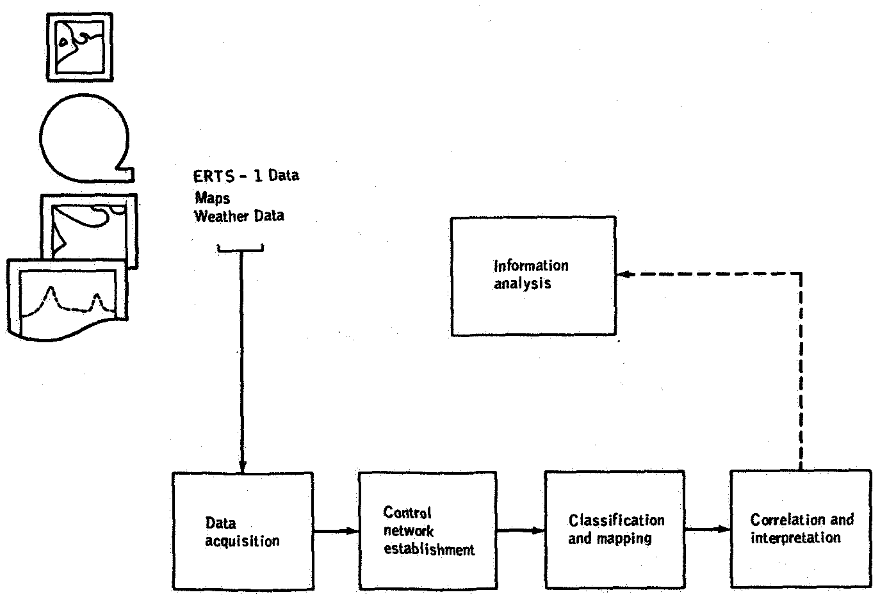

FIGURE 3. - Computer-aided Procedure Sequence of Operation

in computer-generated line printer output showing the location of each point classified as water at the scale specified by the user, a listing of selected incremental geographic coordinates corresponding to latitude/longitude symbols on the computer-generated output, and an optional listing of pixels classified as water.

The computer programs used are DAM.COEF and DAM.CLASSIFY, run in succession in the same computer run for each data set. These programs use an ERTS-1 data tape and the transformation coefficients generated during control network establishment. Each ERTS-1 pixel (picture element) on the tape is individually classified as "water" or "other" based on its spectral values. Mathematical transformation coefficients previously derived are used to compute geographic coordinates for each data element classified as water and to assign each element classified as water to a position on the line printer map. In addition to symbols for each element classified as water, the line printer output maps indicate latitude and longitude intersection points along with "cut-line" symbols ($), "join-line" symbols (the right edge of line numbers on each line printer output strip), and "limits of coverage" symbols (:). These serve as guides in joining together the individual output strips to form mosaics during correlation and interpretation.

Information Correlation and Interpretation

Information correlation and interpretation constitutes the last phase of the computer-aided procedure for using ERTS-1 data to detect and locate areas of surface water. The purposes of correlation and interpretation of the classification and mapping outputs are to mosaic the individual line printer output strips to form a map and to transfer the computer derived information to conventional maps for further analysis.

Figure 4 is a General Highway Map of Washington County, Texas, at a scale of 1:126,720 (1 inch = 2 miles). The map sheet, from the 1968 series, shows Somerville Reservoir and the Brazos River. Figure 5 presents a portion of a correlated computer-generated map at a scale of 1:126,720 corresponding to the area outlined on the highway map. Somerville Reservoir and the Brazos River are shown, as well as numerous other areas of surface water. In addition, Figure 5 shows the results of constructing a mosaic from line-printer output, followed by the annotation of latitude/longitude intersections according to a Geographic Intersection Table provided with the line-printer output. In this case, the user-selected coordinate increments were every 15 minutes. Connecting intersections with lines is optional. The resulting computer-generated map is easily visually correlated to the highway map using the graticules on both maps.

INFORMATION ANALYSIS

Information analysis, i.e., use of the computer-generated information, follows completion of the computer-aided procedure. The purposes of

information analysis are twofold: (1) to evaluate the procedure and verify the results, and (2) to relate information generated by the computer-aided procedure to information required within the National Program of Inspection of Dams. A sequence of steps which might be followed is presented below:

a. Periodically evaluate and verify the procedure by processing data for test areas containing water bodies of known areal extent.

b. Note areas of surface water derived through use of the procedure which are not shown on the selected base maps. These areas may be verified through use of recent aerial photography, helicopter or light plane overflights, or field checks.

c. Select from amended and verified base maps those areas of surface water meriting further consideration within the National Program of Inspection of Dams.

d. Extract the information required for an inventory of dams in the United States under the National Program of Inspection of Dams from the amended base maps for each qualifying area of surface water, and enter on Corps of Engineers from ENG 4474.

SUMMARY AND CONCLUSIONS

Processing ERTS-1 data by utilizing the computer-aided procedure described in this manual will provide an inventory of areas of surface water. The procedure has been evaluated quantitatively using ERTS-1 data corresponding to the study area in East Texas. However, each user should quantitatively evaluate the performance resulting from execution of the procedure using ERTS-1 data corresponding to an area of interest to the user. The inventory of dams deemed to be within the scope of the National Program of Inspection of Dams can be derived from the computer-generated information.

Use of the computer-aided procedure to generate information has the following advantages over information derived from the use of conventional methods:

a. Provides an inventory which is as current as available ERTS-1 coverage and is more complete and accurate than an inventory derived from the use of conventional methods.

b. Cost-effective in comparison with the time and effort expended in the use of conventional methods.

c. Available for immediate implementation to meet the time limitations imposed by Public Law 92-367.

d. Computer programs are compatible with standard computers that range in size from the mini-computer classification to large scale data processing systems.

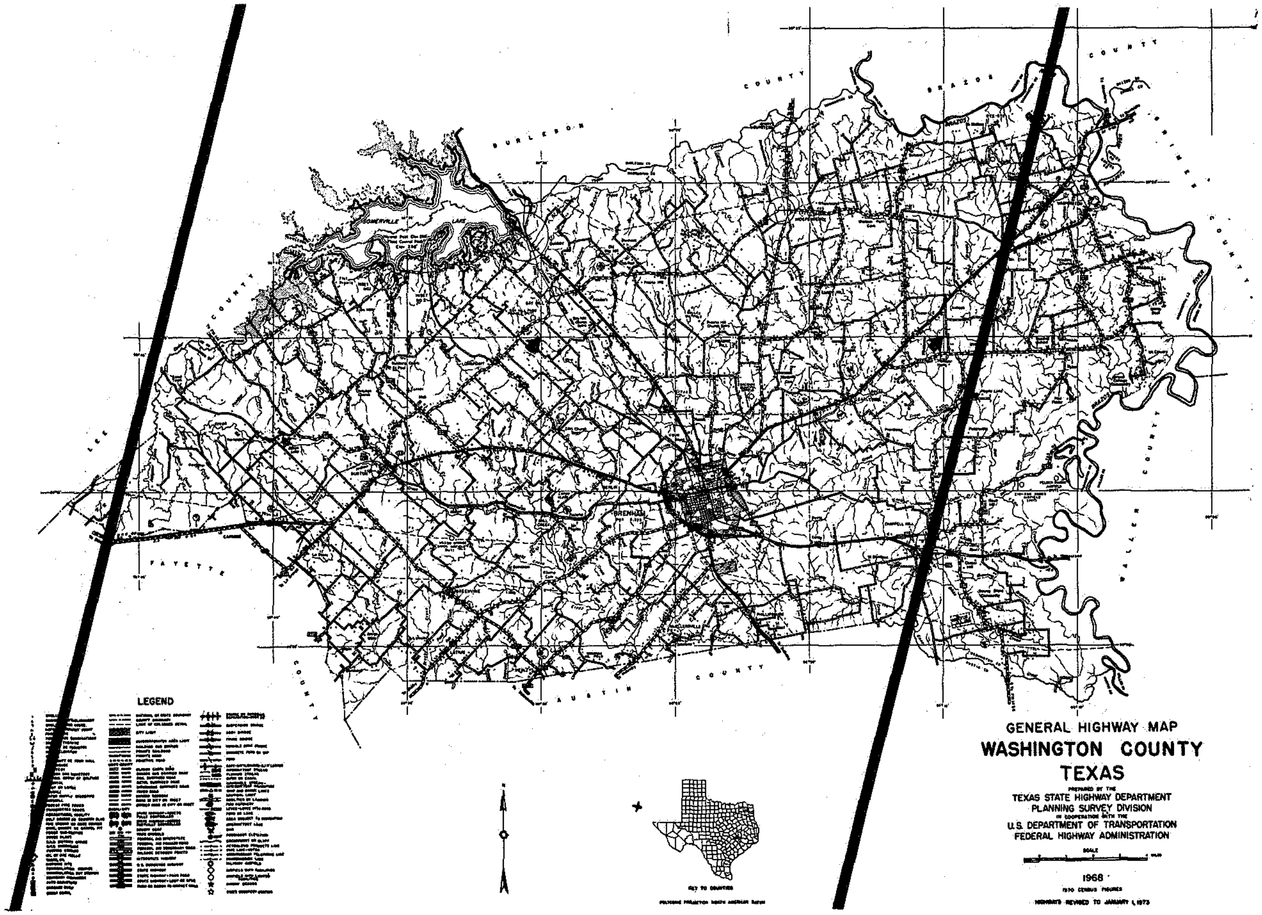

FIGURE 4. - Reduced general highway map of Washington County, Texas (original scale of 1:126,720, 1 inch = 2 miles).

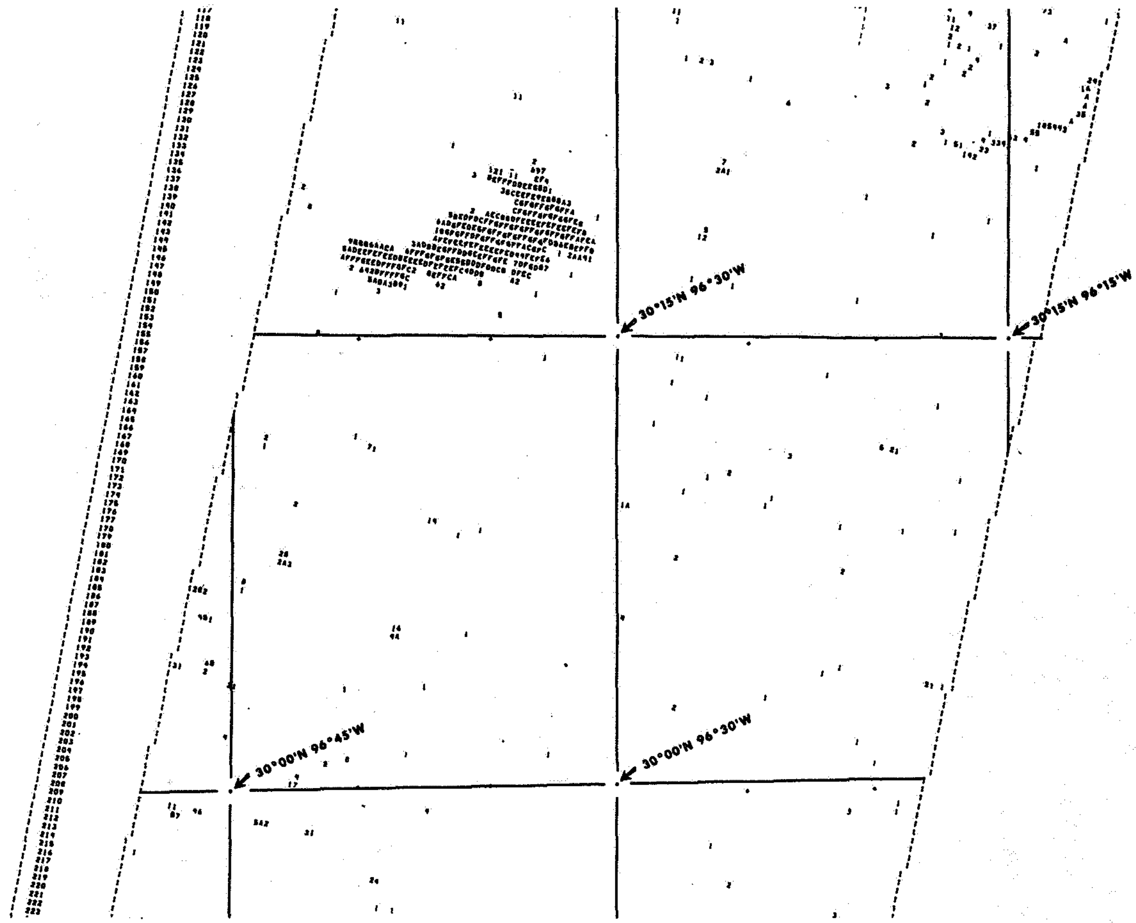

FIGURE 5. - Reduced portion of computer-generated map correlated to Washington County Highway Map (original scale of 1:126,720, 1 inch = 2 miles).

REFERENCES

"Procedures Manual for Detection and Location of Surface Water Using ERTS-1 Multispectral Scanner Data: Vol. II, Data Acquisition," JSC-08638.

"Procedures Manual for Detection and Location of Surface Water Using ERTS-1 Multispectral Scanner Data: Vol. III, Control Network Establishment," JSC-08451.

"Procedures Manual for Detection and Location of Surface Water Using ERTS-1 Multispectral Scanner Data: Vol. IV, Computer Program Description and User's Guide," JSC-08452.

"Procedures Manual for Detection and Location of Surface Water Using ERTS-1 Multispectral Scanner Data: Vol. V, Information Correlation and Interpretation," JSC-08639.

"Development of a Computer-Aided Procedure for the National Program for Inspection of Dams," JSC-08449.

"Development of a Two-Channel Linear Discriminant Function for Detecting and Identifying Surface Water Using ERTS-1 Data," JSC-08450.

"Evaluation of a Computer-Aided Procedure for Detecting Surface Water," JSC-08453.

Paper W 5

DYNAMICS OF PLAYA LAKES IN THE TEXAS HIGH PLAINS

C. C. Reeves, Jr., *Texas Tech University*

ABSTRACT

Three small playa lake basins on the Texas High Plains were originally selected as ERTS-1 test sites to attempt correlation of ERTS-1 imagery with the water balance ecosystem and geology/morphology of the lake basins. Two of the test sites were instrumented with water level recorders, infiltrometers, tensiometers, evaporation pans, totalizing aneometers, weighing rain gauges, and continuous recording microbarograph and hygro-thermographs. However, when initial imagery (under maximum usable magnification) showed that resolution was not adequate for the monitoring of water fluctuations of the small lakes, the 5-mile long large Double Lakes playa complex was instrumented as an alternate test site.

During the period July 1972-August 1973, the Double Lakes playas went from an initial flooded condition (July, 1972 pass) to a partially dry condition (south playa dry, north playa wet, June 19, 1973 pass) to a total dry condition (July 6) to a flooded condition (July 24) to a partial dry condition (August 11). This sequence is portrayed by 16 mm time-lapse film loops constructed from ERTS-1 MSS imagery.

Color composites using an electronic density profile have been particularly useful for distinguishing the exact water area from the muddy areas of the Double Lakes playas, and for determining the salt crust areas. Color composites also portray gradations in water transparency, due to depth fluctuations, suspended sediment or algae, much better than the single MSS bands.

Analysis of Bands 6 and 7 of ERTS-1 MSS imagery, using photographic enlargement and a 32-color density slicer with zoom magnification, shows that lake basins as small as 200 m in diameter (±10 acres) can be reliably classified as being "wet" or "dry", thus supplying the methodology for a rapid, periodic census of surface water. A cost/benefit analysis reveals that the use of MSS imagery for such a census results in a 66 to 200-fold cost reduction when compared to the costs of using other conventional methods. Thus, even the poorest of the arid countries of the world can afford to monitor their ephemeral lakes, enhancing the predictability of extended drought conditions.

INTRODUCTION

The semi-arid and arid lands, which constitute nearly 30 percent of Earth's continental surfaces, are pock-marked by small natural basins, the intensity of which in many areas commonly exceeds 1 per square mile. These basins contain water during wet periods and, as such, frequently constitute the only available source of fresh water for villages, livestock and crops. In countries with the technological "know how," playa lake water often exists as the only natural source for natural and artificial recharge of local aquifers.

The Southern High Plains of West Texas and eastern New Mexico, for example, is now an isolated plateau of approximately 30,000 square miles which receives no ground water recharge except from precipitation (Fig. 1). Yet, over 5 million acres in cultivation makes the Southern High Plains one of the most intensely farmed areas in the United States. This tremendous agricultural economy, based principally on cotton and sorghum with lesser amounts of winter wheat, onions, potatoes and castor beans, has been developed and can only continue to exist because of the regional Ogallala aquifer. Since 1940, some 60,000

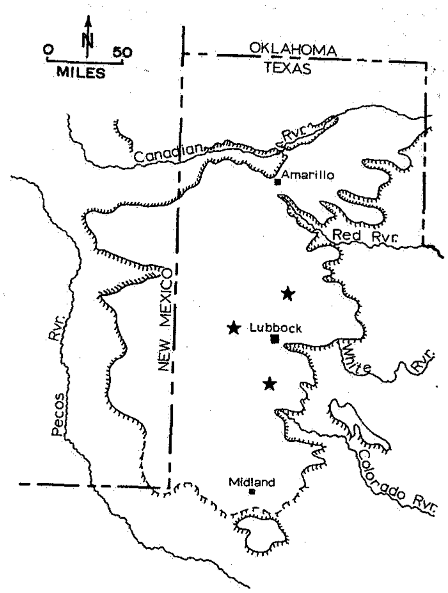

Figure 1 - Index map of Southern High Plains. The stars show the localities of the three original ERTS-1 test sites. The large ERTS-1 Double Lakes test site, Lynn County, Texas, is located near the star south of Lubbock.

irrigation wells have been drilled and have been producing ever increasing amounts of water from the Ogallala aquifer. During the last 30 years the regional water table has fallen over a hundred feet in some areas and certain localities have been completely dewatered in response to this widespread groundwater withdrawal. The depletion of the Ogallala aquifer, and remedial measures to extend the life of the aquifer, has been the subject of studies by several private and governmental agencies (Texas Water Development Board, 1968). Suggestions for extending the life of the aquifer have ranged from the importation of water (from Mississippi or even Canada) to the development of a regional artificial recharge program utilizing the ephemeral playa lake waters.

The prospect of using the playa lake surface water for regional recharge has, of course, been of most immediate interest due to the potpourri of engineering and political problems associated with water importation. Although recharge is in itself expensive, such methods have a long and encouraging history (Tison, 1970), and with the prospect of 80¢ cotton and $4.00 grain, the cost/benefit ratio is rapidly becoming more attractive. Unfortunately, no one knows how many lakes there are at any particular "wet spell", let alone how much such water might be available during a year's time for such a recharge project.

The rational behind our ERTS-1 proposal, which naturally was implemented before present inflated farm prices, was to correlate ERTS-1 imagery with the water balance ecosystem and geology/morphology of several typical playa lake basins on the Southern High Plains. Spatial distribution of soils and time-space distribution of soil moisture and ponded water was to be correlated with the satellite imagery. Such correlations were expected to aid in approximating water loss and changes in storage volume with time as related to meteorologic parameters. Thus, direct application of the study was an inventory of the water budget of a semi-arid playa-type lake system.

METHODOLOGY

The three original test sites, each covering a drainage area of approximately 1,000,000 square meters and having playa areas of approximately 160,000 square meters, were staked on 100 m grids. Soil scientists then took samples, using hand or power augers and probes (Fig. 2) and made profile descriptions at most intersections to produce soil maps of each test site (Fig. 3).

The basins were then drilled with a power auger to determine the thickness and extent of lacustrine fill and the morphology of each basin (Fig. 4 and Fig. 5). A continuous core in the deepest part of each basin was then taken, and samples are now being worked for pollen content and clay mineralogy. The results of the pollen profiles, the clay mineralogy, lacustrine stratigraphy and basin morphology, will allow reasonable assumptions to be made regarding origin(s) and geologic history, of the basins. Vegetation studies are also being conducted on the test sites by an independent investigator, but no data is now available.

Two of the small test sites were initially instrumented with water level recorders, infiltrometers, tensiometers, evaporation pans, totalizing aneometers, weighing rain gauges, and continuous recording microbarograph and hygro-thermographs (Fig. 6) to monitor local weather and to help in correlating the water balance with any resultant ponded storage.

IMAGERY

As expected, initial imagery illustrated that MSS Bands 6 and 7 were best for delineation of water areas in the test site area; however, our initial image of 29 July, 1972 (1006-16522) revealed that resolution of the three original test sites was adequate only for distinguishing the presence or absence of water. Water fluctuations in the small playa-type basins, as seen on succeeding passes (Fig. 7), could not be discerned even

Figure 2 - Using power auger for soil investigation at the Heard Playa test site, Hale County, Texas.

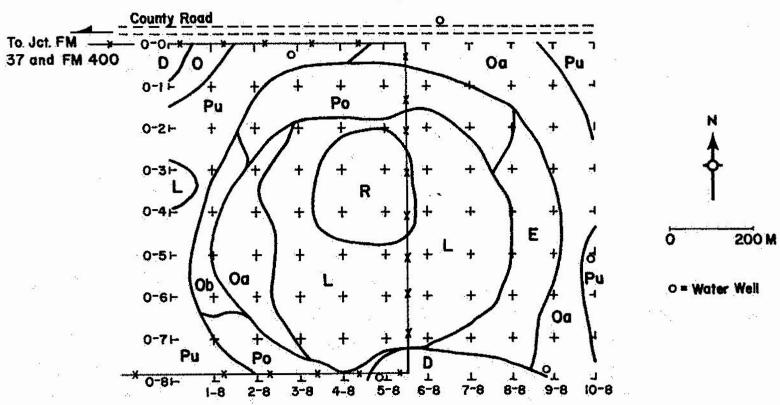

Figure 3 - Soils map of the Heard Playa test site, Hale County, Texas (by J. Goebel). D = Drake, Pu = Pullman, L = Lofton, Oa, Ab = Olton, Po = Posey, R = Randall, E = Estacado.

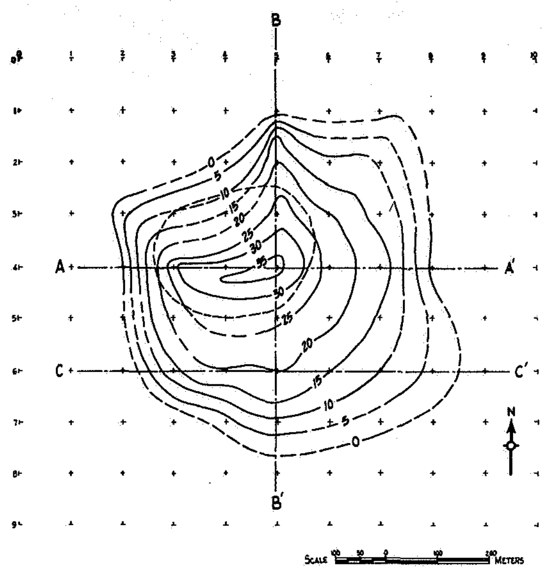

Figure 4 - Map showing thickness of lacustrine fill at the Heard Playa test site, Hale County, Texas, and locations of cross-sections of the basin constructed from drill holes.

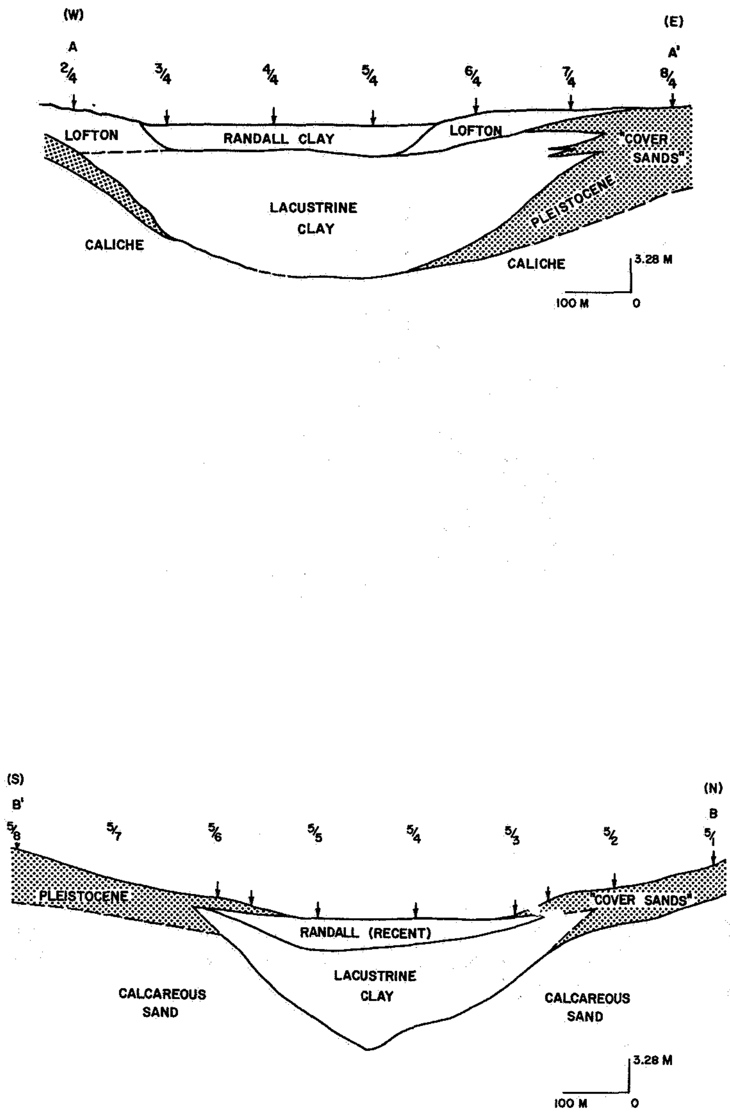

Figure 5 - Cross sections of the Heard Playa test site, Hale County, Texas, and locations of cross-sections of the basin constructed from drill holes.

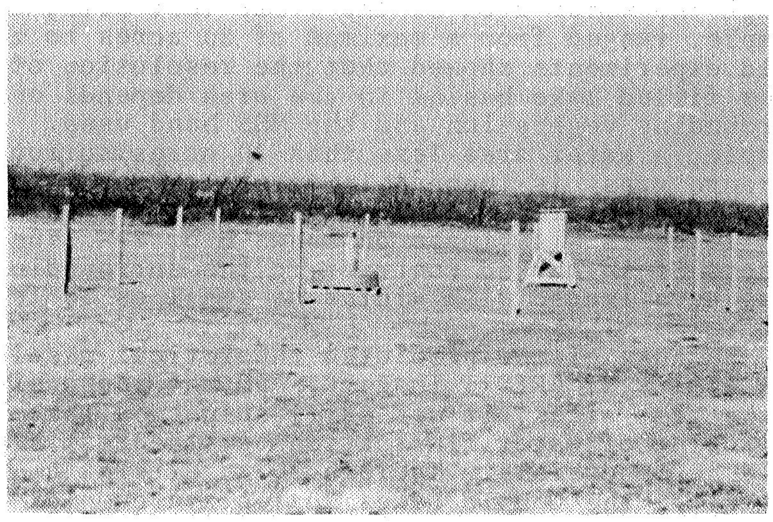

Figure 6 - Weather monitoring instrumentation at the T-Bar test site, Lynn County, Texas.

Figure 7 - View of the T-Bar test site (arrow) Lynn County, Texas, from the 9 October, 1972 pass (1078-16524). Original ERTS-1 scene magnified to maximum usable power.

though the water area of the T-Bar test site, for example, ranged from a maximum of 20 acres to zero. Field experiments showed that the resolution of water-filled lake basins in the area depends on surrounding vegetation and the MSS band used. For example, a water area less than 20 acres surrounded by range grass is impossible to see on Band 4, but in a light-colored soil area, water areas less than 10 acres will image on Bands 6 or 7. Linear objects if in marked contrast to the surrounding area, have imaged with widths as small as 36 feet.

Because of the predicted theoretical resolution limits of ERTS-1 imagery, and the known size of the test sites, it was early suspected that monitoring of water fluctuations at the test sites would be impossible. Therefore, an alternate test site, the Double Lakes dual playa complex of Lynn County, Texas, (Fig. 8), was selected. The Double Lakes site, consisting of a dual playa complex approximately 5 miles long eroded in the lacustrine sediments of an ancestral Pleistocene lake which once covered about 9 square miles, has a drainage area of about 35 square miles. This type of playa basin is representative of the large type saline playas common the the arid and semi-arid areas of Asia, Africa, Australia, South America and the western United States. After receipt of initial imagery, which confirmed our resolution expectations, the instrumentation was removed from one of the original small playa test sites and installed between the playas at the Double Lakes test site.

A soils map and a geologic map (Fig. 9) of the Double Lakes test site were then constructed. The extent of lacustrine fill and general morphology of the basin was determined by outcrop studies and 33 drill holes. The drill holes, totaling 1180 feet, were drilled through the lacustrine fill of the basin to the underlying Cretaceous bedrock. This revealed that the Double Lakes basin formed along an ancient drainage channel which crosses a topographic high on the Cretaceous unconformity (Fig. 10) and is not a sample deflation basin or a sink.

The ERTS-1 satellite first passed over the West Texas study sites on 29 July, 1972. Table 1,

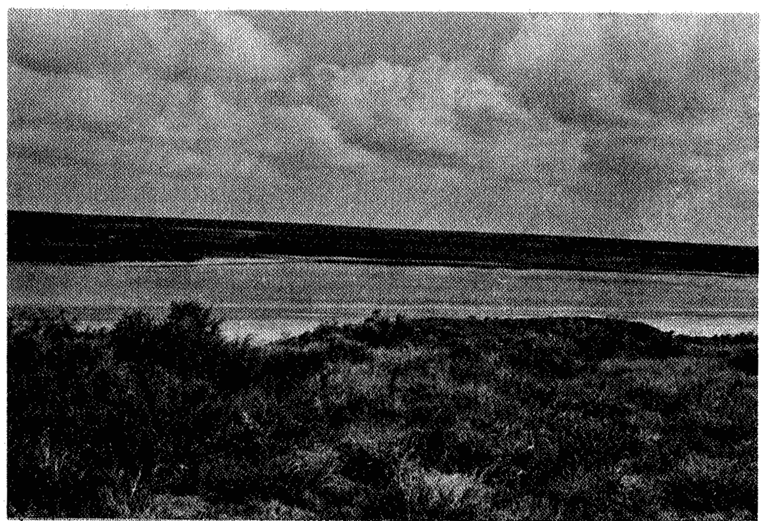

A

B

Figure 8 - Views of the Double Lakes test site, Lynn County, Texas. A = the north playa (view to the northwest, B = the south playa (view to the southwest).

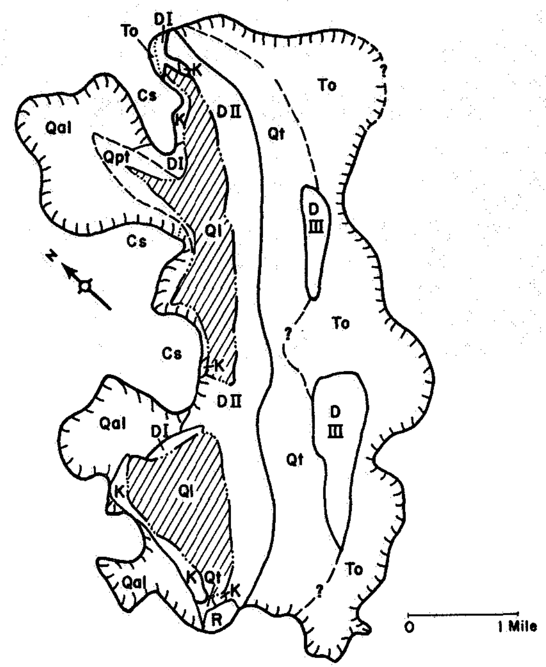

Figure 9 - Geologic map of the Double Lakes test site, Lynn County, Texas. To = Ogallala Formation (Pliocene), Q_T = Tahoka Formation (Pleistocene: Wisconsin), C_S = "Cover Sands" (Pleistocene: Illinoian), D_I, D_{II}, D_{III} = dunes (Pleistocene), Q_{AL} = Quaternary alluvium, Q_{PT} = Pre-Tahokan (Pleistocene: pre-Wisconsin), Q_L = Lacustrine playa (Quaternary: reworked), K = Cretaceous (by J.W. Buchanan, Jr.).

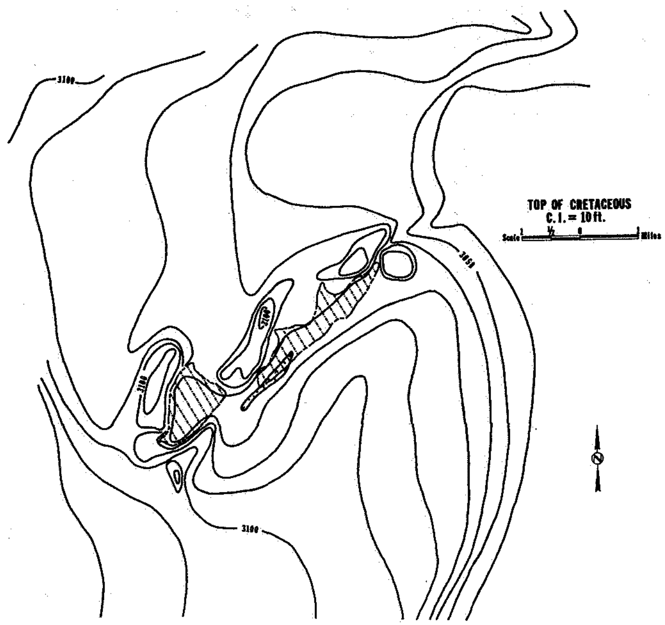

Figure 10 - Structural map on top of the Cretaceous surface at the Double Lakes test site, Lynn County, Texas. Control from irrigation wells and drill holes. The present playas are cross-hatched (by J.W. Buchanan, Jr.).

Table 1 - Summary of ERTS-1 passes over the West Texas test site area. Passes on September 3, 21, October 27, December 20, 1972, January 7, 25, March 2, April 25, May 13, 31, August 29, were not received due to cloud cover. Stars between dates indicate number of intervening passes missed.

DATE	BANDS	ORBIT AND SCENE	SKY CONDITION	QUALITY	COLOR COMPOSITES AVAILABLE
July 29	4,5,6	1006-16522	20% clouds	Fair	No
Aug 16	4,5,6,7	1024-16522	30% clouds	Good	Yes
**					
Oct 9	4,5,6,7	1078-16524	10% clouds	Good	Yes
*					
Nov 14	4,5,6,7	1114-16532	10% clouds	Good	Yes
Dec 2	4,5,6,7	1132-16532	0% clouds	Good	Yes
***					
Feb 12	4,5,6,7	1204-16533	0% clouds	Good	Yes
*					
Mar 20	4,5,6,7	1240-16534	50% clouds	Good	Yes
Apr 7	4,5,6,7	1258-16534	0% clouds	Good	Yes
***					
June 18	4,5,7	1330-16531	0% clouds	Good	No
July 6	4,5,6,7	1348-16525	0% clouds	Good	Yes
24	4,5,6,7	1366-16524	5% clouds	Good	Yes
Aug 11	4,5,6,7	1384-16523	3% clouds	Good	Yes
***					

summarizing the ERTS-1 passes over the study areas, shows that only 52 percent of the passes were useful, there being two periods where 53 days occurred between usable imagery. The greatest number of adjacent scenes received to-date has been the 4 pass sequence of June 18, July 2 and 24, and August 11. It was fortunate that our monitoring program ceases September 1, 1973, for the 3 succeeding passes of August 29, September 16 and October 4 were not usable due to over 70% cloud cover.

During the period July 1972-September 1, 1973, the three original study sites were wet for only a few weeks during the late summer-early fall. The Double Lakes site was flooded from July, 1972 until June, 1973. After drying late in June, the site was again flooded in July and went dry by September, 1973. Monitoring of the Double Lakes site was initiated on December 30, 1973, and continued until September 1, 1973.

STUDY METHODS

ERTS-1 MSS imagery, in 9 x 9 positive format and all available color composites, are being studied by using B & L Zoom magnifiers, photography, a 32-color density slicer, and the time lapse storage and retrieval capability of the Stanford Research Institutes ESIAC (Electronic Satellite Image Analysis Console).

Photography of the MSS color composites, whereby 35 mm slides are taken of select enlarged areas, and then projected on a large screen, have been most useful. Figure 11 illustrates such a sequence from the 7 April, 1973 pass (1258-16534) illustrating how details of the Double Lakes test site can be brought out with such techniques.

Density slicing, using an I^2S unit (Fig. 12), with an Angenieux 10 x 15 Zoom lens and a 2X extender, produces maximum usable magnification on a 17-inch color TV monitor. At small scale the cultivated cotton and sorghum fields, the range land (grasses) and a few of the major soil patterns in the test site area are enhanced by

A

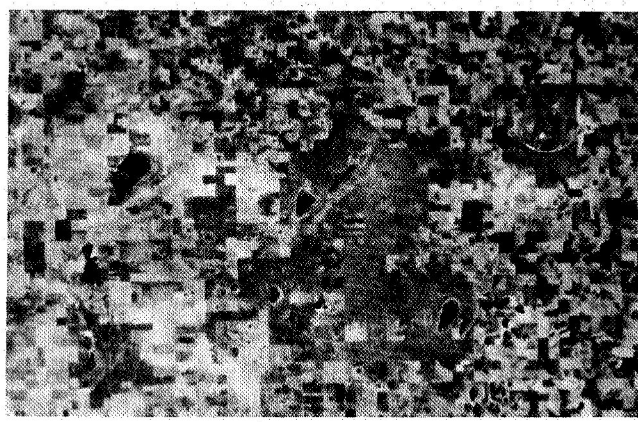

B

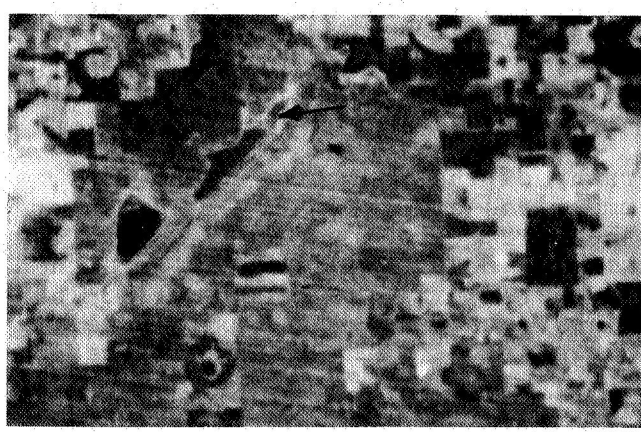

C

Figure 11 - Reproductions of the 7 April, 1973 pass (1258-16534) over the Lubbock, Texas, area. The arrow on A points to the Double Lakes test site which is brought out by photographic enlargement on B and C. Notice differences on water depth between the north and south playa and the isolated muddy spot at the north end of the north playa (arrow on C). Also see Fig. 13B.

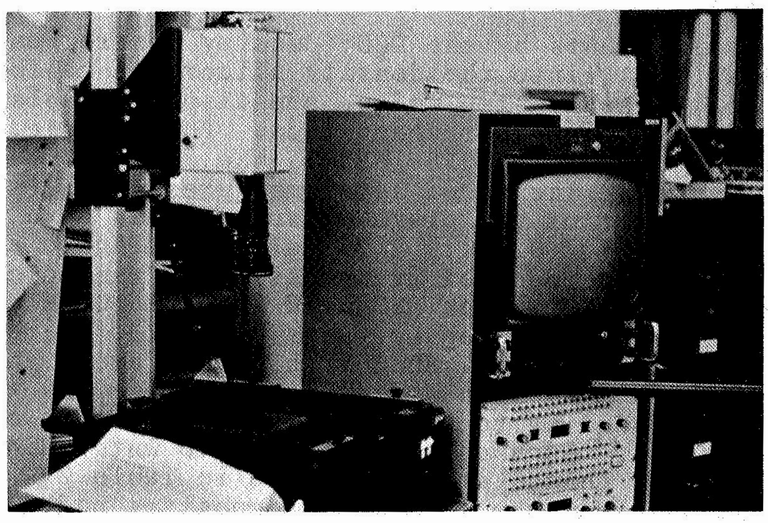

Figure 12 - The I^2S 32-color density slicer with 10 x 15 Angenieux Zoom lens, density control unit (DCU), and electronic planimetry.

density slicing. However, at large scale, density slicing greatly enhances the water in the test site playas and on some views seven different variations can be recorded. Although we first suspected that the density changes were the result purely of changes in water depth, it is possible that suspended load or algae may be a significant factor. Correlation of water quality with ERTS-1 imagery will be examined during the water flood period of 1973-1974.

Measurements by the DCU (density control unit) which is built into the density slicer and calibrated to a photographic step wedge, are also available for determining playa characteristics. For example, on the October 9 view (1078-16524), the density measurement of the 12 inches of water measures +2.05, and the muddy part of the playa measures +1.28 on a density range of 0.15 to 2.30 corresponding to a maximum 70.0 percent of transmission on the color composite. However, on MSS Band 7 Scene 1078-16524 shows density measurements of +1.73 for the salt crusted playa, +1.80 for the muddy area, and +2.15 for the water on a density range of 0.00 to 2.15 corresponding to a maximum of 100 percent of transmission. Such changes related to water depth and seasonal change are summarized in Table 2 and Table 3 from the MSS color composites and MSS Band 7, respectively.

Use of the DCU, whereby a trace of the film density is projected on the TV monitor along the vertical axis of the cursor, has been very useful for pinpointing extent of the water area and extent of the muddy playa (Fig. 13). For example, notice on Figure 13 (9 October, 1972 pass) that the density of the water in the north playa of the Double Lakes test site is fairly uniform, but decreases in intensity to the north, passing into a jagged, sloping intensity zone indicating the muddy part of the playa (arrow). Figure 13B (7 April, 1973 pass) illustrates a localized muddy area (arrow) to the north of the flooded playa, but separated by a salt encrusted playa area. Figure 13C (16 August, 1972 pass) illustrates the flooded playa four months later, showing the same small muddy area north of the

TABLE 2 - Density variations with changes in water depth and season at Double Lakes test site. Measurements made on MSS color composites.

DATE	WATER DEPTH CM	DENSITY READINGS, NORTH PLAYA		
		Deepest Water	Mud Area	Salt Crust
July 29	5.08	CNA	CNA	CNA
Aug 16	22.86	1.10	0.76	0.69
Oct 9	30.48	2.05	1.28	
Nov 14	35.56	1.75	1.46	1.20
Dec 2	40.00	1.70	1.50	1.35
Feb 12	40.64	CO	CO	CO
Mar 20	40.38	1.47		1.13
Apr 7	40.64	1.06	NP	0.85
June 18	2.54	CNA	CNA	CNA
July 6	0.00	NP	NP	1.04
24	2.54	CO	CO	CO
Aug 11	0.00	CO	CO	CO

NP = not present

CO = composite ordered

CNA= composite not available

Table 3 - Density variations with changes in water depth and season at Double Lakes test site. Measurements made on MSS Band 7.

DATE	WATER DEPTH IN CM	DENSITY READINGS, NORTH PLAYA Deepest Water	Mud Area	Salt Crust	REMARKS
July 29	5.08	----	----	----	No Band 7
Aug 16	22.86	+1.68	+1.43	0.93	1 and 2
Oct 9	30.48	2.15	+1.80	+1.73	
Nov 14	35.56	NM	NM	NM	These pictures too dark at density setting for measurement
Dec 2	40.00	NM	NM	NM	
Feb 12	40.64	NM	NM	NM	
Mar 20	40.38	+2.25	----	----	3
Apr 7	40.64	+2.23	+1.89	----	4
June 18	2.54	+1.98	+1.66	1.39	5
July 6	0.00	----	----	1.19	DRY PLAYA
24	2.54	+1.84	+1.64	1.39	7
Aug 11	0.00	----	+1.56	1.17	DRY PLAYA

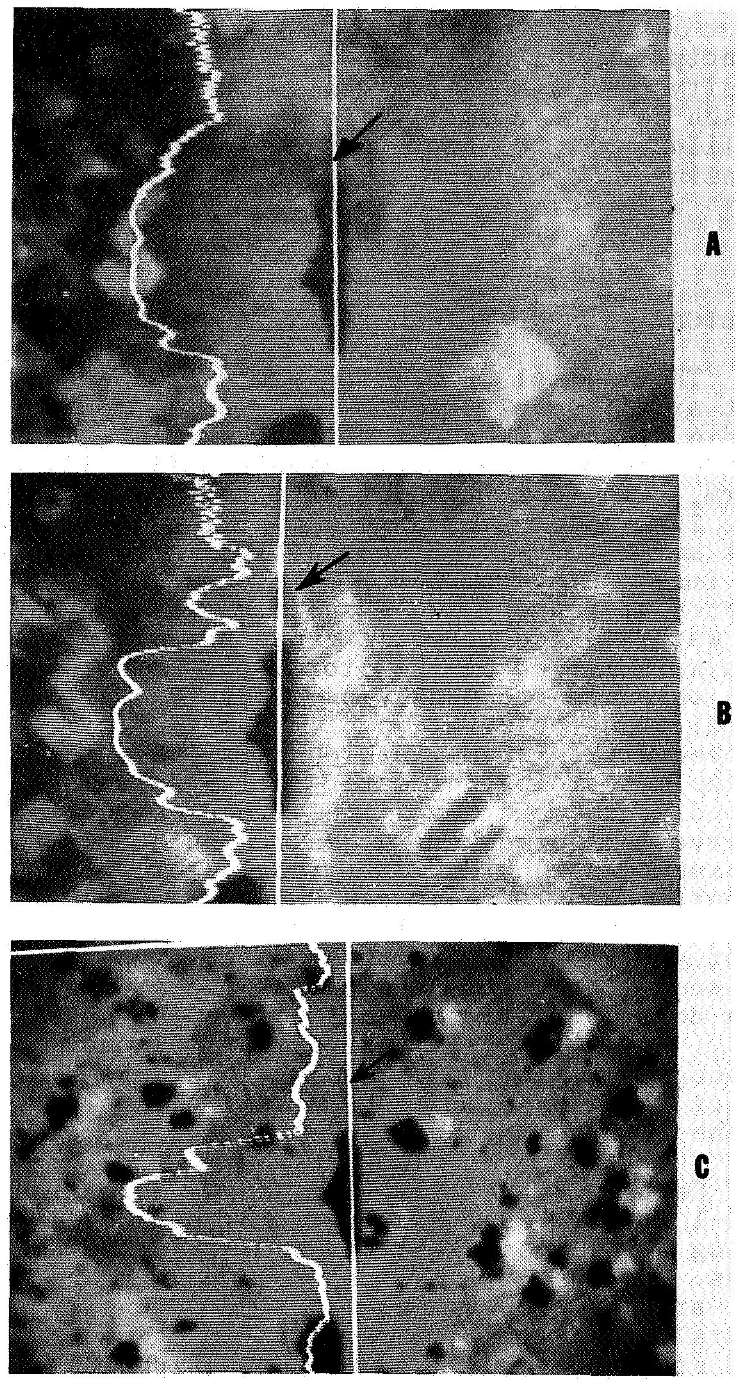

Figure 13 - Density profiles across the north playa of the Double Lakes test site. A = 9 October, 1972 pass (1078-16524), B = 7 April, 1973 pass (1258-16534), C = 16 August, 1972 pass (1024-16522). See Fig. 11A, B, C for regional view of this scene.

e-8

principal water body. However, as indicated by the density curve, moisture content was less. The reason for the constriction in all three density profiles near the neck in the playa is due to a shoaling of the water due to a local high on the playa surface.

APPLICATIONS AND FUTURE POTENTIAL

The initial ERTS-1 imagery over the West Texas test area (29 July, 1972, 1006-16522) contained, on Band 6, the visible wet-soil scar from a local thunderstorm the previous evening (Fig. 14). This storm, with tops at about 8 km and a diameter of only 2.4 km, originated 99 km northwest of Lubbock, thus may have dropped most of its water outside the imaged area. However, although we have no antecedent imagery, we suspect all of the 353 to 447 water-filled playa lake basins within the storm path were filled by the storm. Storm paths have been observed frequently on other scenes (1385-16523), thus observation of isolated storm cells, coupled with ground-truth observations, should refine meteorological water-fall predictions. Secondly, there are very few areas where ground observation networks are dense enough to give an exact geographical distribution of storm extent. ERTS-1 scenes, in MSS Bands 6 and 7, provide a method of quickly determining the exact geometrical pattern of water drop from isolated storm cells as long as the precipitation does not fall too long before the satellite pass. However, it is interesting to note that although the storm of 28 July, 1972, was small and of local extent, the wet soil path also shows on the 16 August (1024-16522) pass.

Certainly, the most exciting application of ERTS-1 imagery, as illustrated by our work, is for taking a lake census in the semi-arid and arid lands. Because of the vast size of the Earth's semi-arid to arid areas, the high intensity of natural basins, the characteristic cumulo-numbus type storm pattern which produces high local runoffs, and the regional lack of potable water,

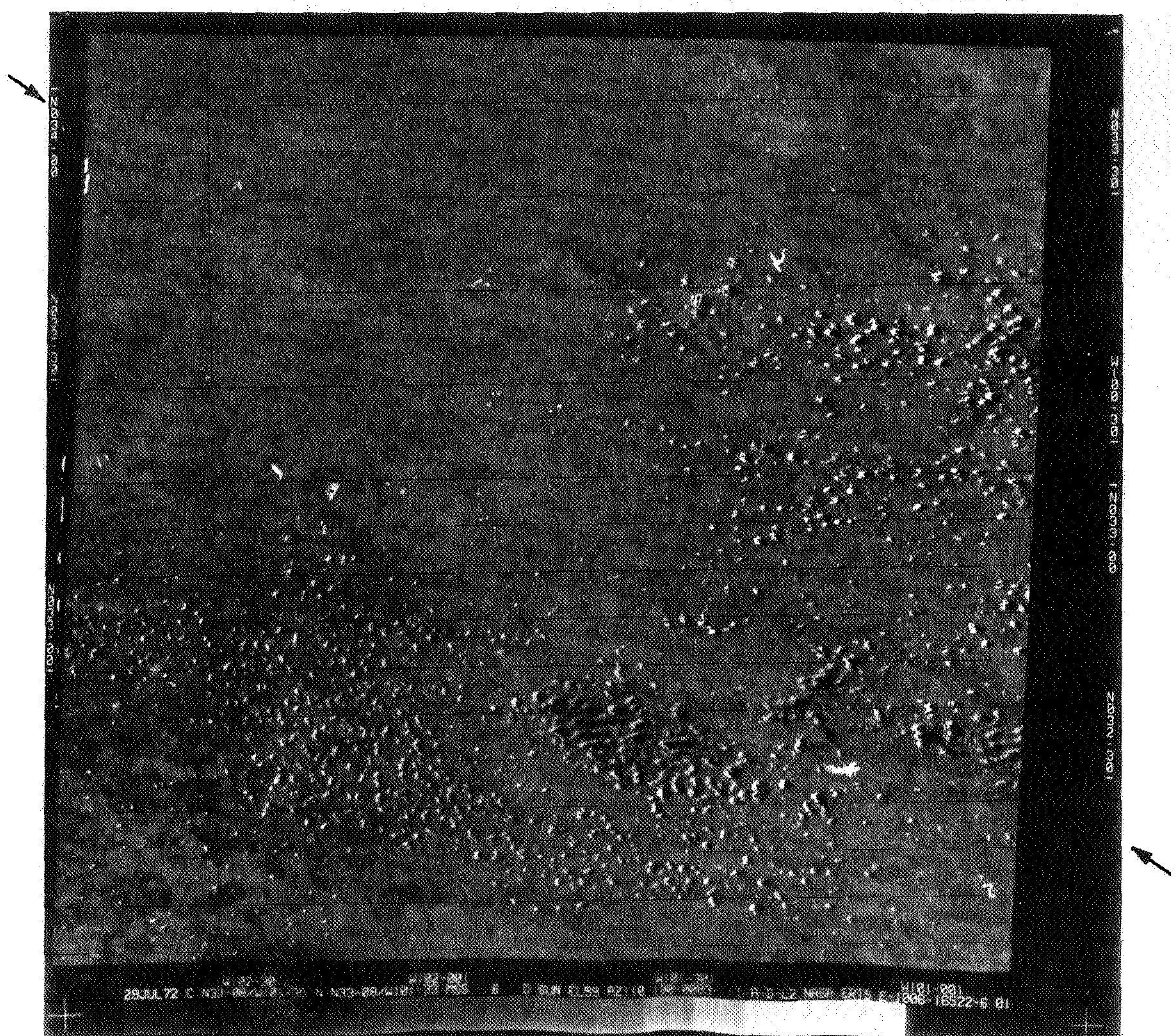

Figure 14 - ERTS-1 scene 1006-16522 (29 July, 1972) of the West Texas study site area. This is a negative print illustrating the storm path passing just southwest of Lubbock, Texas. The trend of the storm path is marked by marginal arrows. The white spots within the path represent small water-filled lake basins. White areas in the eastern and southern parts of the picture are clouds.

a rapid, cheap method to inventory available surface water supplies during various times of the year is a prerequisite to responsible water management. Previously, even in populated areas with ready access such as the Southern High Plains of West Texas, it has not been practical to inventory surface water supplies. For example, consider how many people it would take and what it would cost to count the number of lake basins containing water in a 30,000 square mile area when there are approximately 20,000 such basins. Naturally, in isolated areas the problem is compounded. For instance, in parts of Arizona it recently took two men 7 days to locate, by automobile and walking, only 26 stock tanks (personal communication, C. Brent Cluff, Tucson, 1973).

An example of such a census was the pilot count made, at our request, on scene 1006-16522 (9 October, 1972) by Stanford Research Institute personnel: the count was 6631 water-filled basins! A second count was made by SRI personnel of only those water-filled lake basins on the Southern High Plains, Texas and eastern New Mexico, from parts of eight scenes of MSS Band 7 imagery taken during the Summer and Fall of 1972. This exercise showed 10,036 water-filled lake basins, which by comparison to acreage and volumetric figures (Schwiesow, 1965; Grubb and Parks, 1968), and the high lake levels of 1972, indicates over 500,000 acre/feet of fresh water than in storage (Reeves, 1973a). I might add that certainly 450,000 acre/feet or more of this ponded fresh water was subsequently lost by evaporation, and this in an area where declining ground water supplies are reducing farm land values from \$700/acre to \$125/acre.

A cost/benefit analysis was determined whereby the time/cost of using ERTS-1 imagery (MSS and CCT) for a lake census was compared to the time/cost factors for taking such a census by light airplane, ground survey, and by using conventional aerial photographs (Reeves, 1973b). The most expensive method of conducting the survey, at about \$2.00 square mile, is by using conventional aerial photography, but the use of ERTS-1 MSS and CCT data results in a 200 to 66-fold cost reduction: \$0.01

to $0.03 square mile, respectively, using MSS and CCT data (Table 4). The applicability of using ERTS-1 data for such a lake census was reported to the Texas Water Development Board and the Panhandle Regional Planning Commission. The TWDB is now working on the recognition and practical applications of lake basin recognition in the state by use of ERTS-1 data.

ERTS-1 imagery cannot only be used to count the number of lakes, but when magnified, the water areas in larger lake basins can be accurately measured and monitored. The fluctuations in the water levels may then perhaps be related to the total water budget in the area, allowing more accurate runoff, infiltration, and evapo-transpiration projections. This, of course, is what we are attempting to do at our test sites. Unfortunately, we do not, as yet, have correlations established between our recorded climatic events and the observed lake levels; however, Table 5 presents the measured lake levels by the SRI ESIAC, as derived from MSS imagery, and lake depths from ground truth.

PROBLEMS

Other than loss of passes due to inclement weather, we've found ERTS-1 MSS imagery and color composites of the highest quality. Our principal problems have not been due to hardware but to personnel. Correlation of the multidisciplinary study has been troublesome, and field vandalism involving the removal of 300 lb infiltrometers, the removal of evaporation pan water (by range steers), and the occupation of weather instruments by various "critters" has been exasperating.

The nature of the test site has also presented some difficulties. The larger playa-type lakes often contain only inches of water, but the water may cover thousands of acres, whereas the small type playa lake basins may contain several feet of water. Evaporation and water level changes therefore tend to be much more rapid in the larger type

Table 4 - Cost/benefit analysis of performing a lake census over the Southern High Plains, Texas, using a ground survey (automobile), contract aerial photographs, a light airplane, and ERTS-1 satellite data (MSS and CCT).

	Ground Survey	Aerial Photo-graphs	Airplane Survey	Satellite System MSS	Satellite System CCT
Photo Repro/ Print charges	---	Contract	---	$45	$200 CPU 600 print chg.
Miles traveled	14,000	---	5,000	---	---
Method of travel	automobile	airplane	airplane	satellite	satellite
Maximum[3] Available frequency	4/year	on call	30/year[4]	36/year	36/year
Accuracy	Excellent	Excellent	Poor	Excellent	Excellent
Time-man hrs.	1064/survey	---	60/survey	?	?
Labor cost[2]	$4000	Contract	$1000	$250	$216 CPU
Transportation/Field Expense cost	$2100	Contract	$600	---	---
Photo or map cost	$300	Contract	$300	$5.00	no charge
Scale[1]	1:24,000	1:20,000	1:24,000	1:300,000	1:24,000
Size of area	30,000 sq. mi.	30,000 sq. mi.	30,000 sq. mi.	30,000 sq mi.	30,000 sq. mi.
Average cost/square mile	$0.27/sq. mi.	$2.00/sq mi.	$0.07/sq. mi.	$0.01/sq. mi.	$0.03/sq. mi.
Total cost	$8000	$60,000	$2000	$300	$1000

[1]scale used for mapping or scale of images or CCT data most workable
[2]labor based on man @ $1000/mth or $50/day CPU cost about $54/scene
Printer charge 20¢/page of 66 lines
[3]frequency does not allow for inclement weather
[4]use of one plane only

Table 5 - Results of measuring water areas and mud areas in the Double Lakes test site by the Stanford Research Institutes ESIAC (from 9 x 9 MSS positives, Band 7).

DATE	WATER COUNT		MUD COUNT		LENGTH WATER IN MM.		WATER AREA IN SQ. KM.		MUD AREA IN SQ. KM.		N. PLAYA WATER DEPTH IN INCHES	T-BAR WET OR DRY
	N	S	N	S	N	S	N	S	N	S		
7-29-72	900	1180	340	500	1.5	1.4	0.64	0.83	0.24	0.35	±2.00	DRY
8-16	1990	1640	3400	1730	2.2	1.0	2.26	1.86	3.87	1.97	9.00	WET
10- 9	2196	2335	2396	2932	3.3	1.9	2.50	2.65	2.72	3.33	12.00	WET
11-14	2360	2300	ND	ND	3.0	1.9	2.68	2.61	----	----	14.00	WET
12- 2	2575	2140	ND	ND	3.0	1.8	2.93	2.43	----	----	15.75	DRY
2-12-73			0.14	ND	3.2	1.7		2.22	----	----	16.00	DRY
3-20	2600	2330	ND	2670	3.1	1.7	2.96	2.65	----	3.04	15.90	DRY
4- 7	2680	2015	ND	2060	3.0	1.6	3.05	2.29	----	2.34	16.00	DRY
6-18	940	NONE	1125	850SA	1.5	0.0	1.07	----	1.28	----	1.00	DRY
7- 6	NONE	NONE	NONE	800SA	0.0	0.0	----	----	----	----	0.00	DRY
7-24	900	860	100	920	1.5	1.1	1.02	0.97	1.13	1.04	1.00	DRY
8-11	NONE				0.0	1.0	----				0.00	DRY

Area = $\frac{2(\text{count})}{1756.25}$ SA = salt crust ND = not determinable

playas. For example, on May 30, 1973, the Double Lakes test site contained 7 1/2 inches of water, by June 19 only 1.1 inch, and by June 26 the playa was dry. However, by July 27, the playa again contained 1.0 inch of water, yet the only imagery available of this sequence is the June 18 pass. It is, therefore, inferred that a shorter period for satellite imagery would be of greater value, particularly when working with playa-type lake budgets and meteorological events in semi-arid to arid areas.

REFERENCES

Reeves, C.C., Jr., 1973a, ERTS-1 Imagery for Water Inventory, Southern High Plains, Texas and New Mexico: in press, Proceedings, Amer. Water Resources Asso. Symp. on Remote Sensing, Burlington, Ontario, Canada.

______, 1973b, ERTS-1 Cost/Benefit Analysis Using MSS and CCT imagery for Water Resource Inventory: Amer. Geophys. Union, Fall Meeting, San Francisco.

Texas Water Development Board, 1968, The Texas Water Plan: Summary: Austin, Texas, 50 p.

Tison, L.J., 1970, Inventory of installations for artificial recharge of underground water levels: Inter. Asso. Scientific Hydrology Pub. 87, 762 p.

Paper W 6

WATER-MANAGEMENT MODELS IN FLORIDA FROM ERTS-1 DATA

Aaron L. Higer, *U. S. Geological Survey, Miami, Florida;* Alfred E. Coker, *U. S. Geological Survey, Tampa, Florida;* and Edwin H. Cordes, *U. S. Geological Survey, Miami, Florida*

ABSTRACT

A prototype multiparameter data acquisition network, installed and operated by the U.S. Geological Survey is a viable approach for obtaining near real-time data needed to solve hydrologic problems confronting nearly 2.5 million residents of south Florida. Selected water quantity and quality data obtained from ground stations are transmitted for relay via ERTS-1 to NASA receiving stations in virtual real time. This data-relay system has been very reliable and, by coupling the ground information with ERTS imagery, a modeling technique is available for water-resource management in south Florida. For example, water stage is correlated with water-surface areas to provide water stage-volume relations in near real-time for management decisions concerning the distribution of water to people, fauna, and flora of southern Florida. An overall water-resource model will be generated when the other aspects (stage-seepage, climate, evapotranspiration, water control releases to salt water, etc.) are incorporated.

An ecological model has been designed for the Shark River Slough in Everglades National Park. This model uses areal measurements of water surface from ERTS data in conjunction with an aquatic animal sampling program to determine density of aquatic animals in the Shark River Slough. These data are then used by U.S. National Park Service ornithologists to make decisions for regulation of water during the bird rookery season in Everglades National Park.

INTRODUCTION

The objective of this investigation is to combine the use of the ERTS-1 Data Collection System (DCS) for ground truthing the multispectral scanner imagery (MSS) for the development of two prototype operational surface-water models: (1) Water management model and (2) Ecological model. The final product will be determination of a water budget (Figure 1) for the Everglades basin (Figure 2), Conservation Areas 1, 2, and 3 and Shark River Slough (Figure 3). The hydrologic conditions are now made available on a daily basis to the Federal and State water management agencies that are responsible for management of water within the Everglades. A water budget will be produced on a near real-time basis using a combination of the ERTS-1 MSS and DCS data. Paulson (1), Schumann (2), and Cooper (3) applied similar techniques to operational systems with a DCS capability; Graybell (4) and Deutsch (5) used MSS to determine surface-water distribution. Anderson (6) used the MSS imagery to identify and map vegetative communities within wetlands. Reeves (7) used successive passes of ERTS imagery of playa lakes in the Texas High Plains to demonstrate the dynamics of surface-water distribution within the lakes. However, this current investigation combines an operational ERTS data collection system with the multispectral scanner data.

WATER MANAGEMENT MODEL

The water supply for southeast Florida, with a population of 2.5 million, depends upon the retention of water in four major impoundment areas (Figure 3): (1) Lake Okeechobee, (2) Conservation Area No. 1, (3) Conservation Area No. 2, and (4) Conservation Area No. 3. Shark River Slough, an important source of water for Everglades National Park, at the downstream end of these interconnected water bodies, also depends upon overland flow from adjoining Conservation Area No. 3. An accurate accounting of the amount of water in surface storage is difficult because land-surface profiles are not available. The shallow water depths of 0.3 to 1.0 meter, the flat terrain, the abundant vegetation, and the vast area of 3,600 square kilometers in the Everglades preclude the feasibility of determining accurate volumes by standard methods. In the Conservation Areas and the Shark River Slough, the water does not pond in the usual manner, but slowly flows over the gently sloping land surface.

Several water budget studies for the conservation areas are underway by Federal (U.S. Corps of Engineers) and State water-management agencies (Central and Southern Florida Flood Control District). Elements that need more accurate definition in the existing water budget studies are rainfall, evapotranspiration, seepage losses and surface storage.

The ERTS water management model uses the DCS to provide quantative in situ data on the elevation of the water surface (Figure 4) and MSS data to provide information on the areal extent of the water surface. Knowing the relation between the surface-water area and surface elevation for the range of water levels, the storage can then be calculated (Figure 5). Additionally, knowing the change in storage and the surface inflow and outflow (input and output) from the system it is possible to calculate evapotranspiration and seepage (Figure 6).

At present the DCS data are transmitted from the Everglades stations (Figures 7 and 8) to the satellite and relayed to the two ground tracking stations at Goddard Space Flight Center (GSFC), Greenbelt, Md. and Goldstone, Calif. The data are then transmitted by teletype from GSFC, Greenbelt, Md. (Figure 9) to the Miami Office of the U.S. Geological Survey. The perforated teletype tape is then processed daily through a mini-computer (Figure 10) to convert the data to engineering units and place it into a format that has been requested by the Corps of Engineers. The data are then transmitted to the Corps of Engineers in Jacksonville, Florida by telecopier. The time required for the transmission of data from the Everglades via the satellite, the NASA tracking stations, and the U.S. Geological Survey to the Corps of Engineers is less than 2 hours.

ERTS multispectral imagery of Florida is obtained every 18 days from an altitude of approximately 900 kilometers. This data is transmitted from the satellite to Goddard Space Flight Center or Goldstone Tracking Station in digital format. The digital tapes are then mailed to the Miami Office of the U.S. Geological Survey. Several systems have been used to extract spectral information from these tapes to construct thematic maps. Electronic processing of the ERTS MSS data has been accomplished using the computer facilities of GE Corporation, Stanford Research Institute, Bendix, and IBM Corporation to produce different types of maps by computer.

The DCS part of the model is operational. However, the imagery part of the program is not yet operational because imagery data are not received from NASA on a near real-time basis (approximately 8 weeks after an ERTS pass) and the processing time (Figure 4) may take up to a week per frame. Between February 14 and March 22, 1973 three successive sets of the ERTS-MSS data were combined with existing ground-truth data (Figures 11, 12, and 13) and the DCS data for Conservation Area 1. During this period the water levels were dropping (Figure 14). For February 14 through March 22 the evapotranspiration and seepage, surface water distribution, and storage were for the Conservation Area I (Figures 5 and 6). This trial run indicated that an operational water-management model for the Everglades basin is feasible.

ECOLOGICAL MODEL

Thousands of years of seasonally fluctuating water supply, punctuated periodically with drought or unseasonally heavy rain, resulted in a natural balance of plant and animal communities. Water fluctuations, along with fires and hurricanes, contributed to the shaping of the ecological communities, i.e., the tree islands (composed of woody vegetation) and grassland communities (wet prairies and sawgrass marshes). However, this natural ecological balance is now influenced by a modified water regime, altered by water control within the Kissimmee-Okeechobee-Everglades watershed for flood control, crop irrigation, and coastal urban use. The Central and Southern Florida Flood Control District manages this watershed that contains more than 22,500 kilometers of canals and levees.

An effect of water deficiencies in Everglades National Park is the failure of wood storks (Figure 14) to form rookeries. Wood storks nest in winter at the inner edge of the mangrove belt in the park (south Dale and north Monroe Counties). According to John Ogden, Ornithologist, U.S. National Park Service (oral commun., 1973), the wood storks were successful in 1959, 1960, and 1961, but failed for five successive years (1962-66), when low rainfall in south Florida resulted in prolonged drought in the park.

The success or failure of wood stork rookeries is a significant index of hydrologic conditions in the park. Wood stork studies in Everglades National Park by Kushlan (8) suggested a working hypothesis for establishing the water conditions of Shark River Slough, the largest fresh-water course in the park, needed for successful formation of these rookeries. A prediction of success or failure of the rookeries at the inner edge of the mangrove belt could be made in November of each year with the assistance of processed ERTS data. November marks the beginning of the dry season and precedes the height of rookery formation by approximately 2 months. The prediction can be based on recorded water-level measurements together with a synoptic view of the spatial distribution of surface water and on the density of small aquatic animals collected in quantitative traps (Higer, 9).

The ecological model is designed to relate the wildlife in the Shark River Slough to the availability of food and water. In an ongoing study with the National Park Service over 50,000 aquatic animals have been trapped (Kolipinski, 10). The species numbers and hydrologic data are entered into a digital computer program that provides statistical summaries of species distributions and water depths at point locations in the slough. Time-variant synoptic displays using ERTS-MSS imagery taken concurrently with stage and rainfall data presently being collected from DCS may provide the following information to develop an ecological model (Figure 16):

1. Knowledge of the quantity of water stored in the slough.

2. Knowledge of the spatial distribution of water (Figure 17) in the slough as it relates to available food for the bird rookeries.

3. Quantitative hydrologic data that allow management to know where and when to increase water into the slough from the upstream water storage areas.

4. Ability to predict the number of aquatic animals in the slough and the success or failure of the rookeries, dependent on the hydrologic regime.

DISCUSSION

The importance of the space-relayed data can be shown by a comparison of the accuracy and frequency of that data received through the Miami USGS teletype with data from the existing remote radio transmission systems in southern Florida. The great "line of sight" distances involved in the radio transmitted systems often provides rare and garbled data messages. The frequent meteorologic disturbances in southern Florida prevent the transmission of the accurate synoptic information on rainfall and water stage that is essential in managing the water for optimum values of conservation. ERTS-1 has been providing the USGS with 5 transmissions per day of these parameters and an opportunity to service faulty platform recorders within 24 hours. This enhances the opportunity for a constant flow of information and makes it possible for the U.S. Corps of Engineers to make daily decisions to optimize its water-control policy to conserve a greater proportion of the seasonally deficient water resource.

Sufficient water must be maintained in the Shark River Slough of the Everglades National Park to preserve the aquatic community and the several bird and mammal species which feed primarily on fish. The amount and time of water releases to the park is a management reaction decision based on very limited information on the water storage that may be available to the north of the Park. Small scale thematic maps of water levels provide an accurate evaluation of water distribution. A gradual reduction of water levels prior to bird rookery formation, would result in the concentration of fish in the Shark River Slough that may ensure adequate food for successful hatches of several rare and endangered bird species (Kushlan, 8).

REFERENCES

1. Paulson, R. W., 1974, An Evaluation of the ERTS Data Collection System as a Potential Operational Tool, Open-file, National Aeronautics Space Administration, ERTS-1 Third Symposium, December 10-14, 1973.

2. Schumann, H. H., 1974, Hydrologic Applications of ERTS-1 Data Systems in Central Arizona, National Aeronautics Space Administration, ERTS-1 Third Symposium, December 10-14, 1973.

3. Cooper, Saul, 1974, A Real Time Data Acquisition System by Satellite Relay, National Aeronautics Space Administration, ERTS-1 Third Symposium, December 10-14, 1973.

4. Graybell, Gary and Hull, Forrest, 1974, ERTS-1 Data in Support of the National Program of Inventory and Inspection of Dams, National Aeronautics Space Administration, ERTS-1 Third Symposium, December 10-14, 1973.

5. Deutsch, Morris and Ruggles, F. H., 1974, Optical Data Processing and Projected Applications of the ERTS-1 Imagery Covering the 1973 Mississippi River Valley Floods, 1974, National Aeronautics Space Administration, ERTS-1 Third Symposium, December 10-14, 1973.

6. Anderson, R. R., and Carter, Virginia, and McGinness, G. C., 1974, Applications of ERTS-1 Data to Coastal Wetland Ecology With Special Reference to Plant Communities, Mapping and Typing and Impact of Man, National Aeronautics Space Administration, ERTS-1 Third Symposium, December 10-14, 1973.

7. Reeves, C. C., Jr., 1974, Dynamics of Playa Lakes in the Texas High Plains, National Aeronautics Space Administration, ERTS-1 Third Symposium, December 10-14, 1973.

8. Kushlan, J. A., Higer, A. L., and Ogden, J. C., 1974, The Relationship of Temporal Variations in Water Level to Fish Production and the Reproductive Success of Wood Storks in the Southern Everglades, in review.

9. Higer, A. L., and Kolipinski, M. C., Pull-Up Trap: A Quantitive Device for Sampling Shallow-water Animals: Ecology, Vol. 48, No. 6, Autumn 1966.

10. Kolipinski, M. C., and Higer, A. L., 1969, Some Aspects of the Effects of the Quantity and Quality of Water on Biological Communities in Everglades National Park: Open-file Report, U.S. Geological Survey, 95 pp.

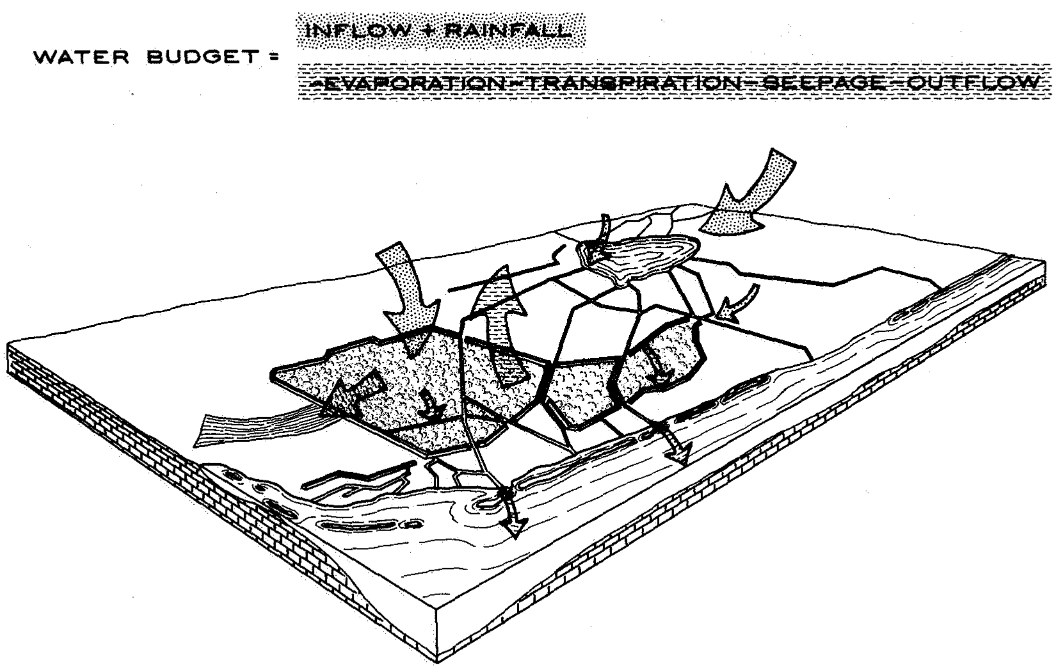

FIGURE 1. Schematic diagram of a water budget for the Everglades water basin.

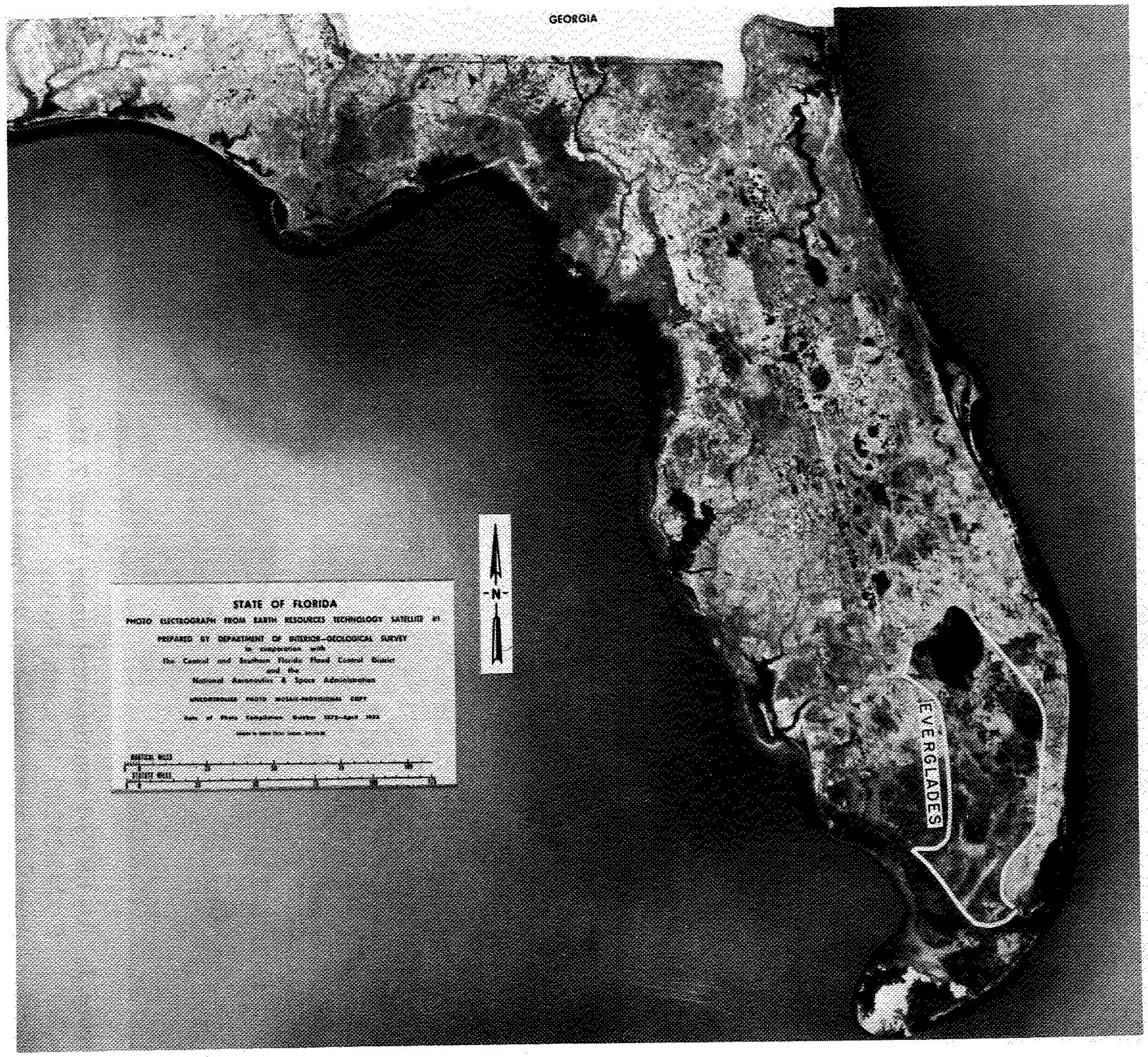

Figure 2. Photo mosaic of Florida, compiled from sixteen ERTS-1 images between October 1972–April 1973 of band 7 of the multispectral scanner. The delineated area is the Everglades water basin.

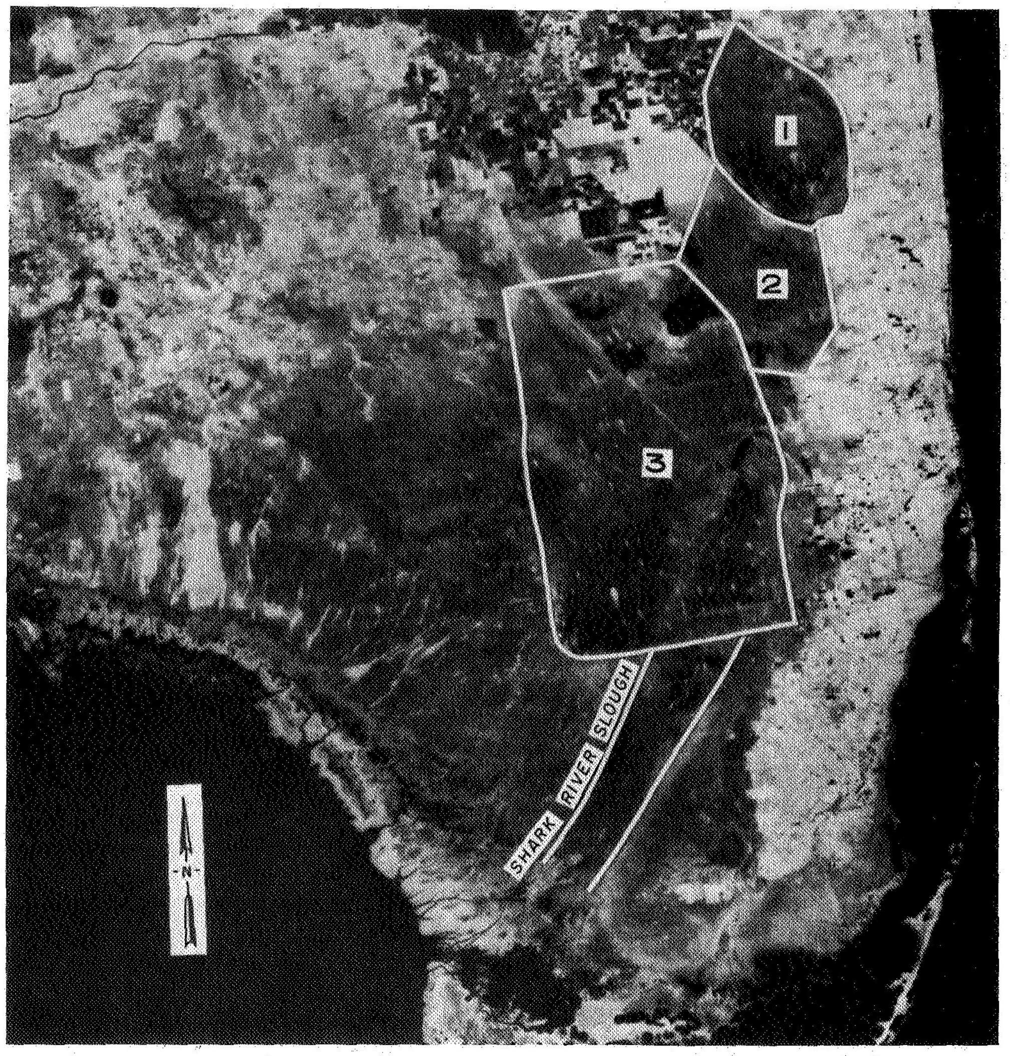

Figure 3. An ERTS-1 multispectral image, band 7, March 22, 1973, NASA, E-1242-15240, of south Florida. The areas outlined are: Conservation Area 1, Conservation Area 2, Conservation Area 3, Shark River Slough, and Lake Okkchobee (southern end can be seen in photo).

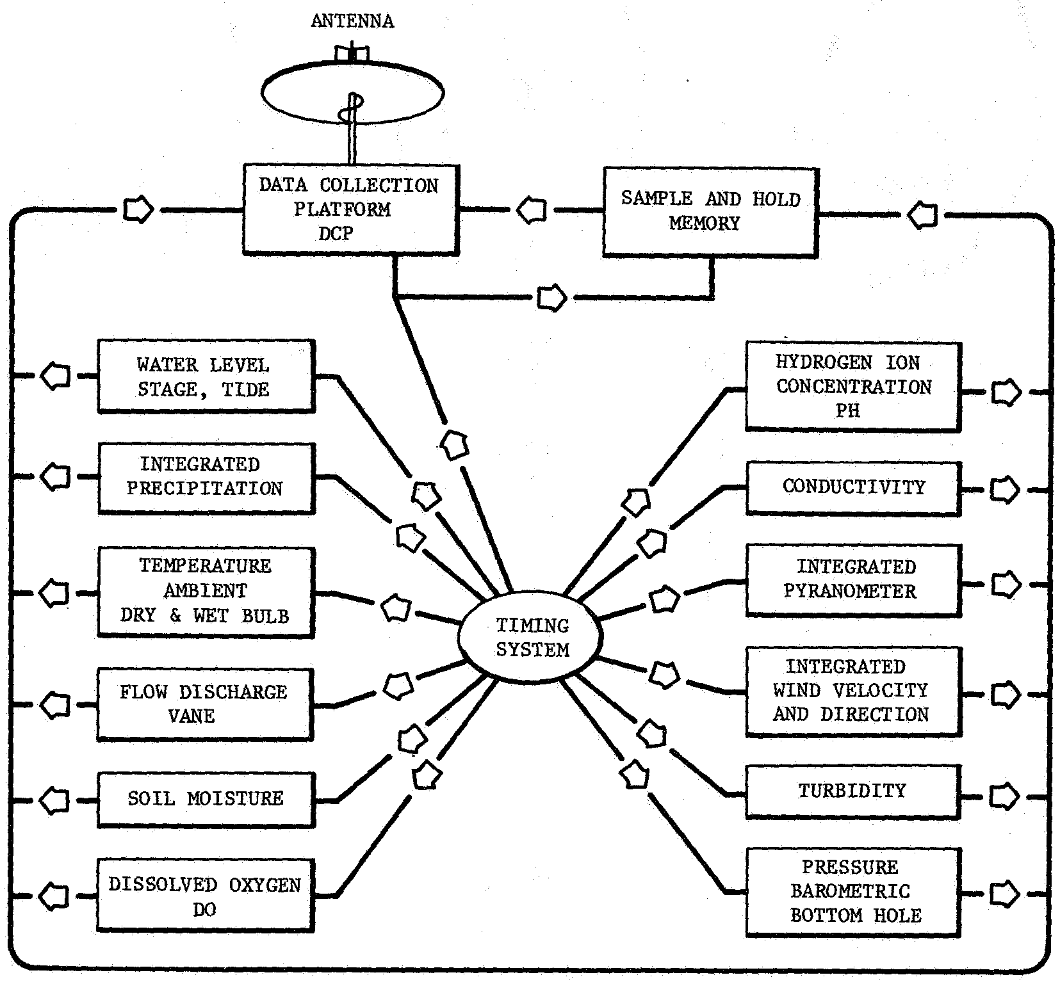

FIGURE 4. A schematic of the proposed system of parameters that are being connected to data collection platforms in the water management areas in Florida. The sample and hold memory system developed by the USGS-EROS Program will allow between 18 and 24 hours of data daily to be collected of the needed parameters to complete a water quality and quantity budget.

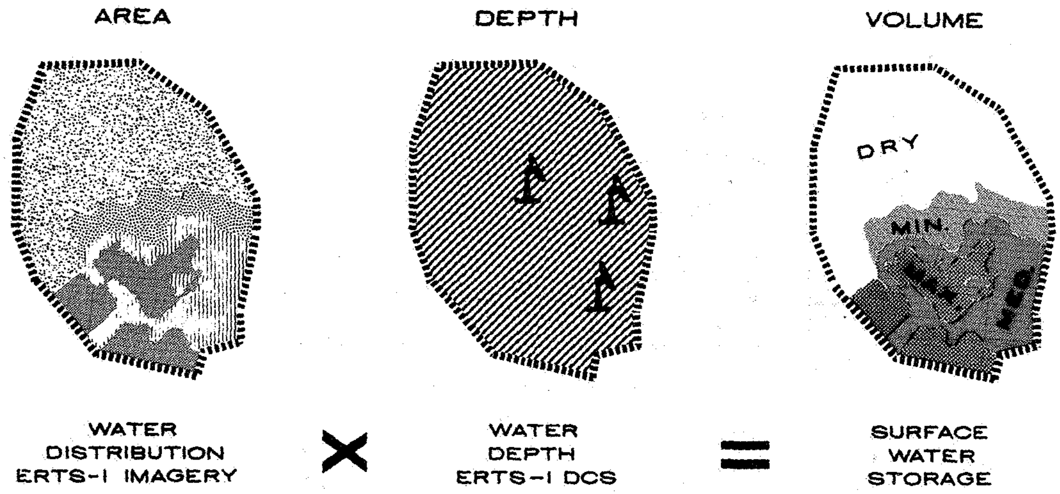

FIGURE 5. Schematic of the application of using space-relayed data to calculate surface water storage. ERTS data of three successive passes on February 14, March 4, and March 22, 1973 of Conservation Area I were used to demonstrate the feasibility of this method of determining surface water storage.

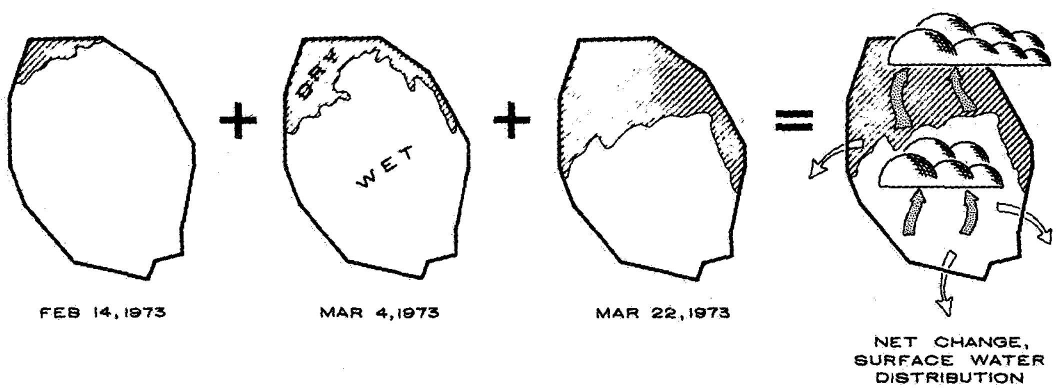

FIGURE 6. Schematic of the application of using space-relayed data to calculate evapotranspiration and seepage. ERTS data of three successive passes on February 14, March 4, and March 22, 1973 of Conservation Area I were used to demonstrate the feasibility of this method of determining evapotranspiration and seepage.

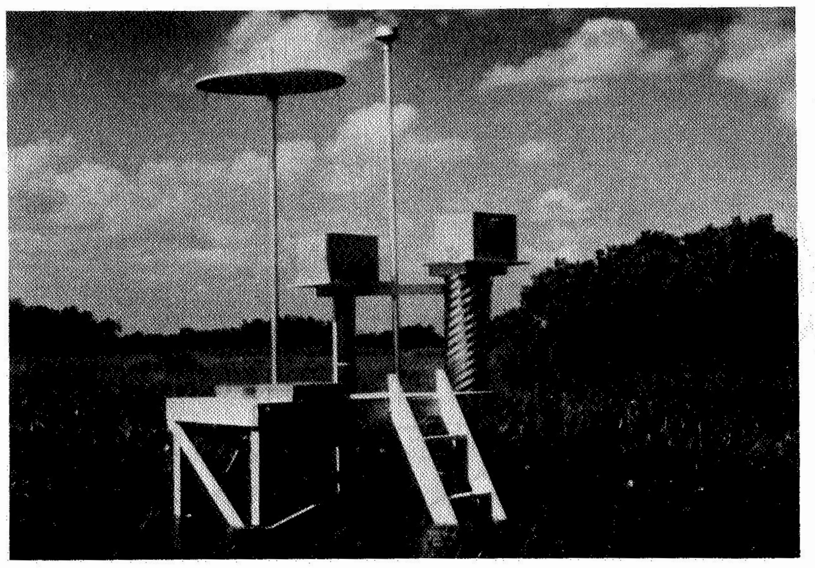

Figure 7. Data collection platform in the Shark River Slough, Everglades National Park. These stations collect and transmit water level and rainfall data for relay by ERTS-1.

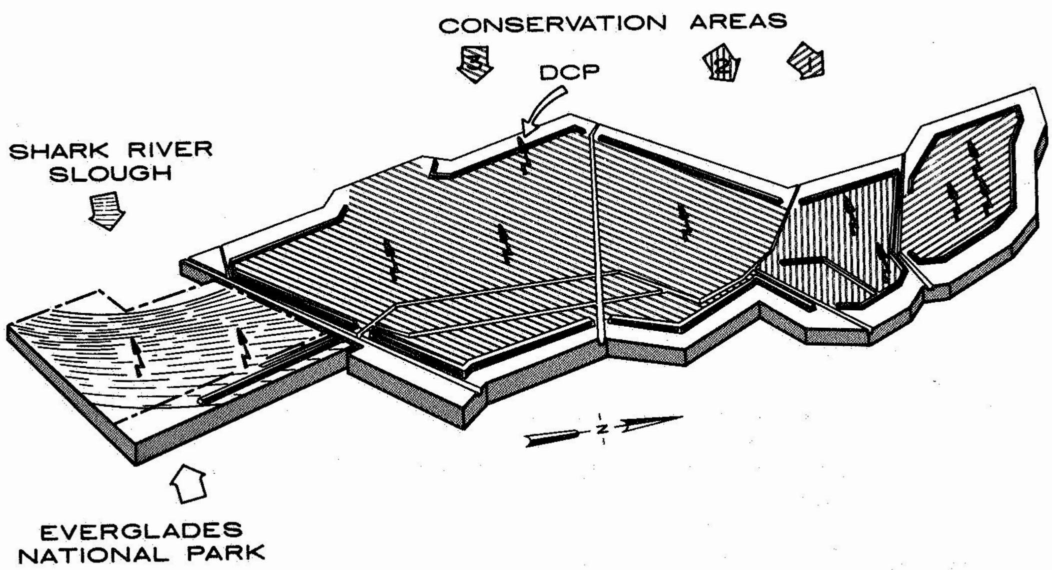

Figure 8. Schematic diagram of the Everglades basin showing relative locations of the data collection platforms (DCP) within the three conservation areas and the Shark River Slough.

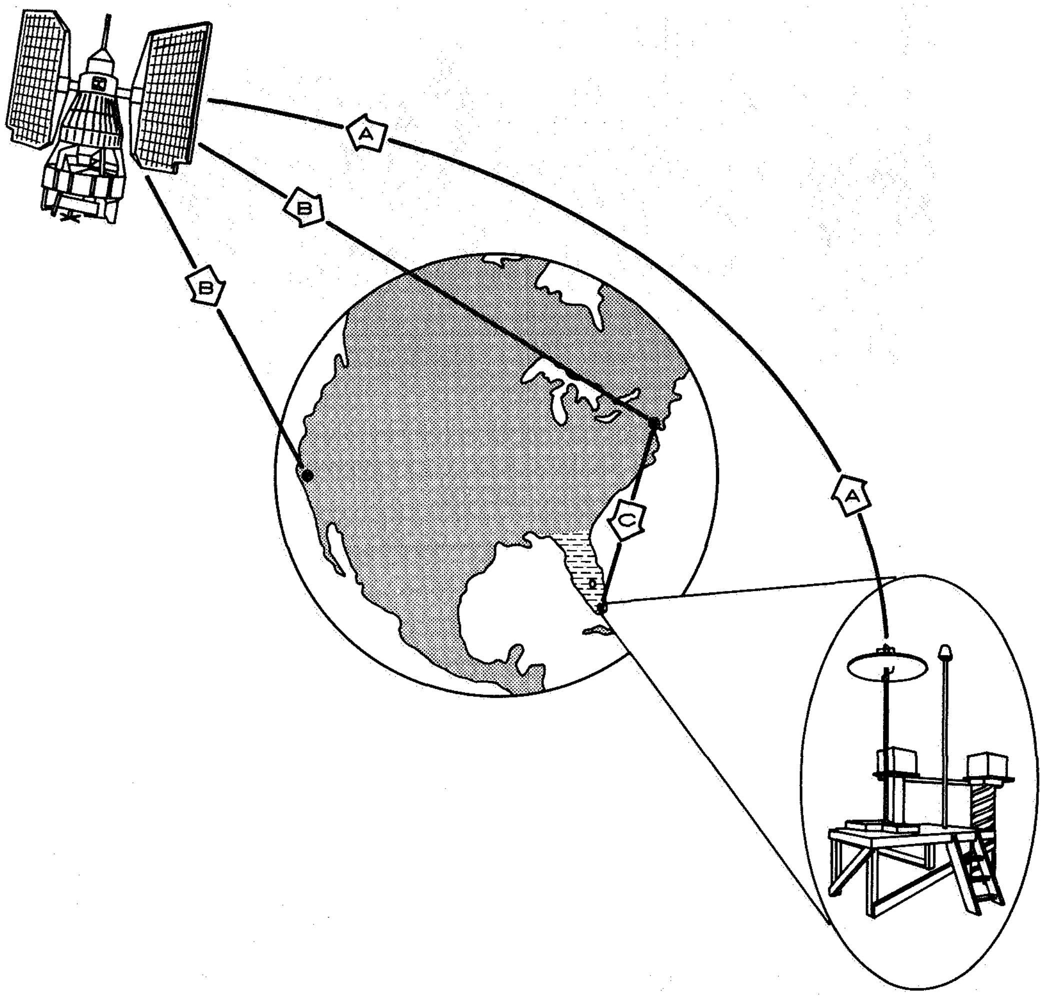

FIGURE 9. Data are transmitted from the Data Collection Platforms in the Everglades (A) via ERTS-1 to NASA tracking stations at Goldstone, Calif. and GSFC, Greenbelt, Md. (B). The data are then transmitted, via NASA communications network, to the Miami Office of USGS (C).

Figure 10. ERTS-1 DCS data are processed with a mini-computer system at the Miami Office of the USGS. The data are then relayed to water management agencies by telephone telecopier.

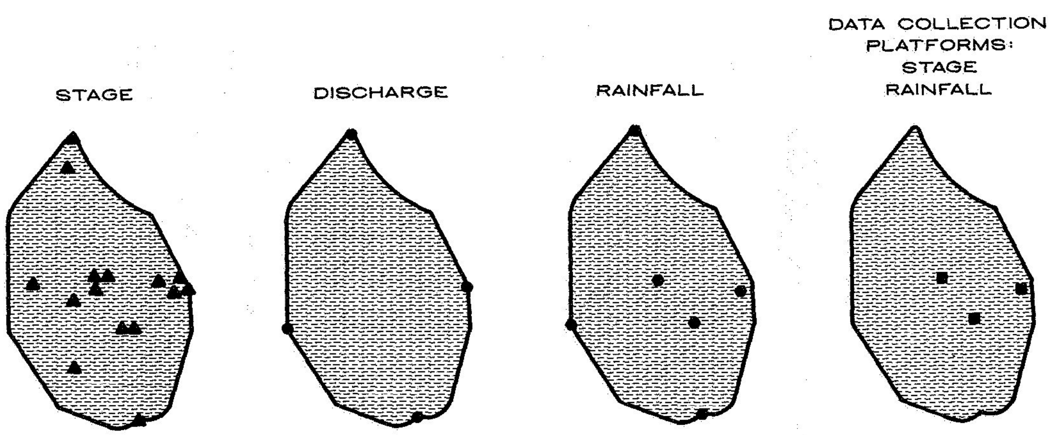

Figure 11. Location of ground truth stations used in the evaluation of the February 4, March 22, 1973 MSS data for Conservation Area 1.

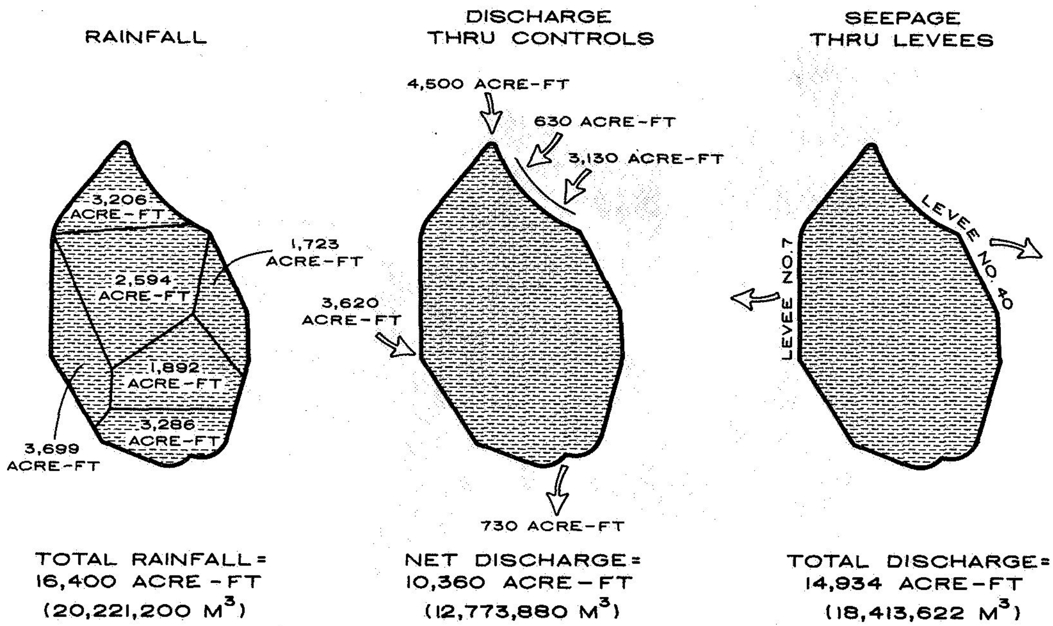

Figure 12. Hydrologic measurements compiled for interpreting the MSS data for February 14, March 22, 1973 in Conservation Area I.

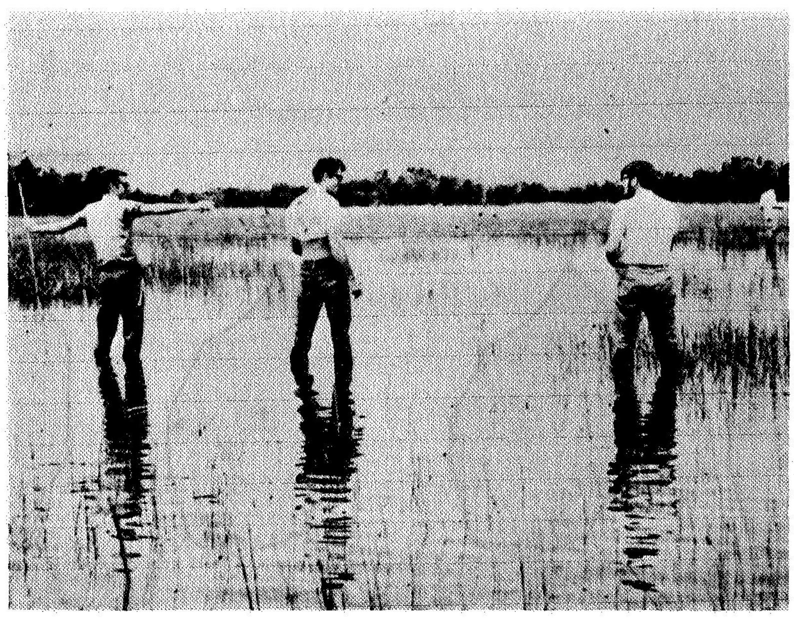

Figure 13. Ground-truth team collecting data such as plant community identification and soil characteristics in Conservation Area I for February 14–March 22, 1973.

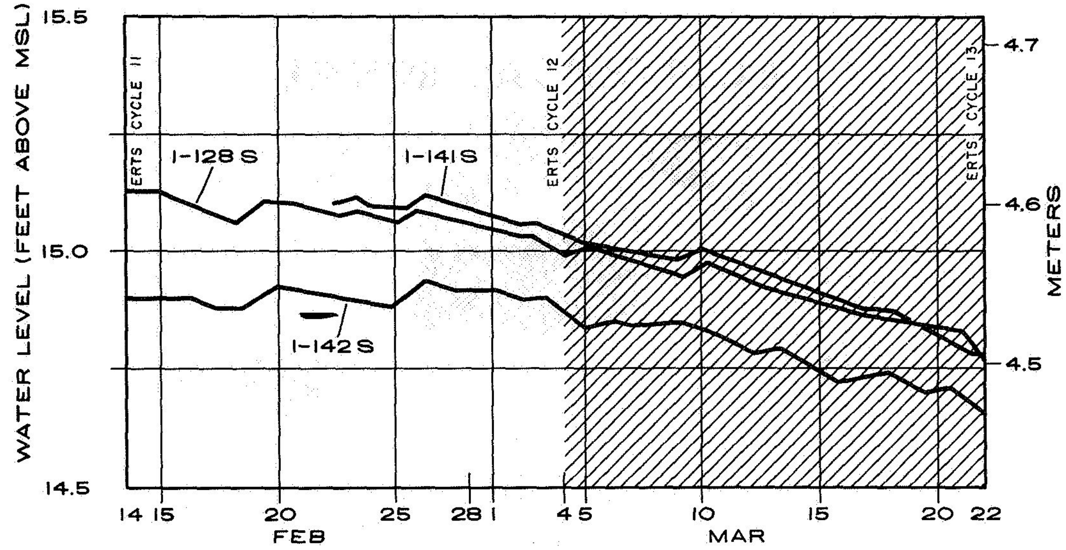

Figure 14. Hydrographs compiled from data relayed from three DCP's in Conservation Area I, February 14–March 22, 1973. During this period there were three passes of ERTS-1 to collect MSS data of Conservation Area I.

Figure 15. Wood storks feeding on small aquatic animals in shallow ponded waters.

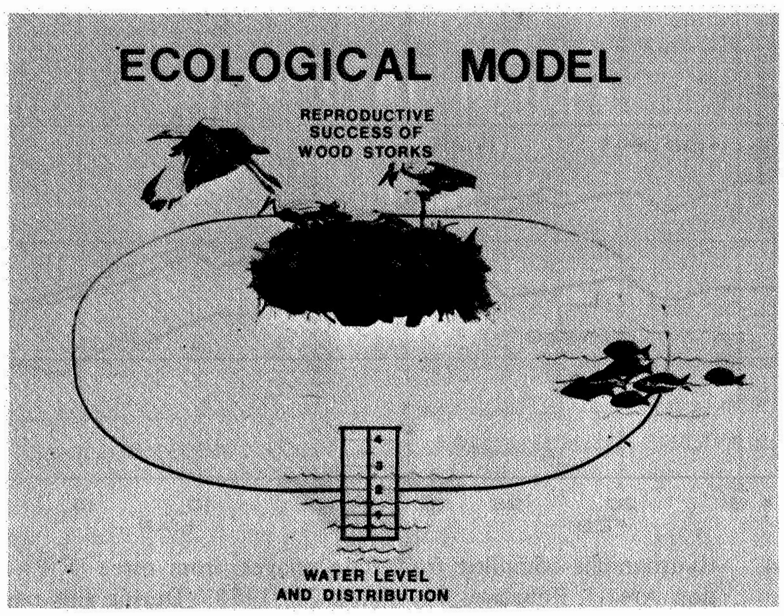

Figure 16. Schematic representing the general concept of the ecological model. The interrelation of surface water distribution and water level, the amount of small aquatic animals available and the wood stork depended on both the hydrologic conditions and the availability of food in order to form successful rookeries.

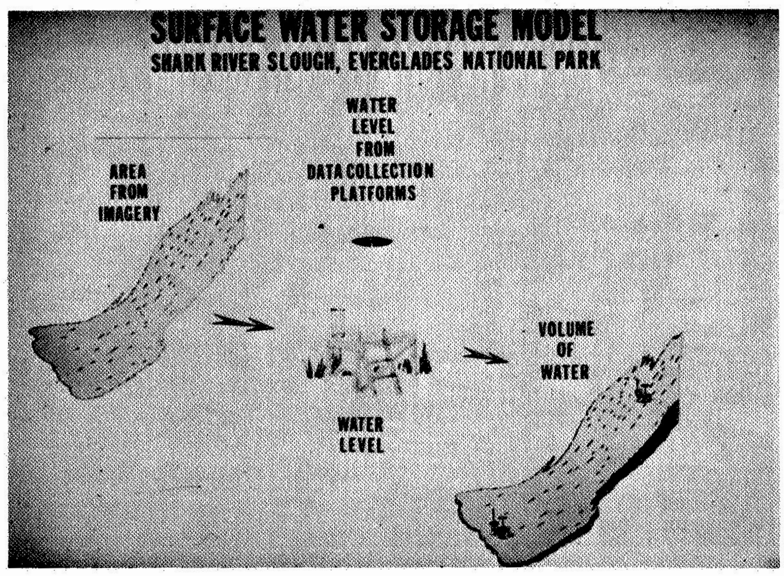

Figure 17. Schematic indicating how the construction or the DCS data and MSS data are used to determine quantity of water distributed in the Shark River Slough.

Paper W 7

MEASURING WATERSHED RUNOFF CAPABILITY WITH ERTS DATA

Bruce J. Blanchard, *(USDA-ARS), Chickasha, Oklahoma*

ABSTRACT

Parameters of most equations used to predict runoff from an ungaged area are based on characteristics of the watershed and subject to the biases of a hydrologist. Digital multispectral scanner, MSS, data from ERTS was reduced with the aid of computer programs and a Dicomed display. Multivariate analyses of the MSS data indicate that discrimination between watersheds with different runoff capabilities is possible using ERTS data. Differences between two visible bands of MSS data can be used to more accurately evaluate the parameters than present subjective methods, thus reducing construction cost due to overdesign of flood detention structures.

INTRODUCTION

Reliable projections of the quantity and rate of runoff from the surface of the land into rivers and streams are difficult to obtain for ungaged watersheds. However, this information is needed in the design of any structure located in the vicinity of a water course; for example, the storage capacity of municipal water supplies and flood detention structures. When projections of runoff are questionable, the storage capacity of such structures is quite often overdesigned. Overdesign not only increases construction costs, but can lead to significant salinization of water stored where high evaporation rates exist.

Examples of overdesign are frequently observed throughout the Great Plains. In the central reach of the Washita River basin, a water supply reservoir for the city of Chickasha was completed in 1958. The history of runoff into this structure for the past 15 years shows that the anticipated runoff exceeded the observed by several times. As a result of the overdesign and other related problems, the salinity of the stored water has increased sufficiently to preclude use as a municipal water supply and even sometimes as an irrigation source.

In an adjacent watershed, Sugar Creek, a study of the response of a large number of flood detention structures to a large storm on September 19-20, 1965 shows that the inflow was only about one-half that expected.

The quantities and rates of runoff that are used to design structures such as these are estimated from various types of watershed runoff models. These models are mathematical equations, generally of an empirical form, based on the drainage area, topography, soil and cover of the subject watershed. Usually, parameters of these models represent drainage area and surface conditions prevailing at the time of a rainfall event. The integrated influence of these characteristics combined with measurable climatological parameters (rainfall, antecedent moisture, rainfall intensity, etc.) can produce reasonable estimates of storm runoff. Efforts have been made to quantify the integrated influence of soils, cover and

surface roughness. However, at the present time, no objective means exists for estimating this influence. Present methods for estimating this influence are tedious, expensive and subject to judgment of the hydrologist.

The problem of subjectivity associated with present methods that are used to derive coefficients of runoff equations may be circumvented by applying digitized data obtained from ERTS. Even though hydrologic analysis based on photographic data obtained from ERTS suffers from the same subjectivity as do the existing methods, data obtained from the multispectral scanner, MSS, on board the satellite can provide digital data that can be incorporated into mathematical equations. This type data is less subjectively biased than are the other types of data.

The ERTS multispectral data is also superior to aerial digital data collected prior to ERTS because the relatively constant sun angle within an ERTS frame, caused by the satellite's sun synchronous orbit, eliminates many of the problems in comparing the spectral reflectance from watershed surfaces. The ERTS data has additional advantages in that there is sufficient spatial resolution to allow the identification of the smallest watersheds of practical interest and yet the number of data points depicting a large watershed are reduced to a manageable number.

DATA REDUCTION

The study site for this experiment is part of an ongoing hydrologic study within the Washita River basin in central Oklahoma. The drainage area in the study reach is 1,130 square miles and contains the 20 watersheds, ranging in drainage area from 20 acres to over 200 square miles, which were selected for study. The 20 watersheds were divided into 2 groups of 10 watersheds each with the distribution of drainage areas as near equal as possible in each group. Group I watersheds were used to distinguish and develop a relationship between the coefficients of a runoff equation and MSS data. Group II watersheds were set aside for verification.

The rainfall-runoff model (equation) selected for evaluation is the one developed by the Soil Conservation Service of the USDA. The equation is:

$$Q = \frac{(P - .2S)^2}{P + .8S}$$

in which $S = \frac{1000}{CN} - 10$

Q is the inches of runoff
P is the inches of rainfall
CN is the curve number, a dimensionless coefficient.

The coefficient (CN) is normally derived from soil, cover and slope data representing the hydrologic condition of the watershed surface for ungaged watersheds. The value of the coefficient can be calculated directly from rainfall and runoff data if the watershed is gaged. The basic objective of this study is to see if the value of the coefficient calculated using the MSS data is closer to the observed value than is the value estimated from the soils, cover and slope data.

Rainfall and runoff data for the 20 watersheds were used to calculate values of the coefficients (CN) for each watershed. The period of record, 1962-1972, depicts below-average rainfall and dry antecedent conditions. Calculated values of the coefficients for the watersheds range from 53.6 to 77.4.

Multispectral data for the watershed areas were obtained from the ERTS scanner for five passes (scenes) of the study area. Each scene represented major changes in soil moisture and vegetative conditions. The first scene, dated September 19, 1972, shows a dry dormant condition with almost no ground cover. The second scene, dated October 25, 1972, provides data with essentially the same ground cover, but extremely wet conditions. The third scene, dated January 23, 1973, showed minor growth in winter wheat fields and wet conditions. The last two scenes, dated April 5, 1973 and April 23, 1973, both showed substantial ground cover for crops, pastures, and timber. One of the growing season scenes was extremely wet and one moderately dry. All scenes were essentially free of clouds.

The MSS data from ERTS were obtained in the form of sequential and adjoining tapes that were laced together with the aid of a computer program, forming a single file for each watershed area. Due to the nature of the problem, it is very important to keep the relative position of the pixels correct and to be able to accurately define its location within a watershed. Without this, coordination of ground truth and spectral response would be impossible. Since the methods used to display the MSS data present a distorted image, the maps used for coordination purposes were digitized so that they could be replotted in the same image as the MSS data.

Data sets for the larger watersheds were obtained by displaying the entire ERTS frame for the area of interest on a Dicomed display. The portion representing the watershed was isolated using the distorted maps and a computer program. The computer program represents the watershed boundary by a series of parallelograms. About 20 parallelograms seem to be enough to adequately define the watershed boundaries (Fig. 1).

Data sets for the small watersheds were more easily obtained by displaying the ERTS data on computer printout and overlaying it with the distorted maps. In all cases, ponds and channels aid significantly in locating specific points on the MSS data maps. Since stream channels are rather difficult to locate in grassland areas, a study of the ERTS data showed that MSS band 5 resolved the stream channels and ponds sufficiently well to position the overlay. However, during the growing season, (MSS band 4 + MSS band 5)/MSS band 6 enhanced the resolution of the stream channels. Although cumbersome, the system described for small watersheds will also work for larger watersheds if a display system is not available.

ANALYSIS OF REDUCED DATA

Since the objective of this study is to see if MSS data can be used to calculate parameters of a runoff equation, several means of relating the two data sets were analyzed. Discriminant analysis, which can be used to study group similarity or difference and relate this to group descriptors, was used to examine the MSS data of the watersheds having extreme differences in observed runoff coefficients. Using a modified multiple discriminant analysis program (Cooley and Lohnes, 1962), good discrimination was observed between these watersheds when MSS bands 4, 5, and 7 were used in the linear discriminant function. The good discrimination was found only in the dry dormant scene, however the same bands also produced the best discrimination in other scenes.

Multiple discriminant analyses considering each of the 10 developmental watersheds as an independent group showed very significant group discrimination. However, the discrimination did not appear to be related to the runoff coefficients. Alternatively, plots of the mean value for each band vs. the observed runoff coefficient were made. Since it appeared that there might be a relationship, all possible combinations of the means were plotted. Two promising relationships were evident. The mean of MSS band 5 (μ_5) minus the mean of MSS band 4 (μ_4) is reasonably well related to the runoff coefficients for the watersheds in Group I (Fig. 2). This relationship is most evident in the dry dormant scene. The combination $\mu_5 + \mu_6 - (\mu_4 + 2\mu_7)$ produces a more consistent relationship when all five scenes are considered.

Both of these relationships were verified on the 10 Group II watersheds, (Figs. 3 and 4). It does not appear that the equation using four bands significantly improves the two-band relation during the dry dormant scene.

In the introduction it was mentioned that runoff from a large number of flood detention structures on Sugar Creek was only about one-half what was expected. Figure 5 shows a comparison between the expected values of the coefficients and the observed values. A comparison of figures 2 and 5 shows that there is considerably less variation in the relationship between the MSS data and the curve numbers than there is between the estimated curve numbers and the observed curve numbers. Predicted coefficients for watersheds in the test group (Fig. 3) have an average deviation of 3.86 from the measured coefficients. Manually calculated coefficients (Fig. 5) have an average deviation of 24.08 from the measured coefficients. The expected curve numbers were calculated subjectively from soils, cover, and topographic data. Thus, it would appear that it may be possible to use MSS data to estimate realistic values for the curve numbers. It may be that coefficients of other runoff models could be predicted equally well.

APPLICATION

The benefit of techniques developed in this study is probably far greater than we can presently estimate. If the relationships found in this study can be applied to impoundment design in the Great Plains area, construction costs can be reduced and the quality of impounded waters can be better protected for municipal and other uses. In fact, the improved quality of the water may eventually become the primary consideration in the southern and western Great Plains.

Two major impoundments in the Washita River basin built in 1958 as multipurpose structures were seriously overdesigned. The net result was evaporation of marginally saline waters until the water supply was not considered suitable for municipal use. At Foss Reservoir in Oklahoma, the U. S. Government has started construction of a multimillion dollar desalinization plant to recover the water supply. At Lake Chickasha, built as a water supply for Chickasha, Oklahoma, salinization of the impounded waters has precluded its use as a municipal supply. With more accurate runoff prediction techniques at the disposal of consulting engineers, it is unlikely that either structure would exist in its present form.

Coefficients of the runoff equation developed from MSS data and shown in figures 3 and 4 for the verification watersheds, more closely approximate the observed values of the coefficients than do those calculated from watershed characteristics (see figure 5 for Sugar Creek). Overprediction of runoff that resulted from using

the coefficients in figure 5 caused design of structures with about twice the storage capacity necessary to contain the design storm runoff. Conservatively, more than 10 percent of the construction costs of these structures could have been saved if a better runoff estimate had been available.

Present soaring construction costs are limiting construction of approved flood detention structures, thus it is essential that the costly overdesign be avoided. This is best accomplished by obtaining accurate runoff estimates. Construction costs of the Soil Conservation Service's program alone approaches 50 million dollars a year on a national scale. A saving of only 5 percent of construction costs (2.5 million dollars) warrants continued and expanded effort in the application of remote sensing techniques to the design of impoundments.

REFERENCES

1. Cooley, W. W. and P. R. Lohnes. Multivariate Procedures for the Behavioral Sciences, pp. 1-211. John Wiley, New York, 1962.

Figure 1. Display of MSS 5 Data for Watershed 512

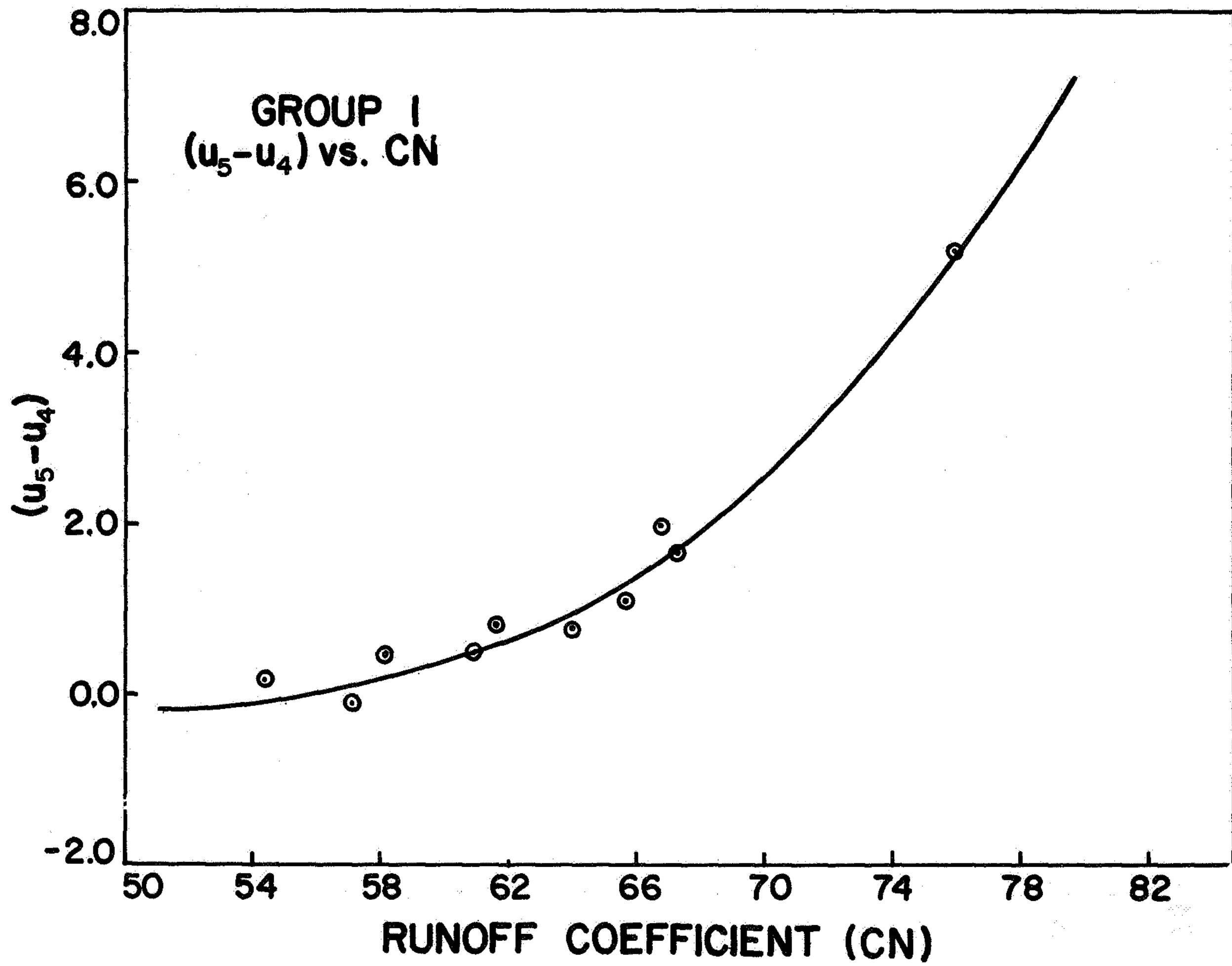

FIGURE 2. RUNOFF COEFFICIENTS (CN) VERSUS DIFFERENCE BETWEEN MEANS FOR MSS 5 AND MSS 4

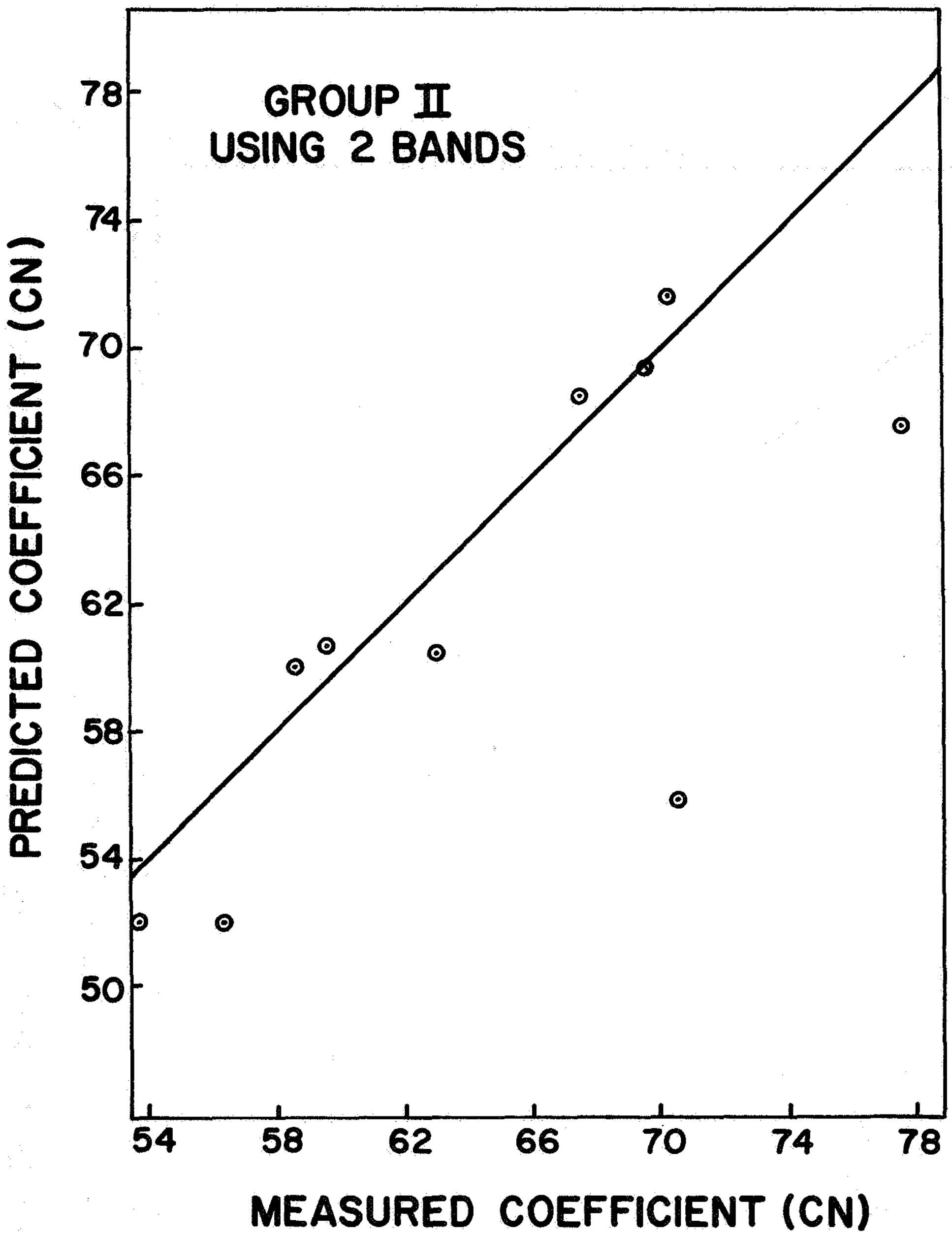

FIGURE 3. PREDICTED COEFFICIENTS BASED ON (μ_5 - μ_4) FOR GROUP II WATERSHEDS

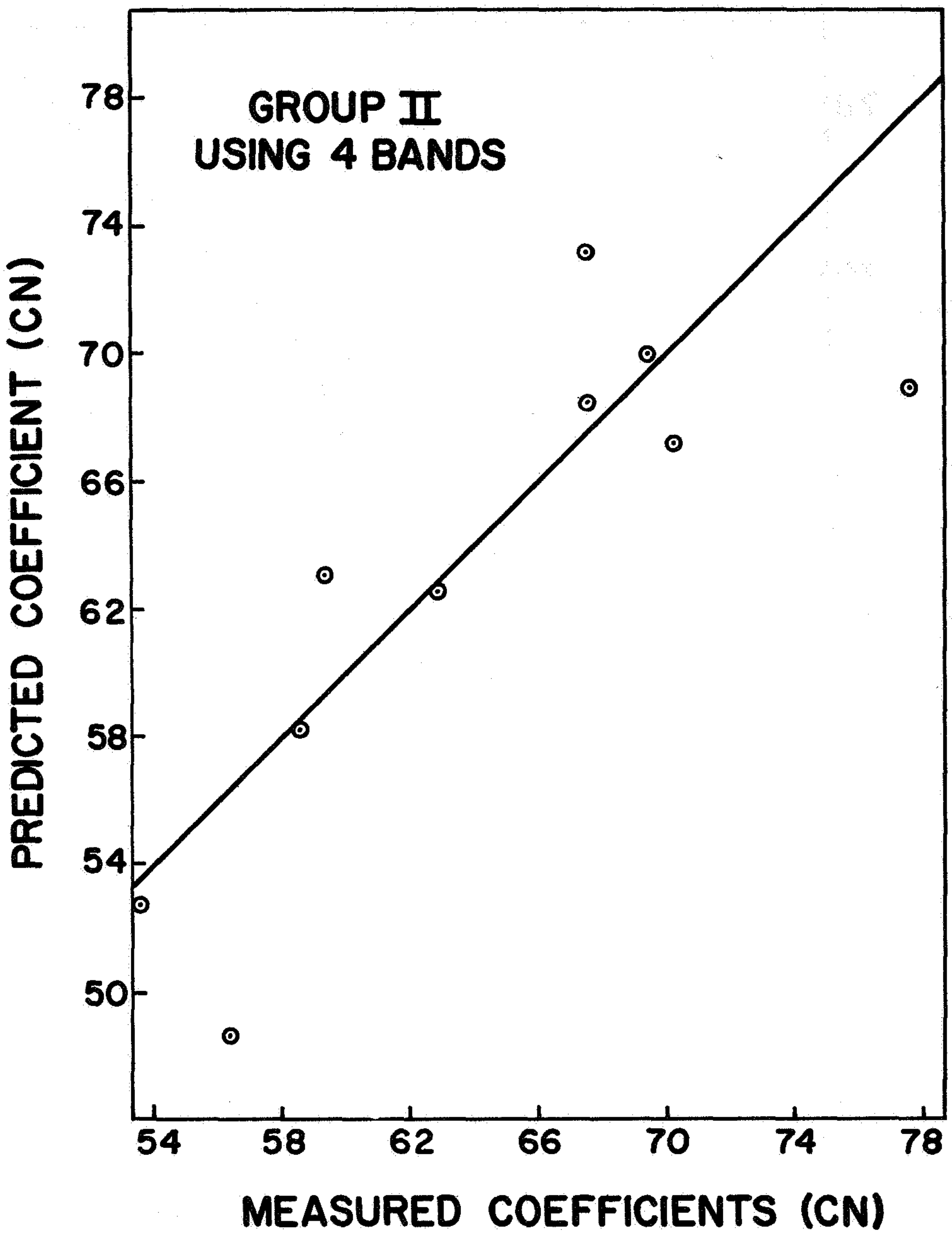

FIGURE 4. PREDICTED COEFFICIENTS BASED ON
$(\mu_5 + \mu_6 - (\mu_4 + 2\mu_7)$

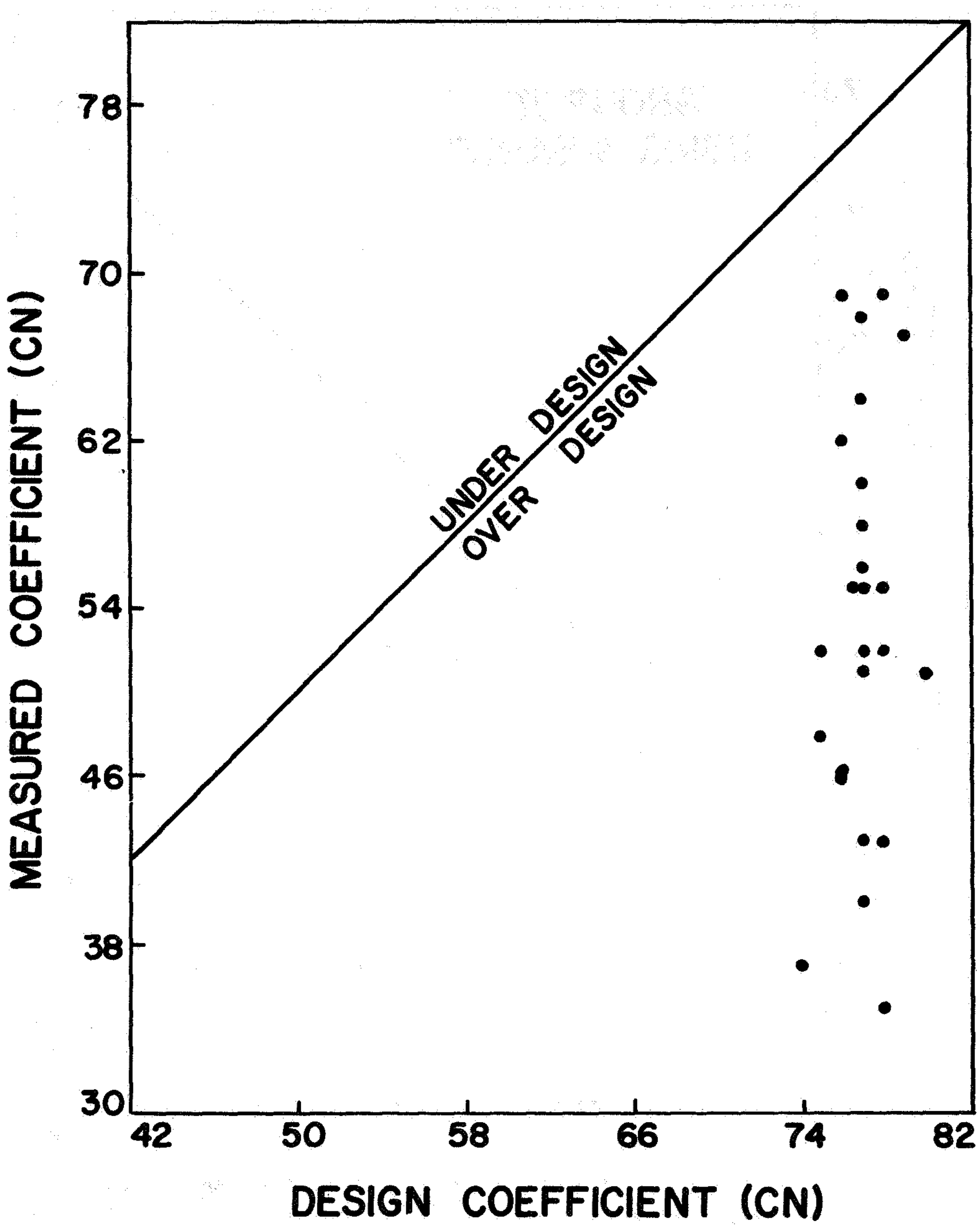

FIGURE 5. COMPARISON OF DESIGN AND OBSERVED COEFFICIENTS (SUGAR CREEK WATERSHED)

Paper W 8

AN EVALUATION OF THE ERTS DATA COLLECTION SYSTEM AS A POTENTIAL OPERATIONAL TOOL

Richard W. Paulson, *U.S. Geological Survey, Harrisburg, Pennsylvania*

ABSTRACT

The Earth Resources Technology Satellite (ERTS) Data Collection System (DCS) has been shown to be, from the users vantage point, a reliable and simple system for collecting data from U.S. Geological Survey operational field instrumentation. It is technically feasible to expand the ERTS system into an operational polar-orbiting data-collection system to gather data from the Geological Survey's Hydrologic Data Network. This could permit more efficient internal management of the Network, and could enable the Geological Survey to make data available to cooperating agencies in near-real time. The Geological Survey is conducting an analysis of the costs and benefits of satellite data-relay systems.

INTRODUCTION

The Data Collection System (DCS) aboard the Earth Resources Technology Satellite (ERTS-1) is being evaluated as a potential operational system for collecting hydrologic data from unattended field instrumentation. The evaluation, which is being conducted by the National Aeronautics and Space Administration (NASA), the Earth Resources Observation System (EROS) Program of the U.S. Department of the Interior, and the U.S. Geological Survey, indicates that it is technically feasible to use earth-orbiting satellites as vehicles for collecting data from field instruments and that there is potential application for operational satellite data-relay systems.

This report contains quantitative measures of DCS performance; the results of a digital computer simulation for estimating the potential of the system; and a discussion of the estimated size, characteristics, and capacity of an operational polar-orbiting satellite data-relay system that could be integrated with U.S. Geological Survey field operations.

OPERATIONAL DCS PERFORMANCE

The ERTS DCS is a communications system that consists of three elements. The elements are a small low-powered battery-operated radio transmitter, which is called a Data Collection Platform (DCP), a radio transponder aboard the ERTS satellite, and ground-receive sites. The polar-orbiting ERTS makes about 14 orbits of the earth daily, and can relay data from a DCP to a ground-receive site whenever both are mutually visible from ERTS, which occurs during a brief period on each of several of the orbits. The DCP transmits a brief data message of 0.04 seconds duration once every 90 or 180 seconds and can communicate with the satellite during several mutual visibility periods daily. The number of mutual visibility periods is primarily a function of geographical position and local terrain interference. Two ground-receive sites, at the Goddard Space Flight Center in Greenbelt, Maryland, and at Goldstone, California, provide good coverage for the contiguous 48 states. They allow data from continental American DCP's to be relayed on 3 to 7 daily orbits during mutual visibility periods lasting 12-14 minutes per orbit. For more information about the ERTS design and orbital characteristics, the reader is referred to the "ERTS Data Users Handbook". Painter and Seitner (1973) provide an excellent and concise summary of overall Data Collection System performance.

The Geological Survey has interfaced DCP's with a number of water-resources instruments such as stream gages, water-quality monitors and ground-water observation wells (Paulson 1973), precipitation and water-stage recorders (Higer - Oral communications), meteorological recorders and snow pillows (Schumann - Oral communications), and geologic instruments such as microseismic recorders and tiltimeters (Ward et al 1973).

Perhaps the most elementary instrument to be interfaced with a DCP is the digital water-stage recorder. Because of the sheer number of digital water-stage recorders in operation, it is worthwhile to examine the interfacing of the DCP to this recorder. The Geological Survey has nearly 18,000 stream-gaging stations, of which approximately 10,000 have digital water-stage recorders. Briefly described, the recorder continuously monitors stream stage via linkage to a float in a stream-connected stilling well. Periodically, at 15- 30- or 60-minute intervals, the recorder punches the real-

time stage value on a 16-channel paper tape--a machine-readable record. When the recorder is interfaced with a DCP, the most recently punched stage value is retained in a 16-bit memory in the recorder. This is the value made available for the DCP data burst which is transmitted at 180 second intervals. Thus, the DCP transmits the most recently punched stage value until it is updated by a new punched value. Figure 1 is a computer summary of the number of times particular hourly values were relayed for one DCP during the 18-day period from day 152 to day 169, 1973. The pattern is closely paralleled by preceding and subsequent 18-day periods. There are two periods during each day when ERTS mutual visibility periods occur, approximately from 24000 to 0400 and 1330 to 1800 Greenwich Mean Time. As there may be 3 or 4 DCP transmissions relayed during one mutual visibility period, a particular value may be relayed several times.

At present, the water-stage value is encoded in the first 16 bits of the 64-bit DCP data message, and the remaining 48 bits are left at zero. A data-storage-and-interface device, being developed by the EROS program, will contain a shift register that will enable the 3 antecedent stage values as well as the real-time value to be encoded in the 16-bit data message. This will help to make full use of the capacity of the DCS.

Figure 2 is the result of a computer simulation of the number of times each hourly value could have been relayed from DCP ID 6115 during the period summarized in Figure 1. It can be seen that about half the hourly values could have been relayed at least once, a few of them 8 or 9 times. The data-storage-and-interface device will have the capacity to store several sets of 64 bits in its memory and cycle them to the DCP for transmission. For example, if two sets of 64 bits were made available sequentially to the DCP after the Nth hour of the day, set one could contain the hourly values from N-3 to N, and set two could contain the hourly values N-7 to N-4. Figure 3 is the result of that simulation. Figure 4 is the result of simulating the availability of 3 sets of 64 bits to the DCP, encoded analogously as before except that 12 values (hourly values N-3 to N, N-7 to N-4 and N-11 to N-8) were made available. In each successive example above the number of unique hourly values transmitted increases, while the maximum number of times that each particular value is relayed decreases. The salient

point is that this DCP, from which about 14 transmissions per day are relayed, has the capacity to transmit virtually all of the daily hourly values if the full capacity of the system is used. All of the hourly values per day comprise about 24 (values) x 16 (bits/value) = 384 unique bits of data, but because of the random nature of the system, about 14 (messages/day) x 64 (bits/message) = 896 bits/day were required to obtain the full daily record.

It is possible to postulate the existence of the ERTS-2 satellite in an orbital plane orthogonal to ERTS-1 and to simulate the availability of data from a stream gage DCP with the interface device, as was done above. The results of that simulation are compared to the single-satellite example in Figure 5. In the two-satellite example, if 2 sets of 64 bits are cycled to the DCP, all of the possible 432 hourly values in the 18-day cycle can be relayed. Not shown in the figure, but obvious in the 2-data-set analysis, is the fact that virtually all of the values were relayed 2 or more times, and that there is redundancy to insure the transmission of all the data. The data rate in a two-satellite case is of the order of 1800 bits per day, which provides the redundancy.

The thrust of this analysis is to demonstrate that if the full capacity of the ERTS-DCS were used at one of these stations, the potential would exist for collecting the quantity of data that the Geological Survey routinely and operationally collects. An operational ERTS-type system would have to guarantee more than 14 transmissions daily with one satellite and probably would have to provide close to 28 average daily transmissions, the two satellite case, to provide the desired redundancy to insure the transmission of all data.

ELEMENTS OF A POTENTIAL OPERATIONAL DATA COLLECTION AND PROCESSING SYSTEM

The U.S. Geological Survey operates a system of water-resources data collection stations that comprise the Hydrologic Data Network. The Network is operated by the Survey in cooperation with local, State, and other Federal agencies and gathers data on a wide variety of environmental phenomena. Many stations in the Network are sites where hydrologic measurements are taken manually at a wide range of temporal intervals, or where water samples are taken for

bacteriological, chemical, or radiological analysis. At many data collection stations in the network, automatic instruments record data on site. The digital-recording stream-gaging station, discussed above, is the most common field instrument in the Network.

The Geological Survey also maintains a national telecomputing network, which consists of computer centers in Washington, D.C., and Reston, Virginia, and nearly 100 remote computer terminals in Survey offices across the country. The Washington, D.C., computer center has an IBM 360/65 computer and the National Center at Reston, Virginia has an IBM 370/155 computer. The Survey also maintains, within the telecomputing network, a National Water Data Storage and Retrieval System into which data from the Hydrologic Data Network are entered and stored via remote terminals.

Thus, the major hydrologic activity of the Geological Survey-the collection, storage, retrieval, and analyzing of hydrologic data-is accomplished through the operation of three basic systems. The Hydrologic Data Network provides data collection, the National Water Data Storage and Retrieval System processes and stores data generated by the Hydrologic Data Network, and a national telecomputing system provides general data processing support for the National Water Data Storage and Retrieval System.

The interface between the Hydrologic Data Network and the data-processing systems is far from being automated in its present conventional operational mode without using the DCS. At intervals measured in terms of weeks, the data from a particular field instrument are retrieved by field engineers and technicians who visit the station, calibrate the instrument, perhaps take supplementary measurements and samples, and conduct general maintenance. The data, many of which are in machine readable form are returned to the office, checked for quality control, transferred onto punch cards or magnetic tape for entry into the computer system. The time lag from time of recording to time of entry into the computer system may be as great as 8 weeks.

The experience that several Geological Survey experimenters have had with the ERTS-DCS indicates that it is technically feasible to interface a large percentage of field instruments in the Hydrologic Data Network with an ERTS-type DCS then, a multi-satellite system could obtain the volume of data now routinely collected by the Network. Conceptually, the

data could be automatically entered into National Water Data Storage and Retrieval System, processed, and disseminated by the telecomputing network for near-real time data use.

One can speculate on the capacity of a polar-orbiting DCS system as an integral part of the data-collection activities of the Geological Survey. The system probably would require about a 20,000 DCP capacity, a daily average DCP that would be easily installed and maintained. The failure rate of the DCP's would have to be less than the failure rate of the field instrumentation, which is of the order of 10 percent per year for digital water-stage recorders. With a multiple polar-orbiting satellite system, the average queuing time for data could be kept below 2 hours. Satellite-relayed data could be received at several regional sites, which would provide good regional DCP coverage and would provide redundancy in ground-receive-site equipment. The data could be processed on site or entered into the telecomputing network for processing. The regional centers would format the DCP data for entry into the basic-data-processing system in the central computer center, and, if required for local or regional applications, perform other more specific data-processing tasks. Thus, an operational DCS could be used to automate the routine data activities for a large part of the Hydrologic Data Network, reducing by orders of magnitude the time lag between water-data collection and its entry into the National Water Data Storage and Retrieval System.

BENEFITS

There are several potential benefits that could be realized by integrating a satellite data-collection system with the operational hydrologic data activities of the Geological Survey.

Satellite-relayed data, summarized and made available via remote computer terminals to Survey district offices, could be used to improve the management of the Hydrologic Data Network. Strategies could be developed for field manpower deployment based upon real-time information from hydrologic instruments. For example, manpower could be deployed to malfunctioning stations or to stations that are recording extraordinary hydrologic conditions where supplementary manual measurements are highly desirable. The emphasis could be shifted to sending personnel where they are most

needed, instead of the present routine station-servicing trips. This could improve the efficiency of expensive manpower, decrease the down time of hydrologic instruments, decrease data loss, and free manpower for new high-priority activities. Also, data from the Network can be made available in near-real time to meet the growing data needs of water-resources management agencies.

An additional significant benefit of a multi-satellite polar-orbiting DCS would be its potential for worldwide use. There would be no added strain on the system if foreign agencies established their own receive-site stations and installed DCP's to monitor their resources. The cost of their installations would be modest and would avoid the necessity of having the large reservoir of technical expertise normally required to install and maintain landline or microwave systems of data collection.

CONCLUSIONS

An operational polar-orbiting-satellite-data-collection system has been shown by the ERTS experiment to be technically feasible. Many of the elements necessary to provide an automatic hydrologic-data-collection and processing system exist in the U.S. Geological Survey. No new significant technology development is required to interface existing instrumentation in the Hydrologic Data Network with existing data-processing systems using a remote data-collection system like the ERTS-DCS. An analysis of the costs and the benefits of an operational satellite-data-collection system is being made by the U.S. Geological Survey.

REFERENCES

NASA, 1971, Earth Resources Technology Satellite Data Users Handbook: NASA Document No. 71DS4249, Goddard Space Flight Center, Greenbelt, Maryland.

Painter, J. Earle, and Seitner, Jack E., 1973, Environmental Monitoring via the ERTS-1 Data Collection System: Proceedings of the American Astronautical Society Conference, 19-21 June, 1973, Dallas, Texas (in Press).

Ward, Peter L., Eaton, Jerry P., Endo, Elliot, Harlow, David, Marquez, Daniel, and Allen, Rex, 1973, Establishment, test and evaluation of a prototype volcano-surveillance system: Symposium on Significant Results obtained from the Earth Resources Technology Satellite-1, Goddard Space Flight Center, New Carrollton, Maryland, March 5-9, 1973, Vol. 1, Section A, pp. 305-315.

Paulson, Richard W., 1973, The Use of the Earth Resources Technology Satellite for relaying hydrologic data in the Delaware River basin: Presented at the 93rd Annual Conference, American Water Works Association, Las Vegas, Nevada, May 17, 1973 (in press).

EROS-NASA
EARTH RESOURCES TECHNOLOGY SATELLITE
DATA COLLECTION SYSTEM
WATER STAGE DATA COLLECTION
AND A SYSTEM OF 1 ERTS-TYPE POLAR-ORBITING SATELLITES
16 BITS OF THE 64 BIT DATA BURST UTILIZED
DCP ID = 6115

****

YEAR	DAY	RANDOM MESSAGE NUMBER OF FIRST TRANSMISSION	HOUR 1	2	3	4	5	6	7	8	9	10	11	12	13	14	15	16	17	18	19	20	21	22	23	24
1973	151																									1
	152	1111	2	4													4	3								
	153	11111	4	5											2		3	2	1							
	154	11111	3	4											1		4		2							
	155	11111	3	2	1										1		3		2							
	156	11111	4		4										2		4		2							
	157	11111	3		4										1	1	3		2							
	158	11111	4		2											2	3		2							
	159	11111	4		4											2	3		1							
	160	1111	4		4											3	3	1								
	161	1111	4		3											4	1	3								
	162	11111	3	2	3											4		3	1							
	163	1111	1	3	1											3		3								2
	164	11111		4	2											3		2								2
	165	11111		4	2											4		4								1
	166	11111		5		2										4		3								3
	167	11111		4		2										3	1	4								3
	168	11111		4		1										1	3	2								2
	169	1111		4													4	4								

1-ENTRIES IN THE HOUR TABLE DENOTE THE NUMBER OF TIMES THAT HOURLY VALUE WAS SIMULATED TO HAVE BEEN TRANSMITTED.

2-ENTRIES IN THE RANDOM MESSAGE TABLE DENOTE THE SEQUENCE NUMBER OF THE FIRST DATA BURST RECEIVED DURING AN ORBIT, AND THE NUMBER OF ENTRIES INDICATE THE NUMBER OF ORBITS THAT DAY.

3-THERE WERE 330 HOURLY VALUES THAT WERE NOT TRANSMITTED SUCCESSFULLY.
THERE WERE 17 HOURLY VALUES THAT WERE TRANSMITTED 1 TIME.
THERE WERE 23 HOURLY VALUES THAT WERE TRANSMITTED 2 TIMES.
THERE WERE 25 HOURLY VALUES THAT WERE TRANSMITTED 3 TIMES.
THERE WERE 28 HOURLY VALUES THAT WERE TRANSMITTED 4 TIMES.
THERE WERE 2 HOURLY VALUES THAT WERE TRANSMITTED 5 TIMES.

Figure 1 - Computer summary of actual data received from a stream-gage DCP

EROS-NASA
EARTH RESOURCES TECHNOLOGY SATELLITE
DATA COLLECTION SYSTEM
SIMULATED HOURLY WATER STAGE DATA COLLECTION UTILIZING A DATA STORAGE INTERFACE MODULE
AND A SYSTEM OF 1 ERTS-TYPE POLAR-ORBITING SATELLITES
1 SETS OF 64 BIT DATA BURSTS SIMULATED
DCP ID = 6115

****

YEAR	DAY	RANDOM MESSAGE NUMBER OF FIRST TRANSMISSION	HOUR 1	2	3	4	5	6	7	8	9	10	11	12	13	14	15	16	17	18	19	20	21	22	23	24
1973	151																						1	3	7	7
	152	1111	6	4										4	7	7	7	3						4	9	9
	153	11111	9	5								2	2	5	7	6	6	3	1					3	7	7
	154	11111	7	4								1	1	5	5	6	6	2	2					3	5	6
	155	11111	6	3	1							1	1	4	4	5	5	2	2					4	4	8
	156	11111	8	4	4							2	2	6	6	6	6	2	2					3	3	7
	157	11111	7	4	4							1	2	5	5	6	5	2	2					4	4	6
	158	11111	6	2	2								2	5	5	7	5	2	2					4	4	8
	159	11111	8	4	4								2	5	5	6	4	1	1					4	4	8
	160	1111	8	4	4								3	6	7	7	4	1						4	4	7
	161	1111	7	3	3								4	5	8	8	4	3						3	5	8
	162	11111	8	5	3								4	4	7	8	4	4	1					1	4	5
	163	1111	5	4	1								3	3	6	6	3	3					2	2	6	8
	164	11111	6	6	2								3	3	5	5	2	2					2	2	6	8
	165	11111	6	6	2								4	4	8	8	4	4					1	1	6	6
	166	11111	7	7	2	2							4	4	7	7	3	3					3	3	7	7
	167	11111	6	6	2	2							3	4	8	8	5	4					3	3	7	7
	168	11111	5	5	1	1							1	4	6	6	5	2					2	2	6	6
	169	1111	4	4										4	8	8	8	4								

1-ENTRIES IN THE HOUR TABLE DENOTE THE NUMBER OF TIMES THAT HOURLY VALUE WAS SIMULATED TO HAVE BEEN TRANSMITTED.

2-ENTRIES IN THE RANDOM MESSAGE TABLE DENOTE THE SEQUENCE NUMBER OF THE FIRST DATA BURST RECEIVED DURING AN ORBIT, AND THE NUMBER OF ENTRIES INDICATE THE NUMBER OF ORBITS THAT DAY.

3-THERE WERE 195 HOURLY VALUES THAT WERE NOT TRANSMITTED SUCCESSFULLY.
THERE WERE 19 HOURLY VALUES THAT WERE TRANSMITTED 1 TIME.
THERE WERE 34 HOURLY VALUES THAT WERE TRANSMITTED 2 TIMES.
THERE WERE 27 HOURLY VALUES THAT WERE TRANSMITTED 3 TIMES.
THERE WERE 47 HOURLY VALUES THAT WERE TRANSMITTED 4 TIMES.
THERE WERE 26 HOURLY VALUES THAT WERE TRANSMITTED 5 TIMES.
THERE WERE 32 HOURLY VALUES THAT WERE TRANSMITTED 6 TIMES.
THERE WERE 25 HOURLY VALUES THAT WERE TRANSMITTED 7 TIMES.
THERE WERE 20 HOURLY VALUES THAT WERE TRANSMITTED 8 TIMES.
THERE WERE 3 HOURLY VALUES THAT WERE TRANSMITTED 9 TIMES.

Figure 2 - Potential capacity of a stream-gage DCP to transmit data if the full 64-bit message is used

FROS-NASA
EARTH RESOURCES TECHNOLOGY SATELLITE
DATA COLLECTION SYSTEM
SIMULATED HOURLY WATER STAGE DATA COLLECTION UTILIZING A DATA STORAGE INTERFACE MODULE
AND A SYSTEM OF 1 ERTS-TYPE POLAR-ORBITING SATELLITES
2 SETS OF 64 BIT DATA BURSTS SIMULATED
DCP ID = 6115

****

YEAR	DAY	RANDOM MESSAGE NUMBER OF FIRST TRANSMISSION	HOUR 1	2	3	4	5	6	7	8	9	10	11	12	13	14	15	16	17	18	19	20	21	22	23	24
1973	151																		1	2	4	4	3	3	3	3
	152	1222	3	2						2	3	3	3	3	4	4	4	2		2	5	5	4	4	4	4
	153	11221	5	3				1	1	3	[illegible]	4	4	4	4	3	3	1	1	2	4	4	3	3	3	3
	154	11112	4	2						2	3	4	4	4	3	3	3	1	1	1	2	3	3	3	3	3
	155	21112	3	2	1					1	3	4	4	4	2	2	2	1	1	2	2	4	4	4	4	4
	156	21211	4	2	2			1	1	3	3	4	4	4	4	3	3	1	1	2	2	4	3	3	3	3
	157	12112	4	2	2					1	4	5	5	5	2	2	2	1	1	2	2	3	3	3	3	3
	158	21112	3	1	1				1	2	3	4	4	4	3	3	2	1	1	2	2	4	4	4	4	4
	159	12112	4	2	2				1	2	3	3	3	3	3	3	2	1		2	2	4	4	4	4	4
	160	1112	4	2	2				1	3	4	4	4	4	3	3	2			2	2	3	4	4	4	4
	161	2221	3	1	1				2	2	4	4	4	4	4	4	2	2		2	3	5	3	3	3	3
	162	11121	5	3	2				2	2	3	4	4	4	4	4	2	2	1	1	2	2	3	3	3	3
	163	1221	2	1					2	2	3	3	3	3	3	3	1	1	1	1	3	4	4	4	4	4
	164	21211	3	3	1				1	1	3	3	3	3	2	2	1	1	1	1	3	4	4	4	4	4
	165	22221	3	3	1				2	2	4	4	4	4	4	4	2	2			3	3	4	4	4	4
	166	21221	4	4	1	1			2	2	4	4	4	4	3	3	1	1	2	2	4	4	4	4	4	4
	167	11211	3	3	1	1			1	2	4	4	4	4	4	4	3	2	1	1	3	3	4	4	4	4
	168	22121	3	3	1	1			1	2	3	3	3	3	3	3	2	1	1	1	3	3	3	3	3	3
	169	2121	2	2						2	4	4	4	4	4	4	4	2								

1-ENTRIES IN THE HOUR TABLE DENOTE THE NUMBER OF TIMES THAT HOURLY VALUE WAS SIMULATED TO HAVE BEEN TRANSMITTED.

2-ENTRIES IN THE RANDOM MESSAGE TABLE DENOTE THE SEQUENCE NUMBER OF THE FIRST DATA BURST RECEIVED DURING AN ORBIT, AND THE NUMBER OF ENTRIES INDICATE THE NUMBER OF ORBITS THAT DAY.

3-THERE WERE 66 HOURLY VALUES THAT WERE NOT TRANSMITTED SUCCESSFULLY.
THERE WERE 59 HOURLY VALUES THAT WERE TRANSMITTED 1 TIME.
THERE WERE 74 HOURLY VALUES THAT WERE TRANSMITTED 2 TIMES.
THERE WERE 107 HOURLY VALUES THAT WERE TRANSMITTED 3 TIMES.
THERE WERE 118 HOURLY VALUES THAT WERE TRANSMITTED 4 TIMES.
THERE WERE 8 HOURLY VALUES THAT WERE TRANSMITTED 5 TIMES.

Figure 3 - Potential capacity of a stream-gage DCP to transmit data if two sets of 64 bits are made available sequentially to the DCP

EROS-NASA
EARTH RESOURCES TECHNOLOGY SATELLITE
DATA COLLECTION SYSTEM
SIMULATED HOURLY WATER STAGE DATA COLLECTION UTILIZING A DATA STORAGE INTERFACE MODULE
AND A SYSTEM OF 1 ERTS-TYPE POLAR-ORBITING SATELLITES
3 SETS OF 64 BIT DATA BURSTS SIMULATED
DCP ID = 6115

****

YEAR	DAY	RANDOM MESSAGE NUMBER OF FIRST TRANSMISSION	HOUR 1	2	3	4	5	6	7	8	9	10	11	12	13	14	15	16	17	18	19	20	21	22	23	24
1973	151															1	3	3	2	2	2	2	2	2	2	2
	152	2121	3	2		1	3	3	3	3	2	2	2	2	2	4	6	5	2	2	2	2	3	3	3	3
	153	13311	4	3	1	2	2	2	2	2	3	3	3	3	3	3	4	3	2	2	2	2	3	3	3	3
	154	33122	2	2	1	2	2	3	3	3	2	2	2	2	2	2	3	2	3	2	2	2	2	2	2	2
	155	21131	2	2	1	2	1	2	2	2	1	1	1	1	3	3	3	3	4	3	3	3	3	3	3	3
	156	23122	2	2	2	2	3	4	4	4	2	2	2	2	2	2	2	2	3	2	2	2	3	3	3	3
	157	33231	2	1	2	2	2	3	3	3	1	1	1	1	3	4	3	2	3	2	2	2	3	3	3	3
	158	32212	1			1	2	3	3	3	3	3	3	3	1	3	3	4	3	2	2	2	2	2	2	2
	159	11112	4	2	3	2	2	3	3	3	1	1	1	1	2	4	3	3	4	3	3	3	2	2	2	2
	160	1223	3	1	2	2	2	2	2	2	3	3	3	3	2	3	2	2	2	2	2	2	3	3	3	3
	161	3123	2	1	2	1	3	3	3	3	3	3	3	3	2	3	3	4	2	2	2	2	3	3	3	3
	162	33312	3	2	2	1	2	3	3	3	3	3	3	3	2	2	2	2	3	2	2	2	2	2	2	2
	163	3211	1	1	1	1	2	2	2	2	2	2	2	2	3	3	3	4	4	4	4	4	1	1	1	1
	164	12121	2	2	2	1	2	2	2	2	1	1	1	1	3	3	3	3	4	4	4	4	2	2	2	2
	165	12212	1	1	2	2	3	3	3	3	2	2	2	2	3	3	3	3	2	2	2	2	3	3	3	3
	166	33112	3	3	3	3	2	2	2	2	2	2	2	2	4	4	3	3	2	2	2	2	4	4	4	4
	167	13332	2	2	2	2	3	3	3	3	3	3	3	3	3	3	3	3	2	2	2	2	4	4	4	4
	168	33311	1	1	1	2	2	2	2	2	1	1	1	1	4	4	4	3	3	3	3	3	1	1	1	1
	169	1213	1	1		2	2	2	2	2	3	3	3	3	3	3	3	1								

1-ENTRIES IN THE HOUR TABLE DENOTE THE NUMBER OF TIMES THAT HOURLY VALUE WAS SIMULATED TO HAVE BEEN TRANSMITTED.

2-ENTRIES IN THE RANDOM MESSAGE TABLE DENOTE THE SEQUENCE NUMBER OF THE FIRST DATA BURST RECEIVED DURING AN ORBIT, AND THE NUMBER OF ENTRIES INDICATE THE NUMBER OF ORBITS THAT DAY.

3-THERE WERE 4 HOURLY VALUES THAT WERE NOT TRANSMITTED SUCCESSFULLY.
THERE WERE 55 HOURLY VALUES THAT WERE TRANSMITTED 1 TIME.
THERE WERE 183 HOURLY VALUES THAT WERE TRANSMITTED 2 TIMES.
THERE WERE 156 HOURLY VALUES THAT WERE TRANSMITTED 3 TIMES.
THERE WERE 35 HOURLY VALUES THAT WERE TRANSMITTED 4 TIMES.
THERE WAS 1 HOURLY VALUE THAT WAS TRANSMITTED 5 TIMES.
THERE WAS 1 HOURLY VALUE THAT WAS TRANSMITTED 6 TIMES.

Figure 4 - Potential capacity of a stream-gage DCP to transmit data if three sets of 64 bits are made available sequentially to the DCP

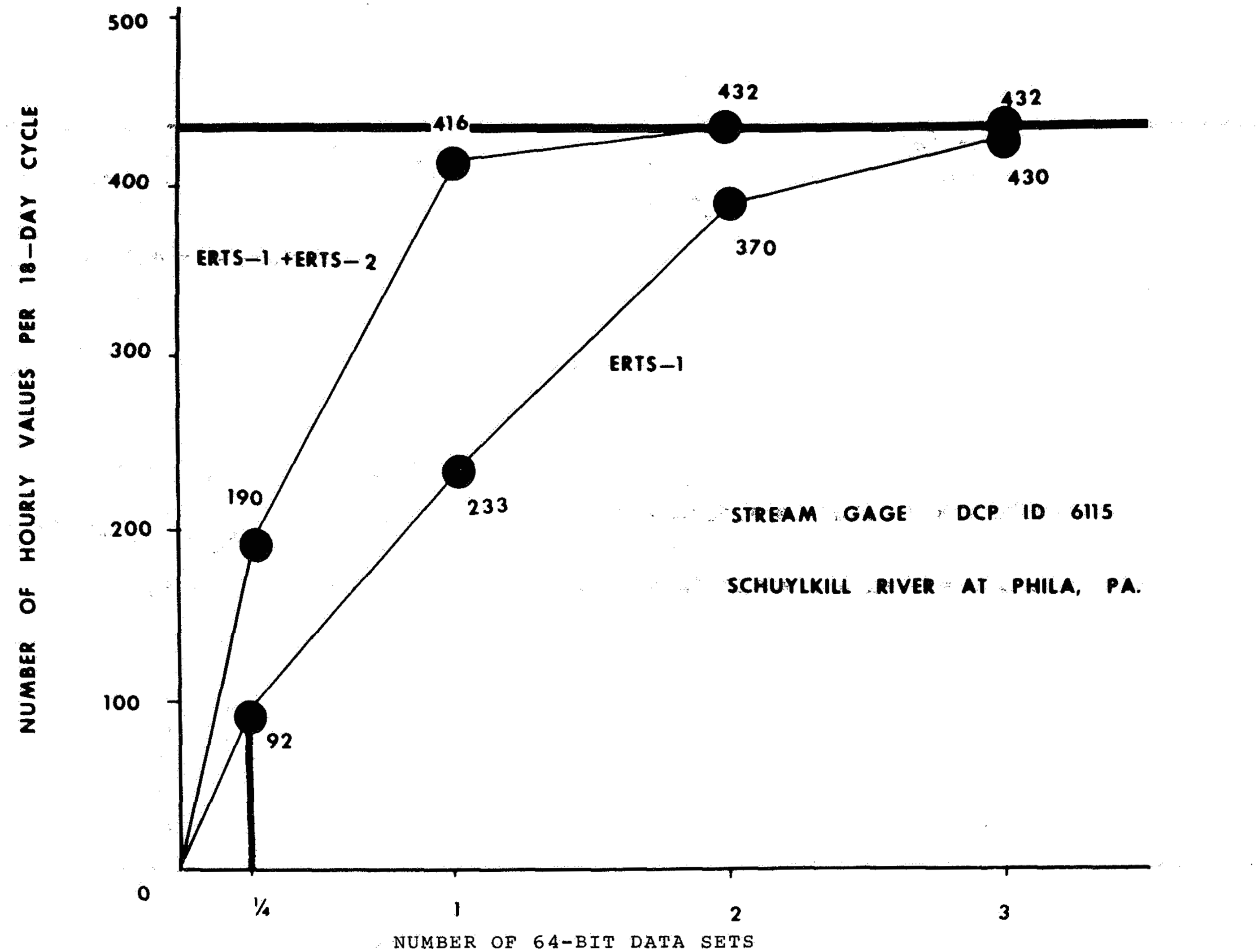

Figure 5 - Potential data-transmission capacity of one or two ERTS-type satellites if a data-storage-and-interface device were attached to a DCP at a stream gage

Paper W 9

RETRANSMISSION OF WATER RESOURCES DATA USING THE ERTS-1 DATA COLLECTION SYSTEM

R. A. Halliday, I. A. Reid and E. F. Chapman, *(Canada – Department of the Environment)*

ABSTRACT

The Water Survey of Canada operates a network of approximately 2400 gauging stations at which water level data are collected. In most cases the water level data are used in conjunction with periodic discharge measurements to produce daily river discharge data. These data may be used for design of structures and works, flow and flood forecasting, project regulation and for pollution control. In many cases it would be desirable to obtain data on a near real time basis. However, the isolated locations of most of the gauging stations have made the cost of land line telemetry prohibitive. Fewer than 100 gauging stations have been equipped with telemetry systems.

Therefore, when the ERTS Data Collection System became available in 1972 it seemed worthwhile to investigate the possibility of using a satellite retransmission system to collect discrete water level readings at least once daily from a few gauging stations and to use these data for operational purposes. In this way a valid assessment with regard to reliability, costs and other aspects of the whole system could be carried out and decisions made with respect to the feasibility and advantages of establishing a much larger network of DCPs dependent on future satellite facilities.

To perform this assessment, nine DCPs were installed in isolated areas of northern and western Canada. It was felt that DCPs in these locations would be exposed to climatic conditions severe enough to provide a check on system reliability. In addition, near real time data from the sites selected would help the Water Survey of Canada meet some of its operational needs.

Water level data are transmitted from all sites and, also, some of the DCPs are used to transmit ice break-up, water velocity, precipitation, air temperature, water stage recorder clock operation or DCP battery voltage. Consideration is being given to transmitting other parameters that would be of value in flood or flow forecasting.

Results of the project have been excellent. There has been no data loss that can be attributed to failure of a DCP although data were lost because of sensor malfunctions. The quality of data collected compares favourably with that of the hard record obtained at the remote sites. Costs of using the ERTS Data Collection System are reasonable.

INTRODUCTION

The Earth Resources Technology Satellite (ERTS-1) was launched on July 23, 1972. This satellite provides for the repetitive acquisition of high resolution multispectral data of the earth's surface on a global basis. In addition, the satellite has the capability of retransmitting data from remote, widely distributed, earth-based sensor platforms to receivers in the United States. This data retransmission capability has been used by the Water Survey of Canada for acquisition of water resources data from nine remote sites on a near real time basis.

The Water Survey of Canada operates over 2400 gauging stations at which water level data are collected. At most stations, the water level data are used to compute river discharge data. These data may be used for the design of structures such as hydro electric power plants and for flow and flood forecasting, project regulation and for pollution control. In many instances, it would be desirable to obtain data on a near real time basis; however because of the isolated locations of most gauging stations, the cost of doing this has been prohibitive. Fewer than 100 gauging stations have been equipped with telemetry systems.

Therefore, when the ERTS Data Collection System was proposed it seemed worthwhile to investigate the possibility of using a satellite retransmission network to collect a discrete water level reading at least once daily from a few gauging stations and to use these data for operational purposes. In this way the dependability, costs and other aspects could be studied and decisions made with respect to the feasibility and advantages of establishing a much larger network of Data Collection Platforms (DCPs) dependent on future operational satellite data retransmission facilities.

This paper discusses site selection, sensors used, field installation of DCPs, data handling, results and future plans.

Site Selection

The sites were selected on the basis that real time data would be very valuable for flow forecasting and other operational purposes. In addition, the severe climatic conditions at the sites would provide a good test of the DCP's performance.

Nine sites were selected for experimentation with satellite retransmission by ERTS. Three of the sites are in southern British Columbia, two in the western arctic, one in northern Saskatchewan, one in the eastern arctic, and two in northern Ontario. These sites are located in northern or mountainous regions. Because of the range in climatic and areal conditions, it is considered that these locations would provide a good test on the operational aspects of the data collection. Table one lists the nine sites now in use.

TABLE ONE

WATER SURVEY OF CANADA GAUGING STATIONS
HAVING ERTS DCPs

	Station Name	I.D.	Lat.	Long.
1.	Duncan River below B.B. Creek	6126	$50^{o}38'$	$117^{o}03'$
2.	Nahatlatch River below Tachewana Creek	6232	$49^{o}57'$	$121^{o}52'$
3.	McGregor River at Lower Canyon	6354	$54^{o}14'$	$121^{o}40'$
4.	Mackenzie River near Wrigley	6260	$63^{o}16'$	$123^{o}36'$
5.	Mackenzie River at Sans Sault Rapids	6366	$65^{o}46'$	$128^{o}45'$
6.	Lake Athabasca at Crackingstone Point	6150	$59^{o}23'$	$108^{o}53'$
7.	Kazan River at Outlet of Ennadai Lake	6353	$61^{o}15'$	$100^{o}58'$
8.	Albany River above Nottick Island	6102	$51^{o}38'$	$86^{o}24'$
9.	Winisk River below Asheweig River	6137	$54^{o}31'$	$87^{o}14'$

Site 1) is in the Columbia River basin. Data are supplied by the Water Survey of Canada to Canadian and United States operating entities who use the information to forecast runoff especially spring runoff when there is an ever present threat of flooding. Also, the Columbia River Basin Permanent Engineering Board uses the information to check operating schedules of the Treaty dams.

Sites 2) and 3) are in the Fraser River basin. Data from these sites are used as an index of tributary inflow into the Fraser River for flood forecasting purposes. In most years the spring runoff on the Fraser presents a flood threat to major population centres.

The principal method of transporting bulk cargo in the western arctic is by means of barges on the Mackenzie River. Because the shipping season is short, it is desirable that barges carry the maximum possible tonnage and yet not be subject to the risk of running aground. The Water Survey of Canada makes predictions of water levels three times weekly for navigational purposes. The real time water level readings from the two Mackenzie River sites (sites 4) and 5)) allow the barge operators to transport the cargo efficiently and economically.

Lake Athabasca (site 6)) is a naturally controlled reservoir augmenting low summer flows in the Slave and Mackenzie Rivers. The wildlife in the area, along with that on an adjoining lake provides the means of livelihood for nearly all the native people in the area. Both the wildlife and native people are now affected by the control exercised by the power development on the connected Peace River. Real time data at Lake Athabasca is considered beneficial for monitoring purposes.

The Kazan River (site 7)) in the barren lands of the eastern arctic is accessible only by chartered air service with the river serving as a landing strip. Flows in this river are representative of conditions in a wide area of the eastern arctic. Therefore, if prevailing river conditions at this site were known, considerable savings might be possible in scheduling hydrometric and other activities in the area. Ice formation

and break-up could be detected and the aircraft equipped with the appropriate landing gear.

The Albany and Winisk Rivers (sites 8) and 9)) are major rivers in northern Ontario that are accessible only by fixed and rotary winged aircraft. A knowledge of river conditions in the area would aid activities in this part of northern Ontario. The two rivers are fairly representative of most rivers in the area and have been under investigation for a major water resources development.

SENSORS

Water Level

Water level is the primary parameter retransmitted from Water Survey of Canada gauging stations by ERTS-1. Two systems are used by the Water Survey of Canada to sense water level. The first is a float and pulley operating in a stilling well that is connected to the river. Where it is not feasible to install or operate a stilling well system, because of climatic or economic reasons, a nitrogen purge system is used to sense the head of water above a fixed orifice near the river bed. The pressure of the head of water over the orifice is transmitted by the pressure exerted on the gas in the bubble tubing to a servo-manometer which converts this pressure to a shaft rotation. At conventional gauging stations the output shaft from the servo-manometer or the float system is connected to a Leupold & Stevens Type A analogue water stage recorder.

At the ERTS DCP sites a Leupold & Stevens Memomark II is used in conjunction with a float or servo-manometer to encode and store the water level as four binary coded decimal digits. This enables water levels ranging from 0000 to 9999 to be transmitted. No interface is needed between the Memomark II and the DCP.

Precipitation and Air Temperature

In co-operation with the Atmospheric Environment Service, Department of the Environment, two Hydrometeorological Automatic Recording and Telemetering Systems (HARTS) were installed to encode and store data from a Fischer-Porter precipitation gauge and a platinum resistance bulb thermometer. Accumulated precipitation to the nearest 0.030m (0.1 ft.) and temperature to the nearest 0.055C° (0.1F°) are encoded for transmittal by ERTS. The HARTS system is described in (Fong, 1973) and has also been used for encoding of snow pillow and wind run anemometer data.

Water Velocity

River velocity is a useful parameter to record especially during those periods when the conventional stage-discharge does not hold. Using stage and recorded velocity data, it is possible to compute river flows at many gauging stations when a stage-discharge curve is not defined. (Strilaeff and Bilozor, 1973).

A Marsh-McBirney electromagnetic meter which has an output voltage of 0 to 1 volts corresponding linearly to a velocity of 0 to 10 feet per second is installed at one site. In order to obtain time averaged data, a velocity integrator has been designed.

"Ice-out" Indicator

A useful piece of information for computation of streamflow data and for planning of hydrometric operations is a knowledge of when the ice moves out of the river at a gauging station. Two methods that use the same principle were designed to detect this ice movement. The first was to connect a 4 1/2 volt battery to light wire, then put this voltage into one of the analogue channels. The battery is frozen into the ice surface of the river so that when the ice moves out, the cable is broken and the voltage level drops to zero. A second version of the same system uses one bit rather than an entire word. In this case a friction type plug is tied firmly near the water's edge with the male side of the plug shorted and connected to a line which is frozen into the ice. When the ice moves out, the plug pulls apart and the bit transmitted changes from a zero condition to a one condition. "Ice-out" indicators were installed at several sites.

DCP Battery Check

A battery check device (Kruus, 1973) has been installed at three sites to monitor the voltage level of the DCP power supply. The voltage of the DCP batteries is scaled to provide a voltage less than 5 volts. In order to conserve the DCP batteries the device is switched on by the data gate signal prior to a transmission. The battery check device uses one analogue channel.

Water Stage Recorder Operation Check

The Leupold & Stevens Type A recorder has very good cold temperature performance characteristics but is subject to clock stoppages at about -50°C (Chapman, 1971). Also, the clocks stop once in a while for reasons other than cold temperatures. Once stopped, it is very unusual for a clock to restart on its own. A method of checking clock operation using a cam and single throw, double pole micro-switch was devised. When the recorder clock is operating two parallel digital bits in the DCP message change from 01 to 10 to 01 and so on every 10 hours. A failure to change indicates that the recorder clock has stopped. A few of these devices are now in operation. One of the authors' chief concerns was to ensure that the device itself would not cause a clock stoppage.

INSTALLATION OF DCPs

The DCPs are installed in regions where severe climatic conditions prevail. Temperatures lower than -50°C can occur at some sites. Also,

wind velocities in the order of 100 km/hr or snow depths of 2 m are possible. None of the sites are in high humidity areas.

Some of the DCPs were heated to protect them from severe temperatures. The method of heating consisted of constructing an insulated compartment of plywood and styrofoam around the instrument. This enclosure is heated using a catalytic propane heater having a 630kJ orifice. One 45.4 kg (100 lb.) tank of propane is sufficient to last three to four months.

Three different DCP power supplies were used. One is a series-parallel combination of 6 rechargeable Union Carbide No. 564 batteries; another is two heavy duty 12 volt lead-acid batteries in series and the last, two snowmobile 12 volt lead-acid batteries in series. A set of air-depolarized carbon zinc batteries that, reputedly, have good low temperature characteristics and long life, have been purchased for installation during the winter of 1973-74.

Figure one shows a typical interior of a gauge house containing a propane tank for the heater, a nitrogen tank for the gas purge system, the Leupold & Stevens Type A-71 recorder, the CAE Aircraft water stage servo-manometer, the Leupold & Stevens Memomark II water level encoder and the General Electric DCP electronic box.

No special precautions were taken in erecting the antennas. Guy wires were used in those cases where strong winds or heavy snow loads were expected. Some antennas have been subject to winds speeds of 80 km/hr or snow loads of 1 m with no damage.

As the DCPs were installed in existing instrument or combined instrument and personnel shelters associated with a gauging station, the installation could be completed very quickly. About two man days were required to install the antenna, connect interfaces to existing sensors and activate the DCP.

The only real problem was getting the DCP on site. In many cases, the bulky shipping carton could not be fitted into aircraft normally used in hydrometric operations. Therefore, the antenna, electronic package and hardware were removed from the carton and the antenna transported with no protection. Fortunately no antennas were damaged. A smaller ground plane would be a definite asset from a transportation viewpoint.

It's noteworthy that, despite the large size of the shipping container, two DCPs were lost during shipment by commercial air carriers.

Figures 2 and 3 show the typical exterior appearance of DCP installations at Water Survey of Canada gauging stations.

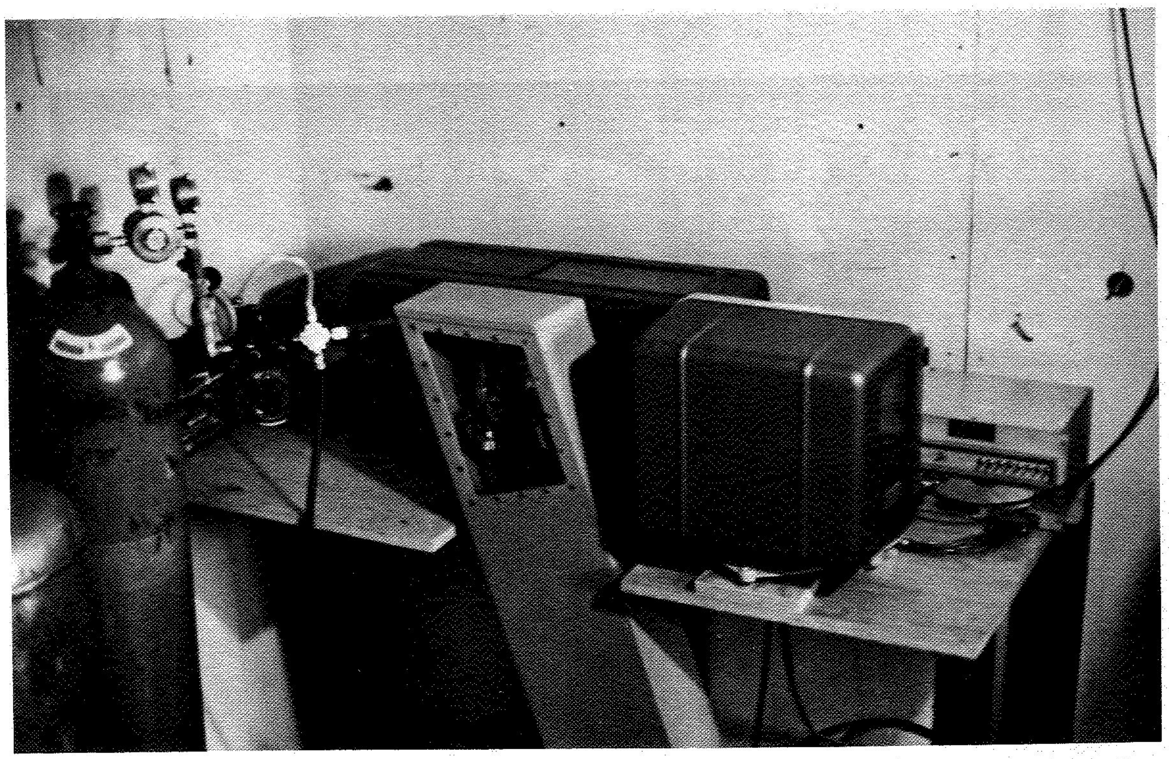

Figure One: Instrumentation Layout in Typical Gauging Station

Figure Two: Typical Instrument Shelter with ERTS DCP Antenna

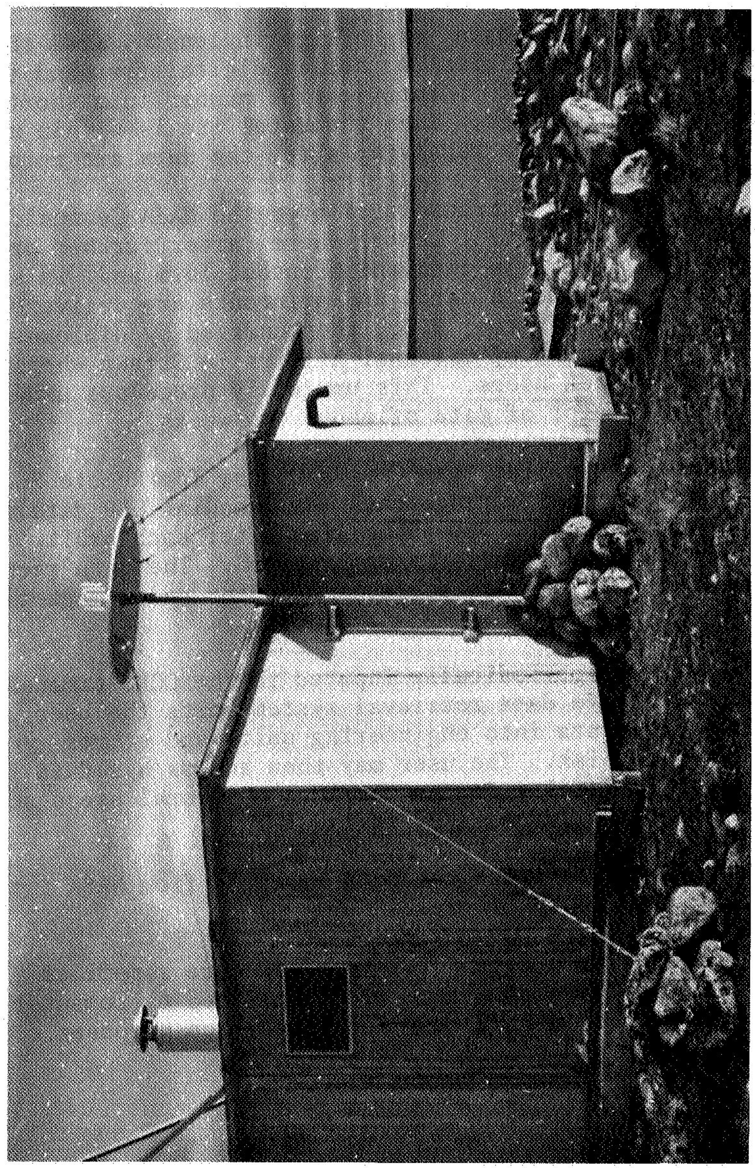

Figure Three: Typical Instrument and Personnel Shelter
with ERTS DCP Antenna

DATA HANDLING AND PROCESSING

The ERTS Data Collection System is composed of three subsystems: the DCP at a remote site, the receiving and transmitting equipment in the ERTS spacecraft, and the receiving site equipment at Goldstone, California and Greenbelt, Maryland.

The DCP accepts eight words of data, eight bits in length, from the user's sensors in analogue, parallel digital or serial digital form and transmits the encoded data along with a DCP identification number in a short burst at 401.55 MHz every three minutes. When the satellite is within mutual view of a transmitting DCP and a receiving site, the data are recovered.

Data received are formatted and transmitted over the NASA Communication System (NASCOM) to the ERTS Control Center where, after further processing, the data are supplied to users in card and printout form and, in some cases, by teletype. The Canadian cards and printouts are delivered to the Canadian Embassy in Washington, D.C., then carried by diplomatic bag to the Canadian Department of External Affairs in Ottawa where the data were mailed to Canadian users. This unwieldly procedure usually results in a delay in receipt of data of about two weeks.

In order to overcome this problem, the Canada Centre for Remote Sensing (CCRS) in Ottawa and NASA made arrangements for Canadian DCP data to be received at CCRS by dedicated telephone line after each orbit. Normally a delay of 30 to 40 minutes is experienced. The data received are recorded simultaneously on a teletype hard copier and a magnetic tape.

At present, these data are periodically inputed to the CCRS time sharing computer system. A software data retrieval system sorts the user platforms, reformats the data into engineering units and stores individual user files on disk. The user may then access his data file using either a teletype or telex remote terminal. Several users across Canada receive data on a daily basis by telex.

Arrangements to automatically input the data received from NASA into the CCRS computer system are in progress.

As data transmitted over the existing teletype line are sometimes degraded, the data received in card form are translated by computer into engineering units to provide a hard copy for comparison purposes.

RESULTS

The nine Water Survey of Canada platforms have been in operation for an average time of one year without experiencing a DCP failure. Two platforms have stopped transmitting because of DCP battery failures but started again when the battery was replaced. Also some platforms have been turned off to move them to different sites.

Four platforms are now installed at sites other than those originally specified in the submission to NASA. (One was never installed at the original location). The platforms were moved to sites where the data would be more beneficial to users and where the platforms would be exposed to more rigorous field conditions. The platforms were relocated once confidence was gained in the ERTS Data Collection System.

The communications link from the DCPs to the NASA Data Processing Facility (NDPF) has been extremely reliable with about 98 percent of the Canadian messages having been assigned the highest confidence level (7). Checks have shown that, when message confidence is 7, the data received via ERTS are identical to the values "seen" by the sensors.

The number of confidence 7 messages from the nine platforms are summarized in table two. All figures are based on the use of the 180 second transmit rate. In this table, transmissions from the same platform received at both Goldstone and Greenbelt at the same time are counted once.

TABLE TWO

SUMMARY OF RETRANSMITTED DATA

Platform Identification	Daily Mean Transmissions for Period of Operation	Transmissions Daily Max.	Transmissions Daily Min.
6126	7	10	3
6232	9	13	4
6354	8/9*	13	3
6260	9/6*	13	4
6366	8/8*	13	4
6150	14	19	6
6353	15	25	7
6102	15	20	6
6137	16	22	6

* two locations

The number of transmissions from a site seems to be dependant on the geographical location and the horizon elevation. Sites surrounded by deciduous trees such as that in figure 2, show no difference in transmission rates from summer to winter. Also the transmission rate seems unaffected by accumulations of over 0.5 m of dry snow on the ground plane. There is some evidence to suggest that the transmissions are attenuated slightly when this snow cover is melting.

A few platforms in the higher latitudes were operated on the 90 second transmission rate for short periods of time until it became apparent that sufficient data would be received at the 180 second rate. It's noteworthy that because of the high latitudes in which the platforms are operated, and despite the long distances to the receivers, that data are occasionally received on 8 orbits a day. Data are frequently received on 7 orbits each day.

The sensors discussed in an earlier section of this paper have all performed well. The main problem has been a failure of the water level encoder to update. This occurs when the encoder clock stops, either because of battery failure or for other reasons. Many batteries associated with the ERTS installations have been left operating until failure in order to evaluate their performance under load at low temperatures.

All of the Water Survey of Canada DCPs are installed in locations where site access is difficult and costly. Because of this, sites are visited as few as five times a year. Therefore when a sensor or other failure occurs at a DCP site several weeks may elapse before repairs can be made. The DCP data can be used to diagnose the problem and appropriate repair parts can be carried in to site. Also, if warrented, a special trip to the site may be scheduled in order to meet data users' requirements.

As ERTS is an experimental system, NASA and other agencies are paying some costs that would normally be charged to users. It is therefore not possible to produce rigorous cost comparisons between data retransmission by ERTS and by other means. Table three shows some approximate costs of installing water level telemetry service at an existing gauging station in southern Canada.

TABLE THREE

APPROXIMATE COSTS OF WATER LEVEL TELEMETRY

	Capital and Installation	Annual Maintenance	Annual Operating
Telephone	\$ 1,400	< \$ 100	\$500
Radio	\$20,000	\$1,000	\$500
ERTS-DCP	\$ 4,500	< \$ 100	low

It should be noted that in most parts of Canada the cost of installing telephone or radio telemetry systems is not economically feasible therefore satellite retransmission is the only means of obtaining water resources data from these areas.

FUTURE PLANS

ERTS Related

The main thrust of the Water Survey's program will be a move towards quasi-operational use of the ERTS Data Collection System. The number of platforms will be increased to about 30 and the DCP memory developed by the U.S. Geological Survey, Water Resources Division will be used at a few sites. Operation of this larger network of DCPs will enable a more thorough analysis of the costs and benefits of satellite retransmission to be carried out.

It is expected that a few additional sensors will be used. The most probable are water temperature and ice thickness. These data are useful for operation of hydrometric data gathering networks and may be of interest to data users.

Beyond ERTS

Additional ERTS platforms will be ordered keeping in mind future developments in the field of satellite retransmission. If the ERTS system fails, these platforms can be easily converted to operate as self-timed units using the Geostationary Operational Environmental Satellite (GOES) Data Collection System. The GOES Satellite, which is expected to be operational in late 1974, will be operated and controlled by the National Oceanic and Atmospheric Administration (NOAA) of the U.S. Department of Commerce.

There are two Canadian satellites under consideration that would have data retransmission capability. The first of these is a low capacity geostationary UHF communications satellite (Walker, Card, Roscoe, 1973). The data retransmission system will be similar in many ways to that of GOES. A feasibility and design study for the platforms, that will be used with the satellite, has been completed under contract to the Canadian Department of Communications.

The second proposed satellite is an earth resources satellite that would be similar to ERTS in many respects. This satellite would have scanning and data retransmission capability. Both of the proposed Canadian satellites could be launched in this decade.

CONCLUSIONS

The original intention of the Water Survey of Canada in participating in the ERTS Data Collection System experiment was to determine if reliable

water level data could be retransmitted twice daily from an isolated location on a near real time basis. It's apparent that the experience since the launch of ERTS-1 has amply demonstrated the technical feasibility of satellite retransmission, at least from low orbiting spacecraft.

The General Electric DCP has proven to be a versatile, rugged piece of hardware and has surpassed original expectations. No interfacing problems have been encountered. The quantity of reliable data gathered by the ERTS DCPs has proven very useful for water resources management and hydrometric field operations.

Canada is a large sparsely populated nation. These factors plus the country's rigorous northern climate and large surface water supply appear to make satellite retransmission of water resources data a logical extension of Space Age technology to the science of hydrometry.

REFERENCES

Chapman, E.F., Low Temperature Tests on Leupold and Stevens Type A-35 Recorders and Recorder Clocks, Technical Bulletin No. 54, Inland Waters Branch, Department of the Environment, Ottawa, 1971.

Fong, H., Hydrometeorological Automatic Recording and Telemetering System, Prototype HARTS-1 (ERTS), Atmospheric Environment Service, Department of the Environment, Toronto, January 8, 1973.

Kruus, Dr. J., A Water Resource Monitoring Platform, Type II Report for Period January to August, 1973, Department of the Environment, Ottawa, October, 1973.

Strilaeff, P.W. and Bilozor, W., Single Velocity Method in Measuring Discharge, Technical Bulletin No. 75, Inland Waters Directorate, Department of the Environment, Ottawa, 1973.

Walker, B.A., Card, M.L., and Roscoe, O.S., 1973, A Planning Study for a Multi-Purpose Communications Satellite Serving Northern Canada, Proceedings, Satellite Systems for Mobile Communications and Surveillance, London, England, March 13-15, 1973.

ACKNOWLEDGEMENTS

The authors wish to thank the many persons in the Department of the Environment who contributed their time and energy to this project. In addition the excellent co-operation of Mr. Howard Edel of the Canada Centre for Remote Sensing, Mr. Duane Preble of the USGS, Gulf Coast Hydroscience Center, and Mr. J. Earle Painter of NASA is gratefully acknowledged.

Paper W 10

ERTS-1 FLOOD HAZARD STUDIES IN THE MISSISSIPPI RIVER BASIN

Albert Rango and Arthur T. Anderson, *NASA/Goddard Space Flight Center, Greenbelt, Maryland 20771*

ABSTRACT

The Spring 1973 Mississippi River flood was investigated using remotely sensed data from ERTS-1. Both manual and automatic analyses of the data indicate that ERTS-1 is extremely useful as a regional tool for flood and floodplain management. Automatic digital analysis using the GEMS system was employed to obtain quantitative estimates of area flooded in small test sites 1225 km^2 in area in St. Charles County, Missouri and the delta region of northwest Mississippi. In the St. Charles County site 265 km^2 (21% of the total area) was calculated to be flooded whereas, in the northwest Mississippi site, 480 km^2 (39%) was inundated with an additional amount of high forest submerged beneath the canopy. In the entire state of Arkansas, manual photo interpretation indicated that 7300 km^2 was inundated with only 630 km^2 flooded along the Mississippi River mainstem. The maximum error of such flood area measurements is conservatively estimated to be less than five percent. Change detection analysis indicates that the flood had major impacts on soil moisture, land pattern stability, and vegetation stress.

Flood hazard identification (i.e., the delineation of flood-susceptible areas) was conducted using photo interpretation techniques in three study areas along the Mississippi River using pre-flood ERTS-1 imagery down to 1:100,000 scale. The flood-prone areas delineated on these images correspond to areas that would be inundated by significant flooding (approximately the 100-year flood). In addition, in northwest Mississippi, the feasibility of objective detection of floodplain features related to flood susceptibility was confirmed using the GEMS system. Flood prone area boundaries obtained from ERTS-1 were generally in agreement with flood hazard maps produced by the U.S. Army Corps of Engineers and the U.S. Geological Survey although the latter are somewhat more detailed because of their larger scale. Initial results indicate that ERTS-1 digital mapping of the flood-prone areas using the Purdue University LARS system can be performed at least at 1:62,500 which is comparable to conventional flood hazard map scales. Direct comparison of the ERTS-1 digital products to conventional flood hazard maps must wait until corrections for image skew can be incorporated into the LARS output format.

ERTS-1 FLOOD HAZARD STUDIES IN THE MISSISSIPPI RIVER BASIN

INTRODUCTION

Floods, both rare and frequently occurring, have caused large amounts of damage to man's interests in floodplain areas throughout history, and he has constantly attempted to reduce this damage through the use of various types of flood prevention techniques. In the United States expenditures for downstream flood control measures grew to about $6,500,000,000 in 1966, however, average annual flood damages continued on an upward trend which began near the turn of the century. Annual flood losses in the United States frequently exceed $1,500,000,000. Projections indicate that annual flood damage will continue to increase markedly until the year 2000 and beyond (Todd, 1970). This projected annual increase is due to the continued encroachment and development by man on the floodplain in areas susceptible to flood inundation. In the United States, it has been estimated that at least 12% of the population lives in areas subject to periodic flooding (White, et al., 1958). Floodplain occupance seems to be increasing at a more rapid rate than the overall population growth rate (Sewell, 1969). Because of economic pressures for development, better means for logically restricting growth in high flood hazard areas and for assessing flood damage where it occurs are needed.

Satellites such as the first Earth Resources Technology Satellite (ERTS-1), with high resolution sensors and repetitive coverage capability, provide promising ways to solve some of the problems associated with mapping the areal extent of flooding and determining general flood susceptibility. ERTS-1 was launched July 23, 1972 into a near polar, 900 km circular orbit. The orbital characteristics of this satellite and the capabilities of the on-board sensors combine to provide a system which is capable of taking remotely-sensed observations over any given point on the earth once every 18 days. Since the launch of ERTS-1, the vast majority of observations have been taken by the Multispectral Scanner Subsystem (MSS) in the visible and near infrared wavelengths. The MSS takes observations in the 0.5-0.6, 0.6-0.7, 0.7-0.8, and 0.8-1.1 μm portions of the electromagnetic spectrum. The ability of the MSS to resolve objects on the earth's surface varies depending upon the geometric characteristics of a given object and its contrast with surrounding features, but generally a spatial resolution capability near 80 meters is available. In the 0.8-1.1 μm spectral region water and/or moist surfaces contrast most sharply with dry soil or vegetated surfaces. Therefore, for mapping of surface water and flood inundated areas, or areas with relatively high soil moisture content, the 0.8-1.1 μm spectral interval is the best of the ERTS-1 wavelength bands.

Although there have been a number of attempts to map flooded areas with aircraft photography, detection of flooding from space has been relatively limited. Probably the best cases until the launch of ERTS-1 were recorded on the Apollo 9 mission in March 1969. Robinove (1971) reported that flooding effects on the Ouachita River could easily be observed whereas Piech and Walker (1972) attempted to map the extent of flooding on the Mississippi River by ratioing the near infrared and visible green bands. ERTS-1 has recently been used to map major floods on the Nishnabotna Rivers in Iowa (Hallberg, Hoyer, and Rango, 1973) and the Gila River in Arizona (Morrison and Cooley, 1973). In both cases correspondence of ERTS-1 derived flood boundaries to boundaries obtained from low altitude photography was excellent. Additionally, more commonly occurring floods have been mapped using ERTS-1 on the James, Appomattox, and Nottoway Rivers in Virginia (Rango and Salomonson, 1973). Flooding in the Mississippi River Basin in 1973 provided an excellent test case for the ability of ERTS-1 to contribute to effective flood management on a major river system.

In the Spring of 1973, streamflow in the Mississippi-Missouri River complex reached the highest flood levels since 1844 in some locations as an estimated 7 to 11 million acres (depending on the source) were flooded from Illinois to Louisiana. The Mississippi River had been running well above normal for most of the winter months due to rainfalls in excess of 200% of normal in particular areas. The flooding situation reached the critical level when a series of spring storms brought additional heavy rains to the entire area in March and April. Four separate crests moved through St. Louis including an all-time record high of 43.3 feet on April 28, 1973. The Mississippi River finally returned to its banks at St. Louis on May 29. Another area hard-hit by flooding was near Vicksburg in the delta region of Mississippi. The levee system along the Mississippi River in this area worked so well keeping the flood water between the levees that its tributaries backed up. Specifically the Yazoo and Big Sunflower Rivers, also running above flood stage and unable to empty into the Mississippi River, caused massive backwater flooding in Northwest Mississippi. Eighty percent of some of the counties in this region were inundated by floodwater. The Yazoo River at Yazoo City, Mississippi did not fall below flood stage until June 26.

Further down the Mississippi River, the U. S. Army Corps of Engineers (USACE), in order to protect New Orleans, had to open the Bonnet Carre flood control spillway on April 8 for the first time in 23 years. Later the Morganza spillway near Morganza, Louisiana also had to be opened to divert excess floodwater from the Mississippi into the Atchafalaya Basin. These flood control systems considerably reduced the effect of flooding in the extreme southern portion of the Mississippi River watershed.

The major economic impact was felt by agriculture, not only because of losses of crops already in the ground throughout the area, but primarily because

farmers were unable to work wet land and plant such spring crops as corn, cotton, and soybeans. As the flooding persisted the planting time for corn and cotton was bypassed and soybeans became the only feasible crop to plant. In some areas such as the Mississippi delta region, the feasibility of planting soybeans was also in doubt because backwater was still in some areas as late as June 28. In addition to agriculture, industry was also affected. As an example, in Louisiana during the flood the state's petroleum industry was losing an estimated $300,000 per day as a result of flooded oil and gas wells.

On April 16, 1973 a special interagency working group on the Mississippi River Basin flooding met to outline proposed tasks to be undertaken by the various interested groups. The final results will be presented in an interagency report on the applicability of remote sensing (primarily using the ERTS-1 and NOAA-2 satellites) to flood management on the Mississippi River. The agencies represented at the April 16 meeting were NASA, USACE, The National Oceanic and Atmospheric Administration (NOAA), and various divisions of the U. S. Geological Survey (USGS). The results presented in this report document the efforts to date at NASA's Goddard Space Flight Center (GSFC) in this interagency study.

FLOOD MAPPING

Mapping of areas inundated by flooding from space using ERTS-1 has been attempted in Iowa, Arizona, and Virginia and proven successful. In general, flood area mapping using only the 0.8-1.1 μm band was used because of the ease with which the flooding effects were evident. For flood maps produced in Virginia using ERTS-1 (Rango and Salomonson, 1973), the estimated error in obtaining flood area measurements is conservatively evaluated to be less than five percent. As a result, it is felt that such flood area mapping on a regional basis is relatively straight forward and should be accomplished with ease for the Mississippi River flood. Both the USACE and the USGS have concentrated on this topic for the interagency study. For this reason NASA/GSFC only studied the feasibility of flood mapping in a few test areas along the Mississippi River. Figure 1 presents a before and after view of the St. Louis, Missouri area and shows flooding in progress on March 31, 1973 on the Illinois, Missouri, and Mississippi Rivers. At the time this image was obtained the Mississippi River was at a stage of 38 feet and rising. One day after the March 31 ERTS-1 image was taken, NASA/GSFC scientists analyzed the scene in about 15 minutes and, through an October 1, 1972 -March 31, 1973 comparison and manual planimetering of the water in the scenes, concluded that approximately 280,000 acres of land had already been inundated.

On the same orbital pass as the March 31, 1973 St. Louis scene, ERTS-1 overflew eastern Arkansas and detected flood effects on the Mississippi River and some of its tributaries (e. g., the White, Black, St. Francis, and Ouachita

Rivers). Congressman Alexander of Arkansas requested NASA to aid him in his own evaluation of the areas affected by flooding in Arkansas. Several composites of the region were made (see Fig. 2), and the area affected by flooding in Arkansas was estimated at 1,800,000 acres, with only 155,000 acres flooded along the Mississippi River mainstem. The rest of the flooding occurred along the tributaries. Apparently the levee system along the Mississippi River was providing adequate protection, whereas flood areas on the tributaries pointed out locations where new or additional flood works might be necessary. Such an evaluation was impossible before the comprehensive, regional coverage from ERTS-1 became available.

In our experience with flood mapping, it was deemed desirable to have a method that would objectively map the flooded region and automatically calculate the area inundated. This would not only allow more consistent mapping to be done but also remove the somewhat laborious manual planimetering step. To do this the General Electric Multispectral Information Extraction System (GEMS), which has the ability to classify water areas according to differences in reflectivity was employed. Figure 3a shows an area in the St. Charles County vicinity as seen by ERTS-1 on March 31, 1973 and used in this analysis. A cursor (small white rectangle) which is variable in size, shape, and location is used for training and subsequent classification. In all, five separate classes of water were obtained and are shown in sequence in Figure 3. Figure 3b shows class 1 in yellow and class 2 in magenta, Figure 3c shows classes 1 and 2 summed in yellow and class 3 in magenta, Figure 3d shows classes 1, 2, and 3 summed in yellow and class 4 in magenta, and Figure 3e shows classes 1, 2, 3, and 4 summed in yellow and class 5 in magenta. The study area shown in Figure 3 measures 1225 km^2. Table 1 presents the results of the calculations of amount of area flooded by different water classes in St. Charles County. The total area flooded in the study area is 265.2 km^2.

Table 1

Total flooded area and sub-class areas as extracted from Figure 3
(St. Charles County, Missouri)

Classification	Percentage of Total Area (%)	Area in km^2
Total study area	100.00	1225.0
Water Class I	3.14	38.4
Water Class II	5.17	63.4
Water Class III	6.48	79.4
Water Class IV	4.10	50.3
Water Class V	2.75	33.7
Total Flooded Area	21.64	265.2

The various classes of water are a result of differences in depth and/or sediment load. Present research is attempting to determine the relations of water depth to the GEMS classification.

GEMS was also used for flood analysis in a backwater area in the Northwest Mississippi delta region. This area, mentioned in the Introduction, is north of Vicksburg, Mississippi. Figure 4a shows the study area on May 5, 1973 under floodwater. The dark red area in the center of the picture running from north to south is the Delta National Forest. Evidence indicates that this forest is also flooded, but all that can be seen is the top of the canopy, except where there is a clearing. The open water in the scene was classified similar to the St. Charles County study area. Figure 4b shows water class 1 in yellow (13.47% or 165.0 km^2) and water class 2 in magenta (16.60% or 203.7 km^2). Figure 4c shows water classes 1 and 2 summed in yellow and water class 3 in magenta (9.17% or 111.2 km^2). The total flooded area in the scene (image area = 1225 km^2) is 479.9 km^2 excluding the area of possible flooding beneath the Delta National Forest. These classifications were performed very rapidly, and it appears that this method is a very efficient means for calculating flooded area.

FLOOD EFFECTS DETECTION

Various effects of the Mississippi flooding can easily be seen from ERTS-1, with changes in surface water area the most striking. In addition abnormal soil moisture levels can be observed as areas of very low near infrared reflectivity. Figure 5 is an ERTS-1 mosaic of the Mississippi River Valley before flooding made from October 1-2, 1972 imagery taken in the 0.8-1.1 μm wavelength band. Figure 6 in comparison is an ERTS-1 mosaic of the same area constructed during and after flooding. This flood mosaic was constructed using 0.8-1.1 μm imagery taken in March and May of 1973. Areas of flooding can be seen as very dark tones, whereas excessive soil moisture is shown as the darker gray tones in the floodplain. The upland areas not affected by excess moisture have a much higher reflectivity. An example of this differential in soil moisture is observed just above center in Figure 6. Crowley's Ridge, an elongated upland area running from north to south just west of the Mississippi River on the floodplain, is very highly reflective and much drier than the surrounding, saturated lowland soils which appear dark. These relative changes in soil moisture can be observed before flooding, during the flood period, and after the recession of flood waters. The monitoring of antecedent soil moisture in this manner provides promise for improving flood forecasting if quantitative values can eventually be attached to these changes. In addition, the monitoring of agricultural fields during flood recession will provide an indication of when plowing and planting may proceed. In the St. Charles County area near infrared reflectivity constantly increased

(surface soil moisture decreased) on consecutive ERTS-1 passes on May 24, June 11, and June 29. Roughly estimating from ERTS-1 observations, initial working of the fields would have been feasible after June 11, 1973.

Some of the more subtle effects of flooding have been observed in the Mississippi River flood test case. Visual evidence that floodwaters have marked erosive potential is shown in Figure 7. This is a before and after flood view of St. Charles County, Missouri. The area shown is approximately 20 miles across. In the October 2, 1972 view agricultural field patterns are striking and very regular, whereas on May 24, 1973 land patterns are drastically changed. The scouring effect of the floodwaters have reworked the agricultural fields in many areas until most are not recognizable. Large swirls or scour scars remain as evidence of the erosive effect of the flowing water. Such a picture enables a rapid, comprehensive assessment of the major areas affected by flooding which was not available before ERTS-1 was launched. Such observations will allow county planners, for example, to focus rehabilitation efforts in the most critical areas without having to wait and assemble incomplete reports from different sources.

During flooding, stream channel changes are likely and as such the Mississippi River was examined with ERTS-1 in that regard. Initial examination using October 1, 1972 and May 5, 1973 imagery did not reveal any channel changes of significance. Examination of ERTS-1 imagery for stream channel changes after flood recession has not been completed and may reveal some subtle changes not visible on the May 5 flood imagery. Major changes on the Mississippi River however, are not likely, probably as a result of the USACE's effective flood control works. A more likely area to observe changes will be on the major tributary streams of the Mississippi River where flood control works are not nearly as comprehensive as on the mainstem. Analysis of this sort is much more complicated and is presently being undertaken.

The effects of flooding on vegetation have been noticed in the delta region of Mississippi. The Delta National Forest, as mentioned earlier, was flooded in May 1973 by backwater from the Yazoo and Big Sunflower Rivers. Using GEMS the flooded vegetation was classified as shown in Figure 4. Figure 4a shows the Delta National Forest as it appears from ERTS-1, Figure 4d shows two classes of flooded vegetation - class 1 in yellow and class 2 in magenta, and Figure 4e shows classes 1 and 2 summed in yellow and class 3 in magenta. In the lower right corner of Figure 4e is a red area that remains essentially unclassified (in a sense class 4). This is an upland forested area that was not affected by flooding. The thin magenta line along the edge of the upland area is delineating flooded vegetation along the base of the upland slope. The reason for the different classes of flooded forest vegetation is most probably due to a combination of vegetation type differences and subtle but important variations in elevation.

Trees in the lower areas of the forest would be better adapted to frequent flooding, whereas those on the slightly higher and drier ground (perhaps natural levees) would be more greatly stressed by this backwater flooding. The monitoring of this area throughout 1973 and 1974 should provide some useful data to foresters on forested vegetation response to and recovery from significant flooding.

FLOODPLAIN MAPPING

Floodplain development cannot be curtailed entirely, but with flood susceptibility inputs for specific areas, zoning can be established so as to considerably reduce losses from floods. Many states already have or are moving toward incorporating into state law some restrictions on floodplain development that are related to the expected areal extent of an arbitrary rare flood. The need for flood susceptibility information has also increased because of Federal legislation such as The National Flood Insurance Act of 1968 (Public Law 90-448). It has been agreed, for example, that the area inundated by the 100 year return period flood should define the regulatory area under The Flood Insurance Act (Sheaffer, Ellis, and Spieker, 1970). Unfortunately, very few communities have been able to have flood hazard reports prepared for their local area and thus be eligible for Federal Flood Insurance. Conventional floodplain mapping is both time consuming and expensive (about \$400-\$6000 per mile according to Wolman [1971]). It appears necessary to develop new methods that are faster and less expensive that could at the minimum be used as supplementary information for extending existing detailed floodplain maps to nearby areas, and possibly be used to provide definitive floodplain information in areas not previously surveyed.

The ERTS-1 mapping of the areal extent of flood inundation as already described in this paper establishes flood hazard zones along a stream associated with a particular recurrence interval. Although the mapping of an occasional flood is an effective way to delineate areas of flood susceptibility on the floodplain, only a few of these major floods occur each year and consequently it would take a considerable length of time to construct an adequate nationwide data base (especially if the 100 year flood was the only return period of interest). A second approach would be to use the comprehensive coverage available from satellites to map features on the floodplain before a flood that may correspond to the limits of major floods. This approach has been attempted with some success using aerial remote sensing by Lee, Parker, and Milfred (1972) in Wisconsin. Burgess (1967) has delineated a number of flood susceptibility indicators that should be useful in airphoto interpretation. Considering the resolution of ERTS-1 and the type of features visible in the imagery a certain number of these flood susceptibility indicators should also be observable from space. The following is an

extracted list of those indicators cited by Burgess (1967) that would likely be useful for floodplain mapping by ERTS-1.

1. Upland Physiography
2. Watershed Characteristics (such as shape, drainage density, etc.)
3. Degree of Abandonment of Natural Levees
4. Occurence of Stabilized Sand Dunes on River Terraces
5. Channel Configuration and Fluvial Geomorphic Characteristics
6. Backswamp Areas
7. Soil Moisture Availability (this could also be a short term indicator of flood susceptibility)
8. Soil Differences
9. Vegetation Differences
10. Land Use Boundaries
11. Agricultural Development
12. Flood Alleviation Measures on the Floodplain

The importance of the development of floodplain mapping using satellite data is many faceted. First of all this type of mapping would be considerably less expensive than current ground survey techniques. Secondly, because of the comprehensive coverage available from ERTS-1 type satellites, many more areas could be mapped in a short period of time. Finally, as a result of ERTS-1 repetitive coverage, floodplain maps could be continually updated to reflect changing land use and cover types. If satellite flood mapping proves feasible, a major step would be made in reducing flood damage losses. As a result of the potential importance and economic saving to be realized, this aspect of floodplain management was concentrated upon by NASA/GSFC personnel.

The Spring 1973 floods in the Mississippi Valley came at an opportune time in regard to satellite coverage. Several high resolution satellites were able to observe the effects of the flood: ERTS-1, NOAA-2, and the U. S. Air Force DAPP satellite (Data Acquisition and Processing Program). Because of its higher resolution and greater number of spectral intervals only ERTS-1 was suitable for floodplain mapping. The Mississippi River flood was used as a study case for a number of reasons. It was a flood on a major U. S. river and as a result the effects were easily visible over an extremely large area. Secondly, without a pre-planned ground truth program, very little ground information is usually available in such a satellite study. It was felt that the availability of ground

observations without pre-planning was maximized on the Mississippi River. Many other federal and state agencies would be involved in flood related studies that could be used as a source of information. Additionally, most river regimes and floodplain indicators found in other sections of the country would probably be found represented along the Mississippi River system. In general it was a very topical test case. There are some disadvantages, however, that should also be mentioned. Most useful floodplain mapping will be done on streams smaller than the Mississippi. As a result an attempt to transfer information obtained in this study to streams in the state of Maryland is now underway. Secondly, because of the comprehensive flood control network along the Mississippi River, the channel is really not free to respond to flood events in a natural way. Because of this confinement, some of the previously listed floodplain indicators may not be pertinent.

Approach

The general approach used in this study is relatively simple. ERTS-1 imagery of the flood was available on a number of dates including March 31, 1973 (western half of valley) and May 5, 1973 (eastern half). Using these data as a base several areas would be selected where significant flooding was known to have occurred. Pre-flood imagery for these same areas would then be examined, in many cases independently, to determine if there are indicators on the floodplain that delineate the areas susceptible to flooding. Different regions would be tested to determine if there is some sort of consistency that would allow the identification of a general set of indicators.

In addition to comparing flood prone areas obtained from analysis of the pre-flood imagery with the actual flooded areas, flood hazard maps are also available for various areas along the Mississippi River. These maps constructed by the USACE or the USGS delineate the areas that would be inundated by a 100 year return period flood (and sometimes the project flood which may be expected to result from the most severe combination of meteorological and hydrological conditions). Although these boundaries may not always be accurate, they provide good large scale data for comparison with the ERTS-1 pre-flood imagery.

The areas selected for study along the Mississippi River on the basis of clear ERTS-1 imagery (both before and after flooding) and available flood hazard maps are as follows; 1) Greenville-Vicksburg-Natchez, Mississippi area, 2) Cairo, Illinois to Memphis, Tennessee area, and 3) St. Charles County, Missouri area. These study areas are outlined in Figure 5. In study areas 1 and 2 various sub areas were used for training purposes, i.e., all available data were used to determine the floodplain indicators that best corresponded to the limits of flooding according to the ERTS-1 imagery and to the 100 year flood boundaries taken from the flood hazard maps. Other sub areas were used as controls, i.e., only

the pre-flood imagery was examined and flood hazard mapping performed from it alone. These ERTS-1 flood hazard maps were then subsequently compared to the USACE and USGS flood hazard maps and the ERTS-1 flood imagery. In study area 3, flood hazard mapping was conducted for the entire St. Charles County area from the pre-flood imagery alone. This also was compared to existing flood hazard maps and post-flood imagery.

These mapping efforts were conducted primarily at an original scale of 1:1,000,000. In study areas 2 and 3, however, some of the ERTS-1 imagery was first enlarged to scales of 1:250,000 and 1:100,000 and the mapping then performed. Additionally, GEMS was used for floodplain mapping at 1:1,000,000 and 1:250,000 scales.

Results

Study area 1 was examined first to explore the general feasibility of using floodplain features visible from space to identify the relative flood susceptibility of a particular area. Using ERTS-1 imagery obtained on September 13, 1972 (ID 1052-16064) it was apparent that the Mississippi delta region north of Vicksburg would be an interesting test case. Using a color composite of this ERTS-1 scene (Fig. 8) several areas of interest were identified. The very light pink tones in the left half of the scene that tend to be located along the smaller rivers in the delta region have been identified as natural levee systems. These structures result when a sediment laden stream floods and the sediment is allowed to settle. The coarsest material is deposited near the stream whereas the fine material remains in suspension longer and finally falls out on the floodplain proper. The coarse material builds up steadily and tends to make the areas along the stream channels 5-10 feet higher than the adjacent, lower-lying bottomlands. The very light pink tones were confirmed as natural levees by comparison with a general soils map of Northwest Mississippi (U. S. Soil Conservation Service, 1972) and through conversations with the personnel of the Vicksburg office of the USACE. These natural levee areas were mapped and appear in yellow in Figure 8. Additionally, the relatively sharp boundary between red and pink tones running north to south near the center is actually the division between older upland geologic structures on the right and younger unconsolidated floodplain materials on the left. This upland boundary with a relative relief of a few hundred feet is very evident because of a sharp vegetation change associated with it. As such it marks a zone of transition between areas of low and high flood susceptibility and consequently was mapped in Figure 8.

Two other flood related significant features were observed in Figure 8. The first is the artificial levee system extending along the Mississippi River and some of its tributaries. These levees are easily observed as light pink lines or areas of sharp vegetation changes and were mapped in Figure 8. Secondary

levees along some of the tributaries were not easily observed in the September 13 image and as a result were not mapped. The other feature is the Vicksburg Industrial Park which is seen as a crescent-shaped, highly reflective region located northwest of Vicksburg. This area has been flood proofed and as such is not very susceptible to flooding.

Observing the same area during flood in Figure 9, which is a diazo color composite of the MSS 0.6-0.7 μm and 0.8-1.1 μm wavelength bands, allows evaluation of the designated non-flood prone areas in Figure 8. It is initially apparent that the upland boundary provides an effective separation between flood prone and non-flood prone lands. Secondly, most of the natural levee system delineated in Figure 8 remains above water whereas the adjacent lowlands are flooded. The exception to this is the area just north of Vicksburg where some of the natural levees have been inundated. This is due to the fact that the backwater was usually deep here—on the order of 20 feet. Although it appears that the artificial levees have generally contained the Mississippi's flow, their effectiveness has been minimized by the backwater encroaching upon them from the rear in many areas. Finally, the Vicksburg Industrial Park in Figure 9 stands out in contrast to the surrounding floodwater as predicted. This simple mapping and comparison was encouraging with regard to the ability of remotely sensed floodplain features to be useful indicators of flood susceptibility. Consequently, we investigated this area in more detail using the GEMS system and also proceeded to map flood prone regions in the specific study areas.

Figure 10a shows a small portion (approximately 1225 km^2) of the September 13 ERTS-1 scene which features the sharp upland boundary (Area 1). The GEMS system was trained on both the upland area and the lower floodplain. The contrasting GEMS classification of the two areas in the scene is shown in Figure 10b. The yellow areas are indicative of upland spectral response and the magenta areas are lowland signatures. Area 2 in Figure 10a, which is also approximately 1225 km , was used to illustrate GEMS classification of two types of natural levee systems. In Figure 10c approximately 9.19% (112.5 km^2) of the GEMS scene is natural levee class 1 (yellow) and 7.50% (92.0 km^2) is natural levee class 2 (magenta). A possible third class of natural levees is evident in the bottom center of the image. These GEMS classifications were enlarged to 1:250,000 scale for analysis.

Figure 11 shows a segment of the May 5, 1973 flooding scene in the same area. The GEMS classification of the natural levees is shown (10.09% or 123.7 km^2), and they are very visible evidence that these areas are not as susceptible to flooding as the surrounding lower areas. The results here indicate that spaceborne remotely sensed data, in combination with an image display and information extraction system, can be used to objectively map flood hazard areas.

With the general success of this approach to mapping floodplain features in mind, attempts were made in each of the study areas outlined in Figure 5 to map features that would serve as indicators of the 100 year flood boundaries. Because study area 2 had a relatively complete set of conventional flood hazard maps along the Mississippi River from Cairo, Illinois to Memphis, Tennessee, it was used initially to evaluate the ability of ERTS-1 to delineate the floodplain areas subject to major flood inundation. Using flood hazard information reports prepared by the USACE at 1:62,500 map scale for the Missouri Water Resources Board from Cairo, Illinois to Midway, Tennessee and USGS flood prone area maps at 1:24,000 and 1:62,500 map scales from Midway, Tennessee to Memphis, a number of specific small study areas were chosen. The following sub areas were chosen for training purposes: Cairo, Illinois to Portageville, Missouri; Caruthersville, Missouri to Randolph, Tennessee; and the Memphis, Tennessee area. Two sub areas were chosen for control efforts, i.e., mapping of the flood hazard areas using only the pre-flood ERTS-1 imagery. These two control sub areas extend from Portageville, Missouri to north of Caruthersville, Missouri and from Randolph, Tennessee to north of Memphis.

Figure 12 presents the actual mapping done in both the training and control sub areas of study area 2. In the training areas the solid lines on either side of the Mississippi River represent the significant flood boundaries (approximately the 100 year flood) constructed using the October 1, 1972 ERTS-1 data in coordination with the May 5, 1973 ERTS-1 flood data and the USACE and USGS flood hazard maps. The training areas were mapped first and very little difficulty was encountered photographically correlating various floodplain features to the expected limits of flooding. Using the knowledge gained in these training exercises the control area flood hazard mapping was attempted using only the October 1 imagery at 1:1,000,000 map scale. The dashed lines indicate the significant flood boundaries (again approximately the 100 year flood) constructed in the control areas. There was no problem in joining these flood hazard boundaries to the connecting training areas. Further, when these control area flood hazard boundaries were compared to the USACE and USGS flood hazard maps the location of the boundaries were identical with only a few minor deviations.

As an example of this comparison, Figure 13 presents both the Portageville control area flood hazard mapping using ERTS-1 data at 1:1,000,000 scale and the USACE 1:62,500 scale flood hazard map of the same area. The square box in the upper left hand section of the ERTS-1 derived flood hazard map corresponds to the same area as shown in the USACE map on the right. One can quickly observe that the USACE flood hazard boundaries are much more detailed than the ERTS-1 boundaries because of the difference in scale. Both boundaries, however, are in close agreement generally, and it appears that the ERTS-1 flood hazard boundaries provide a reasonable approximation of the more detailed and expensive USACE product. There appears to be a minor boundary difference in

the vicinity of the Reelfoot National Wildlife Refuge. This is probably due to a lack of enough ERTS-1 floodplain information in this area, although there is the possibility of some discrepancy in the USACE map. Because the USACE surveys are costly they are mostly confined to the main channel of the Mississippi. The ERTS-1 image used for mapping, however, revealed that because of the entry of a major tributary south of the town of Ridgely, Tennessee combined with a solid line of Mississippi River mainline levees to the west and the upland boundary to the east, the potential for backwater flooding was high. This was not indicated on the USACE map. When the ERTS-1 May 5 flood imagery was examined in this particular area flooded backwater areas existed. This demonstrates one way in which remotely sensed data can be used to update or improve existing flood hazard maps. The areas where backwater flooding is likely have been indicated in Figure 12.

What are the floodplain features visible from ERTS-1 that permit the positioning of these flood hazard boundaries? Generally they are features that have resulted from the occurrence of past floods in a particular area, or from flood protection that a particular region may experience. Specifically they are as follows:

1. Natural levee systems can be distinguished on the Mississippi River floodplain as light tones probably contributed to by soil and vegetation differences.

2. Soil differences can be observed from ERTS-1 and can be used as indicators. Lowland soils indicate areas of flood susceptibility. In the backwater area north of Vicksburg, at least 75% of the flooded areas were areas possessing lowland soil types. The other 25% occurred in areas where the backwater was so deep that all soils were inundated. One problem that is involved here is obtaining imagery from ERTS-1 at a time when soil features can easily be observed.

3. Upland boundaries in the Mississippi Valley are very prominent and can be easily distinguished by strong vegetation contrasts. Vegetation pattern differences are noticeable as is the more lush growth associated with the upland area.

4. Agricultural pattern differences are readily apparent and are mostly a result of the decreased likelihood of flooding behind levee systems. Well organized field patterns indicate the areas not so likely to flood whereas less organization, larger haphazard fields, more wild areas, and heavy vegetation growth indicate the flood prone areas.

5. Artificial levee systems indicate where there is less of a chance of flooding. The public has responded to these improvements by moving in behind the levees with towns and agriculture. The strong contrast

between the organized fields and the non-organized areas tends to enhance the observation of the levee system.

6. Special flood alleviation measures in urban areas such as flood proofing of industrial parks is readily apparent as highly reflective areas. In some of these areas individual buildings can be observed.

7. Channel configuration and possible backwater areas can be observed where major tributaries enter the floodplain of the Mississippi River, especially where the Mississippi is well surrounded by levees.

From our experience on the Mississippi River floodplain, it appears that most effective mapping can be done only after the dormant season arrives in Autumn. Summer vegetation growth in these areas is so lush that the ERTS-1 imagery does not allow much discrimination among surface features. Autumn imagery allows you to map floodplain surface features much more easily. In this regard the October 1 and 2, 1972 ERTS-1 passes over the Mississippi Valley were outstanding. The September 13, 1972 ERTS-1 imagery was also excellent for mapping the natural levee systems in the Mississippi delta region. August 1972 imagery over the Mississippi Valley was clear, however, ability to detect surface features was poor. In general Spring imagery after agricultural fields have been plowed should be best for showing soil differences. The flooding during Spring 1973, however, did not allow confirmation of this hypothesis.

Study area 1 was next selected to test the ERTS-1 flood hazard mapping techniques developed in study area 2 and to verify if the same indicators just listed were pertinent. Two training areas were selected based on availability of USACE flood hazard maps. The floodplain areas near Vicksburg and Greenville, Mississippi were designated training areas because the USACE had compiled flood information reports for these communities. The Natchez, Mississippi area was selected as the control mapping area. The mapping of the Vicksburg area was relatively simple because the major flood susceptibility indicator was the upland boundary which can be easily traced from ERTS-1. It was of interest that the flood proofed Vicksburg Industrial Park and the Mississippi Power and Light Facility were easily mapped, as were elevated Indian mounds along the base of the upland boundary. No difficulties were encountered. The Greenville area was considerably more complex because there were no major topographic boundaries in the vicinity. Results were encouraging, however. The levees protecting the city of Greenville were easily observed by ERTS-1 and provided a definitive way to determine how far Mississippi floodwaters would encroach on the city from the west. The lowland areas subject to flooding behind the levees had distinctly darker tones on the ERTS-1 imagery. Even though the USACE flood hazard map was at 1:10,000 map scale, most of the same flood prone areas could be detected on the 1:1,000,000 scale ERTS-1 imagery. A light tonal area northeast of Greenville that was determined to be not susceptible to flooding is one of the

natural levees (along Deer Creek) previously discussed. The Greenville Harbor Project area can be mapped on both the pre- and post-flood ERTS-1 imagery. The flood imagery is of such high quality that individual buildings can be picked out in this flood proofed area. In both of these training cases the pre-flood ERTS-1 imagery, the USACE flood hazard maps, and ERTS-1 May 5, 1973 flood imagery were all used to determine the ERTS-1 features that were useful indicators of the potential for flooding. They appeared to be the same as established in study area 2.

The control area flood hazard mapping in the vicinity of Natchez was performed, as in study area 2, using only the October 1, 1972 ERTS-1 imagery. This was then compared to the USACE flood hazard maps and the May 5, 1973 ERTS-1 flood imagery in this region to determine the accuracy of the control mapping. The USACE in the Vicksburg District indicate that this May 1973 event was approximately a 75 year return period flood. Figure 14 presents the results of the ERTS-1 flood hazard mapping along the Mississippi River. The significant flood boundaries in Figure 14 corresponded to the 100 year flood boundaries presented by the USACE, except in the area of Catherine Creek which was not easily visible on the ERTS-1 image. This tributary error is indicated in Figure 14 with a dashed line. There are oil fields inside the significant flood boundaries that were inundated by the Spring flood. The conclusion here is that ERTS-1 can be used to construct regional flood hazard maps in this area where additional floodplain information is needed. The next question to be answered is at what map scale can this be done?

Study area 3 included all of St. Charles County, Missouri. Because of the promising results obtained in study areas 1 and 2, it was decided to construct an ERTS-1 flood hazard map for the entire study area using only October 2, 1972 imagery and then compare it with USGS flood prone area maps and ERTS-1 flood imagery. In addition, to help determine the scale at which the mapping can be done, both 1:250,000 and 1:100,000 scale map products were used. It was decided to restrict the floodplain mapping to the areas along the Mississippi, Missouri, and Illinois Rivers. Initially it was apparent that a considerable amount of detail was present on both the 1:250,000 and 1:100,000 scale color composites. More detailed mapping was possible as one progressed from 1:1,000,000 down to 1:100,000 scale images. Figure 15 presents the results of the ERTS-1 flood hazard mapping for St. Charles County at 1:100,000 scale from a color composite print. For comparison examine Figure 16 which is a composite of ten USGS flood prone area maps showing 100 year flood boundaries for most of the same area. Very good correlation exists between the ERTS-1 derived map and the products of the USGS. As indicated in Figure 15 there are a few areas of different interpretations in the positioning of the significant flood boundaries. There are five places where there is a possible error. One of these is a region where a secondary levee system exists which makes the area appear non-flood

prone. Under significant flooding such as the 100 year return period flood it may in fact become inundated. Because the flooding observed by ERTS-1 near St. Charles County did not approach the 100 year frequency, it was not possible to check this out. The other four areas of possible error are most likely just interpretation differences, however, it may be possible that some error exists in the USGS map product. At this time, it is probably best to assume that the errors result from a lack of detail in the ERTS-1 imagery until proven otherwise.

GEMS analysis of the St. Charles County floodplain area produced results comparable to the interpretation shown in Figure 15. It should be mentioned that areas outside the main floodplain were also classified by GEMS as flood prone. Most of these occurred in the St. Louis urban area. Although it is not much of a problem when the study area is restricted to the floodplain, it may be troublesome when using the GEMS classification in an unfamilar area.

Conclusions

ERTS-1 pre-flood imagery of the Mississippi delta region reveals relatively high reflectance areas that correspond to natural levee systems which are 5-10 feet above the average elevation of the floodplain. These areas, which have also been mapped using the GEMS system, are not flood prone as indicated by the May 5, 1973 flood imagery of this area and USACE flood hazard maps. In fact a general mapping of the flood susceptible areas from the September 13, 1972 ERTS-1 data is confirmed by the ERTS-1 flood images. As a result of this exercise, flood hazard mapping using ERTS-1 imagery was attempted in three study areas along the Mississippi River. The areas expected to be inundated by significant flooding (in this case approximately the 100 year flood) were generally delineated successfully, many times from pre-flood ERTS-1 images alone. Most ERTS-1 mapping was done at 1:1,000,000 scale and compared very favorably with large scale flood hazard maps produced by the USACE and USGS. In the St. Charles County area ERTS-1 determination of flood susceptibility was performed at both 1:250,000 and 1:100,000, allowing a much more detailed delineation of the flood prone areas. The floodplain features used as ERTS-1 indicators of flood susceptibility are natural levee systems, soil differences, upland boundaries, agricultural pattern and vegetation differences, artificial levee systems, special flood alleviation measures in urban areas, and backwater areas.

APPLICATIONS

By possessing the ability to rapidly survey the extent of flooding from space with ERTS-1, a new regional flood assessment tool is available. Never before has such a complete picture of flooding on a major stream been observed as was the case with ERTS-1 observations of the Spring 1973 Mississippi River flood.

The value of this new tool for flood management is multi-faceted. First, by having a comprehensive picture of flooding over the whole river valley, the areas of maximum flooding extent can be determined, thus focusing initial relief efforts on these hardest hit areas. This application would be most pertinent in a hydrologically data-sparse, developing country. In the United States, however, the value rests in the fact that the areas of extensive flooding point out locations where additional flood control works may be necessary, e.g., ERTS-1 showed flooding to be more extensive on the Mississippi River tributaries then on the mainstem.

Several Federal agencies (USACE and USGS) have as part of their tasks the job of flood assessment. Using ERTS-1 data they have been able to regionally assess the extent of the Mississippi River flood (e.g., see Deutsch, et al., 1973). Although the regional approach using ERTS-1 will not answer questions about the flooding of specific fields and the exact location of flood boundaries, the results are extremely useful for aiding in the planning of flood recovery efforts. In fact it has been speculated that knowing the general areas where flooding took place will reduce the number of erroneous flood damage claims. It appears that there will still be a need for ground-based high water surveys in specific areas of interest, but even here ERTS-1 has a role to play. Conversations with personnel of the Vicksburg District of the USACE revealed that numerous aircraft flights are usually employed to select the areas for the ground surveys of major flood events. The USACE personnel indicated that the ERTS-1 imagery of the flood would be used to locate these ground survey areas much more economically than previously possible.

Although flood mapping at 1:1,000,000 or 1:250,000 scale performs a useful regional function, it is not sufficient to enable insurance companies to settle claims. The use of the ERTS-1 digital data may help to solve this problem. Our initial early results indicate that digital mapping is possible at the 1:62,500 scale at a minimum (and perhaps even at the 1:24,000 scale). This type of mapping would indeed be approaching a scale commensurate with claim settlements. Improvements to be expected on future earth resources satellites such as higher resolution and increased frequency of coverage will help solve this problem of insurance settlements, improve general flood mapping, and allow more accurate positioning of flood crests in different parts of a river basin.

Other results obtained in this study have implications for improved flood damage assessment. Initial results using the GEMS system in St. Charles County, Missouri and the Mississippi delta region indicate that ERTS-1 may have the ability to detect differing depths of floodwaters. If this is the case, and it is presently being investigated, then the flood damage assessment model used by the USACE would be provided with a new data source. Flood damage is computed on the basis of the kind of development in an area versus the water depth. This water

depth is obtained rapidly, some times by pictures taken from a moving automobile. If results are positive, ERTS-1 data could be incorporated into damage assessment techniques. The fact that ERTS-1 was able to detect differing reflectivities of similar vegetation following flooding provides a possible way of evaluating the extent of flooding under heavy vegetation cover. In addition temporal monitoring of flooded vegetation reflectances will be an aid in evaluating the long term effects of flooding.

Floodplain management research is a topic in water resources which is currently drawing the attention of the Committee on Water Resources Research (COWRR) of the Federal Council for Science and Technology. COWRR has selected this topic as extremely critical and will focus on it in an attempt to outline the research necessary to accomplish major objectives in floodplain management. There is the possibility of COWRR selecting a regional research project area for such a study. The two mentioned possibilities are the Lower Mississippi Basin or the North Atlantic-New England Region. COWRR will consider remote sensing as a possible way of helping meet some of their research goals.

Satellite remote sensing such as that available from ERTS-1 can be used as a regional floodplain mapping and planning tool that will help reduce flood damages. Although some sections of the major floodplains in the U. S. have been surveyed for flood susceptibility, many areas have not and will not be surveyed in the near future. Photographically, ERTS-1 can be used at a scale of 1:100,000 to map flood susceptible areas on floodplains. At this scale ERTS-1 can be used on a regional basis as an input to floodplain zoning. ERTS-1 can locate the areas susceptible to flooding and their relationship to "safe" areas. As such ERTS-1 mapping can be used to guide development, e.g., ERTS-1 could be used to locate the sites of new planned cities like Columbia, Maryland. In areas where towns already exist, further expansion could be more logically regulated. If the desirability of development of a specific area was in question, then ground surveys or low altitude aircraft flights could be made. ERTS-1, however, could eliminate the need for many of these surveys. Currently performed by the USACE or USGS, floodplain ground surveys cost from $400-$6000 per mile depending on the area. Similar surveys from ERTS-1 total only the cost of about one man hour.

In areas where some detailed ground information on the floodplain has been compiled, ERTS-1 data can be used to extend this information into unmapped regions and thus provide preliminary information to help guide development. This would both reduce the cost of surveys and also provide a sensible way to regulate man's ever increasing encroachment on the floodplain. A variation of this approach would be to use ground surveyed areas available from the USACE or USGS as a form of ground truth. Computer programs utilizing ERTS-1 digital data could use these areas as training sites and then extend the analysis into the surrounding

region at the 1:62,500 map scale. This would provide an objective and very cost effective way to use remote sensing as a viable input for floodplain management.

Because the flood hazard boundaries delineated using ERTS-1 data are approximately equal to the 100 year flood boundaries, ERTS-1 could be used to assist in performing surveys necessary for communities to qualify for the Federal Flood Insurance program. Such surveys would have to be performed using ERTS-1 digital data at 1:62,500 map scale. The current average cost for these floodplain information reports is $25,000 (Wolman, 1971). ERTS-1 would allow this cost to be reduced to a small fraction of this figure. Conservatively estimating computer time necessary for the satellite-based survey to be one hour, the ERTS-1 floodplain information report would cost $250.

Legal review has clearly established the rights of states and other governmental units to designate zones of flood hazard on the floodplain. Ordinances setting up such land use regulation must "be reasonable and not arbitrary" (Hogan, 1963). The question then is whether general or regional delineations of flood hazard areas from ERTS-1 will hold up in court. Wolman (1971) more or less answers the question affirmatively when he states "some acceptance of error in drawing boundaries is suggested by the fact that where zones have been established to prevent obstruction of the floodways current guides suggest that the burden of proof should fall on those intending to occupy the adjacent floodplain to demonstrate by engineering survey that their actions will not adversely affect conveyance by the floodway." In other words, ERTS-1 could be used to set up legal floodplain boundaries that would have to be disproved in court by the proposed developer at his expense.

FUTURE WORK

Analysis using the data generated by the GEMS system will be completed in the near future. In coordination with the GEMS work the computer analysis programs available at the Laboratory for the Application of Remote Sensing (LARS) at Purdue University are being used to analyze ERTS-1 data in study areas 1 and 3. Parameters being studied include water depth, water extent, and identification of flood hazard indicators. It appears that mapping of these themes can be accomplished at least at the 1:62,500 map scale. If successful floodplain mapping can be carried out at this scale, a very significant advance will have been made. Computer analysis using the LARS system will be completed by the end of 1973.

Flood management advances are important on rivers like the Mississippi, however, they are even more necessary and challenging on smaller streams. As

a result of this and as part of a continuing effort to cooperate with state agencies in states such as Maryland, results of work done in the Mississippi River Basin will be extended to smaller watersheds in Maryland. One likely candidate is the Patuxent River. Mapping of flood susceptible areas will be performed using ERTS-1 compared with existing flood hazard maps and data available on the extent of major flooding in the summer of 1972.

Flood prediction is an area not yet dealt with in this paper, but it is an extremely important subject. As a result there is currently underway a study to determine the ability of the Electrically Scanned Microwave Radiometer on the Nimbus 5 satellite to monitor changes in soil moisture in the Mississippi River Basin in study areas 1 and 2 of this report. Initial results indicate that there is a general positive correlation between microwave brightness temperatures and surface soil moisture. If these initial results prove to be valid, then flood prediction using remote sensing becomes a greater possibility. Nimbus 5 currently passes over the Mississippi River at least once a day. The results of this study will also be available by the end of 1973.

SUMMARY

The Spring 1973 Mississippi River flood was investigated using remotely sensed data obtained from ERTS-1. The overall analysis of this severe flood has shown that ERTS-1 is extremely useful as a regional tool for flood management. It appears that flood extent mapping can be performed photographically at a scale of 1:100,000 and should be useful to agencies interested in obtaining a rapid, comprehensive assessment of flood damage. Using an image analysis and information extraction system, i.e., GEMS, an automatic and fast determination of the percentage of area flooded in St. Charles County, Missouri and the delta region of Northwest Mississippi was possible. The use of ERTS-1 digital data would allow flood extent mapping to be performed at scales of at least 1:62,500. The observation of flood extent allowed a general evaluation to be made of the effectiveness of flood control works on the Mississippi River and its tributaries in Arkansas. Using GEMS, several different classes of floodwater were obtained in St. Charles County and the Mississippi delta region based on reflectivity differences associated with water depth and/or sediment load variations.

Because the effects of the flood were observed using ERTS-1 repetitive data, reflectivity differences associated with surface soil moisture changes could be monitored in both space and time. Agricultural land patterns were seen to be radically altered by the scouring effects of the floodwater. Major changes in the course of the Mississippi River were not observed initially probably because of the extensive flood control system that exists. Vegetation that was inundated

by floodwater was observed to experience a marked decrease in reflectivity when compared to nearby unflooded vegetation. It was determined using GEMS that various signatures of flooded vegetation existed in the Delta National Forest most likely because of differing tolerances of the vegetation to inundation. It seems that the multi-spectral, repetitive coverage available from ERTS-1 is very useful for change detection.

The mapping of areas susceptible to flooding along the Mississippi River was successfully performed using pre-flood imagery in three separate study areas. The areas subject to inundation by major flooding (approximately the 100 year return period flood) were identified by observation of various floodplain indicators such as natural and artificial levee systems, soil differences, agricultural pattern and vegetation differences, upland boundaries, backwater areas, and special flood alleviation measures in urban areas. The flood prone areas delineated using ERTS-1 were compared to conventional flood hazard maps prepared by the USACE and USGS. The comparison indicated close agreement between the two types of maps with only a few areas of interpretation differences. Most ERTS-1 flood hazard mapping was done photographically at the 1:1,000,000 scale, however, flood susceptibility determinations in St. Charles County, Missouri using ERTS-1 were satisfactorily performed with more detail at scales of 1:250,000 and 1:100,000. Preliminary work with ERTS-1 digital data indicates that this mapping can be performed at a scale of 1:62,500. ERTS-1 because of its comprehensive view can be used on a regional basis as an input to floodplain zoning. In areas where some ground surveys of flood susceptibility have been performed, ERTS-1 data can be used to extend this information into unmapped regions and thus provide preliminary information to guide development. Because the flood hazard boundaries delineated using ERTS-1 data are approximately equal to the 100 year flood boundaries, ERTS-1 could be used to assist in performing surveys necessary for communities to qualify for the Federal Flood Insurance program. In general ERTS-1 should provide a much needed, cost effective tool for increasing our knowledge about the flood susceptibility of floodplain areas.

REFERENCES

Burgess, L. C. N., 1967: Airphoto interpretation as an aid in flood susceptibility determination, International Conference on Water for Peace, Volume 4, Washington, D. C., pp. 867-881.

Deutsch, M., F. H. Ruggles, P. Guss, and E. Yost, 1973: Mapping of the 1973 Mississippi River Floods from The Earth Resources Technology Satellite, Proceedings of the International Symposium on Remote Sensing and Water Resources Management, American Water Resources Association, Proceedings No. 17, Burlington, Ontario.

Hallberg, G. R., B. E. Hoyer, and A. Rango, 1973: Application of ERTS-1 imagery to flood inundation mapping, Proceedings of the Symposium on Significant Results Obtained From ERTS-1, Volume 1, New Carrollton, Maryland, pp. 745-754.

Hogan, T. M., 1963: State flood-plain zoning, De Paul Law Rev., 12, pp. 246-262.

Lee, G. B., D. E. Parker, C. J. Milfred, 1972: Development of new techniques for delineation of flood hazard zones, Part II: By means of air photo interpretation, Partial Technical Completion Report to the Office of Water Resources Research, University of Wisconsin, Water Resources Center, Madison, Wisconsin, 15 pp.

Morrison, R. B. and M. E. Cooley, 1973: Assessment of flood damage in Arizona by means of ERTS-1 imagery, Proceedings of the Symposium on Significant Results Obtained from ERTS-1, Volume 1, New Carrollton, Maryland, pp. 755-760.

Piech, K. R., and J. E. Walker, 1972: Thematic mapping of flooded acreage, Photogrammetric Engineering, 38(11), pp. 1081-1090.

Rango, A. and V. V. Salomonson, 1973: Regional flood mapping from space, manuscript submitted to Water Resources Research, August, 27 pp.

Robinove, C. J., 1971: Remote sensing in geology, hydrology, and geography, Proceedings of the International Workshop on Earth Resources Survey Systems, NASA-SP-283, Volume 1, National Aeronautics and Space Administration, Washington, D. C., pp. 56-66.

Sewell, W. R. D., 1969: Human response to floods, in Water, Earth, and Man edited by R. J. Chorley, Methuen & Co. Ltd., London, pp. 431-451.

Sheaffer, J. R., D. W. Ellis, and A. M. Spieker, Flood-hazard mapping in metropolitan Chicago, U. S. Geological Survey Circular 601-C, Washington, D. C., 14 pp.

Todd, D. K. (ed.), 1970: The Water Encyclopedia, Water Information Center, Port Washington, N. Y., pp. 173-180.

U. S. Soil Conservation Service, 1972: General soils map, Northwest Mississippi, Resource Conservation and Development Project, U. S. Department of Agriculture, Jackson, Mississippi, 1 page.

White, G. F. et al., 1958: Changes in urban occupance of flood plains in the United States, University of Chicago, Department of Geography Research Paper no. 57.

Wolman, M. G., 1971: Evaluating alternative techniques of floodplain mapping, Water Resources Research, 7(6), pp. 1383-1392.

ACKNOWLEDGEMENTS

The authors thank various district offices of the USGS (Water Resources Division) and the USACE for supplying conventional flood hazard maps and reports along the Mississippi River. In addition the Vicksburg District personnel of the USACE were very helpful in providing supplementary ground information on flooding in the Vicksburg area. Mr. Scott Sollers of the USACE (Washington, D. C.) offered many useful ideas in the initial development of this study. The Space Division of the General Electric Company in Valley Forge, Pennsylvania was very helpful in providing the GEMS system for our analysis. Finally, members of the Earth Survey Sciences Office at NASA/GSFC have supported this study through analysis efforts and review of the manuscript.

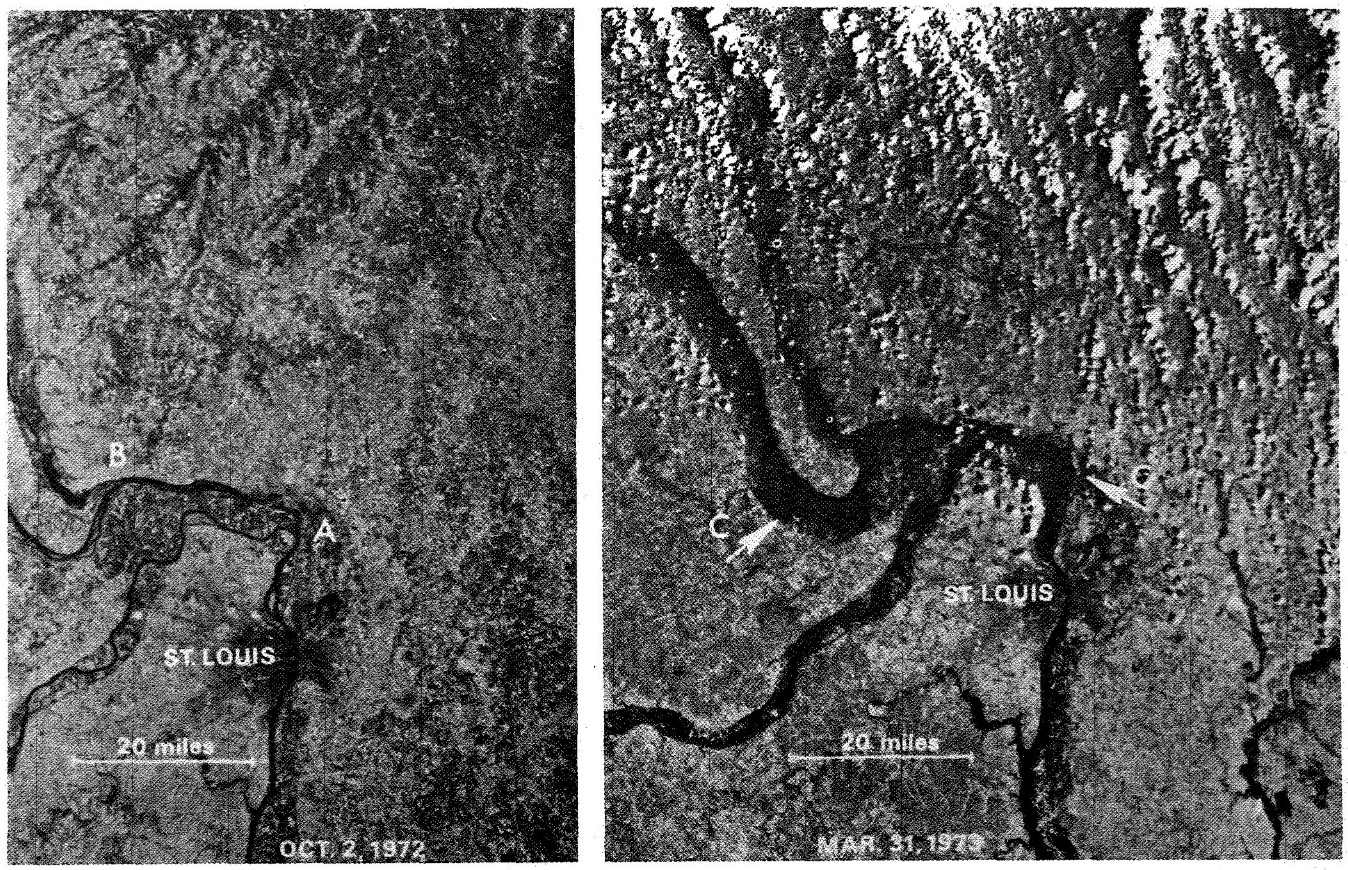

Figure 1. Near infrared (0.8-1.1 μm) views from ERTS-1 taken before and after the Spring 1973 flooding on the Mississippi River in the St. Louis area. (A) and (B) indicate the confluence of the Missouri and Mississippi Rivers and the Illinois and Mississippi Rivers, respectively. (C) indicates areas of significant flooding.

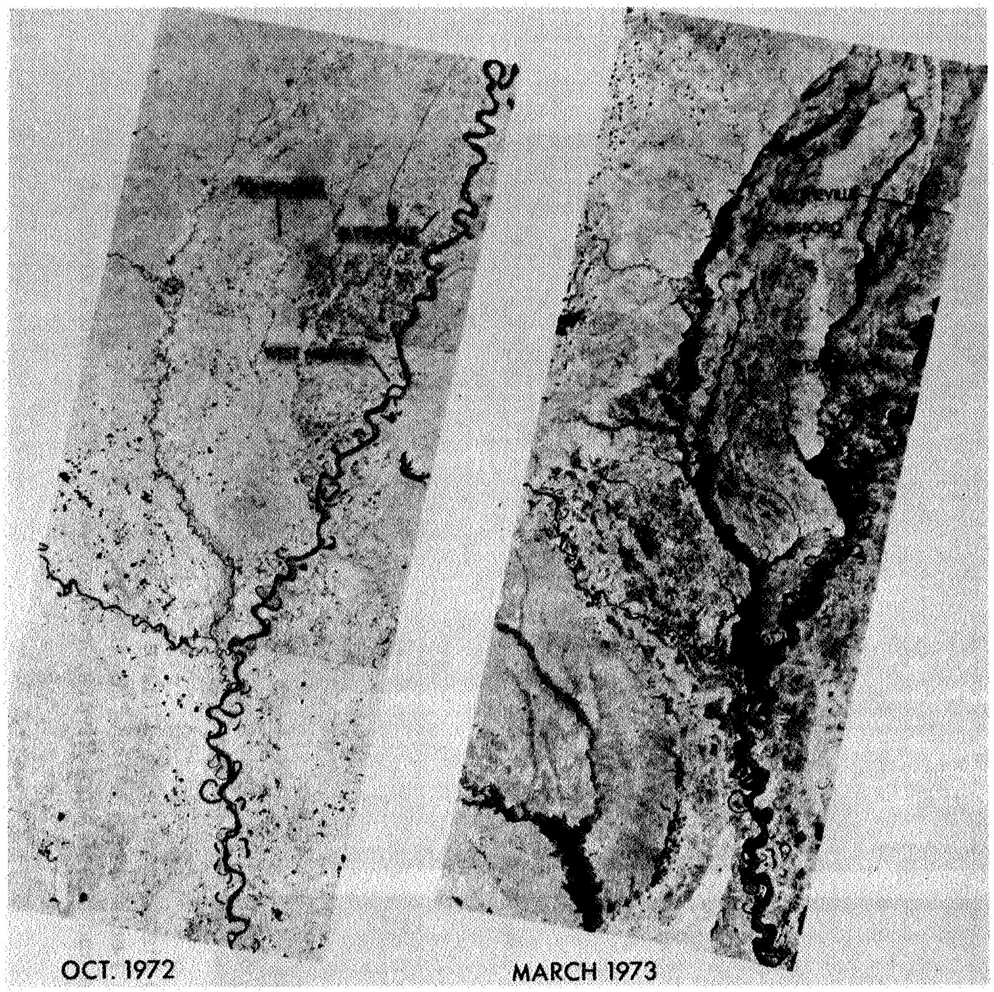

Figure 2. ERTS-1 views Arkansas flooding.

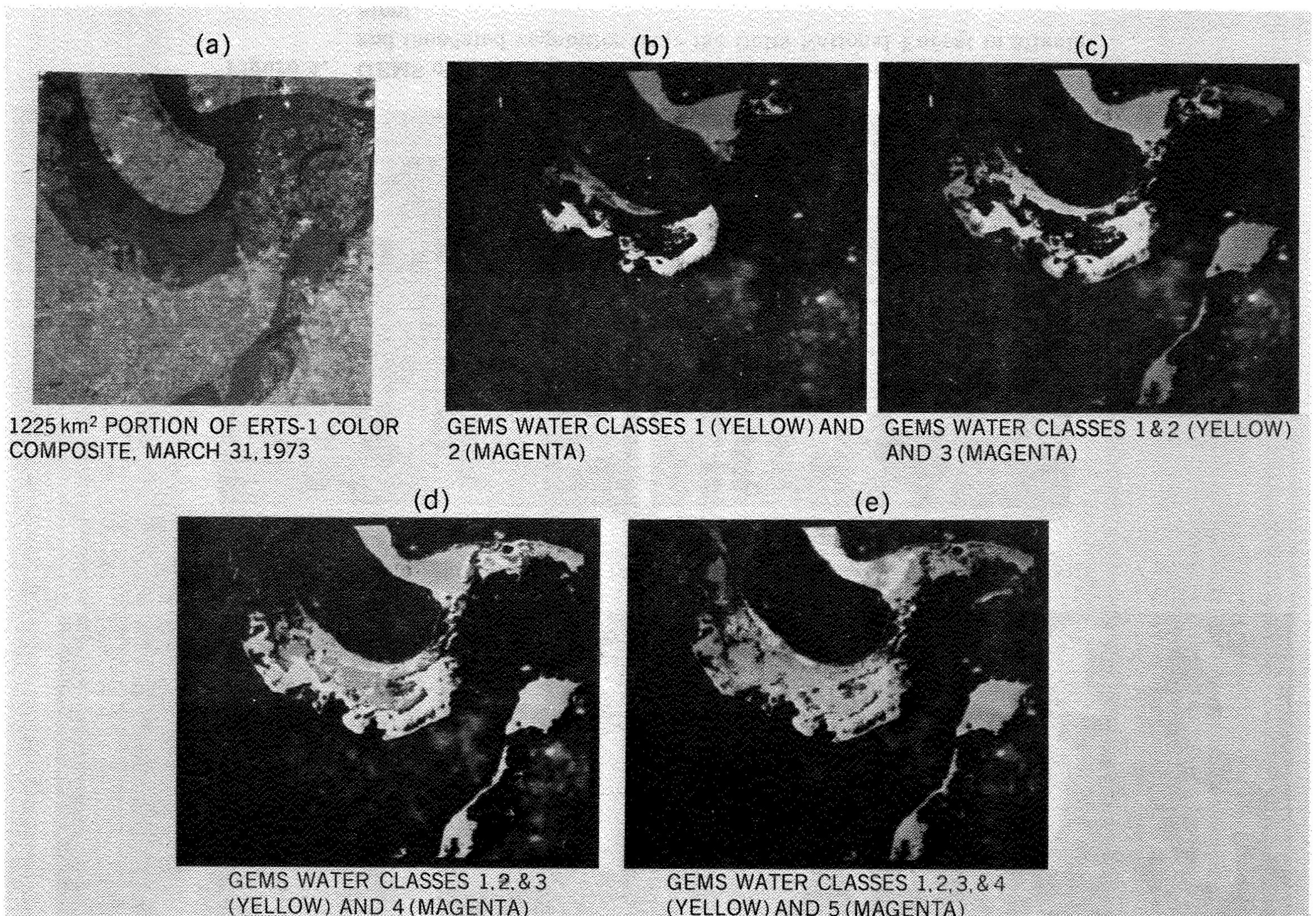

Figure 3. GEMS water classification of ERTS-1 flood data in St. Charles County, Missouri along the Mississippi, Missouri, and Illinois Rivers.

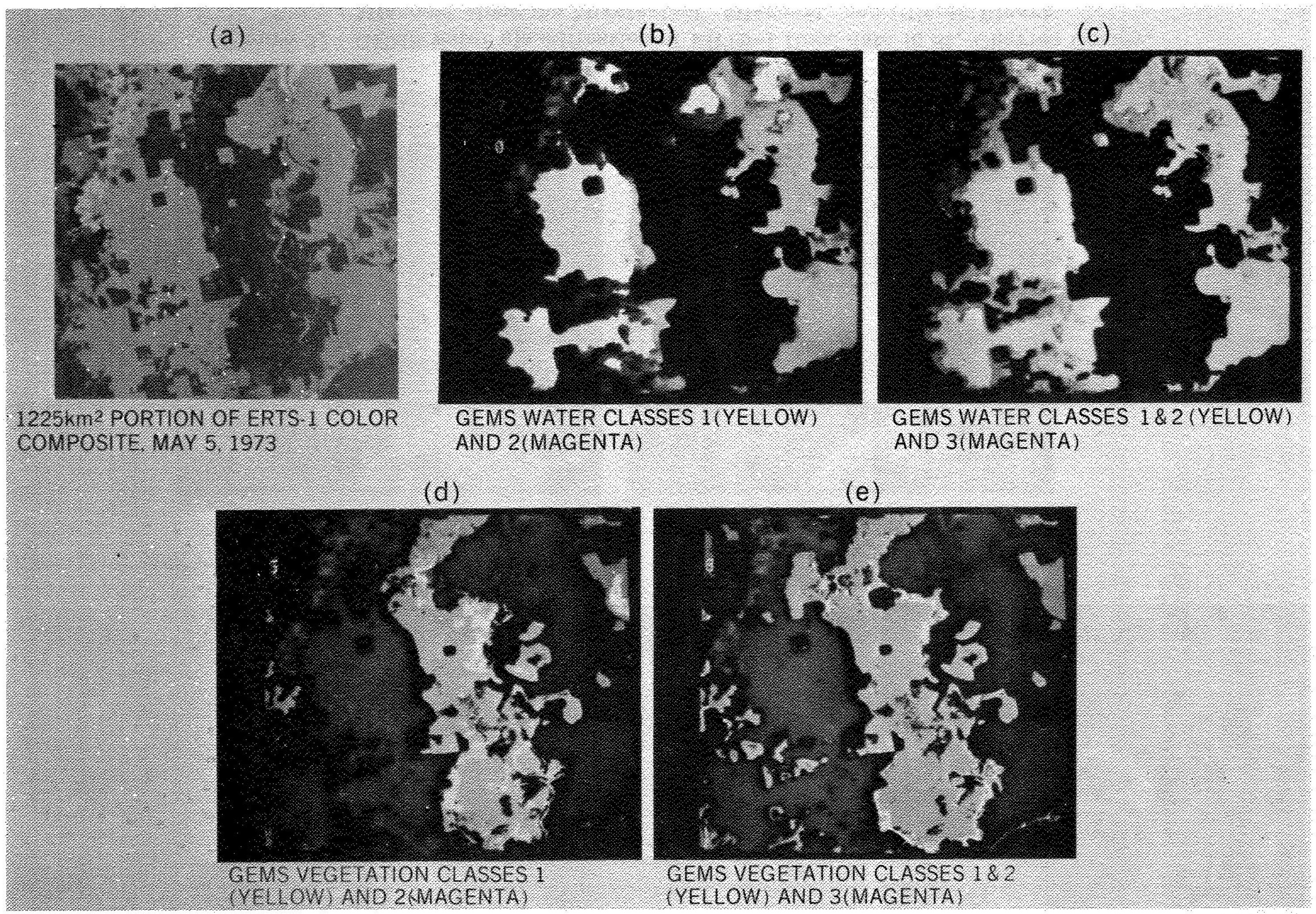

Figure 4. GEMS classification of ERTS-1 data for various types of floodwater and inundated vegetation near the Delta National Forest in Mississippi.

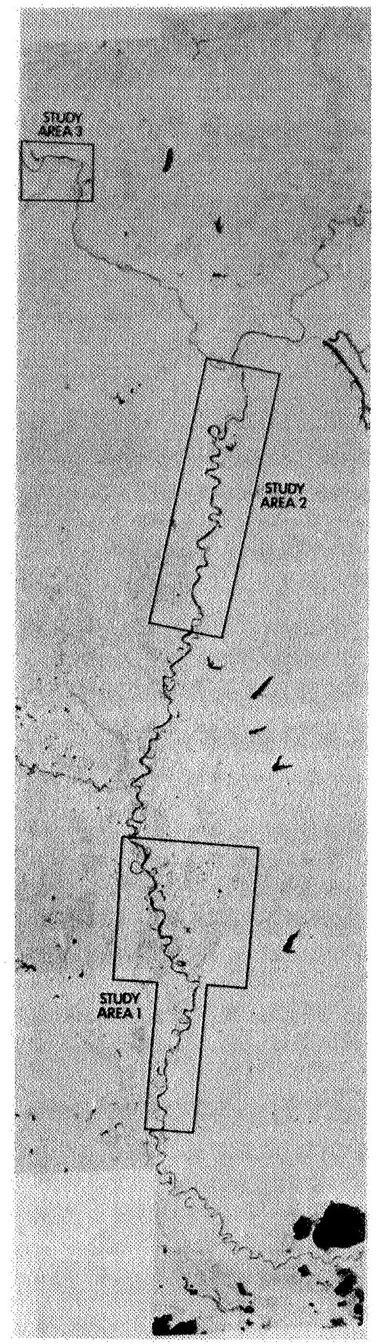

Figure 5. ERTS-1 mosaic of the Mississippi River from St. Louis to New Orleans, October 1 and 2, 1972 (0.8-1.1 μm). Three separate flood-plain study areas are indicated.

Figure 6. ERTS-1 mosaic of the Mississippi River in flood from St. Louis to New Orleans - March 31, May 5, and March 24, 1973 images (0.8-1.1 μm).

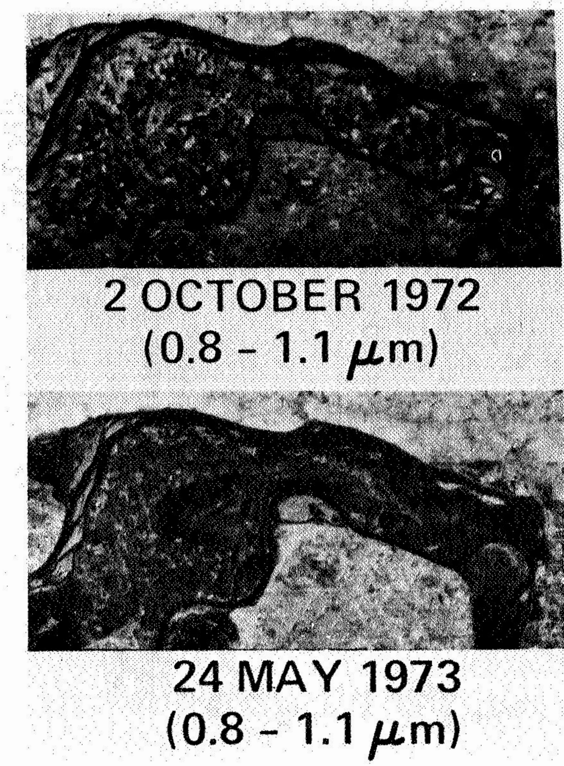

Figure 7. Land pattern changes in St. Charles County, Missouri as a result of floodwater scour effects associated with the Spring 1973 flooding along the Mississippi and Missouri Rivers.

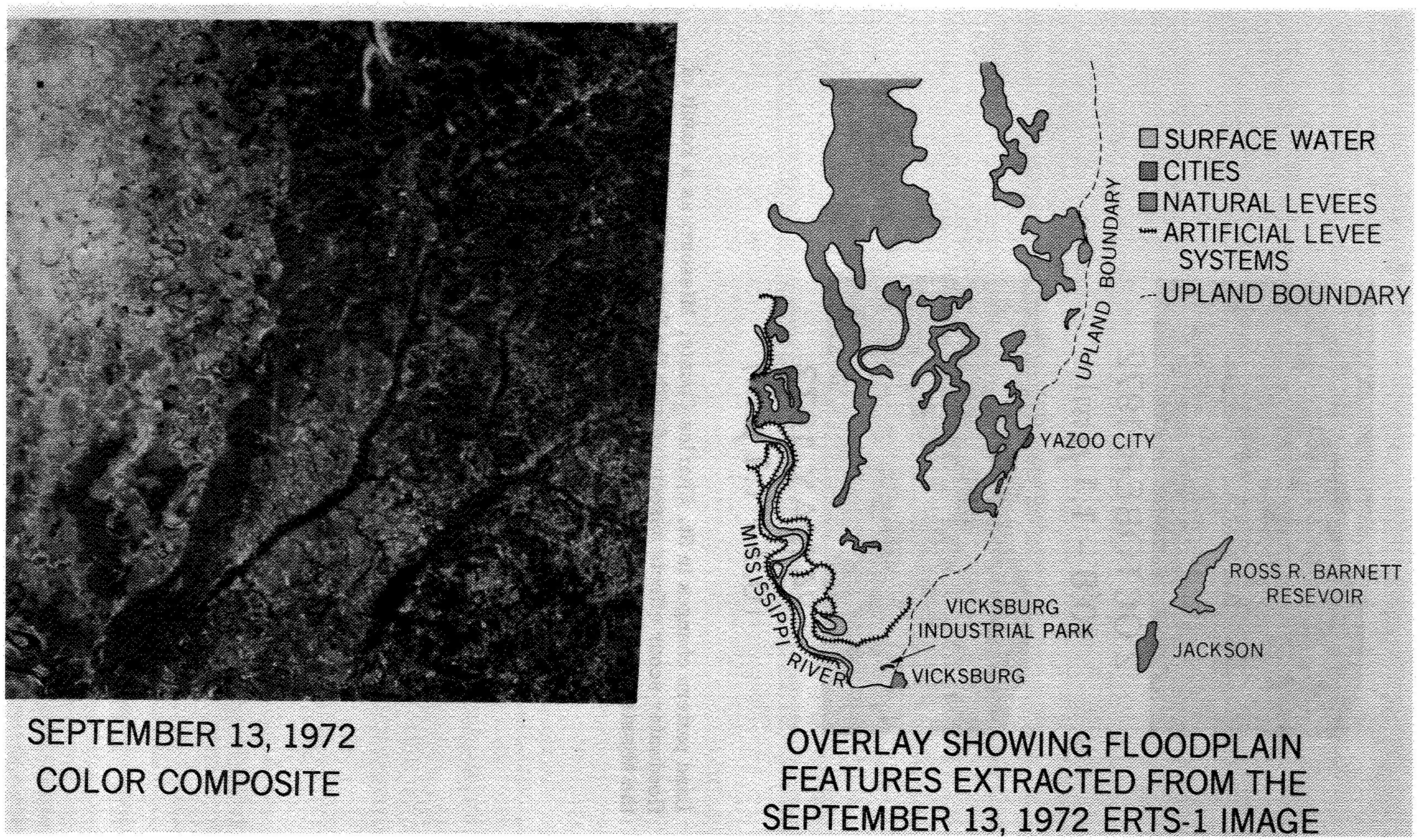

Figure 8. ERTS-1 floodplain mapping along the Mississippi River in the Arkansas-Mississippi-Louisiana area.

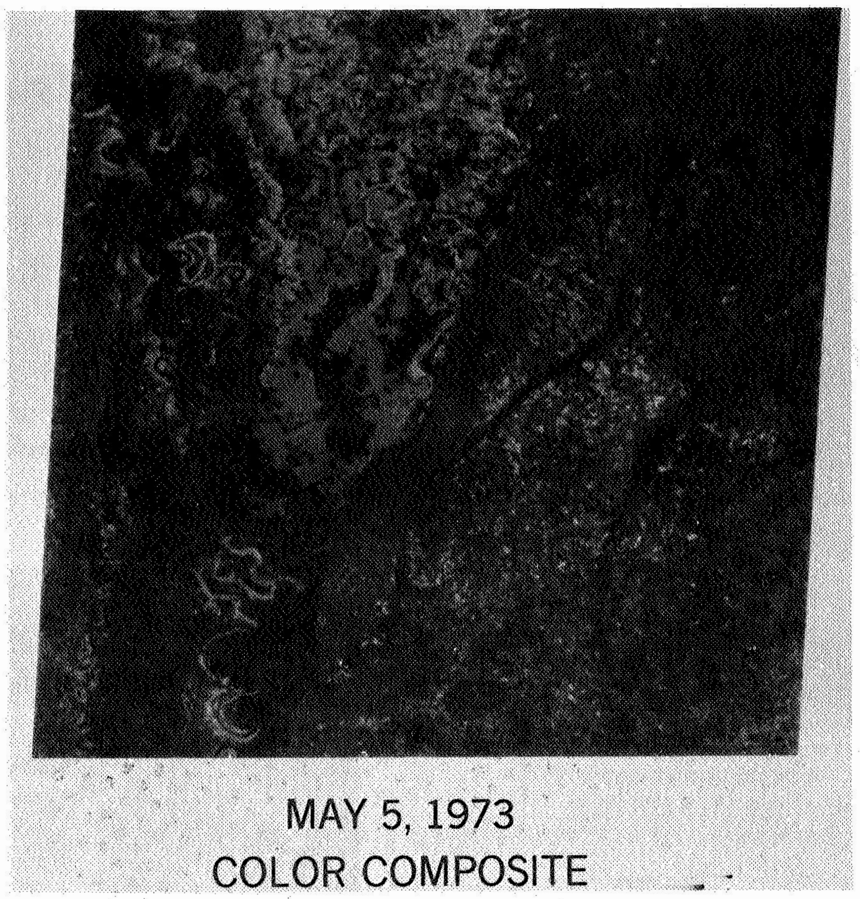

Figure 9. ERTS-1 observations of Spring 1973 flooding on the Mississippi River floodplain in the Arkansas-Mississippi-Louisiana area.

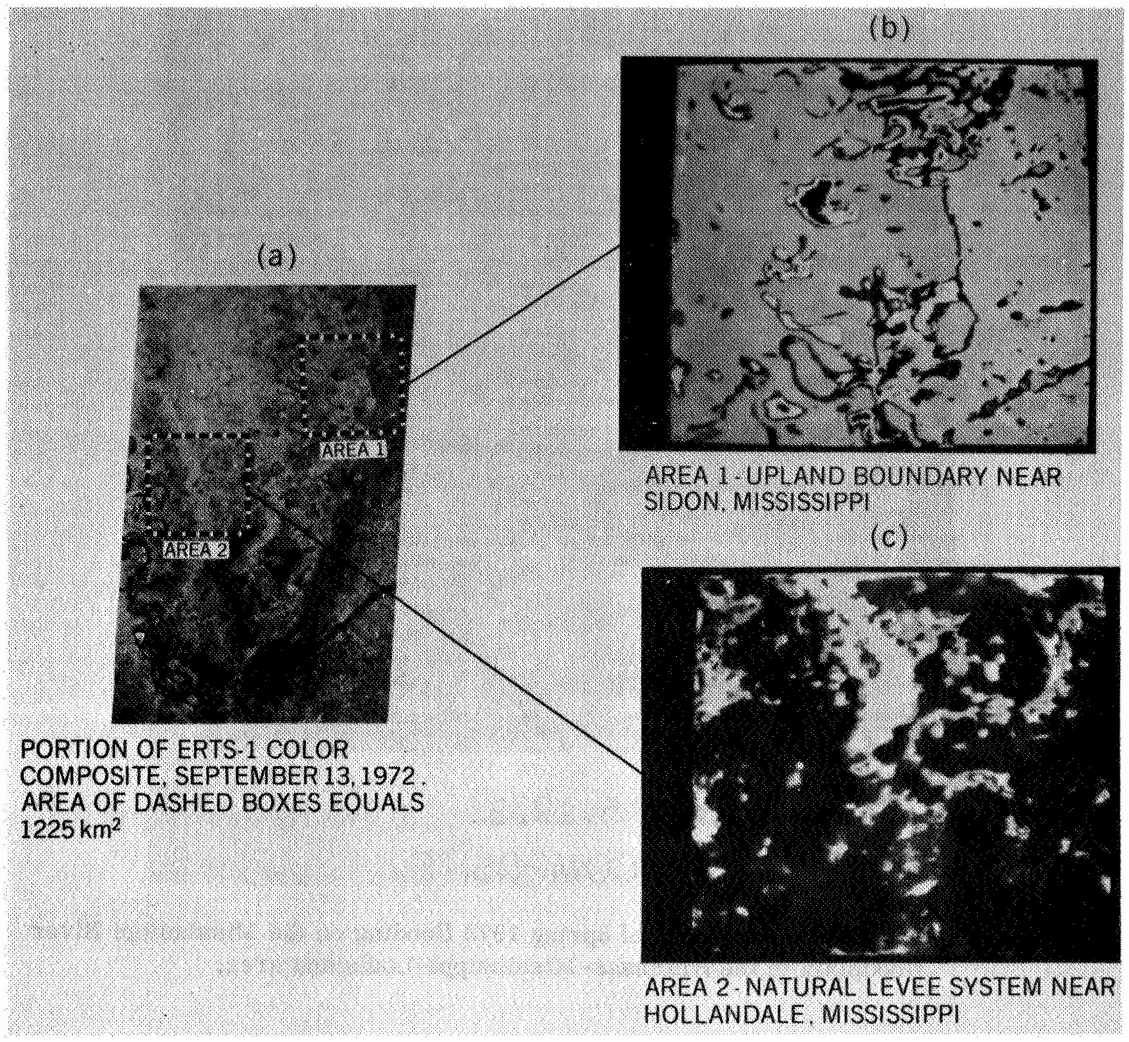

Figure 10. GEMS analysis of upland boundaries and natural levee systems in the Mississippi delta region as imaged by ERTS-1.

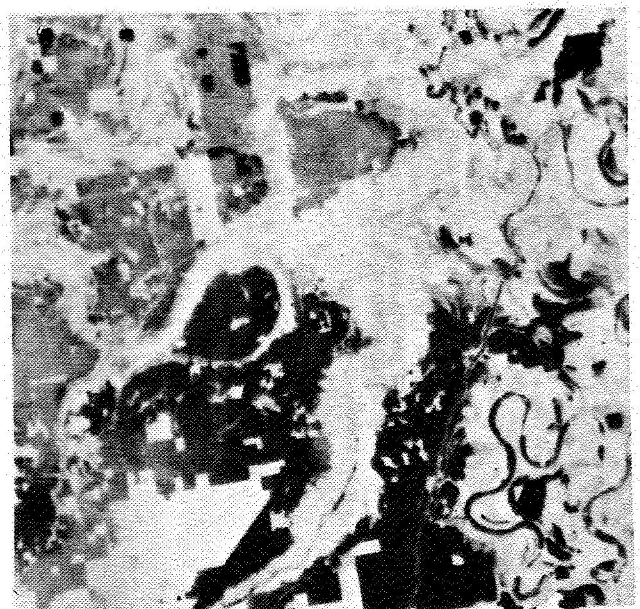
1225 km^2 PORTION OF ERTS-1 FLOOD SCENE MAY 5, 1973.

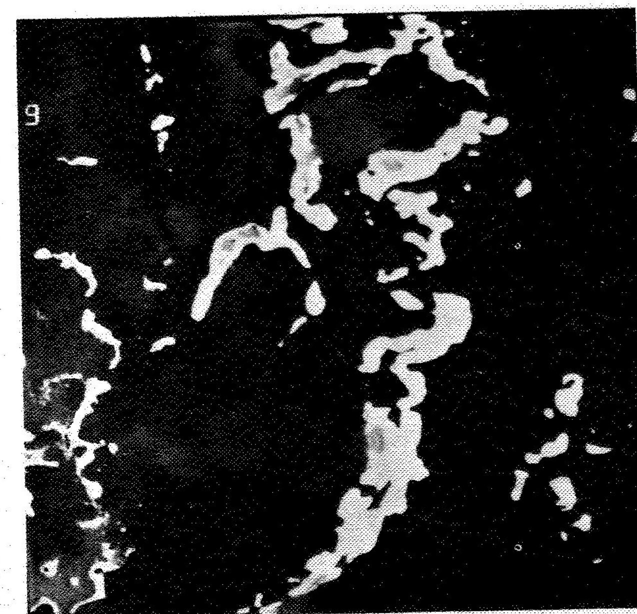

GEMS CLASSIFICATION OF NATURAL LEVEES (WHITE) NEAR LOUISE, MISSISSIPPI

Figure 11. GEMS natural levee classification of ERTS-1 data during flooding in the Mississippi delta region, May 5, 1973.

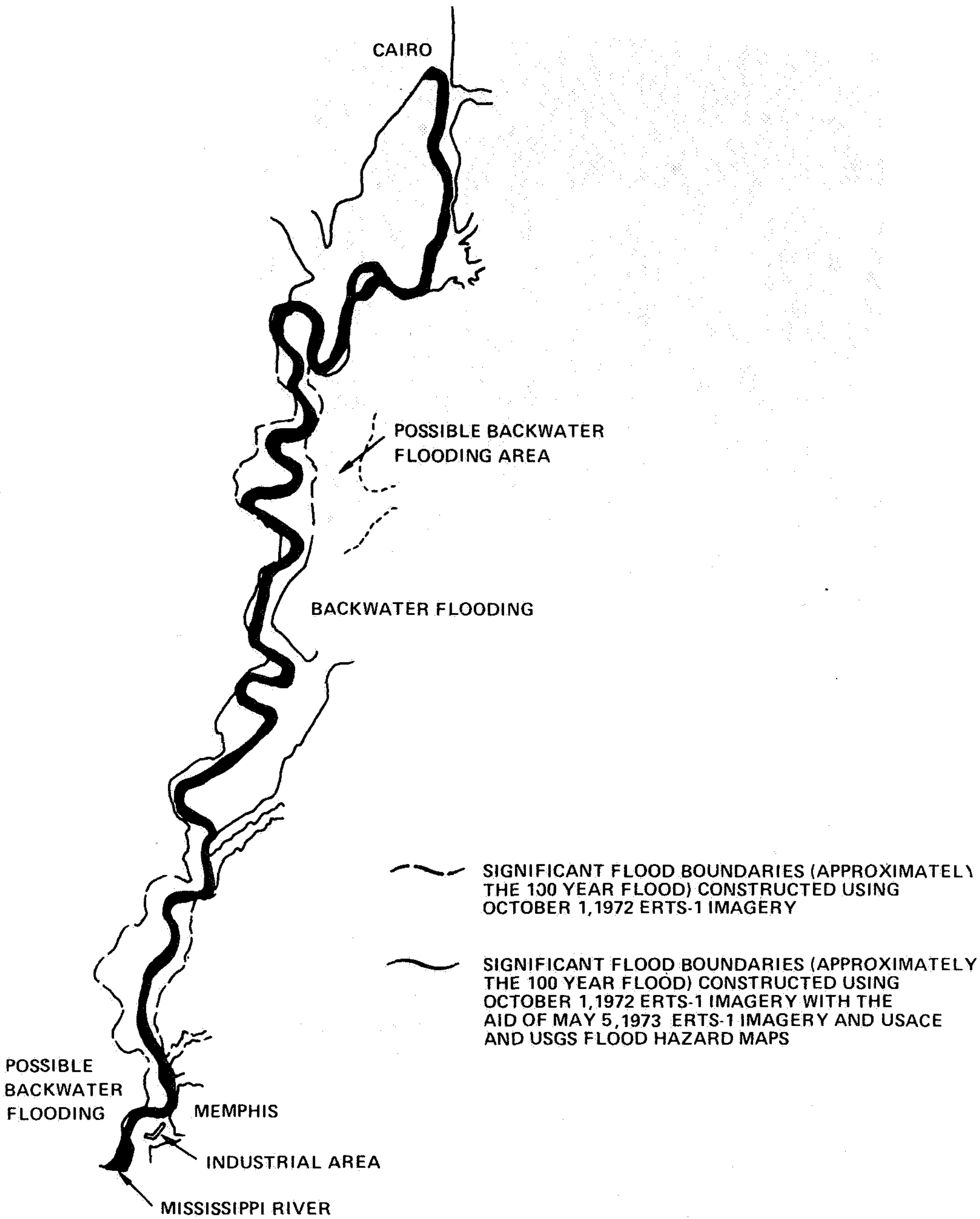

Figure 12. ERTS-1 regional flood hazard mapping at 1:1,000,000 scale from Cairo, Illinois to Memphis, Tennessee.

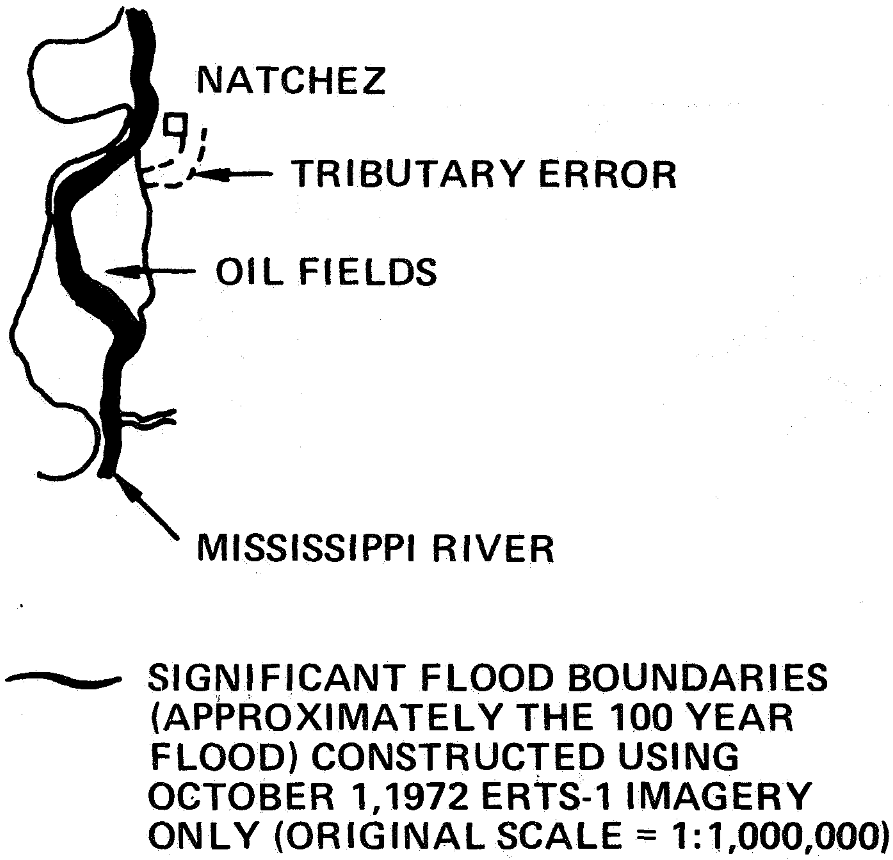

Figure 13. ERTS-1 regional flood hazard mapping in the Natchez, Mississippi area.

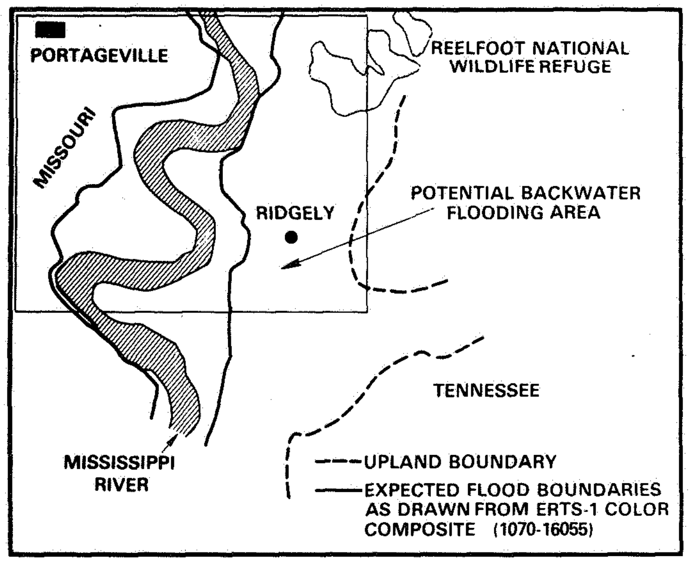

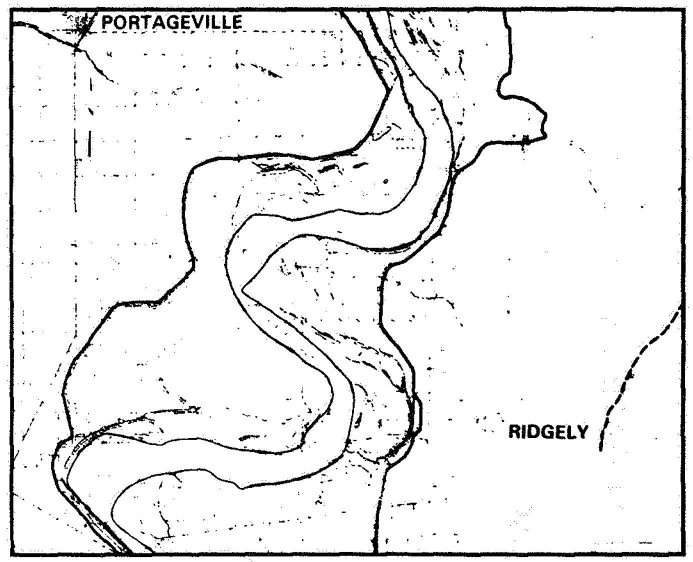

ERTS-1 DERIVED EXPECTED LIMITS OF SIGNIFICANT FLOODING (APPROXIMATELY THE 100 YEAR FLOOD) ALONG THE MISSISSIPPI RIVER.
ORIGINAL SCALE 1:1,000,000

U.S. ARMY CORPS OF ENGINEERS 100 YEAR FLOOD BOUNDARIES.
ORIGINAL SCALE 1:62,500

Figure 14. ERTS-1 derived expected limits of significant flooding (approximately the 100 year flood) along the Mississippi River. Original scale 1:1,000,000.

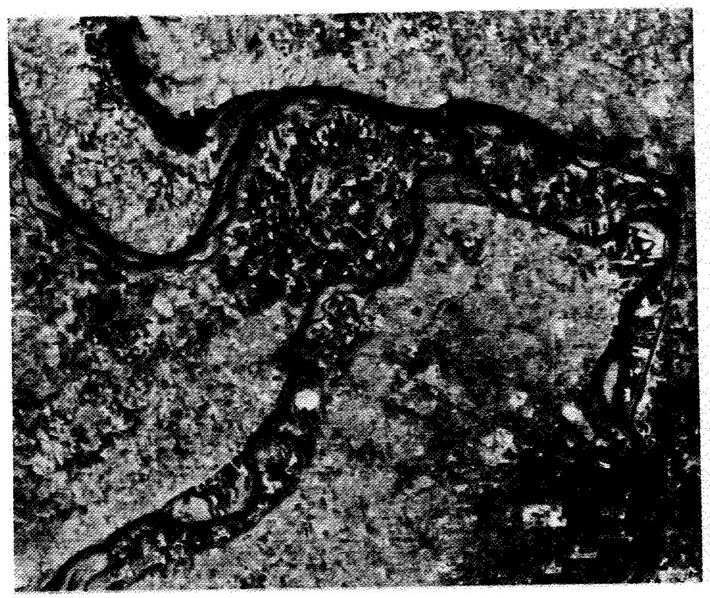

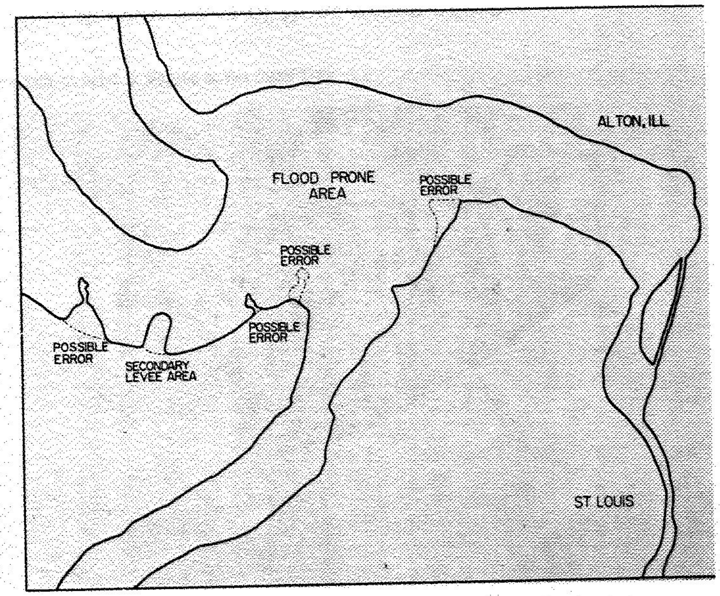

Figure 15. ERTS-1 Flood hazard mapping in St. Charles County, Missouri at a scale of 1:100,000. The areas delineated as flood prone will be inundated by a significant flood (approximately the 100 year flood).

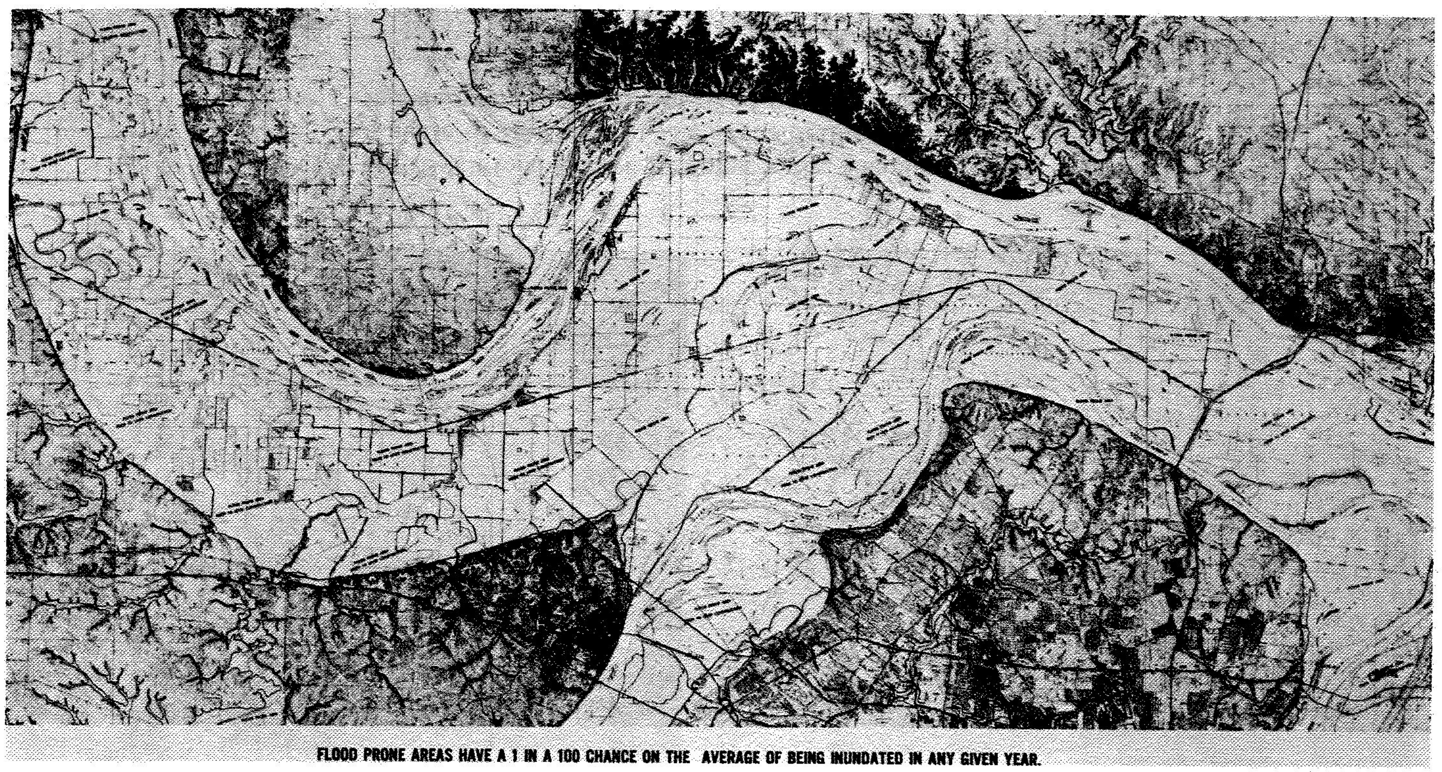

Figure 16. Composite of ten U. S. Geological Survey maps of flood prone areas in St. Charles County, Missouri at an original map scale of 1:24,000.

Paper W 11

OPTICAL DATA PROCESSING AND PROJECTED APPLICATIONS OF THE ERTS-1 IMAGERY COVERING THE 1973 MISSISSIPPI RIVER VALLEY FLOODS

Morris Deutsch and F. H. Ruggles, *U. S. Geological Survey*

ABSTRACT

Flooding along the Mississippi River and some of its tributaries was imaged by the multispectral scanner (MSS) on the Earth Resources Technology Satellite (ERTS-1) on at least three orbits during the spring of 1973. The ERTS data provided the first opportunity for mapping the regional extent of flooding at the time the imagery was acquired. Special optical data processing techniques were used to produce a variety of multispectral color composites which enhanced flood-plain details. One of these, a two-color composite of near infrared bands 6 and 7, was enlarged and registered to 1:250,000-scale topographic maps and used as the basis for preparation of flood image maps. Two specially filtered three-color composites of MSS bands 5, 6, and 7 and 4, 5, and 7 were prepared to aid in the interpretation of the data. The extent of the flooding was vividly depicted on a single image by two-color temporal composites produced on the additive-color viewer using band 7 flood data superimposed on pre-flood band 7 images. On May 24, when the floodwaters at St. Louis receded to bankfull stage, imagery was again obtained by ERTS. Analysis of temporal data composites of the pre-flood and post-flood band 7 images indicate that changes in surface reflectance characteristics caused by the flooding can be delineated, thus making it possible to map the overall area flooded without the necessity of a real-time system to track and image the peak flood waves. Regional planning and disaster relief agencies such as the Corps of Engineers, Office of Emergency Preparedness, Soil Conservation Service, interstate river basin commissions and state agencies, as well as private lending and insurance institutions, have indicated strong potential applications for ERTS image-maps of flood-prone areas.

INTRODUCTION

During the spring of 1973, the Mississippi River Valley experienced some of the most disastrous flooding in recorded history. Tremendous areas of lowland were inundated along the Mississippi River main stem and along a number of major tributaries between St. Louis and the mouth of the river, south of New Orleans. At St. Louis, an all-time high flood crest of 43.3 feet was recorded on April 28, 1973, exceeding the previous record of 43 feet recorded in April 1785. Flood

stage, which is 30 feet at St. Louis, was reached on March 10. The river remained above flood stage at St. Louis for 76 days until it finally receded to bankfull stage on May 24. Hydrographs of the river stages at St. Louis, Memphis, Vicksburg, and Baton Rouge are shown in Figure 1.

Flood inundation mapping, by conventional methods, the techniques of which are well established and understood, is a time-consuming and expensive procedure. Traditionally, either ground surveys or black and white panchromatic photography has been used as a basic tool in flood inundation mapping. During the past several years, however, utilization of new techniques of remote sensing by aircraft- and spacecraft-borne sensors has been gaining increased attention. Myers, Waltz, and Smith (1972), delineated the area flooded by Rapid Creek at Rapid City, South Dakota, using color and color infrared aerial photography and thermal infrared aerial imagery. From some of the early data obtained by the first Earth Resources Technology Satellite (ERTS-1) Benson and Waltz (1973) delineated and measured an area inundated by a severe local rainstorm near Aberdeen, South Dakota. Hallberg, Hoyer, and Rango (1973) reported on the mapping of the Nishnabotna River flood in Iowa; they employed ERTS data collected a week after the flood. They also assessed the value of color infrared photography versus traditional black and white panchromatic photography for flood mapping purposes and found the former to be highly superior. Morrison and Cooley (1973) mapped inundation limits of the Gila River flood in Arizona from ERTS imagery and obtained good agreement with maps prepared from aerial photography and ground surveys.

Early in March, in anticipation of flooding along the Mississippi River, the U.S. Geological Survey made a special request to the National Aeronautics and Space Administration for data from subsequent passes of ERTS-1 over the Mississippi River Valley. Basically, it was desired to be able to map the extent of inundation as quickly as possible, and with a minimum amount of conventional ground observations. It was surmised that specially processed ERTS data could provide hydrologists with a powerful new technique to supplement established methods of flood mapping, thereby for the first time making it possible to accurately map the extent of flooding over very large areas, and to optically depict the flooded area.

On March 31, 1973, ERTS-1 provided the first synoptic view of extensive flooding along two large reaches of the Mississippi River, between St. Louis, Missouri, and Natchez, Mississippi. On May 4 and 5, ERTS-1 sensors imaged a strip of the Mississippi River reaching from midway between St. Louis and Cairo, Illinois, to New Orleans and the Gulf of Mexico. The flood is depicted at its peak within the reach between Cairo and Memphis. The flood peaked at Cairo on May 4 at 14.7 feet above flood stage. Cloud cover over most of the Mississippi River

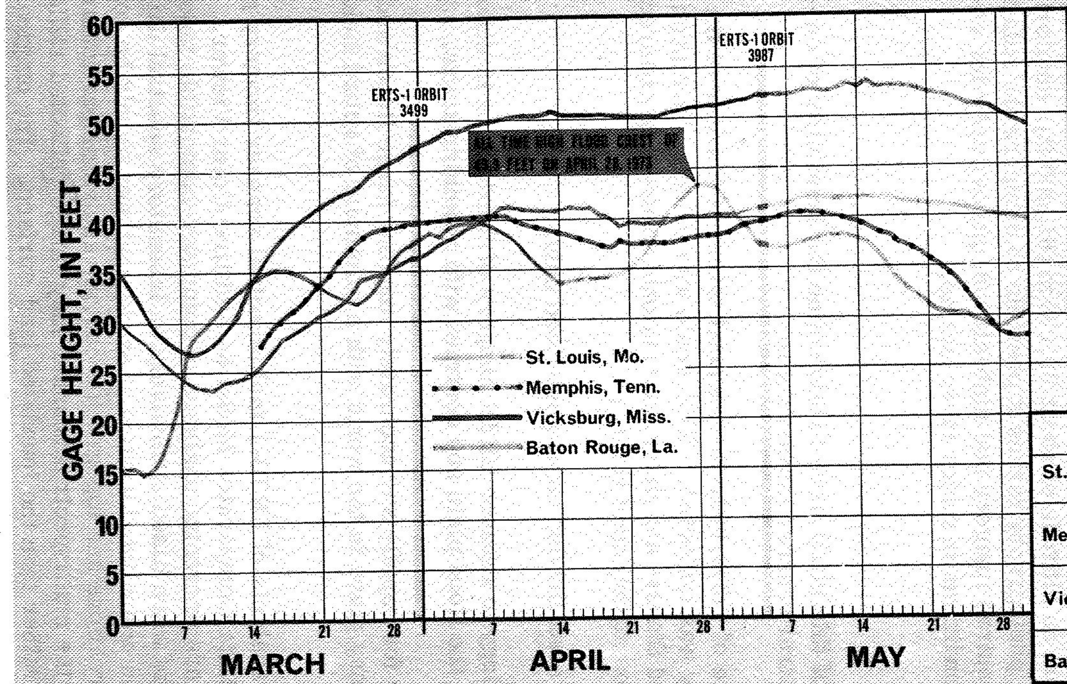

	Flood Stage (Ft.)	Pre-1973 Crests (Ft.)	Pre-1973 Crests (Date)
St. Louis	30	42	April, 1785
Memphis	34	48.7	Feb, 1937
Vicksburg	43	58.4	May, 1927
Baton Rouge	35	47.8	May, 1927

HYDROGRAPHS OF MISSISSIPPI RIVER FLOODS, SPRING, 1973

Figure 1. These hydrographs show that the lower Mississippi River was above flood stage for prolonged periods during the spring of 1973.

Valley below St. Louis on March 30, April 17 and 18, and May 6, prevented consecutive-day coverage over the entire reach from St. Louis to the mouth of the river.

On May 24, 1973, the date that the Mississippi River receded to bankfull stage at St. Louis (Figure 1), ERTS-1 again obtained cloud-free multispectral imagery over the swath imaged on March 31, thus providing a basis for determining the feasibility of mapping the total area flooded employing post-flood data.

On April 12, a NASA U-2 aircraft photographed the flood along the Mississippi River below St. Louis from an altitude of about 20,000 m (65,000 ft), employing color infrared film. The photography makes it possible to compare the relative effectiveness of space-acquired imagery and high-altitude photography for regional mapping of flood conditions in major river basins.

Objectives and Scope

The principal objectives of this study were to determine the feasibility of employing ERTS-1 multispectral scanner (MSS) data to:

- Delineate at a scale of 1:250,000, the regional extent of flooding at the instant the imagery was collected. (This scale was selected inasmuch as as the entire United States—and many international areas—are covered by topographic maps at the same scale.)

- Delineate the total area flooded using post-flood data.

- Develop a methodology to enhance ERTS imagery of flood areas to show maximum detail in the flood plain and contrast with adjoining areas.

- Develop techniques for rapidly and accurately mapping large floods and flood-prone areas any place in the world with a minimum of actual field observation.

This study was limited to analysis of ERTS-1 multispectral scanner imagery projected through a Spectral Data Comparator Model 64 Additive-Color Viewer. Limitations of time and funds prevented analyses of computer-compatible tapes. Flood boundary delineations were based exclusively on laboratory spectral data analysis, although under an operational system spectral analyses should be complemented by ground observations and topographic contour analysis, particularly in forested areas because the multispectral scanner may image reflected radiation from the tree canopy rather than the inundated land surface. The original data used for the analyses in this study were third generation (3G) 70 mm MSS negatives. All of the data were reprocessed to balance the density range and

minimum density in the black and white positives (AG) with respect to each other. This was done to achieve the greatest enhancement of the flood plains in the additive-color projection.

Techniques of data processing, color enhancement of flood features, preparation of two-color temporal composites to display flooded areas regionally, and flood mapping were presented in greater detail at the June 1973 Symposium of the American Water Resources Association on Remote Sensing and Water Resources Management (Deutsch, and others, 1973).

ERTS-1 COVERAGE OF THE 1973 MISSISSIPPI RIVER FLOODS

All of the ERTS data used for this study were obtained by the MSS which images reflected solar radiation from the Earth's surface in four bands of the visible and near-infrared portions of the electromagnetic spectrum, nominally as follows (NASA, 1971):

MSS Band	Wavelength (Micrometers)	Color
4	0.5-0.6	Green-yellow-orange
5	0.6-0.7	Red
6	0.7-0.8	Near-infrared
7	0.8-1.1	Near-infrared

Figure 2 is a mosaic prepared from ERTS-1, MSS band 7 images showing flood inundation over large reaches of the Mississippi River Valley from St. Louis to the Gulf of Mexico. The imagery was obtained by the satellite on March 31 for the western swath including the St. Louis area, and on May 4 and 5 for the eastern swaths. The images were precisely enlarged to a scale of 1:1,000,000. The May 4 and 5 orbital swaths cover about a 2000 kilometer reach of the Mississippi (1,200 river miles) from about half way between St. Louis and Cairo, Illinois, to the Gulf of Mexico. The flood is at its peak along the reach between Cairo and Memphis (see Figure 1). Flooding along the lower Ohio River at its confluence with the Wabash River is also clearly shown. The seven May 5 scenes used in the mosaic were collected during an orbital interval of only 3 minutes. All of the flood data shown in Figure 2 were collected in about 7 minutes.

In order to map the area inundated by any flood, it is obviously necessary to have data on the area normally covered by water. For this critical analysis, data collected by ERTS-1 over the Mississippi River on October 1 and 2, 1972, were obtained from the Earth Resources Observation Systems (EROS) Data Center at Sioux Falls, South Dakota.

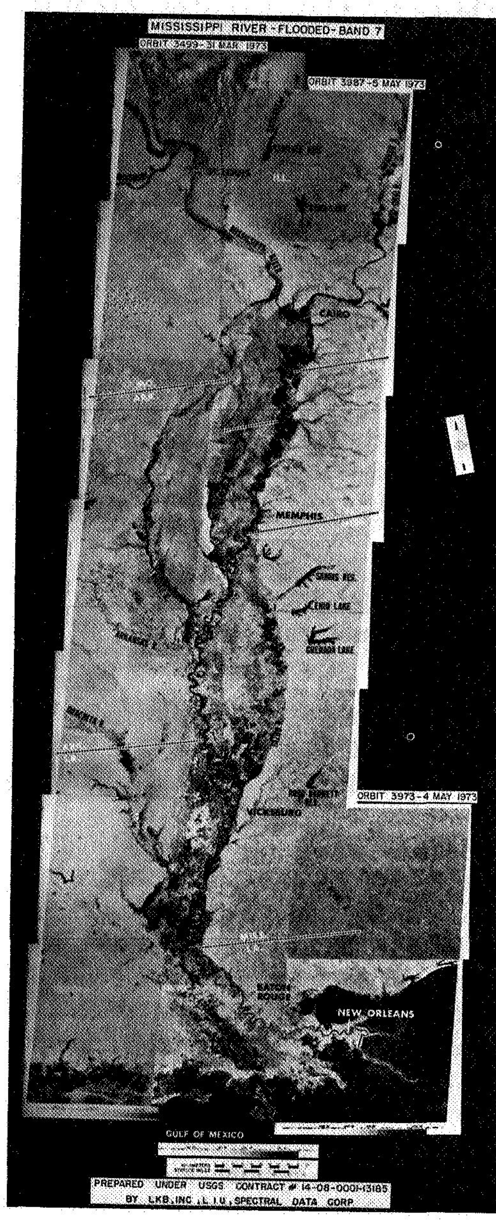

Figure 2. On March 31 and May 4-5, 1973, ERTS-1 imaged the lower Mississippi River Valley in about 7 minutes. This mosaic of band 7 near-infrared images provided the first overall view for the entire region.

Figure 3 is a black and white mosaic of MSS band 7 images recorded by ERTS-1 sensors on October 1 and 2, 1972, which depicts "normal" conditions. The difference in water-covered or wet surface between October 1972 and the 1973 flood period is obvious. Especially noticeable also is the wet flood plain between St. Louis and Cairo, Illinois, and the lower White River above its confluence with the Arkansas River in the lower left image. For the purposes of the present study, covering the reach from about St. Louis to Memphis, data from only seven ERTS scenes in October and seven flood images were needed.

On May 24, the date the Mississippi River receded to bankfull stage at St. Louis, excellent imagery covering the same swath as orbit 3499 on March 31 was obtained. These data provided the basic information needed to determine the feasibility of attaining the second objective of the experiment.

Color Enhancements

From inspection of the "standard" false-color composite of bands 4, 5, and 7 images of the flood area produced by the NASA Data Processing Facility (NDPF) (Figure 4 lower left) it appeared that the flooding was more extensive on the image than was actually the case. The additive-color viewer was hence used to produce two- and three-color enhancements highlighting conditions on the flood plains.

From among the numerous additive-color combinations examined on the viewer screen the following were deemed to be best for detailed flood-plain analysis of mapping.

Rendition "A" (Figure 4, upper left) - Band 5 is projected as blue; band 6 as green; and band 7, filtered to about 60 percent transmission, as red. This rendition was best suited for interpreting the extent of flooded area in relation to rural land use. Morphologic and geologic features are enhanced, and water detail is well preserved. Areas with standing water appear as blue, and wet or saturated soils as brown.

Rendition "B" (upper right) - Band 6 is projected as red, filtered to about 60 percent transmission and band 7 as green. This pictoral rendition prepared from the two near infrared bands was considered the best for differentiating areas of varying degrees of inundation and wetness. This rendition, therefore, was used as the basic source of information from which the flood maps described below were prepared. Standing water appears as red and the wet or saturated flood plain as green.

Rendition "C" (lower right) - Band 4 is projected as blue; band 5 as green; and band 7, filtered to about 40 percent transmission, as red. This pictoral rendition

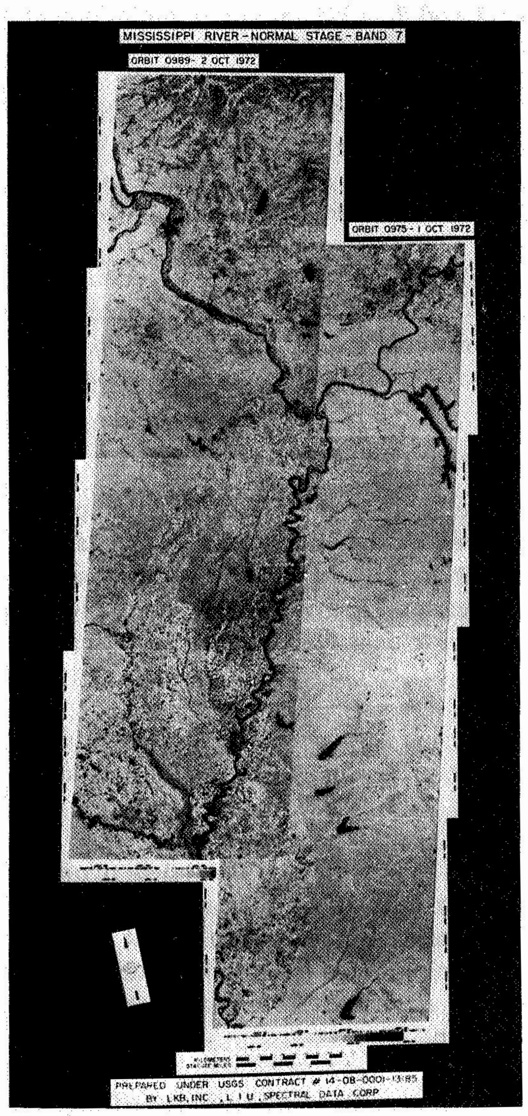

Figure 3. The ERTS flood data were compared with the band 7 near-infrared images used to construct this mosaic depicting "normal" conditions along the Mississippi Valley between St. Louis and the mouth of the Arkansas River on October 1-2, 1972.

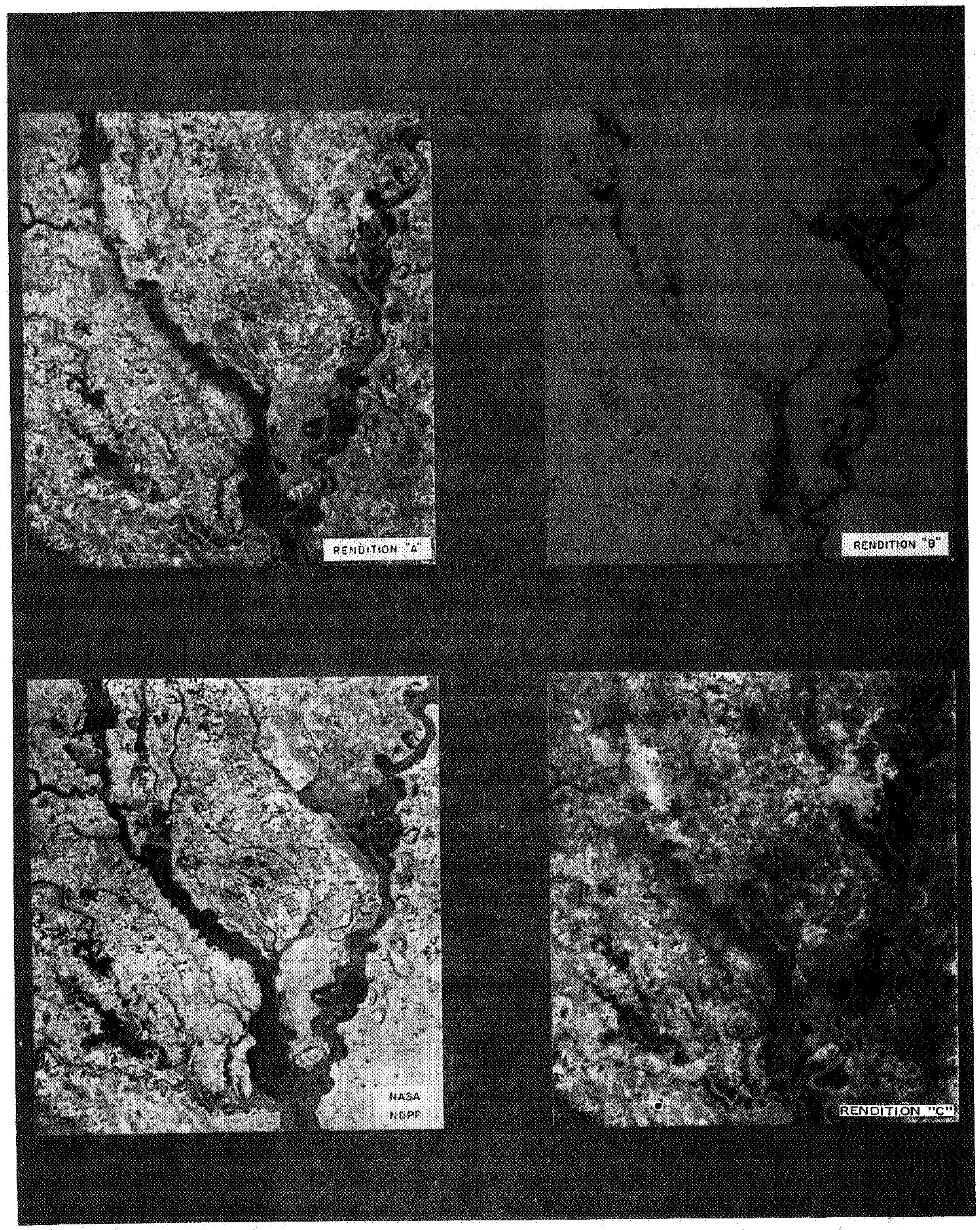

Figure 4. Three specially filtered additive-color enhancements and the "standard" NASA Data Processing Facility color composite were prepared from ERTS-1 multispectral scanner images to study detailed flood-plain conditions north of the confluence of the Mississippi, Arkansas, and White Rivers on March 31, 1973.

is best suited for interpreting flooded areas in relation to urban patterns. While preserving water detail, it enhances cultural detail. In this rendition, standing water is shown in shades of blue or green, and areas of wet or saturated soil appear as brown.

Temporal Composite Display of Flooded Areas

The extent of flooding can be clearly displayed by projecting a pre-flood image and one collected during the flood into a single composite image. Band 7 was used because there is little or no reflection of incident radiation from water in this spectral region, and thus the water appears dark in a positive print.

Figure 5 shows the Cairo, Illinois, area imaged by MSS band 7 on May 5, 1973, in green, and on October 1, 1972, in red. The temporal composite (bottom), prepared by additive projection of the two band 7 scenes, depicts the flooded area in red, as described below. The composite covers only the area of image overlap between the two dates. This image, therefore, shows excellent differentiation between dry soil, saturated soil, and standing water. In a properly processed positive, standing water is very dark, dry soil is relatively light, and saturated soil is intermediate in density. When a non-flood image is projected as red, in register with a flood image projected as green, the composite color image is composed of the following elements:

1. Where there is surface water present on both images, the composite image receives little or no light and is therefore essentially black. This depicts the area normally covered by the river and other surface-water bodies.

2. Where the ground is not covered with water in both scenes, the composite image receives relatively equal amounts of red and green light, and is therefore yellow. This depicts the area unaffected by flood waters.

3. Where there is surface water in the scene projected in green, and dry soil in the scene projected as red, the composite image receives only red light, and is therefore a highly saturated red color. This depicts the area of flood inundation.

4. Where there is water-saturated soil in the scene projected as green, and dry soil in the scene projected as red, the composite image receives red light combined with a lesser amount of green light, and results in a color on a continuum between yellow and red.

It can readily be seen also from Figure 5 that the orbit of the satellite has shifted about 20 miles to west between October and May. Furthermore, the swaths were

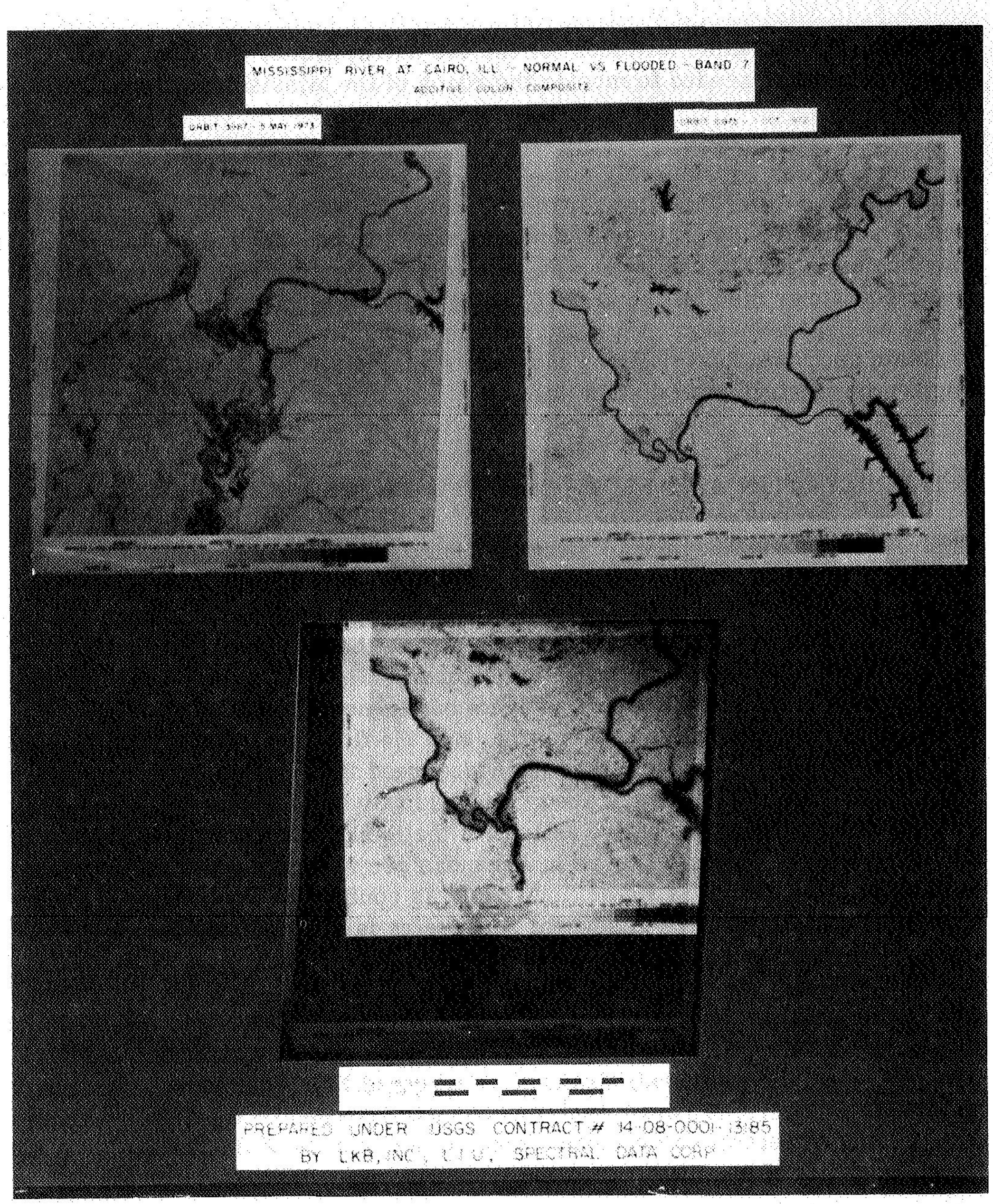

Figure 5. Band 7 images covering the flooded areas (green) were combined with images of the same area collected under "normal" conditions (red) to prepare temporal composites (bottom) such as the one shown here at the confluence of the Mississippi and Ohio Rivers. The extent of flooding is depicted in red; "normal" conditions in black.

not framed at the same latitudes for the two dates; hence, the number of temporal composites needed to mosaic the reach of the Mississippi River was doubled.

In general it was considerably more difficult to register scenes covering the same area for different dates for the temporal composites than it was to register the various bands collected simultaneously for the spectral composites. This may be due in part to differences in side edge distortion caused by the orbital shift, but it may also be due in part to slight attitude difference of the satellite. In any event, inasmuch as the flood plains are relatively linear, it was possible to obtain good registration along those flood plains studied at the expense of slight misregistration in distant areas.

INTERPRETATION AND FLOOD-MAPPING PROCEDURES

Figure 6 is a flood image-map using the Cairo area temporal composite enlarged to a scale of 1:250,000 as an image base. Figure 7 is a mosaic of band 7 temporal composites for the entire study area. Except for cloud shadows, the presence of red depicts water on the surface during the flood period that was not present during "normal" conditions in October. There is major flooding along the Mississippi above St. Louis and at its confluence with the Missouri River. There is also flooding in the Cairo area, and the flood peak is depicted between Cairo and Memphis. In fact, there is widespread flooding throughout the Mississippi River Valley in the study area. The Ohio River is in flood at its confluence with the Tennessee. The entire valleys of the Kaskaskia River in Illinois, and the White and St. Francis Rivers in Arkansas are very wet and locally in flood. In contrast, the Arkansas River (lower left) is confined to its banks. The change in area of surface storage in several reservoirs is clearly depicted by red extensions beyond their pre-flood shorelines.

The initial area selected for flood inundation map preparation was the ERTS image that covered Cairo, Illinois area at the confluence of the Mississippi and Ohio Rivers. The 1:250,000 scale drainage overlays of NJ16-7 (Paducah quadrangle) and NJ16-10 (Dyersburg quadrangle) were superimposed on a 1:250,000 rendition "B" multispectral enlargement, and the perimeters of the flooded area along the main stems of the Mississippi and Ohio Rivers were drafted (Figure 8).

Area measurements that differentiated normal river stage acreage from flooded inundation acreage were computed by subtraction. The wet areas were determined with a Dell-Foster 3-axis Digitizer-Quantitizer. This procedure was repeated to complete the analyses of the extent of flooding along the Mississippi

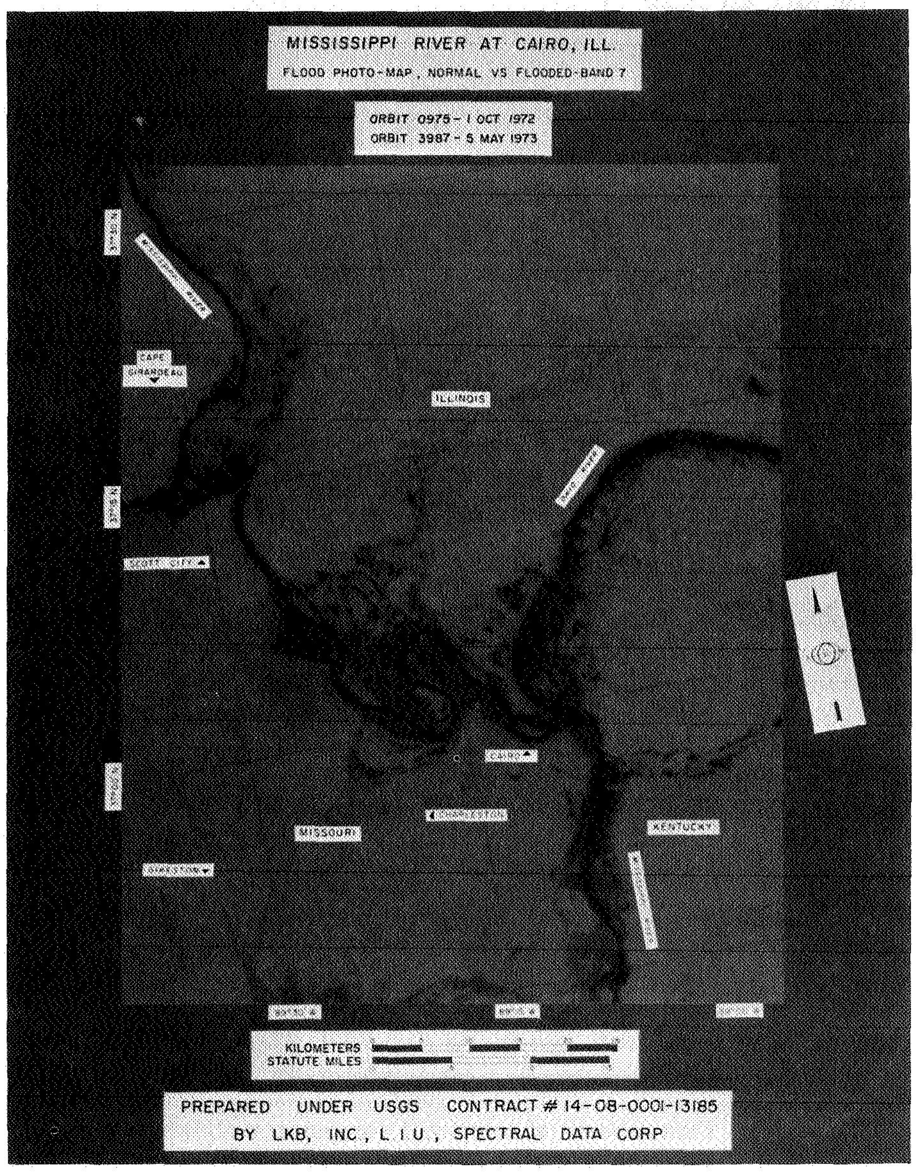

Figure 6. Detailed distribution of flooding in the Cairo, Illinois, area is shown in red on this image map prepared from an enlargement to a scale of 1:250,000 of the temporal composite shown in Figure 5.

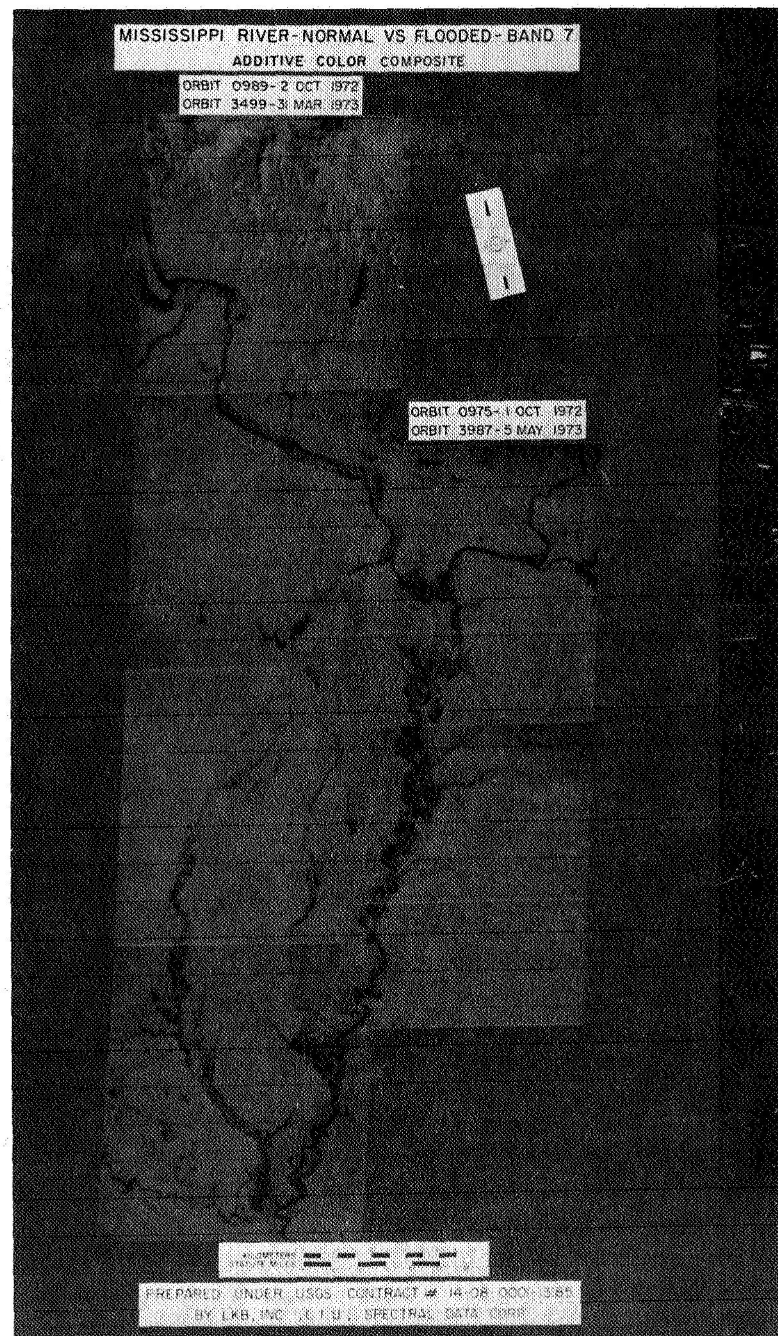

Figure 7. This mosaic of temporal composites shows the extent of flooding in red along the Mississippi Valley between St. Louis and the mouth of the Arkansas River on March 31 and May 5, 1973. "Normal" river conditions and the areal extent of surface water on October 1 and 2, 1973, appear as black.

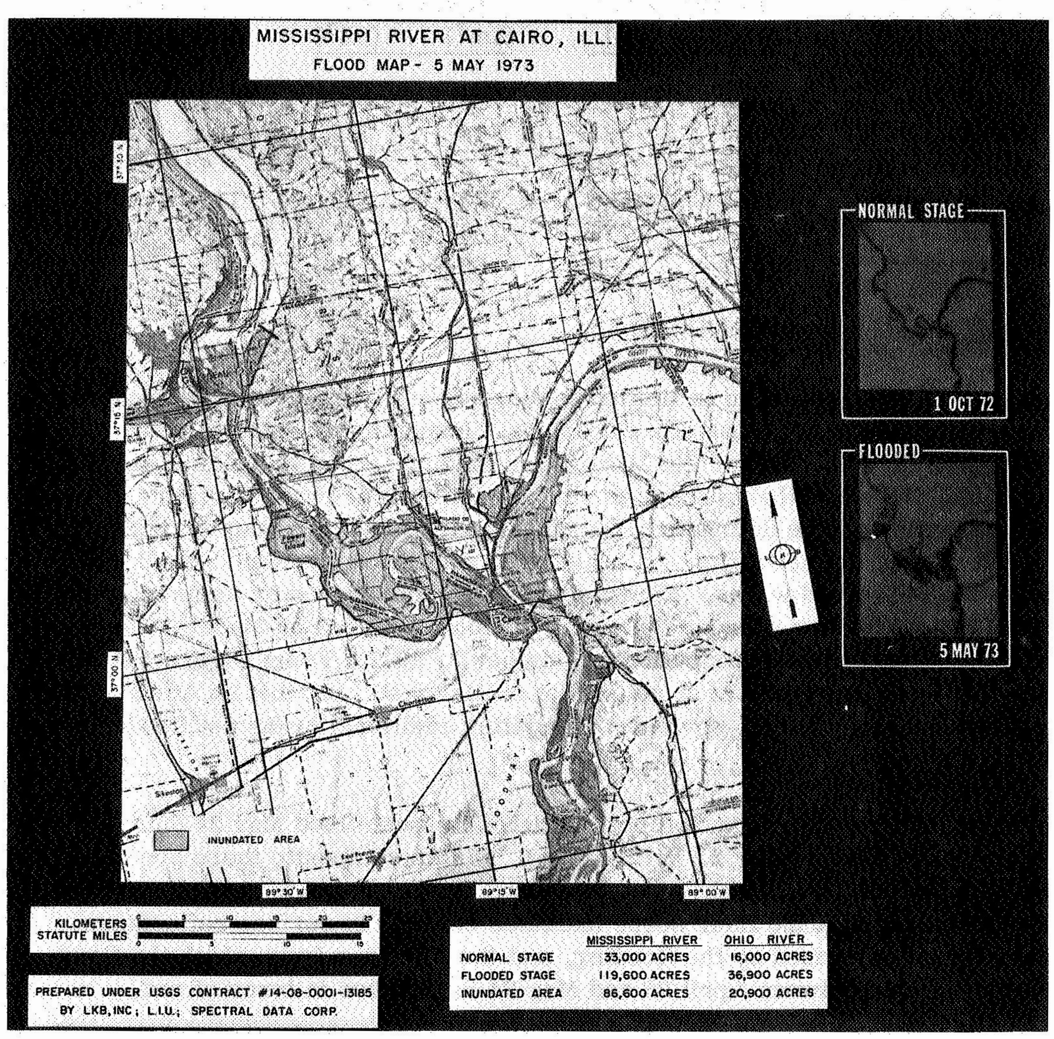

Figure 8. This map showing the extent of flooding along the main stems of the Mississippi and Ohio Rivers near Cairo, Illinois, was based exclusively on band 6 and 7 near-infrared images collected by ERTS-1 on October 1, 1972, and May 5, 1973.

River main stem from St. Louis to the confluence with the Arkansas and White River, with results as follows:

Quadrangle (1 x 2 degrees)	Total Flooded Area (km²)	Total Flooded Area (mi²)	Normal River Area (km²)	Normal River Area (mi²)	Inundated Land Area (km²)	Inundated Land Area (mi²)
St. Louis	805	311	326	126	479	185
Paducah	987	381	344	133	642	248
Rolla	75	29	3	1	73	28
Dyersburg	1474	569	324	125	1150	444
Blytheville	723	279	153	59	570	220
Memphis	412	159	88	34	324	125

Interpretation of Post-Flood Data

Because ERTS-1 coverage is limited to cloud-free coverage once every 18 days, it cannot track the progress of a flood peak. Inspection of data collected by ERTS-1 on May 24, the day the Mississippi River receded to bankfull stage at St. Louis, indicates that changes in surface reflectance characteristics caused by the flooding can be delineated, thus making it possible to map the total area flooded without the necessity of a real-time, continuous system to track and image the peak flood waves. Figure 9 shows an additive-color temporal composite of band 7 images showing the extent of flooding in red on March 31 against normal surface-water distribution on October 2, 1972. From Figure 1 it can be seen that flood stage was at about 38 feet on March 31, but that on April 28 the flood peaked at 43.3 feet, obviously inundating additional areas not flooded on March 31.

Figure 9 also shows a temporal composite of the post-flood May 24 data at St. Louis against the October 2, 1972, image. In this composite there are areas shown in red that are not shown on the March 31-October 2 temporal composite. It is postulated that the later scene indicates changes in surface reflectance characteristics caused by the flooding, and that the area from which the flood waters receded between April 28 and May 24 is depicted in tones of red.

ERTS MSS Imagery Compared with Aircraft Color Infrared Photography

On April 12, 1973, a NASA U-2 aircraft photographed the Mississippi River in flood below St. Louis. Figure 10 shows U-2 photography at St. Louis, Cairo, and Memphis and the areas covered by five frames in relation to the ERTS-1

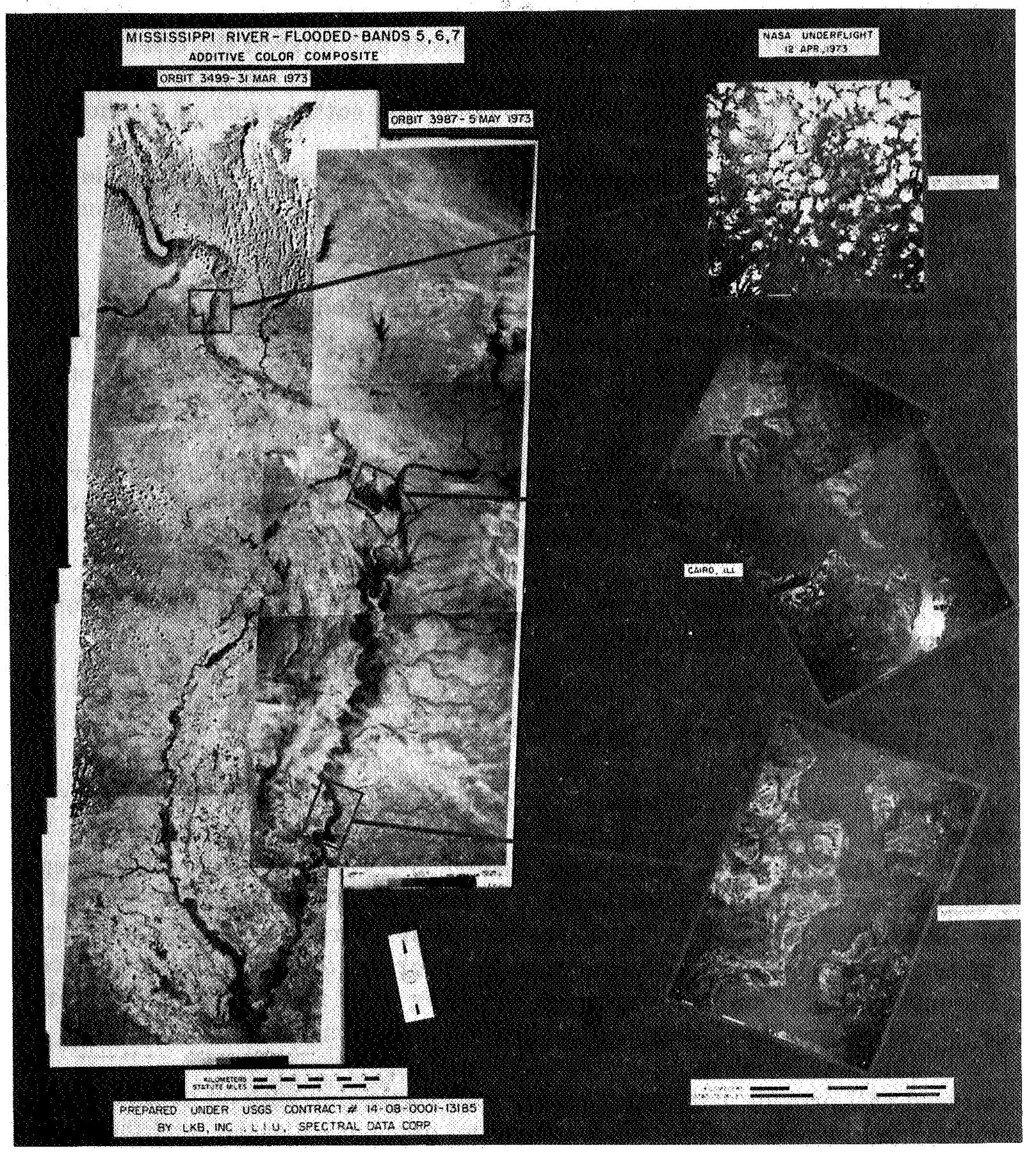

Figure 10. ERTS MSS imagery provides superior synoptic and regional coverage over the Mississippi River between St. Louis and Memphis, but high-altitude aircraft color infrared photography shows greater detail at St. Louis, Cairo, and Memphis.

multispectral imagery. Inspection—but not analysis—of the U-2 data leads to the following observations:

- The U-2 followed the main valley of the river and missed the effects of flooding of the Mississippi on various tributaries. At Cairo the camera angle-of-view was not wide enough to cover the entire width of the flood.

- Where turning with the course of the river, the aircraft caused spatial distortions in the film that would require rectification to permit accurate mapping.

- The multispectral mode of the ERTS data permitted automatic, rapid, and accurate delineation of the flooded area, whereas mapping from aircraft photography would require density slicing or use of photointerpretation techniques.

- ERTS covered the entire region using only a small fraction of the number of frames required by the U-2, which would have been again multiplied were it possible to obtain vertical photography during block coverage.

- The principal advantage of the aircraft data is that it would permit mapping at scales of 1:24,000 and larger.

POTENTIAL FLOOD APPLICATIONS OF ERTS IMAGERY

The technique described in this report offers a relatively simple and economic procedure that can be used to quickly assess areas that have been inundated during recent flood periods. Rango and Anderson (1973) mapped areas susceptible to flooding along the Mississippi River using pre-flood ERTS imagery at scales as large as 1:100,000. These methods will not replace an engineering type of flood evaluation that requires specific information, i.e., depth of flooding in a basement, or the amount of damage resulting from undermined roads, or the degree of damage to mechanical equipment in buildings.

The method will provide regional disaster relief agencies with an overview from which they will be able to determine a first cut damage estimate, and thus be able to dispense assistance in the most expeditious manner.

The regional planner will have a tool to enable him to assess the best use of the flood plains. Housing authorities will be able to determine areas subject to flooding; private lending agencies will be able to evaluate the flood potential of a proposed urban development; flood insurance agencies (private and public) will be able to evaluate flooded areas and be able to assist their customers more

quickly; engineers will be able to quickly evaluate the effectiveness of flood control works and thereby be provided with a prototype model for a river basin.

The list of possible uses of the ERTS-1 evaluation described herein is limited only by the ingenuity of the user.

CONCLUSIONS

Optically processed ERTS MSS imagery provides hydrologists with an important new technique for rapid and inexpensive flood inundation mapping and related studies:

- The areal extent of flood waters over very large reaches of a major river basin can be viewed synoptically.
- Areas in flood can be quantitatively determined by automatic data-processing techniques.
- ERTS imagery can be color enhanced by additive-color techniques to aid in the interpretation of flood conditions and their relation to geologic, physiographic, and urban settings.
- The extent of inundation versus "normal" conditions can be sharply delineated on a temporal basis on single color-composited images.
- The near-infrared bands (6 and 7) on ERTS can be used in combination for interpretation of flood conditions and delineation of flood-water boundaries.
- Bulk-processed ERTS imagery can be used as the basis for area-of-flood inundation mapping for a region at a scale of at least 1:250,000, and probably as large as 1:100,000.
- Optical data-processing of ERTS MSS imagery provided for an extremely fast and inexpensive means of regionally delineating the Mississippi River floods of 1973, and measuring the areal extent of inundation during the course of the floods.
- Regional flood mapping is far more feasible with satellite imagery than with aircraft photography.
- The effects of flooding on the reflectance characteristics of the surface make it possible to delineate areas where flood waters have receded by using post-flood data, thereby eliminating the necessity for continuous

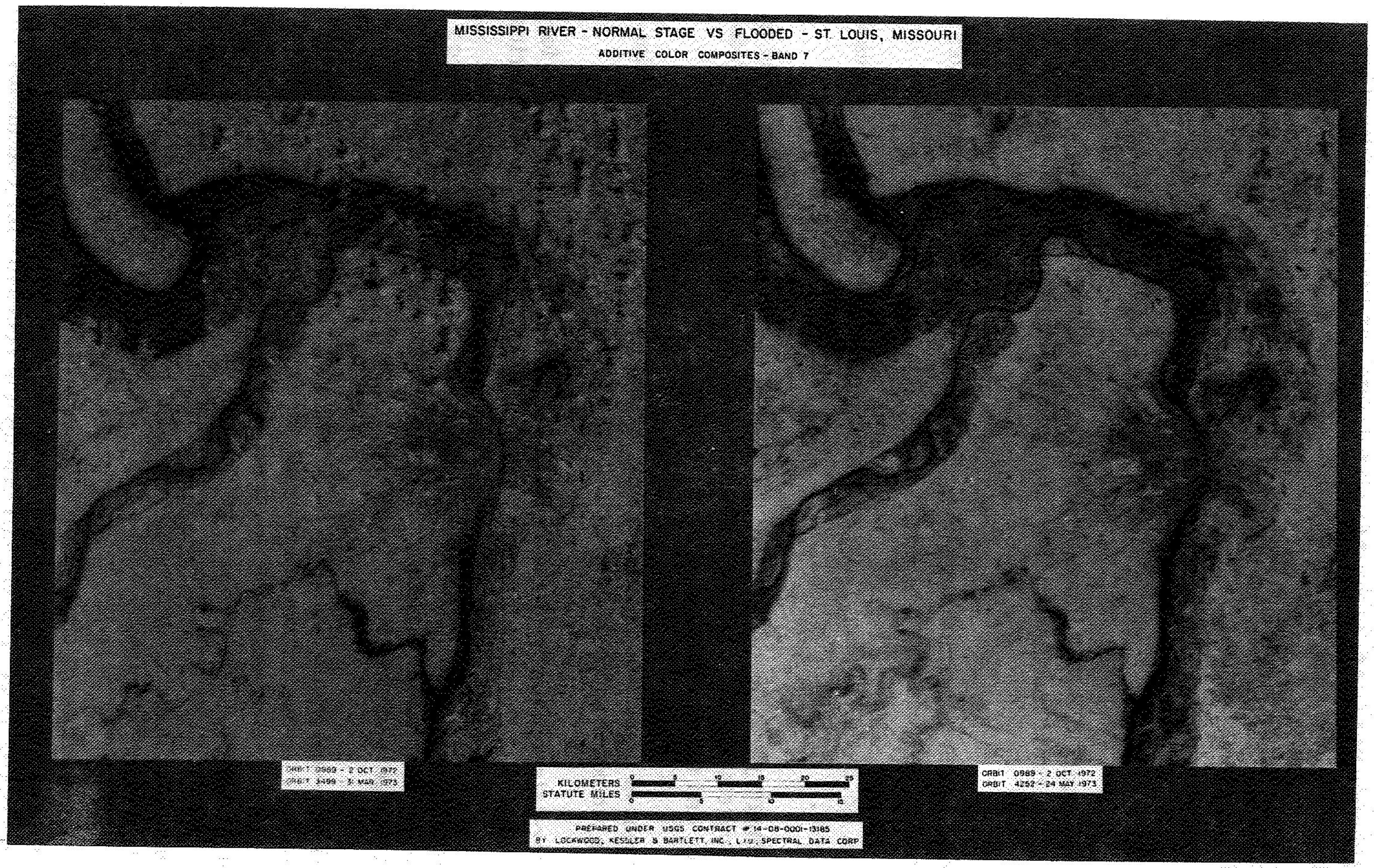

Figure 9. These temporal composites depict flood conditions against "normal" conditions in the St. Louis area where the Illinois and Missouri Rivers join the Mississippi River. On the left, the extent of flooding on March 31, 1973, is shown in red; on the right, red indicates the area from which flood waters receded between April 28 and May 24, 1973.

tracking and imagery of the flood crest and reducing the volume of data required.

- Flood-prone area maps generated from ERTS MSS data have potentially important engineering, economic, disaster relief, and planning applications.

ACKNOWLEDGEMENTS

The authors wish to express their appreciation to Drs. Stanley Freden and Albert Rango of the NASA Goddard Space Flight Center for making the ERTS-1 imagery of the Mississippi flooding available on a priority basis. They are equally indebted to Dr. George Rabchevsky of the Terratek Corporation for his excellent advice and considerable assistance on techniques of color-additive enhancement and false-color reproduction.

Data processing and preparation of illustrations was performed by Mr. Philip Guss of Lockwood, Kessler, and Bartlett, Inc. of Syosset, New York, and Dr. Edward Yost of Spectral Data Corporation of Hauppage, New York, under terms of U.S. Geological Survey Contract 14-08-0001-13185. Their scientific and technical expertise provided the foundation for this study.

REFERENCES

Benson, L.A., and Waltz, F.A., 1973, Monitoring flood damage with satellite imagery: South Dakota State Univ. Remote Sensing Int. Report 73-07, 11 p.

Deutsch, Morris, Ruggles, F.H., 1973, Guss, Philip, and Yost, Edward, Mapping of the 1973 Mississippi River floods from the Earth Resources Technology Satellite: Proceedings no. 17, Am. Water Resources Assoc. Symposium on Remote Sensing and Water Resources Management, June.

Hallberg, G.R., Hoyer, B.E., and Rango, Albert, 1973, Application of ERTS-1 imagery to flood inundation mapping: in Proceedings of the Symposium on Significant Results Obtained from the Earth Resources Technology Satellite, NASA, vol. 1, sec. A., p. 745-753.

Morrison, R.B., and Cooley, M.E., 1973, Assessment of flood damage in Arizona by means of ERTS-1 imagery: in Proceedings of the Symposium on Significant Results Obtained from the Earth Resources Technology Satellite, NASA, vol. 1, sec. A, p. 755-760.

Myers, V.I., Waltz, F.A., and Smith, J.R., 1972, Remote Sensing for evaluating flood damage conditions—the Rapid City, South Dakota flood, June 9, 1972: South Dakota State Univ., Remote Sensing Inst. Report 72-11, 29 p.

National Aeronautics and Space Administration, 1971. Data users handbook—Earth Resources Technology Satellite: NASA Goddard Space Flight Center Document 715D4249.

Rango, Albert, and Anderson, A.T., 1973, ERTS-1 flood hazard studies in the Mississippi River basin: NASA Goddard Space Flight Center Report X-650-73-294, 29 p., 16 figs.

Paper W 12

APPLICATION OF ERTS IMAGERY TO ENVIRONMENTAL STUDIES OF LAKE CHAMPLAIN

A. O. Lind, *(University of Vermont), Burlington, Vermont*

ABSTRACT

ERTS Imagery has provided data relating to a number of environmental and limnological concerns such as water quality, lake flooding and lake ice formation. Pollution plume data provided by ERTS was recently used in the Supreme Court case involving the States of Vermont and New York and a paper company. Flooding of lowland tracts has been a major concern due to a repetitive pattern of high lake levels over the past three years, and ERTS imagery is being used to construct the first series of flood maps of the affected areas. Lake ice development and turbidity patterns have also been studied from ERTS, since these have significance for shore erosion studies.

LAKE CHAMPLAIN AS A RESOURCE

The significance of Lake Champlain to the State of Vermont cannot be overstated since it not only serves to supply water to shore communities, but also functions as a major water playground for the people of Vermont and New York as well as a significant population of tourists from megalopolis. In addition, the natural setting of the lake in a trough between the Adirondack and Green Mountains, provides an aesthetically pleasing sight which seems beyond economic quantification. In order to insure that the lake may continue to serve in these capacities, a number of state and local agencies, of which the University of Vermont is a principal one, are engaged in inventoring and mapping the various physical and biotic features of the lake as well as the interaction between those features and human activity. ERTS has figured significantly in providing information on the lake and its varied shorelines to the extent that some of the results from the ERTS experiment are now being applied in resource management decisions. This paper describes these direct applications, which include water pollution and lake flooding, and assesses the significance of other ERTS-derived limnological information pertaining to turbidity and lake ice.

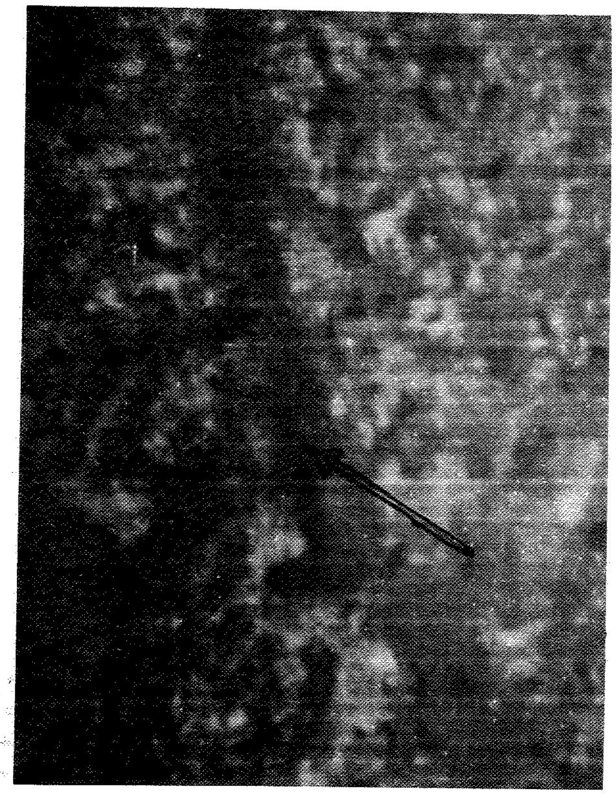

Fig. 1. The April 25, 1973, MSS band 4 rendition of the International Paper Co. effluent pattern which extends into Vermont waters. This 4X enlargement of a portion of image no. 1276-15073 was entered as evidence in the Vermont vs. IPC and New York pollution suit as were other images.

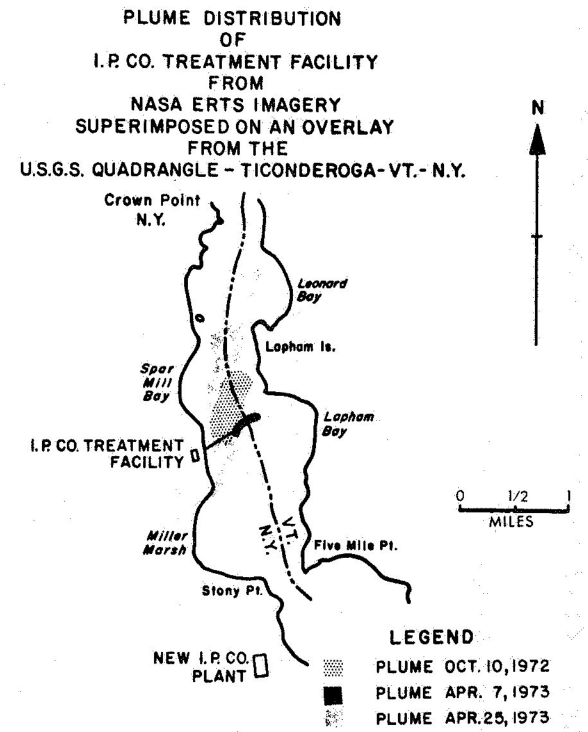

Fig. 2. A composite map of surface effluent patterns emanating from the IPC treatment plant based on three ERTS scenes. This composite was also entered as evidence in the pollution suit.

WATER POLLUTION

Water pollution in Lake Champlain is an especially significant environmental concern to the State of Vermont because it jeopardizes the vital resource qualities of the lake. The degradation of water quality by the International Paper Co. mill just north of Fort Ticonderoga, New York, has been the subject of intense interest by the State of Vermont, and as reported in an earlier symposium paper,[1] the State of Vermont is currently suing the paper company. The State of New York is also a defendant in this case now pending before U.S. Supreme Court Master, Ammi Cutter.

The application of ERTS data in the court action is directed toward delineating the extent of surface water degradation patterns. The relationship of these patterns to the interstate boundary and waters within the State of Vermont is of special concern. With the termination of the initial ERTS project in the early summer of 1973, three ERTS scenes had been studied which revealed the extent of papermill effluent associated with the submerged diffuser pipe extending from the mill's treatment plant.

The first plume of October 10, 1972 (Image No. 1079-15115) was described in earlier reports and has a somewhat oval shape oriented over the diffuser pipe which spreads the effluent linearly at first, but wind and current conditions may cause further surface spread of the effluent pattern. The linear pattern associated with the submerged diffuser was observed during a dye experiment conducted in October, and a more irregular spreading pattern was documented by conventional aerial coverage during the same month. On two occasions in April (1973) the southern arm of Lake Champlain was imaged by ERTS showing two additional patterns. A fairly widespread pattern was observed on April 25 (Image No. 1276-15073) and on April 7 (Image No. 1258-15073) a pattern essentially confined to the discharge pipe area was noticeable. While MSS band 4 proved to be the most useful single band for study of the plume area, multispectral combination of MSS bands 4, 5, and 6, was used to emphasize the plume patterns further.

---

[1]Lind, A., Henson, E. B., and Pelton, J., 1973. Environmental Study of ERTS-1 Imagery: Lake Champlain and Vermont, 2nd NASA ERTS Symposium, New Carrollton, Md.

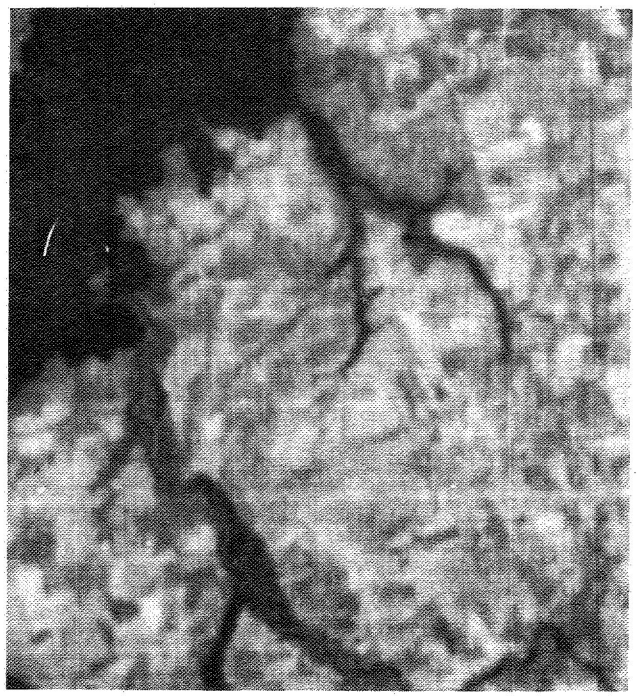

Fig. 3. Low water conditions of October 10, 1972 (lake level at 28.99 m.) in the Otter Creek-Dead Creek area of Addision County, Vermont. MSS band 6. Scale 1:125,000.

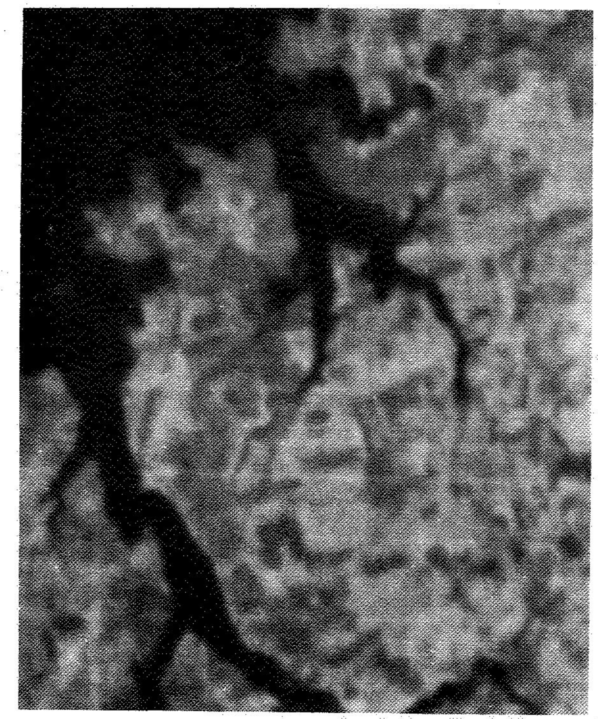

Fig. 4. Contrasting high lake level of April 7, 1973 (30.60 m.) (Scale 1:125,000) in the Otter Creek-Dead Creek area.

The three effluent patterns just described were mapped and overlayed on the USGS Fort Ticonderoga 15-minute quadrangle. This map and the ERTS imageries just described were presented as evidence by the State of Vermont before the special U.S. Supreme Court Master.[2] The imagery and composite plume map were accepted as evidence by the court, and this action therefore marks the first time that satellite imagery and satellite-derived information have been used as evidence in a court of law.

Additional ERTS imagery received just recently is expected to show additional effluent patterns. One example is provided in the August 30, 1973 (Image No. 1403-15111) scene.

LAKE FLOODING

A second major area of concern pertains to the spring flood cycle of Lake Champlain which has reached some record-breaking levels. Generally, lake levels in excess of 30 meters above mean sea-level results in flooding of low-land tracts containing agricultural and residential areas, as well as roads and wild lands. Flooding also occurs along the Richelieu River in Canada which drains Lake Champlain. For three consecutive years, high lake-levels have resulted in damages to flooded areas and the question of possible control of the lake level has been raised. The proposed project is currently under study by the U.S. Army Corps of Engineers, the International Joint Commission, and the Lake Champlain Committee. At this time, there is need for information on the location and extent of flooding. An examination of seasonal ERTS data reveals that an assessment of flooding is possible. Examples are provided for two lowland tracts, namely the Lamoille delta region in Chittenden County and the Otter Creek-Dead Creek area in Addison County. Contrasts between the low lake level of October 10, 1972 (28.99 m.) and the higher lake levels of April 7 (30.60 m.) and April 25 (30.30 meters) are clearly discernible on ERTS coverage in MSS bands 6 and 7. Mapping of shoreline positions is currently in progress on a scale of 1:62,500.

TURBIDITY AND LAKE ICE

Other limnological features of Lake Champlain which have been surveyed through ERTS include turbidity and lake ice.

---

[2]Presented on October 4, 1973, John F. Kennedy Federal Building, Boston, Massachusetts.

Fig. 5. Turbidity patterns at Chimney Point, Lake Champlain on an enlarged ERTS scene (band 4) during early spring (April 7, 1973). The smaller southern, turbid arm of the lake discharges into the larger main lake.

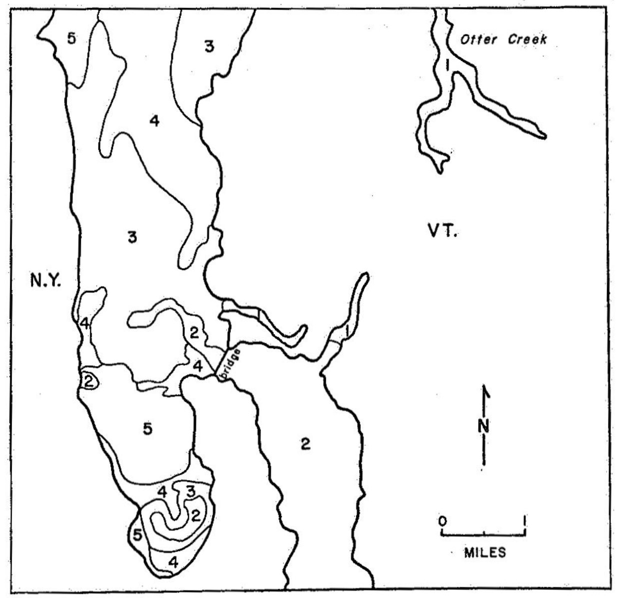

Fig. 6. Turbidity map derived from April 7, 1973, scene (Fig. 5). The following qualitative scale applies: 1. Extremely turbid; 2. Highly turbid; 3. Moderately turbid; 4. Slightly turbid; 5. Negligibly turbid. The relative turbidity is based on color/tone patterns from a multi-spectral viewer rendition of the scene.

Fig. 7. Ice development on Lake Champlain. The slightly enlarged scene from January 8, 1973, MSS band 5 imagery shows various ice types and the extent of open water covered with evaporation clouds,(bottom center).

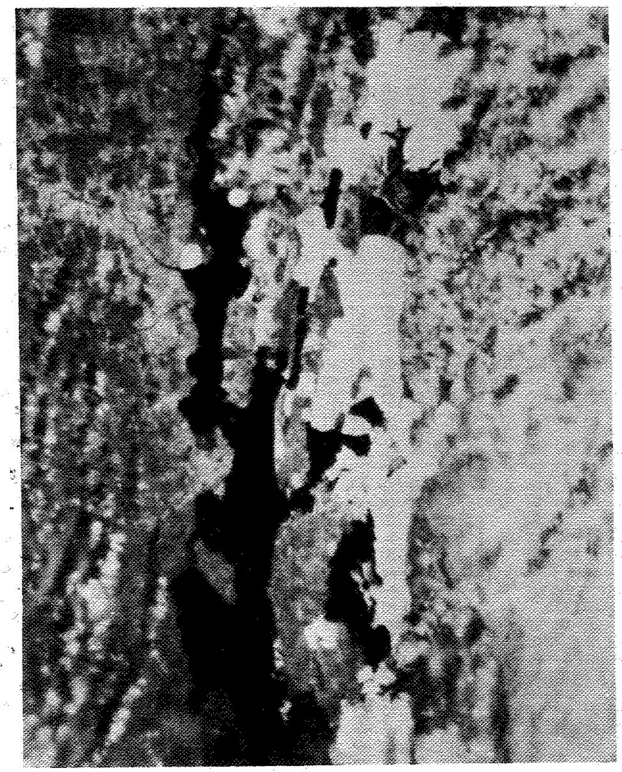

Fig. 8. The pattern of ice break-up as imaged on March 21, 1973, in the northern portion of Lake Champlain (MSS band 6). The remainder of the lake was cloud covered and no other opportunity was available for documenting this phase of lake ice history.

Turbidity patterns are readily seen on all good ERTS images and mapping of these patterns has been attempted in the lake's major turbidity boundary area where the southern turbid arm of Lake Champlain adjoins the clearer waters of the main lake. Other patterns of turbidity are also present and are associated with river and stream outlets or highly erodible shore tracts where emergent lacustrian silts and clays come under wave attack. The latter turbidity patterns appear to be indicative of the rate of shore erosion. ERTS has provided the first real opportunity to survey lake turbidity patterns in some detail and considerable variation in turbidity patterns has been observed. For example, a rather dramatic increase in turbidity extending much beyond expectations was observed in the July 7, 1973, coverage (Image No. 1349-15120). Extensive, heavy rains brought streams in the Champlain Basin to flood stages during the first week in July.

Lake ice, like turbidity, is readily observed on ERTS imagery, and comparisons of winter and spring scenes reveal the pattern of ice build-up and decay. As with turbidity, ERTS has provided a unique opportunity to document ice conditions in Lake Champlain. The detailed mapping of ice patterns is awaiting another freeze-thaw cycle since winter coverage scenes are incomplete. Suitable winter coverage is more difficult to obtain due to extensive winter cloudiness.

SUMMARY

ERTS imagery has significantly benefited both scientific analysis of Lake Champlain and the resource management concerns of the State of Vermont. Application of ERTS-derived data in the U.S. Supreme Court case of Vermont vs. International Paper Company and New York provides evidence for water pollution control. Mapping of seasonal lake flooding gives guidance to major domestic and international resource management agencies contemplating modification of the lake outlet to control lake level. Other, no less important practical applications of the ERTS experiment to limnology, include turbidity and lake ice which can be measured and assessed with satellite data. There is little doubt that the ERTS experiment has provided new dimensions to the study of Lake Champlain, and as long as ERTS is operational, additional perspectives will continue to be generated.

Paper W 13

A REAL TIME DATA ACQUISITION SYSTEM BY SATELLITE RELAY

Saul Cooper, *Chief, Water Control Branch, Department of the Army, New England Division, Corps of Engineers*

INTRODUCTION

The New England region, shown on plate 1, is comprised of several small watersheds, draining hilly terrain. With the high density population centers in the southern three states come the perennial problems of flood damage and flood protection. Because of the high development that has taken place along the main stem of our rivers since the industrial revolution and which has continued in recent years, nearly all our reservoirs are situated on tributaries where time of concentration and reaction time from rainfall to floodflows are short. The New England Division has constructed 35 reservoirs, 37 local protection projects and 4 hurricane barriers to provide not only flood protection but also some of the other multipurpose uses such as recreation, water supply and conservation. We have no storage allocated for power, irrigation or navigation.

In 1969, the New England Division, Corps of Engineers installed an Automatic Hydrologic Radio Reporting Network consisting of 41 remote reporting stations and controlled by a computer to help in regulating this system. It is automatically interrogated at regular intervals, the information is acted upon through several software routines and a complete printout of river stage, discharge, precipitation, etc. for all 41 stations is available in approximately four minutes. This system is shown on plate 2.

PURPOSE

In response to NASA's solicitation for proposals associated with ERTS experiments, we submitted one that was accepted. The overall aim of our experiments is to evaluate the future usefulness of satellites in the performance of coordination and management functions related to the operation of flood control and other multipurpose projects. Our experiments can be divided into two parts: (1) data collection and (2) imagery.

This paper concerns our results to date on the data collection portion

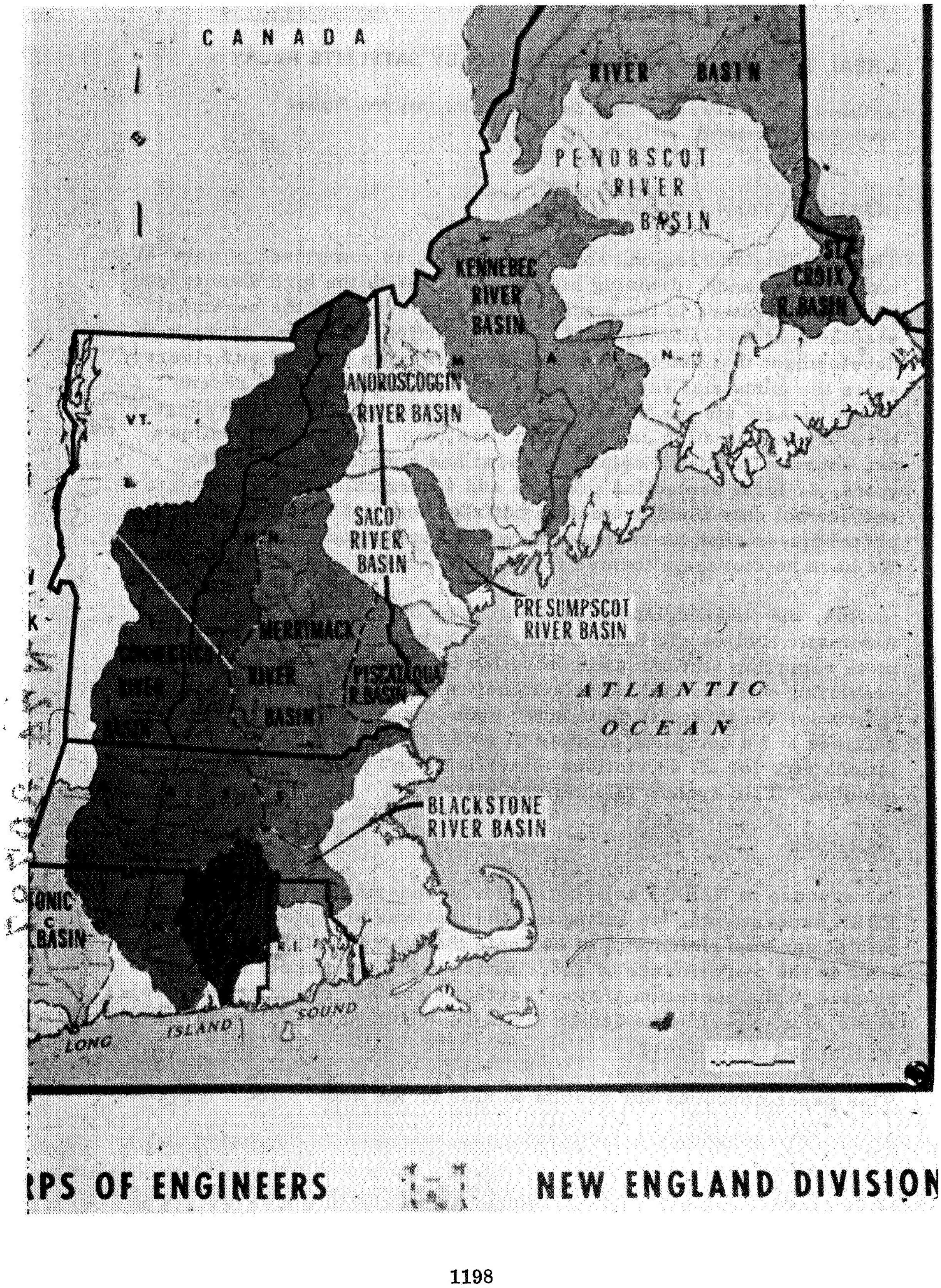

CANADA
RIVER BASIN
PENOBSCOT RIVER BASIN
KENNEBEC RIVER BASIN
ST. CROIX R. BASIN
ANDROSCOGGIN RIVER BASIN
VT.
SACO RIVER BASIN
PRESUMPSCOT RIVER BASIN
MERRIMACK RIVER BASIN
PISCATAQUA R. BASIN
RIVER BASIN
ATLANTIC OCEAN
BLACKSTONE RIVER BASIN
R.I.
LONG ISLAND SOUND
RPS OF ENGINEERS
NEW ENGLAND DIVISION

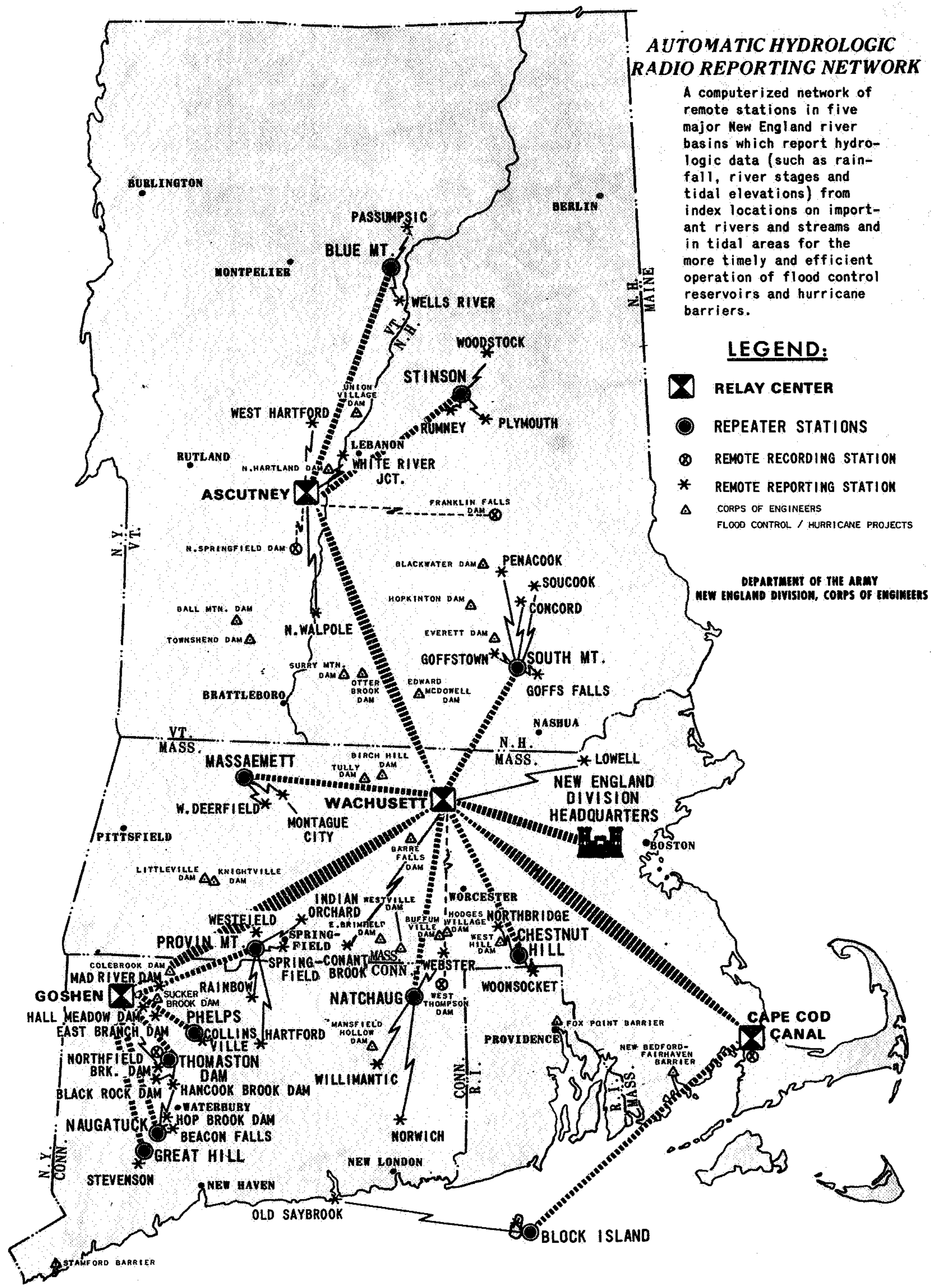
AUTOMATIC HYDROLOGIC RADIO REPORTING NETWORK
A computerized network of remote stations in five major New England river basins which report hydrologic data (such as rainfall, river stages and tidal elevations) from index locations on important rivers and streams and in tidal areas for the more timely and efficient operation of flood control reservoirs and hurricane barriers.
LEGEND:
RELAY CENTER
REPEATER STATIONS
REMOTE RECORDING STATION
REMOTE REPORTING STATION
CORPS OF ENGINEERS FLOOD CONTROL / HURRICANE PROJECTS
DEPARTMENT OF THE ARMY
NEW ENGLAND DIVISION, CORPS OF ENGINEERS
BURLINGTON
MONTPELIER
PASSUMPSIC
BLUE MT.
BERLIN
WELLS RIVER
VT.
N.H.
N.H.
MAINE
WOODSTOCK
STINSON
UNION VILLAGE DAM
WEST HARTFORD
RUMNEY
PLYMOUTH
LEBANON
RUTLAND
N.HARTLAND DAM
WHITE RIVER JCT.
ASCUTNEY
FRANKLIN FALLS DAM
N.Y.
VT.
N.SPRINGFIELD DAM
BLACKWATER DAM
PENACOOK
SOUCOOK
HOPKINTON DAM
CONCORD
BALL MTN. DAM
TOWNSHEND DAM
N.WALPOLE
EVERETT DAM
GOFFSTOWN
SOUTH MT.
SURRY MTN. DAM
OTTER BROOK DAM
EDWARD MCDOWELL DAM
GOFFS FALLS
BRATTLEBORO
NASHUA
VT.
MASS.
N.H.
MASS.
LOWELL
MASSAEMETT
BIRCH HILL DAM
TULLY DAM
NEW ENGLAND DIVISION HEADQUARTERS
WACHUSETT
W.DEERFIELD
MONTAGUE CITY
PITTSFIELD
BOSTON
BARRE FALLS DAM
LITTLEVILLE DAM
KNIGHTVILLE DAM
INDIAN ORCHARD
WESTVILLE DAM
WORCESTER
WESTFIELD
E.BRIMFIELD DAM
BUFFUM VILLE DAM
HODGES VILLAGE DAM
NORTHBRIDGE
WEST HILL DAM
CHESTNUT HILL
PROVIN MT.
SPRINGFIELD
SPRING-CONANT FIELD BROOK
MASS.
CONN.
WEBSTER
COLEBROOK DAM
MAD RIVER DAM
RAINBOW
WOONSOCKET
GOSHEN
SUCKER BROOK DAM
NATCHAUG
WEST THOMPSON DAM
HALL MEADOW DAM
PHELPS
FOX POINT BARRIER
CAPE COD CANAL
EAST BRANCH DAM
COLLINSVILLE
HARTFORD
MANSFIELD HOLLOW DAM
PROVIDENCE
NEW BEDFORD-FAIRHAVEN BARRIER
NORTHFIELD BRK. DAM
THOMASTON DAM
WILLIMANTIC
BLACK ROCK DAM
HANCOCK BROOK DAM
WATERBURY
CONN.
R.I.
R.I.
MASS.
NAUGATUCK
HOP BROOK DAM
BEACON FALLS
NORWICH
N.Y.
CONN.
GREAT HILL
NEW LONDON
STEVENSON
NEW HAVEN
OLD SAYBROOK
BLOCK ISLAND
STAMFORD BARRIER

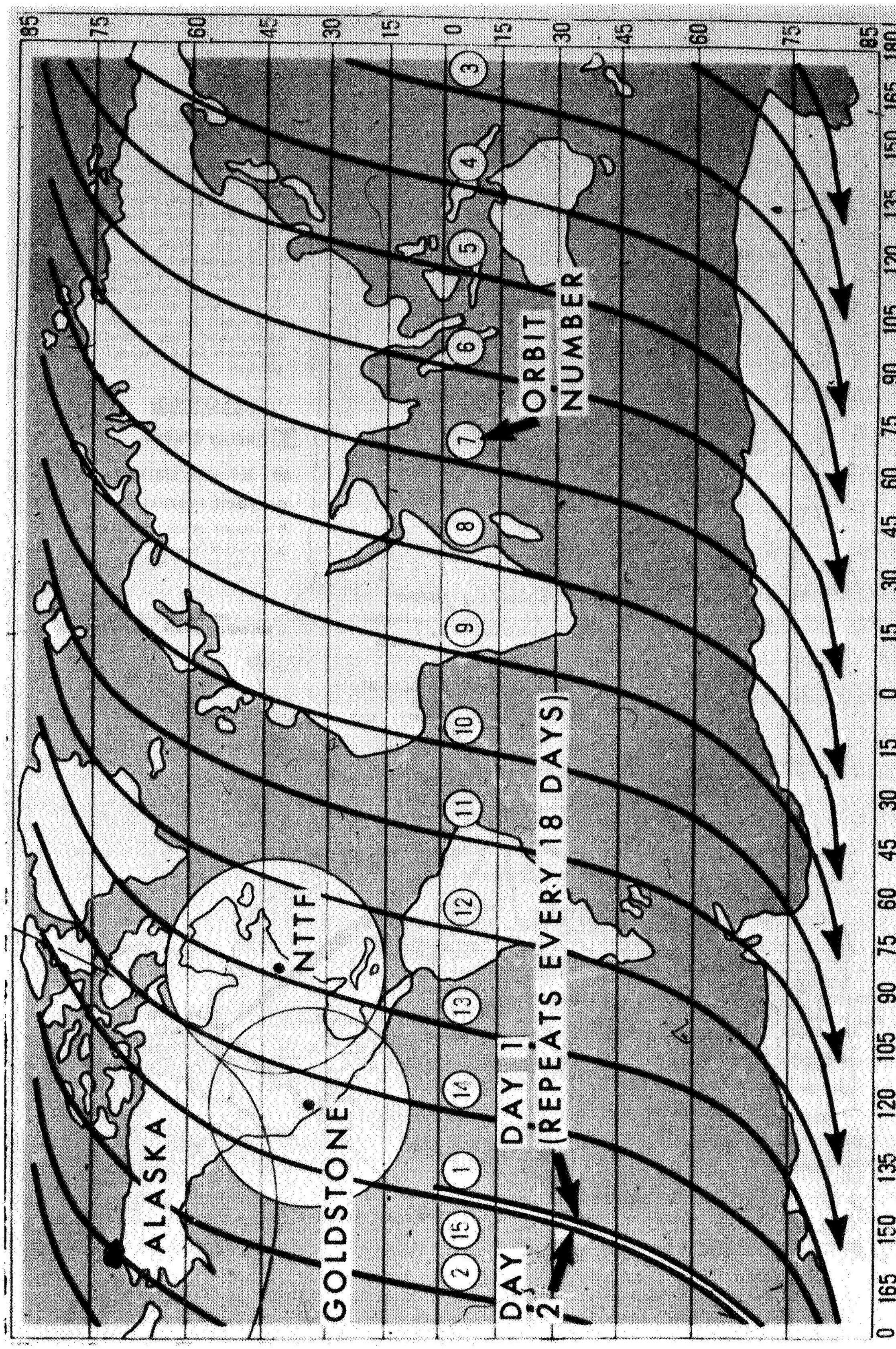

TYPICAL ERTS DAILY GROUND TRACE

ERTS-1 DATA REPORTING STATIONS

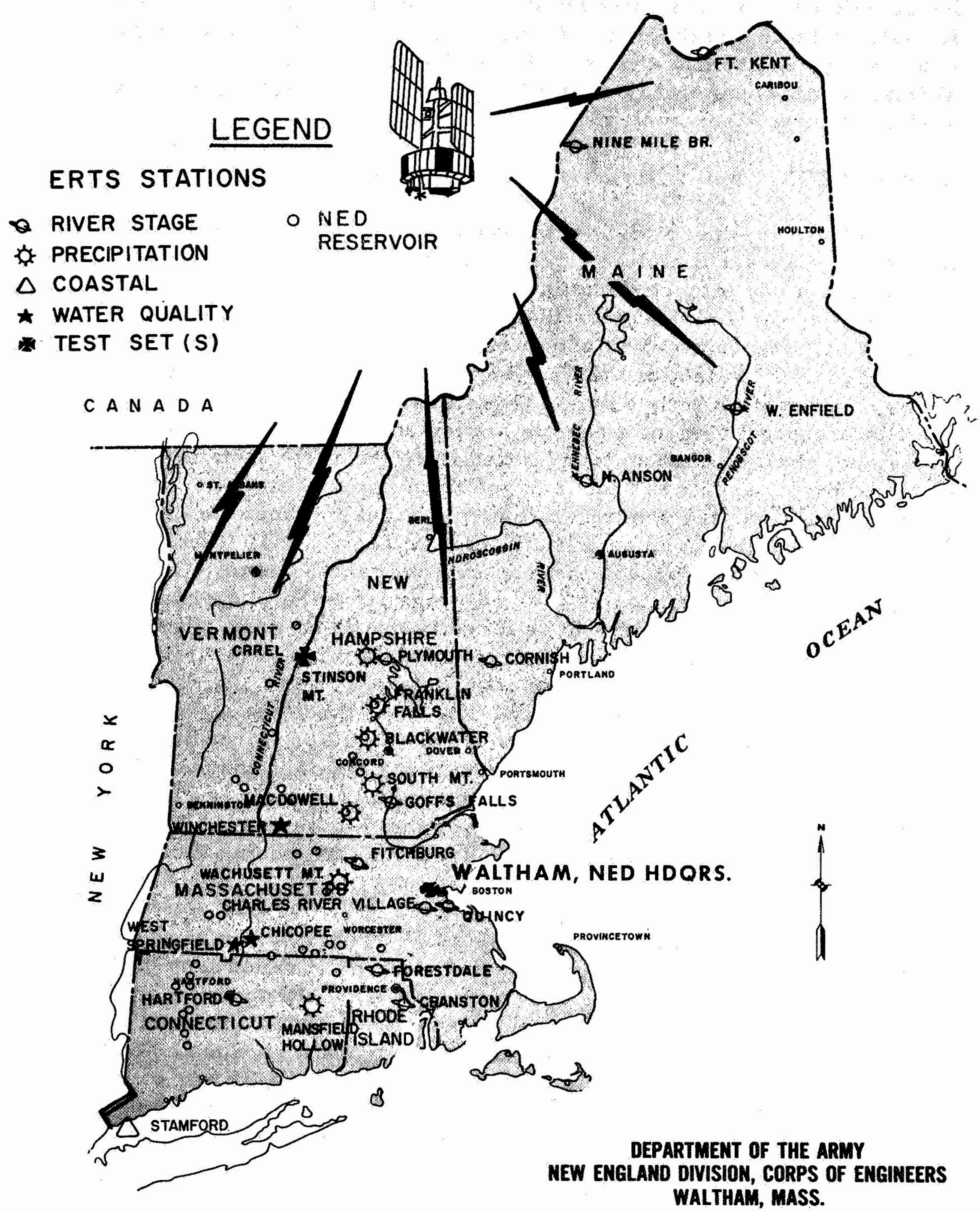

DEPARTMENT OF THE ARMY
NEW ENGLAND DIVISION, CORPS OF ENGINEERS
WALTHAM, MASS.
SEPTEMBER 1973

of our work. Our principal task is to develop statistics that demonstrate the relationship between conventional means of acquiring hydrologic data and the contribution made by using the satellite and its data collection platforms. We are interested in determining the availability, reliability and usability of the data. Of course, the ultimate acceptance or rejection of any such system will rely on its cost relative to other systems available.

DESCRIPTION

The satellite, in a near polar orbit about 547 nautical miles above the earth, makes a complete circuit every 103 minutes and 14 daylight orbits a day (depicted on plate 3). For the imagery portion of the experiment it is mandatory that the spacecraft maintain this exact positioning in order to obtain repetitive coverage every 18 days. For data collection, the spacecraft has to be in view and its antenna directed towards earth. Therefore, whenever the spacecraft is in mutual view of a remote station and either Goddard or Goldstone, the information transmitted from the remote station is received by the spacecraft and relayed to the ground station. In normal operation, the remote station continuously transmits data at 3-minute intervals. The satellite is in view for about 10 minutes between the times it appears and recedes over the horizon. During this period we can obtain up to four readings from the platforms. The spacecraft does not have to be directly overhead to obtain a reading. In addition, we normally receive data when the satellite is orbiting on the tracts immediately east and west of us. Therefore, during daylight hours we can receive data from three separate orbits with up to four readings from each orbit or a total of 12 readings per station. For imagery we are concerned about daylight passes because the cameras are only turned on during this period; but daylight passes over Russia are night passes over our region and the DCS is operational then too; therefore we also receive data during these orbits.

Twenty-seven platforms have been installed throughout the New England area from Fort Kent, Maine to Stamford, Connecticut (the locations of the platforms are shown on plate 4). Although the sites were selected to provide an overall assessment of environmental conditions throughout the New England area, many were located to provide operational data, and some to run in parallel with our own system. Initial platforms were installed in easily accessible locations so that maintenance, if required, would not become too

REAL TIME OPERATIONAL DATA COLLECTION SYSTEM FOR WATER CONTROL USING ERTS-A

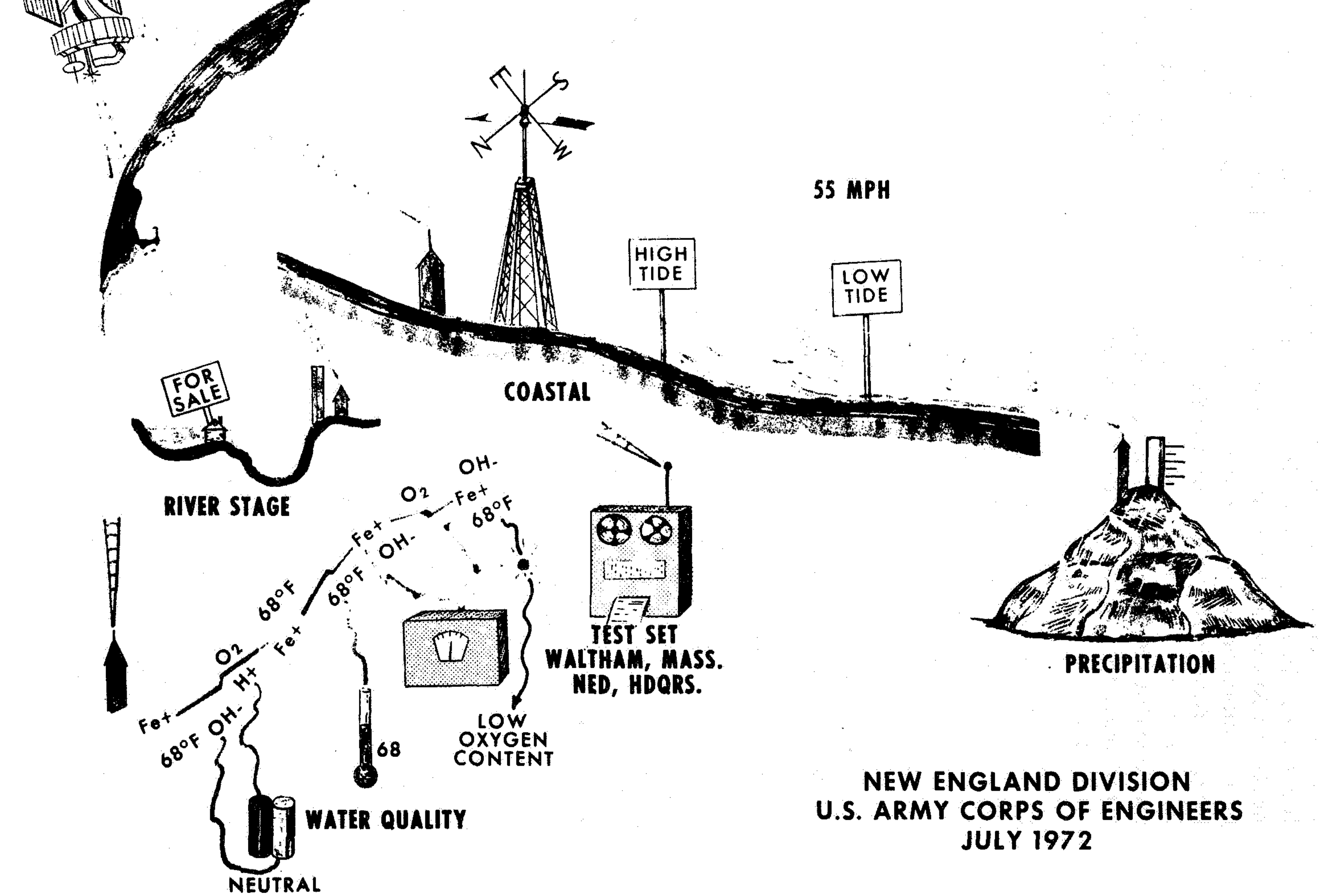

NEW ENGLAND DIVISION
U.S. ARMY CORPS OF ENGINEERS
JULY 1972

burdensome. However, operational experience indicated the equipment was reliable and other platforms were installed in more remote locations. In fact, in May 1973, we experienced record floods in northern Maine and one of the results of a meeting between officials from Canada and the United States was the establishment of a platform at Nine Mile bridge on the St. John River. This is the key index station for forecasting floodflows on the St. John and it is inaccessible during the spring runoff period. ERTS data will be supplied from that station to those responsible for flood forecasts and warnings.

Plate 5 shows the types of parameters being measured, i.e., precipitation, river stage, coastal (wind speed and direction), and water quality (temperature, dissolved oxygen, pH and conductivity).

RESULTS

We have attempted to address the basic questions of availability, reliability and usability. For availability we have used the 18-day ERTS cycle to determine the maximum number of reports possible for each station which is a measure of the field of view for the station. Table 1 shows the results for selected sites. Station to station differences are primarily due to effects of geography such as elevation, tree cover and interference from hills. The high mountain top stations have the best field of view while river stations in the valleys surrounded by high hills have the least. In many instances the platforms have been in view about 90 times during each cycle, or 5 times a day, with the single ERTS-1 satellite.

Due to the experimental rather than operational aspect of the study, DCP servicing has been assigned a low priority. This means that when a DCP failure occurs it may be a matter of weeks rather than days or hours before replacement or repair. Thus, the bias introduced decreases the statistical significance of the results. Perhaps the statistic that best measures DCP reliability is the percentage of good reports to total received. For the period January to June 1973, the average reliability was computed at 98.2 percent and is shown for selected sites on table 2. A report is considered good if it contains a confidence level of seven and any two consecutive messages did not differ by more than 0.2 unit.

MAINTENANCE

Table 3 lists the various types of failures that have occurred to the

TABLE 1

ERTS-1 DCP FIELD OF VIEW STATISTICS

LOCATION	TOTAL POSSIBLE REPORTS PER 18-DAY CYCLE
ST. JOHN R. @ FT. KENT, MAINE	86
PENOBSCOT R. @ W. ENFIELD, MAINE	90
CARABASSETT R. @ N. ANSON, MAINE	80
ANDROSCOGGIN R. @ AUBURN, MAINE	78 LEAST
SACO R. @ CORNISH , MAINE	83
PEMIGEWASSET R. @ PLYMOUTH, N.H.	81
MERRIMACK R. @ GOFFS FALLS, N.H.	88
ST. JOHN R. @ NINE MILE BR., MAINE	90
CHARLES R. @ CHARLES R. VILLAGE, MASS.	79
TOWN BRK. @ QUINCY, MASS.	83
PAWTUXET R. @ CRANSTON, R.I.	81
CONNECTICUT R. @ HARTFORD, CONN.	90
STINSON MT, N.H.	92 MOST
SOUTH MT., N.H.	90
FRANKLIN FALLS DAM, N.H.	89
MAC DOWELL DAM, N.H.	86
STAMFORD BARRIER @ STAMFORD, CONN.	90
ASHUELOT R. @ WINCHESTER, N.H.	82
N. NASHUA R. @ FITCHBURG, MASS.	87
WESTFIELD R. @ W. SPRINGFIELD, MASS.	81
CHICOPEE R. @ CHICOPEE, MASS.	88

TABLE 2

SUMMARY ERTS-1 DCS RELIABILITY STATISTICS (JANUARY-JUNE 1973)

TIME CYCLE	TOTAL NUMBER REPORTS RECEIVED	GOOD REPORTS	PERCENT GOOD÷TOTAL
1/1–1/18	782	771	98.6
1/19–2/5	699	691	99.0
2/6–2/23	663	657	99.0
2/24–3/13	743	734	98.8
3/14–3/31	736	725	98.5
4/1–4/18	825	811	98.3
4/19–5/6	800	786	98.3
5/7–5/24	732	718	98.1
5/25–6/11	758	723	95.5
6/12–6/29	764	753	98.6
	7,502	7,369	98.2

TABLE 3

SUMMARY ERTS-1 DCP FAILURES (THRU JUNE 1973)*

FAILURE	NUMBER OF OCCURRENCES
PROGRAMMER BOARD	5
TRANSMITTER BOARD	1
DIGITAL BOARD	4
FUSE	3
ANTENNA	1
ANTENNA CABLE	2
BATTERY	4
BATTERY CHARGER	2
SENSOR	3
	25

* COVERS 154 DCP-MONTHS, WHERE A DCP-MONTH IS EQUIVALENT TO ONE DCP OPERATING FOR ONE MONTH

platforms and periphery equipment. If we consider only NASA supplied equipment and neglect batteries, battery chargers and sensors then the total number of 16 equipment failures averages out to be one per 10 DCP months of operation. This is very low in comparison to our own automatic hydrologic radio reporting network.

USABILITY

For determining usability of the data, a questionnaire was forwarded to all Corps of Engineers offices requesting information on their present and future plans for automatic real time data collection. Results from this survey indicated that the total number of stations and parameters will not change significantly during the next five years. However, the indication was that almost all stations 4,000 plus or minus should be equipped to transmit in an automatic near real time mode in the near future.

At the present time most hydrologic data is transmitted by voice radio, telephone or teletype. Table 4 shows a comparison of present transmission methods versus the five year projection for automated near real time data collection.

The number of parameters measured will show a slight decrease based on the 5-year projection and this is shown in table 5 where the total number of parameters presently measured is 6,124 and the projected figure is 5,765.

A summary of how often information will be required from the sensors is presented in table 6 and this varies from over 1,450 instantaneous to 40 biweekly reports. Further information is needed to determine how important it may be to obtain real time instantaneous data versus hourly or 3-hourly values in a real time mode.

IMMEDIATE GOALS

Following is a list of our immediate goals:

a. Continuing the evaluation studies of ERTS data collection and imagery with a final report scheduled in August 1974.

b. Updating our ERTS-B proposal as necessary to keep it current.

TABLE 4

CORPS OF ENGINEERS QUESTIONAIRE
HYDROLOGIC DATA COLLECTION

TRANSMISSION

	TELEMARK	VOICE RADIO	TELETYPE AND TELEPHONE	NEAR REAL TIME	TOTAL
NUMBER OF EXISTING FIELD LOCATIONS	623	844	2347	46	3860
5 YR. PROJECTION FOR NEAR REAL TIME DATA	–	–	–	4177	4177

TABLE 5

CORPS OF ENGINEERS QUESTIONAIRE

HYDROLOGIC DATA COLLECTION

NUMBER OF PARAMETERS

	LAKE OR RIVER LEVEL	COASTAL	WATER QUALITY	PRECIPITATION	OTHER	TOTAL
NUMBER OF EXISTING STATIONS	1941	108	344	2230	1501	6124
5 YR. PROJECTION FOR NEAR REAL TIME DATA	2027	181	448	1845	1264	5765

TABLE 6

CORPS OF ENGINEERS QUESTIONAIRE
HYDROLOGIC DATA COLLECTION
TIMING (5 YEAR PROJECTION)

NUMBER OF PARAMETERS

PARAMETERS	CONT.	1 HR	2 HR	3 HR	6 HR	8 HR	12 HR	24 HR	WEEKLY	2 WEEK	TOTAL
RIVER OR LAKE LEVEL	753	497	79		244	325	23	106			2027
PRECIPITATION	310	430	36	351	240	17	100	361			1845
SNOW COVER	84	10	7		319			75	68		563
WIND SPEED &/OR DIRECTION	42	10				8		193			253
PRESSURE	10							16			26
OCEANOGRAPHIC DATA	87							94			181
AIR OR SOIL TEMPERATURE	10	55	3					190		20	278
AIR OR SOIL MOISTURE		65						49			114
WATER QUALITY DATA	154	49		3	8		1	187	26	20	448
EVAPORATION								10			10
SPILLWAY GATE OPENING		15									15
SOLAR RADIATION		5									5
TOTAL	1450	1136	125	354	811	350	124	1281	94	40	5765

c. Continuing our coordination at the working level with all user agencies in order to keep abreast of their requirements and programs.

d. Pursuing the acquisition of a direct downlink for data collection from ERTS. We consider this the next logical step in our evaluation of a complete satellite data relay system and we have submitted a proposal to NASA for participation with us in the establishment of a user acquisition station as a feasibility demonstration.

e. Determining unit costs for remote stations using ground based radio relay systems. We expect NASA to perform systems and cost analyses of dedicated satellite data collection systems for cost comparisons with other available systems.

SIGNIFICANT RESULTS

Significant results on DCS show that the DCP's are reliable and useful and satellite data collection appears feasible on a nationwide basis.

CONCLUSION

The Corps of Engineers is proud to have been selected as a participant in this experiment. We hope our input will help bridge the gap between the scientific and user community. By defining the Corps functional requirements we are assured that any future system, whether ERTS, GOES, or a separate satellite will contain the hardware to best satisfy our needs for automatic data collection.

Paper W 14

HYDROLOGIC APPLICATIONS OF ERTS-1 DATA COLLECTION SYSTEM IN CENTRAL ARIZONA

Herbert H. Schumann, *U. S. Geological Survey, Phoenix, Arizona*

ABSTRACT

The Earth Resources Technology Satellite (ERTS-1) Data Collection System (DCS) was used to relay hydrologic data (streamflow rates, precipitation amounts, soil and air temperature, and snow-moisture content) from remote sites in central Arizona to those responsible for reservoir management. Three U.S. Geological Survey streamflow gaging stations, 1 meteorological station and 2 snow-moisture content installations were equipped with ERTS-1 Data Collection Platforms (DCP's).

By mid-March 1973, the high moisture levels on the Salt and Verde River watersheds, reduced reserve reservoir storage capacity, and a large potential for flooding in the Salt River Valley presented a critical water management situation. Beginning on March 15, 1973, the ERTS-DCS was utilized to furnish near-real time information on snow-moisture content and streamflow rates to the Salt River Project for use in the management and operation of reservoirs on the Salt and Verde Rivers. The Salt River Project, aided by near-real time hydrologic data furnished by both microwave and ERTS-telemetry, was successful in predicting the volume of runoff into the reservoirs. Serious flooding in the downstream Phoenix metropolitan area was prevented by prudent water management.

INTRODUCTION

The inability to accurately measure or monitor rapidly changing moisture conditions over large and remote areas presents serious water-management problems in Arizona and other arid regions of the world. The lack of timely information on the distribution and amounts of precipitation, snow-water content, and streamflow rates cause vexing problems related to multiple-

use reservoir operations that can and have resulted in the loss of valuable water resources, caused millions of dollars worth of downstream property damage and even the loss of life.

The principal objective of the ERTS-1 Data Collection System (DCS) Experiment in Arizona is to test and evaluate applications of near real-time satellite telemetry of hydrologic data to assist in the management of Arizona's water resources. Six ERTS Data Collection Platforms (DCP's) are being used to relay information on streamflow rates, precipitation amounts, snow-moisture content, and air and soil temperatures from remote sites in central Arizona (fig. 1).

The Salt and Verde River watersheds include approximately 34,000 square kilometers (13,000 square miles) of central Arizona, range in altitude from about 400 to 3,900 meters (1,325 to 12,670 feet) above mean sea level, and receive from 25 to 65 centimeters (10 to 25 inches) of annual precipitation (fig. 1). Runoff from the Salt and Verde Rivers is regulated by six reservoirs that are operated by the Salt River Project. These reservoirs furnish hydroelectric power and municipal, industrial, and irrigation water to the Salt River Valley (the Phoenix area) of Maricopa County, Arizona (fig. 1).

UNUSUAL HYDROLOGIC CONDITIONS IN 1972-73

Winter precipitation was 60 and 100 percent above average on the Salt and Verde River watersheds respectively and produced record snowpacks according to the U.S. Soil Conservation Service (fig. 5). The 3.8 meters (150 inches) of snow measured at Mt. Ord on April 1, 1973 was the greatest snow depth ever measured in Arizona.

The record snowfall in central Arizona resulted in the largest amounts of streamflow recorded in the past 53 years on the Verde River and in the past 32 years on the Salt River. The Salt and Verde Rivers combined yielded more than 3.7 cubic kilometers (3 million acre-feet) of water.

HYDROLOGIC DATA COLLECTION

The DCS is being used to relay hydrologic information from remote sites in central Arizona (fig. 1). Three U.S. Geological Survey (USGS) streamflow gaging stations, two snow-moisture content installations (snow pillows), and one meteorological station have been equipped with DCP's (figs. 1, 2, and 3).

Streamflow Information

Three USGS streamflow gaging stations located on the Verde, Gila, and Black Rivers were equipped with digital water-stage recorders, modified for telemetry, and DCP's operating in the digital-parallel mode (fig. 1). These DCP's transmit stream stage information 4 to 5 times per day on the average (stream stage or gage height is the water surface elevation referred to some arbitrary gage datum) (fig. 4).

The DCS, operating in the parallel digital mode, is capable of furnishing significant amounts of streamflow information on a near-real time basis. However, the serial-digital DCS capability, currently under development by the USGS for transmitting streamflow data, should provide data of even greater utility for determining times of flood peaks and the rate of change of streamflow. The ability of the DCS to provide early warning of hydrologic sensor failure is an unexpected and significant benefit. On several occasions DCS-furnished information indicated water-stage recorder failures or other mechanical problems that saved many weeks of valuable streamflow record.

Snow-Moisture Content Information

The snow pillow, located at 2,225 meters (7,300 feet) above mean sea level on Baker Butte northeast of Bartlett Reservoir was equipped with a digital water-stage recorder with telemetry capability and a DCP by the USGS working in cooperation with the U.S. Soil Conservation Service and the U.S. Forest Service (fig. 1). The use of the ERTS DCS to relay snow-moisture content data from this installation is believed to be the first attempt at telemetry of snow data within Arizona (fig. 3).

OPERATIONAL APPLICATIONS

In addition to the DCP the Verde River streamflow gage was equipped with microwave telemetry by the Salt River Project (SRP). On Feb. 21, 1973 the microwave telemetry failed and the SRP requested streamflow information from this station on an emergency basis. The reservoirs on the Verde River were filled to within 95 percent of capacity and it had become necessary to release water to maintain sufficient reserve reservoir storage capacity to protect the downstream Phoenix metropolitan area from major flood damage. Using DCS data received from the NASA Goddard Space Flight Center by telephone, the USGS was able to furnish the SRP with the requested streamflow information within 26 minutes from the time of transmission to the ERTS-1 satellite.

By March 1, 1973, continued high moisture levels on the Salt and Verde River watersheds, reduced reserve reservoir storage capacity, and a large potential for serious flooding in the Salt River Valley presented a critical water management situation. On March 15, 1973, the SRP requested all available data from DCS equipped installations on their watersheds for use in the management and operation of their reservoir system. At the request of the USGS, these data were furnished by the NASA Goddard Space Flight Center directly to the SRP twice daily by telephone between Mar. 15 and May 22, 1973. Using a procedure developed by the USGS for rapid conversion of these DCS data into engineering units, SRP personnel were able to utilize DCS-furnished streamflow and snow-moisture content information operationally in near-real time.

The Salt River Project, aided by near-real time hydrologic data furnished by both microwave and ERTS-DCS telemetry, was successful in predicting the volume of runoff into the reservoirs. Flooding in the downstream Phoenix metropolitan area was prevented by prudent water management. This was accomplished although the watersheds of central Arizona produced the greatest amounts of streamflow recorded in recent years. Flooding did occur on about 810 hectares (2,000 acres) of agricultural lands along the Gila River west of Phoenix (fig. 6).

The large amounts of runoff from the Salt and Verde River watersheds filled the reservoirs and necessitated the release of more than 1.2 cubic kilometers (1 million acre-feet) of water, valued at more than $10,000,000, into the normally dry Salt River channel above the Phoenix metropolitan area. These releases of water caused the closing of many roads across the Salt River in the Phoenix area. These

road closings resulted in an estimated wage and salary loss of $11,000,000 according to the Maricopa County Civil Defense Agency. However, the number and duration of the closings were minimized in part by the utilization of ERTS DCS data.

FUTURE OPERATIONAL APPLICATIONS

Recent research in Arizona indicates that air temperature and precipitation data are needed in addition to snow-moisture content data to more effectively relate snowmelt rates and resultant runoff. Air temperature and precipitation sensors were incorporated in the new DCP equipped snow-water content installation that was established on the Black River drainage in eastern Arizona during the past summer (fig. 1). The Baker Butte snow-moisture content installation has also been equipped with air temperature and precipitation sensors.

During the summer of 1973, three DCP's were relocated on other USGS streamflow gaging stations to better monitor moisture conditions of the Salt and Verde River watersheds during the coming winter runoff season. The DCP from the Verde River gage was installed on the West Clear Creek gage to help study the relationship between runoff and snowmelt rates as indicated by the DCP equipped snow-moisture content site at Baker Butte in the upper West Clear Creek drainage (fig. 1). The DCP from the Gila River gage was relocated on the White River gage above the confluence with the Black River. The DCP from the upper Black River gage was installed on the Black River gage above the confluence with the White River (fig. 1). These gages record about 85 percent of the runoff into the Salt River.

Future plans also include the development of a data handling procedure to furnish water management with near-real time DCS data that has been converted into engineering units. The DCS data will be converted into engineering units by the USGS computer system in Washington, D.C. and will be received in Arizona through a small computer terminal.

SUMMARY AND CONCLUSIONS

The DCS is capable of furnishing significant amounts of hydrologic information on a near-real time basis. The ability of the DCS to furnish early warning of hydrologic sensor failure is an important benefit that can assist in the management of hydrologic data networks and prevent the loss of valuable hydrologic record.

The DCS was utilized to furnish near-real time information on snow-moisture content and streamflow rates to the Salt River Project for use in the management and operation of reservoirs on the Salt and Verde Rivers between Mar. 15 and May 22, 1973. The Salt River Project, aided by near-real time hydrologic data furnished by both microwave and DCS telemetry, was successful in predicting the volume of runoff into the reservoirs. Serious flooding in the Phoenix metropolitan area was prevented by prudent water management.

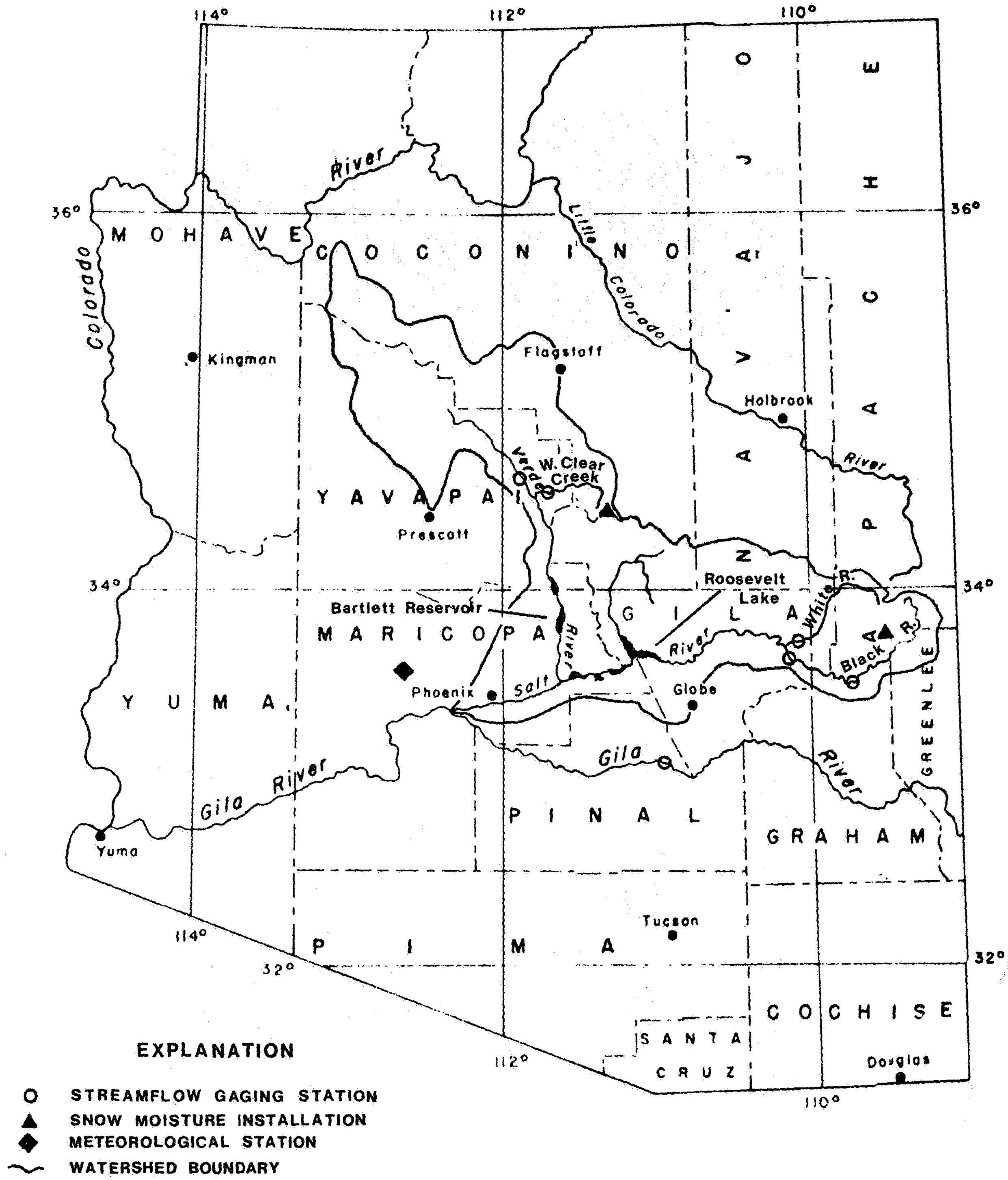

FIGURE 1. --- LOCATION OF ERTS DATA COLLECTION PLATFORMS AND SALT AND VERDE RIVER WATERSHEDS, ARIZONA

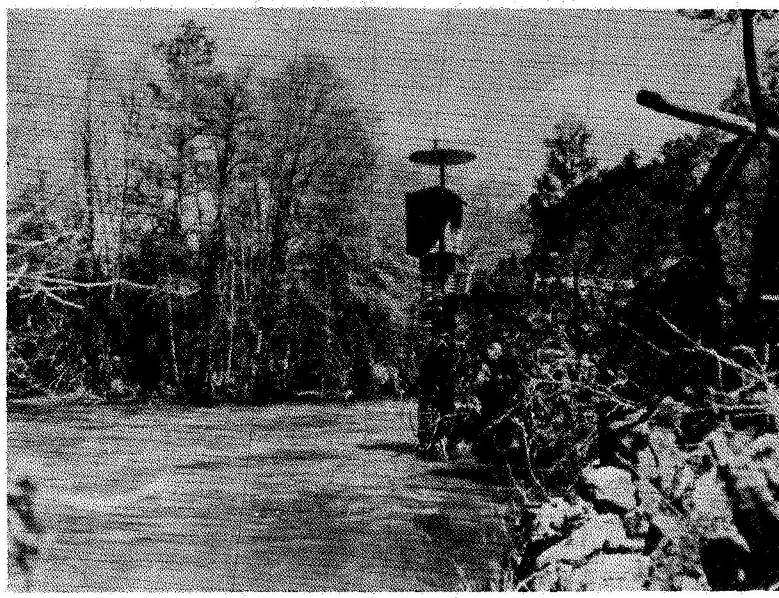

Figure 2. Black River Steamflow Gaging Station Near Point of Pines, Arizona Equipped with ERTS Data Collection Platform

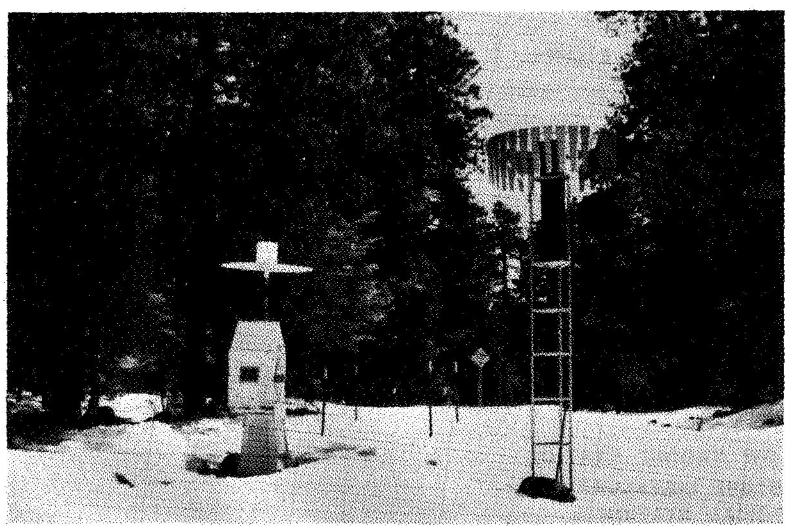

Figure 3. Snow Pillow at Baker Butte, Arizona Equipped With ERTS Data Collection Platform

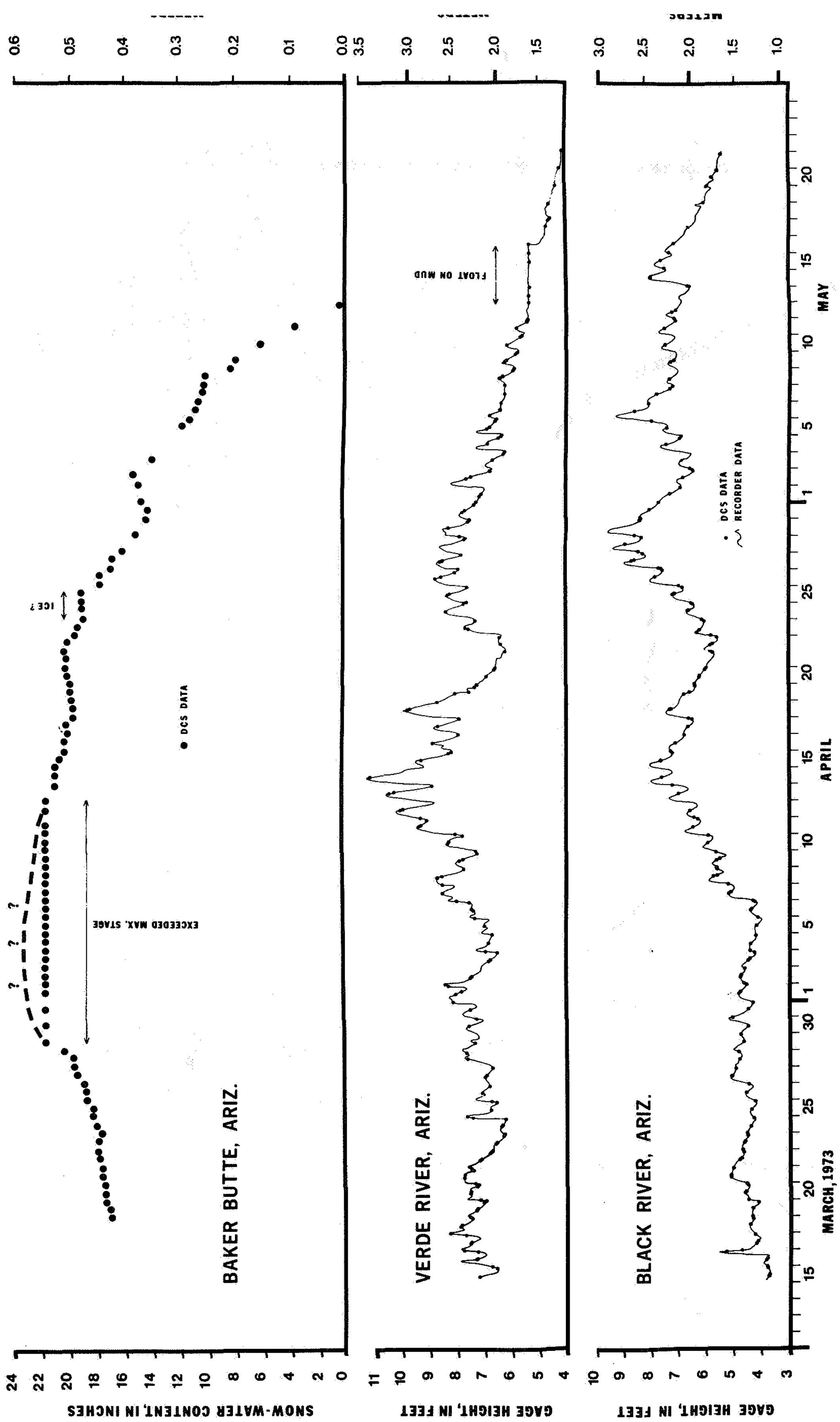

FIGURE 4.—STREAM GAGE HEIGHTS AND SNOW-WATER CONTENT

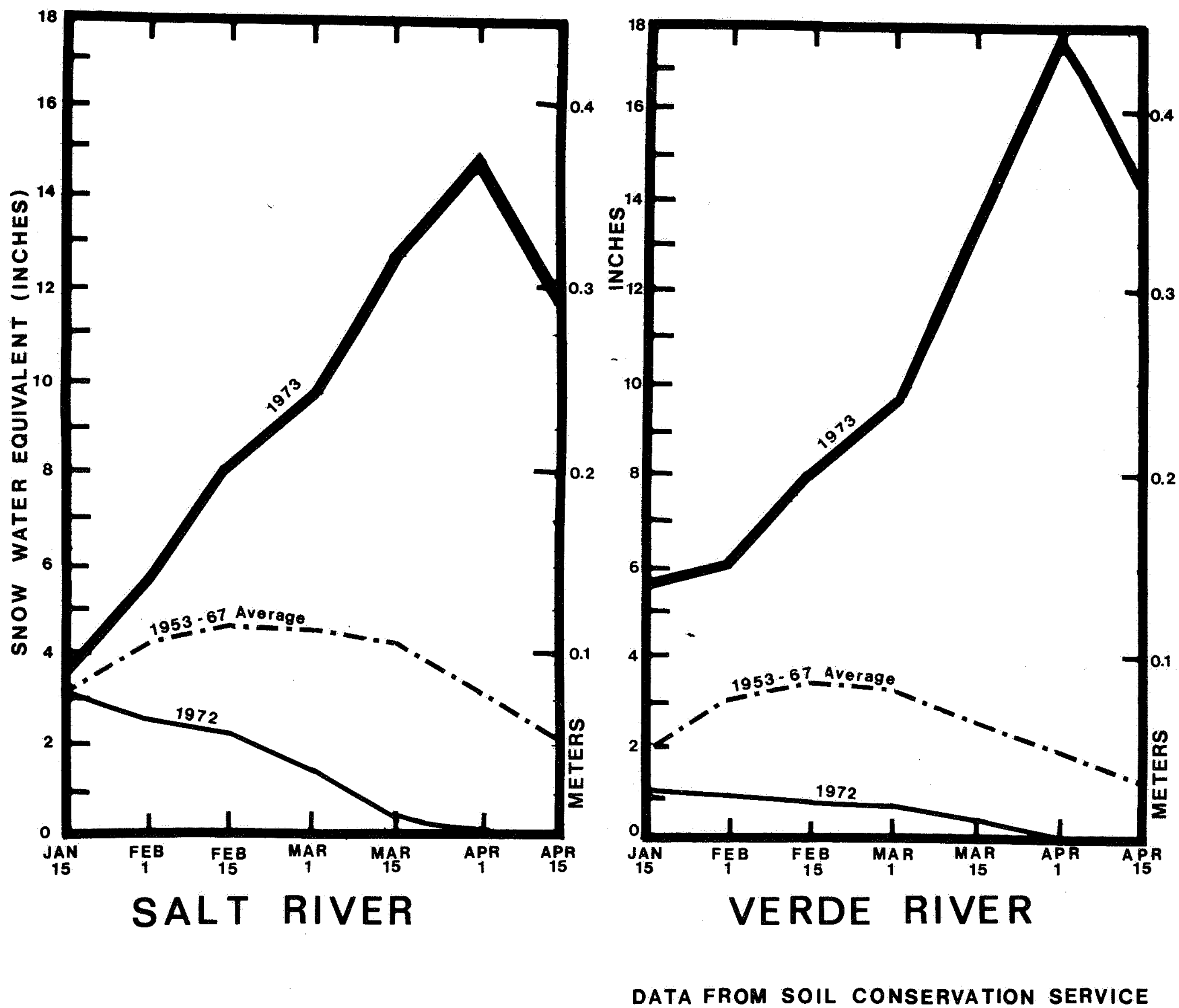

FIGURE 5. — SALT AND VERDE RIVER WATERSHED SNOW-WATER EQUIVALENTS

Figure 6. ERTS-1 Image E-1283-17334-7 Showing Major Reservoirs and Rivers in Central Arizona

Paper W 15

APPLICATIONS OF ERTS DATA TO COASTAL WETLAND ECOLOGY WITH SPECIAL REFERENCE TO PLANT COMMUNITY MAPPING AND TYPING AND IMPACT OF MAN

Richard R. Anderson, Virginia Carter,, John McGinness, *Department of Biology, The American University, Washington, D. C.*

ABSTRACT

Complete seasonal ERTS-1 coverage of Atlantic coastal wetlands from Delaware Bay to Georgia provides a basis for assessment of temporal data for wetland mapping, evaluation, and monitoring. Both MSS imagery and digital data have proved useful for gross wetland species delineation and determination of the upper wetland boundary. Tidal effects and (band to band or seasonal) spectral reflectance differences make it possible to type vegetatively coastal wetlands in salinity related categories. Management areas, spoil disposal sites, drainage ditches, lagoon-type developments and highway construction can be detected indicating a monitoring potential for the future.

A northern test site (Maryland-Virginia) and a southern test site (Georgia-South Carolina), representing a range of coastal marshes from saline to fresh, were chosen for intensive study. Wetland maps were produced at various scales using both ERTS imagery -- bands 5 and 7 -- and digital data -- bands 4, 5 and 7. A Bausch and Lomb Zoom Transfer Scope and various overlay techniques were used with either 9-1/2" black and white transparencies or enlarged black and white prints. Diazo color composites, color enhancement techniques, and multi-spectral manipulation were used to supplement this information.

Data will be useful for coastal wetland inventories, updating acreage estimates, mapping boundaries, detecting seasonal changes, detecting and monitoring man's impact. Resolution limitations allow for mapping to a 1/125,000 scale.

Results are being applied directly to a Dismal Swamp study with U.S. Geological Survey. There is potential application to on-going programs in Georgia and South Carolina and to the Coastal Zone Management Act and a National Wetlands Law.

INTRODUCTION

During the last five years there has been established a clear need for development of a rapid, relatively low cost method for mapping and monitoring coastal wetlands. This period has been one of unprecedented activity by state governments to preserve this sensitive and threatened aquatic ecosystem. Laws regulating the types of activity in wetlands have been passed in almost all Atlantic coastal states. To implement this wetland legislation, coastal wetland mapping efforts have been initiated which utilize a variety of methods. New Jersey, Maryland and South Carolina have been among the most active users of remotely-sensed data as a wetland mapping tool. The New Jersey program (conducted by Anderson and Earth Satellite Corporation) is the most ambitious and will soon complete mapping all the state's coastal wetlands to national map accuracy standards using low altitude color infrared photography. However, this technique is too expensive for many states to use on a routine basis.

The recently passed Coastal Zone Management Act and the proposed National Wetlands Law (H.B. 139) are indicative of increasing awareness within the federal government of the need to protect coastal resources. It may soon be necessary to map and monitor wetlands on a national scale.

With the launch of ERTS-1 in July, 1972, repetitive satellite data first became available for the investigation of earth resources. This research was initiated to determine the feasibility of using these data to monitor and map coastal wetland phenomena. The broad objectives/goals of the research were as follows: Test the usefulness of ERTS data for (1) delineation and mapping of coastal wetlands communities and boundaries; (2) identification of wetland type for management and maintenance of dependent wildlife populations; (3) monitoring of wetlands for natural and man-made reductions in productivity and (4) mapping of shallow waters. The first three objectives have been met using ERTS data. The fourth has not received sufficient experimentation due to high water turbidity in the test sites.

The general study area includes coastal wetlands from Maryland to Georgia. Two principal test sites were established for intensive use of ERTS data. These were in the Chesapeake Bay (Fig. 1) and portions of the coast of South Carolina and Georgia (Fig. 2). For detailed discussion of the vegetational characteristics of these areas reference should be made to a previous paper by the authors (1).

The authors are particularly indebted to the NASA aircraft support programs operated from Ames Research Center, California, and the Johnson Spacecraft Center, Texas. Underflight data have been invaluable as interpretive aids for the ERTS imagery.

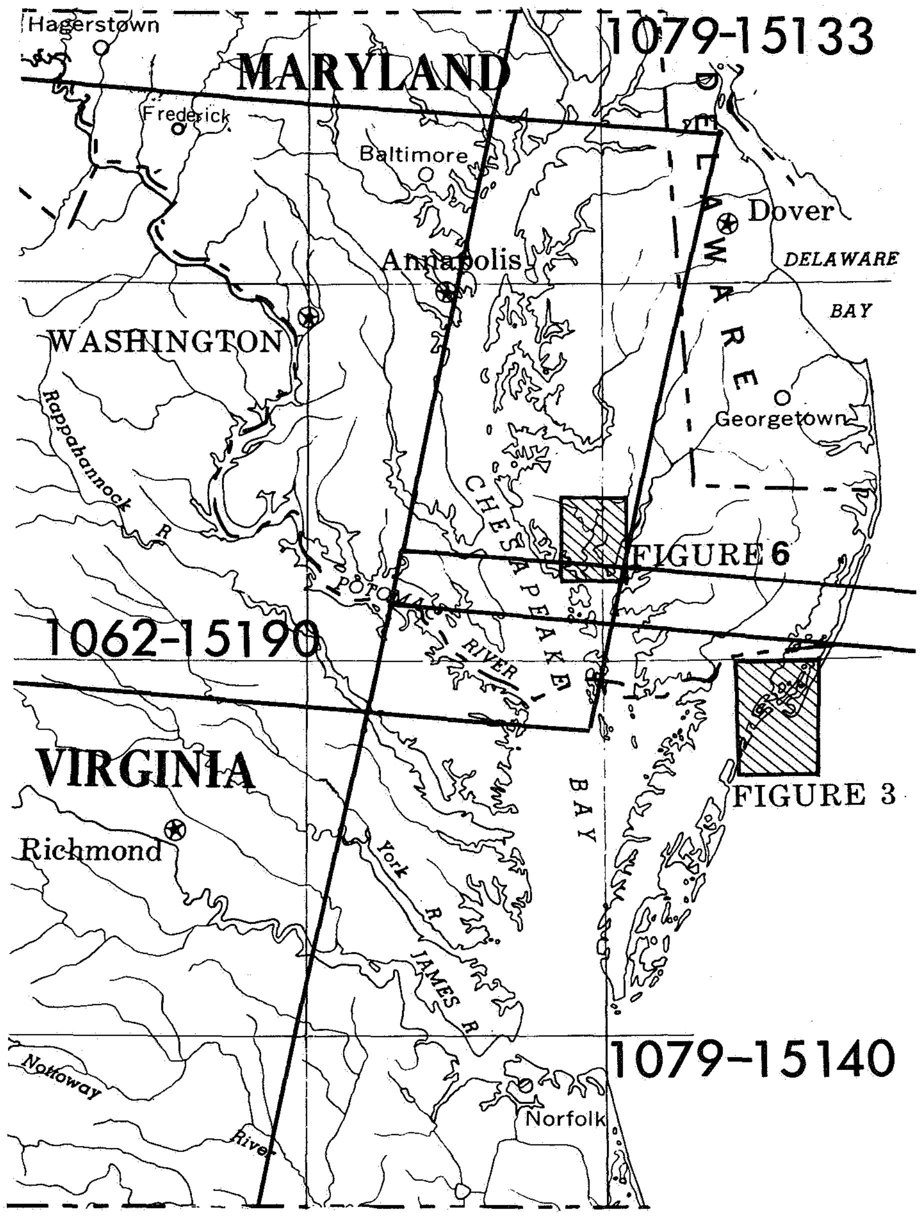

Figure 1. Map Showing location of Chincoteague (Figure 3) and Nanticoke (Figure 6) test sites.

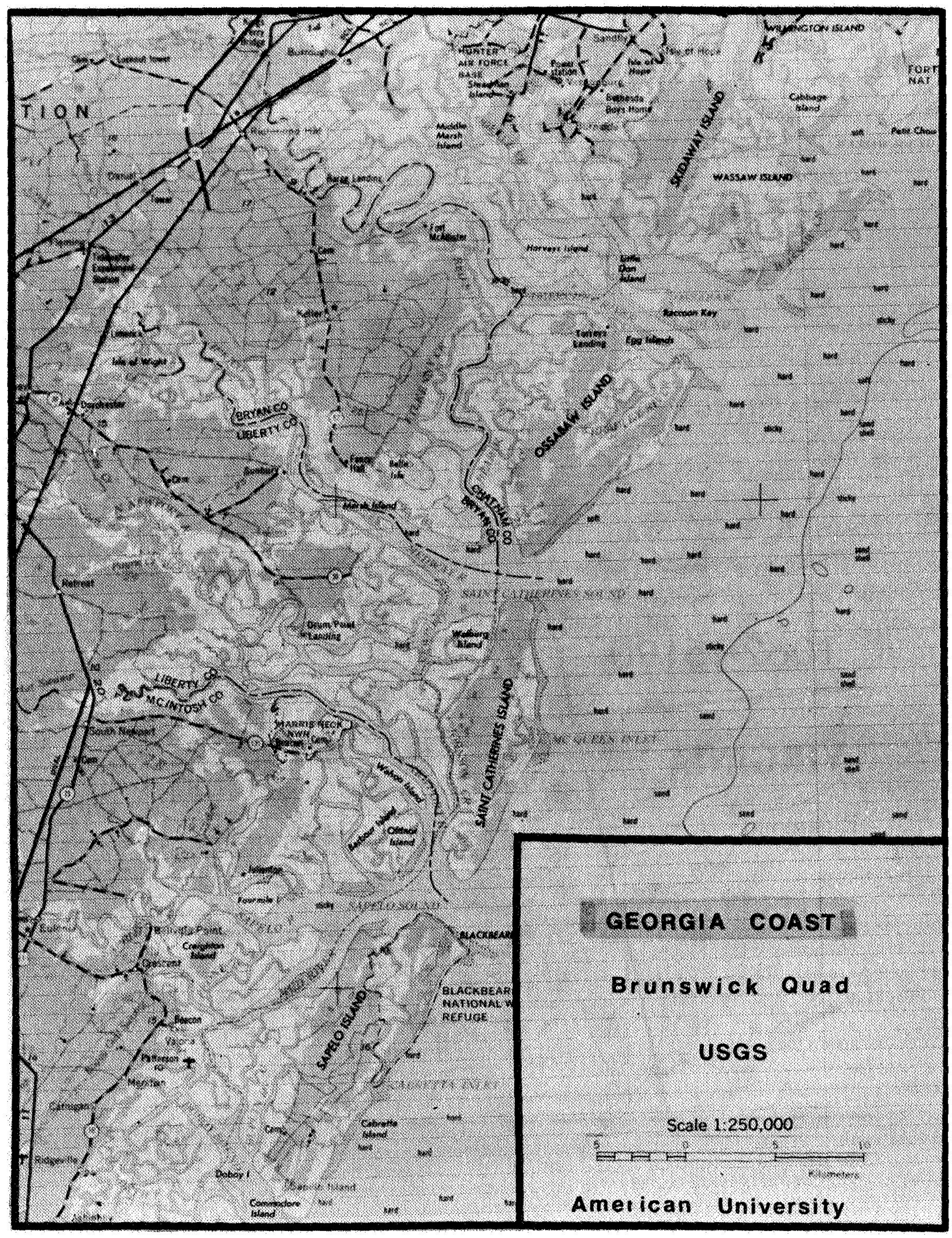

Figure 2. Georgia Test Site

RESULTS OF THE STUDY

I. ERTS Data Interpretation

a. Techniques.

ERTS positive transparencies at a scale of 1:1,000,000 have high resolution and excellent contrast. The film density of coastal wetlands is quite high, especially in MSS 7, making the wetland/upland boundary quite distinct except in tidal freshwater wetlands. MSS 7, supplemented by MSS 5, has proved most useful for preparation of wetland maps by visual interpretation methods using imagery as received. A combination of winter/summer imagery makes it possible to map the upper wetland boundary in tidal freshwater wetlands.

Processing techniques at Goddard Space Flight Center favor the more highly reflective upland features. For this reason special dark room processing has been used to produce negatives and prints favoring interpretation of saline wetland species composition and the land/water interface. Most detail in the uplands is lost at the level of over-exposure needed to map the extent of species like *Spartina alterniflora* which have a large quantity of background water.

A number of data enhancement techniques have been investigated for their usefulness as interpretive aids and for possible automatic interpretation and mapping of wetlands. These techniques are discussed briefly below:

1. Diazo color composites: Color composites using three MSS bands, either standard 1:1,000,000 imagery or enlarged positive transparencies, have been prepared using this inexpensive and rapid technique. Registration of bands is laborious and at times difficult, but the resulting composites successfully enhance selected features.

2. Density slicing: Both Datacolor and Interpretation Systems Incorporated have been used for single band density slicing. These systems have a capability for area measurement which could be extremely useful. However, the ability of these systems to supply area measurements is dependent upon isolation of the feature of interest in a single band. Density slicing is a subjective process and the user must interact with the system to achieve the most effective enhancement of the data.

3. Multispectral analyses: The EROS program has developed an Autographic Theme Extraction System (ATES) located at the EROS Data Center in Sioux Falls. Binary theme extractions from ATES have been used to interpret ERTS imagery of the Dismal Swamp. There are some indications that an automated system will be able to extract coastal wetlands as an isolated theme. One of the system components -- the Multispectral Image Analysis System -- is a versatile machine which combines and displays several ERTS bands simultaneously. Composites may be made from density-sliced bands or positive-negative combinations.

Registration is tedious and there is very little magnification available since the machine is intended to supply basic information to a photographic system.

Some work has been done using the Stanford Research Institute's ESIAC; but while the analysis of seasonal or temporal data is of interest to us, our output from the system is not quantitative. The 2 band ratioing capability of the system is presently under investigation.

In addition to imagery, a limited quantity of ERTS digital data have been analyzed using the ERTS_ANALYSIS SYSTEM (2) developed by J. Schubert at Goddard Space Flight Center (NASA). The system accesses ERTS-CCT's directly and produces a geographically referenced printer-plot map of analyzed data at a scale of 1:20,000. A marsh vegetation analysis algorithm for use with this system was developed from ISCO field spectral reflectance measurements and ground truth data.

b. Effects of tidal stage and season on image interpretation.

1. Tidal stage: Images taken over the Georgia coast, Ossabaw Island area, on different dates were analyzed for effects of tidal height on imagery interpretation in wetlands. In addition, ERTS images and U-2 photography from different dates over Charleston, S.C., area were examined to check the interpretation of the Georgia images and to examine tidal effects in the upper reaches of tidal rivers. The approximate time of imagery relative to high or low tide, tidal height above mean low water and tidal range were calculated using the *Tide Table, High and Low Water Predictions for East Coast of North and South America*, 1972 and 1973, published by NOS (NOAA).

Figure 3 is an MSS 7 image of the Ossabaw Island test site on the Georgia Coast taken at low tide. Drainage patterns are very clear and a high berm or levee where mud flat and plant species *Borrichia frutescens* and *Spartina alterniflora* predominate, can be resolved. Separation and delineation of major species associations is difficult at this tidal stage.

Figure 4 is an MSS-7 image of the same area taken at high tide. The berm area ("C") is discernable and species separation is easier than in the image taken at low tide. There is good differentiation between low growth and high growth forms of *Spartina alterniflora*. The areas of high growth *S. alterniflora* occur at creek-side and creed-end and are light in tone. Low growth forms of *Spartina alterniflora* occur on higher ground, but grow so sparsely that the water background affects scene reflectance. Areas containing predominantly *Juncus roemarianus* can be separated from those containing predominantly *Spartina alterniflora* at this tidal stage since an overall light reflectance is characteristic of *Spartina alterniflora* areas where large amounts of background water are present. Fresher marshes containing *Spartina cynosuroides* and associated species have a higher reflectance than the more brackish *Juncus* marshes and may also be separated on this image. The upper wetland boundary is difficult to delineate inland because of the high reflectance of fresh water species.

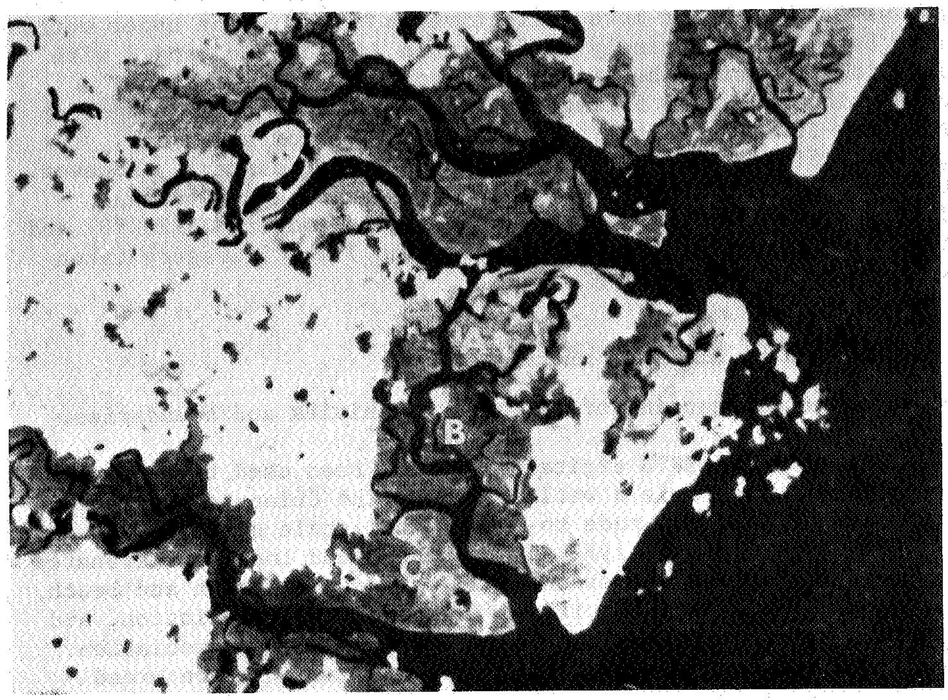

Figure 3. 1010-15322-7, Aug. 2, 1972, Low Tide

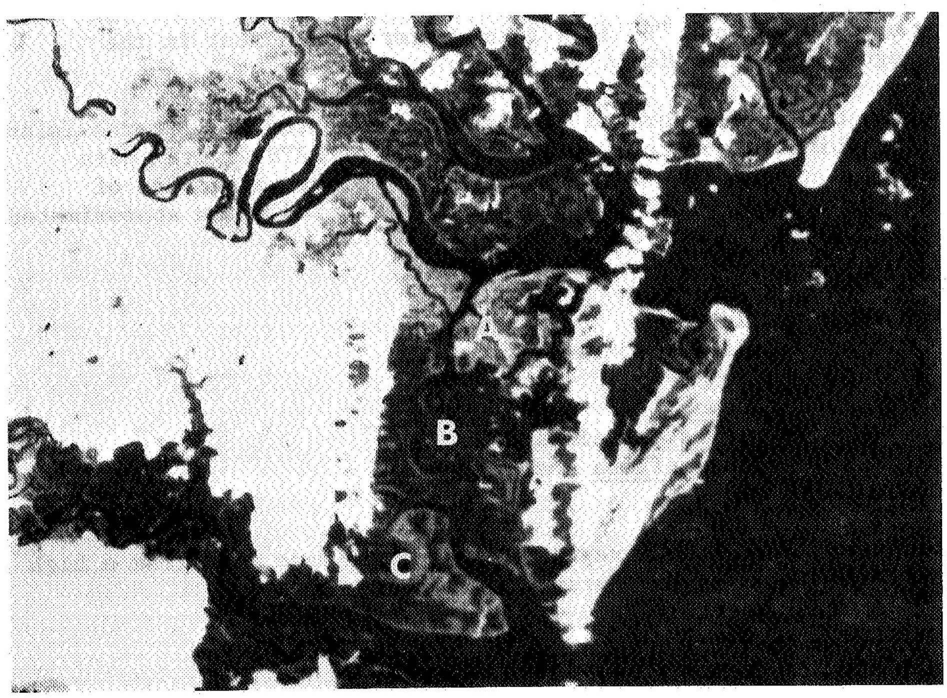

Figure 4. 1046-15324-7, Sep. 7, 1972, High Tide

Ossabaw Island, GA showing A. Juncus roemarianus, B. Spartina alterniflora, and C. Berm.

2. Season: Seasonal change is not a critical factor in interpreting saline wetlands once growth of all species has begun. However, as the water becomes fresher, the species mixture becomes more complex and the vegetative cover more reflective in the IR. The upper wetland boundary becomes increasingly difficult to identify in band 7 with distance inland during the growing season. Supplementing the interpretation with band 5 imagery aids delineation since the marsh shows a grey-level reflectance distinguishable from spoil and agricultural fields (lighter) and water or woods (darker). However, the best method using B/W imagery is to delineate upper wetland boundaries on band 7 of winter or early spring imagery (3/23/73) and to attempt species discrimination using band 7 and 5 imagery taken midway to late in the growing season.

II. Achievement of Research Objectives

a. Delineation and mapping of wetland communities and boundaries.

Both ERTS imagery and ERTS digital data have been used to accomplish this objective. Fig. 5 is a wetland map of the Chincoteague salt marsh complex in Virginia made to an original scale of 1:250,000 using MSS 7 (1079-15140 Sept. 7, 1972) and a Bausch and Lomb Zoom Transfer Scope. Four categories are shown: (1) upland vegetation and beach, (2) water, (3) *Spartina alterniflora*/*Salicornia* sp. association, and (4) *Spartina patens*/*Distichlis spicata*/*Iva frutescens* association. The upper wetland boundary is generally sharp except where broad transition zones exist. The marsh-water interface is sometimes difficult to determine in areas interlaced with numerous small tributaries or sparse patches of vegetation. "A" is an accreted area of sand and marsh not shown in the USGS 1:250,000 map published in 1946. "B" and "C" are spoil areas and "D" is a fresh water impoundment in the Chincoteague Wildlife Refuge.

Fig. 6 is a computer-generated vegetation map of the small marsh island within the Chincoteague test area. Analysis of ERTS digital data makes maximum use of grey-level resolution. Eight categories of marsh vegetation and marsh features were identified at an approximated scale of 1:20,000. These categories are:

1 - water
- sandy mudflat
/ organic mudflat, sparsely vegetated
_ spoil
I *Iva frutescens*
P *Spartina patens* association
A *Spartina alterniflora* association
? unidentified

For comparison, Fig. 7 is a reproduction of the same area from a high altitude color infrared photograph.

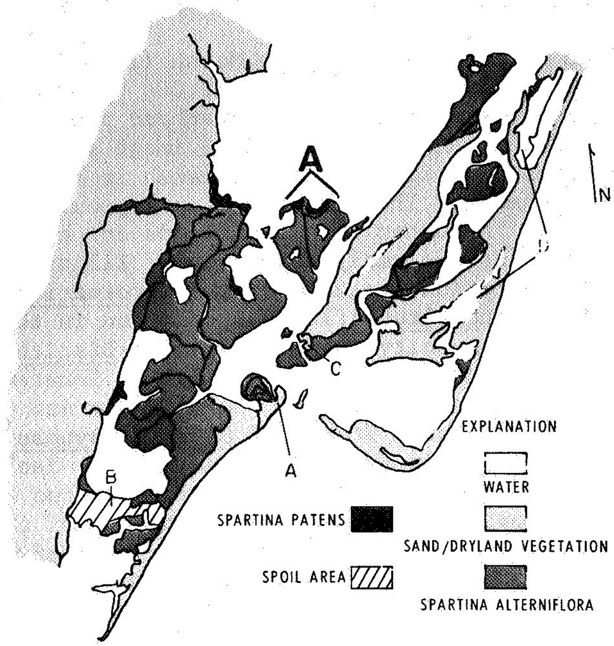

Figure 5. Wetland Map of Chincoteague Marsh

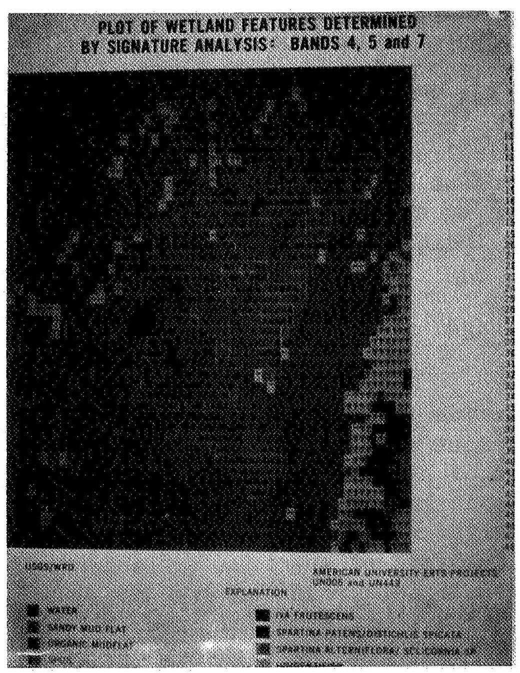

Figure 6. Computer Generated Map of Area A

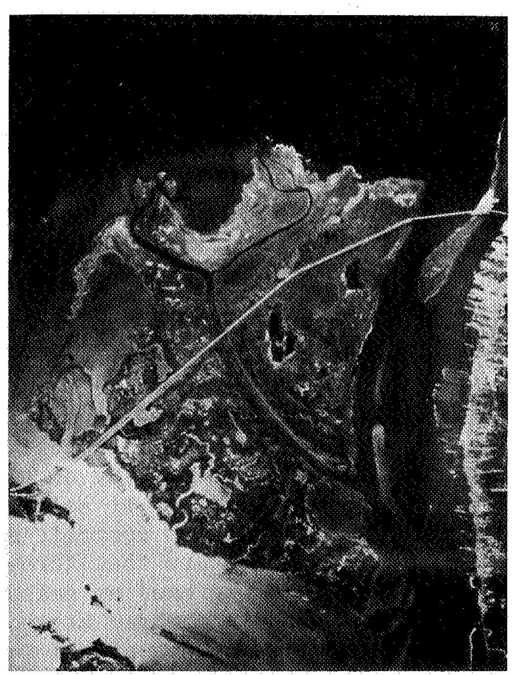

Figure 7. Color IR Aerial Photo of Area A

Refinement of the signature analysis algorithm should improve the mapping capability and allow extrapolation to other salt marshes with similar vegetative associations. Those along the Atlantic Coast and in other countries such as southern England would be prime candidates.

Fig. 8 is a wetland map of the Nanticoke Marsh (1079-15133, MSS7, Oct. 10, 1972) made at an original scale of 1:250,000 by overlaying the 1:1,000,000 scale image enlarged with an overhead projector. Fig. 9 is an enlargement of the same area from ERTS image # 1349-15134-7, June 1, 1973. Species composition in this marsh is typical of a brackish water environment. The area shown is approximately 10 miles long and 5 miles wide. A number of tree islands dot the marsh, the largest of which contains the small community of Elliots' Island, Maryland. Wetland vegetation includes a Juncus roemarianus/Scirpus sp.(three square)/Spartina alterniflora association in the lower marsh areas. The high marsh community, Spartina patens/Distichlis spicata/ Iva frutescens/Baccharis halimifolia, is primarily located along the edges and near the single road. Toward the northern end of the marsh, the water becomes less saline. Stands of Spartina cynosuroides occupy the stream margins within this portion of the marsh. Isolated stands of Phragmites communis occur, but they are generally too small to be detected on the ERTS imagery. Because the signature of the dominant low marsh species Juncus roemarianus is close to that of water, it is difficult to delineate the marsh-water interface within the marsh itself.

Mapping at a scale of 1:250,000 is adequate for the general delineation of large marshes and for rather gross plant species associations. Enlargement of the imagery to a scale of 1:125,000 provides additional information when processing is done to enhance the contrast in denser parts of the images. Overlays can be made directly from the prints which show the marsh-water interface and upper wetland boundary clearly. Where broad successional zones exist, these can also be mapped and smaller plant communities, occasionally less than 25 meters in diameter, can be identified in high contrast areas. In addition, open and vegetated ditches dug for drainage or agriculture can be recognized and indicated on the map. Further enlargement of the imagery is not productive unless the optics of the enlarging system are exceptionally good. The use of digital data is clearly indicated where detailed mapping is desired.

b. Identification of wetland type for management and maintenance of dependent wildlife populations.

The categorization of tidal wetlands according to salinity gradients is valuable information to wildlife management agencies. Plant species composition varies depending on the amount of salt in the water or soil. The general range of salt tolerance is known for most wetland plants. Hence, species composition may be inferred from salinity categories. It appears that through the analysis of spectral reflectance differences (band to band or seasonal) on ERTS data, one can type coastal wetlands into three categories: saline, brackish and fresh. The boundaries among these tend to be indistinct but generalizations on the extent of each type may be made.

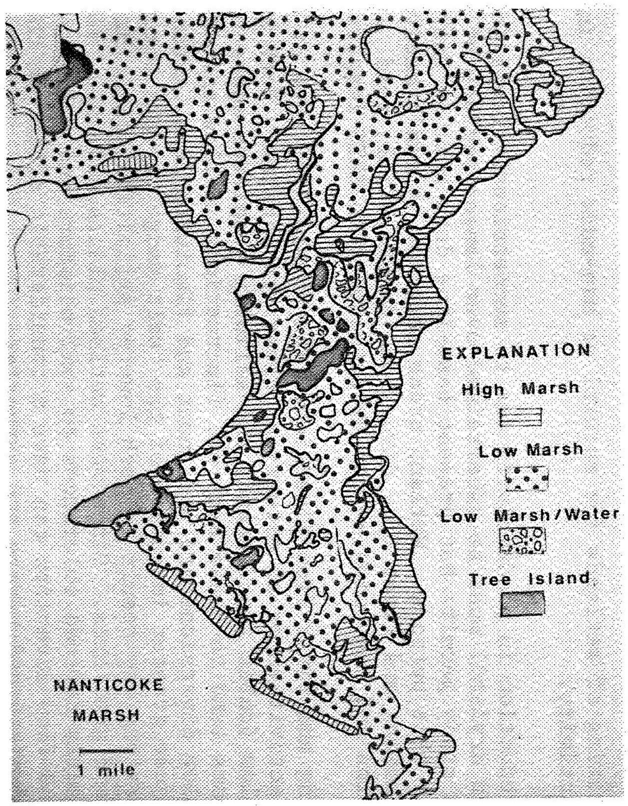

Figure 8. Wetland Map of the Nanticoke Marsh

Figure 9. Enlargement of ERTS Image 1349-15134-7
June 1, 1973

Fig. 10 is part of the 10/12/72 band 7 (1081-15264) image of the Charleston, S.C., area showing the coastal marshes inland to Lake Moultrie. The city of Charleston is primarily located on 2 large masses of land which jut southward into Charleston Harbor. Proceeding inland from the coast along the Wando, Cooper, Ashley and Stono Rivers, the water becomes progressively less saline and the vegetation changes accordingly. Because of the tidal ebb and flow, broad transitional areas of vegetation exist and exact boundaries are difficult to place. Fig. 11 is a wetland map of the area made from ERTS images 1081-15264-5,7 and 1243-15274-7 using a Bausch and Lomb Zoom Transfer Scope to compile at a scale slightly larger than 1:250,000.

Three categories of marsh were identified:

Category 1. Salt marsh containing predominantly *Spartina alterniflora* with subdominants present in varying amounts, usually at or near the upper wetland boundary.

Category 2. Near-saline to brackish marsh containing predominantly *Juncus roemarianus* with stream channels bordered by *Spartina alterniflora* at the more saline and *Spartina cynosuroides* at the fresher end.

Category 3. Brackish to fresh marsh containing large stands of *Spartina cynosuroides* along stream margins with *Scirpus americanus* or *olneyi* (three-square) or *Juncus roemarianus* often filling in the remaining area. Subdominants include *Scirpus* sp., *Zizania aquatica* (wild rice), *Juncus* sp. As the water becomes fresher, *Sagittaria* sp. (arrowhead), *Nuphar advena* (yellow water lily), *Pontederia cordata* (pickerelweed), *Peltandra virginica* (arrow arum), *Lilaeopsis chinensis*, and *Typha* sp. (cattail), become co-dominants with *Spartina cynosuroides*.

c. Monitoring of wetlands for natural or man-made reduction in productivity.

Natural reduction in productivity due to successional trends (e.g. wetland to dryland) must be ascertained over longer periods of time than this study permits but present base-line data will be extremely useful for this purpose. Wetland areas affected by man's activities such as damming and river flow diversion, dredge, fill, road construction and lagooning -- can be detected with ERTS imagery.

1. Damming and river flow diversion: The physical effects of each of these activities on an estuary or river are similar. Both alter rate of flow (cubic feet/second) and salinity gradients along coastlines. Dams tend to cause seasonal fluctuations in flow and salinity, whereas flow diversions are permanent and fluctuate less. Reductions in flow cause greater intrusion of the "salt wedge" up the estuary. Flow diversions may result in much lowered salinities, altering mixing patterns and gradients. Since most wetland plants and animals have rather clearly defined tolerances to soil moisture and salinity, damming and flow diversion can have a considerable effect on the biology of disturbed rivers and estuaries.

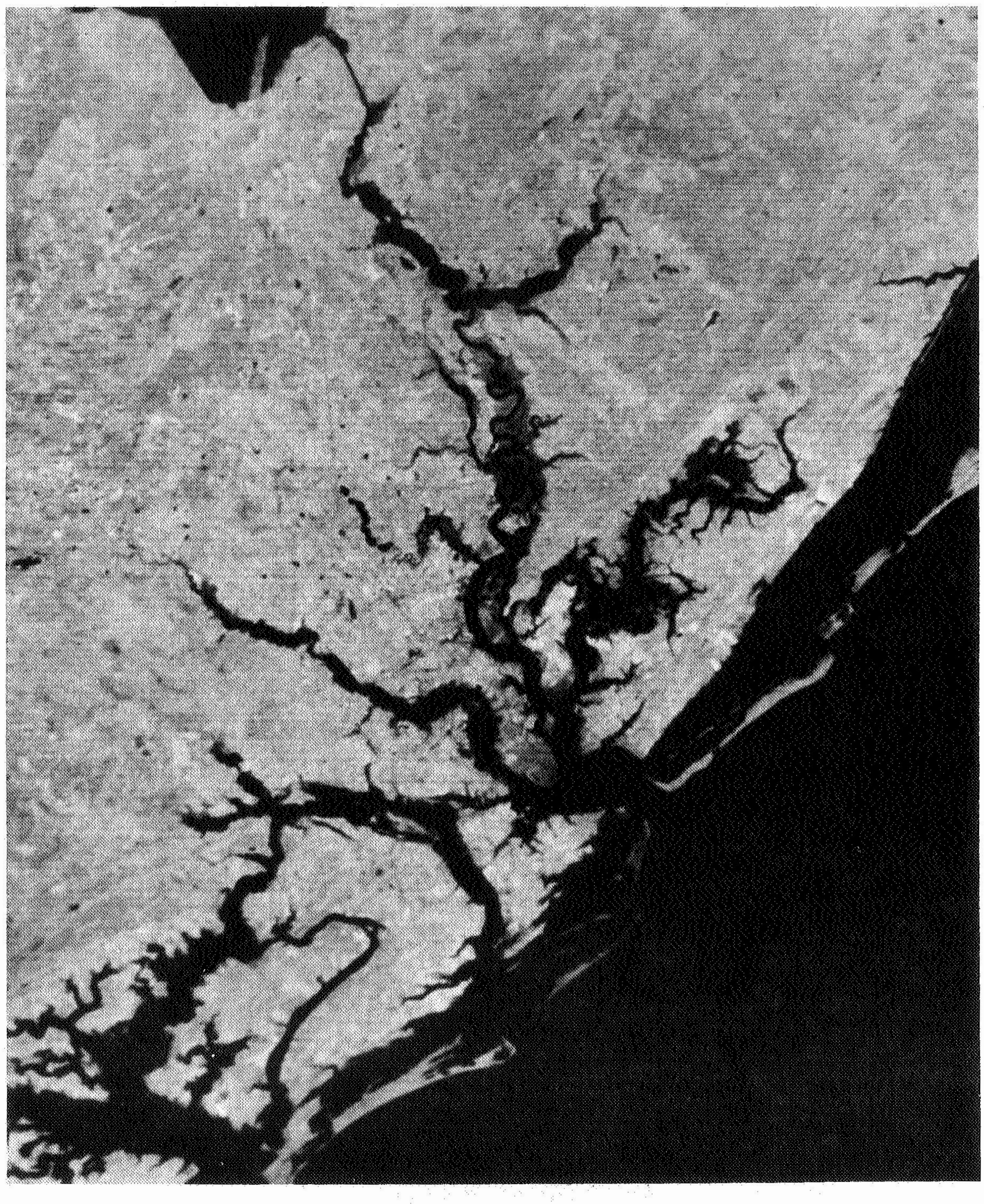

Figure 10. ERTS Image 1081-15264-7 Charleston, S. C.

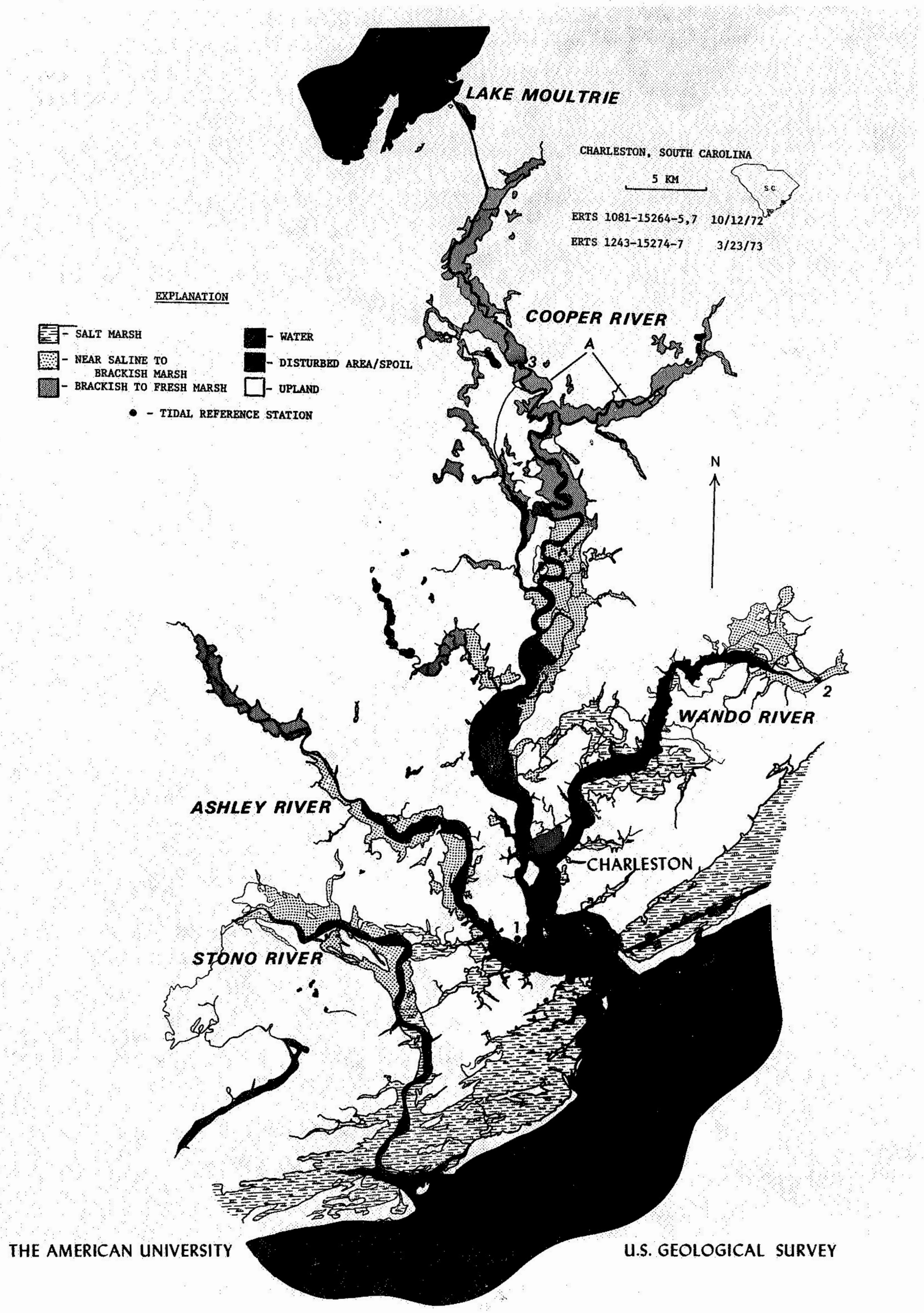

Figure 11. Wetland Map of Charleston, S. C. Area

Figs. 10 and 11 (Charleston, S.C.) show the head of the Cooper River south of Lake Moultrie to be split into two branches (A on Fig. 11). This area initially presented a complex interpretation problem since it appeared that the natural water levels were being affected by events other than tidal. Examination of the 8/19/72 imagery when "predicted" tide height was relatively low (as calculated from tide tables) showed that the riverine drainage channel could be delineated as it appears in the wetland map. However, imagery on 10/12/72 and 3/23/73 and color IR photography on 9/22/72 at differing "predicted" tide heights from high to low show the marsh adjacent to the channel to be flooded with only the vegetation along the original channel levees showing a strong vegetative signature. A field check on 5/19/73 showed standing water in many of the areas shown in the map as marsh.

A search of the literature revealed that prior to construction of the Santee-Cooper project of the South Carolina Public Service Authority in 1942, the annual freshwater inflow to the Charleston Harbor Estuary from the Cooper River was 72 cubic feet/second (3). The annual inflow is now 15,000 cubic feet/second, which accounts for flooding of areas that were previously marsh. As a result of this project, sedimentation in the navigation channel has increased from about 180,000 to 10,000,000 cubic yards per year, solid and domestic wastes are trapped in the estuary, and the salinity regime has been drastically altered. A proposed Corps of Engineers project (4) will redirect some of the water thus altering the estuarine environment again.

2. Dredge, fill and drainage activities: Since wetlands are low lying frequently or permanently flooded lands, they must be altered to make them habitable for man. Dredging of spoil from a portion of the wetland or from river channels and depositing on another portion to elevate for more suitable building sites is a common practice along the eastern coastline. The practice of ditching for wetland drainage has also been extensively used to control mosquito populations. These activities permanently alter wetlands to drylands and there is a need to routinely monitor them. Analysis of ERTS data shows an excellent capability for monitoring dredge, fill and ditching activities.

Areas of spoil disposal are illustrated on Fig. 3 and also Fig. 11. They show as highly reflective zones within the less reflective, undisturbed wetland.

3. Lagooning for waterside homes: This problem is particularly acute in Maryland, Delaware and New Jersey. Spoil removed for lagoon production is placed on the wetland for building sites. Fig. 12 is an ERTS image of a portion of the New Jersey coast. Lagooning is easily observed as well as other dredge and fill activities.

4. Highway construction: The impact of this activity is the impediment of water flow to wetlands above the location of bridges, etc. Typical highway construction across wetlands results in filling to the point of river or stream crossing, bridging, and then filling to the opposite shoreline. The restriction of water flow to the

bridge only results in greater flooding of the wetlands below and less flooding above the bridge.

Fig. 13 shows construction of highway I-95 along the Georgia coast. Wetland filling is easily observed. Changes in species composition above and below wetland crossings may be monitered with ERTS.

d. Mapping of shallow waters.

High turbidity in the test sites precluded mapping with early imagery. Insufficient experimentation with more recent imagery prevents us from attaining this objective.

USER IMPLICATIONS

The authors feel that the usefulness of ERTS data for general coastal wetland mapping has been demonstrated. There is now a need to apply these techniques in on-going programs at the state level. Preliminary discussions are underway with the states of South Carolina and Georgia. A cooperative effort between The American University and the U.S. Geological Survey in the Dismal Swamp of North Carolina illustrates a user oriented approach to our wetland research.

ERTS imagery and high altitude color IR underflight photography have been used in a comprehensive study of the Great Dismal Swamp and Dismal Swamp Canal. The purpose of this congressionally authorized (1972) study is to assess the feasibility and desirability of preserving and protecting the swamp and canal. Atlernative uses for the land and water resources comprising the swamp are also to be evaluated. Eight government agencies are participating in this study. ERTS imagery provides a synoptic view of the entire 210,000 acres of viable wetland included in the study area. The Feb. 13 image clearly defines surface water input and outflow. Autographic Theme Extraction (EROS-ATES) has been used to separate areas of standing water and dryer areas of the swamp. Color IR photography has been used for study site delineation ground truth site selection for vegetative study, hydrologic data acquisition, and vegetation mapping.

ERTS data have great potential for monitoring results of water level manipulation in the Dismal Swamp. About 49,000 acres of the swamp presently comprise the Dismal Swamp Wildlife Refuge and it is hoped that additional acreage may be acquired. Management of the refuge will include some regulation and management of the hydrologic regime. The effects of this management should be easily monitored by repetitive imagery which can detect vegetative stress and standing water.

REFERENCES

1. Anderson, R. R., Carter, V., and McGinness, J., ERTS-1 Investigation of Wetlands Ecology, Type II Report, Nov. 1972 - May 1973, Goddard Space Flight Center.

2. Schubert, J. S., and MacLeod, N. H., 1973, Vegetation Analysis with ERTS Digital Data: A New Approach, unpublished report (available from Biology Department, The American University).

3. Ketchum, Bostwich H., 1972, The Water's Edge: Critical Problems of the Coastal Zone, MIT Press, Cambridge, Mass.

4. Water Resources Development by the U.S. Army Corps of Engineers in South Carolina, U.S. Army Engineer Division, South Atlantic, 1969.

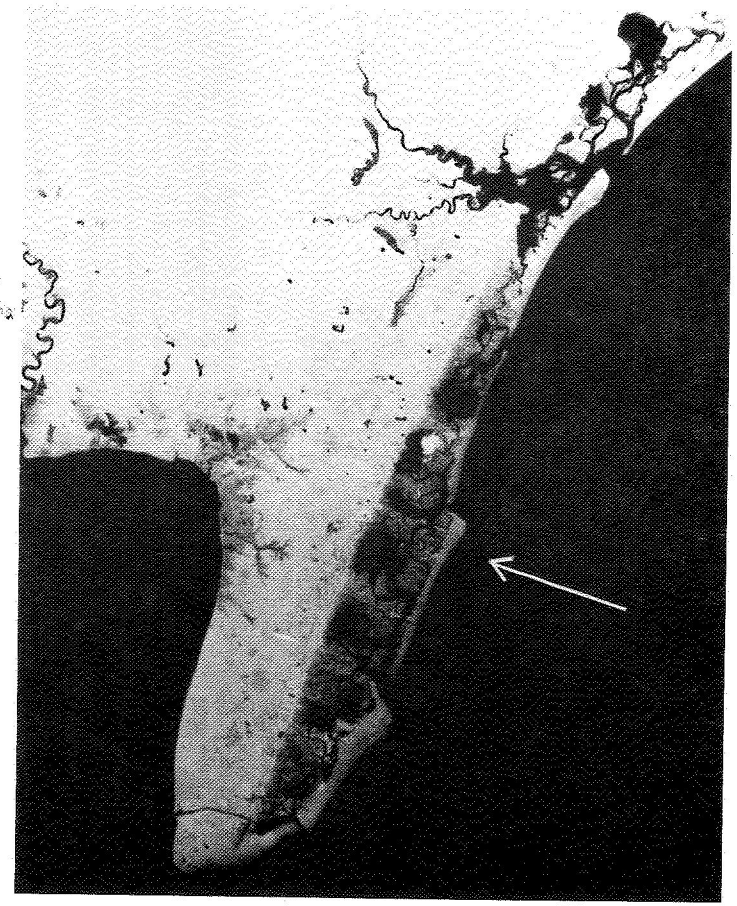

Figure 12. 1349-15134-7 New Jersey Coast Lagooning

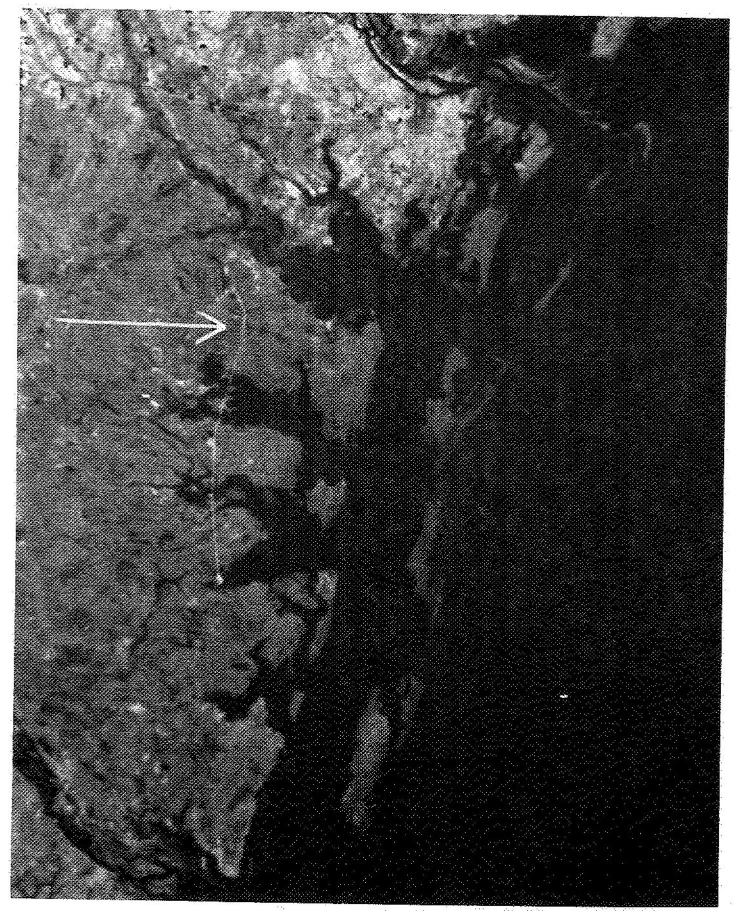

Figure 13. 1243-15280-7 Georgia Coast Highway Construction

Paper W 16

INVENTORIES OF DELAWARE'S COASTAL VEGETATION AND LAND-USE UTILIZING DIGITAL PROCESSING OF ERTS-1 IMAGERY

V. Klemas, D. Bartlett *(College of Marine Studies)*, R. Rogers and L. Reed
(Bendix Aerospace Systems Division)

ABSTRACT

Digital analysis of ERTS-1 imagery was used in an attempt to map and inventory the significant ecological communities of Delaware's coastal zone. Eight vegetation and land use discrimination classes were selected as follows:

1. *Phragmites communis* (Giant Reed grass)
2. *Spartina alterniflora* (Salt marsh cord grass)
3. *Spartina patens* (Salt marsh hay)
4. Shallow water and exposed mud
5. Deep water (> 2 meters)
6. Forest
7. Agriculture
8. Exposed sand and concrete

Canonical analysis showed that classification accuracy was quite good with *Spartina alterniflora*, exposed sand - concrete, and forested land - all discriminated with between 94% and 100% accuracy. The shallow water-mud and deep water categories were classified with accuracies of 88% and 93% respectively with all errors in classification occurring as one water category being classed as the other, a condition which is neither surprising nor bothersome with the overlap which these two classes exhibit no matter what the measurement technique used. *Phragmites communis* showed a classification accuracy of 83% with all confusion occurring with *Spartina patens* which may be due to use of mixed stands of these species as training sets. Discrimination of *Spartina patens* was very poor (accuracy = 52%) due to difficulties in locating large, pure stands of *S. patens* for use as training sets. Classification accuracy for agriculture was also very poor (51%). Limitations of time and available class-memory space resulted in limiting the analysis of agriculture to very gross identification of a class which actually consists of many varied signature classes. If crop inventory had been the primary objective of the study, substantially better results could have been achieved in discriminating agricultural land categories.

Abundant ground truth was available in the form of vegetation maps compiled from NASA-RB-57 color and color infrared photographs. Blow-ups of portions of the thematic maps digitally derived from ERTS data showed very good correlation with known sites. Cal-comp plots of thematic data at scales up to 1:24,000 showed good cartographic precision when overlayed onto existing maps. It is believed that with further refinement of training set selection, sufficiently accurate results can be obtained for all categories producing a useful planning and management tool.

INTRODUCTION

Work carried out over the past two years at the University of Delaware indicated that the coastal zone of Delaware and, in particular, its extensive tidal wetlands offer a unique opportunity to evaluate ERTS-1 sensing capabilities and the feasability of using digital processing techniques to map and inventory coastal vegetation and land-use. Major vegetation species found in the tidal wetlands have been shown to be easily distinguishable at ERTS scale.[4] Furthermore, human alterations of the coastal zone were easily recognized since such alterations typically involve removal of vegetative cover resulting in a change of spectral signature.[4] The superior spectral resolution of the CCTs as compared with a single band or composite imagery has indeed provided good discrimination through digital analysis of the CCTs with the added advantage of rapid production of thematic maps and data.[5]

Digital Techniques

Computer software, techniques and procedures used to transform ERTS CCT's into the land use maps and data described here were developed in the Bendix Earth Resources Center. The nucleus of this center is a Digital Equipment Corporation PDP-11/15 computer with 32K words of core memory, two 1.5M-word disk packs, two 9-track 800 bpi tapes transports, a line printer, a card reader and a teletype unit.

Transforming ERTS CCT's into thematic data is a four step process, performed as follows:

1. Locate Training Areas - In defining the location of training areas, the CCT containing the areas of interest is screened on the color-coded TV monitor. The signal range of interest within the band chosen as having the best target-background contrast is displayed in 16 color slices. When the test site of interest appears on the monitor, the CCT is stopped and the scene is mapped out by the line printer. Then, utilizing available ground truth, the training areas are identified on the grey scale printout and their locations recorded. (See Figure 1) The locations of the training areas are then conveyed to the computer by the investigator, using the resolution element number and scan-line number of the upper-left and lower-right corner of each training area.

FIGURE 1

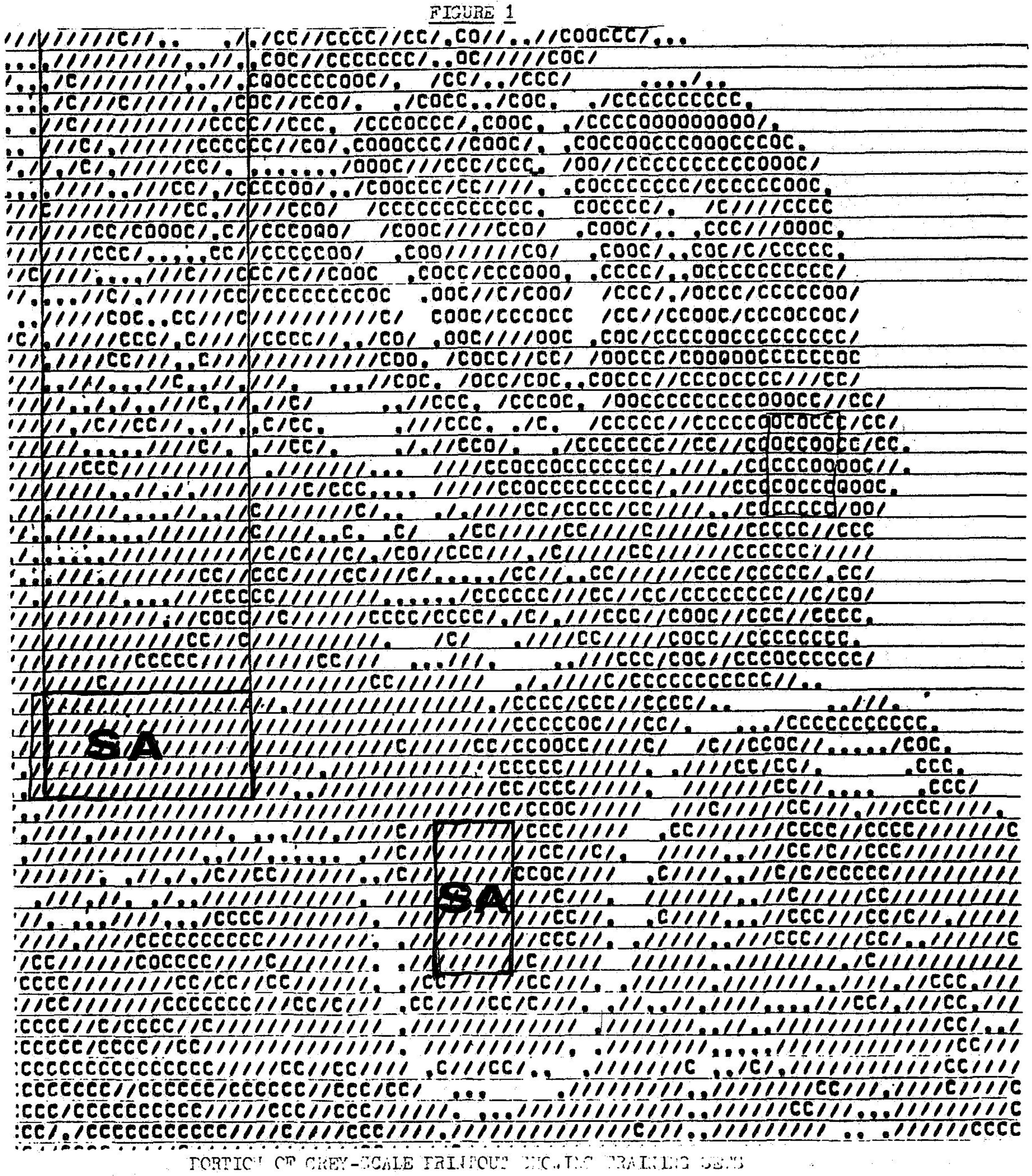

PORTION OF GREY-SCALE PRINTOUT SHOWING TRAINING SETS SELECTED FOR *Spartina alterniflora* (SA). Band 7.

TABLE 1

CANONICAL ANALYSIS: TARGET GROUP IS 10 SPARTINA ALTERNIFLORA

INCLUDED VARIABLES 1(MSS 4) 2(MSS 5) 3(MSS 6) 4(MSS 7)

MEANS	38.20833	22.35417	67.54166	91.16666	(PERCENT REFLECTANCE)
STD DEV	1.56741	1.73194	4.48593	5.19352	
DETERMINANT	0.183281E 04				

EIGENVALUES

1	1537.34155
2	34.52617
3	2.68026
4	1.45123

CANONICAL VARIABLES		1	2	3		1	2	3
CONSTANTS		-20.015	-20.026	-8.726				
VAR	IVN	COEFFICIENTS				CONTRIBUTION		
1	1	0.350	0.134	0.530	MSS 4 -	2.192	0.842	3.326
2	2	0.453	-0.124	-0.359	MSS 5 -	3.140	0.856	2.486
3	3	0.002	0.003	-0.061	MSS 6 -	0.038	0.058	1.089
4	4	-0.040	0.191	0.006	MSS 7 -	0.824	3.974	0.132

CANONICAL VARIABLES EVALUATED AT GROUP MEANS

	WEIGHT	1	2	3
GROUP 1	1.000	7.167	-1.746	0.250
GROUP 2	1.000	29.190	-4.525	-0.542
GROUP 3	1.000	80.844	5.351	0.070
GROUP 4	1.000	6.144	-3.182	-0.675
GROUP 5	1.000	17.440	-7.190	-0.074
GROUP 6	0.000	4.671	-13.039	1.220
GROUP 7	0.000	6.450	-16.796	2.642
GROUP 8	1.000	45.826	-5.642	0.543
GROUP 9	1.000	4.561	-7.475	0.333
GROUP 10	0.000	-0.000	0.000	0.000

FIGURE 2A

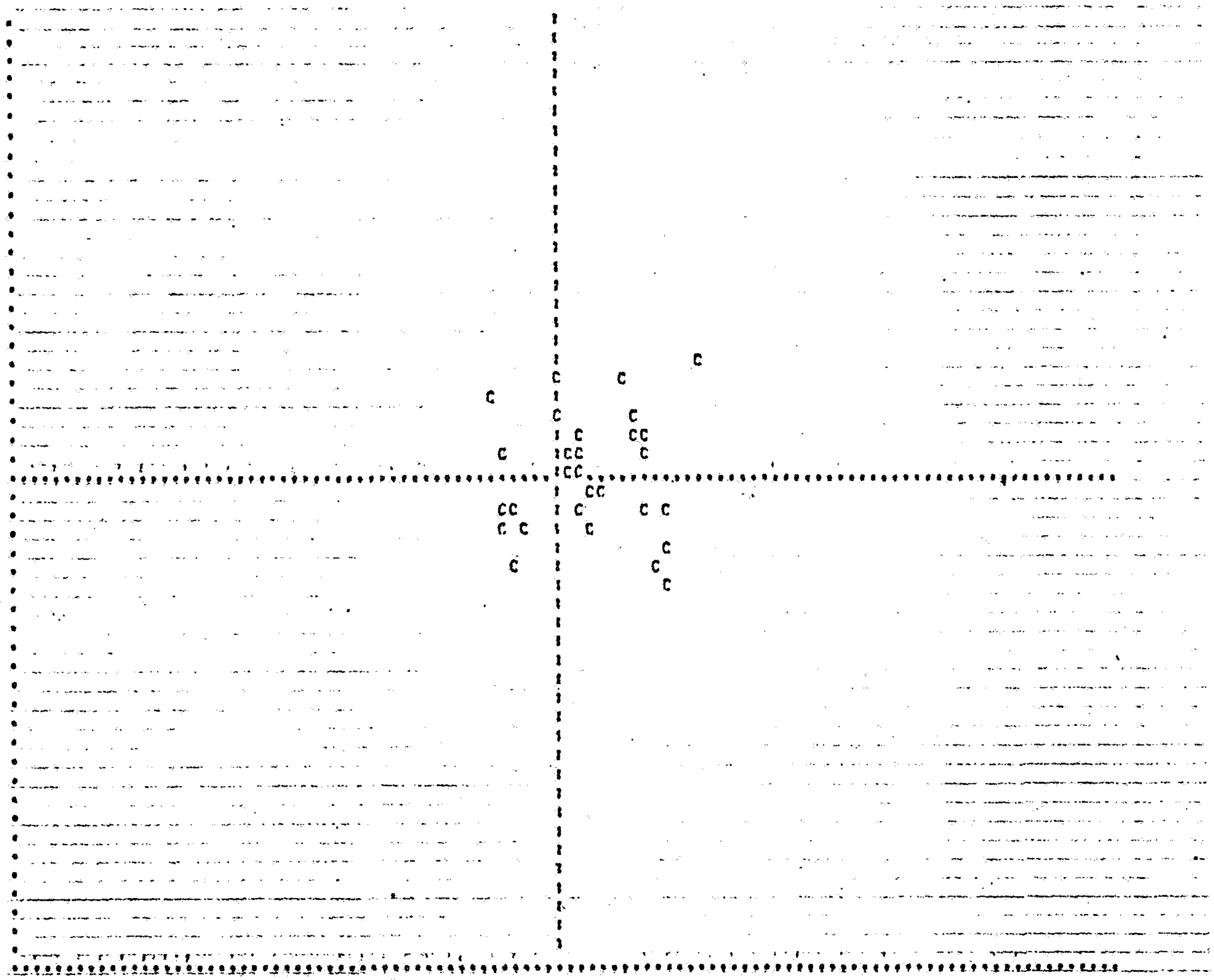

LINE PRINTER SCATTER DIAGRAM SHOWING TARGET GROUP "C" (*SPARTINA ALTERNIFLORA*) PLOTTED IN CANNONICAL SPACE.

FIGURE 2B

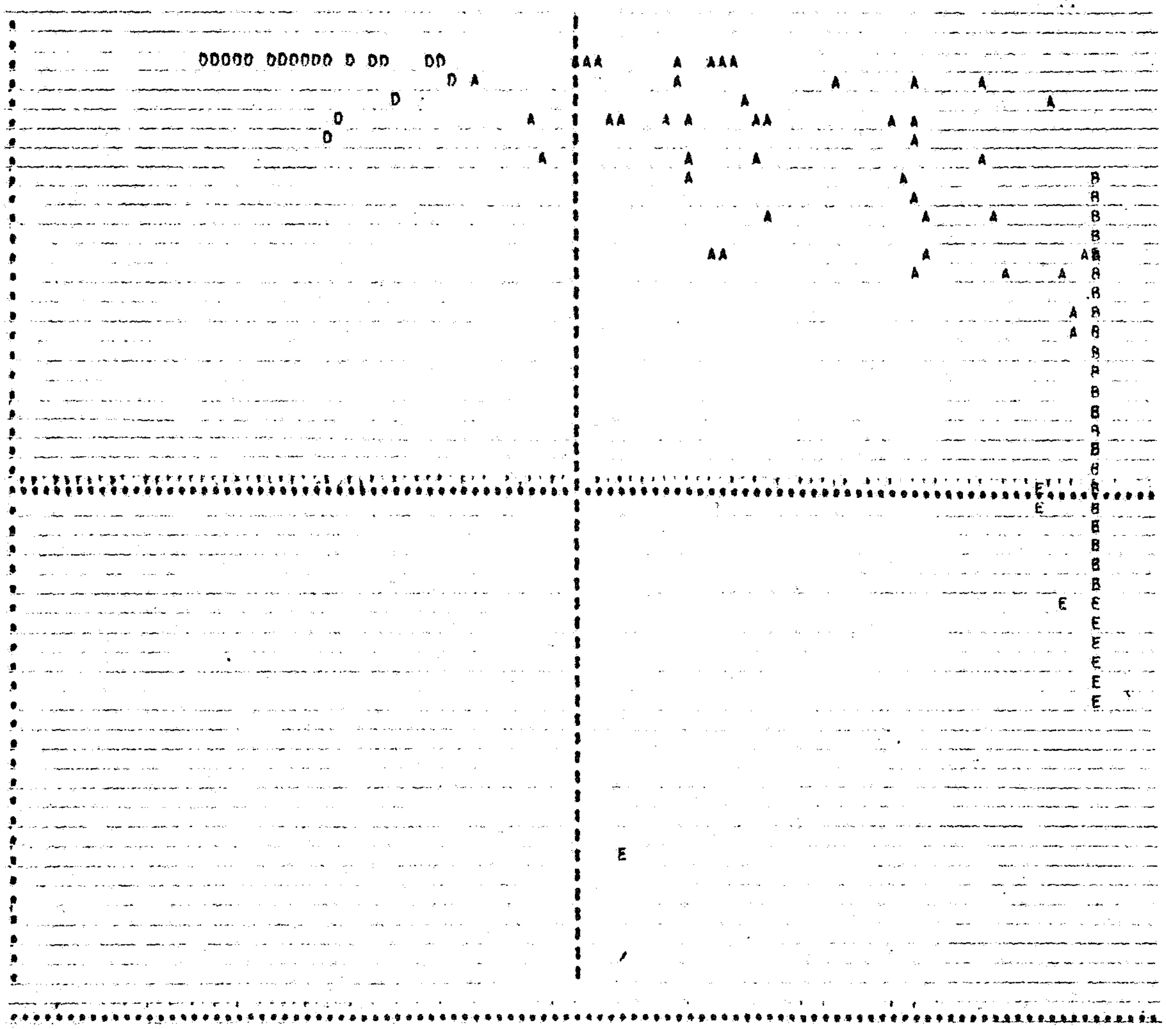

LINE PRINTER SCATTER DIAGRAM SHOWING SEPARABILITY OF TARGET CATEGORY "C" (SPARTINA ALTERNIFLORA) AS PLOTTED IN FIGURE 2A FROM BACKGROUND CATEGORIES "A","B","D" AND "E".

TABLE 2

CLASSIFICATION TABLE

GROUP	CLASSIFIED AS GROUP 0	1	2	3	4	5	6	7	8	9	10	
1	0.00000	82.53968	0.00000	0.00000	17.46032	0.00000	0.00000	0.00000	0.00000	0.00000	0.00000	<u>PHRAGMITES</u> <u>COMMUNIS</u>
2	0.00000	0.00000	51.66667	4.16667	6.66667	0.00000	16.66667	0.00000	0.83333	20.00000	0.00000	AGRICULTURE #1
3	0.00000	0.00000	2.94118	97.05882	0.00000	0.00000	0.00000	0.00000	0.00000	0.00000	0.00000	BARE SAND
4	0.00000	43.54839	0.00000	0.00000	51.61290	0.00000	0.00000	0.00000	0.00000	4.83871	0.00000	<u>SPARTINA</u> <u>PATENS</u>
5	0.00000	0.00000	0.00000	0.00000	0.00000	100.00000	0.00000	0.00000	0.00000	0.00000	0.00000	AGRICULTURE #2
6	0.00000	0.00000	0.00000	0.00000	0.00000	0.00000	88.23529	11.76471	0.00000	0.00000	0.00000	SHALLOW WATER - MUD
7	0.00000	0.00000	0.00000	0.00000	0.00000	0.00000	6.57895	93.42105	0.00000	0.00000	0.00000	DEEP WATER (>2M.)
8	0.00000	0.00000	0.00000	0.00000	0.00000	0.00000	0.00000	0.00000	100.00000	0.00000	0.00000	CONCRETE
9	0.00000	0.00000	0.00000	0.00000	5.55556	0.00000	0.00000	0.00000	0.00000	94.44445	0.00000	FOREST
10	0.00000	1.04167	0.00000	0.00000	0.00000	0.00000	0.00000	0.00000	0.00000	0.00000	98.95834	<u>SPARTINA</u> <u>ALTERNIFLORA</u>

computer decisions on areas where ground truth is avialable, the investigator can rapidly determine the effectiveness of the decision processing.

4. Produce Decision Data Products - The decision analysis may be presented in a number of ways, including:

a) The area covered by each category in terms of percent of total area processed, acres and square kilometers. (See Table 3).

b) Color-coded decision imagery showing any or all of the categories at any convenient scale.

c) Cal-comp or Gerber plots of any category, geometrically corrected and plotted at a map scale specified by the investigator. (See Figure 3).

RESULTS

The primary objective of the analysis was to map and inventory the significant ecological communities of Delaware's coastal zone. To this end, eight vegetation and land use discrimination classes were selected as follows:

1. Phragmites communis (Giant Reed grass)
2. Spartina alterniflora (Salt marsh and grass)
3. Spartina patens (Salt marsh hay)
4. Shallow water and exposed mud
5. Deep water (2 meters)
6. Forest
7. Agriculture
8. Exposed sand and concrete

Canonical analysis showed that classification accuracy was quite good with Spartina alterniflora, exposed sand - concrete, and forested land - all discriminated with between 94% and 100% accuracy. (See Table 2). The shallow water-mud and deep water categories were classified with accuracies of 88% and 93% respectively with all errors in classification occurring as one water category being classed as the other, a condition which is neither surprising nor bothersome with the broad transitions one often finds between two categories so poorly delineated. (See Table 2). Phragmites communis showed a classification accuracy of 83% with all confusion occurring with Spartina patens which may be due to use of mixed stands of these species as training sets. (See Table 2). Both species occupy similar environments within the coastal zone. Analogue multispectral analysis done previously indicates that these species will be separable after refinement of training sets.[1] Discrimination of Spartina patens was very poor (accuracy = 52%) due, almost certainly, to difficulties in locating large, pure stands of S. patens for use as training sets. (See Table 2). Classification accuracy for agriculture was also very poor (51%). (See Table 2). Limitations of time and available class-memory space

2. Develop Target Characteristics - Inputting the training area coordinates (boundaries) to the computer permits the ERTS spectral measurements within these boundaries to be extracted (edited) from the CCTs and placed into computer disk files. One file is established for each different land use or vegetation category. The data in each file is then processed to obtain a numerical descriptor to represent the spectral characteristics of each category of interest. The descriptors presently include the mean signal and standard deviation for each band and the covariance matrix taken about the origin, which includes the four MSS bands. (See Table 2).

3. Evaluate Target Characteristics and Classification Techniques - Once the numerical descriptions which define the spectral characteristics of each land use category of interest are determined, the operator executes the "canonical analysis" program. This program derives, for each land use category being sought, a set of "canonical coefficients". In the decision processing phase discussed later, these coefficients are used by the computer to form a linear combination of the ERTS measurements to produce a "canonical variable" whose amplitude is associated with the probability of an ERTS measusrement being from the target sought. A set of canonical coefficients are derived for each category of interest. (See Table 1).

Before producing decision data on a complete ERTS CCT, a number of tests are applied to evaluate the computer's capability of performing the desired land use classification. One test is to play back the data from the training edits, which were previously placed on the computer disk file, and to compute and display the canonical variables in the form of "scatter diagrams". (See Figures 2a and 2b). A pair of scatter diagrams, are generated for each set of canonical coefficients, i.e., for each vegetation category. The set of canonical coefficients which define a vegetation category are used to produce a canonical space plot. The same coefficients map the background (i.e., other land use categories) into the same canonical space. These plots aid the investigator in determining the degree of separability being obtained between the target and background categories.

Another test of the canonical coefficients is to proceed to use them in the decision processing but to limit the data processed to that which is well known, i.e., the training data which was previously edited and stored on the disk file. Processing this data and keeping an accurate record of decisions permits a classification accuracy table to be developed which provides the investigator with a quantitative measure of the classification accuracy achieved by the canonical coefficients in the decision processing. (See Table 2). The percentage of each target group which would be classified as another target group is shown thus identifying the areas where signature overlap may introduce errors into the decision processing.

A final test of the canonical coefficient is to play back the ERTS CCT and to assign a color code to the computer decisions which are displayed to the investigator on the TV monitor. By viewing the

resulted in limiting the analysis of agriculture to very gross identification of a class which, in Delaware, actually consists of many, varied signature classes. There is no doubt in the investigators' minds that if crop inventory had been the primary objective of the study, substantially better results could have been achieved in discriminating agricultural land categories.

Abundant ground truth was available in the form of vegetation maps compiled from NASA-RB-57 photography and in the photos themselves - both color and color-IR. Blow ups of portions of the thematic maps digitally derived from ERTS data showed very good correlation with known sites. Cal-comp plots of thematic data at scales up to 1:24,000 showed excellent cartographic precision when overlayed onto existing maps. (See Figure 3).

It is believed that with further refinement of training set selection, sufficiently accurate results can be obtained for all categories, producing a useful planning and management tool.

TAPE 2

ERTS PROCESSOR 31-AUG-73 05:51:58

ERTS SCENE ID - 1079-15133
DATE OF SCENE - 10OCT72
CENTER OF SCENE - N38-53/W075-21
SUN COORDINATES - EL39 DEGREES
AZ149 DEGREES
SPACECRAFT HEADING - 191 DEGREES
STARTING SCAN LINE = 1
ENDING SCAN LINE = 1500

CATEGORY	PERCENT OF TOTAL	ACRES	SQ. KM.
UNCLASSIFIED	7.27	95166.81	446.08
PHRAGMITES	11.66	152705.42	715.78
AGRICULTURE	20.30	265884.31	1246.28
INDUSTRIAL	1.16	15165.12	71.08
PATENS	25.16	329502.78	1544.48
MUD LADEN WATER	3.39	44379.63	208.02
WATER	12.43	162775.97	762.98
ALTERA FLORA	4.54	59460.66	278.71
TREES	14.10	184713.00	865.81
TOTALS	100.00	1309753.75	6139.21

PROGRAM RUN TIME = 01:58:33

TABLE 3

FIGURE 3

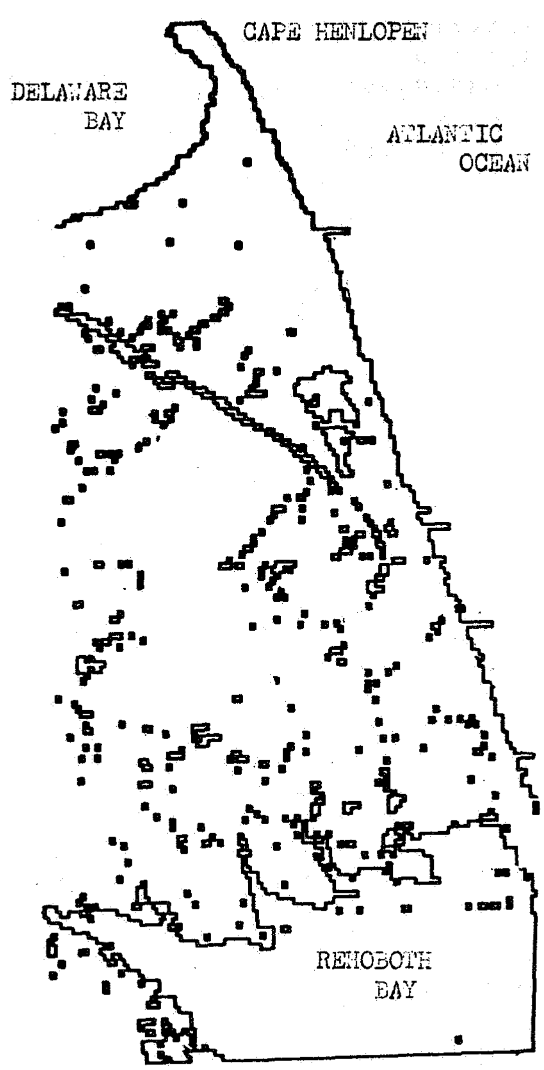

CAL-COMP PLOT OF WATER BOUNDARIES IN AREA OF CAPE HENLOPEN, DELAWARE

SCALE = 1:85,000

REFERENCES

1. Klemas, V., Daiber, F., Bartlett, D., Crichton, O., Fornes, A., Application of Automated Multispectral Analysis to Delaware's Coastal Vegetation Mapping, American Society of Photogrammetry Annual Meeting, Washington, D. C., March 11-16, 1972.

2. Reimold, R. J., Gallagher, J. L., and Thompson, D. E., -- "Remote Sensing of Tidal Marsh" in Photogrammetric Engineering, Am. Soc. of Photogrammetry, 1973.

3. Wobber, F. T., and Anderson, R. R. -- "Operational Wetlands Mapping Using Multiband Aerial Photography" in Coastal Mapping Symposium, Am. Soc. of Photogrammetry, 1972.

4. Klemas, V., Bartlett, D., Daiber, F., Mapping Delaware's Coastal Vegetation and Land Use from Aircraft and Satellites, A.S.P., Symposium on Remote Sensing in Oceanography, Orlando, Fla., October 2-5, 1973.

5. Rogers, R. H. and Reed. L. E., (1973), "Automated Land Use Mapping from Spacecraft Data" - Bendix Special Report #4097.

Paper W 17

EVALUATION OF REMOTE SENSING AND AUTOMATIC DATA TECHNIQUES FOR CHARACTERIZATION OF WETLANDS

Robert H. Cartmill, *(NASA) Johnson Space Center, Earth Resources Laboratory, Mississippi Test Facility, Bay St. Louis, Mississippi*

ABSTRACT

This evaluation has been conducted in the Atchafalaya River basin of South Central Louisiana. This is a humid area of heavily forested swamps with a large volume of flow mostly from a diversion of the lower Mississippi River.

Techniques to obtain enlarged imagery from computer compatible tapes of ERTS data without photographic enlargemnet is explained and illustrated. Techniques of extraction of environmental information from single bands and multiband pattern recognition procedures is explained and evaluated. A comparison of pattern recognition classifications of the Atchafalaya Basin by aircraft multispectral scanner and ERTS MSS data is made. Data for this comparison were gathered within three weeks of each other in the winter of 1973. Scorecards of the accuracy of the classifications are presented.

Recommendations are made concerning the utilization of each sensor platform to perform specific tasks of wetlands characterization.

INTRODUCTION

The study area is the lower portion of the Atchafalaya River basin indicated by the blocked area of ERTS frame 1070-16073 of October 1, 1972, shown in Figure 1. The basin is located about sixty miles west of New Orleans in south-central Louisiana. This basin has been leveed on either side by the U.S. Army Corps of Engineers. They have also constructed two diversions from the Mississippi River into the basin. As a result approximately one-third of the flow of the Mississippi River with its attendant sediment load passes down the Atchafalaya. The impact of this large flow of water through a small coastal river system has been large. The most obvious result has been the deposition of a sediment in the basin creating new land at the rate of about three square miles per year.

The climate of the region is humid with rainfall averaging about 64 inches per year. During the summer the climate is typical of the humid tropics with early morning buildup of cumulus clouds and afternoon thunderstorms. Killing frosts do occur but only very late in the year. Cloud cover statistics prepared by Brown (1970) yield an expected value of cloud free ERTS passes in one year of 4.19. During the first year of this study we obtained three cloud free passes.

The area is almost uninhabited but possesses numerous oil fields. It is also the largest producing region of crawfish in the country supplying large portions of the Louisiana market for this delicacy. Figures 2, 3, and 4 show typical scenes of the area. The lighter colored trees in Figure 4 are water tupelos which have lost their leaves at the time the picture was taken (October).

The objectives of the study are shown in Table 1.

RESULTS

Our first step in the data processing is to manufacture a simulated color IR picture on a nine-inch film strip from the computer compatible tapes as shown in Figure 5. This is done by selecting three bands (1, 2 and 4) of the four ERTS bands and assigning each of them a color (blue, green, and red). The three bands become channels of data that are projected onto the image plane of a film recorder which generates the composite image. By repeating elements and scan lines the picture can be made to any convenient scale. Figure 6 shows an enlargement of a picture of a portion of the basin. These enlargements can be then contact printed and mosaiced to produce large scale pictures of the area. These pictures can be used for standard photo interpretation and are used to locate training samples for the pattern recognition programs.

The second step in the data processing is to produce thematic maps or elementary classifications of the area by use of very simple computer programs. Figure 7 shows a density map produced from band 3 of ERTS frame 1070-16073. Here a certain count range was given a different color--0-15 counts, dark blue; 16-25 counts, yellow, etc. Notice that by this method the clear lake water can be readily separated from the sediment-laden river water. However, use of one channel blurs the discrimination of the agricultural areas and is insufficient for forest species identification. Figure 8 shows a thematic map (open water) of the basin produced by using digital data from bands 1 and 4 of ERTS frame 1286-16083. We believe that this technique developed by the Johnson Space Center at Houston removes most of the ambiguities in identifying water. A simple two-dimensional decision rule is used to divide the space into two domains--water and other. These techniques have been shown to be adequate to detect and monitor the accretion of new land in the basin.

The third and final data processing effort is to use a modified version of the Purdue pattern recognition programs to produce surface classification maps of the study area. One of the objectives of the study is to compare ERTS data with lower altitude aircraft MSS data. We are also endeavoring to determine the limits of the different number of classes which can be discriminated by each sensor platform.

The aircraft has one great advantage in this humid area over the ERTS platform in that it can be dispatched to gather data when weather conditions are suitable In addition, the aircraft scanner at the altitude flown 6100 meters (20,000 feet) has a resolution of 12 meters vs. the ERTS resolution of 79 meters.

Figures 9 and 10 show the results of the aircraft classifications. These figures illustrate one of the principal disadvantages of wide angle (80°) aircraft scanners. Notice the island shown in Figure 9 which is classified as tupelo trees. Figure 10 shows the same island as seen on the adjacent flight line. Now it has been classified as cypress trees. The reason is that the MSS spectral signatures of the two species are nearly identical despite the fact that the photograph shown in Figure 4 shows a marked contrast. In Figure 9 the scanner was viewing the sunlit side of the trees and in Figure 10 it was viewing the shady side. This difference in illumination was sufficient to change the classification between the two flight lines. This problem has been discussed in detail in a paper by Cartmill and Boudreau (1973). This difficulty has not been encountered in the small angle ERTS data.

Fortunately this did not present overwhelming difficulties as the U.S. Forest Service groups these two water-loving species together for purposes of inventory. Figures 11 and 12 show a comparison between the aircraft and ERTS classifications of the same portion of the basin. The aircraft data was gathered on January 15, 1973, and the ERTS data on February 4, 1973. The classes and color coding are the same and the difficult cypress and tupelo trees have been grouped together. The same training samples were used for both classifications. There are obviously some areas of disagreement between the two classifications, but the general features agree well with one another. The two figures also illustrate the effects of element resolution size on the detail of classification.

Tables II and III represent the training field classification scorecards of each data set. These classification percentages probably represent the upper limit of classification accuracy we can achieve using our present techniques at this time of year with dormant vegetation and low sun angle. Most of the classification errors occurred between different classes of the same general materials. One species of tree being classed as a different species, for example. Combining the different classes into broader groupings will yield accuracies approaching ninety percent.

POSSIBLE USES

The Earth Resources Laboratory has made numerous contacts with state and federal agencies who have management responsibilities in the basin. At present these agencies have not had sufficient time to evaluate the full potential uses of these space-derived products. Table IV shows a list of some of the more promising uses for these products.

CONCLUSIONS AND RECOMMENDATIONS

Table V presents the tentative conclusions and recommendations derived from the analysis of the data to the present time.

References

Brown, S.C., February 1970, "Simulating the Consequence of Cloud Cover on Earth-viewing Space Missions", Bul. of the Amer. Met. Soc., Vol. 51, No. 2.

Cartmill, R.H. and Boudreau, R.D., May 1973, Study of Atmospheric Effects and Illumination in Multispectral Data (A Case Study of the Atchafalaya River Basin, Flight of October 29, 1971.) Earth Resources Laboratory Report 050, Johnson Space Center, Houston, TX.

TABLE I OBJECTIVES

GENERAL OBJECTIVES

A. DETERMINE THE USEFULNESS OF VARIOUS SENSORS AND THEIR ASSOCIATED PLATFORMS TO CHARACTERIZE WETLANDS.

B. DEVELOP AUTOMATED TECHNIQUES TO PROCESS THE LARGE VOLUMES OF DATA GATHERED BY THE SENSORS WITH EMPHASIS ON MSS COMPUTER COMPATIBLE TAPES.

SPECIFIC OBJECTIVES

A. MONITORING OF ACCRETION AND EROSION.

B. DETERMINATION OF SALT WATER INTRUSION IN MARSH AREAS BY PLANT SPECIES IDENTIFICATION.

C. LOCATING AND IDENTIFYING AQUATIC PLANTS.

D. DETERMINATION OF CERTAIN WATER CHARACTERISTICS.

E. FOREST AND OTHER PLANT SPECIES IDENTIFICATION.

TABLE II CLASSIFICATION SCORECARD
OF THE AIRCRAFT MSS TRAINING SAMPLES

Class	Percent Correctly Classified	Percent Misclassified	Percent Unclassified
River	68	25	7
Lake	83	6	11
Cypress-Tupelo	67	16	17
Mixed Forest	72	16	12
Willow	66	26	8
Scrub Forest	--	--	--
Water Hyacinth	90	1	9
Bare Fields	83	14	3
Marsh	61	24	15

Overall percentage correctly classified - $\frac{\text{6628 correct}}{\text{9104 total}} \times 100 = 72.8\%$

TABLE III CLASSIFICATION SCORECARD
OF THE ERTS TRAINING SAMPLES

Class	Percent Correctly Classified	Percent Misclassified	Percent Unclassified
River	69	30	1
Lake	71	24	5
Cypress-tupelo	94	0	6
Mixed forest	52	28	20
Willow	73	2	25
Scrub forest	88	12	0
Water hyacinth	96	4	0
Bare fields	100	0	0
Marsh	89	11	0

Overall percentage correctly classied - $\frac{\text{670 correct}}{\text{865 total points}} \times 100 = 77.5\%$

TABLE IV
Potential Uses of ERTS Products for
Wetlands Management

User	ERTS Product	Potential Use
Atchafalaya Basin Div. La. Dept. of Public Works	1. Large scale ERTS simulated color IR maps. 2. Thematic map (water) from ERTS CCT's.	1. Location of dry campsites for recreation development 2. Location of the boundaries of wildlife refuge.
Forest Resources Survey Southern Forest Experiment Station Forest Service U.S. Dept. of Agriculture	Classification of ERTS CCT data.	Tally of total forested area in each county for inventory estimates between 10 yr. formal inventories
La. Forest Commission	Classification of ERTS CCT data	Forest mapping of the state.
Lower Ms. River Forecast Center, National Weather Svc., NOAA, U.S. Dept. of Commerce	1. Thematic map (water) 2. Large scale ERTS simulated color IR maps.	Definition of stage-flow rating curves and volume of overbank storage
New Orleans District, U.S. Army Corps of Engineers	1. Large scale ERTS simulated color IR maps.	1. Definition of the flow regime in complex channel systems. 2. Determination of areas of likely sediment deposition. 3. Penetration of River outflow into marsh areas
	2. Thematic map (water)	Determination of limits of innundation for flood damage calculations
	3. Classification of ERTS CCT data.	Issuance of permits to alter navigable channels.

TABLE V TENTATIVE CONCLUSIONS AND RECOMMENDATIONS

CONCLUSIONS

A. ERTS MSS DATA CAN PROVIDE MONITORING OF ACCRETION PROCESSES IN SWAMP AREAS.

B. AIRCRAFT COLOR IR PHOTOGRAPHY HAS SUPERIOR ACCURACY TO AIRCRAFT MSS DATA WHICH IN TURN IS BETTER THAN ERTS MSS DATA IN LOCATING AQUATIC PLANTS BECAUSE OF THE BETTER RESOLUTION.

C. ERTS MSS DATA CAN DIFFERENTIATE BETWEEN SEDIMENT LADEN RIVERS AND CLEAR LAKES USING SIMPLE ONE CHANNEL DENSITY SLICES.

D. ACCURATE FOREST SPECIES IDENTIFICATION IN SWAMP AREAS WAS NOT OBTAINED BY EITHER ERTS OR AIRCRAFT IN THE FALL AND WINTER. THE GREATER RESOLUTION OF THE AIRCRAFT DATA DID NOT IMPROVE THE CLASSIFICATION. FOREST COULD BE ACCURATELY MAPPED FROM OTHER VEGETATION.

RECOMMENDATIONS

A. GREAT CONSIDERATION SHOULD BE GIVEN TO CLOUD COVER STATISTICS AND SATELLITE OVERFLIGHT FREQUENCY BEFORE INTEGRATING SATELLITE DATA INTO AN ENVIRONMENTAL MONITORING SYSTEM. THIS WOULD INCLUDE SUCH ITEMS AS DETERMINING THE EFFECTS OF A VEGETATION ERADICATION PROGRAM, CALCULATION OF THE PERCENT OF HARVEST, THE LIMITS OF FLOOD INUNDATION, ETC.

B. SIMPLE PROCESSING PROCEDURES OF ERTS MSS DATA CAN YIELD MUCH VALUABLE INFORMATION AND ARE WELL WITHIN THE CAPABILITIES OF MANY USERS. THIS WOULD INCLUDE SINGLE BAND ANALYSIS OR TWO BAND DECISION RULES USING A STANDARD COMPUTER PRINTOUT.

C. VEGETATIONAL ANALYSIS SHOULD BE DONE BY USE OF ALL AVAILABLE BANDS WITH PATTERN RECOGNITION TECHNIQUES.

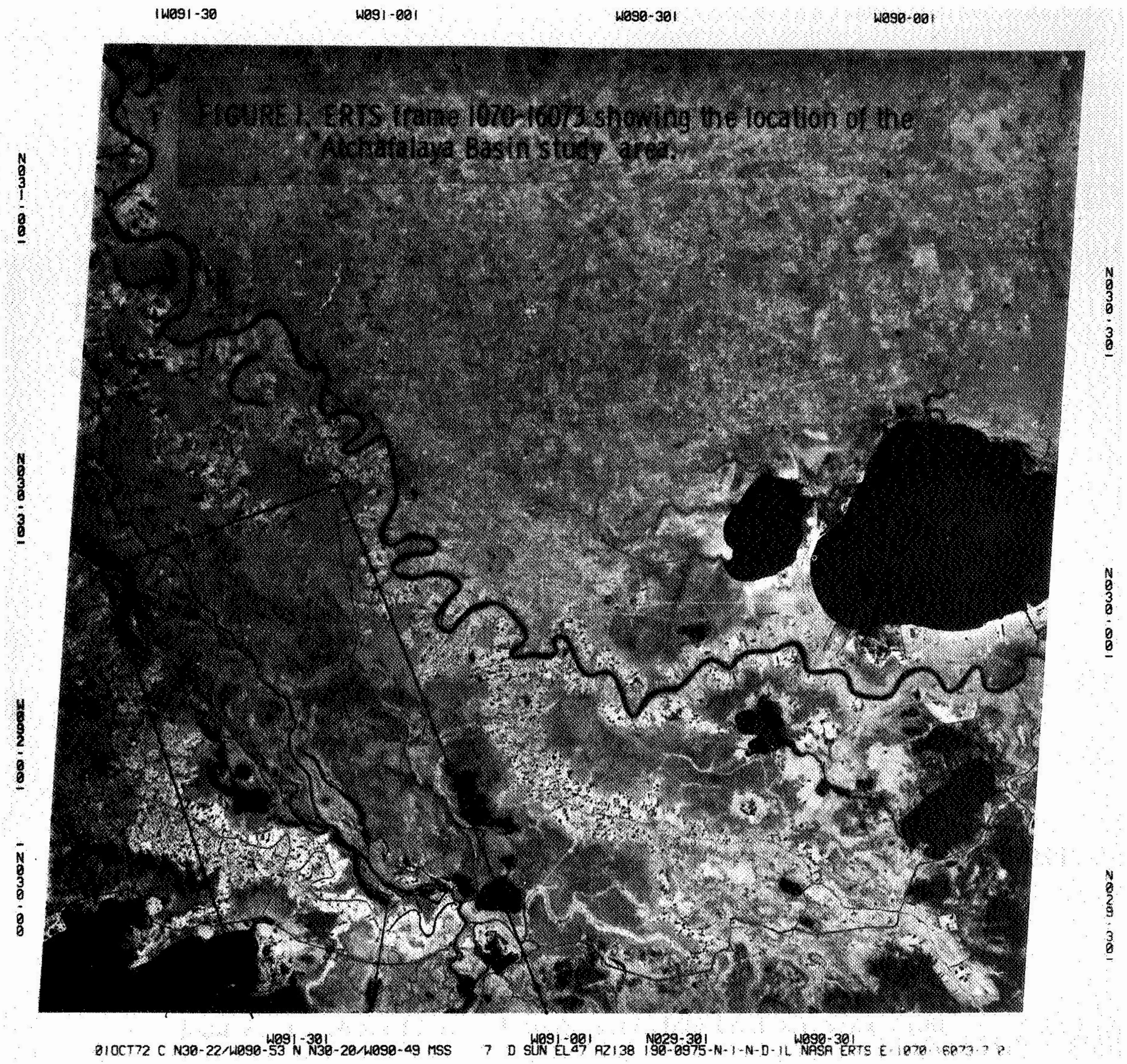

Figure 1. ERTS Frame 1070-16073 Showing the Location of the Atchafalaya Basin Study Area

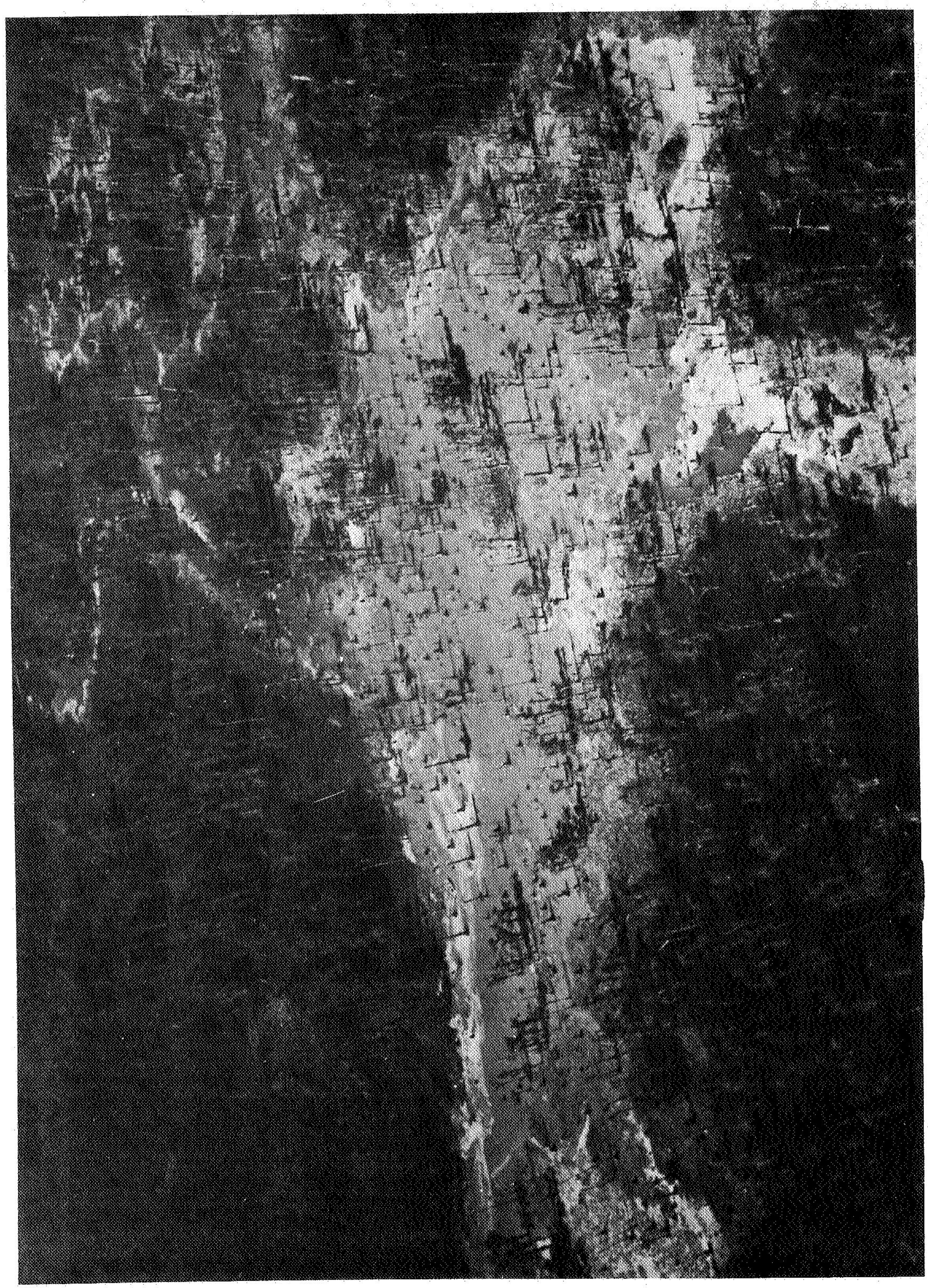

Figure 2. Low Level Aerial Photograph of the Swamp Area of the Basin

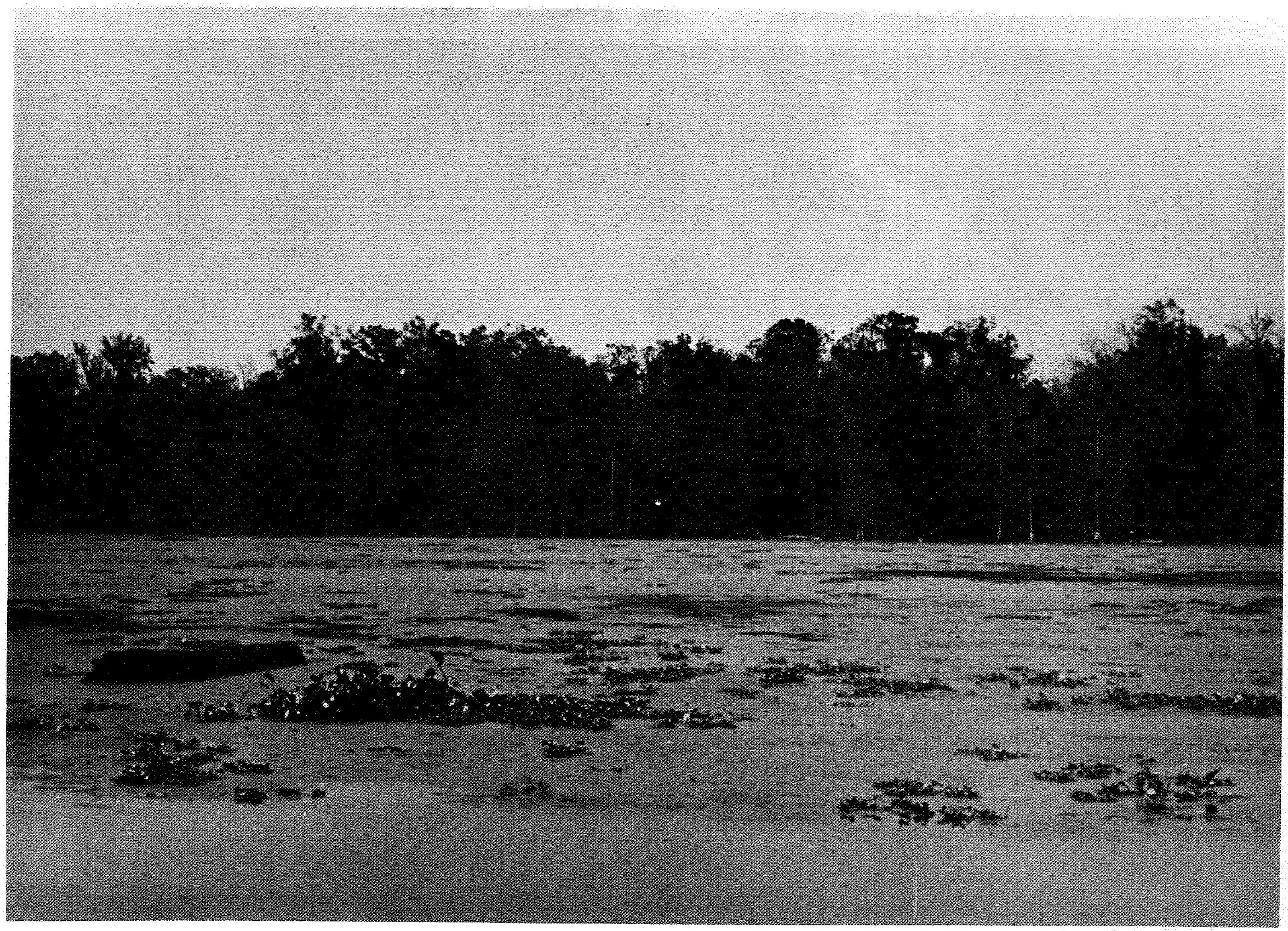

Figure 3. Ground Level Photograph of a Small Lake Covered With Duckweed and Water Hyacinth

Figure 4. Low Level Aerial Photograph of the Forested Area of the Basin

Figure 5. Computer Derived Simulated Color IR Map Made from the Computer Compatible Tapes of ERTS Frame 1070-16073, October 1, 1972

Figure 6. Large Scale Computer Derived Simulated Color IR Map Made from the Computer Compatible Tapes of ERTS Frame 1286-16083, May 5, 1973

Figure 7. Computer Density Map Derived from Band 3 Digital Data (CCT's) of ERTS Frame 1070-16073, October 1, 1972

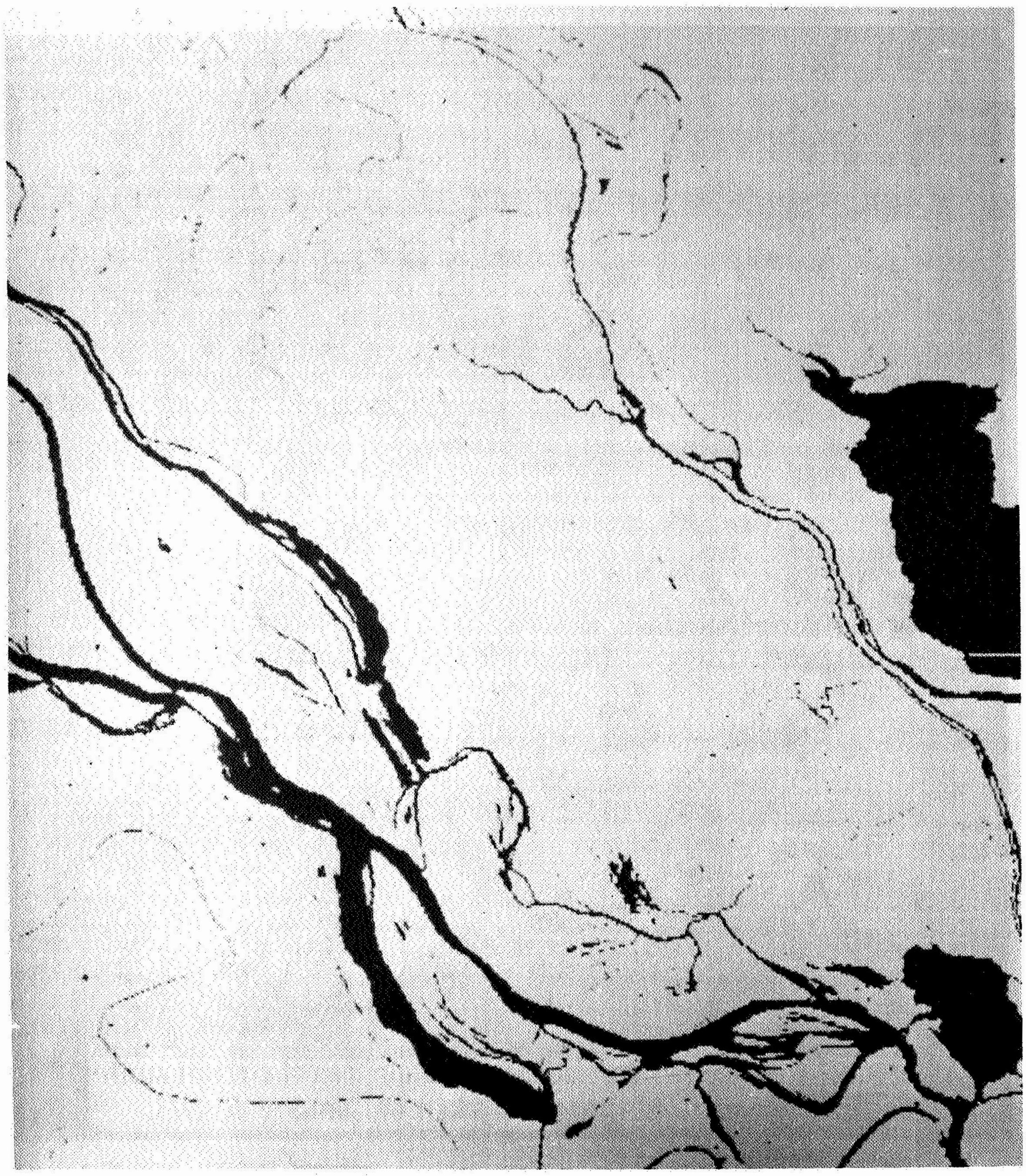

Figure 8. Themic Map (Water) Derived from the Digital Data (CCT's) of ERTS Frame 1070-16073 by Use of a Two Band (1&4) Decision Curve

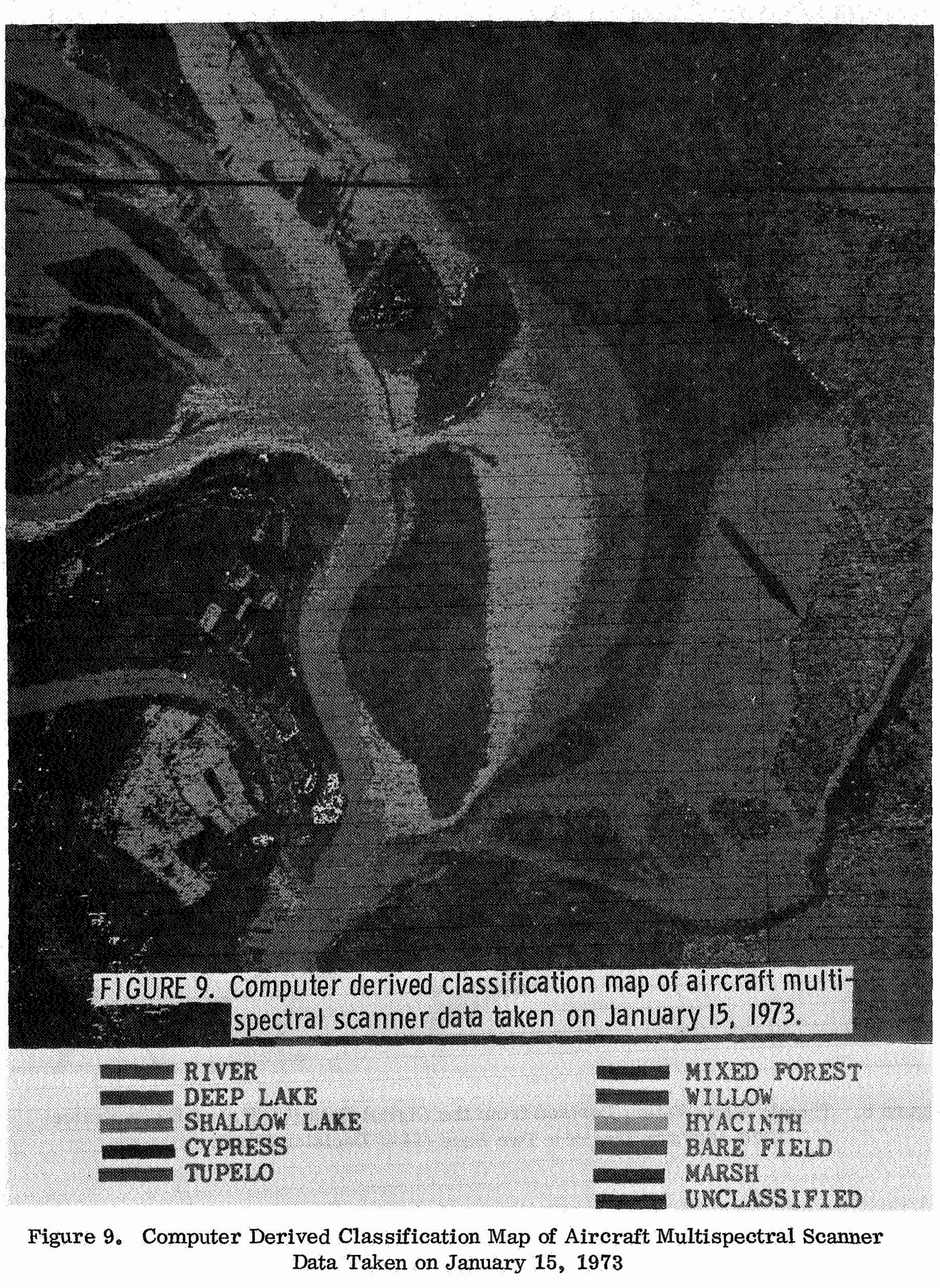

Figure 9. Computer Derived Classification Map of Aircraft Multispectral Scanner Data Taken on January 15, 1973

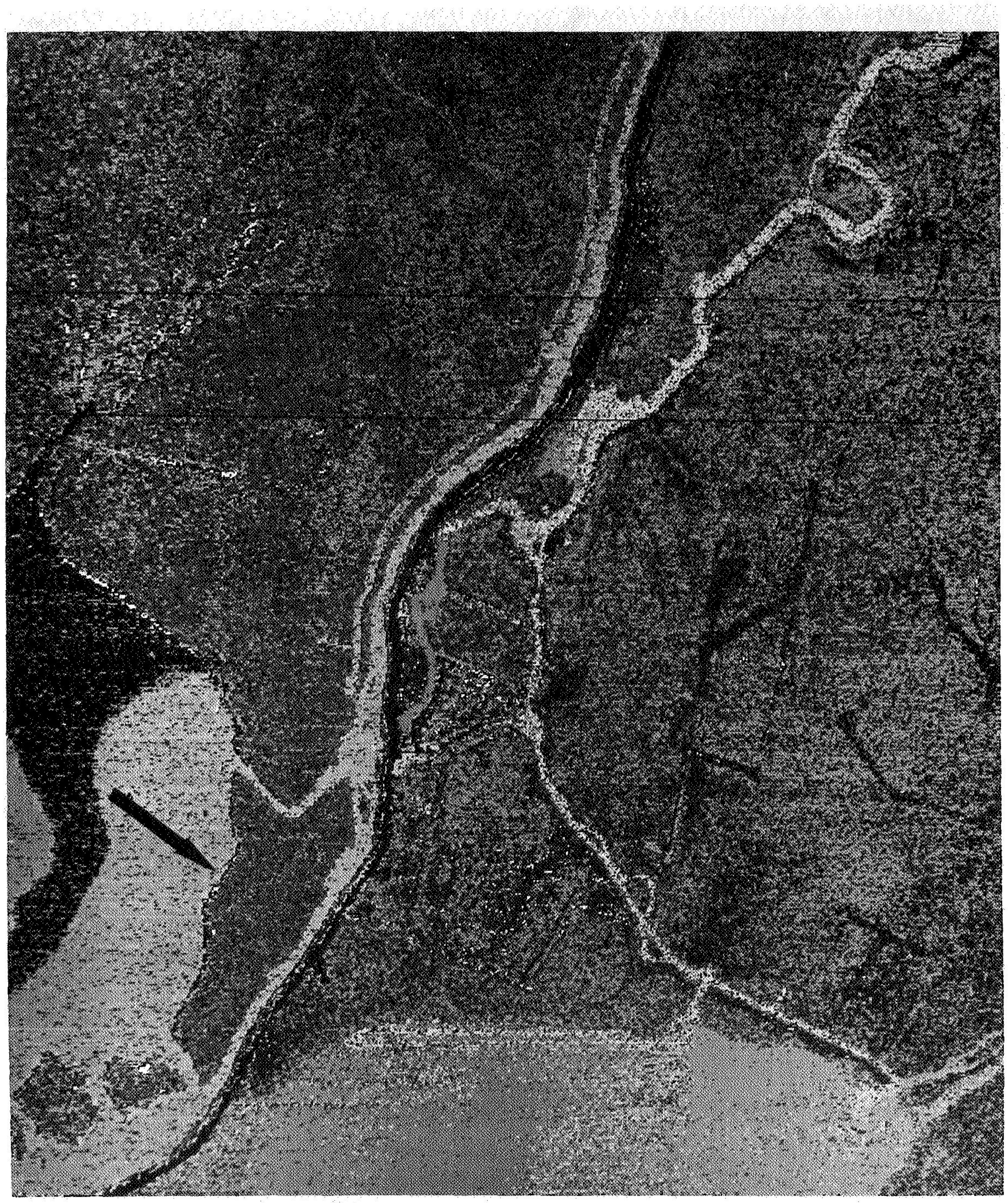

Figure 10. Computer Derived Classification Map of Aircraft Multispectral Scanner Data Taken on the Adjacent Flight Line Shown on Figure 9

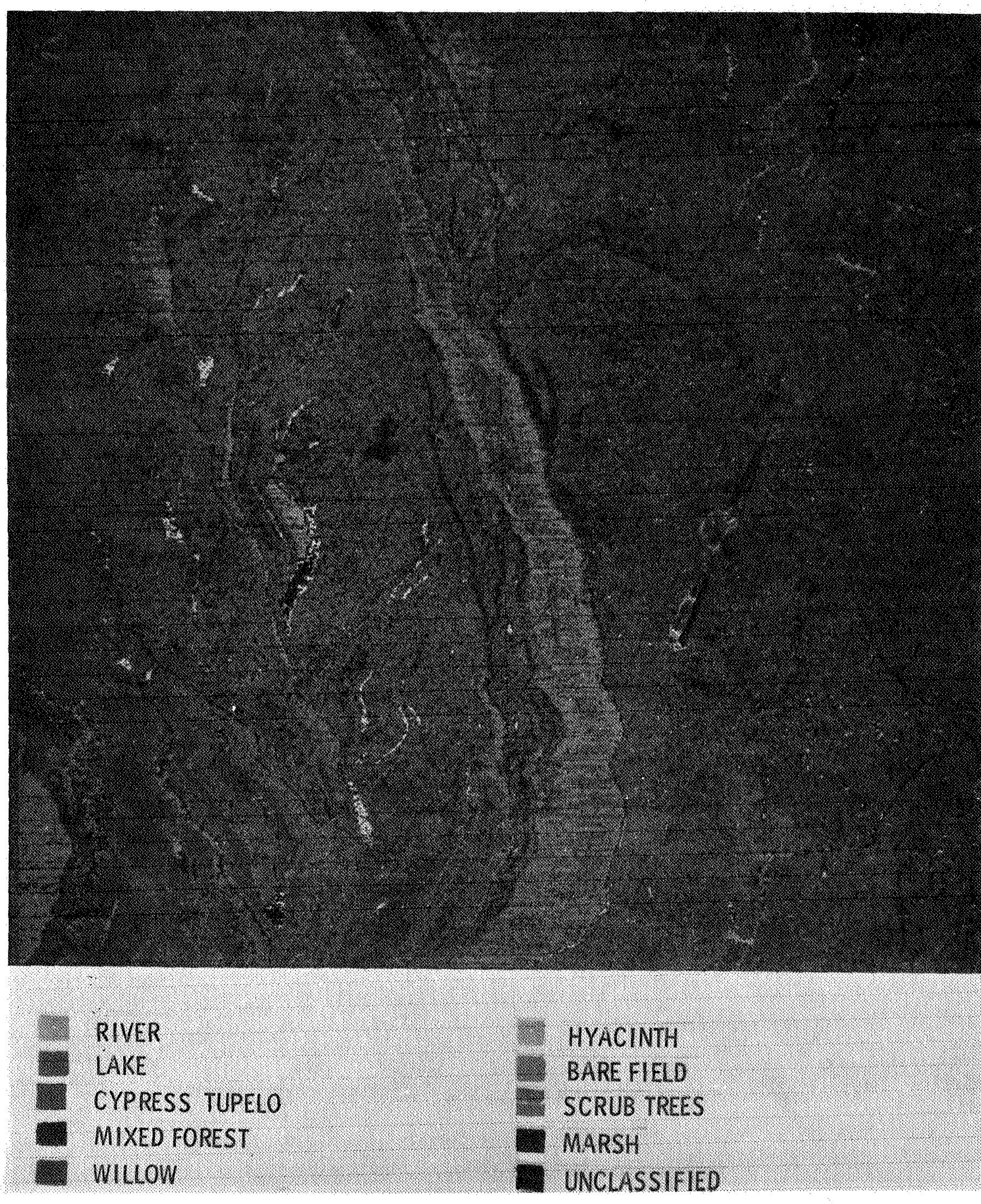

Figure 11. Computer Derived Classification Map of Aircraft Multispectral Scanner Data Taken on January 15, 1973

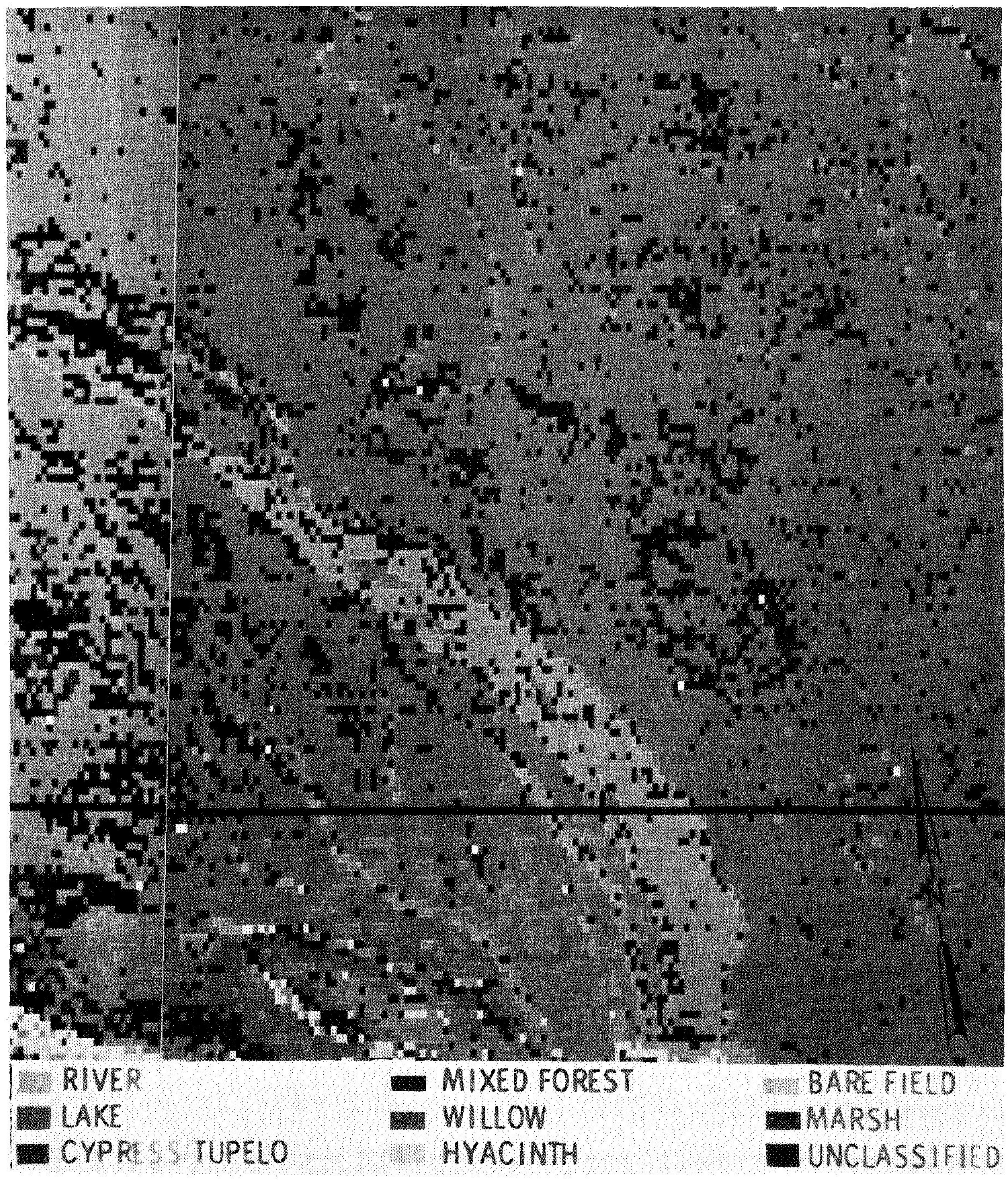

Figure 12. Computer Derived Classification Map of ERTS Frame 1196-16082, February 4, 1973

MARINE RESOURCES

Paper M 1

RELATIONSHIPS BETWEEN ERTS RADIANCES AND GRADIENTS ACROSS OCEANIC FRONTS

George A. Maul, *Atlantic Oceanographic and Meteorological Laboratories, National Oceanic and Atmospheric Administration, Miami, Florida,* Howard R. Gordon, *Department of Physics, Optical Physics Laboratory, and Rosenstiel School of Marine and Atmospheric Science, University of Miami, Coral Gables, Florida*

ABSTRACT

A time series of the Loop Current in the Gulf of Mexico, covering an annual cycle of growth, spreading, and decay, has been obtained in synchronization with ERTS. Computer enhanced images, which are necessary to extract useful oceanic information, show that the current can be observed either by color or sea state effects associated with the cyclonic boundary. The color effect relates to the spectral variations in the optical properties of the water and its suspended particles, and is studied by radiative transfer theory. Significant oceanic parameters identified are: the probability of forward scattering, and the ratio of scattering to total attenuation. Several spectra of upwelling diffuse light are computed as a function of the concentration of particles and yellow substance. These calculations compare favorably with experimental measurements and show that the ratio of channels method gives ambiguous interpretative results. These results are used to discuss features in images where surface measurements were obtained and are extended to tentative explanation in others.

INTRODUCTION

Remote sensing of the ocean in the visible region of the spectrum is being explored for a variety of reasons. Maximum insolation at 475 nm provides a natural energy source for passive sensors. A minimum in the attenuation coefficient for water may allow a passive measurement of some oceanic properties as a function of depth. Variations in the spectra of upwelling light at these wavelengths can be attributed to variations in pigment forming molecules such as in phytoplankton and to variations in the concentration of scattering particles such as suspended sediments. Strongly baroclinic currents in the subtropics and tropics can be detected by change in the optical properties across their boundaries when infrared techniques fail due to isothermal surface conditions. Patterns of man's activities in and on the ocean have near surface manifestations which change the nature of upwelling visible radiance.

The social significance of oceanic observations from a vehicle such as ERTS has recently been summarized by Maul (1974a). Discussions in the present paper are limited to a study of the dominant feature of the Gulf of Mexico circulation, that portion of the Gulf Stream System called the Loop Current. This intense current transports vast amounts of thermal and kinetic energy into the basin through the Yucatan Straits. Temporal and spatial variability in the flow (figure 1) was studied as part of the ground truth time-series which followed the anti-cyclonic turning from Yucatan to the Florida Straits. Some dynamical results were reported by Maul (1973a) and will not be discussed here. As a purely descriptive oceanographic study however, these data have significance in hurricane intensification studies such as by Leipper and Volgenau (1970); the investigation of the Florida east coast red tide (Murphy, *et al.*, 1973) used these ship tracks and a supporting ERTS image to document their arguments; the environmental impact of a recent accidental jettisoning of cyanide canisters following a ship collision in the Gulf of Mexico is being studied using these data (Corwin and Richardson, 1974). Continued reconnaissance of this current pattern is significant in our understanding of, and reaction to, the transport, which affects fishing industries, marine transportation, and public health.

ERTS OBSERVATIONS OF OCEANIC FRONTS

The location of the cyclonic boundary of the Loop Current was obtained by tracking the 22°C isotherm at 100 meters depth using expendable bathythermographs. The pathline of this

isotherm is of the order of 20 kilometers to the right (facing downstream) of the surface frontal zone (Hansen and Maul, 1970). This, coupled with ship observations of chlorophyll-a, surface temperature, volume scattering function, and sea state, provides the baseline measurements to insure that the interpretations to follow are well founded. Figure 2 is a temperature-depth profile across the current along a suborbital track during a satellite transit; surface observations are at the top of the figure. This summarizes the general conditions of increasing temperature and salinity and decreasing chlorophyll and scattering when crossing the boundary into the current and serves to orient them to the indicator isotherm. These observations confirm (Maul and Hansen, 1972) that changes in all these properties occur simultaneously, allowing an increase in confidence when a recognition decision is made using several variables.

Diffuse reflectance from beneath the ocean, which is defined as the ratio of upwelling to downwelling irradiance, measured just above the surface, is rarely more than 0.05. Reflectance from the ocean's surface, which is independent of diffuse reflectance, can be comparable or even substantially larger depending on sea state, and this has been shown by Maul (1973b) to be a useful indicator of the current. Reflectance from clouds and agricultural scenes is sometimes an order of magnitude greater than from the ocean, even in the 500-600 nm wavelength (λ) region. In order for the NASA Data Processing Facility (NDPF) to produce an image for an average scene radiance, the ocean signal is compressed into the lowest few gray scales. This is clearly illustrated in figure 3 which is a scanline plot across the boundary of the Loop Current from the multispectral scanner. The large spikes in all four channels (MSS 4 upper) are clouds; there seems at first glance to be very little change in digital number (DN), which is proportional to radiant intensity, as a function of the sample number. However, careful examination shows that the average value of the DN at samples greater than number 950 is slightly larger than those before this point. It will be seen that this marks the transition to higher radiances caused by increased sea state in the current.

In order to graphically display this small change over a two-dimensional region, computer enhancement is necessary. Contrast stretching for the ocean scene is accomplished by first studying the frequency distribution of DNs in a training area on the image; the area is selected to be representative of the ocean away from land and is large enough to be statistically significant. As seen from figure 3, such a histogram

would be strongly bimodal due to clouds. Selection of the upper (DN_u) and lower (DN_l) cutoff can be set at $\pm$ 2 standard deviations about the ocean mode; in this case $9 \leq DN \leq 13$ was used. It should be noted that each image will have different cutoff values and that the final image is quite sensitive to the range of DN chosen (Charnell *et al.*, 1973). The general expression for computing the stretch variable (ζ) is:

$$\zeta = M\left[\frac{DN_u - DN}{DN_u - DN_l}\right]^n \quad (\text{for } DN_l \leq DN \leq DN_u) \tag{1}$$

where M is the maximum value allowed by the output device, and n is an arbitrary integer exponent. Equation 1 produces a negative of the input digital image; positive whole integers n, further stretch the low radiance values encountered in the ocean. The graphic result of using equation 1 on the data from which figure 3 was taken is given in figure 4.

Figure 4 is a negative print of an area due north of the Yucatan Straits using MSS 5 data. Computer enhancement in this iamge uses only five gray scales of the 128 levels available; all values below DN_l are set to 127 and all above DN_u are set to 0. The boundary between the resident Gulf waters (left) and the current (right) is seen as a transition from light to dark tones respectively. Since the radiance levels in the ocean are so low, the oceanographer *must* resort to computer enhancement as this example shows.

Figure 5 is another enhancement of the Loop Current boundary using MSS 5 where $7 \leq DN \leq 15$ and $n = 2$. In this negative image of the western Florida Keys, water from Florida Bay extends into the Florida Straits and is entrained by the Loop Current. The current boundary in both figures 4 and 5 was delineated by surface vessel tracks during the day of the satellite transit. Notice that the current is darker in tone (higher in radiance) in figure 5. This is caused by the dominance of surface reflection due to higher sea state in the current in figure 4, as compared to higher reflectance due to particles in the Florida Bay water in figure 5.

SOME THEORETICAL CONSIDERATIONS

At this point it is useful to consider in detail the processes contributing to the radiance spectrum $N(\lambda)$ at the position of the satellite. Solar radiation incident at the top the atmosphere is absorbed and scattered in the atmosphere. Some radiation is scattered back into space without striking the

ocean contributing a radiance $N_s(\lambda)$ at the satellite. The rest (which is not absorbed) will interact with the ocean. This interaction can yield upwelling radiance above the ocean in three ways: 1) specular reflection from the surface; 2) diffuse reflection from foam (bubbles) on or just beneath the ocean surface; and 3) the diffuse reflection from water molecules and suspended particles in the water. Of these the first two phenomena are closely related in that they depend on the sea state, while the third source of radiance is essentially independent of sea state. The specular reflectance from the rough ocean surface can be computed by the methods of Cox and Munk (1954) in terms of the wind speed and incident radiance distribution. The diffuse reflectance from white caps can be approximately accounted for by assuming they are "white", Lambertian, and have an albedo of 1 so that they contribute uniform upwelling radiance just above the surface given by

$$H_0(\lambda)\,\frac{f}{\pi}$$

where f is the fraction of the scene covered by the white caps and $H_0(\lambda)$ the irradiance incident on the sea surface. The third source of radiance, that from beneath the surface, is the most difficult to compute and will be discussed in detail below. We can write the radiance at the satellite as

$$N(\lambda) = N_s(\lambda) + \gamma(\lambda) N_{ss}(\lambda) + \alpha(\lambda)\; N_d(\lambda) \tag{2}$$

where $N_{ss}(\lambda)$ is the contribution at the surface due to reflection from the surface and white caps, N_d is the diffuse radiance just above the surface due to photons that have penetrated the ocean, $\alpha(\lambda)$ and $\gamma(\lambda)$ are atmospheric transmittance factors for N_d and N_{ss}. $\alpha(\lambda)$ and $\gamma(\lambda)$ are in general not equal since the radiance distribution (variation with angle) of N_{ss} and N_d are different. It is possible for photons to be reflected from the surface, backscatter from the atmosphere into the ocean, and scatter back into the atmosphere. Photons which do this we consider to be a part of N_d. It should be stressed at this point that $N_d(\lambda)$ in the above equation is the *only* source of radiance that contains information about conditions beneath the sea surface such as the concentration and composition of suspended particles and dissolved organic material. A thorough understanding of the dependence of $N_d(\lambda)$ on the basic optical properties of the water and its constituents is required in order to obtain *quantitative* information about the constituents of the ocean from measurements of $N_d(\lambda)$. The remainder of this section is devoted to relating $N_d(\lambda)$ to these optical properties.

We shall assume that the radiance distribution incident on the sea surface is given, and that the radiance is transmitted from the ocean to the satellite in a known manner given by $\alpha(\lambda)$ and $\gamma(\lambda)$ in equation 2. This reduces the problem to that of taking a known downwelling radiance distribution just above the sea surface, and computing the distribution (just above the surface) of the upwelling radiance. As mentioned above, radiant energy interacting with the ocean can be absorbed by water, suspended particles, and dissolved organic material commonly called yellow substance with absorption coefficients a_w, a_p, a_y respectively and scattered by the water and particles with scattering coefficients b_w and b_p (scattering by the yellow substance appears to be negligible). The total attenuation coefficient, c, for these interactions is given by

$$c = c_w + c_p + c_y \tag{3}$$

where

$$\begin{aligned} c_w &= a_w + b_w, \\ c_p &= a_p + b_p, \\ c_y &= a_y \end{aligned} \tag{4}$$

are the beam attenuation coefficients of the water, particles, and yellow substance. The scattering is further characterized by the phase function, $P(\theta)$, which relates to the intensity of radiation, $dJ(\theta)$, singly scattered from a small sample volume, dv, when illuminated by an incidence irradiance, H_0, through

$$P(\theta) = \frac{dJ(\theta)}{(H_0 dv) b}$$

$$2\pi \int_0^{\pi} P(\theta) \sin\theta \, d\theta = 1 \tag{5}$$

The total phase function for water and particle scattering is

$$P(\theta) = \frac{(b_w P_w(\theta) + b_p P_p(\theta))}{(b_w + b_p)}$$

where P_w and P_b are the phase functions due to water only and particles only respectively. It is convenient to further define the forward (F) and backward (B) single scattering probabilities by

$$B \equiv 1 - F$$

$$F \equiv 2\pi \int_0^{\pi/2} P(\theta) \sin\theta \, d\theta \tag{6}$$

and the single scattering albedo by

$$\omega_0 \equiv \frac{b}{c} \tag{7}$$

Hence it is clear that

$$B = \frac{(b_p B_p + b_w B_w)}{(b_p + b_w)} \ , \tag{8}$$

$$\omega_0 = \frac{(b_w + b_p)}{(a_w + a_p + a_y + b_p + b_w)} \ , \tag{9}$$

and in general, $$0 \leq \omega_0 \leq 1 \ .$$

It should be noted that *all* of the above quantities depend on wavelength (λ). The transfer of radiation in the ocean is governed by the radiative transfer equation which has been discussed in detail by Chandrasekhar (1960) and Preisendorfer (1965). Gordon and Brown (1973) have computed the diffuse reflectance (upwelling irradiance/incident irradiance) just above a flat *homogenous* ocean as a function of its optical properties by a Monte Carlo technique. Using a combination of the parameters which arise naturally from the quasi-single scattering model (Gordon 1973), Gordon, Brown and Jacobs (in preparation) show that the diffuse reflectance (R_d) can be written

$$R_d = 0.179x + 0.0510x^2 + 0.1710x^3 \tag{10}$$

where
$$X \equiv \frac{B\omega_0}{(1-\omega_0 F)}$$

R_d is to first order independent of the distribution of the incident irradiance. It should be emphasized that the above equation does *not* include the irradiance specularly reflected from the sea surface or white caps, i.e. R_d is the contribution to the reflectance from photons which penetrate the surface and are multiple scattered back into the atmosphere. Preliminary computations (Gordon and Brown unpublished) indicate equation 9 is also valid for a moderately rough surface. The radiance distribution above the sea surface (due to photons scattered out of the ocean) is only weakly dependent on ω_0 , and thus the radiance at any viewing angle will in first order vary with ω_0 , and B in the same fashion as R_d. Hence, it is sufficient to study the influence of the optical properties of the ocean on R_d alone.

Equation 9 shows that the important oceanic parameters are ω_0 and B, and so the observed reflectance spectrum, R_d (λ), can be explained entirely through a knowledge of ω_0 (λ) and B(λ). Conversely under *optimum* conditions, only $\omega_0(\lambda)$ or B(λ) can be deduced from R_d and then only if *one* of these quantities is already known. The situation appears quite depressing when it is realized that $\omega_0(\lambda)$ is only imperfectly known even for pure water and to our knowledge there are no measurements of $B_p(\lambda)$ and $\omega_0(\lambda)$ for various kinds of suspended particles. Hence at the present time it is difficult to interpret $\omega_0(\lambda)$ and B(λ) even if both could be extracted from $R_d(\lambda)$ measurements. This underscores the necessity of laboratory experimentation to determine these optical properties for various ocean constituents such as marine phytoplankton, and suspended mineral particles, for adequate interpretation of oceanic "color". If the optical properties of the constituents are known, then it is theoretically possible to determine their concentrations through observations of $R_d(\lambda)$ as is discussed in several examples below.

We shall now examine a particularly simple problem of interpretation, that of determining the concentration of suspended material in the absence and presence of yellow substance. The particles are assumed to be nonabsorbing, and their scattering coefficient is assumed to be independent of wavelength [cases where b_p = (const.) λ^{-n} with $n \leq 1$ have also been investigated and yield results not dramatically different from the n = 0 case]. These calculations will *not* apply at all to locations with particles containing absorbing pigments such as phytoplankton in the water, since Mueller (1973) and Gordon (1974) have shown that scattering from such particles varies *strongly* with wavelength near the pigment absorption bands.

In order to use equation 10, $B(\lambda)$ and $\omega_o(\lambda)$ in equations 8 and 9 must be determined. We shall follow Tyler, Smith and Wilson (1972) and use for b_w and B_w values experimentally computed for sea water continuously filtered for 18 hours (Petzold 1972), rather than theoretical computations of these quantities for pure water. We do not feel comfortable with this, however, on the above basis they have estimated the absorption spectrum of "clear natural water", and since we use their $a_w(\lambda)$ spectrum this assumption is essential for consistency. It is thus assumed that $B_w = 0.1462$ and $b_w = 0.008 m^{-1}$ at 550 nm, so

$$b_w = 0.008 \left[\frac{550}{\lambda}\right]^4 m^{-1}$$

To find B_p, Petzold's measurements of $P(\theta)$ from the Tongue of the Ocean (TOTO), San Diego Harbor (SDH), and Off Shore California (OSC) at 530 nm have been used. Assuming the above for B_w and b_w, the contribution from water is subtracted yielding the B_p values listed in Table 1 (ω_o is given in the parenthesis and ω_o for filtered sea water at this wavelength is 0.136).

TABLE 1

Derived Values of B_p for the Indicated Locations

TOTO	SDH	OSC
0.0165 (.59)	0.0186 (.82)	0.00966 (.59)
0.0158 (.25)	0.0194 (.83)	0.00836 (.55)
0.0130 (.26)	0.0169 (.91)	0.00836 (.55)

From Table 1 it is clear that B_p not only varies considerably from one location to another, but also varies considerably for a single region. This is unfortunate in that for small ω_o, R_d is directly proportional to $\omega_o B$ and ω_o and B are then *equally* important in determining R_d for these cases. We shall assume that Table 1 gives the range of variation of B_p to be expected in natural waters, however this is probably not the case. Furthermore we will assume B_p (and B_w) is independent of wavelength.

Since a_p is taken to be zero, and the $a_w(\lambda)$ estimate of Tyler, Smith and Wilson is to be used, only $a_y(\lambda)$ remains to

be considered. This is taken from Jerlov (1968, Page 56) and is parameterized by

$$a_y(\lambda) = a_y e^{0.0145(550-\lambda)}$$

where λ is in nm. Reasonably high concentrations of yellow substances in the open ocean have $a_y \simeq 5 \times 10^{-3} m^{-1}$ (i.e., near Galapagos Islands) however, a_y can be much larger in coastal regions.

Using the above and equation 10, we have computed $R_d(\lambda)$ called Reflectance (0,-) in the figures, as a function of b_p/b_w (proportional to the concentration of suspended particles) for various values of B_p and a_y. The results are given in figures 6 through 10.

Figure 6 shows the R_d for $\lambda = 550$ nm as a function of b_p/b_w and B_p. The linearity of R_d with b_p/b_w is to be noted. These results clearly demonstrate the importance in knowing B_p for a quantitative determination of the particle concentration from R_d (which is measured at the *sea surface*). Figure 7 shows spectra of R_d again for various values of b_p/b_w but now with $B_p = 0.0165$. These spectra have the same general shape as those observed by Tyler and Smith (1970) just beneath the surface in Crater Lake, but are not in quantitative agreement even when the loss due to transmittance through the water surface is considered. Basically the difference is that quantitative agreement requires too large a value of b_p/b_w. This could be due to the value of B_p used, the fact B_p is assumed to be independent of wavelength, or inaccuracies in their estimated $a_w(\lambda)$ on which the present calculations are based. In any event the computations can be used as a guide for examining ERTS related data. Figure 8 shows the influence of yellow substance on the reflectance for the case with $b_p/b_w = 128$ and $B_p = 0.0165$. The major influence of the yellow substance is to depress the blue region of the reflectance spectrum. All of these results are summarized in figures 9 and 10, where the reflectances have been integrated over the ERTS MSS channels 4 (figure 9) and 5 (figure 10) for various B_p and a_y as a function of b_p/b_w. It is seen that the yellow substance influences the reflectance in MSS 4 only at very high concentrations (for the open ocean) and essentially plays no role in the MSS 5 reflectance. Therefore, for suspended particle concentrations, it appears that MSS 5 is best with MSS 4 only slightly degraded by the dissolved organic materials. It should be emphasized again that the above discussion refers only to the case of no phytoplankton (chlorophyll)!

We now turn to the problem of estimating b_p/b_w or some related quantity from satellite observations. Since the above calculations are only for the case of negligible phytoplankton (chlorophyll) concentrations we must find criteria from which to choose which ERTS channels will satisfy this constraint. Also unless only MSS 5 is used we expect yellow substances to be important especially in coastal regions where river runoff, etc., may be considerable. Furthermore there is the additional problem that the reflectance depends on B_p which is also unknown, as will as b_p/b_w. We have developed a method which partially overcomes some of these problems. Considering the radiances observed in MSS 4 and 5, we have approximately

$$N_4 = \alpha_4 N_{d_4} + \gamma_4 N_{ss_4} + N_{s_4}$$
$$N_5 = \alpha_5 N_{d_5} + \gamma_5 N_{ss_5} + N_{s_5} \qquad (11)$$

where α_i and γ_i ($i = 4, 5$) are the fractions of N_{d_i} and N_{ss_i} (measured at the sea surface) that reach the sensor. It is assumed that α_i and γ_i are constant over an ERTS Frame (if they vary in a known way, their influence is easily accounted for and will not be discussed further). Now from the theory

$$N_{d_4} = k_4 \frac{b_p}{b_w}$$
$$N_{d_5} = k_5 \frac{b_p}{b_w} \qquad (12)$$

where k_4 and k_5 are essentially independent of b_p/b_w, but depend directly on B_p. Taking the horizontal gradient, ∇_H, of equation 11 using equation 12 we find

$$\nabla_H N_i = k_i \alpha_i \nabla_H \left(\frac{b_p}{b_w}\right) + \gamma_i \nabla_H N_{ss_i} \qquad (13)$$

since N_{s_i} is nearly constant over a frame ($\nabla N_{s_i} = 0$). The last term in equation 13, $\nabla_H N_{ss_i}$, is the horizontal gradient of the reflected radiance from the sea surface. This is nearly zero everywhere except where the sea state changes dramatically with horizontal distance (for example in figure 4). Nearly everywhere on the frame then, $\nabla_H N_{ss_i} = 0$, so

$$\frac{\nabla_H N_4}{\nabla_H N_5} = \frac{k_4 \alpha_4}{k_5 \alpha_5} \qquad (14)$$

Again α_4/α_5 is constant (or slowly varying) over the scene; so almost everywhere in the frame, variations in $\nabla_H N_4/\nabla_H N_5$ are the result of variations in k_4/k_5. Now if B_p is constant, or if the "mean" B_p is constant in each wavelength band, this would imply that essentially only the concentration of scattering particles varies over the frame, i.e. not the nature of particles or their size distribution. In this case, k_4/k_5 would be constant. Hence essentially k_4/k_5 will vary, if the nature or size distribution of the particles varies over the frame (B_p changes), or if the yellow substance concentration varies considerably over the frame, which would force k_4 to vary independently of k_5. Thus if we find

$$\frac{\nabla_H N_4}{\nabla_H N_5} = \text{Const} \tag{15}$$

it is reasonable to expect that *only* the particle concentration changes over the frame. In this case

$$\nabla_H N_4 \text{ or } \nabla_H N_5 \sim \nabla_H \text{ (particle concentration)} \tag{16}$$

Note here that these relations should also apply to scenes containing phytoplankton if they are the dominant scatterers; but for mixtures of phytoplankton and suspended white particles, one would expect equation 15 to be violated over a scene if the relative concentrations vary drastically. To reiterate, if 15 holds, probably only the particle concentration varies over the frame, and 16 can be used to measure the gradient of its concentration. Since B_p is unknown, the actual concentration is indeterminate without ground truth to better than a factor of two, since this is the assumed uncertainty in B_p. Several examples of the use of the above ideas for analysis of ERTS data are presented below.

DISCUSSION

Equation 16 was applied to MSS 4 and MSS 5 data in figure 11. This computer enhanced negative image of the Cape Hatteras region shows what appears to be large gradients in suspended sediment. The Gulf Stream apparently has entrained particles from Rayleigh Bay and is carrying them out to sea. Along the scanline shown we have computed

$$\frac{\partial}{\partial x}\left[N_4\right] = g\,\frac{\partial}{\partial x}\left[N_5\right] + h \tag{17}$$

properties of the individual components with wavelength is known.

As an example of this, the spectra given in figure 12 were integrated over the MSS 4, MSS 5, and MSS 6 filter functions. A series of numerical tests were then made of ratios, differences, and sums to see if the three water types could be distinguished at the sea surface. It was quite easy to distinguish on the basis of such calculations between the Gulf Stream waters and the coastal waters, and between the coastal waters and the plankton bloom; however it was *not* possible to distinguish between the Gulf Stream and the plankton bloom. This suggests, as the theory implies, that for these data the ratio test (MSS 4/MSS 5) is not likely to be successful in specifying the chlorophyll-a concentration. Further, since the sea surface component, N_{SS}, (λ), spectrally alters N (λ), numerical tests (ratios, differences *etc.*) are *invalid* indicators of oceanic properties.

Probably the most efficient method of determining the concentration of the constitutents in the ocean will be to compare theoretical and experimental spectra, adjusting the constitutent concentrations in the theoretical spectra until agreement is found. This of course requires a basic understanding of the optical properties of the constitutents which can be derived only from careful *in situ* and laboratory experiments. It seems that at the present time much energy and money is being expended to try and use optical methods to locate and study materials with nearly unknown optical properties suspended or dissolved in a medium with only poorly known optical properties. This must be overcome before significant progress can be made.

A final interpretation of oceanic observations from ERTS is given in figure 13 which is a computer enhanced MSS 6 negative image of southeastern Florida. The dark lineation parallelling the coast in the upper portion of the image is a zone of high reflection caused by locally increased N_{SS} along the edge of the Florida Current. The increase in surface reflectance is probably caused by surface wave interaction with the cyclonic boundary and is not bottom influence. This further explains the edge effect and supports the discussion on the local dependence of $\nabla_H N$ on $\nabla_H N_{SS}$ only given above. Another example of the dominance of N_{SS} is the bright slick areas (low N) off the Virginia Key sewer treatment plant. This is probably caused by the dampening of the glitter causing capillary waves in the oil film associated with the organic slick. The slick, which has drifted south past the popular Key Biscayne beaches, offers an explanation of the narrow lineation off shore in the Florida Straits: a passing oil tanker heading south which is pumping her bilges would cause

where the least squares values for g=0.38 and h=0.00, and the linear correlation coefficient, r, is 0.66. The coefficient of determination, r^2, which is the ratio of the explained variation from the mean (by the least squares line) to the total variation, is 44%. Physically this means that this image *may* not be useful for determining particle concentrations because B_p, ω_o (i.e. a_y), or b_p/b_w may be changing. The extent to which this holds true in natural waters is unknown; this will be extensively tested in the New York Bight area where turbidity measurements are being made by NOAA vessels concurrent with ERTS transits.

The data of figures 7 and 8 can be compared to measurements of upwelling irradiance. Data given in figure 12 were observed using a ¼-meter Ebert spectroradiometer from 3 meters above the surface; these observations were made during the time frame of figure 5 and represent the water types shown in that image. All spectra were carefully selected to represent the same downwelling irradiance, sea state, sun angle, cloud cover, and absence of bottom influence. Specular reflection due to waves were minimized by preselecting ten spectra with similar shapes. After digitizing the records, averages and standard deviations (σ) were computed at each wavelength; if values exceeded the average by 1σ, they were rejected and a new mean computed. Absolute values of the spectra are traced to NBS through the 2-meter integrating sphere at NASA's Goddard Space Flight Center.

As the chlorophyll-a concentration increases, the spectral peak shifts to longer wavelengths in similarity with the computed data in figure 8. This is not to say that the chlorophyll-a and the yellow substance produce *quantitatively* similar results; in general they will not. What it does imply is that the broad absorption bands in pigments such as chlorophyll and yellow substance at shorter wavelengths ($\leq$600 nm) produce *qualitatively* similar effects in the spectra. When other factors are equal, increasing the concentration of pigments will cause a decrease in the radiance in MSS 4 only. In nature however, such as in a plankton bloom or in a river plume, increased amounts of chlorophyll are normally accompanied by increased particle concentrations (organisms which contain the chlorophyll) as well as yellow substances (decay products of the plankton), and increased amounts of "white" suspended particles in the river plume case. The radiances in MSS 4 and 5 will in these cases vary in a manner which will depend again on the relative concentration of the constitutents, and since a and b vary almost independently, the reflectance signature, which depends on $\omega_o(\lambda)$ and $B(\lambda)$ is not unique and can be unraveled only when the variation of the optical

a similar feature on the image. Thus ERTS could be useful in patrolling coastal waters for such illegal acts which affect the nearshore water quality.

CONCLUSIONS

The spectral properties of the oceanic front associated with the Loop Current have been studied by ship and satellite observations and by radiative transfer theory. It is seen that computer enhancement is required to extract useful information from the ERTS data for the ocean scene. The current boundary can be detected by changes in the surface reflectance, N_{ss}, as well as the diffuse reflectance, N_d, from below the surface; N_d however is dependent on both B and ω_o, and thus the spectral interpretation of ocean color *requires* surface truth measurements for meaningful results. Particle concentrations, which can delineate currents, can be estimated in MSS 5 if the ratio $\nabla_H N_4 / \nabla_H N_5$ is reasonably constant over a scene. MSS 4 is strongly influenced by yellow substance, and particle estimation based on these data are invalid in many coastal zones. Water mass identification using ratios or differences of MSS 4, 5, and 6 data have no validity in either theory or observation in the Gulf of Mexico. Finally, it must be emphasized that the spectrum of upwelling radiance just above the surface is a function of both N_d and N_{ss} and that N_{ss} frequently dominates.

ACKNOWLEDGEMENTS

We wish to acknowledge the assistance of R. L. Charnell and R. M. Qualset for many fruitful discussions and computer programming. This work was in part supported by NASA contract S-70246-AG.

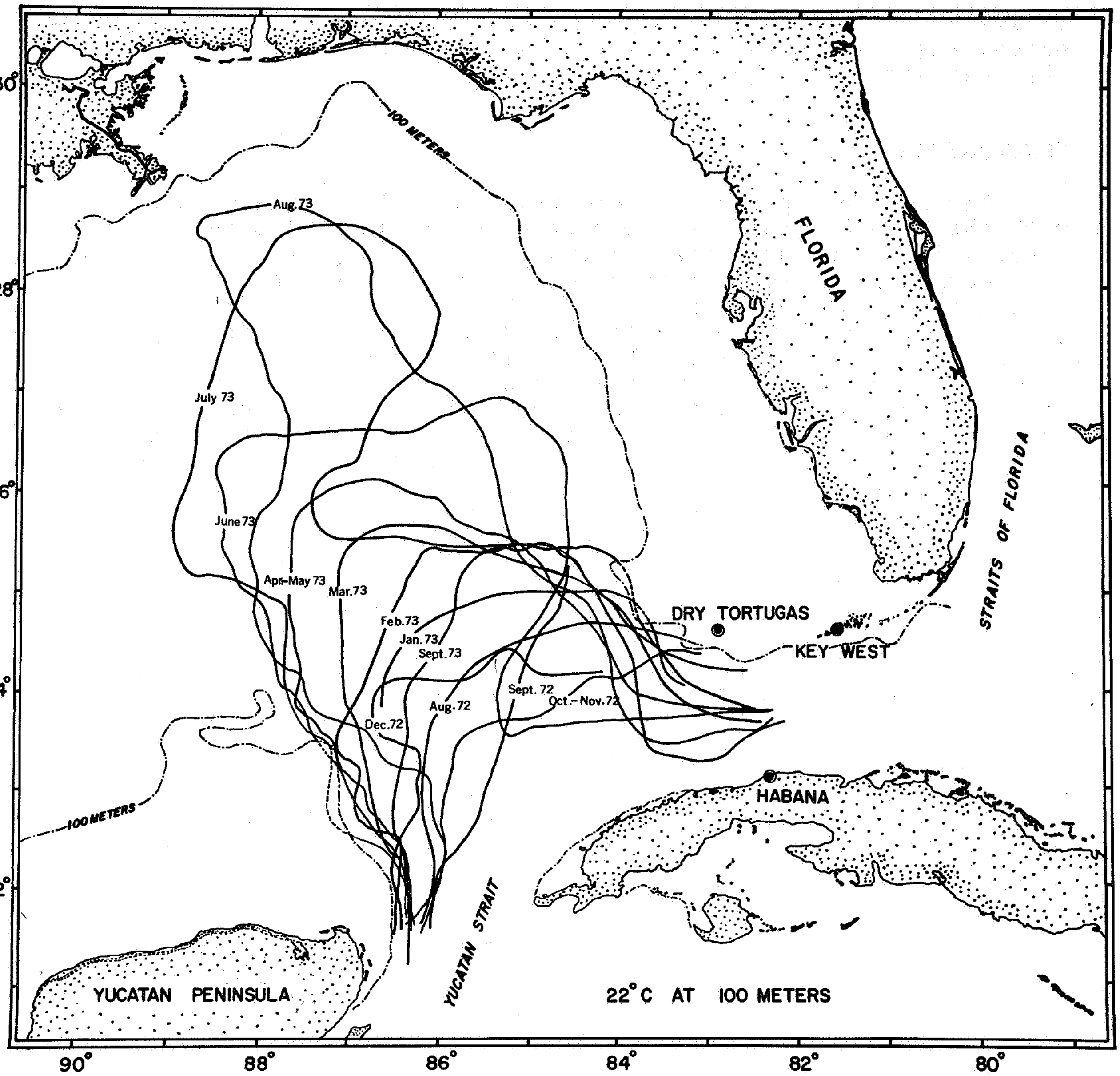

Figure 1. Time series of the Loop Current in the Gulf of Mexico, August 1972-September 1973. The pathlines are the location of the 22°C isotherm at 100 meters depth. Each cruise was synchronized with ERTS passes over the area every 36 days. The indicator isotherm was located by expendable bathythermographs from a surface vessel; this isotherm is approximately 20 kilometers to the right of the cyclonic edge facing downstream.

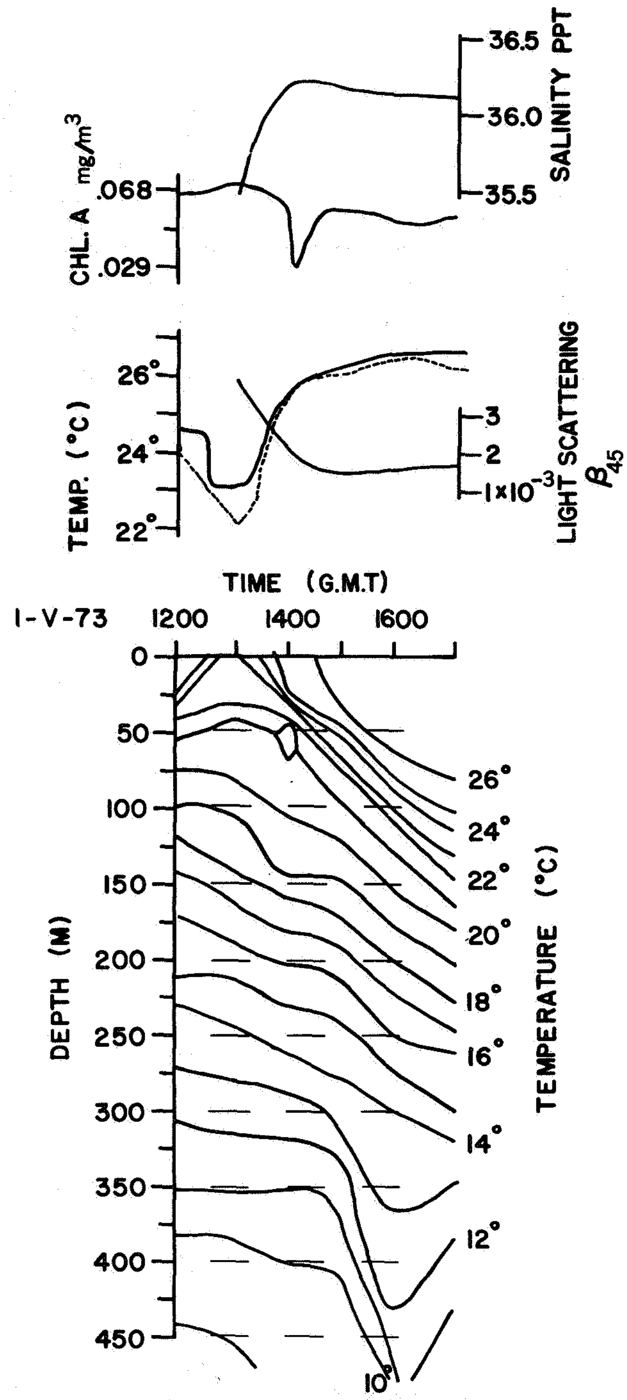

Figure 2. Cross section of the Loop Current taken by ship along a suborbital track on the day of ERTS transit. Section shows typical increase in salinity and temperature (dashed-radiometric, solid-bucket) when crossing into the current. Similarly chlorophyll-a and volume scattering function at 45° (436nm light) decrease. The temperature-depth section shows the relation between the 22°C at 100 meters and the surface frontal zone (at ca. 1330 GMT). Horizontal scale is 5 hours travel time at 9.8 knots or 90 kilometers.

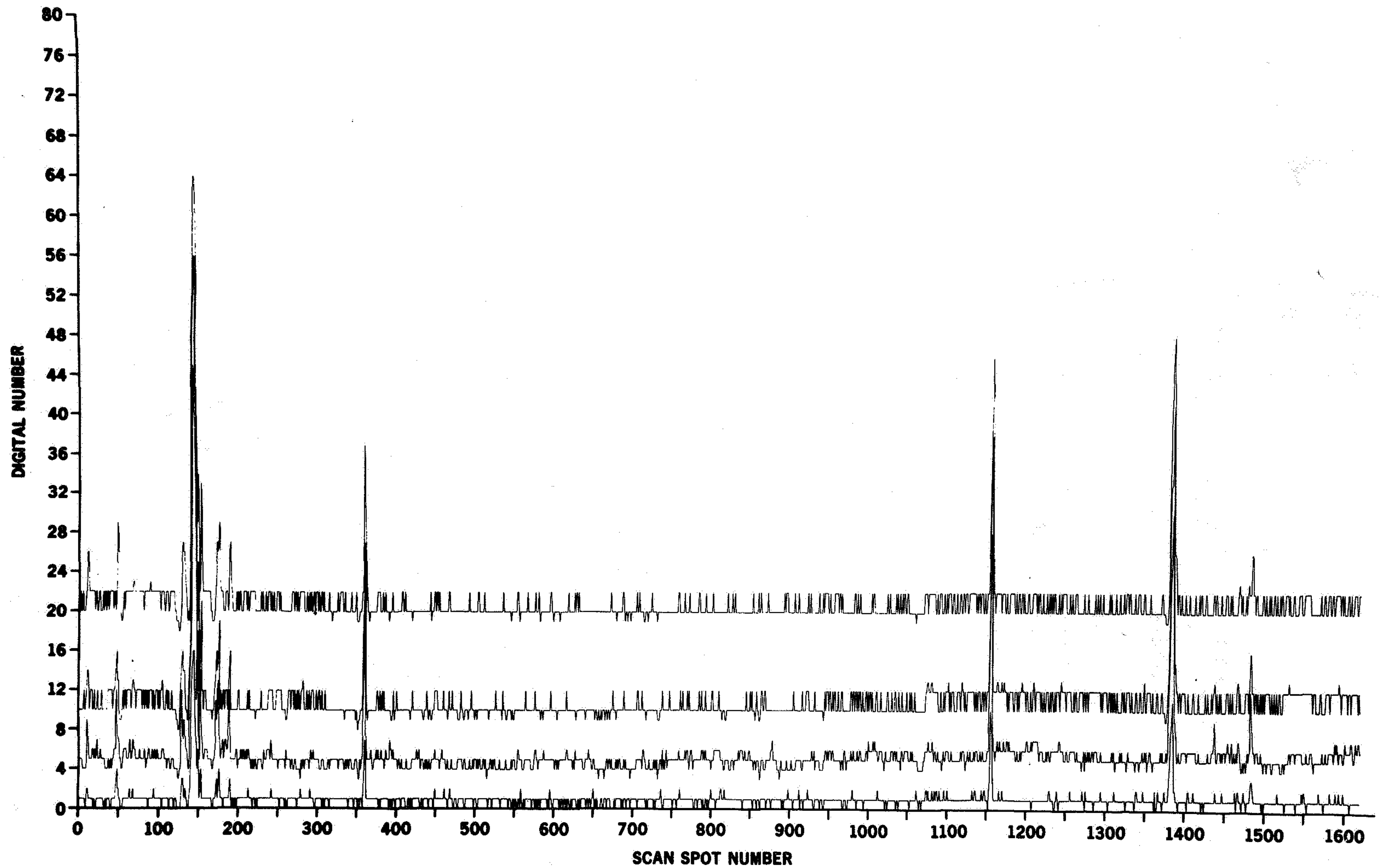

Figure 3. ERTS scanline plot across the Loop Current front. Top scanline is MSS 4, next MSS 5, MSS 6, and MSS 7 on the bottom. The large energy spikes are clouds. At scan spot number 950 there is an increase in the average value of the digital number of 1 or 2; this marks the cyclonic edge of the current.

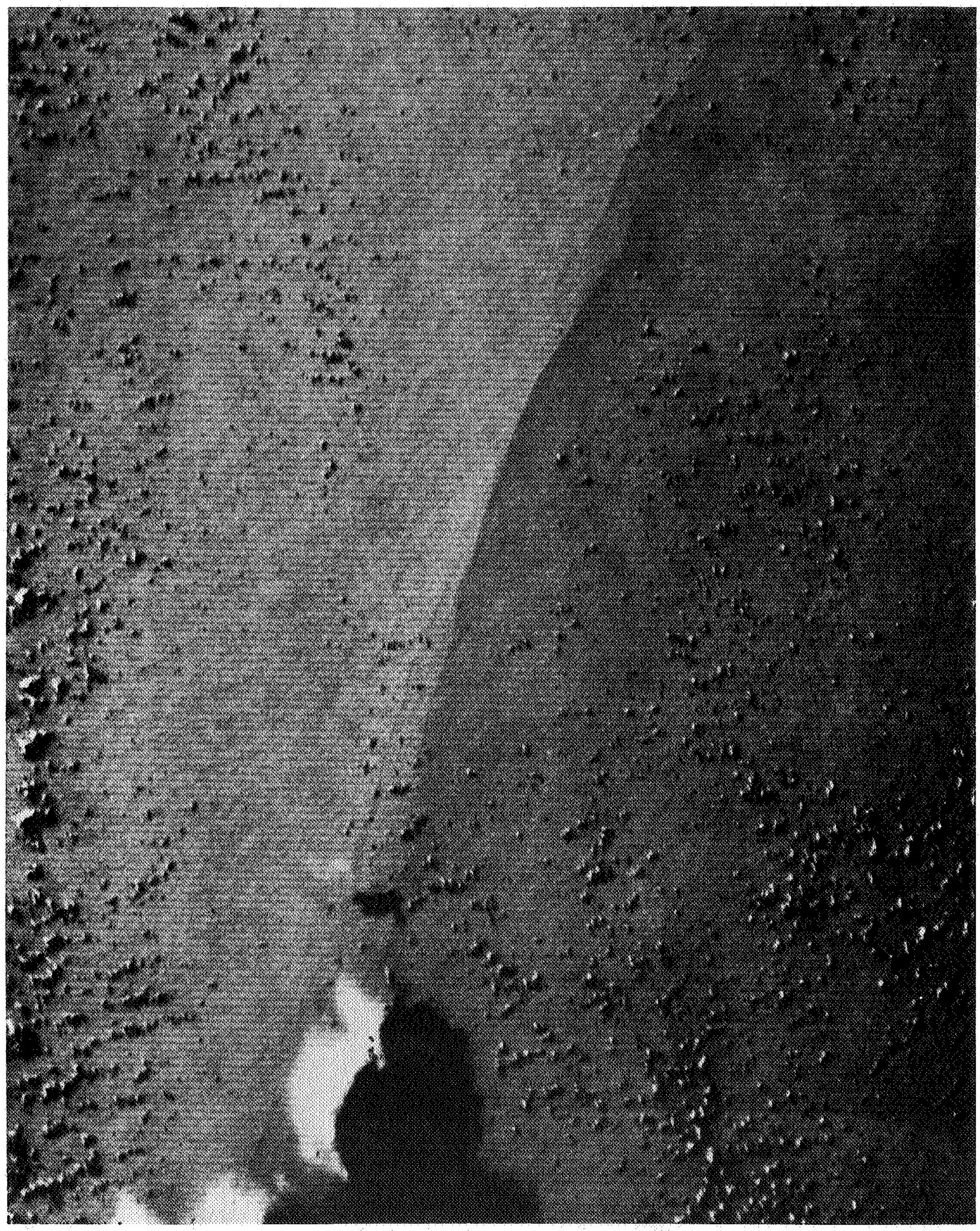

Figure 4. Negative print of computer enhanced ($9 \leq DN \leq 13$; n = 1) MSS 5 image of the cyclonic boundary of the Gulf Loop Current. Surface vessel track confirmed the location of the current to be the darker shade (higher radiance) region on the right hand side of the image (ERTS ID 1065-15411). Scanline plot in Fig. 4 horizontally passes through the middle of the scene. Horizontal distance across the image is 90 kilometers.

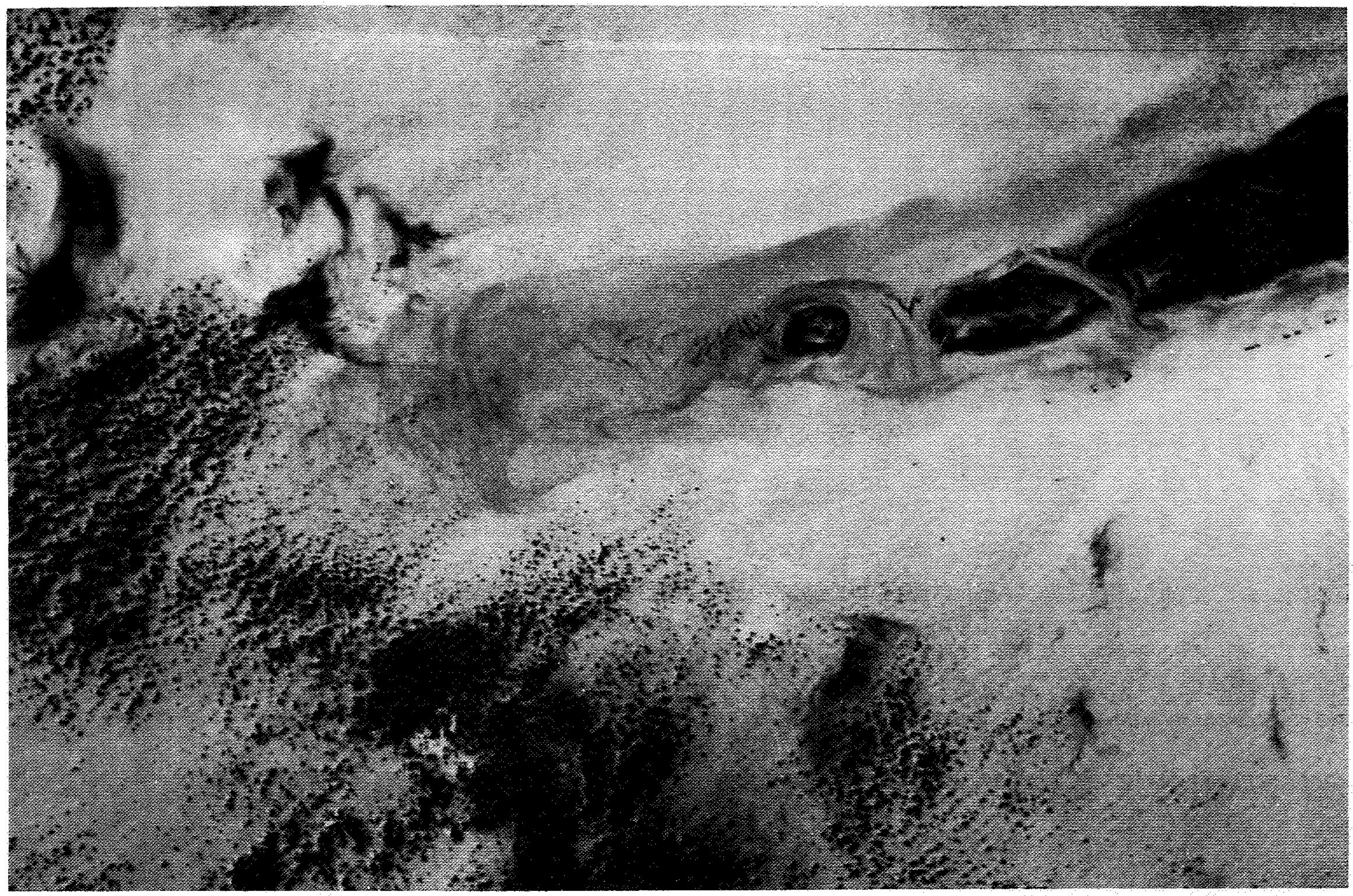

Figure 5. Negative print of computer enhanced ($7 \leq DN \leq 15$; n = 2) MSS 5 image of Marquesa Key and Key West (ERTS ID 1099-15293). Change in radiance southwest of Marquesa from dark to light marks the ship-located boundary between the higher intensity Florida Bay water and the lower intensity Gulf Stream. Bottom depth is in excess of 100 meters and thus does not contribute to the radiance. Horizontal distance across the image is 135 kilometers.

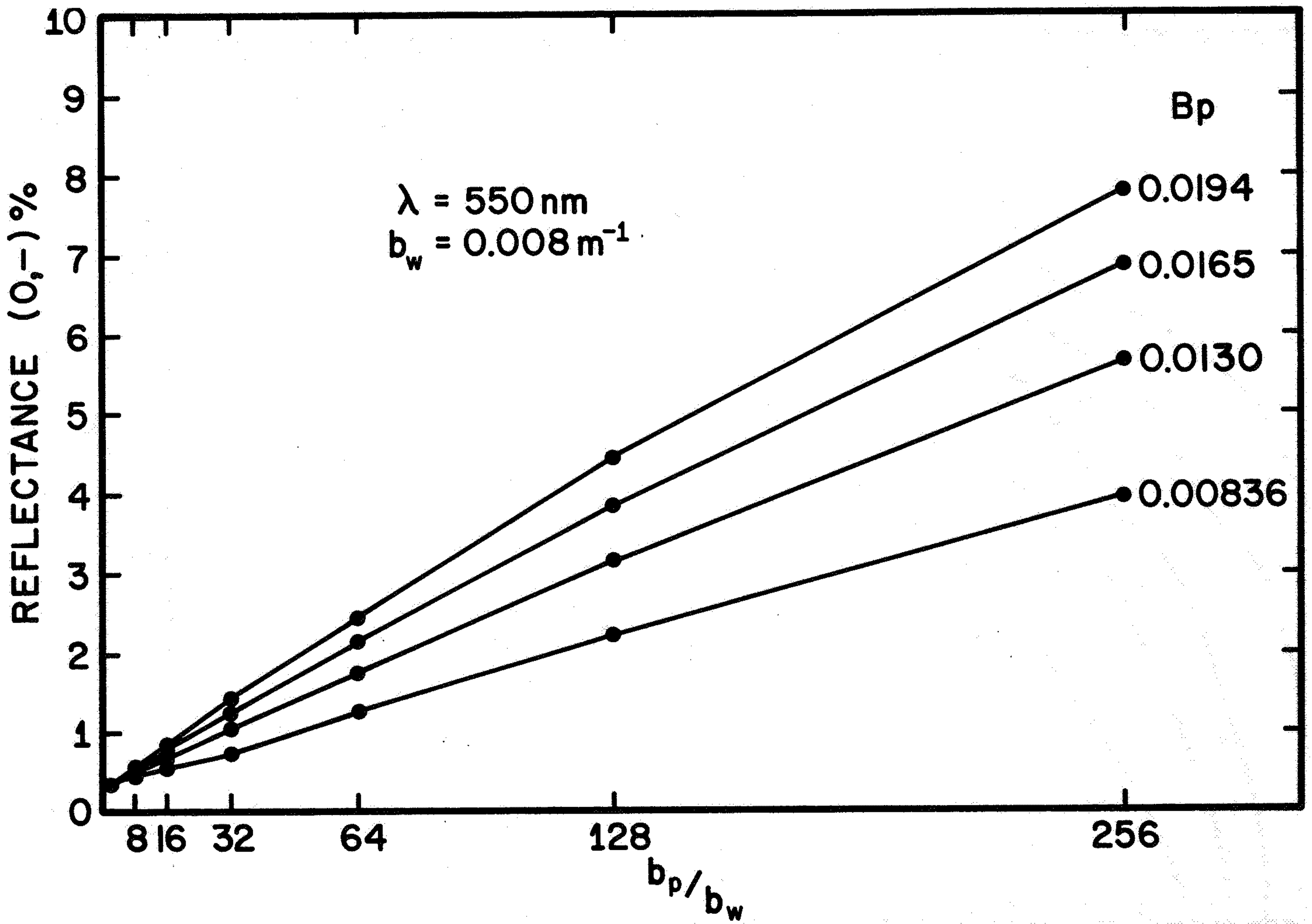

Figure 6. Computed reflectance in percent at the sea surface as a function of the ratio of the particle scattering coefficient to the water (only) scattering coefficient for 550nm. The value of the fraction of backscattered light due to particles (B_p) for each curve is given on the right hand side.

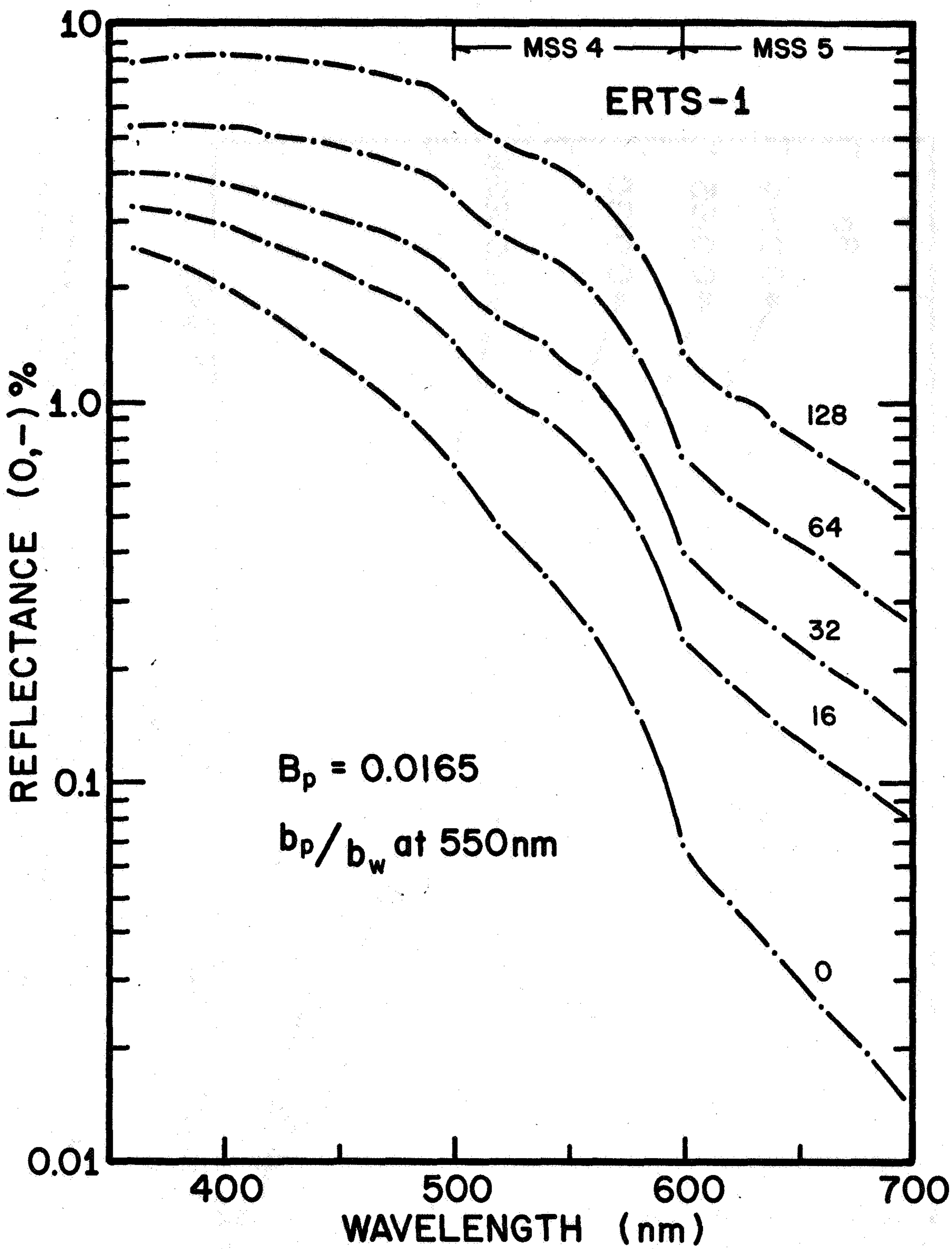

Figure 7. Computed reflectance in percent at the sea surface as a function of wavelength for various values of the ratio of the particle scattering coefficient to the water scattering coefficient. Note the wavelength dependence in these spectra of changing the particle concentration.

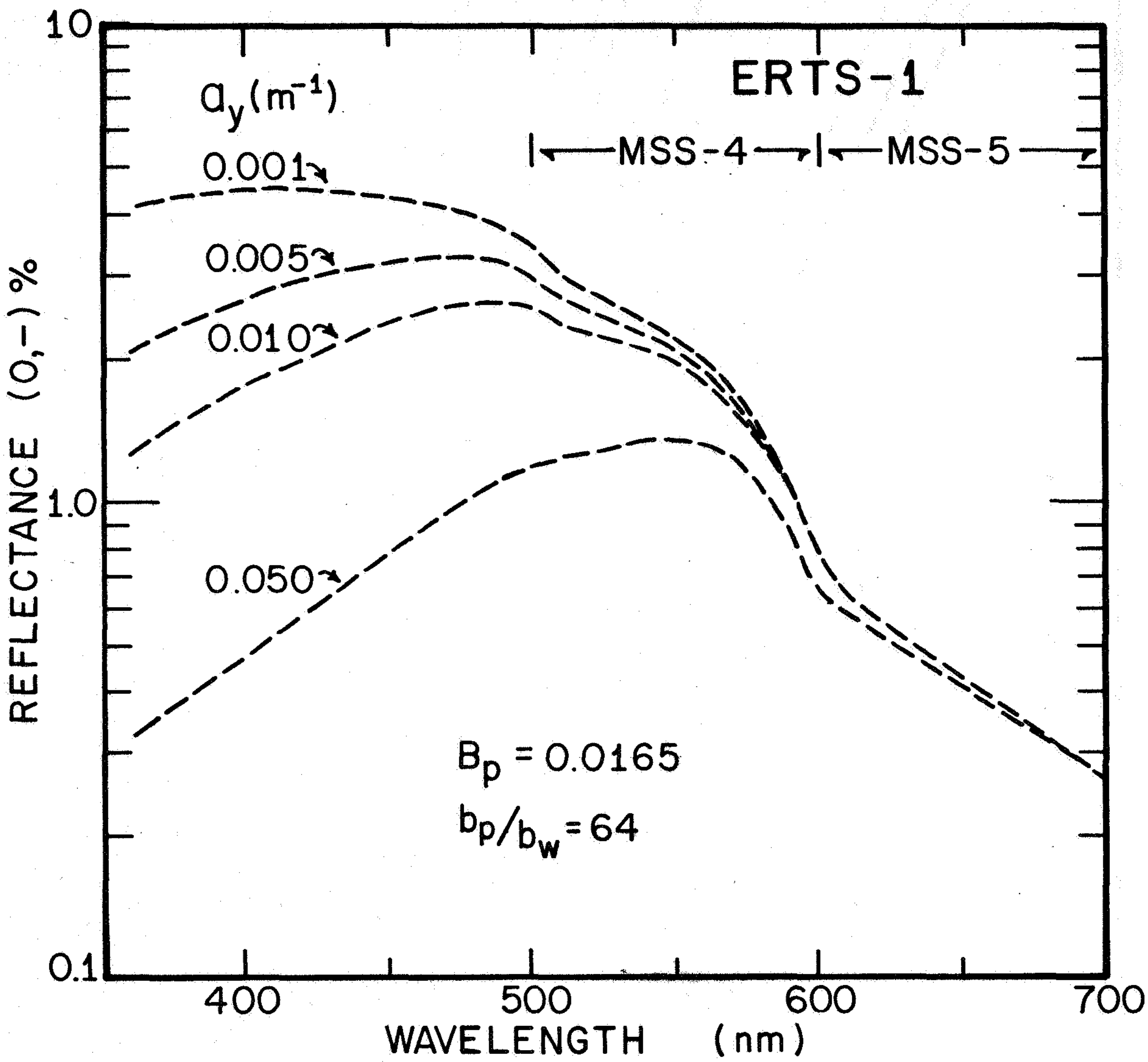

Figure 8. Computed reflectance spectra, in percent, at the sea surface. The ratio of the particle to water scattering coefficients (b_p/b_w) and the fraction of backscattered light are 128 and 0.0165 respectively. Values of the absorption coefficient due to yellow substance (a_y) are listed on the left hand side. Note the shift of the spectral peak to longer wavelengths with increasing a_y.

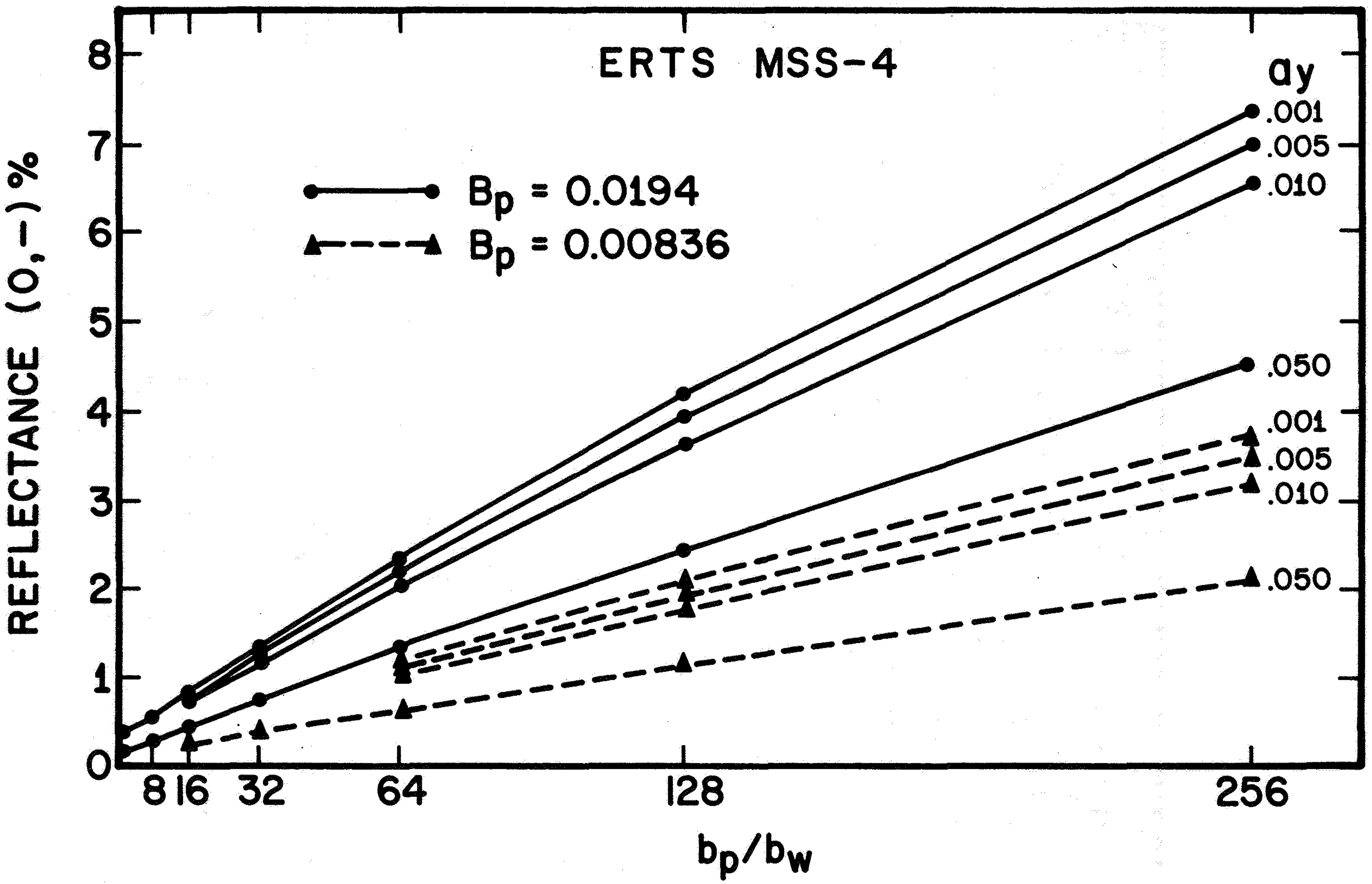

Figure 9. Computed reflectance in percent at the sea surface as a function of the ratio of the particle to the water scattering coefficients integrated over the spectral response of the MSS 4 filter (0.5-0.6μm). Values of the absorption coefficient due to yellow substance (a_y) are listed along the right hand side. Note the linearity depends on both a_y and the fraction of backscattered light, (B_p).

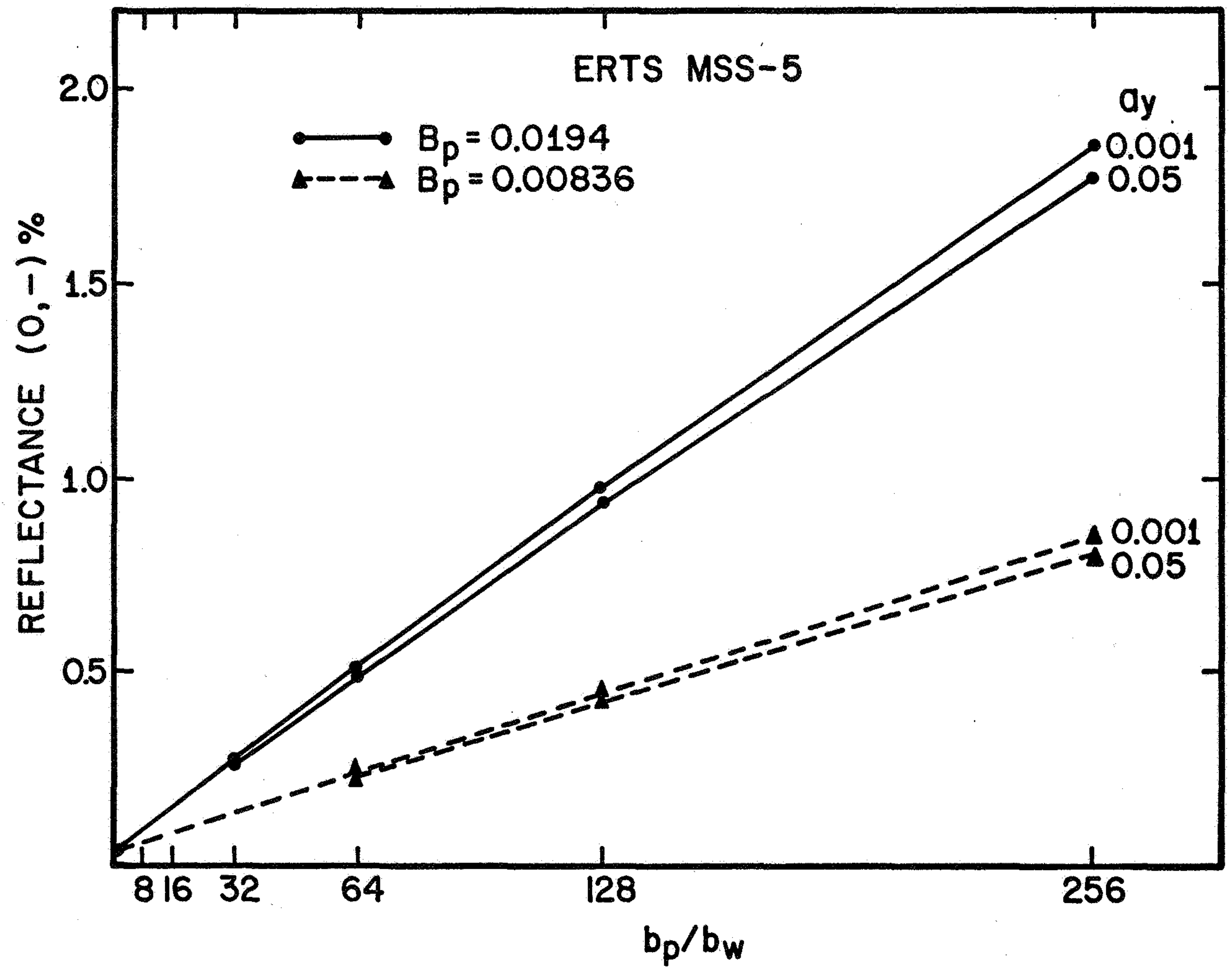

Figure 10. Computed reflectance at the sea surface, in percent, as a function of the particle to water scattering coefficient ratio, integrated over the response function of the MSS 5 filter (0.6-07 μ m). Values of the absorption coefficient due to yellow substance (a_y) are listed along the right hand side. Note the linearity is not strongly dependent on a_y but only on the fraction of backscatter light, B_p.

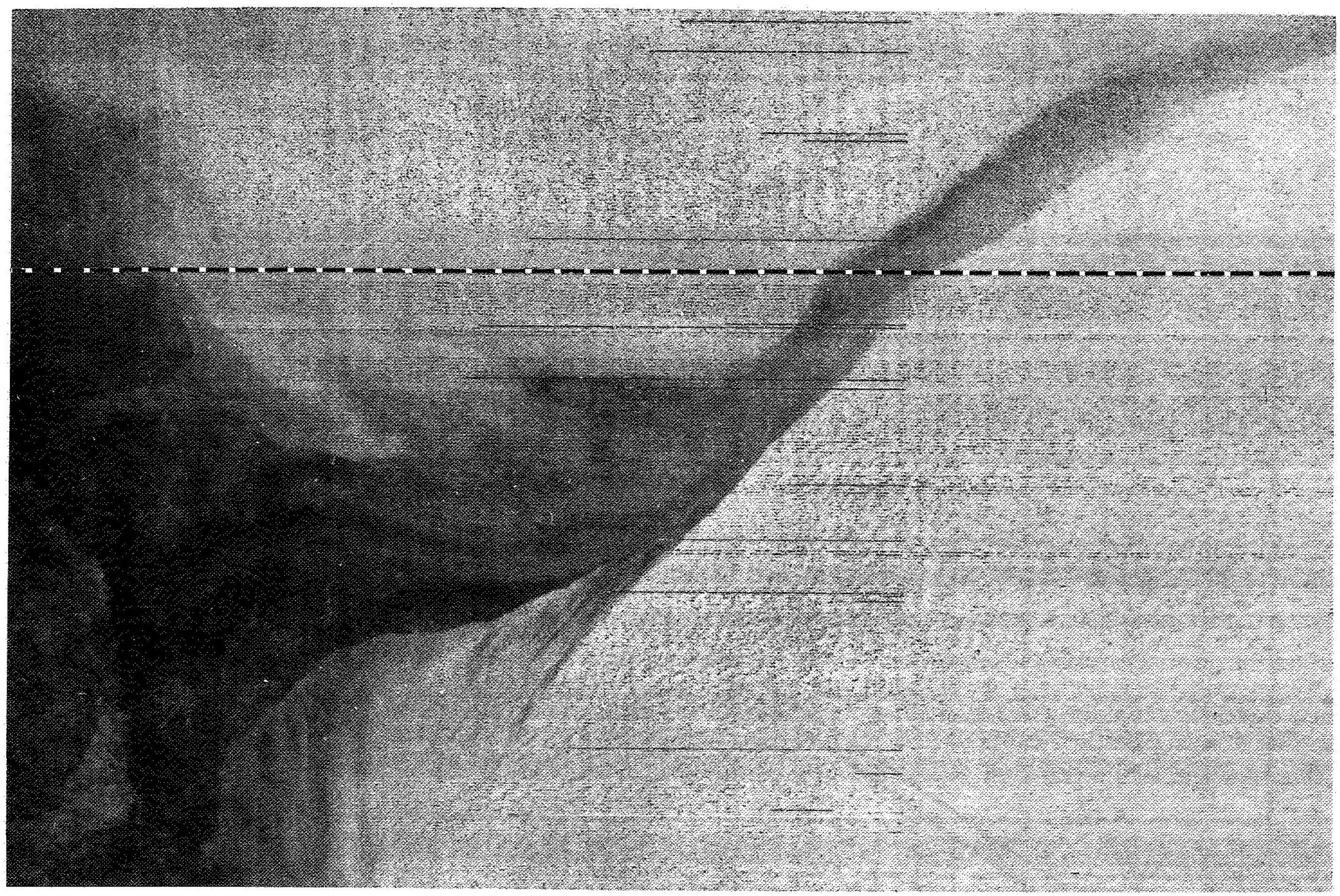

Figure 11. Contrast stretched ($4 \leq DN \leq 12$; $n = 2$) negative image of the ocean area offshore of Cape Hatteras (ERTS ID 1132-15042). The Gulf Stream can be seen as the bright area to the south of the entrained sediment from the coastal estuaries. The least squares fit of eq. (17) was done along a scanline north of the Cape and extending from nearshore, through the suspended sediment and into the current. Extensions of this plume were observed for 150 kilometers further east on other ERTS images. Horizontal distance across the image is 135 kilometers.

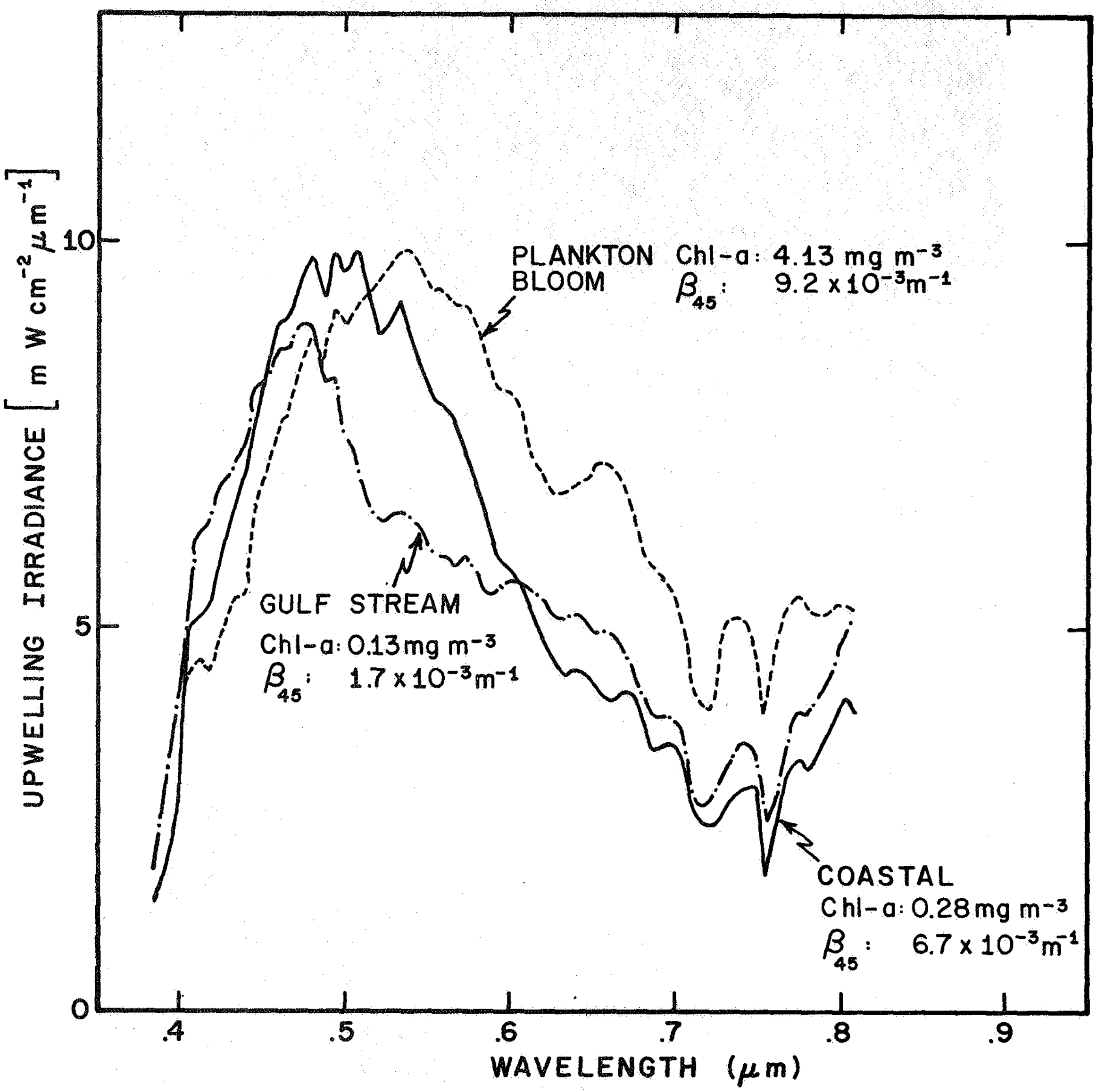

Figure 12. Observed upwelling spectral irradiance in the Gulf of Mexico, November 1972. The three spectra represent typical observations during the time series, and whow the shift of the dominant wavelength to larger values with increased surface chlorophyll-a. The volume scattering function, $\beta 45$, is for blue (436nm) light.

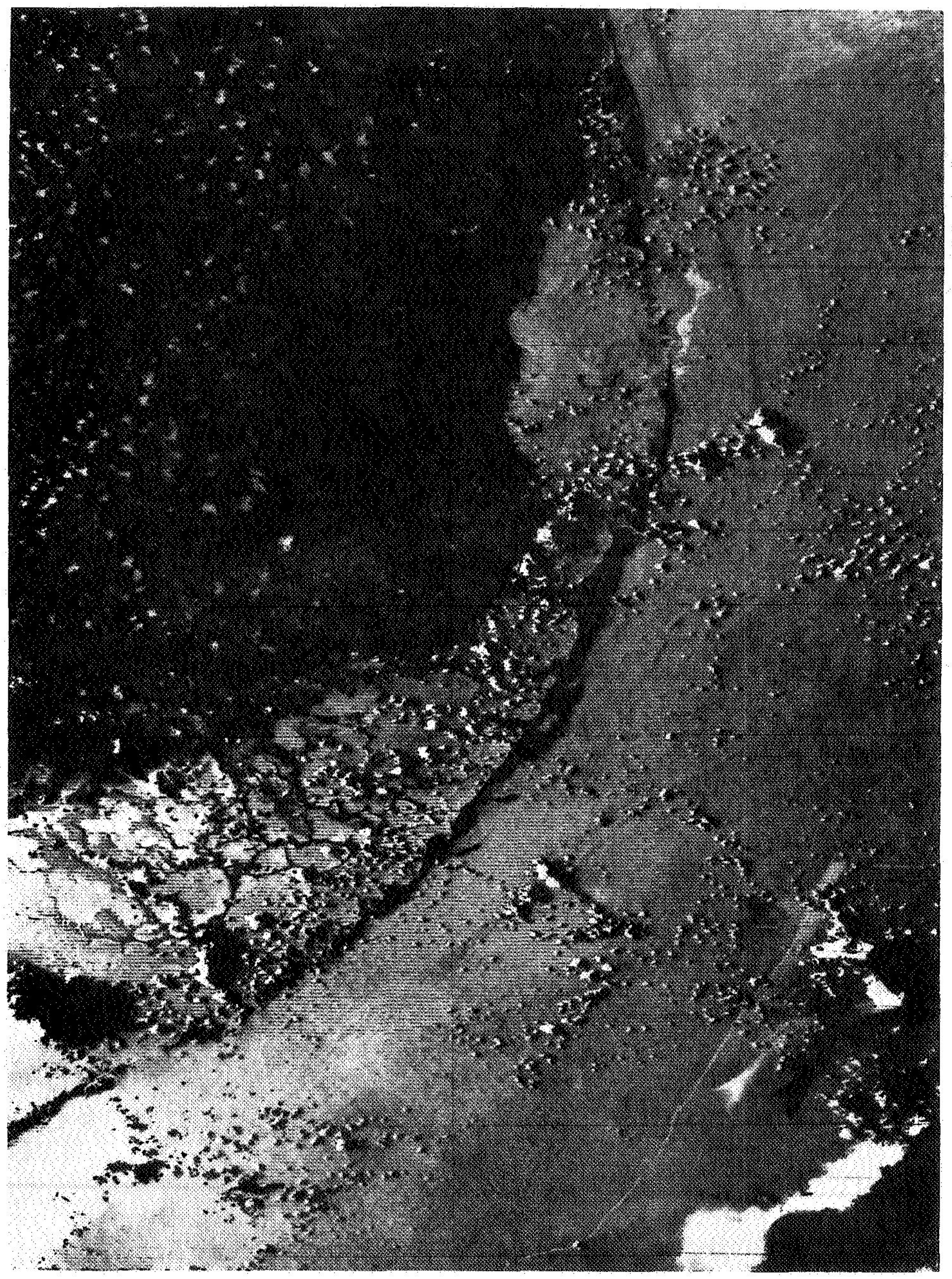

Figure 13, Negative print of computer contrast stretched ($7 \le DN < 15$; n = 2) ERTS image of South Florida (ERTS ID 1026-15230). The Florida Current can be seen as a line of dark lineation parallel to the coast; bottom is essentially invisible in this MSS 6 scene. A ship can be seen by its characteristic V-shaped wake just offshore of Miami Beach. Possibly the Virginia Key sewer outfall area can be observed by its low reflectance due to an organic slick. Horizontal distance across the image is 90 kilometers.

REFERENCES

Chandrasekhar, S. (1960). Radiative Transfer, Dover, New York, 393 pgs.

Charnell, R. L., G. A. Maul, and R. M. Qualset (1973). Paper presented October 3, 1973, ASP-ACSM Fall Convention, Orlando, Florida.

Corwin, T. L. and H. R. Richardson (1974). Preliminary report to the Commandant of the Coast Guard on the Gulf of Mexico Cyanide Barrel Spill, Daniel H. Wagner Associates, Paoli, Pennsylvania 19301, 36 pgs.

Cox, C. and W. Munk (1954). J. Opt. Soc. Am., 44(11), pp. 838-850.

Gordon, H. R. (1973). Appl. Opt., 12, pp. 2804-2805.

Gordon, H. R. and O. B. Brown (1973). Appl. Opt., 12, pp. 1549-1551.

Gordon, H. R. (1974). To be published in J. Opt. Soc. Am.

Hansen, D. V. and G. A. Maul (1970). Remote Sensing of Environment, 2, pp. 161-164.

Jerlov, N. G. (1968). Optical Oceanography, Elsevier, New York, pg. 56.

Leipper, D. F. and D. Volgenau (1970). Transactions, A.G.U., 51(4), pg. 310.

Maul, G. A. and D. V. Hansen (1972). Remote Sensing of Environment, 2, pp. 109-116.

Maul, G. A. (1973a). Transactions, A.G.U., 54(4), pg. 310.

Maul, G. A. (1973b). Symposium on Significant Results Obtained from the Earth Resources Technology Satellite-1. NASA SP-327, Vol. I (B), pp. 1365-1375.

Maul, G. A. (1974a). COSPAR: Space Research XIV, pp. 335-347.

Mueller, J. L. (1973). PhD. Dissertation Oregon State University, Corvalis, Oregon, 239 numbered leaves.

Murphy, E., K. Steidinger, B. Roberts, J. Williams, and J. Volley (1973). Submitted to Limnology and Oceanography.

Petzold, T. J. (1972). Volume Scattering Functions for Selected Ocean Waters, Scripps Institution of Oceanography, Visibility Laboratory SIO Ref. 72-28, 82 pgs.

Preisendorfor, R. W. (1965). Radiative Transfer on Discrete Spaces, Permagon, New York, 462 pgs.

Tyler, J. E. and R. C. Smith (1970). Measurements of Spectral Irradiance Underwater, Gordon and Breach, New York, 103 pgs.

Tyler, J. E., R. C. Smith, and W. H. Wilson, Jr. (1972). J. Opt. Soc. Am., 62(1), pp. 83-91.

Paper M 2

OCEAN INTERNAL WAVES OFF THE NORTH AMERICAN AND AFRICAN COASTS FROM ERTS-1

John R. Apel, Robert L. Charnell, *Atlantic Oceanographic and Meteorological Laboratories, NOAA, Miami, Florida 33149*

Abstract

Periodic features observed in the ocean portions of certain ERTS-1 images have been identified with reasonable certainty as surface manifestations of oceanic internal gravity waves. A series of images taken over the New York Bight, commencing with the 16 July 1972 overpass and continuing on into autumn of 1973, has shown the internal waves to be present when summer solar heating stratifies the water sufficiently well to support such oscillations. When fall and winter wind action mixes the shelf water down to the bottom, the waves no longer appear. In the Bight, the wavelengths range from approximately 400 to 1000 m, with the wave field being most sharply delineated near the edges of the continental shelf, at the mouth of the Hudson Canyon. They appear in packets consisting of several waves separated by 10-15 km, which propagate up on the shelf and disappear.

The internal wave dispersion equations have been solved for the water conditions existing in the area and wave refraction patterns calculated. This shows the waves to be highly refraction-oriented by the bottom topography near the Hudson Valley and the packets to be separated by approximately twelve hours--one semidiurnal tidal period. They also disappear about where the water depth equals the mixed layer depth.

An explanation of the sources and sinks for the internal waves is that they are "daughter" waves generated for a few hours during the peak current velocity by the long-wavelength baroclinic tide occurring at the edges of the continental shelves and island arcs. They then propagate with very low phase speeds, of order ¼ to ½ m/s, to be absorbed in the bottom sediments where the wave breaks on the shelf. On a worldwide basis, this process can account for a significant portion of the 3 x 10^{12}-watt loss in rotational energy of the earth-moon system and the attendant lengthening of the day.

The waves have also been detected off the east and west coasts of Africa, where the wavelengths approach 4 km. On the western continental shelf, they appear in packets separated by 30-40 km and are highly phase-oriented parallel to the bottom shelf topography. Once again, twice-daily generation by tides in the highly stratified water can account

for the six packets observed in the image. On the African east coast, where the continental shelf is narrow and the water deep, very little topographic orientation is apparent; the waves appear to have near-random phase, in agreement with shipborne measurements of open-ocean internal wave coherencies.

Digital image processing is necessary to bring out the subtle image brightness changes which the waves cause in an ERTS scene. Two-dimensional Fourier transforms have been computed for individual wave packets. Power spectra taken from space series sampled in the direction of the propagation vector reveal the shelf waves to be coherent narrow-band processes, while the open-ocean waves are nearly incoherent.

Figure Captions

1. New York Bight on 16 August 1972; the computer-enhanced negative print shows oceanic internal waves in southeast corner.

2. Internal wave patterns superimposed on continental shelf bottom topography, showing wave packets separated by 12 hours' propagation time and guided by Hudson canyon up to 30-fathom contour.

3. Detailed characteristics of one internal wave packet having 400- to 500-m wavelengths (left side); two-dimensional Fourier transform of left scene, with axes proportional to wave vector components.

4. Schematic of internal wave generation at shelf edge, propagation and absorption where top of thermocline intersects bottom at 30 fathoms.

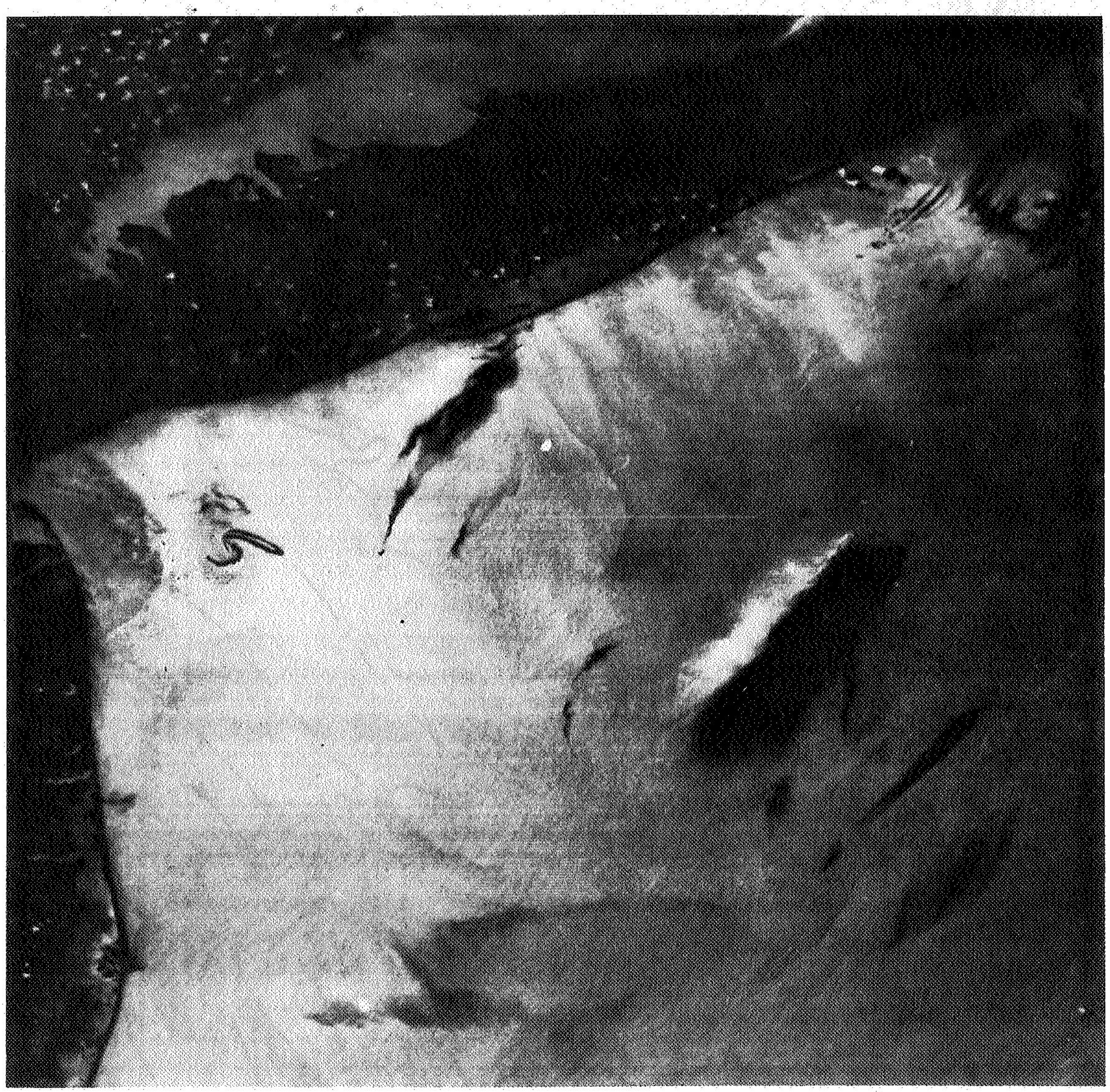

Figure 1

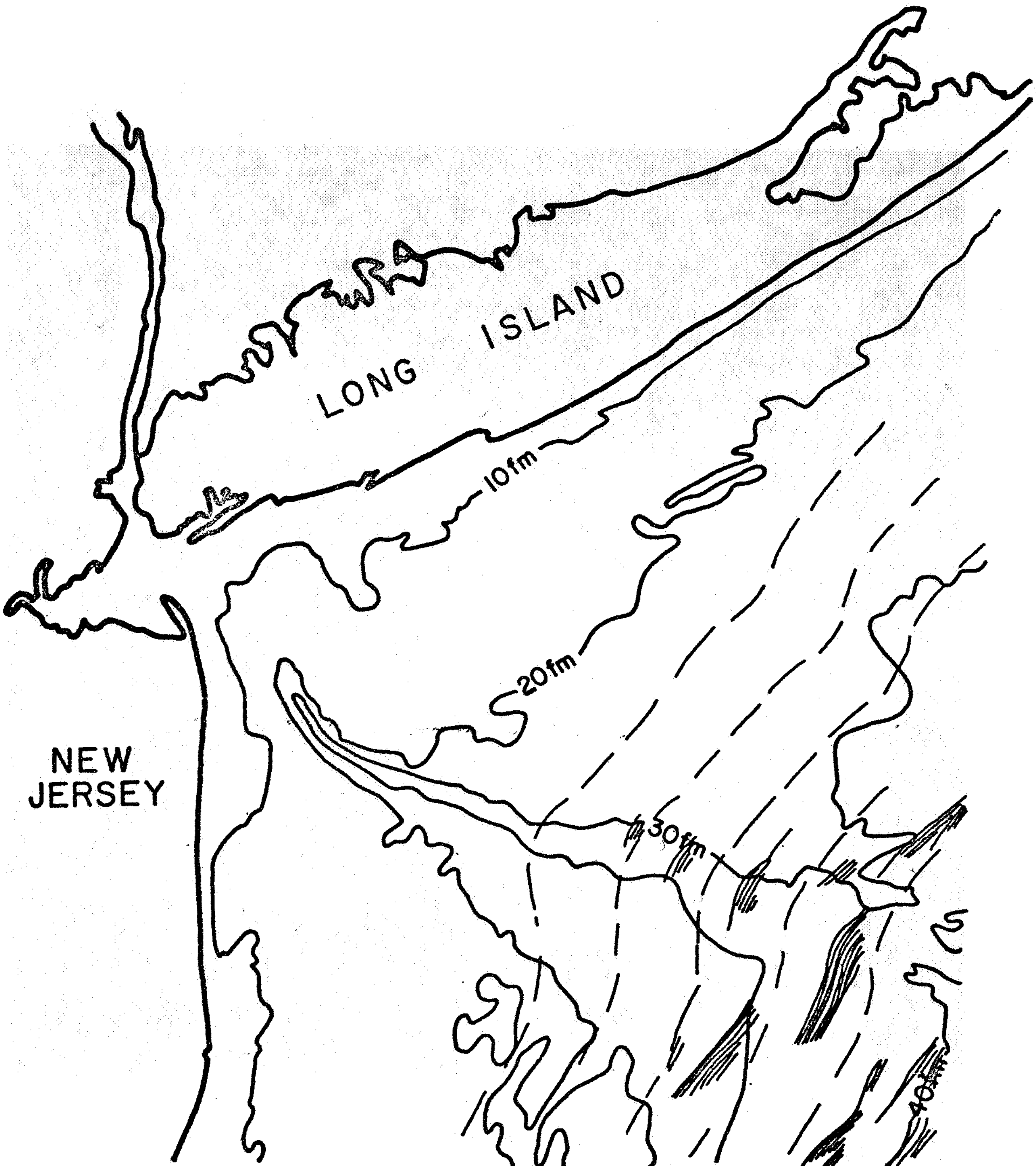

Figure 2

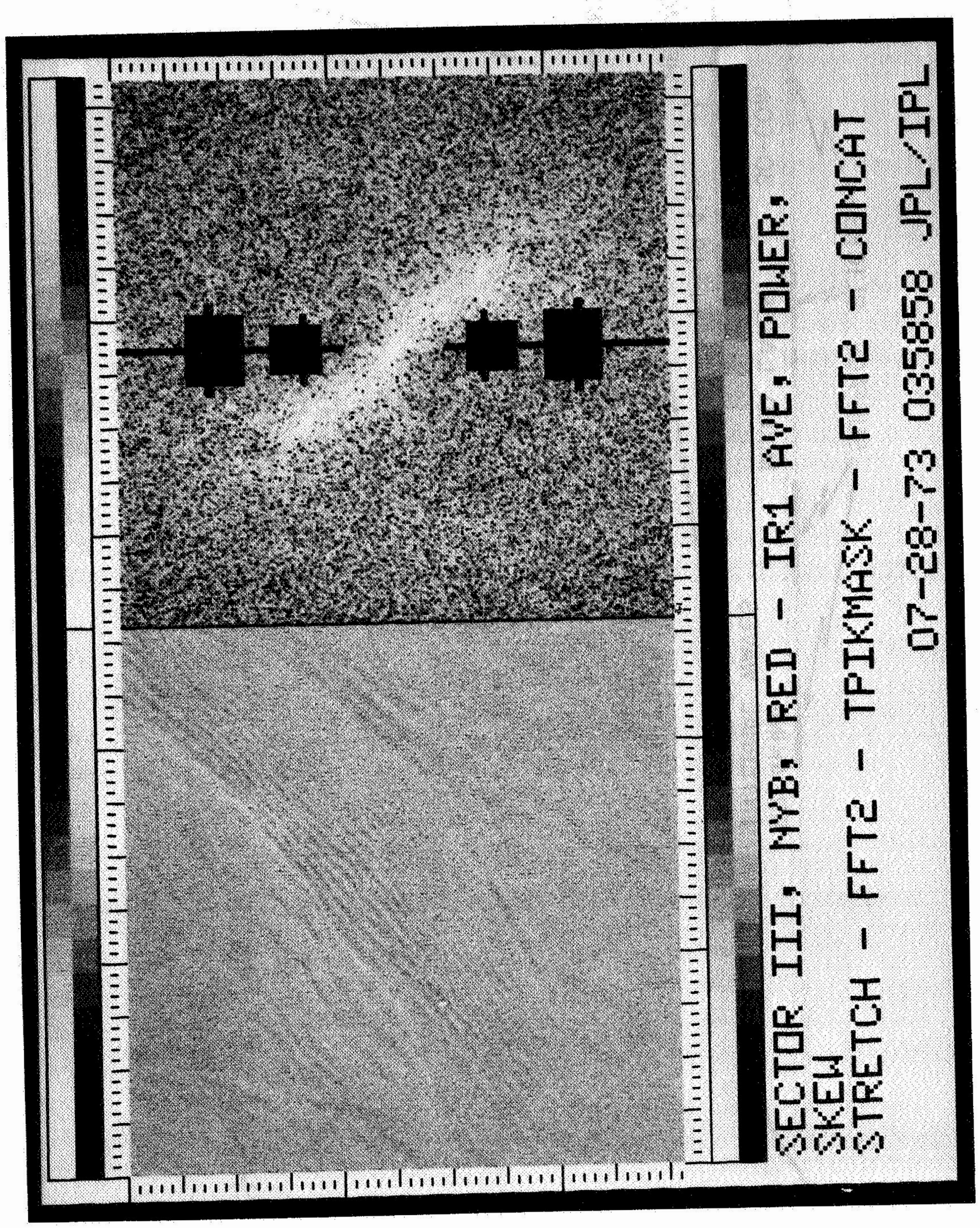
SECTOR III, MYB, RED - IR1 AVE, POWER,
SKEW
STRETCH - FFT2 - TPIKMASK - FFT2 - CONCAT
07-28-73 035858 JPL/IPL

Figure 3

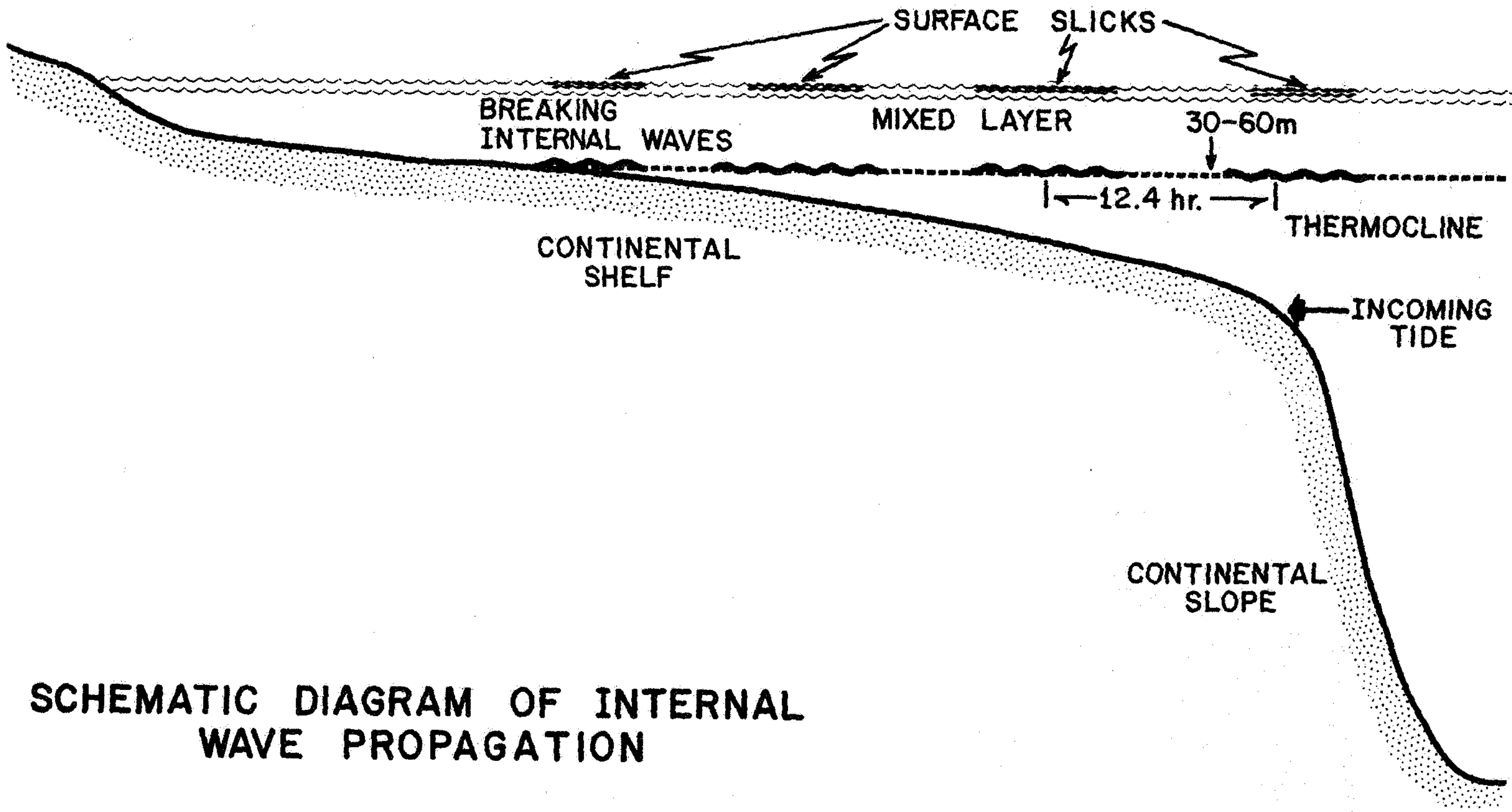

SCHEMATIC DIAGRAM OF INTERNAL WAVE PROPAGATION

Figure 4

Paper M 3

A REVIEW OF INITIAL INVESTIGATIONS TO UTILIZE ERTS-1 DATA IN DETERMINING THE AVAILABILITY AND DISTRIBUTION OF LIVING MARINE RESOURCES

William H. Stevenson, *NOAA, National Marine Fisheries Service, Mississippi Test Facility, Bay St. Louis, MS 39520;* Andrew J. Kemmerer, *NOAA, National Marine Fisheries Service, Washington, D.C. 20235;* Buddy H. Atwell, *NASA, Earth Resources Laboratory, Mississippi Test Facility, Bay St. Louis, MS 39520;* and Paul M. Maughan, *Earth Satellite Corporation, 1747 Pennsylvania Avenue, Washington, D.C.*

INTRODUCTION

The National Marine Fisheries Service has been studying the application of aerospace remote sensing to fisheries management and utilization for many years. This report summarizes NMFS/NASA Project Number 240. Details are available in the final report by Stevenson and Pastula. This 15-month study was initiated in July 1972 to determine the reliability of satellite and high altitude sensors to provide data about oceanographic parameters in coastal waters; demonstrate the use of remotely sensed oceanographic information to predict the distribution and abundance of adult menhaden; and, demonstrate the potential of using satellite acquired information for improving the harvest and management of a fishery resource. The study focused on coastal areas in the north central portion of the Gulf of Mexico including parts of Alabama, Mississippi and Louisiana (Fig. 1). The area used in the final analysis was limited to the Mississippi Sound, which is approximately 145 kilometers (90 miles) long and 16 kilometers (10 miles) wide, has an average water depth of about 3.7 meters (12 feet), and in general characterizes an estuarine environment.

A small industrial fish, commonly called menhaden, was selected as the target species (Fig. 2). This fish supports the largest volume commercial fishing industry in the United States and is a major source of protein for animal feed as well as oils and solubles for several hundred other uses. The menhaden is a surface schooling fish, spending most of its life within the coastal environment. They are harvested by fishing vessels operating in concert with low-flying fish-spotter aircraft (Fig. 3), captured by half-mile-long fence-like nets called purse seines (Fig. 4), and carried to the processing plants (Fig. 5) in modern transport ships (Fig. 6). Menhaden were selected as the target species for a variety of reasons including: (1) their surface schooling pelagic nature which makes them well suited to satellite and aircraft remote sensing, and (2) they support an important commercial fishery actively pursuing advanced technology to solve varied problems confronting the industry.

*NOAA, National Marine Fisheries Service, Mississippi Test Facility, Bay St. Louis, MS 39520
**NOAA, National Marine Fisheries Service, Washington, D.C. 20235
†NASA, Earth Resources Laboratory, Mississippi Test Facility, Bay St. Louis, MS 39520
††Earth Satellite Corporation, 1747 Pennsylvania Avenue, Washington, D.C.

PROJECT MANAGEMENT RATIONALE

The multidiscipline project was organized along technical disciplines of remote sensing, oceanography, fisheries biology and resource utilization. Management responsibilities for each discipline were assigned to one or more of the Government or industry groups who participated as co-investigators. In addition, state, federal and private fishing companies provided resources or data to the project. One of the most important results of this project, in the opinion of the principal investigator, was a demonstration of the magnitude of organization, planning, logistical support, data management and technical support required to insure the success of remote sensing projects in fisheries. Details of these facets have been published by Stevenson and Vanselous (1973).

DATA ACQUISITION SUMMARY

Data acquisition activities were divided into four discipline groups: remote sensing, oceanography, resource biology and utilization. Remote sensing data were obtained by both satellite and aircraft. Water color, as a function of wavelength, and surface turbidity patterns were obtained with the ERTS-1 multispectral scanner (MSS). Water color, turbidity, sea surface temperature, surface current patterns, and limited surface salinity were obtained by aircraft-supported sensors concurrently with selected ERTS-1 overpasses.

Oceanographic surface data were taken at 95 stations in the Mississippi Sound to provide a sampling density of one station per 29 square kilometers. Parameters measured included water color, turbidity (secchi disc transparency) surface temperature, currents, salinity, chlorophyll a, sea state and water depth.

Fisheries resource distribution and abundance data were provided primarily by low-altitude aerial photography. This information was periodically augmented by nighttime, low-altitude, low-light-level television surveys and commercial fish spotter pilot reports. Data obtained were school location, species, school size and number.

Utilization or harvest data were obtained from three commercial fishing vessels throughout most of the fishing season. Measurements were taken at the time and location of capture or attempted capture of a menhaden school. Data collected included water color, turbidity (secchi disc transparency), surface water temperature, salinity, catch location, species, size of catch, number of catches or sets made.

The acquisition system was designed to obtain similar data from more than one source. This provided the necessary redundancy to compare data obtained by different discipline techniques.

DATA ANALYSIS AND RESULTS SUMMARY

Analysis of the data followed two distinct avenues. Intra-discipline analysis was made to provide an internal check on the validity of the information within its own discipline. Inter-discipline data analysis was carried on concurrently to determine if correlations existed between the remotely sensed environmental data and the surface water environment, the environment and menhaden distribution and availability, and finally fish distribution and commercial fishing activities. Standard statistical, oceanographic, and image analysis techniques were used and have been reported elsewhere (Kemmerer and Benigno, 1973; Kemmerer et al., 1974; Weldon, 1973; Maughan, Marmelstein and Temple, 1973).

Results of the analyses clearly demonstrate the feasibility of using data from satellite-supported environmental sensors to predict fish distribution under at least one set of conditions. It must be emphasized that the results presented in this report should be considered tentative. Additional tests are needed to confirm them and determine their applicability for other geographic areas and biological conditions.

ERTS-1, MSS Band 5 imagery contained density levels which correlated with menhaden distribution patterns (Fig. 7). A portion of MSS Band 5 imagery from August 7, 1972, covering the western Mississippi Sound was analyzed by superimposing the locations of 23 photographically detected menhaden schools on it. Water imagery densities were divided into two density ranges and color enhanced. All menhaden schools were found to lie in the less dense range (Fig. 8). These density levels were further shown to correlate significantly with sea-truth measurements of secchi disc transparency and water depth, two parameters which also were shown to correlate significantly with menhaden distribution along with water color and salinity. Independent tests of these relationships using oceanographic and biological data taken at or near sites of commercial menhaden capture corroborated them. A correlation between chlorophyll _a_ and menhaden distribution appears valid, but could not be substantiated with available data. There appeared to be little or no correlation between sea surface temperature and menhaden distribution.

Eight empirical multiple regression models which predict menhaden distribution in the study area were constructed from combinations of four oceanographic parameters (water depth, secchi disc transparency, surface salinity, and Forel-Ule color). A number of interpretations and presentation methods can be applied to model products and one of them was applied to the data collected on August 7, 1972 (Fig. 9) to predict menhaden distribution in Mississippi Sound. Model products were divided into three categories: high, moderate and low potential. The interpretation applied to these categories is related to relative probability. In high potential areas, the probability of fish capture is higher than in moderate or low potential areas. Incomplete commercial fishing reports from August 7, 1972 indicate most, if not all, fishing occurred in the high potential areas. The importance of the models is not that they are an end in themselves, but that they demonstrate a potential means or direction through which remotely sensed oceanographic information can be used to provide menhaden distribution information on a real time basis.

POTENTIAL APPLICATIONS

Potential applications of the results from this study cannot be completely identified in this report; however, three areas are recognized: commercial fishing, resource assessment and environmental monitoring. Utilizing linear models to predict water transparency directly from ERTS-1, MSS, Band 5 digital data as an input to the menhaden distribution prediction models, the identification of good fishing areas for commercial operations may be possible. When one considers that menhaden are distributed over roughly a 12,000-square-nautical-mile area in the Gulf of Mexico, the importance of being able to sort out those areas which have a high probability of successful fishing should be obvious.

Another potential use of the menhaden distribution prediction models appears to be as an aid to developing efficient sampling designs for resource assessment purposes. Seldom is it practicable to sample 100 percent of an area because of time and budgetary constraints. Instead, sampling designs often are predicated on a priori knowledge about the resource such that most of the sampling can be done in areas where most of the fish are expected to be. For example, usually only about 20 percent of the Mississippi Sound had "high potential" ratings for menhaden during the study period. If one were reasonably cautious and decided to expend 5 times as much sampling effort per unit area in "high potential" areas as in "moderate" and "low" areas, a decrease of up to 64 percent in total survey coverage could be realized based upon model predictions. The breakdown in sampling effort admittedly is arbitrary and would change depending on how well the models perform and whether or not their predictive capability can be improved upon through additional data inputs.

We have shown that relationships exist between certain oceanographic parameters and the distribution of menhaden, and that these relationships may have potential application for commercial fishing and resource assessment. Conventional methods of obtaining these measurements synoptically over an area the size of Mississippi Sound (1000 square miles), however, are prohibitive. For these measurements to satisfy the needs of the prediction models, they have to be obtained within a 2-hour time period and, because of the spatial dynamics of Mississippi Sound, are needed on a 1/2-mile grid basis to accurately describe conditions within the Sound. To estimate the number of boats required to obtain these data by conventional methods several simplifying assumptions were made: (1) the Sound is rectangular 10 mi. x 100 mi.; (2) typical vessels used to make measurements of this type travel at a speed of 10 knots; and (3) the time required on a station is 15 minutes. Under these conditions at least 660 vessels would be required to collect enough raw data to satisfy the requirements identified during the course of this study. The alternative is to measure the oceanographic parameters remotely from satellite or aircraft.

The present state-of-the-art in remote sensing of water quality parameters, based on the research of others as well as our own, indicates that the measurement of surface water temperature from aircraft is operational. Methods to measure salinity, chlorophyll and turbidity remotely from aircraft are being developed and improved upon. Enough work has been done to offer encouragement regarding

the continued development of methods to increase the accuracy and precision of these measurements from aircraft and extend some or all of them to a satellite sensing capability (See Thomann 1973, Atwell 1973, and Weldon 1973). Although remote techniques for measurement of all oceanographic and biological parameters of interest are not completely developed, the advantages of a synoptic coverage of large areas make remote sensing the only realistic method of data gathering for fishery models of the type developed in this project. Future applications will be identified by continued studies of this type carried out in close and active participation with commercial and scientific personnel who have the ultimate responsibility to manage and utilize marine fisheries resources.

REFERENCES

Atwell, B. H. 1973. Mississippi Sound Remote Sensing Study, Report II. NASA Earth Resources Laboratory, Report No. 091, Bay St. Louis, MS

Kemmerer, A. J. and J. A. Benigno. 1973. Relationships between Remotely Sensed Fisheries Distribution Information and Selected Oceanographic Parameters in the Mississippi Sound. Symposium of Significant Results Obtained from ERTS-1, Goddard Space Flight Center, Greenbelt, Maryland; NASA; March 5-9.

Kemmerer, A. J., J. A. Benigno, G. B. Reese, and F. C. Minkler. 1974. A Summary of Selected Early Results from the ERTS-1 Menhaden Experiment. Fishery Bulletin, U. S. Department of Commerce, NOAA/NMFS (In Press) Seattle, Washington.

Maughan, P. M., A. D. Marmelstein, and O. R. Temple. 1973. Application of ERTS-1 Imagery to the Harvest Model of the U.S. Menhaden Fishery. Symposium of Significant Results Obtained from ERTS-1, Goddard Space Flight Center, Greenbelt, Maryland; NASA; March 5-9.

Stevenson, W. H. and E. J. Pastula, Jr. 1973. Investigations Using Data from ERTS-1 to Develop and Implement Utilization of Living Marine Resources. Final Report, NASA Project No. 240, GSFC ID No. CO 321. NASA Goddard Space Flight Center, Greenbelt, Md. 20771.

Stevenson, W. H. and T. M. Vanselous. 1973. Remote Sensing Data Management from a User's Viewpoint. Amer. Astro. Soc. 19th Annual Meeting, International Congress Space Benefits, AAS Paper No. 73-152, June.

Thomann, G. C. 1973. Remote Measurement of Salinity in an Estuarine Environment. Remote Sensing of Environment Vol. 2 No. 4.

Weldon, J. W. 1973. Remote Measurements of Water Color in Coastal Waters. NASA/Earth Resources Laboratory/MTF Internal Report No. 083, August.

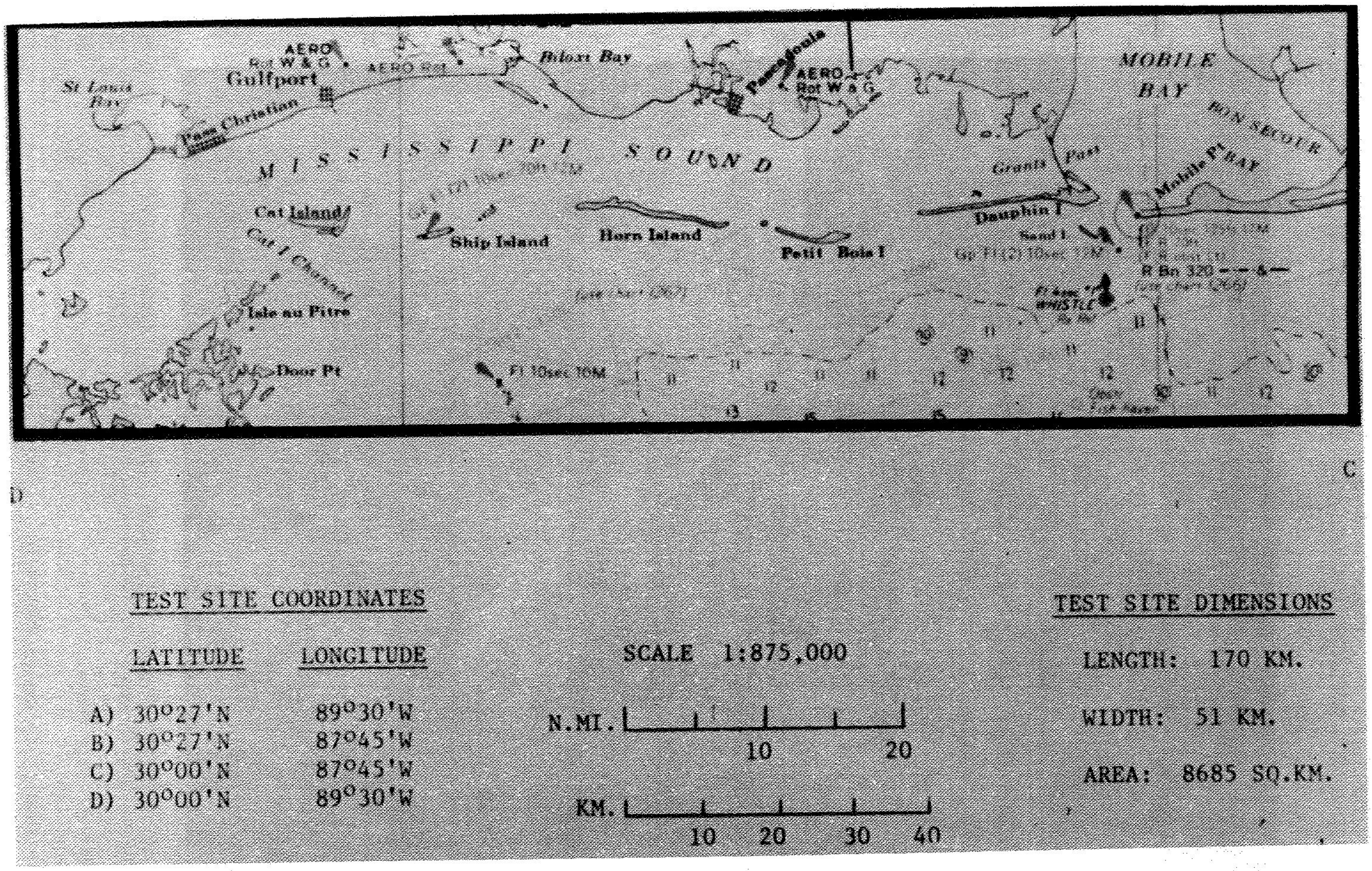

Fig. 1. Project 240 test area in North Central Gulf of Mexico.

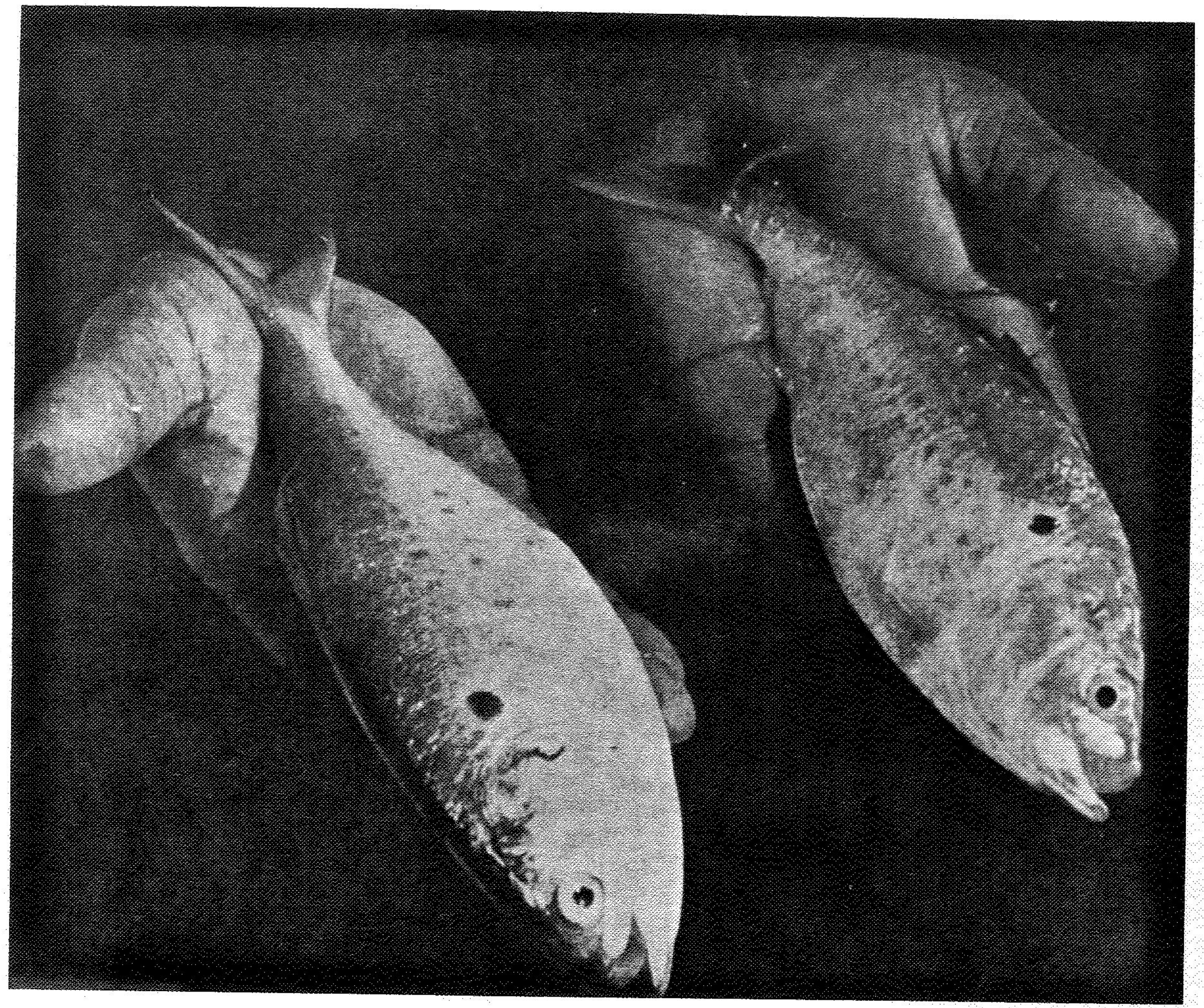

Fig. 2. Project 240 target fish species, Menhaden, (Brevoortia patronus).

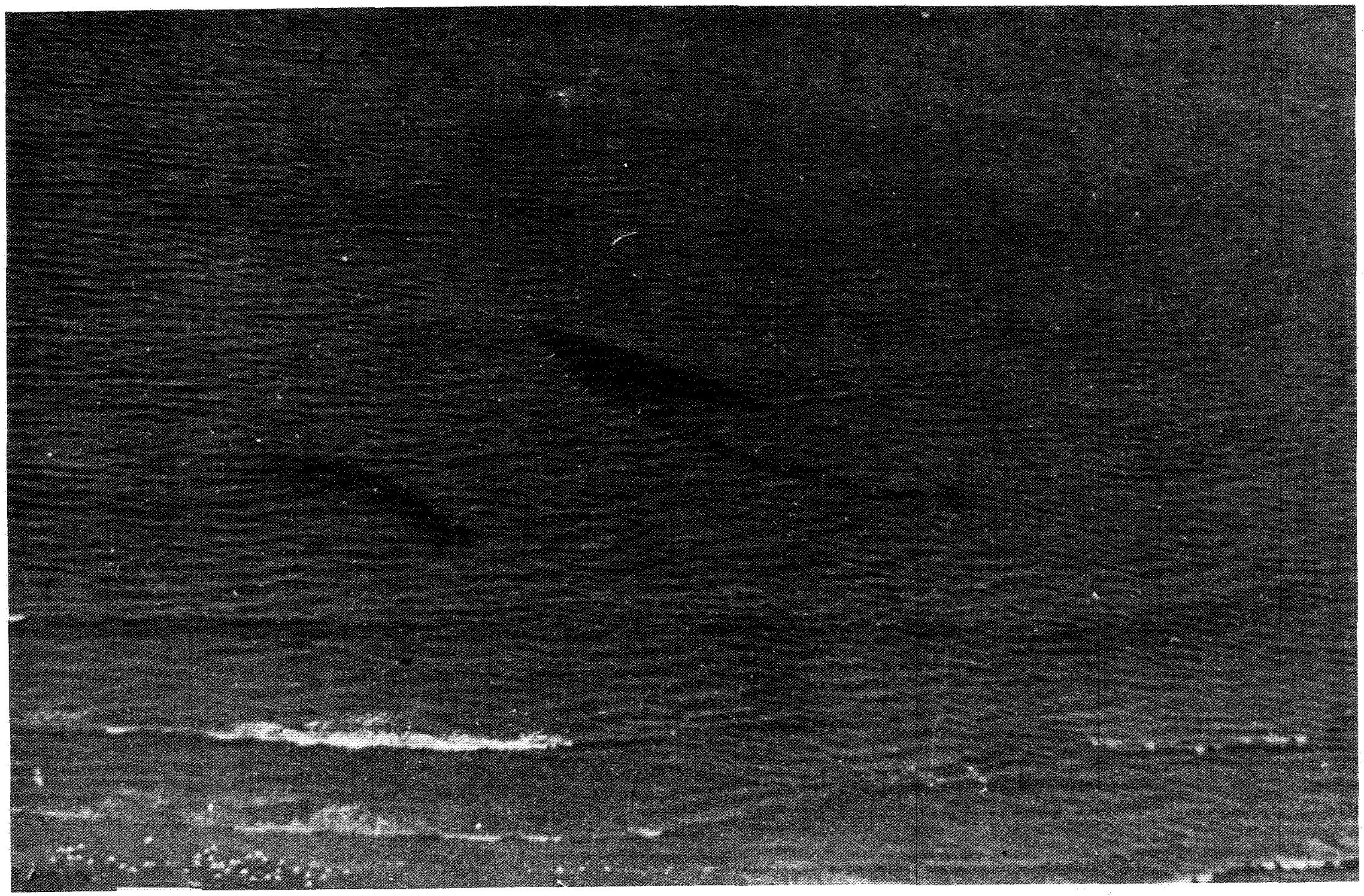

Fig. 3. Menhaden school in Mississippi Sound observed from fish spotter aircraft at 500 ft. altitude.

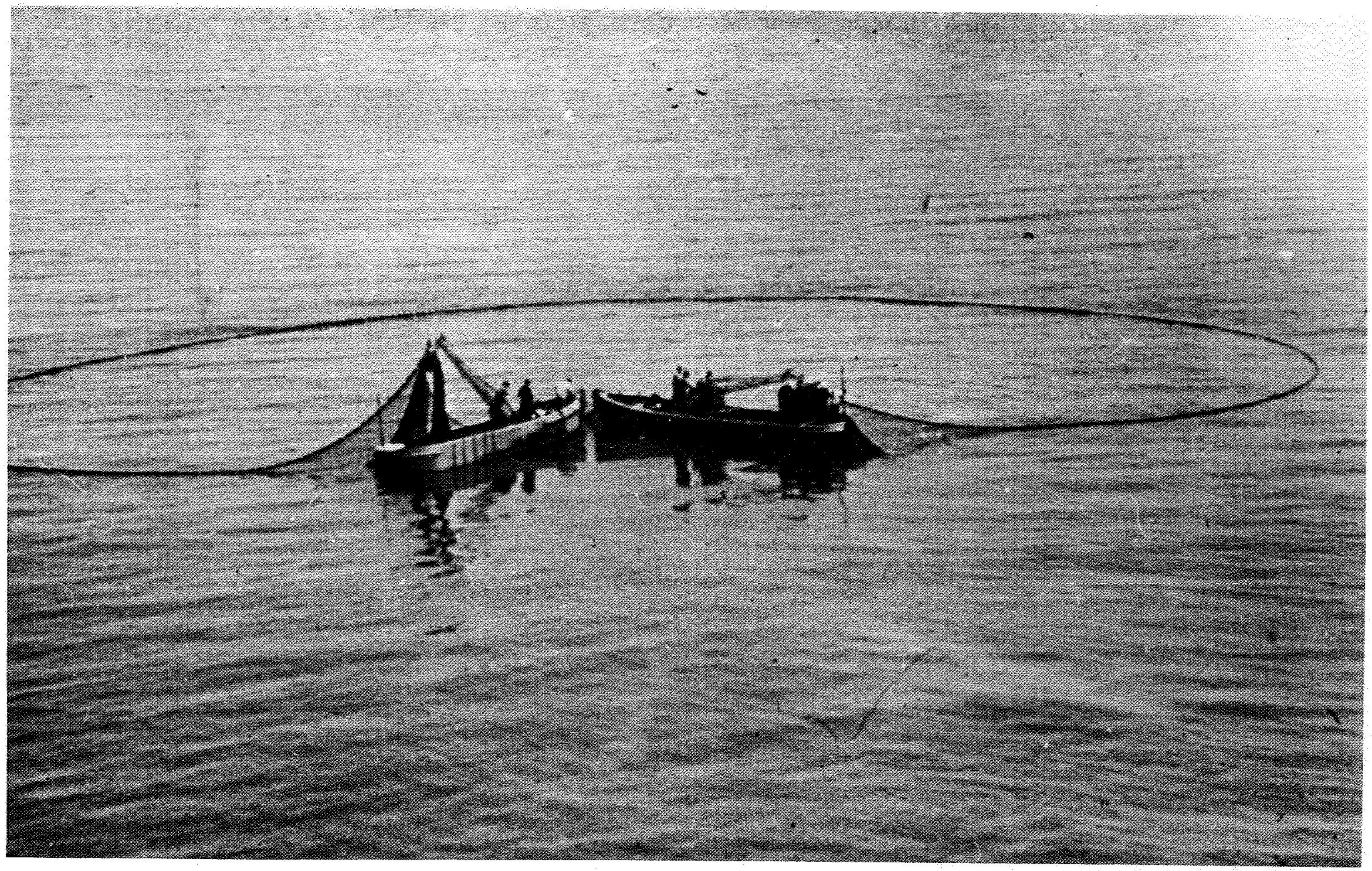

Fig. 4. Menhaden Purse Seine operated from two catcher boats. The seine is set around the school of fish forming a fence from the surface to the bottom.

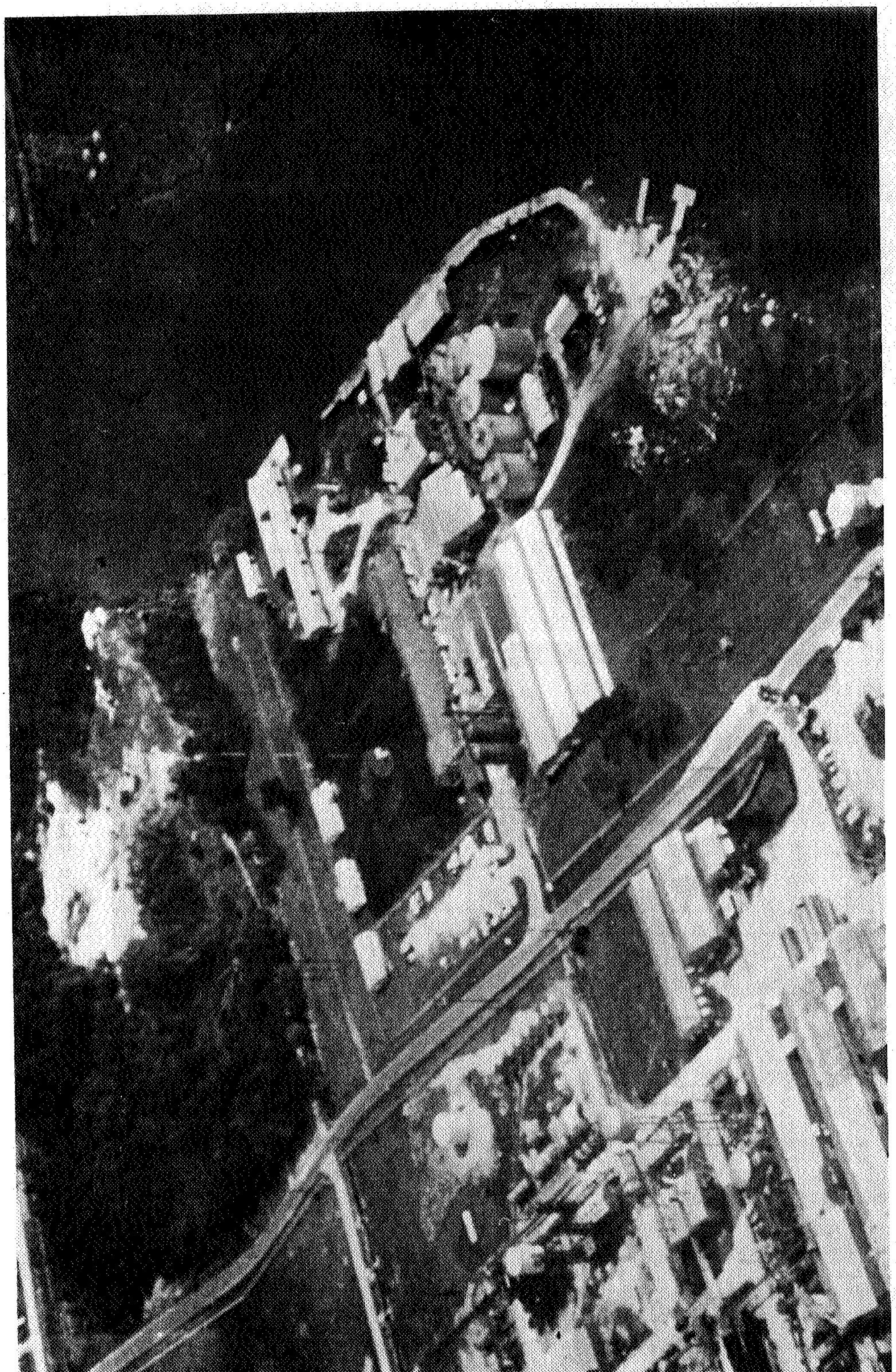

Fig. 5. Modern menhaden processing plant located at Moss Point, Ms.

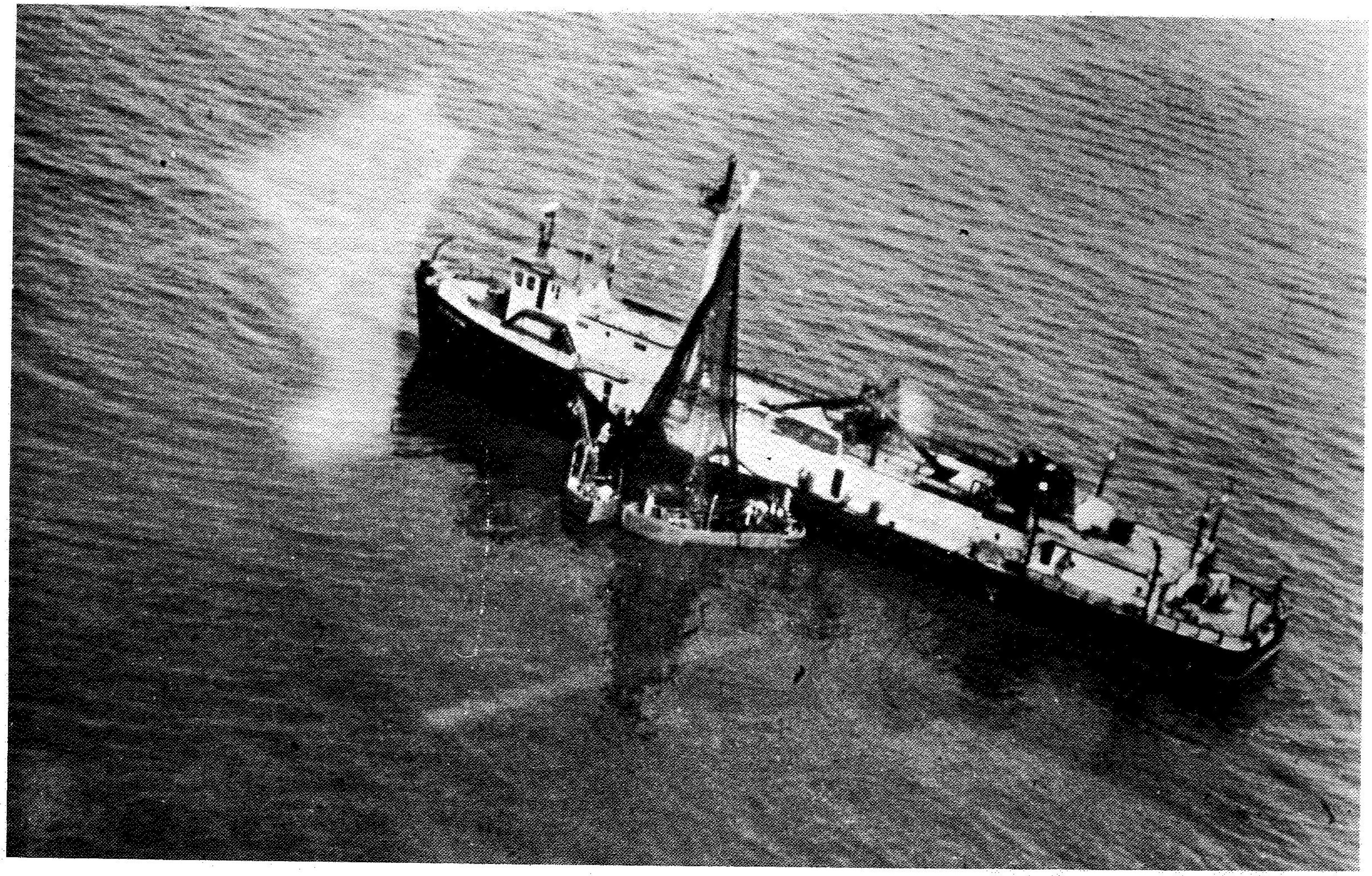

Fig. 6. Modern menhaden transport ship. Catcher boats with fish in net are along side to transfer the fish from the net to the ship.

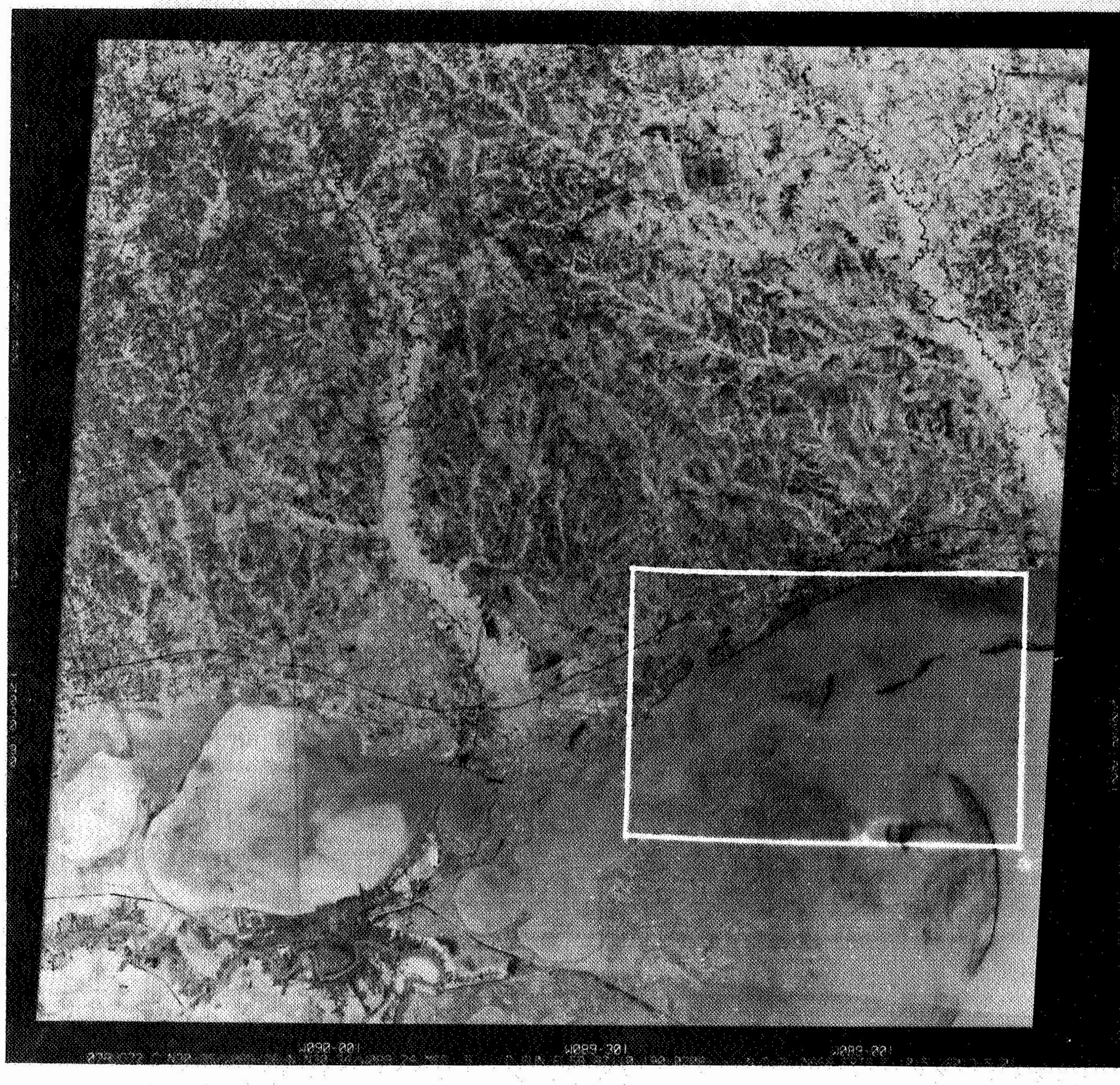

Fig. 7. ERTS-1 MSS Band 5 Image of western Mississippi Sound. The inset area was enlarged for analysis of fish distribution and water density relationships.

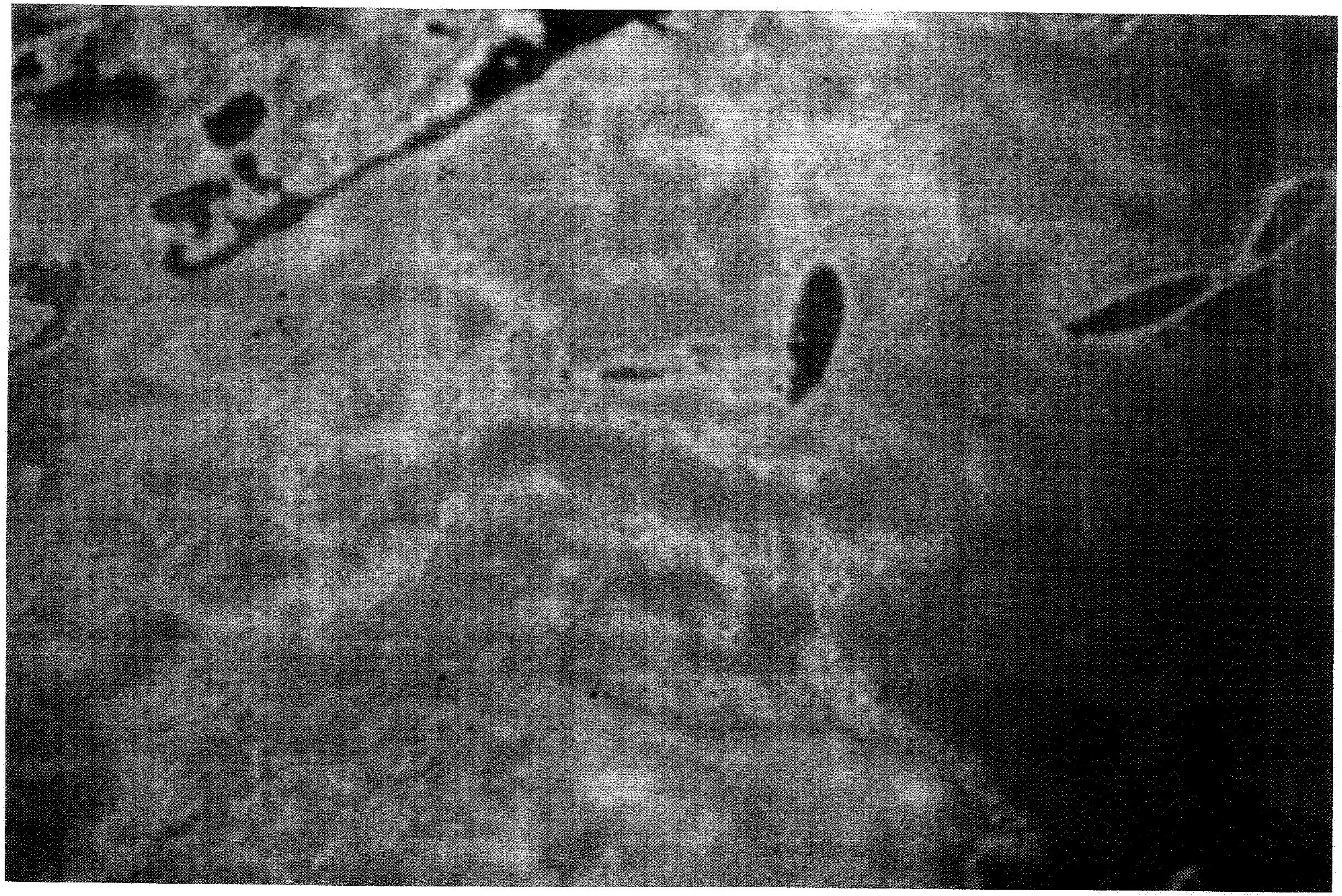

Fig. 8. Color enhanced ERTS-1 MSS Band 5 image. Orange shaded area represents low density areas of the image. Schools of menhaden are shown as black dots. From Kemmerer, Benigno, Reese and Minkler, 1973

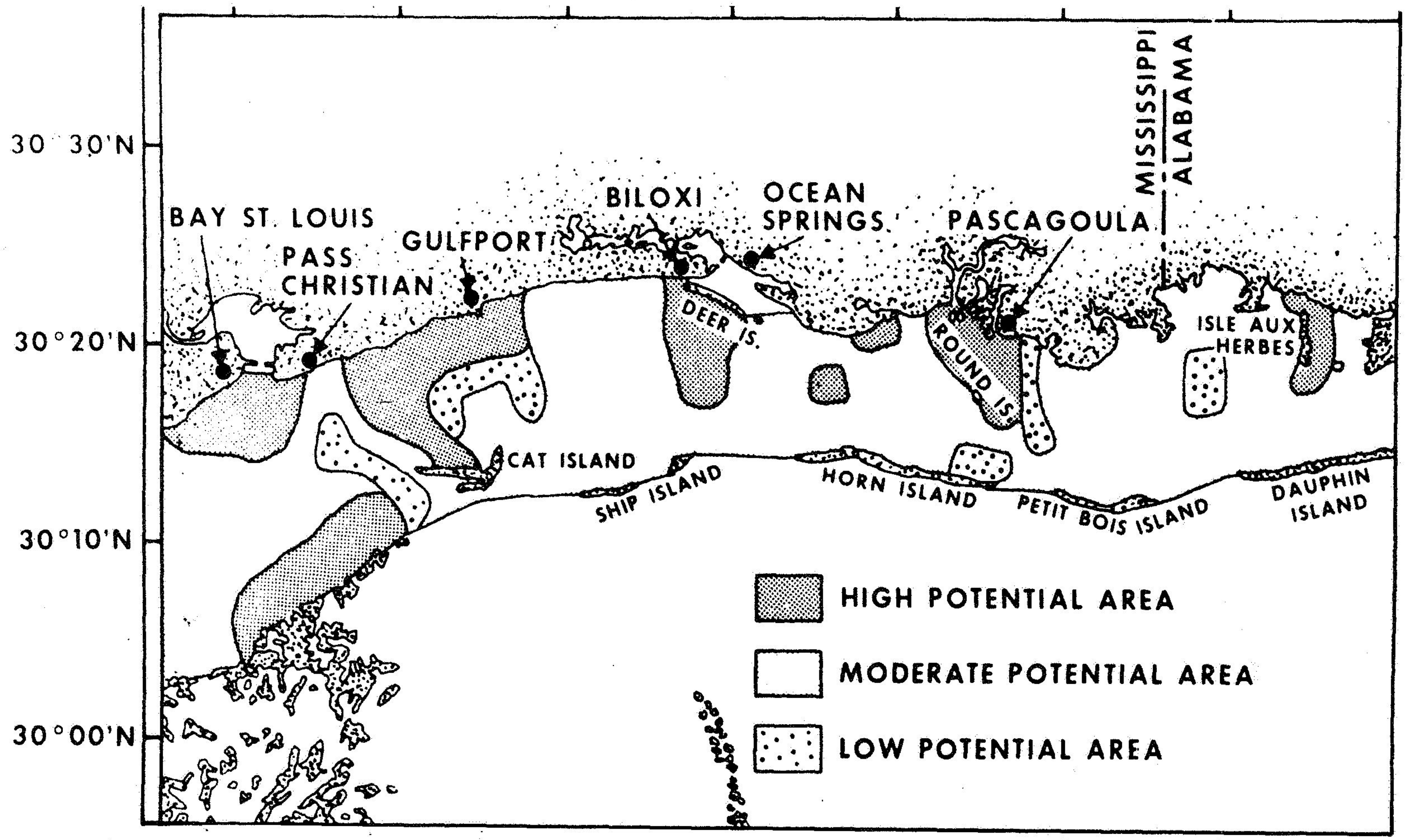

Fig. 9. Empirical regression model presentation of menhaden occurrence probability in Mississippi Sound. From Kemmerer, Benigno, Reese and Minkler, 1973.

Paper M 4

UPDATING COASTAL AND NAVIGATIONAL CHARTS USING ERTS-1 DATA

Fabian C. Polcyn and David R. Lyzenga, *Environmental Research Institute of Michigan*

ABSTRACT

A successful processing algorithm for extracting water depth information from ERTS data has been developed. Depth charts for two geographical areas have been constructed representing different solar illumination and water transparency conditions. Absolute depth calculations for water depth to 4.5 fathoms have been demonstrated for the Little Bahama Bank. Depth Charts also were constructed using data in Band 4 and 5 of the ERTS-1 MSS for areas in Lake Michigan. This data represented a low sun angle, poor light transmission in water conditions and gave useful results to 200 meters. In both cases, the ERTS map represented an update in shallow water detail in comparison with available navigation charts for the areas tested.

Present processing costs to provide MSS depth charts are estimated to be on the order of $1.50 per sq. mile. The updating of navigation charts for areas hazardous to shipping is an achievable direct application. The technique is available for world wide use. The International Hydrographic Office has called on countries to improve and update their navigation charts. One billion dollars per year is the estimated loss by the world shipping industry with several millions attributed to losses due to inaccurate navigation charts.

In the United States, the U.S. Lake Survey, The U.S. Coast and Geodetic Survey, NAVOCEANO and National Ocean Survey are agencies that will benefit directly from this capability. Other agencies dealing with erosion problems, sand transport, beach gradients, effects of new harbor construction, storm damages to near shore properties and time changes in beach recreation properties will be beneficiaries of this remote sensing technique.

The frequency of coverage of ERTS data should provide a baseline data set for all of the critical areas. Aircraft multispectral data collected in conjunction with satellite coverage could also be used to establish calibration areas of water depth for the satellite map but they also could be used in those areas where higher resolution is desired.

INTRODUCTION

The history of navigation and shipping is filled with examples of ship losses due to collisions with unchartered shoals or with shoals whose positions were known only approximately. The International Hydrographic Office has expressed concern over the status of navigation charts around the world and has called upon the world community to assist in providing more reliable chart information.

In a similar fashion, near shore processes in coastal waters provide a dynamic environment for change aided by man's own rearrangements of the shoreline through his construction of harbors, recreation beaches, power generation plants sites, marinas and local erosion abatement devices. There is need for a monitoring technique with capability both for wide area updating of charts and for the timely assessment of storm induced changes along coast lines. The successful launch and operation of ERTS-1 and the subsequent telemetry of multispectral data from around the globe covering 10,000 sq. nm per frame every 18 days makes it possible to conceive of such a needed monitoring system. A successful processing algorithm for extracting water depth information from ERTS data has been developed. Depth charts for the Little Bahama Bank and for a section of the Michigan-Wisconsin coastline have been constructed as test cases using band 4 and band 5 of ERTS-1 multispectral scanner.

BENEFITS

One of the benefits that can be predicted from the use of satellites in mapping the oceans is in helping improve nautical charts where better location and depth information of shoals would help reduce ship casualties. Additional benefits might be in helping to shorten commercial shipping routes and increased safety. The reduction in commercial ship casualties would reduce losses of life, cargo, and property. An estimate of the average losses for the U.S. is given in Table I showing it running over $90 million per year. On a world wide basis, the U.S. shipping is about 10% of the total for commercial ships of 100 or more gross tonnage so that about 1 billion dollars is the estimated world loss. The number of vessels involved and the primary cause of the U.S. ship casualties are given in Table II (Reference 1.) At least one loss category is directly attributed to inaccurate depth information. It is possible that other loss categories might be indirectly reduced with better navigation charts. This might arise by reducing calculated risks or by shortening shipping routes. In any event, the estimated loss on a world basis that might be reduced is estimated at a few million dollars per year.

A similar case could be made for benefits to be derived in providing timely information for the control of erosion processes in the near shore environments. Homes, commercial properties, recreational areas built near shore are subject to erosional losses due to changing water level and wave action. Transport of sand and erosion of bluff lines can be monitered by remote sensing. Surface currents can be mapped by temperature and turbidity gradients. Near shore depths can be mapped by satellites and aircraft remote sensors. The monitoring of effective shoreline erosion control devices would be possible on an area large basis over which such shore processes operate.

EXPERIMENTAL RESULTS

Figures 1, 2, 3 cover three different times for which ERTS-1 obtained data over the Little Bahama Bank near Grand Bahama Island. From the comparison of density change in Band 4, those phenomena which are transient in character can be separated from the more stable features. In this test site, a number of shifting sand bars occur and a number of ships wrecks have been indicated on the charts. Also can be seen are high turbidity, linear features which upon further investigation were found to be associated with the location of fishing sites since the action of a number of fish produced the high sand suspension zones that stretched for 1 to 3 miles due to currents. Figures 4 and 5 taken from 2000 ft. in a light aircraft record the differences in character between shifting sand shoals and high turbidity fishing sites.

Using a multispectral technique involving two channels of information e.g. bands 4 and 5 in the case of ERTS-1 (Reference 2.) a depth chart for the Little Bahama Bank was computed with depth down to 10 meters displayed. Figure 6 and Figure 7 show the comparison between the available chart and the computer generated ERTS-1 depth map for the area. The depth code is given as follows

Red	M	0-1 meters	Blue	.	3-5 meters
	X	1-2 meters		*	5-7 meters
	=	2-3 meters		X	7-9 meters
				M	over 9 meters

The technique uses the different water penetration characteristics of colors in the blue green and red wavelengths. For the ERTS-1 analysis, green and red wavelength were employed. Further improvements in depth calculations can be expected when blue wavelengths are available from satellite sensors.

A second site involving a coastline in Lake Michigan was used to demonstrate the depth mapping capability of ERTS-1 is a different water transparency situation. Also, a lower sun angle was involved since data frame 1089-16090 was used. The solar zenith angle of 60 degrees and the relatively higher attentuation coefficient for this area permitted a theoretical maximum depth of 2.77 meters. Because of noise, variations in detector response, the maximum depth that can be reliably computed for this particular circumstance was 2 meters. At higher solar elevations, a greater depth can be measured. For the Bahama example a higher sun angle and clearer water permitted depth to 9 meters to be measured for ERTS-1 frame 1079-15165.

Figures 8 and 9 show the results obtained in Lake Michigan near Green Bay. Of particular note is the mapping of the underwater shoals at Fish Island (lower right) which were not seen in band 7, could likely to be mistaken for land above water in band 4 but were calculated to be 1.5 meters underwater by the multispectral ratio technique. (See Figure 9) Figure 10 shows how the ratio values in band 4 and 5 were related to water depth. On the depth map a code involving 2 red symbols for 0-1 meter and 1-1.5 meters and two blue symbols for the range 1.5-2 meters and greater than 2 meters was used.

The demonstration of shoreline depth mapping suggests the application of this technique to the problems referred to earlier involving changes in beaches and in erosion processes.

The costs of processing ERTS-1 Frames for depth information based on present analysis techniques amounted to about \$1.50 per sq. mile. The updating of navigation charts is an achievable direct application of ERTS-1 technology. Processing programs have been developed which provide the capability to assign geographical coordinates to each resolution element of ERTS so that location of shoals could be defined to within one-half resolution element.

SUMMARY

The successful measurement of water depth from satellites and aircraft (Reference 3) suggests that a combined system for measurement of hazardous shoals or for monitoring changing coastlines can be devised in which each sensor platform does its primary function. Large areas can be mapped to 10 meter depths by satellite sensors. Aircraft sensors could be employed where higher spatial resolution is required. Ships collecting depth soundings in the conventional way would have to be used only in the high turbidity areas where no bottom reflection is obtained or for deep ocean soundings.

Satellite data provides additional information besides depth and location. The transport phenomena of near shore processes can be mapped on a scale consistent with the size of currents and tidal actions.

Agencies such as the U.S. Lake Survey, U.S. Coast and Geodetic Survey, U.S. Army Corp of Engineers, State Water Resource Commissions should benefit from this new technology.

REFERENCES

1. G. J. Zissis, et. al, Design of a Study to Evaluate Benefits and Cost of Data from the First Earth Resources Technology Satellite (ERTS-A), Report No. 11215-1-F, Willow Run Laboratories of the Institute of Science and Technology, the University of Michigan, Ann Arobr, July 1972.

2. F. J. Thomson, et. al, ERIM Progress Report on Use of ERTS-1 Data, Report No. 193300-16-P, Environmental Research Institute of Michigan, Ann, Arbor, July 1973.

3. W. L. Brown, F. C. Polcyn, A. N. Sellman, and S. R. Stewart, Water-Depth Measurement by Wave Refraction and Multispectral Techniques, Report No. 31650-31-T, Willow Run Laboratories of the Institute of Science and Technology, The University of Michigan, Ann Arbor, August 1971.

TABLE I

ESTIMATED U. S. LOSSES THROUGH U. S. COMMERCIAL SHIP CASULTIES

	1966	1967	1968	1969	1970	1971
Vessel	95,139,000	53,080,000	63,206,000	68,267,000	69,274,000	78,961,000
Cargo	7,454,000	9,801,000	5,186,000	10,269,000	17,360,000	6,629,000
Property	3,131,000	12,262,000	12,676,000	7,926,000	10,629,000	8,911,000

This table has been constructed using fiscal year figures published in the following issues of the <u>Proceedings of the Marine Safety Council</u>: December, 1966; November, 1968; December, 1969; December, 1970; December, 1971.

TABLE II

NUMBER OF VESSELS INVOLVED IN U. S. COMMERCIAL SHIP CASUALTIES -- PRIMARY CAUSES

Primary Cause	1966	1967	1968	1969	1970	1971
Personnel Fault	550	551	984	1,193	1,300	1,325
Calculated Risk*	257	386	307	124	22	10
Restricted Maneuvering Room	210	177	50	32	31	22
Storms-Adverse Weather	374	202	446	253	274	370
Unusal Currents	50	34	70	46	57	19
Sheer, Suction, Bank Cushion	36	31	34	57	3	4
Depth of Water Less than Expected	100	63	110	76	54	50
Failure of Equipment	311	376	540	610	510	524
Unseaworthy-Lack of Maintenance	340	323	135	133	86	81
Floating Debris-Submerged Object	153	157	97	151	172	151
Inadequate Tug Assistance	137	105	34	63	30	14
Falt on Part of Other Vessel or Person	746	947	1,142	1,333	1,304	1,435
Unknown-Insufficient Information	29	23	62	112	220	147
TOTAL	3,293	3,030	4,0001	4,183	4,063	4,152

The source of the figures is the same as for Table III-1.
*Before 1969, 'Error in Judgment-Calculated Risk', rather than just 'Calculated Risk'.

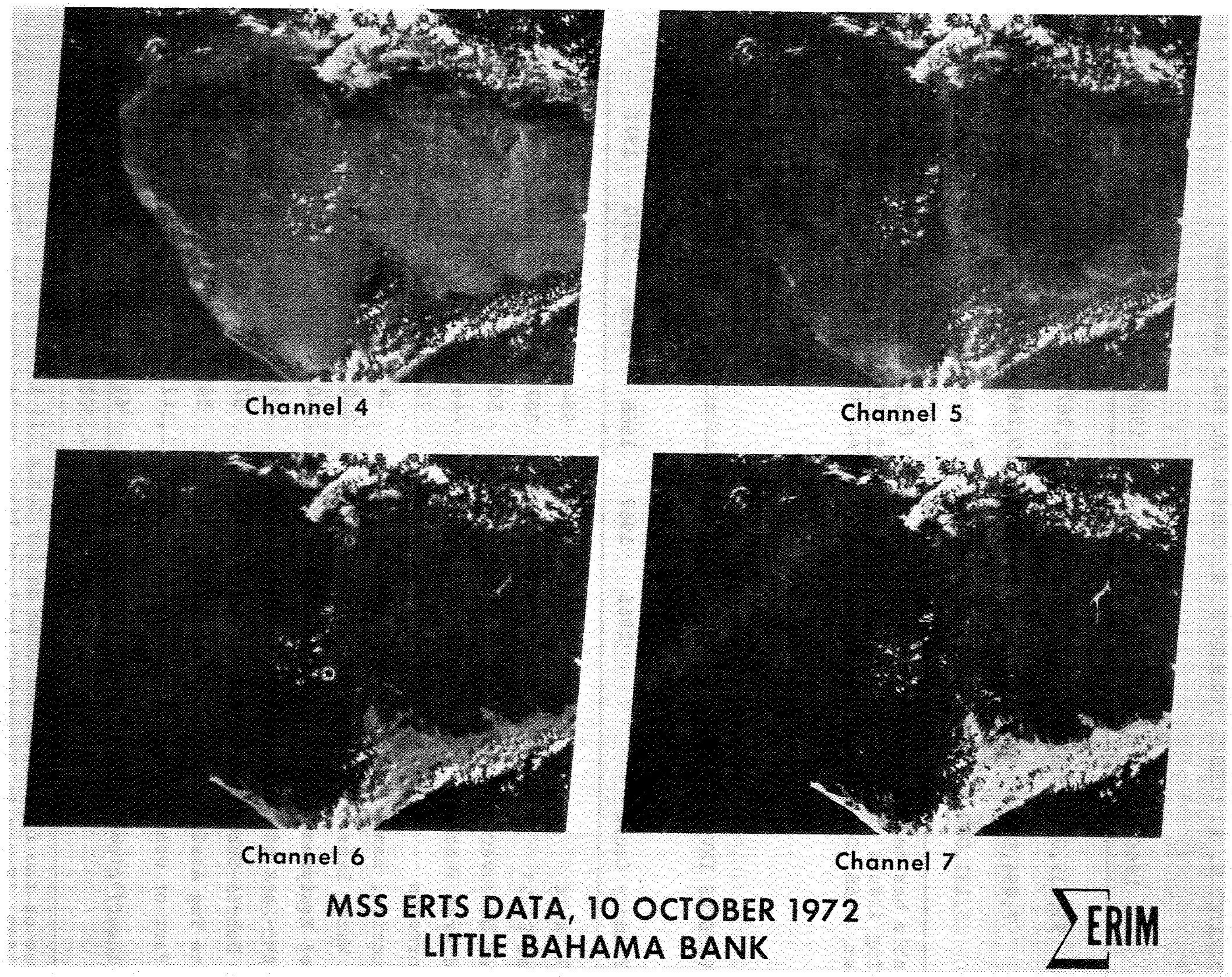
Channel 4
Channel 5
Channel 6
Channel 7
MSS ERTS DATA, 10 OCTOBER 1972
LITTLE BAHAMA BANK
ERIM

FIGURE 1

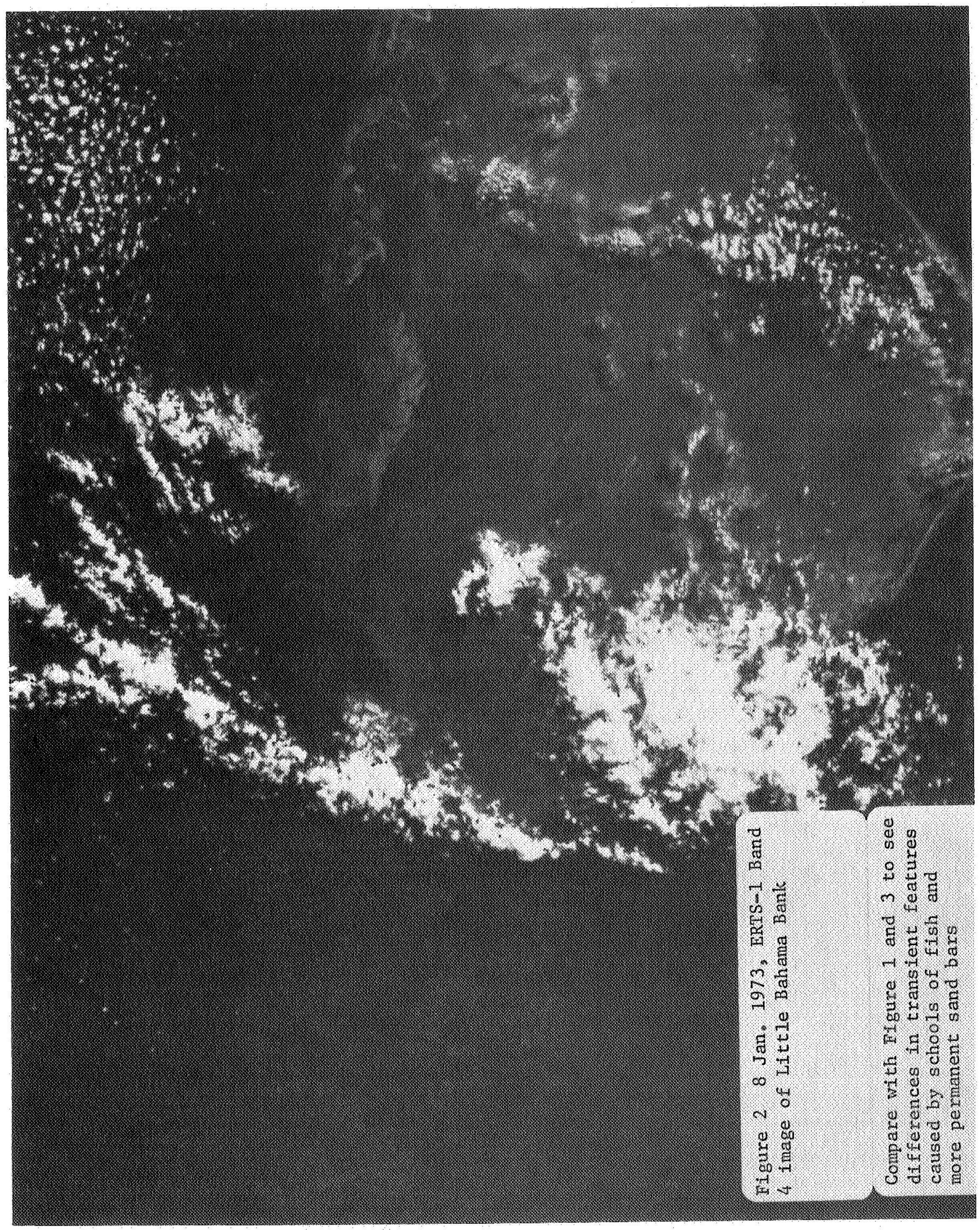

Figure 2 8 Jan. 1973, ERTS-1 Band 4 image of Little Bahama Bank

Compare with Figure 1 and 3 to see differences in transient features caused by schools of fish and more permanent sand bars

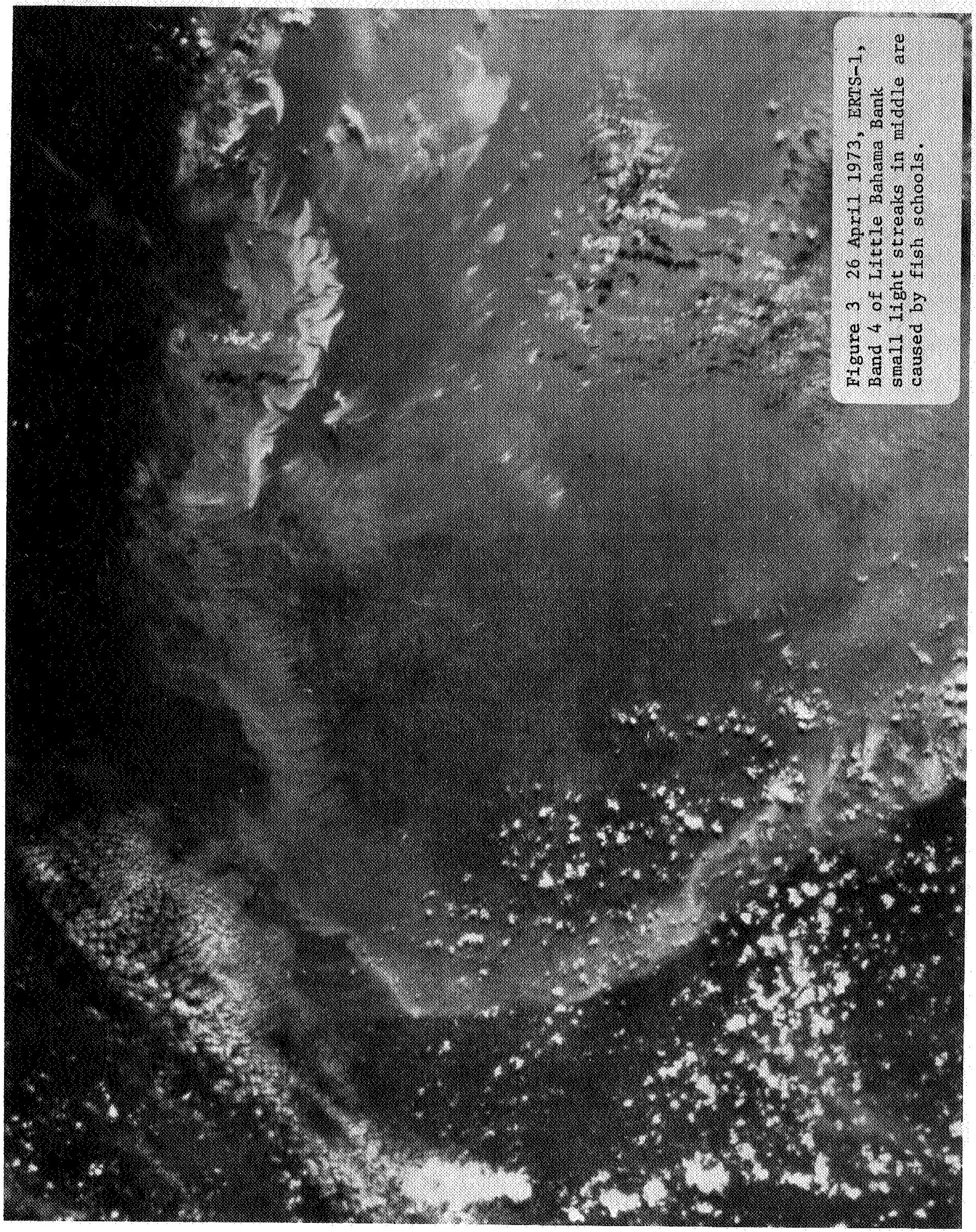

Figure 3 26 April 1973, ERTS-1, Band 4 of Little Bahama Bank small light streaks in middle are caused by fish schools.

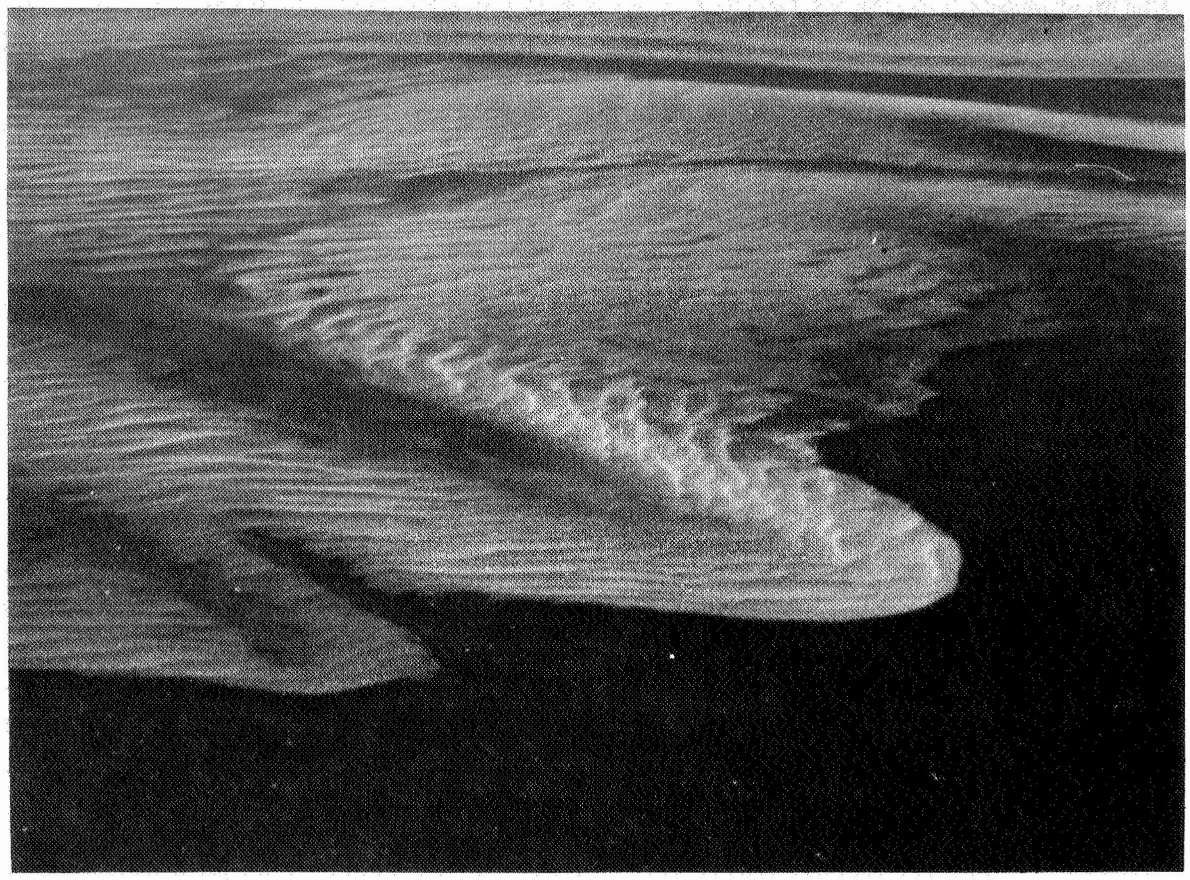

Figure 4 Photograph of sand bars near Walker Cay, Little Bahama Bank, Nov. 1973, 2000 ft. altitude Approximate Scale 1:2500

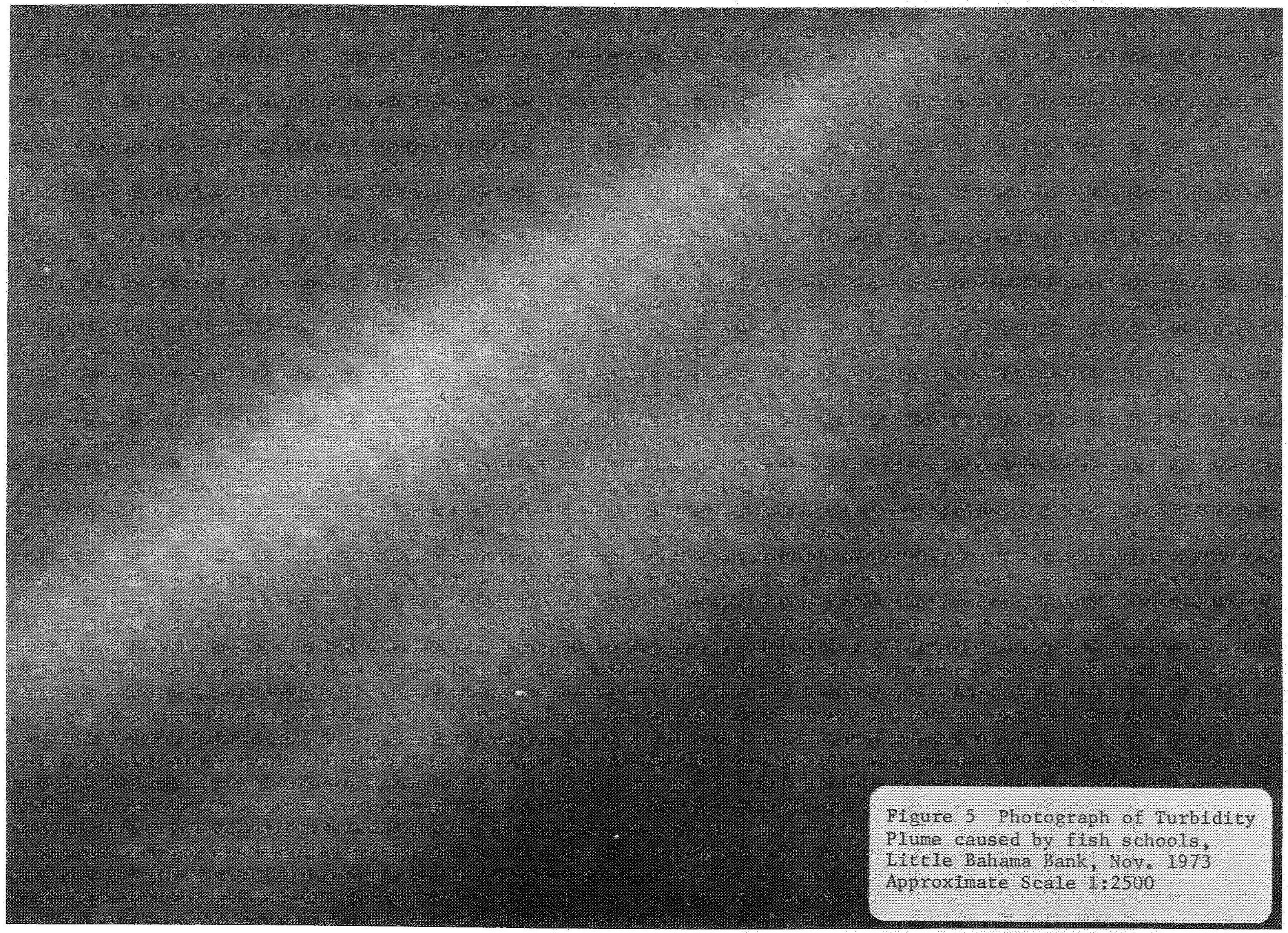

Figure 5 Photograph of Turbidity Plume caused by fish schools, Little Bahama Bank, Nov. 1973 Approximate Scale 1:2500

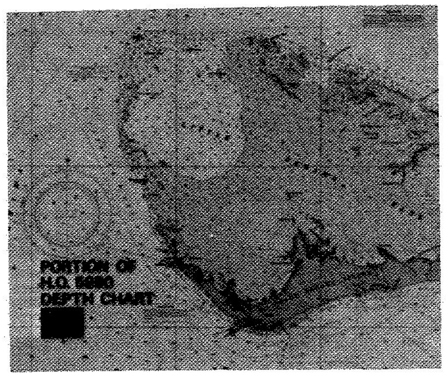

Figure 6 Portion of H.O. 5990 Depth Chart for Comparison to ERTS-1 Map

Figure 7 Computer generated absolute depth map constructed for Little Bahama Bank using multispectral ratio technique
See text for depth chart

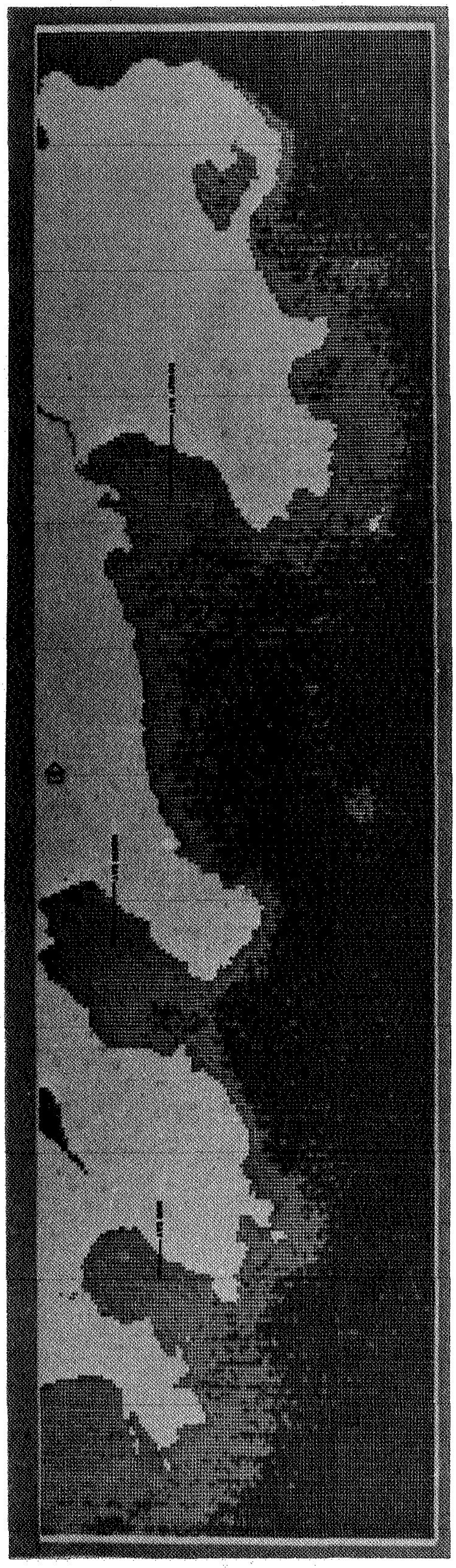

Figure 8 Depth map made by Multispectral Ratio Technique from ERTS Frame 1089-16090, Northwest Lake Michigan

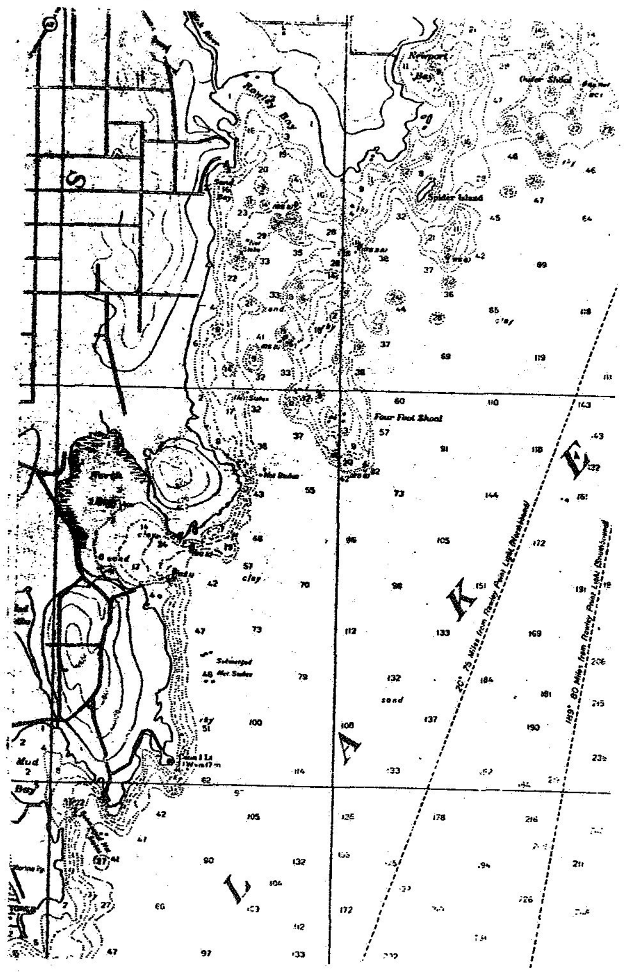

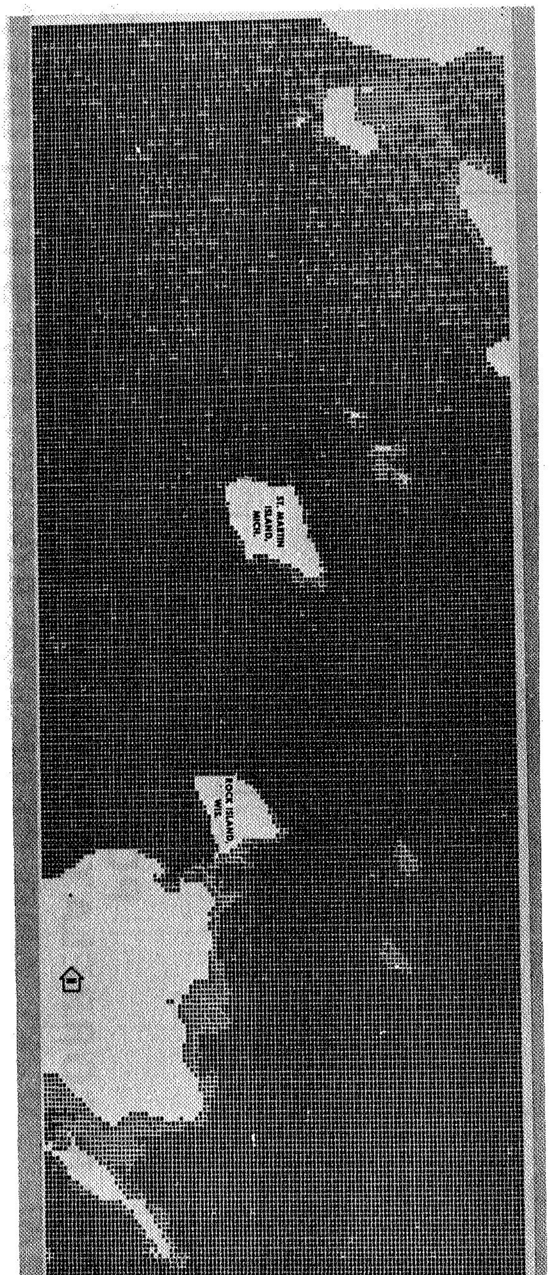

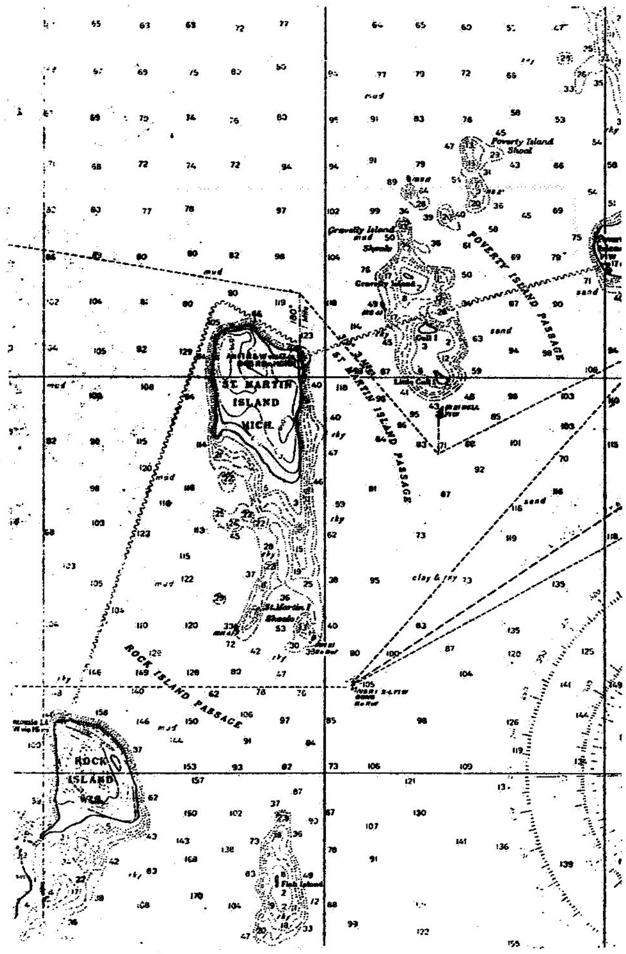

Figure 9 ERTS-1 Depth Map and chart for passage area from Lake Michigan into Green Bay

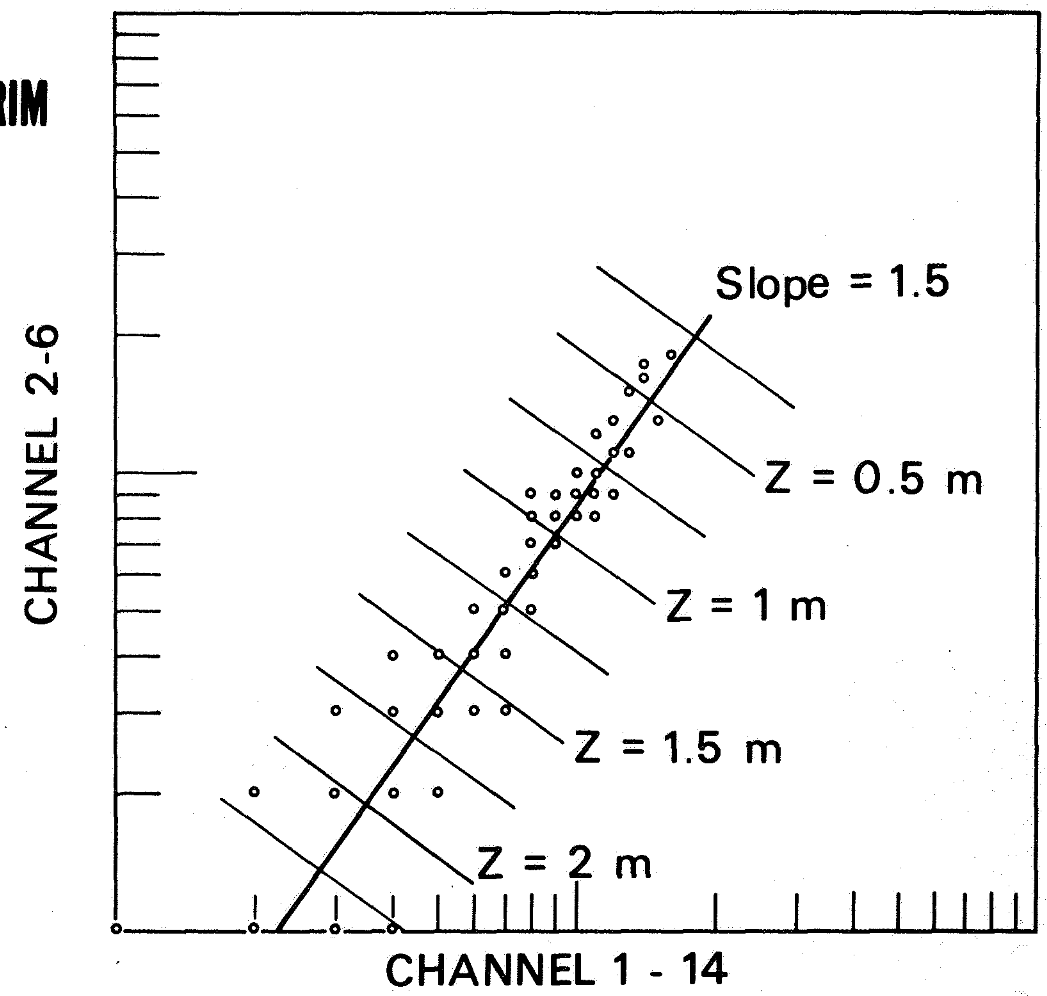

FIGURE 10 **POINTS ON LOG-LOG PLOT, SHOWING LINEAR CORRELATION BETWEEN $LOG(V_1 - V_{S1})$ AND $LOG(V_2 - V_{S2})$, AND DECISION BOUNDARIES FOR DEPTH**

Paper M 5

SEDIMENT CONCENTRATION MAPPING IN TIDAL ESTUARIES

A. N. Williamson and W. E. Grabau, *Environmental Systems Division, Mobility and Environmental Systems Laboratory, U.S. Army Engineer Waterways Experiment Station, P.O. Box 631, Vicksburg, Mississippi 39180*

ABSTRACT

An analytical procedure has been developed that considers the ERTS-1 multispectral scanner as a reflectance spectrophometer. ADP techniques requiring only very limited computer capability are utilized to search the data defining the spectral reflectance characteristics of a scene on a pixel-by-pixel basis, identify each pixel whose spectral reflectance matches a reference spectrum, and generate maps that identify pixel locations where spectrum matches occur and identify the spectrum that was matched. If the reference spectra are known to represent a specific condition on the ground, a map of the distribution of that condition can be output as a dimensionally accurate overlay to maps of any selected scale. Two applications are described in this report: (1) mapping the distribution of water masses exhibiting specific suspended sediment concentrations; and (2) determining the location and delineation of surface water bodies in the southeastern U. S.

The techniques described in this paper are currently being successfully used in connection with U. S. Army Corps of Engineers' projects to map the land area inundated by the 1973 spring flood in the Lower Mississippi River Valley, map sediment distributions in Lake Pontchartrain (in Louisiana) as a result of opening the Bonnet Carre Floodway during the spring flood, and inventory lakes and reservoirs in the states of North Carolina, South Carolina, Georgia, Florida, Alabama, Iowa, Louisiana, West Virginia, and Kansas in connection with the National Dam Safety Program.

INTRODUCTION

Technical Objectives and Long-Range Goals

A long-range goal of the Corps of Engineers (and a number of other agencies) is to develop the capability of predicting the dispersal of water constituents (i.e., sediments, nutrients, pollutants, salinity, etc.) in estuaries. If such predictive capabilities were available, it might eventually lead to methods of predicting, and managing, the biological populations in the estuary and related waters.

Attempts to develop estuarine dynamics models has clearly demonstrated that it will be necessary to monitor the movements of the various

water masses (i.e., the discharges of the various rivers as well as inflowing marine waters) through the system in order to validate the models. Ideally, this implies a set of synoptic records of conditions within the estuary and related waters over some period of time. While this kind of record is effectively impossible to obtain with conventional methods, the ERTS-1 offered the possibility of a practical method, provided that the ERTS multispectral scanner could be used to achieve two specific capabilities. These two capabilities can be stated as research objectives, as follows:

a. To determine the feasibility of using ERTS-1 digital data for mapping the planimetric distributions of suspended sediment concentrations in estuarine waters; and

b. To determine whether different sediment types could be differentiated, by exploiting their differences in spectral reflectance.

Conceptual Plan

In considering the nature of the problem, it seemed obvious that the methods used to identify types of sediments, and to map the distributions of their respective concentrations, would have to be completely objective. That is, no determination should be based on subjective interpretation, because prior experience with remote sensing systems had clearly demonstrated that it was impossible to define recognition criteria in such a way that the criteria were used by all interpreters in the same way.

The requirement for objective procedures dictated that the entire interpretive process be based on mathematical manipulation of the digital data recorded on computer compatible tapes (CCTs). The research plan which was actually followed is presented in fig. 1 in diagrammatic form. In the context of this plan, the multispectral scanner (MSS) aboard ERTS-1 can be thought of as a reflection spectrophotometer that senses and records the spectral reflectance and/or emittance of a scene on a pixel-by-pixel basis. In our terminology, a pixel (or picture element) is the area over which radiant power is integrated and measured. As illustrated in fig. 2, each pixel on the ground is represented by a corresponding pixel in each of the spectral bands of the MSS. By placing the values for a pixel in each spectral band into juxtaposition, as shown in fig. 2, a crude reflectance spectrum for the corresponding area on the ground can be defined.

It is worth noting at this point that the spectrum, as recorded by the MSS, is indeed crude. As an example the "real" reflectance spectrum illustrated at the top left of fig. 2 is generalized by the ERTS-1 MSS into the "histogram" shown at the top right of fig. 2. The radiant energy in each band is then converted into a voltage by the

sensing element, and that voltage is then recorded in digital form, as illustrated in the bottom right of fig. 2. This generalization has important implications with respect to analytical interpretive processes.

The analytical concept which was finally used was based on the premise that a given material on the surface would always yield the same reflection spectrum, as seen from satellite altitude, provided that certain conditions were met. These conditions are as follows:

a. The constituents of the material were constant. For example, if the material is a soil, the conditions would not be met if the soil moisture content changed.

b. The surface expression of the material was the same. For example, if the material was water, it would not be expected to look the same under substantially different wave conditions.

c. The reflectance geometry must be similar. For example, it would be expected that a significant change in sun angle would affect the reflectance spectrum.

d. The atmospheric composition was the same. Significant changes of absorbtion and scattering occur as a result of changes in aerosol content of the atmosphere, and thus a change in type or density of haze would change the spectral composition of radiation reaching the satellite.

If the above conditions could be met, then it follows that the spectral data, as sensed by the satellite, could be correlated directly with conditions on the surface, with the implication that identical spectral records obtained by the satellite would imply identical conditions on the surface. For the purposes of this report, this means that a specific type and concentration of suspended sediment would be represented by the same spectrum throughout any one ERTS-1 scene, since all four of the conditions specified above (with the possible exception of condition b) would be met. Condition b, identity of surface expression, might not be met, since it would be all too likely that wave conditions would vary somewhat even within the same estuary. As a result, it should not be expected that exact spectrum matches would in fact occur. However, if acceptable limits of variation could be established, it would be a simple matter to convert the reflectance spectra as measured by the satellite into concentration of suspended sediment on a pixel-by-pixel basis throughout an ERTS scene. The result would be a map of the distribution of suspended sediments, by concentration classes, produced by a completely automated process.

There are serious inadequacies in this procedure. By far the most important of these is that it provides little if any predictive capability. That is, the correlations used to map sediment concentrations

the scene obtained on the next orbital pass, because all four of the conditions previously specified may be different. That is, the type of sediment may be somewhat different, the sea state may be different, the sun angle may be different, and the atmospheric composition may be different. In view of the number of possible variables, it is unlikely that the same correlations will be valid for any extended period.

A far more definitive plan which, if successful, would have resulted in significant predictive capability, was abandoned early because of rapidly mounting costs. This plan is presented in diagrammatic form in fig. 3. Had we been able to follow this plan, the product would have been a capability for predicting the spectral composition of various sediment concentrations, as seen by the ERTS-1, for any set of atmospheric and sea state conditions. With that as a basis, the ERTS-1 digital data could then have been used to map sediment concentrations without the necessity for the elaborate ground control required by the existing procedure.

DATA COLLECTION AND ANALYSIS

Selection of Study Areas

In order to keep the scope within reasonable limits, a very limited number of test areas within the Chesapeake Bay region was chosen. The Chesapeake itself was chosen primarily because State, local, and Federal agencies are intensely concerned over the health of the Bay. Eventually four river estuaries and the Chesapeake and Delaware Canal, as indicated in fig. 4, were chosen as test areas. The selection criteria were as follows:

a. Each river drainage basin should exhibit an array of soil types unlike any other in the set; or

b. Each river should incorporate a unique source of industrial waste.

In detail, the specific reasons were as follows:

a. Area 1: York estuary. The drainage basin includes large sections of the Piedmont and the coastal plain, but does not extend to the slopes of the Blue Ridge. Further, there is a major industrial complex at West Point.

b. Area 2: Rappahannock estuary. The drainage basin includes the eastern slopes of the Blue Ridge, the entire width of the Piedmont, and only a narrow slice of the coastal plain.

c. Area 3: Wicomico estuary. The drainage basin includes a portion of the south central Delmarva Peninsula, which has soils closely

resembling those in the Choptank drainage basin, but there is a major food-processing industrial complex at Salisbury.

d. Area 4: Choptank estuary. The drainage basin includes much of the north and central Delmarva Peninsula, without any large sources of industrial effluents.

e. Area 5: Chesapeake and Delaware Canal. This area was chosen primarily for two reasons. First, to determine whether the exchange of water between the Chesapeake and Delaware Bays via the canal would be detected; and second, to determine whether a feature as narrow as the canal would yield valid spectral reflectance data. Theory suggested that features at least three pixels wide might be required, because atmospheric scattering would "contaminate" the pixels at the edge of a water surface.

It was hoped that the suspended sediments and/or industrial wastes in the four river sites would differ enough to produce four distinctive spectral reflectance "signatures."

Computer Considerations

It seemed to us, in considering the problems involved in automatic interpretation, that not everyone who wanted to play the game would have access to a giant computer. Accordingly, it was decided that the analytical procedures would be designed to fit on as small a computer as possible. As a result, all processes described in this report were achieved with PDP-15 computer with 16K of core memory and two disc storage units.

Ground Control Data

One of the primary requirements was to establish the spectral reflectance characteristics of the various water bodies at, or close to, the time of a selected ERTS overpass, and to collect water quality data at those times and places, to serve as a basis for correlation. Ground control data collection stations were selected in the York, Rappahannock, Wicomico, and Choptank Rivers and the Chesapeake and Delaware (C&D) Canal. ERTS-1 overpasses were supported by collection of ground truth data at 72 stations on 10 October and 63 stations on 28 October. As weather conditions precluded collection of data on the Choptank River on 28 October, data were collected at 11 stations on the Choptank on 29 October. Where local conditions permitted, the following parameters were measured: suspended material concentration, water temperature, conductivity, turbidity, dissolved oxygen, current velocity/direction, spectral transmittance, secchi depth, and pH. A typical sampling pattern is illustrated in fig. 4a.

A data collection platform (DCP) connected to a water quality analyzer for monitoring temperature, conductivity, pH, and dissolved oxygen and a multichannel recorder connected to sensors for monitoring water temperature, wind speed and direction, rainfall, and incident and reflected solar radiation were used to collect data at one station in the Choptank River and one in the Rappahannock.

It had originally been intended to take spectral reflectance data at each ground control site using an instrument specifically designed to measure radiant energy through the same four windows used by the ERTS-1 (fig. 5). Thus, excluding the effects of the optical path through the atmosphere, and assuming that the area contained in the field of view of the ground control instrument is the same as that of the ERTS-1 the ground control reflectance spectra should be the same as the spectra measured by the satellite. Unfortunately, we were not able to get delivery of the special instrument until after the conclusion of the field program. We attempted to obtain both down-welling and reflected radiation data by using a bread-board consisting of eight broad-band radiometers, four pointed upward and four downward. They were filtered to accept radiation in approximately the four ERTS bands. It proved to be impractical to keep the system in calibration, and that, along with serious filter problems, resulted in very patchy and unreliable data. As a result, no near-surface spectral data were used in the analyses.

Reference Reflectance Spectra

The location on the surface of a single pixel cannot be fixed with absolute accuracy. The possible accumulated errors from all causes adds up to about 300 m. However, in most cases the errors partially compensate for each other, so that the average error is somewhat less than 100 m. The practical effect of this is that a sediment concentration sample cannot positively be identified as coming from within a single pixel; the best that can be done is to argue that it probably comes from one of a possible matrix of about nine pixels, as illustrated in fig. 6.

Fortunately, the areas of distinctive water masses in the Chesapeake estuaries are quite large, so that an examination of the reflectance spectra of the nine pixels in the "potential error matrix" shows then to be closely similar. Exceptions occur, of course, when the sample point happens to be close to the edge of a sediment "cloud." Our procedure was to select the spectrum of that pixel which most closely resembled its neighbors as the reference spectrum. That is, if seven of the nine spectra closely resembled each other, while two did not, the spectrum which was assumed to represent the sample point was taken to be one of the seven. Since virtually all of the energy in Band four (0.8-1.1 μm) was absorbed by the water, the selection was based entirely on the records of Bands 1, 2, and 3.

Since it was originally intended to model the energy exchange processes through the entire system, as described in fig. 3, there were some real advantages to be gained by converting the ERTS-1 CCT data into radiance values. The original concept had been to match the actual radiance spectrum of a water body, measured near the ground, with the radiance spectrum of that body as recorded by the ERTS-1 MSS. Then, if it could be demonstrated that reflectance spectra, as measured near the ground, correlated with type and amount of suspended sediment, it should be possible to convert a reflectance spectrum as measured by the ERTS-1 into concentration of suspended sediment. This scheme, however, requires that the near-ground spectra be "corrected" for the effect of the atmosphere. As is well known, a bundle of energy starting at the bottom of the atmosphere does not emerge unscathed at the top. Certain wavelength components are absorbed, and others are scattered in various ways in varying degrees. Furthermore, those effects are by no means constant; they may change on very short notice as a function of atmospheric composition. The amounts of particulates, both solids and liquids, suspended in the atmosphere are of particular importance.

This problem is of considerable military as well as civilian interest, and as a result there are a number of models that predict the effects of atmospheric conditions on electromagnetic radiation. One of the best that is available for use was written by McClatchey et al at Air Force Cambridge Research Lab.[1]

This scheme foundered on our inability to obtain reliable near-ground spectral data. As a result, we fell back to a much less satisfying procedure, but one which still looked forward to a coupling between satellite and ground observations, when and if ground observations become available. The scheme included back-calculating from the NASA tape values to obtain predictions of near-ground radiance spectra. This was done by using NASA-provided data on gain settings, and atmospheric transmittance values obtained by manipulating the AFCRL atmosphere effects model, in the equation shown in fig. 7. In theory, the product of this equation is the spectrum that would be read by a near-ground radiometer. All subsequent manipulations of spectral data were made on the basis of radiance values obtained in this way.

When all of the ground control data points (i.e., measures of suspended sediments as obtained from samples of the water) were plotted against the reference spectra as selected according to the procedure previously described, the result is as illustrated in fig. 8. The center

---

[1] McClatchey, R. A., Fenn, R. W., Selby, J. E. A., Votz, F. E., and Garing, J. S., "Optical Properties of the Atmosphere," AFCRL Report 71-0279, U. S. Air Force Cambridge Research Laboratories, Bedford, Massachusetts, May 1971.

of the three lines on the graphs is the calculated regression line. The two dashed lines labelled "error band" have nothing to do with the standard deviation of the regression line; instead, the lines define the limits of potential error introduced by instrumental variation in the ERTS MSS. Those errors are approximately $\pm$ 2 percent of full scale. With this in mind, a "perfect" correlation would be one in which all of the sample points fell inside the error band.

Given the correlations between sediment concentration and spectral composition as indicated by the Rappahannock data, it is possible to establish reference spectra. These cannot, of course, be simply a list of three radiance values, one for each band for each suspended sediment concentration; instead, they must be ranges of values, and a certain amount of what might be called "engineering judgement" had to be invoked in order to arrive at them. The result of this largely subjective process, as applied to the Rappahannock data, is illustrated in fig. 9.

It should be noted that the spectral "signatures" of the suspended materials in the various estuaries are not as distinct as had been hoped. For example, if the correlation bands for the York and Rappahannock rivers are placed on top of each other, as in fig. 9a, the bands at lower end of the suspended material concentration scale (i.e., below about 15 mg/l) overlap so completely that discrimination between sediment types is clearly impractical. However, at concentrations between 15 mg/l and 25 mg/l, Band 3 provides some measure of discrimination, and at concentrations above about 25 mg/l, both bands 2 and 3 separate, and thus provide discrimination. Thus, while the discriminatory powers of the spectral signatures are far from absolute or ideal, they still permit identifications over a part of the range of interest.

Tape Processing Procedures

The input to any digital computer must be a set of digital data. In the case under discussion, the initial data store consists of a set of magnetic tape furnished by NASA. As everyone knows, the NASA tapes are formatted in such a way that all four MSS bands are mixed on one tape. In order to perform any significant processing, and still stay inside the core memory constraints of our computer, it was necessary to rewrite the tapes such that one tape contained all data for one spectral band, with the pixels following each other in sequence (fig. 10). It is, of course, not as simple as fig. 10 indicates, but the diagram conveys the general idea.

There was one more basic complexity which had to be resolved. ERTS-1 computer compatible tapes are received with "radiance" values for bands 1, 2, and 3 recorded in a "decompressed" mode. (Values for band 4 are recorded in so-called "linear" or "compressed" mode.) What this means is that the numbers on the CCT'S vary between 0 and 124 for bands 1 and 3,

and between 0 and 122 for band 2. Band 4 numbers can be used directly. To obtain "true" radiance values, the CCT numbers must be converted into values on a scale ranging from 0 to 63. Unfortunately, the conversion is nonlinear (fig. 11), with complex curves, so that the transform can only be achieved with tables provided by NASA. Early instructions for achieving this transformation were a bit confusing; later information has clarified the situation so that it is no longer a problem.

With this correction made, each pixel value is, in effect, scaled to a number between 0 and 63 (which can be thought of, somewhat inaccurately, as representing a grey level on film), and recorded on the WES format as a 12-bit word. In this manner, the six most significant bits in each word are allowed to remain free for further use (fig. 12).

As has already been noted, Band 4 (the near-infrared band, 0.8-1.1μm) values measured over water bodies are very low, normally less than 0.20 mw/cm^2-SR. As indicated in fig. 13, the "water" values contrasted sharply with those measured over land. Band 4 therefore provided a convenient way to digitally mask or identify values corresponding to land areas in Bands 1, 2, and 3 data, where land/water separations were not always clearly defined. The general procedure is illustrated in fig. 13. The Band 4 data were scanned pixel by pixel, and in every case in which the radiance value was less than 0.2 mw/cm^2-SR, a binary "1" was placed in the first bit position of the 12-bit word containing the pixel value (see fig. 12). This identified every "water" pixel in the data array.

The Band 1, 2, and 3 tapes were then processed using the Band 4 mask to edit out all "land" pixels, leaving a data file consisting of new tapes on which were stored only "water" pixels. The purpose of this exercise was to save computer time by reducing the number of pixels that had to be processed. A line printer output of a portion of one of the edited tapes is shown in fig. 14; the blank area in the lower left is Greys Point on the Rappahannock. The numbers are radiance values (mw/cm^2-SR x 0.01).

Spectrum Matching

With radiance values of all four bands available on a pixel-by-pixel basis, it is now possible to define the radiance spectrum of each pixel. For example, fig. 15 illustrates the radiance spectrum of the pixel outlined in the upper left corner. Fig. 15 is a portion of a printout of Band 1; there is of course a similar printout for Bands 2, 3, and 4. Putting the radiance values for the indicated pixel in juxtaposition results in a radiance spectrum, as illustrated by the bar graph insert in the middle of the figure. In actual fact, of course, the numbers defining the spectral composition of each pixel are not printed out, except for the production of illustrative material, as in this case. Instead, they are consolidated in a data file on a disc, with a format that contains the xy position of each pixel, and the radiance values

of Bands 1, 2, and 3. Band 4 radiance values are not normally stored, since they are always effectively zero.

The next step is to classify each pixel in the data file in terms of the reference spectra. The computer program compares the radiance value of each band for each pixel and determines which class it falls into. In effect, the result is a matrix, as illustrated in fig. 16. For example, the radiance value for Band 1 in the example is 1.14, and this fits into class 1; the value in Band 2 is 0.39, which fits into class 1. However, the value for Band 3 is 0.20, which fits into both classes 1 and 2, as shown in the matrix. The pixel is said to be classified when there is a fit (i.e., an "X" in the matrix) in all three bands in any one class. When this condition is met, the program assigns a map symbol and a class value to that pixel. Upon the completion of the pixel-by-pixel comparison, there is in effect a new data file containing the location class number and map symbol of each pixel. If a pixel spectrum does not fit any of the reference spectra, that pixel is defined as unclassified, which is in effect a fifth category.

OUTPUT PRODUCTS

This file can then be used to print out a map of the distribution of suspended sediment classes, as illustrated in fig. 17. Note especially the zeros, (which represent "no classification") and note that they occur most commonly near the shores. There may be at least two reasons for this:

a. Shallow water, so that reflectance from the bottom is contaminating the reflectance from the water.

b. Small-scale sediment clouds may be occuring in the near-shore zone as a result of shore-line erosion.

The basic data file can also be used as input to a film-writer, which can construct a photomap showing sediment concentration classes as shades of grey. In this procedure, an optical density is assigned to each sediment concentration class. In this case, the values listed in fig. 18 were used. The result is illustrated in fig. 19. Note that in this one only three classes of sediment concentrations were used.

One thing that should perhaps be mentioned is that the photomap in fig. 19 fits precisely on a 1:250,000 Defense Mapping Agency Series V502 map. This may not strike a responsive chord, but achieving near-perfect registry with digital data is not a trivial task. There are two classes of problems.

a. There are a number of distortions in the MSS tapes. They arise because of slight inaccuracies in satellite attitude controls, earth

rotation during the scanning period, uncertainties about precise orbital path, and many others. These must all be removed before an image derived from the MSS tapes can be brought into registry with a map.

b. The ERTS-1 MSS does not record a square pixel; instead, the pixel is approximately 57.2 m wide in the east-west direction and 79.1 m long in the north-south direction. The ratio of width to length is approximately 1 to 1.4. The difficulty is that the standard film writer (such as our Optronics machine) "writes" with a perfectly square pixel. The result is that it is impossible to write a dimensionally accurate image directly from a NASA tape with a standard film writer. We were able to achieve near-perfect registry by subdividing what we now call the "NASA pixel," with its dimensions of 57.2 by 79.1 m, into 35 "WES pixels," each having a dimension of 11.84 by 11.84 m. To compensate for the error which accumulates in the north-south direction (3.78 m per row of NASA pixels), a false line of WES pixels is inserted at specified intervals. The result is, for example, a transparent overlay that fits very closely over a base map, so that the map-overlay combination can be used directly for position location and the like.

SPIN-OFF PRODUCTS

The near-total absorption of the near-infrared energy by water has proven to be a highly useful characteristic. In theory, this characteristic should permit the identification of any open water surface having an area greater than that of one ERTS-1 pixel (about 4,525 m^2). In practice, because there is a low probability that a pixel will fall directly over a small water surface, the water surface must have an area in excess of about 27,000 m^2 before it is detected with reasonable certainty. This characteristic has been exploited in support of the National Dam Safety Program. The problem revolves around the fact that there are tens of thousands of small reservoirs in the United States, and that the locations of many of them are not a matter of public record. Thus, a quick and reasonably reliable method had to be found for locating all (or at least nearly all) such reservoirs.

In support of this program, the WES used the water surface masking technique, which is a variation of standard density-slicing procedures, using the Band 4 digital data. The masking out of land areas, as previously described, is used to generate a tape that identifies all "water" pixels, as illustrated in fig. 13. At the same time, the data are corrected for positional errors; that is, the positions of the pixels are adjusted so that an image produced from the tape will be rectified as fully as possible. An image of the waterbodies is then printed out with an Optronics image-writer, which results in a transparent film-base overlay (fig. 20), which can be photographically enlarged to some convenient scale, such at 1:250,000.

There are two difficulties at this point. First, the rectification is rarely perfect, and second, the image projection is not the same as the map projection. While the errors in position location of a single pixel introduced by these characteristics are only on the order of 2000 m at a maximum, that error is still too large if one is on the ground driving along a country road looking for a one-pixel reservoir. The next step is therefore to locate the corner coordinates of the image (or the pixel array) by fitting water bodies on the overlay to water bodies on the reference map. This subjective process takes only a few minutes. Then, with the latitudes and longitudes of the corner points of each strip known, the tapes are then rectified to the map projection, and a new tape is written. This tape is then used to print a second-generation overlay, which matches the map quite closely. Fitted to AMS 1:250,000 maps, the maximum positional errors are about 300 m.

In addition to the map overlays, the field agencies are provided with an inventory listing (fig. 21). This list identifies every discrete water body by latitude and longitude, and accompanies that identification with an estimate of surface area. These two data sets are made possible by a computer program that we call the "contiguity routine." It must be recalled that the computer has only 16,000 words of core memory, with two disc attachments. The contiguity routine places the first scan line in memory, where it may be thought of as a line of zeros and ones, as in fig. 22. Each individual "water" pixel is placed in a separate file on a disc, so that in the example, pixel 1-3, (line 1, pixel number 3) is in one file, pixel 1-7 is in another file, and so on. Scan line 2 is then placed in memory, and a search routine is then initiated. All pixels occupied by zeros are passed over, since they represent land. However, the discovery of a 1 in pixel 2-6 initiates a search routine:

Step	Question	Response	Action
1	Is pixel 1-5 a 1	No	Go to step 2
2	Is pixel 1-6 a 1	No	Go to step 3
3	Is pixel 1-7 a 1	Yes	Place pixel 2-6 in the same file as pixel 1-7; go to pixel 2-7 and resume search

The effect of this routine is to assemble a separate file for each group of pixels that meet the contiguity criteria: pixels are contiguous if they occupy diagonal positions or adjacent positions.

Upon completion of the search of scan line 2, scan line 1 is dropped from memory and scan line 3 is placed in memory (fig. 23.) The search routine will detect the fact that the files holding pixels 2-6 and 2-10 are connected by a line of contiguous pixels in line 3. When this occurs,

the two files are consolidated in a new file on the disc. After all scan lines have been searched, the disc contains a separate file for each water surface, and the number of entries is equivalent to the number of pixels, which in turn can be used to calculate an approximate surface area. This process requires 1-2 hrs of computer time per ERTS scene depending upon the number of water surfaces in the scene.

The latitude and longitude which appears on the inventory list is the position of the pixel at the midpoint of the longest line of pixels in the file, representing the water body (fig. 24).

This same density-slicing routine, again using Band 4, was also used to provide the Corps of Engineers with a transparent overlay of inundated areas along the Lower Mississippi and its tributaries during the 1973 flood (fig. 25). These overlays are invaluable in matters relating to damage evaluation, estimation of floodplain storage, and the like.

SUMMARY

The analytical procedure considers a multispectral remote sensor as a reflectance spectrophotometer. ADP techniques requiring only very limited computer capability are utilized to search the data defining the spectral reflectance characteristics of a scene on a pixel-by-pixel basis, identify each pixel whose spectral reflectance matches a reference spectrum, and generate maps that identify pixel locations where spectrum matches occur and identify the spectrum that was matched. If the reference spectra are known to represent a specific condition on the ground, a map of the distribution of that condition can be output as a dimensionally accurate overlay to maps of any selected scale. Two applications are described in this report: (1) the distribution of water masses exhibiting specific suspended sediment concentrations in four estuaries around Chesapeake Bay; and (2) the location and delineation of surface water bodies in the Southeastern U. S.

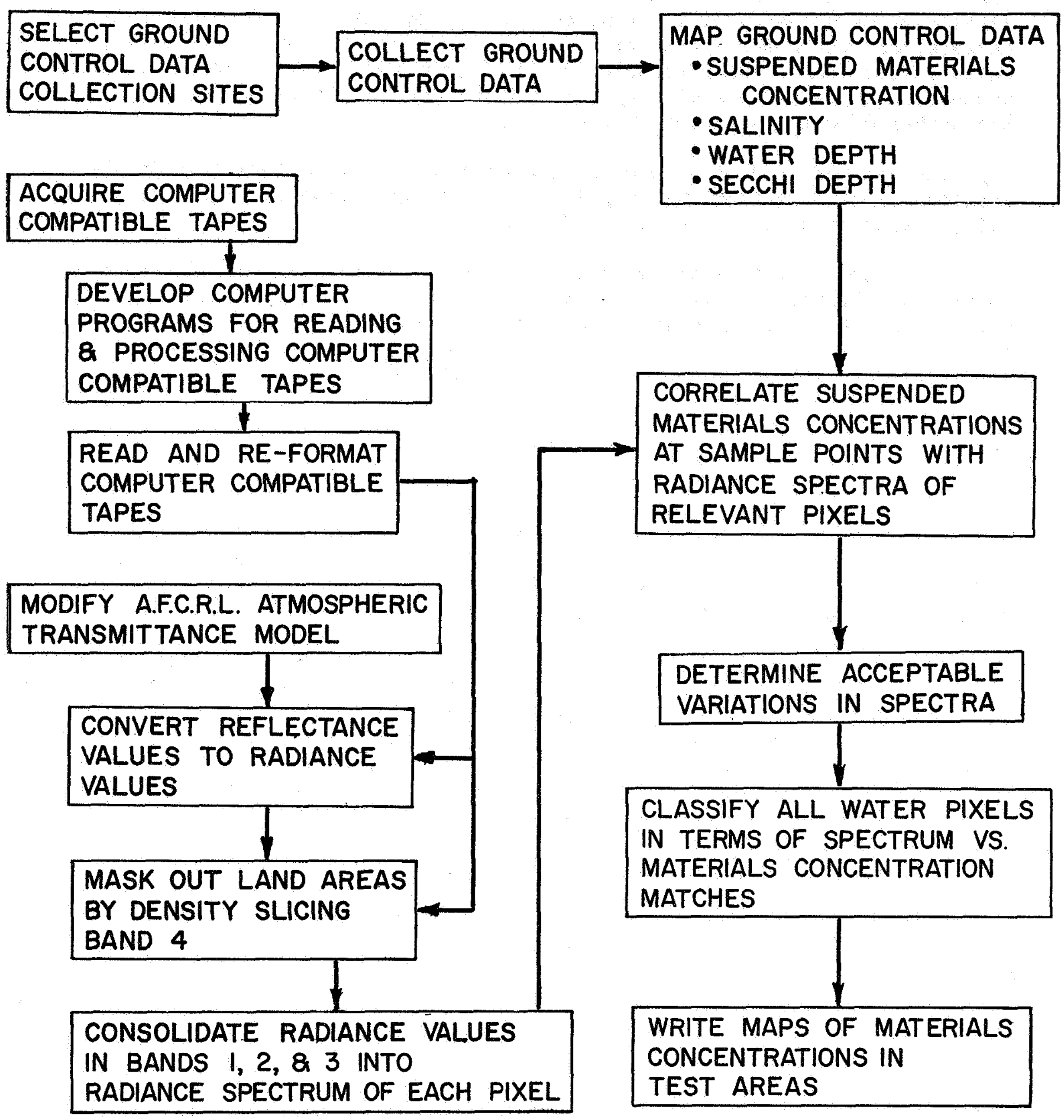

Fig. 1. Flow diagram of research plan

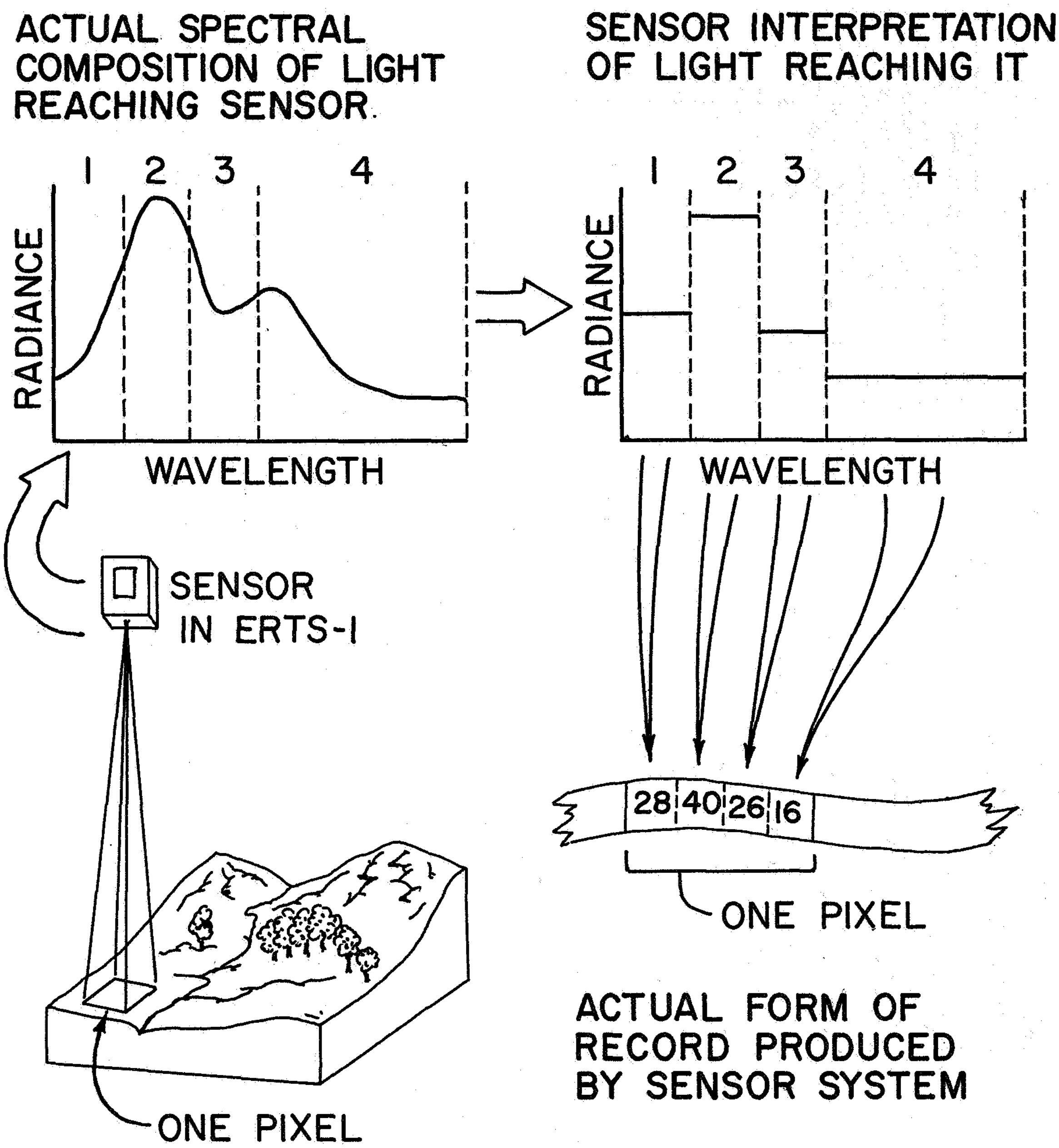

Fig. 2. Data recording sequence in satellite sensor system

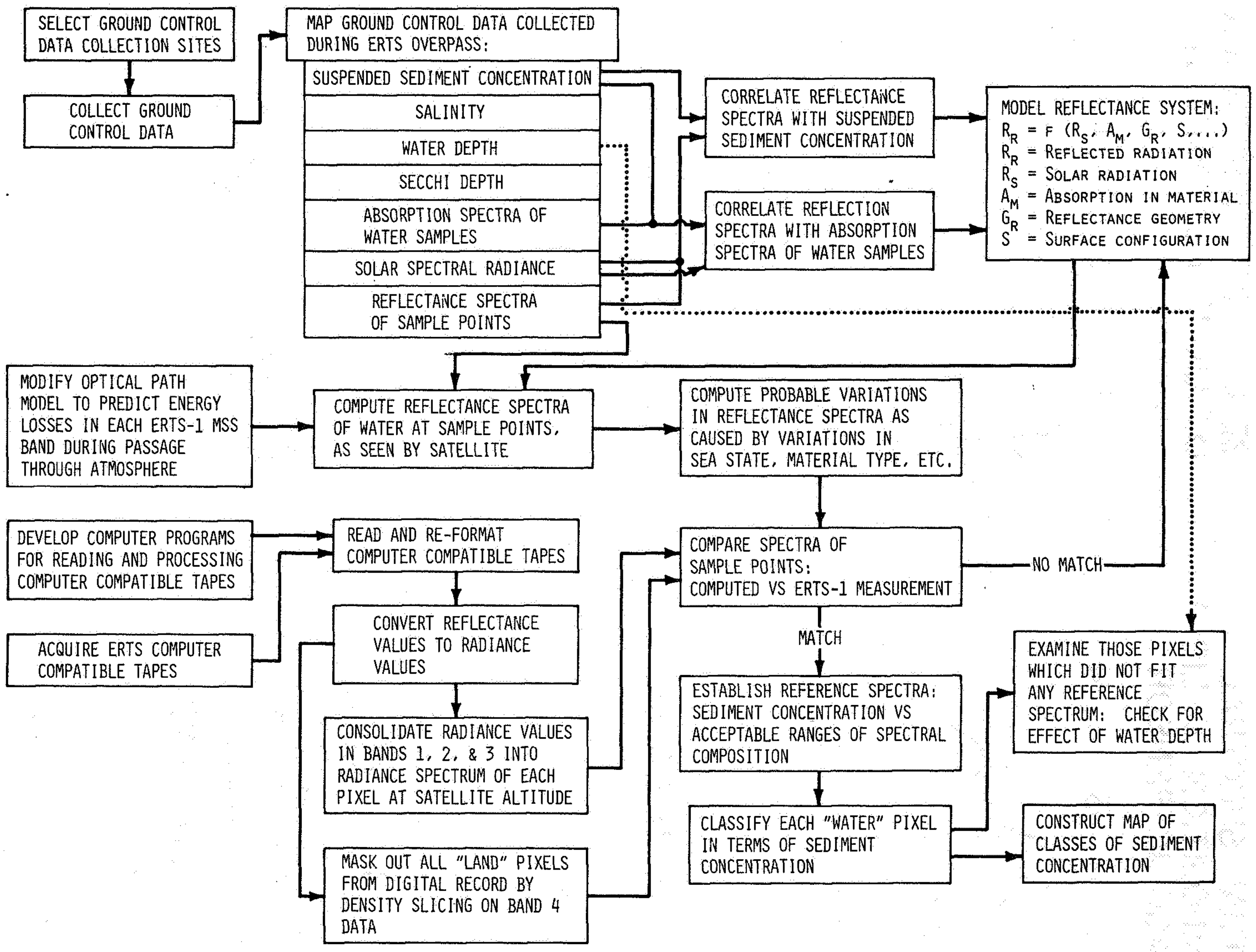

Fig. 3. "Ideal" research plan

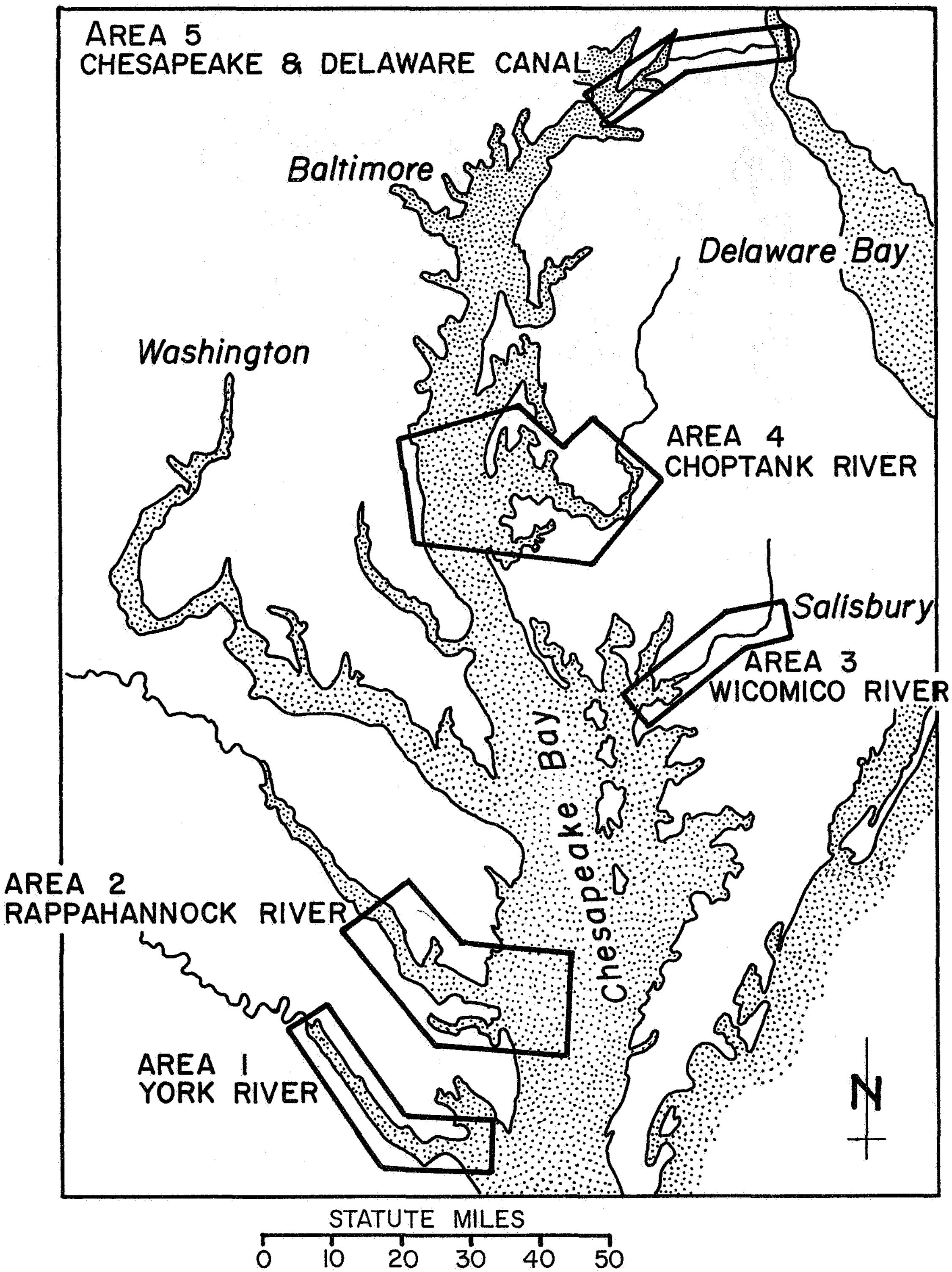

Fig. 4. Location map, Chesapeake Bay study areas

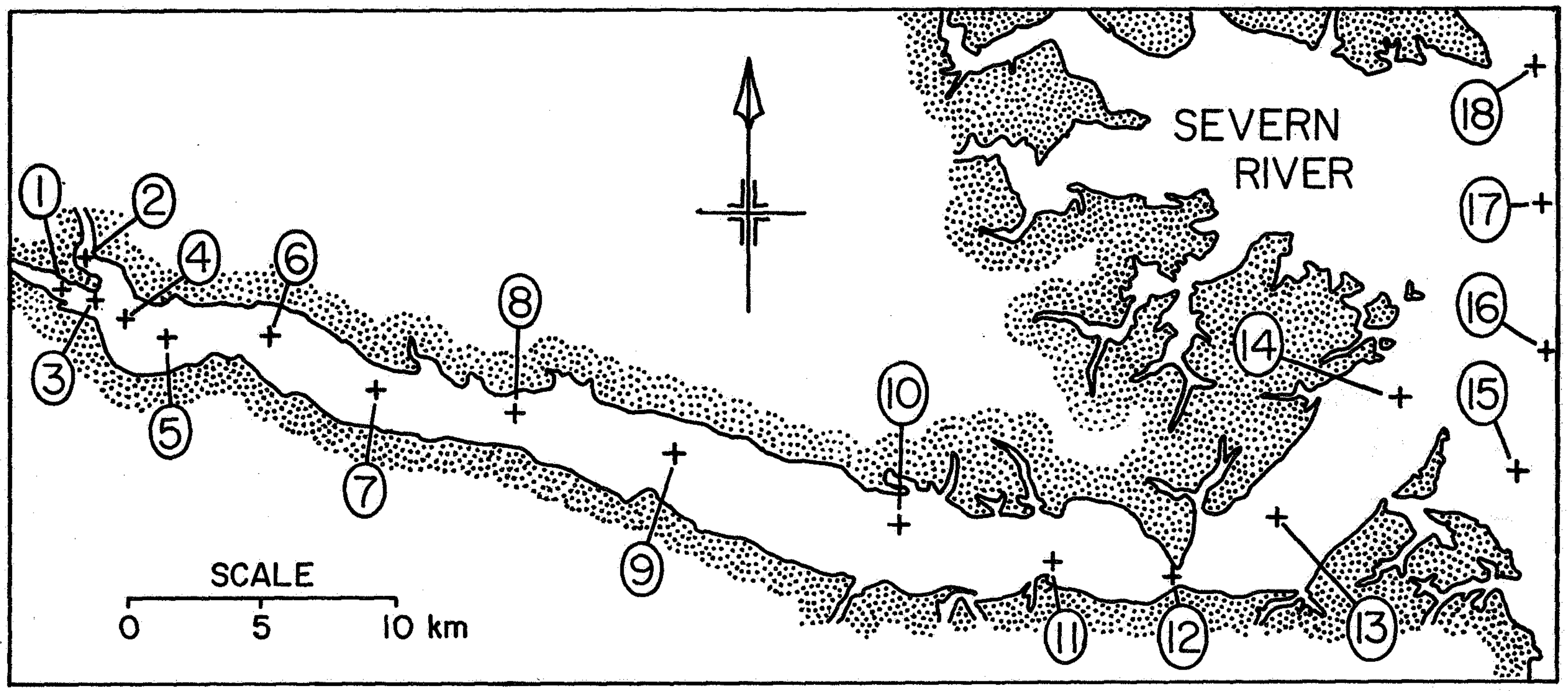

Fig. 4a. Location of ground control points in York River

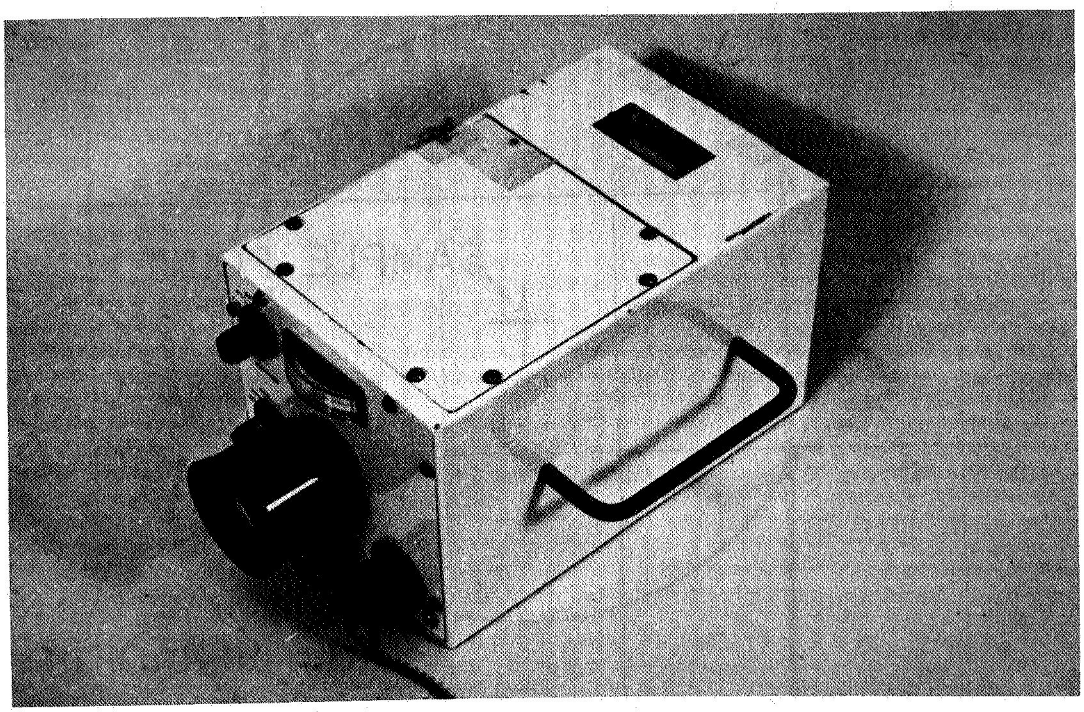

Fig. 5. Radiometer for ERTS-1 Studies

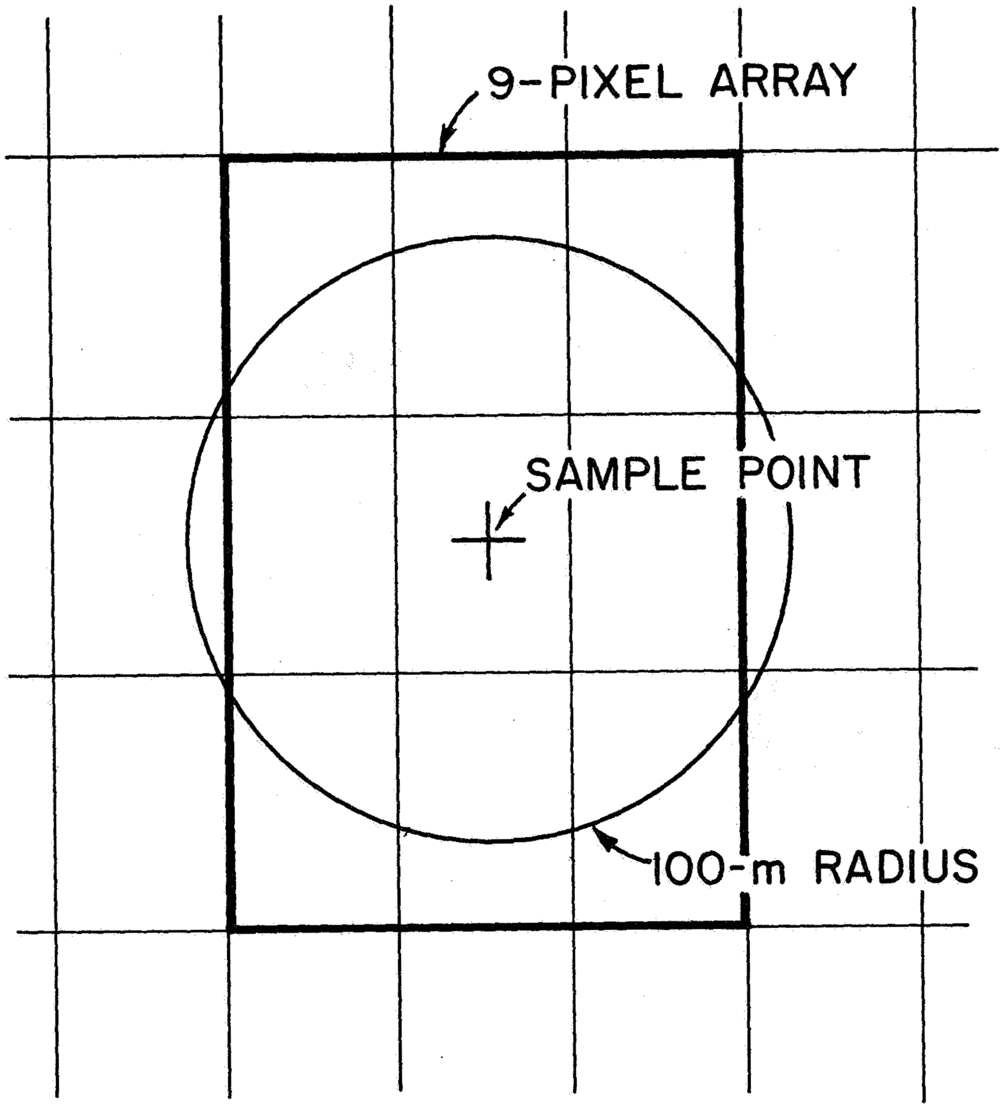

Fig. 6. Positioning error

$$H = \frac{x \cdot M_i}{63 \cdot T_i}$$

WHERE: H = radiance in mw/cm²-SR

x = value from computer compatible tape (CCT)

M_i = gain setting (from NASA)

T_i = atmospheric transmittance (from AFCRL model)

$M_1 = 2.48$	$T_1 = 0.69$
$M_2 = 2.00$	$T_2 = 0.75$
$M_3 = 1.76$	$T_3 = 0.68$
$M_4 = 4.60$	$T_4 = 0.76$

Fig. 7. Conversion of CCT values to radiance values

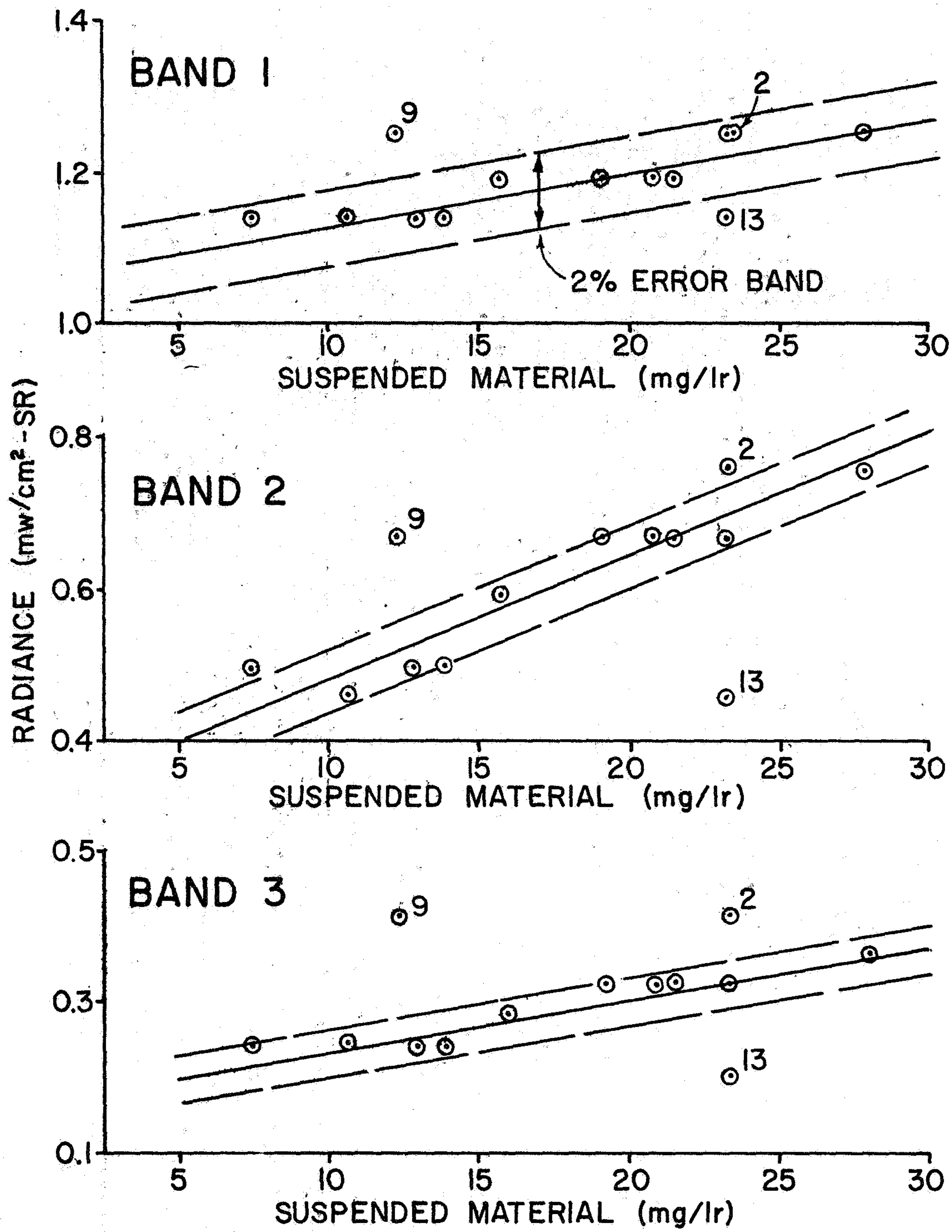

Fig. 8. Radiance vs. suspended material - York River estuary

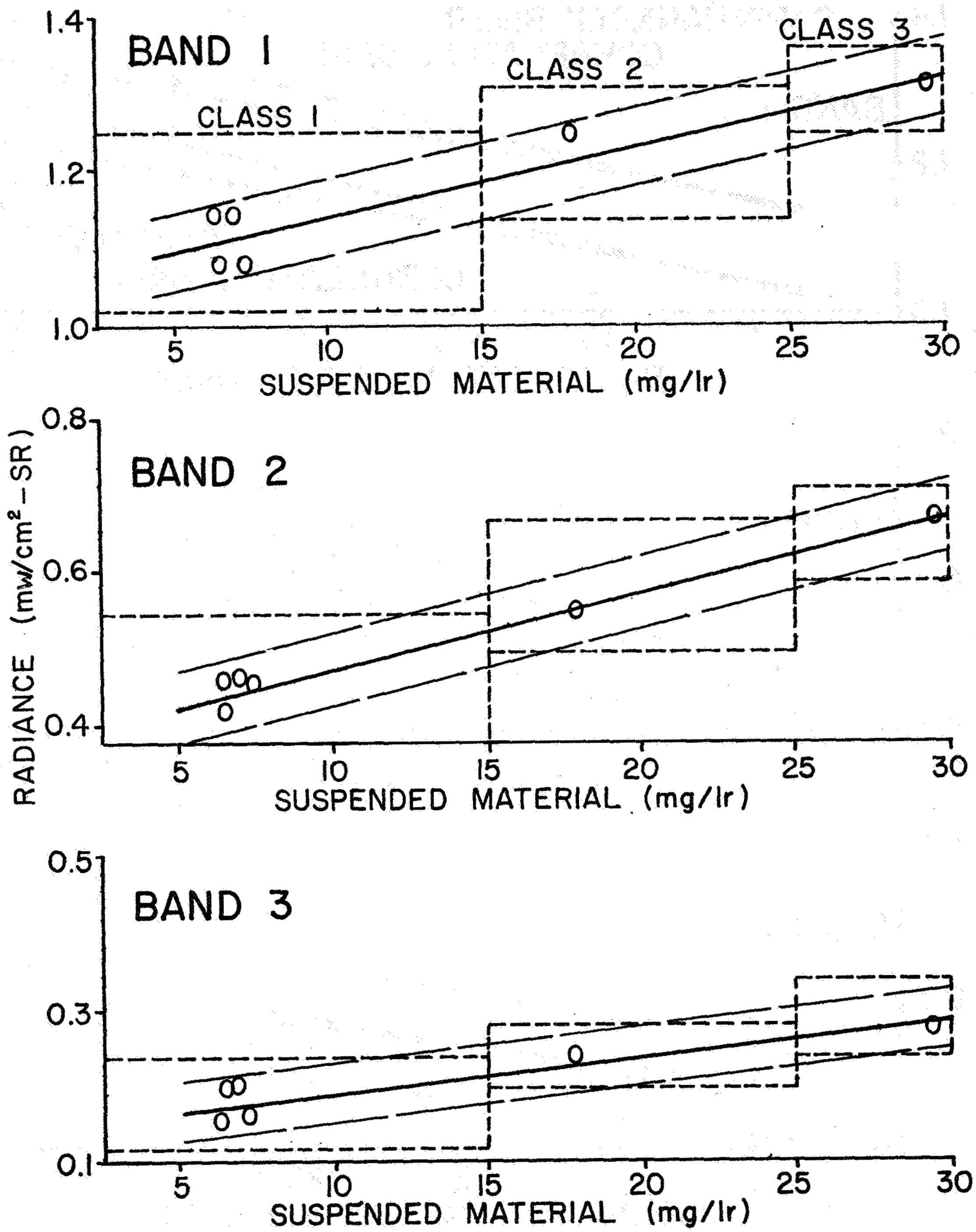

Fig. 9. Radiance vs. suspended material - Rappahannock River estuary

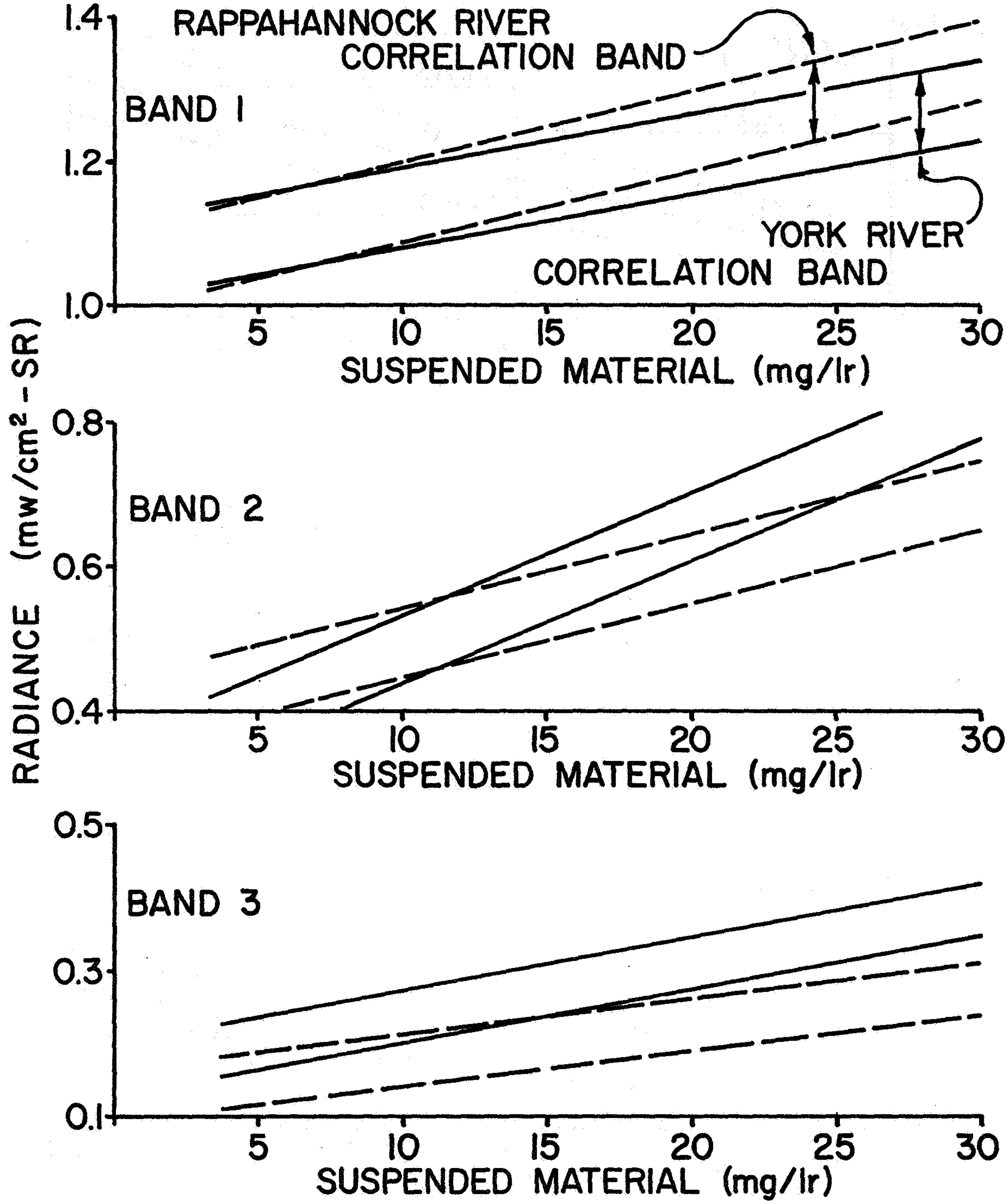

Fig. 9a. Comparison of radiance signatures of York and Rappahannock Rivers

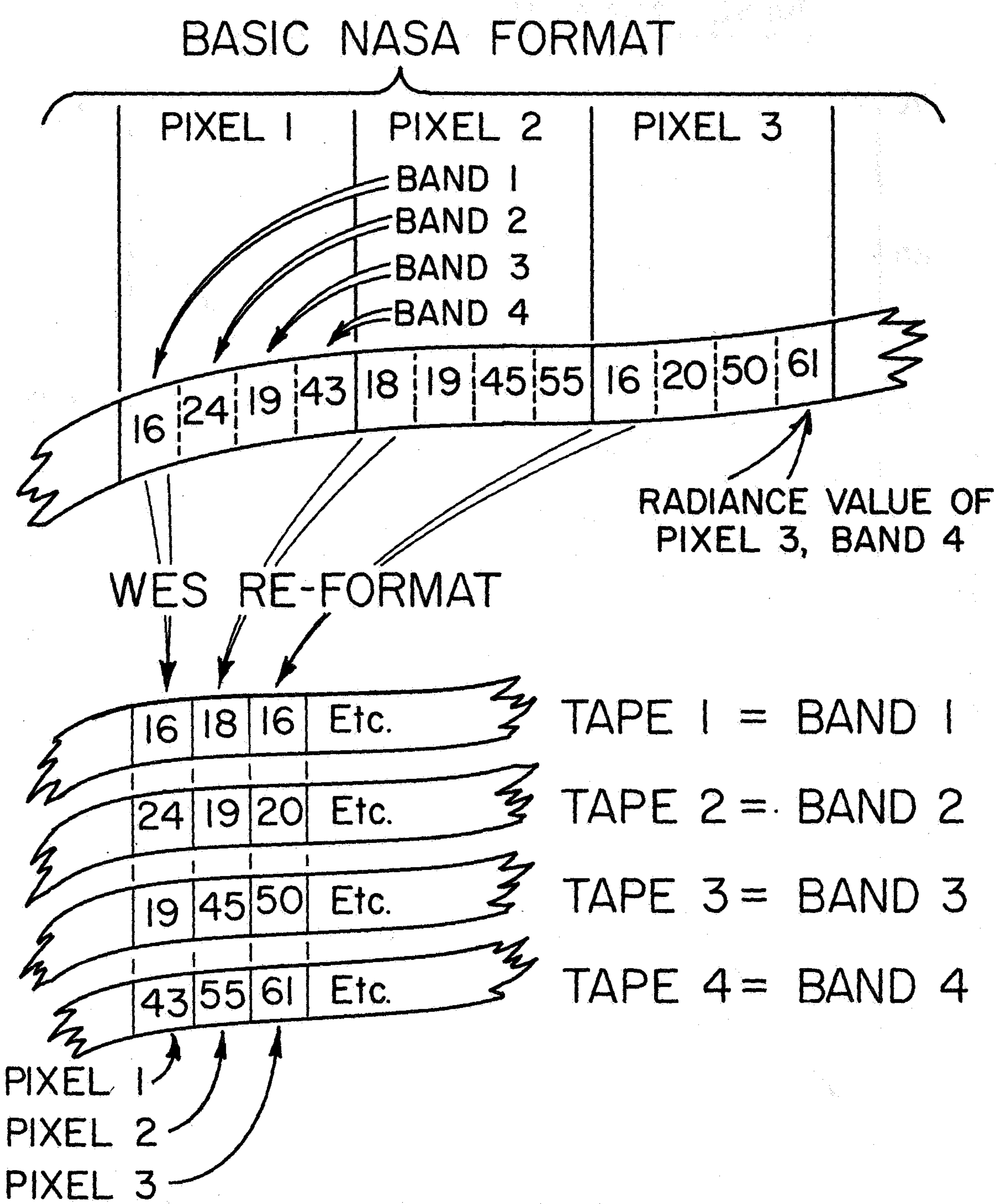

Fig. 10. Conversion of NASA format to WES format

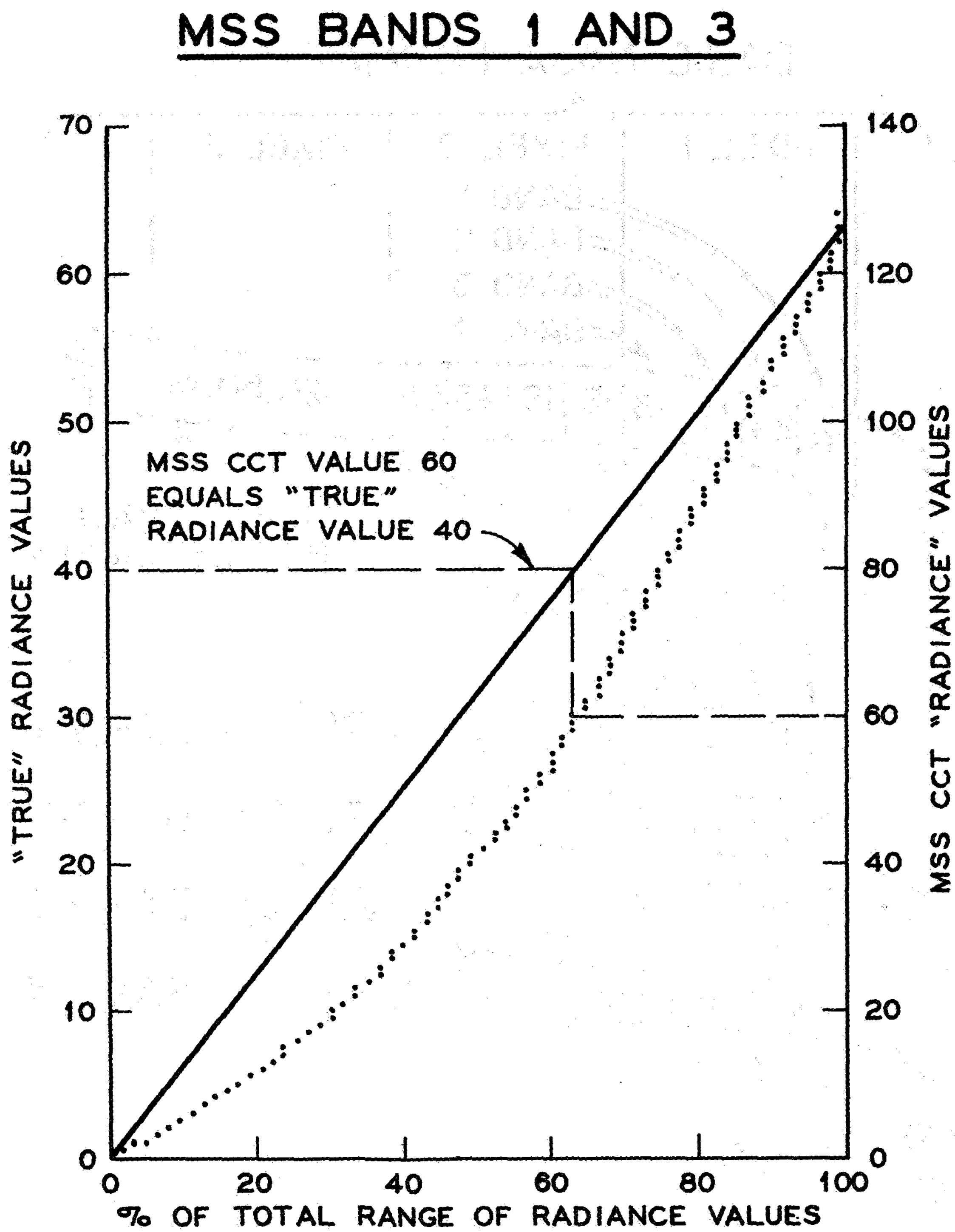

Fig. 11. Conversion of CCT radiance values to "true" radiance values

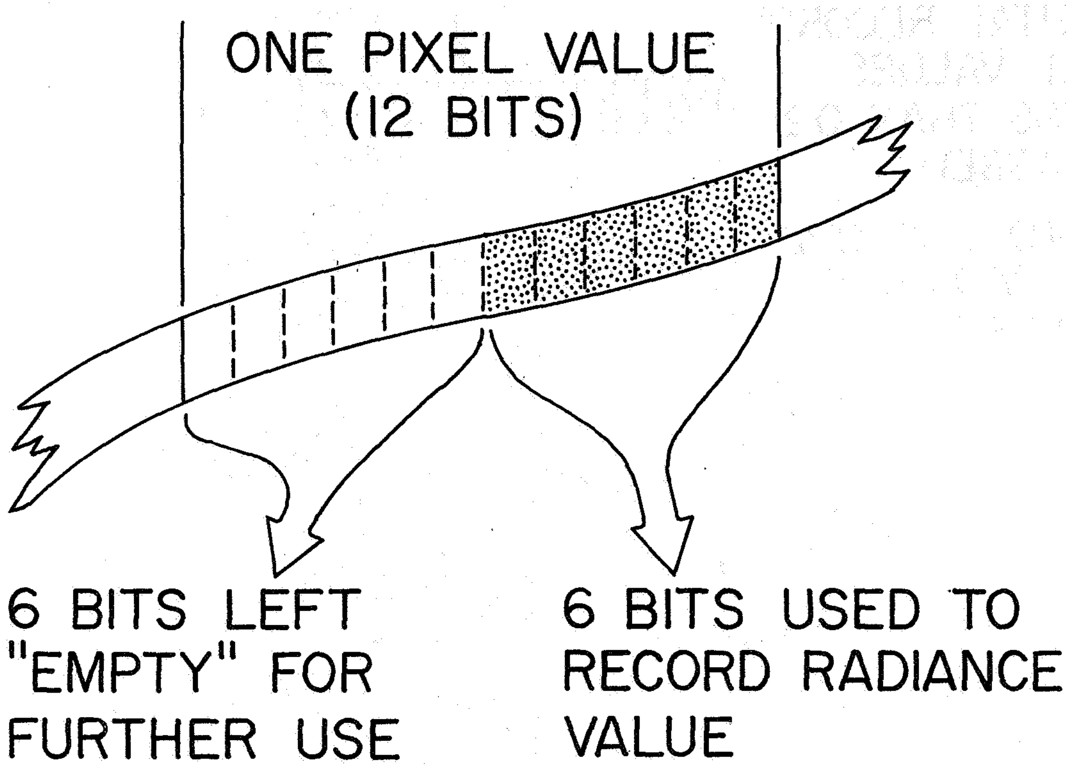

Fig. 12. Iniital utilization of 12-bit word

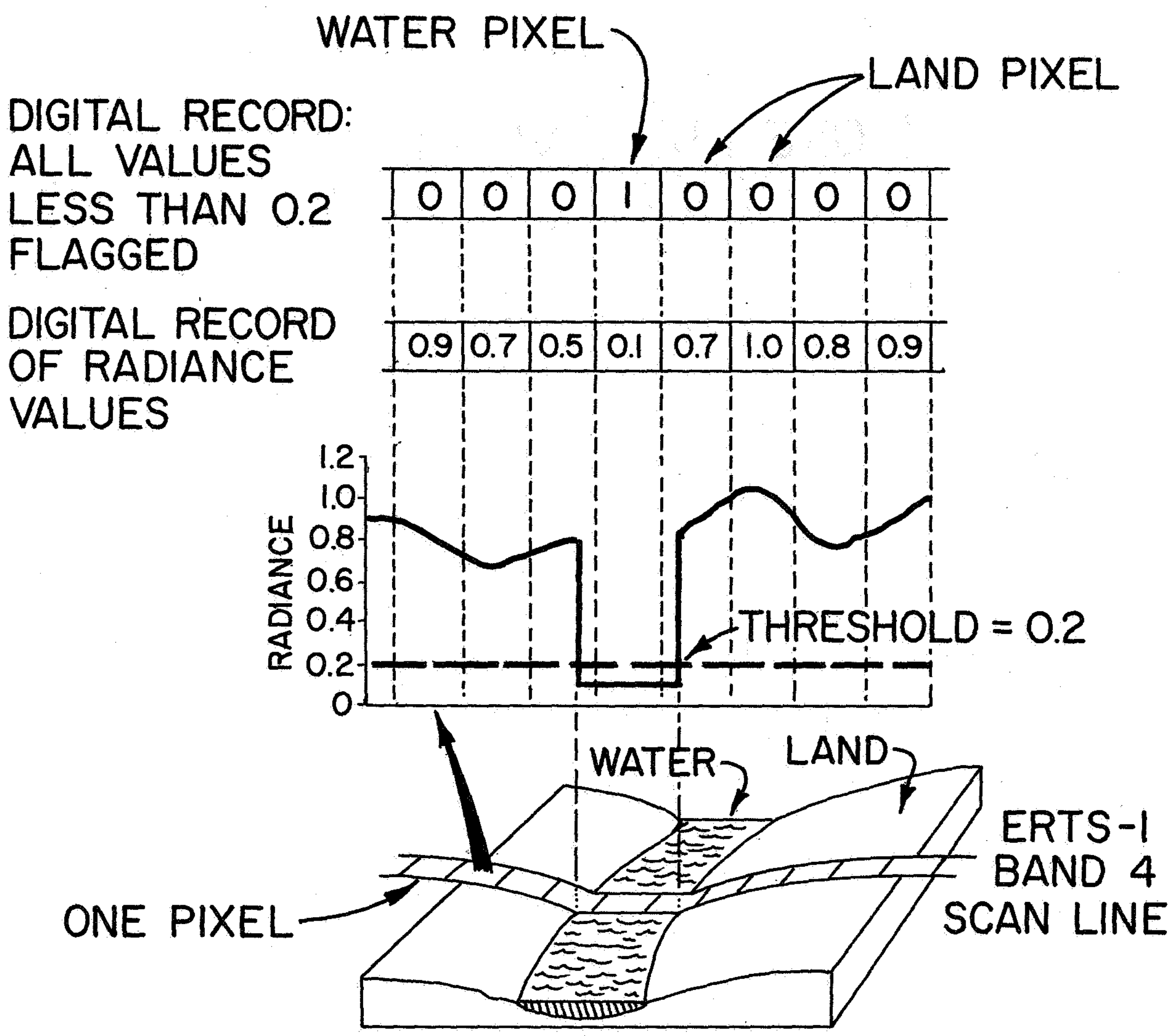

Fig. 13. Water pixels vs. land pixels

```
                    154. 154. 154. 154. 142. 142. 142. 142. 131. 131. 142. 131.
136. 136. 142. 154. 142. 142. 154. 142. 154. 136. 142. 136. 136. 125. 125. 125.
          148. 159. 159. 159. 159. 165. 159. 159. 148. 148. 148. 148. 142. 142.
          154. 154. 154. 159. 154. 154. 154. 154. 154. 154. 148. 136. 136. 136.
          142. 148. 159. 159. 148. 142. 148. 148. 159. 148. 142. 136. 136. 136.
148. 148. 131. 148. 131.           148. 154. 154. 154. 148. 148. 148. 148. 131.
142. 142. 154. 142.                142. 142. 142. 154. 154. 154. 142. 142. 142.
                                   154. 142. 142. 142. 142. 136. 136. 136. 136.
                                        148. 159. 148. 159. 148. 142. 142. 142.
                                             154. 154. 154. 148. 148. 148. 148.
                                             148. 148. 148. 148. 142. 136. 142.
                                             148. 148. 154. 148. 131. 131. 131.
142. 142. 131.                               154. 154. 154. 142. 142. 131. 131.
136. 136. 131. 131. 136. 131. 136. 131. 142. 136. 142. 142. 136. 131. 131. 136.
142. 142. 148. 142. 125. 142. 142. 142. 125. 142. 148. 148. 142. 142. 142. 125.
                         148. 136. 136. 148. 148. 154. 148. 136. 136. 136. 136.
                         142. 142. 136. 142. 142. 142. 136. 136. 136. 136. 136.
```

Fig. 14. Masking out land mass

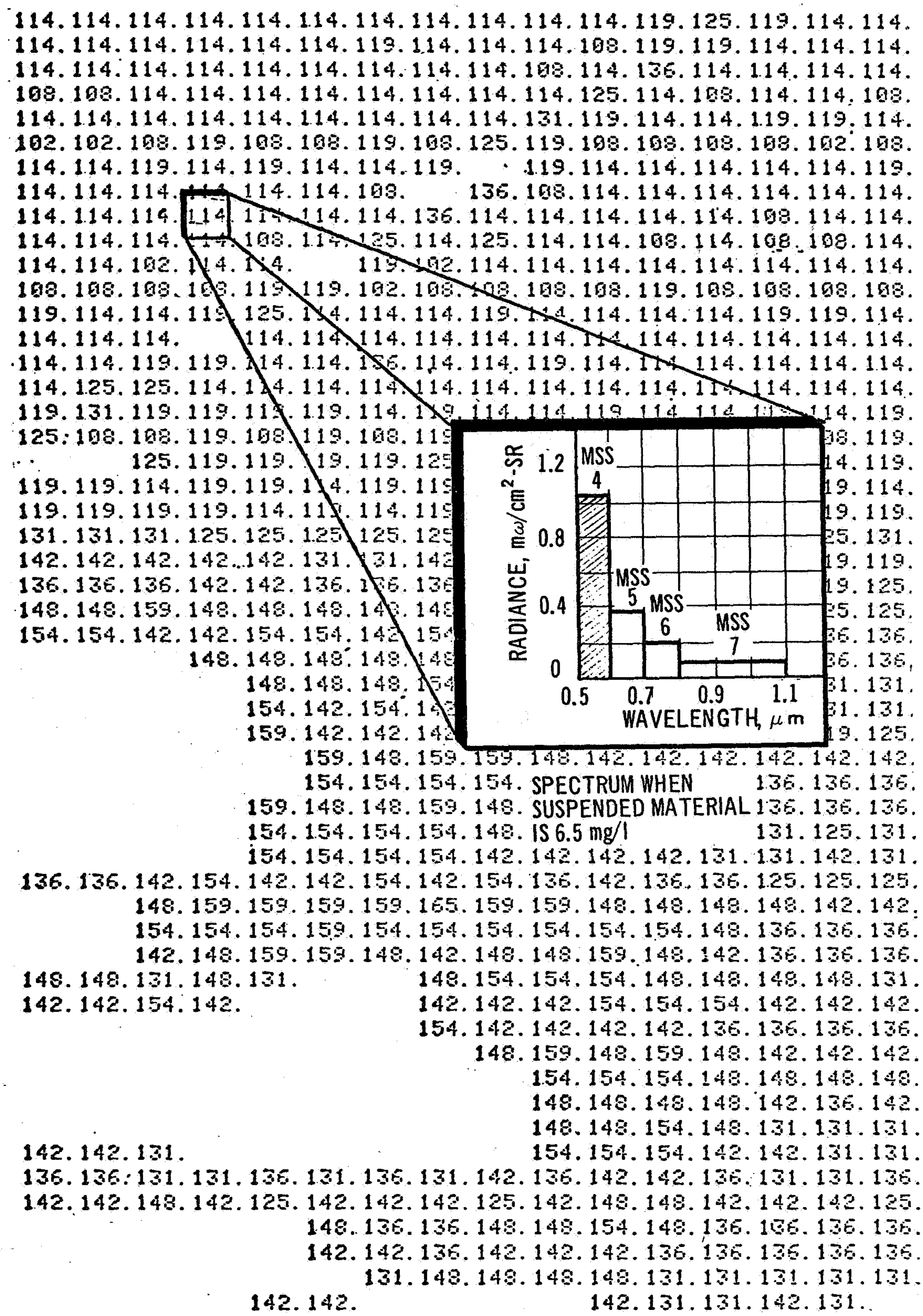

Fig. 15. Assembly of radiance spectra

	RADIANCE (mw/cm²-SR) ERTS-1 MSS BAND			CONCENTRATION OF SUSPENDED SEDIMENTS (mg/lr)	MAP SYMBOL	CLASS
	1	2	3			
REFERENCE SPECTRA	1.02–1.31	0.38–0.55	0.08–0.28	0–10	-	1
	1.36–1.48	0.46–0.71	0.16–0.32	10–20	+	2
	1.48–1.59	0.76–0.84	0.28–0.32	20–30	*	3
	1.48–1.59	0.76–0.84	0.36–0.41	>30	#	4
					O	UNCLASS.
PIXEL VALUES	1.14	0.39	0.20	0–10	-	1
					ASSIGNED TO PIXEL BY COMPUTER PROGRAM	

CLASSIFICATION MATRIX

SEDIMENT CONCENTRATION CLASS \ BAND NO.	1	2	3
1	X	X	X
2			X
3			
4			

Fig. 16. Classification of pixels

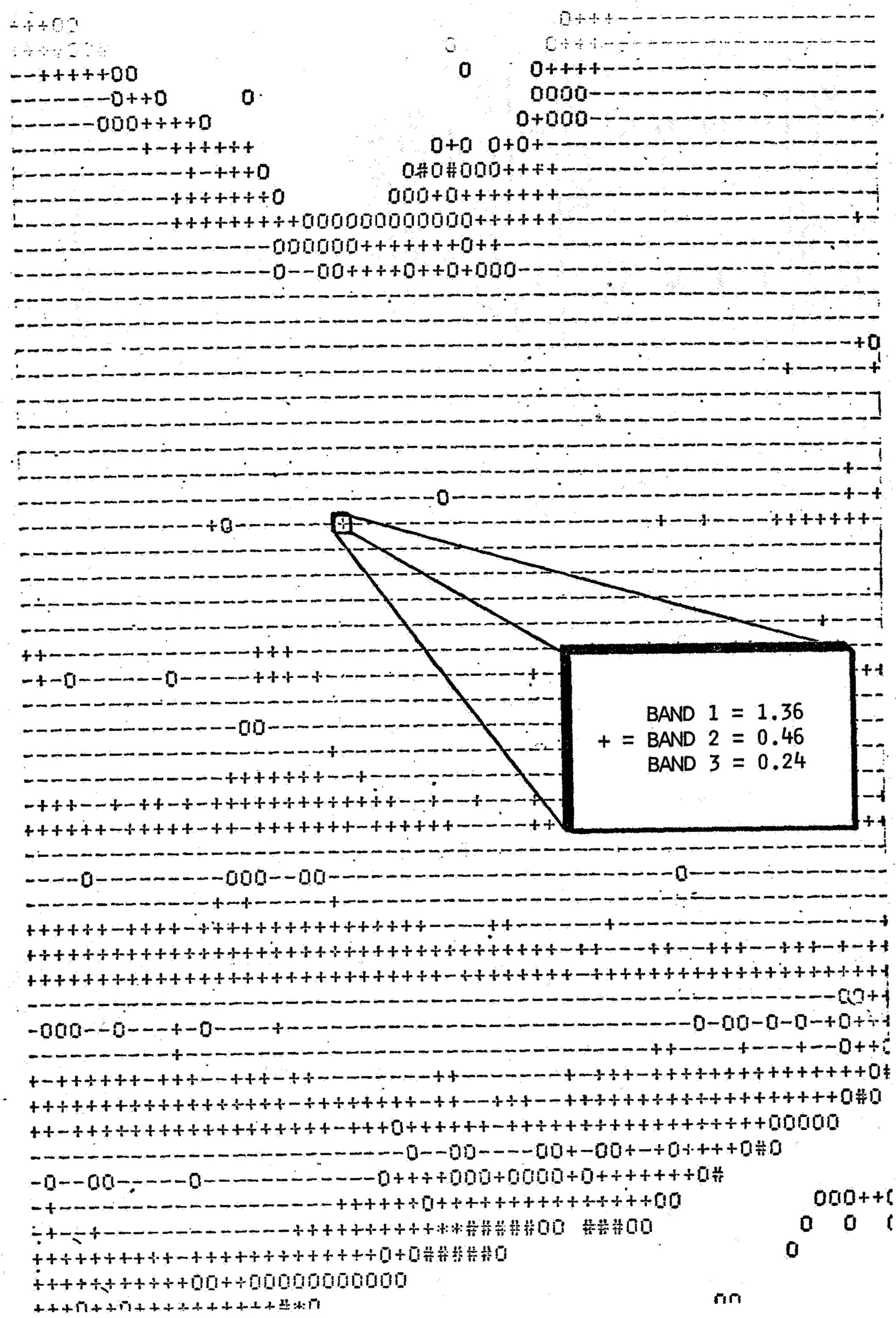

Fig. 17. Computer generated map

SEDIMENT CONCENTRATION CLASS	OPTICAL DENSITY
UNCLASSIFIED	3.0
1	1.68
2	1.08
3	0.49
LAND	0.0

Fig. 18. Optical densities used as photomap of York River

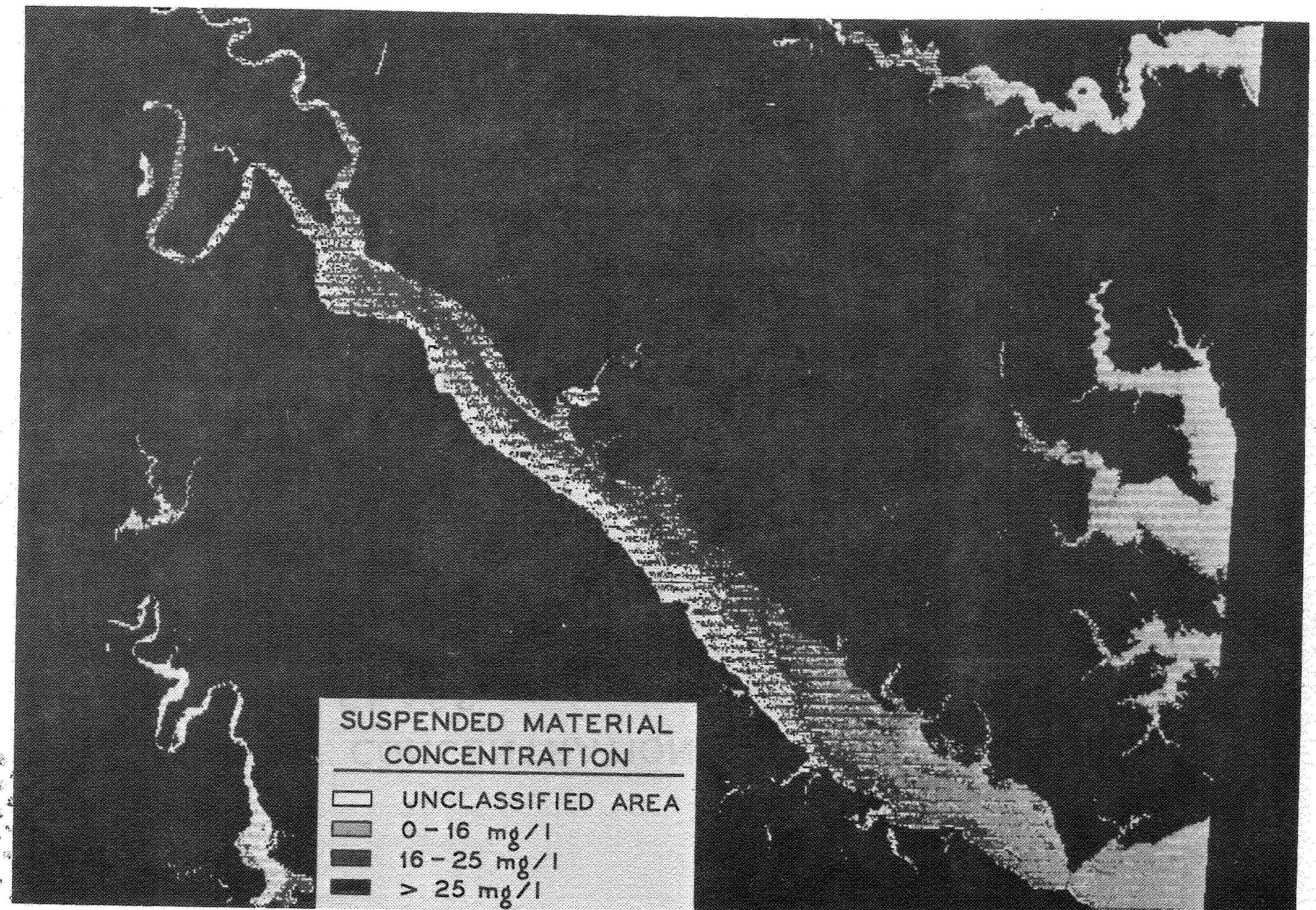

Fig. 19. Photomap showing concentrations of suspended material

Fig. 20. Sample overlay showing surface water bodies

LATITUDE DEG MIN	LONGITUDE DEG MIN	PIXEL COUNT	EST. SURFACE ACRES
N35- 9.6	W 82-21.4	45.	50.
N35- 7.0	W 82- 4.8	1.	1.
N35- 9.2	W 82-18.9	2.	2.
N35- 9.6	W 82-21.7	1.	1.
N35- 9.6	W 82-21.9	3.	3.
N35- 6.3	W 82- 1.1	1.	1.
N35- 6.2	W 82- 1.0	1.	1.
N35- 9.5	W 82-21.9	1.	1.
N35- 8.8	W 82-17.6	2.	2.
N35- 6.2	W 82- 0.8	19.	21.
N35- 9.4	W 82-21.9	6.	7.
N35- 6.2	W 82- 1.6	2.	2.
N35- 6.1	W 82- 1.3	27.	30.
N35- 9.4	W 82-22.1	1.	1.
N35- 6.0	W 82- 0.7	10.	11.
N35- 6.7	W 82- 5.3	1.	1.

Fig. 21. Sample printout of inventory of surface water bodies

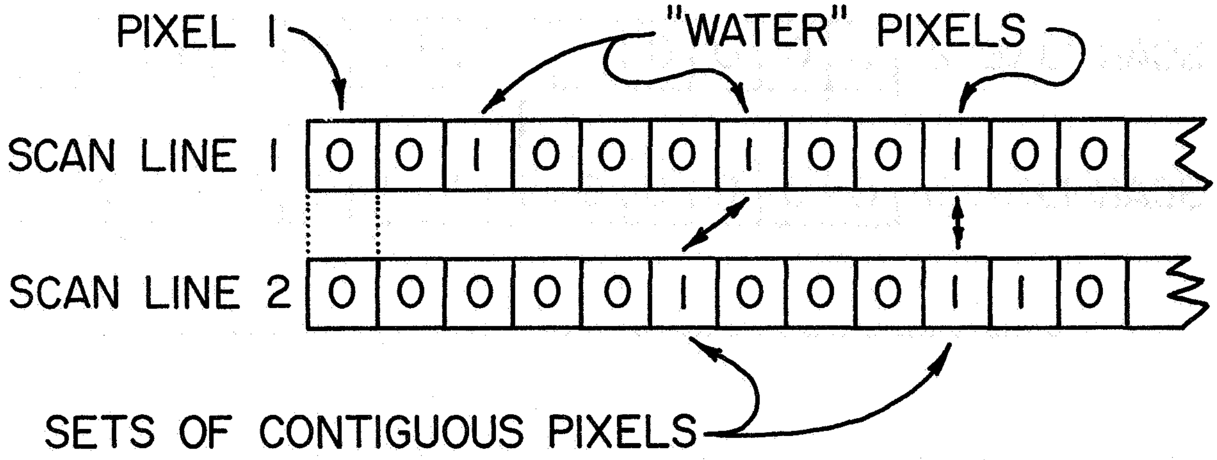

	FILE A	FILE B	FILE C
FILES ESTABLISHED FOR SCAN LINE 1	1 - 3	1 - 7	1 - 10
FILES AFTER SEARCH OF SCAN LINE 2	1 - 3	1 - 7 2 - 6	1 - 10 2 - 10 2 - 11

Fig. 22. The contiguity rule

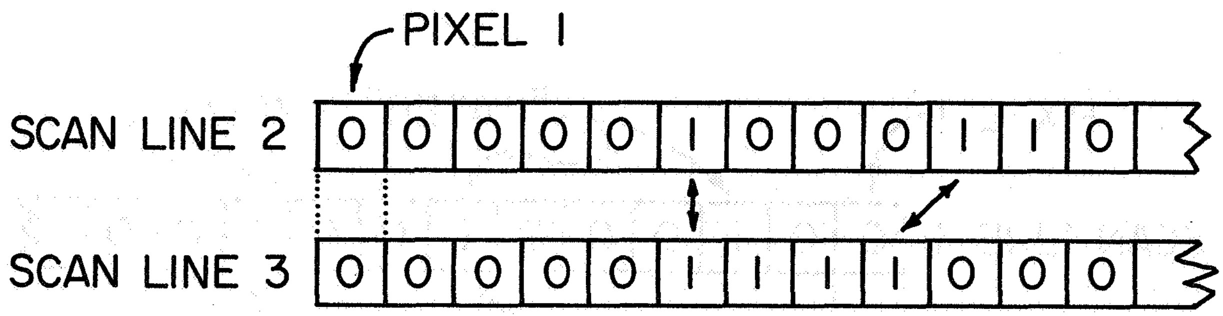

STATUS OF FILES AFTER SEARCH OF SCAN LINE 2	FILE A 1 – 3	FILE B 1 – 7 2 – 6	FILE C 1 – 10 2 – 10 2 – 11	
STATUS OF FILES AFTER SEARCH OF SCAN LINE 3	FILE A 1 – 3	FILE B	FILE C	FILE D 1 – 7 1 – 10 2 – 6 2 – 10 2 – 11 3 – 6 3 – 7 3 – 8 3 – 9

Fig. 23. File consolidation

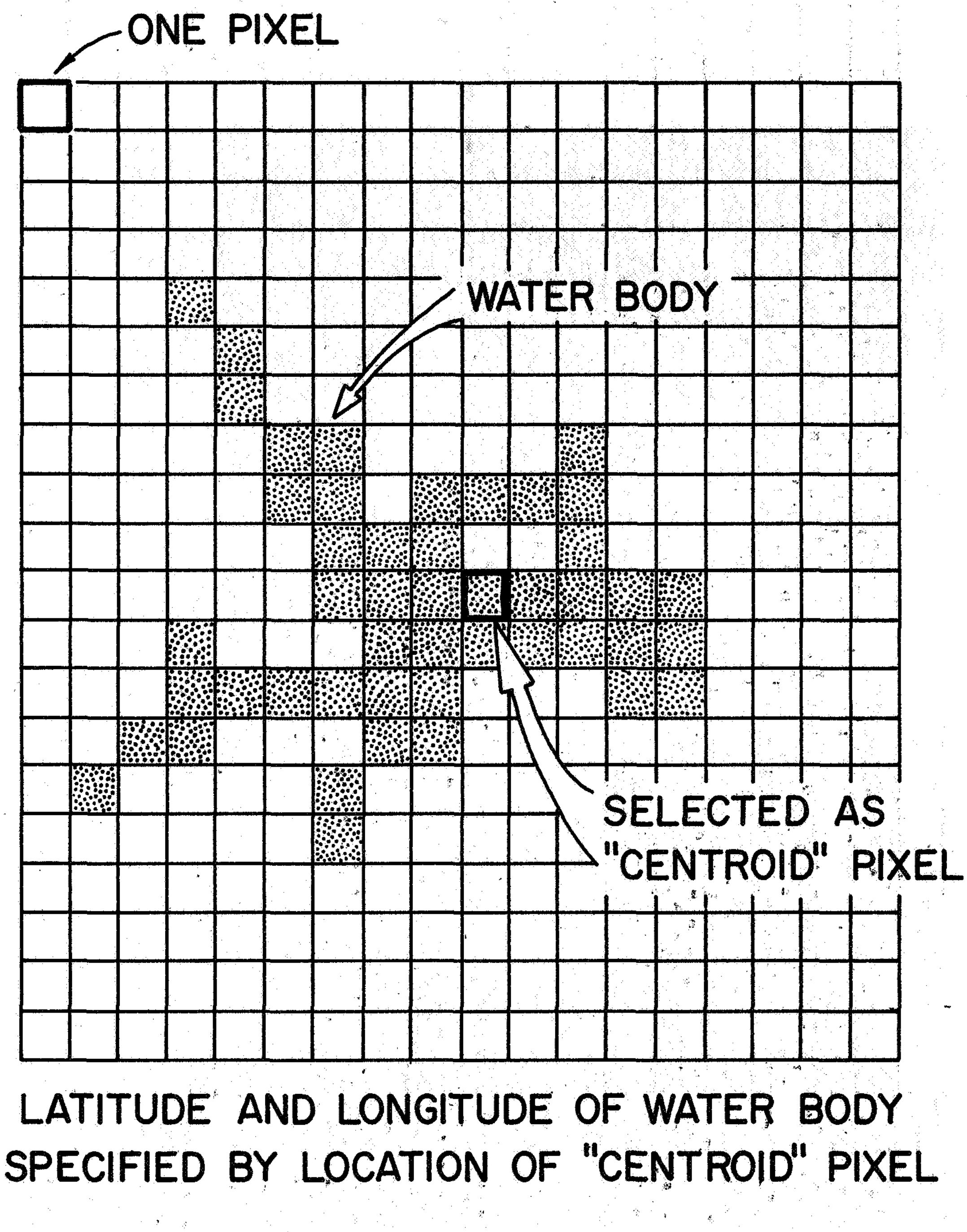

Fig. 24. Selection of "centroid" pixel

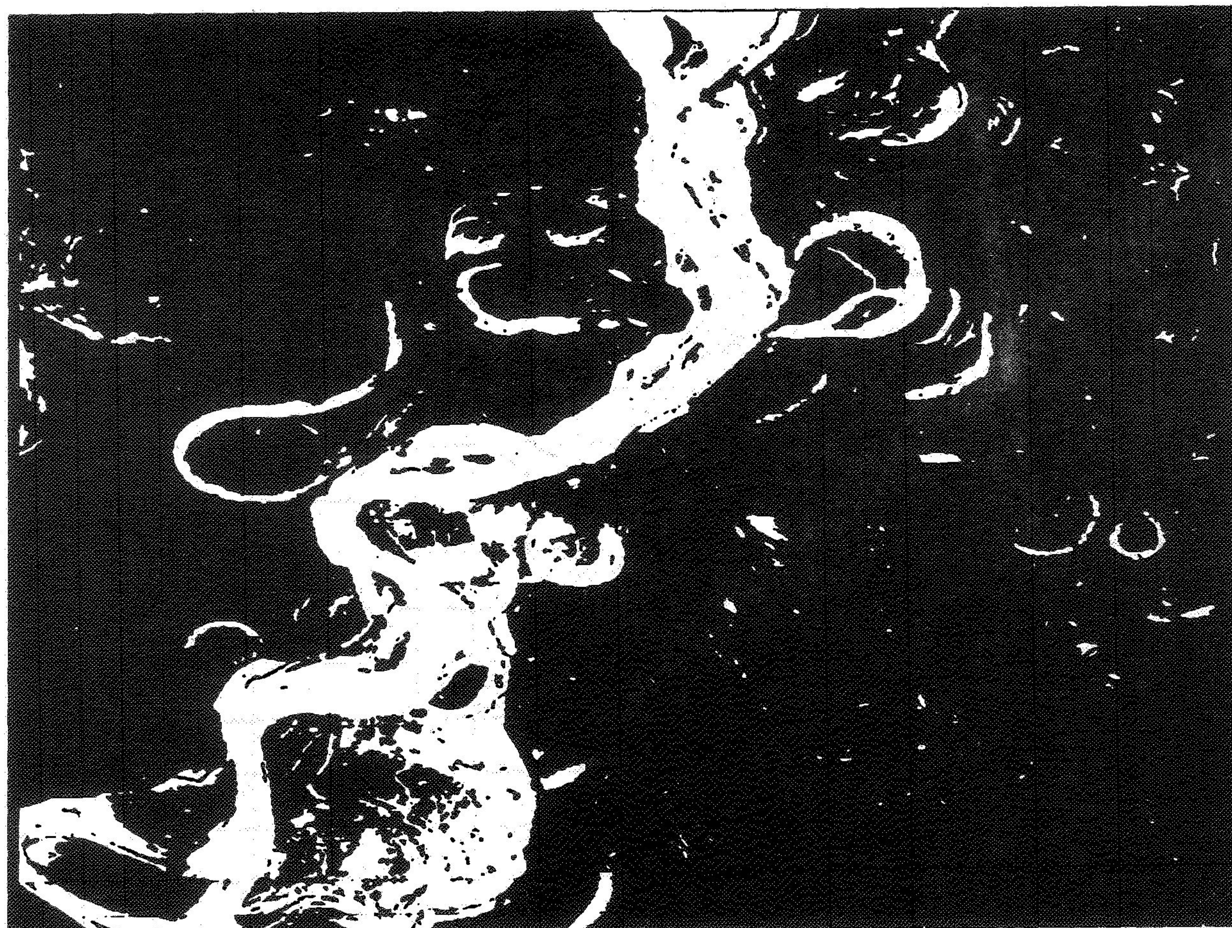

Fig. 25. Sample overlay of flood in Lower Mississippi River Valley

Paper M 6

MONITORING COASTAL WATER PROPERTIES AND CURRENT CIRCULATION WITH ERTS-1

V. Klemas, M. Otley, C. Wethe, *University of Delaware, Newark, Delaware,* and R. Rogers, *Bendix Aerospace Systems Division, Ann Arbor, Michigan*

ABSTRACT

Imagery and digital tapes from nine successful ERTS-1 passes over Delaware Bay during different portions of the tidal cycle have been analyzed with special emphasis on turbidity, current circulation, waste disposal plumes and convergent boundaries between different water masses. ERTS-1 image radiance correlated well with Secchi depth and suspended sediment concentration. Circulation patterns observed by ERTS-1 during different parts of the tidal cycle, agreed well with predicted and measured currents throughout Delaware Bay. Convergent shear boundaries between different water masses were observed from ERTS-1. In several ERTS-1 frames, waste disposal plumes have been detected 36 miles off Delaware's Atlantic coast. The ERTS-1 results are being used to extend and verify hydrodynamic models of the bay, developed for predicting oil slick movement and estimating sediment transport.

INTRODUCTION

Imagery and digital tapes from nine successful ERTS-1 passes over Delaware Bay during different portions of the tidal cycle have been analyzed with special emphasis on turbidity, current circulation, waste disposal plumes and convergent boundaries between different water masses. (NASA-ERTS-1 I.D. Nos. 1024-15073, 1079-51533, 1133-15141, 1187-15140, 1205-15141, 1294-15083, 1349-15134, 1385-15131, 1403-15125, respectively). During ERTS-1 overpasses ground truth has been collected for a total of twelve boat and helicopter transsects across the bay, including measurements of Secchi depth, suspended sediment concentration and size, transmissivity, temperature, salinity, and water color. Three U-2 and four C-130 overflights took place during the same time period. Small aircraft equipped with clusters of filtered film cameras were used to underfly each ERTS-1 overpass.

PHYSICAL CHARACTERISTICS OF DELAWARE BAY

The Delaware Bay Estuary is a relatively prominent coastal feature which bounds the Delmarva Peninsula on its northern side. The geography of this region, including the locations of several convenient reference points, is shown in Fig. 1. Trenton, New Jersey is generally taken

to define the upper limit of the estuary, so that its total length is over 130 miles.

Fresh water input to the system is derived mainly from the Delaware River at an average rate of 11,300 cfs which, in terms of volume flow, ranks this as one of the major tributaries on the eastern coastal plain. Together with this large volume of fresh water, the river also discharges a heavy load of suspended and dissolved material, since its effective watershed encompasses an area typified by intensive land use, both agricultural and industiral (Oostdam, 1971). Seaward of the Smyrna River, the bay undergoas a conspicuous exponential increase in both width and cross-sectional area so that the strength of the river flow is rapidly diminished beyond this point. Ketchum (1952) has computed the flushing time of the bay (defined in this case as the time required to replace the total fresh water volume of the bay) to be roughly 100 days. Seasonal variations in river flow cause this figure to fluctuate within a range of from 60 to 120 days. Consequently, river flow is not a significant factor in determining the current pattern in the bay except in the consideration of time-averaged flow. In terms of short-period studies it is mainly important as a source of suspended sediment and contaminants.

The seaward boundary of the bay extends from Cape May southeast to Cape Henlopen -- a distance of eleven miles. Tidal flow across this boundary profoundly affects the dynamic and hydrographic features of the entire estuary. The effect is especially pronounced toward the mouth where conditions are generally well mixed. The dynamic behavior of the tides is closely approximated by the cooscillating model described by Harleman (1966). In this model, the upper end of the estuary is assumed to act as an efficient reflecting boundary. Consequently, the actual tidal elevation at any given point is a result of the interaction of both a landward directed wave entering from the ocean and a reflected wave traveling back down the estuary. The tidal range is a maximum at the reflecting boundary and decreases toward the mouth in a manner dependent upon the relative phase of the two components. Observations of the tide at Trenton show a 7-foot range compared to a 4-foot range at the mouth. A relative maximum appears at roughly the location of Egg Island Point where the phase relationship is temporarily optimal. An important consequence of this behavior is the occurrence of strong reversing tidal currents in the Delaware River. The tidal wavelength as computed by Harleman, is 205 miles, so that both peak currents and slack water may occur simultaneously at either end of the bay.

The tidal flow is also modified by the bay's rather complex bathymetry (Fig. 1). Most prominent are several deep finger-like channels which extend from the mouth into the bay for varying distances (Kraft, 1971). Depths of up to 30 meters are present, making this one of the deepest natural embayments on the east coast. The channels alternate with narrow shoals in a pattern which is shifted noticeably toward the southern shore. On the northern side, a broad, shallow mudflat extends from Cape May to Egg Island Point. Considerable transverse tidal

shears result from these radical variations in bottom contours. As a consequence, a marked gradient structure may form normal to the main axis of the bay as a function of tidal phase. This intrinsic two-dimensional character, together with the complex, superimposed time variations, represents an almost insurmountable task when it is confronted with the tools of conventional hydrographic surveys. The problem is ready-made, however, for the techniques of high-altitude photography.

VISIBILITY OF SUSPENDED SEDIMENTS

Extensive investigations of suspended sediments in Delaware Bay and laser transmission tests in a test tank facility have been conducted respectively by (Oostdam, 1970, and Hickman, 1972). The results can be summarized as follows:

- suspended sediments in Delaware Bay averaged 30 ppm. During July-August the average sediment level was 18 ppm.

- turbidity increased with depth in the water column, except during periods of bloom, when surface turbidities at times exceeded those at greater depths.

- suspended sediment concentration gradients were greater during ebb than during flood because of greater turbulence and better mixing during flood stage.

- the turbidity decreased from winter to summer.

- marked increases in turbidity which were observed during May and September were caused mainly by plankton blooms.

- suspended sediments were silt-clay sized particles with mean diameters around 1.5 microns.

- the predominant clay minerals are chlorite, illite and kaolinite.

- reflectivities for the Delaware Bay sediments were measured to be about 10%.

At the time of the ERTS-1 overpasses, Secchi depth readings ranged from about 0.2 meters near the shore up to about 2 meters in the deep channel. Preliminary "equivalent Secchi depth" measurements with green and red boards indicated that neither "color" exceeded the readings obtained with the white Secchi disc. Therefore it is quite unlikely that the bottom will be visible in any of the ERTS-1 channels and, at least in Delaware Bay, most of the visible features will be caused by light reflected off the surface or backscattered from suspended matter.

"Red" filters, such as the Kodak Wratten No. 25A, have frequently been used in aerial photography to enchance suspended sediment patterns (Klemas et al., 1973, Bowker et al., 1973). In Delaware Bay red filters have been particularly effective for discriminating light-brown sediment-laden water in shallow areas from the less turbid dark-green water in the deep channel.

Figures 2 and 3 contain microdensitometer scans between Cape Henlopen and Cape May at the mouth of the bay. ERTS-1 images taken in bands 4, 5, and 6 were scanned, and grey scales equalized, to enable comparison on the same set of coordinate axes. Band 5 is clearly most sensitive to suspended sediment features. Even in band 5, however, the sediment patterns are caused by only four to five neighboring shades of grey in the negative transparencies and about twice that number in the digital tapes.

CORRELATION WITH MEASURED WATER PROPERTIES

During ERTS-1 overpasses ground truth was being collected with boats and helicopters along the three transsects across the bay shown in Figure 4, including measurements of Secchi depth, suspended sediment concentration, transmissivity, temperature, salinity, and water color. The correlation between ERTS-1 MSS band 5 image radiance, Secchi depth and sediment concentration is shown tentatively in Figure 5. These measurements, including salinity and temperature shown in Figure 6, were obtained during the ERTS-1 overpass on January 26, 1973. Note the sharp discontinuities in salinity and temperature near aquatic boundaries.

During flood tide at the mouth of the bay, considerable correlation was found between the depth profile and image radiance, as shown in Figure 7. During flood tide most of the sediment in suspension seems to be locally generated over shoals and shallow areas of the bay resulting in a higher degree of backscatter from shallower waters.

CURRENT CIRCULATION PATTERNS

Since suspended sediment acts as a natural tracer, it is possible to study gross circulation in the surface layers of the bay by employing ERTS-1 imagery and predicted tide and flow conditions. Adjacent to ERTS-1 pictures, Figures 8, 9, 10, 11, and 12 contain tidal current maps for Delaware Bay. Each ERTS-1 picture is matched to the nearest predicted tidal current map within $\pm$ 30 minutes. A closer match was not attempted at this point, since quantitative comparison would require comprehensive current measurements over the entire bay at the time of each satellite overpass -- a feat not attainable with limited resources. The current charts indicate the hourly directions by arrows, and the velocities of the tidal currents in knots. The Coast and Geodetic Survey made observations of the current from the surface to a maximum depth of 20 feet in compiling these charts.

The satellite picture in Figure 8 was taken two hours after maximum flood at the entrance of Delaware Bay on October 10, 1972. The sediment pattern seems to follow fairly well with the predicted current directions. A strong sediment concentration is visible above the shoals near Cape May and in the shallow nearshore water of the bay. Peak flood velocity is occurring in the upper portion of the bay, delineating sharp shear boundaries along the edges of the deep channel. At the time of this ERTS-1 picture, the wind velocity was 7 to 12 miles per hour from the north.

Figure 9 represents tidal conditions two hours before maximum flood at the mouth of the bay observed by ERTS-1 on January 26, 1973. High water slick is occurring in the upper portion of the bay, resulting in less pronounced boundaries there as compared to Figure 8. The shelf tidal water is not rushing along the deep channel upstream anymore as in Figure 8, but is caught between incipient ebb flow coming down the upper protion of the river and the last phase of flood currents still entering the bay. The sediment plume directions in Figure 9 seem to show flood water overflowing the deep channel and spreading across the shallow areas towards the shore. On the morning of December 3, 1972, there was a steady wind blowing over the bay at 7 to 9 miles per hour from the west.

About six months later, on July 7, 1973, the ERTS-1 overpass shown in Figure 10 occurred during the same part of the tidal cycle as that shown in Figure 9. Since river flow differs in the winter and summer, Figures 9 and 10 enable one to compare the effect of river flow and wind effects with identical tidal conditions. The body of water having a higher radiance seen about 20 miles offshore in Figure 10 has not yet been explained.

As shown in Figure 11, on August 12, 1973, ERTS-1 passed over Delaware Bay one hour before maximum ebb at the mouth of the bay. In addition to locally suspended sediment over shallow areas and shoals observed in Figures 8 and 9, plumes of finer particles are seen in Figure 11 parallel to the river flow and exiting from streams and inlets off New Jersey's and Delaware's coastlines. Shear boundaries along the deep channel are still visible in the upper portion of the bay; however, they are beginning to disappear as slack sets in, resembling conditions in Figure 9. At the time of the overpass, the wind was from the north-northeast at about 11 miles per hour, possible causing the streaks in the ocean off New Jersey's coastline.

The satellite overpass on February 13, 1973 occurred about one hour after maximum ebb at the capes. The corresponding ERTS-1 image and predicted tidal currents are shown in Figure 12. Strong sediment transport out of the bay in the upper portion of the water column is clearly visible, with some of the plumes extending up to 20 miles out of the bay. Small sediment plumes along New Jersey's coast clearly indicate that the direction of the longshore current drift in that area is towards the north. The wind velocity at the time of the satellite overpass was about 7 to 9 miles per hour from the north-northwest.

SHEAR BOUNDARIES AND SALINITY WEDGES

Boundaries or fronts (regions of high horizontal density gradient with associated horizontal convergence) are a major hydrographic feature in Delaware Bay and in other estuaries. Fronts in Delaware Bay have been investigated using STD sections, dye drops and aerial photography. Horizontal salinity gradients of 4% in one meter and convergence velocities of the order of 0.1m/sec. have been observed. Several varieties of fronts have been seen. Those near the mouth of the bay are associated with the tidal intrusion of shelf water (Figure 12). The formation of fronts in the interior of the bay (Figure 8) appears to be associated with velocity shears induced by differences in bottom topography with horizontal density difference across the front influenced by vertical density difference in the deep water portion of the estuary. Surface slicks and foam collected at frontal convergence zones near boundaries contained concentrations of Cr, Cu, Fe, Hg, Pb, and Zn higher by two to four orders of magnitude than concentrations in mean ocean water. (Szekielda, Kupferman, Klemas, Polis, 1972), Figure 14, (Band 5, I.D. Nos. 1024-15073) obtained by ERTS-1 on August 16, 1972 contains several distinct boundaries. The southern-most boundary, as shown in Figure 15 is of particular interest, since it has frequently been observed from aircraft (Figure 16) and at the time of the ERTS-1 overpass. Divers operating down to depths of 6 meters noted increases in visibility from about half a meter to two meters as the boundary moved past their position.

WASTE DISPOSAL PLUMES

Careful examination of Figures 17 and 18 disclosed a fish-hook-shaped plume about 40 miles east of Cape Henlopen caused by a barge disposing acid wastes. The plume shows up more strongly in the green band than in the red band. Since some acids have a strong green component during dumping and turn slowly more brownish-reddish with age, the ratio of radiance signatures between the green and red bands may give an indication of how long before the satellite overpass the acid was dumped. Currently acid dumps are being coordinated with ERTS-1 overpasses in order to determine the diffusion and movement of the waste materials along the continental shelf.

IMAGE ENCHANCEMENTS AND DIGITAL MAPS

Color density slicing and optical additive color viewing techniques were employed to enhance the suspended sediment patterns. Grey tone variations were "sliced" into increments and different colors assigned to each increment by using the Spatial Data Datacolor 703 System at NASA's Goddard Space Flight Center. Color density slicing helped delineate the suspended sediment patterns more clearly and differentiate turbidity levels. Density slicing of all four MSS bands gave an indication of relative sediment concentration as a function of depth, since the four bands penetrate to different depths ranging from several meters to several centimeters, respectively.

Additive color composites of bands 4 and 5 were prepared by Photo-Science, Inc. using the photographic process silver-dye bleaching. This process bleaches out spectral separations of each MSS band to produce the color composite. The additive color rendition is then reproduced on Cibachrome CCT color transparencies. Comparison of the composite with the equivalent band 5 image in Figure 8 indicates that the composite does not contain more suspended sediment detail than the individual band 5 image. For similar reasons, composites prepared with the International Imaging Systems Mini-Addco Additive Color Viewer, Model 6030 did not improve contrast beyond what was attainable in band 5 directly.

ERTS-1 digital tapes are currently being used by Bendix Aerospace Systems Division to prepare annotated sediment concentration maps of the bay. Ground truth from at least one transsect is used to annotate the maps.

CONCLUSIONS

ERTS-1 image radiance (microdensitometer traces) correlated well with Secchi depth and suspended sediment concentration. While only four concentration levels were extracted from transparencies, up to twice that number were obtained on sediment concentration plots derived from the MSS tapes directly. MSS band 5 seemed to give the best representation of sediment load in the upper one meter of the water column. Color density slicing helped delineate the suspended sediment patterns more clearly and differentiate turbidity levels. Density slicing of all four MSS bands gave an indication of relative sediment concentration as a function of depth, since the four bands penetrate to different depths ranging from several meters to several centimeters, respectively.

Circulation patterns observed by ERTS-1 during different parts of the tidal cycle, agreed well with predicted and measured currents throughout Delaware Bay. During flood tide the suspended sediment as visible from ERTS-1 correlated well with the depth profile. ERTS-1 imagery is now being used to extend and verify a predictive model for oil slick movement in Delaware Bay.

Convergent shear boundaries between different water masses were observed from ERTS-1, with foam lines containing high concentrations of lead, mercury and other toxic substances. Several varieties of fronts have been seen. Those near the mouth of the bay are associated with the tidal intrusion of shelf water. Fronts in the interior of the bay on the Delaware side appear to be associated with velocity shears induced by differences in bottom topography. In several ERTS-1 frames, waste disposal plumes have been detected 40 miles off Delaware's Atlantic coast.

Applications of these results to relevant problem areas are listed in Table 1.

TABLE 1

PARAMETERS DISCRIMINATED AND CORRELATED	APPLICATION TO COASTAL RESOURCES MANAGEMENT
1. SUSPENDED SEDIMENT CONCENTRATION Band 5 correlated best with concentration and Secchi depth (transmissivity, temperature, salinity, color).	To verify and extend sediment transport model of Delaware Bay and monitor water quality. (U.D. and EPA).
2. CURRENT CIRCULATION PATTERNS Good agreement with predicted current circulation as a function of tide and wind during 9 good overpasses.	To extend and verify predictive model for oil slick movement in Delaware Bay. (U.D. and NSF-RANN).
3. WATER MASS BOUNDARIES Foam lines along convergent boundaries with toxic substances.	Boundaries used to modify hydrodynamic model of bay; toxic substances affect oyster beds. (U.D. and State).
4. WASTE DISPOSAL PLUMES Greenish acid plume 36 miles off coast most visible in band 4.	Sludge and acid dumps coordinated with ERTS-1 overpasses to study dispersion of wastes dumped along continental shelf. (U.D. and EPA).
5. WETLANDS VEGETATION Maps of Delaware's wetlands completed showing 6 vegetation species and 3 other properties.	To develop marsh relative value model and plan wetlands development. (U.D. and State).
6. LAND USE AND ENVIRONMENTAL IMPACT About 10 coastal land use categories mapped using ERTS digital tapes.	To monitor land use, its impact on marsh environment, and coastal erosion. (U.D. and State).

REFERENCES

Bowker, D. E., P. Fleischer, T. A. Gosink, W. J. Hanna and J. Ludwich, Correlation of ERTS Multispectral Imagery with Suspended Matter and Chlorophyll in Lower Chesapeake Bay, paper presented at Symposium on Significant Results Obtained from ERTS-1, NASA Goddard S.F.C., Greenbelt, Maryland, March 5-9, 1973.

Harleman, D. R. F., Tidal Dynamics in Estuaries, Estuary and Coastline Hydrodynamics, ed., A. T. Ippen, McGraw-Hill, Inc., New York, 1966.

Ketchum, B. H., The Distribution of Salinity in the Estuary of the Delaware River, Woods Hole Oceanographic Institute, Ref. No. 52-103, 38 pages, 1952.

Klemas, V., W. Treasure and R. Srna, Applicability of ERTS-1 Imagery to the Study of Suspended Sediment and Aquatic Fronts, paper presented at Symposium on Significant Results Obtained from ERTS-1, NASA Goddard S.F.C., Greenbelt, Maryland, March 5-9, 1973.

Klemas, V., R. Srna and W. Treasure, Investigation of Coastal Processes Using ERTS-1 Satellite Imagery, paper presented at American Geophysical Union Annula Fall Meeting, San Francisco, California, December 4-7, 1972.

Kraft, J. C., A Guide to the Geology of Delaware's Coastal Environment, College of Marine Studies Publication, University of Delaware, 1971.

Kupferman, S. L., V. Klemas, D. Polis, and K. Szekielda, Dynamics of Aquatic Frontal Systems in Delaware Bay, paper presented at A.G.U. Annual Meeting, San Francisco, California, April 16-20, 1973.

Nat. Aer. Space Admin., Data Users Handbook, Earth Resources Technolgy Satellite, GSFC Document 71504249, 15 September 1971.

Oostdam, B. L., Suspended Sediment Transport in Delaware Bay, Ph.D. Dissertation, University of Delaware, Newark, DE, May, 1971.

Ruggles, F. H., Plume Development in Long Island Sound Observed by Remote Sensing, paper presented at Symposium on Significant Results Obtained from ERTS-1, NASA Goddard S.F.C., Greenbelt, Maryland, March 5-9, 1973.

Sherman, J., Comment made at NASA Marine Resources Working Group Meeting GSFC, Greenbelt, Maryland, March 9, 1973.

Szekielda, K. H., S. L. Kupferman, V. Klemas and D. F. Polis, Element Enrichment in Organic Films and Foam Associated with Aquatic Frontal Systems, Journal of Geophysical Research, Volume 77, No. 27, September 20, 1972.

U. S. Department of Commerce, Tidal Current Charts - Delaware Bay and River, Environmental Science Services Administration, Coast and Geodetic Survey, Second Edition, 1960.

U. S. Department of Commerce, Tidal Current Tables, Atlantic Coast of North America, National Oceanic and Atmospheric Administration, National Ocean Survey, 1972 and 1973.

Hickman, G. D., J. E. Hogg and A. H. Ghovanlou, Pulsed Neon Laser Bathymetric Studies Using Simulated Delaware Bay Waters. Sparcom, Inc., Technical Report #1, September 1962, pp. 10-13.

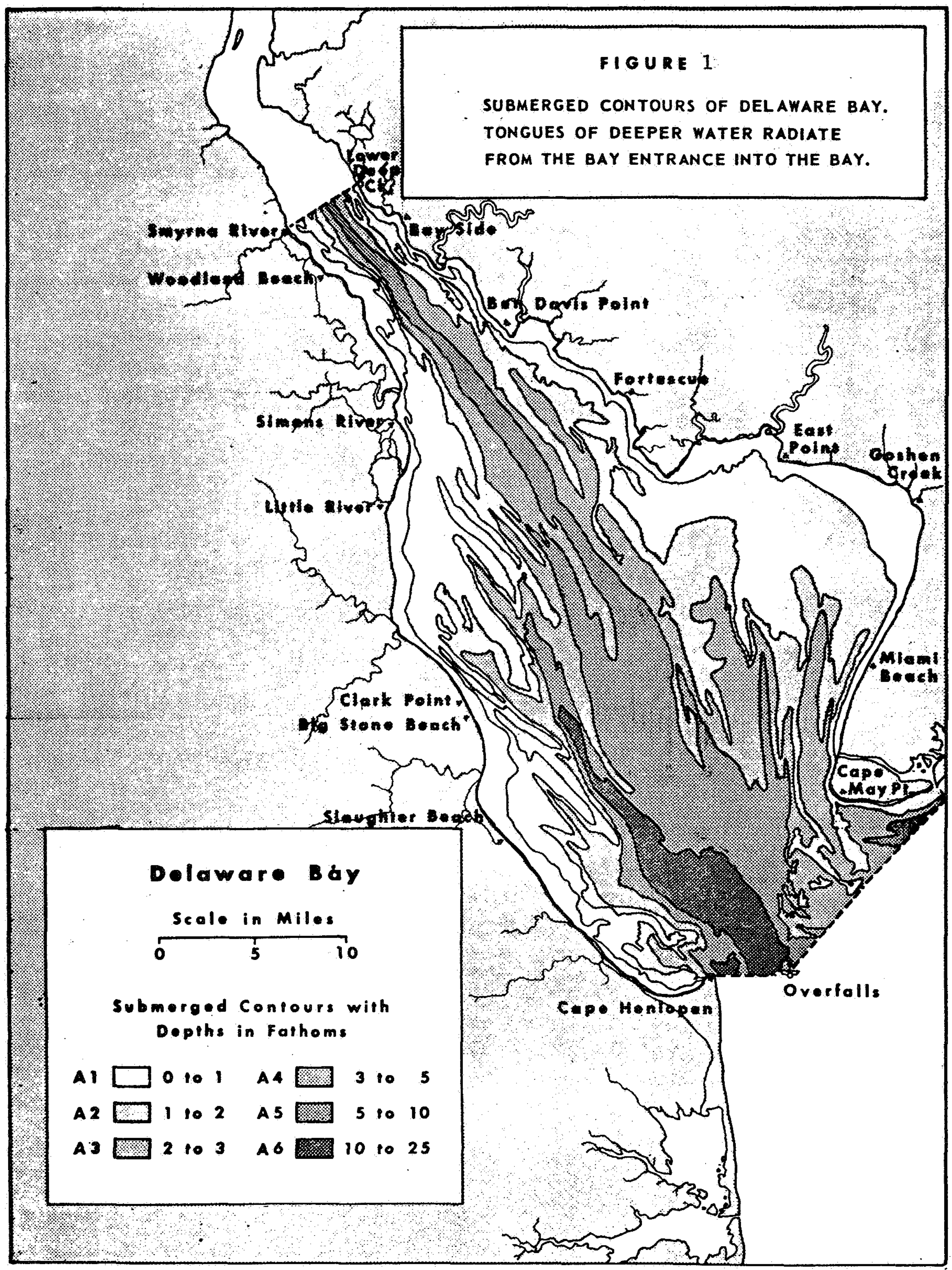
FIGURE 1
SUBMERGED CONTOURS OF DELAWARE BAY. TONGUES OF DEEPER WATER RADIATE FROM THE BAY ENTRANCE INTO THE BAY.
Smyrna River
Woodland Beach
Bay Side
Ben Davis Point
Fortescue
Simons River
East Point
Goshen Creek
Little River
Miami Beach
Clark Point
Big Stone Beach
Cape May Pt.
Slaughter Beach
Overfalls
Cape Henlopen
Delaware Bay
Scale in Miles
0
5
10
Submerged Contours with Depths in Fathoms
A1 0 to 1
A2 1 to 2
A3 2 to 3
A4 3 to 5
A5 5 to 10
A6 10 to 25

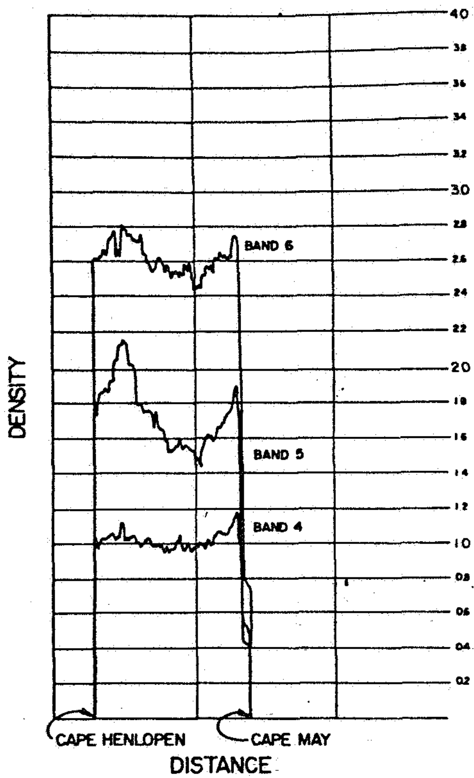

Figure 2 - Positive transparencies.

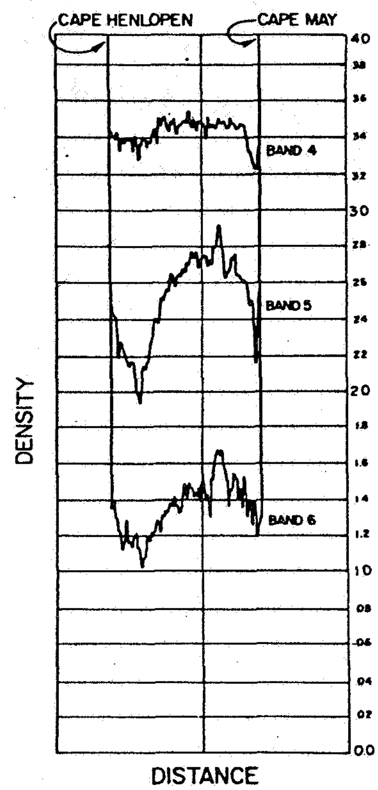

Figure 3 - Negative transparencies.

Microdensitometer traces of October 10, 1972, ERTS-1 imagery from Cape Henlopen, Delaware to Cape May, New Jersey, using MSS bands 4, 5, and 6.

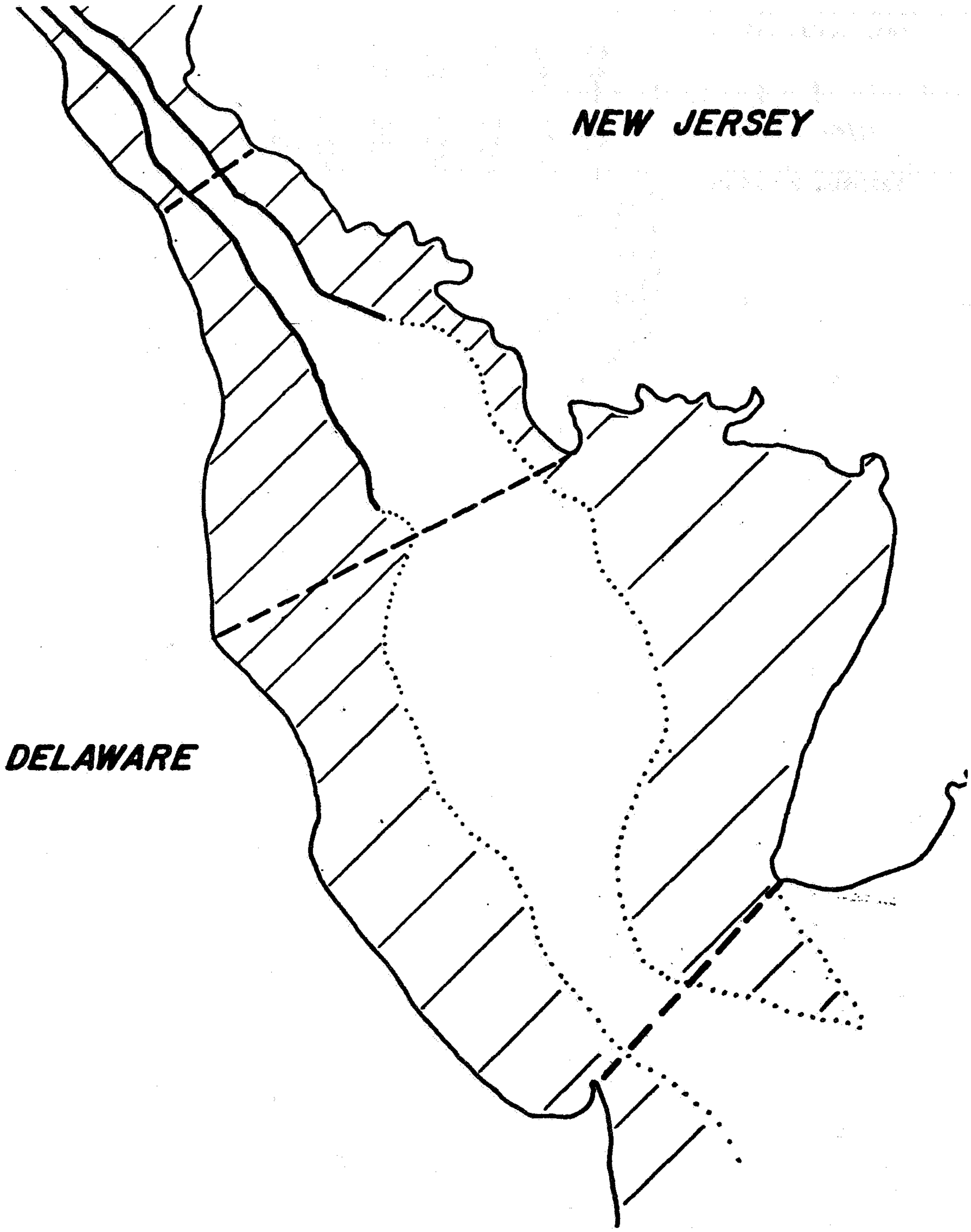

Figure 4. Helicopter and boat transsects across Delaware Bay along which Secchi depth, sediment concentration, transmissivity, temperature, salinity and water color were measured during ERTS-1 overpasses.

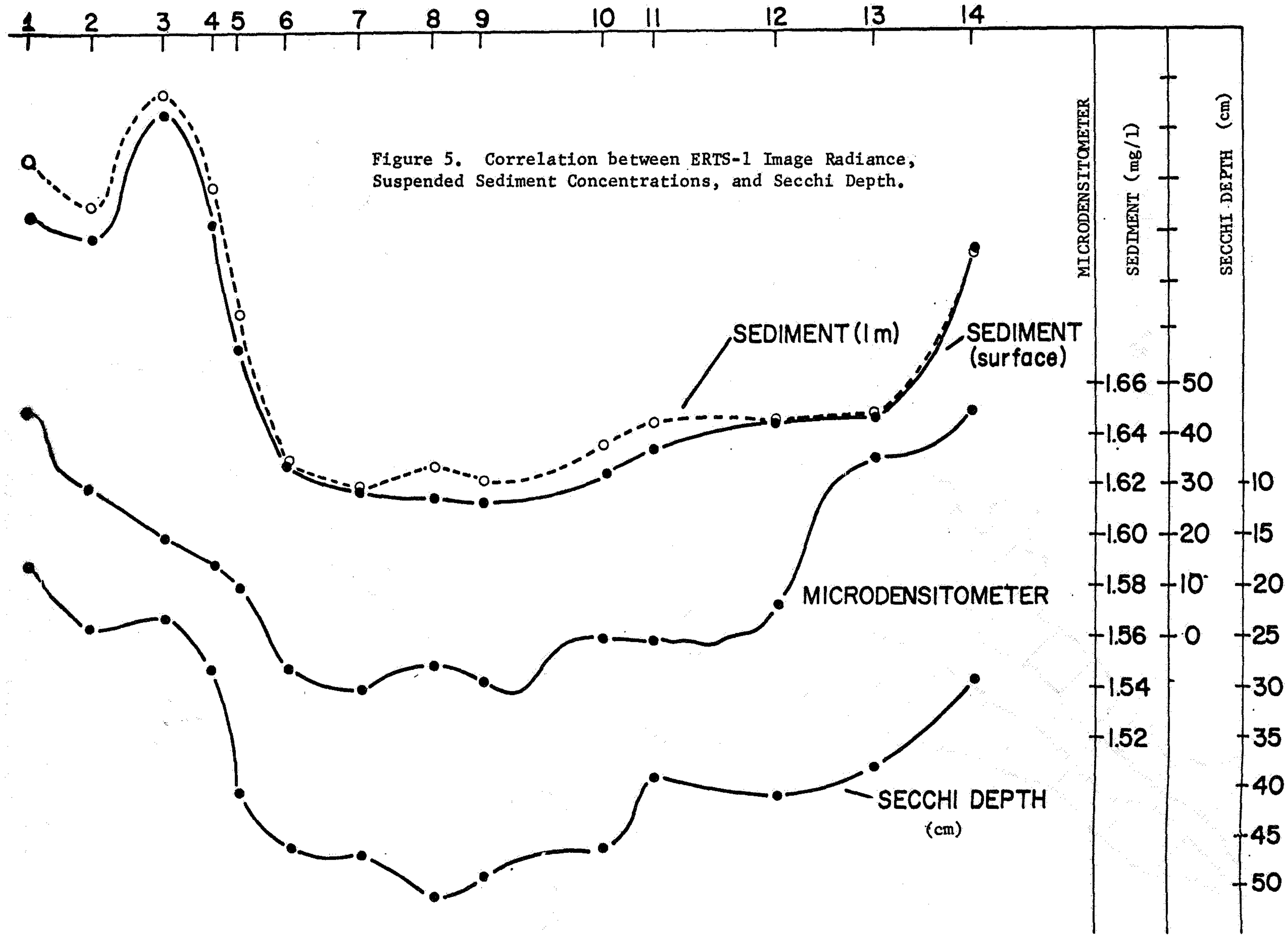

Figure 5. Correlation between ERTS-1 Image Radiance, Suspended Sediment Concentrations, and Secchi Depth.

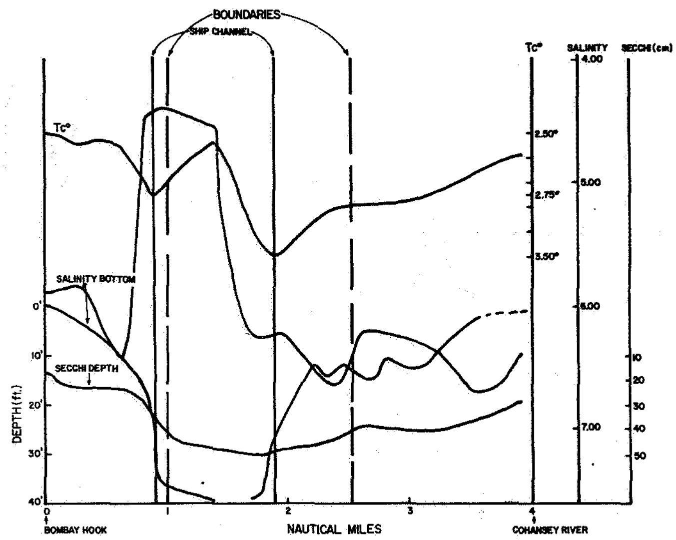

Figure 6. Temperature, salinity Secchi depth and bottom profiles across the upper transsect of the bay during ERTS-1 overpass on January 26, 1973.

Figure 7. ERTS-1 image radiance (microdensitometer trace) and depth profile across the mouth of Delaware Bay during flood tide.

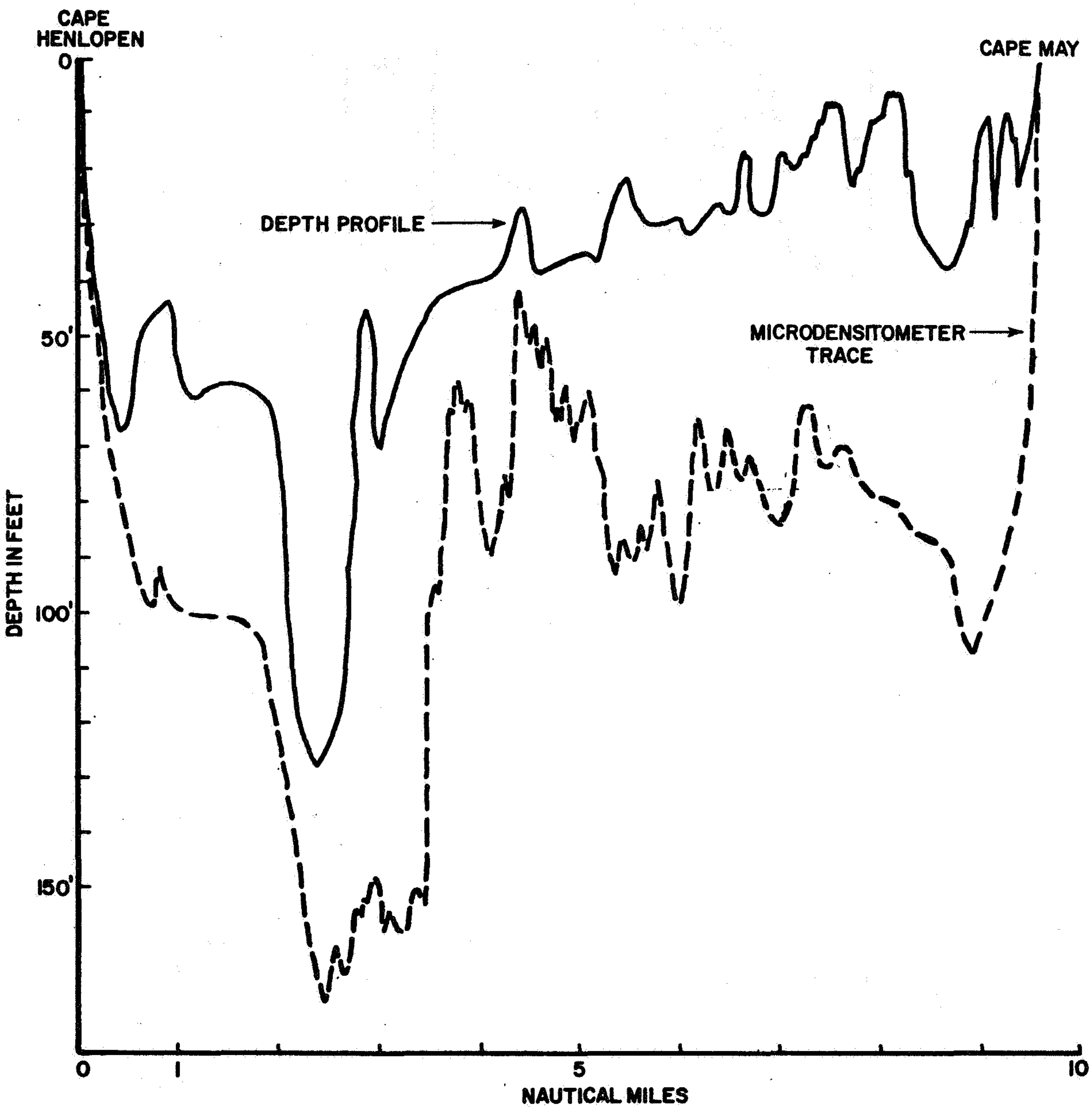

MICRODENSITOMETER TRACE FROM CAPE HENLOPEN, DEL. TO CAPE MAY, N.J.
ERTS-1 ID. 1024-15073 (BAND 5) AUG. 26, 1972

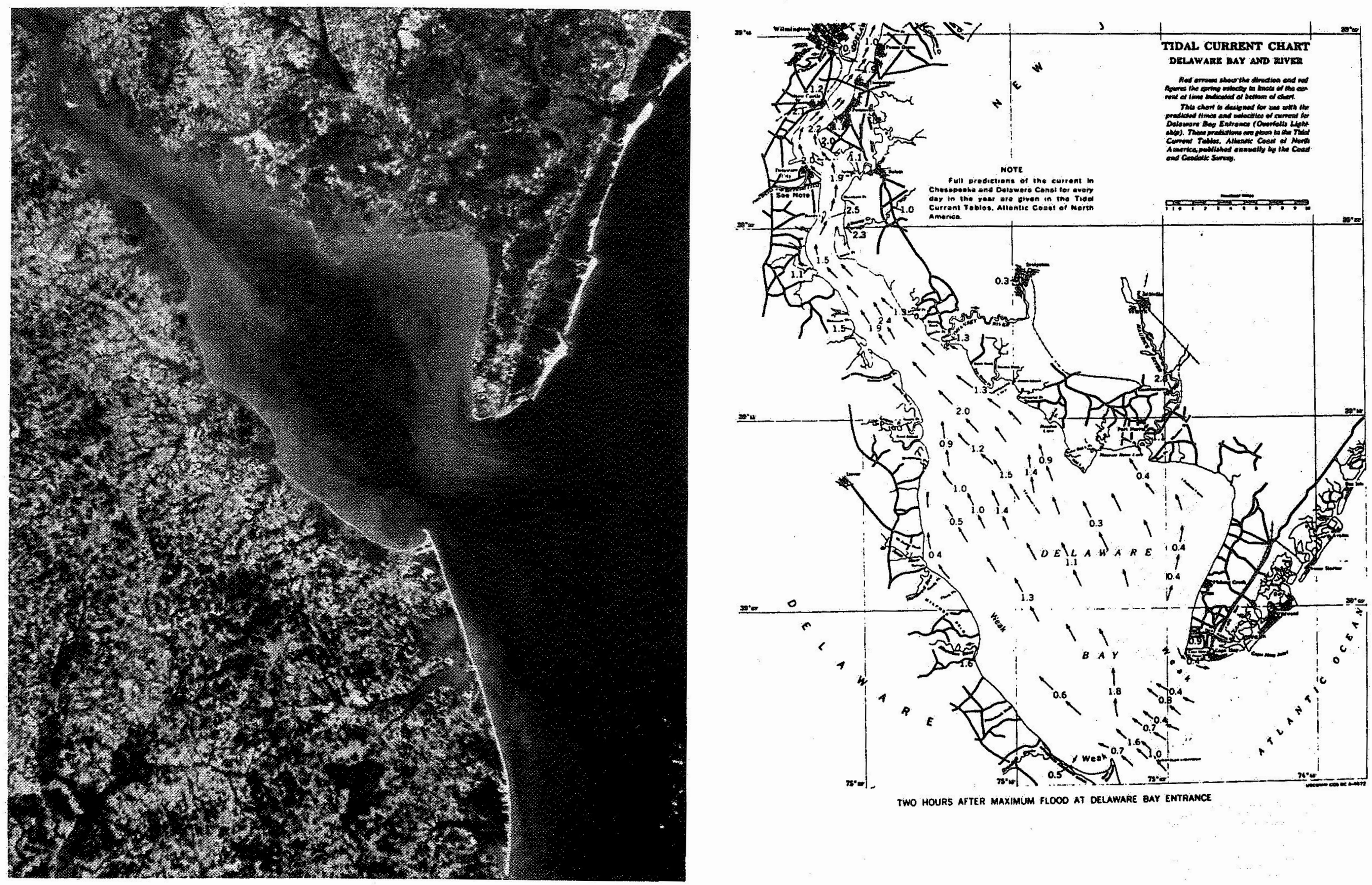

Figure 8. ERTS-1 image of Delaware Bay obtained in MSS band 5 on October 10, 1972 and tidal current map. (I.D. No. 1079-15133.)

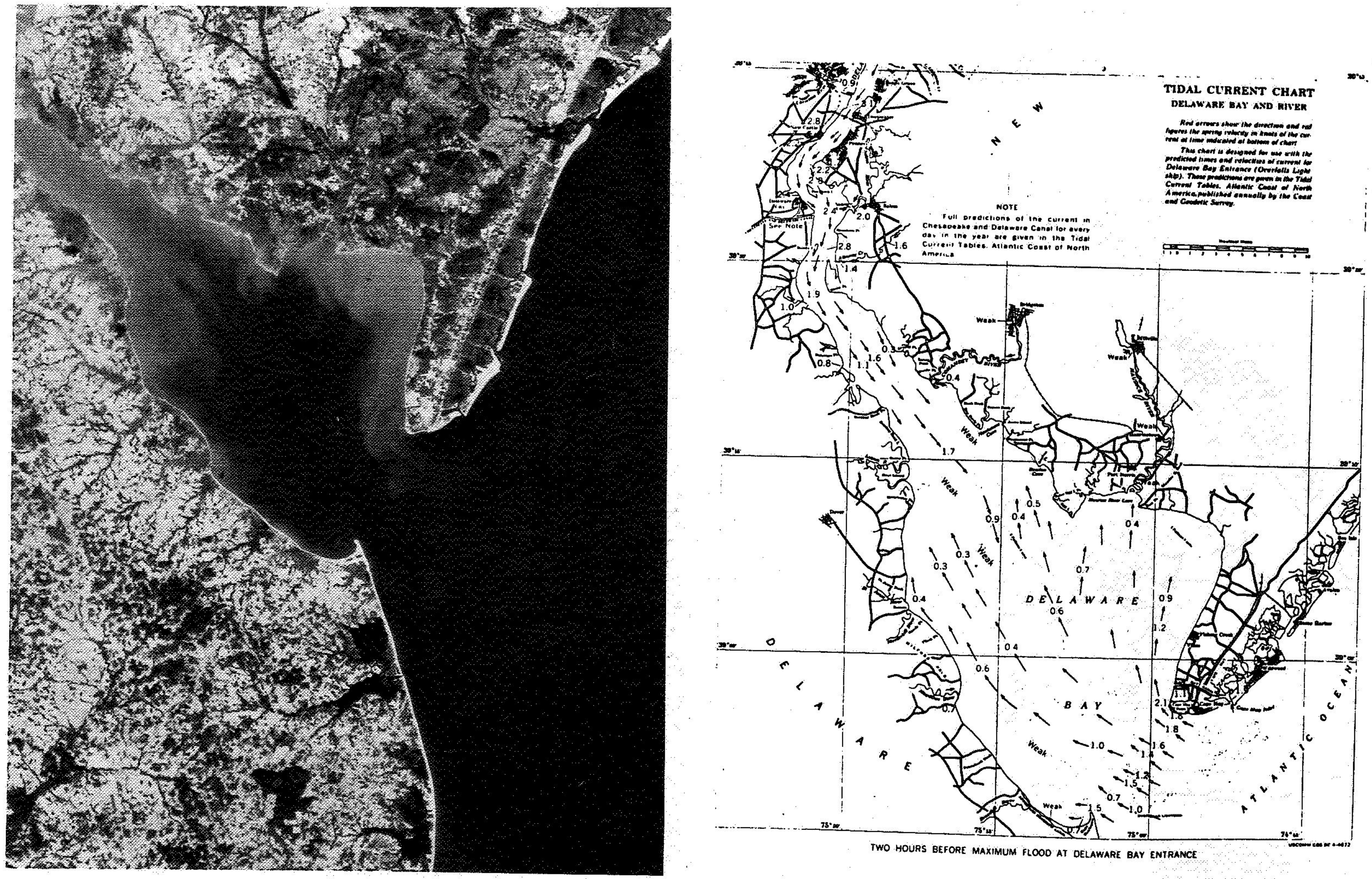

Figure 9. ERTS-1 image of Delaware Bay obtained in MSS band 5 on January 26, 1973 and tidal current map. (I.D. Nos. 1187-15140).

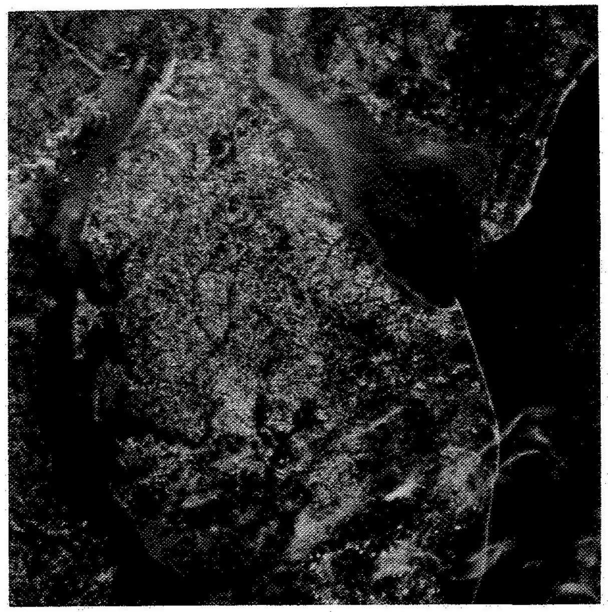

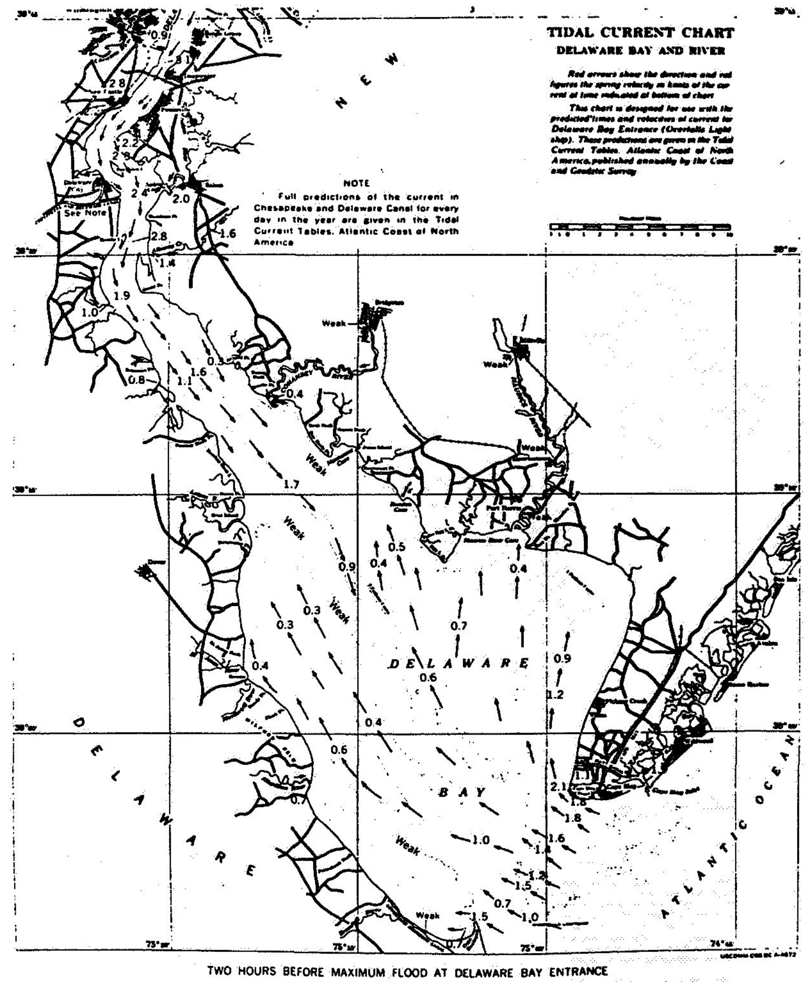

Figure 10. ERTS-1 image of Delaware Bay obtained in MSS band 5 on July 7, 1973 and tidal current map. (I.D. Nos. 1349-15134.)

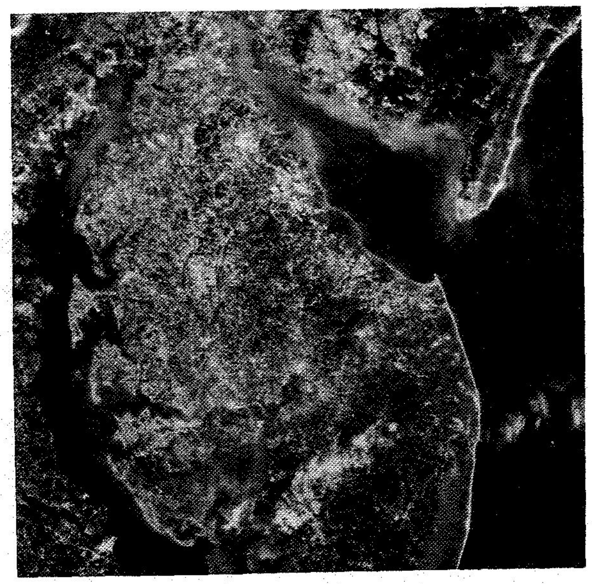

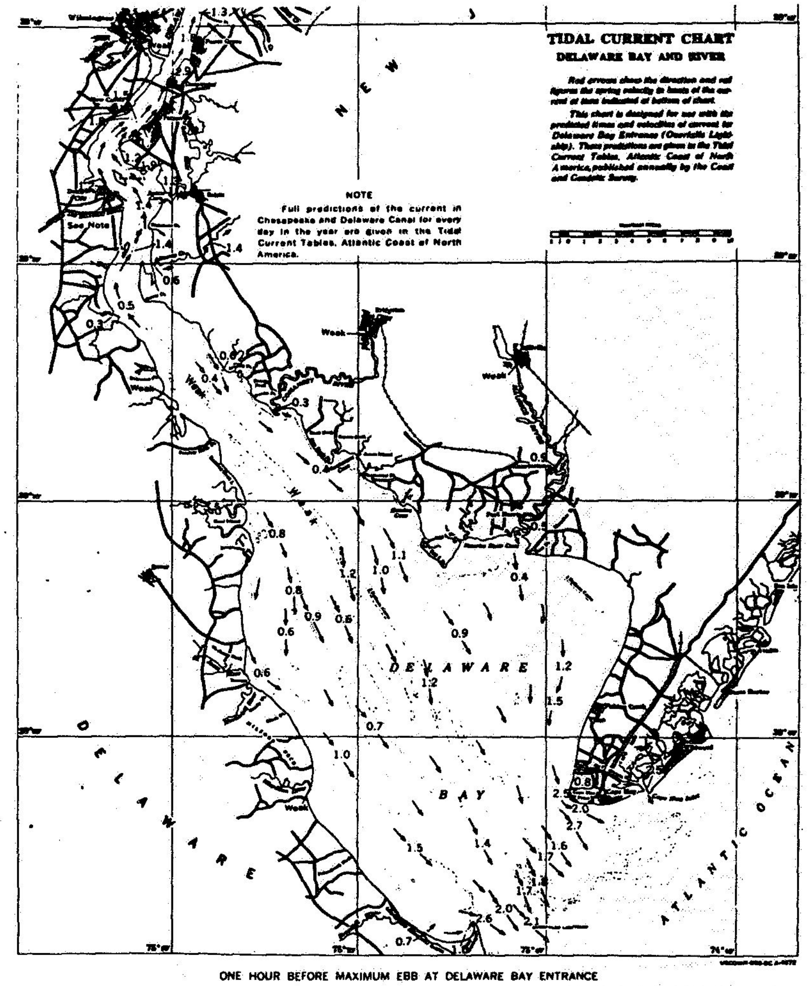

Figure 11. ERTS-1 image of Delaware Bay taken with MSS band 5 on August 12, 1973 and tidal current map. (I. D. Nos. 1385-15131.)

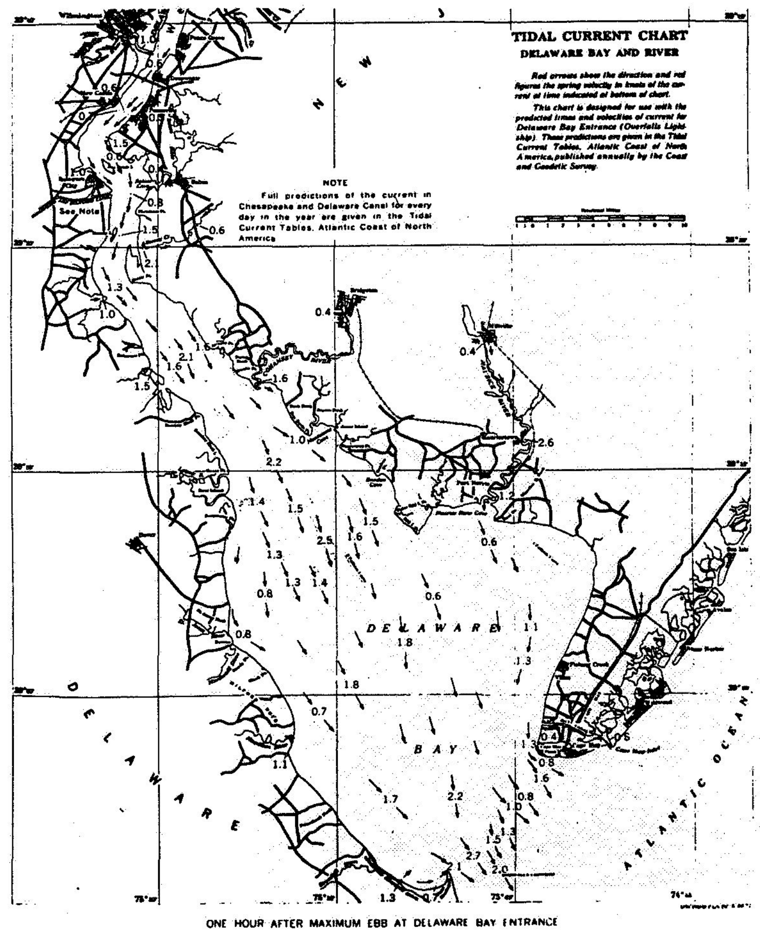

Figure 12. ERTS-1 image of Delaware Bay obtained in MSS band 5 on February 13, 1973 and tidal current maps. (I.D. Nos. 1205-15141.)

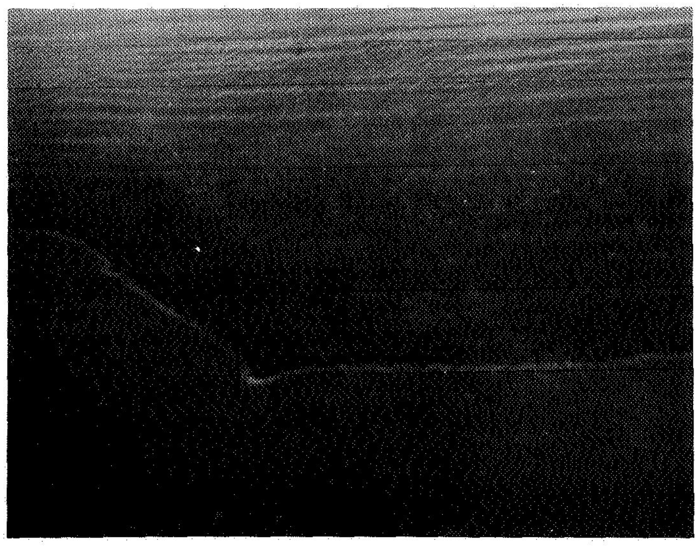

Figure 13. Frontal system caused by higher salinity shelf water intruding into Delaware Bay.

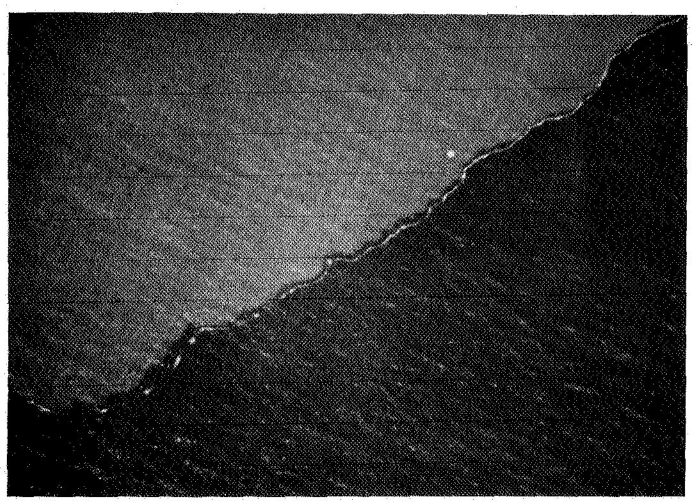

Figure 16. Aerial photograph from 9000 feet altitude of foam-line at boundary between two different water masses off Delaware's coast.

Figure 14. ERTS-1 image of the mouth of Delaware Bay showing several water mass boundaries and high concentrations of suspended sediment in shallow waters. (Band 5, August 16, 1972, I.D. 1024-15073).

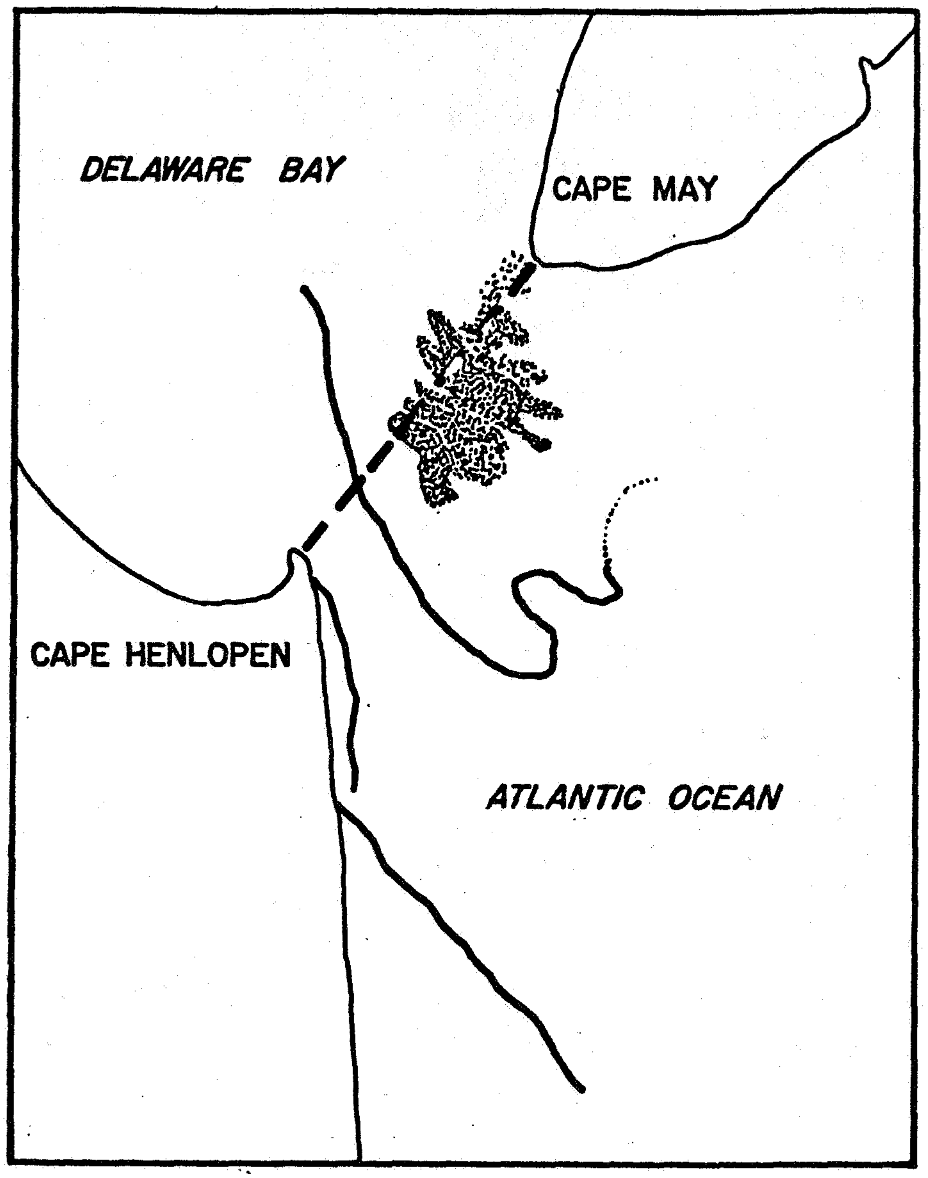

Figure 15: Aquatic boundaries and suspended sediment plumes identified in the ERTS-1 image of August 16, 1972, shown in Figure 14.

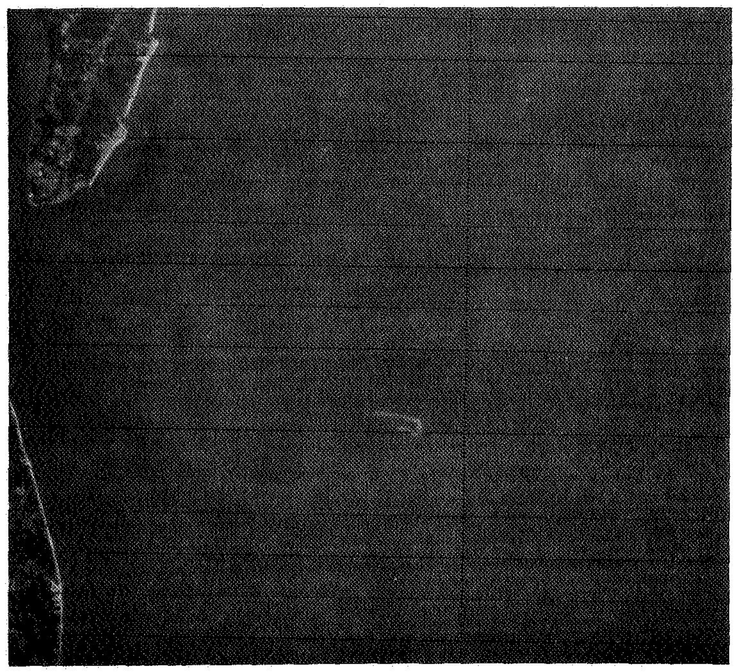

Figure 17. Acid waste dumped from barge about 40 miles east of Indian River Inles appears clearly as a fishhook shaped plume in MSS band 4 image of January 25, 1973.

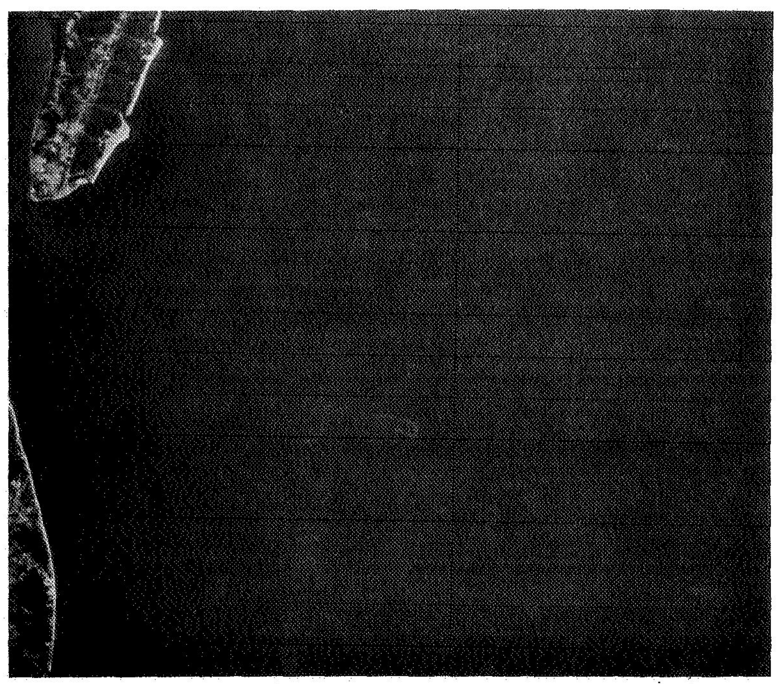

Figure 18. Due to its predominantly greenish component, the acid plume shows less contrast in band 5.

Paper M 7

CALIFORNIA COASTAL PROCESSES STUDY

Douglas M. Pirie, *Corps of Engineers, San Francisco District* and David D. Steller, *Geosource International Inc., Seal Beach, California*

ABSTRACT

This paper presents preliminary findings and applications derived from ERTS-1 satellite imagery of the nearshore coastal processes of the California coast. The study objectives are to analyze nearshore currents, sediment transport, and estuarine and river discharges along the California coast thru the use of synoptic and repetitive imagery from ERTS as well as aircraft underflights and surface data.

The major conclusions that are described in detail in this paper are as follows: (1) Distinct seasonal patterns for sediment transport as a function of the oceanic current systems and coastal morphology have been identified. (2) Large scale sediment plumes from intermittent streams and rivers extend offshore to previously unanticipated ranges. Areas where these plumes contain possible contamination from onshore activities can be traced in detail. (3) Computer generated contouring of radiance levels from computer-compatible tapes result in charts that can be used for determination of surface and nearsurface suspended sediment distribution. (4) Flying spot scanner enhancements result in details of nearshore features. (5) Data from this ERTS study is providing significant information for coastal planning and construction projects.

INTRODUCTION AND SUMMARY

The objectives of this ERTS study are to analyze nearshore currents, sediment transport, and estuaries and river discharges along the California coast through the use of synoptic, repetitive imagery from the Earth Resources Technology Satellite (ERTS). During ERTS overpasses, airborne and sea truth data are collected for comparing and confirming details of nearshore processes that are detected on ERTS imagery. Four test sites along the California coast (San Francisco, Monterey Bay, Santa Barbara Channel, and Los Angeles) are emphasized during the interpretation of the overall ocean surface dynamic structure. Major effort is being placed on four analysis techniques: (1) mosaic analysis of three California coast ocean seasons using visual and densitometer analysis of suspensates to determine surface dynamics, (2) computer contouring investigation of radiance level distribution, (3) investigation of the

relationship between ERTS scene radiance levels and suspended sediment content, and (4) use of flying spot scanner enhancements to facilitate detection and interpretation of subtle suspended sediments. At numerous locations, the nearshore features are also investigated utilizing both aerial photography (high and low altitude) and sea truth data. Sea truth is collected by the principal and co-investigators and supplemented primarily by data from the University of Southern California, the Office of Naval Research, the University of California at Santa Cruz, and the National Park Service.

One of the major results of this study is the ability to detect the source and movement of sediments in the nearshore and offshore zones. This sediment interpretation capability results from analyzing the ERTS-MSS green bank imagery. Included are three mosaics of the California coast which were assembled for specific ocean current seasons. Contrast between clear ocean water and sediment-laden water is possible through both visual interpretation of tone contrast and through enhancement techniques. These processes are applied to the transparencies and computer compatible tapes (CCT). Distribution of sediments from riverine discharge and coastal erosion is possible along the coast out to distances of 160 km and more. A complex interrelationship of energy sources including wind, tide and current modified by bottom topography and atmospheric conditions governs the movements of coastal waters. These transitory processes acting over an area as large as the California coast presents a complex analysis problem whose solution is significantly aided using ERTS imagery. The ability to detect current direction and horizontal distribution, upwellings, current blockage, offshore movements, gyres, sediment source and nearshore and offshore current reversals represents a valuable new contribution to coastal information and U.S. Army Corps of Engineers operations.

Along the California coast, the dominating factor in nearshore processes dynamics is the California Current which moves generally southeast. In the winter the northward-directed nearshore Davidson Current moves opposite to the south-moving California Current further offshore. This northward flow in winter (mid-November to mid-February) is attributed to the seasonal change in the wind patterns across California, Oregon and Washington. The effect of this seasonal coastal current movement is brought out in detail in ERTS imagery analysis. About halfway through February another major change in wind direction annually initiates the phenomena of nearshore Coriolis force upwelling resulting in the Upwelling Period. During this period the prevailing coastal winds are from the northwest and tend to increase the speed of the surface current and maintain the flow parallel to the coast. In some areas immediately adjacent to the coast, the southward component of the winds is often increased. When this occurs, the influence

of the eastward component of the wind on the surface layer becomes insufficient to prevent the surfacing of the deeper layer cold water that has built up against the coast. This effect seems to be intensified south of capes and points which extend out toward the California Current stream. Along the California coast, as noted in the ERTS imagery, upwellings occurs near Cape Mendocino, Point Conception and Crescent City during March and July. The cooler upwelling waters are often rich in nutrients with a result that phytoplankton blooms often occur in this period. The third mosaic presented, is titled the Transition Period and includes available imagery near the end of the Upwelling Period and before the Oceanic Period, which dominates from mid-July to mid-November.

The detectability of nearshore processes and open ocean current is largely dependent upon the amount and distribution of suspensates in the coastal waters. In addition to the use of the common interpretative techniques for coastal processes (i.e., densitometer, additive color, photographic density enhancement), three major methods of analysis have been developed. The first method is to use the suspended sediment samples and transmissometer data to calibrate and compare radiance levels found in the ERTS imagery. This analysis is used in conjunction with the CCT contouring in order to analyze sediment distribution in the test areas of interest. The second technique is to use the flying spot scanner (FSS) to convert tape to film. This technique is utilized to expand the restricted ERTS signal dynamic range that corresponds to suspensates in coastal waters. It amplified the signal range prior to recording, so the features of interest are emphasized in the played-back enhancement. The third technique is the use of the NASA computer compatible tapes (CCT) in playback enhancements and in the contouring of radiance levels. The contours are related to sediment content in the coastal and offshore areas as determined by sea truth collections and data analyses. In each case, these techniques have resulted in the enhancement of subtle or nondetectable (by human eye) signal levels in the ERTS data.

Identification of important processes operating in a coastal environment and understanding their relative importance and mutual interactions are prime requirements in interpreting coastal water dynamics and in designing coastal structures. This study is developing the details of nearshore processes as well as the dynamics of the three ocean seasons. Investigations of the ocean season currents have been going on for years, but essentially no simultaneous data source as extensive as ERTS has been available. The use of the ERTS information in analyzing present and future coastal study sites is of primary value to the U.S. Army Corps of Engineers.

DAVIDSON CURRENT PERIOD

The complex movements of the various surface currents which occur during the Davidson Current Period are illustrated in Figure 1. The information for this plot comes from repetitive ERTS coverage, several aircraft flights

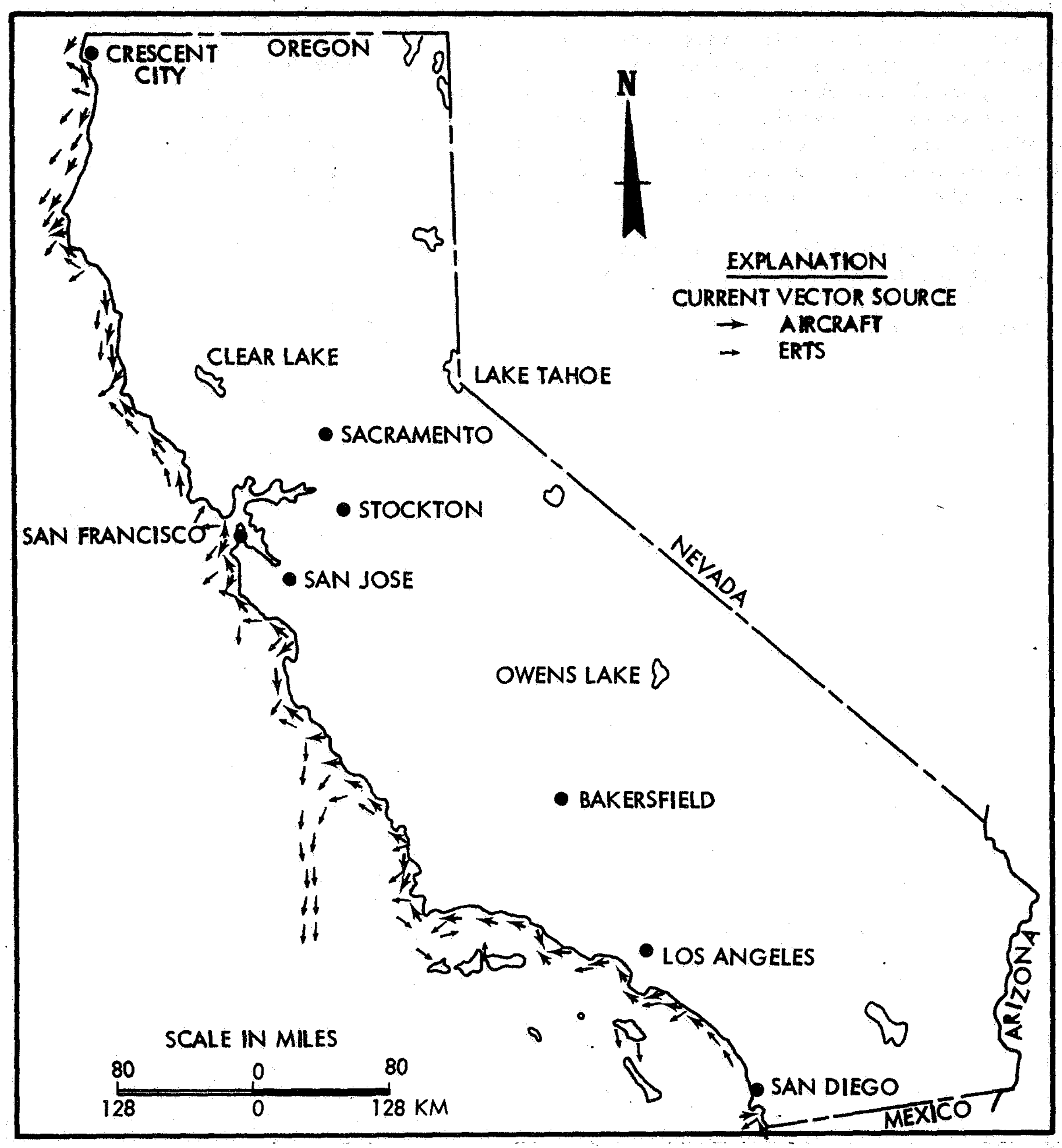

Figure 1. Davidson Current Plot. Nearshore and Coastal Currents Determined from MSS Band 4 (5000 - 6000 Å) Imagery During the November 1972 - January 1973 Period. ERTS Imagery was Supplemented by U-2 and Low Level Aircraft Photography and Sea Truth **Data**

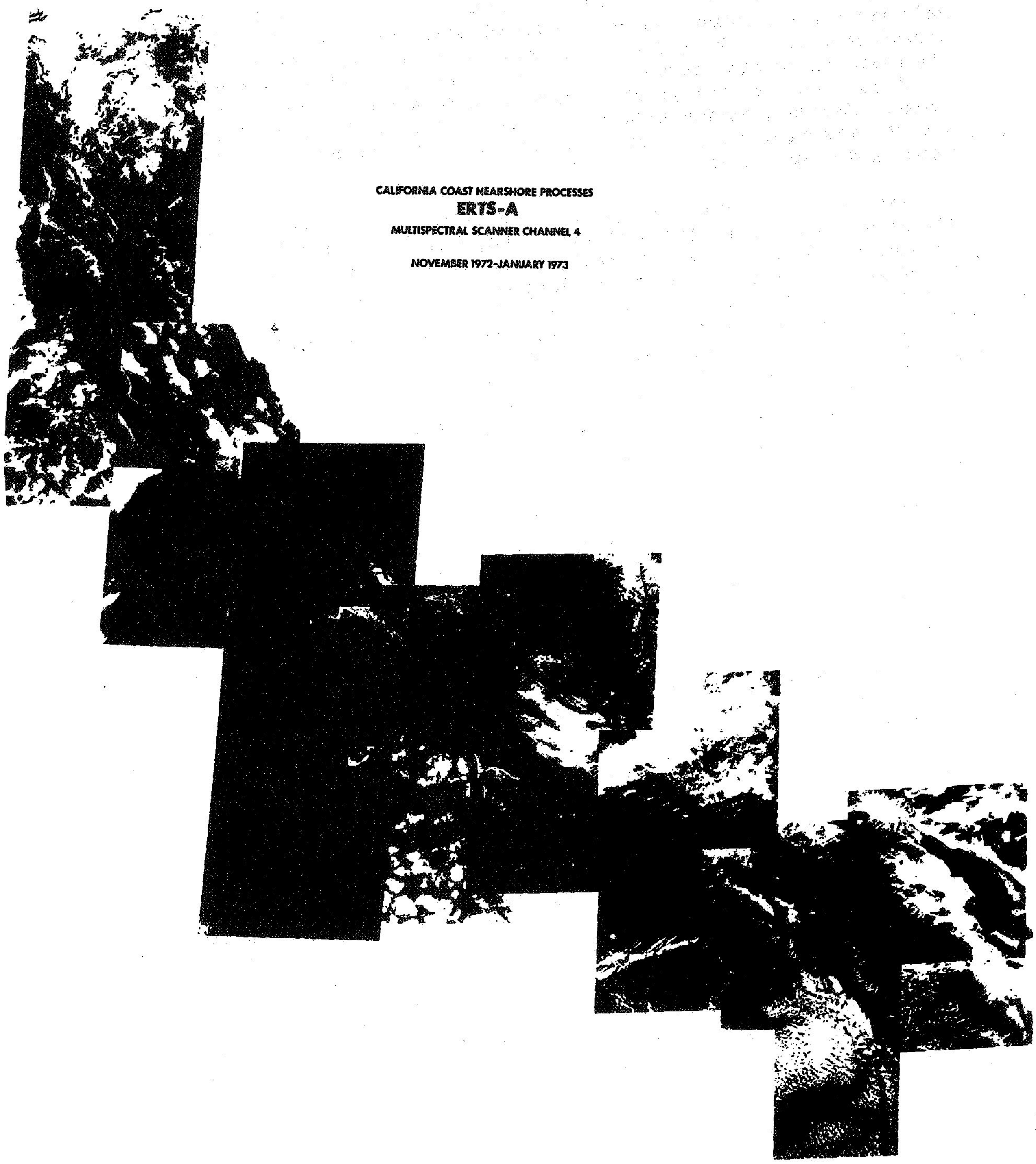

Figure 2. Davidson Current Period Mosaic

and sea truth sources. Figure 2 is a mosaic of channel 4 (5000-6000 A) ERTS imagery which includes scenes judged to most clearly delineate the relative concentrations and dispersal of suspended sediment. The time period covered by these figures is mid-November 1972 - February 1973. The main influencing current on the coast is the California Current which is a part of the great clockwise circulation of the North Pacific Ocean. However, during this period each year, the Davidson Current -- a north moving counter-current--is the dominant inshore transporter of water and suspensates.

The Davidson Current is generally a deep counter-current below 200 meters which flows to the northwest along the coast from Baja California to some point beyond Cape Mendocino. It brings warmer, more saline water great distances northward along the coast. When the north winds are weak or absent in late fall and early winter this counter-current forms at the surface, well to the inshore side of the main stream of the California Current. The evidence for this current is visible on the mosaic and indicated by the temperature contours and current measurements collected from this area. The temperature contours in the eastern Pacific bend to the north along the coast during the height of the Davidson Current activity with the most dramatic changes taking place in February.

In general, the Figure 2 mosaic of this period illustrates the greatest concentration of nearshore northern moving sediments offshore to a distance of 5 to 9 km. At several points along the coast the movement is blocked by large gyres which appear to carry significant volumes of sediment off-coast where they are then transported southward by the California Current. At Pt. Conception a relatively small blockage takes place, but off Pt. Lopez 67 km south of Monterey an extensive offshore movement of sediment takes place. Initial transport here is in the southwest direction to a point about 96 km off the coast where movement changes to the south. Small scale gyres are present near Pt. Año Nuevo, Devils Slide, Pt. Arena, Pt. Delgada and off Humboldt Bay. In each case a counterclockwise gyre is present which carries north-moving nearshore sediments offshore into the south-moving California Current. No attempt has been made to estimate the significant amount of offshore sediment movement occurring during the Davidson Current period.

In the Los Angeles Harbor area material from the Los Angeles, San Gabriel and Santa Ana Rivers are being moved offshore and westward by the influence of the Davidson Current. Inside the harbor itself an east-southeastward current is in effect. Once outside the Los Angeles breakwater a slow moving westward current appears to dominate the nearshore sediment movement. Off Santa Catalina Island, however, transport is in the southeast direction indicating a surface current reversal in San Pedro Channel. Suspended sediments in Santa Monica Bay ring the

bay with a 5 to 8 kilometer wide border. This ring of sediment appears to be escaping the bay area to the west around Pt. Dume. This agrees with the general Davidson Current pattern.

In the Santa Barbara Channel between Port Hueneme and Anacapa Island the westward current domination is observed. The pattern with minor modifications continues to the west of Carpinteria. A counterclockwise gyre is present just east of Santa Barbara and is moving sediment offshore 6 to 8 kilometers. Off Pt. Conception the California Counter-Current in the area between the mainland and the Channel Islands, as described by Drake (1972), appears to pick up these particules and transports them offshore in a complex pattern where they are influenced by the California Current.

The Monterey Bay surface waters are reported to be exceedingly uniform during the Davidson Current period (CCOFI, 1958). The extreme temperature difference between any pair of stations averages a little less than 1°C. No regular pattern of temperature distribution is discernible. The general northern trend of the suspended sediment, however, appears to continue in Monterey Bay as noted on the ERTS imagery. From the area of the Elkhorn Slough north and northwest to Santa Cruz a large gyre of material is present. Little of this material appears to be escaping the confines of the Bay. The blockage of suspensate movement from the Bay appears to be blocked by the counterclockwise gyre activity that is present off Pt. Ano Nuevo.

In the Gulf of the Farallones which encompasses the majority of the San Francisco test cell, a complex surface current and sediment transport system is present. A large clockwise gyre is present off the Golden Gate reaching from the Lake Merced area northwest to the vicinity of Duxbury Pt. Near Lake Merced a nodal point is present separating the large gyre just mentioned from a smaller gyre present off Pacifica. From Duxbury Pt. to Drakes Bay the current appears to be moving sediment in a northwest direction. Near Drakes Bay this current meets a counterclockwise moving current which generally moves around Pt. Reyes. Just north of Pt. Reyes at the mouth of the Russian River the distinct northerly effect of the Davidson Current is illustrated. The majority of the movement takes place within 5 to 7 kilometers of the coast.

The overall effect of the current along the California coast can be viewed in detail on the ERTS imagery. Although the general changes in current direction have been known for some years the complexities within the general currents have not been recorded in detail. Near the coast the effect of the irregular coastline and varying depth governs detailed transport and current direction. This topography and the winds, which sometimes reinforce and sometimes oppose the current, and the significant vertical motion in the region of upwelling and possible oscillations of

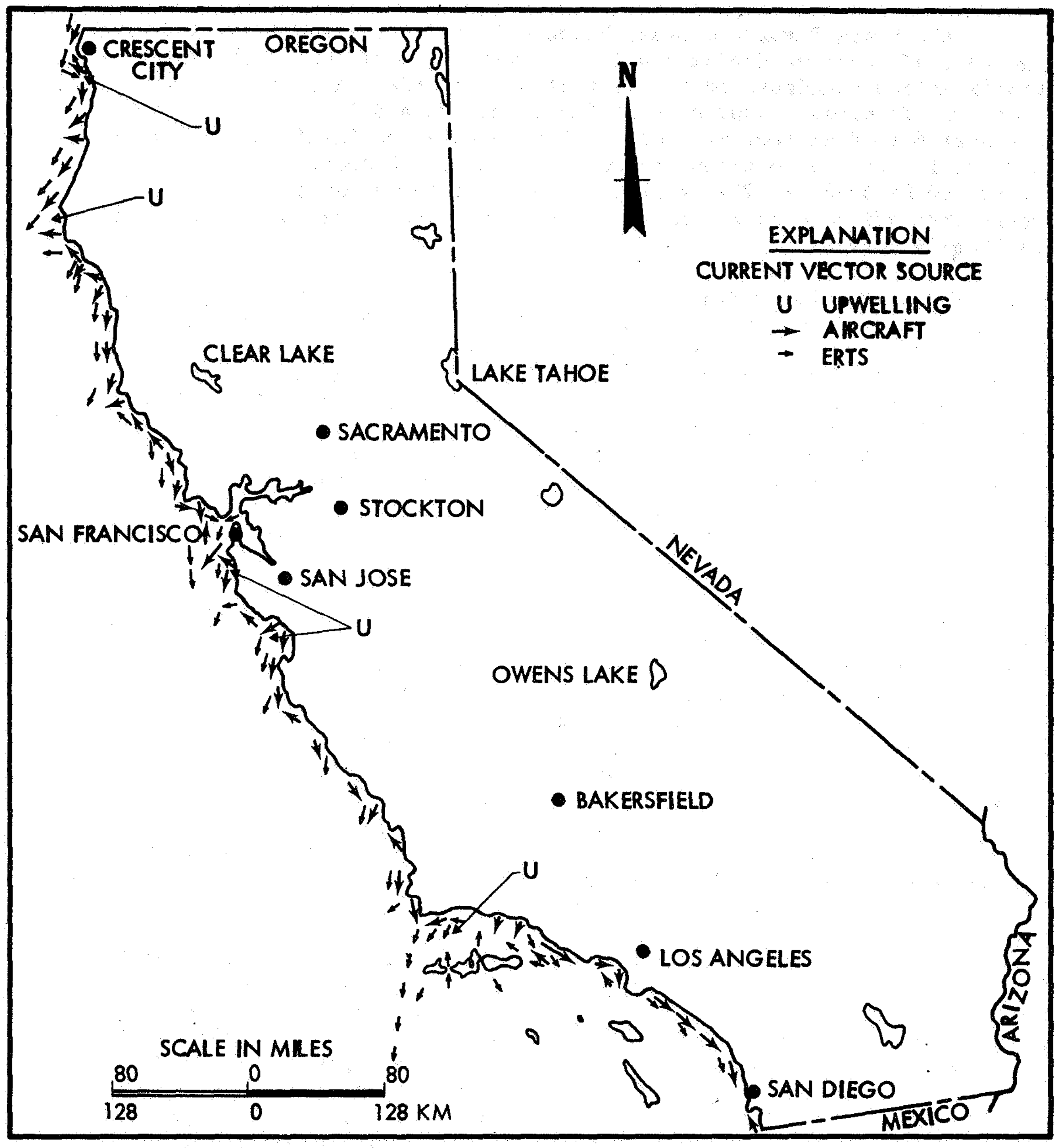

Figure 13. Upwelling Period Current Plot. Nearshore and Coastal Currents Determined from MSS Band 4 (5000 - 6000 Å) Imagery, U-2 and Low Level Aircraft Photography and Sea Truth

Figure 4. Upwelling Period Mosaic

internal waves, all combine to make the measurement of current complex. The synoptic ERTS view of currents as indicated by sediment tracers presents a unique capability to the coastal investigator.

UPWELLING PERIOD

The Upwelling Period is a markedly seasonal phenomena which takes place generally from mid-February to July. An Upwelling Period Current Plot, Figure 3, resulted from analyzing the ERTS imagery mosaic, Figure 4, for the March-April 1973 period. This mosaic is assembled from ERTS channel 4 (5000-6000A) frames. The imagery was picked for clarity and visible suspended sediment content which is utilized as a tracer for studying current movement.

During the Upwelling Period winds parallel to the coast and the Coriolis force move waters offshore allowing deeper ocean water to surface. This effect seems to be intensified south of capes and points which extend out into the current stream and above submarine canyons. On the current plot these processes illustrated as upwellings are located at Crescent City, Cape Mendocino, south of Pt. Conception, Half Moon Bay and Monterey Bay. These colder upwelling waters are often rich in nutrients with the additional result that plankton blooms occur. This is often accompanied by increases in the fish population and is of great interest to the fishing industry.

During the April 16-30, 1973 period, a gradual warming was taking place along the coast with the exception of the Cape Mendocino area. An extensive upwelling extended from near Crescent City to the south of San Francisco and was a variation from the general warming trend. Similar type features on a more local scale were detected by studying offshore tonal changes on the ERTS imagery. Confirmation of coastal processes of this period resulted from aircraft and sea truth measurements similar to those taken during the Davidson Current period.

The effect that upwelling has on the nearshore coastal sediment transport is emphasized and illustrated on the ERTS imagery mosaic. In reviewing historical data on upwelling, it is noted that the exact location of these features are not predictable. The importance of this information to both the understanding of nearshore processes and to the fishing industry is apparent.

TRANSITION PERIOD

The Transition Period mosaic consists of a description of sediment transport and coastal currents for the California coast during the period May-July 1973. This period embraces the end of the Upwelling Period, thus we call it a Transition Period. The excellent imagery available represented an opportunity to analyze the coastal waters surface dynamics between the slowing of the upwelling and the nearshore dominance of the California

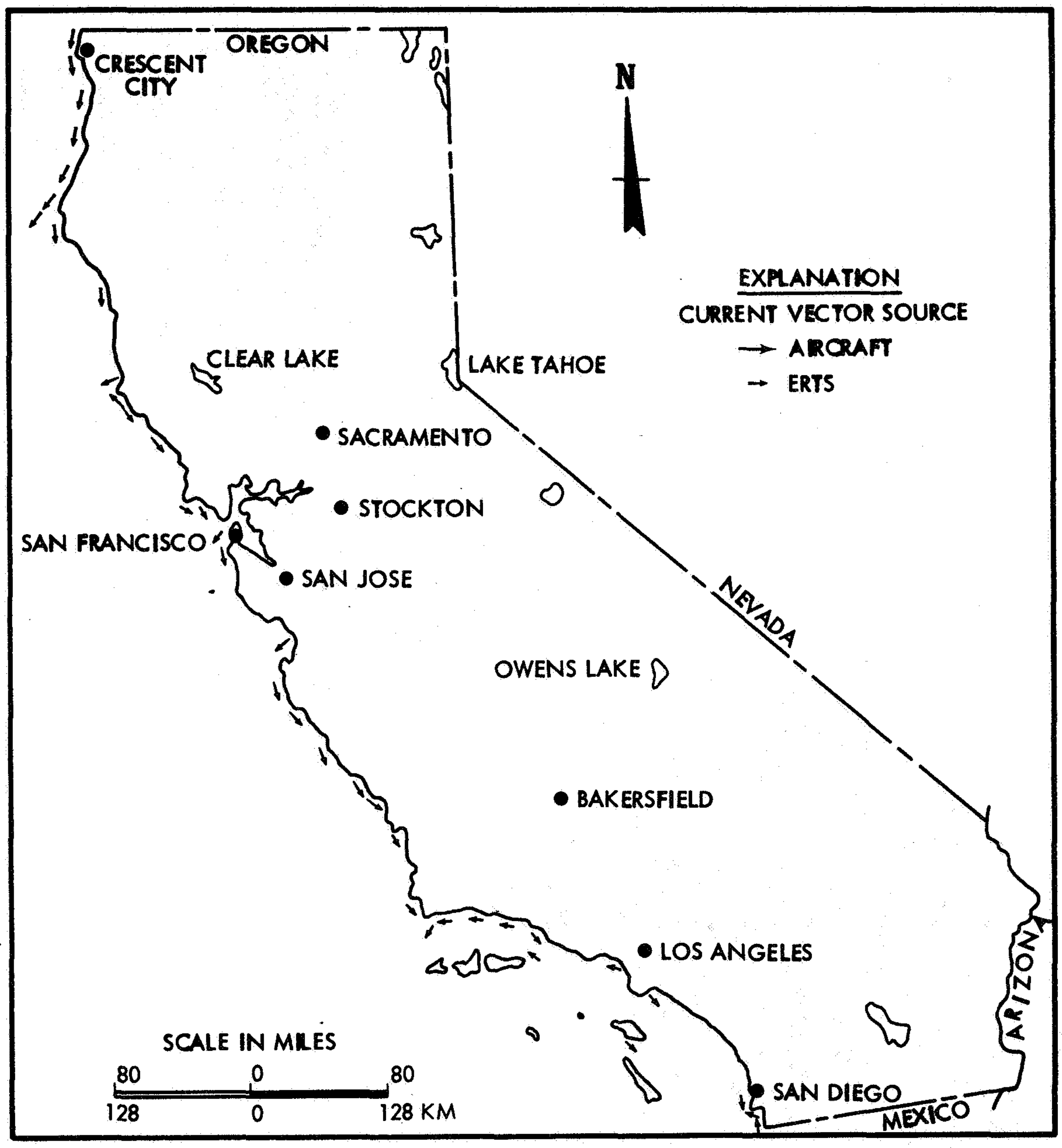

Figure 51. Transition Period Current Plot. Nearshore and Coastal Currents Determined from MSS Band 4 (5000 - 6000 Å) Imagery During the May to July 1973 Period. This represents the Last Two Months of the Upwelling Period and the Beginning (Late July) of the Oceanic Period. Seasonal Lack of Offshore Sediments During This Period Results in Fewer Plotted Currents

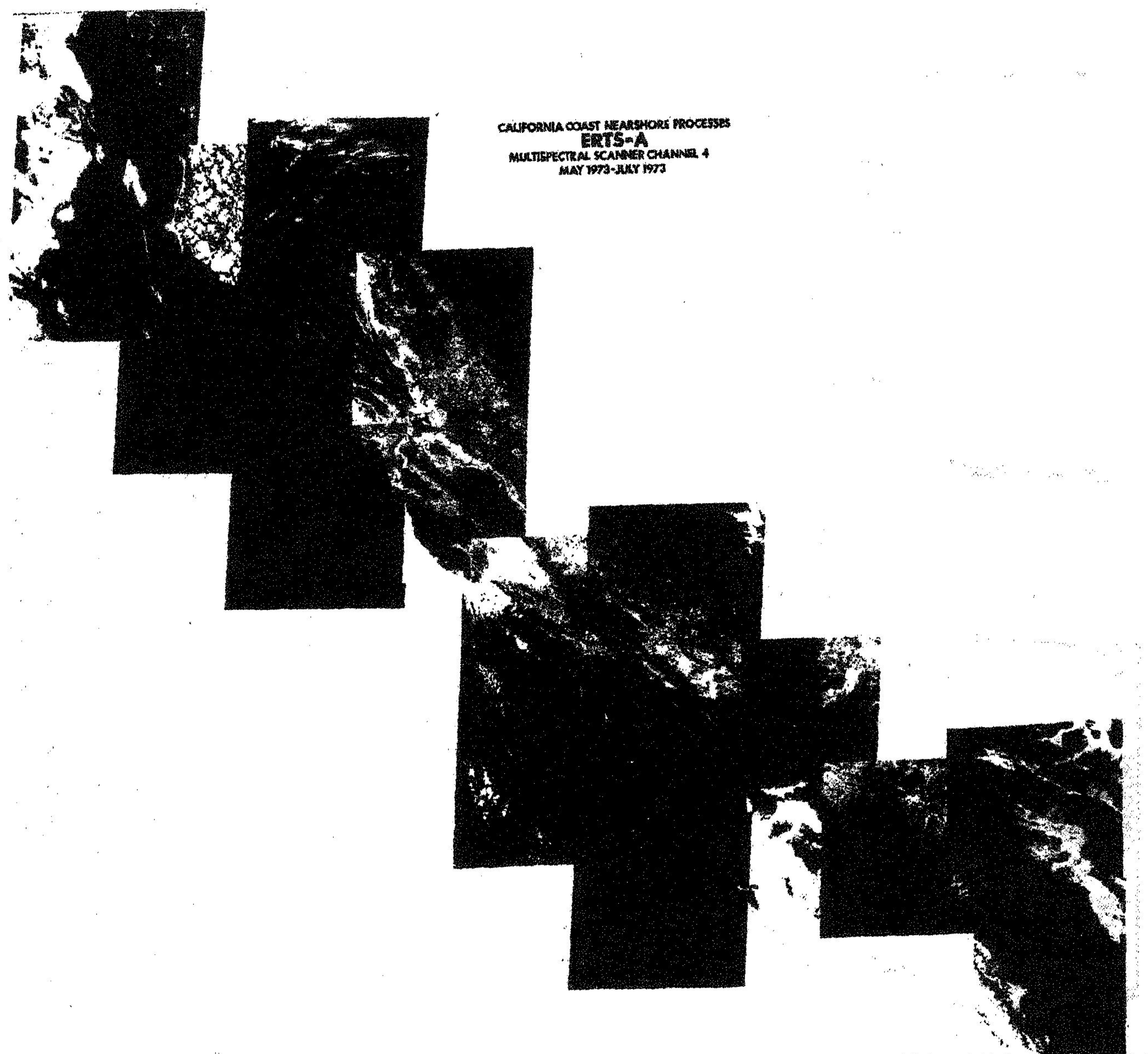

Figure 6. Transition Period Mosaic

Current. As shown on Figure 5, the current along the California coast was generally south during the Transition Period. The mosaic of this period (Figure 6), however, illustrates several areas which were not following this simplified pattern.

Analysis of the Transition Period mosaic indicates several areas of complex offshore sediment transport and gyre activity. These include: Cape Mendocino, Pt. Arena, the Gulf of the Farallones, Pt. Conception, Palos Verdes Peninsula and San Diego. The period represented by this mosaic corresponds to the dry season along the majority of the coast. For this reason there is less riverine discharge and less suspended sediment in the nearshore and offshore area. Erosion of beaches and sea cliffs by longshore currents and storm waves plus natural summer stream runoff still provide sufficient material for detection by ERTS. The major data source for this period's current plot was primarily from ERTS since few aircraft flights occurred during May and June.

The California Current which is always present off the California coast and which is coming into inshore dominance during this period is an eastern Pacific boundary current. It can be described as a meandering, diffuse southward flow, with short-term variations in speed that are of the same order as the mean speed itself. This current which starts south from the area of the Aleutian Islands is modified by upwelling, solar heating, river discharge and exchange with estuaries and embayments. The complex meanderings and changes which occur along the path of the California Current are at least partially detectable by analyzing these ERTS images.

SUSPENDED SEDIMENT ANALYSIS

On a seasonal basis, stable sediment patterns are observed to persist for several weeks with minor changes. *In situ* measurements of suspended sediment as a function of depth and lateral extent show these patterns to be extremely complex in three-dimensional development. Such sediment clouds with either a sharp or diffuse boundary at an intermediate depth, will reflect or back scatter a disproportionate amount of light, thus confounding the film density/sediment load determination. Color of the sediment cloud may be used to identify and assign an appropriate statistical weight in the image merging program, but the morphology of the turbidity cells is complex. Also along the California coast, coastal mountain ranges normally cause surface winds to parallel the coast in an equator-ward direction, thus producing a dominantly offshore sweep for the sun-warmed surface waters. The colder subsurface waters rise to produce both thermal and suspended sediment-type gradients.

What is of concern here is to attempt a calibration of film density in terms of absolute seiment load. Color and turbidity are very much

interrelated in that the particulates which cause water to be turbid themselves selectively absorb and scatter visible energy. Turbidity in water results from the presence of particulates, either organic or inorganic in nature, while color can sometimes be attributed to scattering and absorption by dissolved materials or by the water molecules. A basic definition of turbidity is that it is a means of expressing that optical property of a sample which results from rapid attenuation of light by scattering and absorption by particulates. Although some investigators feel that the weight-concentration of suspended matter in the given optical path is infeasible to correlate with turbidity, the basic problem (illustrated in Figure 7) is showing that normalized transmittance is due to the scatter type (i.e., in the lagoon, in the surf zone, or ocean). A lesser effect (i.e., a few percent per meter) is due to the specific sediment load (e.g., reference curves M3 and M5 of Figure 7).

On the other hand, curves such as Figures 8 and 9 indicate that this may not be correct since it shows an excellent agreement. Indeed, logic tells one that the concentration of particulates in the path will be the dominating factor in a long path length. Size, shape and refractive index are possibly not as important as once thought in terms of scattering. Hence, most oceanographers utilize suspended sediment concentration (organic plus inorganic) as a measure of turbidity. In situ measurements made with a 30 cm Secchi disk, in extremely turbid San Francisco Bay waters show strong correlation of sediment loads to the 4500 Å band film density readings.

The closest ERTS band analog is at 5000 Å. Apparently, the 5000 A band indicates the position of the sediment cloud where the mean density change of the total suspended sediment in water is on the order of 10 milligrams/liter on a volumetric average over the water column.

In deeper water, a critical hypothesis to test is if the net increase in suspended sediment contributes dominantly to the backscattered light. In this case, higher reflectances due to multiple sediment layers at varying depths would be confounded with increased backscatter due to an increase in total suspended sediment.

Since a wide range of sediment samples and simultaneous aerial photography were available from an ONR Bathymetry Study for Portugese Bend and Inspiration Cove on Palos Verdes Peninsula near Los Angeles, they were chosen to test this hypothesis. These waters represent the "median" coastal seeing environment. Although in general, the Portugese Bend sediment load was observed to increase with water depth, both concave and convex gradients as well as linear, increased with depth and were characteristic of individual stations in the raw sample data. These data ranged from a high of 44.9 mg/l to a low of 0.3 mg/l. It should also be noted that these particular data correspond to a period of runoff of terregenous sediment due to rain during the preceding week. Comparison of film isodensity traces

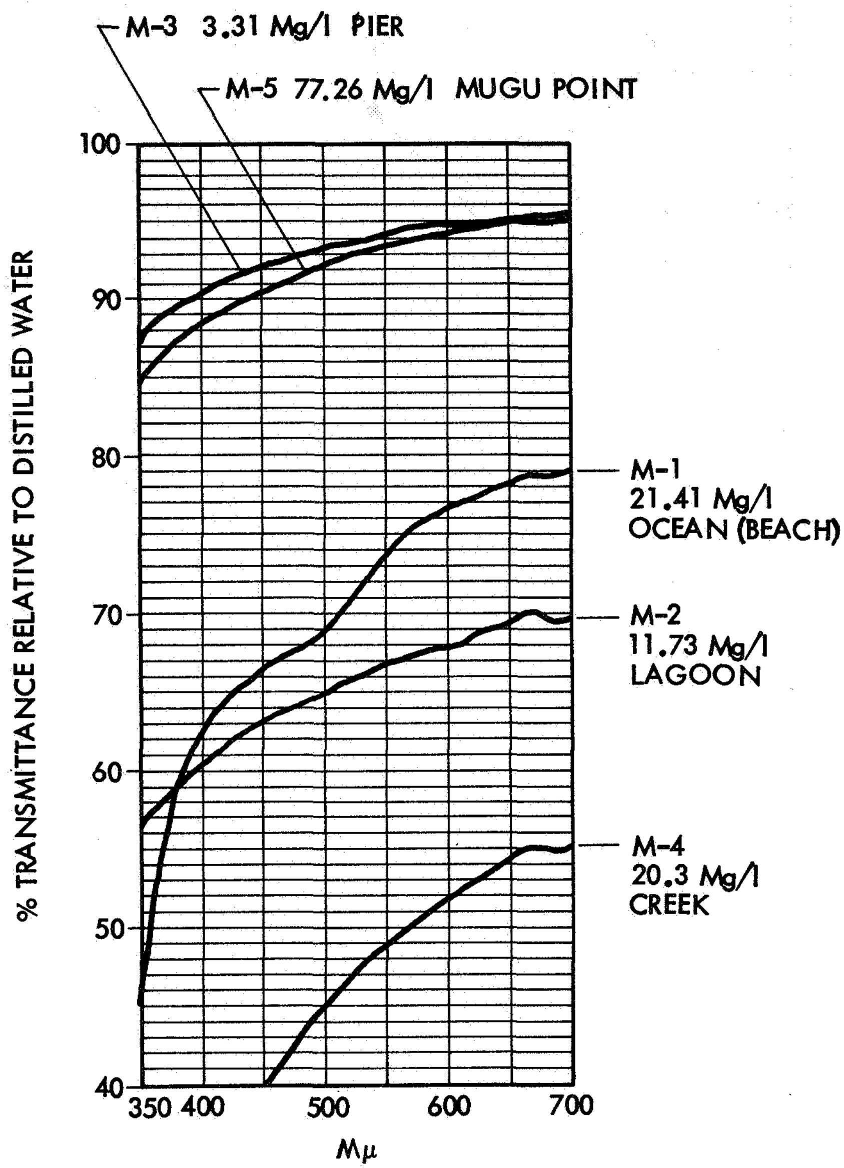

Figure 7. Mugu Lagoon & Ocean Water Sediment Loads and Spectral Transmittance

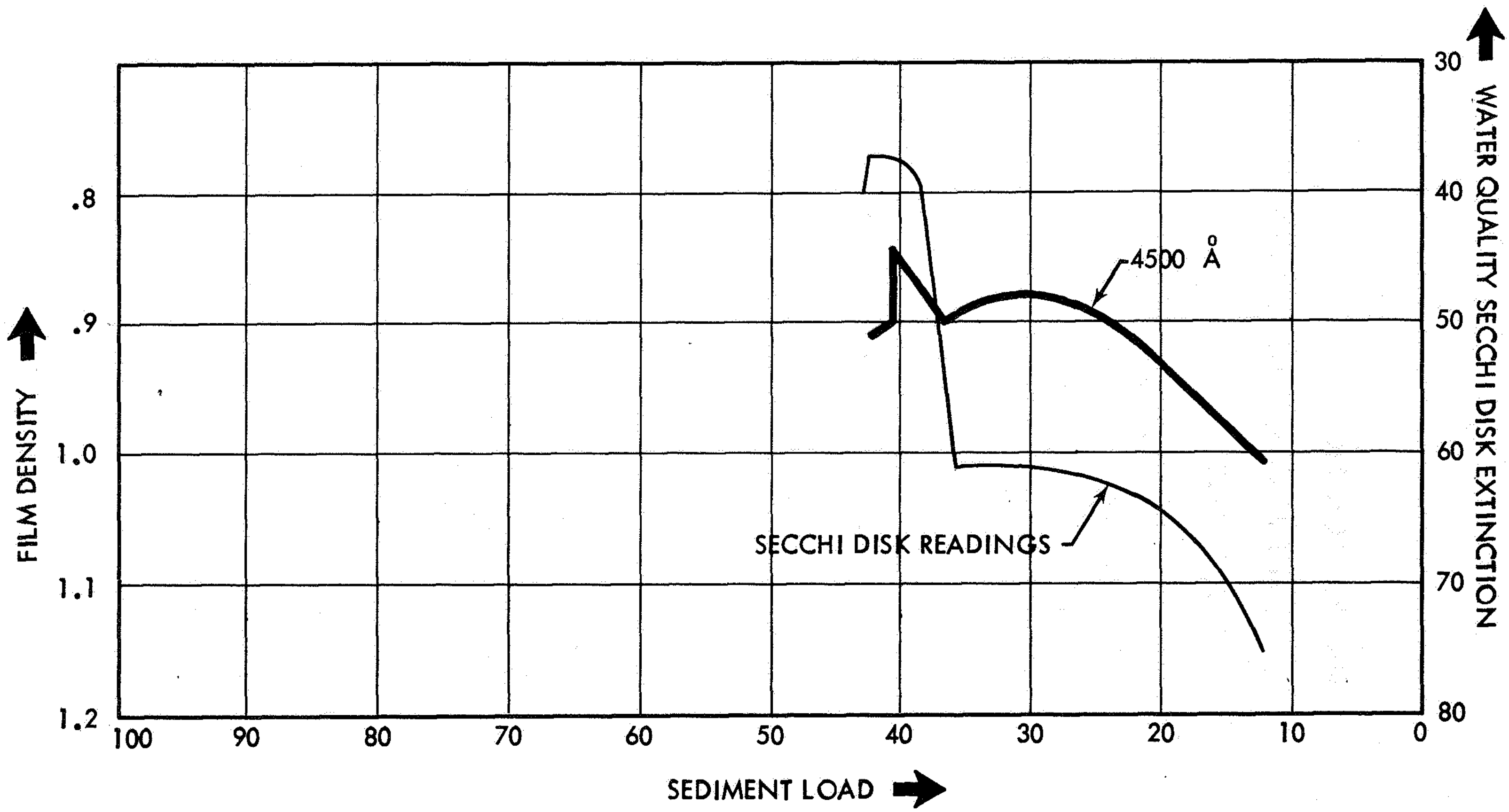

Figure 8. Film Density Vs. Sediment Load & Optical Extinction

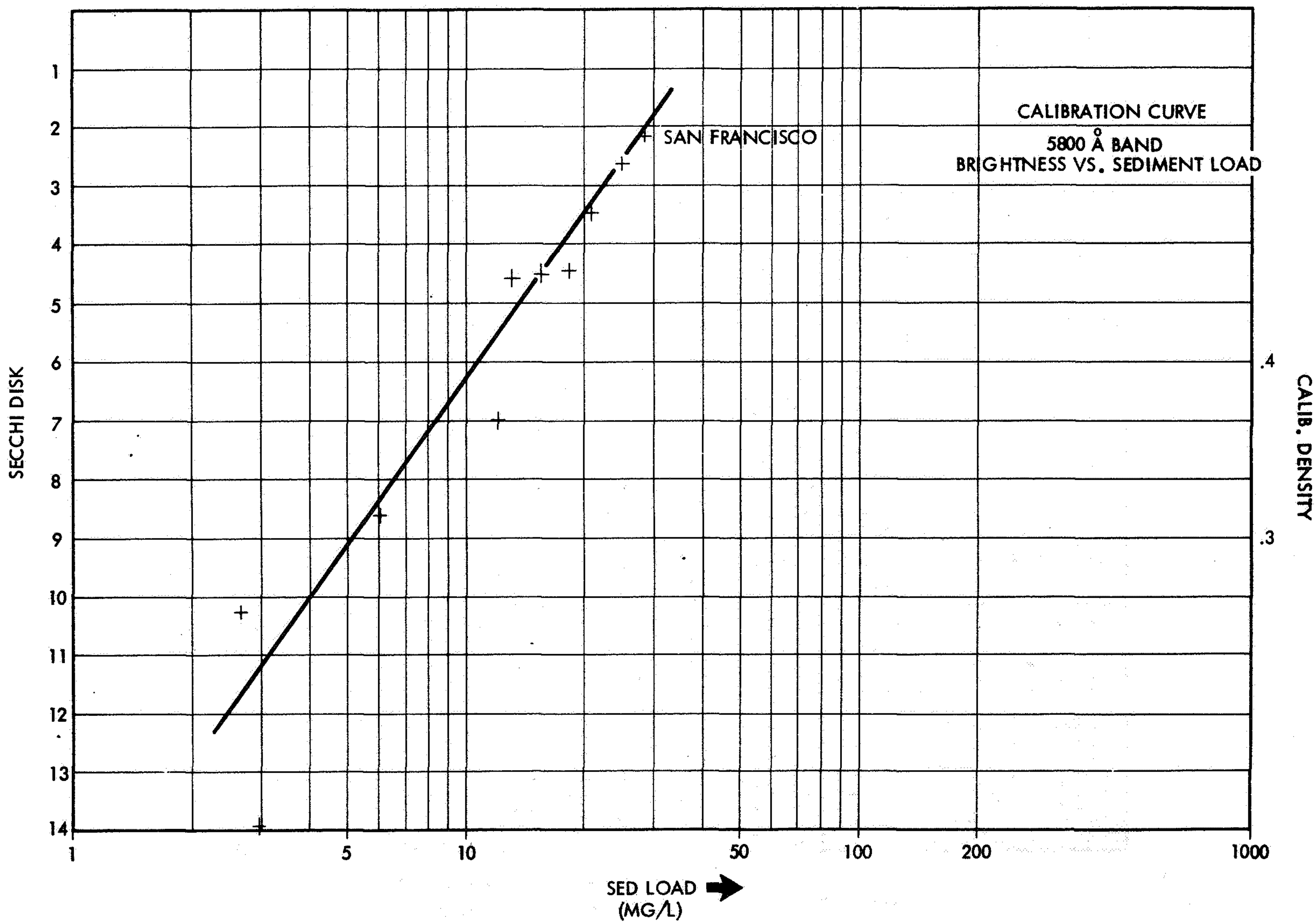

Figure 9. Calibration Curve for Sediment Load Vs. Film Density in Median California Coastal Waters (Film GAMMA = 1)

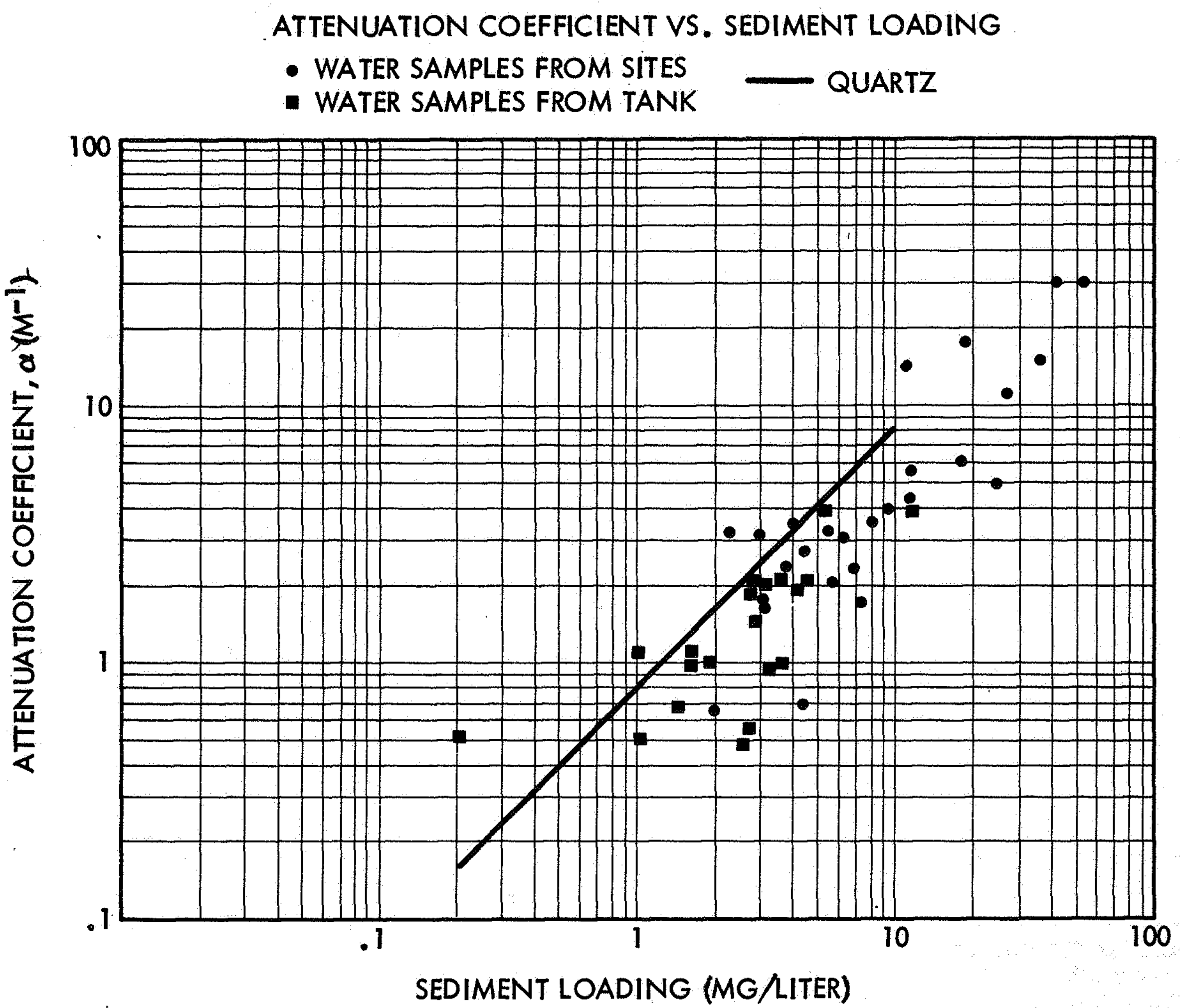

FIGURE 10. ATTENUATION OF BLUE-GREEN LIGHT VS. SEDIMENT LOADING
GHOVANLOU, ET AL 1973

over the sampled area with suspended sediment anomalies at depth showed neither a significant correlation nor anticorrelation. Hence, in the absence of a more extensive sampling grid, simple volumetric averages of sediment load were computed from the water sample analysis. (These ranged from 16 to 4 mg/l.) These showed a "break" at approximately the 6 meter depth contour corresponding roughly to a 10 mg/l decrease in sediment seaward. A visible scum line was also observed in the photography in this vicinity, evidently marking the boundary between these two water types.

These data were employed to derive the film density/sediment load calibration shown in Figure 9. The same calibration was applied to NASA frame 1108-18014-4, Figure 11. Initially it was noted that the negative supplied by NASA did not have the stated densities on its stepwedge. Table 1 provides the recalibration performed.

TABLE 1

Drakes Sediment Level	
Station No.	Mg/l
600	1.1
601	.56
602	2.51 (Avg)
603	3.6 (Avg)
604	15.3
613	0.5
651	4.3
654	3.1
655	4.4

Step	1108-18014-4 Negative (Reference Figure 11)	
	Density (Macbeth)	NASA
15	0.18	0.40
14	0.40	1.31
13	0.62	1.48
12	0.76	1.75
11	0.86	1.87
10	0.96	1.96
9	1.04	2.04
8	1.08	2.10
7	1.14	2.16
6	1.20	2.21

Comparison to the surface sediment sample measurements made by Drake (1972) is given in Table 1. Figure 11 gives the location of Drakes sample stations. These represent milliport filter residues for surface water samples collected in January 1969. Despite the time gap, these are seasonally comparable times and show a reasonable correlation. Note in particular Station 604

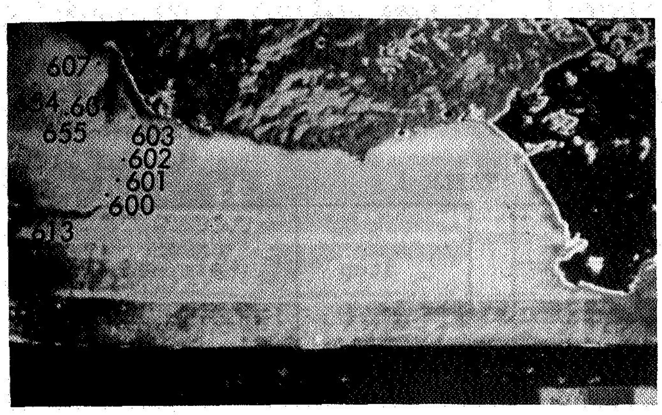

(NASA ERTS Frame 1108-18014-4)
8 November 1972

Sediment Load
Key: (Interpolated from Figure 9)

Dark Blue	-	1- 2 mg/liter	
Medium Blue	-	2- 3 mg/liter	
Light Blue	-	3- 4 mg/liter	
Light Green	-	4- 8 mg/liter	insensitivity may be due
Dark Green	-	8-15 mg/liter	to reciprocity failures.

Figure 11. Tentative Mapping of Near-Surface Suspended Sediment from ERTS Imagery

of Figure 11 which shows 15.3 mg/l in Drakes data versus 8-15 mg/l estimated from the ERTS frame (Figure 11) and the sediment load film brightness relationship derived from airborne data (Figure 9). Further testing and sampling to determine the accuracy of this methodology is now underway.

FLYING SPOT SCANNER ENHANCEMENTS (FSS)

Imagery, enhanced and improved for nearshore sediment detection and delineation, has been recorded on film from NASA computer compatible tapes (CCT). Geosource's modified flying spot scanner (FSS) system is used to convert NASA digital data to hard copy film. This film writing/reading system uses a high resolution CRT as a light source for data processing. A spot size of 0.7 mils can be achieved when normal brightness and signal levels are employed.

Data on a 9-track 800 BPI tape is directly applied to the system at a real time rate. Recorder playback clocks are used to discretely position the CRT spot through one of five fixed digital rasters.

Horizontal and vertical deflection is provided from two 12-bit digital to analog converter (DAC's). The Z-axis modulation of the CRT's intensity is performed after digital to analog conversion of the video. Video gain and level manipulation are controlled through a wide bandwidth video amplification stage to provide signal levels yielding optimum film gamma for every scene.

Enhancement Technique

NASA Original Bulk Imagery displays the scene's dynamic range within the film's available gamma range. Typically, however, the sediment features which are of particular interest on this nearshore processes study are represented in only a small portion of this gamma or density range. Thus, the sediment features have a relatively low contrast as compared with that which can be achieved during film recording. Figure 12 portrays a typical example of how the contrast of sediment features can be enhanced. Part (a) of the figure is a direct print from a MSS band 4 negative. The scene displays a nominal contrast with white or light clouds in the northeast corner and a dark density or black in the ocean regions. This print was exposed on poly contrast Kodak paper with a No. 3 filter to increase the contrast of offshore sediment features.

The (b) part of Figure 12 is a print from the negative recorded on the FSS using the analog preprocessing technique. A comparison between the matching images immediately illustrates the advantages of controlled playback exposures. NASA imagery must be recorded on film in such a way that all signal levels are within the film's density range. It would not be practical or desirable for NASA to generate negatives with exposures

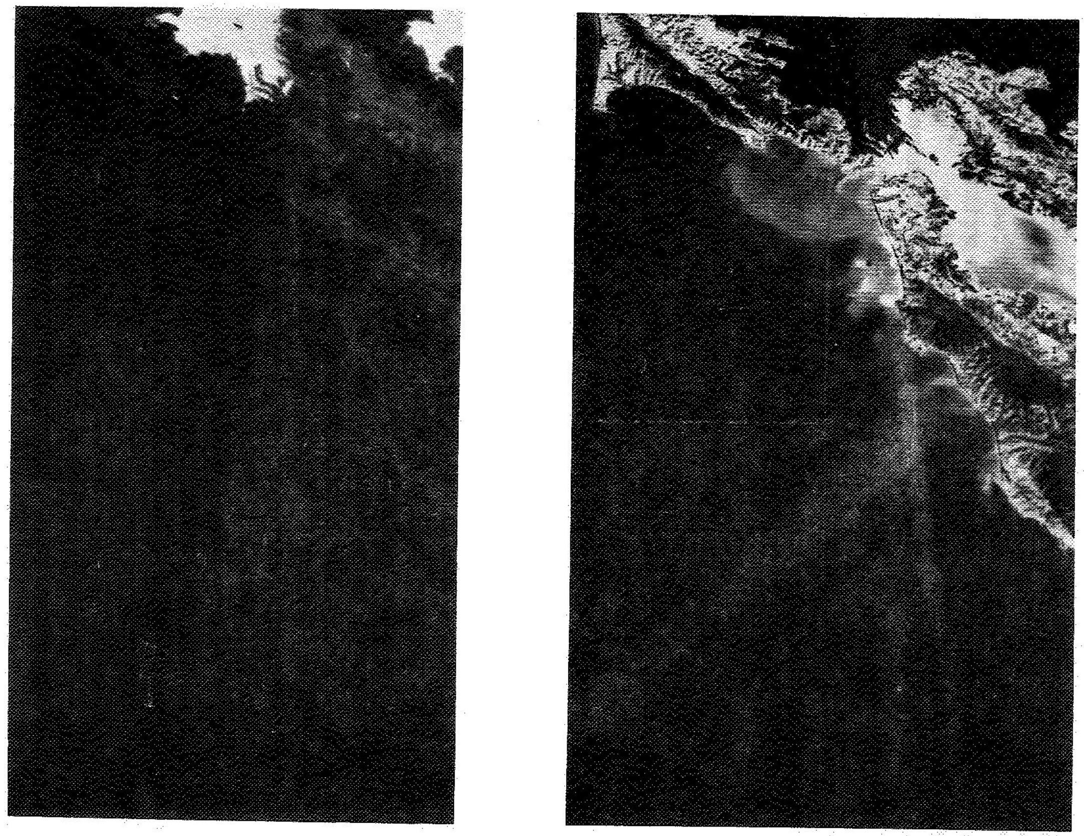

(a)
1130-18235-4 ORIGINAL

(b)
1130-18235-4 FSS

Figure 12. San Francisco FSS Enhancement
Scene 1130-18235-4

Note gyre in the Gulf of the Farallones and offshore sediment movement south of Half Moon Bay (in b).

optimized for only selected portions of any scene's signal range. However, for special features of interest, such as offshore suspended sediment, its signal range is limited and relatively small.

This small signal range can be amplified prior to recording as demonstrated here so that maximum contrast between sediment features can be realized. To contrast-enhance features within any scene, two signal processing techniques are available in the FSS system. One method employs standard analog amplification methods (Analog Preprocessing Technique) to control the signals gain and DC level setting. The alternate method is a hybrid digital/analog technique. In this method the eight-bit parallel digital data is shifted at the input to the digital to analog converter (D/A) to achieve the appropriate gain. By this second method, discrete steps in gain of 2/1 can be applied to the input signals. The D/A output is then fed through a unit gain analog amplifier where DC offset is controlled. In the application of either of these techniques for enhancing ERTS scenes, particular problems may present themselves. Thus, a more detailed discussion of these techniques in a total system context is presented below.

1. Analog Preprocessing Technique

The exposure of the FSS negatives is a function of numerous parameters and systems settings (CRT voltage or brightness, signal levels, scan rate and raster size, lens aperture, and film characteristics, etc.). To reduce the effect and randomness of these variables, an analysis of FSS system performance was undertaken as they applied to ERTS data reduction. It is necessary to understand at this point that all parameters and settings have been standardized or fixed for the ERTS data task. This approach of formulating a standard system configuration and data reduction procedure is necessary so that consistent optimum high quality products can be produced. Additionally, the processing time has been reduced to a minimum. All other parameters being fixed, the film exposure is now only a function of the signal levels present at a system monitoring point. This point is in the video chain at the output of the analog video preprocessing amplifier prior to being input to the electron beam video drive amplifier. A signal swing from 0 to 0.5 V will result in a log film density of 0.41 to 2.25

The digital data from the tape deck is converted to analog signal for preprocessing prior to film recording. The video amplifiers are used to control the signal gain and DC level so that the signal levels are within the 0 to 0.5 volt range. For a normal exposure, the total signal range of any scene is adjusted so that it is within this voltage window. To enhance the contrast sediment features, the signal levels are increased by virtue of the analog gain controls so that the video signals representing sediment features swing from

0 to 0.5 V. As noted above, the application of this analog gain to enhance features presents an additional problem. This problem is that signals from other features, such as land, beach, etc., have also been amplified. These signal levels are larger than the maximum desirable signal level of 0.5 V. Recording of this amplified full dynamic range signals would result in poor imagery, as well as presenting potential damage to the CRT. The large signal levels present two problems. Firstly, these larger signals could saturate the post amplification stages of the video amplifiers, thus causing holdover of the video signals in regions of land-water interfaces. Secondly, and more important, the excessive signal level will overdrive the CRT brightness. This would result in an increased CRT spot size, internal light scattering, and thus a fogging in the imagery. To eliminate these problems a signal limiter has been incorporated into the video chain. Gain can be applied to the video signal, but the output signal range is fixed to 0 to 0.5 V. This gain, applied to the raw video, results in contrast enhanced sediment feature in the final film negatives. The amount of enhancement is a function of the gain applied.

2. Hybrid Digital/Analog Technique

The second preprocessing technique available for contrast enhancement employs all the capabilities and system settings as described in the analog discussion. The single exception is digital gain. It must be remembered that to perform contrast enhancement, one must control signal levels, and this must be done within system constraints, thus, the limiter function. In the analog case, the gain is continuously controllable from 0 to 100. Thus, it is difficult to repeat amplifier settings, or to specify differences between settings. This is not to say that the system cannot be calibrated to get such information. However, additional steps are required. The digital techniques allow us to apply gain in discrete multiples of two. This technique then yields the same results, signal gain, but in known multiples. The procedure is simple and straightforward assuming a basic knowledge of digital to analog converters.

The two techniques described above are those used to control signal gains. Other techniques are available for application to the analog signal. These include non-linear amplification, thresholding, and differentiation. Each technique yields an enhanced image; however, for sediment detection and delineation, contrast enhancement yields the optimum results.

FSS Modification and Improvement

The analysis referred to in the above text has improved the data product as recorded on the FSS system. Extensive analyses was directed toward isolating problem areas in the FSS system which in the past prevented

producing imagery displaying resolution that improved on prints from NASA original negatives. In the past, the FSS system has been used to generate imagery with enhanced sediment features (e.g., gain control was used to increase the contrast of the sediment anomalies).

This analysis resulted in isolating three major problem areas: (1) CRT dynamic focus, (2) the recording lens, and (3) the recording film. The dynamic focus power supply was readjusted so that the CRT spot remains focused at all points on the CRT face. Additional shaping circuits were incorporated and a complete adjustment made to yield an optimum dynamic waveform. Secondly, a new recording lens was installed into the system. The result was an increase in the modulation transfer function of the optics and a sharp image plane. Care was taken during installation to achieve a critical focus in the image plane. The third problem area was the film used for recording. Additionally, the recording procedure was standardized to reduce the time required to playback an image. Candidate films were reviewed based on their characteristic curves, granularity, and spectral sensitivity. Additionally, a requirement for red light insensitivity to make handling easier was imposed. The film picked was Kodak TRI-X Ortho type 4163*. Test exposure and processing times were tried to determine a standardized procedure. This resulted in a relationship between input voltage levels and film densities. The following table shows this relationship:

Input Voltage Level	Log Film Density
0	0.41
0.1	1.03
0.2	1.50
0.3	1.93
0.4	2.15
0.5	2.23

*Processed in D-19 at 68 F for 7 minutes.

Data from CCT of frame 1183-18105-4 was used during the first test runs. These runs showed another problem. If the signal levels of interest are between signal levels, both above and below their levels, the signals larger than those of interest become too large as gain was applied to the signal. These signal levels actually become large enough to damage the CRT phosphor or the light level increase to a point which results in fogging of adjacent data. To remedy this problem, a signal limiter was incorporated into the video section of the FSS. This is displayed on the imagery as a fold-over condition as illustrated by the black clouds in Figure 12-b. As the signals level increases to this safety threshold, the film image is increasing in density. Once the signal increased past this level, the resulting density is folded over to clear and remains there until the signal level falls below the safety threshold level.

The incorporation of the above modifications and procedures resulted in improved FSS imagery. The new imagery displays resolution comparable to NASA originals. Thus, enhanced data can be recorded with little reduction in resolution.

COMPUTER PROCESSING OF CCT

Digital processing activity for this study consists of two major efforts: (1) develop the software and techniques to convert bulk CCT's to formats compatible with existing hardware and software systems and (2) develop the software to interface ERTS digital tapes with contouring programs to generate radiance contour maps for use in determining near surface suspended sediment in the California nearshore areas of interest. The primary objective of this processing is to provide a means for analyzing coastal sediment distribution.

MSS bulk CCT's provided by NASA are organized into groups of tapes which depict a scene approximately 185 kilometers square. There are four tapes of each scene containing multispectral information on one strip 46 kilometers wide.

The software programs developed convert these bulk CCT's to a flying spot scanner (FSS) compatible tape produced for each spectral band. To achieve this compatibility certain conventions were adopted as illustrated in Figure 13 and described below.

The FSS line format requires that input data be organized in lines of lengths of 256, 512, 1024, 2048, 4096 points (bytes) each. A 46 km strip from bulk tape consists of lines with 870 points (bytes) each. The 1024 byte line length required by the FSS was achieved by adding to the data, dummy bytes at the end of each line.

Similarly, the standard number of lines selected for scenes to be reproduced on the FSS was fixed at 1024. Since each 46 km strip is 2340 lines, the adopted convention results in three blocks of data per spectral band for each strip. The last block actually consists of only 292 data lines, the remaining 732 lines are dummy data lines inserted during processing.

Figure 14 is a photograph of a 46 km strip reproduced and enhanced on the FSS from bulk CCT data (note the block sizes). This is a direct reproduction of the bulk CCT data and has not been corrected to any degree. Future software developments will include the incorporation of de-skewing options to the FSS compatible tape generation programs. The overlay shown depicts the area selected for subsequent processings. This figure and all others showing CCT data were generated using spectral band 4 tapes since they have been previously identified as having the best reflectance characteristics for identifying suspended sediment in ocean waters.

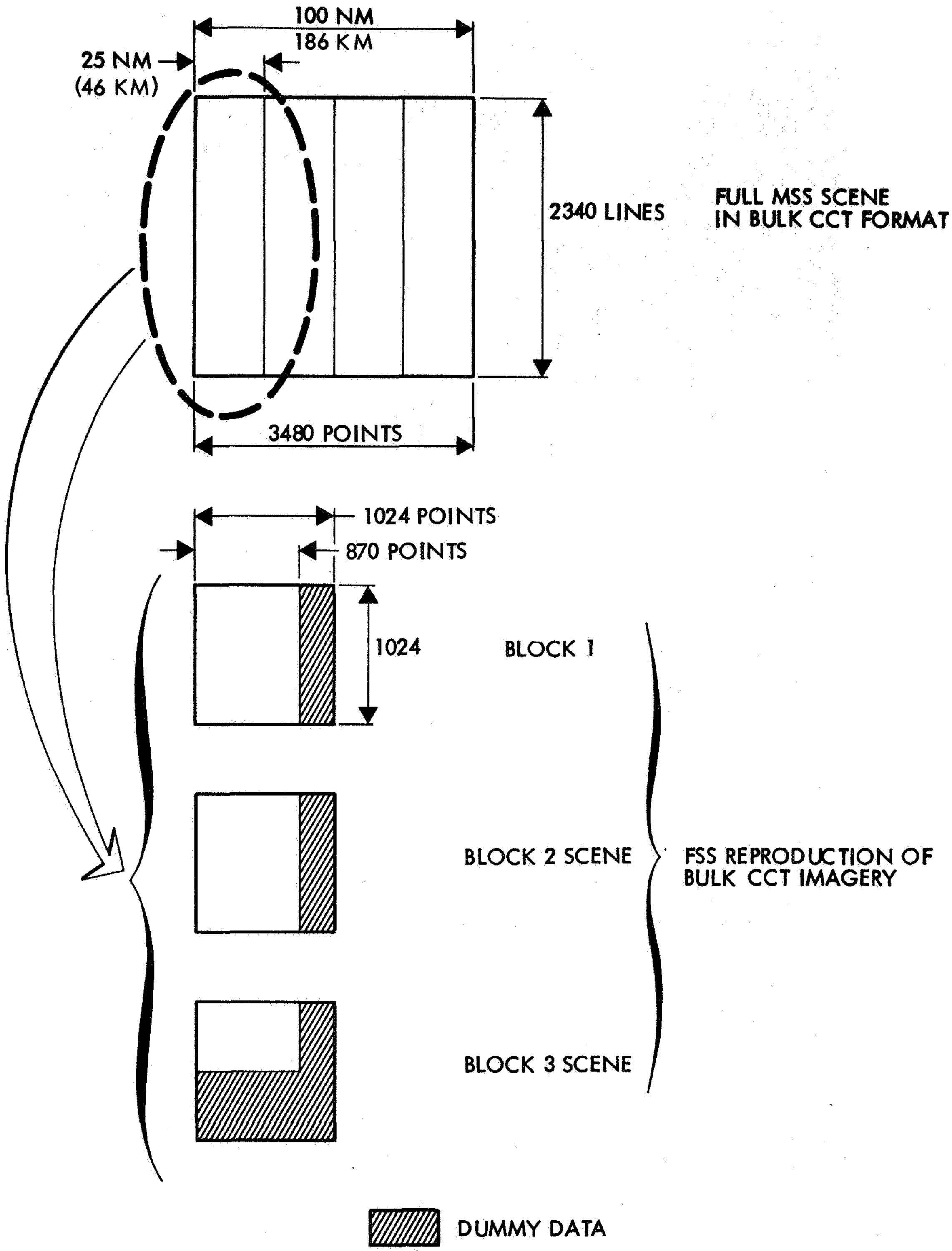
100 NM
186 KM
25 NM
(46 KM)
2340 LINES
FULL MSS SCENE IN BULK CCT FORMAT
3480 POINTS
1024 POINTS
870 POINTS
1024
BLOCK 1
BLOCK 2 SCENE
BLOCK 3 SCENE
FSS REPRODUCTION OF BULK CCT IMAGERY
DUMMY DATA

Figure 13

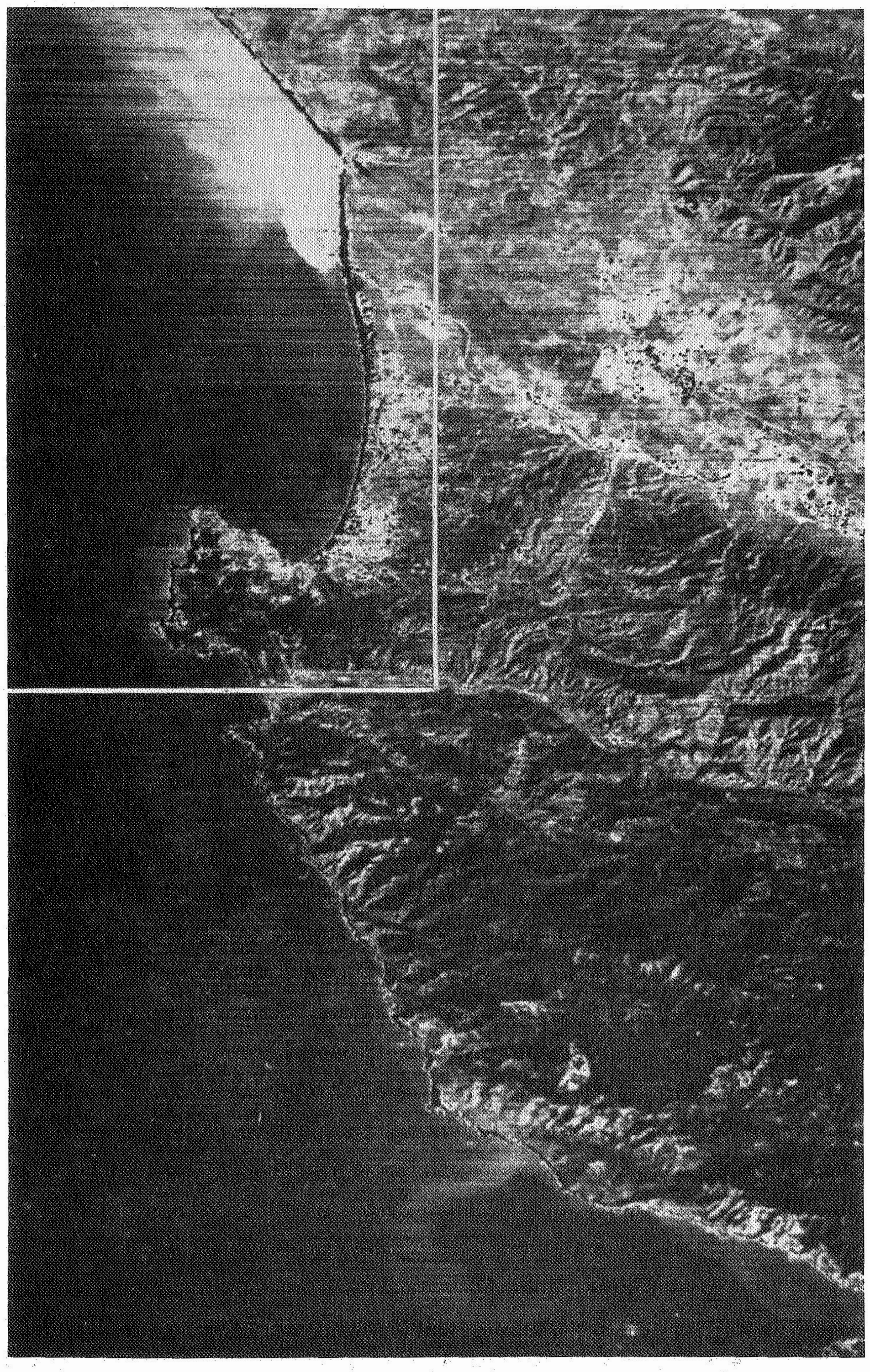

Figure 14. FSS Enhancement of Monterey Bay
Area of contour map Figure 15 shown - Scene 1183-18182-4. January 22, 1973.

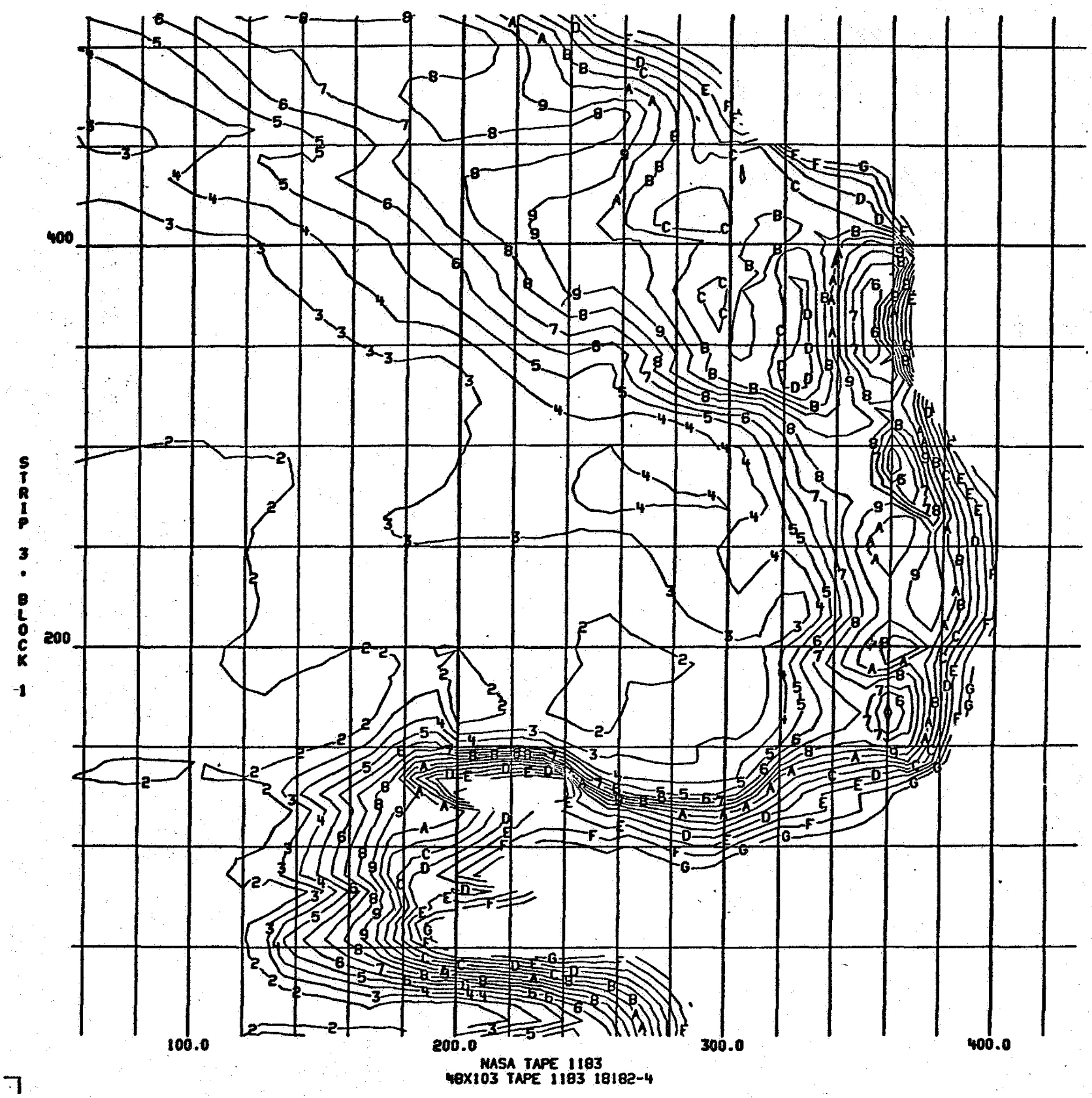

Figure 15. Monterey Bay Contour Map

CONTOURING PROGRAMS

The contouring programs were used to generate plots of reflectance contours around the Monterey Peninsula as shown in Figure 14 as well as other California sites. Briefly, this contouring process requires the following steps.

1. Spectral Channel Selection - A specific rectangular area within the 1024 x 1024 scene can be selected during the sampling process. The contouring program is sized to accept a maximum of 4900 data points.

2. Area Size Selection - By appropriately designating the sampling rate, areas of various sizes can be selected for contouring. For example, a 1024 x 1024 block represents a 46 x 46 km area. Therefore, a square array of data points (64 points long on each side 64 x 64 = 4096) can represent the full scene (46 x 46 km), 1/4 th scene, 1/8 th, 1/16 th or 1/32 nd depending on whether a sampling rate of 16, 8, 4, 2 or 1 is selected.

3. Digital Dump Selection - The data points representing the area selected are punched on data cards and may also be dumped on the line printer for verification.

4. Data Smoothing - Once a specific data block has been selected, a smoothing program is used to operate on the data. This involves using multiple regression surface fitting technique that eliminates scattering in the data values. This approach yields a set of data values which when contoured will reflect large area sedimentation patterns rather than localized variations.

5. Annotation Selection - During the contouring and annotation process, several formatting parameters can be specified: (a) a grid is superimposed on the contours and may be located to represent latitude and longitude lines; (b) the ratio of physical distance covered by equal numbers of points in the X and Y directions may be specified; this is useful in working with bulk data since 185 km in the X direction is represented by 3480 points while only 2340 points represent 185 km in the Y direction. This distortion may be corrected in the contoured plot by simply specifying this ratio.

A step external to the above process was incorporated in the generation of the contours shown in Figure 15. This consisted of using spectral band 7 as a reference to generate the shoreline. The characteristics of this band are such that the reflectance levels of land features are significantly

higher in value than reflectance levels of water features (typically, water reflectivity value range is 0 to 3 and land reflectivity values range from 11 to 15), therefore the shoreline can be easily discerned. A digital printout of band 7 was used to locate the shoreline on a similar printout of the identical area in band 4. The land mass was then masked and assigned a large reflectance value that would produce a distinct contour in the final output.

APPLICATIONS

Numerous potential sites along the California coast are being considered for coastal or river construction. Although each site requires a thorough ground survey, it is evident that analysis of ERTS imagery results in valuable input to an overview of the coastal dynamics. The possible effect of a dam on California's Mad River is a good example. A study by the Corps of Engineers of the ocean beaches in the vicinity of the Mad River mouth (near Humboldt Bay, California) was made with the purpose of developing a conceptual model of the coastal processes in the area and forecasting the effects of a proposed upriver dam. Included in the Mad River analysis was an interpretation of ERTS imagery for seasonal changes in nearshore currents and sediment transport. This interpretation resulted in knowledge of details of offshore as well as nearshore surface dynamics. As ERTS coverage continues, it will be possible to build accurate and comprehensive historical records for such sites. In many studies, this type of historical data is not available for use in monitoring existing coastal phenomenon or for planning future coastal modifications.

Some of the projects along the California coast for which large sums of money are spent yearly by the Corps of Engineers are: dredging, harbor design and development, placement of groins and shore protection projects. Since the first Corps project in California, the improvement of San Diego Harbor in 1852, there has been a continued variety of coastal improvement programs. The dredging of Santa Cruz Harbor, Ventura Marina, Channel Island Harbor and Oceanside Harbor currently costs $1.5 million per year. The placement of groins along Newport Beach was a $2-million project. Maintenance of Humboldt Bay waterway presently runs about $100,000 per year and a recent reconstruction of the bay protective structure cost about $10 million. It is not presumed that all these dollars will be saved by the new data from the ERTS study, but it is expected that the resulting nearshore processes information will result in more effective use of the dollars spent. For example, the placement of new breakwaters, if warranted from the study of sediment transport, could eliminate or reduce the dredging costs of port facilities. The analysis of riverine discharge might result in plans to eliminate or reconsider upriver waterway construction resulting in a continual supply of sediment for the beach areas. This study will also benefit the public by providing information for the engineering of new harbor or beach protective construction that will reduce storm drainage costs to private and public facilities.

In addition to the utilization of ERTS data in the Mad River study, the Corps of Engineers has applied preliminary ERTS data to a study of the Russian River beaches to determine erosion and environmental effects due to possible losses of sand transport. In the West Coast Deepwater Port Facilities Study ERTS imagery was found effective in the analysis of environmental effects that could accompany oil spills, thereby allowing the positioning of proposed anchorage sites to minimize environmental damage. The cooperative study of the Salinas River watershed area has been using ERTS to determine the distribution of contaminates from the river in Monterey Bay and the California Coastal Commission is utilizing our ERTS reports for long range planning of the coastal zone. From remote sensing data derived from ERTS as well as aircraft, the most effective positioning of the dredged material from the maintenance dredging of Crescent City Harbor, California, was determined. These are only a few of the applications for which ERTS data have been utilized.

An important Federal application of ERTS to be realized in the near future is in conjunction with the dredged material disposal studies where the surface distribution of heavy metals, pesticides and organics that are present in silt and clay matrices can be forecasted; and, with other types of monitoring, the possible environmental effects will be resolved. This same type of application is appropriate for stream, river, estuarine and outfall effluent monitoring.

Finally, with ERTS-A data covering the monthly and seasonal variations of the nearshore currents as well as with possible future satellite data, the computer programs designed to analyze littoral drift along the California coast will be modified to include the nearshore seasonal current drift component necessary to increase the accuracy of sand transport prediction.

CONCLUSIONS

The objectives of this study have been to analyze nearshore currents, sediment transport, and estuary and river discharges along the California coast through the use of imagery from the ERTS satellite. During ERTS overpasses, airborne and sea truth data have been collected for comparing and confirming details of nearshore processes that are detected on ERTS imagery.

The major conclusions that have been described in this paper are as follows: (1) Distinct seasonal patterns for sediment transport as a function of ocean current systems and coastal morphology are being identified. (2) Large scale sediment plumes from intermittent streams and rivers extend offshore to heretofore unanticipated ranges. Areas where these plumes contain possible contamination from on-land activities can be traced in detail. (3) Computer generated contouring of radiance levels from NASA-CCT, result in charts that can be used in the determination of surface and nearsurface suspended sediment distribution. (4) Flying Spot Scanner enhancements result in excellent detailing of nearshore

features and (5) Data from this study is providing significant information for coastal planning and construction projects.

ACKNOWLEDGMENTS

Acknowledgment is gratefully made to the National Aeronautics and Space Administration (NASA), and the Corps of Engineers, U.S. Army, for access and permission to use this study material. The views of the authors do not purport to reflect the position of the National Aeronautics and Space Administration or the Corps of Engineers, Department of the Army, or Department of Defense.

Contents of this paper are not to be used for advertising or promotional purposes. Citation of trade names does not constitute an official endorsement or approval of the use of such commercial products.

REFERENCES

CCOFI, 1958, California Cooperative Oceanic Fisheries Investigations: Progress Report, 57 p.

Drake, David Edward, 1972, Distribution and Transport of Suspended Matters, Santa Barbara Channel, California, unpubl. Ph. D. dissertation, University of Southern California, Los Angeles, 356 p.

Drake, David E. and Donn S. Gorsline, 1973, Distribution and Transport of Suspended Particulate Matter in Hueneme, Redondo, Newport and La Jolla Submarine Canyons, California: Contribution #316, Dept. of Geological Sciences, University of Southern California, Los Angeles.

Ecker, Richard, 1973, Personal communication on study of Mad River mouth and adjacent beaches: U.S. Army Engineering District, San Francisco, California.

Ghovanlou, A.H., G.D. Hickman, and J.E. Hogg, 1973, Laser Transmission Studies of East Coast Waters: Tech. Rpt. #2, Sparcom Inc., 49 p.

Hodder, D.T., 1973, Coastal Bathymetric Plotting: Space Division, Rockwell International, SD 73-SA-0131, 53 p.

Hodder, D.T. and M.C. Kolipinski, 1973, Airborne and Satellite Remote Sensing of Anacapa Island for Hydrology and Aquatic Biology: 13th International Technical Scientific Meeting on Space, Rome, Italy, 8 p.

Ingle, Jr., James C., 1966, The Movement of Beach Sand: Elsevier Pub. Co., 221 p.

Inman, Douglas L. and Borchard M. Brush, 1973, The Coastal Challenge: Science, V. 181.

Jones, James H., 1971, General Circulation and Water Characteristics in the Southern California Bight: Southern California Coastal Water Research Project, 37 p.

Kolpack, R.L. (editor), 1971, Biological and Oceanographical Survey of the Santa Barbara Channel Oil Spill, Vol. 11, Physical, Chemical and Geological Studies, Allen Hancock Foundation, University of Southern California, Los Angeles, 477 p.

Natland, M.L. and Kuenen, P.H., 1951, Sedimentary History of Ventura Basin, California, and the Actions of Turbidity Currents, p. 66-107 in Hough, J.L., Ed., Turbidity Currents and the Transportation of Course Sediments to Deep Water: Soc. Econ. Paleontologists and Mineralogists Spec., Pub. No. 2.

Scruton, P.C. and D.G. Moore, 1953, Distribution of Surface Turbidity off Mississippi Delta: Am. Assoc. Petroleum Geologists Bull., V. 37, p. 1067-1074.

Shepard, F.P. and K.O. Emery, 1941, Submarine Topography off the California Coast, Canyons and Tectonic Interpretation: Geol. Soc. America Spec. Paper 31, 171 p.

Specht, M.R., D. Needler, and N.L. Fritz, 1973, New Color Film for Water Photography Penetration: Photogrammetric Engineering, p. 359-369.

1971, Dredge Disposal Study for San Francisco Bay and Estuary: U.S. Army Engineering District, San Francisco, California, 32 p.

1973, The Ecology of the Southern California Bight, Implications for Water Quality Management: Southern California Coastal Water Research Project, 531 p.

Paper M 8

THE UTILIZATION OF ERTS-1 DATA FOR THE STUDY OF THE FRENCH ATLANTIC LITTORAL

Pierre G. Demathieu *(Institut Géographique National)* and Fernand H. Verger *(Laboratoire de Geomorphologie), Paris, France*

ABSTRACT

The French Atlantic Littoral (FRALIT) programme uses ERTS-1 data to study coastal geomorphology and waters. ERTS-1 gives an overall picture of the phenomena for the first time due mainly to channel 4 data, but the other channels also contribute valuable complementary data on superficial waters. These studies have already resulted in accurate maps of the mud transported south-westwards from the mouth of the River Loire.

1. The Objectives of the FRALIT Programme.

The FRALIT programme is concerned with the study of the French Atlantic coastal regions and these investigations of shoreline phenomena cover not only marine waters and currents and the sediments they transport but also the land regions, coastal sediments, sea marshes, and the foreshore zone.

2. The Investigators and their Equipment.

The following expert groups are participating in these studies:
(a) Geomorphological Laboratory, Ecole Pratique des Hautes Etudes, directed by Prof. F. Verger, which has headquarters in Paris and a laboratory in Dinard, Brittany.
(b) Institut Géographique National, Paris, particularly its Remote Sensing Service directed by Mr. P. Demathieu, together with assistance from other groups such as the Data Processing Service as well as the Aerial Surveys Department which maintains 12 aircraft including a Falcon Jet Mystere 20 specially equipped for remote sensing.
(c) Pedology Laboratory, University of Poitiers, directed by Professor J. Dupuis.
(d) Geographical Laboratories of the University of Nantes and the University of Amiens directed respectively by Mr. Pinot and Mr. Regrain.

A wide range of facilities are thus available to the research team and in addition it has access to computers and stations in the field as well as aircraft and photographic processing laboratories.

3. Investigation Procedures.

In the preliminary studies attempts were made to use all possible methods, including both normal visual photointerpretation and photographic and optical data processing procedures, e.g. equidensities, densitometry, construction of a colour display console, as well as digital processing. This first phase lasted from November 1972 when the first images were received, until September 1973. Since then attempts have been made to make more intensive use of those techniques which seemed to be the most promising, particularly digital data processing. The first programmes dating from April 1973, when the first computer compatible tapes were received, were simple ones. They were written for channel by channel statistical comparisons, correlation studies of pairs of channels and listings showing a single zone as imaged by a single channel, or several channels combined in a previously defined manner. We are now writing more complex programmes using training processes, e.g. a training phase supervised by field data and an unsupervised phase for studying the structure of the spatial data. We have also specially processed the data for water regions and we hope to be able to establish a correlation between the variations of the derivative of the spectra, the turbidity stratification and the bathymetric contours, but we have not yet made sufficient progress to present any results.

4. Results

The study of ERTS-1 images has enabled us to make digital maps of various geographical elements on the continent using their spectra but, in general, the results could have been obtained by normal methods. ERTS-1 data are also useful for up-dating or renewing the existing cartography.

On the other hand, ERTS-1 data have been shown to be a completely novel way of investigating dynamic sedimentology processes occurring all along the French coastline included in the FRALIT programme. Up to the time the ERTS-1 data arrived we only had rather incomplete information on the turbidity of the coastal waters. The light-sensitive seaweeds, e.g. laminariae, on the rocky bottom of the Loire estuary, do not grow more than 10-15 metres below the lowest waters and are evidence of the strong turbidity of the waters in that region. Sporadic, non-simultaneous and discontinuous observations had earlier been made with the Secchi disks, but only in fine weather, which resulted in an imperfect survey of the turbidity distribution.

The ERTS-1 satellite produced the following important images in a cloudless sky of the South Brittany coastal regions:

A:	25 September 1972	10 66	10 294
B:	8 March 1973	12 28	10 305
C:	9 March 1973	12 29	10 363

This material is particularly interesting because images A and B, although taken nearly six months apart, enabled us to view the same region under similar tidal conditions, i.e. end of ebb tide at the time of strong spring tides (coefficients 0.92 and 1.00 respectively) and similar meteorological conditions, i.e. NE winds, anticyclone (pressure 1025 and 1036 mb respectively). However, for image A the Loire was at extremely low water (river flow 135 cubic metres/sec) whereas for image B the Loire was at the end of a flood period (river flow 800 cubic metres/sec).

A comparison of images B and C obtained on two consecutive days under somewhat similar hydrological and meteorological conditions enabled us to study the turbidity front off the Loire estuary. The two pairs of multispectral images on all four MSS channels were of sufficiently good quality for us to make the following deductions:

1. The Loire gives rise to a 12km plume beyond St-Nazaire during low water and to a 100 km plume when in flood. Channels 4 and 5 were used to determine turbidity which, being very strong, completely masked the bottom response. There was no correlation whatsoever between the bathymetric contours and the channel 4 and 5 data anywhere in the strong turbidity zone. Beyond that region the sea-bottom was so deep that it could not even contribute to the image on MSS channel 4. Fig. 1 shows the distribution of the turbidity regions as well as the sea currents at the time the image was obtained and also an hour beforehand.

2. The sea currents, as shown on images A and B, carry sediments coming from the Loire away towards the south-west. In addition, these currents also reactivate the sediments on the tidal flats of Bourgneuf Bay supplied during rising tide by the material already brought from the Loire. The general migration towards the south-west is also accompanied by complex motions around Noirmoutier Island, where some of the sediments pass around the northern end of the island whilst the rest pass by the narrow Fromentine Inlet and spread out in a plume over a large part of the Fromentine tidal delta. This sedimentary plume is much less noticeable when the Loire has not been flowing fast prior to the period when the image was taken.

3. One can see a real turbidity front on the MSS channel 4 data, which corresponds to depths of about 50 metres without there being any real link between the isobath and the iso-turbidity.

5. Conclusion.

We could have also mentioned other analyses but we decided to limit ourselves here to an account of studies carried out in a single region on a well-defined topic for which ERTS-1 has provided data which would have been impossible to obtain by normal methods.

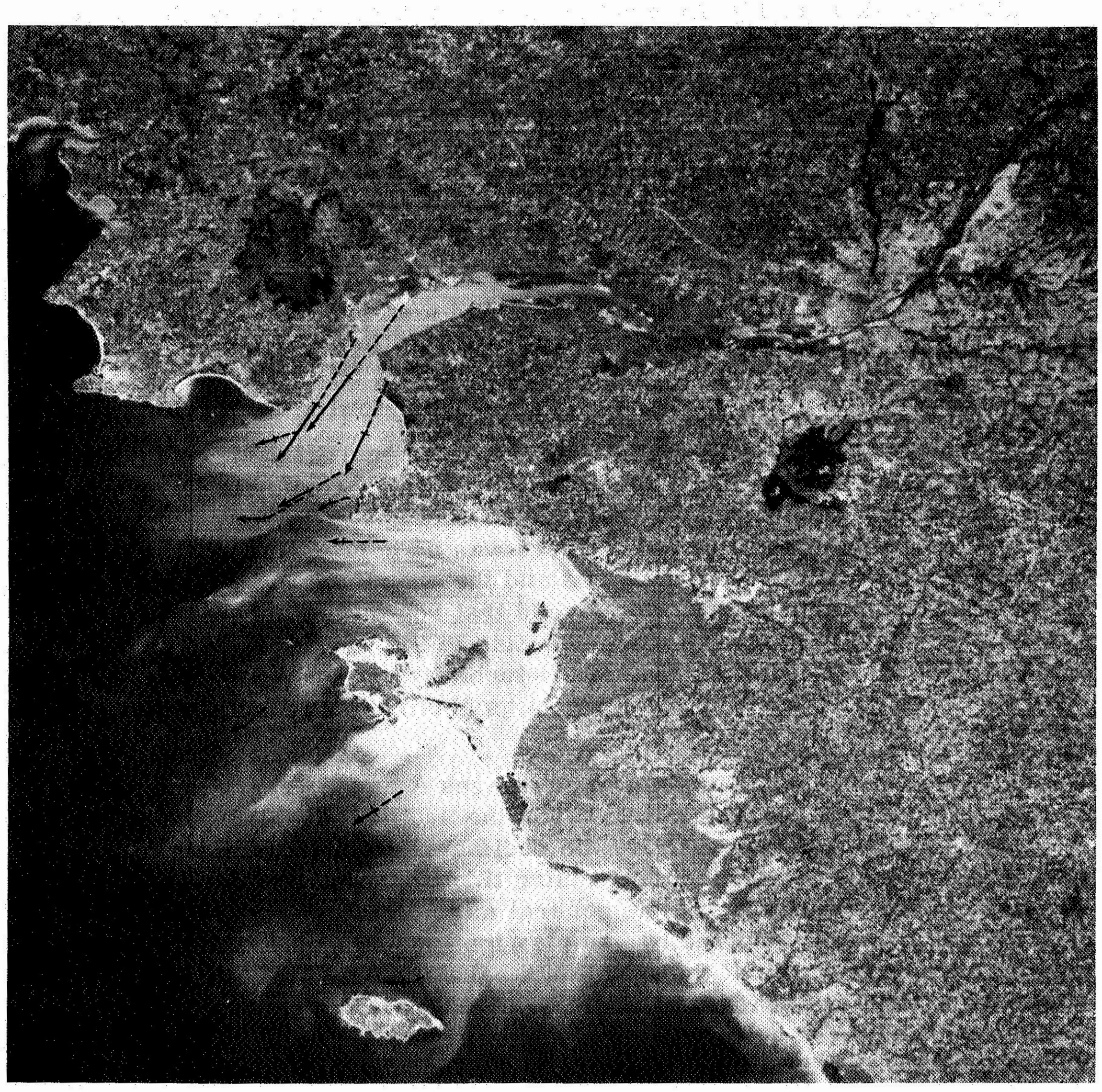

Vitesse des courants de marée

1 heure avant

au moment du passage

échelle $1^{cm} = 1^{m}/sec.$

Figure 1.

Paper M 9

ERTS IMAGERY APPLIED TO ALASKAN COASTAL PROBLEMS

F. F. Wright, *Marine Advisory Program, University of Alaska, 142 E. 3rd Avenue, Anchorage, Alaska 99501,* G. D. Sharma, D. C. Burbank, *Institute of Marine Science, University of Alaska, Fairbanks, Alaska 99701,* and J. J. Burns, *Alaska Dept. of Fish and Game, 1300 College Road, Fairbanks, Alaska 99701*

ABSTRACT

Along the Alaska coast, surface water circulation is relatively easy to study with ERTS imagery. Highly turbid river water, sea ice, and fluvial ice have proven to be excellent tracers of the surface waters. Sea truth studies in the Gulf of Alaska, Cook Inlet, Bristol Bay, and the Bering Strait area have established the reliability of these tracers. ERTS imagery in the MSS 4 and 5 bands is particularly useful for observing lower concentrations of suspended sediment, while MSS 6 data is best for the most concentrated plumes. Where satellite-synchronous sea truth was available, optical density slicing techniques have been developed to permit the quantitative discrimination of suspended sediment concentrations. Ice features are most clearly seen on MSS 7 imagery; fracture patterns and the movement of specific floes can be used to map circulation in the winter when runoff is restricted, if appropriate allowance is made for wind influence. Current patterns interpreted from satellite data are only two-dimensional, but since most biological activity and pollution are concentrated near the surface, the information developed can be of direct utility. Details of Alaskan inshore circulation of importance to coastal engineering, navigation, pollution studies, and fisheries development have been clarified with satellite data. ERTS has made possible the analysis of circulation in many parts of the Alaskan coast which were extremely difficult to study using standard oceanographic techniques.

(Paper not available at time of printing)

Paper M 10

MONITORING ARCTIC SEA ICE USING ERTS IMAGERY

James C. Barnes and Clinton J. Bowley, *Environmental Research and Technology, Inc., Lexington, Massachusetts 02173*

ABSTRACT

Because of the effect of sea ice on the heat balance of the Arctic and because of the expanding economic interest in arctic oil and other minerals, extensive monitoring and further study of sea ice is required. The application of ERTS data for mapping ice is evaluated for several arctic areas, including the Bering Sea, the eastern Beaufort Sea, parts of the Canadian Archipelago, and the Greenland Sea. Interpretive techniques are discussed, and the scales and types of ice features that can be detected are described. For the Bering Sea, a sample of ERTS imagery is compared with visual ice reports and aerial photography from the NASA CV-990 aircraft.

INTRODUCTION

Nearly a decade ago, relatively low resolution video imagery from earth satellites was already being used to acquire useful information on arctic sea ice distributions. In fact, it was at that time that Fletcher (1966) stated that the "observational barrier" in the Arctic was crumbling primarily under the impact of satellite observation systems. Now, ERTS-1 is providing multispectral data at a resolution that has not previously been available. Techniques being developed using ERTS data will lead eventually to the use of operational satellite systems to collect ice data on a far more complete and economical basis than has heretofore been possible.

The requirement for extensive monitoring and study of sea ice is emphasized by recent interest in the economic exploitation of arctic regions. Exploration for oil and other minerals will, in itself, require increased shipping in arctic waters, demanding increasingly accurate ice-condition forecasting. The modern demands of the Canadian ice advisory service are summarized by Markham (1973).

Detailed scientific study of sea ice is being accomplished through efforts such as Project AIDJEX, the Arctic Ice Dynamics Joint Experiment, the purpose of which is to gain a quantitative understanding of the interaction between the fields of motion of the atmosphere, the pack ice, and the liquid

ocean. (Division of Marine Resources, 1970). Several scientists have pointed out that because of the critical effect of sea ice on the heat balance of the Arctic, the amount of ice may be an important and possibly a key factor in the climate of the northern hemisphere (Fletcher, 1966; Maykut and Untersteiner, 1969; and Committee on Polar Research, 1970). In another report, Fletcher (1968) states that the seasonal patterns of surface heat exchange over oceanic regions, which are directly related to ice distribution, are the most important factors to monitor in both the Arctic and Antarctic.

APPLICATION OF SATELLITE DATA

Since the time of Fletcher's remarks concerning the impact of satellite observations on the Arctic, numerous studies have been conducted to develop techniques to apply satellite data to marine resources problems. Studies such as those reported by McClain and Baliles (1971) and Barnes, Chang, and Willand (1972) have demonstrated that useful ice information could be derived from the visible and thermal IR measurements made by existing meteorological satellites. Now, through the improved NOAA-2 operational system even greater use of spacecraft-acquired data for sea ice analysis is being made (McClain, 1973; Wiesnet, 1973).

This paper describes an investigation to evaluate the application of ERTS-1 data for detecting and mapping arctic sea ice. The specific objectives of the investigation were to determine the spectral bands most suitable for detecting ice, to measure the scale and types of ice features that can be detected, and to develop interpretive techniques for differentiating ice from clouds and for mapping ice concentrations. Ice features have been mapped for several arctic areas, including the Bering Sea, the eastern Beaufort Sea, parts of the Canadian Archipelago, and the Greenland Sea. Preliminary results of the analysis of the initial ERTS data sample from the 1972 late summer and early fall seasons have been presented by Barnes and Bowley (1973a; 1973b).

INTERPRETIVE TECHNIQUES AND IDENTIFICATION OF ICE TYPES

Ice can be identified in all of the MSS spectral bands because of its high reflectance and can be distinguished from clouds through a number of interpretive keys, as discussed in the earlier paper. Experimentation has shown that the photographic processing of prints from the original 70 mm negatives can be important for ice detection, since exposures selected to retain detail in bright, snow-covered land areas may result in the loss of significant ice features. Because of this, much of the data analyzed in the study were reprocessed. In the reprocessing procedure, the images were usually enlarged to a scale of 1:500,000; this scale was found to be the most conveinient for interpreting ice features. Identification of ice types has

been made, based on variations in reflectance and the shapes and sizes of the patterns. Differences in reflectance between the shorter wavelength bands (MSS-4 and MSS-5) and the near-IR band (MSS-7) have been found very useful for differentiating ice types and for determining characteristics of the ice surface. For example, in some of the earliest ERTS images from late July 1972, ice in Crozier Channel and Kellett Strait along the coasts of Prince Patrick and Melville Islands (see map, Figure 1) appears very dark in the MSS-7 band. Because of the differences in reflectance in the MSS-4 and MSS-7 images, these areas are believed to be areas where the ice surface is covered by melt water. As pointed out by McClain (1972), even a thin film of water on the ice can cause a sharp drop in reflectance in the near-IR portion of the spectrum, whereas in the visible the reflectance does not change significantly.

An even more striking example is seen in imagery of the same area in late June 1973 (Figures 2 and 3). On this date daytime temperatures at Mould Bay, located on Prince Patrick Island, are reported to be well above freezing, so that the snow-cover on the ice is quite likely melting. Canadian ice observers who have overflown these areas report that during the summer many of the bays and inlets are characteristically covered with considerable melt water. As also seen in Figure 3, however, within the areas of low reflectance, the ice is intersected by bright linear patterns, many of which can also be identified in the imagery from the previous summer. The interpretation of these patterns is that leads or cracks too small to be resolved by the satellite have permitted the water on the sea surface to drain away; in the vicinity of the cracks, which develop in preferred locations from year to year, the ice becomes drier once again, and the reflectance in the near-IR increases.

The use of multispectral data to distinguish between puddled areas and areas of open water, and to identify ice type, is further illustrated in Figures 4 and 5. In these images showing ice along the east coast of Greenland near 77°N, distinct differences in the sea ice characteristics in the two spectral bands can be seen. The ice in the eastern part of this scene appears much brighter in the MSS-4 band than in the MSS-7. Closer to the coast, the area of very close and consolidated pack ice has a nearly uniform reflectance in the MSS-4 band, whereas in the MSS-7 band the individual ice floes are distinctly brighter than the surrounding ice. This is particularly evident in the ice adjacent to the shore lead, which appears fairly bright in the MSS-4 band, but is nearly black in the MSS-7 band. Because this is not an area of solid ice cover, such as shown in the previous example, the lower reflectance in the near-IR is presumably due to brash or rotten ice, where water is on and around the ice elements.

SEQUENTIAL ICE OBSERVATIONS

Detection of Leads in the Beaufort Sea

ERTS imagery from several passes during the period from the first of April through mid-June 1973 covering the Beaufort Sea in the area 72-80°N and 126-150°W has been examined. This area contains compact (10/10) and very close (9/10 to less than 10/10) pack ice, but even in the early April data extensive leads can be seen, some being as much as 180 km or more in extent. In these early spring images, complex patterns are evident, with newer leads often intersecting older refrozen leads. As the spring season progresses, the pack ice undergoes deformation from large ice fields into smaller ice floes.

In the imagery of 1 April, a large lead that is about 50 km wide at the widest point exists near 74°N, 140°W. Distinct tonal variations are evident within the lead. The differences in tone can be distinguished in both the visible and near-IR spectral bands, and are presumably representative of the gradual refreezing of the lead through formation of grey and grey-white ice. Twenty days later, on 21 April, the same lead can be seen, although it has narrowed considerable to a maximum width of only 20 km. On this date, the entire lead appears to contain grey-white ice. Within the grey-white ice, small shearing leads are visible; the dark tone of these features indicates either open water or nilas ice. Finally, in an image of 7 May, the lead can barely be distinguished as only a very small difference in reflectance is detectable between the refrozen lead and surrounding ice.

Mapping Ice Changes in the Eastern Beaufort Sea

Ice movement and deformation in the eastern Beaufort Sea near Prince Patrick Island and the mouth of M'Clure Strait can be mapped throughout the spring season through use of ERTS imagery. Early in the spring, in imagery on 8, 10, 11, and 28 April, a quasi-permanent flaw lead can be observed just west of Prince Patrick Island. The lead separates fast ice along the coast and in M'Clure Strait from pack ice to the west. In the April imagery, all land and ice surfaces are snow covered and, therefore, appear smooth. The images for 8 April and 11 April are shown in Figures 6 and 7.

Significant changes in the configuration of the lead can be mapped from the imagery. On the 8th, the maximum width of the lead is 4 km; two days later, it has widened to a width of 10 km near Prince Patrick Island and almost 30 km at M'Clure Strait; one day later, on the 11th, the maximum width is as much as 35 km. Later in the month the widening continues, so that on 28 April the lead is as much as 50 km wide. As the lead opens, new ice formation is also evident. On the 10th and 11th, the low reflectance

indicates the formation of grey ice, whereas on the 28th the higher reflectance in the western portion of the lead indicates that much of the ice has become grey-white. On each date the area of new ice formation is along the immediate eastern edge of the lead. Ice floes, judged to be either first-year or multi-year ice because of their high reflectance, are also embedded in the newer ice within the lead.

The same area can be observed again in imagery on 2 and 3 May. During the short interval since the previous observation (28 April), ice conditions have changed dramatically. The lead has now closed in again and is full of ice floes, with very little grey or grey-white ice evident. Changes continue to take place, and by the next ERTS cycle (17 May) the lead has once again reopened in the area south of Prince Patrick Island. In these three observations, the formation of a giant floe (more than 150 km across) can also be traced. The floe develops from fractures that can be detected on the 2nd and 3rd of May, and can be identified in later data on 20 May and 6 June. By the last date, the floe has become surrounded by a broken ice field containing much smaller floes, and surface features can now be seen on the floe.

Monitoring Ice Deterioration in Amundsen Gulf and M'Clure Strait

Through repetitive ERTS coverage during mid-June, ice deterioration can be monitored in Amundsen Gulf and M'Clure Strait. On 10, 12, and 13 June the eastern part of Amundsen Gulf is observed, and on 16, 18, and 20 June M'Clure Strait is observed. In both areas the ice appears to be in a state of rapid deterioration. The ice surface is covered with various patterns indicative of puddling and thawing, and ice breakup is occurring in Amundsen Gulf and at the western end of M'Clure Strait. Shore polynyas exist along Banks Island, particularly at the mouths of the rivers. In Amundsen Gulf, the movement of ice floes over the 4-day period can be observed. Surface weather charts indicate that temperatures throughout the Canadian Northwest rose well above freezing during the month of June.

CORRELATION BETWEEN ERTS IMAGERY AND AERIAL ICE OBSERVATIONS

The Bering Sea Expedition (BESEX) presented an opportunity to correlate ERTS imagery with aerial observations, both in the form of visual ice reports and aerial photography. BESEX, a joint effort between the USA and USSR, was conducted during the period from mid-February through early March 1973. The primary area of interest extended southward from St. Lawrence Island to beyond the edge of the pack ice. During the experiment some 14 flights were made by the NASA CV-990 aircraft, operating out of Elmendorf Air Force Base in Anchorage; on all flights numerous on-board experiments were conducted including nearly continuous vertical viewing aerial photography.

During the BESEX period ERTS data were collected on a total of four passes over the Bering Sea. On two dates, 27 and 28 February, the ERTS passes crossed the easternmost part of the Bering Sea in the Nunivak Island area; on 6 and 7 March, the passes crossed St. Lawrence Island and the prime BESEX area of interest. In the ERTS imagery of 6 March, a portion of which is shown in Figure 8, an area of low reflectance, apparently grey ice, extends southward from St. Lawrence Island. Along the immediate south coast of the island, a band of open water exists. Over the open water small streaks of stratus cloud can be seen, although the ice to the south appears to be cloud-free. To the north and to the southeast of St. Lawrence brighter ice floes exist, surrounded by the grey ice. Numerous fractures and leads cut through the bright (first-year and multi-year) ice and the surrounding grey ice. Differences between the apparent grey ice and the older ice are especially noticeable in the MSS-7 imagery.

Aerial photography of a part of the area covered by the ERTS imagery on 6 March (Figure 8) is shown in Figure 9. Although the aerial photographs were taken on the previous day, many ice features in the photography can also be detected by ERTS. For example, areas of young fast ice (grey and grey-white) as small as about 200m in width can be seen along the coast of the island; similarly, numerous shearing leads are in evidence. In fact, it appears that all of the significant ice features visible in the aerial photography can be detected in the ERTS imagery.

The commentary by the ice observer onboard the CV-990, given in the Navigational Flight Data report, is also in remarkably good agreement with the ice conditions deduced from the ERTS data, even though the flight is a day earlier. To the north of St. Lawrence the observer reports generally 80% first-year and multi-year ice and 20% grey ice. Where the observer reports simple shearing leads, leads are detectable in the imagery. Also, the north coast of the island is reported as having compacted ice; in the imagery, the ice in that area does appear solid, quite different from the ice south of the island.

As the flight approaches the western end of St. Lawrence Island, the commentary indicates that the amount of first-year and multi-year ice is decreasing and that the ice ahead is mostly grey ice; the location of the ice boundary separating these different ice types in the ERTS imagery corresponds almost exactly with the location where the above comment was made. After crossing the island, the observer reports all grey ice a few days old, some of which has undergone deformation in the form of stretching to the southwest. This observation confirms the ice type deduced from the ERTS data; furthermore, leads indicative of stretching of the ice can be seen in the imagery.

The ice conditions displayed in the ERTS imagery on 7 March are very similar to those of the previous day. On the 7th, however, the stratus streaks have increased, obscuring some of the grey ice south of St. Lawrence Island. Farther south some ice features can be detected, but much cloudiness exists.

One segment of the CV-990 flight on this day follows the southern boundary of the grey ice, an area that is cloud-free. The observer reports a vast expanse of grey ice, and then reports running into a stratus deck; the comment is made that the "stratus streaks are due to open water along the south shore of St. Lawrence." Thus, this commentary verifies exactly the ice and cloud conditions apparent in the ERTS imagery.

CONCLUSIONS

The results of the investigation demonstrate that ERTS imagery has substantial practical application for monitoring arctic sea ice. Ice features as small as 80-100m in width can be detected, and the combined use of the visible and near-IR imagery is a powerful tool for identifying ice types. In the eastern Beaufort Sea, the combination of ERTS orbital overlap and a high incidence of cloud-free conditions during the spring assures a high frequency of repetitive satellite coverage. With this repetitive coverage, the deformation and movement of ice features could be mapped throughout the early April to late June period.

Ice features that can be identified in ERTS imagery include: the distinction between grey, grey-white, and older forms of ice, as well as the distinction between ice floes and surrounding brash ice; the growth and deterioration of leads; the formation of new grey ice within leads; the deterioration of the ice surface as evidenced by the formation of puddled areas and flooded ice; linear dry areas within flooded ice fields caused by the drainage of melt-water; and icebergs embedded in fast ice or close pack ice detectable by their shadows.

Data from ERTS passes crossing the Bering Sea in early March have been compared with ice observations collected in the Bering Sea Expedition (BESEX). On two flights of the NASA CV-990 aircraft, the ice conditions in the vicinity of St. Lawrence Island reported by the onboard observer are in remarkably close agreement with the ice conditions mapped from the corresponding ERTS imagery. The ice identified in ERTS imagery and substantiated by the aerial observer include the locations of boundaries between areas consisting of mostly grey ice and of mostly first and multi-year ice, the existence of shearing leads, and the occurence of open water with the associated development of stratus cloud streaks. Moreover, it appears that essentially all of the significant ice features near St. Lawrence Island visible in the aerial photographs taken from the CV-990 can also be detected in the ERTS imagery. It seems entirely feasible, therefore, that ERTS imagery could be used to replace some currently flown aerial surveys, at a considerable cost saving.

REFERENCES

Barnes, J.C. and C.J. Bowley, 1973a: Use of ERTS Data for Mapping Arctic Sea Ice, Symposium on Significant Results Obtained from the Earth Resources Technology Satellite-1, NASA SP-327, pp. 1377-1384.

Barnes, J.C. and C.J. Bowley, 1973b: Mapping Sea Ice from the Earth Resources Technology Satellite, Arctic Bulletin, 1 (1), pp. 6-13.

Barnes, J.C., D.T. Chang, and J.H. Willand, 1972: Image Enhancement Techniques for Improving Sea Ice Depiction in Satellite Infrared Data, Journal of Geophysical Research; Oceans and Atmospheres Edition, 77 (3), pp. 453-462.

Committee on Polar Research, 1970: Polar Research, A Survey, National Research Council, National Academy of Sciences, Washington, D.C.

Division of Marine Resources, 1970: Arctic Ice Dynamics Joint Experiment, Report No. AIDJEX - Bull-1, University of Washington, Seattle.

Fletcher, J.O., 1966: "Forward", Proc. of the Symposium on the Arctic Heat Budget and Atmospheric Circulation, Memorandum RM-5233-NSF, The RAND Corporation.

Fletcher, J.O., 1968: The Polar Oceans and World Climate, Proc. of the Long-Range Polar Objectives Conference, U.S. Department of Transportation, Washington, D.C.

Markham, W.E., 1973: Modern Demands on the Canadian Ice Advisory Service, Paper 3.12, Presented at Interdisciplinary Symposium on Advanced Concepts and Techniques in the Study of Snow and Ice Resources, Monterey, California.

Maykut, G.A. and N. Untersteiner, 1969: Numerical Prediction of the Thermodynamic Response of Arctic Sea Ice to Environmental Changes, Memorandum RM-6093-PR, The RAND Corporation.

McClain, E.P., 1973: Some New Satellite Measurements and Their Application to Sea Ice Analysis in the Arctic and Antarctic, Paper 5.2, presented at Interdisciplinary Symposium on Advanced Concepts and Techniques in the Study of Snow and Ice Resources, Monterey, California.

McClain, E.P., 1972: Detection of Ice Conditions in the Queen Elizabeth Islands, Proc. of Symposium on Earth Resources Technology Satellite-1, September 29, 1972, National Aeronautics and Space Administration.

McClain, E.P., and M.D. Baliles, 1971: Sea Ice Surveillance from Earth Satellites, Mariners Weather Log, 15 (1), pp. 1-4.

Wiesnet, D.R., 1973: "The Role of Satellites in Snow and Ice Measurements," Page 5.1, presented at Interdisciplinary Symposium on Advanced Concepts and Techniques in the Study of Snow and Ice Resources, Monterey, California.

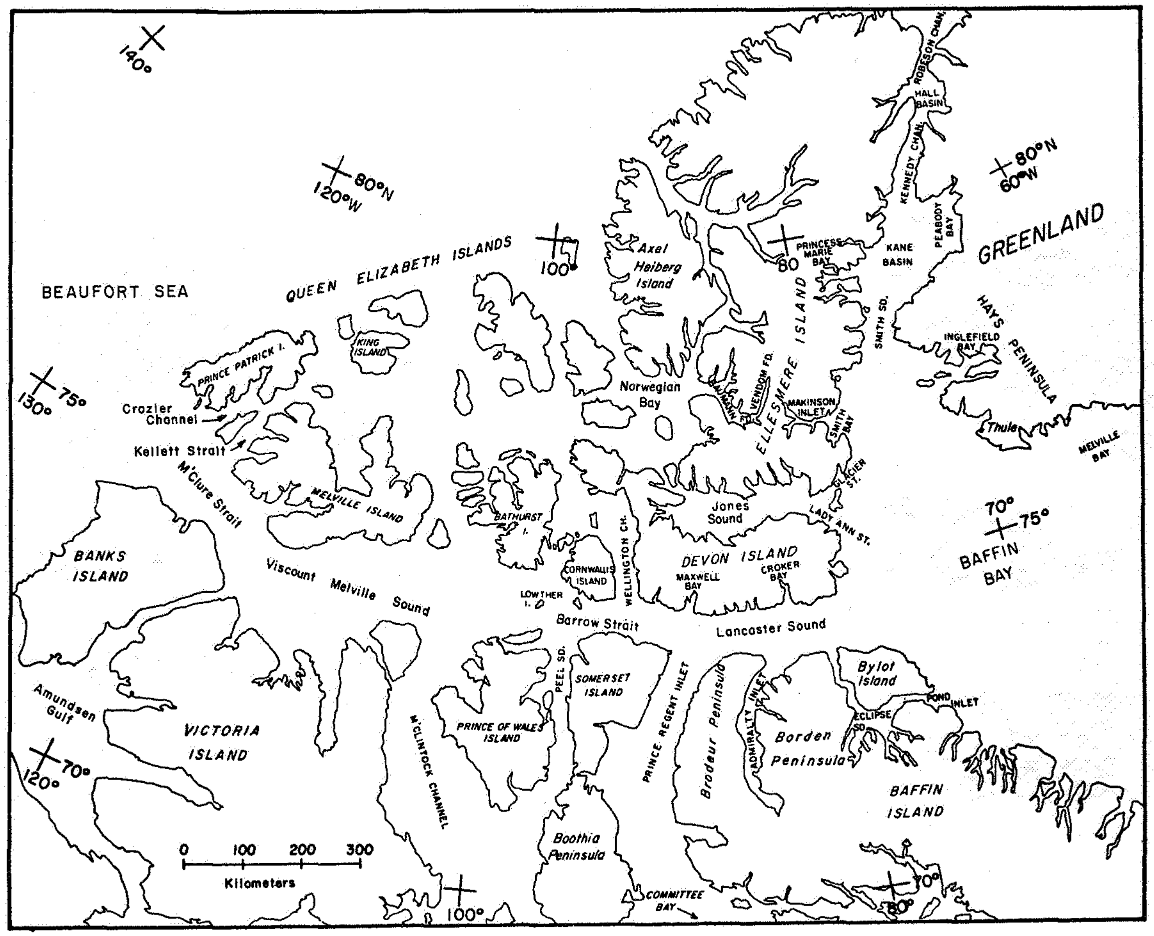

Figure 1 Map of Arctic showing area from eastern Beaufort Sea to Baffin Bay

Figure 2 ERTS MSS-4 (visible) image showing ice in Crozier Channel and Kellett Strait just north of M'Clure Strait, 18 June 1973 (ID No. 1330-20064). Prince Patrick Island is at the left, Melville Island at the right.

Figure 3 ERTS MSS-7 (near-IR) image corresponding to the MSS-4 image shown above. Dark patterns in the near-IR image are related to surface melt water.

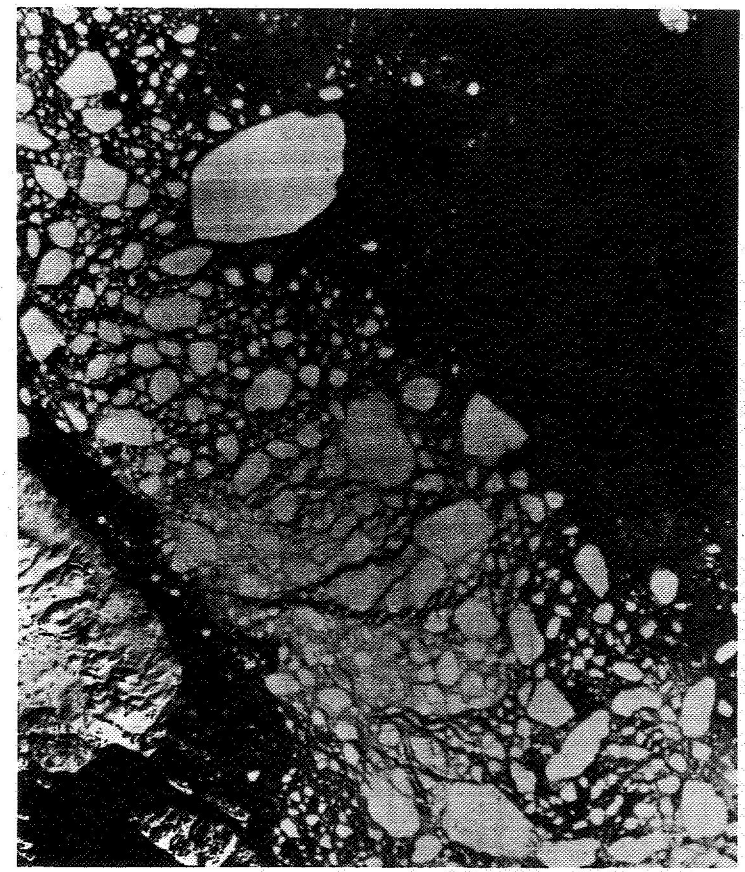

Figure 4 (left) ERTS MSS-4 (visible) image showing ice along the east coast of Greenland near 77°N, 25 September 1972 (ID No. 1064-13342). Germania Land and Store Koldeway are at left.

Figure 5 (right) ERTS MSS-7 (near IR) image corresponding to the MSS-4 image shown above. Note the differences in reflectance of ice features as compared to the visible data.

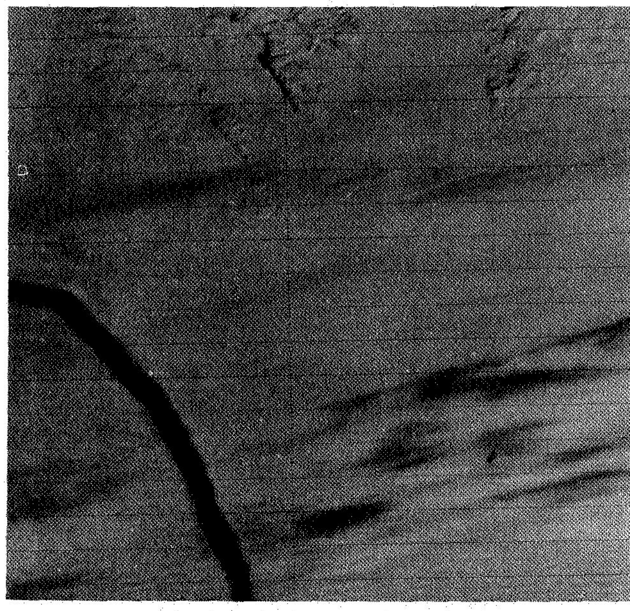

Figure 6 ERTS MSS-7 image showing lead in eastern Beaufort Sea near Prince Patrick Island, 8 April 1973 (ID No. 1259-20130).

Figure 7 ERTS MSS-7 image showing approximately the same area as in Figure 6, 11 April 1973 (ID No. 1262-20302). Note growth of lead and formation of new grey ice within lead that has occurred in three-day period.

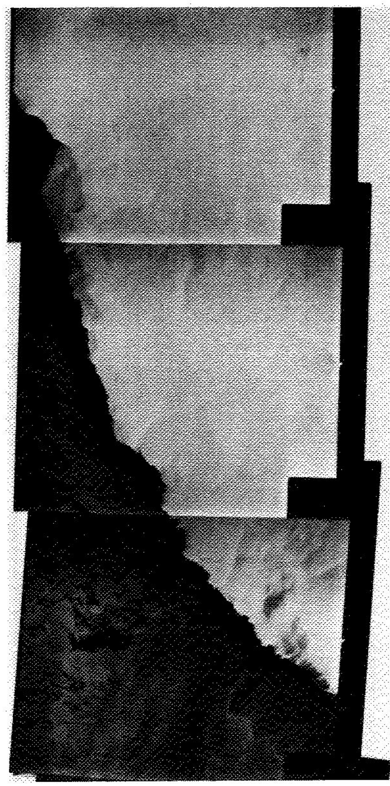

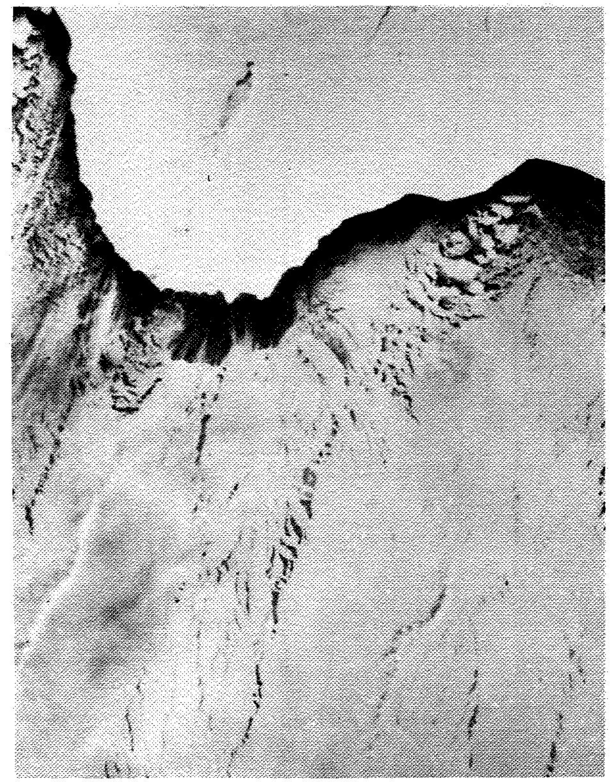

Figure 8 (left) ERTS MSS-7 image showing ice in Bering Sea near St. Lawrence Island, 6 March 1973 (ID No. 1226-22171).

Figure 9 (right) Aerial photographs covering a portion of the area shown in above ERTS image (Figure 8) along coast of St. Lawrence Island. Photographs were taken by NASA CV-990 aircraft on 5 March 1973.

Paper M 11

APPLICABILITY OF ERTS TO ANTARCTIC ICEBERG RESOURCES

John L. Hult and Neill C. Ostrander*, *The Rand Corporation, Santa Monica, Cal. 90406*

ABSTRACT

This investigation explores the applicability of ERTS to (a) determine the Antarctic sea-ice and environmental behavior that may influence the harvesting of icebergs, and (b) monitor iceberg locations, characteristics, and evolution. Imagery sampling in the western Antarctic between the Peninsula and the Ross Sea is used in the analysis. It is found that the potential applicability of ERTS to the research, planning, and harvesting operations can contribute importantly to the glowing promise derived from broader scope studies for the use of Antarctic icebergs to relieve a growing global thirst for fresh water. Live Antarctic readout will permit timely acquisition of imagery on every orbital pass, which will be necessary to achieve adequate glimpses through the 80 percent cloud cover. Thermal sensor bands will provide coverage in daylight or darkness. Several years of comprehensive monitoring will be necessary to characterize sea-ice and environmental behavior and iceberg evolution. Live ERTS services will assist harvesting control and claiming operations and offer a means for harmonizing entitlements to iceberg resources. The valuable ERTS services will be more cost effective than other means and will be easily justified and borne by the iceberg harvesting operations.

INTRODUCTION

This investigation uses data from the first Earth Resources Technology Satellite (ERTS-1) [1] to determine the characteristics, abundance, and accessibility of Antarctic iceberg resources and also to evaluate the potential role and application of ERTS types of sensing systems to the future harvesting of Antarctic resources.

*Any views expressed in this paper are those of the authors. They should not be interpreted as reflecting the views of the Rand Corporation or the official opinion or policy of any of its governmental or private research sponsors. This paper is derived from a condensation of *Applicability of ERTS For Surveying Antarctic Iceberg Resources*, by J. L. Hult and N. C. Ostrander, The Rand Corporation, R-1354-NASA/NSF, November, 1973. The original work was supported jointly by NASA's ERTS program and by the Office of Exploratory Research and Problem Assessment of the National Science Foundation.

Preliminary studies of broader scope have exposed the potentially attractive global use of Antarctic icebergs for fresh water and cooling. [2,3] As population soars and standards of living increase, the fresh water deficiencies in certain areas of the world are rapidly becoming acute. Those areas that are particularly concerned include the Pacific Southwest United States, and parts of Mexico, Chile, Australia, the Middle East, and North Africa. In some of these arid regions, water may be available by transferring it from river basins with abundant water or by desalting seawater. However, the costs of transferring or desalting, which may be \$100 or more per 1000 m^3 (or per acre-ft)[1] tend to put severe limits on such use.

For the thirsty areas of the world, the possibility of using Antarctic icebergs as a fresh water resource might become a very attractive prospect. The crucial problem is to devise a technology that can deliver melted iceberg water at much less cost than either desalting or inter-basin transfers, while at the same time ensuring acceptable environmental impact of such operations.

The idea of using Antarctic icebergs has been considered and even tried a number of times during the past century. Theoretically, icebergs could be floated to any point accessible by a deep water route (at least 200 m of water depth).

The abundance of icebergs has long been recognized (annual yield of about 1,000,000 million cubic meters or 1000 million acre-ft). If a way can be found to move the icebergs and control their melting so as to deliver, say, 10 percent of the *annual* yield economically, this operation could potentially satisfy the water demands of an urban population of 500 million (with a usage of 200 m^3 per person). The potential direct economic impact of fully exploiting 10 percent of the annual yield is estimated to be as much as \$10 billion annually.

Past exploration of the Antarctic has indicated that a major portion of the sea ice that forms and builds up during the dark winter months thaws out during the daylight season. By March of each year most of the tabular icebergs naturally formed from the ice-shelf discharges are accessible for acquisition and export operations. Although the *sea* ice is generally less than 2 m thick (compared with a few hundred meters for most tabular, fresh water icebergs), the area of sea ice formed and thawed each year is thousands of times the total area of icebergs and about ten times the mass. Thus sea ice is a major factor to contend with in the acquisition of icebergs. Its moderating influence on the climate (together with that of the continental icecap) is so dominating over that of the icebergs that little climatic effect would be expected, even with the removal of most of the annual iceberg yield. It should be possible to process icebergs for high quality fresh water and thermal pollution abatement without adverse effects on the global or Antarctic climate.

[1]An acre-ft of water is a quantity sufficient to cover one acre with water a foot deep. This is approximately 1,234 m^3 = 1.234 $k \cdot m^3$.

In order to get a better understanding of the feasibility of moving icebergs and controlling their melting, a model of the transport operations from the Ross Sea to Southern California was made. The available environmental data on currents, winds, and temperatures were included in the model. Although these data are very crude and limited, they are adequate to test the preliminary feasibility. The model shows that the transport effort required need not be very sensitive to the winds, can benefit from the currents but is not dependent on them for feasible operations, is not too sensitive to the route selected, and will require insulation of the icebergs for acceptable survival en route to the Northern Hemisphere. The Coriolis forces,[2] which are proportional to the momentum (mass × velocity) and the sine of the latitude, provide the principal resistance to the transport operations. These forces are applied at right angles to the velocity and require a large fraction of the transport effort to counteract their effects, particularly at more southerly latitudes.

The cost of delivering the icebergs will be determined by the design of the transport operations and the configuration of the iceberg "trains." Narrow trains (300 to 600 m wide) are desirable because they are estimated to reduce the net Coriolis effects on the icebergs. Also, when these trains are propelled at an angle with respect to the resultant velocity, they can more effectively obtain "lift" to counteract Coriolis forces. An asymptotic minimum transport effort per unit of iceberg is approached for iceberg "trains" longer than about 20 km. Greater lengths increase the mass, transport resistance, and insulation costs proportionately. The costs of insulation can be estimated without specifying many of the details of operational techniques for applying the insulation, which need to be tested by experience. Essentially, the iceberg surfaces exposed to ablation from the flowing seawater can be wrapped by unrolling plastic film that is designed to trap pockets of melt water to form a quilting of still water between the iceberg and the flowing seawater. Quilt-water thicknesses of 3 cm will limit the iceberg melting to less than 10 percent per year.

The operational cost of delivering a large iceberg train (1.22×10^{13} kg) to California on a one-year cycle is estimated to be about \$8 per 1000 m^3 (\$10 per acre-ft). It is also estimated that designing operations for more nearly optimum speed or better train configurations will not significantly reduce these rates. On the other hand, these delivery costs should approximately hold for a variety of operations that would depart significantly from the asymptotic one that was costed.

The conceptual illustrations in Fig. 1 show a possible operational configuration with electrically driven propellers distributed along, and harnessed to, the train convoy. Also shown is a possible test configuration using more conventional tugs to pull a small three-piece iceberg train.

[2] Coriolis forces tend to deflect an object moving in the Northern Hemisphere to the right and one moving in the Southern Hemisphere to the left.

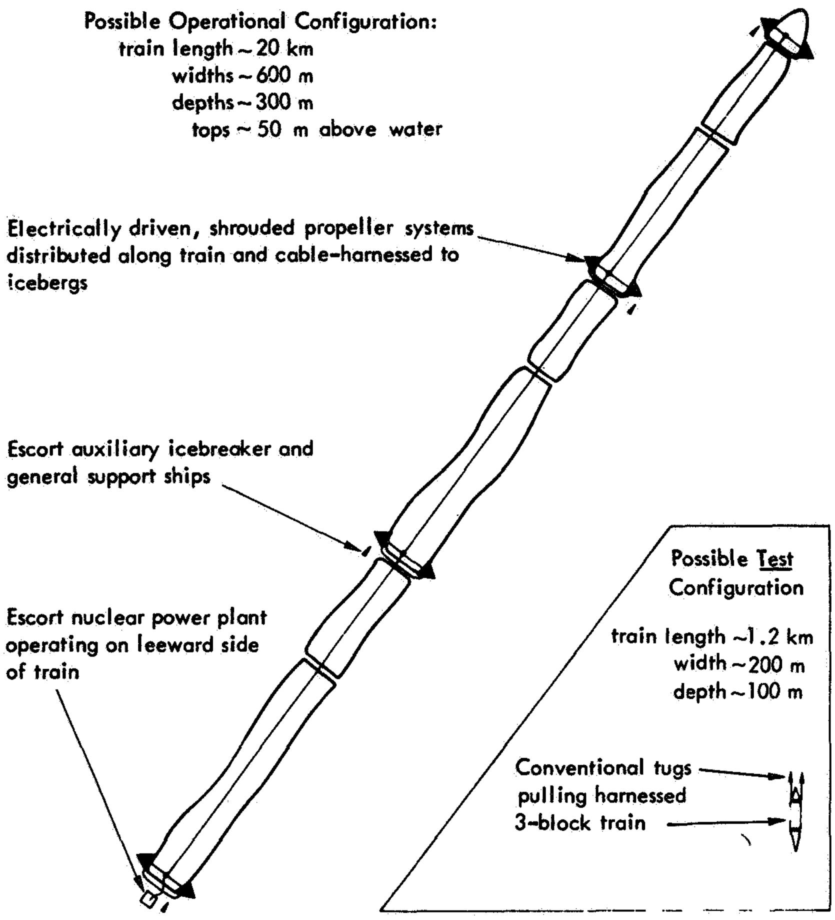

Fig. 1—Conceptual illustrations

Before designing and developing an operational system, and for refining cost estimates, a test program with icebergs would be desirable to: determine the nature of the submerged surfaces of tabular icebergs; test techniques for insulating and harnessing icebergs; measure the transport environment and performance; determine how well the Coriolis forces can be controlled; and test the performance of modeling to simulate operational control and performance.

The conversion of the icebergs for fresh water and heat sink was explored in a very preliminary way in order to uncover promising concepts and to estimate cost limits based on general physical principles. This exploration indicated that iceberg conversion to fresh water at sea level should be achievable in a variety of ways for about \$8 per 1000 m^3. A preliminary engineering study and comparison of the more promising conversion techniques is needed to develop better cost estimates and the basis for the design of test systems for evaluating alternative approaches for operational systems.

The total costs of Antarctic iceberg transport, conversion to water, and delivery to wholesale distribution terminals in coastal areas appear to be of the order of \$24 per 1000 m^3 (\$30 per acre-ft). This would be less costly and would require less energy expenditure than interbasin water transfers of a few hundred kilometers or desalting or costly water reclamation operations. Furthermore, nuclear energy could be used, thus eliminating competition for fossil fuel resources. Fresh water from icebergs should therefore become an attractive alternative for areas close to deep seawater access routes.

Before any large-scale operational use of Antarctic icebergs is implemented, there should be a comprehensive assessment of the potential societal and environmental impacts. A preliminary exploration of a variety of such factors reveals no obvious insurmountable obstacle. The factors to be investigated include: the international acceptability of exploiting Antarctic icebergs; the en route environmental constraints; the acceptability of terminal operations; the demand for iceberg water and the integration of its delivery system with other established systems for furnishing fresh water; icebergs as reservoirs and recreation areas; and the risk involved in implementing iceberg water resource systems. The more avenues that are explored, the more promising the concepts seem to become. However, a more refined assessment can be made when the potential operations become better defined, and when specific terminal applications can be examined in detail.

The objectives of this investigation were to explore the applicability of ERTS to (a) determine the Antarctic sea-ice and environmental behavior that may influence the harvesting of icebergs, and (b) monitor iceberg locations, characteristics and evolution. A very limited imagery sampling of portions of the western Antarctic was scheduled to collect data on cloud-cover obstruction, the capability to monitor and assess sea-ice behavior, the ability to distinguish and measure iceberg characteristics, and the general topographic surveillance capabilities of the ERTS system in the Antarctic environment. The results from ERTS-1 imagery are described in the next section. This is followed by a section on ERTS system potential which treats: live imagery, thermal and micro wavelengths, sea-ice behavior and iceberg evolution, tactical harvesting information, claiming and monitoring service, entitlements to Antarctic iceberg resources, and economical potentials for ERTS.

RESULTS FROM ERTS-1 IMAGERY

The applicability of ERTS for surveying Antarctic iceberg resources was evaluated by studying images of the ocean and coastal areas of the Western Antarctic between the Antarctic Peninsula and the Ross Sea. The test site was bounded by the four coordinate corners in clockwise order: 65°S, 160°E; 65°S, 75°W; 75°S, 75°W; 79°S, 160°E. Imagery was obtained only from November 1972 through March 1973. No cloud-cover limitations were specified, and imagery from bands 5 and 7 of the Multispectral Scanner (MSS) covering wavelengths of 0.6 to 0.7 and 0.8 to 1.1 micrometers, respectively, was used in the analyses. Most of the analyses were made with bulk black and white, 9.5-in. positive paper prints of band 7; however detailed visual measurements of iceberg surface dimensions were made from 70-mm positive transparencies which were readily magnified to a scale of about 1:150,000.

The ERTS systems are described in detail in the *Data Users Handbook*. [1] The principal deficiency of the ERTS-1 experimental system for this investigation was the lack of live readout in the Antarctic which could eliminate delays and permit much more imagery collection than is feasible by storage on board the satellite. Imagery for more than 900 scenes was interpreted in this investigation. The scene centers were plotted on a map of Antarctica as illustrated in Fig. 2. They were fairly well distributed over the originally defined test area. However, the analyses revealed that the useful *coverage* (openings in cloud cover) *was spotty both geographically and temporally*. For the purposes of analysis and to facilitate cataloging, the Antarctic was partitioned into sectors along orbital parallels as illustrated in Fig. 2.

All the imagery analyzed was obtained during the period from 16 November 1972 to 27 March 1973 and can be found listed in *Earth Resources Technology Satellite, Cumulative Non-U.S. Standard Catalog No. N-9*. [4] Imagery obtained for this investigation that contained useful information other than cloud coverage has been described and submitted to the Image Descriptor Data Bank file under one or more of the following descriptors: Ice, Sea Antarctic; Icebergs, Antarctic; Antarctic Topography.

CLOUD COVER

Previous data on cloudiness in the Southern Hemisphere indicate a total cloudiness that reaches maximum values in the coastal regions surrounding the Antarctic continent. [5] Climatologically, the mean cloudiness exceeds 80 percent most of the year over most of the region extending 1000 km north of the coast. Climatology also indicates that cloudiness is the most extensive during the daylight season when it persists to the high interior regions of the Antarctic with 50 percent likelihood as compared with perhaps only 20 percent during the night season. The primary area of interest for the harvesting of iceberg resources is in the regions of drift ice where cloud cover greater than 80 percent appears to persist, and it becomes essential to determine the potential utility of sensors that must exploit openings in cloud cover as well as to examine the characteristics of the openings themselves.

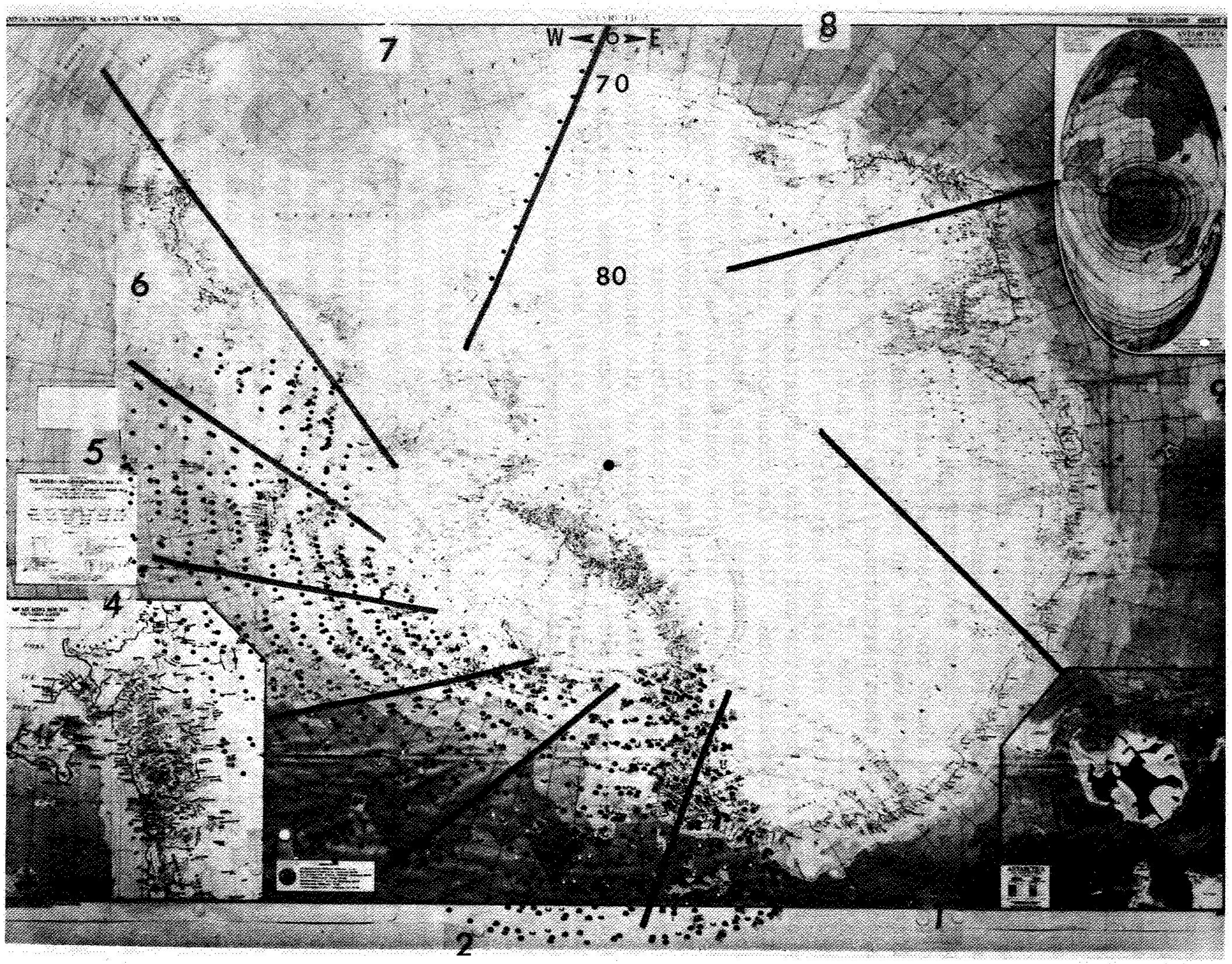

Fig. 2 — Division of Antarctica into 9 sectors and distribution of images

Cloud-cover information was obtained from more than 900 Antarctic scenes that were interpreted according to the authors' subjective estimation of the fraction of the scene area over which the obscuration was sufficient to degrade the ability to find icebergs and to measure their dimensions at the full resolution capability of the sensors. These interpretations can be compared with the cloud-cover values assigned to more than 2900 Antarctic scenes (including those interpreted in this study) in the *Cumulative Non-U.S. Standard Catalog No. N-9*. [4] Most frequently the scene areas were totally obscured and there was no question that the cloud cover was complete. Some scene areas had very thin cover through which the general nature of the sea ice below could easily be discerned, but the contrast needed to find imbedded icebergs and measure their dimensions was obscured. Such areas were interpreted to be cloud-covered. However, any scene with 90 percent or more of cloud cover through which a positive determination could be made about the presence or absence of sea ice below was arbitrarily assigned a value of 90 percent cloud cover. The cloud cover of scenes was then partitioned into categories of 0-40, 50-80, 90, and 100 percent. Some of the tabulated data of cloud cover over drift-ice areas within the study test site are illustrated in Fig. 3. They are tabulated by sector and sector combinations and by time period and time period combinations. Also the cloud-cover interpretations as defined for this study are compared with the catalog listings. The catalog listings of cloud cover are the routine subjective impressions of the processing crew that was operating at the time; they do not represent any precise interpretation of any particular cloud-cover definition, especially for the highly ambiguous scenes of the Antarctic involving so much cloud cover over the snow and ice. The scene-to-scene comparisons of cloud cover by the interpretations of this study are frequently at great variance with the catalog listings; however, the averages seem to have fairly consistent differences.

The season average of cloud cover over drift ice in sectors 2 through 6 as interpreted in this study was 0.84. The corresponding average as obtained from the catalog listing was 0.74. The season average of cloud cover over fixed ice for the same sectors was 0.70 as interpreted in this study and 0.60 as obtained from catalog listings. Similarly, the season average of cloud cover over drift ice in sector 1 as interpreted in this study was 0.91 whereas the corresponding average obtained from catalog listings was 0.81. Thus the averages of cloud cover as interpreted with the definitions of this study are about 0.1 greater than the corresponding averages obtained from the catalog listings. From the data it is concluded that for the daylight period from November 1972 through March 1973, the cloud cover over most of the drift-ice areas where iceberg harvesting operations are most promising exceeded 0.8 as interpreted by the definitions of this study. This is in substantial agreement with the climatological cloud cover described in other references, [5] which also indicate only very slight reductions in cloud cover over the drift-ice areas during the seasons of darkness.

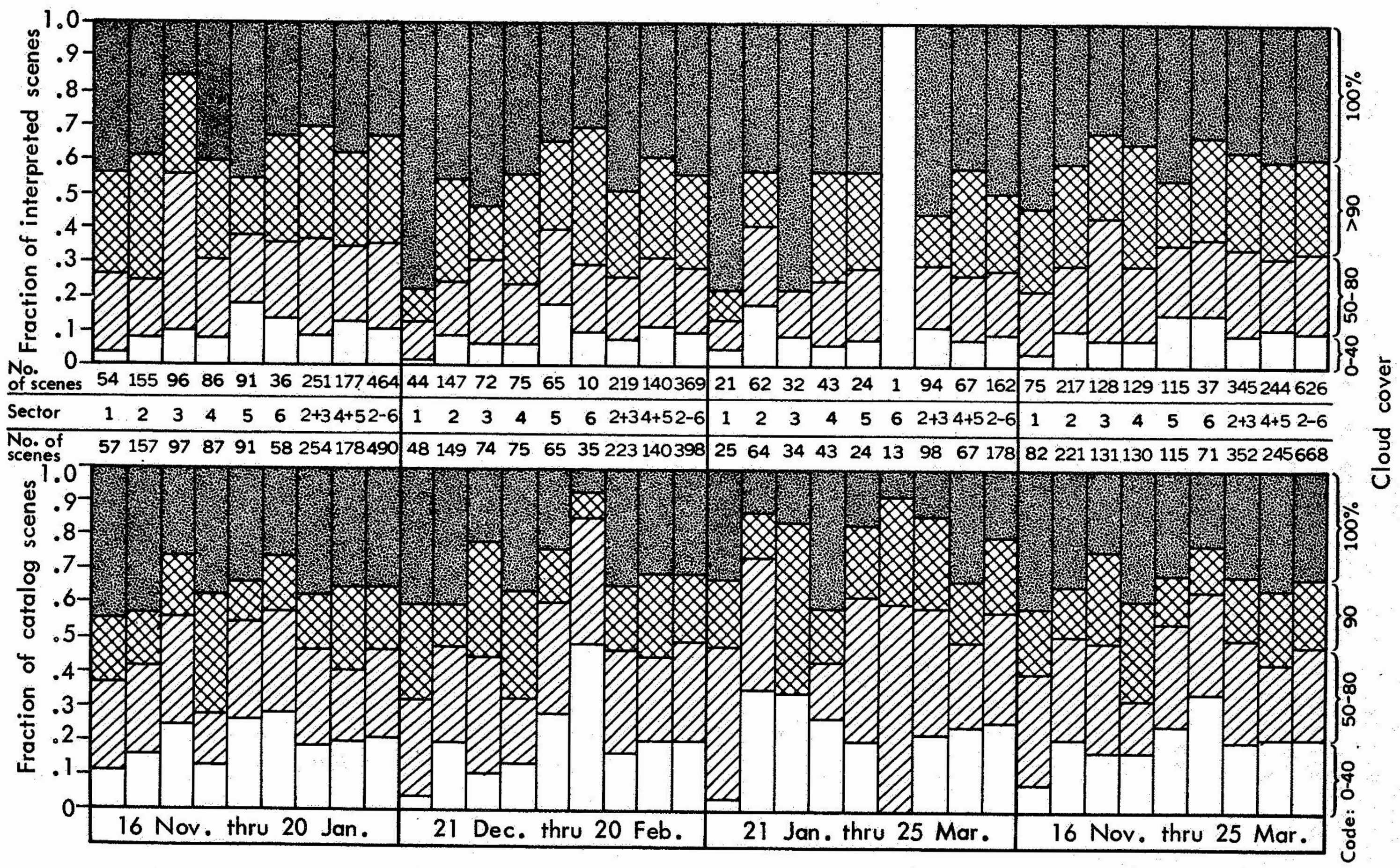

Fig. 3—Cloud-cover comparison over drift-ice areas: (Special interpretation and catalog, various period combinations)

There was inadequate sampling of scenes to provide conclusive evidence of cloud-cover variation with period or with sector. However, there seems to be a slight tendency for increased average cloud cover in the middle of the daylight season compared with the ends, and for decreased average cloud cover in sectors in which drift-ice areas extend farther south (sectors 2 and 3 including the Ross Sea and sector 7 including the Weddell Sea).

It is difficult to define the characteristics of the "openings" to be expected in the prevailing cloud cover over Antarctic iceberg scenes of interest. However, most open areas are comparable to or smaller than a scene of 185 km diameter, and in the small sample of this type of data there seemed to be no recognizable correlation between openings on scenes obtained 24 hours apart with average geographical overlap of 0.7 between scenes. Thus it is assumed that if complete imagery was obtained on every ERTS pass, the cloud-cover openings on successive passes would be statistically independent events, and the probability of a cloud-cover opening in all the potential ERTS images over a specified iceberg area should range between 0.3 and 0.7 in each 18-day cycle (or in each 9-day period when using a thermal sensor capable of operating in the dark during either the ascending or descending nodes). This estimate assumes a cloud-cover average between 0.8 and 0.9 and a day-to-day scene overlap between 0.7 and 0.8.

SEA ICE

In order to harvest Antarctic icebergs efficiently and to assemble them into trains for movement to using areas, it will be necessary to contend with the sea ice that surrounds Antarctica and the icebergs most of the time. The seasonal and geographical extents of the Antarctic sea ice have been described in various publications. [5,6] Also valuable are the historical accounts of sea-ice obstructions to navigation in these regions. [7] The descriptions of the various forms of ice that may be encountered and how they evolve are helpful to the understanding of the nature of this barrier to the otherwise easy access to the densest iceberg clusters. [8] ERTS types of observations over several years with scene sampling at nearly every orbital-pass opportunity should provide a valuable record of sea-ice behavior that could be very useful in planning the harvesting of iceberg resources. The very limited sampling obtained with ERTS-1 (less than 10 percent of the opportunities for October through March) was inadequate for a comprehensive interpolation of the sea-ice behavior over a daylight season. A much more complete sampling over two or more years and preferably over the full year (in darkness as well as daylight) seems highly desirable to gain a confident understanding of the sea-ice behavior and its potential influence on ocean operations in the Antarctic.

The sea ice observed in the portion of the western Antarctic from which this investigation obtained imagery consisted of a huge belt extending more than 1000 km northward from the coast in the early daylight season. By February, after erosion during a few months of the daylight season, the northern edge of the sea-ice belt had receded to about 70° south latitude over much of the western Antarctic lying within the test site.

At the same time the ice belt seemed to withdraw from the coast in many areas, with considerable erosion of coastal fast ice. The dissolution of the belt from both north and south seemed to be most severe in the Ross Sea in the vicinity of 180° longitude, where the belt separated in February to open the Ross-Ice-Shelf front and much of the coast eastward to the Getz Ice Shelf (~130°W) to access without the necessity of breaking through the belt. Most of the Bellingshausen Sea and Amundsen Sea east of Cape Dart on Siple Island seemed to be closed off throughout the season by the sea-ice belt. However, the belt became the narrowest in this sector and would have required breaking through about 300 km or less of belt width to reach open-water areas near the coasts. The behavior of the belt seemed to be more consistent with that depicted in Ref. 5 than in Ref. 6; however, it may change from year to year without always following a detailed standard pattern.

During the daylight season when the sea-ice-belt width is receding, the deteriorating ice debris along the northern edge of the belt appeared to feather out into wisps as viewed with ERTS resolution. The central portion of the belt may be consolidated into a continuous snow-covered surface that may crack and then break up into floes of mixed and varied sizes and erosion shapes.

Icebergs that calve from the ice shelves and glacial ice streams along the coast may become locked up in coastal fast ice for years, but they tend to leak out of their locked-up coastal clusters and diffuse northward through the sea-ice belt. Most of the icebergs become locked into huge floes in the central portions of the belt for periods of one or more seasons. However, many icebergs may break loose, especially near the edges of the belt or near large fractures or leads, and plow through the sea ice or sweep it up in front of them as the iceberg is driven by deeper sea currents.

The collection and harnessing of icebergs into long trains will probably be easiest along the northern edge of the belt or in the open-water areas inside (south) of the belt where these operations would not need to contend with crowding sea-ice stresses. The greater density of the iceberg clusters near the coast would facilitate the formation of large trains with more favorable characteristics. Once a train of icebergs has been formed in open coastal waters, it may be feasible in some situations to propel it so as to plow through the belt. The thrust required to move the train in open waters will be large compared to that provided by natural currents in these regions. The train should, therefore, have a considerably greater capacity to plow through the belt than do the naturally imbedded icebergs. Techniques need to be developed for controlling the train when attempting to plow through the sea-ice belt in order to move it in the desired direction and avoid collisions with icebergs that are locked in or are themselves moving through the belt.

ICEBERG CHARACTERISTICS

The iceberg characteristics that were of greatest interest in this investigation were the effective widths available that would permit harnessing icebergs snugly together into long trains. Eight dense cluster areas representative of western Antarctica between the Ross and Bellingshausen Seas were selected and the maximum widths of the icebergs and their topside areas were tabulated. Individual visual measurements were made of each iceberg on a projected image with a scale of about 1:150,000. The widths were measured perpendicular to the dimension that appeared to offer the best opportunity for in-line harnessing of each iceberg into train formation. Figures 4 and 5 illustrate the various types of clusters.

Figure 4 shows a cluster of icebergs locked into the fast ice off Cape Colbeck (eastern edge of Ross Sea at the lower right). The much deeper and higher (~50m) icebergs stand out in relief against the fast ice and are easily recognized and measured under magnification. Also included in this sample are a number of icebergs in open water west of the locked-in cluster. In the open water the shadows of the higher icebergs do not provide recognizable signatures for distinguishing them from sea ice. However, tabular icebergs (large icebergs with flat tops) tend to break into pieces with crisp looking edges similar to the pieces of a broken window pane, as distinct from the eroded looking edges of many sea-ice floes. Also, the currents at the much greater depth of icebergs tend to move them differently from sea ice and they will frequently dam up or sweep out the sea ice to leave an open-water signature behind them. This is illustrated by the two icebergs, each about 6 km long by 1 km wide, that are about 15 km off the western tip of the fast ice containing the cluster of icebergs (the scene width is approximately 185 km). These two large icebergs were originally joined together end-to-end to form a single ship-shaped iceberg about 12 km long. In this scene, they are sweeping south the melting sea ice, including a bright eroded ice floe of comparable size within their swath. There are a number of other smaller icebergs in the open water to the south and between the pack ice and the fast ice that were also included in the data sample.

Figure 5 shows many clusters of icebergs in or near the fast ice, south and west of Thwaites Iceberg Tongue. One sample of dimensional statistics was taken from icebergs in the open water on the western edge of the fast ice, and a much larger sample was taken from the icebergs locked in the interior of the fast ice. In both cases, all large multple-layered ice-berg clumps were excluded so that the statistics of the basic layering widths of the Thwaites source would not be distorted.

Figure 6 displays the statistics of iceberg characteristics obtained from the eight areas sampled. The distribution of iceberg widths is illustrated in terms of the fraction of the total topside area of the sample of ice-bergs for each 0.1 km of width interval. Each sample area is identified by a geographical name and the ERTS frame from which it was selected. The

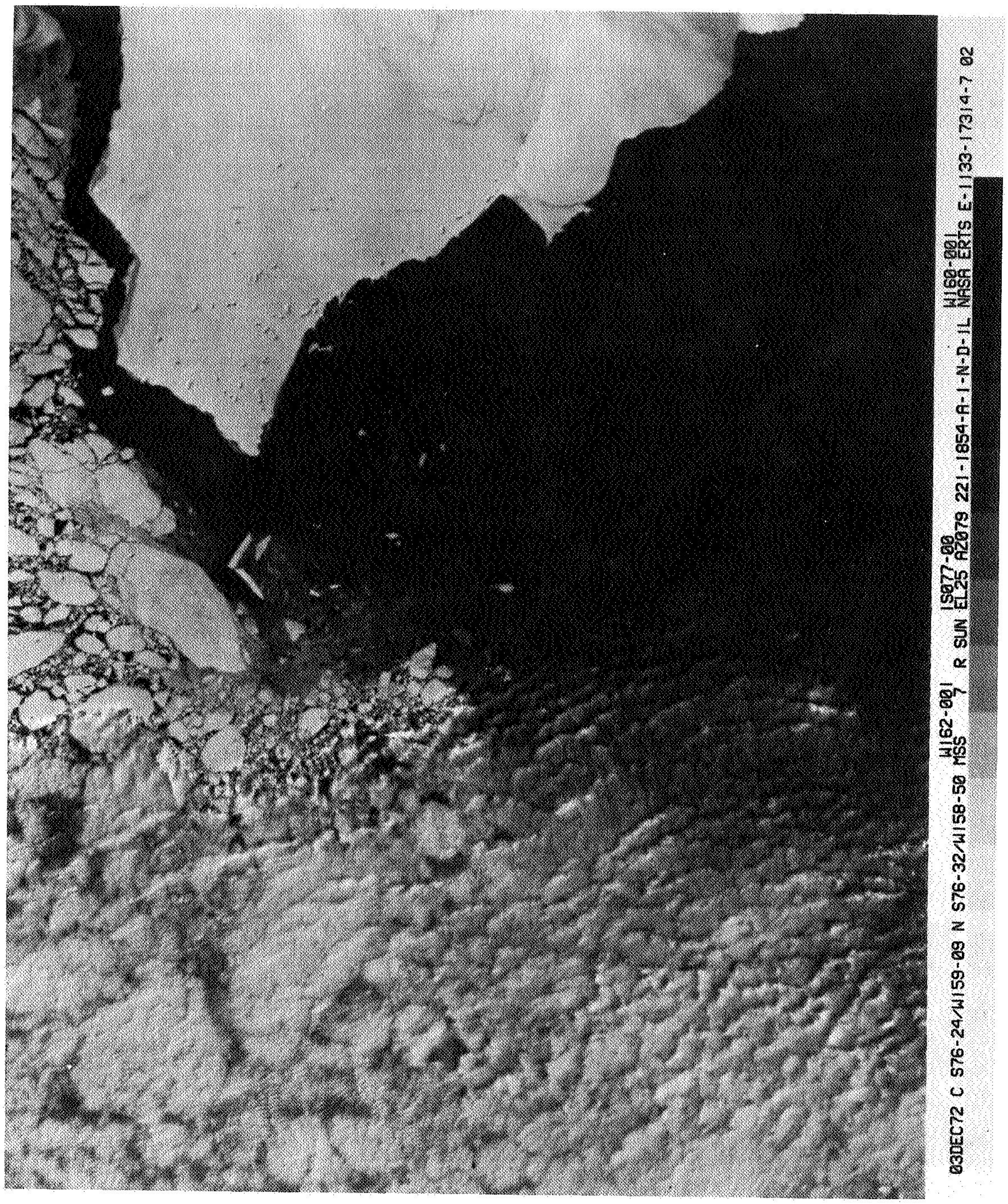

Fig. 4 — Iceberg cluster off Cape Colbeck

Fig. 5 —Iceberg clusters south and west of Thwaites Iceberg Tongue

total number of icebergs included in each sample is given as well as the number in each interval (above the bars). The total topside area of the icebergs in the sample is given in km^2.

Figure 6a, from a sample in Fig. 4, seems to indicate a bimodel distribution. However, major portions of the areas in the 1.0 and 1.1 intervals are derived from the two large icebergs--each about 6 km long--mentioned previously in connection with Fig. 4. If these two exceptional icebergs were excluded from the sample, it would subdue the distribution peak near 1.0 and reduce the average area per iceberg to about 0.6 km^2, which would be more comparable with Figs. 6b and 6c.

The sample represented in Fig. 6d, which comes from north of the tip of Thwaites Iceberg Tongue, is anomalous in its distribution of large widths and of an average area per iceberg of 1 km^2. The source of these icebergs is not known, but the shapes and large widths are not characteristic of those from Thwaites.

The small samples represented in Figs. 6e and 6f come from the northern edge of the sea-ice belt. They are biased toward smaller and narrower icebergs, which might be expected for these more northerly samples of icebergs that are probably older and more eroded than those near the coasts.

The icebergs in Figs. 6g and 6h were selected from the Thwaites area discussed with Fig. 5. Sample g is the one from near the western edge of the fast ice and may include some icebergs from other sources than Thwaites. The large sample, h, comes from the interior fast ice and should be a pure representation of Thwaites source characteristics.

The sample statistics of Fig. 6 indicate that until a substantial fraction of the annual iceberg yield is harvested, it may not be necessary to use icebergs of greater than 0.5 km width. However, if the samples of Fig. 6 are representative of all the Antarctic iceberg yield, it may be necessary to harvest icebergs up to 0.8 km wide if much more than half of the annual yield is to be used.

Inadequate data precluded an attempt to inventory the total mass of icebergs in the Antarctic, the annual yield, or the average or typical life of icebergs. The great abundance of icebergs that was observed was not inconsistent with a possible mass balance between the accumulation of precipitation in Antarctica and its discharge to the sea, which has been estimated to yield an average of 10^{12} m^3 of icebergs per year. [2] However, the data samples do indicate that there may be great variability in the life and evolution of the icebergs after they have been calved. In some areas they become trapped near the coast for many years and probably melt much more slowly than icebergs that are swept into oceanic gyres and experience significant current gradients over their immersed depths as they circulate through the belt of sea ice. The significantly smaller dimensions of the icebergs found in the

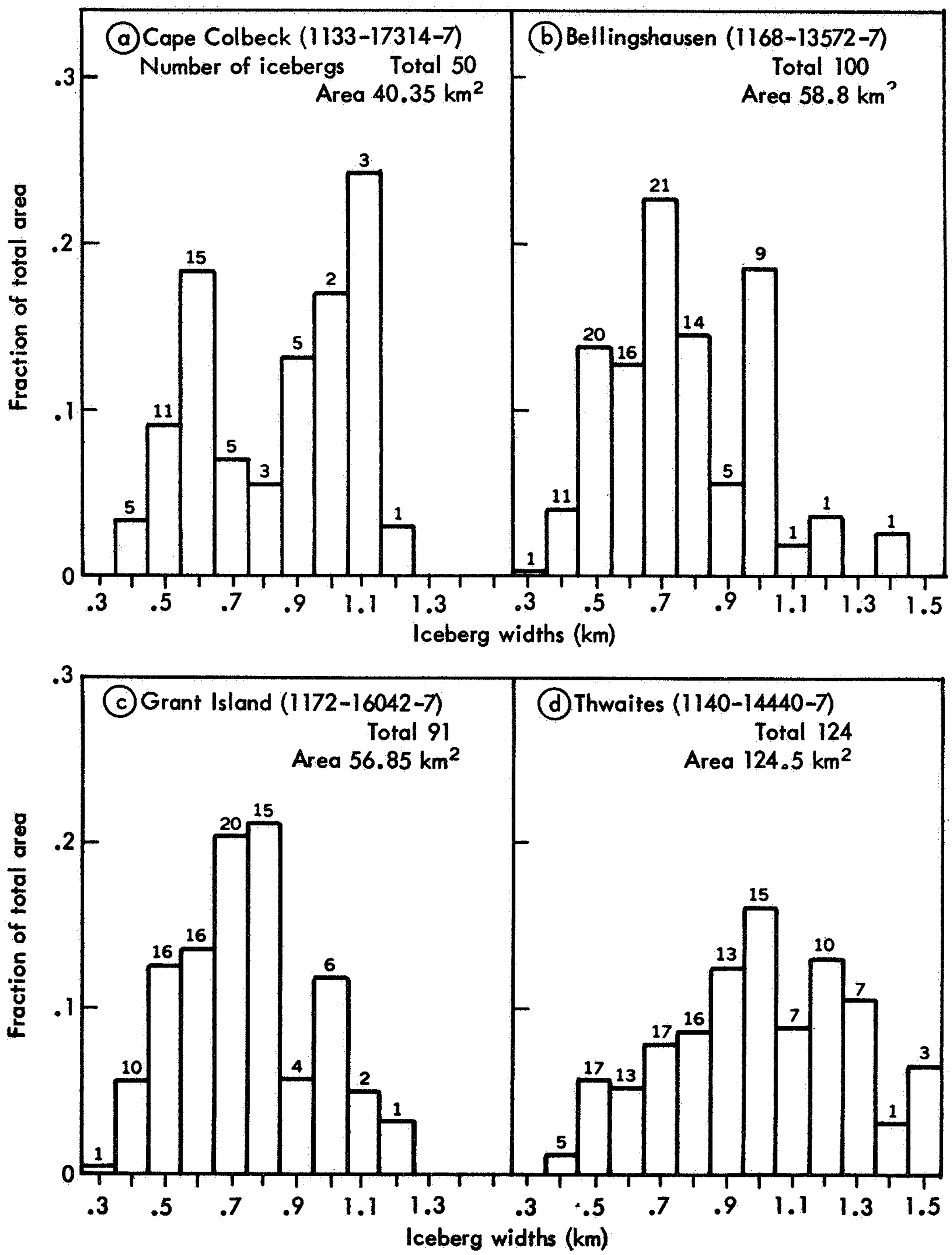

Fig. 6 — Distribution of iceberg widths in sampled areas

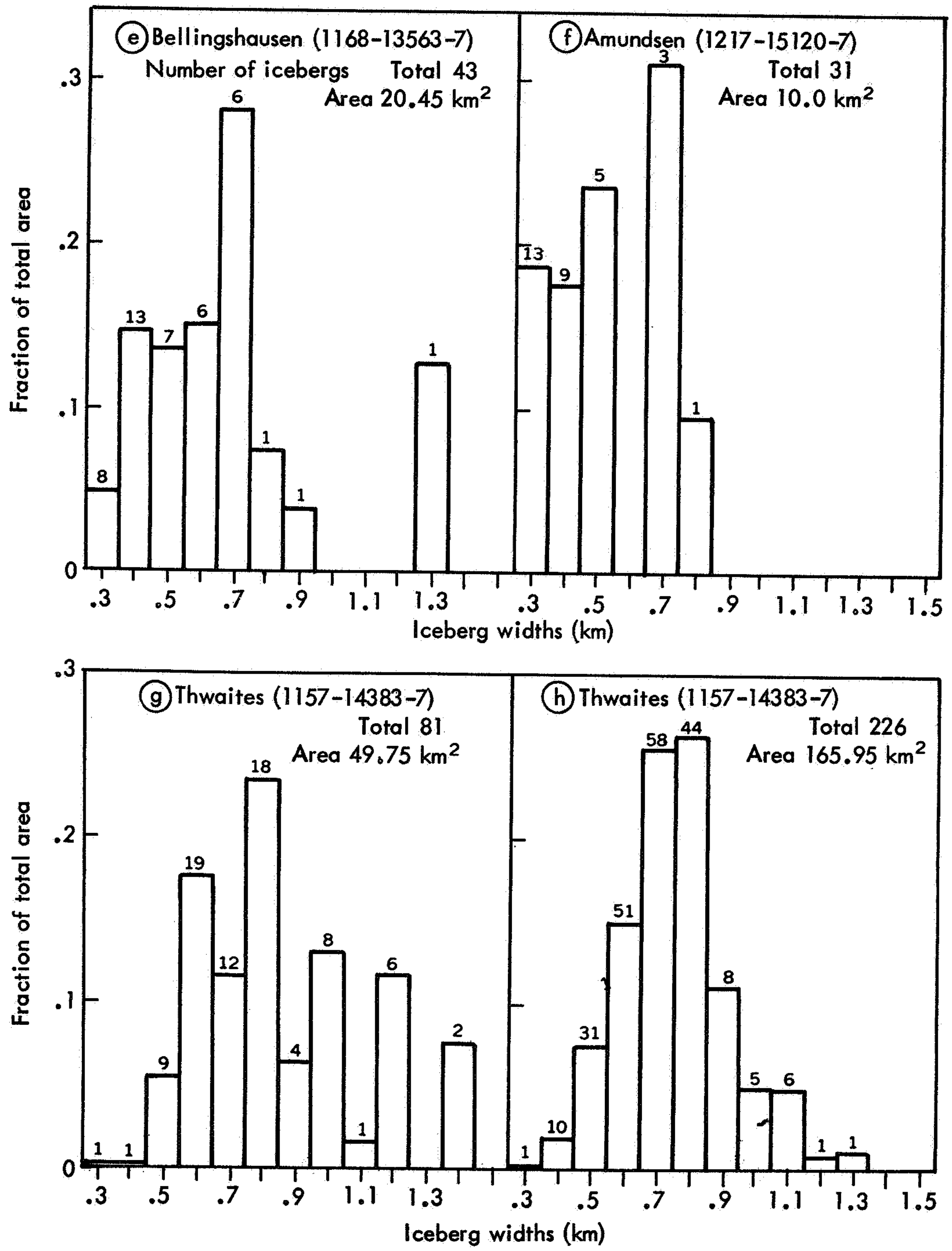

Fig. 6 — Continued

northern edge of the belt as compared with those near the coast indicate that the melting life of the average iceberg in a circulating gyre may be comparable to the circulating period of the icebergs.

The imagery from ERTS-1 did not provide any accurate means of determining height or thickness of icebergs. The shadows produced on surrounding sea ice give an approximate order of magnitude for the height of many of the icebergs ($\sim$50 m). However, more accurate determination from satellites will probably require different sensors (such as thermal imaging devices that could measure temperature differences with height, or radio waves using ranging techniques). There probably is some relationship between the thickness of glacial ice streams entering the ocean water and the characteristic widths at which the icebergs tend to break off. Also, the entering flow inclination, tides, and seasons may be influential factors. Additional ERTS data, especially from high-resolution thermal sensors, together with correlation with ground truth, seem desirable for reliable estimates of iceberg thickness.

Some iceberg characteristics, such as the nature and smoothness of the melting submerged surfaces and the expected variations with source and environmental history, will probably never be known without direct physical measurements. Much additional valuable information for achieving efficient harvesting operations will best be gained by experience in the operating environment.

ANTARCTIC TOPOGRAPHY

In addition to the information about iceberg resources that was obtained from ERTS imagery, considerable topographical information was obtained that may be useful for mapping and other Antarctic interests.

A complete listing of images that contain topographical information unobscured by cloud cover may be obtained from the Image Descriptor Data Bank file under the descriptor: Antarctic Topography.

ERTS SYSTEM POTENTIAL

The limited Antarctic imagery that was obtained for this investigation is adequate to extrapolate with reasonable confidence what the ERTS system could be in application to Antarctic iceberg resources. This estimate could be confirmed with suitable system modifications to planned experiments including those with ERTS-B.

LIVE IMAGERY

The principal advantages of live (real-time) imagery obtained with Antarctic readout stations are that it would be possible to collect complete imagery from every orbital pass over Antarctica and it could

be made available for immediate use. This would eliminate the storage capacity limitations and reliability problems of spaceborne video recorders. Also, the information could be made available soon enough to be of tactical value in the control of harvesting operations.

There are a number of ways that live readout might be provided in Antarctica. Synchronous satellite relay could make live readout possible almost anywhere on earth. This could require the development and operation of the relay satellites and considerable modification to current ERTS designs, but it may be the ultimate solution. An earlier solution that could be made compatible with current ERTS configurations would be to provide a readout station on board a ship that could be moved to provide the service wherever it was needed. Or earth stations could be installed at suitable locations such as McMurdo station for year-round operation. It appears that such a site alone could provide live readout for most of Antarctica except for coastal and drift-ice areas in the sector of eastern Antarctica between the Weddell Sea and the Amery Ice Shelf. It could provide excellent coverage for readout of stored data because it could follow *every* orbital pass for a relatively long time. Therefore, it could obtain stored readout with very small delays from many areas that it could not reach for live readout.

An alternative to live readout for alleviating the deficiencies of the initial experimental ERTS system relative to Antarctic imagery would be to greatly increase the capacity and flexibility of the recording system. This might require improving the earth station network for readout of stored data in addition to increasing the recording capability in the satellite. A site at McMurdo may be an attractive augmentation that would permit much live readout as well as transmission of most of the stored data on every orbital pass.

The initial investment required to install a readout station near McMurdo is estimated to be comparable to the Fairbanks, Alaska installation--about $500,000. A crew of 35 has proved satisfactory to provide four operating shifts of eight men each. If a "quick look" facility is to be provided, an initial investment of about $100,000 would be added. It is estimated that about $1.5 million per year will be required to cover the annual operating expenses and to recover the initial investment costs during its useful life. If the filtered imagery is to be transmitted to potential users by synchronous satellite relay, it may not increase greatly the costs of the McMurdo station if a suitable site is selected that is within a satisfactory look angle to the relay satellite, but the communication relay costs must be added as a part of the total user costs.

THERMAL AND MICRO WAVELENGTHS

A thermal wavelength band (10.4 to 12.6 micrometers) is planned for inclusion in ERTS-B. With imagery from this band it may be possible

to measure small surface temperature differences day or night. Such a capability may greatly aid in distinguishing icebergs from sea ice and may even permit height determinations of icebergs by temperature differences. Approximately the same ground resolution would be desirable at thermal wavelengths as is provided with the other wavelength bands. Also, approximately the same cloud-cover limitations will apply. Because most of the cloud cover in Antarctica consists of particles that are large compared to these wavelengths, the cloud cover is not expected to provide significantly greater openings at thermal than at the shorter wavelengths. The thermal band is used to record the one-way thermal emission from the surface, and the cloud cover attenuates or darkens this emission. At the shorter wavelength bands, the observations are of scattered sunlight and the brightness of the cloud-scattered sunlight degrades any contrast that might otherwise filter through the cloud cover. However, the distinction between the ways in which the bands obtain imagery is not expected to make any great operational difference in the effects of cloud cover. On the other hand, the many more observation opportunities available with the thermal band (every pass, independent of solar illumination) will permit obtaining two to six times as many glimpses through cloud openings and will enable monitoring throughout the year.

Microwaves could penetrate cloud cover, and the reflections from the top and bottom of ice have been used to measure ice-shelf thicknesses by ranging techniques from aircraft. However, these techniques are not yet feasible from ERTS and the angular resolution achievable at these ranges and wavelengths would not be very useful for observing most individual icebergs. However, synthetic aperture radar techniques could be used from aircraft or satellites to provide high resolution surface mapping independent of cloud cover or solar illumination. Although these techniques may not soon be available on operational ERTS type of satellites, they could be employed with aircraft to greatly reduce the flight effort required with sensors that are obstructed by cloud cover.

SEA-ICE BEHAVIOR AND ICEBERG EVOLUTION

In order to plan the operational harvesting of icebergs it is important to understand sea-ice behavior and iceberg evolution. Much of this knowledge could be obtained by monitoring and following iceberg processes over several yearly cycles of seasons in the areas of interest. Since this should be done prior to operational harvesting, the cost of obtaining the information should be treated as research cost to be recovered during the years of harvesting operations. It does not seem important to have a "quick-look" capability for this type of information. However, in order to achieve usefully complete coverage through the prevailing cloud cover, it would be desirable to obtain imagery on nearly every pass opportunity. The very limited sampling of part of western Antarctica that was accomplished with ERTS-1 will be useful for correlation with more comprehensive data that might be obtained in the next few years. Comprehensive satellite imagery should be buttressed with ground truth information that might be obtained from a test program to acquire, harness, insulate, and tow real (though small) icebergs in Antarctica. Only then

would it be possible to design and invest in operational systems with the necessary confidence.

TACTICAL HARVESTING INFORMATION

Tactical information for aid in acquiring icebergs and controlling the harvesting operations should be timely, and timeliness could be achieved with live readout and a "quick-look" capability. Each operational harvesting expedition could include this capability as an integral part of its facilities. Alternatively, it could be accomplished at a common central station, e.g., McMurdo, and the useful processed information could be forwarded to the harvesting expeditions by satellite relay. In either case, the costs of obtaining the information would be an operational expense that legitimately should be charged to the harvesting operations.

CLAIMING AND MONITORING SERVICE

When there is the possibility of independent harvesting operations competing for icebergs, a claiming procedure that will permit efficient planning and harvesting will be needed. This might be accomplished by practices established in other situations, e.g., staking claims perhaps a year or two in advance, or stationing a man on board so that the ice "ship" is not abandoned. However, a more attractive way of claiming might be to coordinate and monitor the claiming with ERTS imagery. This method could be used to coordinate the claiming early enough to permit efficient planning for harvest without excessive claiming effort or resource waste. The claiming service would be a legitimate operational harvesting expense, and the charge could be determined by the quantity or value of icebergs claimed.

ENTITLEMENTS TO ANTARCTIC ICEBERG RESOURCES

The Antarctic icebergs are a continuous yield resource. They simply melt and return to sea water without a direct benefit to mankind if they are not harvested and used in the process. They are part of the international waters and should be available to anyone as an extension of the freedom-of-the-seas doctrine. Furthermore, it would seem desirable to avoid the tradition practiced for water entitlements in parts of the world in which indefinite claims are established by the first to perfect their rights, so that future new needs may be denied if the resources are not adequate.

It is suggested that the claiming and monitoring service with satellite imagery be extended to include auction of the icebergs, with any surplus revenues used to increase the harvest and equalize the costs. The auction and claiming could be once a year, sufficiently in advance of the harvesting season to permit adequate planning and preparation for the operations. This method of granting entitlement to icebergs should secure the greatest economic benefits from this resource, and it would not deny anyone future access.

ECONOMIC POTENTIALS FOR ERTS

About $1.5 million per year is estimated to be necessary to maintain a continuous ERTS readout and "quick-look" station in Antarctica. This would permit using the full capabilities of ERTS-1 and ERTS-B on every orbital pass to provide a wealth of information about Antarctica in general, in addition to that of primary value for the harvesting of icebergs. Also, a station near McMurdo would be able to read out any stored information on every ERTS orbit. This might permit greatly increased world-wide use of the image storage capability of ERTS by relieving readout constraints.

The estimated revenue requirement to procure and place an operational ERTS into orbit and control its operation will probably be between $5 and $10 million annually. However, the Antarctic harvesting of icebergs should only be assessed its fair share of this revenue requirement.

The total cost of delivering iceberg water to the final user or distributor is estimated to be about $24 per $k{\cdot}m^3$. [2] This is only a small fraction of the cost of desalting sea water or of long distance interbasin transfer. Therefore it is not expected that iceberg water will suffer serious competition from these other sources even if the price is raised considerably. However, the demand for iceberg water for agricultural uses is expected to be very elastic about this point, and to supply the agricultural demands it will be necessary in most cases to reach the scale that will permit the attractive prices that have been estimated for iceberg water. Therefore, it is felt that the iceberg harvesting systems may only be able to afford an additional assessment of a few percent of the delivery price for the water before the demand might be seriously affected, i.e., large volume demand might fall rapidly with increasing assessments above about $1 per $k{\cdot}m^3$ for ERTS aid.

If 10 percent of the annual yield of Antarctic icebergs were harvested, an assessment of $0.10 per $k{\cdot}m^3$ would produce an annual revenue of about $10 million, which would be adequate to compensate for the share of ERTS operating costs. However, since early harvesting operations may commence at only 1 percent of the annual yield and some research and development costs should be assumed by the iceberg harvesting operations, it would seem appropriate to begin assessing iceberg harvesting operations at a rate between $0.1 and $1.0 per $k{\cdot}m^3$.

In order to obtain as much useful imagery with optical sensors on board high altitude aircraft as might be obtained with full use of ERTS, at least 10 aircraft passes would be required for each ERTS pass to achieve a comparable coverage. The most suitable aircraft for such a task would require at least 1,000 hours of imaging flight every 24 hours in order to duplicate the ERTS coverage. Although a feasible basing and operational plan has not been conceived, an operating fleet of more than 120 aircraft and 400 flight crews would be required to maintain such operations over an extended period of time. This would be a prodigious and costly operation compared to that required with ERTS (at least 10 to 100

times as great an effort). Even with a likely requirement for coverage of only portions of the Antarctic, the task of doing it with optical sensors on board aircraft seems much larger than full coverage by satellite.

If satsisfactory coverage could be obtained with synthetic aperture radar on board aircraft, it may be possible to do so for limited operations at costs comparable with the full use of ERTS. The capabilities and costs of both techniques need test and evaluation in order to select the appropriate operational role of each.

The costs of not having the equivalent of ERTS imagery for harvesting of icebergs in the Antarctic are also difficult to assess. Small bootleg operations would be possible without paying an ERTS toll. However, it should be very difficult to achieve dependable competitive operations or obtain user commitments with any operation that would try to harvest without coordination through an ERTS information system established for this purpose.

SUMMARY AND CONCLUSIONS

This investigation is one of a series exploring various aspects of the feasibility of using Antarctic icebergs as a global fresh water resource. Related investigations that have explored concepts for transporting and using the icebergs indicate great promise for this continuous yield resource. However, icebergs of appropriate size and shape must be available for assembly into trains for economical transport, and methods must be found to cope successfully with the surrounding sea ice. Also, ways of harmoniously harvesting this international resource must be developed. These problems have been the concern of this investigation.

The results from ERTS-1 for the period from November 1972 through March 1973 reveal a general prevailing cloud cover more than 80 percent of the time over the Antarctic coastal and sea areas of interest. However, openings in the cloud cover can be exploited to piece together imagery of a large fraction of the earth's surface off Antarctica every few weeks, if every ERTS imaging opportunity is taken.

The sea-ice belt girding Antarctica was very evident, but there was insufficient imagery to refine previous descriptions of its seasonal behavior. Many images of iceberg clusters were obtained that confirm the general abundance and dimensional characteristics of icebergs and that identify differing characteristics with different sample areas. However, the sea-ice and iceberg environment should be comprehensively and continuously monitored for several years in order to acquire enough information to confidently plan and design efficient iceberg harvesting operations. A wealth of additional information for mapping, resource exploration, and research can also be obtained when imagery for iceberg resources is collected.

The potential application for ERTS would be greatly enhanced with live Antarctic readout to enable the timely acquisition of complete imagery

on every orbital pass. Also, use of thermal bands should provide better imagery in daylight or darkness throughout the year. With these improvements in ERTS performance, the long-term monitoring for planning and design as well as the quick-use requirements for control of harvesting operations and the registering of claims and entitlements could be achieved. ERTS has capabilities that could support new concepts for claiming service and establishing entitlements that would drastically reduce the costs, conserve the resources, harmonize the operations, and reserve the opportunity for anyone to acquire any entitlement in the future.

The iceberg harvesting operations can easily bear the costs of the ERTS services that appear to be essential to the success of economical large-scale use of the continuous Antarctic iceberg yield that otherwise melts and returns to sea water without benefit to man in the process.

REFERENCES

1. *ERTS Data Users Handbook*, NASA Goddard Space Flight Center, Greenbelt, Maryland.

2. Hult, J. L., and N. C. Ostrander, *Antarctic Icebergs as a Global Fresh Water Resource*, The Rand Corporation, R-1255-NSF, October 1973.

3. Weeks, W. F., and W. J. Campbell, *Icebergs as a Fresh Water Source: An Appraisal*, Cold Regions Research and Engineering Laboratory, Hanover, N. H., Research Report 200, January 1973.

4. *Earth Resources Technology Satellite, Cumulative Non-U.S. Standard Catalog No. N-9*, NASA Goddard Space Flight Center, Greenbelt, Maryland, May 31, 1973.

5. Newton, Chester W. (ed.), *Meteorology of the Southern Hemisphere*, American Meteorological Society, Meteorological Monographs, Vol. 13, No. 35, November 1972.

6. *Atlas Antarktiki* (Atlas of Antarctica), published in 1966 in Moscow by the Main Administration of Geodesy and Cartography, Ministry of Geology USSR. Translated in *Soviet Geography: Review and Translation*, Vol. 8, nos. 5-6, May-June 1967, American Geographical Society, Lane Press, Burlington, Vermont.

7. *Sailing Directions for Antarctica, Including the Off-Lying Islands South of Latitude 60°S*, H. O. Pub. No. 27, U. S. Navy Hydrographic Office, 2d ed., 1960.

8. *Oceanographic Office Observers Manual: Ice Observations*, H. O. Pub. 606-d, U. S. Navy Oceanographic Office, rev. ed., 1968.

ENVIRONMENT SURVEYS

Paper E 1

THE USE OF ERTS-1 IMAGERY IN AIR POLLUTION AND MESOMETEOROLOGICAL STUDIES AROUND THE GREAT LAKES

Walter A. Lyons, *Air Pollution Analysis Laboratory* and Richard A. Northouse, *Robotics and Artificial Intelligence Laboratory, College of Engineering and Applied Science, The University of Wisconsin-Milwaukee, Milwaukee, Wisconsin 53201*

ABSTRACT

ERTS-1 images continue to be highly useful in studies of: (1) long range transport of air pollutants over the Great Lakes, (2) the mesoscale atmospheric dynamics associated with episodic levels of photochemical smog along the western shore of Lake Michigan, (3) inadvertant weather modification by large industrial complexes. Also unusual wave patterns in fogs and low stratus over the Great Lakes are being detected for the first time due to the satellites high resolution.

1. INTRODUCTION

The Air Pollutional Analysis Laboratory of the University of Wisconsin-Milwaukee is engaged in a major EPA-supported study of mesoscale pollution transport phenomena along the western shore of Lake Michigan. Though this project, which involves use of instrumented Cessna 336 (operated with the Wisconsin Department of Natural Resources), pilot balloon and tetroon wind measurements, a nine station air quality monitoring network, helicopters, etc., was begun prior to the launch of ERTS-1, the satellite has been playing an increasingly large role in understanding the complex mesoscale meteorological processes which result in frequent adverse air quality levels in the Gary-Chicago-Milwaukee corridor. In addition, a National Science Foundation grant, in support of the International Field Year for the Great Lakes (IFYGL), has greatly benefitted from the ERTS-1 program. The project involves the compilation of a one-year mesoscale cloud census and solar radiation climatology for Lake Ontario. The high resolution images of ERTS have enabled unambiguous determinations of cloud types and systems with a precision unobtainable with any current operational meteorological satellite. Furthermore, several unexpected mesoscale cloud structures have been detected and are under intensive study. In essence, the meteorological content of ERTS imagery is almost limitless, and except for manned spacecraft photography, provides the most significant source of information for cloud studies available.

2. LONG DISTANCE POLLUTION TRANSPORT ACROSS A LARGE LAKE

Air pollution meteorologists have, often for lack of better information, tended to consider the air pollution levels in a given air quality control region (AQCR) to be solely the result of emissions within that region. This concept of a "regional air shed" has long prevailed in the formulation of control strategies for any given AQCR, including the seven counties of Southeast Wis-

consin. Yet for several years it had been "guesstimated" that perhaps 10% of Milwaukee's suspended particulates originate from the Chicago-Gary area. On 1 October 1972, an ERTS-1 image (ID No. 107016041) of southern Lake Michigan revealed smoke plumes from several major industrial clusters at the southern end of Lake Michigan streaming more than 60 km northeastwards over the lake before disappearing beneath a cloud deck (Fig. 1 a,b). This clearly established that, at least during the spring through early fall, when air masses are warmer than the relatively cold lake surface, that these particulate plumes can travel great distances over the lake with comparatively little diffusion. It also lends great credance to the hypothesis that Milwaukee citizens frequently might breathe significant dosages of the pollutants emitted by Gary, Indiana over 160 km away. Experience has shown that these plumes can be best seen (over water) in either band 5 or 6 (Fig. 1b). A more theoretical discussion of plume contrasts over a water surface is given by Lyons and Pease (1973).

On 14 October 1973, another image (ID No. 144816023) over the same region again showed the same phenomena - except this time no cloud cover obscured the plume's track. Figure 2 shows several major plumes advecting in southwesterly flow towards the Michigan shoreline. After initial spreading (due to residual turbulence generated over the heated land), the plumes show little further dilution and cross the lee shoreline in the Benton Harbor, Michigan area (110 km fetch). As these plumes moved overland, they almost certainly underwent continuous fumigation to the surface about 5 to 10 km inland, undoubtedly causing high levels of pollution at the surface. Needless to say, Michigan air pollution control authorities, had they monitored this region, might very well have been at a loss to explain such readings in an area relatively free of local sources. The shoreline fumigation problem of the Great Lakes is discussed in depth by Lyons and Cole (1973) who also present a numerical method for modeling

its effects. The meteorological and legal ramifications of such widespread interregional pollution transport are now, with the help of ERTS, beginning to be understood.

3. THE LAKE BREEZE AND AIR POLLUTION

During summer 1973 a large field project was conducted in Milwaukee to study the detrimental effects of the lake breeze circulations on shoreline air quality. Fig. 3 is a map of the field operations areas superimposed over the 17 July 1973 ERTS image (blowup of Milwaukee region). Lake breezes cause high air pollution in shoreline areas for several reasons: (1) limited mixing depths associated with intense low-level inversions as cool lake air moves inland, (2) continuous fumigation of elevated plumes from such shoreline sources as power plants, and (3) recirculation of pollutants within the lake breeze cell wind patterns (Lyons and Olssen, 1973). The various observations taken this day indicated a classic lake breeze (penetrating about 5-10 km inland at 1000 LST). Eulerian (pilot balloon) and Lagrangian (optically tracked tetroons) wind field measurements showed a 500m deep inflow layer capped by the typical westerly return flow current aloft. The Lagrangian air trajectory measurements suggested the expected circular motion of air (and pollutants) over the shoreline region. The surface air quality monitoring network plus the instrumented Cessna 336 aircraft measurements produced the expectedly high levels of particulates and sulfur oxides. What was not expected, however, was that readings of photochemical oxidants (ozone) at several stations within the lake breeze reached alert levels (greater than 10 PPHM for 4 hours or more) and peak values approached 30 PPHM (especially on 18 July 1973, when similar conditions prevailed). The southeast Wisconsin region had not been presumed to have sufficiently large emissions of the primary pollutants (hydrocarbons and oxides of nitrogen) to result in such

high levels of ozone. The immediate reaction of the writers was to consider the Chicago metropolitan region a major contributor of these pollutants. This notion was at first resisted by some area officials. However, the ERTS-1 image (ID No. 135916094 and 135916100) for 17 July 1973 (Fig. 4) shows a distinct band of cumulus clouds stretching from Chicago to Milwaukee. These clouds mark the lake breeze front. By considering the air trajectories obtained that day by the tetroons, it now appears quite likely that morning rush hour automotive exhausts from Chicago did indeed become trapped within the lake breeze cell, and travelled in a long helical trajectory northwards. With the measured northwards component of the wind, it appears entirely plausible that Chicago pollutants could have reached Racine and Milwaukee by afternoon, adding significantly to the photochemical smog levels. The immediate question is then raised: how is the southeast Wisconsin AQCR to alleviate a photochemical smog episode by a plan of curtailing the industrial and automotive emissions in its region if a significant portion of the offending pollutants originate in another jurisdiction?

4. INADVERTANT WEATHER MODIFICATION BY INDUSTRIES

Lyons and Pease (1973) reported on a case where the smoke plumes from the Chicago-Gary industrial complex obviously appeared to be "seeding" winter cumulus cloud bands over Lake Michigan, causing them to be better developed, brighter, and potentially greater producers of snow. Continued monitoring of this region continues to reveal examples of "inadvertant weather modification" by man's activities. On both 16 July 1973 and 3 August 1973 (ID No. 135816042, ID No. 137616041) northeasterly winds were blowing onshore in the Chicago area. Since the particular air masses were relatively cool for the season, the usual intense low level inversions were not present over the lake. Stability in the lower 1000m of the atmosphere was probably close to dry adiabatic. Thus cumulus cloud formation could be expected to begin shortly after the air advected in-

land over the much warmer ground surfaces. This was indeed found (Fig. 5a, b), but so were several distinct lines of well developed cumulus clouds which obviously had their origins over several major industrial complexes (mostly steel mills).

Such phenomena have been suspected, but the ERTS imagery incontrovertibility shows that major plumes can modify and induce convective cloud development both during the winter and summer months. On neither day did the clouds grow to precipitation states. Yet the well publicized LaPorte, Indiana excess precipitation anomaly (Changnon, 1968) has frequently been ascribed to the "seeding" effects of the Chicago-Gary industrial effluents. ERTS thus provides one more piece of evidence which may eventually prove the correctness of this hypothesis.

6. MESOSCALE GRAVITY WAVES IN STRATUS CLOUDS

During the spring, Lake Michigan water temperatures rise very slowly, so that often overlying air masses might be as much as 30°C warmer. This condition results in almost persistent shallow (100-200m) but intense "conduction inversions" over the lake. If the airmass dewpoints are higher than the lake surface temperature, shallow fogs often form. These may cover much of the lake surface, and will often drift inland several miles before being dissipated by heating from the warm ground. ERTS images have, not unsurprisingly, revealed many of these fog masses over the Lakes during spring and summer months. But what has now been discovered in the ERTS imagery are frequent extremely complex mesoscale wave motions in the fog and stratus cloud decks. On 18 April 1973 (Id No. 126916101) such a fog bank was observed over Lake Michigan from Milwaukee north to the Door County, Wisconsin peninsula (Fig. 6). A fine network of intersecting wave patterns in the fog is visible, with wave trains often at right angles to one another. The initial interpretation of these images is in-

triguing. Intense internal gravity waves are being generated near the top of the surface based inversion (about 100m), presumably due to strong wind shears present there. These waves then propagate and those which strike the shoreline bluffs are reflected much like water waves in a pool. While there is no theoretical reason why such cannot happen, this is perhaps one of the first and most graphic examples of this atmospheric process. A numerical model of the actual conduction fog formation process has now been developed. It is now possible to compute at least the gross temperature and moisture profiles associated with these highly modified lake air masses.

7. FUTURE STUDIES

In the near future it is hoped to obtain "ground truth" measurements of suspended particulate levels in the Chicago-Gary smoke plumes using the instrumented aircraft simultaneously with ERTS overflights. Future goals include development of reliable methods for estimating diffusion statistics over water for major plumes and also possibly making direct estimates of atmospheric particulate loadings from ERTS data. The UWM Robotics and Artificial Intelligence Laboratory is currently beginning experiments with ERTS digital tapes to see if pattern recognition and cluster analysis methods can be used to automatically detect, (1) suspended particulate air pollution over water, (2) glaciated (ice) versus supercooled liquid water cloud types (for possible detection of inadvertant cloud seeding by anthropogenic ice nuclei sources).

8. ACKNOWLEDGMENTS

Portions of the research supported by the State of Wisconsin Department of Natural Resources, the National Aeronautics and Space Administration (NASA-21736), Environmental Protection Agency (Grant R800873), and the National Science Foundation (Grant GA-32208).

9. REFERENCES

Lyons, W. A. and S. R. Pease, 1973: ERTS-1 Views the Great Lakes, NASA Goddard Space Flight Center, Symposium on Significant Results Obtained from ERTS-1, March 5-9, 1973, pp. 847-854.

Lyons, W. A. and L. E. Olsson, 1973: Detailed Mesometeorological Studies of Air Pollution Dispersion in the Chicago Lake Breeze, Monthly Weather Review, May, pp. 387-420.

Lyons, W. A. and S. R. Pease, 1973: Detection of Particulate Air Pollution Plumes from Major Point Sources using ERTS-1 Imagery, Bulletin of the American Meteorological Society, November.

Changnon, S. A., Jr., 1968: The LaPorte Anomaly - Fact or Fiction?, Bulletin of the American Meteorological Society, Jan., pp. 4-11.

Lyons, W. A. and H. S. Cole, 1973: Fumigation and Plume Trapping on the Shores of Lake Michigan During Stable Onshore Flow, Journal of Applied Meteorology, April, pp. 494-510.

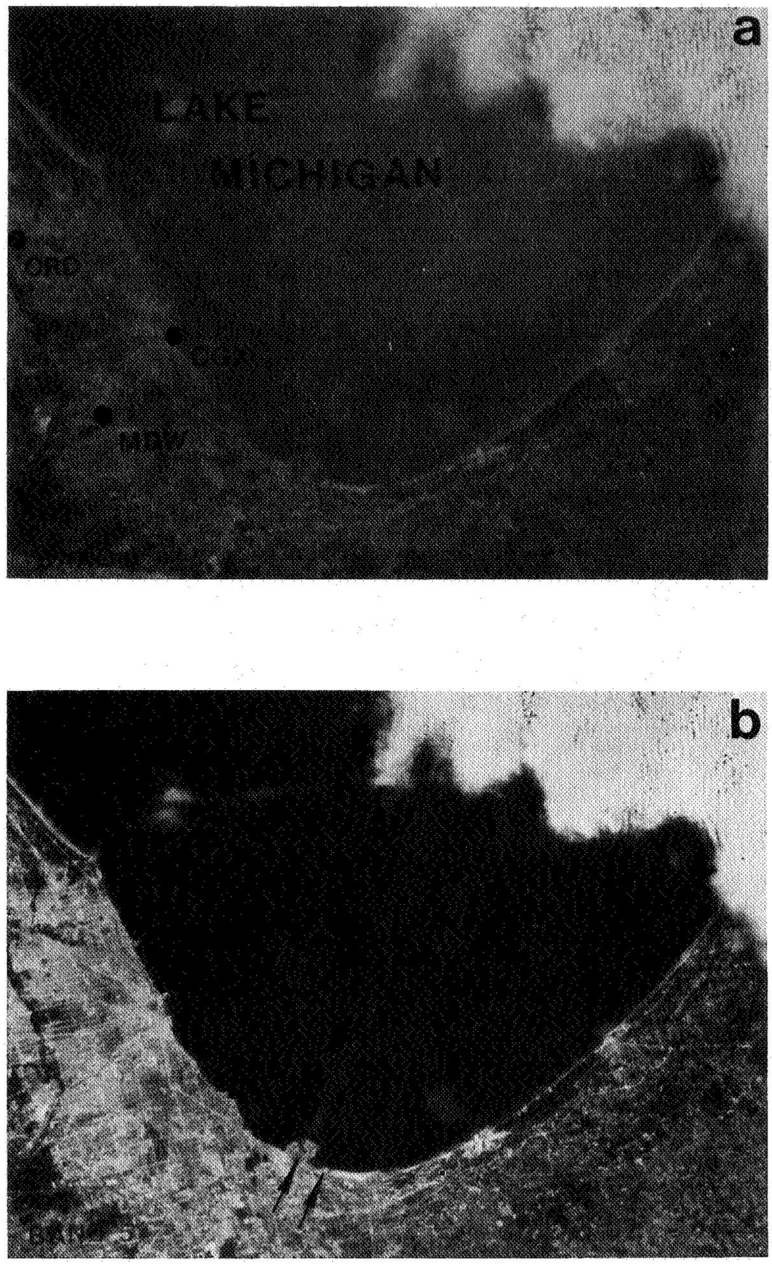

Figure 1 - ERTS-1 images over southern Lake Michigan, 1 October 1972 for band 4 (top) and band 5 (bottom). Plumes of smoke from major industries can be clearly seen extending for more than 60 km to the northeast over the lake in band 5. The general lack of image contrast in the 0.5-0.6 micrometer region makes the plume virtually invisible.

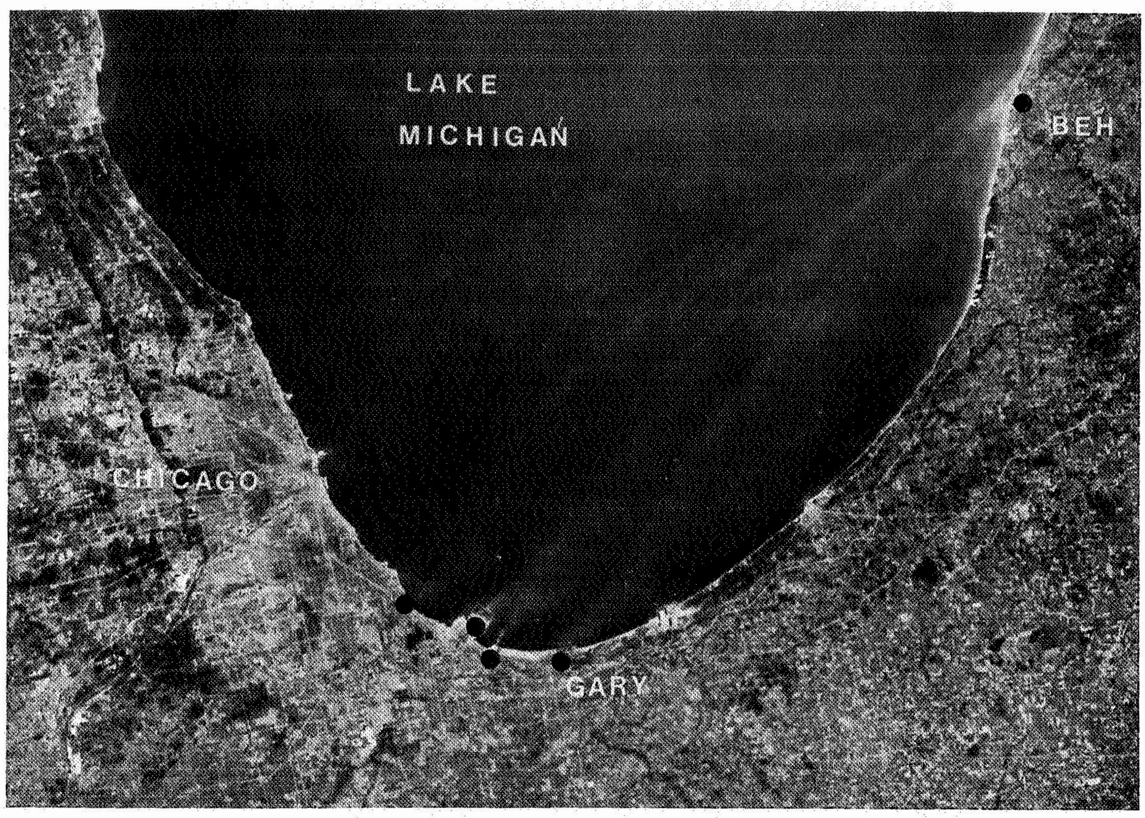

Figure 2 - Southern Lake Michigan area, 14 October 1973, band 5, showing plumes of smoke from the Chicago-Gary complex travelling the entire lake and crossing the downwind shoreline near Benton Harbor, Michigan (BEH).

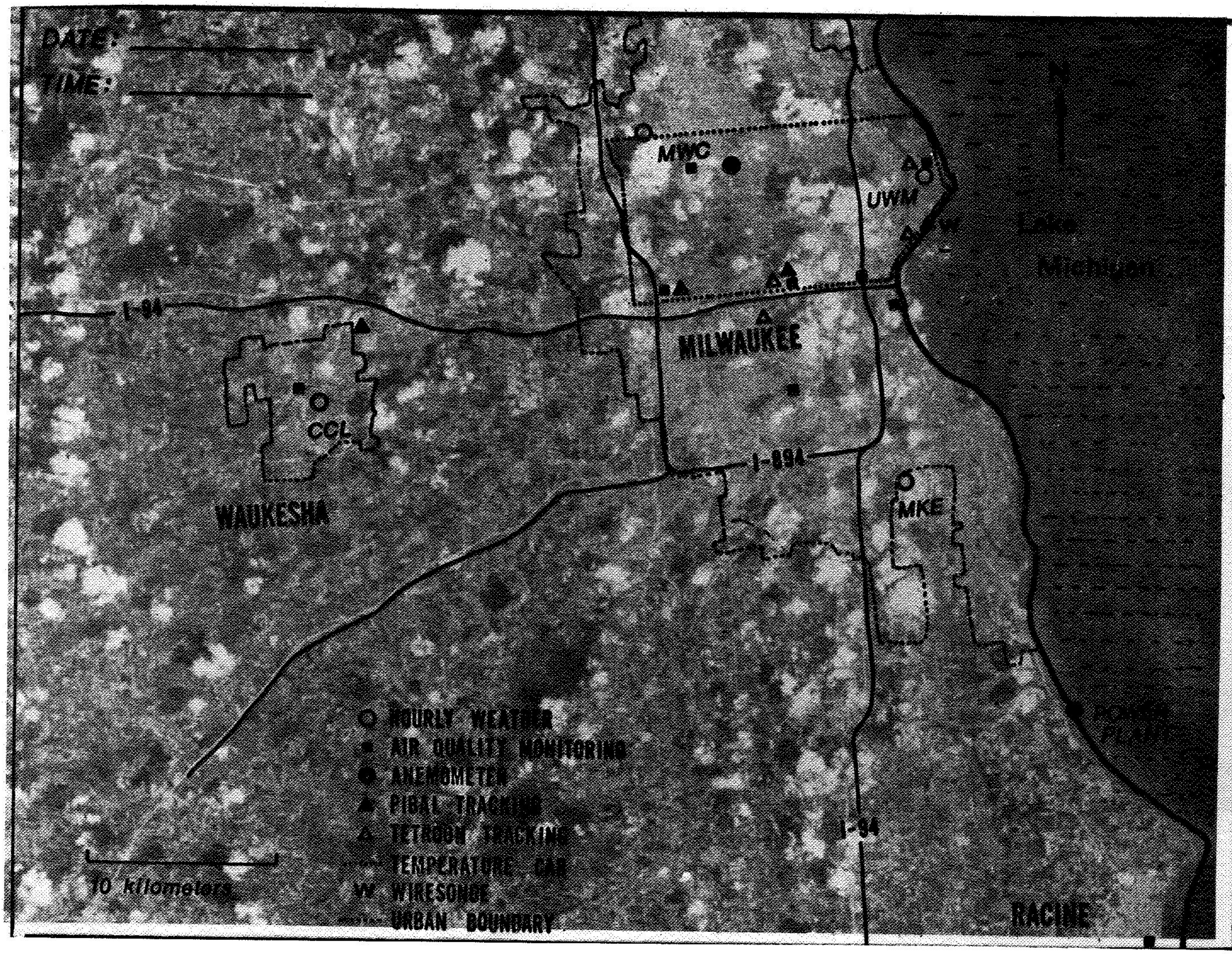
DATE:
TIME:
N
Lake Michigan
MWC
UWM
W
MILWAUKEE
I-94
I-894
CCL
WAUKESHA
MKE
POWER PLANT
RACINE
HOURLY WEATHER
AIR QUALITY MONITORING
ANEMOMETER
PIBAL TRACKING
TETROON TRACKING
TEMPERATURE CAR
W WIRESONDE
URBAN BOUNDARY
10 kilometers

Figure 3

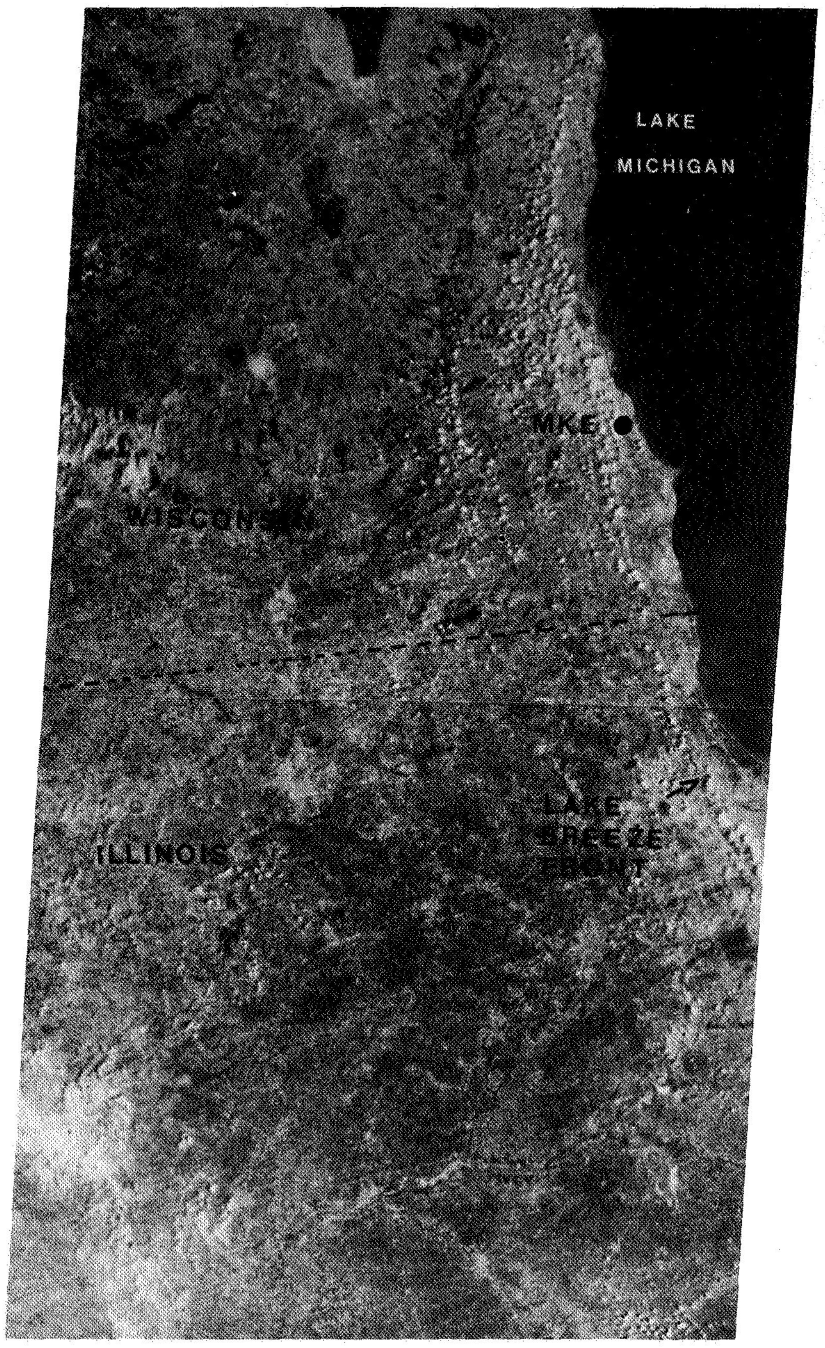

Figure 4 - The western shore of Lake Michigan from the northern portion of Chicago to Sheboygan, Wisconsin, band 5, 17 July 1973. Visible is the line of cumulus clouds marking the lake breeze front during a period of high photochemical oxidant levels in shoreline areas.

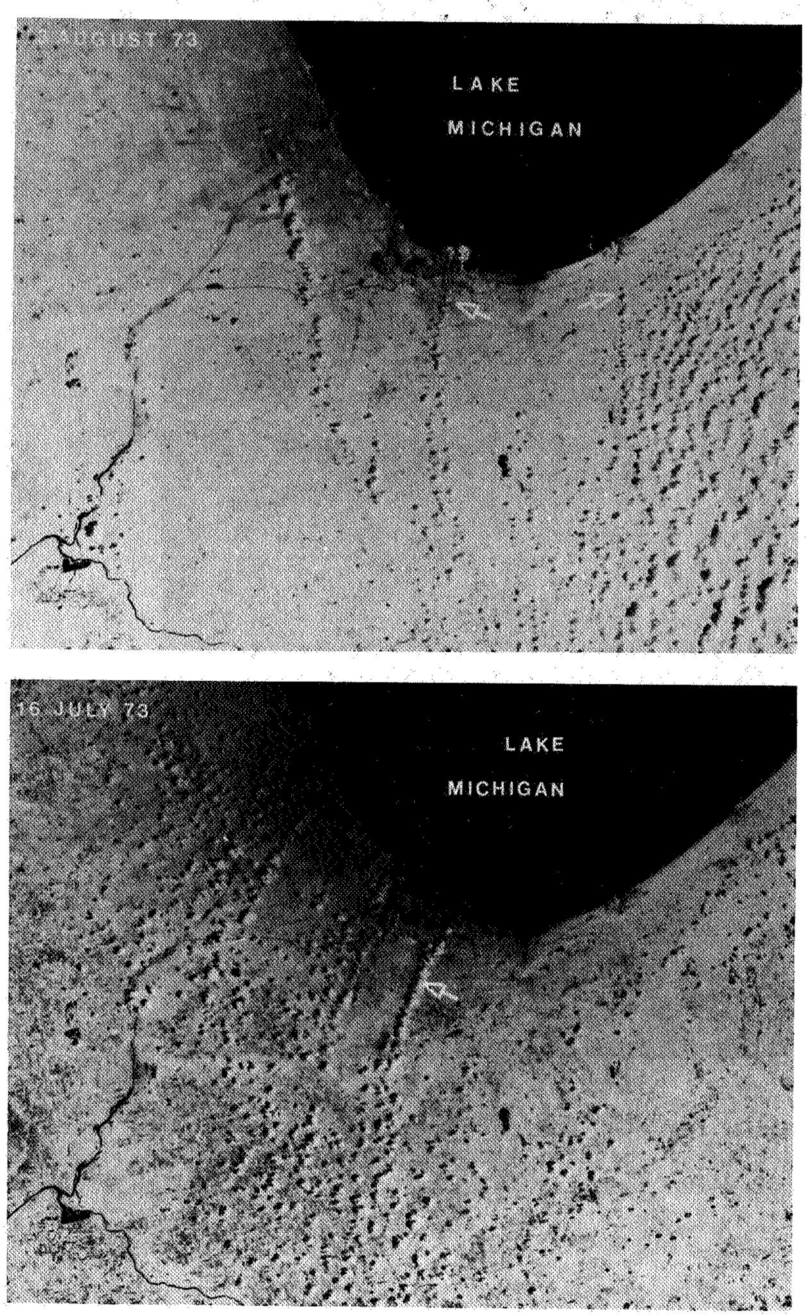

Figure 5 - Views of the greater Chicago area on 3 August 1973 (top) and 16 July 1973 (bottom). Lines of cumulus clouds generated by industrial activity indicated by arrows. Both scenes band 7.

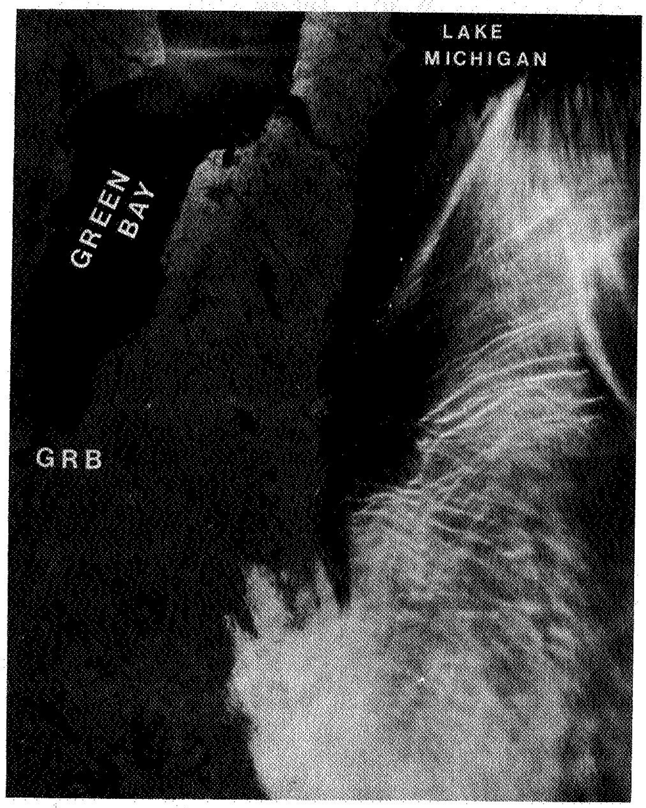

Figure 6 - Shallow fog over western Lake Michigan (southern Green Bay in upper left), band 6, 18 April 1973. Patterns reveal trains of complex intersecting internal gravity waves within inversion layer.

Paper E 2

A METHOD TO MEASURE THE ATMOSPHERIC AEROSOL CONTENT USING ERTS-1 DATA

Michael Griggs, *Science Applications, Inc., 1200 Prospect Street, P.O. Box 2351, La Jolla, California 92037*

ABSTRACT

The apparent gradual increase of particles in the atmosphere has received considerable attention in recent years due to the possible effect of atmospheric aerosols on the earth's climate. The ERTS-1 satellite offered the opportunity of determining the feasibility of monitoring the atmospheric aerosol content on a global basis, as suggested by theoretical studies, which showed a linear relationship between the upwelling earth-atmosphere radiance and the aerosol content. This relationship was investigated at two test sites, San Diego and the Salton Sea, using the MSS radiance data, with ground-truth observations of the aerosol content being made with a Volz photometer at the time of the satellite overpasses. Significant results, relating the radiance over water surfaces to the atmospheric aerosol content, have been obtained. The results indicate that the MSS channels, 4, 5 and 6 centered at 0.55, 0.65 and 0.75 μm have comparable sensitivity, and that the aerosol content can be determined within $\pm$ 10% with the assumed measurement errors of the MSS. The accuracy of the aerosol content measurement could be increased by using an instrument specifically designed for this purpose.

INTRODUCTION

The scientific community (e.g. SCEP[1] and SMIC[2]) has become increasingly aware in recent years of the importance of atmospheric aerosols and their optical properties in possible climate modification. The aerosols in the atmosphere consist of man-made and natural particles, and it is the man-made contribution due to combustion added to the natural (dust, sea spray, forest fires and volcanic dust) background that is generally considered to be important in determining climatic changes. However, the man-made contribution on a global scale is quite small; estimates range from a negligible amount[3] to about 6% of the natural background[4]. (Of course, on a local scale, e.g. the Los Angeles basin, man-made particles can far exceed the

natural concentration.) It may well be that global changes in the natural background are more important than man-made particles. With the increased cultivation of land and activities of man in arid areas, the background level of aerosols is likely to increase.

McCormick and Ludwig[5] presented evidence of a worldwide buildup of atmospheric aerosols which could increase the earth albedo resulting in a cooling of the earth-atmosphere system. This effect would counteract the postulated increase of temperature in the lower atmosphere due to the "greenhouse effect" of the increased CO_2 emissions by human activities. In fact, there has been a decrease in the mean annual air temperature since about 1945 at mid latitudes, suggesting that the aerosol pollution effect is greater than that of the CO_2 increase. However, the effects of aerosols and CO_2 are more complex than suggested above, so that their effects on climate are not readily predicted. For instance, Robinson[6] points out that the earth may self-regulate its temperature by the variation of cloud amount: the higher temperatures, due to the CO_2 "greenhouse effect", lead to a higher water content in the lower atmosphere, which may increase the cloud amount; this increases the albedo, thereby decreasing the temperature. Robinson concludes there is no justification for forecasting a final equilibrium temperature due to an increase in CO_2 content, until atmospheric models are significantly improved to include the cloud cover as a variable.

In addition to the uncertainties in the climatic effects of CO_2, the cooling effect of aerosols suggested by McCormick and Ludwig may not be correct. Charlson and Pilat[7], Atwater[8] and Mitchell[9] have shown that since aerosols absorb and scatter, they may produce warming or cooling, depending on the ratio of absorption to scattering.

Thus, it is clear that considerably more work on the complex problem of modeling the atmosphere and on the optical properties of aerosols is needed before the long term effects of man-made pollution can be predicted. Since these problems will not be solved in the near future, it is important to initiate global measurements of aerosols on a continuous basis to monitor any changes.

We have shown in earlier theoretical studies[10] that it should be possible to make satellite observations of the aerosol content of the atmosphere from radiance measurements. The launch of ERTS-1 offered the opportunity of investigating these theoretically derived relationships with actual satellite data.

These relationships were investigated using MSS data at two test sites, San Diego and the Salton Sea, with ground truth being obtained with ground-based Volz photometer measurements of the aerosol content.

APPROACH

The approach to the investigation has been an empirical one based on theoretical calculations for model atmospheres. To make the computations manageable, certain approximations about several parameters, such as the aerosol size distribution and the underlying surface reflectance, have to be made. Hence, in the real atmosphere, model conditions are never realized, so that deviations from the theoretical relationship are expected. Thus, an empirical investigation has been conducted using the theory to provide insight into the extremes of values which may be encountered.

The relationship between radiance over water surfaces and the aerosol content has been studied using the satellite radiance measurements obtained from the ERTS-1 digital data, and the ground-truth measurements of the aerosol content made with a Volz photometer at the time of selected ERTS overpasses.

Relationship of Radiance and Aerosol Content

Calculations of the radiance backscattered from the earth-atmosphere system, as seen from space have been published by Plass and Kattawar.[11,12] These calculations, using Monte Carlo techniques, consider multiple scattering of all orders, and take into account aerosol scattering and ozone absorption. Examination of the results of Plass and Kattawar shows that the outgoing radiance varies with aerosol content, and is most sensitive when the underlying surface albedo is low. The ocean, which covers much of the earth, has a low albedo at high sun angles and provides a suitable underlying surface for aerosol measurements. The calculations also indicate that the longer wavelengths are more sensitive to aerosol changes. At shorter wavelengths the Rayleigh optical thickness is comparable to, or greater than, the aerosol optical thickness, so that changes in the aerosol content have less effect.

In order to further investigate the effect of aerosols on the upward radiance over a calm water surface, Plass and Kattawar[13] made some special calculations for us, in a separate study[10], for several aerosol vertical distributions. The calculations showed a result of great

importance for satellite observations of the upward radiance: the upward radiance depends strongly on the total number of aerosols, but not on their vertical distributions. Thus, measurements of the upward radiance can be directly related to the total vertical aerosol content and hence the global loading.

The three wavelengths (0.7 μm, 0.9 μm and 1.67 μm) considered show comparable sensitivity to aerosol changes. However, the relative normalized radiance is less at the longer wavelengths, and since the incoming solar flux decreases at longer wavelengths the absolute radiance level decreases rapidly with increasing wavelength (the absolute radiance at 1.67 μm is about 6% of that at 0.7 μm).

These results are used to determine the relationship between the upward radiance, measured by MSS channel 6, and the aerosol content of the atmosphere for various sun angles. A simple linear relationship is shown, in Figure 1, to exist between radiance and the aerosol content. These straight lines are based on only two values of aerosol content, but a linear relationship may be established by considering four data points for zero albedo[11,12]. It is seen that a 1 percent change in radiance is equivalent to about 1.5 percent change in aerosol content.

Potential Problem Areas

The preceding discussions are based on theoretical calculations which use a model atmosphere, model aerosol properties, and assume a smooth water surface or a Lambertian surface. Since these model conditions are never realized in practice, empirical relationships between the satellite data and the aerosol content have been investigated. However, two potential problems must be considered, although as shown later in the discussion of the results, they do not appear significant.

Sun Glitter. If the ocean were perfectly smooth as assumed in the calculations, an image of the sun would be seen at the specular reflection angle, and the only upwelling surface radiation observable at other look angles from space would be the diffuse sky radiation reflected from the ocean surface and the radiation scattered up from below the ocean surface. As the smooth ocean surface is increasingly disturbed, a glitter pattern becomes increasingly larger about the specular point. At sun zenith angles greater than about 30° the glitter effect has been considered negligible (except for very rough seas) at the nadir point. However, measurements by Hovis (private communication from R. Fraser) suggest that this assumption is not correct, so that the ocean surface radiance at the nadir is not known accurately.

Surface Reflectance Gradients. The calculations of Plass and Kattawar assume an underlying surface of constant reflectivity extending to infinity. However, the radiances in this program are obtained over water adjacent to a land surface of higher reflectivity, and radiation reflected from the land is scattered into the atmosphere above the water so that the apparent radiance above the water is different from the calculated theoretical value in the vicinity of the boundary.

DATA ANALYSIS METHODS

The investigation has utilized the radiances measured by the MSS, and the aerosol content measured by ground-based observations with a Volz photometer at the time of several ERTS overpasses.

The data for the four MSS channels were received as bulk processed black and white 9. 5 in. positive prints and transparencies, and as bulk processed digital 7-track computer compatible tape, selectively ordered after viewing the black and white products.

To extract the radiance data from the computer compatible tapes (CCT), a program was written to read data in prescribed geographical areas from the tapes on a CDC 6400. The areas of interest for analysis are chosen by viewing the black and white products, and selecting areas, about 6 km on a side, within the test sites free of obvious clouds, or effluents in the water. The word counts are printed out for each area, and can be converted to radiance using the MSS calibration data. The data are then examined, and an area about 300 x 300 m, in which the radiance is essentially uniform, is selected, and the average radiance estimated for each MSS band.

Measurements of the aerosol content were made with a Volz sun photometer[14] at both test sites at times of selected ERTS overpasses at the Salton Sea/ desert site, and at every overpass at San Diego as weather permitted.

RESULTS

Significant results were obtained in analyzing the ERTS digital data and the ground-truth measurements. A linear relationship, as predicted by theory, was found to exist between the MSS radiances over water surfaces and the aerosol content of the atmosphere.

Volz Data

During the program there were twenty-two ERTS overpasses at each of the test sites. Six trips were made to the Salton Sea/desert test site to make ground-truth measurements, and data were obtained on five occasions; cloud cover prevented the taking of data on just one occasion. It was planned to make Volz photometer measurements for each overpass at San Diego, but the overpasses coincided with cloud cover with surprising frequency, and data were obtained on only five occasions. The Salton Sea ground-truth measurements were always made on the shoreline at Bombay Beach on the east side of the sea. The San Diego observations were made in different locations each time, but always close to the ocean.

The results of the measurements are given in Figure 2, and show that in general the aerosol content was less than the value given by Elterman[14] in his 1964 model atmosphere (Elterman's model aerosol distribution corresponds to a 25 km visibility at the surface). The measurements on a few of the days show quite rapid changes, which are greater than the instrument error. They could possibly be due to the movement of undetected thin clouds between the sun and the observer, although all these variable measurements were taken in apparently completely clear sky conditions. The variations are probably due to the movement of air cells with different aerosol content in the lower atmosphere.

Radiance-Aerosol Relationship (Water Surface)

The investigation of the radiance-aerosol relationship over water surfaces is based on eight data points, four over the Pacific at San Diego, three over the Salton Sea, and one[16] over the Atlantic off the coast of North Africa, where measurements of the aerosol content are available. The radiance values are normalized to a sun angle of $\mu = 0.45$, using a correction based on the theoretical variation with sun angle given in Figure 1; it is assumed that the correction is the same for each channel. The correction is greater than 5% only for the three points with high sun angle.

The normalized radiances for all four MSS channels are plotted against the aerosol content in Figure 3. The aerosol content is given in terms of the Elterman 1964 model vertical aerosol optical thickness; i.e., the aerosol content is given by the ratio (measured aerosol optical thickness at wavelength λ/model aerosol optical thickness at wavelength λ). It is seen that, as predicted by theory, a linear relationship exists for all four channels, being best for MSS 5 and MSS 6. MSS 6 shows excellent agreement with the theoretical relationship shown in Figure 1, suggesting that

the model is very reasonable, particularly for zero aerosol content (i. e., a pure molecular atmosphere). The results for MSS 7 are given only to illustrate the low radiance values discussed above, and even though a linear relationship is indicated, this channel is not considered useful for determining the aerosol content. The results for MSS 4 show more scatter of points about the mean curve than for the other channels. The reason for the larger scatter in this channel is not readily obvious, since the radiance errors are not significantly different from the other channels. Possibly this channel is more sensitive to changes in the water reflectance due to the presence of effluents, chlorophyll, or other suspended material in the water, although on the one occasion when effluents were obviously present in the Salton Sea, the radiance in MSS 4 was closer to the mean curve than in the other channels.

Effluents were clearly apparent on 5-5-73 when ground-truth measurements were made, and on subsequent imagery of the Salton Sea during the summer months. The effluents, which are presumably due to irrigation run-off, were not observed during the winter months, when there is more rain and it is cooler, thus requiring less irrigation. These effluents result in variable high radiances over the water surface. To analyze the data for 5-5-73, an area exhibiting the lowest values of radiance was selected, but as seen in Figure 3, the radiances appear too high for the measured aerosol content, expecially for MSS 5 and 6. The effluent pattern is more apparent in the photographic images at shorter wavelengths. However, the data point for MSS 4 shows less deviation from the previous data than at the longer wavelengths. In addition, the spectral variation of radiance has the same basic shape as other data. Thus, the spectral behavior of this effluent, and its effect on aerosol observations is not completely consistent, and further studies of this type of data are required. However, it is clear that care should be taken in using data from bodies of water where effluents occur on an intermittent basis. The data may be readily screened by visual examination of the photographic images.

Analysis of Potential Problem Areas

No evidence of sun glitter has been visually observed on the ERTS photographic data received during the program. (Sun glitter was observed on the photographic data from the NASA aircraft overflight at 2000 ft altitude on 5-23-73, but was not identifiable on the ERTS data for the same time). All of the data at the San Diego and Salton Sea test sites were obtained over relatively calm seas, so that the sun glitter might be expected to be minimal. However, the one data point in Figure 3 for the Atlantic Ocean was obtained over rough seas, with seven foot waves and winds of

about 20 knots being reported. Presumably, sun glitter should be apparent under these conditions. However, it is seen in Figure 3 that this point does not significantly deviate from the linear relationships for the San Diego and Salton Sea data. Thus it is believed that nadir observations will not be significantly affected by sun glitter, although more rough sea data are needed to draw any firm conclusion.

It was suggested earlier that observations at two wavelengths might be used to eliminate a sun glitter problem if it should occur. In order to investigate this possibility the spectral variations of the upwelling radiance over water surfaces have been plotted. Figure 4 shows the results for several ERTS overpasses at the Salton Sea. These values are not normalized, and higher radiances are expected for higher sun elevations for a given aerosol content. Within the errors of the MSS radiance measurements, there are no obvious spectral differences from one overpass to the next, at least at the MSS wavelengths, even for the 5-5-73 data when effluents were present. However, there appears to be a tendency at sun elevations below about 50° for the radiance decrease from MSS 5 to MSS 6 to be less than at high sun elevations. Similar spectral variations are found for the data at the San Diego test site.

The effect of surface reflectance gradients was determined by examination of the digital data in the San Diego coastal regions and at the Salton Sea. It was found that the radiance over the water surface is higher immediately at the water-land boundary, but rapidly decreases and reaches a uniform value within about 1300 ft of the boundary. Thus, the effects of scattering from the adjacent high albedo land appears to be negligible beyond about 1300 ft from the shoreline. The water radiance data used for the preceding radiance-aerosol study were all obtained beyond 1300 ft from the shoreline, where the radiance was uniform.

Error Analysis

The results of the analysis of the radiance-aerosol content relationship contain uncertainties due to inherent instrument errors, and due to the assumptions necessary in the data interpretation. These uncertainties are discussed below.

Volz Photometer Errors. Flowers et al,[14] in comparing the Volz photometer with a standard photometer, found that values of aerosol optical thickness greater than about .240 (i.e., an aerosol content of 1.13 N), can be measured with an accuracy of ± 5%, and for an optical thickness near .100 (.47 N), an accuracy of about ± 10% applies. It is presumed that similar errors apply to the measurements made in this program with our Volz photometer.

A further error is possible in using the Volz data in this investigation due to the fact that the Volz measurement was never made directly over the water surface where the ERTS radiance measurement is made. It has been assumed that the atmosphere has been homogeneous over the area including the Volz and the radiance measurements. This may not always be a good assumption since the Volz data in Figure 2, on occasion, show variations over a short time period, greater than the instrument error, suggesting the movement of air cells with different aerosol content. This type of error cannot be readily estimated, but could be checked in a future program, using several photometers in the test site area.

ERTS Radiance Errors. Fraser[17] has made calculations of the noise equivalent radiance for each of the MSS channels based on preflight calibrations. No inflight calibrations have been reported, and it is assumed that the preflight ones apply throughout this program. Fraser's results are reproduced in Table 1, with the values of the full scale radiance, and NER in radiance units added for clarity. If the radiance-aerosol content relationship in Figure 3 is assumed to be correct, then the NER results in a $\pm$ 10% error in determining the aerosol content in the useful channels MSS 4, 5 and 6.

CONCLUSIONS

Significant results, relating the radiance over water surfaces to the atmospheric aerosol content, have been obtained. The results indicate that the MSS channels 4, 5 and 6 centered at 0.55, 0.65 and 0.75 μm have comparable sensitivity, and that the aerosol content can be determined within $\pm$ 10% with the assumed measurement errors of the MSS. The fourth channel, MSS 7, is not useful for aerosol determination due to the water radiance values for this channel generally being less than the instrument noise. The accuracy of the aerosol content measurement could be increased by using an instrument specifically designed for this purpose. In an independent study[18] we designed a simple instrument in which the radiance could be measured to $\pm$ 1% accuracy resulting in a $\pm$ 1.5% error in the aerosol content.

This radiance-aerosol content relationship can provide a basis for monitoring the atmospheric aerosol content on a global basis, allowing a baseline value of the global burden of aerosols to be established. This baseline could be established more rapidly from satellite measurements than from a network of ground-based observations, and probably with considerable cost savings. In addition, this technique could provide a method

for monitoring the particulate emissions of SST's, by making observations in the vicinity of flight corridors, such as over the North Atlantic. It should be possible to look at the ocean through the flight corridor and alongside it, to measure the difference, due to the SST's, in the aerosol content.

ACKNOWLEDGMENTS

The author is indebted to G. D. Hall for making some of the ground-truth measurements, to M. R. Schoonover for providing the computer analysis of the tapes, and to C. B. Ludwig, W. Malkmus, E. R. Bartle, and R. S. Fraser for helpful discussions.

REFERENCES

1. "Study of Critical Environmental Problems (SCEP)", MIT Press (1970).

2. "Study of Man's Impact on Climate (SMIC)", MIT Press (1971).

3. M. T. Ellis and R. F. Pueschel, Science 172, 845 (1971).

4. G. M. Hidy and J. R. Brock, Second International Clean Air Congress, Washington, D. C. (Dec. 1970).

5. R. A. McCormick and J. H. Ludwig, Science 156, 1358 (1967).

6. G. D. Robinson, "Long-Term Effects of Air Pollution", Center for the Environment and Man, Inc., Hartford, Rept. No. CEM 4029-400 (1970).

7. R. J. Charlson and M. J. Pilat, J. Appl. Meteor. 8, 1001 (1969).

8. M. A. Atwater, Science 170, 64 (1970).

9. J. M. Mitchell, Jr., J. Appl. Meteor. 10, 703 (1971).

10. C. B. Ludwig, M. Griggs, W. Malkmus and E. R. Bartle, "Monitoring of Air Pollution by Satellites", NASA CR-112137, (In Press).

11. G. N. Plass and G. W. Kattawar, Appl. Opt. 7, 1129 (1968).

12. G. N. Plass and G. W. Kattawar, Appl. Opt. 9, 1122 (1970).

13. G. N. Plass and G. W. Kattawar, Appl. Opt. 11, 1598 (1972).

14. E. C. Flowers, R. A. McCormick and K. R. Kurfis, J. Appl. Meteor. 8, 955 (1969).

15. L. Elterman, in "Handbook of Geophysics and Space Environments", S. L. Valley, Ed. (McGraw-Hill Book Co., New York, 1965).

16. R. Fraser, Private Communication. Dr. Fraser determined the radiance, and the Volz measurement was made from a NOAA ship.

17. R. Fraser, Private Communication.

18. "Monitoring of Air Pollution by Satellites (MAPS)", Phase I Report, Contract NAS1-12048, Science Applications Report SAI-73-564-LJ, (June 1973).

TABLE 1

The noise equivalent radiance (NER) of MSS for ocean observations. Also, the ratio of the standard deviation in sensor response to atmospheric turbidity changes to the NER. The mean sensor output (V), the standard deviation (σ), and NER are expressed in percentage of full scale sensor response (after Fraser[17]).

Spectral Band in μm	Surface Reflectivity	$\bar{V}$	σ	SNR	$\bar{V}$/SNR	σ/NER	Full Scale Radiance (mw/cm^2/sr)	NER mw/cm^2/μm/sr
0.5-0.6 (MSS 4)	0.02	12	1.4	22	0.6	2.5	2.48	.15
	0.10	23	1.1	40	0.6	1.9		
0.6-0.7 (MSS 5)	0.02	8	1.4	9	0.9	1.5	2.00	.18
	0.10	22	1.0	22	1.0	1.0		
0.7-0.8 (MSS 6)	0.02	7	1.0	11	0.6	1.6	1.76	.11
	0.10	22	1.0	25	0.9	1.1		
0.8-1.1 (MSS 7)	0.02	4	0.5	3	1.0	0.5	4.60	.15
	0.10	10	0.4	10	0.9	0.4		

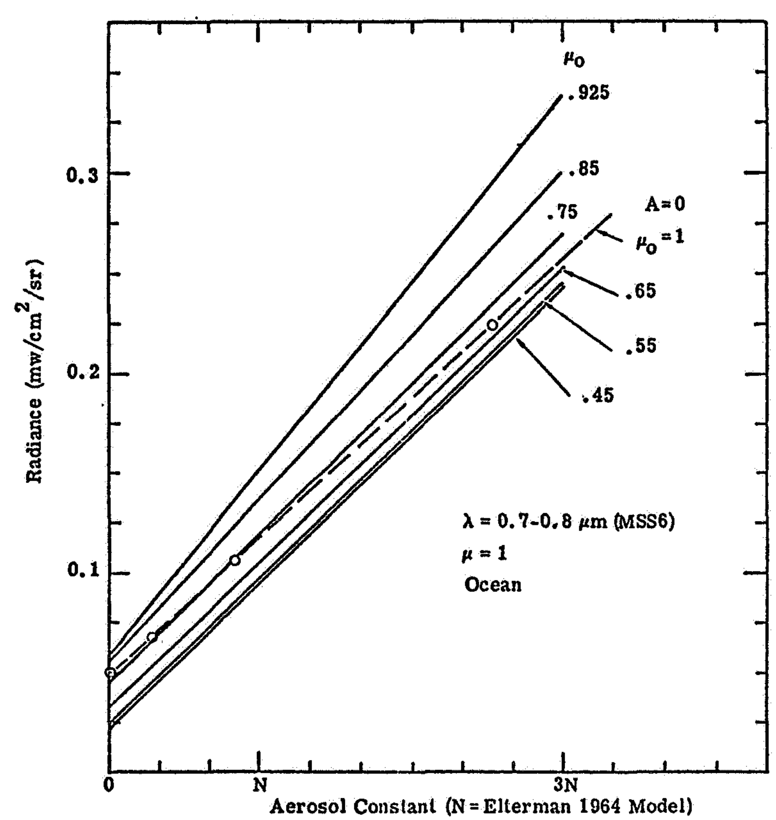

Fig. 1. Theoretical Radiance vs. Aerosol Content for MSS 6

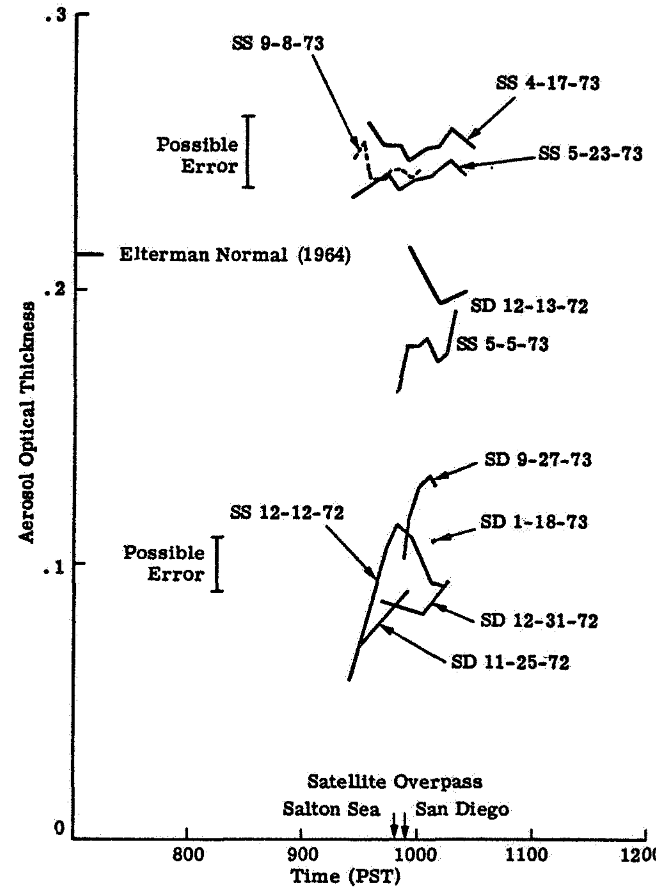

Fig. 2. Volz Data

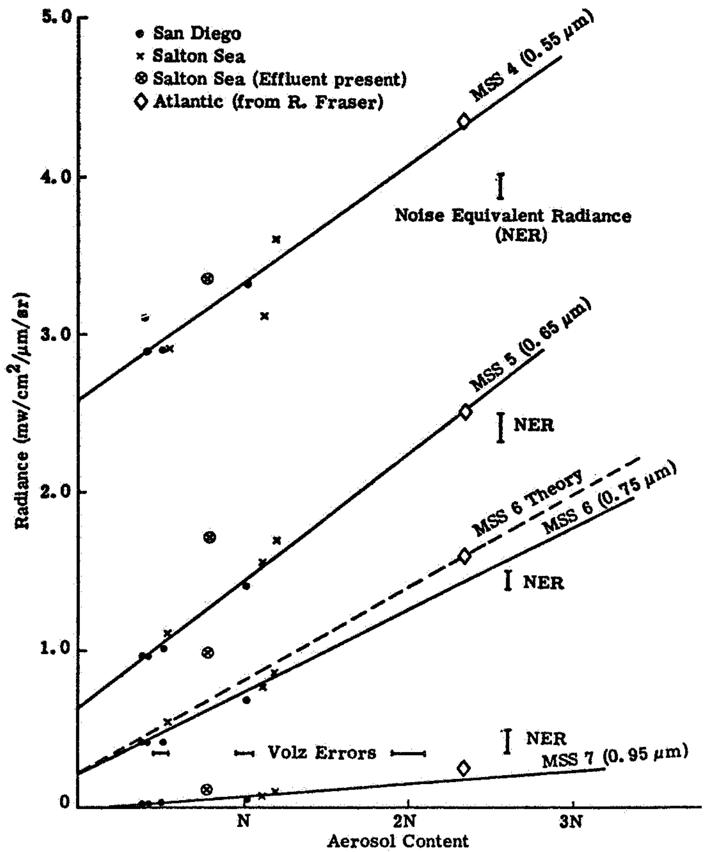

Fig. 3. Measured Radiance vs. Aerosol Content Over Water Surfaces (Normalized to sun angle $\mu = .45$)

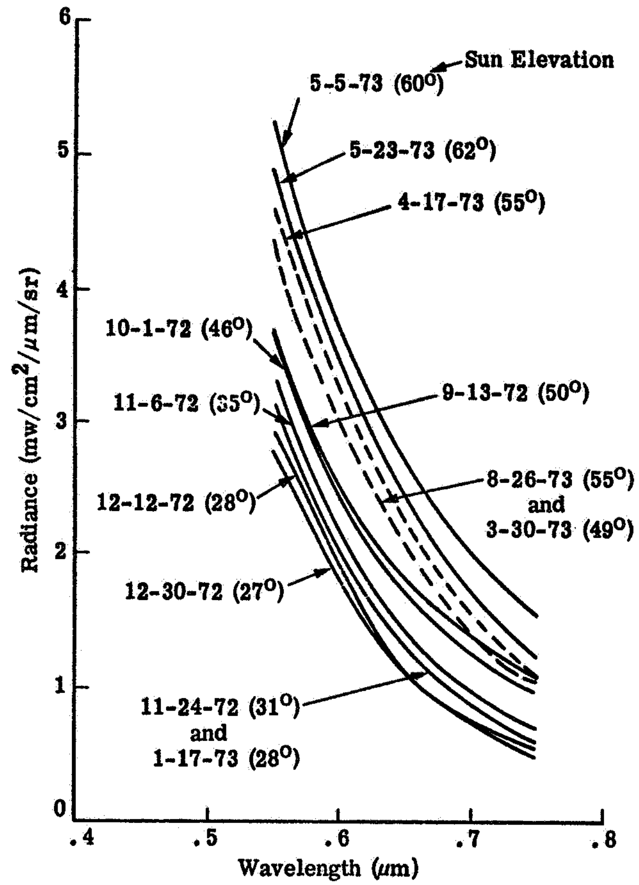

Fig. 4. Salton Sea Water Radiance vs. Wavelength

Paper E 3

AUTOMATED STRIP-MINE AND RECLAMATION MAPPING FROM ERTS

Robert H. Rogers and Larry E. Reed, *Bendix Aerospace Systems Division, Ann Arbor, Michigan* and
Wayne A. Pettyjohn, *Ohio State University, Department of Geology, Columbus, Ohio*

ABSTRACT

Using computer processing techniques, it is possible to produce geometrically-corrected maps of the coal strip mines in East-Central Ohio by utilizing ERTS-1 CCTs. Several target categories can be drawn by a computer-controlled pen on film that will accurately overlay a base map of any scale selected by the operator. For each overlay, the computer can generate a table that shows the area of each target category in square kilometers, acres, or percent of total area.

INTRODUCTION

The area encompassed by this investigation includes five counties in eastern Ohio that comprise nearly 3,000 square miles. The counties; Muskingum, Coshocton, Guernsey, Tuscarawas, and Belmont; have been disrupted by coal mining since the early 1800s. Strip mining, which generally began before the 1920s, has been practiced in all of them. The total area of stripping operations in each county was quite large during the period from 1914 to 1947, but was insignificant when compared to the area stripped from 1948 to the present time.

On-site examination of individual mines, and particularly older mines, is hindered by (1) a lack of adequate mine map coverage; (2) deeply eroded, non-existent, or blocked access roads; (3) lack of accurate or adequate records; (4) the great total size of the stripped area; (5) strip mine reclamation planting along roads that obscures adjacent barren land; and (6) dated aerial photographic coverage.

From the earliest days of mining until 1948, little thought was given to the detrimental effects of coal mining on the environment. However, reclamation techniques required by 1948 legislation resulted in some grading and planting of trees and forage on soil banks although, in some areas, the soil was too toxic for replanting. In view of the stricter laws passed by the state legislature in 1973, reclamation is proceeding, not only more rapidly, but much more effectively.

Various agencies within the Ohio state government collect certain types of coal-mining data. There is, however, little or no coordination between agencies; automatic data processing is non-existent; and various filing systems approach the choatic. Consequently, reports available to the public are severely dated, commonly inaccurate, and difficult to acquire.

ENVIRONMENTAL EFFECTS OF STRIP MINING

In addition to large areas that are disrupted to such an extent that they are no longer productive, strip-mining has caused severe ecologic effects. These include the erosion of bare or sparsely vegetated spoil banks and the discharge of highly mineralized water. Sediment eroded from mined areas tends to fill streams and reservoirs which, in turn, leads to flooding, decreased storage area, and the choking of vegetation. Water that discharges from spoil banks and underground mines generally has a low pH and is highly mineralized.

MAJOR TARGET AREA

Although several specific areas have been examined, a very large mine in Southeastern Muskingum County, owned and operated by the Ohio Power Company, was chosen for detailed examination. The mine, although very irregular, is nearly 14 km (9 miles) long and as much as 8 km (5 miles) wide (see Figure 1).

Mining and reclamation at this mine is proceeding at a very rapid rate. Air photographs indicate that there was no stripping in the area in 1950. By 1965, however, about 1.6×10^7 square meters (4,000 acres) had been disrupted and, by 1971, strip mining had devastated close to 4.5×10^7 square meters (11,000 acres) in a single mining area (see Figure 1). A similar pattern occurred in several other Ohio counties.

Because of the more stringent 1972 Ohio strip-mine bill, reclamation now proceeds, in many areas, at the same rate as the mining. In fact, grading equipment may be operating just behind the giant mining machinery.

Aerial photographs of the Northern part of the Ohio Power Company area were taken in May of 1972. The area was examined in the course of field work in June of 1973. In several parts of the mine, there is no comparison between the landscapes that appear on the 1972 photography and the condition that existed only 13 months later (see Figure 2). Many of the strip mine lakes had been filled, graded, and planted as a part of the reclamation program.

Examination of several water quality parameters in lakes, reservoirs, and streams throughout the region indicates a wide range in concentration, both in space and time (see Figure 2). Furthermore, the quality cannot be readily predicted from one area to another or, for that matter, from one impoundment to the next in the same mine. Consequently, a detailed regional analysis of water quality characteristics cannot be adequately accomplished without a monumental budget.

ERTS-1 DATA PROCESSING

Local, state, and federal agencies must have repetitive coverage of mining areas and the capability for rapidly evaluating each situation. They also must be able to quickly determine areas of mining reclamation and progress or viability of replanted vegetation, at least on an annual basis. This, presently, cannot economically be done by ground teams, and aerial photographs rapidly become outdated.

In response to the urgent need for a faster and more economical means of generating strip mine and reclamation maps, this study is evaluating the suitability of using ERTS computer compatible tape (CCT) for automatic mapping. The procedure uses computer target "spectral recognition" techniques as a basis for classification. To implement these techniques, a computer is provided with a number of samples of ERTS measurements (training sets) for each target category of interest.

Once the numerical descriptions which define the spectral characteristics of each target category are determined, the operator executes the "canonical analysis" program. The program derives, for each target category being sought, a set of "canonical coefficients". In the decision processing phase, the coefficients are used by the computer to form a linear combination of the ERTS measurements to produce a "canonical variable" whose amplitude is associated with the probability of an ERTS measurement being from the target sought. A set of canonical coefficients are derived for each target category of interest.

In decision processing, the probability of an ERTS measurement arising from each one of the different target categories of interest is computed for each ERTS spatial resolution element, and a decision based on these computations is reached. If all probabilities are below a threshold level specified by the operator, the computer is permitted to decide that the target viewed is unknown (an unclassified category).

Before producing decision data on a large amount of ERTS data, a number of tests are applied to evaluate the computer's capability of performing the desired target classification. The tests include generating scatter diagrams, generating classification accuracy tables, and viewing the results of processed data on a TV monitor. In the test site, the classification accuracy was greater than 95% (see Table 1).

Table 1. Classification Accuracy Table

CLASSIFICATION TABLE 12-OCT-73 10:11:59

REJECTION LEVEL = 0.100000 PER CENT

TNG SET	PER CENT CLASSIFIED AS GROUP 0	1	2	3	4	5
1	0.000	97.872	0.000	2.128	0.000	0.000
2	0.000	1.587	98.413	0.000	0.000	0.000
3	0.000	4.545	0.000	95.455	0.000	0.000
4	0.000	0.000	0.000	0.000	100.000	0.000
5	0.000	0.000	0.000	0.000	0.000	100.000

PROGRAM RUN TIME = 00:00:21

Designation	Target
1	Stripped earth
2	Water with sedimentation
3	Partially reclaimed earth
4	Vegetation
5	Water without sedimentation

DECISION DATA PRODUCTS

Decision products developed for this investigation, using the 21 August 1972 ERTS-1 CCTs, include a printout table showing the area covered by each target category, decision imagery, and decision map overlays. The target classifications include stripped earth and major areas of erosion, partially reclaimed earth and minor areas of erosion, vegetation, deep (clear) water, shallow (turbid) water, and unclassified areas. Decision imagery, although not geometrically-correct, is produced rapidly and provides an immediate view of the processed scene. Decision-map overlays are geometrically-corrected and will directly overlay a UTM map coordinate system at any scale selected by the operator.

The canonical coefficients defining each of the five categories was applied to process that portion of the CCTs covering the Ohio Power Company's surface mining operation. The first step in the decision processing resulted in a new or processed CCT, which contains a code for each spatial element designating it as one of the categories. From this processing, Table 2 was generated, showing the area coverage of each category in terms of percent of total area processed, square kilometers, and acres.

Table 2. Area Table

ERTS PROCESSOR 15-OCT-73 09:01:32

ERTS SCENE 10 - 1029-15361
DATE OF SCENE - 21 AUG 72
CENTER OF SCENE - N39-25/W081-00
SUN COORDINATES - EL53 DEGREES
AZ130 DEGREES
SPACECRAFT HEADING - 191 DEGREES
TAPE NUMBER - 1
STARTING SCAN LINE = 450
ENDING SCAN LINE = 950

CATEGORY	PERCENT OF TOTAL	ACRES	SQ. KM.
UNCLASSIFIED	4.47	20293.15	82.12
STRIPPED EARTH	0.74	3343.62	13.53
DIRTY WATER	0.80	3610.80	14.61
RECLAIMED EARTH	3.95	17928.80	72.55
VEGETATION	89.67	406771.91	1646.13
CLEAN WATER	0.38	1704.79	6.90
	------	---------	-------
TOTALS	100.00	453653.06	1835.84

PROGRAM RUN TIME = 00:23:23

Notable, on the list of categories shown, are the two water and two disturbed-earth categories. Water without sediment includes deep or clear water such as that found in reservoirs; water with sediment represents shallow or murky water, characteristic of shallow rivers and strip-mine-associated lakes. The two disturbed earth categories, stripped earth and partial reclamation, need little explanation except for some definition of partial reclamation. Partially reclaimed land may represent areas where reclamation, either natural or man-made, is proceeding very slowly, and usually less than 40% of the area is covered with vegetation. It also may represent recently mined areas where there has been a significant amount of spoil-bank grading, as well as planted sites where the vegetation may cover 0 to 100% of the area.

Table 2 also shows that stripped earth makes up 0.74% of the total area processed or 13.53×10^6 square meters (3,344 acres). It can readily be seen that this type of data product could be especially valuable when a quantitative measure for new stripping is needed, to determine progress of reclamation, and to measure changes brought about by surface mining.

The tape produced for decision processing was also used to generate 70-mm imagery wherein each image shows only a specified category at a scale of 1:1,000,000. This imagery is geometrically (spatially) identical to the data on the decision CCT and on the CCT provided by NASA from which it was produced. Since the tape if from bulk processing, some geometrical errors exist and are carried over into the decision imagery. Also, the CCT data provided from the NASA bulk processing is not corrected for earth rotation, consequently, the decision imagery will not directly overlay a UTM map coordinate system.

A method of recording all computer classifications, each represented by a different color, onto a single image, was also evaluated. To accomplish this, three images, representing the three primary colors (red, green, and blue) and containing all target classes in shades of gray, are produced. Using an additive color process, a composite image, in which each target class is assigned a distinctive color, is created. An example of this process, showing a large portion (about 1.8×10^9 square meters or 700 square miles) of Muskingum County and the Ohio Power Company's operations in that area, is shown in Figure 3.

To produce data that will directly relate to a map, a method for correcting the decision CCT for earth rotation and other geometric errors was developed. A second CCT, with these geometric corrections applied in a format suitable for driving a Gerber plotter, was recorded. This tape, when played back on the computer, causes a geometrically-corrected map of each target category to be drawn on film at a scale specified to the computer by the investigator. The pen drawings were used to produce color-coded overlays for an AMS series map of the same scale.

Figures 4 through 7 are photographs of computer-produced transparent maps, from the Gerber plotter, that overlay a 1:250,000 scale AMS map. The two water classifications are shown in Figure 4, stripped earth is shown in Figure 5, partially reclaimed land in shown in Figure 6, and a composite of all the classifications is shown in Figure 7. The overlay technique was found to be particularly useful for updating base maps and, more importantly, for detecting and identifying changes; i.e., change detection between the base maps and ERTS-1 data.

At this time, analyses of the accuracy of classifications have been confined largely to analyses of classification tables generated from data from the training areas. To be truly objective in analyzing accuracy, the final output products must also be evaluated with other areas not used in the computer training process. This was accomplished by comparing classification results with available maps, ground-survey data, and aerial photographs.

Figure 8 is a mosiac of the Ohio Power Company's strip-mine operation, generated from photographs acquired by the NASA C-130 aircraft on 7 September 1973. By comparing Figures 7 and 8, it is evident that the target categories are classified correctly in nearly all cases. Especially noticeable is the accuracy with which small lakes, a product of the mining operation, were classified.

A direct comparison between aerial photography and the stripped earth decision image plot of a part of the mine is shown in Figure 9. This illustration shows, not only that there is close agreement between the two techniques, but also that there have been some significant changes in mining areas between 21 August 1972 and 7 September 1973.

Thus far, this investigation has demonstrated the feasibility of using ERTS-1 CCTs for mapping and monitoring strip mining. The technique is rapid, accurate, and very inexpensive when compared to standard methods using aerial photographs and ground teams.

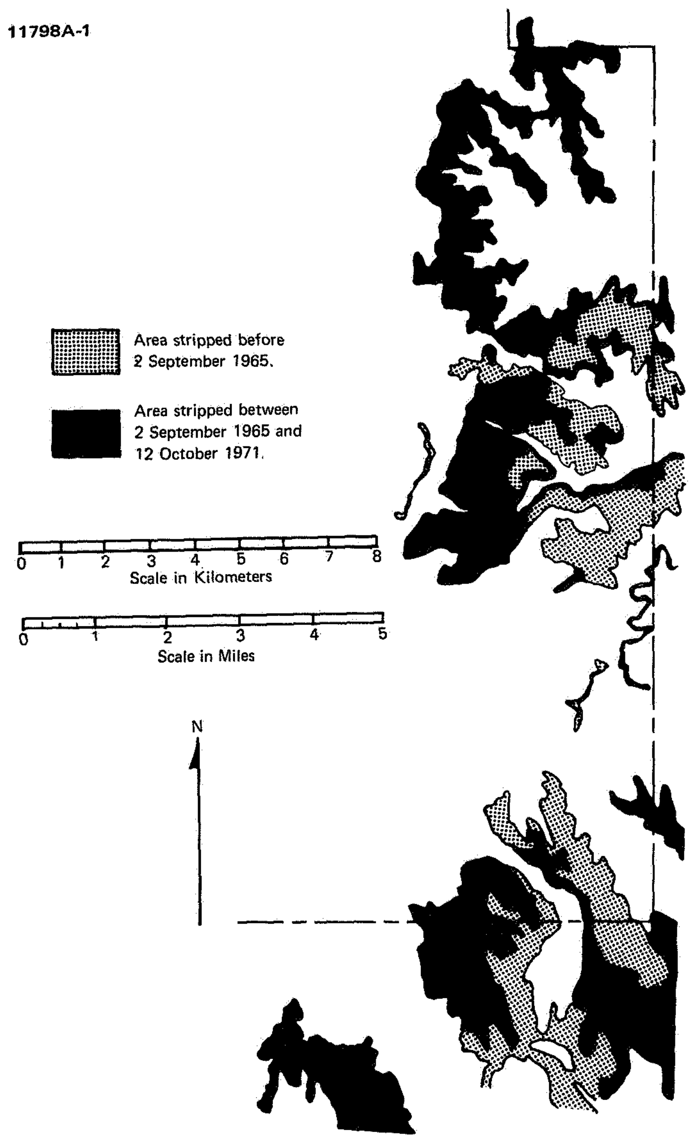

Figure 1. Strip-Mined Area in Muskingum County

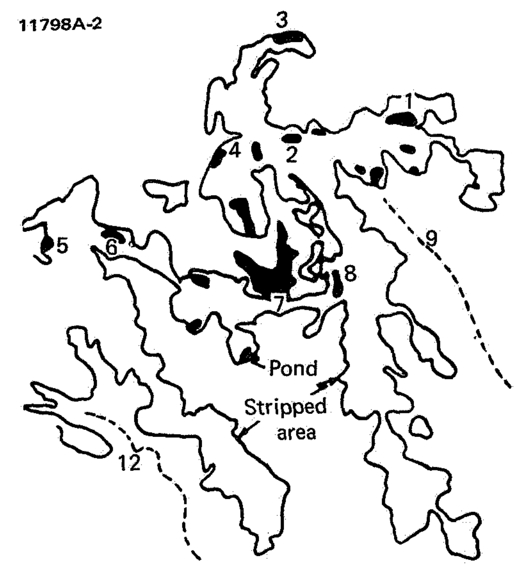

Site	
1	Pond, nonexistent
2	Pond, pH-9.7 conductance-750
3.	Lake, nonexistent
4.	Lake, nonexistent
5.	Lake, nonexistent
6.	Pond, pH-9.3, conductance-580
7	Lake, pH-8.9, conductance-600
8.	Pond, pH-3.1 conductance-1900
9.	Stream, pH-8.2, conductance-775
12.	Stream, pH-8.5, conductance-700

Base from May 9, 1972 air photograph
Field check on August 9, 1973

Figure 2. Water Quality and Reclamation Data in the Northeastern Part of

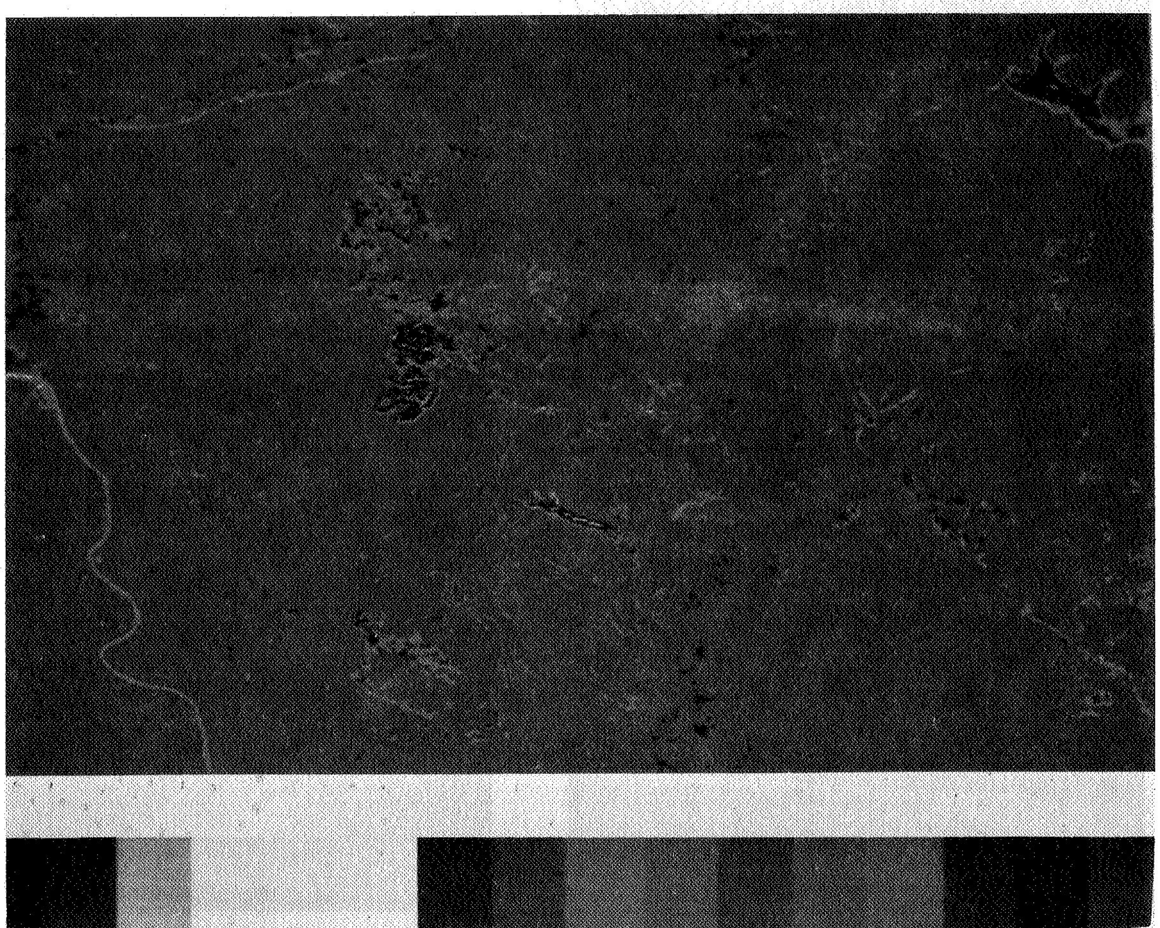

Classifications:

Red - Stripped Earth and Major Sources of Erosion

Yellow - Partially Reclaimed Earth and Minor Sources of Erosion

Green - Vegetation

Lt. Blue - Shallow Water or Water with Sedimentation

Blue - Deep Water or Water without Sedimentation

Black - Unclassified

Figure 3. Decision Imagery Representing a Large Part of the Study Area Based on the 21 August 1972 ERTS-1 CCT

Figure 4. Overlay of Both Computer-Generated Water Categories on a 1:250,000 Scale Base Map

Figure 5. Overlay of Computer-Generated Stripped Earth Category on a 1:250,000 Scale Base Map

Figure 6. Overlay of Computer-Generated Partially Reclaimed Category on a 1:250,000 Scale Base Map

Figure 7. Overlay of All Computer-Generated Categories on a 1:250,000 Scale Base Map

Figure 8. Aerial Photo-Mosaic of Southeastern Muskingum County, Ohio, and the Ohio Power Company Strip Mine

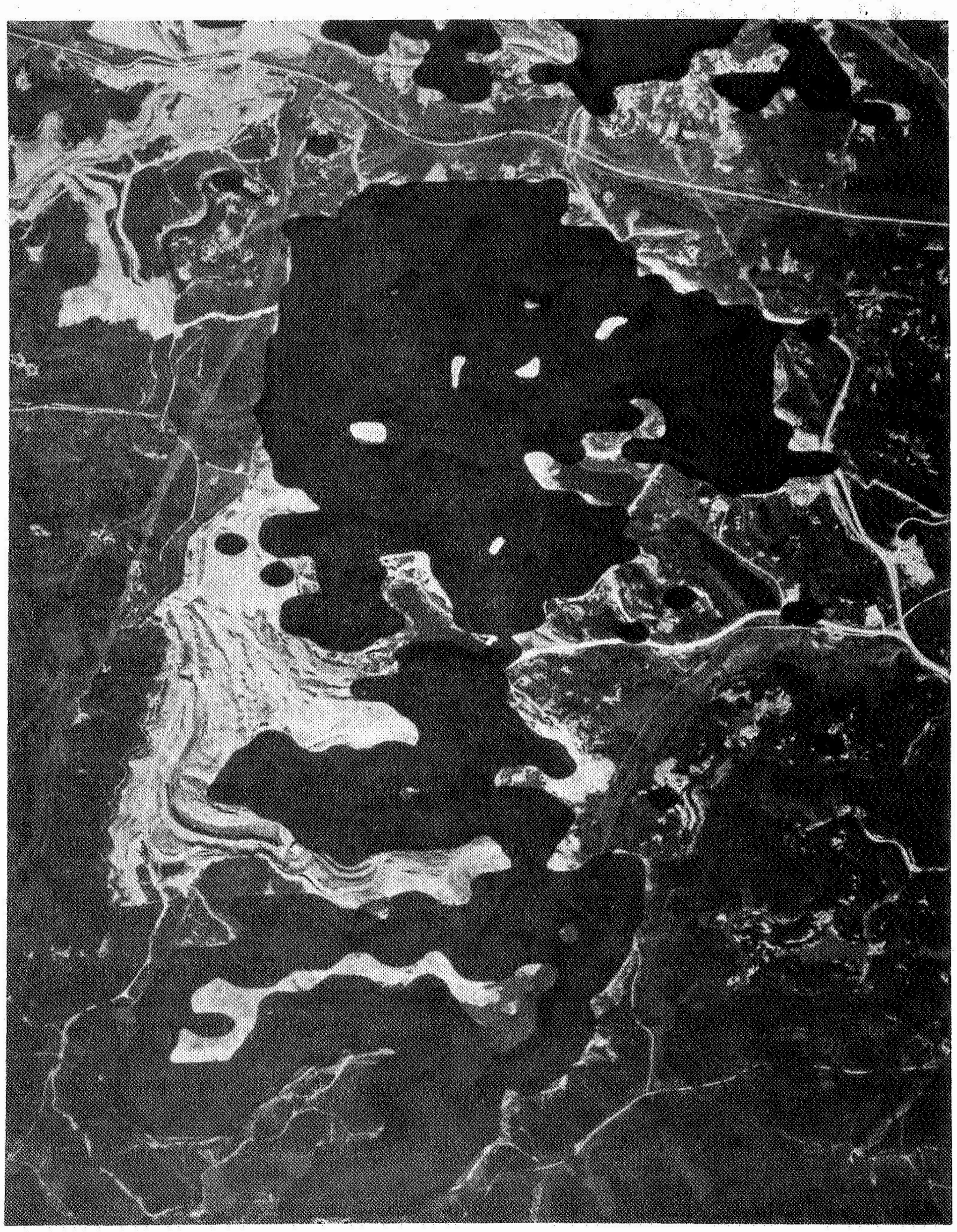

Figure 9. Overlay of Stripped Earth Category on Aerial Photograph of Southern Part of Ohio Power Company Mine Taken on 7 September 1973 by NASA C-130 Aircraft

Paper E 4

SIGNIFICANT APPLICATIONS OF ERTS-1 DATA TO RESOURCE MANAGEMENT ACTIVITIES AT THE STATE LEVEL IN OHIO

D. C. Sweet and P. G. Pincura, *(Department of Economic and Community Development);* C. J. Meier, *(Department of Natural Resources);* G. B. Garrett, *(Ohio Environmental Protection Agency);* and L. Herd, *(Department of Transportation), State Government of Ohio;* and G. E. Wukelic, J. G. Stephan and H. E. Smail, *Battelle Columbus Laboratories*

ABSTRACT

According to Dr. David C. Sweet, Director of the Ohio Department of Economic and Community Development and Principal Investigator of the Ohio ERTS and Skylab Programs, "The Ohio satellite effort is a major step towards wise resource management necessary for balanced development in Ohio". Described herein are techniques utilized and the progress made in applying ERTS-1 data to (1) detecting, inventorying, and monitoring surface mining activities, particularly in relation to recently passed strip mine legislation in Ohio; (2) updating current land use maps at various scales for multiagency usage, and (3) solving other real-time problems existing throughout the various Ohio governmental agencies. General conclusions regarding current user views as to the opportunities and limitations of operationally using ERTS-1 data at the state level are also noted.

INTRODUCTION

The purpose of the NASA ERTS experimental program is to assess remote sensing from a satellite as a technique for inventorying, monitoring, and eventually managing the earth's resources. The tremendous success of this program to date in generating unique data on natural and cultural resources the world over is well known. However, how much and how soon the public benefits from this space capability depend upon how effectively this new data resource can be absorbed into the mainstream of all government, public, and private planning and decision making functions bearing on the utilization and management of the earth's resources. This presentation summarizes progress made, techniques utilized, and limitations encountered in using ERTS-1 data

for resource management in a state such as Ohio having highly diversified industry, agriculture, and geography as well as limited remote sensing experience and capabilities.

Ohio, with NASA funding assistance, is making a comprehensive, multi-disciplined assessment of the state-level utility of ERTS data. Major participating organizations are:

State Agencies

- Department of Economic and Community Development (DECD, Lead Agency)
- Department of Natural Resources (DNR)
- Ohio Environmental Protection Agency (OEPA)
- Department of Transportation (DOT)
- Public Works
- Ohio State University (OSU)

Others

- Battelle Columbus Laboratories (BCL)-Technical Support Contractor
- NASA/Goddard Space Flight Center (GSFC)-Technical Monitor
- NASA/Lewis Research Center (LeRC)-Scientific Monitor

Since its establishment in July, 1972 this statewide, ERTS user program has encompassed (1) user awareness, (2) application analysis, and (3) utility assessment activities. A brief summary of the status and accomplishments within each of these functional program categories follows.

USER AWARENESS

User familiarization with remote sensing technology, ERTS imagery, and earth resources discipline developments is necessary if experimentally identified application opportunities are to become operational realities. To meet this need major emphasis in the Ohio program has been placed on encouraging all levels of government planners, researchers, and decision makers to actively participate in ERTS data analysis and evaluation activities. This approach serves to expose potential state users as to ERTS capabilities, while providing an insight to their existing data needs and problems which ERTS data must accommodate to be of maximum state benefit. To date over 150 state-agency personnel have participated in this user-awareness exercise.

To educate potential state ERTS data users across the total spectrum of on-going state activities as to the nature of the NASA ERTS program in general and the Ohio program in specific an "Ohio-ERTS Data Users Handbook" was distributed to all major potential state users in early 1973. The handbook also contains reproductions and descriptions of the more usable ERTS frames received for Ohio.

And finally to promote ERTS throughout the public sector, State of Ohio and Battelle personnel have made numerous public presentations, hosted several press conferences, and continue to assist students interested in ERTS data utility.

APPLICATION ANALYSIS

Figure 1 shows a portion of the Remote Sensing Applications Laboratory at Battelle which is used in concert with state researchers and planners for the routine analysis of incoming ERTS data. Major equipment in this facility as well as that located at state agencies used in the acquisition and/or analysis of on-site, aircraft, or spacecraft data are listed in Table I.

Fig. 1. View of a Portion of the Data Analysis Equipment Used by Battelle and State of Ohio Personnel to Analyze ERTS Data on Ohio

TABLE I.

DATA ACQUISITION AND DATA ANALYSIS EQUIPMENT
CURRENTLY BEING USED ON THE OHIO-ERTS PROGRAM

	BATTELLE	
32-Color Viewer	Spatial Data Systems, Inc.	Qualitative & quantitative evaluation of ERTS imagery by converting densities to desired color
Multispectral Viewer Model 20	Spectral Data Corp.	Overlay of up to 4 ERTS images to produce color composites and to enhance specific image features
Multiple Interpretation Module (MIM)	Richards Corp.	Viewing, comparison, magnification and mensuration of ERTS and aircraft imagery
Spectral Radiometer & Recorder	ISCO	Collecting ground-truth radiometric "spectral signatures"
70-mm Multispectral Cameras	Hasselblad	4-camera array used for acquiring aerial multispectral data
K-17 & K-24 Aerial Cameras	Fairchild	Acquire aerial underflight data
	DNR	
K-17 Aerial Camera	Cessna	Acquire aerial underflight data
	OEPA	
Ohio National Guard Helicopter	--	Available upon request to monitor areas of environmental concern
Grant request submitted for purchase & operation of remote sensing aircraft	--	"
	DOT	
Nistri-Analytical Stereoplotter	Nistri-Bendix	Mapping & plotting from ERTS & aircraft photography
K&E Grid Digitizer	K&E	Mapping & plotting from ERTS or aircraft photography
Twin-Engine Plane	Beechcraft	Acquiring aerial photography
6" Zeiss RMK-A	Zeiss	Acquiring aerial photography

In the Ohio-ERTS program, application analyses are concentrated in the discipline areas of environmental quality, land use planning and mapping, and agriculture and forestry. The status of the ERTS-1 individual application candidates under examination and their significance to state resource management functions are noted in Table II. The applications range in scope from a single department's interest in soil erosion in a highly localized area to multidepartmental interests in statewide land-use trends. In this presentation, the analytical efforts employed and results obtained in evaluating the usefulness of ERTS multidate and multispectral data to Ohio surface mining and land-use interests will be described in detail. Status of studies of other application candidates and the results of several real-time, problem-solving exercises will be only briefly noted.

Surface Mining

State Need

Surface mining in Ohio is a major industry requiring more and more state attention. Foremost among current state efforts relate to legislative improvements in surface-mining controls. For example, in April, 1972, Ohio enacted a more rigid strip-mine law containing provisions for:

- Determining and holding reclamation bonds
- Establishing and enforcing reclamation requirements
- Monitoring the status of the strip-mining activity and assessing environmental degradation.

To effectively enforce this law the state must have the capability and resources to:

- Inventory past strip-mine activity, both reclaimed and unreclaimed
- Inventory current strip-mine activity
- Determine condition of unreclaimed land and type of reclamation practice required to restore it
- Verify data and reclamation plans contained in strip-mining permit applications.

Thus, the emergence of ERTS was quite timely if data could be used to inventory, monitor, and assess stripping and reclamation activities.

Application Results

Utilizing the equipment at the Battelle Remote Sensing Applications Laboratory, we have looked at ERTS-1 MSS imagery, aircraft photos, and on-site radiometric (spectral) signatures of the same strip-mined areas. Conclusions

TABLE II.

MAJOR ERTS-1 DATA APPLICATION CANDIDATES
UNDER EXAMINATION IN OHIO

Application Area	State Need	Potential State Value
Surface mining	> 1/4 million acres affected	Help implement 1972 strip-mine law
Land use	Multiagency priority problem	Provide periodic statewide views of major land-use changes
Air quality	Ohio EPA interest	Test computer model by monitoring smoke plumes
Mapping	Current maps needed at all agency levels	Provide photo base maps
Sanitary land fills	> 1,400 illegal sites estimated	Detect illegal and/or new sites
Floodplains	50% of Ohio cities subject to flood damage	Help define and enforce statewide regulatory law
Outdoor recreation	50 state parks exist--major expansion program underway	Help select new recreation sites
Lake Erie	Pollution and sedimentation studies by OEPA and DNR coastal zone management	Improve state water quality planning and enforcement activities
Mineral estimates	Ohio Geological Survey	Determine remaining coal reserves
Acid mine drainage	To detect surface water seepage into nonactive underground mines in southeastern Ohio	Prevent vegetative and wildlife destruction
Metropolitan areas	Transportation network/ residential densities	Aid in land-use legislation & transportation planning
Soil studies	Soil erosion problems	Enhance water quality, land value, and agricultural productivity
Agriculture & forestry	To inventory crop and timber acreage	Improve agriculture and forestry resources

thus far are that ERTS MSS imagery can indeed be utilized to inventory (within the accuracy limitations of scale) the extent of strip mining in Ohio. Assessment of the condition of the stripped terrain is problematical but can be done effectively. Monitoring the actual activity of strip mining can be done provided a sufficient time has elapsed, and usable imagery is obtained. Obviously aircraft photographs can provide greater precision of measurement and interpretation, but at a far greater cost in both data collection and analysis.

Figure 2 shows a typical complete ERTS-1 scene of southeastern Ohio (Band 5) with strip-mined areas clearly discernible even at the 1:1000,000 scale. Figure 3 compares enlargements of a 13 km long (~ 4,000 acres) strip-mine area for Bands 5 (visible) and 7 (near infrared) showing the capacity of Band 7 to detect standing bodies of water.

By comparing aerial underflight panchromatic photography of strip-mining areas at a scale of 1:24,000 with ERTS imagery blown up to the same scale it was found that the examination of ERTS Bands 5 and 7 in some instances yields more information than the comparative aircraft photography. This was the case for at least two features: water and residual vegetation in the strip-mine area. The image density slicing viewer can discern 25-30 density differences in a single strip-mine area which may eventually be relatable to spoil bank materials, high walls, and other features appearing in a typical Ohio strip mine (see Figures 4a-c).

Since a strip-mine area is obvious by the removal of the so-called overburden or original vegetation, the restoration of such an area can be monitored by the increased recovering of such base areas. Older strip-mine areas under reclamation are best discerned on ERTS Band 7. They distinguish themselves by a less dense vegetation cover than the surrounding areas covered by original vegetation and by a large number of small ponds and lakes. Strip-mine areas over 30 years old have been observed. Analyses of areas under reclamation are made by comparing the area under reclamation with newly strip-mined land (0 percent reclamation) and original vegetation (100 percent). Degrees of reclamation are then made as 0-25 percent, 25-50 percent, 50-75 percent, and 75-100 percent.

Using the built-in electronic planimeter capability of the Spatial Data Image Density Slicing Viewer, and standard planimetric techniques, an effort was undertaken to demonstrate that (1) the unreclaimed strip-mine areas could be enhanced to the exclusion of any other terrain feature using ERTS imagery, and (2) that an accurate area calculation was possible in a relatively short period of time. A test survey of areas strip mined and areas reclaimed was made of Harrison County in eastern Ohio using Band 5 of an ERTS-1 image. The resulting area calculation achieved in this survey corresponds quite favorably to Department of Natural Resources Data as shown in Table III.

A one year comparison study of a major strip mining area located in eastern Ohio was undertaken to demonstrate the value of repetitive ERTS-1 imagery in a land-use monitoring capacity. The study site chosen was a controversial area where two of Ohio's major mining shovels had moved into during January, 1973. The comparison was made between a portion of the MSS Band 5 image of 21 August 72 shown in Figure 5a and a portion of the MSS Band 5 image

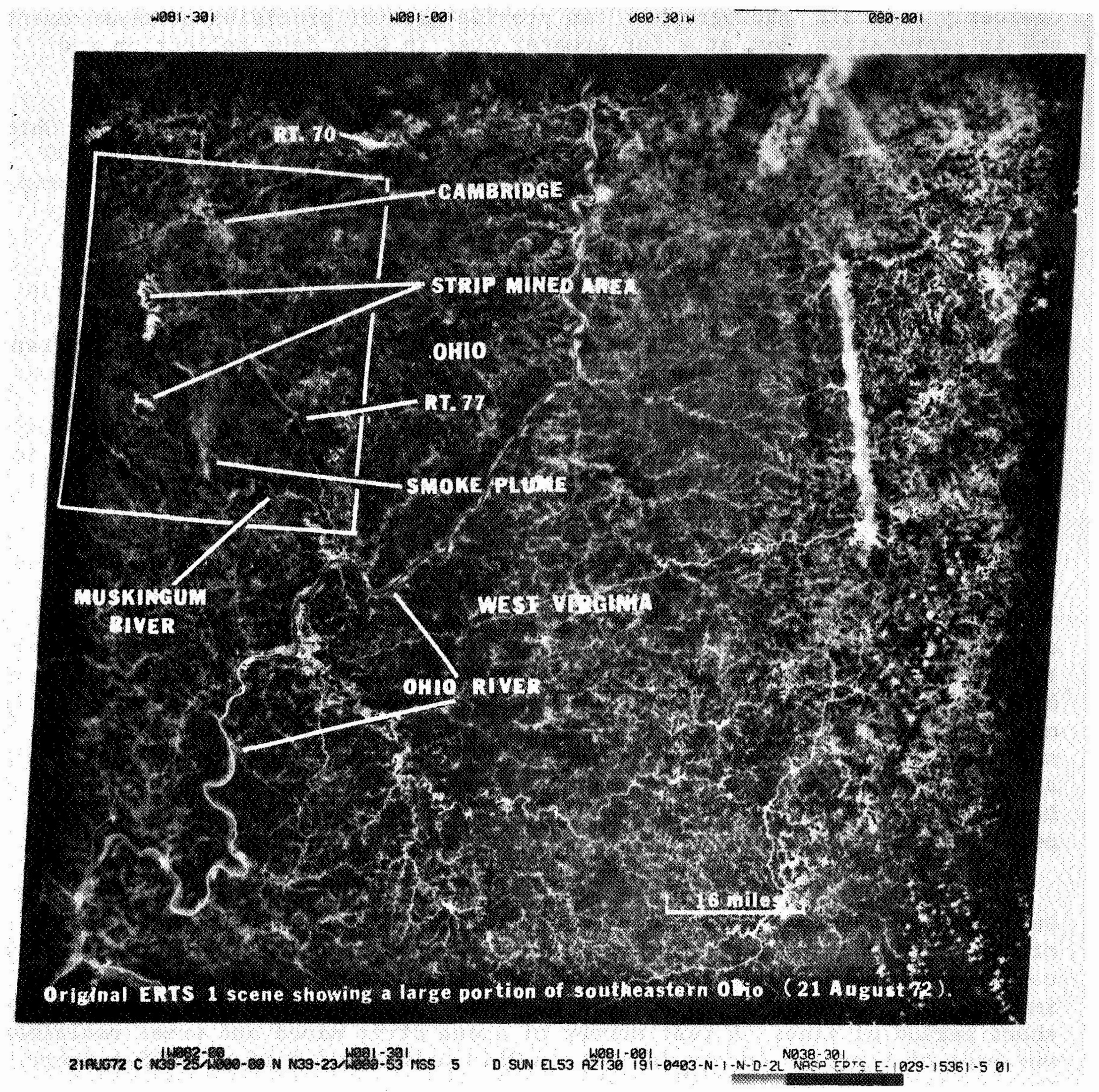

Fig. 2. Typical ERTS-1 (Band 5) scene of southeastern Ohio showing how pronounced strip-mining areas appear.

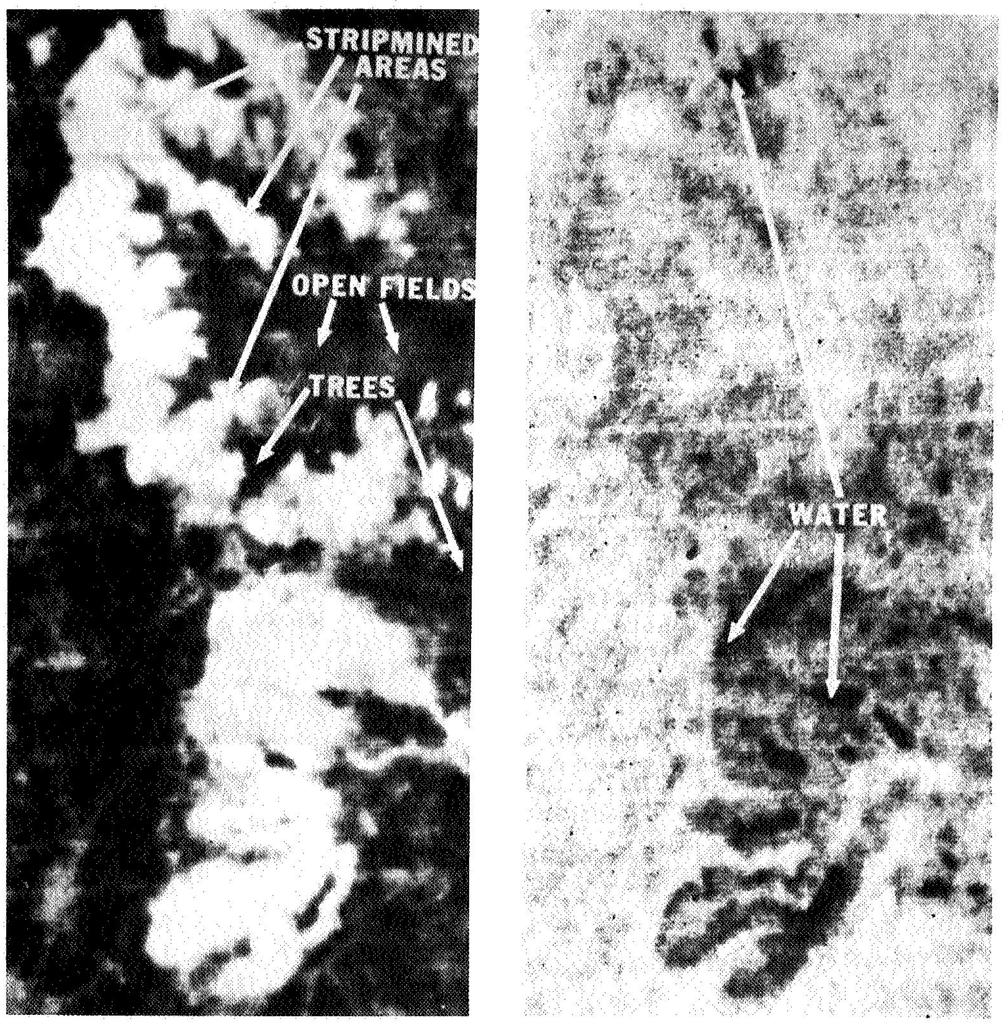

Fig. 3. Comparison of strip-mine areas as seen on ERTS-1 Band 5 (left) and Band 7.

Fig. 4a. 1:24,000 USGS topographic map sheet (reduced by 1/2 original format) showing typical active Ohio strip-mine area.

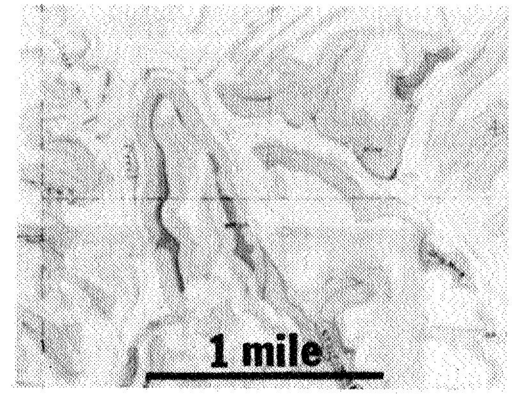

Fig. 4b. 1:24,000 aircraft photo of the same strip-mine area. Photos such as these were used to demonstrate that ERTS imagery has sufficient image quality and area fidelity to perform strip-mine inventories (photo by NASA Lewis Research Center).

Fig. 4c. Electronically magnified and enhanced ERTS-1 MSS Band 5 image of the same area. Note similarity to aircraft photo above.

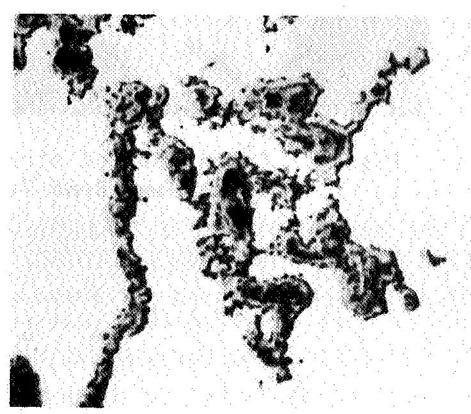

TABLE III.

COMPARISON OF STRIP-MINE AREA ESTIMATES FOR HARRISON COUNTY, OHIO		
Total Land Area -- 258,000 Acres		
	ODNR	ERTS-1
% of strip-mined land	19.01	18.4
Area affected	49,064 acres	47,472 acres
% of unreclaimed strip-mined land	6.8	6.2
Area unreclaimed	17,603 acres	15,996 acres

of 3 September 1973 shown in Figure 5b. During the one-year period over 400 acres of land were effected.

The capacity of ERTS to be utilized as a tool for effectively monitoring Ohio's strip mining activities being demonstrated by this and Dr. Pettyjohn, et al., programs is both significant and timely because of the public trust implications so important to the growing environmental protection-energy crisis dilemma existing in Ohio and throughout the nation at large.

Because of the state's interest in establishing legislation to control all surface mining (All Minerals Bill pending in the Ohio General Assembly), we are currently looking at the feasibility of extending the demonstrated capability of ERTS to detect and inventory strip mining to other surface-mining operations in Ohio. Figure 6 shows how surface radiometric signatures of typical gravel pits, limestone quarries, and strip mines in Ohio differ from one another. Figure 7 demonstrates the capacity of ERTS data to detect various types of such surface mining operations in northern Ohio by comparing ERTS data to an existing 1:250,000 topographic map for the same region.

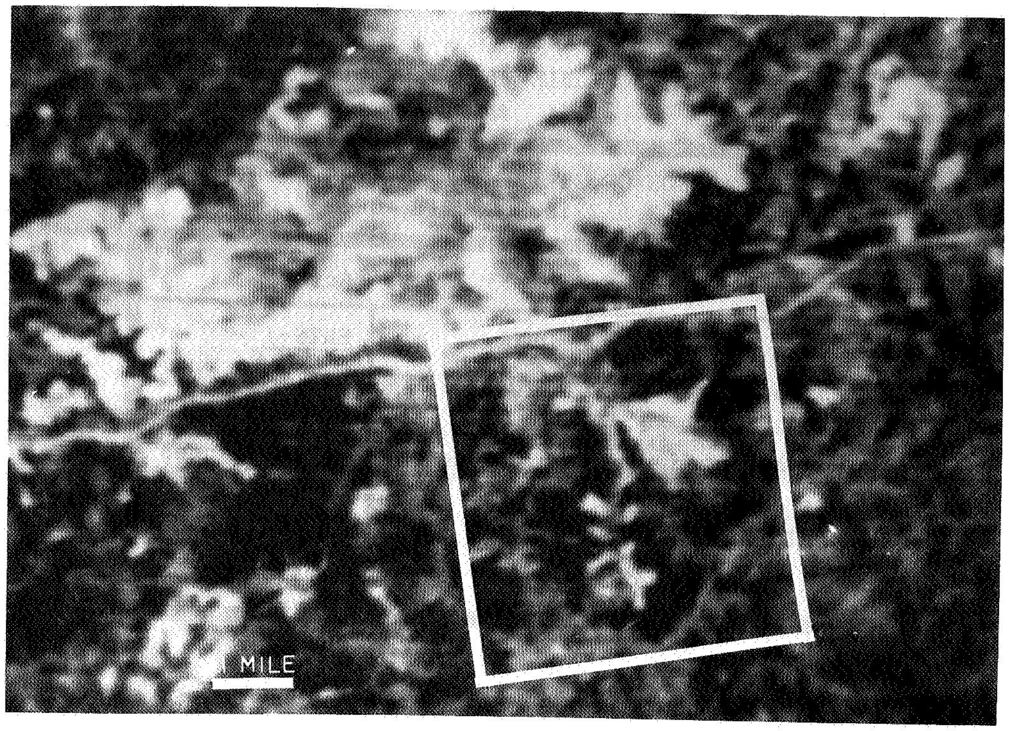

Fig. 5a. 21 August 1972 ERTS-1 MSS Band 5 photo showing a heavily strip mined area in eastern Ohio.

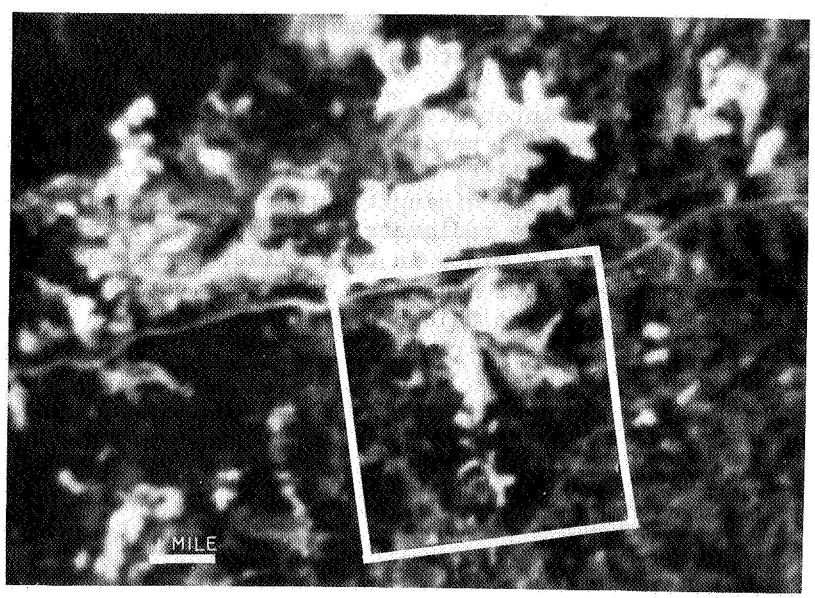

Fig. 5b. 3 September 1973 ERTS-1 MSS Band 5 photo of same area shown in Figure 5a revealing the extent of strip mining occurring during a one-year period.

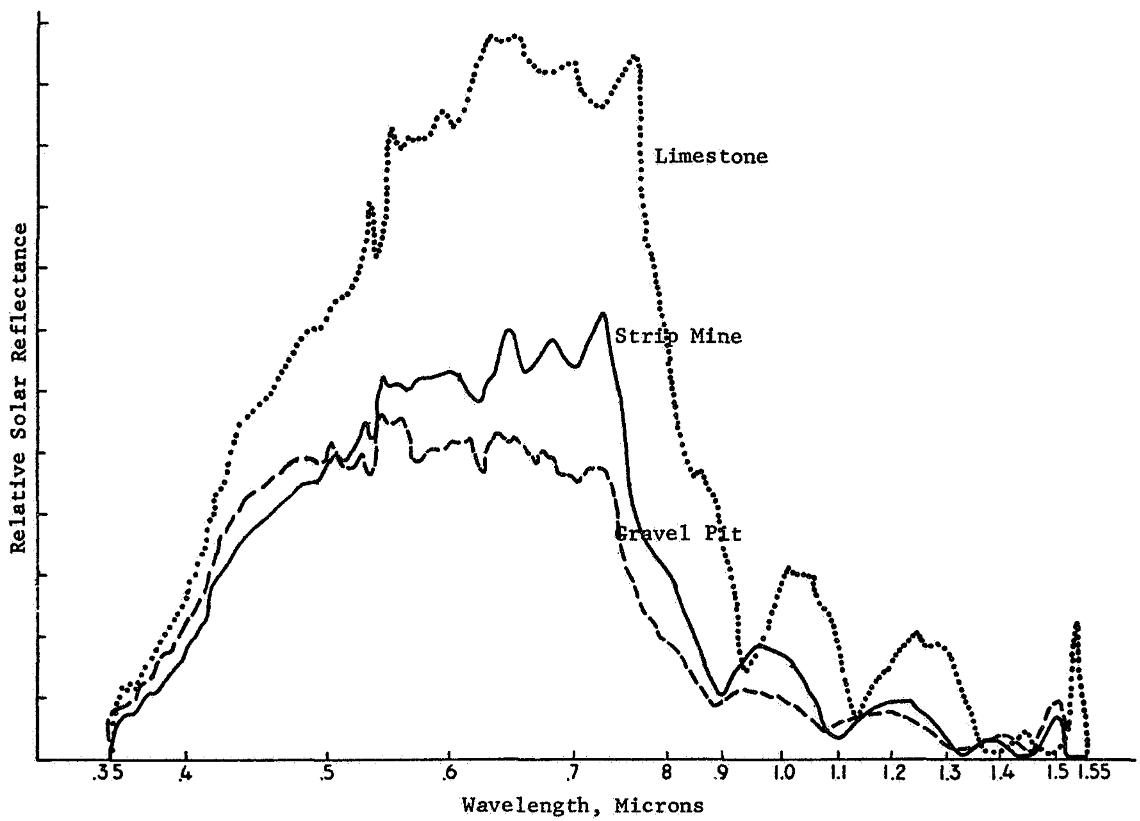

Fig. 6. Comparison of relative reflectance curves of limestone quarry, gravel pit, and strip mine operations in Ohio. These data indicate definite differences in the reflectance characteristics of the visible portion of the electromagnetic spectrum. Such data are necessary for distinguishing types of surface-mine operations in Ohio using ERTS data.

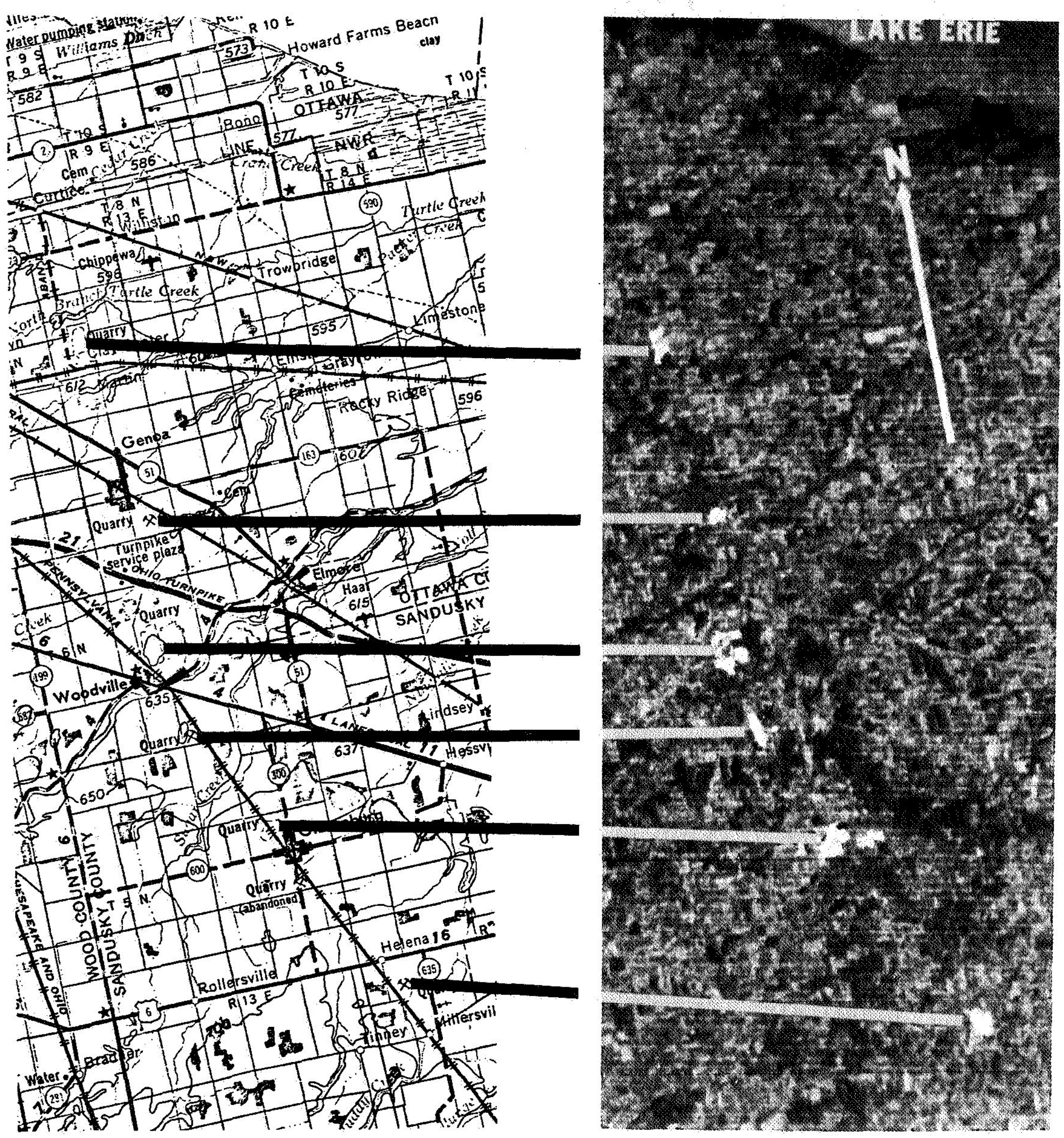

Fig. 7. Correlation of topographic map sheet and ERTS-1 photo of 27 March 73 showing the locations of surface mines in northern Ohio. (Scale: 1:250,000)

Land Use

State Need

Ohio, like every other state, has increasing multiagency requirements for the periodic preparation of a relatively inexpensive statewide inventory of the land and natural resources for use in general planning, land-use decision making, and new legislation preparation. A serious attempt to fulfill this land use data need was undertaken as the objective of the 1960 Ohio land use study. Utilizing existing 1940 to 1960 data and USGS 1:24,000 topographic maps this study produced tabulated land use data and generalized 1:250,000 and 1:500,000 scale land use maps. The land use maps were then compared to aerial photographs collected from 1958 to 1964 for accuracy determination. This 1960 Ohio land use map was completed over a three year period at a cost of approximately $110,000 excluding the costs of obtaining the aerial photography. Although the tabulated land use data provided a much needed detailed land use information base, the study and particularly the maps have been found to be inaccurate in numerous areas. Accordingly, a high-priority state interest exists relative to the extent, accuracy, and cost of using ERTS data to periodically update such land-use information.

Application Results

Preliminary evaluation of the usable ERTS-1 existing for all parts of Ohio, indicates that the data are more than adequate for periodically mapping and inventorying major surface natural and cultural features at scales of 1:24,000 and smaller and at less cost and with better accuracies than with previous techniques. Efforts to date have demonstrated the types of ERTS data analysis techniques and products that can be made available on an operational basis for solving land-use problems, for general land use planning, and for meeting the longer range requirements of the pending National Land Use Policy Act.

Since it was not the intent of the Ohio ERTS program to develop a land use classification scheme, a prominent scheme developed and used by the U. S. Geological Survey was adopted. An outline of this classification scheme is shown in Table IV, and the level to which each major classification has been evaluated thus far for Ohio-ERTS land-use interests is shown on the right side of the table. The feasibility of using ERTS data for land use activities in photographic and computerized formats is demonstrated in the following series of enlarged and color enhanced ERTS-1 photographs of the Columbus, Ohio, metropolitan area shown in Figures 8a-d.

As illustrated in Figure 9 several black and white mosaics and a color mosaic of the entire state of Ohio from 40 x 40 ERTS images are being assembled by the Department of Transportation and the Department of Economic and Community Development. The mosaics have been placed in many departments of the state for planning and management activities. The significance of the mosaics, is, that for the first time, a comprehensive/synoptic overview of Ohio's many diverse environmental, natural, and cultural surface features and

TABLE IV.

OHIO LAND-USE FEATURES DISCERNIBLE ON ERTS-1 IMAGERY

USGS Land Use Classification System for Use With Remote Sensor Data*		ERTS, Analysis Status (Includes Levels 1 & 2)
Level I	Level II	
01. Urban and Built-up Land		
	01. Residential	TBD**
	02. Commercial and Services	TBD
	03. Industrial	TBD
	04. Extractive	Yes
	05. Transportation, Communications, and Utilities	Yes
	06. Institutional	TBD
	07. Strip and Clustered Settlement	Yes
	08. Mixed	Yes
	09. Open and Other	Yes
02. Agricultural Land		
	01. Cropland and Pasture	Yes
	02. Orchards, Groves, Bush Fruits, Vineyards, and Horticultural Areas	TBD
	03. Feeding Operations	TBD
	04. Other	TBD
03. Rangeland		
	01. Grass	N/A***
	02. Savannas (Palmetto Prairies)	N/A
	03. Chaparral	N/A
	04. Desert Shrub	N/A
04. Forest Land		
	01. Deciduous	TBD
	02. Evergreen (Coniferous and Other)	TBD
	03. Mixed	Yes
05. Water		
	01. Streams and Waterways	Yes
	02. Lakes	Yes
	03. Reservoirs	Yes
	04. Bays and Estuaries	Yes
	05. Other (Ice and Snow)	Yes
06. Nonforested Wetland		
	01. Vegetated	Yes
	02. Bare	Yes
07. Barren Land		
	01. Salt Flats	N/A
	02. Beaches	TBD
	03. Sand Other Than Beaches	TBD
	04. Bare Exposed Rock	TBD
	05. Other	TBD
08. Tundra		
	01. Tundra	N/A
09. Permanent Snow and Icefields		
	01. Permanent Snow and Icefields	N/A

* "A Land-Use Classification System for Use With Remote Sensor Data", J. R. Anderson, E. E. Hardy, & J. T. Roach, Geological Survey Circular, 671, Washington, D. C., 1972.

** TBD = To be determined by future analysis.

*** N/A = Classification not applicable to Ohio.

Fig. 8a. 1:48,000 aircraft index photo sheet of 17 April 72 of a recently urbanized area in northeastern Columbus, Ohio.

Fig. 8b. An electronically magnified portion of an ERTS-1 MSS Band 5 photograph of 3 November 72 of the area.

Fig. 8c. An eight-character computer print-out demonstration product derived from the ERTS-1 MSS Band 5 computer compatible tape of 3 November 72 of the area.

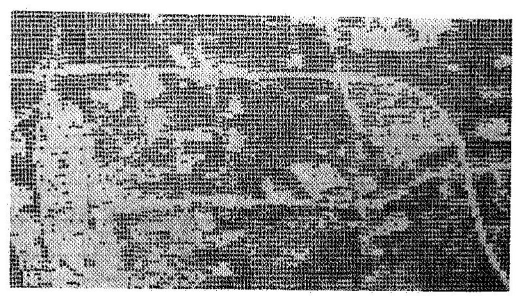

Fig. 8d. Magnified and color enhanced portion of an ERTS-1 MSS Band 5 photograph of 3 November 72 superimposed on a 1964 1:24,000 USGS topographic map sheet of the area. The recently urbanized areas are highlighted to illustrate the capability of ERTS imagery to accurately identify land-use changes.

Fig. 9. ERTS-1 MSS Band 5 Photomosaic of the State of Ohio
Original Scale: 1:250,000.

their interrelationship can be viewed at once. Such a synopic overview is being utilized, for example, by the Ohio Power Siting Commission for selecting new power plant sites and alternative power transmission corridors as they attempt to wisely manage Ohio's energy supplies and resources.

Other

In addition to the above major application analysis activities, several real-time, problem-solving exercises in which ERTS data utility were examined can be cited:

Agriculture and Forestry

In response to the provisions of pending federal land use legislation, the passage of Issue I in Ohio which permits lower agricultural property assessments, and other various pressures that indicate a need to formulate a state land use program, The Department of Economic and Community Development has recently initiated an in-depth study to include historical background research, policy formulation, and data collection activities relative to prime or unique agricultural land in Ohio. In this prime agricultural land study, it is anticipated that ERTS data will be used to aid in formulation of an operational definition of prime agricultural land, in determination of the location of such lands in Ohio, and in the assessment of the interrelationship of prime agricultural lands to environmental, economic, and social parameters such as open space, market distribution centers, and urban sprawl.

As shown in Figure 10 a thematic map demonstration product of the major forested areas in southeast Ohio was derived from ERTS data and has been made available to the Ohio Biological Survey to support their concentrated study of the entire Scioto River Basin for the U. S. Army Corps. of Engineers.

Although the transparency clearly illustrates the significant changes that have occurred in southeastern Ohio's forestry resources since 1968 (when compared to 1:250,000 topographic map) the importance lies in the generation of a new ERTS data product type potentially useful for providing dynamic statewide views of natural and cultural features in single and/or combined formats.

For selected study-site areas, the transparency is over 95 percent accurate for mature forested areas in excess of 25 acres, and although the accuracy has not as yet been determined for extrapolated regions, it appears comparable to the USGS 1:24,000 maps and more accurate than the 1:250,000, especially for urbanized areas.

Lake Erie

Ohio EPA researchers are seriously interested in using satellite photography for Lake Erie water quality management practices. Figures 11a and 11b show the ability of ERTS to provide a repetitive overview of Lake Erie pollution and sedimentation plumes heretofore unavailable. From a preliminary analysis of repetitive scenes, OEPA personnel are optimistic that ERTS data may significantly improve understanding of the complex and dynamic characteristic of Lake Erie and make more accurate modeling possible. In addition to a better definition of nearshore and offshore developments, OEPA personnel are interested in evaluating such specific correlations as: littoral drift/lake dispersions, algae masses, temperature phenomena, and water level (for coastal zone management, which is also of high interest to the Department of Natural Resources).

Synoptic winter-time imagery provided by ERTS-1 has likewise provided a new insight into the characteristics of Lake Erie ice conditions. Because of ice conditions, shipping activities on Lake Erie have been limited to the

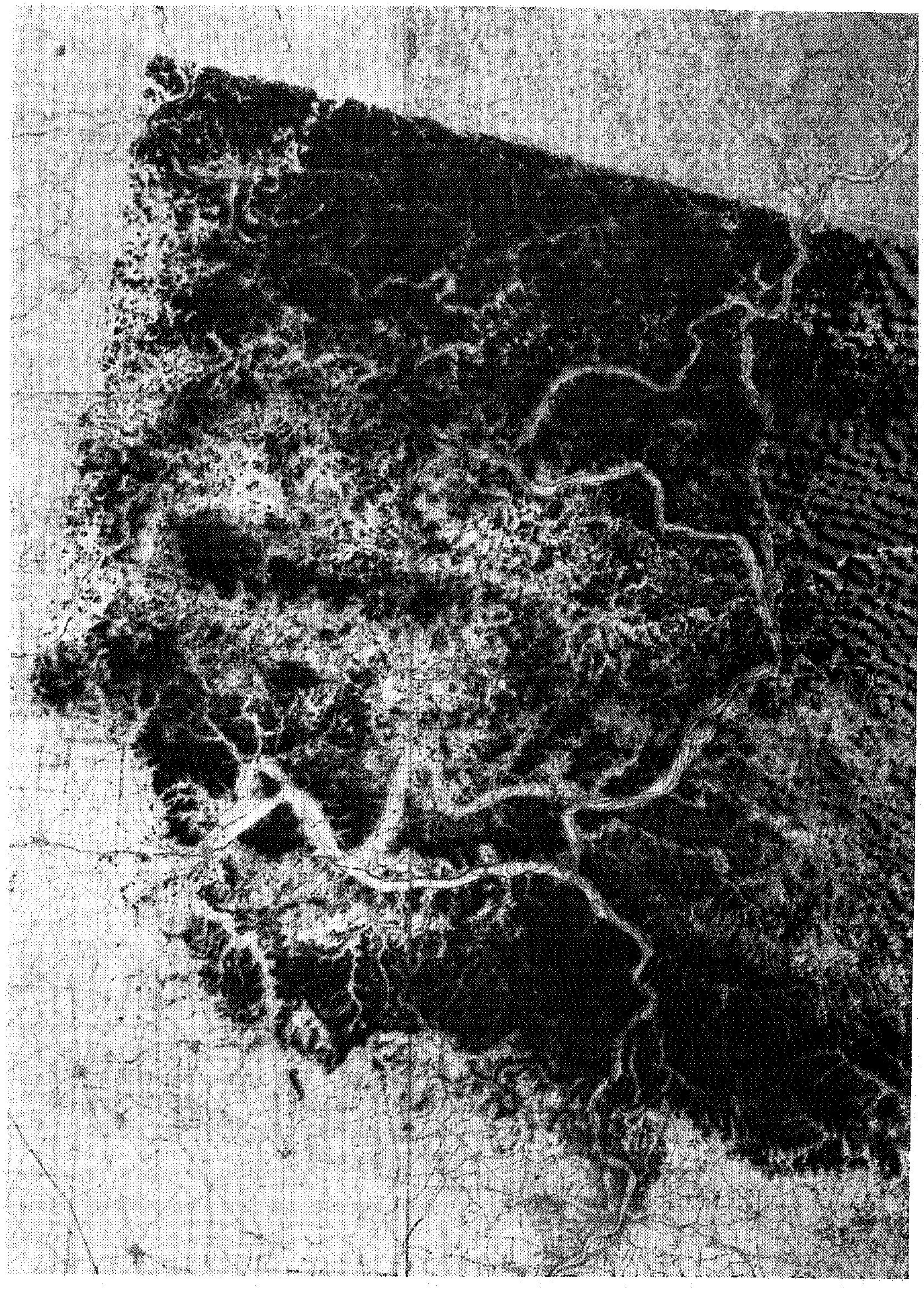

Fig. 10. Southeastern Ohio forestry transparency demonstration product overlaid onto existing 1:250,000 USGS topographic map sheets.

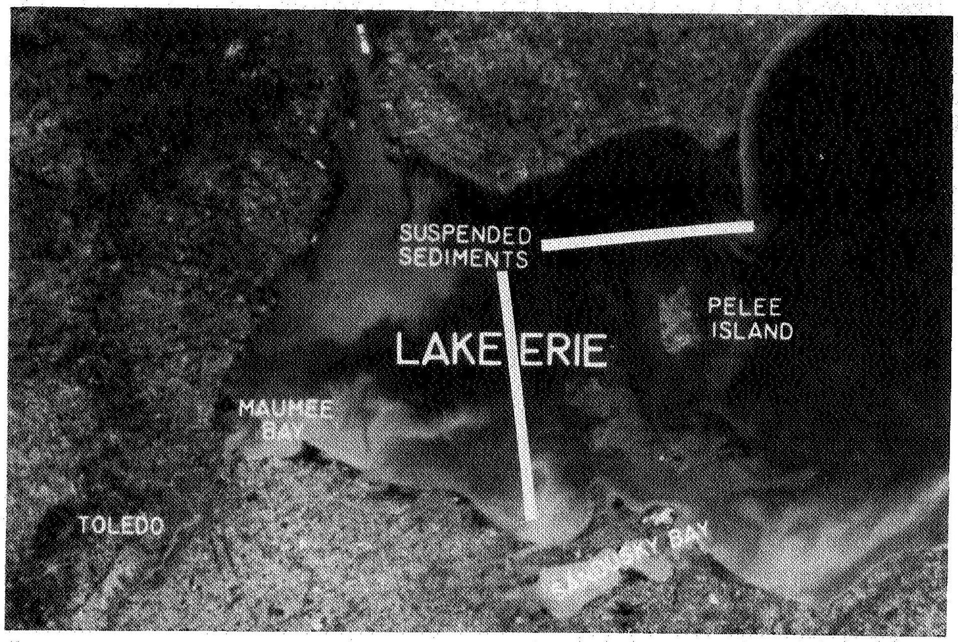

Fig. 11a. ERTS-1 photo of 27 March 73 showing sedimentation patterns in western Lake Erie (Band 5, 6,000-7,000 A). Note that the Sandusky Bay land areas appear partially inundated (see Fig. 11b for comparison).

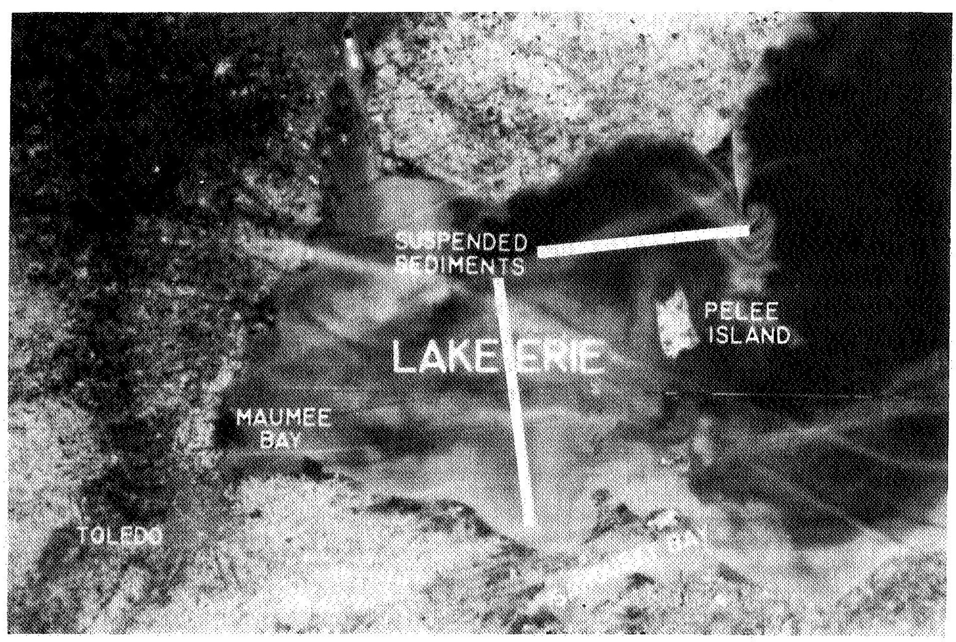

Fig. 11b. ERTS-1 photo of 14 April 73 showing sedimentation patterns in western Lake Erie. Also note that water in Sandusky Bay area has receded (see Fig. 11a for comparison).

nine warmer months of the year in the past. However, as illustrated in Figure 12, ERTS-1 imagery of February 18, 1973 revealed that shipping on Lake Erie could possibly occur on a year-wide basis with some assistance by ice cutters. The Ohio Departments of Transportation and DECD are pursuing this interest.

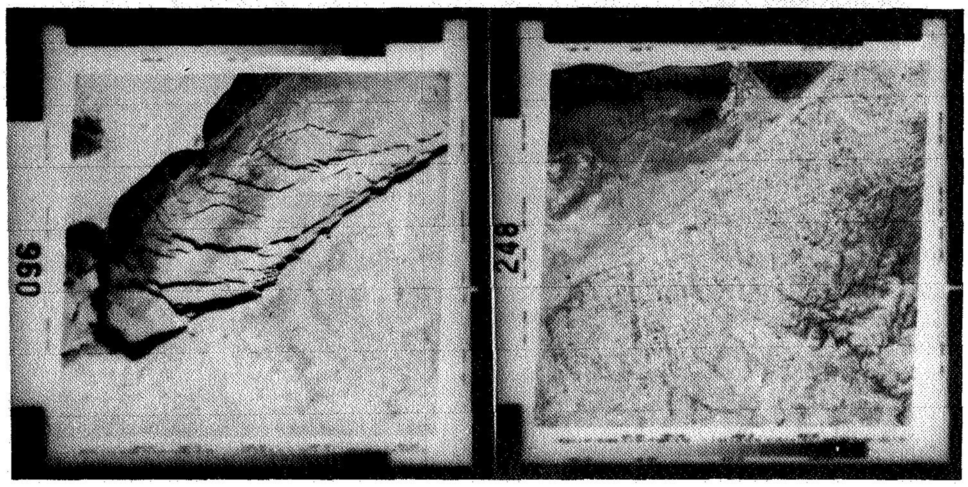

Fig. 12. Successive ERTS-1 photos of 17 and 18 February 73 showing ice conditions on Lake Erie.

DCP Demonstration Activity

In addition to the ERTS imagery analysis, a single DCP has been used in the Ohio-ERTS program to demonstrate the utility of the ERTS Data Collection System (DCS) for potential state use in an operational mode. The platform was installed in December, 1972 and operated until late July, 1973, except for one outage due to lightning damage, which required shipment of the platform to Wallops Island for repair. The platform has been interfaced with a Schneider Model RM 25 Robot Monitor, which senses seven water quality and five meteorological parameters. An ERTS utility demonstration report is being prepared describing and summarizing the results of this experiment for use of state personnel in evaluating the potential operational utility of the DCS.

Transportation Planning

The Department of Transportation is looking at satellite data from both transportation planning and support to other agencies from the viewpoint of base maps. They hope to eventually use up-to-date ERTS base maps for general land and soil studies, land development plans, tax information, geological/construction implications, noting the availability of existing surveys, and as an aid to determine updating requirements for USGS topographic map series.

Sanitary Land Fill Detection

At the request of OEPA personnel a preliminary assessment of the ability of ERTS imagery to provide an inventory of sanitary land fills (many illegal) throughout the state was undertaken. However the resolution of current ERTS imagery was found inadequate for this application.

Abandoned Mines Study

The capability of ERTS to detect areas mined many years ago has been used by the Ohio Geological Survey to determine how much of certain coal seams remain to be mined. In this study, rather than a time-consuming search of old permit records, ERTS photography was used to determine if certain suspected areas had been strip mined years ago.

The Department of Natural Resources has also begun studies on the seepage of surface water into old underground mines in southeastern Ohio and the resulting acid mine water pollution. ERTS imagery has been used to detect possible wet areas in which surface water is prominent by vegetative patterns and vegetation differences which may be due to adverse affects of such pollution.

Floodplain Monitoring

Department of Natural Resources is interested in determining to what extent ERTS data could be used to detect new developments encroaching upon the floodplain and from this the extent to which the repetitive nature of orbital survey data could be used to monitor the floodplains. Approximately 50 percent of Ohio's cities are periodically subjected to flood damage. Results will be important to the ability to enforce statewide floodplain regulations under legislative consideration in Ohio.

Air Pollution

Since major smoke plumes are discernible in ERTS imagery, the Ohio EPA plans to use ERTS data on the location, movement, and confluence of smoke plumes to test computer air motion models being developed for use in state wide major air pollution control practices.

Education

The Ohio State University is cooperating with participating State government agencies and BCL in pursuing the educational implications of ERTS data applications. Specialized workshops, interdepartmental seminars, and formal courses have been organized in which ERTS and aircraft data on Ohio are being utilized.

UTILITY ASSESSMENT

The major requirement of the Ohio-ERTS program is to assess the potential state value of ERTS data applications. The State of Ohio, through Battelle Columbus Laboratories, has demonstrated ERTS-1 data use opportunities to officials at the federal, state, regional, and local levels. Representatives of nearly every facet of Ohio environmental protection, resource management, and land use planning have witnessed the potential utility of ERTS data as applied to their discipline interest, and the reaction has been extremely favorable and enthusiastic.

As a response to almost daily requests from various planners throughout Ohio to have ERTS-1 capabilities and data use possibilities explained and demonstrated, and to assist in making the final state utility assessment, the Department of Economic and Community Development is planning a statewide, ERTS workshop to be held in late January. All planners and officials from state agencies, regional planning organizations, and local planning and policy departments will be invited to review the potential utility of ERTS data established to date, and to test the appropriateness of ERTS data to their particular problem-solving needs and interests. In this way, not only will ERTS-1 data utility receive the maximum exposure, but also direct involvement in real-time problem-solving experiments will provide tangible and retainable evidence for planners to consider when integrating the role of ERTS in their future plans and programs.

In addition, participants will be specifically requested to contribute to:

(1) Assessment of the potential state benefit inherent in the use of ERTS data developed during the workshop as well as that contained in demonstration products prepared in the application areas of surface mining, land use, and agriculture and forestry.

(2) Determination of the operational implications of Ohio-ERTS data user progress made to date.

SUMMARY

Although progress to date has been significant and swift, the application of remotely-sensed data and particularly satellite data has only just begun in Ohio state government. The development and operational employment of specific techniques and applications for state government is very difficult, time consuming, and most important, quite expensive. Ohio for one simply cannot afford to develop this technology on its own.

These meetings are a great help in exchanging ideas, techniques, and findings. Certainly, a key challenge existing at the state user level is the establishment of procedures for translating ERTS data into families of useful products that can be effectively absorbed into on-going decision making activities. State government is doing its job, perhaps not as effectively as

we would like, but it is doing the job. Thus, the general philosophy among many state officials is "Why should we bother with this stuff?", or "How will it help me do my job better?", and these are indeed valid questions to which we must effectively respond. The days of ill-defined practices, and equipment developed at great expense are giving way to austere but effective management and utilization of data. Collection technology is far ahead of utilization (data reduction) technology as is evidenced by the vast amount of imagery that has never been utilized even superficially.

Accordingly, we must try to arrange for increased budgeting at all levels of government to accelerate the application and utilization of existing and anticipated remote-sensing data. To create a larger, state-user demand for remote-sensing products and services requires that application efforts in the near future be as <u>specific</u> and <u>inexpensive</u> as possible.

REFERENCES

RESOURCE MANAGEMENT IMPLICATIONS OF ERTS-1 DATA TO OHIO, David C. Sweet and Terry L. Wells, State of Ohio, Department of Economic and Community Development, and George E. Wukelic, Battelle Columbus Laboratories, Symposium on Significant Results Obtained From the Earth Resources Technology Satellite-1, Goddard Space Flight Center, New Carrollton, Maryland, March 5-9, 1973.

APPLICATIONS OF REMOTE SENSING TO RESOURCE MANAGEMENT AT THE STATE LEVEL, D. C. Sweet, C. J. Meier, T. L. Wells, G. B. Garrett, and L. Herd, State Government of Ohio and G. E. Wukelic, J. G. Stephan, and H. E. Smail of Battelle Columbus Laboratories, Symposium on Management and Utilization of Remote Sensing Data, American Society of Photogrammetry, Sioux Falls, South Dakota, October 29-November 2, 1973.

Paper E 5

ERTS IMAGERY AS A SOURCE OF ENVIRONMENTAL INFORMATION FOR SOUTHERN AFRICA

Douglas T Williamson and Brian Gilbertson, *Spectral Africa, P.O. Box 2, Randfontein. Rep. of South Africa*

ABSTRACT

Southern Africa is faced with a variety of environmental problems that reflect the different states of development of countries in the region. The task of the environmental planner is in many instances complicated by a lack of basic resource information. The acquisition of the necessary data is often impeded by shortage of trained personnel and lack of funds, particularly in developing nations of the region.

This paper describes the range of environmental problems in Southern Africa and shows specific examples of how ERTS type imagery can materially assist in solving these problems. These examples demonstrate that ERTS type data will be of substantial value to both the industrialized and the developing nations of Southern Africa, provided that problems of availability and user education are overcome.

INTRODUCTION

The indices of table 1 show that the countries of Southern Africa are at different stages of economic development.

TABLE 1

Economic Status of Countries in Southern Africa vs. USA.
(Source: UN Yearbook, 1971)

Country	Area km^2	Population density per km^2	Gross Domestic Product US$ x 10^6	Per Capita GPD US$	Per Capita National Income US$
Botswana	569 800	1	67	110	96
Lesotho	30 344	30	82	92	95
Rhodesia	389 362	14	1 454	276	252
S. Africa	1 221 043	17	17 373	838	728
Swaziland	17 366	23	80	208	162
U.S.A.	9 363 393	22	969 574	4 734	4 274

The problems that these countries face tend to reflect their economic status. The developing nations face the task of inventorying natural resources and allocating these resources among different strategies of exploitation and development. The more developed countries to some extent share this problem but must also cope with the environmental effects of industrialization.

The development of resources and the solution of environmental problems is an urgent matter in Southern Africa. As in other parts of the world populations are increasing rapidly. Rhodesia's population, for instance, is expected to double within 16 years, South Africa's within 25 years. These populations will require additional resources for their maintenance, let alone their social and economic advancement. It is thus important that all resources be efficiently exploited to maximize benefits from non-renewable resources and to enhance productivity of renewable resources. This will require precise knowledge of existing resources and surveillance of renewable resources to detect avoidable degradation.

The resource information requirements of Southern Africa are summarised in the first column of table 2.

TABLE 2

Areas of Applicability for ERTS Imagery

PROBLEM	ADVANTAGES OF ERTS TYPE IMAGERY	OPTIMUM COVERAGE
Problems of Planning		
a. Resource Inventory	Regional coverage, ease and speed of interpretation.	Full seasonal coverage
b. Resource Allocation	Display of geographic and ecological relationships over a wide area.	Full seasonal coverage.
c. Environmental Impact Studies	Regional coverage, ease and speed of interpretation	As required
Problems of Control		
a. Detection of Resource Degradation	Repetitive coverage over large areas	Seasonal
b. Monitoring changes in land use	Repetitive coverage over large areas	Every 3-5 years
c. Possibly, Monitoring industrial & urban pollution	Repeated regional coverage allowing extrapolation of data gathered in small areas on the ground	As often as possible, optimum daily

Environmental knowledge of Southern Africa is inadequate in important respects. Soil and vegetation mapping, for example, have for the most part been completed in only the broadest outlines. In addition, the acquisition of environmental data is often impeded by shortage of trained personnel and lack of funds. ERTS-imagery provides a means of remedying some of these inadequacies. In the next section we discuss specific applications of ERTS-imagery to environmental problems of importance in Southern Africa. One example from many has been selected from each of the categories of table 2.

ENVIRONMENTAL INFORMATION FROM ERTS IMAGERY

Resource Inventory: Figure 1 shows ERTS image 1053-07510, and was chosen to illustrate the utility of ERTS imagery for resource inventory. It covers a large portion of the Chobe National Park, Botswana. This part of Northern Botswana has a semi-arid climate but adjoins two major water resources, the Okavango Delta and the Chobe-Linyanti River Complex. Portion of the Kwhai drainage from the Okavango is visible in the lower left hand corner of the image. The Chobe-Linyanti complex can be seen in the upper right hand corner of the image. Intersting geological features which are clearly depicted are the fault line bounding the Okavango system and the Mababe Depression, which was formerly a lake.

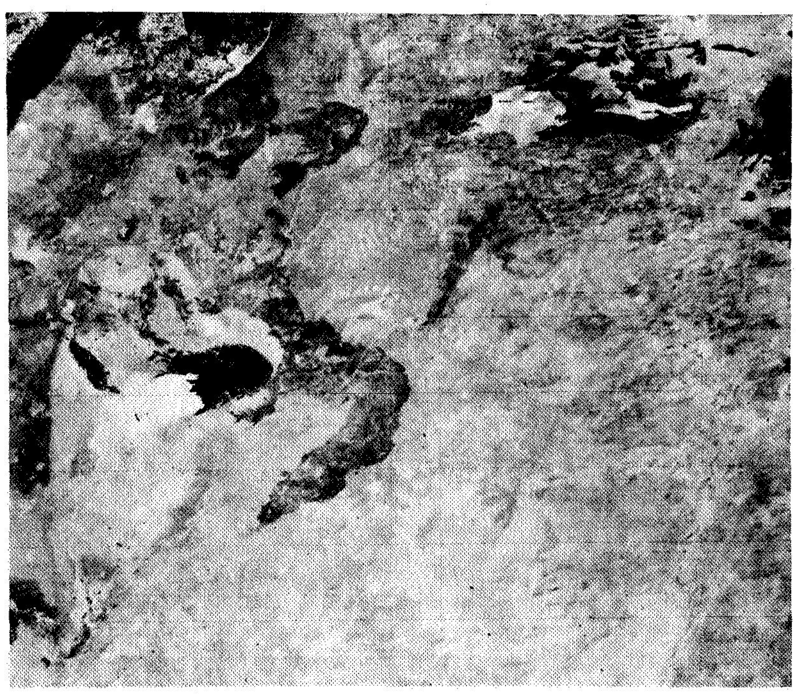

FIG. 1 : NASA ERTS E-1053-07510

The image provides an insight into the distribution and areal importance of the natural vegetation types. Aquatic vegetation, as in the Chobe Linyanti Complex in the upper right hand corner of the image is a striking red-brown colour. Colour tonal differences further allow differentiation between areas of open and closed woodland (dark and light brown tones), mosaic of trees and grassland (patchy brown and white to pale areas), and grassland (pale and white areas). The black and discoloured olive sections show the massive extent of dry-season burning in this part of the world.

Resource Allocation: The Chobe National Park image of figure 1 also illustrates the application of ERTS-data to problems of resource allocation. A clear insight into geographic and ecological relationships is desirable for the allocation of land resources to different land use practises. Figure 1 graphically portrays drainage patterns and the distribution of surface water and natural vegetation. This regional perspective of important relationships will facilitate the task of deciding upon the the land use practise to be adopted in particular areas.

Environmental Impact Studies: It is impossible to implement development programmes without some measure of disturbance to natural communities and ecosystems. However, it is essential that development of one resource should not be needlessly destructive of other resources, and for this reason environmental impact studies before development is undertaken are desireable.

In another paper (Williamson and Gilbertson, 1973) it was shown that ERTS imagery can be applied to this end. An image of the Knysna coast was studied to determine the likely effect of a freeway development.

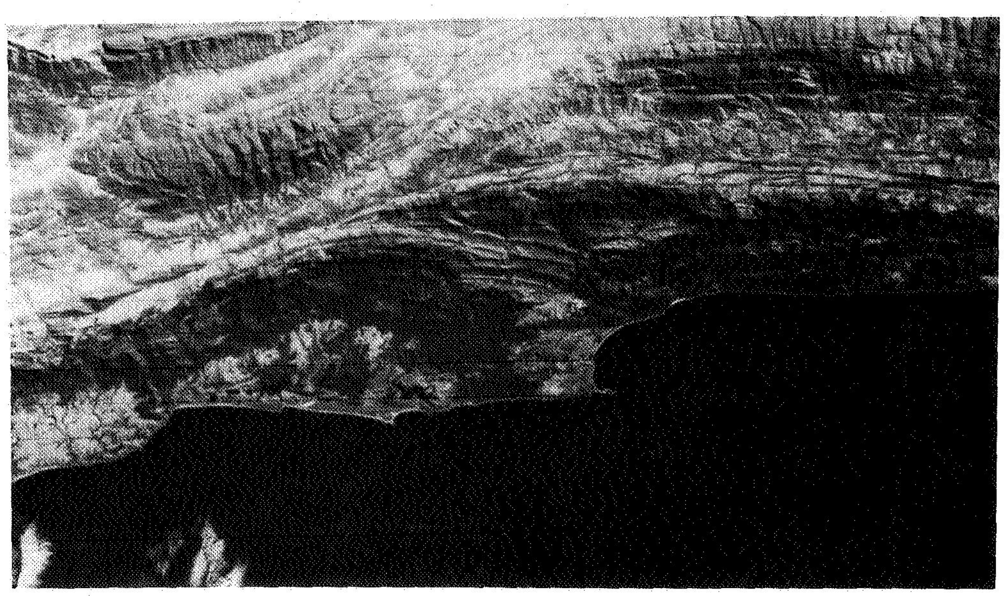

FIG. 2 : ERTS E-1231-07452

The image enabled an estimate of the impact of the development to be made rapidly and with a satisfactory degree of accuracy. Offical estimates of likely damage to indigenous forests of the region were from 0.024% to 0.25%, the estimate based on the ERTS image was 0.20%.

Detection of Resource Degradation: A portion of southern, central Rhodesia is shown in figure 3. The dark band running from the top towards the bottom of the image, slightly left of centre is an important geological structure, the Great Dyke. Around the lower end of the Great Dyke and curving away and back toward it on the right are paler areas with sharply defined edges. On maps of the same scale as the image the edges of these pale areas register with the boundaries of the African Tribal Trust lands. In the pale areas severe overgrazing has decimated the natural vegetation.

FIG. 3 : NASA ERTS IMAGE E-1103-07291

This type of degradation is widespread in Southern Africa. Frequently it is accompanied by the drying up of perennial watering points because ground water is not replenished due to increased run off through lack of vegetative covering. The ability to detect and control such deterioration is vital if lands are to remain sufficiently productive to support the burgeoning population of the developing world.

Monitoring changes in Land Use: The Knysna image of figure 2 also illustrates the utility of ERTS imagery in monitoring changes in land use practise. Comparison of this image and an adjacent one with existing maps revealed that areas of natural grassland and low shrub were being replaced by plantations of introduced coniferous trees. The ERTS images also showed the encroaching freeway development which was not mapped.

Monitoring Pollution: Figure 4 shows part of the Witwatersrand complex. The position of the city of Johannesburg is marked with an A, and a line of minedumps stretch from east to west. Wind and water erosion of these dumps is an environmental hazard which is controlled largely by establishing a cover of vegetation on the dumps. Varying degrees of vegetative cover can be distinguished on the image.

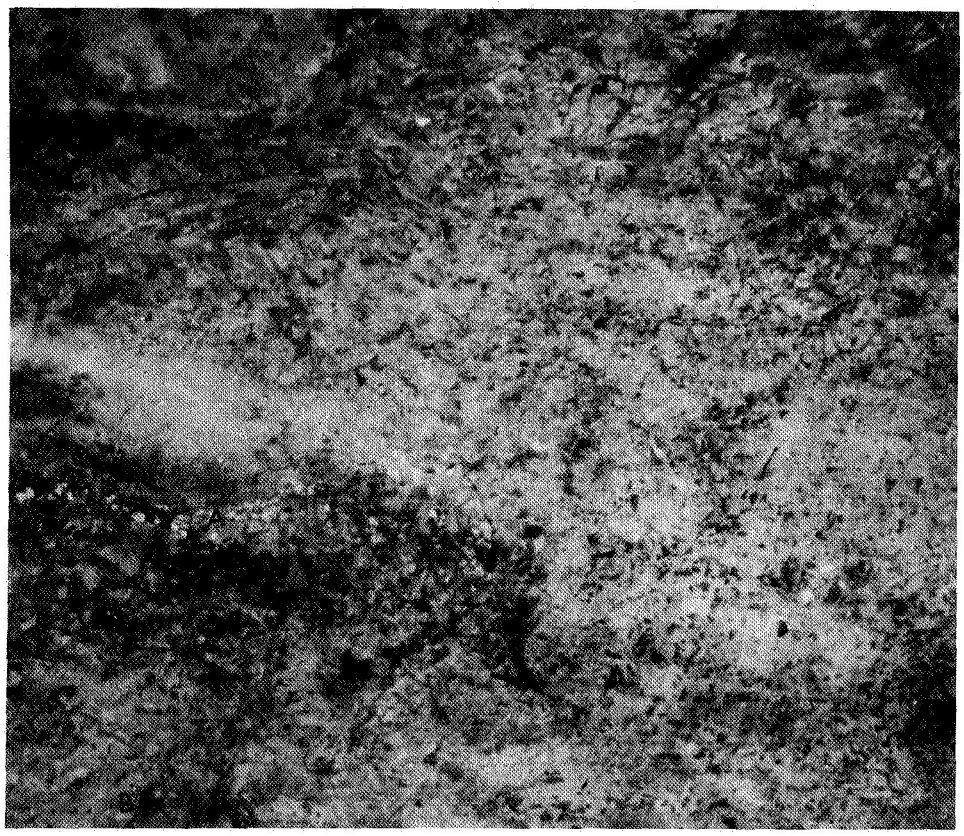

FIG. 4 : NASA ERTS-IMAGE E-1049-07301

The wastes and smoke of a large steel factory near the Vaal river are visible south of Johannesburg, at a point marked B. Large areas of haze can also be seen to the North and East of Johannesburg. Grass fires contribute largely to this but urban and industrial smog may also be contributing factors. This cannot be confirmed because conditions were not monitored at the time of the satellite's overpass but it is worth noting that the satellites coverage of the Witwatersrand may enable measurements of air quality made at strategic points to be extrapolated to provide a picture of air quality over the entire region.

DISCUSSION

The unique advantages of ERTS imagery that emerge from the preceding discussion are summarised in column 2 of table 2. It is clear that the main benefits lie in the fields of large area inventory and planning, and in environmental surveillance on a regional basis. It is useful to compare the costs of ERTS-data in these roles with those of more conventional methods.

Table 3 presents a data users point of view, and compares the costs of aerial photography and ERTS imagery over a large region. It is clear that a substantial economic saving is offered by the ERTS data. Further economies occur in the interpretation phase. For example, regional geological (Viljoen, 1973) and vegetative (Williamson, 1973) mapping programs in Southern Africa have already shown that a good deal of time can be saved via the utilization of ERTS-data.

TABLE 3

Comparison of approximate costs (in US$) of aerial photography vs. ERTS imagery for coverage of an area 45 000 km^2

Item	ERTS 1:250 000	Black & White 1:40 000 aerial	Aerial Colour 1:40 000
Number of prints required to cover area.	2	1 500	1 500
Cost of acquiring existing photography.	18	Governm. 300 Commerc. 1000	7 500
Cost of photography that must be undertaken by user	-	33 000	43 000
Cost of laydown of uncontrolled mosaic	-	5 500	5 500
Cost of photography of uncontrolled mosaic.	-	1 000	1 700
Total cost if photography existence	18	7 000	15 000
Total cost if user must undertake photography	-	40 000	50 000

The cost benefits to the data user emphasize the value of the ERTS-type imagery. However, the extent to which such imagery will come into widespread use in Southern Africa for the planning and control problems of table 2 will depend not only on cost, but obviously also on the availability of imagery of acceptable quality and frequency.

In problems of planning it is desirable that the data base be as complete as possible. One requirement is that cloud-free ERTS-1 coverage of the entire area be available. This goal has already been achieved to a large extent, though not entirely, as is shown in figure 5. Furthermore, since repetitive imagery can enhance the value of the data, and in fact provide unique information (Grootenboer, 1973) it is also desirable that seasonal coverage be available. As yet no area of Southern Africa has received cloud-free coverage over four seasons (see figure 6.)

In problems of control the timing of the coverage is of principal interest. Consequently, further ERTS-type programs, with carefully selected coverage cycles, will be required for these applications. The third column of table 2 comments on the coverage cycle requirements of specific types of resource problem.

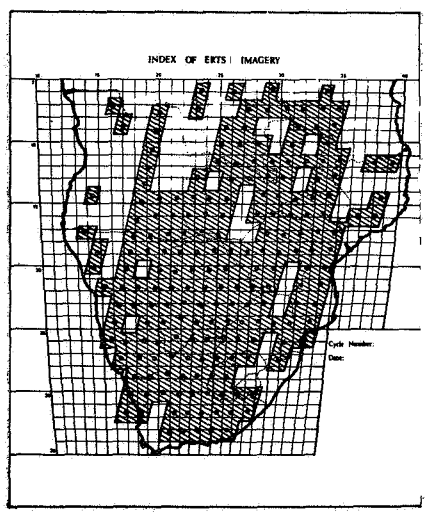

FIG. 5 : One-time Cloud-free coverage, NASA "good" rating.

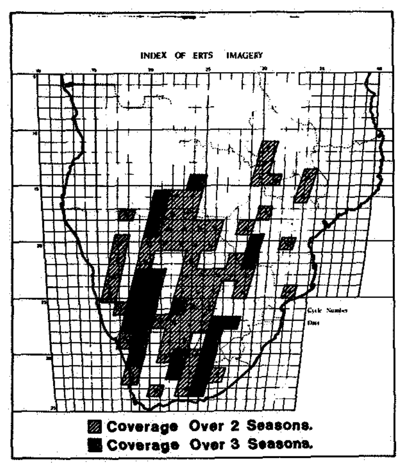

FIG. 6 : Seasonal Cloud-free coverage, NASA "good" rating.

Finally it should be noted that future use of ERTS data will also depend on the education of potential data users regarding the application techniques. The reaction of many potential users of ERTS data is to ask for greater resolution. Often this is unnecessary, and stems only from prior experience with conventional aerial photography. Effective demonstration of results will be required to overcome this obstacle.

CONCLUSIONS

The developing countries of Southern Africa face a variety of environmental problems. Important information required in approaching some of these problems can be obtained from ERTS-type imagery. For planning applications, ERTS-1 has already provided a sound data base of cloud-free imagery over most of Southern Africa. However, some gaps in the coverage still remain, and a desirable extension would be complete seasonal coverage. The applications in problems of control have been demonstrated, but the eventual value will depend on the availability of repetitive coverage from future ERTS projects. Finally, an intensive user education program is needed if the long-term benefits are to be maximised.

If these problems of availability and user education are overcome it is probable that ERTS type data will be of substantial value to both the industralized and the developing nations of Southern Africa.

REFERENCES

Grootenboer, Jan
1973, "The Influence of Seasonal factors on the Recognition of Surface Lithologies from ERTS imagery of the Western Transvaal". NASA Symposium on Significant Results from ERTS-1, December 10-14.

Viljoen, R.P.
1973, ERTS-1 imagery as an aid to the understanding of the Regional Setting of Base Metal Deposits in the North West Cape Province, South Africa. NASA Symposium on Significant Results from ERTS-1. December 10-14.

Williamson, D.T.
1973, Vegetation Mapping from ERTS-1 imagery of the Okavango Delta and

Williamson, D.T. and Gilbertson, B.
1973, Application of ERTS imagery in Estimating the Environmental impact of a Freeway through the Knysna Area of South Africa. NASA Symposium on Significant Results from ERTS-1. December 10-14.

Paper E 6

APPLICATION OF ERTS IMAGERY IN ESTIMATING THE ENVIRONMENTAL IMPACT OF A FREEWAY THROUGH THE KNYSNA AREA OF SOUTH AFRICA

Douglas T Williamson and Brian Gilbertson, *Spectral Africa, P.O. Box 2, Randfontein. Rep. of South Africa*

ABSTRACT

In the coastal areas north-east and south-west of Knysna, South Africa, lie natural forests, lakes and lagoons highly regarded by many for their aesthetic and ecological richness. A freeway construction project has given rise to fears of the degradation or destruction of these natural features.

We investigated the possibility of using ERTS imagery to estimate the environmental impact of the freeway and found that

(a) All threatened features could readily be identified on the imagery and their position in relation to the proposed freeway route was immediately obvious.

(b) It was possible within a short time to provide an area estimate of damage to indigenous forest which matched official estimates based on more protracted studies.

(c) In several important respects the imagery has advantages over maps and aerial photos for this type of work.

(d) The imagery will enable monitoring of the actual environmental impact of the freeway when completed.

We concluded that ERTS imagery, with its regional coverage, ease and speed of interpretation, will streamline environmental impact studies of this scope with likely economic benefits.

INTRODUCTION

The coastal area of South Africa around Knysna is one of the country's most valuable recreational resources. It is endowed with natural lakes, lagoons and estuaries and in this area are found the relics of once extensive, indigenous montane forests. Tourism is the major industry.

In April 1973 it was announced that a large freeway was to be developed through the Knysna area. The project was criticized on the grounds that it would destroy natural features and irreversibly diminish the aesthetic and hence the recreational value of the countryside.

Many conflicting views were expressed about the likely repercussions of the project and it became obvious that a rapid and objective means of assessing the impact of the development was desirable. It was therefore decided to investigate the applicability of ERTS type imagery to this sort of problem.

METHODS AND RESULTS

The objective of the study was to determine whether ERTS imagery could be used to identify natural features threatened by the freeway, and to provide a quantitative estimate of the likely areal extent of damage to the indigenous montane forest. A colour composite in the conventional false colour mode was prepared from ERTS-1 image 1231-07452 at a scale of 1:500 000, and is reproduced as figure 1.

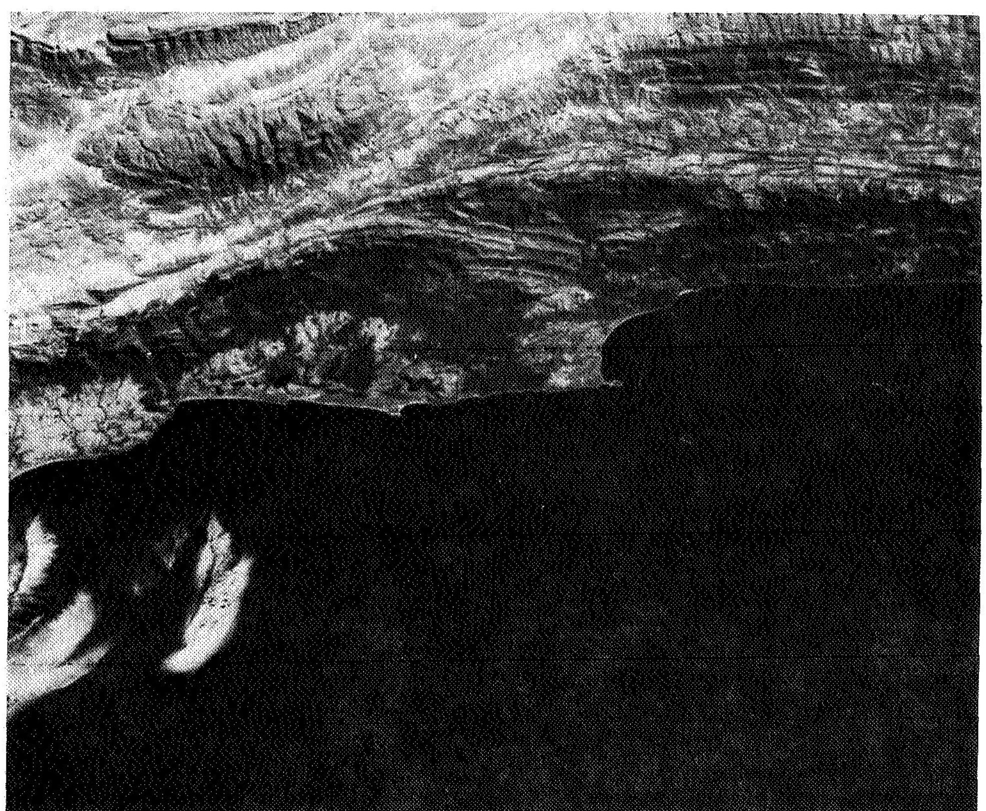

FIG. 1 : ERTS-1 image of the Knysna Area.

To identify threatened features, the freeway route was established from press releases and, with the aid of a Planvariograph, a tracing was produced of the route and the coastline at the same scale as the ERTS image. This tracing was superimposed on the Knysna image, and vulnerable features that could be detected along the course of the road were noted.

In this way a number of vulnerable features were identified. Four estuarine ecosystems were found to lie in the path of the freeway. These productive systems are endangered by siltation caused by accumulation of silt and debris around the pillars carrying the freeway across the estuary. It was also found that the freeway will pass through two areas of indigenous forest. Construction of the road will obviously necessitate clearing of a broad swathe through these areas. Another vulnerable feature identified was an area of dense vegetation covering coastal dunes that will be traversed by the freeway. The importance of the vegetation is that it stabilizes the dunes and there is a danger that disturbing it will result in subsidence and wind and water erosion.

The list of vulnerable features so prepared was compared with features mentioned in various statements on the controversy. This comparison established that we had been able to identify all features for which fears had been expressed by protestors with a first-hand knowledge of the area.

To estimate the likely extent of damage to the indigenous forest it was necessary to first estimate the area of these forests and the width of the path of freeway construction. As ground truth we used government topographical maps, on which some vegetation boundaries are marked, and in this way identified areas of indigenous forest on the ERTS image. In the process of identifying these areas many differences were observed between mapped vegetation and the ERTS image. These differences were investigated by examining black and white aerial photography and by ground inspection. They were found to be the result of a change in land use where areas of natural grass and shrub had been replaced by plantations of introduced coniferous trees. The revised ground truth was used to determine the location of indigenous forests and their areas were measured using a compensating planimeter.

The area to be destroyed by construction was firstly measured on an adjacent ERTS image which showed the encroaching freeway development, and a mean width of 130 meters was obtained. Measured on the ground with a steel tape the mean width was only 52 meters. Because the instantaneous field of view of the ERTS MSS subtends an earth-area square of approximately 80 meters on a side, an exaggerated reading for a high contrast feature such as the road is not unexpected.

From these measurements of freeway width and forest area it was estimated that approximately 0.20% of the indigenous forest would be destroyed by the construction of the freeway. Two official estimates of 0.024% and 0.25% were quoted in the press. Government spokesmen were reported to have said that 4 years were spent in considering the route of the freeway. The present study occupied but a few weeks.

It is worth noting that the ERTS image presents a permanent record of the forest prior to the freeway construction. Comparison with subsequent satellite imagery will allow the actual impact of the freeway to be determined. This will be valuable for the investigation of similar environmental hazards in the future.

DISCUSSION

It is obvious that maps or aerial photography could be used for an environmental impact study. However, our study of the Knysna image has convinced us that ERTS type imagery has advantages for this type of work over both maps and aerial photography.

It has the advantage over maps that it presents far more information than the typical map does and so promotes an integrated approach to planning. Satellite imagery has the further advantage that it is a more nearly contemporoneous record of existing conditions than maps are. For example, the government topographical maps used in this study took 5 to 6 years to produce. Contemporaneity is a particularly important consideration where dynamic features such as vegetation are in issue.

The advantage of satellite imagery over aerial photography is that it is physically and conceptually easier to handle. Tens or hundreds of aerial photographs are required to provide the same coverage as an ERTS image and to give comparable ease of regional interpretation. These must be made into a mosaic, which will still be far larger and more laborious to interpret than an ERTS image. The synoptic coverage of satellite imagery makes information far more accessible to the interpreter's immediate consciousness. This accessibility of information is particularly valuable in circumstances where it is important that a wide range of factors be considered.

SUMMARY AND CONCLUSION

The coastal area around Knysna is one of South Africa's most valuable recreational resources. A projected freeway development through the area has been criticised as a likely degrading influence upon the region.

A study was undertaken to establish whether ERTS type imagery could provide an objective estimate of the environmental impact of this development. A number of estuarine ecosystems, areas of indigenous forest and a stretch of coastal dunes covered by a protective mat of vegetation were found to be in the path of the freeway. A quantitative estimate was made of the likely areal extent of damage to the indigenous forest. This estimate fell within the range of official estimates.

It was concluded the ERTS imagery provides a perspective which facilitates the investigation of the type of environmental hazard inherent in the Knysna freeway development.

Paper E 7

APPLICATIONS OF ERTS-1 IMAGERY TO TERRESTRIAL AND MARINE ENVIRONMENTAL ANALYSES IN ALASKA

D. M. Anderson, H. L. McKim, W. K. Crowder, R. K. Haugen, L. W. Gatto, T. L. Marlar, *U. S. Army Cold Regions Research and Engineering Laboratory, Hanover, New Hampshire 03755*

ABSTRACT

ERTS-1 imagery provides a means of distinguishing and monitoring estuarine surface water circulation patterns and changes in the relative sediment load of discharging rivers on a regional basis. This information is being used to produce a data base useful in regional planning and in the development of management programs as required by the Coastal Zone Management Act of 1972. It also will aid local fishing industries by augmenting currently available hydrologic and navigation charts.

The interpretation of geologic and vegetation features resulted in preparation of improved surficial geology, vegetation and permafrost terrain maps at a scale of 1:1 million utilizing ERTS-1 Band 7 imagery. This information will be further utilized in a route and site selection study for the Nome to Kobuk Road in central Alaska.

Large river icings along the proposed Alaska pipeline route have been monitored. Sea ice deformation and drift northeast of Point Barrow, Alaska has been measured during a four day period in March and shorefast ice accumulation and ablation along the west coast of Alaska is being mapped for the spring and early summer seasons. These data will be used for route and site selection, regional environmental analysis, identification and inventory of natural resources, land use planning, and in land use regulation and management.

INTRODUCTION

Two of the greatest problems in arctic and subarctic environmental research have been the absence of long-term observational data and sparse geographical coverage. Studies of synoptic environmental events over regional-sized areas have been either impossible or prohibitively expensive. Problems of resource utilization have recently been dramatized in Alaska, where a severe lack of basic environmental data and understanding has collided with rapidly mounting pressures for extensive

development of extractive industries, transportation systems, and population centers. The existing information on river, lake, and coastal hydrology, and on the distribution, properties and behavior of permafrost terrain is insufficient for an understanding of the various environments and their interrelationships. The history of construction and technological development in these areas dramatically illustrates the difficulties caused by environmental extremes and the possibility of serious unforeseen consequences of disturbing established environmental equilibria.

Two examples illustrate the point. The proposal to construct a trans-Alaska pipeline several years ago created an urgent need for general and specific information on the environment across the entire state. Voluminous data were obtained, but at a high cost, and with a great effort by many individuals. Some of the data, especially that pertaining to route selection and regional patterns of soils, vegetation, and the distribution of permafrost could have been acquired at a considerable savings of money and manpower had ERTS imagery been available.

Now that the decision to begin construction on the pipeline has been made, this need has again become critical. The top three research topics identified recently by the Alaska Oil and Gas Association are: 1) ice forces, features and movements, 2) permafrost distribution and behavior, and 3) landfast ice surveys. The need to develop remote sensing methods to rapidly map the distribution and properties of sea ice, permafrost and shorefast ice in Alaska was given high priority at the Second International Conference on permafrost held this summer in Yakutsk, Siberia and is being highlighted by a National Science Foundation ad hoc committee on priorities in permafrost research. Accurate, up-to-date maps of permafrost and shore fast ice are urgently needed in final route selections, selection of pumping stations and off-shore loading facility sites, and the planning and implementation phases of pipeline and facilities construction.

The second example of a situation where the availability of ERTS imagery could have resulted in cost savings and better utilization of resources is the harbor construction at Dillingham. Following construction, it was discovered that siltation rates were so high that they threatened to render the new facility useless within a short time. Continuous dredging is required to maintain the harbor throughout the ice-free season. A more favorable site could have been selected and a serious and expensive problem avoided had better information on the regional and local circulation patterns been available. Similar projects in other localities are in the planning stages. Based on the results reported here, it is clear that information to help avoid such difficulties is now available.

The objectives of this investigation are:

1. To develop application of ERTS-1 imagery in a synoptic study of surface circulation patterns, tidal flat configuration, suspended sediment distribution and water mass boundaries in Cook Inlet.

2. To utilize ERTS-1 imagery in the analysis of the relationships between the distribution of permafrost terrain on a regional scale and geologic, vegetative and other environmental factors.

3. To identify and interpret the physical and cultural features representative of the major physiographic provinces of Alaska for the purpose of demonstrating the effectiveness of ERTS-1 imagery in cold regions research and engineering.

As indicated above, coastal processes were analyzed in Cook Inlet (area 4, Fig. 1). Surface circulation patterns, tidal flat configuration, suspended sediment distribution and water mass boundaries were mapped from MSS bands 4 and 5 imagery. A 10-scene photo mosaic of a 153,400-km^2 area in north-central Alaska (area 3, Fig. 1) was constructed for a regional environmental analysis from MSS band 5 imagery. Seven surficial geology, eight vegetative cover and four permafrost terrain units were defined and delineated on this photo mosaic. Permafrost units were differentiated and delineated from tonal and textural patterns related to surficial geology and vegetation. The distribution of shore fast ice along the Alaskan coast was examined from Point Barrow to Cap Krusenstern (area 2, Fig. 1) using imagery acquired during the March 1973 ERTS passes and an analysis was made of the deformation of the Arctic pack ice north of the Alaskan coast from Point Barrow to Harrison Bay (area 1, Fig. 1).

COASTAL PROCESSES IN COOK INLET

Cook Inlet is a large tidal estuary in southcentral Alaska. It is oriented in a northeast-southwest direction and is approximately 330 km long and increases in width from 37 km in the north to 83 km in the south. The inlet is bordered by extensive tidal marshes, lowlands with many lakes, and mountains. Anchorage, the state's most populated city, is located at the head of Cook Inlet and is the center of transportation, commerce, recreation and industry. The use of Cook Inlet as a water route to this growing urban area will increase as the development of the regional resources continues. The estimated petroleum and gas reserves of the Cook Inlet area are 7.9 billion bbl and 14.6 trillion cubic feet, respectively (Crick, 1971). Coal deposits in the Beluga River region are estimated at more than 2.3 billion tons (equivalent to approximately 7 billion barrels of oil) (Evans et al, 1972). In view of present acute energy requirements rapid development of this potential is inevitable.

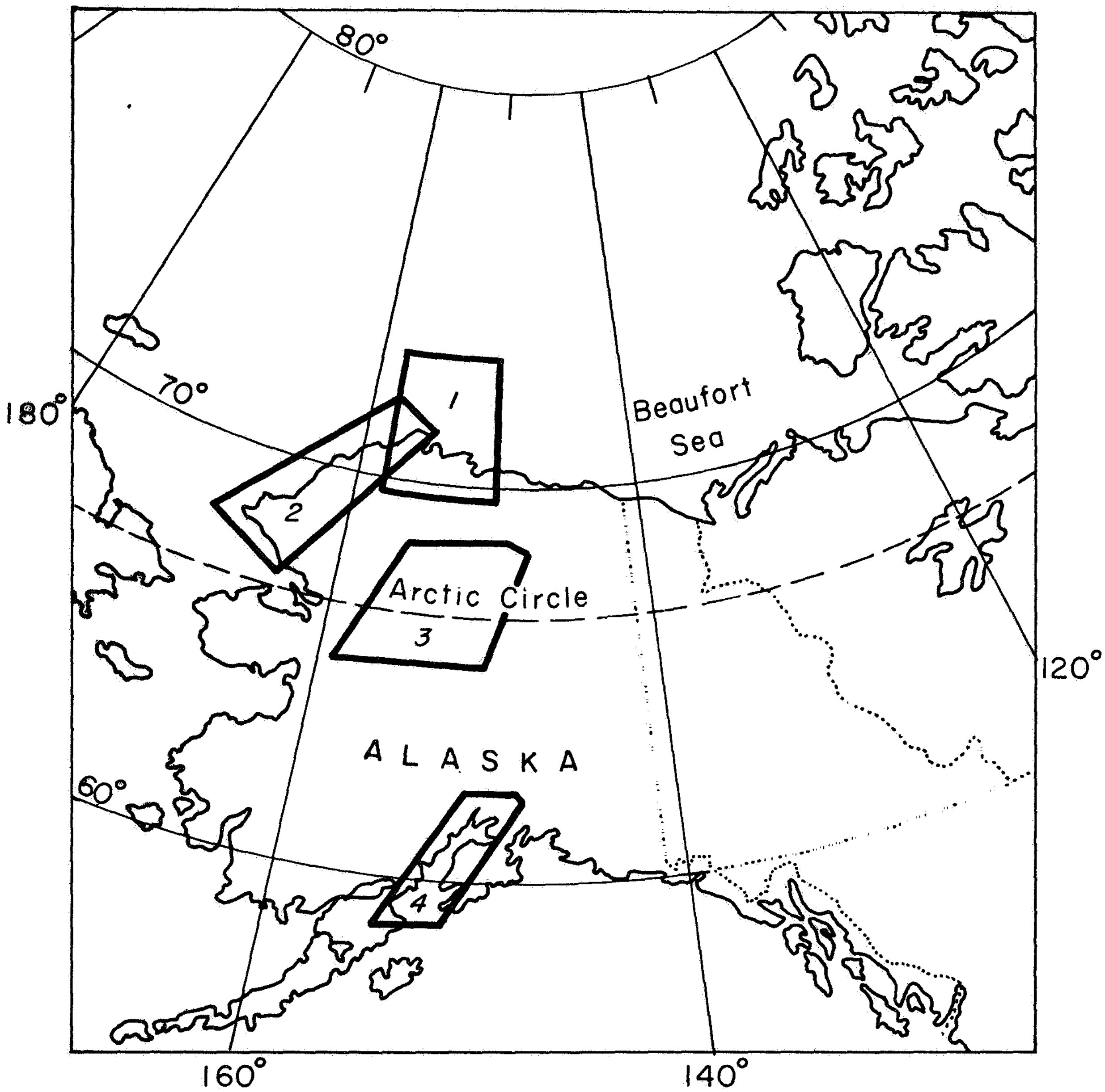

Figure 1 Site Location Map

Trading Bay, on the western side of the inlet has 14 oil and gas producing platforms around Middle Ground Shoal. It is the major site of petroleum production in the Cook Inlet area. An oil refinery and a tanker terminal are located at Nikiski 15 miles across the Inlet and a tanker terminal is also located at the mouth of the Drift River approximately 30 miles southwest of Trading Bay. Numerous submarine pipelines cross the inlet and several crude oil gathering facilities are located along the coast. Additional offshore platforms, coastal facilities and tanker terminals will be constructed as petroleum production increases and as the southern portion of the inlet is developed. Increased utilization of the coastline will follow as facilities are constructed in support of the petroleum industry.

The environmental effects of the regional development must be considered in formulating future plans for the region. The present amounts and types of pollution in the inlet will increase so the capability of the inlet to disperse the additional pollutants must be determined. Suspended sediment is currently the dominant pollutant in the inlet. It is estimated that in newly developed areas as much as 20,000-30,000 times more sediment is produced than in natural undisturbed areas (Environmental Currents, 1972). The following rivers contribute the greatest amount of sediment to the inlet - Knik, Matanuska, Susitna, Beluga, MacArthur, Drift and Tuxedni. The watersheds of these rivers are now the areas of greatest utilization and future use will increase their sediment production.

Other sources of inlet pollution are the coastal towns. With completion of the Asplund Water Pollution Control Facility the sewage from the Greater Anchorage Area Borough is treated prior to being discharged into the inlet near Point Woronof. This project is the single most important environmental protection measure so far undertaken in the Anchorage area (Alaska Construction and Oil, 1973). The remaining cities and villages bordering the inlet discharge untreated sewage directly into the inlet.

Petroleum pollution in the inlet originates from numerous sources: 14 producing offshore platforms, the Drift River, Arness or Nikiski tanker terminals, submarine and coastal pipelines, the gathering and handling facilities along the coast and wastewater effluent from the Standard Oil and Tesboro refineries. Approximately 9500-17500 bbl/yr or 0.3% (Kinney, et al., 1970a) of the total crude produced is accidentally spilled but, to date, the spills have not been obviously detrimental to coastal areas. From January through April 1972, 5 spills occurred in the inlet as a result of accidental disconnects at tanker terminals with evidences of the spills disappearing in 3-4 days (Kinney, et al, 1970a). Because of the high surface turbulence and mixing, oil spills rarely reach shore; they simply evaporate and disperse as they move up and down the inlet with the high tidal fluctuations.

Petro-chemicals from the Phillips liquified natural gas plant and the Collier Chemicals ammonia plant at Nikiski are introduced in the inlet. The effluent outfalls from these plants are located in a region of high turbulence. Dilution of the wastes is rapid and concentrations remain below harmful levels even during the low runoff winter months (Rosenberg, et al., 1967).

The movement and strength of ice in Cook Inlet is another particularly important aspect of the inlet environment to be considered when offshore construction is planned. The inlet ice is seasonal and remains for approximately 4 months of the year. It is fine- to medium-grained (1mm-4mm) with a salinity of .4-.6% and a ring tensile strength of 10-20 kg/cm^2. The inlet ice exists as large floes which are commonly greater than 320 meters across with individual blocks generally less than 1 meter thick. Pressure ridges up to 6 meters in depth occasionally form (Blenkarn, 1970). The large floes move up and down the inlet with the 6-8 knot currents which are produced by 9-meter semidiurnal tides. The regional circulation patterns that move the ice floes within Cook Inlet are controlled primarily by the interaction between the semidiurnal tides and the Coriolis force.

Using suspended sediment in the inflowing fresh water as a tracer, the current patterns have been distinguished in MSS bands 4 and 5 imagery. The distinction between the saline, oceanic water in the southeastern portion of the inlet and the fresher sediment-laden, inlet water in the northern and southwestern portions has been used to detect changes in the sediment distribution and movement of the water masses.

Figure 2a shows differences in the main boundary between the oceanic and fresh water in the southern inlet on two successive days. The boundaries separate the two major water types during low tide at Anchorage and high tide at Seldovia. The irregularity of the western portion of these lines may be due to the upwelling of cold, saline oceanic water that occurs in the western portion of the inlet (Kinney et al. 1970b; Evans et al. 1972). The northern portion of the 4 November boundary is also quite irregular, possibly due to a similar cause. Some estuaries are characterized by a salt water wedge that moves headward along the bottom while the fresh water outflow moves over the wedge and out the estuary (Bowden 1967). In Cook Inlet a subsurface tongue of oceanic water progresses headward and moves up the shoaling bottom of the inlet to the latitude of Tuxedni Bay where it rises to the surface south of Kalgin Island during flood tide (Kinney et al. 1970b). The upwelling waters appear as a large area of clear water surrounded by sediment-laden water. This process produces a zone of high nutrient concentration in the photic zone at this location. This may be significant to the fishing industry since certain species of fish may tend to concentrate in this high nutrient area. Changes in the boundary over an 18-day cycle are shown in Figure 2b. These boundaries are generally

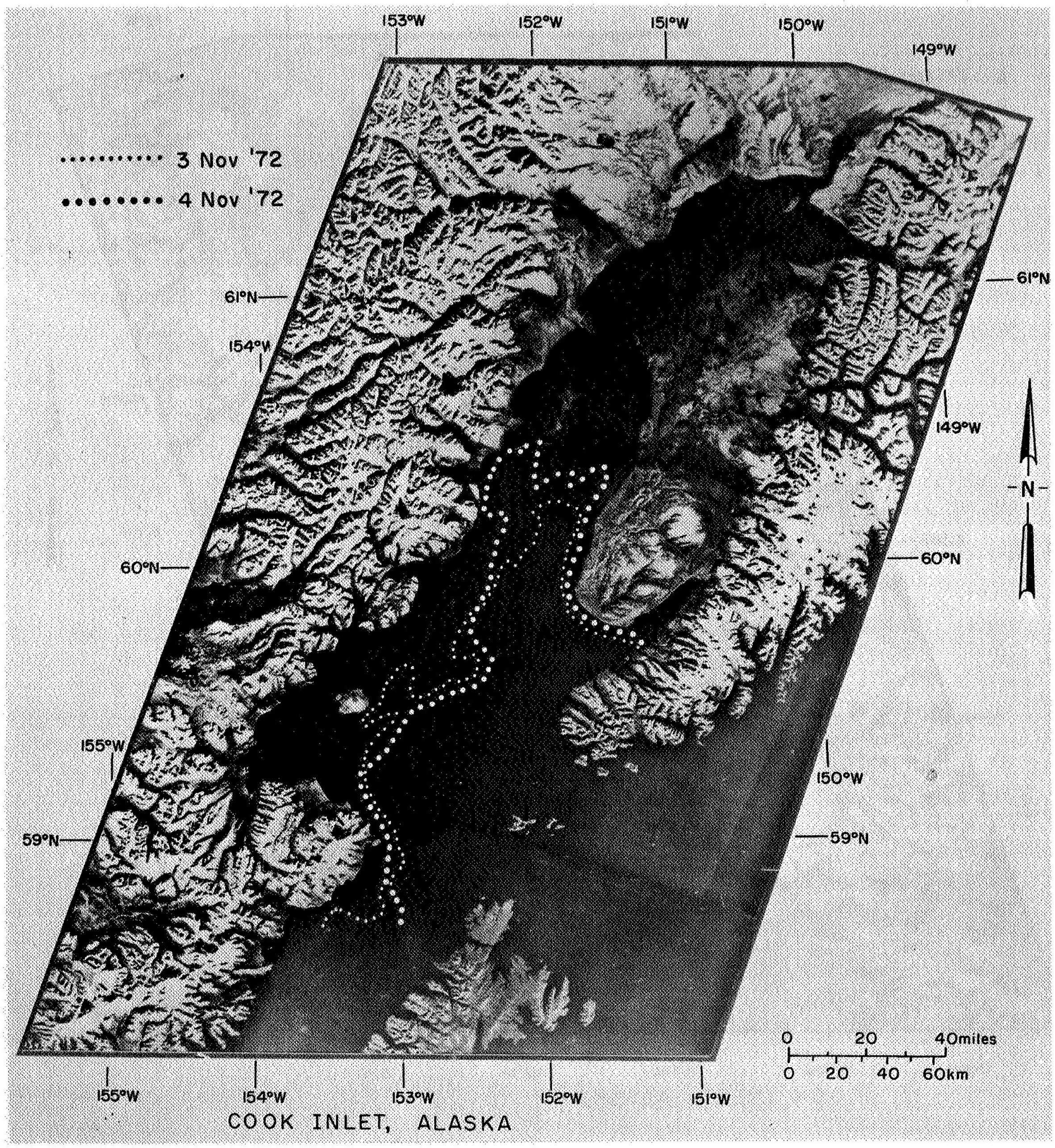

a. Daily changes.

Figure 2. Boundaries separating oceanic and inlet water (from Anderson, et al., 1973).

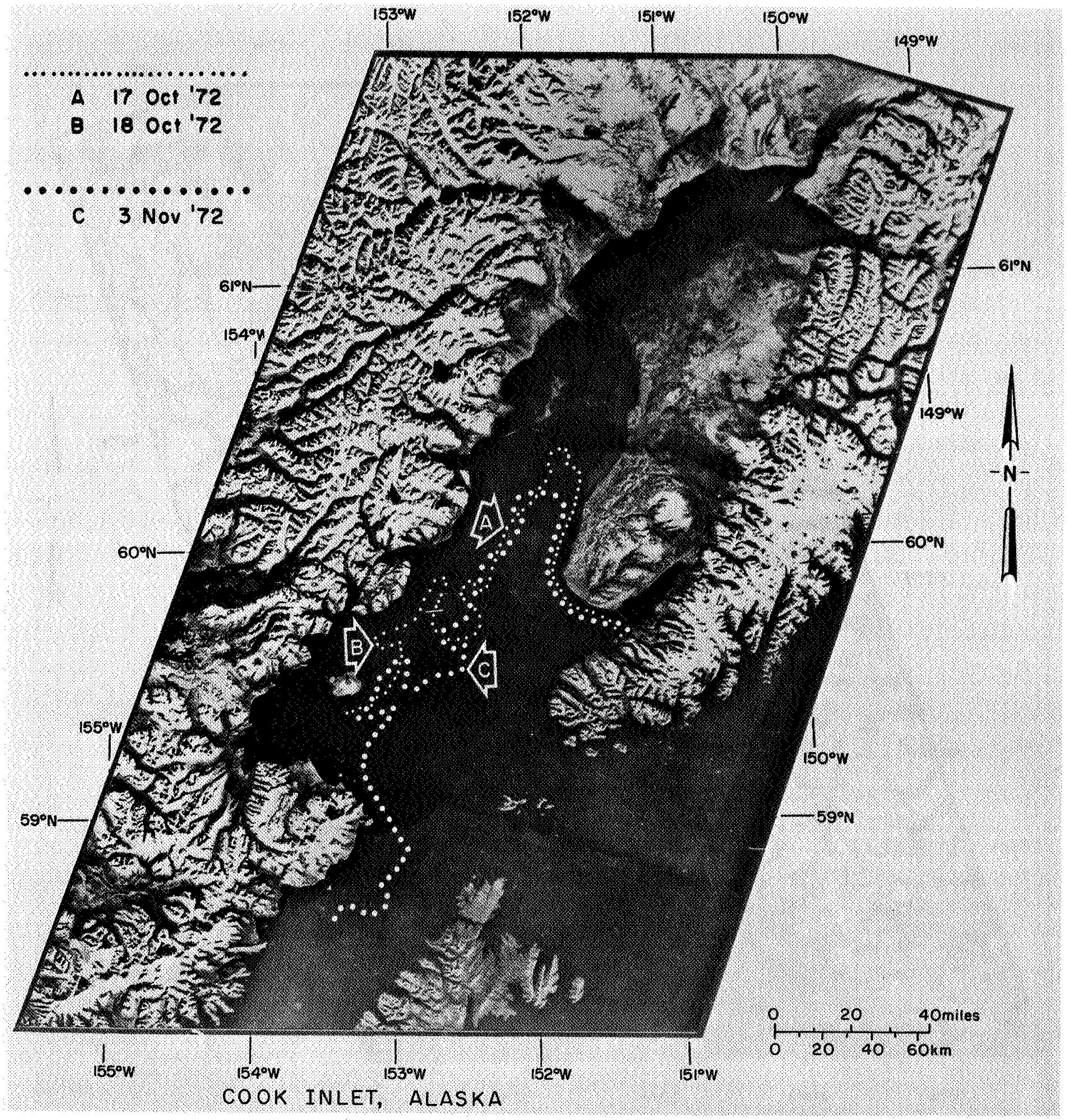

b. Changes over 18-day period.

Figure 2. (Continued)

comparable to those in Figure 2a. Although changes in the sediment distribution and surface circulation produce some obvious alterations in the regional distribution of water types, the overall relationships appear to persist with time.

REGIONAL ENVIRONMENTAL ANALYSIS

The first usable ERTS-1 images for our investigation were obtained during orbit 30 on 25 July 1972. Since then more than 3,000 individual scenes have been reviewed. Those images that are relatively cloud-free and taken at acceptable sun elevations have been used to construct a number of photo mosaics of areas chosen for detailed analysis.

The surficial geology was mapped on the 1:1 million scale photo mosaic (Fig. 3) with the aid of stereo pairs and other available ground truth. Seven recognizable units were defined (Fig. 4). Bedrock (b) consists of in-situ bedrock and very coarse, rubbly bedrock colluvium primarily confined to steep slopes and mountain crestlines. Bedrock-colluvium (bc) is composed of coarse- to fine-grained deposits occurring on moderate to steep slopes in mountainous terrain and rolling uplands which have minor scattered bedrock exposures restricted to the uppermost slopes and crestlines. Alluvial-glaciofluvial deposits (Qag) are fine- to coarse-grained sediments derived from reworked glacial and alluvial deposits, morainal deposits, till, and outwash gravels and sands. These deposits occur in part on modified morainal topography and large alluvial terraces. Fluvial-lacustrine deposits (Qfl) consist of fine-grained sands and silts associated with abandoned floodplains and low-lying terraces. They may include windblown sand and silts. Undifferentiated alluvial deposits (Qal) are fine- and medium-grained alluvial fan, terrace, stream and eolian deposits. Fluvial deposits (Qfp) are fine- and medium-grained silts and sands, generally well rounded, associated with modern floodplains and low-lying terraces. Eolian deposits (Qe) are fine-grained windblown sediments, deposited on gently to moderately sloping hills and low-lying flatlands and include areas of actively drifting dunes.

The units defined for mapping the surficial geology and the surficial geology map made from the ERTS-1 imagery at 1:1 million scale were subsequently compared to USGS Miscellaneous Geologic Investigations Maps at a scale of 1:250,000 (Cass 1959, Patton 1966, Patton and Miller 1966, Webber and Péwé 1970) and the 1:1.5 million scale Surficial Geology of Alaska map (Karlstrom et al 1964). From these comparison, it was established that the surficial geology map made from ERTS-1 imagery correlated favorably with the published 1:250,000 maps and is superior to the 1:1.5 million map.

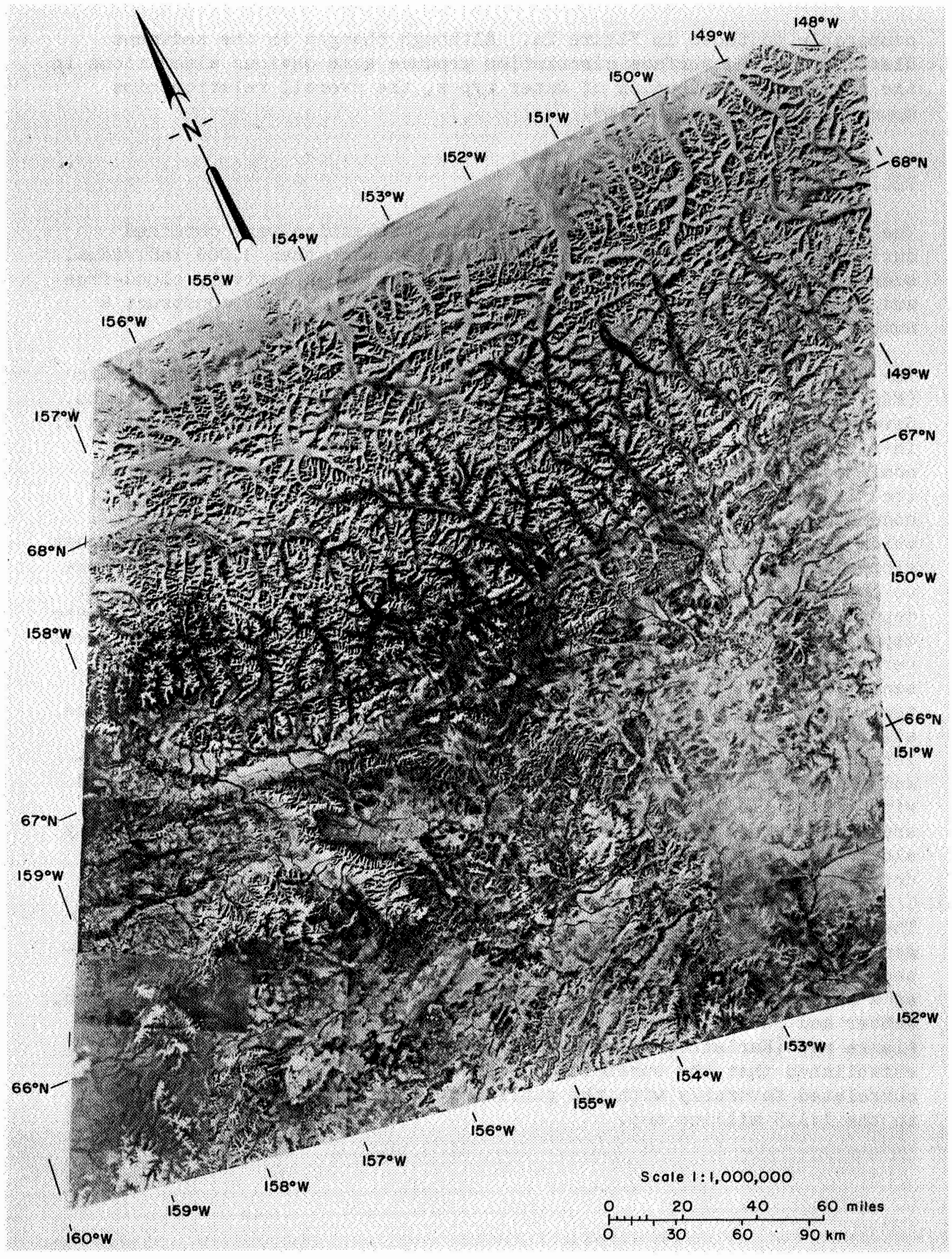

Figure 3. Uncontrolled photo mosaic of 153,000 km^2 area in north-central Alaska.

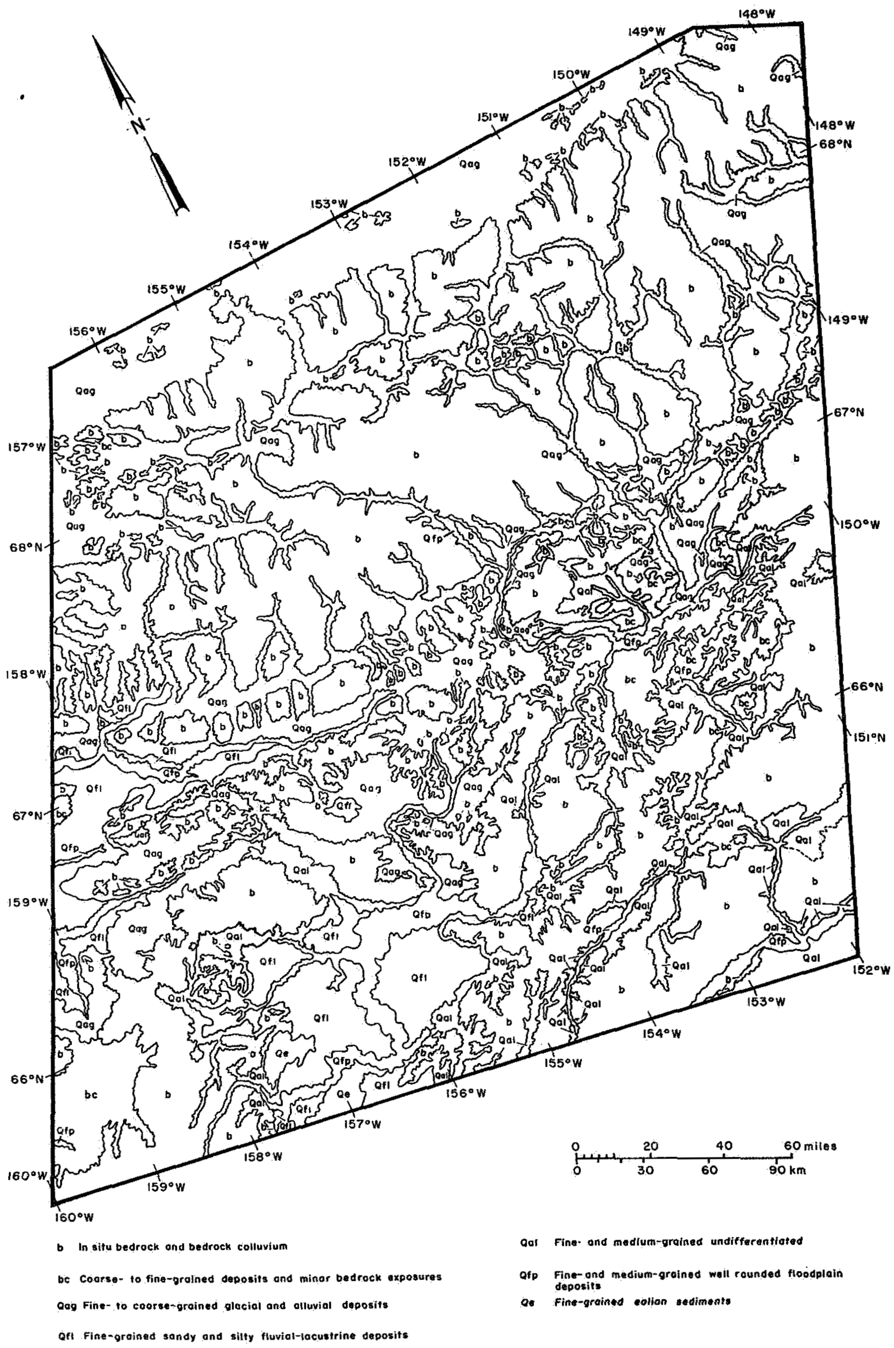

Figure 4. Surficial geology map of north-central Alaska.

Vegetation

Vegetation is one of the most important indicators of the permafrost characteristics of an area, but the relationship is complex (Hopkins et al. 1955). Vegetation primarily influences permafrost terrain by affecting the atmosphere-lithosphere, thermal exchange and the moisture regime in the soil (Trytikov 1959). Vegetation retards soil warming in the summer and cooling in the winter, but the depth of the active layer also depends on other variables, such as the depth of winter snow and drainage conditions during summer. Vegetation type and density in a permafrost region are most directly related to soil type and drainage conditions. The value of a map of vegetation patterns lies in its relationship to the depth of seasonal thaw. The vegetation association - depth of thaw relationship where permafrost is present in the discontinuous permafrost zone is shown in Table 1.

Table 1. Relationship between vegetation association and depth of thaw (Hopkins et al. 1955).

Vegetation	Depth of thaw (m)
Tall willows on floodplain	2.4
Mixed alder, willow, white birch	1.2
Mixed stands of white spruce and white birch	0.6 - 0.9
Black spruce in tundra or muskeg	0.3

Vegetation differences are apparent on the MSS imagery primarily through tonal rather than textural patterns. The tonal differences are related to vegetation density and species composition. Eight density levels have been identified and mapped (Fig. 5). Ground truth was obtained from existing mapping by Spetzman (1963) and from oblique photography from a small aircraft by the investigators. Tall to moderately tall, closely spaced spruce-hardwood forest (Fc) consist of white and black spruce with paper birch, aspen, and balsam poplar on moderately to well-drained sites such as active floodplains, mountain slopes (especially southern slopes) and highland areas. The second plant association (Fou) has basically the same species as the closely spaced spruce-hardwood forest (Fc) except the vegetative cover appears less dense. Also the Fou unit has an ecological setting similar to Fc but it extends to somewhat less favorable habitats. Open black spruce forest (Fo) has stunted, open tree growth which includes tamarack, white birch and white spruce in addition to the dominant black spruce. Thick moss,

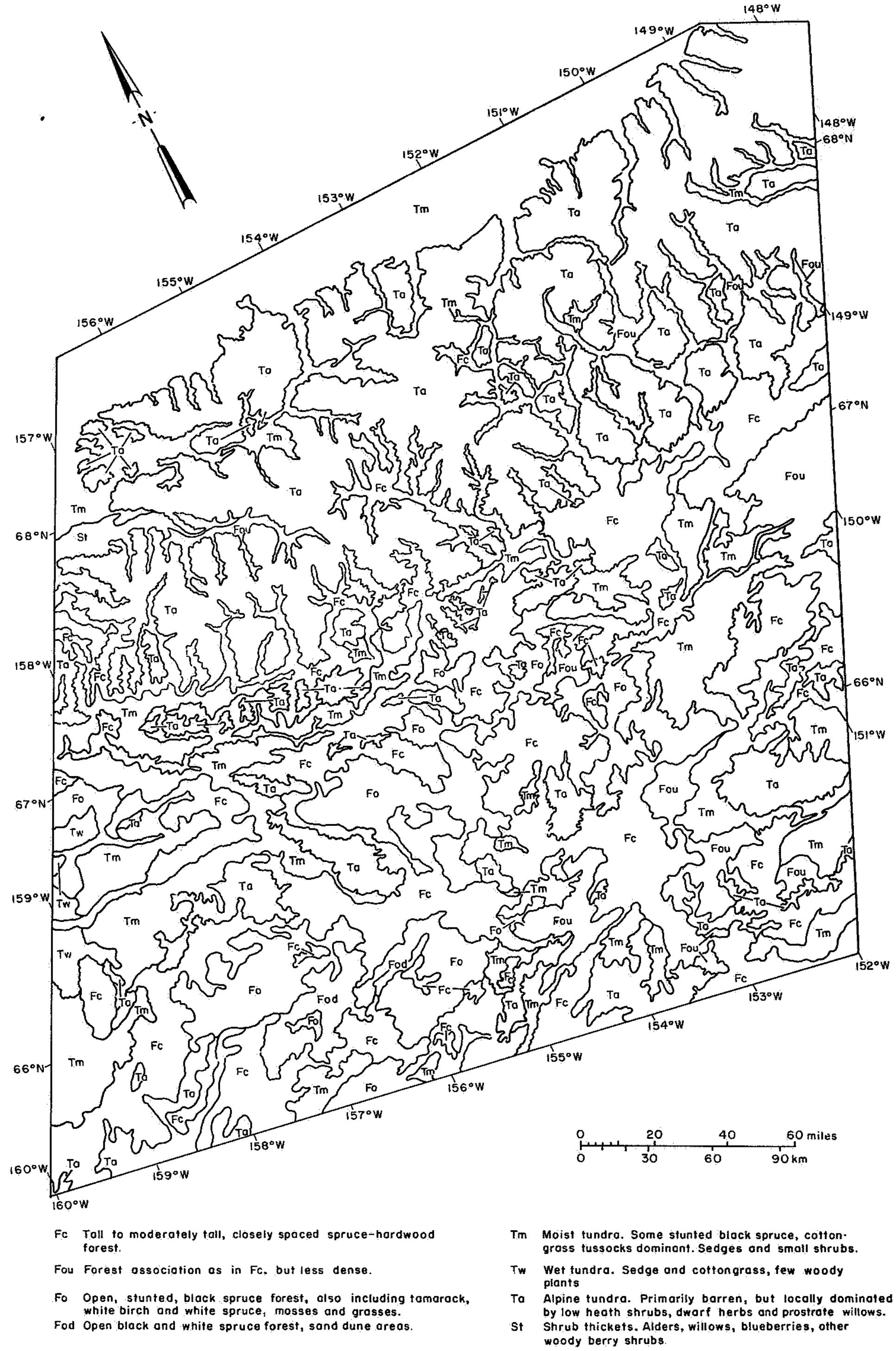

Figure 5. Vegetation map of north-central Alaska.

grasses and heath comprise the ground cover. Open black and white spruce forest (Fod) is confined to several isolated areas where the forest has overgrown and stabilized sand dunes. This forest tends to be open, but is better drained and not as stunted as within the Fo class. Moist tundra (Tm) occupies vast areas of poorly to moderately drained topography. It contains some stunted black spruce within the southern two thirds of the study area. Cottongrass tussocks are the dominant vegetation form, with sedges and dwarf shrubs where tussocks are absent. Wet tundra (Tw) consists of sedge and cottongrass with few woody plants. This association is distinguished from Tm by the presence of many thaw lakes and wet areas. Shrub thickets (St) are dense thickets of alders, willows, blueberries and other woody, berry shrubs found in coastal areas and floodplains north of the timberline. Extensive areas of this association in the northern foothills are indicated on existing vegetation maps. However, a distinctive pattern is not visible in the ERTS mosaic because of an extensive snow cover existing at the time this imagery was acquired. Alpine tundra (Ta) is primarily barren, but locally dominated by low heath shrubs, prostrate willows and dwarf herbs. This association is generally found at elevations over 600 m.

Permafrost

Permafrost is formally defined solely on a temperature basis. It is rock or soil material, with or without moisture or organic matter, that has remained continuously below 0°C for two or more years (Ferrians 1969). It occurs where the depth of winter freeze exceeds the depth of summer thaw, and is classified into two broad categories: continuous and discontinuous. In the continuous permafrost zone (Fig. 6), permafrost lies beneath all land areas, but it is absent directly beneath large water bodies, which provide a sufficient heat reservoir to keep underlying materials unfrozen (Williams 1970). The thickness of permafrost in this zone ranges from several hundred feet in the south to an extreme of more than 600 m. in northern Alaska. The boundary that separates these two zones is theoretically distinct but imperfectly located. Climatically, it approximates the mean southern position of arctic air in summer (Bryson 1966), it is close to the southern limit of the tundra (MacKay 1972) and is the effective limit of active ice-wedges and pingos (Péwé 1966). The discontinuous permafrost zone is a complex mosaic of frozen and unfrozen ground with permafrost thickness decreasing in a southerly direction.

Permafrost is a major environmental factor in Alaska and other high latitude regions. The existence of permafrost is the result of complex interactions among environmental factors such as local microclimate, plant cover, the insulating qualities of the organic and vegetative layers, texture and moisture content of the soil, surficial geology and

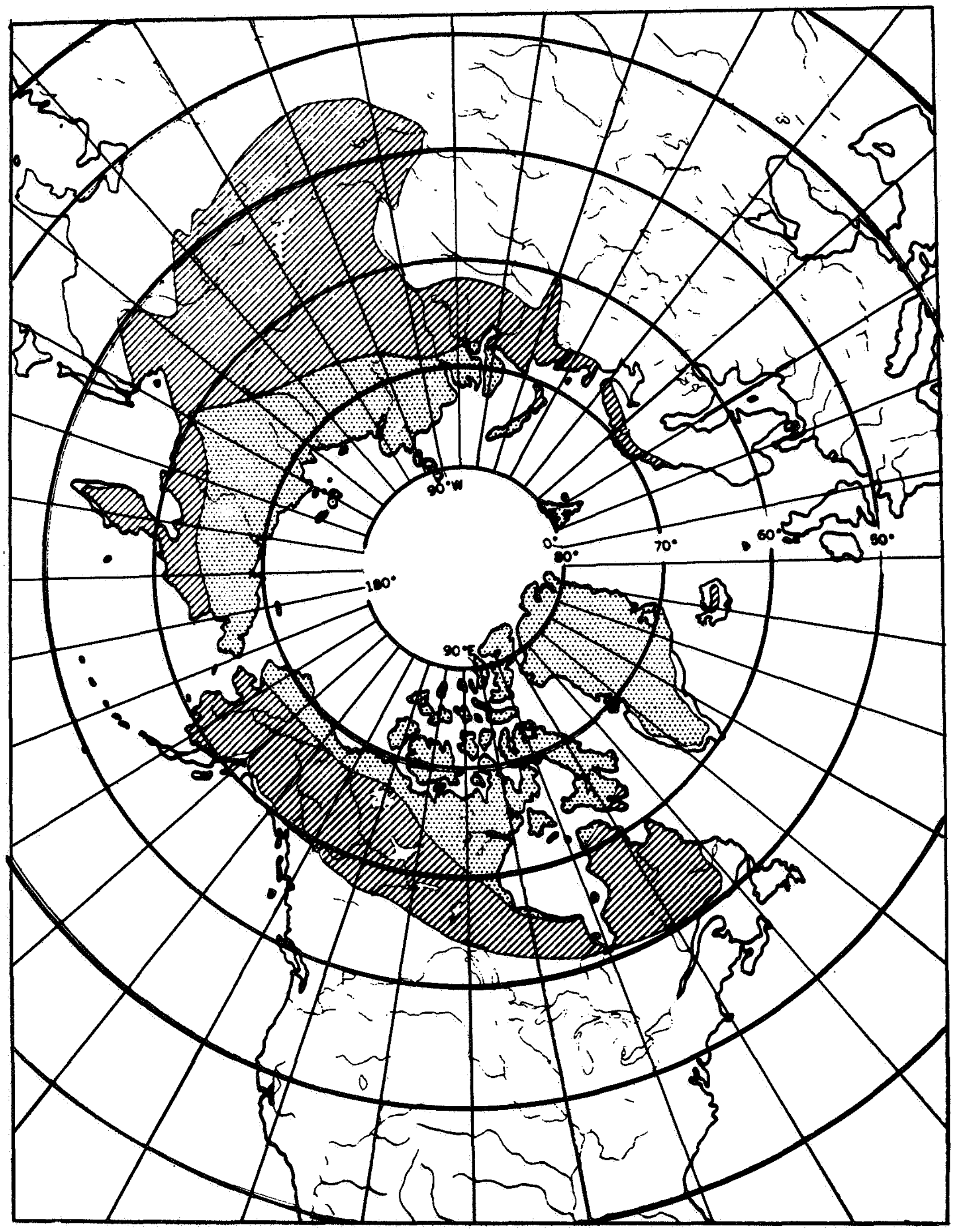

Figure 6. Geographic distribution of permafrost: stipled area is continuous permafrost zone: lined area is discontinuous permafrost zone (from Ferrians, 1969).

topographic position. Figures 7 and 8 illustrate typical permafrost settings and the nomenclature in current use.

In central Alaska the distribution of permafrost is discontinuous because the present climate in this area is near the threshold values for the continued existence of permafrost. Only in well-protected locations such as north facing slopes, shaded valley bottoms, or high elevations within the region does permafrost exist. Minor changes in the thermal regime, whether natural or man-induced, can produce major alterations in permafrost landscapes.

Existing maps of permafrost distribution are general, primarily because of the lack of extensive, detailed data (Ferrians 1969). The delineation of the boundaries supporting permafrost mapping units by conventional aerial photography has been found to be difficult, requiring extensive ground studies to confirm. There is no precedent study in which permafrost terrain has been classified utilizing imagery of the scale and resolution available with ERTS. Consequently, it could not be known in advance the extent to which the more subtle tonal and textural changes on the MSS images might show large scale patterns not discernible in aerial imagery and useful in differentiating among the various types of permafrost terrain. The ERTS-1 MSS imagery exceeded expectation in this respect. Large scale patterns easily identifiable on the imagery include thermokarst topography, icings (naleds, aufeis), beaded drainage, and permanent ice fields. Smaller features, such as pingos/palsas, ice wedge polygons, solifluction lobes, nivation terraces, and stone polygons and stripes could not be identified at the resolution afforded by the multispectral scanner system.

As shown in Figure 9, four permafrost terrains have been mapped based on the interpretation of surficial geology and the probable depth of thaw inferred from the vegetative association. Other mapping criteria, temperature and permafrost properties, are not observable on the ERTS imagery and were not used in the permafrost terrain mapping. The bedrock (m) terrain is characterized by a thaw depth of 0.3 - 1.0 m except on south-facing slopes where thaw depths may exceed 2 m and a few scattered taliks. Soils are coarse-textured and shallow. Alpine vegetation occurs on the highest, steepest area with black spruce and paper birch on the north-facing slopes. The principal trees on south-facing slopes are white spruce, paper birch, quaking aspen and alder. The alluvium-colluvium (u) permafrost terrain has a thaw depth of <0.5 m in areas of poor drainage and 0.5 - 2.0 m and numerous taliks on moderately to well-drained slopes. Fine-grained, shallow soils occur on steep slopes and medium- to fine-grained, deep soil on gentle slopes. Alpine vegetation occurs on summit positions and black spruce and paper birch on north-facing slopes. White spruce, quaking aspen and alders are found on the south-facing slopes. Moist tundra occurs on poorly drained footslope positions. The active floodplain (l_1) terrain is characterized

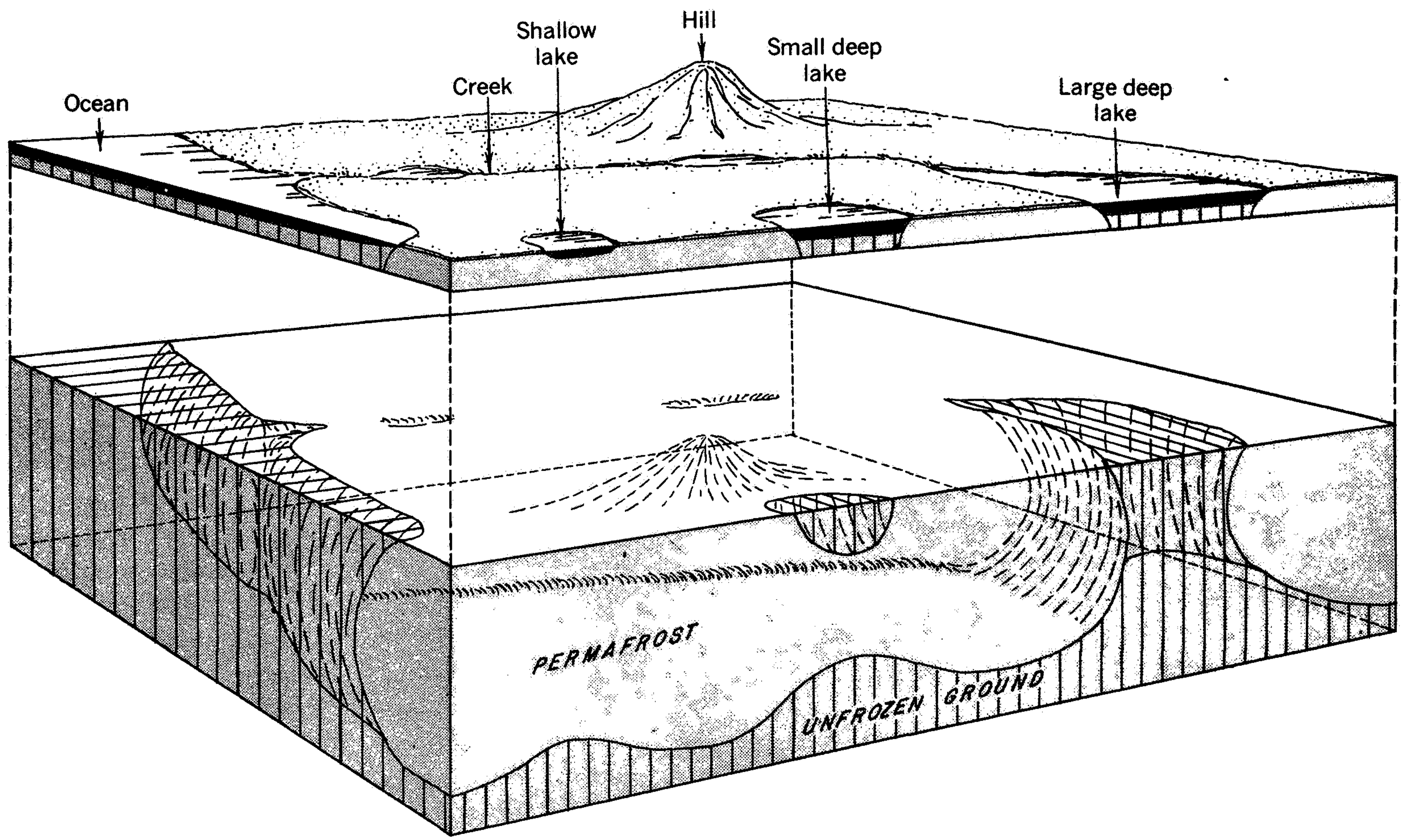

Figure 7 The effect of surface features on the distribution of permafrost in the continuous permafrost zone (after Lachenbruch, 1968, p. 837).

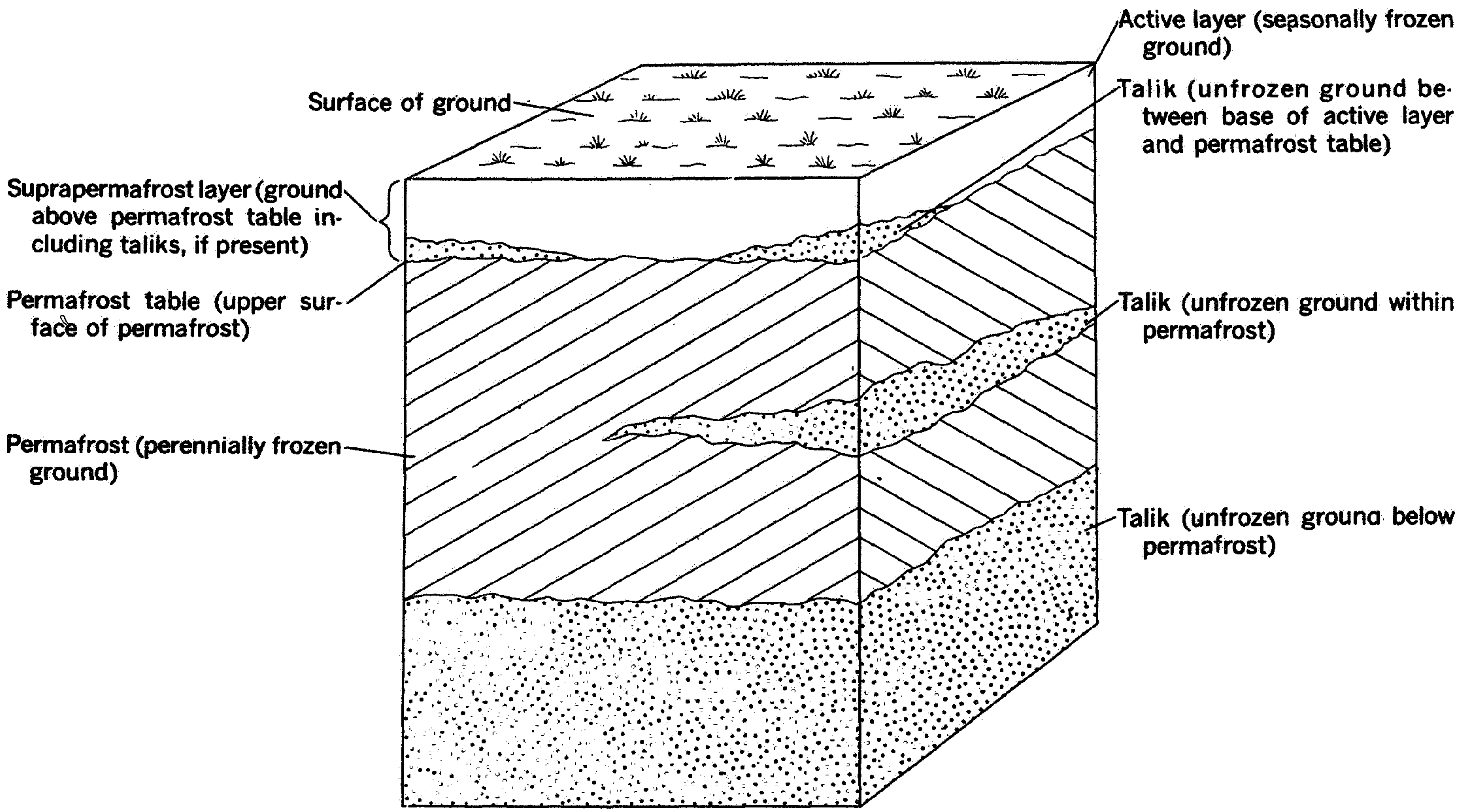

Figure 8. Occurrence of taliks in relation to the active layer, suprapermafrost zone, permafrost table, and permafrost (from Ferrians, et al, 1969).

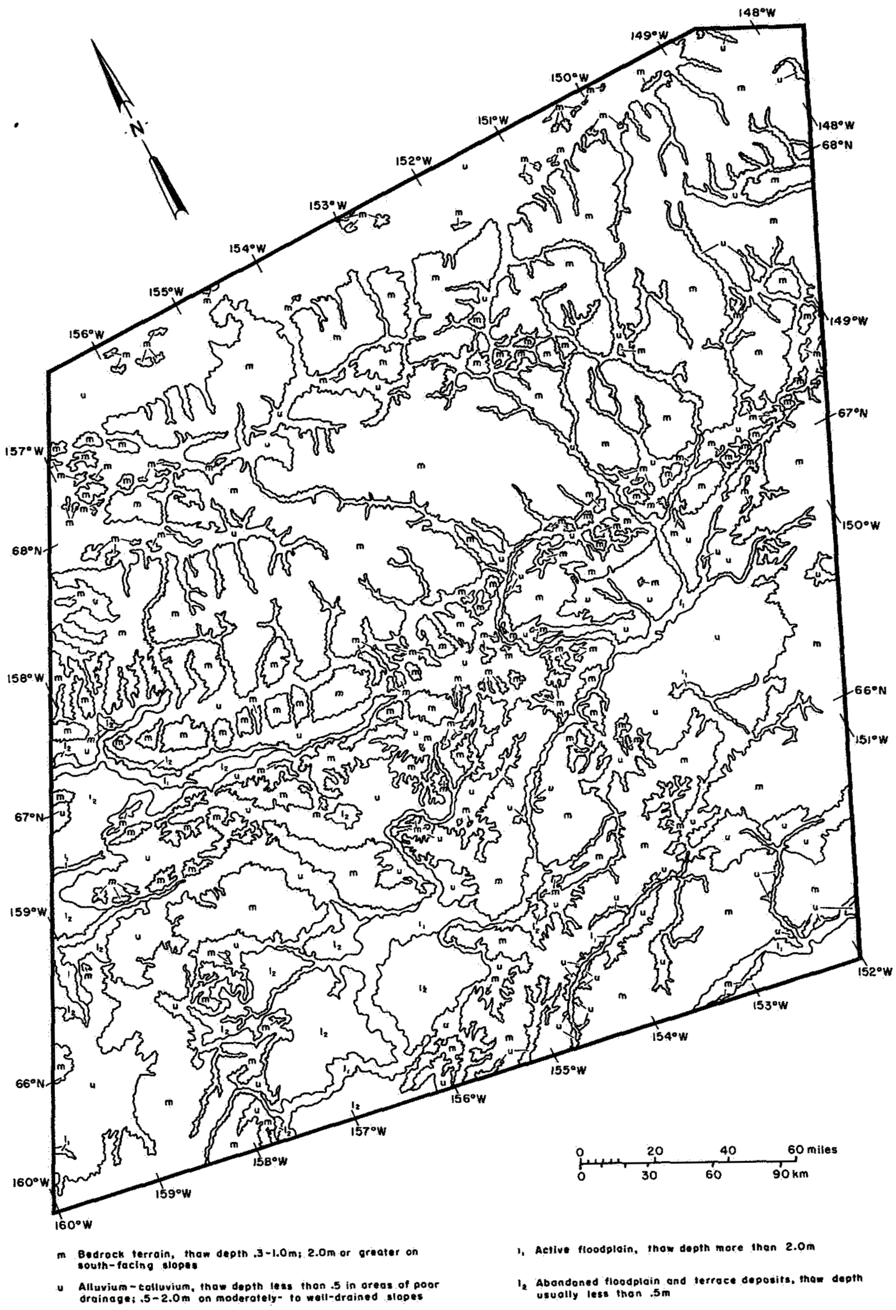

Figure 9. Permafrost terrain map of north-central Alaska.

by numerous taliks, a thaw depth of more than 2.0 m, and fine-grained, deep soils. Balsam poplar, paper birch and white and black spruce dominate. The fourth permafrost terrain unit, abandoned floodplain and terrace (1_2), is characterized also by numerous taliks but contains many small thaw lakes. Soils are fine-grained and shallow with permafrost occurring at depths usually less than 0.5 m. Vegetation includes moss, lichens, low lying shrubs and black spruce. Using these criteria, a permafrost terrain distribution map was prepared with considerably greater detail than that previously available. It is quite feasible by extending these techniques, to rapidly produce improved more detailed permafrost maps than those presently in existence.

ICINGS

Icings (naleds, aufeis) are masses of surface ice characteristic of permafrost terrain formed during the winter by continual or successive freezing of ground water that finds its way to the surface in rivers or springs (Muller 1947). Repetetive overflows become layers of stratified ice, often creating very large masses. During the late stages of formation the ice mass often extends considerably beyond the boundaries of the normal stream channel. In such cases, icings can become hazardous. Icings may spread over or encroach upon roads, for example. Also ice blocked drainageways may lead to washout of embankments during spring thaw (Carey 1973). Icings tend to occur at the same locations from year to year, although the amount of icing development varies considerably. The ability to survey and monitor the occurrence of icings by satellite imagery in uninhabited areas will provide valuable information for final selection of the Alaska pipeline route.

The principal environmental factors influencing icing development include precipitation prior to freeze up which influences streamflow during the winter, the depth of snow during the winter which influences the depth of frost penetration in the ground, and temperature regimes during late winter and early spring when icing formation usually occurs. The effectiveness of ERTS imagery in defining seasonal changes in the ice cover of water bodies was quickly demonstrated. Large river icings were not observed in the interior of Alaska during the 1972-1973 season, but on the North Slope of the Brooks Range, many icings were located, identified and monitored through two or more satellite passes. During the formation in late winter and spring, water overflowing ice surfaces appears as a very dark tone against the white snow background on MSS band 7 imagery. Later, after the snow cover has disappeared, icings appear white in all bands and contrast sharply with the surrounding landscape. A number of icings were observed along the proposed Alaskan pipeline route from Prudhoe Bay to the Brooks Range (Fig. 10). Along the Echooka River, a tributary of the Sagavanirktok River, an icing some

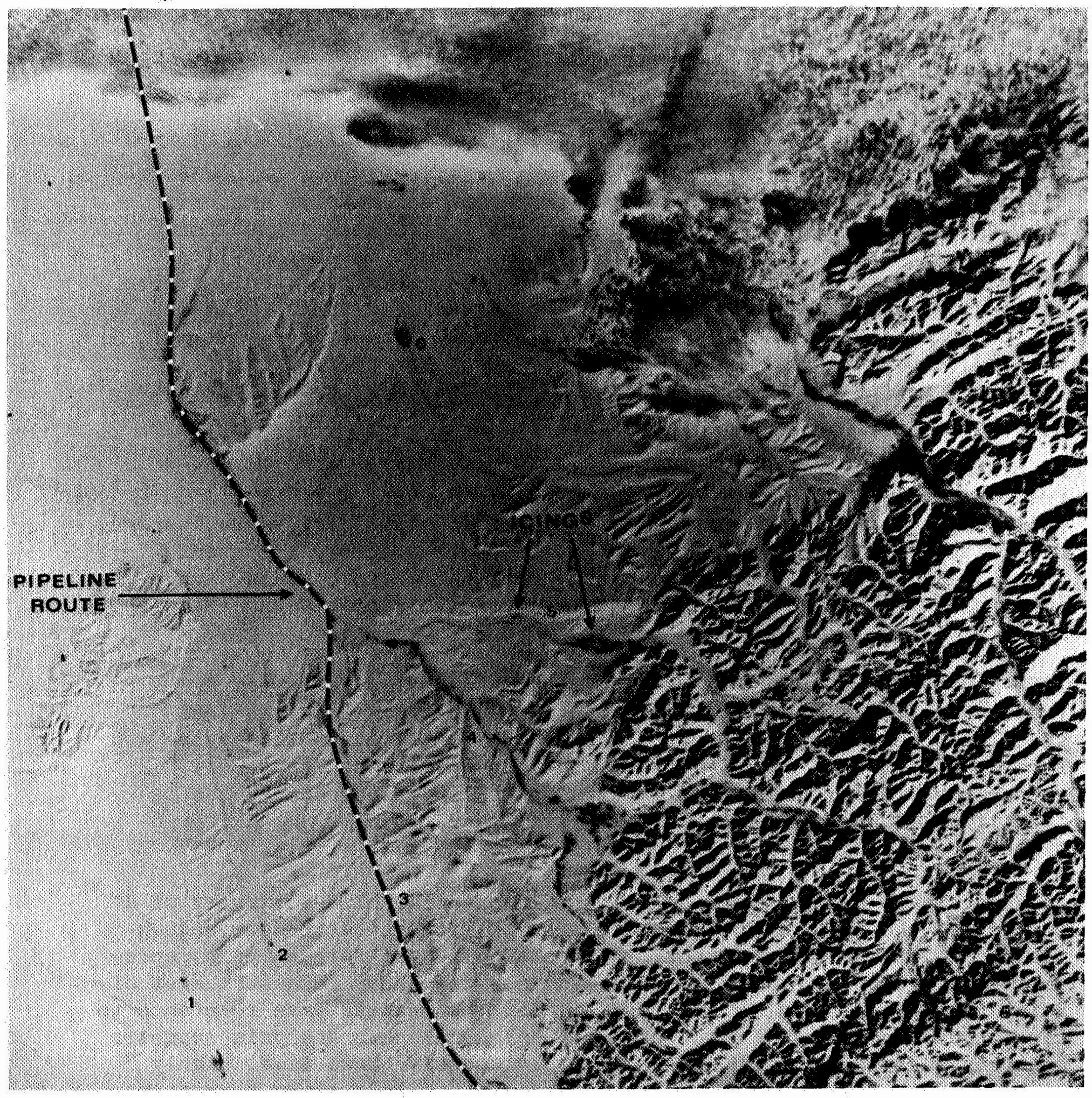

Figure 10. Proposed pipeline route in relation to known icings
(ERTS MSS band 7 image, 1251-21123).

16 feet in thickness is visible on the ERTS MSS band 7 image (ID 1251-21123). Other icings are identified on the Kaparuk (1), Toolik (2), Sagavanirktok (3), Ivishak (4), Echooka (5) and Shaviovik (6) Rivers (Fig. 10). Many of these are seen to persist throughout the year. A knowledge of their location and seasonal dynamics is useful in planning routes and scheduling construction activity on the Alaskan North Slope and the Arctic Coastal Plain.

SEA ICE/SHORE FAST ICE

Development of the North Slope oil reserves together with offshore docking facilities and northern sea transportation routes has generated a need for a rapid method of assessing sea ice deformation and drift. Measurements of this type are needed in the formulation of realistic prediction models. Three particular types of data are especially in demand: 1) data on ice deformation across the shear zone region where the moving pack impacts and grinds against stationary shore fast ice, 2) the formation, distribution and persistence of the shore-fast ice, and 3) sequential deformation measurements on a variety of spatial scales at representative locations to determine the regional characteristics of the ice velocity field.

Prior to ERTS-1, satellite sensors did not have sufficiently high resolution for measurements of ice deformation, thus investigations utilizing meteorological satellite data have been primarily qualitative. Even with this limitation, however, it has been possible to detect gross ice boundaries, calculate albedo maps on synoptic scale, and improve our knowledge of the heat balance of the Arctic Ocean (Wendler 1973).

ERTS-1 provides, for the first time, regional scale multispectral imagery with sufficiently high resolution to perform detailed ice studies. Preliminary analysis has shown that the various ice types and features, fast ice, pack ice of various concentrations, brash ice, rotten ice, leads, fractures, puddled areas, and flooded ice, can be identified (Barnes et al. 1973) and first year floes may be differentiated from multiyear floes (Campbell et al. 1973).

In an analysis using high resolution multispectral ERTS-1 imagery of a portion of the Beaufort Sea, it has been possible to determine sequential positions on the ice pack. The data collected for analysis represent a four-day deformation sequence across the shear zone northeast of Point Barrow, Alaska (Fig. 11a and b), and the results have relevance to the boundary conditions used for drift calculations. Analysis suggests that the pack is behaving as a relatively cohesive mass (i.e. highly viscous) with slippage over a narrow region ($\sim$50 km) at the boundaries.

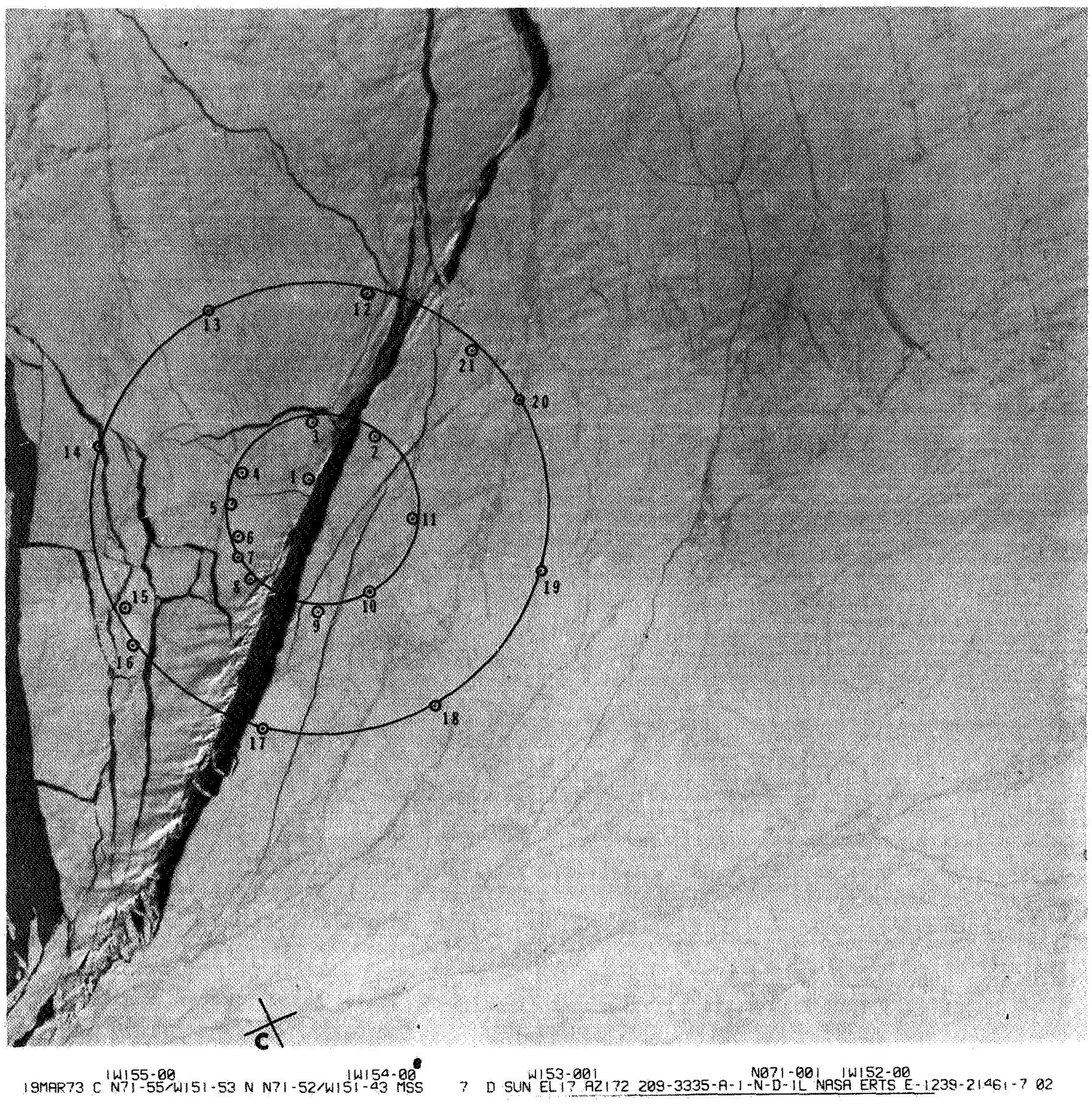

a. Nested strain arrays shown on ERTS MSS band 7 scene 19 March 73.

Figure 11. Arctic ice pack northeast of Point Barrow, Alaska (Crowder, et al., 1973)

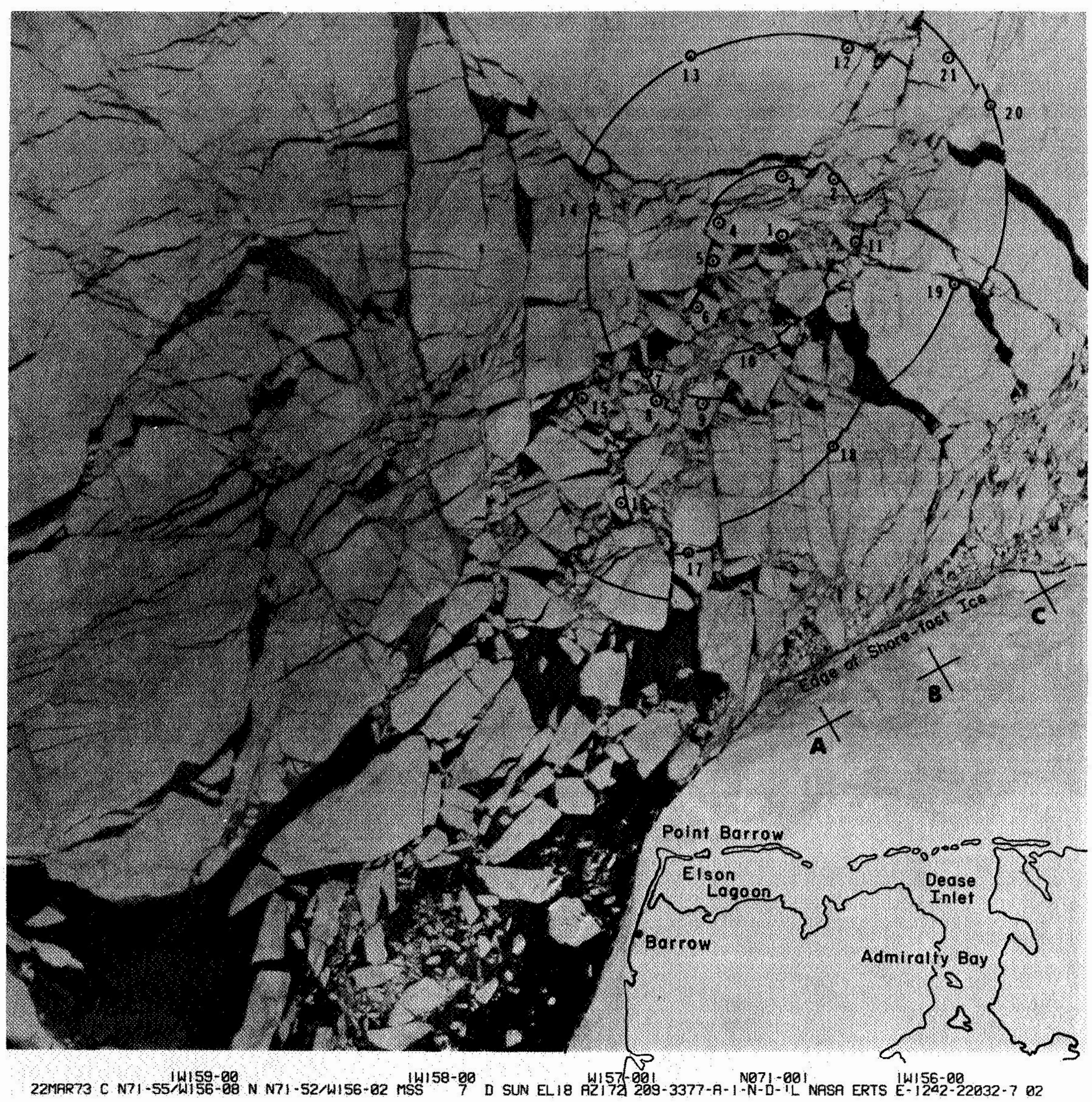

b. Deformation and drift strain of nested strain arrays on March 73 scene.

Figure 11. (Continued)

This indicates that the assumption of no slip at the boundary coupled with a single viscosity model is probably not tenable for the arctic ice pack (Crowder, et al. 1973).

This study, recognizing certain limitations, illustrates how satellite imagery may be used to assess regional deformation and drift of arctic pack ice. The most serious limitation is the difficulty of obtaining sequential, cloud-free imagery coincident with the occurrence of significant deformation.

The distribution of shorefast ice along the Alaskan coast from Point Barrow to Cap Krusenstern as shown in imagery acquired during March 1973 is shown in Figure 12. Compilation and analysis has made clear that the formation and persistence of shorefast ice is easily monitored with ERTS sequential imagery. If compiled in an atlas of shorefast ice distribution as a function of season, such data could be valuable in guiding the planning and construction of navigational and shore facilities.

APPLICATIONS ACHIEVED

The application of satellite imagery in describing and interpreting aspects of arctic and subarctic environments for proper utilization and management of earth resources was addressed in this investigation. ERTS imagery has been used to improve thematic mapping of estuarine processes, vegetation and geomorphic and geologic features. Major estuarine, circulation patterns, water masses, areas of sediment deposition and the distribution of tidal flats were identified and mapped in Cook Inlet. The distribution of permafrost terrain was mapped for a 153,400 km^2 area in north central Alaska. The methods employed were similar to those of previous work but the regional scale map produced had considerably greater detail. As a part of the permafrost mapping, more detailed surficial geology and vegetation maps were also made. These results will be directly applicable to route and site selection, particularly for the Nome to Kobuk Road in western Alaska. Permafrost mapping will also be useful in regional environmental interpretation and urban and land use planning, regulation and management in developing areas of Alaska. The location and monitoring of large river icings in northern Alaska was also accomplished and related to problems of route selection and regional planning.

The anticipated need for information on ice patterns and movements for purposes of navigation and construction of offshore facilities led to an analysis of sea and shorefast ice in the Arctic Ocean. The synoptic, regional perspective of ERTS imagery is well suited to the measurement of sea ice deformation. A spatial deformation analysis was done for a four day period in March 1973 which represents the first successful application of satellite imagery for this purpose. Shorefast ice accumulation and breakup along the western coast of Alaska was also mapped.

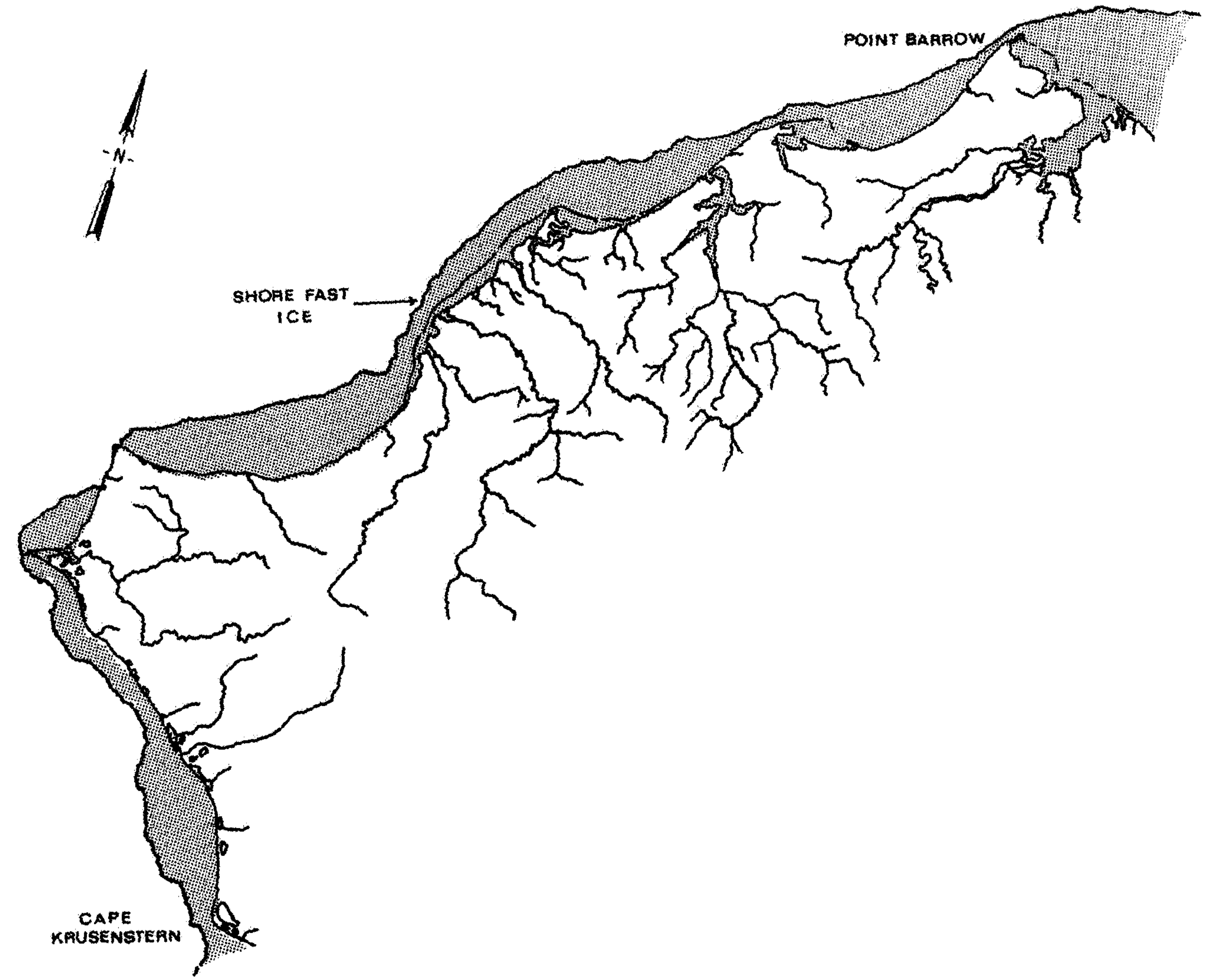

Anderson et al.
(26)

Figure 12. Shore fast ice from Point Barrow to Cape Krusenstern (March imagery).

The direct applications of ERTS imagery to an operational requirement of the Corps of Engineers was achieved in a concurrent investigation. The Corps of Engineers was required to institute a program for the inspection and inventory of dams throughout the United States as a result of public law 92-367, passed on 9 August 1972. In response to a request by the Office of the Chief of Engineers, members of this ERTS investigation team compiled and published a manual on "The Use of ERTS-1 Imagery in the National Program for the Inspection of Dams" (McKim, et al. 1972). This manual described a photointerpretation technique for identifying and inventorying water bodies six acres or larger with ERTS-1 imagery. The approach presented was clearly shown to be the most practical and economical method of accomplishing the requirements of the National Program for Inspection of Dams.

POTENTIAL APPLICATIONS

A number of potential applications of ERTS-1 imagery in a wide variety of earth resources studies have been recognized. These potential uses are directly applicable to the requirements of the Congressional Acts which form the basis for the principal civil works mission responsibilities of the Corps of Engineers. These Acts, listed according to subject area, are as follows:

1. Recreation

   Federal Water Project Recreation Act, 1965
   Land and Water Conservation Act, 1965
   Outdoor Recreation Act, 1963

2. Environmental Impacts

   National Environmental Policy Act, 1969

3. National Program for Inspection of Dams, 1972

4. Urban and Land Use Planning

   Forest Conservation Act, 1960
   Corps Urban Study Mission

5. Flood Plain/Inventory Mapping

   Flood Plain Control Act, 1936-1960

6. Shore Line and Beach Erosion

   River and Harbor Act, 1962 and 1968
   Coastal Zone Management Act, 1972

7. Water Quality

Fish and Wildlife Coordination Act, 1946-1958
Federal Water Pollution Control Act, 1948-1972
Water Supply Act, 1958

Specific examples of ERTS investigations that contribute to work presently being performed under one or more of these Acts include: snow and ice surveys relating snowmelt to stream runoff and delineation of areas where ice creates engineering problem and hazards; floodplain mapping which will provide pertinent information in urban planning; monitoring aquatic pollution and relating the measured parameter to land use practices; preparation of microzonation maps for seismic risk evaluations used in planning and guiding construction activities; compiling baseline data for maritime projects and coastal zone management programs; and in the interpretation of coastal processes. The results obtained from these remote sensing investigations can be used in conjunction with information acquired by conventional means in developing improved data collection procedures.

SUMMARY AND RECOMMENDATIONS

The ERTS-1 mission provides for the first time a means of analyzing terrestrial and marine phenomena on a regional basis. Previously these analyses were not feasible because of expense or lack of suitable data. Improved synoptic mapping of estuarine, surface circulation patterns, suspended sediment distribution and water mass boundaries has been accomplished in Cook Inlet. Also more detailed surficial geology and vegetation maps were prepared at a scale of 1:1,000,000 for a 153,400 km^2 area of north-central Alaska. Based on the interpretation of surficial geology and the probable depth of thaw inferred from vegetation associations, a permafrost terrain map of the same area was prepared with considerably greater detail than previously available maps. Several large river icings were monitored along the proposed Alaskan pipeline route from Prudhoe Bay to the Brooks Range. Sea ice deformation and drift northeast of Point Barrow were measured during a four day period in March. Shorefast ice accumulation and ablation along the west coast of Alaska was mapped for the spring and early summer seasons. In addition applications have been developed in all phases of this investigation and potential uses proposed.

Based on the experience of this investigative team, it is considered appropriate to make some general recommendations on future NASA satellite applications programs. First, ERTS-1 should be fully utilized as

long as it is operational. Consideration should be given to delaying the ERTS-2 mission until its sensor package can be significantly improved or augmented. Second, there is a need to emphasize and improve provisions for technology transfer within user organizations. Greater awareness and participation from the operational personnel of user agencies is needed. This is a responsibility of the user agencies but NASA should take the lead in stimulating a greater awareness of this requirement. Third, a provision for direct downlink for users of DCP's would enhance the utility of this system for many present and potential users by streamlining the data handling system. Finally, the logical culmination of the ERTS program would be the establishment of geostationary, operational satellites, as has been proposed in the GOES program. The geostationary satellites should include, among other sensors, high resolution MSS sensors, directable zoom capability for coverage of localized phenomena, and a direct downlink for a data collection system.

REFERENCES

Alaska Construction and Oil. (1973) Big Anchorage sewer job nears completion, p. 45-48.

Anderson, D.M., L.W. Gatto, H.L. McKim, A. Petrone. (1973) Sediment distribution and coastal processes in Cook Inlet, Alaska, Proceedings of the ERTS-1 Symposium, Goddard Space Flight Center, 5-9 March, p. 1323-1339.

Barnes, J.C. and C.J. Bowley. (1973) Mapping sea ice from the Earth Resources Technology Satellite. Arctic Bulletin 1(1): 6-13.

Blenkarn, K.A. (1970) Measurement and analysis of ice forces on Cook Inlet structures, Offshore Technology Conference, April 22-24, p. 365-378.

Bowden, K.F. (1967) Circulation and diffusion. Estuaries, Amer. Assoc. for the Advancement of Science, Wash., D.C., Publ. No. 83, p. 15-36.

Bryson, R.A. (1966) Air masses, streamlines and the boreal forest. Geographical Bulletin, vol. 8, p. 228-269.

Campbell, W.J., P. Gloersen, W. Nordberg and T.T. Wilheit. (1973) Dynamics and morphology of Beaufort Sea ice determined from satellites, aircraft, and drifting stations. NASA Rpt. No. X-650-73-194.

Carey, E.K.L. (1973) Icings developed from surface water and ground water. U.S. Army Cold Regions Research and Engineering Laboratory Monograph 111-03.

Cass, J.T. (1959) Reconnaissance geologic map of the Melozitna quadrangle, Alaska. U.S. Geological Survey. Misc. Geol. Inv. Map 290, scale 1:250,000.

Crick, R.W. (1971) Potential petroleum reserves, Cook Inlet, Alaska - In Future Petroleum Provinces, North America, A.A.P.G. Memoir 15, v.I. p. 109-119.

Crowder, W.K., McKim, H.L., Ackley, S.F., Hibler, W.D. and D.M. Anderson (1973) Mesoscale deformation of sea ice from satellite imagery (preprint) Symposium on Advanced concepts and Techniques in the Study of Snow and Ice Resources, December 2-8, 1973.

Environmental Currents. (1972) Environmental Science and Technology, vol. 6, no. 12, p. 965.

Evans, C.D., E. Buch, R. Buffler, G. Fisk, R. Forbes and W. Parker (1972) The Cook Inlet environment, a background study of available knowledge. Resource and Science Service Center, University of Alaska, Anchorage, Alaska.

Ferrians, O.J. (1969) Permafrost map of Alaska. U.S. Geological Survey, Misc. Geol. Inv. Map I-445, scale 1:2,500,000.

Ferrians, O.J., R. Kachadoorian and G.W. Greene (1969) Permafrost and related engineering problems in Alaska, U.S.G.S. Prof. Paper 678, 37 p.

Hopkins, D.M., T.N.V. Karlstrom and others (1955) Permafrost and ground water in Alaska. U.S. Geological Survey, Prof. Paper 264-F, p. 113-146.

Karlstrom, N.V. and others (1964) Surficial geology of Alaska. U.S. Geological Survey, Misc. Geol. Inv. Map I-357, scale 1:1,584,000.

Kinney, P.J., D.K. Button, D.M. Schell, B.R. Robertson and J. Groves. (1970a) Quantitative assessment of oil pollution problems in Alaska's Cook Inlet: Report R-169-16, Institute of Marine Sciences, University of Alaska, College, Alaska, 116 p.

Kinney, P.J., J. Groves and D.K. Button (1970b) Cook Inlet environmental data: R/V Acona cruise 065-May 21-28, 1968, Inst. of Marine Science Report R-70-2, University of Alaska, Fairbanks, Alaska.

Lachenbruch, A.H. (1968) Permafrost in Fairbridge, R.W., ed. The Encyclopedia of Geomorphology: New York, Reinhold Publishing Corp., p. 833-839.

MacKay, R.S. (1972) The world of underground ice. Annals of the Association of American Geographers, vol. 62, no. 2, p. 1-22.

McKim, H.L., T.L. Marlar and D.M. Anderson (1972) The Use of ERTS-1 Imagery in the National Program for the Inspection of Dams. USACRREL Special Report 183.

Muller, S.W. (1947) Permafrost or permanently frozen ground and related engineering problems. Ann Arbor, Michigan: J.W. Edwards, Inc., 231 p.

Patton, W.W., Jr. (1966) Regional geology of the Kateel River quadrangle, Alaska. U.S.G.S. Misc. Geol. Inv. Map I-437, scale 1:250,000.

Patton, W.W., Jr. and T.P. Miller (1966) Regional geologic map of the Hughes quadrangle, Alaska. U.S.G.S. Misc. Geol. Inv. Map. I-459, scale 1:250,000.

Pewe, T.L. (1966) Paleoclimatic significance of fossil ice wedges. Biuletyn Peryglacjalny. no. 15, p. 65-73.

Rosenberg, D.H., D.C. Burrell, K.V. Natarajan and D.W. Hood. (1967) Oceanography of Cook Inlet with special reference to the effluent from the Collier Carbon and Chemical Plant: Report R67-5, Institute of Marine Science, University of Alaska, College, Alaska, 80 p.

Spetzman, L. A. (1963) Terrain study of Alaska, Part IV: Vegetation. Military Geology Branch, U. S. Geological Survey.

Trytikov, A.P. (1959) Perennially frozen ground and vegetation. In Principles of geocryology Part II, Engineering geocryology, Chapter XII. Academy of sciences of the U.S.S.R., V.A. Obruchev Institue of Permafrost Studies, Moscow, p. 399-421.

Webber, R.R. and T.L. Pewe (1970) Surficial and Engineering geology of the central part of the Yukon-Koyukuk Lowland, Alaska. U.S.G.S. Misc. Geol. Inv. Map I-590, scale 1:125,000.

Wendler, G. (1973) Sea ice observation by means of satellite. J. Geophys. Res., 78(9).

Williams, J.R. (1970) Groundwater in the permafrost regions of Alaska, U.S. Geological Survey, Prof. Paper 696, p. 18-20.

Paper E 8

AN INTERDISCIPLINARY STUDY OF THE ESTAURINE AND COASTAL OCEANOGRAPHY OF BLOCK ISLAND SOUND AND ADJACENT NEW YORK COASTAL WATERS

Edward Yost, *Long Island University;* R. Hollman, J. Alexander and R. Nuzzi, *New York Ocean Science Laboratory*

ABSTRACT

ERTS-1 photographic data products have been analyzed using additive color viewing and electronic image analysis techniques. Satellite data were compared to water sample data collected simultaneously with the data of ERTS-1 coverage in New York Bight. Prediction of the absolute value of total suspended particles can be made using composites of positives of MSS bands 5 and 6 which have been precisely made using the step wedge supplied on the imagery. Predictions of the relative value of the extinction coefficient (-$\bar{K}$) can be made using bands 4 and 5. Thematic charts of total suspended particles (particles per litre) and extinction coefficient (-$\bar{K}$) provide scientists conducting state and federal water sampling programs in New York Bight with data which improves the performance of these programs.

INTRODUCTION

A program was conducted to locate and identify New York coastal water masses using ERTS-1 imagery in conjunction with ship sampling. One of the prime objectives of this research project was to develop techniques for analyzing ERTS satellite photographic data products which would provide quantitative surface water data of use to oceanographers. The real usefulness of ERTS for oceanography depends on the quantitative data which can be extracted from the image data provided by the satellite.

The dynamics of the Block Island Sound and New York Bight coastal waters were the focus of interest. On-going state and federal programs are being conducted in these areas using conventional ship sampling techniques. The use of ERTS data in these programs has three important contributions:

1. Revising the locations of ship sampling stations and timing of the collection of such data.

2. The extension of sample data over the entire water area between and beyond the sampling stations.

3. Repetitive acquisition of data in the absence of ship sampling.

The New York Bight results are reported herein. Two predominant features dominate this coastal water area, the effluent from the Hudson River and the sludge dumping dispersion patterns. The concepts of flow and mixing patterns in the Bight are being revised in light of the ERTS-1 data. The dumping of treated sewage material in the Bight is a source of controversy as to the extent of its impact on the biota. Satellite imagery offers a convenient and unique method of monitoring such dispersion.

SHIP SAMPLING PROGRAM

Twenty-seven cruises were conducted in the New York Bight, Block Island Sound and in Peconic Bay during the fall of 1972 and spring-summer of 1973. Each cruise consisted of from one to twenty ships. The locations of the sampling stations are shown in Figure 1.

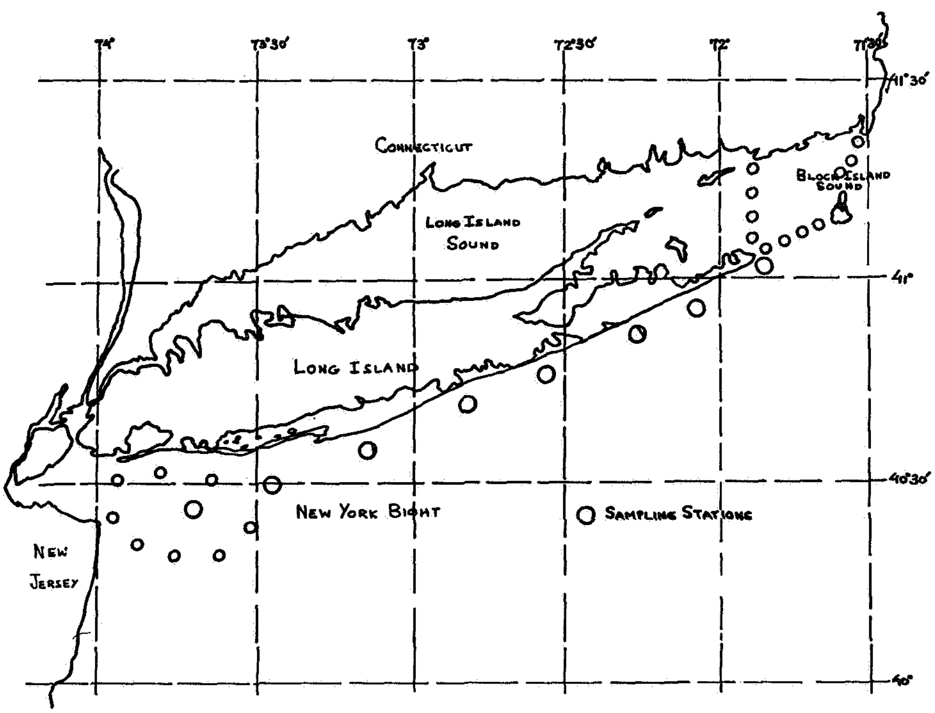

Figure 1. Ship sampling stations in New York coastal waters.

Typically, each of the transects was occupied for a complete tidal cycle being sampled from four to six times. Samples were obtained at six depths in 5 litre Niskin bottles for chemical and biological analysis.

Physical parameters of salinity, temperature, and extinction were measured at each station.

Four critical surface parameters were selected for correlation with the ERTS-1 imagery:

-- Average extinction coefficient ($-\bar{K}$)
-- Total suspended particles (particles/litre)
-- Total cell counts (particles/litre)
-- Chlorophyll a (mg/litre)

These data along with temperature (°C) and salinity (0/00) were collected during the satellite day for subsequent correlation with the ERTS-1 imagery. Since each sampling station could not be occupied at the exact instant of the satellite overpass, the data were adjusted to the tidal cycle which existed at the time of the ERTS-1 satellite pass.

IMAGE ANALYSIS PROCEDURES

The approach used for analysis of the ERTS-1 imagery with respect to water characteristics was:

1. Use water sample data to develop image analysis procedure for each pair of image-water sample data.

2. Use the techniques thus developed on a second ERTS-1 date and compare the results with the water sample data with this second date.

Positive images were made from the ERTS-1 31 May 1973 negatives to bring out maximum water detail (Yost et al, 1972). These positives were placed in a Spectral Data Model 64 additive color viewer. Three brightness readings were made of the image of each sampling station using a Photo Science Spot Brightness meter. The black-and-white image brightness of MSS bands 4, 5, 6, and 7 was thus obtained and a regression analysis performed with respect to: average extinction coefficient, total suspended particles, total cell counts, and chlorophyll a.

On the basis of this analysis, composite bands were selected for subsequent analysis. In the New York Bight, combined positive images of MSS bands 4 and 5 were found to be best for the measurement of extinction coefficient and positive images of bands 5 and 6 best for the measurement of total suspended particles.

Semi-automatic classification of water characteristics was achieved by interface of a Spectral Data Model 703 density slicer with the Spectral Data Model 64 viewer. The composite screen image was "sliced" and the video display used to construct a chart of the water characteristics being analyzed. Figure 2 shows the arrangement of the instrumentation used for analysis of the ERTS imagery.

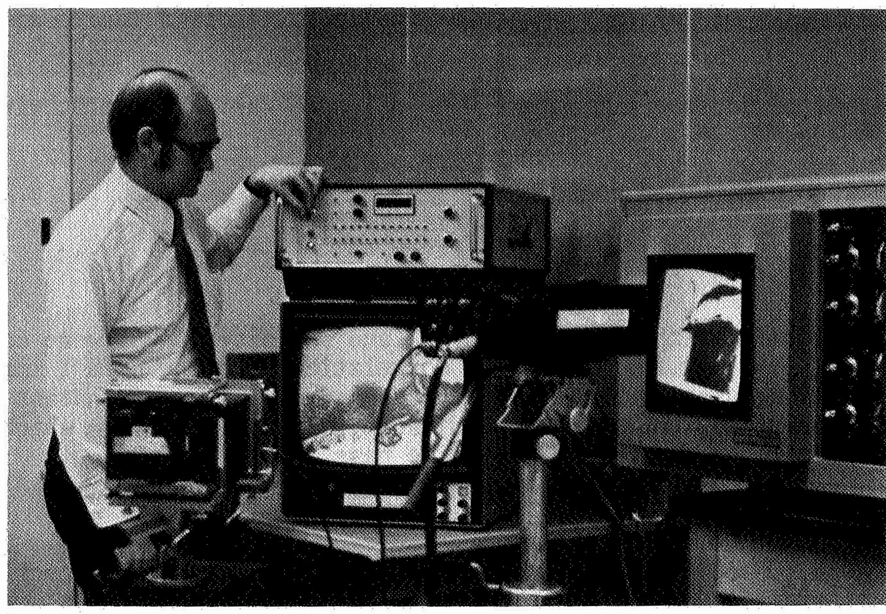

Figure 2. Spectral Data additive color viewer and Spectral Data density slicer used together to analyze ERTS imagery.

TOTAL SUSPENDED PARTICLES

ERTS-1 imagery acquired over New York Bight on 31 May 1973 was analyzed. A portion of this image is shown in Figure 3.

Figure 3. ERTS-1 MSS Band 5 of New York Bight, 31 May 1973.

The brightness of the projected reprocessed positive image was measured at each of the nine New York Bight sampling stations on each of the four individual MSS bands. Table 1 shows the image brightness and associated water data.

Sta. #	N. Lat.	W. Long.	Image Brightness ft. lamb. MSS Bands 4	5	6	7	av. $-\bar{k}$	Surface Total part./litre x10^6	Total cell ct./litre x10^3	Chloro a mg/l.
1	40°32'.4	73°56'.6	3.9	3.5	5.9	8.7	.14	274	149	4.1
2	40°32'.4	73°58'.0	4.0	2.9	5.0	7.9	.67	1665	1738	14.8
3	40°29'.2	73°59'.6	4.1	3.6	5.8	8.1	.93	2677	1134	17.2
4	40°25'.1	73°56'.0	3.4	2.2	4.8	8.6	.44	1119	1997	19.7
5	40°24'.4	73°51'.3	3.7	2.3	4.0	7.5	.30	939	865	8.9
6	40°23'.0	73°48'.2	2.9	1.5	3.3	5.6	.43	609	724	20.1
7	40°25'.5	73°45'.0	3.0	1.5	3.2	5.6	.50	923	1063	6.4
8	40°30'.0	73°44'.0	3.4	1.9	3.9	7.3	.54	561	1138	14.9
9	40°33'.8	73°48'.6	4.2	2.3	4.9	8.9	.53	478	280	5.5

Table 1
New York Bight - 31 May 1973
ERTS-1 Image Brightness and Water Sample Data at Nine Stations

The relation of screen brightness in each band and total suspended particles was plotted and a linear regression line plotted for each. These relationships are shown in Figure 4.

Single band images show little relationship between total particles and image brightness, although band 5 is the best of the four bands. However, when positive images of bands 5 and 6 are combined, a significant relationship between image brightness and total particles is achieved as shown in Figure 5.

A comparison of the regression lines for the individual ERTS-1 MSS bands and the composite MSS bands 5 and 6 for 31 May 1973 is shown below:

Band	Wavelength	Regression Line	Correlation Coefficient
4	.5 - .6μ	y = 3.48 + .02x	.01
5	.6 - .7μ	y = .67 + .13x	.61
6	.7 - .8μ	y = 4.04 + .05x	.35
7	.8 -1.1μ	y = 7.40 + .02x	.10
5 & 6	.6 - .8μ	y = 4.45 + .18x	.92

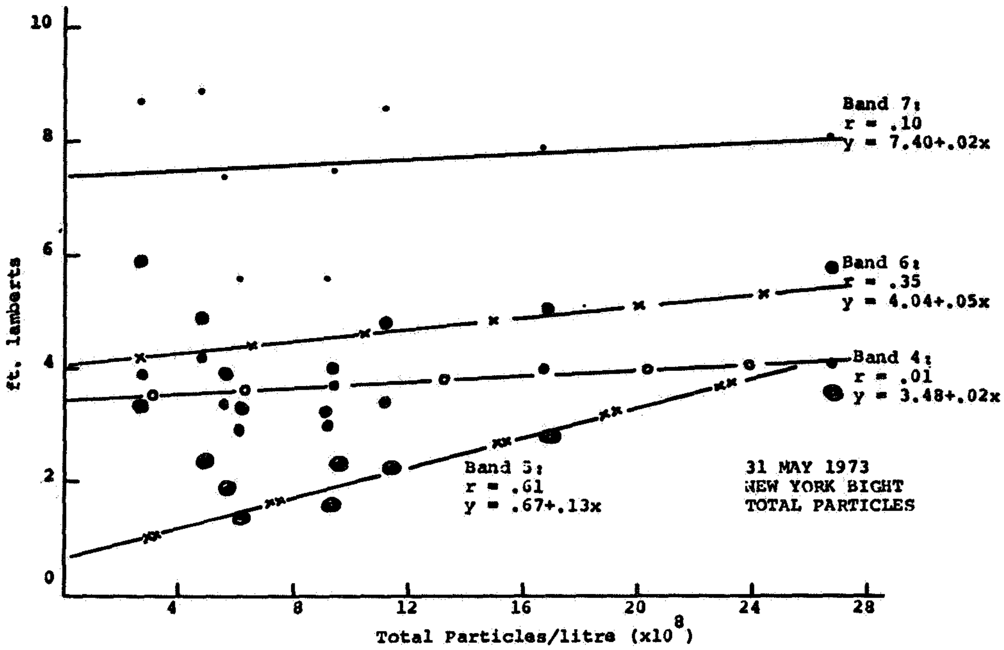

Figure 4. 31 May 1973 - New York Bight. The relationship of total particles and brightness of four ERTS-1 MSS bands.

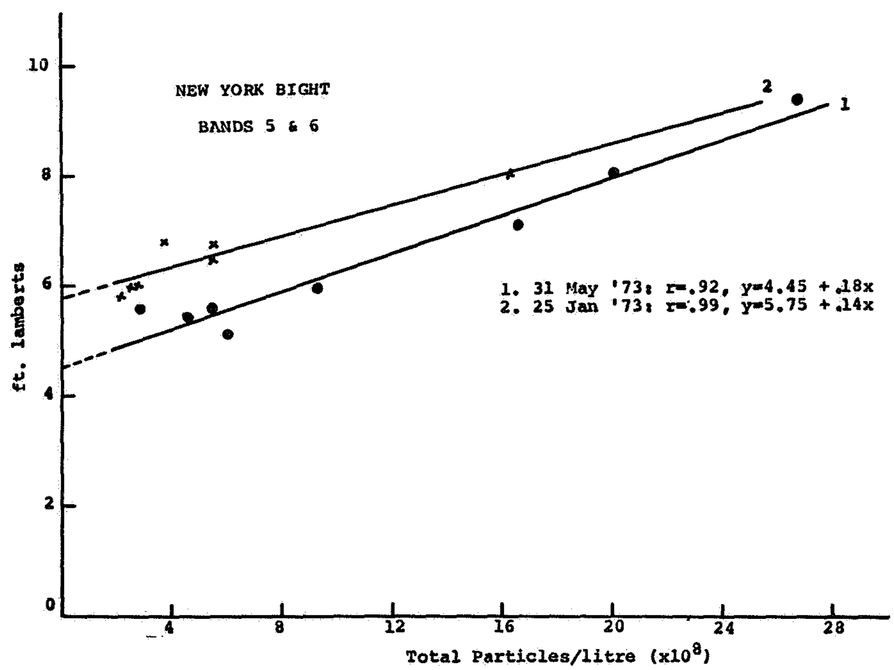

Figure 5. 25 Jan. 1973 and 31 May 1973 - New York Bight. The relationship of total particles and image brightness of composite of ERTS-1 MSS bands 5 and 6.

In computing the above regression lines, y (the dependent variable) is image brightness and x (the independent variable) is total suspended particles (particles per litre $x10^8$).

The validity of using an additive color combination of reprocessed positive images of ERTS bands 5 and 6 for obtaining quantitative measurement of total suspended particles was evaluated by using the same image analysis techniques on the 25 January 1973 ERTS images of New York Bight. After performing the analysis, a regression of the image data on the water sample data obtained on that date was made. These results are shown in Figure 5 above.

By using more precise controls on the reprocessing of the positive imagery from the ERTS negatives through utilization of the step wedge calibration provided, a general relationship between image brightness and total particles exists which can be used for quantitative measurement. This relationship is shown in Figure 6.

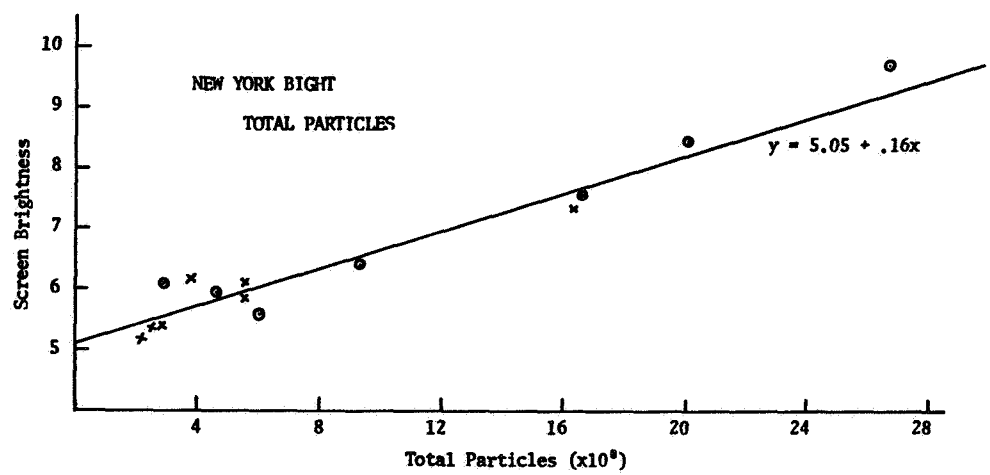

Figure 6. 25 January 1973 and 31 May 1973 - New York Bight. The relationship of total particles with image brightness of accurately processed positive composites of ERTS MSS bands 5 and 6.

Figure 7 shows the predicted value of total particles using a composite of ERTS MSS bands 5 and 6 which have been carefully reprocessed as positives, and the actual values measured by ship sampling.

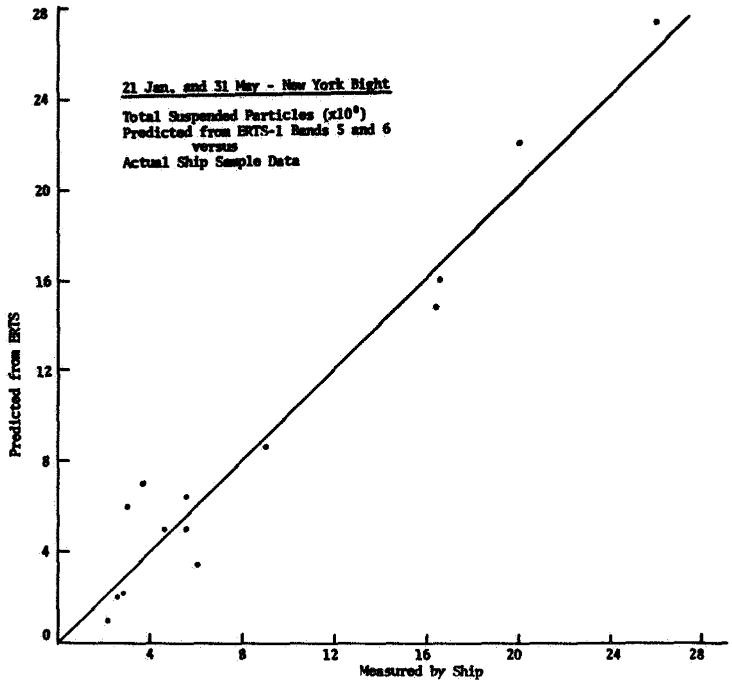

Figure 7. Total suspended particles predicted by ERTS measurements versus actually measured particles.

It should be emphasized that the above is a prediction of the <u>absolute</u> value of total suspended particles, <u>not</u> the relative value.

EXTINCTION COEFFICIENT

An analysis similar to that discussed above was performed for determining the extinction coefficient ($-\overline{K}$) from the ERTS-1 imagery. A statistical analysis of the individual bands showed that positives of bands 4 and 5 could be used to predict <u>relative</u> values of the extinction coefficient. Figure 8 shows the results for ~~25 January~~ and 31 May 1973; variability in the slope of the regression line is believed to be due to atmospheric effects. Figure 8 shows the step wedge density versus the brightness of the 31 May 1973 positives used.

The relationship between screen brightness and extinction coefficient measured by ship sampling is shown in Figure 9 on the following page.

By using the density slice attached to the additive color viewer, a visual display of the relative extinction coefficient was made. This technique is used for the analysis of all ERTS data of New York Bight and Block Island Sound. Figure 10 is a black-and-white reproduction of the screen image and Figure 11, the thematic chart made for the image.

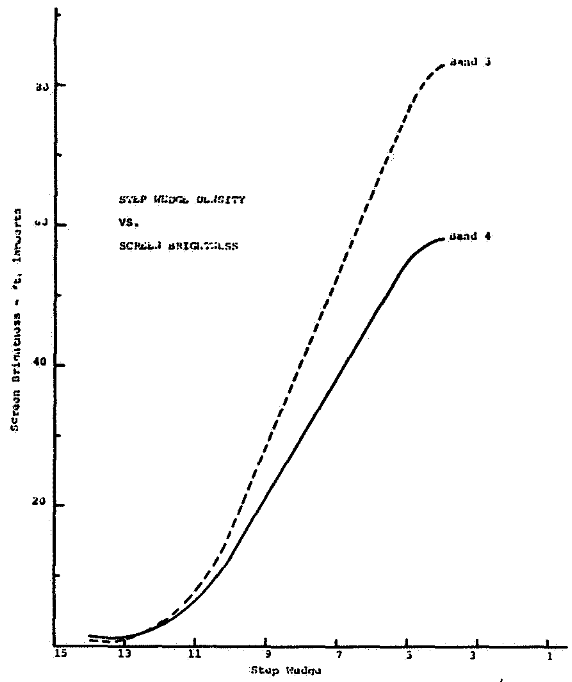

Figure 8. Step wedge density vs. screen brightness of Bands 4 and 5 used to determine extinction coefficient for 31 May 1973.

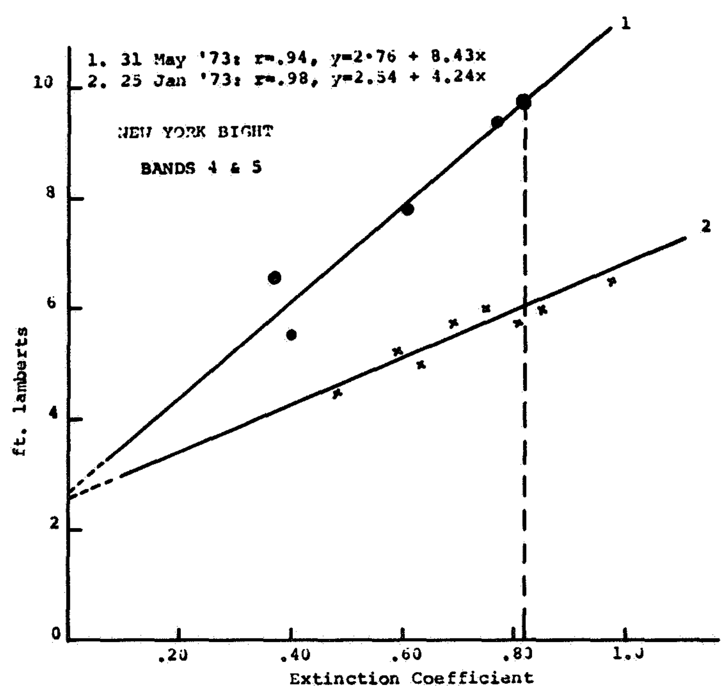

Figure 9. 25 January and 31 May 1973 - New York Bight. Screen brightness of Bands 4 and 5 versus extinction coefficient measured by ship sampling.

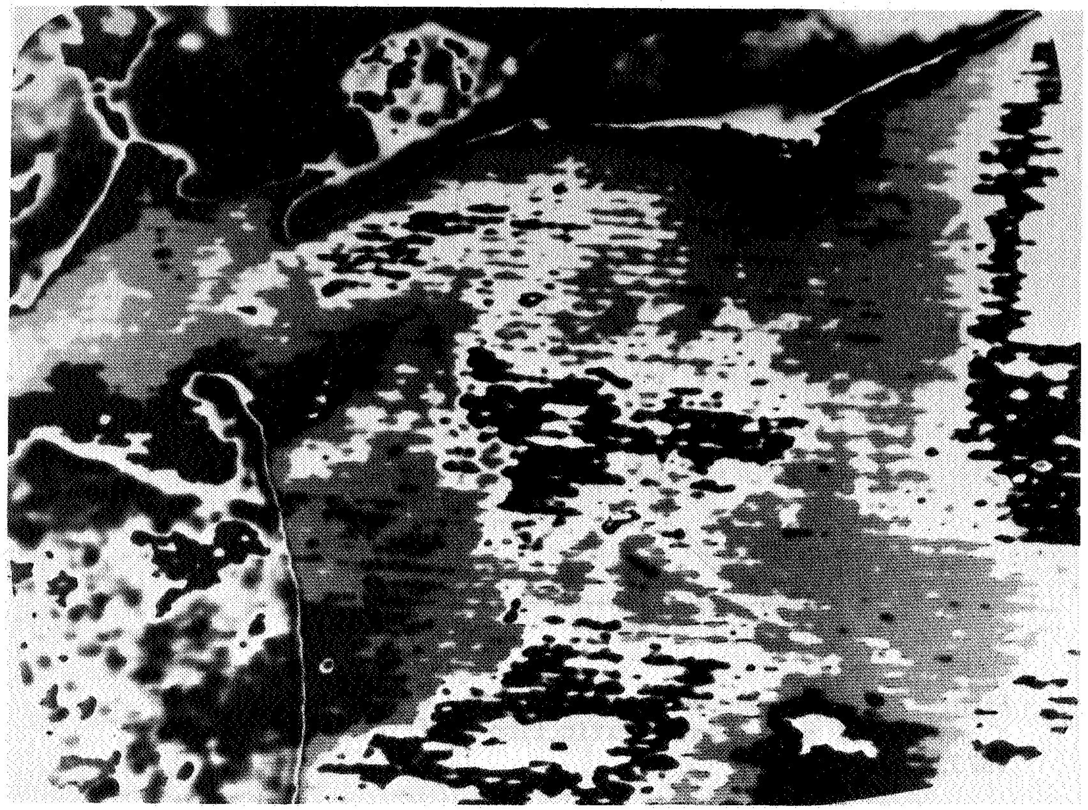

Figure 10. Electronic density analysis of extinction coefficient: ERTS-1 Bands 4 and 5, 31 May 1973 - New York Bight.

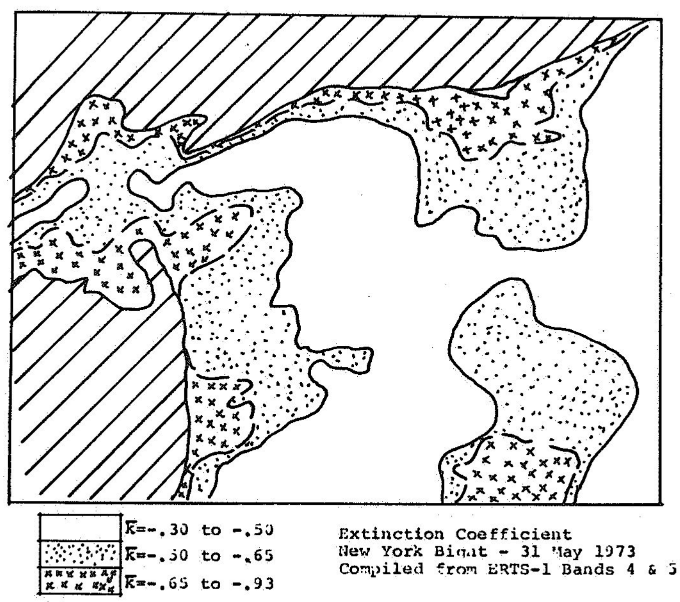

Figure 11. Thematic chart of extinction coefficient made from ERTS-1 bands 4 and 5 of New York Bight, 31 May 1973.

TOTAL CELL COUNTS AND CHLOROPHYLL A

An analysis of ERTS-1 imagery and ship sampling shows that only gross approximations of total cell counts and chlorophyll a are possible in New York Bight waters, although better relationships appear to exist in Block Island Sound. Figure 12 shows the typical relationship of image brightness and chlorophyll a.

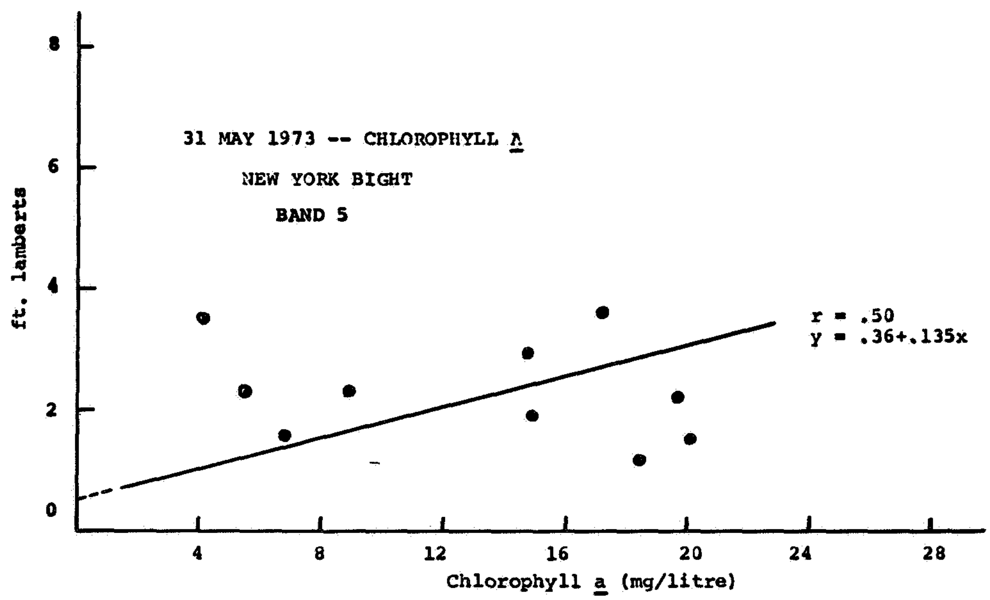

Figure 12. 31 May 1973 - New York Bight. ERTS-1 Band 5 image brightness versus chlorophyll a.

CONCLUSIONS

Predictions of the absolute value of the number of total particles contained in New York Bight can be made using ERTS-1 bands 5 and 6 which have been carefully reprocessed to bring out maximum water detail.

Predictions of the relative extinction coefficient of New York Bight waters can be made using ERTS-1 bands 4 and 5. Atmospheric effects in band 4 apparently cause variability in image characteristics which prevent absolute measurements from being attained.

Display of these bands in an additive color viewer provides the scientist with a color composite in which variations in color are related to total particles or extinction coefficients.

An electronic density slicer can be used with an additive color viewer to provide semi-automatic thematic charts of total particles or extinction coefficient.

Charts of these basic water characteristics derived from ERTS-1 should be incorporated in any ship sampling program to establish ship sampling stations, periodicity of sampling, and extend ship sampling data on a continuous basis.

REFERENCES

Yost, Edward, R. Kalia, S. Wenderoth, R. Anderson, and R. Hollman (1972): "The Estuarine and Coastal Oceanography of Block Island Sound and Adjacent New York Coastal Waters", ERTS-1 Symposium Proceedings, Goddard Space Flight Center, Greenbelt, Maryland.

Paper E 9

AIRCRAFT AND SATELLITE MONITORING OF WATER QUALITY IN LAKE SUPERIOR NEAR DULUTH

James P. Scherz, *Associate Professor, Civil and Environmental Engineering Department, University of Wisconsin, Madison;* Michael Sydor, *Associate Professor of Physics, University of Minnesota, Duluth, Minnesota;* and John F. Van Domelen, *Research Assistant, Institute for Environmental Studies, and Ph.D. Candidate, University of Wisconsin, Madison*

ABSTRACT

Satellite images and low altitude aerial photographs often show vivid discolorations in water bodies. These aerial images are just pretty pictures unless one knows to which water quality parameters the discolorations correlate and how this correlation can be reliably made. Extensive laboratory analysis shows that water reflectance, which causes brightness on aerial images, positively correlates to the water quality parameter of turbidity, which on a particular day correlates to suspended solids. Work with low altitude photography on three overcast days and with ERTS images on five clear days provides positive correlation of image brightness to the high turbidity and solids which are present in Lake Superior near Duluth over 50% of the time. Proper use of aerial images would have shown that an $8,000,000 drinking water intake constructed in the midst of this unpotable, turbid water should have been located 6 miles north in clear, usable water. Noise effects such as skylight reflection, atmospheric effects, and depth penetration also must be understood for operational use of remote sensing for water quality monitoring and are considered in the paper.

SUMMARY AND OVERVIEW

Do ERTS images of water bodies show important water quality parameters or are they just pretty pictures? In the same tone, do conventional aerial photographs of water bodies show important water quality parameters or are they just pretty pictures? If such aerial images do correlate to important water quality parameters, then which parameters; and how can these correlations be quantitatively and reliably made?

This paper describes work which concludes that aerial image brightness directly correlates to the water quality parameter of turbidity which in turn is caused by suspended solids. The paper describes reflectance analysis of water samples in the laboratory, correlation of water quality to low altitude aerial photos taken on three overcast days, and correlation to ERTS imagery taken on

five clear days. "Noise" factors of bottom effects, surface reflection, and atmospheric effects are also considered in this paper. Enough is now understood so that aerial photographs and satellite images can be used as effective tools for water quality work.

An example of such potential use is in Lake Superior near Duluth, Minnesota, and Superior, Wisconsin, where an $8,000,000 water intake was constructed to obtain drinking water from Lake Superior. No water filtration was planned because of the clearness of Lake Superior water. The location engineer used traditional locating procedures which did not include properly acquiring aerial photography nor properly utilizing existing aerial photographs taken from 1939 to 1969, on file in the city of Superior.

The intake, when completed, provided water too turbid for drinking water standards over 53% of the time. Aerial photos and ERTS images likewise show turbid water runoff from several rivers which stays in the area of the intake over 50% of the time. A lawsuit of the city which built the intake against the location engineer provided the means of gathering much of the data contained in this paper pertaining to correlating water quality to low altitude photography. NASA support at the University of Minnesota, Duluth, and at the University of Wisconsin, Madison, provided the means of doing the laboratory reflectance analysis of the water samples and correlating water quality to ERTS imagery.

The lawsuit was settled out of court so remote sensing evidence was not introduced into court on this case. It is clear however, if in the future a locating engineer correctly utilizes aerial or ERTS imagery, such water intakes should be located in clear and not turbid water. In such cases, if aerial imagery is correctly utilized, taxpayers and the engineer will be rewarded with successes and spared such multimillion dollar blunders.

CORRELATION OF WATER QUALITY TO LOW ALTITUDE PHOTOGRAPHY

Figure 1 shows an ERTS image of the SW end of Lake Superior and the cities of Duluth, Minnesota and Superior, Wisconsin. In the figure, the dark part of the lake is the very clear water for which Lake Superior is so famous. The light colored part of the photo is muddy, turbid water caused by storm runoff from several rivers along the south shore of the lake. An X marks the spot where an $8,000,000 water intake was located to obtain the clear Lake Superior water. As can be seen the location engineer placed his intake several miles too far south thereby missing the clear water. Aerial photos on file at Superior since 1939 and ERTS images show this turbid water in the vicinity of the intake over 50% of the time and clear water a few miles to the north. (Such

Figure 1. ERTS Satellite Image taken 12 August 1972 showing the south west end of Lake Superior near Duluth. Note the dirty water. An X marks the spot where an $8,000,000 water intake was located which when put into operation produced turbid unusable water.

aerial images should be utilized when one is locating such water intakes to assure that they are located in clear and not turid water.)

In order to ascertain just what water quality parameters correlate to the brightness of the ERTS image, water samples were collected on 4 November 1972 after a 2-inch rain storm and simultaneous aerial photos were taken from a small fixed wing aircraft (5). The skys were completely overcast and the flight altitude was limited to about 1000 feet above the water. This data was collected by Professor Scherz and John Van Domelen in conjunction with the lawsuit concerning the intake.

The water samples were analyzed for total solids, volatile solids, suspended solids, dissolved solids, turbidity, and color. Also light was shown down on the top of the water samples and the percent reflectance* and transmittance of these samples were determined at different wavelengths. The change in reflectance and transmittance was then compared to the different water quality parameters.

Also the brightness of all colors on resulting aerial photos were analyzed with a modification of the equipment as was used to obtain the reflectance and transmittance of the water samples. Figure 2 shows a schematic of the apparatus used to obtain the volume reflectance and the brightness of the photos (1, 4, 5).

Figure 3 shows the resulting volume reflectance curves of several different water samples and their corresponding values of turbidity and suspended solids. One can see from Figure 3 that there is indeed a positive correlation between volume reflectance and turbidity and suspended solids. If one takes the volume reflectance at some color (say red) and plots that against turbidity and suspended solids, a reflectance-turbidity curve results. Figure 4 shows this curve for the water samples shown in Figure 4 along with many other collected and synthetic samples. One will note that for values of suspended solids and turbidity found in the field on 4 November 1972, (values to the left of point A in Figure 4), that there is indeed a linear relationship between volume reflectance and turbidity with a slope of about 30°. This means if one can measure the reflectance, the turbidity can be obtained by use of the curve. For clear water samples to the left of point B on Figure 4 there is a reversal in the curve caused by light striking a shiny bottom of the sample tube and returning to the surface of the water sample. This reversal to the left of point B was corrected on later work by putting in a light-absorbing black bottom in the sample tube. The general shape of the curve in Figure 4 is similar to other curves obtained from analyzing paper mill waste and lake waters containing various amounts of algea (1, 4).

When the brightness of the photos were analyzed and plotted against turbidity, this plot was also a straight line but considerably higher than the laboratory data (Figure 4).** The photos in addition to showing the volume reflection also show

*This lab reflectance is called volume reflectance. When done right, it contains no effects of the bottom of the sample tube nor reflection of overhead light from the air-water interface.

**In the laboratory the percent reflectance was compared to a barium sulfate reflectance standard. From the photo the reflectance of the water was compared to a styrafoam panel or other object of known reflectance located somewhere in the frame.

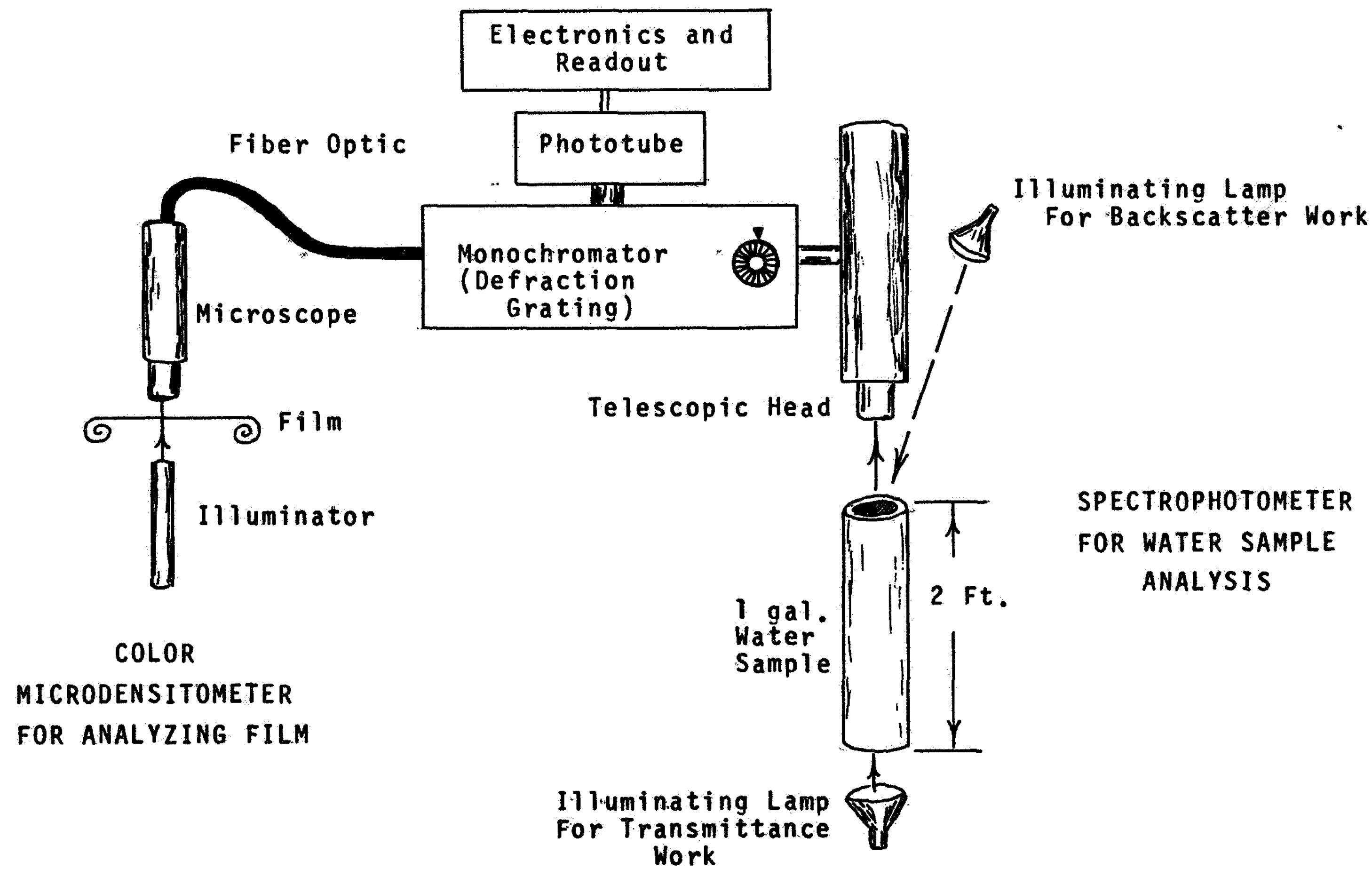

Figure 2. Schematic of Equipment used to Analyze Film and Water Samples

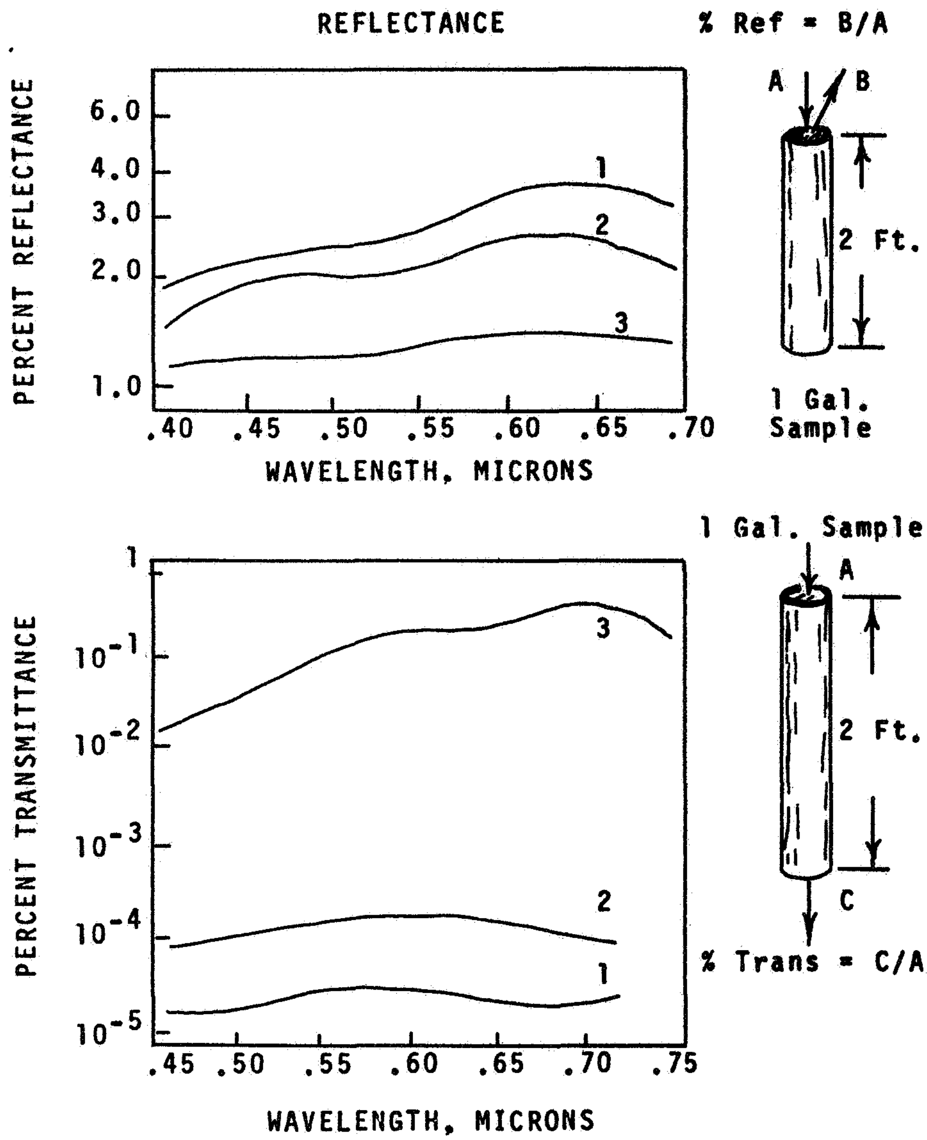

Water Sample	Turbidity	Suspended Solids
1	87	76
2	56	46
3	23	17

Figure 3. Reflectance and Transmittance Curves for Water Samples Collected near Duluth on 4 November 1972.

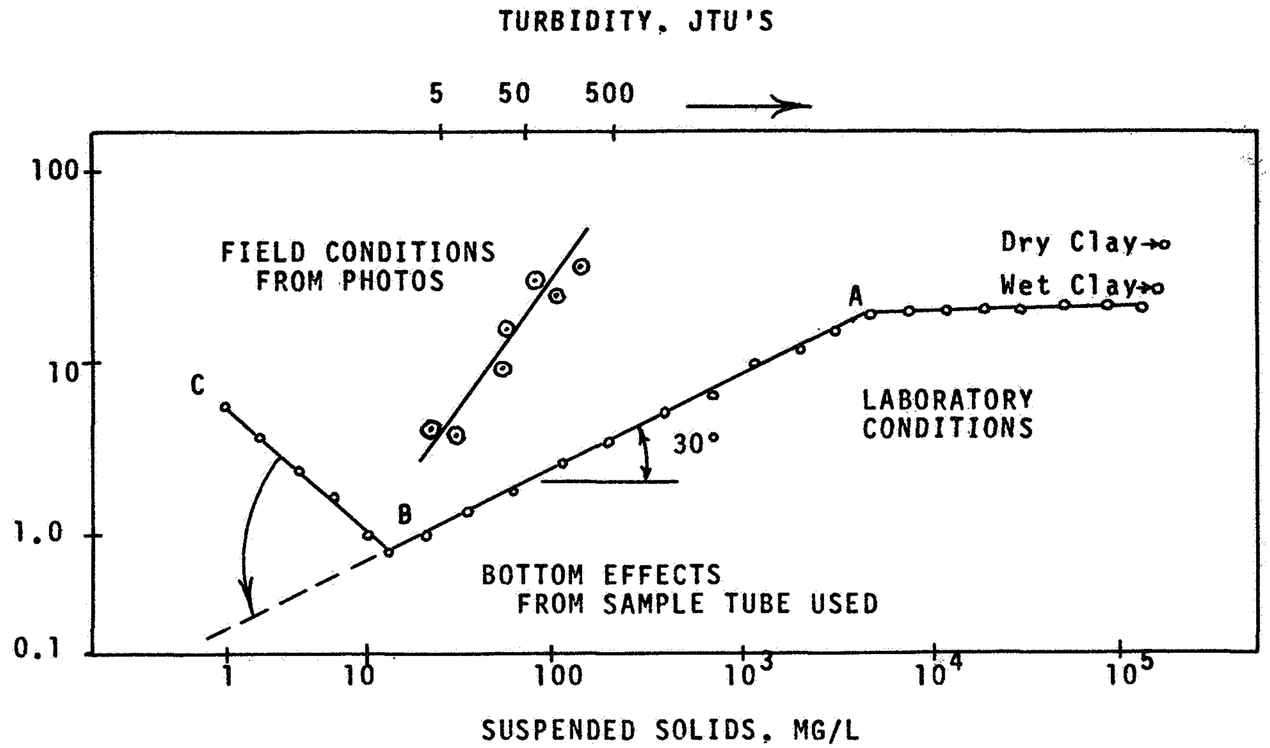

Figure 4. Volume reflectance from laboratory analysis, and apparent reflectance from the photo analysis plotted against turbidity and suspended solids. This curve shows the relationship for the red part of the spectrum. Clay of the type in the water from Figure 3 was successively diluted to almost distilled water to obtain this curve. Effects of a shiny sample tube bottom cause the curve reversal between B and C. Further work with an absorbing black bottom remedied this reversal. The vertical displacement between the curve for field conditions and lab conditions is primarily due to the fact that skylight reflection and path luminance is present on the photos but not present in the lab analysis.

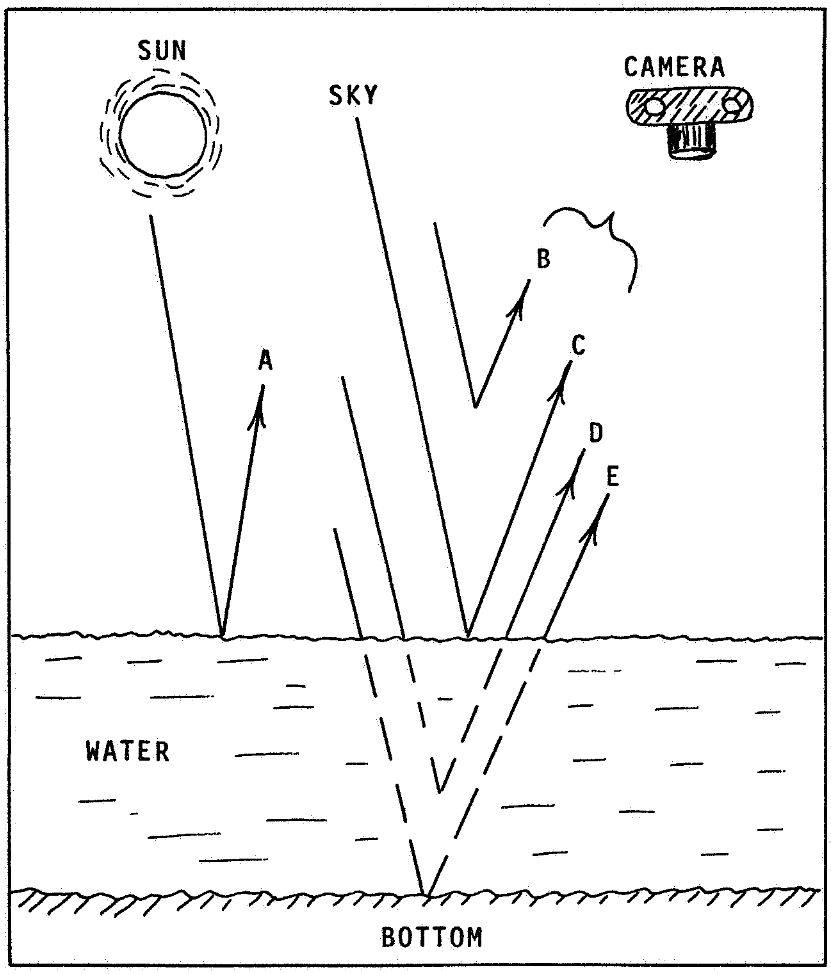

A = Surface Reflection of the Sun
B = Atmospheric Scatter
C = Surface Reflection of the Sky
D = Volume Reflectance of the Water
E = Bottom Effects

Note: Both Atmospheric Scatter, B, and Surface Reflection of the Sky, C, cause the apparent reflectance of an aerial photo to be higher than the laboratory analysis, which measures only volume reflectance, D. It must be assured that bottom effects, E, are insignificant and that there is no sun reflection, A, in the area of the photo being analyzed.

Figure 5. Components of light showing on an aerial image caused by various interactions of light in, on, and through the water.

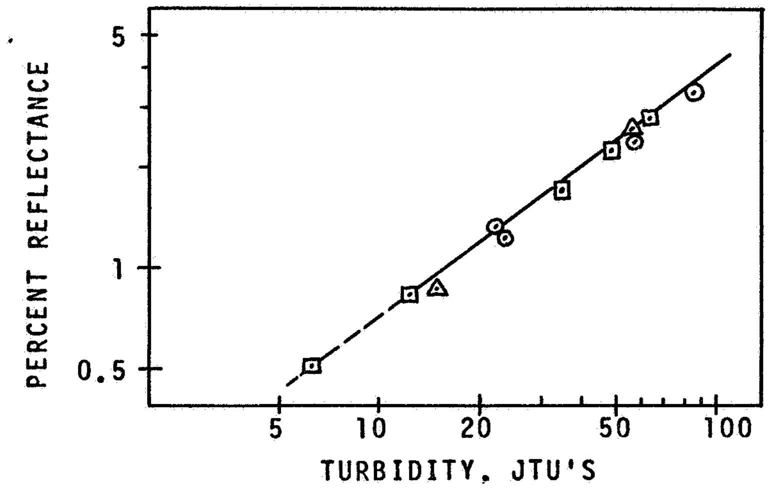

Reflectance vs. Turbidity

⊙ = Water Samples Collected 4 November 1972
(2 days after a heavy storm)
△ = Water Samples Collected 17 November 1972
⊡ = Water Samples Collected 23 November 1972

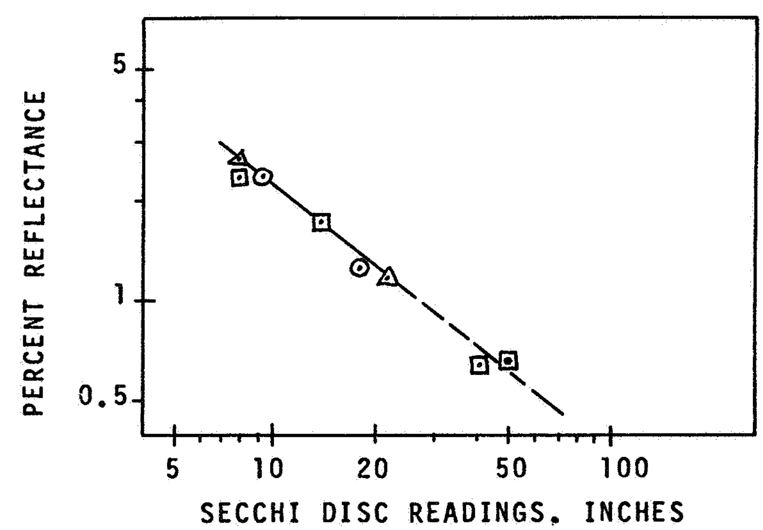

Reflectance vs. Secchi Disc Readings

Figure 6. Laboratory Reflectance versus Turbidity and Secchi Disc Readings for all of the water samples collected during the 3 days in November, 1972. The location is dirty water in Lake Superior near Duluth in the area shown in Figure 1.

versus Secchi disc readings is a very important curve because if one obtains reflectance from an aerial image, this curve will indicate how far into the water the image is sensing and whether bottom effects are significant. From the curve in Figure 6 the maximum Secchi disc reading is about 3 meters. For the aerial image shown in Figure 1, the depth to bottom in this area is from 15 to 25 meters. Therefore the light areas in Figure 1 definitely do not contain bottom effects.

The turbidity is caused by light scattering from suspended solids in the water. However, a large number of small particles or a small number of large particles can cause the same value of turbidity. Also the shape of the particles have an effect. The relationship therefore between turbidity and suspended solids changed between 4 November to 23 November as the character of the suspended solids changed due to differential settling. Figure 7 shows a plot of suspended solids versus turbidity for all three days. One will note that for any one day there is indeed a good correlation between turbidity and suspended solids but that this correlation changes from day to day. If one were not overly concerned with high precision, an average curve could be drawn for the three days and approximate suspended solids values as well as turbidity could be obtained from analysis of aerial photos. If this is done the values of suspended solids obtained from turbidity on the curve would probably not be in error by more than about 30% (See Figure 7).

For November 4, 17, and 23 the reflectance-turbidity curves from the aerial photos vary considerably apparently due to different skylight and atmospheric effects for the different days. Therefore, for low altitude photography, until a universal method is found to account for skylight reflection and atmospheric effects, it appears that a few simultaneous water samples are necessary to obtain the vertical position of the reflectance-turbidity curve for that particular aerial overpass. Once that is done, turbidity and solids can be mapped over the entire area photographed. It is the water pollution parameter of turbidity that quantitatively correlates to the aerial image brightness. To whatever extent suspended solids correlate to turbidity on a particular day, suspended solids can also be mapped from the aerial image brightness.

One can also correlate the concentration of solids and turbidity to the ratio of the brightness of say red/green from a color photo. This ratio is also effected by the skylight reflection and changes from day to day although the waste concentration may not (2, 4). The skylight reflection problem is presently being investigated by John Van Domelen at the University of Wisconsin.

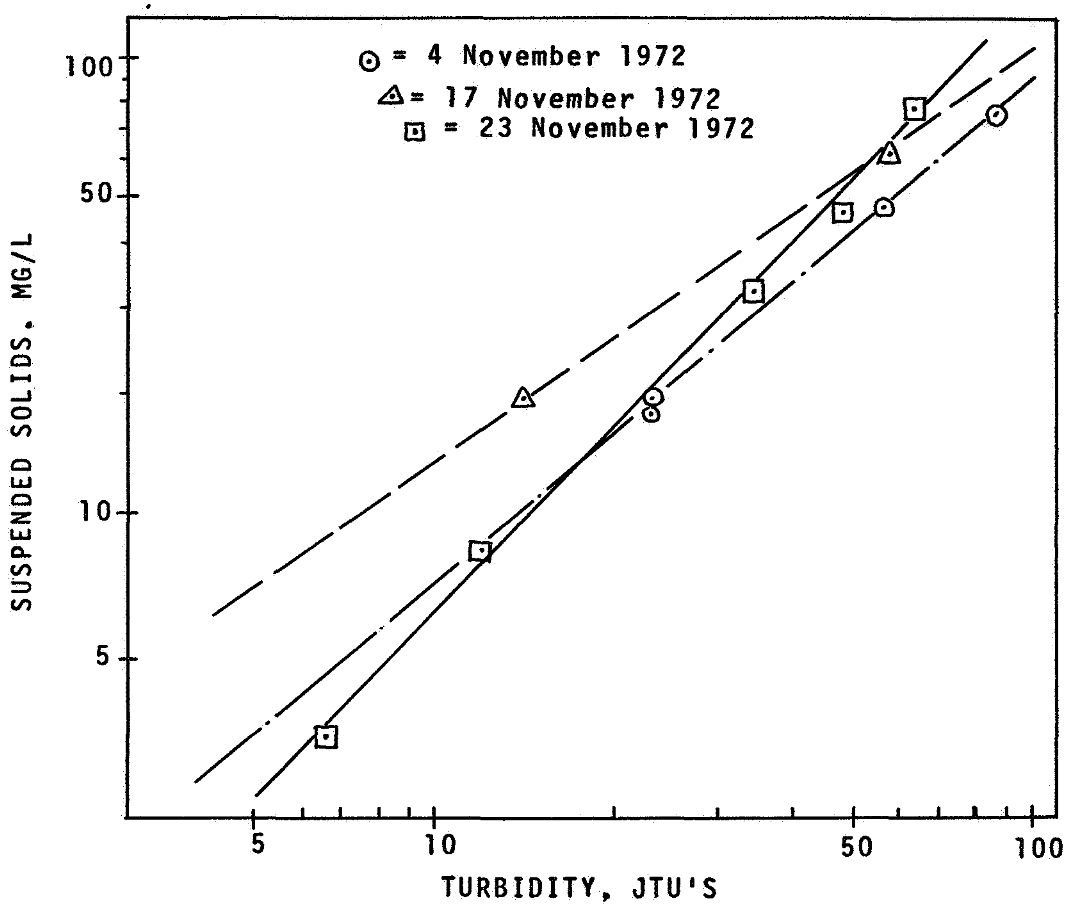

Figure 7. Plot of Suspended Solids versus Turbidity for all of the water samples collected in dirty water in Lake Superior near Duluth in November 1972.

CORRELATION TO ERTS IMAGERY

The only difference between correlating between water quality and a low altitude photo, and between water quality and a satellite image is the atmosphere in between. Also whereas the low altitude photo can be taken under conditions varying between clear to completely overcast, a usable ERTS image only occurs on a relatively clear day. The skylight reflection (C) in Figure 5 from above the satellite is a constant so the only variable from day to day is the path luminance (B) in Figure 5.

In the upper portion of the full ERTS frame shown in Figure 1 lies the city of Ely, Minnesota. The U. S. Forest Service is interested in classifying the lakes in this area as to various stages of lake enrichment or eutrophication. Consequently water samples were gathered from three lakes in the area: from a very clear lake, an enriched lake, and one partially enriched. These water samples were analyzed for reflectance and transmittance and for turbidity and suspended solids. The brightness of the lakes as they appeared on the ERTS image was analyzed on the microdensitometer. In Figure 8 the percent reflectance from the lab and the ERTS image are plotted against turbidity and suspended solids. One will again note the same characteristic curve as in Figure 4 with the ERTS image data higher than the lab curve. There is again a good correlation between image brightness and turbidity and suspended solids and also with the Forest Services Eutrophication Classification. The turbidity and the solids that cause it in this case are caused by algea which in turn are caused by the nutrient enrichment which varies from lake to lake. The types of algea also vary from lake to lake. Green algea live in lakes with high concentrations of dissolved oxygen while blue algea are often most prevalent in lakes where there is little oxygen. A wavelength ratio analysis of aerial images might well also indicate the predominant type of algea. This is an area which needs more research.

The curves in Figure 8 appear impressive but the water samples were not collected simultaneous with the ERTS overflight in this case. There was almost a year between the image and the sampling; some water samples simultaneous with ERTS overflight are needed for positive correlation between the water and the satellite.

Professor Sydor and his students at the University of Minnesota, Duluth, were able to collect water samples of the muddy Lake Superior water simultaneous with ERTS overpasses on four days in the summer of 1973. These images were very valuable in their work of ascertaining the current patterns in Lake Superior near Duluth.

These water samples were analyzed for suspended solids and turbidity. The resulting ERTS images were analyzed on an image density slicer at the University of Minnesota and the density values at the sample points were compared to the density of the step wedge on the image. The resulting exposing brightness was then compared to the percent of maximum exposing brightness using the internal calibration of the ERTS camera. These resulting values can then be compared to percent reflectance obtained in the lab and from the low altitude photos. Additional water samples were analyzed at the University of Wisconsin for corresponding volume reflectance values. Figure 9 shows the resulting reflectance obtained from the ERTS image on the four days compared

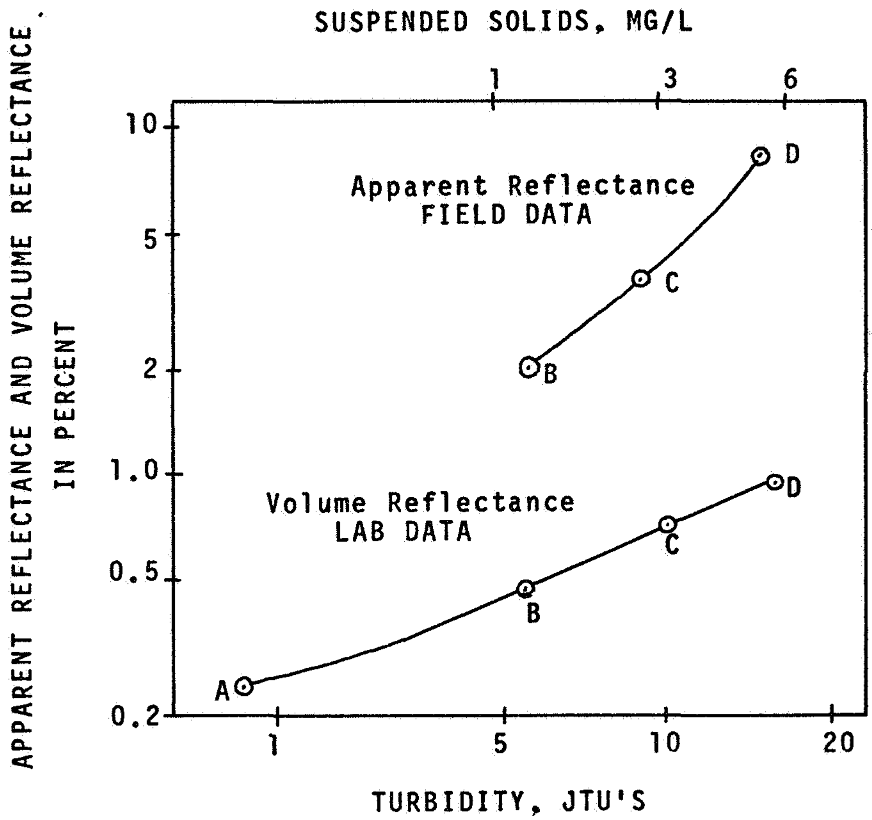

Figure 8. Volume Reflectance from analyzing water samples in the lab and apparent reflectance from ERTS imagery plotted against turbidity and suspended solids. The three lakes analyzed are classified in three different stages of enrichment or Eutrophication as follows:

Sample	Lake	U. S. Forest Service Classification
A	Distilled Water	NA
B	Snowbank Lake	Oligotrophic (clear)
C	Ensign Lake	Mesotrophic (Middle Stage)
D	Shagawa Lake	Eutrophic (enriched)

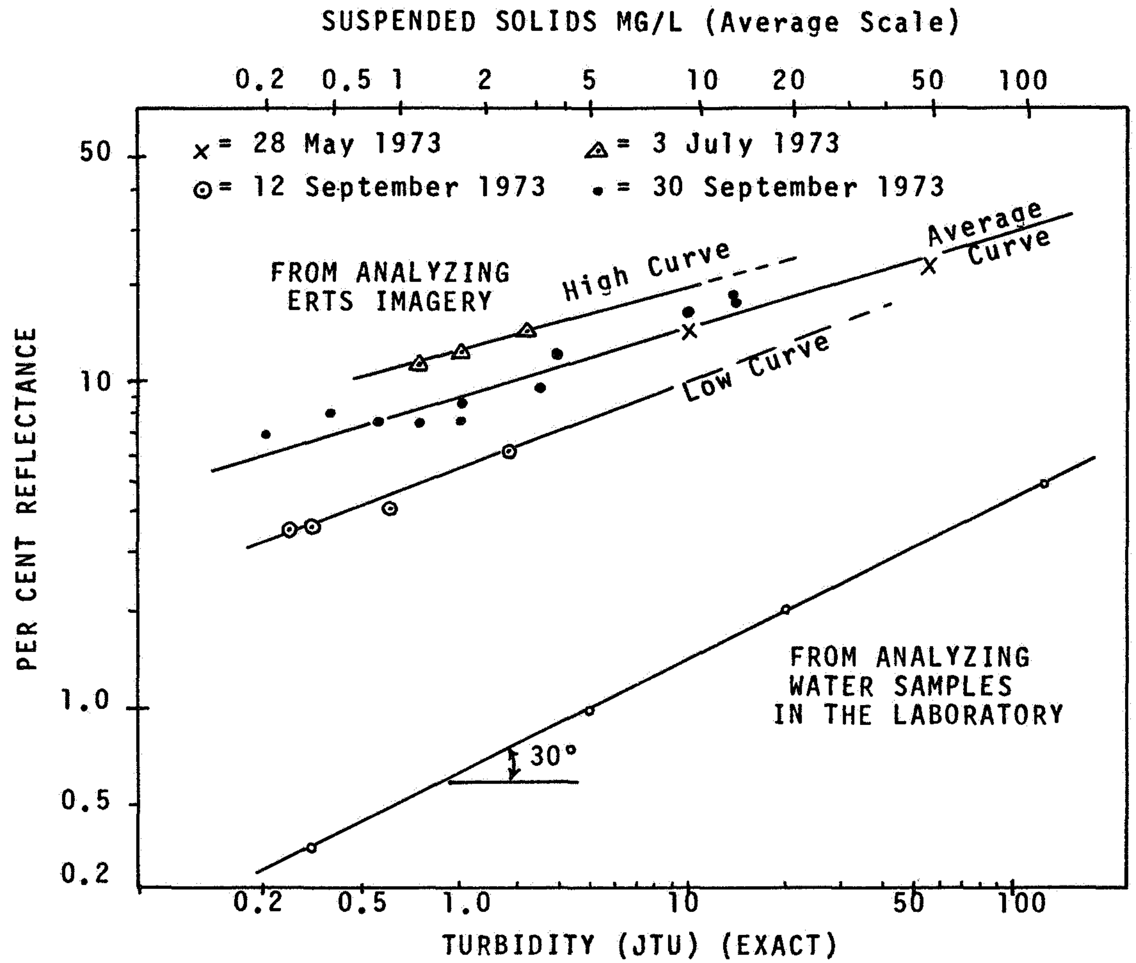

Figure 9. Volume Reflectance from laboratory analysis and Apparent Reflectance from ERTS Imagery for the water in Lake Superior near Duluth, Minnesota

to the lab volume reflectance. It is obvious from the curve that although all four days were clear there is some difference in path luminance for the different days. The third of July appears to have been a hazy day. Nevertheless an average curve for the four days establishes the variation of reflectance with turbidity and thus it can be used to find the relative turbidity in the area for any ERTS image, and the absolute turbidity if but one in situ measurement is available to establish the vertical position of the curve for that particular day. Figure 10 shows a suspended solids contour map made by using the average curve from Figure 9 and two in situ turbidity and suspended solids measurements taken at the time of this ERTS overflight. Both samples agree with the average curve. Expected errors in values of turbidity or solids due to deviation of any point from the established curve for a particular day is perhaps no more than 10 to 20% (See Figure 9). This is about comparable to errors expected in water sample gathering and analysis techniques. A map showing concentration of turbidity would appear quite similar to the map for suspended solids shown in Figure 10. The argument can be made that the image brightness exactly correlates to turbidity only and that suspended solids measurements may be in error up to about 30% due to various relationships between turbidity and suspended solids (See Figure 7). This is true but when one notes that the drinking water standards for maximum turbidity are 5 (JTU) and that the water intake in Lake Superior (Figure 1) was obtaining water for drinking with turbidity of as high as 100 (JTU) the design of the intake can be said to be in error by over 20 times or 2000%. If conventional engineering design can be off by 2000%, and if ERTS images are accurate to ±20% or 30%, then it is obvious that aerial remote sensing can greatly improve present engineering performance. It is time that aerial remote sensing is used as a valuable tool for water quality investigations.

ACKNOWLEDGEMENTS

The authors gratefully acknowledge the following: the City of Cloquet, Minnesota for their assistance in field data acquisition and analysis, to NASA Grant No. NGL 50-002-127 for Multidisciplinary Research in Remote Sensing at the University of Wisconsin, Madison, and to NASA Grant No. NGL 24-005-263 for Remote Sensing Research at the University of Minnesota, Duluth; to Army Corps of Engineers Grant No. DACW-37-74-C-0014; to Dr. Kenneth Holtje and the U.S. Forest Service for their support in gathering field data near Ely, Minnesota; to Mr. Kirby Stortz; Wayne Maanum and Professors Merle Meyer and Dwight Brown from the University of Minnesota at Minneapolis for use of their apparatus; to Professor James L. Clapp and staff at the University of Wisconsin Institute for Environmental Studies for administrative assistance and to Steven Klooster for his contributions toward workable instrumentation and procedures; to Bill Johnson for his contributions to water analysis; and to all others who contributed their talents and efforts on this project.

the reflection of the skylight, or clouds in this case. The lab results show no reflection of clouds so these values are lower. When one looks into a store window he sees not only what is in the showcase but also his own face or perhaps a street light reflecting back at him. So it is with the sun, sky and clouds from the surface of a water body. It was concluded that this shift between the lab curve and the field curve was primarily caused by skylight reflection from the surface of the water and atmospheric scatter which is also called path luminance.

Figure 5 shows a sketch of the interaction of light with water. The volume reflectance of Figure 4 which correlates to turbidity and suspended solids in just the part (D) in Figure 5. The aerial image also shows, (A) the reflection of the sun. This can be avoided however, by correctly pointing the camera or using that part of the image which does not contain the sun glitter. Some energy (E) can penetrate to the bottom of the water body and return to the camera. These are unwanted bottom effects. About 99% of the energy reaching the camera comes from above the depth of the Secchi disc reading* (3). Therefore, bottom effects can be eliminated by assuring that Secchi disc readings are less than the depth to bottom in the area under investigation or working with longer IR wavelengths which penetrate only a few inches into the water.

Atmospheric scatter or path luminance (B in Figure 5) and that energy from the sky which reflects from the air-water interface (C) are always present on an aerial photo and causes the shift between the aerial image data and the lab data as shown in Figure 4. As long as the sky is uniformly clear or overcast the value of skylight reflection (C) is uniform and can be uniformly subtracted out.

The muddy water collected on 4 November 1972 and caused by the storm two days prior, remained in the SW end of Lake Superior for over 3 weeks. On 17 November 1972, samples and aerial photos were again taken, and again on 23 November 1972. Lab analysis of the water samples and photo analysis were repeated on these dates similar to what was done to the data from 4 November 1972.

When the data from these three days were combined it was only the water quality parameter of turbidity that completely correlated to volume reflectance for all days. Figure 6 shows the plot of volume reflectance versus turbidity for these three days. Since the Secchi disc reading is just a crude field method of obtaining turbidity, reflectance also plots well against the Secchi disc reading for these three days and this is also shown in Figure 6. The plot of reflectance

*The Secchi disc is a white disc that is lowered into the water until it is no longer visible. This depth is known as the Secchi disc reading.

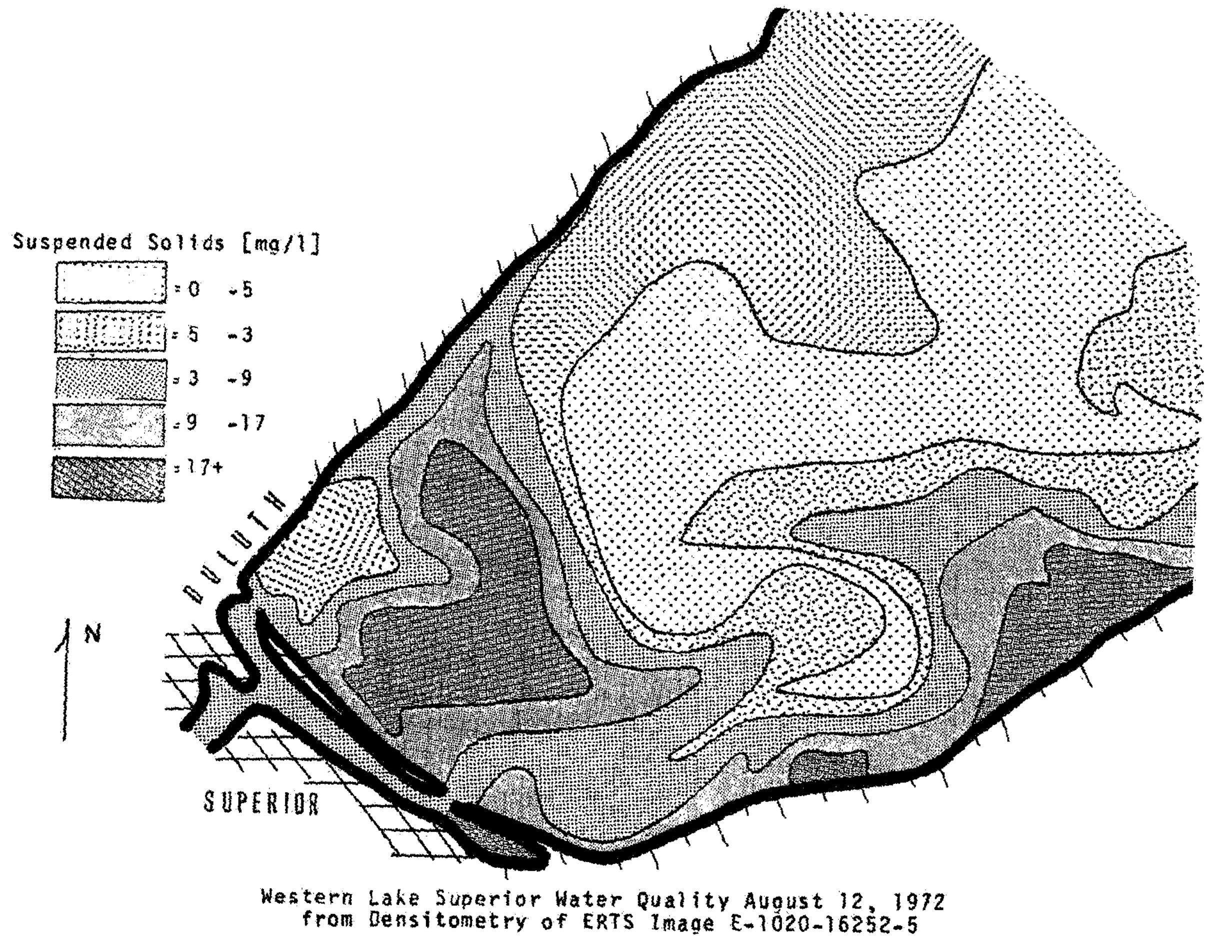

Figure 10. Contour lines of equal suspended solids obtained from analyzing the brightness of the ERTS image from Figure 1 and using the curve shown in Figure 9. An almost identical contour map results for Turbidity.

REFERENCES

1. Klooster, Steven A., and Scherz, James P., "Water Quality Determination by Photographic Analysis," Report No. 21, Institute for Environmental Studies Remote Sensing Program, Department of Civil and Environmental Engineering, University of Wisconsin, Madison, Wisconsin, August, 1973. Also Proceedings of 2nd Annual Conference on Remote Sensing of Earth Resources, March 26-28, 1973, at University of Tennessee Space Institute, Tullahoma, Tennessee.

2. Piech, Kenneth R., and Walker, J. E., "Photographic Analysis of Water Resource Color and Quality," Proceedings, 37th Meeting of American Society of Photogrammetry, Washington, D. C., March 1971.

3. Scherz, James P., "Development of a Practical Remote Sensing Water Quality Monitoring System." Proceedings, 8th International Symposium on Remote Sensing of Environment, Ann Arbor, Michigan, October, 1972.

4. Scherz, James P., Klooster, Steven A., and Van Domelen, John F., "Aerial and Satellite Photography-A Valuable Tool for Water Quality Investigation." Proceedings, ASP-ACSM 1973 Fall Convention, Walt Disney World, Orlando, Florida, October 2-5, 1973.

5. Scherz, James P. and Van Domelen, John F., "Lake Superior Water Quality Near Duluth from Analysis of Aerial Photos and ERTS Imagery." Proceedings, International Symposium on Remote Sensing and Water Resources Management, June, 11-14, 1973, Burlington, Ontario, Canada.

6. Standard Methods for Examination of Water and Waste-water, 13th Edition, Turbidity, pp. 349-355, American Public Health Association, 1015 Eighteenth St., N. W., Washington, D. C.

Paper E 10

QUANTITATIVE WATER QUALITY WITH ERS-1*

Harold L. Yarger, James R. McCauley, Gerard W. James and Larry M. Magnuson, *Kansas Geological Survey, University of Kansas, Lawrence, Kansas 66044;* and G. Richard Marzolf, *Division of Biology, Kansas State University, Manhattan, Kansas 66502*

1.0 ABSTRACT

Analyses of ERTS-1 MSS computer compatible tapes of reservoir scenes in Kansas along with ground truth show that MSS bands and band ratios can be used for reliable prediction of suspended loads up to at least 900 ppm.

The major reservoirs in Kansas, as well as in other Great Plains states, are playing increasingly important roles in flood control, recreation, agriculture, and urban water supply. Satellite imagery is proving useful for acquiring timely low cost water quality data required for optimum management of these fresh water resources.

2.0 INTRODUCTION

The dominant limnological feature of the Great Plains today takes the form of reservoirs constructed by the U.S. Army Corps of Engineers and the U.S. Bureau of Reclamation. The primary influence on the reservoir ecosystem is the suspended material and chemicals carried in by streams and rivers. The authors are studying ERTS images of Kansas reservoirs to determine the feasibility of monitoring these water quality indicators by satellite. The reservoirs throughout the state (Figure 1) which should be representative of most Great Plains reservoirs, are located in a variety of physiographic regions such as the glaciated region in the northeast, the valleys and scarps in the southeast, the dissected plateau and alluvial plains areas in central Kansas, and the high plains in the west.

Two reservoirs, Perry and Tuttle Creek, have been singled out for close study. Approximately ten water samples from each reservoir are collected during each cloud-free ERTS overpass and analyzed for concentrations of inorganic suspended and dissolved solids, organic suspended and dissolved solids, chlorophyll, potassium, phosphate, and nitrate ions. In addition, secchi disc and temperature measurements are taken at each sampling station. The two reservoirs are distinct in terms of adjacent outcropping rocks and land use. Perry drains

*Work supported, in part, by NASA contract NAS5-21822

a recently glaciated region in the cornbelt of eastern Kansas. Tuttle Creek drains the Flint Hills area to the west which is outcropping Cretaceous and Permian rock. The dominant land use is seasonal grazing and small grains. A later phase of this project will be to test any predictive relations derived from Perry and Tuttle Creek on other reservoirs in Kansas.

Kansas reservoirs are typically shallow and thus are susceptible to mixing by strong winds which are a characteristic climatic feature of this region. Wind generated currents are of sufficently high velocity to maintain a sizable fraction of the silts and clays in suspension and the result is turbid water (mean light extinction coefficient $\sim$2.5 meters^{-1}). Accordingly, reflected energy detected by ERTS is primarily influenced by the suspended load (the predominant fraction of which is inorganic material).

Figure 2 summarizes imagery and ground truth acquisitions for Perry and Tuttle Creek reservoirs during the first 25 ERTS passes over the state of Kansas, which covers the period July 25, 1972 to Oct. 2, 1973.

Water samples were collected for 16 of the 23 cloud free reservoir passes. Conditions such as ice cover, high wind and mechanical failure prevented sample collection for the remaining 7 cloud free passes. This report is based primarily on the analysis of computer compatible tapes CCT's) from 11 reservoir passes with ground truth which includes sun angles above the Horizon of 25° to 62° (Figure 3). Qualitative analyses of ERTS-1 9.5" positive transparencies appear in earlier presentations (Yarger, 1972 and 1973).

3.0 Sun Angle Effects

The multispectral scanner (MSS) in ERTS records light reflected from a scene illuminated by an admixture of sunlight and skylight (Figure 4). On relatively clear days the spectral shape of the illumination remains fairly constant throughout the year. However, the intensity, angle of incidence, and path length through the atmosphere depend on sun angle (angle above horizon). The reflectance levels from the concrete dam at Tuttle Creek Reservoir, a target with constant spectral reflectance, demonstrate a strong sun angle dependence in all MSS bands (Figure 5). As has been suggested by Vincent (1972), the sun angle dependence is suppressed by plotting band ratios instead of absolute levels (Figure 6). The three other possible ratios, not plotted in figure 6, also show a flat response to change in sun angle. Ratioing essentially removes the effect of unequal illuminating intensities caused by the continuously changing sun angle from one ERTS pass to the next. Since the ratio curves for the dam are flat, the angle of incidence and atmospheric scattering of

reflected light are not important factors, at least for a concrete target.

Water reflectance levels do not exhibit as strong a dependence on sun angle, but there is a significant measureable effect (see Figure 7 for band 5 example). As for concrete, the absolute, reflectance levels for water decrease with lower sun angle. In addition, the correlation (or slope) between reflectance level and suspended solids, in the range 0-90 ppm, appears to depend on sun angle. On the other hand, the magnitudes of MSS5/MSS4 ratios are indistinguishable for the three different sun angle passes (Figure 8). The slopes (ratio vs. suspended solids) for the two low sun angle passes remain fairly flat. A dark object subtraction on each band before ratioing, as suggested by Vincent (1972), does not significantly change the slopes of the three passes. Dark object subtraction, which is the absolute level detected by ERTS minus level of darkest object in scene, should suppress atmospheric scattering effects present in the ratios. These results indicate that the slope dependence on sun angle is probably not due to atmospheric scattering. It is perhaps due to water column reflectance dependence on illuminator angle of incidence.

There were no obvious anomalous conditions during the low sun angle passes such as high wind or chemical concentration. Lower temperatures should not significantly effect water volume reflectance (Scherz, 1971). Reflectance levels from the 8 passes with sun angle $\gtrsim 45°$ exhibit much weaker dependence on sun angle, but ratioing neverless improves correlation with suspended load, particularly for bands 4 and 5. The 3 passes with sun angle $\lesssim 40°$ exhibit lower correlation with suspended load, but the suspended load range 20 to 60 ppm is small compared to the range 0 to 900 ppm for all the data. More points at higher suspended load and low sun angle are needed to statistically confirm a band ratio-suspended solids correlation dependence on sun angle. For the remaining discussion it is assumed that, after ratioing, sun angle dependence is relatively unimportant.

4.0 CCT Correlations with Ground Truth

Digital levels for each water sample were extracted from the CCT by locating the sample station coordinates on a CCT generated gray level map, then averaging 9 pixels centered around the coordinate which corresponds to a 240 x 240 meter square area on the water surface.

Band 4 shows no correlation beyond $\sim$50 ppm and is useful only for relatively clear water (Figure 9). This green band penetrates the water column more than the other bands (Figure 4), but as a consequence encounters a large amount of scattering material which

produces saturation or maximum scattering at levels $\gtrsim$50 ppm. Band 5 is correlated with somewhat higher turbidites ($\lesssim$80 ppm) but its response to suspended load is quite similar to band 4 (Figure 10). Band 5 ratioed with band 4 (Figure 11) improves suspended load correlation and is roughly linear in the range of 0 to 80 ppm with RMS residual of 12 ppm (Figure 12). All regression analysis in this report was done with horizontal axis as the dependent variable and vertical axis as the independent variable.

Band 6 and the ratio band 6/band 4 display good correlation with suspended load over the entire range of 0 to 900 ppm (Figure 13 and 14). A smoothly varying polynomial fit yields an RMS residual of 31 ppm. A similar fit (not shown) to the non-ratioed curve in figure 13 yields an RMS residual of 48 ppm, so that a significantly better fit was achieved by ratioing. As is the MSS5/MSS4 ratio, the MSS6/ MSS4 is linearly related to suspended solids in the region $\leq$100 ppm. The response of band 7 (not shown) and band 7/band 4 (Figure 16) to suspended load is somewhat weaker than the other ~~bands but~~ is definitely correlated with accuracy level $\sim$50 ppm.

Figure 17 is an example of a suspended solids contour map of Tuttle Creek Reservoir (August 14,1972) which was produced using a correlation curve between band 5 and suspended solids. The curve (not shown) was derived from four high sun angle passes which yielded an RMS residual of 5 ppm.

Band ratio correlations with secchi depth (or maximum light penetration depth) are shown in figures 18, 19, and 20. The MSS5/MSS4 ratio is able to predict secchi depth (or water clarity) to within $\pm$ 20 cm. to at least a 1 meter depth, which is the limit of this investigation. The ratios MSS6/MSS4 and MSS7/MSS4 yield reliable results for the more turbid water conditions corresponding to secchi depth in the range 0 to 40 cm and 0 to 20 cm respectively.

A study of ratio curves for MSS6/MSS5, MSS7/MSS5, and MSS7/MSS6 (not shown) indicates that these ratios are not very useful for correlation with suspended load or secchi depth.

It appears that gray levels obtained from electronic slicing of 9.5" black and white ERTS images will yield similar quantitative correlation with suspended load with nearly the same accuracy. This part of the investigation is still underway.

Also underway is an attempt to look for any slight correlations with other water quality parameters such as chlorophyll and the algal nutrients. So far MSS5/MSS4 ratios show no obvious correlation with chlorophyll concentrations up to 10 μ g/liter.

5.0 Conclusions

Inorganic suspended load is the dominant influence on reservoir reflection levels. MSS band ratios derived from CCT's can be used for reliable prediction of suspended load up to 900 ppm during at least the high sun angle warmer months and perhaps the entire year (see discussion on sun angle). The ratio MSS5/MSS4 is useful in the range 0 to 80 ppm with accuracy on the order of 10 ppm. The ratios MSS6/MSS4 and MSS7/MSS4 are useful from 0 up to at least 900 ppm, which is the limit of this investigation, with accuracies of 30 ppm and 50 ppm respectively.

It is obvious that MSS band correlation with other water quality parameters such as chlorophyll and the algal nutrients will be slight if detectable at all. This part of the investigation is still underway.

References

1. Vincent, Robert K., "An ERTS Multispectral Scanner Experiment for Mapping Iron Compounds": Proceedings of the Eighth International Symposium on Remote Sensing of Environment, Ann Arbor, Michigan, Oct. 2-6, 1972, pp. 1239-1243.

2. Scherz, James P., "Monitoring Water Pollution by Remote Sensing": Journal of the Surveying and Mapping Division, ASCE, vol. 97, no. SU2, Proc. Paper 8550, Nov. 1971, pp. 307-320.

3. Yarger, H.L., et.al., "ERTS-1 Study of Reservoirs in Kansas": Proceedings of the Eighth International Symposium on Remote Sensing of Environment, Ann Arbor, Michigan, Oct. 2-6, 1972, pp. 1477-1490.

4. Yarger, Harold L. et., al., "Water Turbidity Detection Using ERTS-1 Imagery": Symposium on Significant Results Obtained from the Earth Resources Technology Satellite-1, Goddard Space Flight Center, March 5-9, 1973, pp. 651-658.

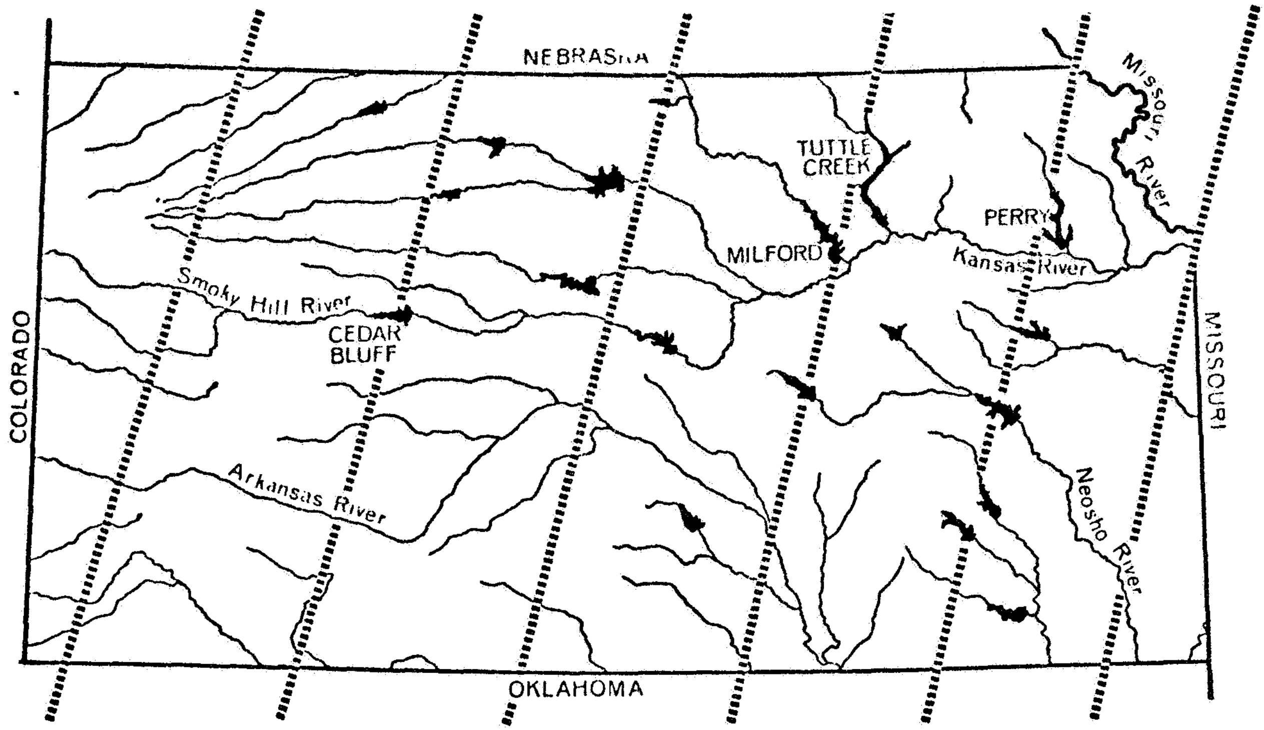

Figure 1. Reservoirs in Kansas

CATEGORY	PASSES	%
TOTAL RESERVOIR PASSES	50	100
CLOUD FREE PASSES	23	46
CLOUD FREE PASSES WITH GROUND TRUTH	16	32
CLOUD FREE PASSES WITH GROUND TRUTH AND IMAGERY	15	30
CLOUD FREE PASSES WITH GROUND TRUTH AND CCT'S	11	22

FIGURE 2. DATA ACQUISITION SUMMARY.

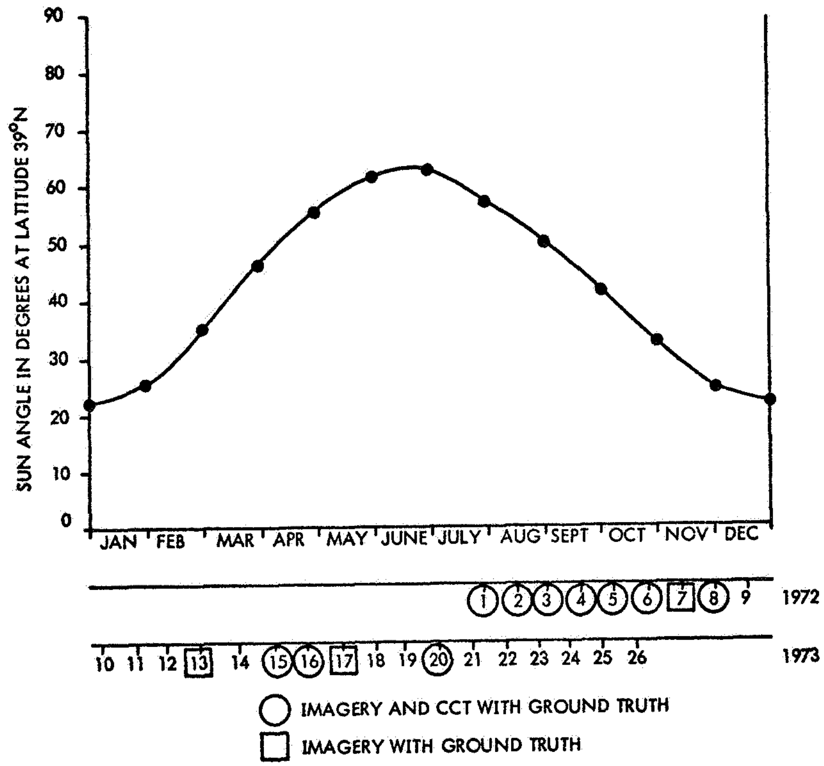

FIGURE 3. DATA ACQUISITION vs SUN ANGLE.

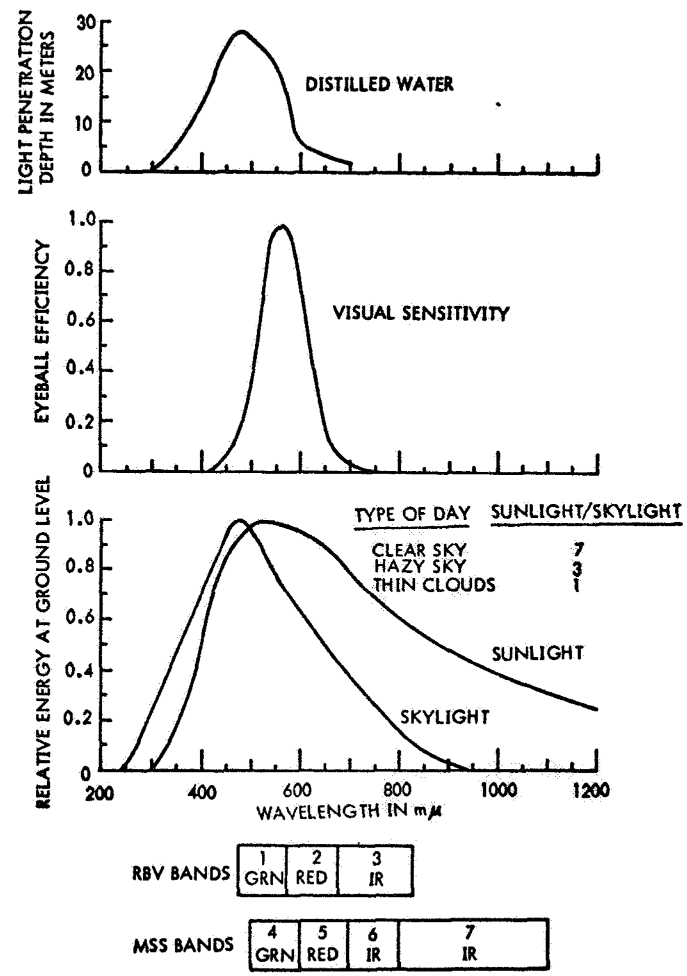

FIGURE 4. RADIANCE vs WAVELENGTH.

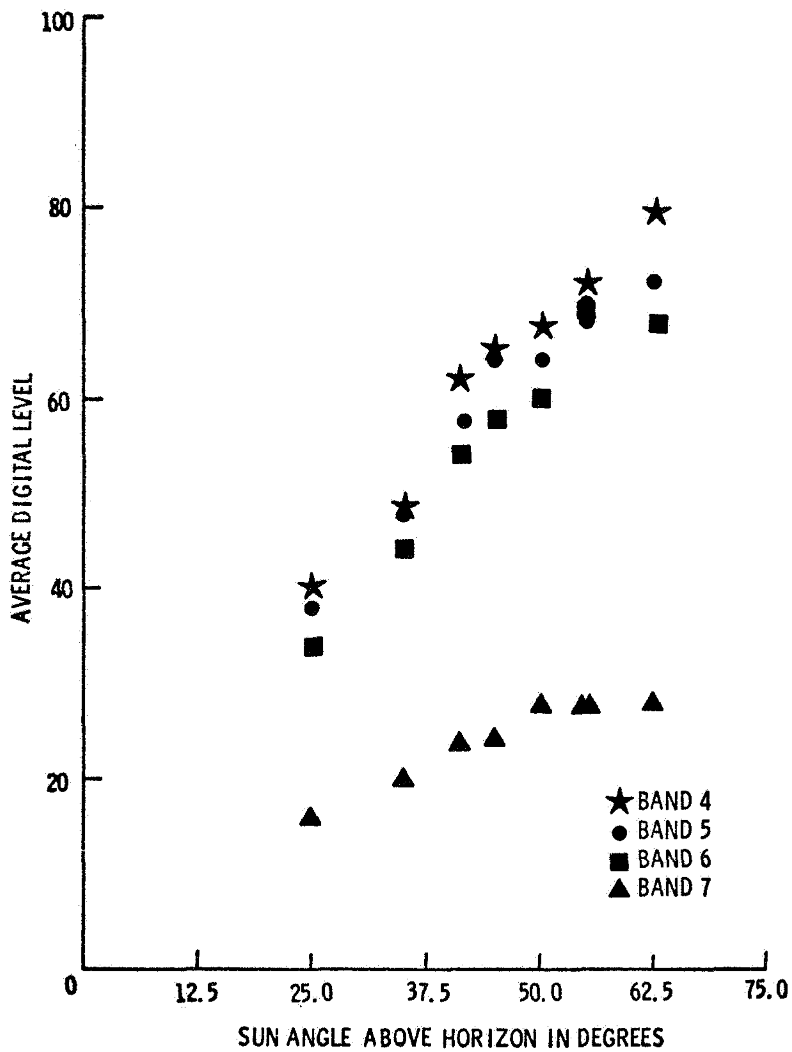

FIGURE 5. MSS DIGITAL LEVELS FROM CCT VS. SUN ANGLE FOR TUTTLE CREEK CONCRETE DAM.

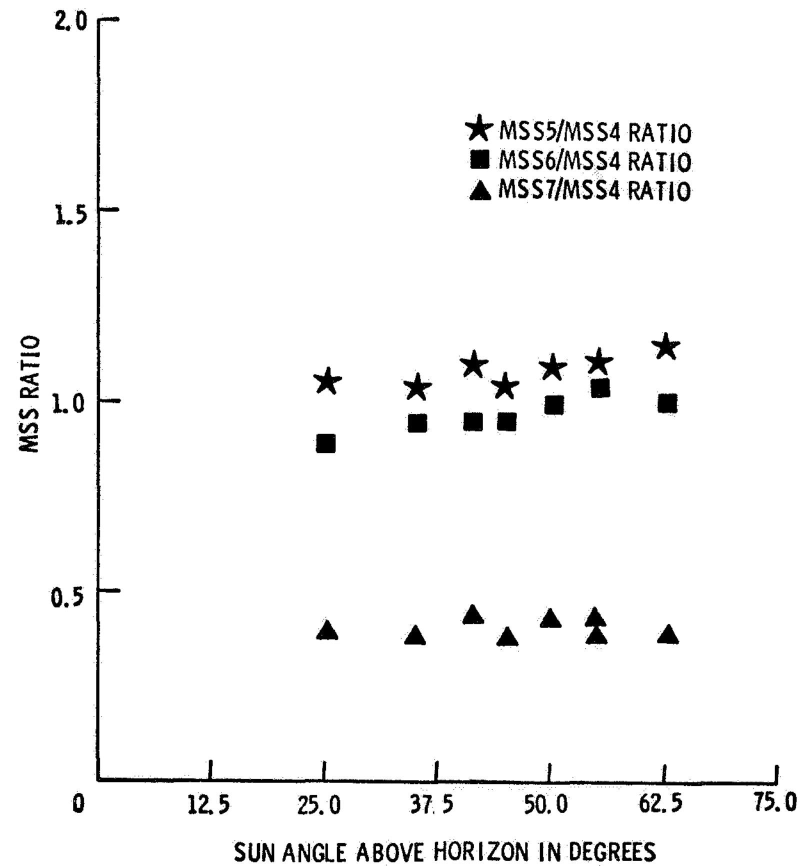

FIGURE 6. MSS BAND RATIOS FROM CCT VS. SUN ANGLE FOR TUTTLE CREEK CONCRETE DAM.

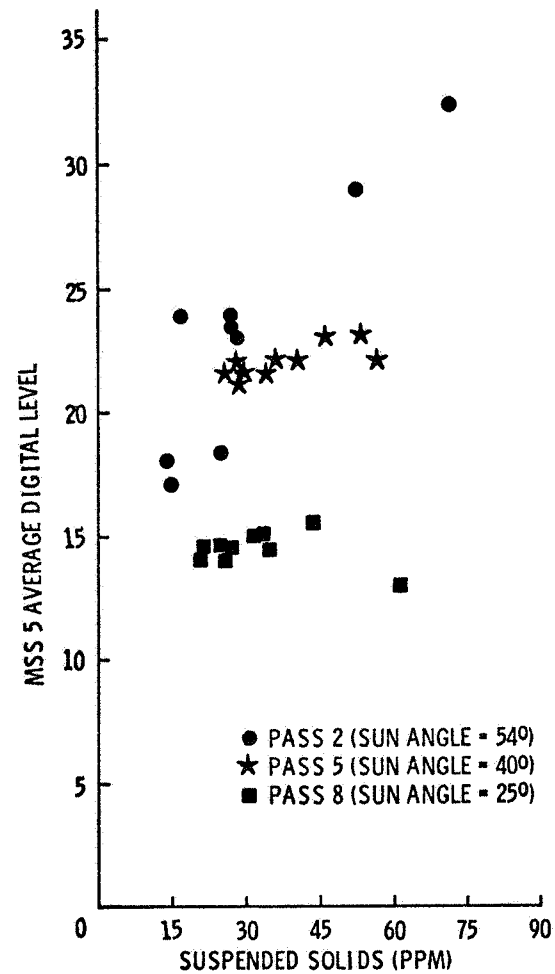

FIGURE 7. MSS5 DIGITAL LEVELS FROM CCT VS. SUSPENDED SOLIDS FOR 28 WATER SAMPLES FROM 3 ERTS-1 PASSES.

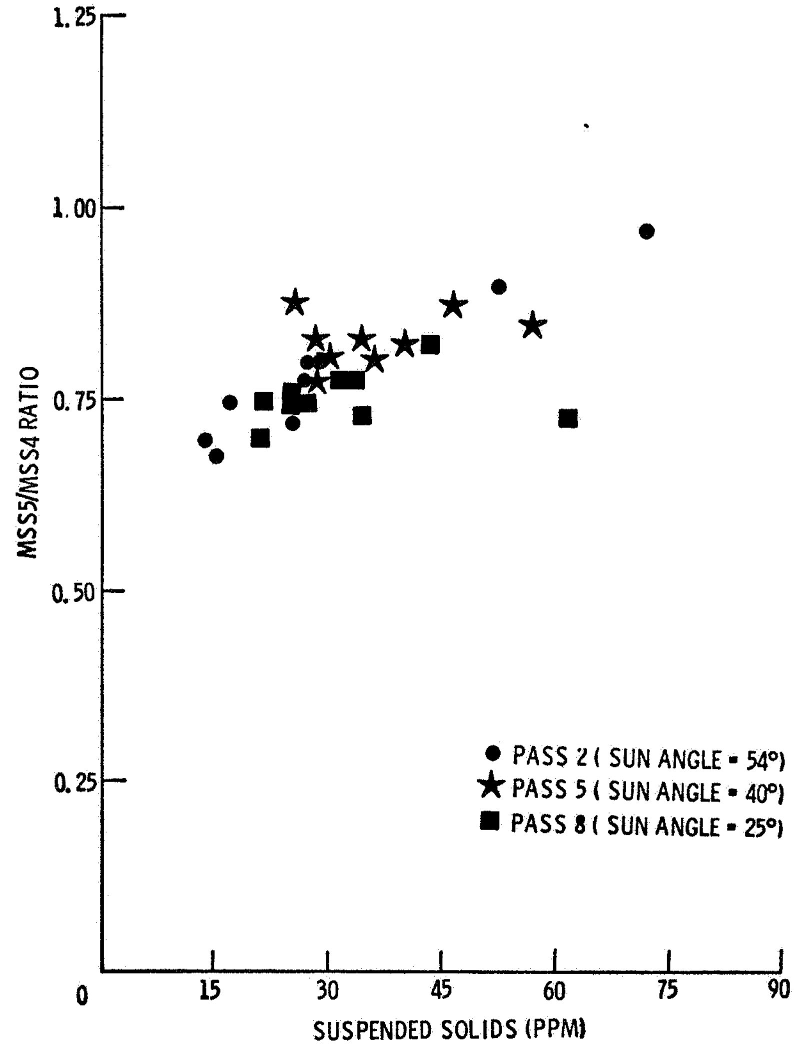

FIGURE 8. MSS5/MSS4 RATIO FROM CCT VS. SUSPENDED SOLIDS FOR 28 WATER SAMPLES FROM 3 ERTS-1 PASSES.

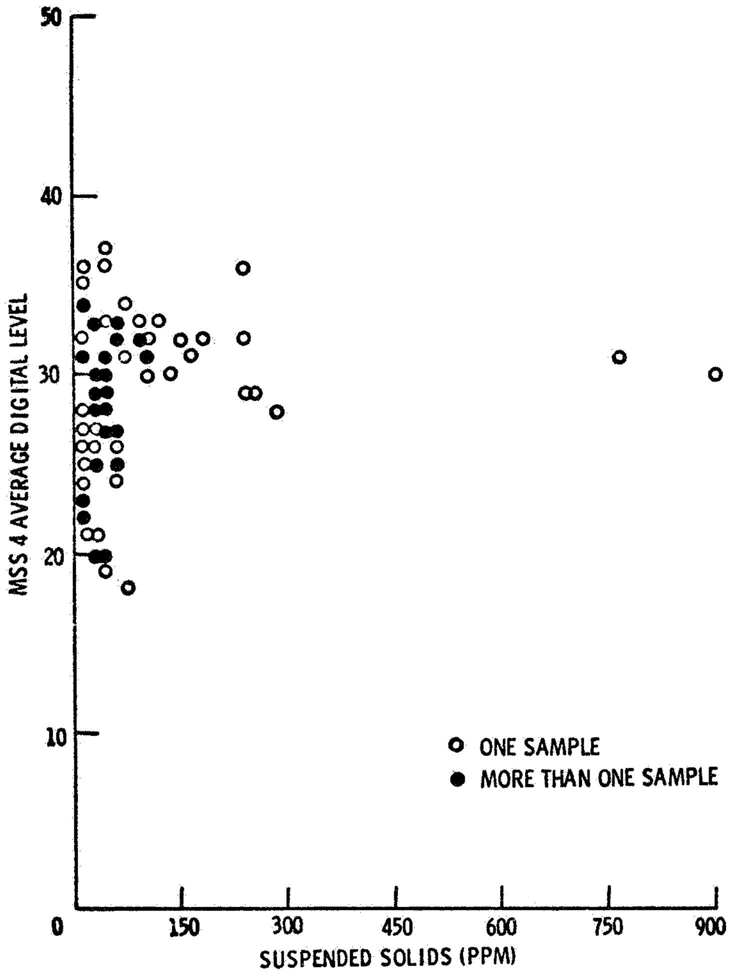

FIGURE 9. MSS 4 DIGITAL LEVEL FROM CCT VS. SUSPENDED SOLIDS FOR 108 WATER SAMPLES FROM 11 ERTS-1 PASSES.

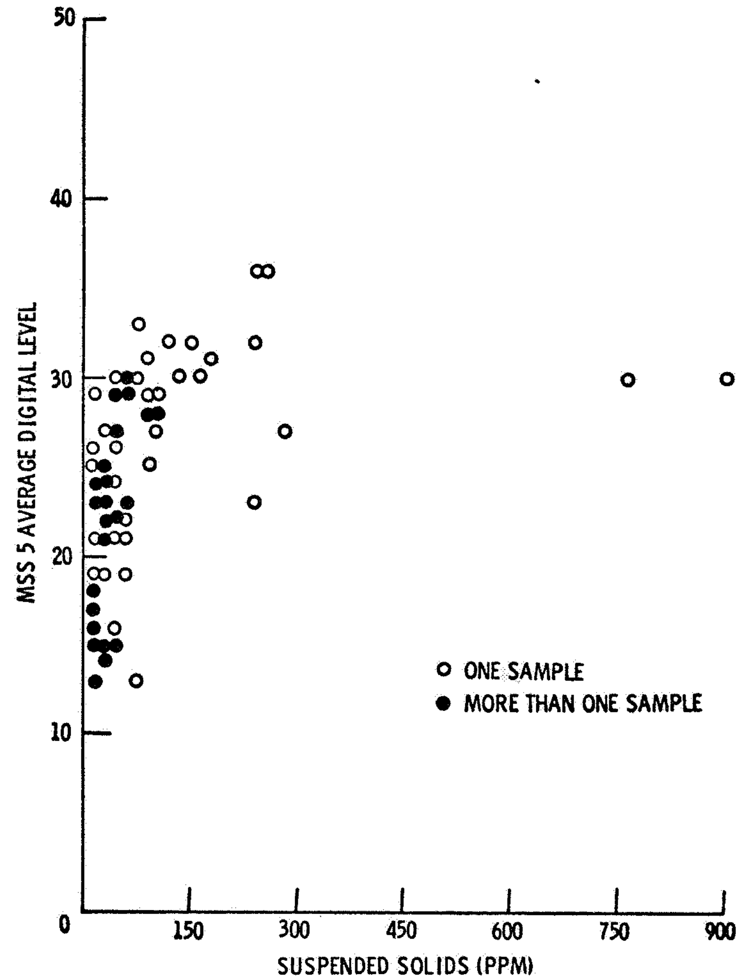

FIGURE 10. MSS 5 DIGITAL LEVEL FROM CCT VS. SUSPENDED SOLIDS FOR 108 WATER SAMPLES FROM 11 ERTS-1 PASSES.

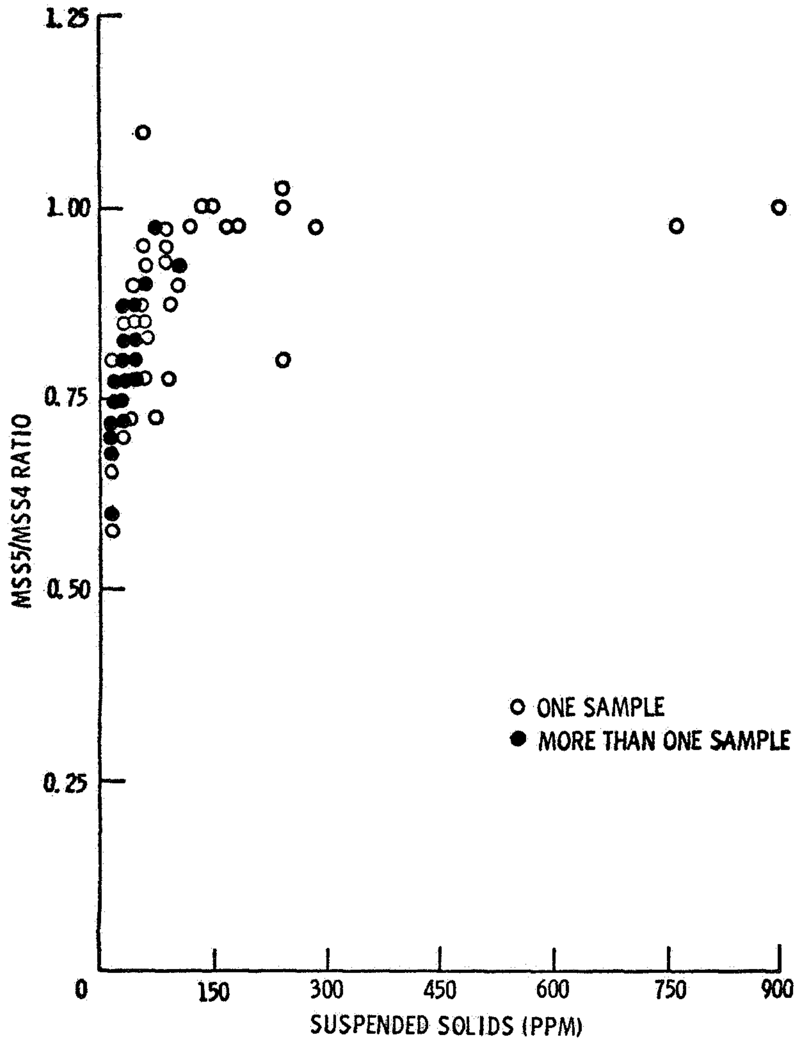

FIGURE 11. MSS5/MSS4 RATIO FROM CCT VS. SUSPENDED SOLIDS FOR 108 WATER SAMPLES FROM 11 ERTS-1 PASSES.

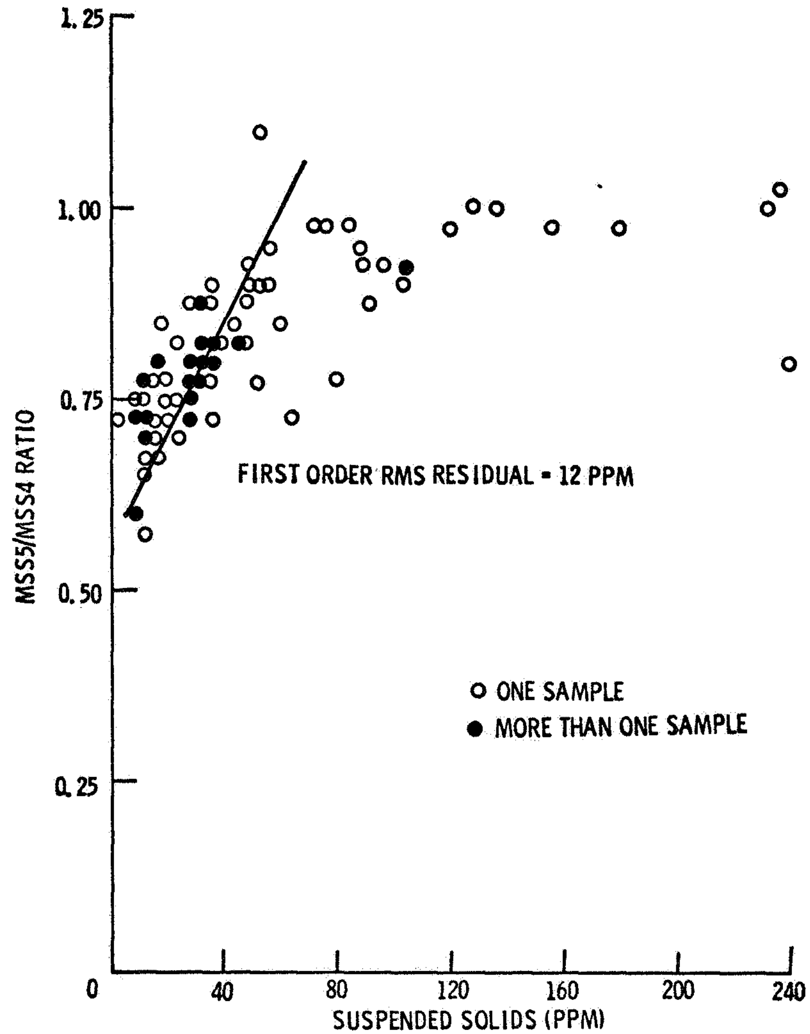

FIGURE 12. MSS5/MSS4 RATIO FROM CCT VS. SUSPENDED SOLIDS FOR 108 WATER SAMPLES FROM 11 ERTS-1 PASSES.

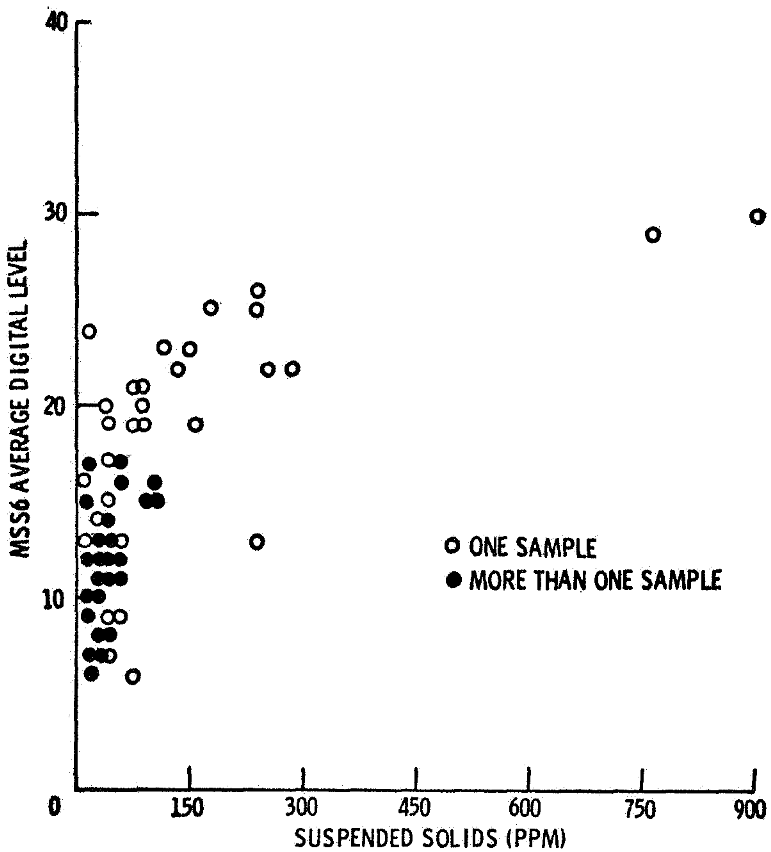

FIGURE 13. MSS6 DIGITAL LEVEL FROM CCT VS. SUSPENDED SOLIDS FOR 108 WATER SAMPLES FROM 11 ERTS-1 PASSES.

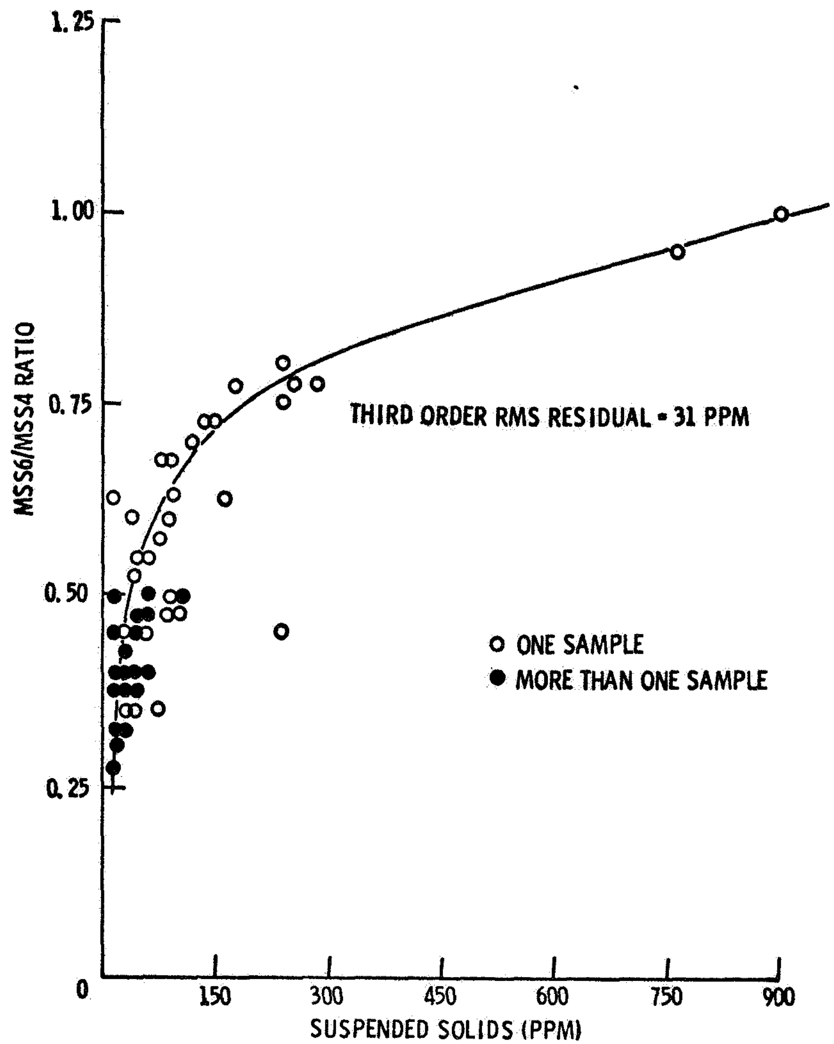

FIGURE 14. MSS6/MSS4 RATIO FROM CCT VS. SUSPENDED SOLIDS FOR 107 WATER SAMPLES FROM 11 ERTS-1 PASSES.

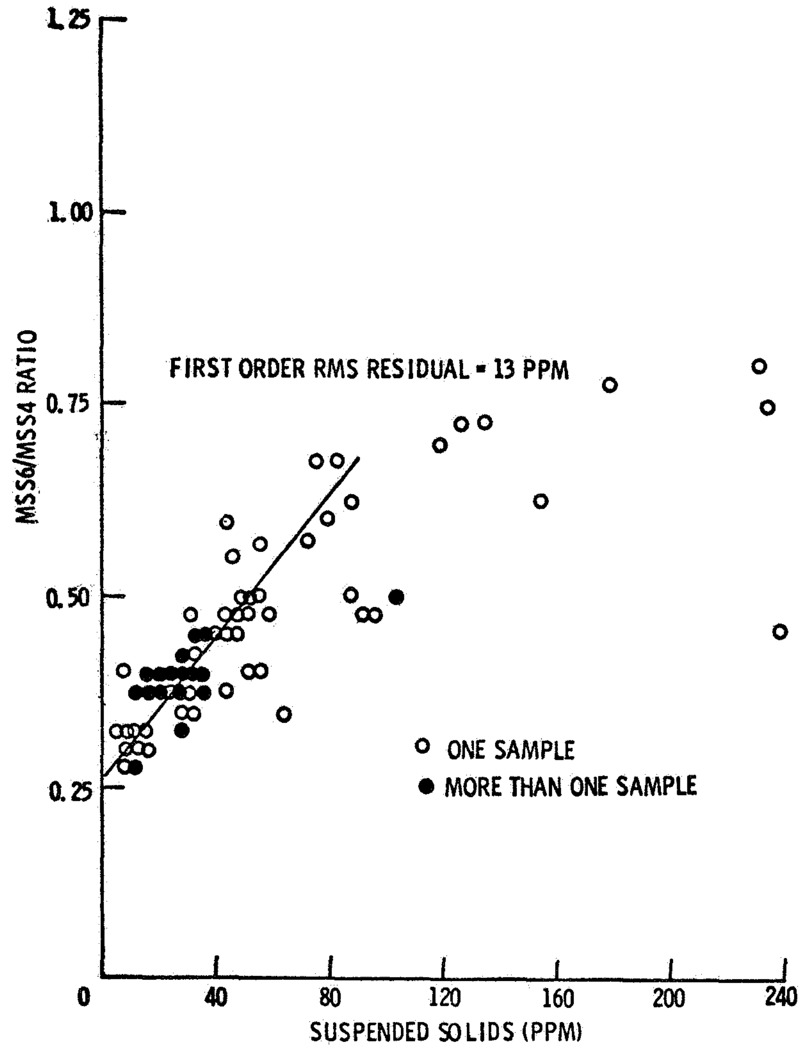

FIGURE 15. MSS6/MSS4 RATIO FROM CCT VS. SUSPENDED SOLIDS FOR 97 WATER SAMPLES FROM 10 ERTS-1 PASSES.

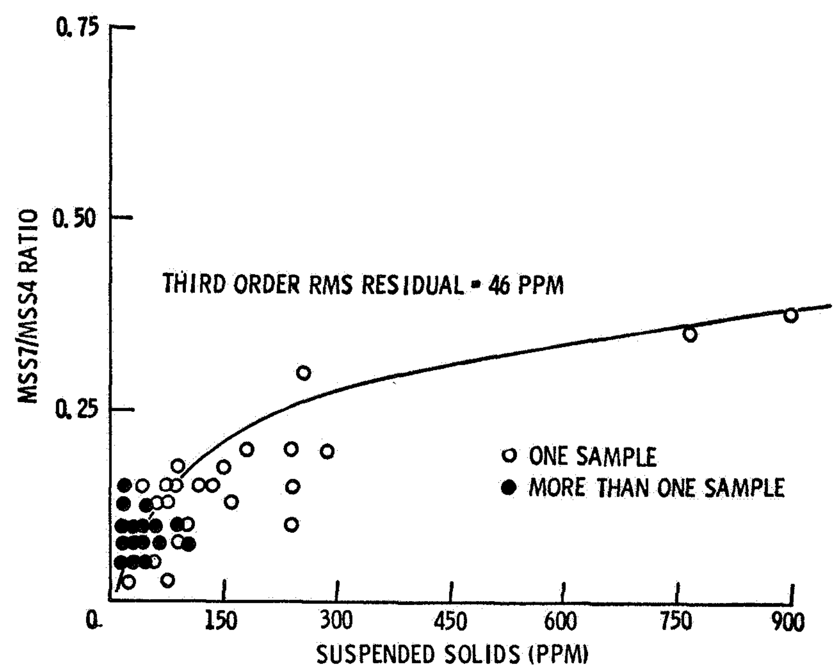

FIGURE 16. MSS7/MSS4 RATIO FROM CCT VS. SUSPENDED SOLIDS FOR 108 WATER SAMPLES FROM 11 ERTS-1 PASSES.

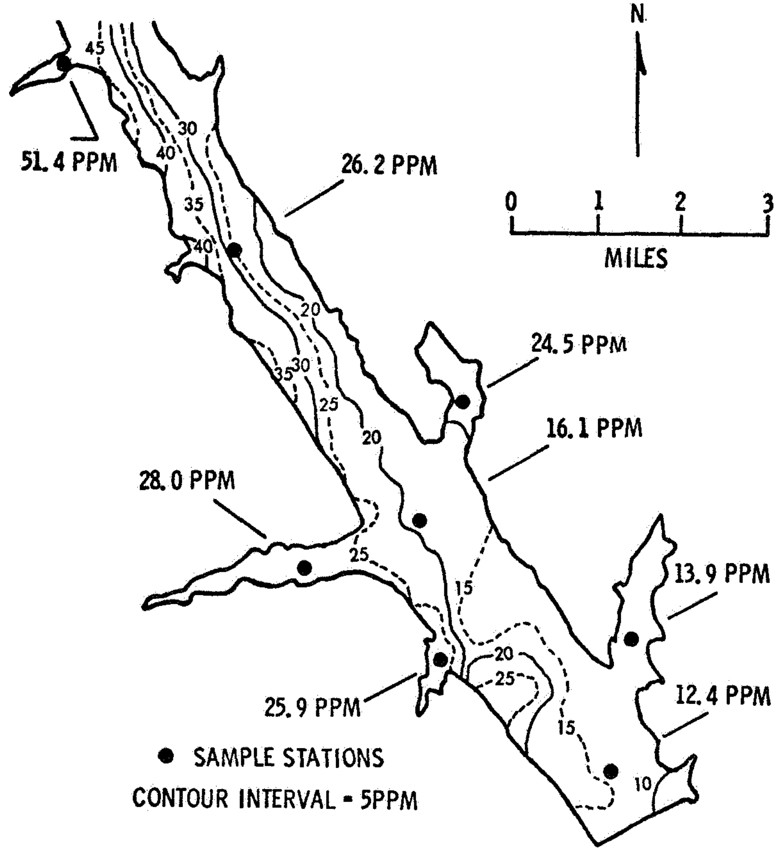

FIGURE 17. SUSPENDED SOLIDS CONTOUR MAP OF TUTTLE CREEK RESERVOIR (AUGUST 14, 1972 ERTS-1 ID NO. 1022-16391-5) DERIVED FROM CCTS (MSS 5) FOR 4 ERTS-1 PASSES.

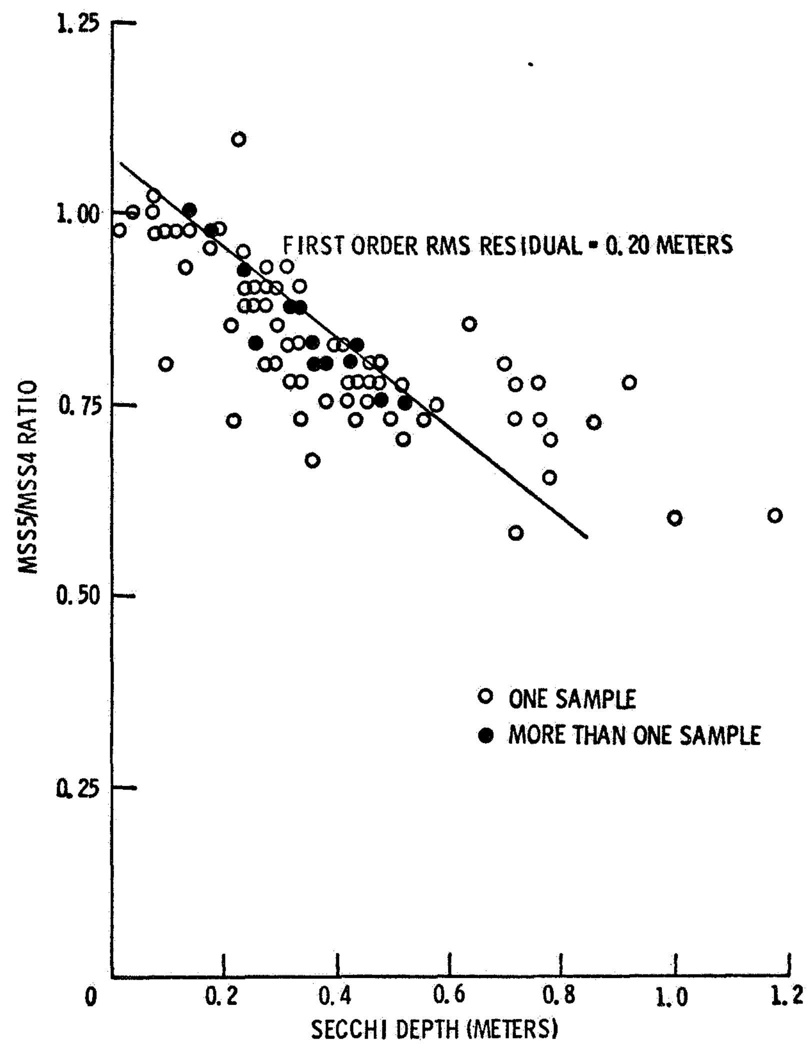

FIGURE 18. MSS5/MSS4 RATIO FROM CCT VS. SECCHI DEPTH FOR 97 SAMPLE STATIONS FROM 10 ERTS-1 PASSES.

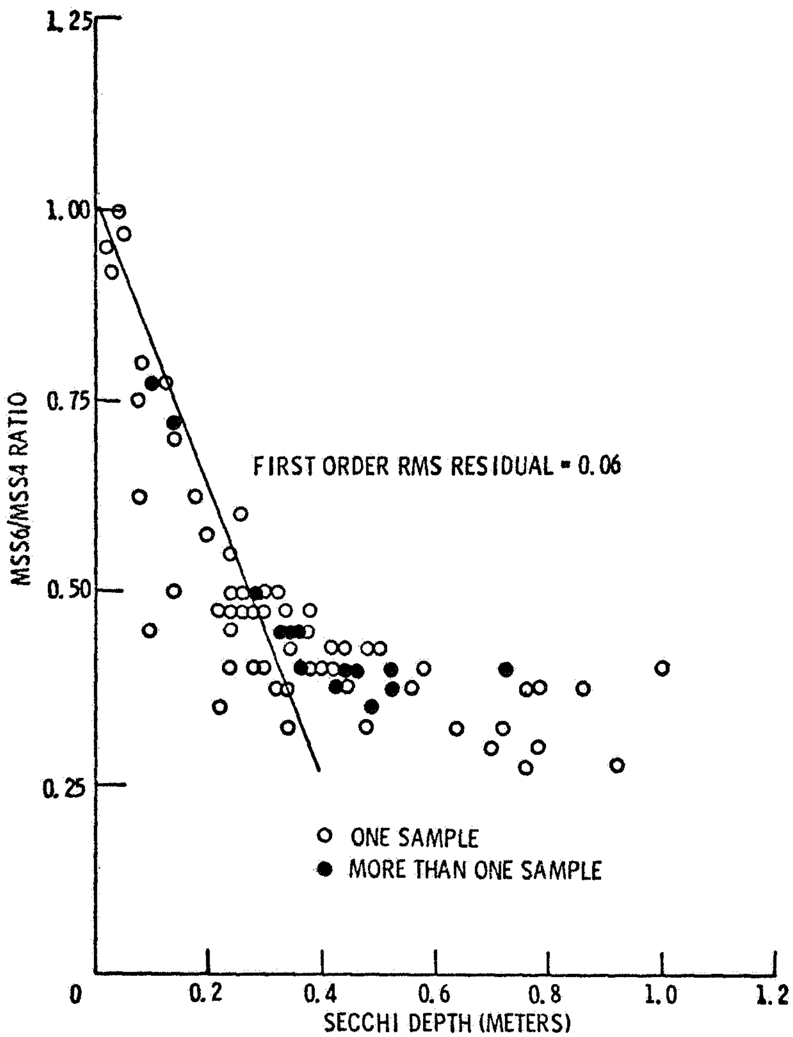

FIGURE 19. MSS6/MSS4 RATIO FROM CCT VS. SECCHI DEPTH FOR 96 SAMPLE STATIONS FROM 10 ERTS-1 PASSES.

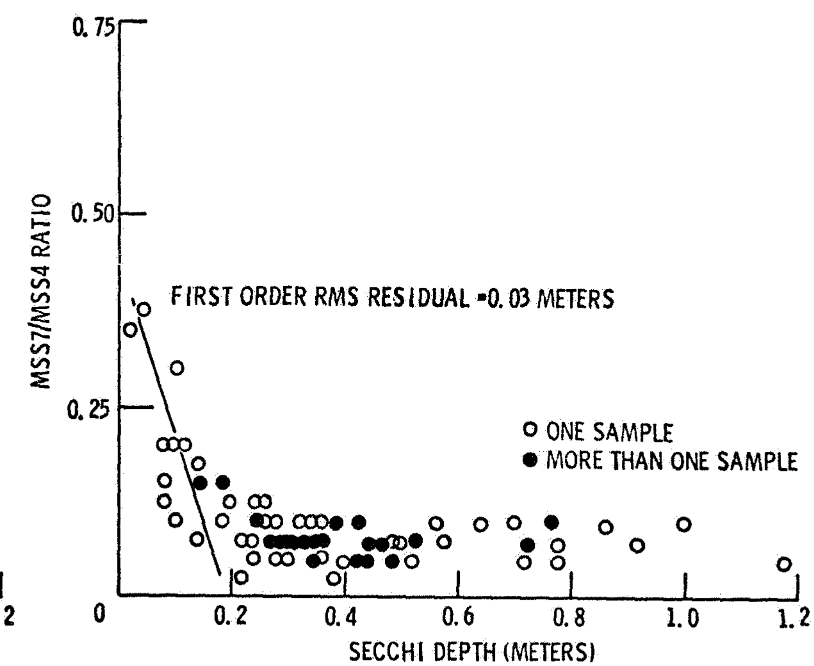

FIGURE 20. MSS7/MSS4 RATIO FROM CCT VS. SECCHI DEPTH FOR 97 SAMPLE STATIONS FROM 10 ERTS-1 PASSES.

Paper E 11

AN EVALUATION OF THE USE OF ERTS-1 SATELLITE IMAGERY FOR GRIZZLY BEAR HABITAT ANALYSIS

Joel R. Varney *(Philco-Ford Corp.)*, John J. Craighead and Jay S. Sumner, *Montana Cooperative Wildlife Research Unit, University of Montana, Missoula, Montana*

ABSTRACT

Improved classification and mapping of grizzly habitat will permit better estimates of population density and distribution, and allow accurate evaluation of the potential effects of changes in land use, hunting regulations, and management policies on existing populations. Methods of identifying favorable habitat from ERTS-1 multispectral scanner imagery were investigated and described. This technique could reduce the time and effort required to classify large wilderness areas in the Western United States.

INTRODUCTION

As man encroached on wilderness that formerly comprised much of the western United States, the grizzly bear declined in numbers and disappeared from many areas where it was once abundant. In order to preserve and manage the remaining populations it is imperative that we thoroughly understand the relationship between the grizzly and its environment, and use this knowledge when making land use and wildlife management decisions.

Considerable data on grizzly bear ecology have been gathered during the course of a 13-year study of these bears in the Yellowstone ecosystem (Refs. 1-7). This population constitutes one of the few sizeable populations remaining in the United States outside of Alaska. Recent research work at the Montana Cooperative Wildlife Research Unit has placed increasing emphasis on habitat evaluation and integration of habitat data with accumulated knowledge of the grizzly's food habits, home range, movements, and population dynamics. The result will be a better understanding of grizzly bear habitat usage and requirements. It will also permit more accurate estimates to be made of population density and distribution, and allow wildlife managers to predict the effects of land use changes (logging, construction of roads, etc.) on existing bear populations. Grizzly bear habitat can be evaluated to determine if grizzlies can be reintroduced and survive in habitat from which they have been eliminated.

The development of remote sensing techniques of land use and habitat evaluation using aerial photography, multispectral scanning, sidelooking radar, active or passive microwave imaging, and other methods, has been

rapid in the last few years. These techniques have great potential for reducing both the effort and cost of surveying the inaccessible and extensive wilderness areas that comprise favorable grizzly bear habitat. This report evaluates the use of one of these techniques, multispectral imaging from earth-orbiting satellites.

Viewing equipment for analyzing ERTS-1 multispectral images was recently acquired by the University of Montana Geology Department as part of an Earth Resources Program contract with the National Aeronautics and Space Administration (Applicability of ERTS-1 to Montana Geology, NAS5-21826; R.M. Weidman, Principal Investigator). This provided us with an opportunity to compare ERTS-1 imagery with habitat data gathered for the U.S. Forest Service and Montana State Fish and Game Department during the summer of 1972 (Ref. 11). Our comparison of multispectral images with habitat data have enabled us to come to some conclusions about the usefulness of this technique and to identify some promising areas for further investigation.

IMAGERY COVERAGE OF MONTANA AND STUDY AREA

The coverage of ERTS-1 MSS imagery for Montana is shown in Figure 1. The satellite moves from north to south along the paths shown as dotted lines.

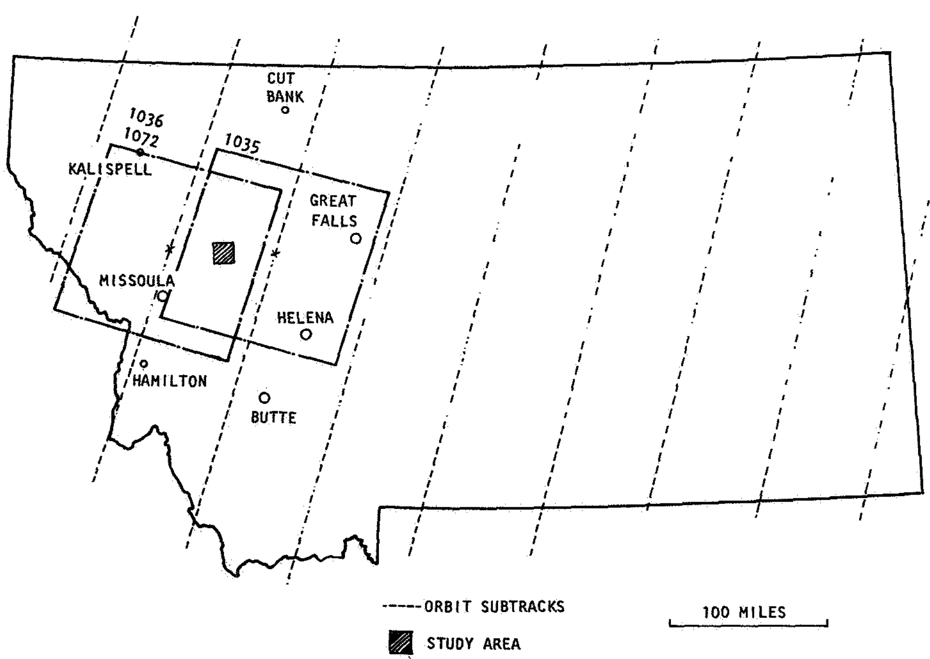

Fig. 1: ERTS-1 coverage of Montana and study area

Images are taken at approximately 160 km (100 mile) intervals along each path. Adjacent paths are covered on successive days, moving from east to west. The same orbit path is repeated at 18-day intervals.

Since each image is roughly square and covers an area measuring 185 km (115 miles) on each side, there is about 10% north-south overlap on successive frames taken in each orbit, and about 40% overlap on frames taken on successive days from adjacent orbits. It is thus possible to obtain side-lap stereo viewing of most areas with images taken in adjacent orbits.

The location of the study area is shown in Fig. 1, along with the coverage of the images that were used in our evaluation. These images were selected by checking the NASA indexes (ERTS U.S. Standard Catalog, NAS1.48:972) and by examining the print file maintained by the Geology Department. Coverage began after launch of the satellite in July 1972 and continues up to the present. The time of greatest interest to us was from July to November 1972. This included the period when personnel were in the field obtaining ground truth data. Satellite imagery obtained during this period is listed in Table I. Although coverage of the study area occurred every 18 days, many images were unusable because of cloud cover. One set of images in August and one in October were cloud-free, and were selected for evaluation. Frame 1036-17571 (Aug. 28) was used for most of the vegetation analysis. This frame and frame 1072-17571 (Oct. 3) were used together to examine time-lapse effects in the appearance of vegetation and snow cover. Frame 1035-17513 (Aug. 27) and frame 1036-17571 (Aug. 28) were used together for side-lap stereo viewing.

TABLE I
ERTS-1 IMAGERY OF STUDY AREA
July-Nov. 1972

Date	Frame	Cloud Cover	Subsatellite Point		Sun Angle Elev.	Sun Angle Az.
8-10	1018-17571	10%	47.12°N	113.88°W	51.7°	137.3°
8-27*	1035-17513	0	47.28	112.43	47.1	142.7
8-28*	1036-17571	0	47.30	113.80	46.0	143.0
9-15	1054-17571	60	47.33	113.77	41.2	148.6
10-2	1071-17513	10	47.51	112.23	35.3	153.3
10-3*	1072-17571	10	47.43	113.72	35.0	153.5
10-20	1089-17515	0	47.38	112.35	29.3	156.8
10-21	1090-17574	70	47.33	113.80	29.0	156.9
11-7	1107-17521	30	47.26	112.45	23.8	158.7
11-8	1108-17575	40	47.26	113.85	23.5	158.8
11-25	1125-17522	40	47.32	112.46	19.3	159.2

* Frames selected for evaluation

STUDY AREA

The 135 sq km (52 sq mi) study area is in the center of the newly-formed 970 sq km (240,500 acre) Lincoln-Scapegoat Wilderness which is 120 km (75 mi) west of Great Falls, Montana. It lies within the Lolo National Forest and is bordered by the Bob Marshall Wilderness area on the northwest. Elevations in the study area range from 1700 to 2800 m (5600 to 9200 ft), with over half of the area above 2400 m (8000 ft). The relative isolation and light use of the area, combined with specific vegetation and topographic characteristics, make it a favorable habitat for grizzlies. Between July 29 and September 15, 1972, the area was type-mapped for food plants utilized by grizzlies. A population survey of grizzlies, black bear, and other mammals and birds was made over a somewhat larger area at the same time (Ref. 11).

GRIZZLY HABITAT CRITERIA

A study of the food habits and habitat requirements of grizzlies in the Yellowstone ecosystem (Ref. 5) indicates that the following criteria are important for the maintenance of a grizzly population:

1. Space

   The home ranges of grizzly bears may encompass areas up to 3900 sq km (1500 sq mi). Large wilderness areas or de facto wilderness areas of national parks and national forests provide the required area.

2. Isolation

   Grizzlies conflict with man and his livestock, and have been eliminated from developed areas. Areas where bears remain and potential habitat for re-introduction of grizzlies is isolated and should receive only light recreational and livestock use. Roads and extensive trails degrade grizzly habitat.

3. Food

   An abundance of natural foods must be available from April to November, and must be sufficiently varied so that occasional annual deficiencies of one or more sources do not jeopardize the population. Basic foods are carrion, ungulates, rodents, berries, pine nuts, green vegetation, bulbs and tubers, and in some situations, fish.

4. Vegetation types

   A wide range of vegetational types characterize prime grizzly bear habitat. A mixture of timber and alpine meadows provide the bears with places to forage, socialize, and breed. Alder

C46

thickets, lodgepole downfalls, and other dense vegetation are preferred bedding sites. Large tracts of undisturbed timber provide protection and seclusion.

While other factors may influence a population in a particular situation, those cited above are the ones which were given primary consideration in our investigation.

HABITAT ASPECTS THAT CAN BE INVESTIGATED WITH ERTS-1 IMAGERY

Information about many of the important features of grizzly habitat can be obtained from ERTS-1 imagery. The high altitude from which the images are taken allows accurate mapping directly from photographs. The repetitive coverage obtained every 18 days is useful in investigating seasonal changes in vegetation and snow cover. The imagery is ideally suited for evaluating general topographic character and identifying broad classes of vegetation in existing or potential grizzly habitat.

The large scale of the images also results in some disadvantages. The resolution limit is about 100 m, which restricts the kinds of information which can be obtained. For example, isolated trees, most roads, and small patches of vegetation or other features less than about 8000 sq m (2 acres) in extent cannot be seen on the imagery. However, vegetation classes can be distinguished (forest vs. meadow), but identification of particular species within a class (pine vs. fir) is generally not possible at present.

We identified several ways in which ERTS-1 imagery can be either a useful supplement to other techniques or offers significant advantages or cost savings over other habitat analysis methods. These include determination of general vegetation character, simple land use classification, and identification of a major food species (whitebark pine). Monitoring seasonal vegetation changes and observing the extent and altitude of snow cover at intervals throughout the year also proved feasible. These are discussed in more detail in RESULTS.

IMAGE ANALYSIS METHODS

Most image analysis was done with a color-additive viewer using positive transparency enlargements (23 x 23 cm, scale 1:1,000,000) of the multispectral scanner scenes. Portions of these transparencies encompassing the study area, 8 x 10 cm in size, were cut out and mounted in 70mm glass and metal slide holders. The area covered is illustrated in Fig. 2 and was designated Scene 1.

The prepared slides for each of the four MSS bands were then placed in a Spectral Data Corporation Model 64 Multispectral Viewer. Red, green, blue, or white light of variable intensity was projected through each of the four

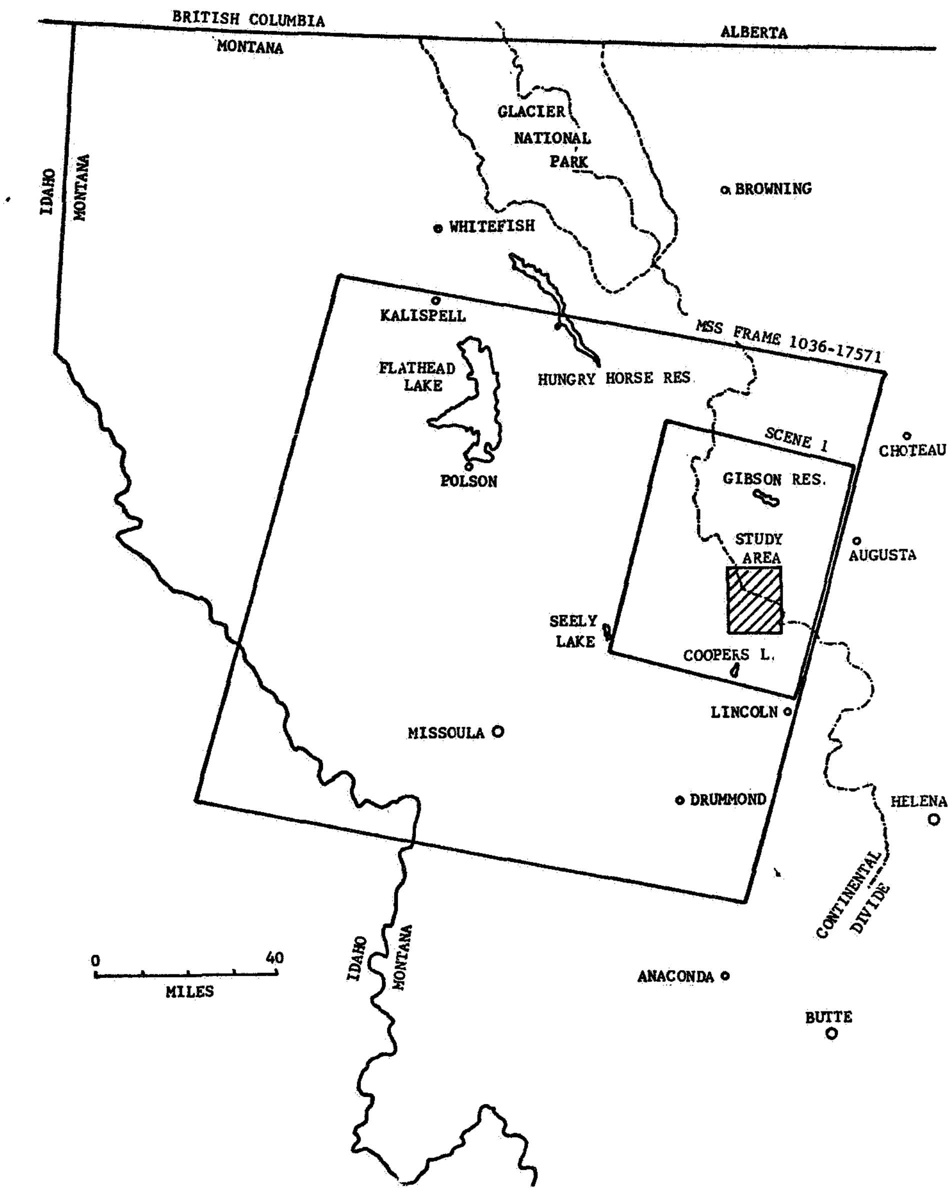

Fig. 2: Boundaries of MSS frame, area displayed on color-additive viewer (scene 1), and study area

transparencies to form a color composite image on a 23 x 23 cm ground glass viewing screen. The viewer optics provide a x3.37 enlargement of the slide, giving an image scale of 1:297,000 on the viewing screen. After adjustments to place all four images in register, various combinations of band, colors, and light intensities can be set up to give maximum enhancement to features of interest in the composite image.

After obtaining the desired scene display by appropriate adjustments, the image was permanently recorded by photographing the viewing screen with a 35mm camera and Type B High Speed Ektachrome film. The resulting slides could later be examined, projected, or used to make prints as required.

A 23 x 23 cm transparent overlay was prepared for the viewer screen to aid in identifying major topographic features and landmarks. A convenient and low cost method of making such overlays consisted of copying a portion of a 1:250,000 scale USGS topographic map on a Xerox 7000 electrostatic copying machine at the #2 reduction setting (84.5%) and then making a 1:1 thermographic overhead projection transparency from this reduced-size copy. The resulting overlay matched the image scale on the viewing screen within 1% and allowed forest boundaries, drainages, mountains, and other features to be easily identified.

A composite aerial photograph map of the study area was also prepared from Forest Service 1:15,840 black and white panchromatic photographs to aid in identifying small features not shown on the topographic map.

A Bauch & Lomb model ZT-4 Zoom Transfer Scope was used to draw vegetation maps from the 35mm slides of color composite images and to superimpose topographic maps on the images for identification of major features and determination of snow cover elevation.

RESULTS

Image color effects

Conclusions similar to those of other investigators (Refs. 8-10) were reached after evaluating the comparative utility of the four MSS images, both individually and in combinations.

The two infrared bands (band 6, 0.7 to 0.8 μm; band 7, 0.8 to 1.1 μm) were very similar in appearance, with rivers and lakes showing black and growing plants in light tones. They reduced the dark tones of forested areas normally apparent in visible light so that the topography of the scene was very clear. Band 5 images (0.6 to 0.7 μm, red) most closely approached the appearance of normal aerial photographs; forests and growing vegetation appeared in dark tones and dry vegetation in light tones. Band 4 images (0.5 to 0.6 μm, green) were the least useful for vegetative mapping and had a slightly hazy appearance due to atmospheric scattering, but were the best for identifying snow cover.

A combination of bands 5 and 7 gave the finest detail for vegetative mapping. Adding band 4 to these two gave greater subtlety of color but resulted in a slight reduction in detail, both because of the haze effect and the additional difficulty of adjusting three images for perfect registration instead of two.

Simulated false-color infrared images were obtained by illuminating band 4 with blue light, band 5 with green, and band 7 with red. Band 6 was usually not used because of its similarity to band 7. In these images growing vegetation appears in various shades of red. A simulated normal-color image could be obtained by projecting band 4 in blue, band 5 in red, and band 7 in green. The resulting image shows growing vegetation in exaggerated shades of green and was slightly easier for inexperienced observers to classify accurately.

Scene illumination effects

The transparencies supplied by the EROS data center are photometrically accurate, having densities which correspond to absolute scene brightness. As a result, scenes obtained during winter months at high latitudes are often very dark. Two effects are responsible for this darkening: one is the lower average illumination level due to oblique lighting; the other is the presence of many more shadows in areas of uneven topography.

Sun angles above the horizon for imagery of the study area were summarized in Table I. They vary from 52° on August 10 to 19° on November 25.

We found that vegetation mapping was more difficult in mountainous areas with November imagery than with August imagery. North- and northwest-facing slopes received much less light at low sun angles than south-facing ones, and resulted in tone variations that were larger than those used to discriminate between vegetation types in bright evenly-illuminated areas. Discrimination within large sloping areas illuminated at very low angles was poor because of the general dark tone, and no details could be distinguished in full shadow.

Determination of general vegetation character

High alpine meadows appear in light red or pink in the simulated false-color infrared images and can be easily identified and distinguished from the timbered areas which are a darker red or grayish-red. Large areas can be quickly examined on the images and those portions with combinations of forest and meadows, favorable grizzly bear habitat, can be noted for further examination.

Classification of habitat quality by type and intensity of land use

Areas that have been identified as possible bear habitat by the initial examination of vegetation character can be further classified by eliminating

those portions that are heavily used by man and grading the remaining area by a measure of land use intensity.

An overlay can be prepared for the satellite image which shows all settlements, agricultural land, grazing land, logging or mining activity, roads, and trails in the area. Areas within a certain radius of settlements and residences, all agricultural land, and a strip adjacent to roads and trails with width proportional to traffic volume are eliminated. Grizzlies tend to avoid such areas, and those who do not are usually eliminated in the eventual bear-man conflicts which result. The remaining area is considered to be potentially suitable habitat for further evaluation. A simple example of one possible type of overlay is shown in Fig. 3. Urban areas, agricultural land, and grazing land are usually easily identifiable on the satellite imagery by their characteristic colors and can be mapped directly. Roads and trails are generally not visible; their locations must be obtained from maps. The width of the excluded strips adjacent to them can be determined from traffic counts, visitor statistics, and other sources.

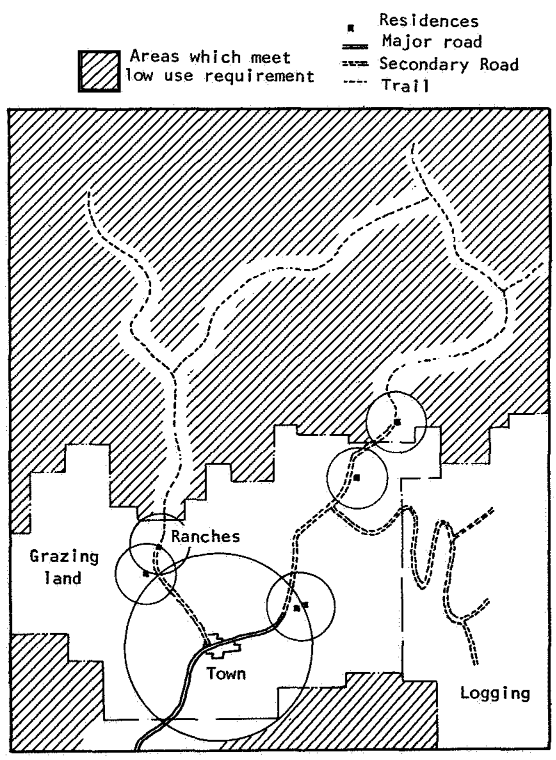

Fig. 3: Example of a use-intensity overlay

Before this method can be used it will be necessary to establish an approximate scale factor for the excluded high-use areas; on trails, for example, the width of the excluded strip would be a certain number of meters per visitor man-day. Such scales would be, initially at least, rather arbitrary. An analysis of Yellowstone Park visitor use would probably provide the best starting point since better records of both bear and human distribution exist there than any other area. The resulting scales would need to be modified in some respects for habitat evaluation outside of national parks. This classification method could not be expected to be accurate in any absolute sense, but would permit use intensity in various areas to be compared with one another and rankings of habitat quality to be made.

Identification of whitebark pine

Examination of the color composite image of the study area with the color-additive viewer did not reveal any distinctive variations in color or tone that would permit differentiation of the various tree species from one another. However, we found that a combination of tree cover imagery and altitude information permitted reasonably accurate identification of whitebark and limber pine, important food species for grizzly bears.

The ground survey showed that whitebark pine (*Pinus albicaulis*) and limber pine (*Pinus flexilis*) occurred predominantly on higher ridges in the study area, usually above 2100 m (7000 ft) elevation. The approximate distribution of these pines is shown in Fig. 3 of Ref. 11. Both species were considered as whitebark pine for classification purposes.

A projection mask was prepared from a topographic map which showed all areas above 2100 m in black. This image was combined (using white light) with the false-color infrared (Fig. 4) or normal-color images in the color-additive viewer. The resulting false-color image is shown in Fig. 5. In this image timbered areas above 2100 m appear dark red, and can be easily identified and mapped. A simulated normal-color image of the study area is shown in Fig. 6.

Timbered areas mapped from the false-color or normal-color images are shown in Fig. 7 in relation to the distribution of whitebark pine observed on the ground. The area covered by whitebark pine is 30.6 sq km, and the high elevation timbered areas identified from satellite imagery cover 44.3 sq km (excluding the two southernmost areas, which were not checked in the ground survey). The crosshatched common area is 25.4 sq km. If the ground survey were entirely accurate, 57% of the high elevation timbered area shown on the imagery was whitebark pine, and 83% of the total whitebark pine area was included within the boundaries mapped from the imagery. This is a reasonably good result, especially considering the simplicity of the method and the limited accuracy of the ground survey.

Fig. 4: Simulated false-color infrared image of scene 1 as displayed on color-additive viewer. Growing vegetation appears in shades of red.

Fig. 5: Scene 1 with high-altitude overlay superimposed in white light. Only the areas above 7000 ft remain visible.

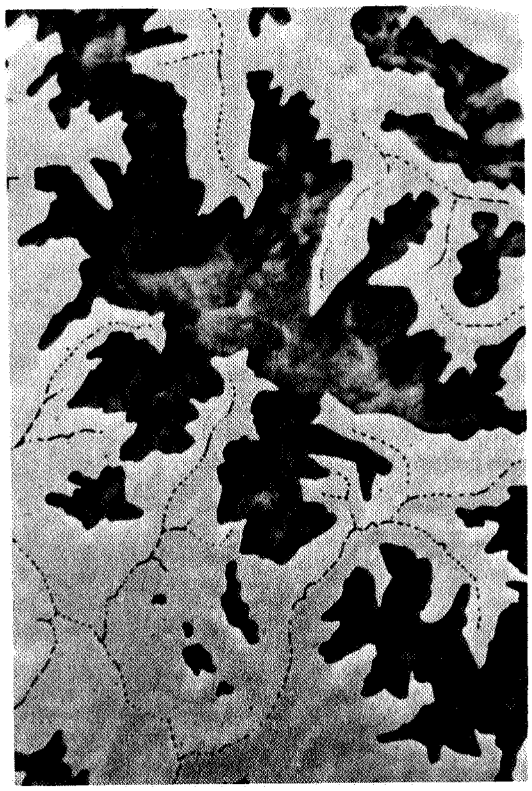

Fig. 6: Simulated normal-color image of study area with high altitude overlay superimposed. Growing vegetation appears in shades of green.

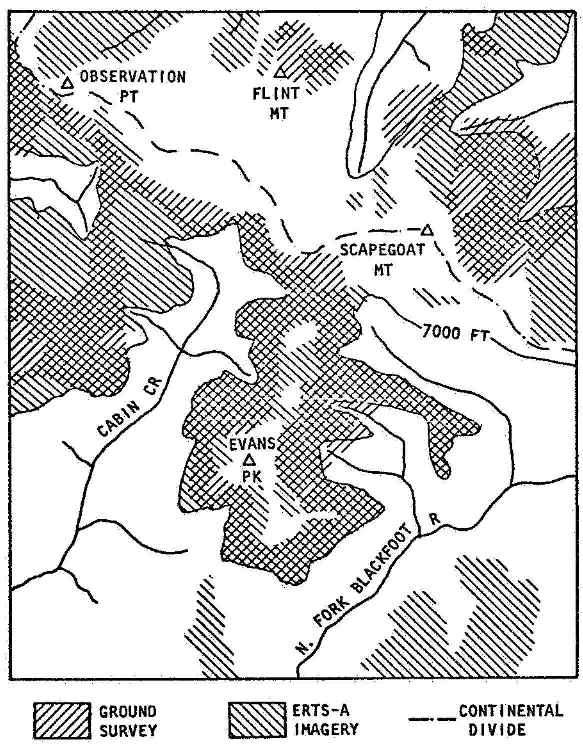

Fig. 7: Distribution of white-bark pine observed on the ground compared with high altitude timbered areas mapped from satellite imagery.

Other factors beside altitude which influence where whitebark pine occurs include aspect, exposure, soil type, and available moisture. On north-facing slopes they were often found at lower elevations than on south-facing slopes. More accurate estimates of distribution could be made using satellite imagery by incorporating such factors into the discrimination process.

Identification of shrubs, grasses, and herbs

Other important plant food items in the study area utilized by the grizzly include huckleberry and grouseberry (*Vaccinium spp.*), tubers of *Claytonia spp.* and *Lomatium spp.*, and several other herbs and grasses. These occur as low shrubs growing as understory among larger trees or small plants in open areas.

It was not possible to identify any of these species from the satellite imagery alone. Open alpine meadows could be easily distinguished from timber stands, but particular species of vegetation in the meadows could not be separated. Mapping the area and extent of the meadows may provide sufficient data to allow an accurate estimate of the amount of tuberous and other foods available, since the general composition of alpine meadow vegetation varies relatively little. It can be reasonably assumed, for example, that the amount and distribution of *Claytonia spp.* and *Lomatium spp.* determined by sampling in one location would be representative of other alpine areas within the ecosystem.

The understory species (*Vaccinium spp.*) were, of course, not visible at all. Understory typing would probably be limited to identifying likely areas for sampling by ground observers.

Some discrimination between visible vegetation types should be possible on the basis of association with indentifiable species (whitebark pine), altitude, soil type, topography (exposure), or a combination of these factors.

Since green plants are easily distinguished from dry or dead ones by their high reflectance in the infrared bands and the resulting appearance in false-color or normal-color images, a series of scenes at 18-day intervals can be used to determine the time of appearance of new growth in the spring, and drying and dying of vegetation in the late summer and fall. To the extent that this is species-specific, it provides an additional type discrimination factor. Other investigators have found that this is a promising technique for distinguishing coniferous trees from hardwoods, and for identifying some species of hardwoods and agricultural crops (Ref. 12).

Mapping snow cover

Information about snow conditions is helpful in studies of the grizzly, since it determines the bear's hibernation behavior and influences the availability of food in the spring and fall.

Snow appeared most distinctively in bands 4 or 5, where it had highest contrast with surrounding snow-free terrain. Although clouds and snow had about the same brightness, they could generally be distinguished without difficulty because of characteristic differences in shapes and because of the shadows that accompanied clouds. The boundaries of snowcovered areas are easily distinguished on bare or lightly-vegetated terrain. They become more difficult to see in heavy timber. These observations agree with the findings of other investigators (Refs. 9, 13, 14).

A time-lapse technique proved to be very useful in determining changes in snow cover over a period of time. Two band 4 images of the same area, one taken in August and one in October, were superimposed on the viewer. The August image was illuminated with red light, the October image with green. In areas where no changes in tone had occurred during the time between the images were taken, the resulting composite was a neutral greenish-gray. Areas that were lighter in the October image appeared red, and areas that were darker appeared green.

The resulting effect is illustrated in Fig. 8. Areas covered by snow in October which were not covered in August are bright red and can be easily distinguished. Examination of this image with a topographic map overlay shows that the snow level on October 3 was at 2400 m (2300 m on north-facing slopes) in the 4200 sq km area shown.

Additional data for vegetation type mapping can be obtained from snow cover information, since it is closely related to moisture conditions. Differential rates of melting and the resulting changes in snow field boundaries can provide data about exposure and average temperature that will help discriminate between some types of vegetation that are indistinguishable on the basis of appearance alone. The appearance and flowering of certain plant species is closely related to snow field boundaries, so the location of these boundaries can indicate the type of vegetation and the general phenology in these areas.

DISCUSSION

The results of this brief investigation show that ERTS-1 multispectral scanner imagery can be of considerable value in habitat analysis. Useful information about several aspects of the grizzly's environment can be obtained with minimal cost and effort from a few hours spent examining the imagery. The authors have not had prior photointerpretation experience, and so we may have overlooked information (of which other investigators are already aware) that could be obtained from the imagery. We plan to continue evaluating this technique in ongoing programs where habitat data are needed.

We feel that satellite imagery is most valuable at present as a supplement to, not a replacement for, field observations by personnel on the ground. Limitations in image resolution and in the kinds of information that can be obtained from multispectral scanning allow much room for error if used alone. The imagery can be used, however, to perform a great deal

Fig. 8: Composite image of scene 1 with superimposed altitude overlay. Recent snow appears bright red.

of initial screening and to select those areas where field effort can be most productively concentrated. In surveying wilderness areas to locate suitable habitat for reintroduction of grizzlies, for example, large portions could be eliminated from consideration on the basis of the imagery alone with high confidence. Field work can then be focused on the remaining locations which appear to meet minimum requirements. Examination of satellite imagery at the beginning of a study should thus allow an effective sampling strategy to be developed which will minimize the field effort and overall program cost.

Using the techniques described, we could rapidly survey the three largest ecosystems in the western United States (Yellowstone, Selway-Bitterroot, and Bob Marshall) to determine the location and extent of favorable grizzly habitat, to assist in making more accurate estimates of the present grizzly population in these areas, and to locate the most promising sites for reintroduction. Such information is badly needed and could be obtained with comparatively modest funding. Together with the extensive data on grizzly food habits, movements, ranges, and general bear ecology that has already been gathered, such a survey could provide several western states with a basis for evaluating their hunting regulations and harvest, and provide both state and federal agencies with better data than is now available to consider when making management and land use decisions.

Satellite remote sensing methods are a valuable addition to the tools of the wildlife researcher and manager in their present state of development. The usefulness of the data from ERTS-1 will expand in the near future, as other researchers develop analysis methods to increase the types and quality of data that can be obtained from the images. This effort should result in additional techniques that would be useful in habitat analysis. Remote sensing will become increasingly valuable in wildlife research and management as equipment with improved resolution and additional spectral bands becomes available on future satellites.

ACKNOWLEDGEMENTS

The imagery analysis described in this report was supported by National Aeronautics and Space Administration grant NGR 27-002-006. Dr. Robert Weidman made available to us the multispectral viewing and cartographic equipment and provided much assistance and helpful advice. Ground truth was obtained from a habitat survey of the Scapegoat Wilderness Area sponsored by the U.S. Forest Service and the Montana State Fish and Game Department, and conducted by the Montana Cooperative Wildlife Research Unit.

REFERENCES

1. Craighead, J.J., and F.C. Craighead Jr. 1971 Grizzly bear - man relationships in Yellowstone National Park. BioScience 21(16):845-847.

2. Craighead, J.J., F.C. Craighead Jr., and H.E. McCutchen. 1970. Age determination of grizzly bears from fourth premolar tooth sections. J. Wildl. Mgmt. 34(2):353-363.

3. Craighead, J.J., M. Hornocker, and F.C. Craighead Jr. 1969. Reproductive biology of young female grizzly bears. J. Reprod. Fert. Suppl. 6:447-475.

4. Craighead, J.J., and F.C. Craighead Jr. 1967. Management of bears in Yellowstone National Park. Mimeo rept., Mont. Coop. Wildlife Res. Unit. 118 pp.

5. Craighead, J.J., J. Sumner, and F.C. Craighead Jr. (in prep.). Food habits of grizzly bears in the Yellowstone ecosystem.

6. Craighead, J.J., M. Hornocker, W. Woodgerd, and F.C. Craighead Jr. 1960. Color-marking grizzly bears. Trans N. Amer. Wildl. Natur. Resour. Conf. 25:347-363.

7. Hornocker, M.G. 1962. Population characteristics and social and reproductive behavior of the grizzly bear in Yellowstone National Park. Unpubl. thesis, University of Montana. 94 pp.

8. Heller, R.C., R.C. Aldrich, F.R. Weber, R.S. Driscoll. 1973. Inventory of Forest and Rangeland and Detection of Forest Stress. Progress Report, Sept.-Oct. 1972. NASA-CR-128485, N73-11313. 11 pp.

9. Barnes, J.C., and C.J. Bowley. 1973. Use of ERTS data for mapping snow cover in the western United States: progress report, June-Dec. 1972. NASA-CR-130336, N73-17299. 22 pp.

10. Tueller, P.T. 1973. Use of satellite imagery for wildland resource Evaluation. Progress Report. NASA-CR-129130, N73-12353. 14 pp.

11. Sumner, J., and J.J. Craighead. 1973. Grizzly Bear Habitat Survey in the Scapegoat Wilderness, Montana. Mimeo rept. Mont. Coop. Wildlife Res. Unit. 67 pp.

12. Dethier, B.E. 1973. Phenology satellite experiment: progress report, Aug. 1972-Feb. 1973. NASA-CR-131318, N73-21334. 48 pp.

13. Weller, G. 1973. Survey of the seasonal snow cover in Alaska: Bimonthly progress report. NASA-CR-131232, N73-20398. 4 pp.

14. Meier, M.F. 1973. Evaluate ERTS imagery for mapping and detection of changes in snowcover on land and on glaciers: progress report. NASA-CR-131020, N73-19374. 3 pp.

Paper E 12

UTILITY OF ERTS FOR MONITORING THE BREEDING HABITAT OF MIGRATORY WATERFOWL

Edgar A. Work, Jr., *Environmental Research Institute of Michigan, Ann Arbor, Michigan,*
David S. Gilmer, A. T. Klett, *Bureau of Sport Fisheries and Wildlife, Northern Prairie Wildlife Research Center, Jamestown, North Dakota*

ABSTRACT

Since 1968 the Bureau of Sport Fisheries and Wildlife (BSF&W) and the Environmental Research Institute of Michigan have cooperated on developing applications of remote sensing to the management of migratory waterfowl. Basically, this work has been concerned with (1) the assimilation of data on surface water conditions so that the data can be used as an index of annual waterfowl production, and (2) the collection of data on land use and wetland quality so that a measure of habitat carrying capacity is obtained. To date, our efforts have been directed toward utilizing ERTS to monitor surface water conditions. An example of a model used for predicting the annual production of mallards (*Anas platyrhynchos*) is presented. The data inputs to this model and the potential for acquiring these data using ERTS are described.

1. INTRODUCTION

The Bureau of Sport Fisheries and Wildlife of the U. S. Department of the Interior is the government agency responsible for the coordinated management of migratory waterfowl in accordance with treaties with Canada, Mexico, and Japan. Approaches to the management of waterfowl populations are two-fold: (1) habitat management and preservation, and (2) population management, including the establishment and administration of hunting regulations. Management of habitat implies preservation through acquisition and lease arrangements, regulation of land use, and manipulation or treatment of certain features to enhance habitat quality. In this context, remote sensing offers a tool for monitoring changes in land use habitat quality and for evaluating land areas for acquisition. On the other hand, management of populations by the administration of hunting regulations is a more direct approach, has a rapid impact, and occurs on an annual basis. In order to be effective, it requires a rapid assimilation of stochastic data.

Annual waterfowl hunting regulations are established to allow for a reasonable level of harvest by hunters while insuring the survival of an adequate number of birds to sustain a viable breeding population the following year. In order to establish annual hunting regulations, the magnitude of the fall flight of birds must be predicted. Figure 1 indicates the stochastic data and sequence and timing of events utilized for this prediction. Note that aside from input data to this model which are based on a direct count of individual ducks and broods, numbers and changes in numbers of ponds are considered. In particular, Crissey (1967) has emphasized that there is a significant correlation between the abundance of prairie water bodies and the subsequent size of the North American duck population. Note too that adjustments, based upon an ecological assessment of wetland abundance and quality and trends associated with long and short term land use, may be possible prior to regulation formulation.

Evaluations of aircraft remote sensing techniques for gathering waterfowl habitat information have been conducted (Burge and Brown, 1970; Nelson, et al., 1971; Work and Thomson, in press). To date our ERTS investigation has been concerned with identifying and mapping prairie ponds and lakes (Work, et al., 1973).

2. BREEDING POPULATION AND PRODUCTION SURVEYS

From Fig. 1, it becomes apparent that estimating the fall flight of waterfowl is critically dependent upon appraisals of the magnitude of the breeding population and annual production of young. Of these two factors, changes in production influence the size of the fall flight more than do changes in breeding population (Crissey, 1957). Current waterfowl breeding ground surveys evolved from an experimental survey first conducted in 1947. Crissey (1957), Stewart, et al., (1958) and more recently Henny, et al. (1972) and Pospahala, et al. (in prep.) discuss the operational aspects of the breeding ground surveys.

Average continental distribution of breeding and wintering ducks is illustrated in Fig. 2. The wintering range is widespread, extending beyond the North American continent into parts of Central and South America. Most of the primary duck breeding habitat in North America is located in the southern portions of the prairie provinces and northwestern Canada, the Dakotas and parts of Alaska. Habitat conditions in these areas greatly influence the annual continental waterfowl population.

Estimates of waterfowl breeding population and production are obtained using a dual sampling approach. The first sample consists of a series of transects which are flown by light aircraft in May and July of each year. Sampling transects and strata are illustrated in Fig. 3. Strata were delineated on the basis of expected waterfowl population density, habitat type, and expected variability of the estimates. Over 2.2 million square kilometers of the breeding range are sampled during each survey. Approximately 53,000 transect kilometers are flown at an altitude of 30 to 45 meters. The survey crew normally consists of a pilot and an observer. Together they count and when possible, identify ducks by species over a 400-meter wide strip in May and a 200-meter wide strip in July. Ponds are counted over a 200-meter wide strip in both May and July (Henny, et al., 1972, Pospahala, et al., in prep.). Each crew member records his count on a tape recorder and later the same day transcribes this information onto summary sheets.

The second sample consists of certain air/ground transects which serve to adjust for biases encountered in the first sample (aerial survey). Specifically, these biases are a result of the inability of the aerial crew to see and count all birds present on the ground, to identify all birds with equal ability, and to identify and classify all wetlands. The results of the aerial survey plus appropriate corrections are converted to estimates of birds or broods per square mile and these numbers are then expanded according to the number of square miles in the sampling unit. The survey as carried out in May yields an estimate of the size of the breeding population. This population component must be reduced by a certain amount to account for normal summer mortality (predation, disease, and accidents) when estimating the fall flight (Geis, et al., 1969).

3. PRODUCTION MODELS

In estimating that portion of the fall flight which is made up of the current year's production, additional analysis are required; Geis, et al., (1969) described a mathematical model (Fig. 4) for estimating mallard production. The mallard was chosen because: (1) it is the most abundant and widespread waterfowl species in North America and is nearly always killed in greater numbers than any other species (Anderson and Henny, 1972); (2) a large amount of ecological data is available for the species; and (3) populations of several other dabbling duck species are affected by many of the same factors as the mallard.

The Geis, et al. prediction model was developed from a multiple regression analysis based upon 13 years of data. Data from both the May and July surveys are utilized in this model. Referring to Fig. 4, the quantities, X_1 and X_3, potentially may be obtained using remote sensing techniques and automatic processing. X_2 can only be obtained from visual observations made during the May survey, while X_4 is derived from visual observations made in July.

More recent analyses have indicated that it may be possible to redesign the model and eliminate use of the brood index (X_4) (private conversations 29 October and 10 December 1973, D. R. Anderson, Migratory Bird and Habitat Research Laboratory, Bureau of Sport Fisheries and Wildlife, Laurel, Maryland). If this is possible, greater emphasis will be placed on the July pond count and this could be effectively accomplished using remote sensing techniques.

Application of these techniques will improve the accuracy of pond counts, and other factors such as pond area and perimeter could be incorporated into a model which might further improve production estimates. The July survey usually lasts until late in the month; however, the results of this survey must be available in early August for use in establishing hunting regulations. Automatic processing of remote sensing data is appropriate for insuring rapid availability of survey information.

4. SURFACE WATER SURVEYS USING ERTS DATA

The current ERTS-1 program conducted by the Bureau of Sport Fisheries and Wildlife in cooperation with the Environmental Research Institute of Michigan is concerned with mapping surface water in May and July. This work involved the adaptation to satellite data of techniques previously developed for use with aircraft scanner data. Because the launch date for the ERTS-1 satellite was delayed until mid-1972, it was necessary to defer the bulk of this investigation until a May and July sequence of data was available from the 1973 season. However, to test the feasibility of pond mapping by means of satellite data, July 1972 ERTS tapes were processed upon receipt (Work, et al., 1973). We are presently processing a 1973 May and July sequence of data. This processing and the subsequent evaluation will complete the next phase of our study.

A portion of the July 1972 surface water recognition map representing about three percent of an ERTS frame is shown in Fig. 5. The area shown is located in central North Dakota and includes a portion of the Missouri Coteau region. The Coteau is a stagnation moraine area featuring many small ponds and lakes and a non-integrated drainage system, which contains some of the best waterfowl breeding habitat in North America.

The data presented in Fig. 5 have been assembled from several computer output strips each having the standard 132-column format. When generated with a general purpose computer, this type of information display is both time consuming to assemble and unwieldly to handle if the scene is larger

than a small fraction of an ERTS frame. For our purposes, the data has generally greater value if it is presented in terms of statistical tables. Figure 6 illustrates statistical tabulations for ponds and lakes for the ERTS scene illustrated in Fig. 5. The upper table itemizes all ponds recognized in a portion of the scene and delineates the location of each pond based on a coordinate system using scan line and point numbers. The latitude and longitude of each water body is also listed. It is also possible to list (not illustrated) each pond's perimeter and a factor related to the complexity of its shape. A size frequency distribution of ponds in the entire scene is presented in the lower tabulation (Fig. 6). With these types of listings, it is possible to obtain separate tabulations by strata.

5. SPATIAL RESOLUTION OF THE DATA

Figure 7 compares water recognition maps of ponds and several smaller lakes generated from both satellite and aircraft data. Using the aircraft data as a basis of comparison, it is apparent that the satellite data renders a reasonable facsimile of ponds in the size class of Big, Clark, and Fish Lakes. However, many of the smaller ponds are not recognized and other ponds and lakes are not accurately represented in areal extent. Because each ERTS pixel (picture element) is 79 x 57 meters or about 0.45 hectares (1.1 acres), water bodies in the less than 0.9 hectare range are recognized only conditionally. This resolution anomaly is partly a result of the sensor's line scanning and pixel sampling geometry and the random occurrence of surface water with respect to the sampled pixel.

Figure 8 shows an example of boundary effect in the delineation of pond margins. The dashes represent pixels having low reflectance values which are not low enough to be classified as water. Some of these boundary elements may be attributed to marsh vegetation and/or mud flat margins; both of these exhibit low reflectance characteristics. These boundary elements probably also contain some water. This causes the acreage of ponds to be underestimated because, in our present binary selection, we are classifying pixels as either totally water or not water.

Improvements in resolution would increase the accuracy of our analysis. In the primary waterfowl breeding range, a majority of the ponds are less than one acre in size. Techniques exist which can detect or predict the existence of smaller ponds and improve the size estimates of larger ones. One technique has been proposed by Malila and Nalepka (1973) in which it is possible to estimate the proportion of materials contained in each pixel by taking advantage of the multispectral data-gathering capabilities of ERTS. This permits a more accurate determination of the area covered by each material. The technique has been termed "proportion estimation" and is basically a method for performing fractional-pixel recognition as contrasted to whole-pixel recognition. Figure 9 illustrates the application of the Malila-Nalepka technique to the delineation of lakes in a Michigan test area. Both whole-pixel recognition and proportion estimation recognition are shown.

In the case of proportion estimation, the density of the recognition symbol is proportional to the amount of surface water in that pixel. For comparison of results, an aerial photo was used to determine the actual number of lakes and their cumulative area. The comparison indicates that proportion estimation has provided more accurate results than those available using the conventional whole pixel recognition. However, this improvement requires more complex processing and greater training time for the computer.

The joint use of satellite and aircraft data in a properly designed multistage sampling plan could improve the precision of pond number and area estimates. This approach can be used independently or in addition to the proportion estimation method. Multistage sampling would take advantage of the detailed information provided by aircraft sensors in conjunction with the synoptic and more economically obtained satellite data.

6. CONCLUSIONS

Waterfowl breeding-ground surveys conducted twice each year by the BSF&W extend over a vast region of the U. S. and Canada. Data from these surveys are used to estimate waterfowl production by means of a mathematical model. Counts of May and July ponds are some of the variables used in this model. Annual production estimates are used to predict fall flights of ducks. This information is then used for establishing waterfowl hunting regulations. Our work to date indicates that satellite remote sensing techniques hold considerable promise for the accurate and rapid assessment of waterfowl breeding habitat, especially changes in pond numbers and distribution. Development of an operational system utilizing satellite sensors as a primary source of data appears to be a realistic goal for the future.

7. LITERATURE CITED

Anderson, D. R. and C. J. Henny. 1972. Population ecology of the mallard: I. A review of previous studies and the distribution and migration from breeding areas. U. S. Fish and Wildlife Service, Bureau of Sport Fisheries and Wildlife, Resource Publication 105. 166 pp.

Burge, W. G. and W. L. Brown. 1970. A study of waterfowl habitat in North Dakota using remote sensing techniques. Willow Run Labs., Inst. of Sci. and Technol., The University of Michigan, Ann Arbor, Tech. Rep. No. 2771-7-F, 61 pp.

Crissey, W. F. 1957. Forecasting waterfowl harvest by flyways. Trans. N. Am. Wildl. Conf. 22:256-268.

Crissey, W. F. 1969. Prairie potholes from a continental viewpoint. Saskatoon Wetlands Seminar. Canadian Wildl. Serv. Report Series. 6:161:171.

Geis, A. D., R. K. Martinson, and D. R. Anderson. 1969. Establishing hunting regulations and allowable harvest of mallards in the United States. J. Wildl. Mgmt. 33(4): 848-859.

Henny, C. J., D. R. Anderson, and R. S. Pospahala. 1972. Aerial surveys of waterfowl production in North America, 1955-71. U. S. Fish and Wildl. Serv., Bur. of Sport Fish. and Wildl. Special Scientific Rept. Wildlife No. 160. 48 pp.

Malila, W. A. and R. J. Nalepka. 1973. Advanced processing and information extraction techniques applied to ERTS-1 MSS data. in Proc. Third ERTS Symposium held by NASA/Goddard Space Flight Center at Washington, D. C., December 10-14, 1973 (this publication).

Nelson, H. K., A. T. Klett, and W. G. Burge. 1970. Monitoring migratory bird habitat by remote sensing methods. Trans. N. Am. Wildl. and Nat. Resour. Conf. 35: 73-84.

Pospahala, R. S., A. R. Brazda, R. C. Hanson, G. H. Jensen, K. D. Norman, G. Pospichal, M. M. Smith, and J. F. Voelzer. (in prep). Aerial surveys of waterfowl breeding populations in North America, 1955-1973. Special Sci. Rept. Wildl. Series. U. S. Fish and Wildl. Serv.

Stewart, R. E., A. D. Geis and C. E. Evans. 1958. Distribution of populations and hunting kill of the canvasback. J. Wildl. Mgmt. 22(4): 333-370.

Work, E. A. Jr., D. S. Gilmer, and A. T. Klett. 1973. Preliminary evaluation of ERTS-1 for determining numbers and distribution of prairie ponds and lakes. in Proc. Symposium on Significant Results Obtained from the Earth Resources Technology Satellite-1, held by Goddard Space Flight Center at New Carrollton, Maryland, March 5-9, 1973. Vol. I, Sect. A, pp. 801-808.

Work, E. A. Jr. and F. J. Thomson. (in press) A study of waterfowl habitat in North Dakota using remote sensing techniques: phase II. Report No. 101000-12-F, Environmental Research Institute of Michigan, Ann Arbor.

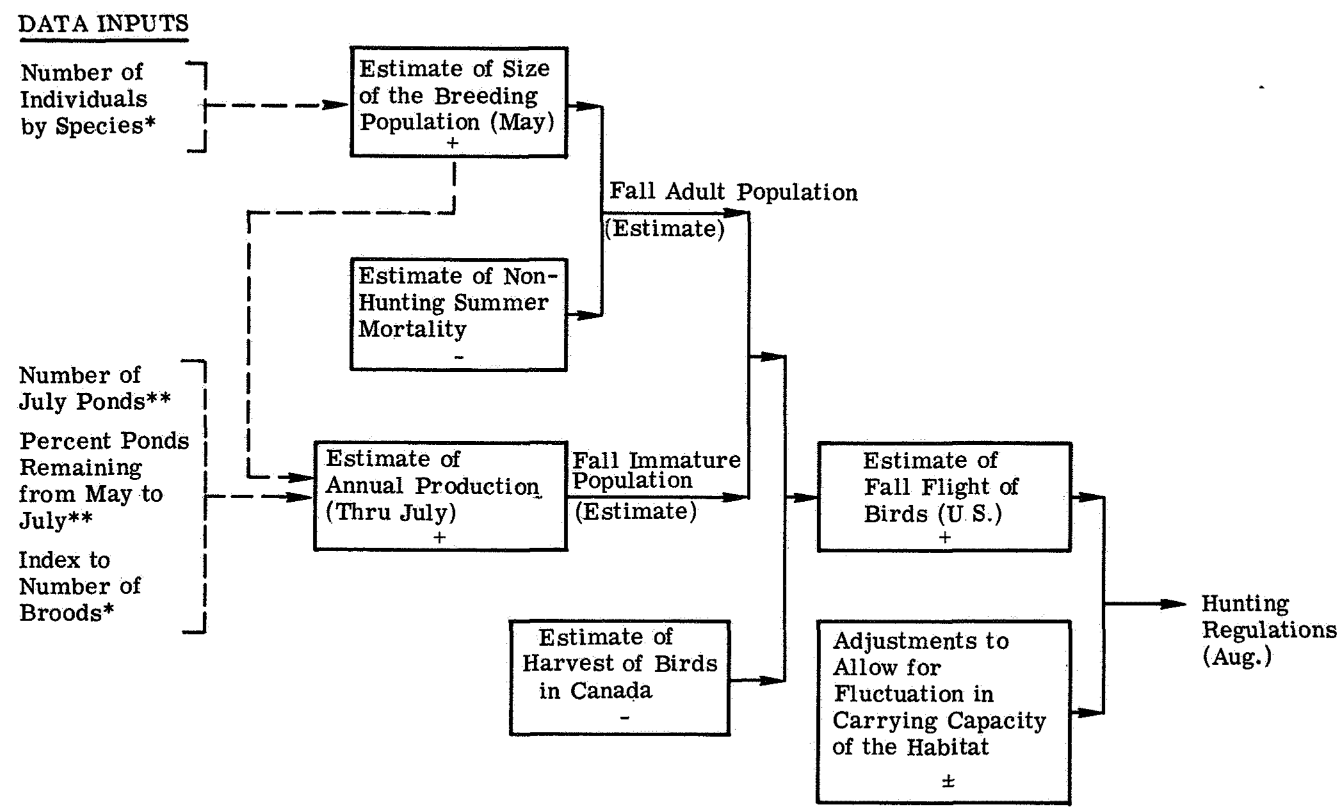

FIGURE 1

DETERMINING HUNTING REGULATIONS BASED UPON THE ESTIMATED MAGNITUDE OF THE FALL FLIGHT OF MIGRATORY WATERFOWL

*Obtained from aerial observations and adjusted based on selected ground counts

**Obtained from aerial observations —data potentially derived using remote sensing techniques

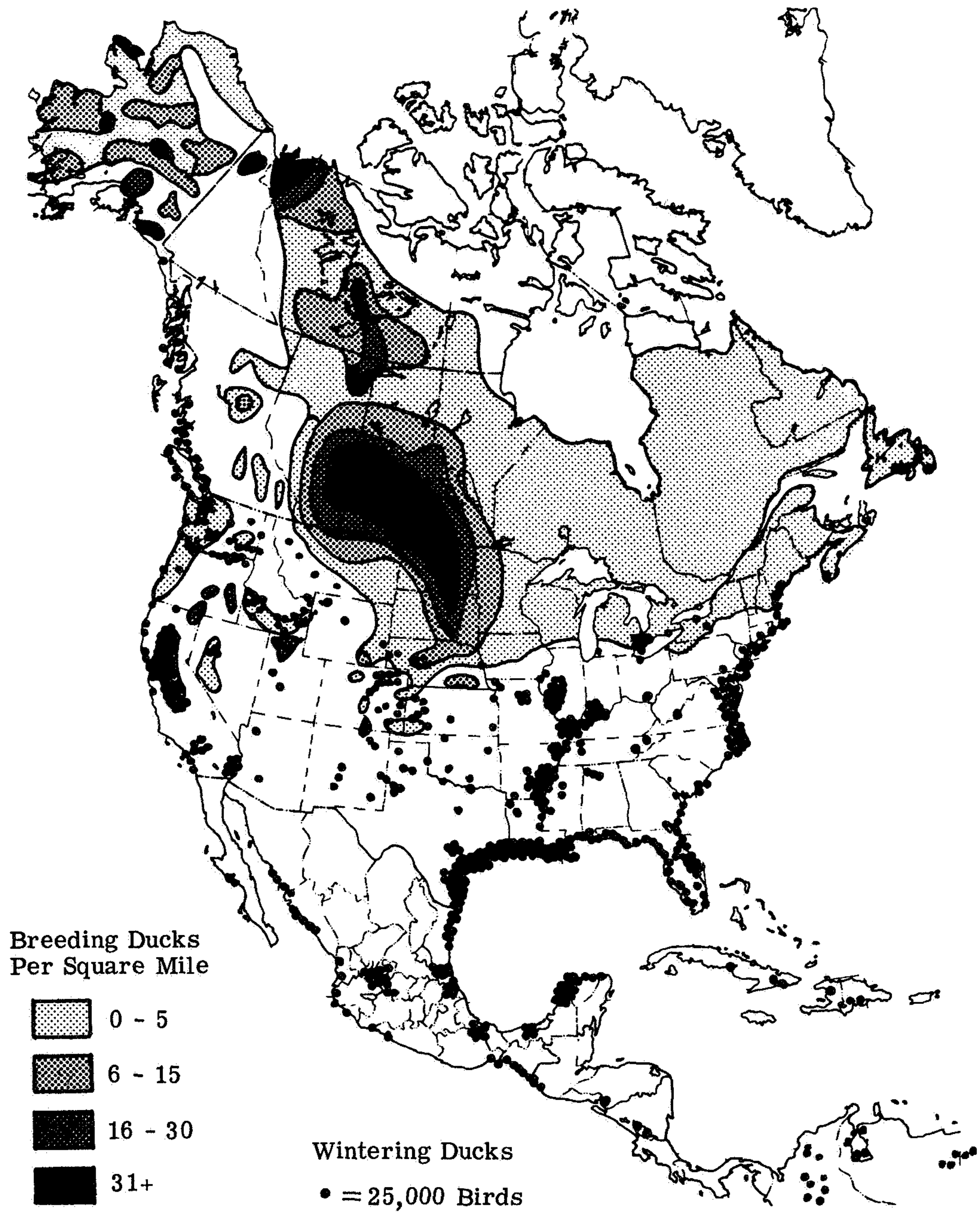

FIGURE 2
AVERAGE DISTRIBUTION OF NORTH AMERICAN
BREEDING AND WINTERING DUCKS

Courtesy BSF&W
U.S. Dept. of Interior

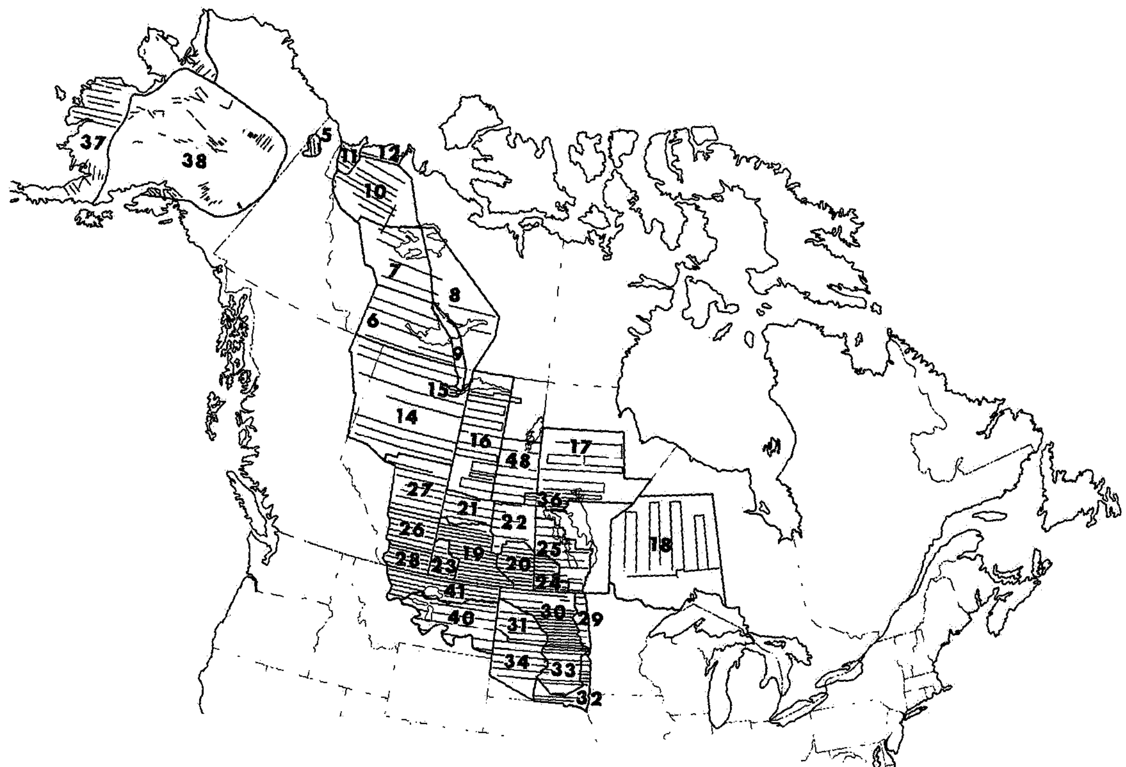

FIGURE 3.

TRANSECTS AND STRATA FOR AERIAL WATERFOWL BREEDING POPULATION AND PRODUCTION SURVEYS

BSF&W
Dept. of the Interior

$$\hat{Y} = 7.926 + 1.468\,X_1 - 0.624X_2 - 0.028X_3 + 0.016\,X_4$$

where $\hat{Y}$ = Predicted number of mallard young (millions)

X_1 = July ponds (millions)

X_2 = continental mallard breeding population (millions)

X_3 = percent of ponds remaining from May to July

X_4 = index to number of broods (thousands) unadjusted

EXAMPLE OF A MODEL FOR PREDICTING
ANNUAL PRODUCTION OF YOUNG MALLARDS*

*After Geis, A. D., R. K. Martinson, and D. R. Anderson (1969)

FIGURE 4

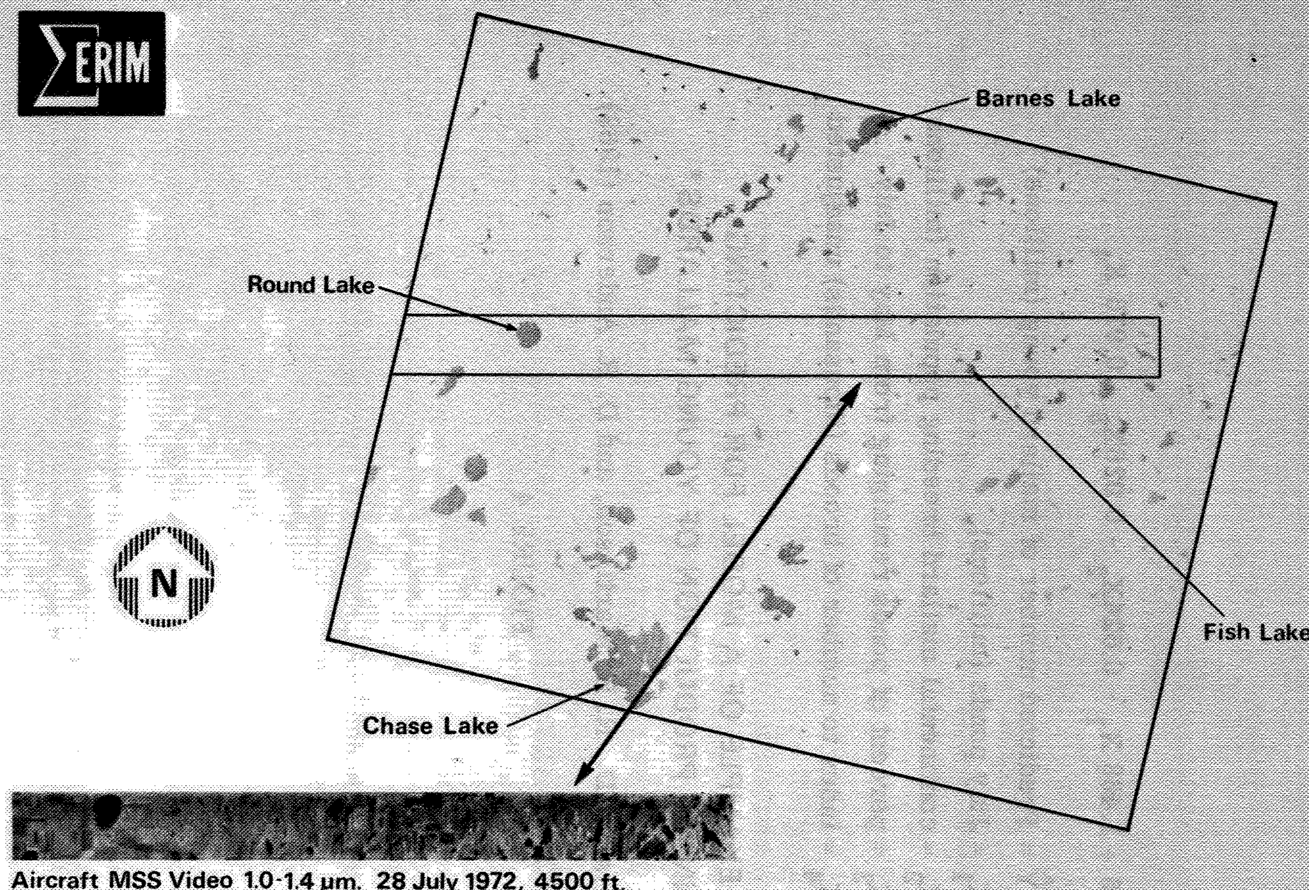

Figure 5
DIGITAL WATER RECOGNITION MAP OF APPROXIMATELY 3% OF AN ERTS FRAME

DATA COLLECTED 31 JULY 1972 • C N45-17/W099-27 • TAPE C, LINES 1140-1540, POINTS 1-610

```
31JUL72 C N47-17/W099-27 N N47-17/W099-25 1008-16594- SUN EL53 AZ134 193-0111-G-1-N-D-0-3-AS1 H ERIM  (ERTS DATA)

   SCENE      NORTH DAKOTA   LINES  1141 THRU  1540     POINTS      1 THRU   610

        SCENE AREA=   424 SQ. MI.
                  =  1099 SQ. KM.

        PIXEL LENGTH=  79 METERS  PIXEL WIDTH=  57 METERS

        MODE= NORMAL
        POINTS COUNTED IF VOLTAGE LIES BETWEEN      .00 AND      9.10 VOLTS

TABULATION OF RECOGNIZED WATER BODIES
```

SCAN LINE	POINT	LAT	LONG	AREA (ACRES)	AREA (HECTARES)
1141	414	47.239N	99.197W	7.868	3.184
1141	457	47.233N	99.165W	1.115	.451
1141	463	47.233N	99.160W	1.115	.451
1142	84	47.279N	99.437W	5.618	2.274
1142	450	47.234N	99.170W	3.355	1.358
1144	418	47.236N	99.194W	4.491	1.818
1144	482	47.228N	99.147W	1.115	.451
1145	329	47.247N	99.259W	37.114	15.020
1145	436	47.233N	99.181W	2.240	.907
1146	55	47.279N	99.458W	1.115	.451
1147	359	47.241N	99.239W	3.356	1.358
1147	398	47.237N	99.209W	1.115	.451
1148	92	47.274N	99.433W	7.877	3.188
1148	450	47.229N	99.172W	5.605	2.268
1149	341	47.243N	99.252W	46.075	18.647
1150	154	47.265N	99.388W	1.115	.451
1150	333	47.243N	99.258W	2.241	.907
1150	353	47.240N	99.243W	5.608	2.270
1150	479	47.225N	99.152W	2.240	.906
1151	260	47.251N	99.311W	1.115	.451
1151	391	47.234N	99.216W	1.115	.451
1152	52	47.276N	99.463W	1.115	.451
1154	11	47.280N	99.493W	2.246	.909
1154	270	47.248N	99.305W	14.604	5.910
1154	435	47.227N	99.185W	4.470	1.809
1156	225	47.252N	99.338W	4.485	1.815
1156	365	47.234N	99.237W	3.367	1.363
1156	388	47.231N	99.221W	1.115	.451
1156	410	47.229N	99.203W	2.241	.907
1157	360	47.235N	99.240W	2.241	.907
1157	534	47.213N	99.114W	1.115	.451

```
31JUL72 C N47-17/W099-27 N N47-17/W099-25 1008-16594- SUN EL53 AZ134 193-0111-G-1-N-D-0-3-AS1 H ERIM  (ERTS DATA)

   SCENE      NORTH DAKOTA   LINES  1141 THRU  1540     POINTS      1 THRU   61

      DISTRIBUTION OF LAKES IN THE SCENE BY AREA
```

AREA (ACRES)	AREA (HECTARES)	FREQUENCY
.25 TO .50	.10 TO .20	
.50 TO 1.00	.20 TO .40	
1.00 TO 2.00	.40 TO .81	159
2.00 TO 3.00	.81 TO 1.21	86
3.00 TO 4.00	1.21 TO 1.62	46
4.00 TO 6.00	1.62 TO 2.43	56
6.00 TO 8.00	2.43 TO 3.24	36
8.00 TO 10.00	3.24 TO 4.05	18
10.00 TO 15.00	4.05 TO 6.07	31
15.00 TO 20.00	6.07 TO 8.09	18
20.00 TO 25.00	8.09 TO 10.12	12
25.00 TO 30.00	10.12 TO 12.14	7
30.00 TO 40.00	12.14 TO 16.19	16
40.00 TO 50.00	16.19 TO 20.23	8
50.00 TO 75.00	20.23 TO 30.35	7
75.00 TO 100.00	30.35 TO 40.47	10
100.00 TO 150.00	40.47 TO 60.70	10
150.00 TO 200.00	60.70 TO 80.94	4
OVER 200.00	OVER 80.94	9

FIGURE 6.

EXAMPLE OF DIGITAL COMPUTER PRINTOUT OF POND AND LAKE STATISTICS FOR THE VICINITY OF WOODWORTH, NORTH DAKOTA USING ERTS-1 DATA COLLECTED AT 1659 GMT ON 31 JULY 1972

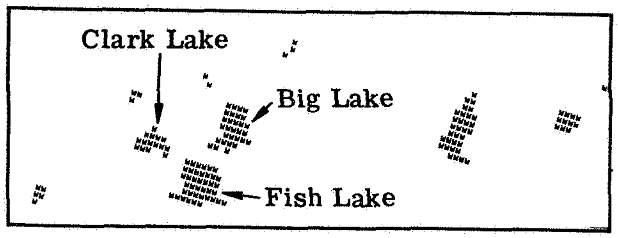

(a) Processed ERTS Water Recognition
(Data of 1659 G.M.T., 31 July 1972)

N

(b) Processed Aircraft Water Recognition from
4500 ft (Data of 1358 G.M.T., 28 July 1972)

1 statute mile

FIGURE 7
COMPARISON OF DETAILS IN ERTS-1 AND AIRCRAFT RECOGNITION MAPS OF PONDS AND LAKES NEAR WOODWORTH, NORTH DAKOTA

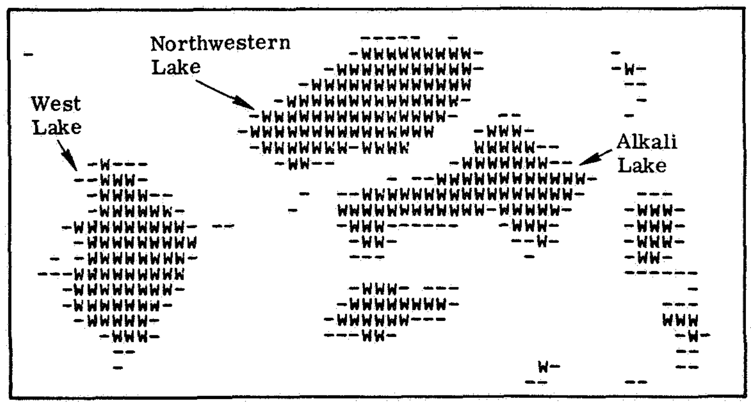

1 mile

'W' = Water
'-' = Water/Marsh Vegetation/Soil

FIGURE 8.
EXAMPLE OF BOUNDARY EFFECT ASSOCIATED WITH RECOGNITION MAP OF LAKES NEAR WOODWORTH, NORTH DAKOTA USING ERTS-1 DATA COLLECTED AT 1659 GMT ON 31 JULY 1972

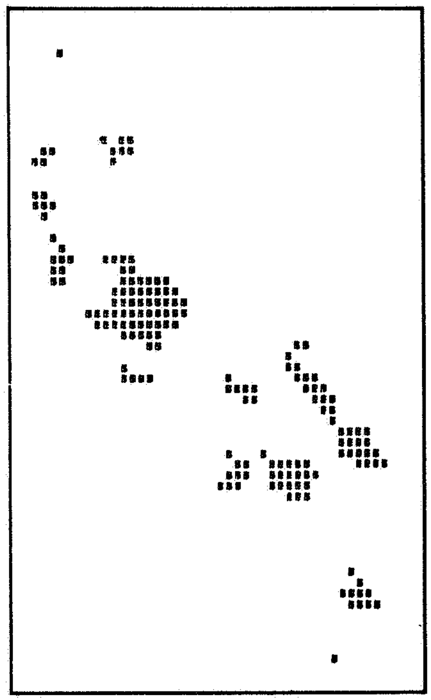

Map of Water Bodies Using
Whole Pixel Recognition

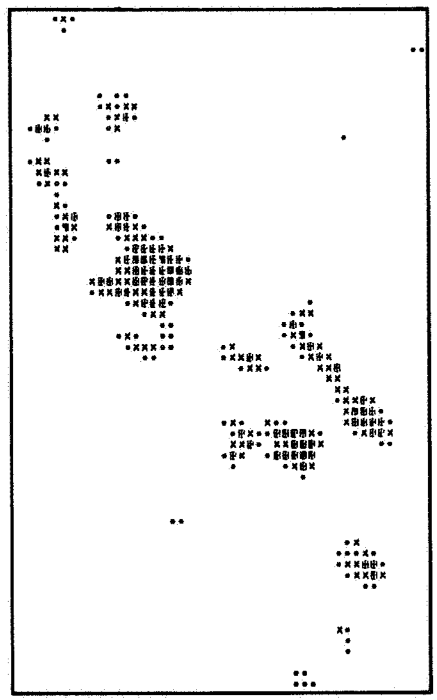

Map of Water Bodies Using
Fractional Pixel Recognition
(Proportion Estimation)

	Whole Pixel Recognition	Fractional Pixel Recognition (Proportion Estimation)	Photo Interpretation
Number of Water Bodies Detected	13	18	19
Total Water Area ($meters^2$)	879,120	1,006,739	1,041,958

FIGURE 9.
COMPARISON OF PROCESSING TECHNIQUES FOR ERTS MSS DATA FOR MICHIGAN LAKES TEST AREA

INTERPRETATION TECHNIQUES

Paper I 1

TECHNIQUES FOR COMPUTER-AIDED ANALYSIS OF ERTS-1 DATA, USEFUL IN GEOLOGIC, FOREST AND WATER RESOURCE SURVEYS

Roger M. Hoffer* and Staff**

ABSTRACT

Forestry, geology, and water resource applications were the focus of this study, which involved the use of computer-implemented pattern-recognition techniques to analyze ERTS-1 data. The results have proven the value of computer-aided analysis techniques, even in areas of mountainous terrain.

Several analysis capabilities have been developed during these ERTS-1 investigations. A procedure to rotate, deskew, and geometrically scale the MSS data results in 1:24,000 scale printouts that can be directly overlayed on 7 1/2 minute U.S.G.S. topographic maps. Several scales of computer-enhanced "false color-infrared" composites of MSS data can be obtained from a digital display unit, and emphasize the tremendous detail present in the ERTS-1 data. A grid can also be superimposed on the displayed data to aid in specifying areas of interest, such as avalanche tracks or areas of burned-over timberland. Temporal overlays of six sets of data have allowed both qualitative and quantitative analysis of changes in the areal extent of the snowpack.

Computer-aided analysis of the data allows one to obtain both cover-type maps and tables showing acreage of the various cover types, even for areas having irregular boundaries, such as individual watersheds. Spectral analysis of snow and clouds, water and shadow areas, and forest cover of varying overstory density have revealed several important results.

* Laboratory for Applications of Remote Sensing, Purdue University, West Lafayette, Indiana

** Personnel involved in this study were from both the Laboratory for Applications of Remote Sensing, Purdue University and from the Institute of Arctic and Alpine Research, University of Colorado, Boulder, Colorado.

This study was supported by NASA Contract NAS5-21880 and by NASA Grant NGL 15-005-112.

INTRODUCTION

This is an interdisciplinary study designed to test the applicability of computer-aided analysis techniques to identify, classify, and map major cover types in the Colorado Rocky Mountains, using multispectral scanner data from ERTS-1. Emphasis has been placed upon a development of analysis techniques useful for processing ERTS-1 data to meet geologic, forest and water resource applications objectives.

Previous work has proven the value of computer-aided analysis of remote sensor data using pattern recognition techniques, but most of this work has been restricted to areas having little topographic relief (1,2,3). It was believed that variations in aspect and slope would have a significant impact upon the spectral response measured by the ERTS-1 scanner. If computer-aided analysis techniques are to be utilized on an operational basis, the relationships between topographic relief and spectral response must be determined. Therefore a key aspect of this study has been the evaluation of computer-aided analysis techniques, to determine their operational utility in areas of mountainous terrain, where so many of our valuable water, forest, and geologic resources are located.

Several different analysis techniques have been developed which have allowed more effective use of ERTS-1 data in the various discipline applications of importance. The major techniques developed are as follows:

- Reformat data to place a full ERTS frame onto a single data tape.
- Display system grid to aid in location of the specific areas of the data tapes.
- Computer-aided enlargement capabilities.
- Geometric correction and scaling.
- Irregular boundary delineation for obtaining area calculations.
- Multiple overlays of digital data.
- Merging of classification results to show temporal change.
- Shadow mapping program as an aid in data interpretation.

The following paragraphs will briefly describe some of the more important of these analysis techniques that were developed and the manner in which they were utilized to meet the objectives of the various discipline groups.

DATA REFORMATTING AND DISPLAY SYSTEM GRID

The original four data tapes containing a single frame of ERTS-1 data are reformatted and the data is placed on a single 1600 b.p.i. data tape. No changes are made in the radiometric quality of the data. This procedure allows easier and more convenient analysis of the data in various portions of a single frame.

After reformatting, the usual procedure has been to go through an enhancement sequence in which individual channels of ERTS data are displayed on the LARS digital display unit and photographed through appropriate filters to produce a false color-infrared composite image of the frame or portion of the frame of interest. To assist in defining the location on the data tape of a particular area of interest, a procedure was developed to superimpose an X-Y grid on the data being displayed. Such a grid can have any desired degree of detail, since every Nth line and Mth column of the investigator's choosing can be displayed. For example, if the entire frame were being displayed, usually a grid of every 200 lines and 200 columns would be superimposed on this data, as shown in Figures 1 & 2. On enlargements of the ERTS data a much finer grid system could be utilized, as for example, every 20th line and column. In some cases, a one square mile grid has been found to be extremely useful. Similarly, one could superimpose a latitude and longitude grid onto the data, if this were more convenient for the investigator.

COMPUTER-AIDED ENLARGEMENT OF DIGITAL DATA

One data processing capability that has proven to be of particular importance in our investigations involves use of the digital data tapes to display data at enlarged scales. Since the digital display unit has the capability of displaying about 800 pixels per line and 500 lines of data, to fit an entire ERTS frame on the screen requires that only 5th line and 5th column initially be displayed. An example of this was shown in Figure 1. Then, by starting with a certain line and column number of the users choice, one can display a subset of the entire frame of data for example, every third line and column, or every line and column as shown in Figures 3 & 4. The next step in enlarging a designated area would involve displaying every ERTS resolution element as two pixel elements along each line of data displayed, and repeating the display of that line of data. In effect, this causes every ERTS resolution element to be displayed as four pixel elements on the display unit. This results in a considerable enlargement of the ERTS data,

as shown in Figure 5. One can also go to 16 pixel elements per resolution element but at this scale the data becomes somewhat blocky in appearance, as seen in Figure 6.

We have found that by enlarging the ERTS data with these digital techniques, a large amount of detail can be seen in the ERTS data. In many cases this detail cannot be seen on the original ERTS imagery or even on 1:250,000 scale photographic enlargements of the original imagery. It is our belief that by using the digital computer to display individual resolution elements of ERTS data, one can obtain a great deal more information than would be possible through normal optical enlargements of the original imagery. There is a tremendous amount of detail present in the ERTS data that is not evident and will simply be missed if one is limited to working with the 1:1,000,000 scale imagery format. This fact has had a significant impact on many of our studies. In developing materials to use in working with the U.S. Forest Service and various state and county land use agencies, we could display the ERTS data at scales large enough to show forest burned areas and avalanche tracks (Figure 7). Location and delineation of such avalanche tracks is of great importance in land use planning activities in these mountain areas, because of the number of houses being built in and near the bottom of these highly hazardous areas.

GEOMETRIC CORRECTION AND SCALING

A particularly significant procedure to allow effective analysis of the ERTS-1 data involves the geometric correction and scaling of the MSS data. This program involves five steps, in which a 1200 line by 1200 column block of data is rotated, deskewed, and rescaled to the users' specifications (4). Use of the system corrected data tapes allows these geometric correction steps to be done without loss in radiometric quality of the data. The only input required for this program, along with the reformatted data tape, is the latitude and longitude of the center point of the data frame involved. The usual output is a geometrically corrected data tape which, if every line and column are displayed on the line printer, allows one to obtain a 1:24,000 scale gray scale printout, oriented with north at the top. Use of this scale allows the analyst to overlay the printout directly on 7 1/2 minute U.S. Geological Survey topographic maps, or other 1:24,000 scale maps and images. This has proven to be extremely beneficial in helping the investigator locate particular, small features of interest, or to define known boundary lines (such as roads) that may not be particularly obvious on the ERTS data. In our studies, we found that proper evaluation of our forest cover classification results from the ERTS data would have been nearly impossible without the use of geometrically corrected and scaled data. This was due to the great difficulty experienced in reliably locating particular

stands of forest cover on the uncorrected ERTS data.

Figure 8 shows a portion of an uncorrected computer printout in which the Vallecito study area has been outlined. The U.S. topographic maps of this 1 1/2 quadrangle study area were overlayed by an acetate sheet and many of the features which could be easily delineated on the map and could also be seen on the gray scale printouts of ERTS imagery were defined (Figure 9). Next, the data was put through the geometric correction and scaling routine and a gray scale printout of this study area was produced. The acetate overlay obtained from the topographic map was then overlayed on the computer printout and the high degree of accuracy of the geometric correction and scaling procedure can be shown (Figure 10). All of the features previously delineated from the topographic map are clearly defined in the same positions on the printout of the ERTS data.

APPLICATION OF ANALYSIS TECHNIQUES TO COVER TYPE MAPPING

As indicated previously, many of the analysis techniques were developed in order to satisfactorily carry out our analysis of ERTS-1 data. One of the major thrusts of the investigation involved ecological inventory, with emphasis on forest cover type mapping. Discussions with U.S. Forest Service personnel indicated as immediate need for general cover type mapping (Level 1) as shown on Table 1, and also the need for maps of various forest types (Level 2 of Table 1). The Forest Service also indicated that many of their planning activities require various levels of detail, much of which could largely be met by maps showing the Level 1 and Level 2 cover types. Several other groups also indicated a similar need for vegetative cover type maps. These included the National Park Service (who needs such information for long range planning and for evaluating and aiding in policy decisions on the use of lands under their jurisdiction), the Bureau of Land Management (who are particularly interested in an inventory of vegetative cover types and present land use, and were also interested in lands having potential for oil shale development), the Division of Wildlife for the Colorado State Government, and several land use planning groups.

Computer-Aided Analysis Results

Based upon input provided by the various user agencies, concerning vegetative cover type mapping, we have emphasized determination of the accuracy and reliability for using computer-aided analysis techniques to map cover types defined by Level 1 and Level 2 categories.

Much of the analysis has involved a four quadrangle area around Lemon and Vallecito Reservoirs in the San Juan Test Site. Detailed cover type maps were prepared, using the WB-57 photography

provided by NASA. Field crews then selected 168 test areas to use in assessing the accuracy of the classification results and for studying slope-aspect-stand density relationships. Classification results indicated that in spite of very distinct variations in spectral response due to the effects of slope, aspect, and differences in density of the forest stands, the various Level 1 categories of cover type could be identified to better than 80% accuracy in most cases. The exception to this was the non-agricultural land, which includes meadows and tundra lands. These were classified as forest cover in many cases. Classification results for the test fields defined within the four quadrangle study area are shown in Table 2. These test field results are a means to quantitatively indicate the classification accuracy obtained over the entire study area.

Classification to the Level 2 degree of refinement has shown many variations in spectral response among the coniferous forest cover groups because of the effects of varying slope, aspect, and density of the forest stands. There appears to be a high degree of correlation between aspect, slope, and density in the spectral response. The interrelationships between these factors are still being studied. It appears that models will have to be developed to take such interrelationships into account before accurate classification can be obtained for the Level 2 categories of coniferous forest cover.

ANALYSIS TECHNIQUES APPLIED TO SNOW MAPPING AND WATER RESOURCE SURVEYS

Computer-aided analysis of ERTS-1 data involving water resource applications has involved several studies including the following:

- Mapping and tabulating the areal extent of snow cover
- Overlaying multiple passes of ERTS data and mapping and tabulating the temporal change in snow cover
- Assessing the capabilities to spectrally differentiate snow from clouds using ERTS-1 data
- Studying and characterizing the reliability of mapping surface water distribution, given the spatial characteristics of ERTS-1 data
- Studying the temporal aspects of freezing and thawing of mountain lakes.

Snow-Cloud Separability

Interpretation and analysis of many data sets have indicated that the detectors on the ERTS-1 satellite system tend to saturate when the scanner is looking at either snow or clouds. Therefore, one cannot reliably separate these two cover types using the dynamic range and spectral characteristics available in ERTS-1 data. (preliminary work with SKYLAB data does indicate that these materials can be easily differentiated in the middle infrared wavelengths, including 1.55 - 1.75 micrometers.)

To quantitatively illustrate the inability to separate clouds from snow, several areas of cloud cover and snow cover were defined on a small portion of one data set, as shown in Figure 11, and the spectral characteristics of these areas were summarized using the statistics processor of the LARSYS programs. Table 3 shows the mean plus or minus one standard deviation for several areas which are identified as cloud cover and several areas identified as snow cover on each of three different dates. A relative response level of 128 indicates saturation level for Channels 4, 5 and 6 of ERTS data and a relative response level of 64 indicates saturation in Channel 7. As can be seen from Figure 12, both snow and clouds tend to saturate all four detectors on two of the dates examined and approach the saturation level for the third date. Thus, the areal extent of snow cover cannot be reliably determined with ERTS-1 data sets in which moderate amounts of cloud cover is present. In many cases, clouds can be identified by their shadow effects, but this does not appear to be a reliable technique.

Digital Data Overlay To Map And Assess Temporal Changes in Snow Cover

Utilizing cloud-free data sets, we made use of our computer-aided analysis techniques to map and tabulate acreages of snow cover in the San Juan Test Site area. Six different data sets were involved in this study, as indicated in Table 4. These data sets were digitally overlaid to produce a single data tape containing 24 channels of data (four channels from each of the six data sets involved). A program was then developed to allow the snow cover changes from one date to the next to be mapped. The output was in the form of a color-coded image, indicating areas in which snow is present on both data sets, areas in which snow was not present on either data set, and areas of change from non-snow to snow, and from snow to non-snow.

Next, a program was developed to allow delineation of an irregular boundary, such as an individual watershed, on the ERTS data. The Animas Watershed near Howardsville, Colorado was utilized in this phase of the study. Initially the boundary was defined using U.S. topographic maps. By overlaying the 1:24,000 scale computer printouts of ERTS data directly on the map, the same boundary was defined as a series of X-Y coordinates

for the ERTS data. Using an average figure of .453 hectares (1.12 acres) per ERTS resolution element, the total area within the watershed was calculated to be 14,706 hectares (36,311 acres). This can be compared to the acreage figure of 35,776 acres which was published in the U.S. Geological Survey literature. The error of 1.5% between these two figures could be attributed to many different sources, the most probable ones being error in the average area figure utilized for each ERTS resolution element or a human error in defining the watershed boundaries of the ERTS data.

Areal calculations for the amount of snow cover within the Animas Watershed on each of the six dates involved in the study indicated that some of the early fall snows had resulted in a broad, shallow snow cover which then partially melted during the late fall before the major snowpack build-up throughout the winter months. By 18 May 1973, only 19% of the area was still snow covered and the following ERTS pass on the 5th of June indicated only 12 1/2% snow cover in the Animas Watershed. Unfortunately, key data sets in March and April were not useable because of the cloud cover. It does appear, however, that reasonably reliable techniques have been developed and are available to provide much of the information needed by the several agencies involved in monitoring and predicting water yield from the snowpack in the upper mountain watershed areas.

GEOLOGIC ANALYSIS AND INTERPRETATION OF ERTS-1 DATA

In the geologic and geomorphic studies, results have indicated a close correlation between the surface cover of vegetation and the geomorphologic characteristics of the area, as was expected. Thus, use of computer-aided analysis techniques to map the surface vegetative features can be followed by manual interpretation of the data by qualified geomorphologists to produce useful geomorphologic maps of the area. Manual interpretation of much of this data is required in order to effectively take into account the spatial characteristics of the data, since our current computer-aided analysis techniques are primarily involved with the spectral features of the data.

In one of the most exciting potential applications of this combination of manual and machine-aided analysis techniques, a study was made to define areas of primary interest for further, more detailed geologic exploration for mineral deposits (5). In this study, the computer is used to produce enhanced large scale infrared composites from the ERTS-1 data tapes. Three geologists then used manual interpretation techniques to define all lineaments that could be discerned in the data. Comparison of these results produced a single lineament map showing only those lineaments that all three analysts had mapped (Figure 13). A grid was then superimposed upon this map and the number of lineament intersections within each cell of the grid were

tabulated and an iso-lineament intersection map was developed. Known mineral deposits were plotted upon the iso-lineament map (Figure 14). A good relationship was observed between the location of a large number of lineament intersections and the known mineral deposits. One particular area of interest showed a large number of lineament intersections where mineral deposits were not known to exist. Field work by the geologists involved indicated that this did appear to be an area of high potential for further geologic exploration. It was later found that another team of geologists, using conventional techniques, had also defined this same area as one of extremely good potential for more detailed geologic exploration. Additionally, a mineral exploration company had already made plans to do more detailed study of this particular area, because of their belief that the area defined in our study of ERTS data is one of high geologic potential.

It would thus appear that the use of this relatively simple technique could offer tremendous geologic potentials for defining areas of interest for more intensive conventional geologic exploration.

SUMMARY AND CONCLUSIONS

In summary, several different analysis techniques have been developed to allow for more effective utilization of ERTS-1 data and computer-aided analysis techniques. The analysis of ERTS-1 data has been directed toward geologic, forest and water resource applications, in accordance with the needs of several user agencies. Contact has been established with many different user agencies and, as appropriate ERTS-1 analysis results are generated, these materials are being utilized as a basis for further discussions on the potential application of ERTS-1 data to meet particular user agency needs. Of particular interest are the contacts that have been established with the following agencies:

- U. S. Forest Service
- National Park Service
- Bureau of Land Management
- Several Colorado state governmental groups
- Several state and county land use planning groups.

In many cases, use of computer-aided techniques to enhance and enlarge ERTS-1 data is of particular interest (e.g. imagery showing avalanche tracks such as shown in Figure 7, forest burn areas, areas of timber clearcutting, and many other land use changes). In many other cases, the ability to tabulate the

areal extent of certain features which can be defined and mapped on the ERTS imagery is of most value to the user agency. The ability to overlay multiple data sets is of particular value for mapping and tabulating temporal changes of various surface conditions. The results obtained thus far during this investigation have proven the value of computer-aided analysis techniques, even in areas of mountainous terrain. Although tentative, many of these conclusions can be summarized as follows:

- Reasonable accuracy (80-90%) can be achieved in areas of rugged relief for Level 1 cover type or land use classification, using machine-aided analysis techniques.

- In mountainous areas, spectral response of Level 2 forest cover types is significantly influenced by variations in stand density, aspect, and slope as well as differences between species.

- Snow cover and clouds cannot be reliably differentiated on a spectral basis in ERTS-1 data, due to detector saturation and available spectral range.

- Similar spectral response is found for many water bodies, terrain shadow areas, and cloud shadow areas, thereby making spectral differentiation difficult, particularly in the infrared wavelengths.

- Computer-aided analysis techniques are very effective for determinations of area and temporal variations of snow cover, over entire regions or individual watersheds.

- Geomorphological features can be effectively mapped with ERTS data through the use of a combination of computer-aided and manual interpretation techniques, and also utilizing knowledge of the vegetative preferences for certain parent materials, slopes, and aspects.

- Delineation of geologic lineaments and domal features can be done very effectively with ERTS data due to the synoptic view, even in heavily vegetated areas, and offers economic potential for mineral resource exploration.

- Analysis of ERTS-1 data could not have progressed satisfactorily without the development of geometric correction and other data handling and analysis techniques.

LITERATURE CITED

1. Landgrebe, D. A., R. M. Hoffer, F. E. Goodrick, and staff. 1972. "An Early Analysis of ERTS-1 Data." Proceedings of the NASA Symposium on ERTS-1, Goddard Space Flight Center, September 29, 1972, pp. 21-38. Also available as LARS Information Note 092972, 21 pp.

2. Hoffer, R. M., P. E. Anuta, and T. L. Phillips. 1972. "ADP, Multiband and Multiemulsion Digitized Photos." Photogrammetric Engineering, 38(10):989-1001.

3. Rohde, Wayne G., Charles E. Olson, Jr. 1972. "Multispectral Sensing of Forest Tree Species." Photogrammetric Engineering, 38(12):1209-1215.

4. Anuta, P. E. 1973. "Geometric Correction of ERTS-1 Digital Multispectral Scanner Data." LARS Information Note 103070, 24 pp.

5. Levandowski, Donald W., T. W. Jennings, and T. W. Lehman. 1973. "Applications of ERTS Imagery to Mapping of Geologic Features Favorable to the Localization of Ore Deposits in North - Central Nevada." Paper presented at the Annual Meeting of the Geological Society of America and Related Societies, Dallas, Texas, November 14, 1973.

ACKNOWLEDGEMENTS

Personnel from LARS and INSTAAR who need to be particularly recognized for their contributions to this paper include Richard Mroczynski, project coordinator for LARS; Tina Cary, Michael Fleming, Donald Levandowski, and Terry Lehman, who were involved in various aspects of the data analysis; Dr. Jack Ives, principal investigator of the sub-contract to INSTAAR, Dr. Paula Krebs, project coordinator for INSTAAR, and Debbie Keamerer, research ecologist. Many other personnel from both LARS and INSTAAR have been involved in this research, and their contributions are gratefully acknowledged.

Table 1. Cover Type Categories Utilized in Computer-Aided Analysis of ERTS-1 Data in the San Juan Mountain Test Site.

General	Level 1	Level 2
FOREST	Conifer	Pinyon-Juniper Ponderosa Pine Douglas and White Fir Spruce-Fir Krummholtz Colorado Blue Spruce
	Deciduous-Conifer	Douglas and White Fir, Ponderosa Pine, and Aspen
	Deciduous	Cottonwood-Willow Alpine Shrub Oak-Shrub Oak Aspen
HERBACEOUS	Agricultural	Cultivated Crops Cultivated Pasture Pasture
	Non-Agricultural	Meadow Tundra Wet Meadow
NON-VEGETATED	Rock and Soil	Exposed Rock Exposed Soil
	Shadow	Ridge Shadow Cloud Shadow
	Water	Clear Turbid
	Snow	Snow Only Snow-Forest Mix
	Cloud	Cloud
	Urban	Urban

Table 2. Test Class Performance for Four Quadrangle Test Site in San Juan Mountains.

			Number of Samples Classified Into							
Group	No of Samps	Pct. Corct	Conifer	Decid	Non-Ag	Agri	Cloud	Shad	Bare	Water
1 Conifer	2031	83.0	1686	180	154	0	0	10	1	0
2 Decid	459	81.7	75	375	6	2	1	0	0	0
3 Non-Ag	276	62.0	60	44	171	0	0	0	1	0
4 Agri	60	86.7	0	8	0	52	0	0	0	0
5 Cloud	123	99.2	0	1	0	0	122	0	0	0
6 Shad	135	96.3	5	0	0	0	0	130	0	0
7 Bare	105	90.5	0	0	2	0	0	0	95	8
8 Water	236	97.9	0	0	0	0	0	0	5	231
TOTAL	3425		1826	608	333	54	123	140	102	239

Overall Performance (2862/3425) = 83.6

Average Performance by Class (697.2/8) = 87.1

168 Test Fields = 3% of Total Area (1554 Hectares or 3836 Acres)

Table 3. Comparison of Spectral Response of Clouds and Snow Using ERTS-1 Data.

	Channel 4 (0.5-0.6μm)	Channel 5 (0.6-0.7μm)	Channel 6 (0.7-0.8μm)	Channel 7 (0.8-1.1μm)
Clouds	126.6 ± 2.3[1]	126.2 ± 2.8	118.2 ± 6.8	55.6 ± 6.7
Snow	125.4 ± 5.2	125.0 ± 5.6	116.2 ± 10.2	51.2 ± 9.0

[1]Numbers indicate mean relative response ± 1 standard deviation using a combination of approximately 3000 data resolution elements, representing several areas of clouds and snow on each of these dates (1 Nov. '72, 6 Dec '72, and 18 May '73). Saturation level is 128 for Channels 4, 5, and 6, and is 64 for Channel 7.

Table 4. Snow Area Calculations for the Animas Watershed near Howardsville, Colorado

Date of ERTS-1 Data Utilized	Hectares (Acres) of Snow Cover Within the Watershed[1/]		Percentage of Watershed Covered by Snow
1 Nov. 1972	11,193	(27,636)	76.1%
19 Nov. 1972	10,040	(24,791)	68.3%
12 Jan. 1973	9,206	(22,731)	62.6%
30 Jan. 1973	10,027	(24,757)	68.1%
18 May 1973	12,876	(31,771)	87.5%
5 Jun. 1973	11,911	(29,411)	81.0%

[1/]Total area of Animas Watershed = 14,695 hectares (36,611 acres), based on ERTS-1 data calculations, and 14,478 hectares (35,776 acres) reported by U.S.G.S., indicating a difference of only 1.5%.

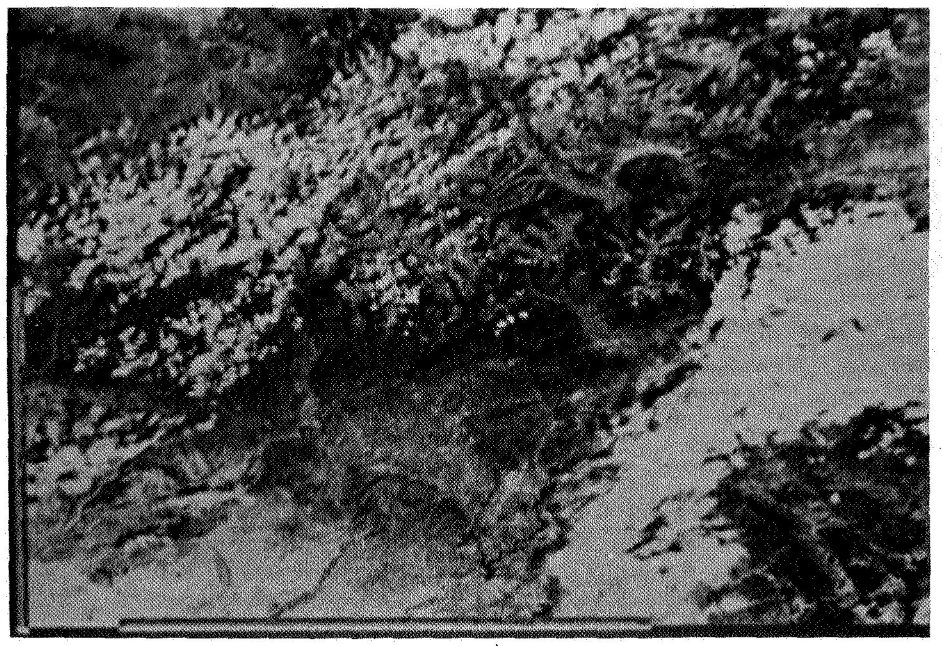

Figure 1. Color-infrared composite of September 8, 1972 ERTS-1 data from the San Juan Test Site in southwestern Colorado, taken from the LARS Digital Display Unit. The scale lines indicate a 100 kilometer (62 statute miles) length. Two different scale lines are necessary because rectangular ERTS-1 data elements are being displayed as square picture elements on the digital display.

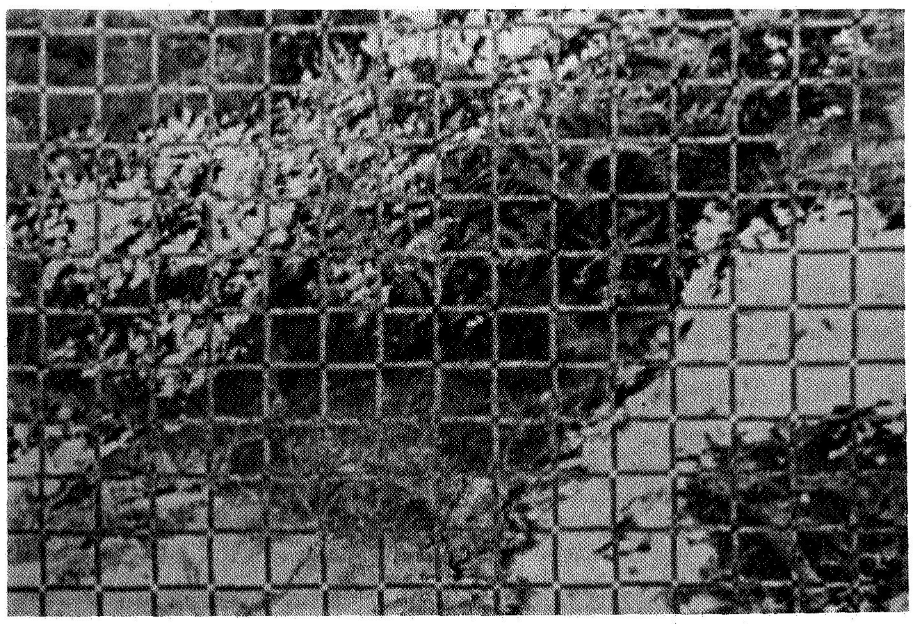

Figure 2. A grid having an interval of 200 lines and 200 columns was superimposed on the data shown in Figure 1, enabling analysts to easily determine the line and column coordinates of specific areas of interest.

Figure 3. A portion of the data shown in Figure 1 has been enlarged by using every third line and column of data. The scale lines indicates a 100 kilometer distance, giving a horizontal scale to this illustration of 1:800,000. Further enlargement is shown in Figures 4, 5, and 6.

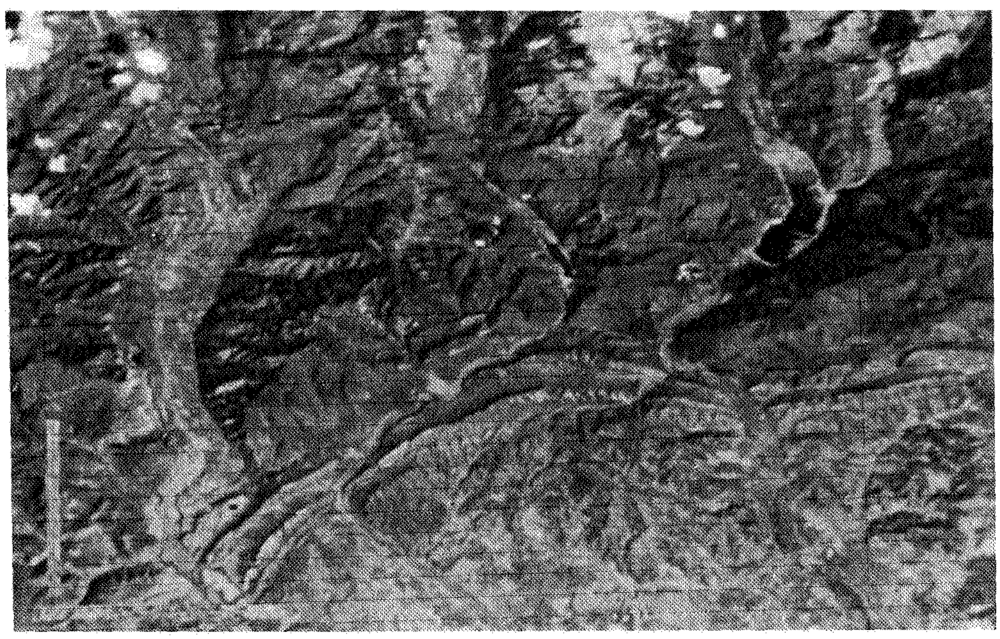

Figure 4. Further enlargement of the data displayed in Figures 1 and 3 shows Vallecito Reserovir and the surrounding area in more detail. Every line and column of data is displayed. The scale lines here represent only a 10 kilometer distance. Horizontal scale of this illustration is approximately 1:300,000.

Figure 5. One fourth of the data displayed in Figure 4 can be displayed onto the full screen by using four pixels per data point. The scale lines again indicate 10 kilometers, giving this figure a horizontal scale of approximately 1:143,000.

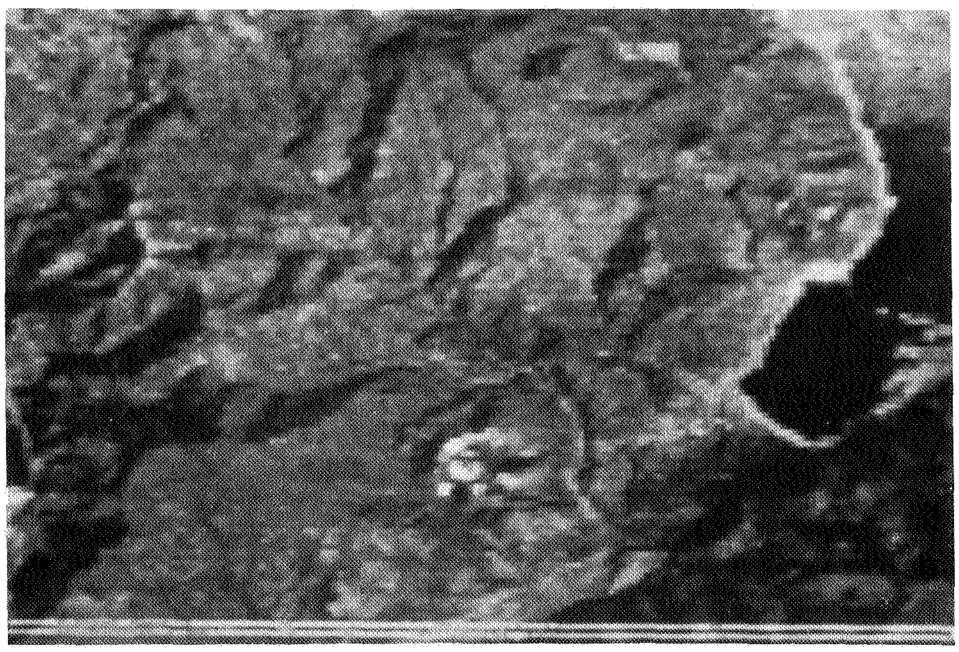

Figure 6. Maximum enlargement capability, in which each ERTS resolution element is displayed as 16 pixel elements on the digital display. Horizontal scale of this illustration is approximately 1:72,500.

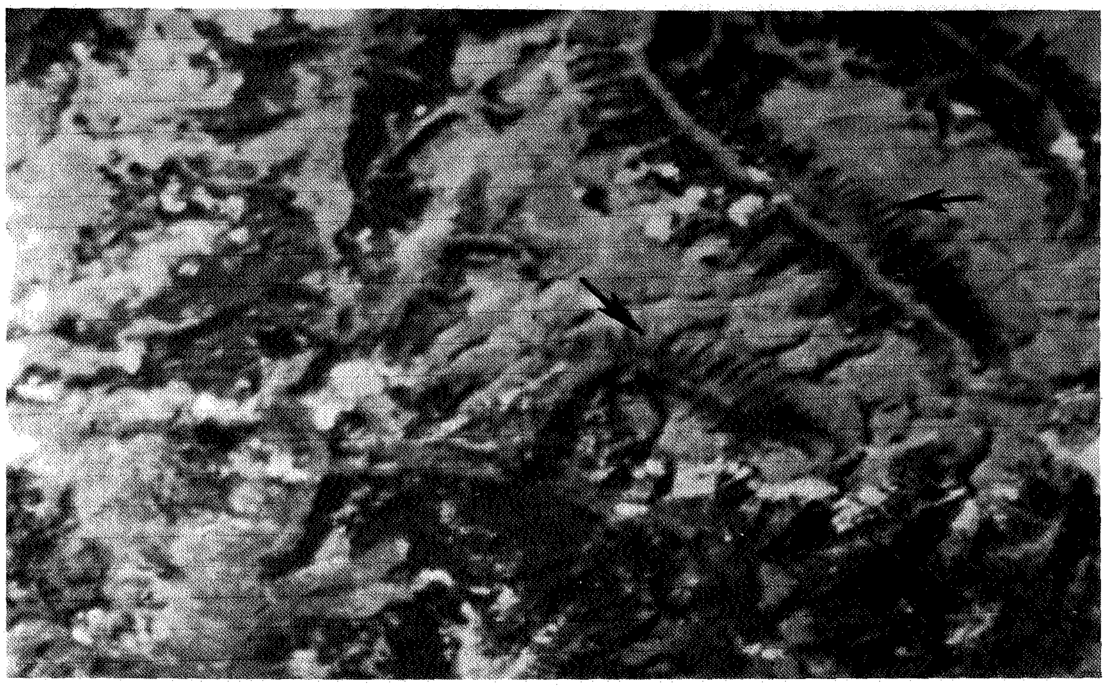

Figure 7. Enhanced color infrared composite of ERTS-1 imagery from the LARS digital display unit, showing avalanche track locations. The scale of this illustration is approximately 1:150,000. This data was obtained on September 8, 1972. Similar enlargements have allowed forest clear-cuts and burned areas to be delineated. Such computer-aided enhancement and enlargement capabilities offer many advantages for effective utilization of ERTS data in various application areas.

Figure 8. Uncorrected printout of ERTS data showing the Vallecito study area delineated by the heavy boundary. Compare this to the same data after it has been geometrically corrected and scaled, as shown in Figure 10.

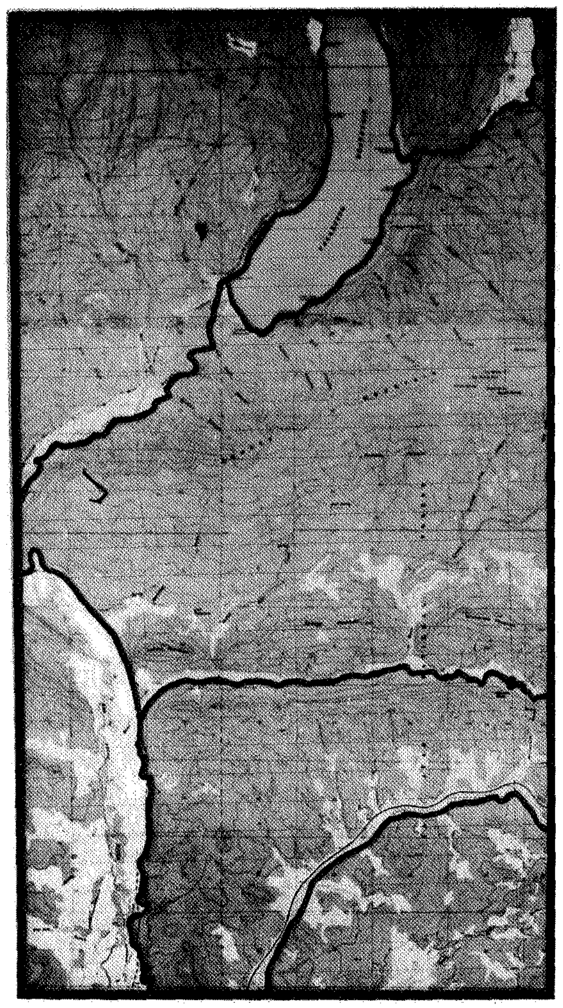

Figure 9. U.S. Geological Survey topographic maps of the Vallecito study area. Dominant features which could be easily delineated on both the topo maps and the ERTS data were delineated on an acetate overlay.

←

Figure 10. Geometrically corrected and scaled computer printouts of ERTS-1 data of the Vallecito study area. The scale of this printout is 1:24,000. The acetate overlay made from the U.S.G.S. topo map was superimposed on the computer printout, allowing one to verify the accuracy of the geometric correction and scaling process.

→

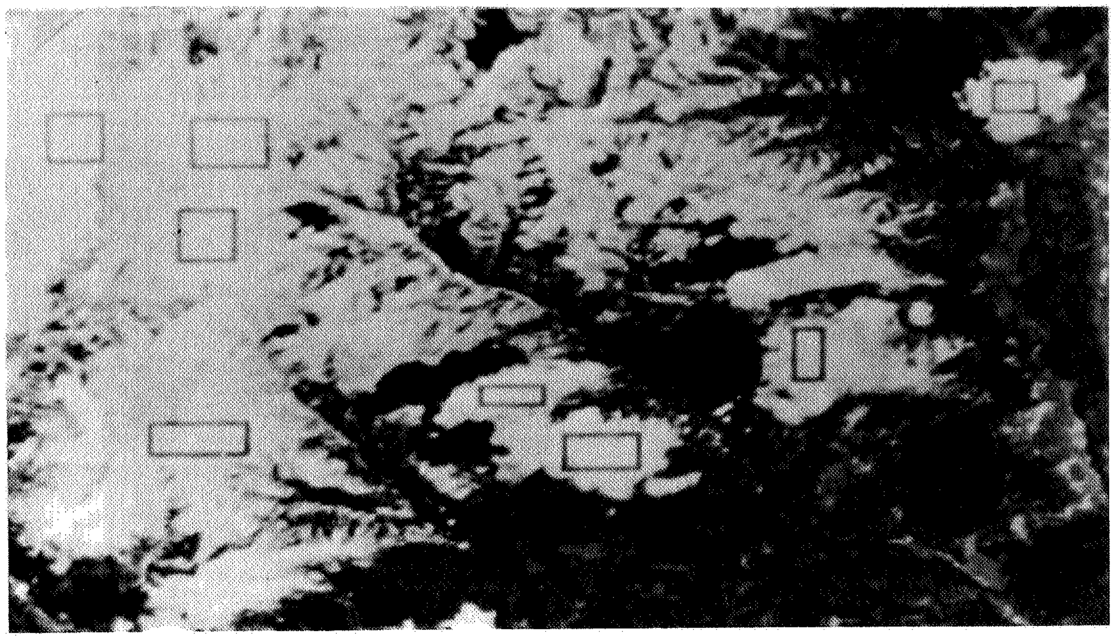

Figure 11. Color infrared composite of ERTS data from the digital display unit, with snow and cloud areas delineated. The four rectangular areas on the left designate snow cover, while the four areas on the right are cloud cover. Comparisons of the spectral response are shown in Figure 12.

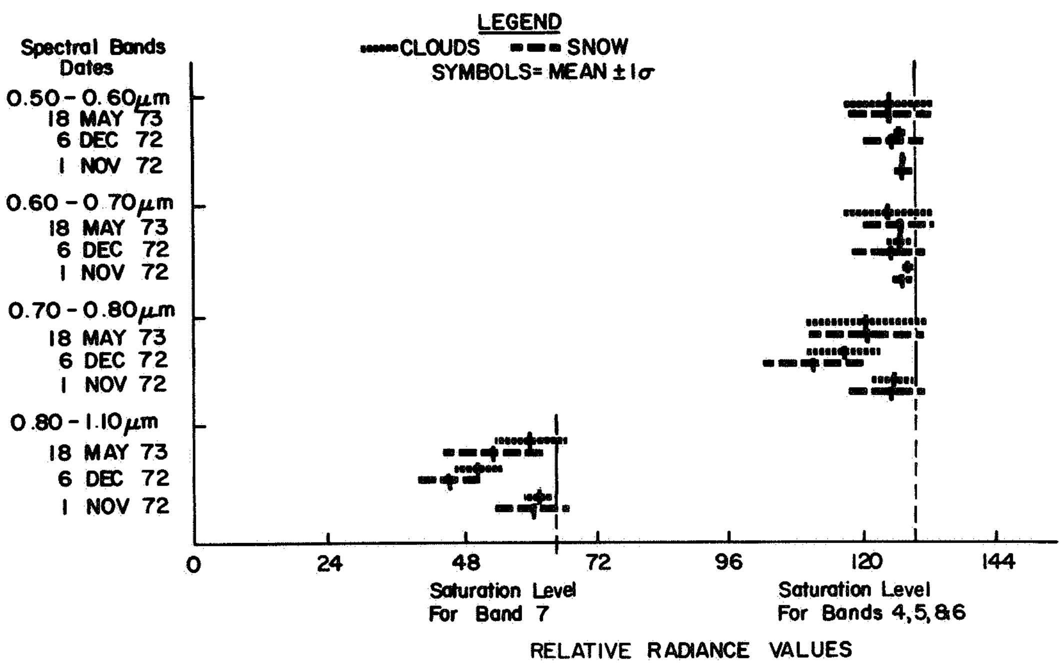

Figure 12. Spectral comparison of clouds and snow using ERTS-1 data from three different dates. Saturation level was reached in nearly all data sets and the similarity of response indicates lack of spectral separability between these two cover types.

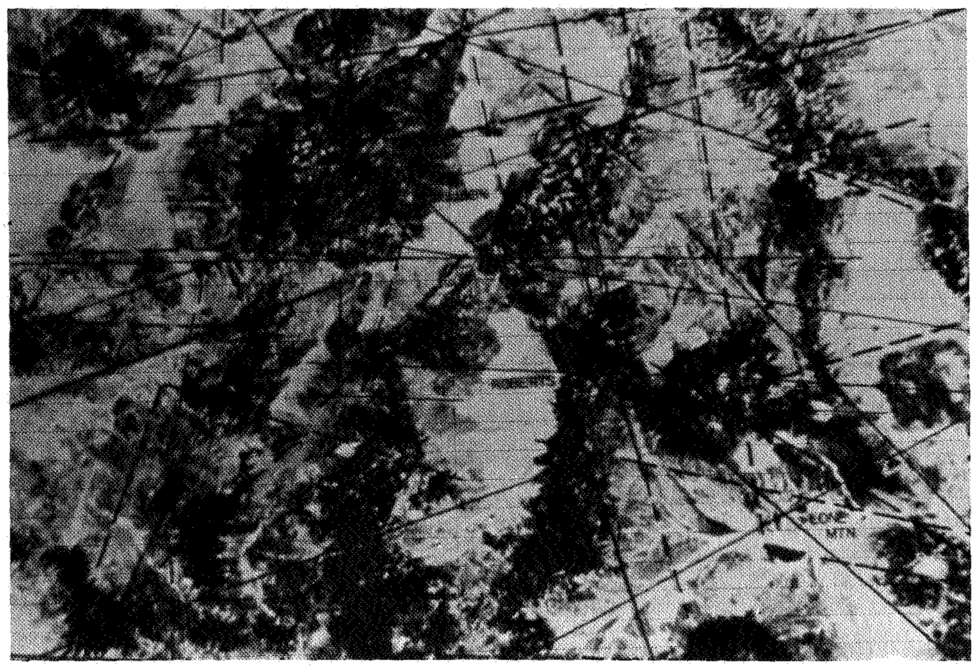

Figure 13. Computer enhanced color infrared composite of ERTS data with lineaments mapped by all three geologists analyzing this data set. A grid was superimposed upon this map and lineament intersections were tabulated for each cell.

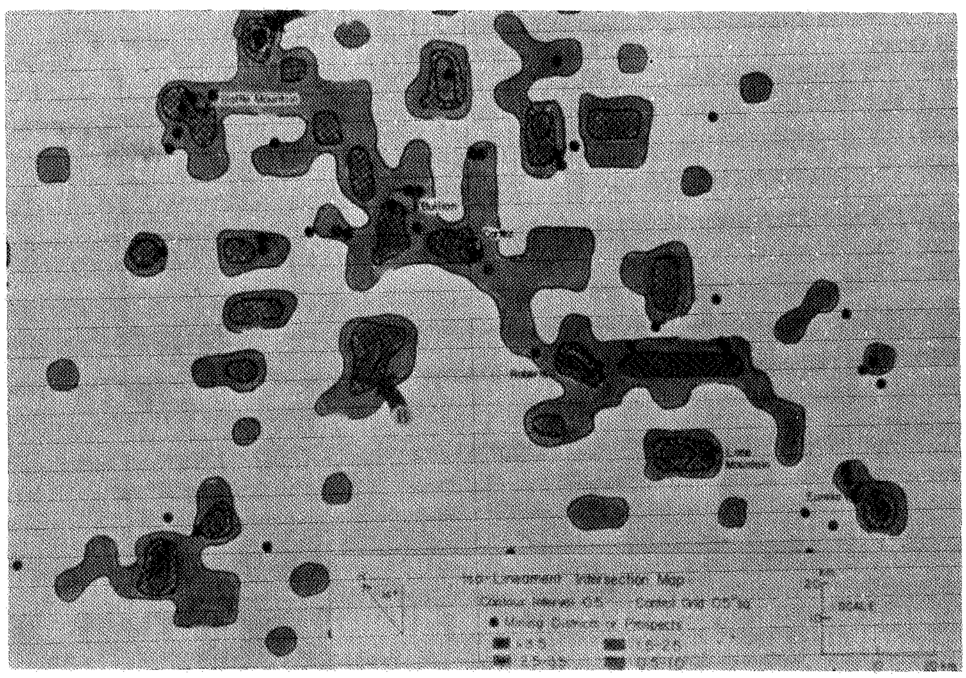

Figure 14. Iso-lineament intersection map and overlay of known mineral deposits. Good relationship was observed between the areas with frequent lineament intersections and known mineral deposits.

Paper I 2

MULTISPECTRAL COMBINATION AND DISPLAY OF ERTS-1 DATA

Vidal Raphael Algazi, *Department of Electrical Engineering, University of California, Davis, California 95616*

ABSTRACT

Standard NASA color composites combine the most relevant 3 bands from the 4 MSS bands available. An alternate approach is to extract the principal components of the data by a linear transformation of the 4 bands. This approach leads to a low dimensionality representation of ERTS-1 data with the least degradation, in the mean square sense, of the radiometric accuracy. The technique has been applied with success to ERTS-1 MSS data for several geographic areas in California. For all examples considered the mean square representation error is less than one percent. By combining this dimensionality reduction which our previous results on image enhancement for visual display, color composites are obtained which contain and display most of the information provided by the ERTS-1 sensors.

INTRODUCTION

A significant problem in the use of ERTS-1 data is the extraction of information pertinent to each application and the presentation of that information in a form most suitable to users.

When the information is to be displayed for visual study by an observer, then the problem can be reduced to two independent steps:

1. Dimensionality reduction, an objective procedure which attempts to preserve most of the ERTS-1 information in a smaller number of components.
2. Display of the reduced number of components for "optimum" visibility by an observer.

A specific dimensionality reduction technique has been applied to ERTS-1 data for several geographical areas in California and distinct types of Earth Resources.

In the display of the reduced number of components, consideration has to be given to properties of the human visual system and the statistics of the data to be displayed. Our previous work on digital image enhancement (1) is applied to this problem to generate color composite which contain and display most of the information provided by the ERTS-1 sensors.

MULTISPECTRAL DATA COMBINATION: PRINCIPAL COMPONENTS ANALYSIS AND DIMENSIONALITY REDUCTION

The motivation for extracting the most significant three spectral components from the 4 spectral MMSS bands of ERTS-1 is that the space used for display, the perceptual space, has only 3 dimensions corresponding to the 3 primary colors.

Generally, the problem of processing and display of multispectral data is to map a set of N spectral components $\{I_k\}$ into a 3 dimensional perceptual space. A common approach is to choose the "best" three I_k's out of N.

Another approach, described briefly here, is to apply a set of invertible transformations to the multispectral data and then to choose the best subset of transformed components.

Let $\underline{I}'$ be the set of transformed spectral components.

We write

$$\underline{I} = [A]\underline{I}' \tag{1}$$

in which [A] is an NxN matrix, corresponding to a linear transformation of $\underline{I}'$ into $\underline{I}$. The columns of [A] are taken to be orthonormal vectors.

Assume that L<N components of $\underline{I}'$ are used and the others discarded. By entering N-L zero components into $\underline{I}'$ we form a new vector $\underline{I}''$ which generates by (1)

$$\hat{\underline{I}} = [A]\underline{I}'' \tag{2}$$

$\hat{\underline{I}}$ is an approximation to $\underline{I}$. The goodness of the approximation is measured in a mean-square sense.

$$\varepsilon_L = E[||\underline{I} - \hat{\underline{I}}||^2] = E[\sum_k (I_k - \hat{I}_k)^2] \tag{3}$$

for a given L, a question of interest is the optimum choice of the set of transformed components $\underline{I}'$ and therefore of the transformation matrix [A].

The solution to this problem for the criterion of (3) is known as the decomposition into principal components or as the Karhunen-Loeve representation of $\underline{I}$, reported in the literature. Let $[\mu]$ be the covariance matrix of the data, then the vectors $\underline{e}_k$, k=1, ...N columns of the matrix A are obtained by solving the matrix equation

$$[\mu]\underline{e}_k = \lambda_k \underline{e}_k \tag{4}$$

in which the λ_k's are positive numbers, also to be determined. Equation 4 is the formulation of a classical mathematical problem with known solution. The λ_k's and $\underline{e}_k$'s are denoted eigenvalues and eigenvectors of matrix $[\mu]$ respectively.

Once the λ_k's and the $\underline{e}_k$'s are obtained, the transformed vector $\underline{I}'$ is obtained by the matrix operation

$$\underline{I}' = [A]^T\underline{I} \tag{5}$$

From $\underline{I}'$, one obtains $\underline{I}$ back by (1) since

$$[A]^T[A] = [I] \tag{6}$$

in which [I] is the identity matrix.

The mean-square error approximation of equation (3) is expressed easily in terms of the λ_k's. It can be shown that

$$\varepsilon_L = E(\sum_k (I_k - \hat{I}_k)^2) = \sum_{k=1}^{L} \lambda_k \tag{7}$$

Since $\hat{\underline{I}}$ is obtained by retaining only L of N transformed components $\{I_k'\}$, one can readily determine, from the λ_k's, the mean-square error incurred by discarding N-L components.

Note that the choice of the transformation matrix [A] and the resulting mean-square error (7) are dependent on the covariance matrix [μ] and thus on the data used in the estimation of [μ]. In the case of ERTS-1 data we expect significant variations in the covariance matrix with the type of natural resource and the seasons.

APPLICATION TO ERTS-1 DATA *

We have applied the approach just outlined to ERTS-1 data, and the results are interesting, both in terms of the small mean-square error caused by the dimensionality reduction, as well as for the examples of enhanced images we have obtained.

We examined the mean-square error introduced by a dimensionality reduction for 3 areas of California: The Buck Lake region, a wildland area; the farmland south of Isleton; the East Bay cities which include part of San Francisco Bay and some woodlands. Two questions of interest are: What is the percent mean-square error introduced by a dimensionality reduction? What are the corresponding eigenvectors and thus corresponding spectral combination used?

The answer to these questions can be obtained from the Tables 1, 2 and for two of the 3 geographic areas.

The normalized covariance matrix (correlation coefficient matrix) indicates the pairwise linear similarity and correlation of the data for the 4 spectral components. As noted earlier MSS bands 4 and 5 and MSS bands 6 and 7 are highly correlated in all cases.

The variances of spectral components are also given (within a scale factor) to indicate their relative ranking. Ratio of variances range from 3 to 1 to 8 to 1.

---

* See References 5 and 6 for additional discussion of principal component analysis applied to Remote Sensing Data.

$$
\begin{bmatrix}
1.0000 & .9356 & .5097 & .3341 \\
.8356 & 1.0000 & .4317 & .2429 \\
.5097 & .4317 & 1.0000 & .9633 \\
.3341 & .2429 & .9633 & 1.0000
\end{bmatrix}
\quad [\rho] \text{ Normalized Covariance Matrix}
$$

$$
\begin{matrix} 109 & 283 & 791 & 600 \end{matrix} \quad \text{Variances}
$$

Table 1

BUCKS LAKE
1002 - 10125

$$
\begin{bmatrix}
.8685 & -.4939 & -.03927 & .001917 \\
.07850 & .1941 & -.6708 & .7114 \\
.4659 & .8220 & -.05041 & -.3232 \\
.1492 & .2060 & .7388 & .6240
\end{bmatrix}
\quad [A]^T, \text{ Rows are Eigenvectors}
$$

$$
\begin{matrix} 9.278 & 10.79 & 325.1 & 1439. \end{matrix} \quad \{\lambda_k\} \text{ Eigenvalues}
$$

$$
\begin{bmatrix}
1.0000 & .9537 & .2323 & .0187 \\
.9537 & 1.0000 & .1226 & -.0881 \\
.2323 & .1226 & 1.0000 & .9629 \\
.0187 & -.0881 & .9629 & 1.0000
\end{bmatrix}
\quad [\rho] \text{ Normalized Covariance Matrix}
$$

$$
\begin{matrix} 467 & 947 & 860 & 411 \end{matrix} \quad \text{Variances}
$$

Table 2

FARMLAND SOUTH OF ISLETON
1003 - 18175

$$
\begin{bmatrix}
.1515 & .0120 & -.5699 & .8074 \\
.8118 & -.5689 & .0208 & -.1292 \\
-.2358 & -.4330 & .6859 & .5349 \\
.5120 & .6990 & .4517 & .2123
\end{bmatrix}
\quad [A]^T \text{ Rows are Eigenvectors}
$$

$$
\begin{matrix} 7.540 & 25.16 & 1186. & 1467. \end{matrix} \quad \{\lambda_k\} \text{ Eigenvalues}
$$

Turning to the eigenvalues and using (7) we have the following table for percent error due to dimensionality reduction

	Bucks Lake	Isleton	East Bay
1 component discarded	.52	0.28	0.81
2 components discarded	1.13	1.21	2.1

Table 3

Entries are percent mean-square error

We see that in all cases, by linear transformation, it is possible to generate 3 equivalent components which represent the 4 spectral MSS bands with less than one percent error.

The relatively larger mean-square error for the East Bay image, which contains a substantial area of water, suggests that significantly different results may be obtained by handling the water area separately.

To test this hypothesis we processed the East Bay image and also a large image of the Bay Area containing water land and partial cloud coverage. The principal component analysis was carried out separately on land water, and clouds. The separation of these distinct areas is done quite well by using a threshold on MSS 7 radiometric data to generate a water area mask since in the infrared the reflectivity of water is very low. Clouds are also easy to remove by thresholding.

For the East Bay Image we have the results of Table 4. This table shows markedly different results for water and land in that the spectral combinations (eigenvectors) needed for optimal dimensionality reduction are quite different. Also dimensionality reduction is significantly less effective, for water then it is for land.

$$\begin{array}{cccc l}
352 & 290 & 544 & 725 & \text{Variances (MSS 4,5,6,7)} \\
\end{array}$$

$$\begin{bmatrix} -.32 & .06 & .74 & -.58 \\ -.60 & .76 & -.20 & .15 \\ .68 & .60 & -.70 & -.40 \\ .26 & .24 & .63 & .69 \end{bmatrix} \quad \text{Eigenvectors} \qquad \text{Land only}$$

$$\begin{array}{cccc l}
23.1 & 25.4 & 541 & 1322 & \text{Eigenvalues} \\
\end{array}$$

80	35	4	8.5	Variances (MSS 4,5,6,7)	

$$\begin{bmatrix} .07 & -.16 & .98 & -.02 \\ .07 & -.10 & .00 & .99 \\ -.48 & .85 & .18 & .12 \\ .87 & .49 & .02 & -.02 \end{bmatrix} \quad \text{Eigenvectors} \qquad \text{Water only}$$

3.7	8.3	14	101	Eigenvalues

Table 4

East Bay Cities. Principal Component Analysis

Thus, although from the eigenvectors of Tables 1 and 2 it appears that some fixed combination of spectral components may lead to acceptable results in all cases, Table 4 indicates that the issue has to be examined more carefully with regard to each specific objective.

DISPLAY OF THE SIGNIFICANT DATA

When the data has been reduced to 3 principal components, it remains to combine these components in a color composite which provides acceptable visual descrimination of the information contained in the data.

One has to choose first the color primaries, or color coordinates to which the principal components will be assigned. The statistics of each principal component (histogram) can then be used to maximize the average visibility of the data.

In the assignment of color primaries we have considered an assignment of Red, Green and Blue coordinates to the principal components. The examination of the eigenvectors, for each specific geographic area, allows an assignment which matches as closely as possible the conventional color assignments of the standard NASA color composites of ERTS-1 data.

Other assignments of color primaries have been considered. These assignments try to exploit more fully the space of visual perception and visual discrimination and the large differences in the variances of the principal components. One possible choice is to assign the component with the largest variance to luminance and the two other components to chrominance. In several examples this approach is dissappointing and leads to flat images. Further work is underway on this basic problem in the display of multispectral data, which is due to the high correlation of the sensor outputs themselves.

After all data transformations, best use is made of the perceptual space available by enhancement of each display component as discussed in [1]. Thus, histograms are generated and a nonlinear mapping of data values I_{RD}, I_{GD}, I_{BD}, to display values I_{RV}, I_{GV}, I_{BV} is done using the relations.

$$I_{RV} = g_R \, (I_{RD})$$

$$I_{GV} = g_G \, (I_{GB}) \tag{8}$$

$$I_{BV} = g_B \, (I_{BD})$$

and

$$g_R(I_{RD}) = K_1 \int_{-\infty}^{I_{RD}} [f_R(x)^{1/2} \, dx + K_2 \tag{9}$$

in which $f_R(x)$ is the histogram of the data assigned to Red and K_1 and K_2 are chosen to match the range available for display. Similar mappings are used for the green and blue signals.

DISCUSSION OF THE RESULTS AND CONCLUSIONS

Dimensionality reduction by principal component analysis, exploits, in an optimal way, the redundanc and correlation which exists in ERTS-1 data. The results presented here for distinct geographic areas indicate that it is possible to represent with 3 principal components the 4 band MSS ERTS-1 data with little loss of radiometric accuracy. Since this approach depends on statistics or average properties of the data, some care is needed in assessing the relevance of a global transformation and of global measure of approximation to each specific application.

The separation of ERTS-1 data into land, water and clouds, which is possible with fairly simple techniques, is important in the analysis and display of ERTS-1 data. In particular Table 4 indicates that water and land may require different transformations and for the purpose of display it certainly appears desirable to enhance water separately because of the small range of data values recorded.

We note also that the results presented here did require a radiometric correction of the digital data to reduce or eliminate stripping. The technique used for sensor response equalization has been reported [2].

Principal component analysis established a firm theoretical basis for multispectral data combination, but requires an algorithm adapted to the data been processed. Some of our results indicates that a fixed multispectral combination, not dependent on specific statistics but suggested by statistical analysis, may be satisfactory in many cases. A detailed study is needed to determine and assess such a multispectral combination in applications.

In applications, dimensionality reduction is of use in automatic classification or in the study of images by photo-interpreters. Personnel of the Center for Remote Sensing Research at the University of California, Berkeley [3] have used some images enhanced and displayed by techniques previously reported [1] to detect and classify total commercial conifer in the Sierra Nevada in California, by photo interpretation. Other work on the delineation of sediments in water has also been done [4]. Results are indicative of the merits of the enhancement

technique and it is expected that combining dimensionality reduction with image enhancement will provide significantly better results.

AN ILLUSTRATIVE EXAMPLE

As an example of multispectral data combination and display we processed a large portion of the San Francisco Bay area, 1165-18175. The first image, Figure 1, shows MSS bands 4, 5, 7 enhanced and combined. In Figure 2, we show the result of processing the 4 MSS bands. Principal components are extracted separately for land and water and the corresponding transformation applied. Clouds are not processed. A composite image is generated by juxtaposition of subimages. The composite images appears to convey a large amount of information, but a detailed study remains to be done.

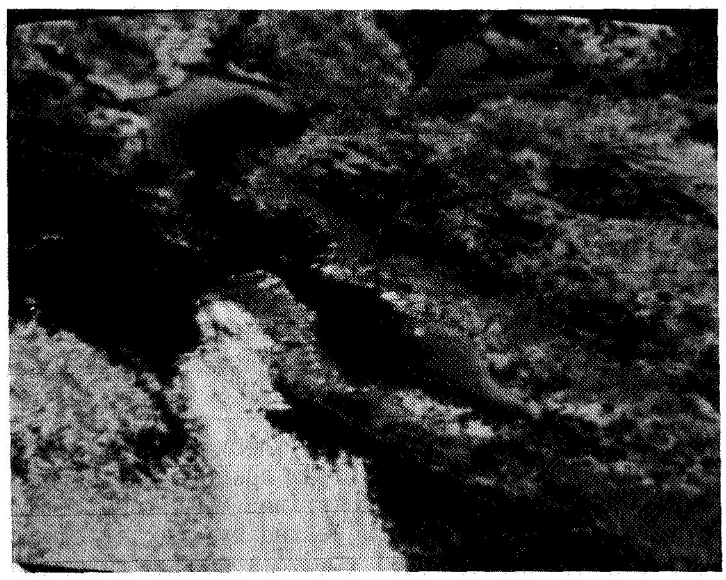

Figure 1. Bay Area 1165-18175
MSS 4,5,7 Enhanced

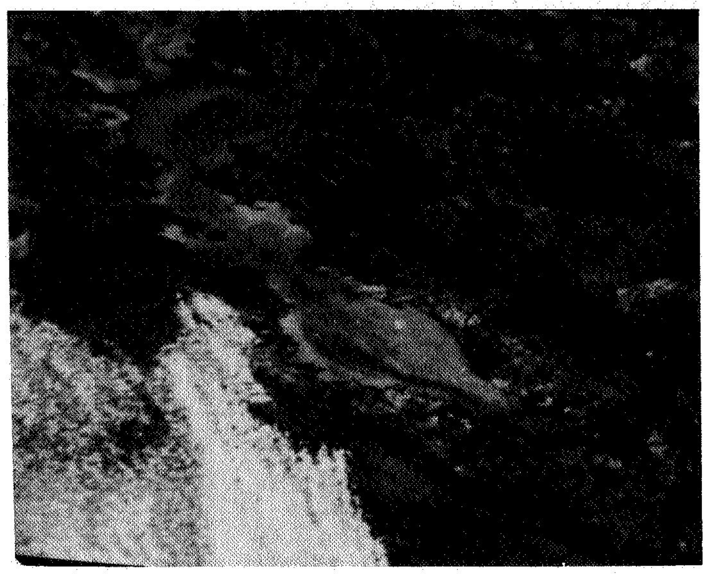

Figure 2. Bay Area 1165-18175

MSS 4,5,6,7 Principal Components, Enhanced

REFERENCES

1. V. R. Algazi. "A Digital Enhancement of Multispectral MSS Data for Maximum Image Visibility", Proceedings of Symposium on Significant Results of ERTS-1, March 1973, NASA-SP-327, pp. 1169-1178.
2. V. R. Algazi. "Nonlinear Equalization and Calibration of MSS Sensors Response", "An Integrated Study of Earth Resources in the State of California using ERTS-1 Data", Annual Report, July 30, 1973. Chapter 8, Appendix 1.
3. G. Thorley et al. "An Integrated Study of Earth Resources in the State of California using ERTS-1 Data", Annual Report, July 30, 1973, Chapter 3. "ERTS-1 Data as an Aid to Resource Management in Northern California".
4. Robert H. Burgy. "Application of ERTS-1 Data to Aid in Solving Resources Management Problems in the State of California", Proceedings of Symp. on Significant Results from ERTS-1, March 1973. X650-73-127, pp. 151-166.
5. R. M. Haralick and I. Dinstein. "An Iterative Clustering Procedure", IEEE Transactions on Systems, Man and Cybernetics, Vol. SMC-1, No. 3, July, 1971, pp. 275-289.
6. P. S. Ready and P. A. Wintz. "Information Extraction, SNR Improvement, and Data Compression in Multispectral Imagery", IEEE Transactions on Communications, Vol. COM-21, no. 10, October 1973, pp. 1123-1131.

Paper I 3

AFFINE TRANSFORMATIONS FROM AERIAL PHOTOS TO COMPUTER COMPATIBLE TAPES

F. G. Peet *(Canada Centre for Remote Sensing, Ottawa, Canada)*, A. R. Mack *(Canada Department of Agriculture, Ottawa, Canada)* and L. S. Crosson *(Canada Department of Agriculture, Saskatoon, Canada)*

ABSTRACT

During the development of a project to estimate wheat production, it became necessary to pull data, corresponding to particular fields in a test site, off an ERTS computer compatible tape. Aerial photographs and topographic maps were on hand for the test site. A method was devised, using an affine transformation, to relate the aerial photographs or topographic maps to the tapes. One can thereby access data on the tape corresponding to regions covered by only a few pixels. The theory can be used for the registration of two tapes for the same area and for the 'geometric correction' of images.

INTRODUCTION

A project is underway to estimate total crop production in Western Canada. Fourteen test sites have been set up containing in total approximately 2,000 fields. These test sites are 2 x 10 miles and lie on generally flat plains. To study the ERTS signals over such a large number of fields a rapid and accurate method of accessing the data for each field on ERTS computer compatible tapes (CCT's) is required. In addition, it is necessary to study the daily variations, where possible, and the 18 day variations in the signals for each field. This task is easier if one can register two ERTS computer compatible tapes for the same ground area, for otherwise one essentially has 10,000 separate fields with which to deal. It is nearly impossible to do either of these jobs using ERTS photos, computer maps or tape dumps of the test sites or any combination of these. Therefore another approach is required.

We seek then,

a) a method of rapidly and accurately extracting data for particular ground features, ranging in area from a few acres to two or three hundred acres, from an ERTS computer compatible tape.

b) a method of registering two ERTS computer compatible tapes for the same ground area.

BACKGROUND OR THE THEORY OF THE METHOD

a) Observation or Necessary Requirement

By a computer map is meant the computer printout obtained when symbols assigned to the numbers sent down by the satellite are printed out. The coordinates of any pixel on such a map specify uniquely the location of that pixel on a CCT. If one knows the location of a feature on a computer map, one knows its location on a computer compatible tape. The observation (or necessary requirement) is that lines (e.g. roads) which are parallel on the considered aerial photos or on the topographic maps are also parallel on the corresponding computer maps. The dark lines in Figures 1 and 2 illustrate roads which are parallel on both the aerial photo and the CCT.

b) Fact

The transformation which maintains the condition of parallelism is an affine transformation*, the general form of which is the following:

$$x = a_1 u + b_1 v + c_1$$

$$y = a_2 u + b_2 v + c_2$$

where u and v could represent the coordinates of a point on the photograph and x and y could represent the coordinates of the point on the computer map.

This fact and the observation are the foundations of the method.

c) Deductions from a) and b)

i) One can use an affine transformation to transform points from the aerial photograph (or topographic map) to the computer map or equivalently to the CCT, if lines parallel on the former are parallel on the latter.

ii) If (i) is applicable to two different CCT's of the same area then these two computer maps or equivalently two CCT's can be registered using an affine transformation because of the group properties of such transformations.

iii) If (i) is applicable to an ERTS image then 'geometric corrections' can be performed, if desired, using affine transformation on that image.

*Guggenheimer, H.W., Differential Geometry, McGraw-Hill, N.Y.

IMPLEMENTATION OF THE METHOD

a) Extracting Required Data from a CCT

Six to eight, or more, easily identifiable points (called control points) are located on both the computer map and aerial photo (or topographic map). The coordinates of both sets of points are given to the computer and a least square analysis is performed to estimate the parameters of the affine transformation. The feature coordinates are then digitized (by which is meant the automatic measurement and recording of the coordinates) and the transformation is applied by the computer to obtain the coordinates on the CCT in terms of line number and pixel number. In the wheat project case the feature is the given field and the feature coordinates are the field vertices.

b) Registering Two Computer Compatible Tapes

To study the time development of the signals, that is, to study daily changes, where possible, and 18 day changes in the signal for a given feature, considerable work is saved if one can register two CCT's. Assume that the feature location is known on the first CCT and unknown on the second CCT. Six to eight control points are located on the corresponding computer maps. The coordinates of both sets of points are given to the computer which performs a least squares analysis to estimate the parameters of an affine transformation from the first CCT to the second CCT. This transformation is then applied to the known feature coordinates on the first CCT to give the feature coordinates on the second CCT. This method also saves considerable storage space, for, in the case of the wheat project, rather than storing 2,000 field coordinates for each site, it is just necessary to store 6 transformation parameters.

RESULTS

Figure 3 shows an aerial photograph with some of the field boundaries outlined on it. Figure 4 shows a computer map (or equivalently a CCT) with field boundaries obtained by applying an affine transformation to the aerial photo of Figure 3. The vertices of the fields on the computer map are within a pixel of their expected location.

SUMMARY

Affine transformations can be used to transform points from aerial photos or topographic maps to points on CCT's provided that lines which are parallel on the former are also parallel on the latter. To do this one digitizes (automatically measures and records) the coordinates of the features of interest on the aerial photo or topographic map. The transformation is then applied by the computer to these digitized coordinates to obtain the coordinates of the feature on the CCT.

If the method of the previous paragraph is applicable to two CCT's then these two computer compatible tapes can be registered with an affine transformation because of the group properties of such transformations. To locate features on a second CCT if their location on a first CCT is known one just applies the transformation to the feature coordinates on the first CCT.

If the method of the second last paragraph is applicable to a given ERTS image, then, if desired, one can perform 'geometric corrections' on that image with an affine transformation.

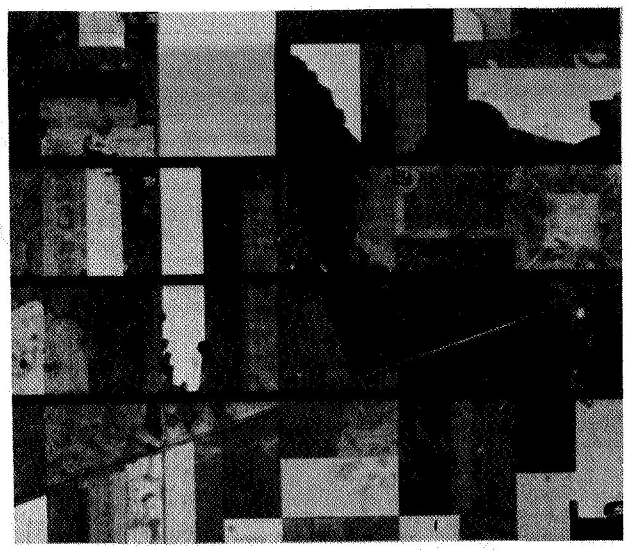

Figure 1
The dark lines are parallel roads

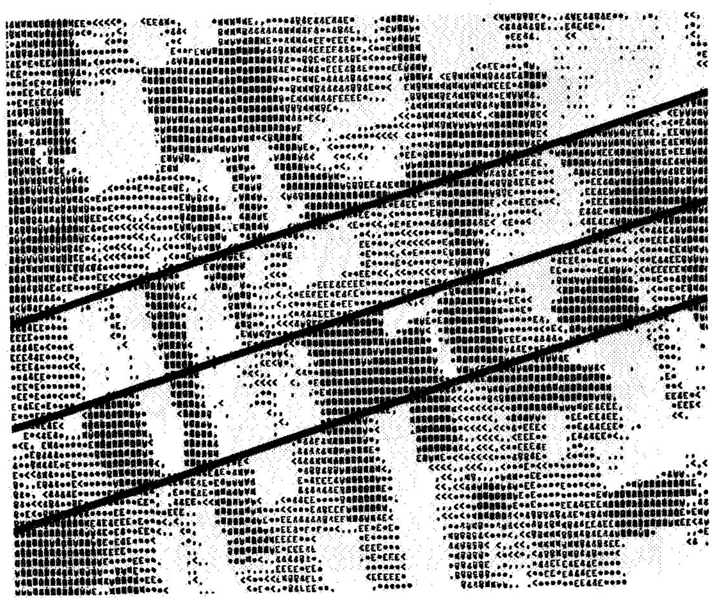

Figure 2
The black lines represent the same roads shown in Figure 1

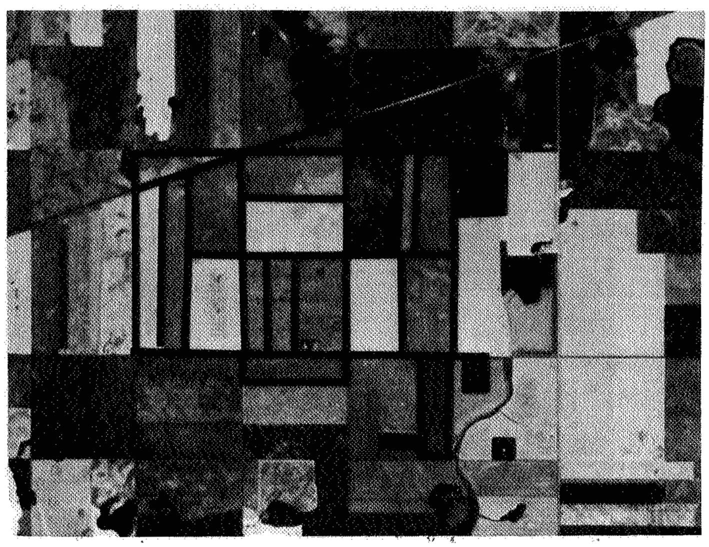

Figure 3

The dark lines correspond to field boundaries

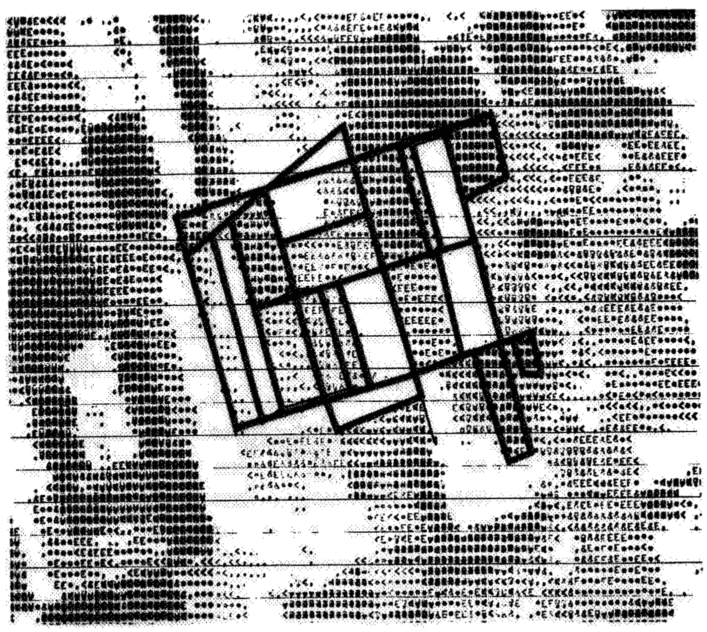

Figure 4

The dark lines are the result of transforming the field boundaries of Figure 3

Paper I 4

ESIAC: A DATA PRODUCTS SYSTEM FOR ERTS IMAGERY (Time-lapse Viewing and Measuring)

William E. Evans and Sidney M. Serebreny, *Stanford Research Institute, Menlo Park, California*

ABSTRACT

An Electronic Satellite Image Analysis Console (ESIAC) has been developed for visual analysis and objective measurement of Earth Resources Imagery. The system is being employed to process imagery for use by USGS investigators in several different disciplines studying dynamic hydrologic conditions. The ESIAC provides facilities for storing registered image sequences in a magnetic video disc memory for subsequent recall, enhancement, and animated display in monochrome or color. The unique feature of the system is the capability to time-lapse the ERTS imagery and/or analytic displays of the imagery. Data products have included quantitative measurements of distances and areas, brightness profiles, and movie loops of selected themes.

The applications of these data products are identified and include such diverse problem areas as measurement of snowfield extent, sediment plumes from estuary discharge, playa inventory, phreatophyte and other vegetation changes. A short movie is presented to demonstrate some uses of time lapse presentation that have been employed in these investigations. A comparative ranking of the electronic system in terms of accuracy, cost effectiveness and data output shows it to be a viable means of data analysis.

INTRODUCTION

This article presents some of the information products and their applications to earth resources investigators that have been obtained at SRI as a participant in the NASA ERTS-1 investigations (Contract NAS 5-21841. Under this contract SRI is providing support to the U.S. Department of Interior, Geological Survey (Water Resources Division) program in Dynamic Hydrology, which is comprised of a number of highly diverse disciplines and areas of interest (see Figure 1). The SRI role in this program is to:

- provide information on dynamic hydrologic phenomena of interest to the ERTS investigators,

- determine requirements and costs for future on-site electronic data processing.

The goal of SRI's participation is

- to develop methods of dynamic information extraction and processing that might be common to all ERTS investigators, with emphasis on the use of image time-lapse sequence and electronic multi-spectral image change detection procedures.

In the pursuit of these purposes SRI has had an on-going development program over the past two years of an interactive system called Electronic Satellite Image Analysis Console (ESIAC) for information retrieval and data processing from ERTS data.* A recent photograph of the ESIAC is shown as Figure 2.

In brief, the basic objective of the ESIAC system is twofold: To enhance or delineate the phenomena of interest and extract quantitative measurement of it. Experience under this contract has indicated that, on occasion, the display function alone can contribute enough to understanding of the phenomena that no more output information is required, but in the vast majority of cases there was a need for the second function -- that of extracting quantitative measurements from the imagery.

ESIAC CAPABILITIES

ESIAC provides an operator/analyst with a means for scanning the imagery and placing selected portions of it in temporary storage for detailed review, enhancement, and analysis. The principal image enhancement technique in the ESIAC is rapid sequential presentation of registered images -- time lapse series, flicker comparisons, and the like. Additional image enhancement capability is provided through contrast and polarity manipulation, easy scale changes (zoom), and false color display of multispectral imagery. The storage memory is a 16-inch analog magnetic video disc recorder fitted with two moving head channels; each channel capable of storing up to 300 addressable 525-line television frames. Quantitative measurements of distances, areas, and signal amplitues are made under operator guidance and may be output in digital form.

---

*Wm. E. Evans and Sidney M. Serebreny, Analysis of ERTS Image Using Special Electronic Viewing/Measuring Equipment; Proceedings of Symposium on Significant Results Obtained From the Earth Resources Technology Satellite, NASA/GSFC, Volume 1, Part B, pp. 1211-1218, March 5-9, 1973.

Recently, three important new capabilities were achieved through additions to ESIAC circuitry:

- Two Dimensional Color Space Display

This display is an oscilloscope with matched wideband x and y deflection amplifiers, connected as shown in Figure 3. This arrangement provides a dynamic version of the two-dimensional diagram frequently used for studying two-band radiometric data. It is particularly useful for (a) identifying amplitude and spectral characteristics of "training" regions in ERTS data, and (b) adjusting the various thresholding, slicing, and ratioing controls to make thematic extractions.

While any two synchronous video signals can be so displayed, a typical situation is for the ESIAC to be used to display a time lapse sequence of additive pseudo-color images derived from two different MSS channels. A particularly useful combination for many analysis tasks is to display on the color monitor one of the infrared images (MSS 6 or MSS 7) in red and one of the visible images (MSS 4 and MSS 5) in the complementary color, cyan. While normal TV display is being scanned in conventional rectangular raster fashion, the spot on the x-y oscilloscope is being continuously positioned in accordance with the instantaneous responses in the two image channels being studied. (We refer to the normal TV display as the "image space display" and to the x-y oscilloscope display as the "color space display".) All points in the image which generate equal responses in the two channels will be distributed ("mapped") along a 45° diagonal line in the x-y color space display. Zero response for both channels defines the origin in the lower left corner. In one mode of operation, the brightness distribution over the color space display provides a measure of the color or energy distribution for the entire image; that is, two-band video information is converted into a two dimensional scatter diagram. Scenes containing significant areas of snow or clouds, for example, produce maps showing appreciable energy distributed along the "neutral" diagonal. A heavily vegetated scene on the other hand, will generate a scatter diagram ("map") with most of its energy above and to the left of the diagonal (see Figure 4). Water bodies normally map into the lower right region.

By providing intensification (z axis modulation) to the color map display only during the cursor-intersection period, any designated portion of the ERTS image becomes identifiable on the color map and its color coordinates (percent response in each of the two channels) can be read (Figure 5). Leaving the cursor positioned over a vegetated area while cycling through a long sequence of registered images provides a rapid and dramatic portrayal of the changing spectral responses of the vegetation patch as its proceeds through its seasonal changes.

• Grey-scale storage during vertical retrace

The ability to store a calibration greyscale step tablet on the same video disc track as the main image permits the storing of the grey-scale and annotation block from an ERTS frame during vertical retrace period of the television signal. This results in a valuable saving in recording capacity on the magnetic disc. Further, when the main image area is being used to display a magnified (zoomed in) segment from a full ERTS frame, the pertinent radiometric calibration data for the frame at zero zoom is still available (by "rolling" the image vertically to display the normal vertical blanking interval).

Any gain, dc offset, or amplitude comparison experienced by the main signal during the storage and reproduction process is also experienced by the calibration waveform.

The desired effect of having the reference data show at 0^{o}, 45^{o} and 90^{o} on the color space display is achieved by recording the two grey scales slightly misregistered in the vertical direction. Because of the intentional misregister, there will be a brief period (several scan lines) during which only the Band 6 grey scale will be scanned, another brief period during which only the Band 5 grey scale will be scanned, and a third brief period during which both grey scales are scanned simultaneously. It is during this latter period that a color image space display will show a neutral grey scale, and the 45^{o} diagonal line will be generated on the x-y (color space) display.

By reading the x and y coordinates of an area relative to the axial dots generated by steps on the film grey scale tablet (interpolating when necessary), two-band radiometric values for the area can be specified in terms of absolute values; e.g., in Watts-Meter^{-2}-Steradian^{-1}, with a minimum error due to amplitude non-linearities in the photographic and TV processing steps.

• Semiconductor binary memory (scratchpad memory)

This equipment provides editing and storage of single frames of binary imagery (thematic masks). The additional memory capacity frees both disc channels for use as the data source for time-lapsed color displays, as well as overcoming an annoying operating restriction that previously existed. Some examples of binary thematic masks that can be generated are shown in Figures 6-8.

All of these highly interactive additions to the ESIAC analysis capability should be of significant help to investigators interested

in converging upon a quantitative description of the dynamics of a phenomenon of interest to them. Decisions about the efficacy of various thresholding, slicing, and ratioing algorithms can be made while watching the results on a registered time series of scenes displayed immediately, and simultaneously, in both image-space and color space. Once a suitable classification algorithm has been found, first-order quantitative results for each scene can be read quickly from the ESIAC area-measuring readout. Then, if the ultimate in precision is required, and Computer Compatible tapes are available, the same algorithm can be programmed for digital processing of the CCT's with reasonable assurance that the results will be meaningful.

SERVICES AND PRODUCTS

The services rendered by SRI in this program include both advisory consultation on information retrieval, and data products derived from specific instructions of the participating investigators. Naturally, advisory consultation between SRI and the investigator played a large role at the onset of the investigation, particularly in reaching a balance between what investigators wanted from ERTS imagery and what could be successfully extracted and objectively measured from the imagery that was of significant value to the objectives of the individual USGS investigators.

Some of the products generated on the ESIAC and provided to the USGS investigators in the Dynamic Hydrology program, to date, have been as follows:

1. Animated Scene Imagery (monochrome or color)
    a. Feature delineation
    b. Scene overlays
2. Binary Overlay of Themes for
    a. Area Measurements
    b. Feature Enhancement
3. Radiometry
    a. Single band radiance vs distance profiles
    b. Two-band scatter diagram displays
        1) Entire scene
        2) Selected segments

It is important to note that, with the ESIAC, all such displays can be time-lapsed.* The most apparent progress was made when the individual Principal Investigators could work interactively with ESIAC at SRI. However, the equipment was also used to advantage in preparing photographic products (movies, overlays, and hard copy) for reports, presentations and more leisurely study.

Many problem areas remain to be resolved before one can consider that the quantitative measurements of given themes are accurate. For example:

- snow is relatively easy to measure if the image is well illuminated. However, snow illuminated at low angles, or in shadow, can be missed or confused with rock or soil, plus the fact that the spectral signature of snow can be modified by protruding trees. Determining the extent of snow cover in a specific drainage basin to useful accuracies presents a special problem in that it requires precise registration to a known geographic outline.

- the identification of vegetation can be hampered by the fact that the classical spectral signatures may be diluted to an unknown degree by the ground reflectance.

- the analysis of imagery over water is made difficult by the presence of low radiance in all spectral bands. Weak sedimentary plumes are easily confused with haze, smoke or thin clouds. In many of the problems, however, the ability to view the imagery and/or the spectral response of the desired scene in time lapse mode often is of great analytical aid. Other difficulties include signal/noise problems which sometimes dictate the use of negative photographic originals. In addition, poor quality imagery, due to inferior photoprocessing, can affect the quantitative measurements of area or edge delineation.

The foregoing problems only exemplify the many that had to be, and still have to be, considered by the individual investigators before the data reduction products supplied can fully serve the objectives of their research. Consequently, this interactive rapport between SRI personnel and the other principal investigators forms a very important part of the

*A movie also will be presented that illustrates the type of data products obtained through the use of ESIAC but, in particular, demonstrates the value of time-lapse to the interpretation of ERTS data.

services provided to the USGS investigators and it includes such areas as determining what are significant displays (both static and time lapse) to them, as well as determining what formats are required or can be helpful to their specific problems.

APPLICATIONS

In this paper we are only listing applications in brief form. They are discussed in greater detail in the reports of the individual investigators.

- Snow Field Dynamics (Dr. Mark F. Meier)
    1. Measurement of snowpack area
    2. Temporal changes in snowpack for derivation of snowpack depletion curves
    3. Prediction of streamfow (including reservoir inputs) for
        a. Hydroelectric power potential
        b. Flood control
        c. Irrigation

- Desert Vegetation Dynamics (Dr. Raymond M. Turner)
    1. Range-readiness for livestock grazing
        a. Distribution of ephemeral vegetation areas
        b. Short-term changes in vegetation covered areas
    2. Diagnosis of insect plague potential through the distribution of precipitation as inferred by vegetation spectral response.

- Estuarine Dynamics (Mr. Fred Ruggles)
    1. Data base for modeling of
        a. Heated water discharge
        b. Dredging and shipping effects
        c. Special dump locations
        d. Water quality control
    2. Input to New England Basin Planning Commission study for the preservation of Long Island Sound. (Three million dollar planning study of activities in a water body that serves some 12 million people)

- Fresh Water Dynamics (Dr. E. Pluhowski)
    1. Shoreline and beach erosion
    2. Navigation channel planning and maintenance

3. Water quality as affected by
   a. Man's activity
   b. Extraneous water courses

- Playa Lake Dynamics (Dr. C. C. Reeves)

  1. Assessment of available water supply for irrigation ground-water recharge
     a. Census of playa lakes
     b. Temporal changes in water supply

  2. Small scale hydrologic balance evaluations

- Watershed Dynamics (Mr. E. P. Hollyday)

  1. Interaction of open, vegetation, snow and massed-works-of-man within a drainage basin
  2. Modeling criteria for basin hydrologic response to precipitation

Consideration of the data products that, to date, have been extracted from the ERTS imagery via ESIAC indicates that it has useful application to many programs in dynamic hydrology beyond those of the Water Resources Division.

COST EFFECTIVENESS

A principal objective of our research program is to determine time and cost parameters for various types of ERTS image analysis, particularly those which require a significant amount of human interpretive skill. Tasks that we have encountered to date can be broadly classified as follows:

Principal Identification Criteria	
1. Overall Radiance 2. Spectral Signature	Machine Excells
3. Spatial Brightness Contrast 4. Spatial Color Contrast	Man Excells
5. Temporal Variations of numbers 1, 2, 3, and 4	Man-Machine Excells

Detailed figures will not be available until the end of the study, but the gross trends depicted in Figure 9 are already apparent.

Electronic viewing/measuring equipment should not be regarded as competing with photographic prints in cost, convenience, and image quality or with computer processing of digital tapes in the precision of fully objective measurements. Although the equipment described here provides capabilities that extend surprisingly far into the realms of both these mutually exclusive techniques, its greater and virtually unique utility lies in providing rapid and extremely versatile coverage of a large middle ground of analysis tasks, particularly those that can benefit from sequential or simultaneous display of numerous images and from interactive guidance by the scientific investigator. For this purpose, we have evolved a system that we believe provides reasonable trade-offs among the competing factors of operating simplicity, processing volume, accuracy, maintainability, and cost.

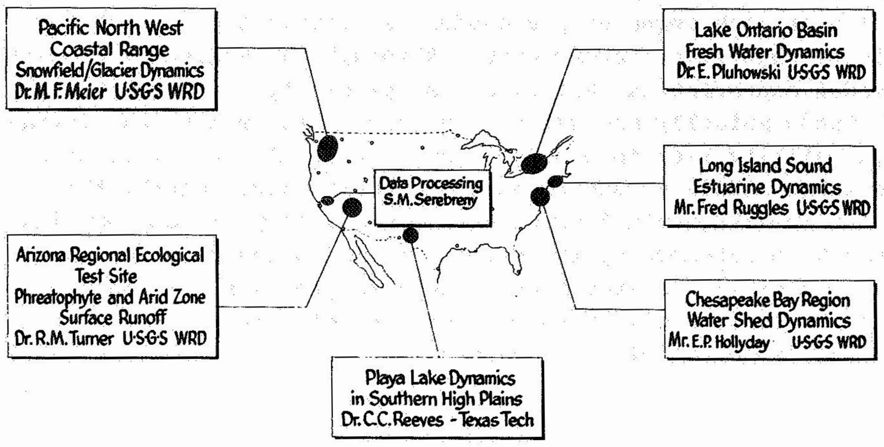

FIG. 1 PROGRAM IN DYNAMIC HYDROLOGY

FIG. 2 PHOTO OF ESIAC

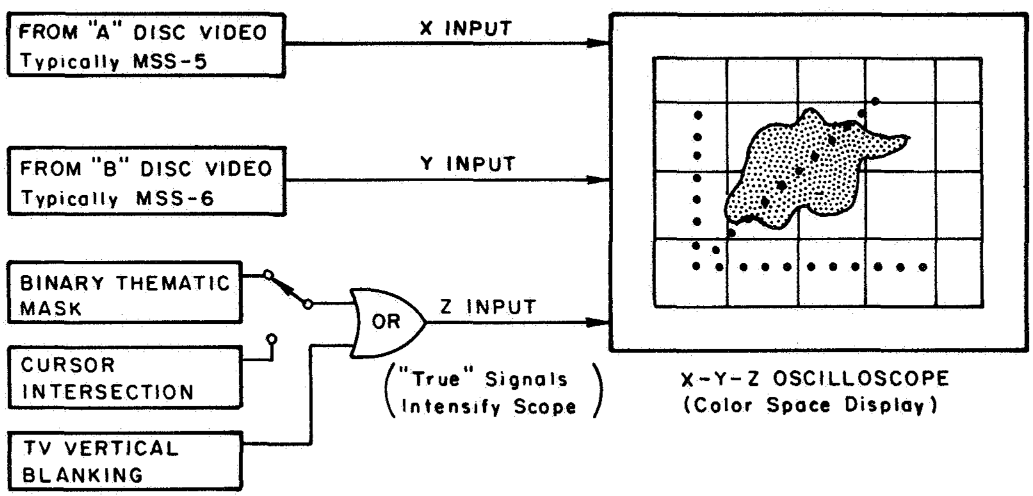

FIG. 3 OSCILLOSCOPE CONNECTIONS FOR COLOR MAPPING DISPLAY

a) PHOTOGRAPH OF IMAGE SPACE DISPLAY (color TV monitor) FOR PORTION OF ERTS SCENE 1261-15274 SANTEE RIVER SWAMP, SOUTH CAROLINA 10 APRIL 1973 (MSS-7 SHOWN IN RED, MSS-5 IN CYAN. PICTURE HEIGHT = 53 km)

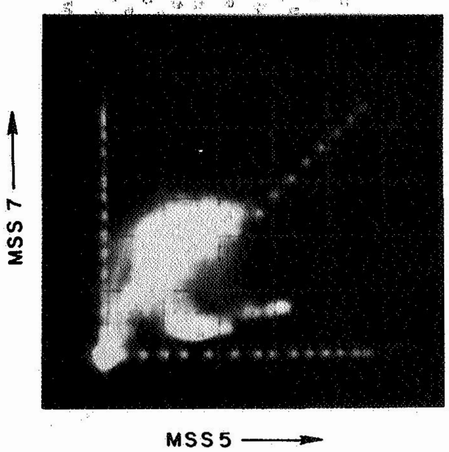

b) COLOR SPACE DISPLAY FOR SCENE OF (a)

Note heavy concentration of energy in the mid-brightness red region above and to the left of the 45° diagonal.

Note also two lesser energy concentrations in the mid and low brightness cyan region below the diagonal.

Dots on axes are from ERTS gray scale tablet (not visible in panel a).

FIG. 4 TWO ALTERNATIVE DISPLAYS OF ERTS MULTISPECTRAL DATA (Each can be Viewed in Time Lapse on ESIAC)

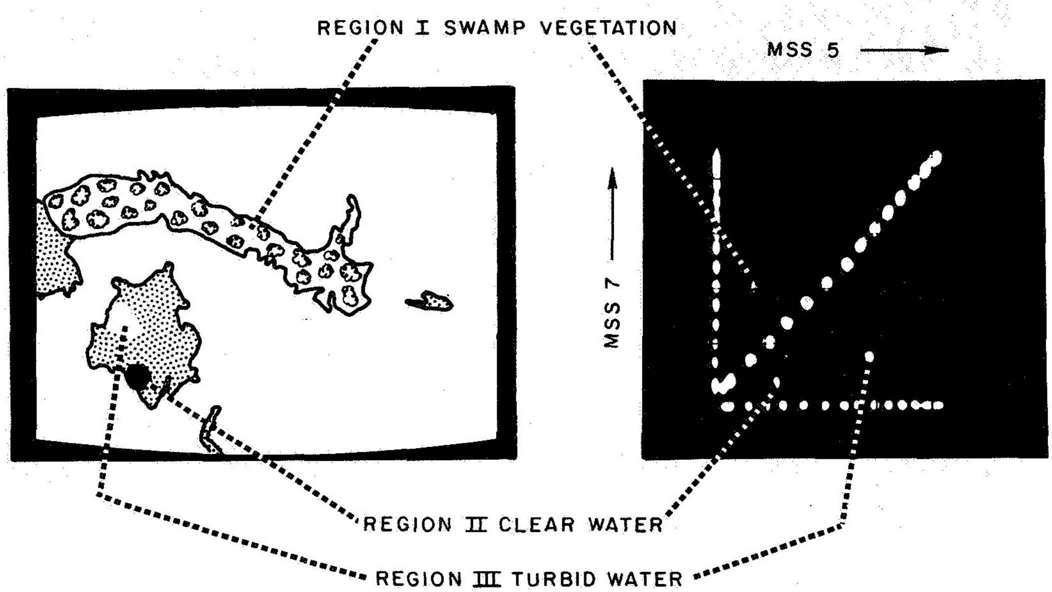

FIG. 5 COLOR SPACE DISPLAY OF SPECTRAL SIGNATURES FROM THREE SELECTED SMALL GEOGRAPHICAL REGIONS WITHIN SCENE OF FIG. 4

(a) MT RAINIER, WASH. 8 OCTOBER 1972
1077-18-260-5

(b) MT RAINIER, WASH 14 NOVEMBER 1972
1114-18-322-5

(c) CONTINOUS TONE DISPLAY OF DATE TO DATE IMAGE DIFFERENCING (MSS-5) 14 NOVEMBER-8 OCTOBER 1972

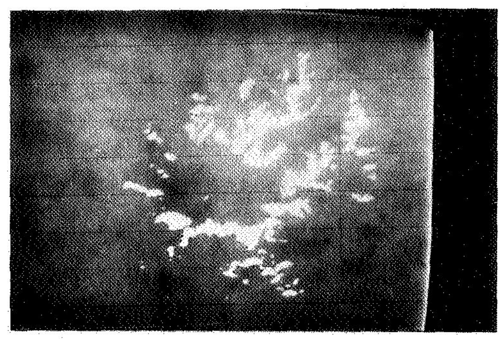

(d) 14 NOVEMBER-8 OCTOBER 1972 BINARY MASKS OF WHITE REGIONS OF FIG. C

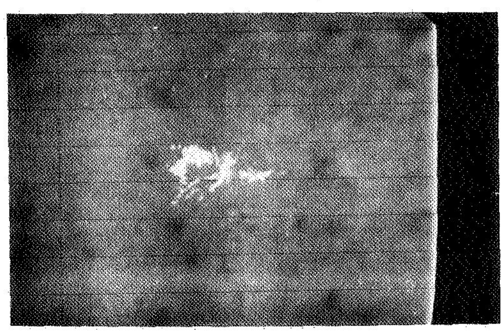

(e) 8 OCTOBER-14 NOVEMBER 1972 BINARY MASKS OF BLACK REGIONS OF FIG. C

FIG. 6 DETERMINATION OF AREAL DISTRIBUTION OF SNOW USING MASKS OF BRIGHTNESS ABOVE THRESHOLD, 2 SEPTEMBER 1972 (BAND 4, .5-.6μ)

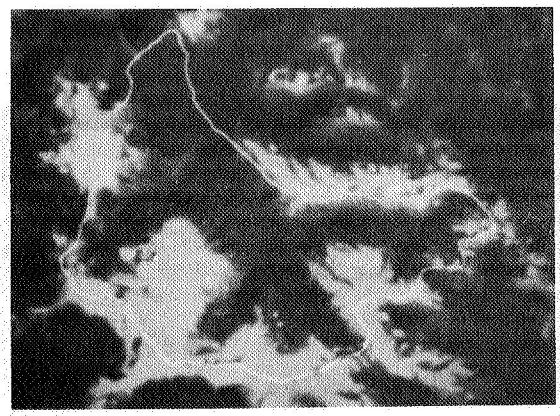

MSS-4 IMAGE 26.8Km HIGH SECTION OF E1041-18253-4. (Thunder Creek Drainage Basin Outline Superimposed)

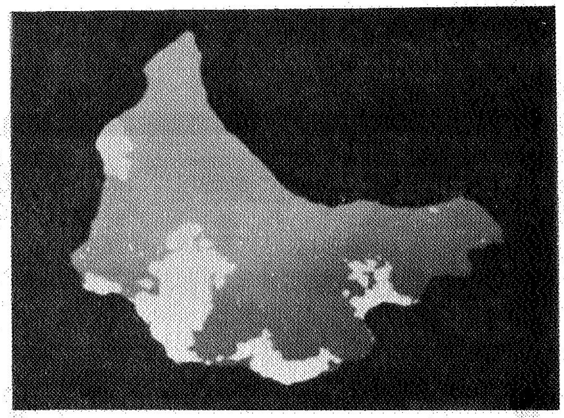

GRAY STEP 10 17.4% OF BASIN

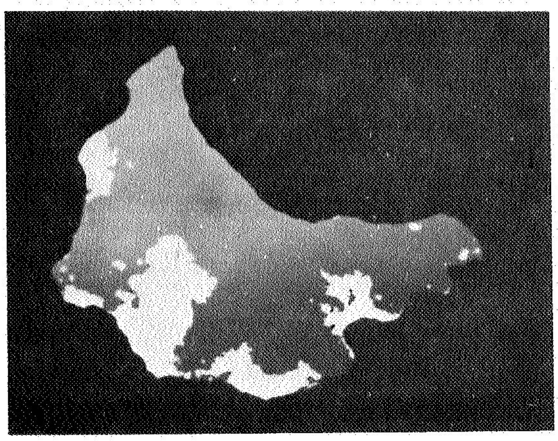

GRAY STEP 8 21.8% OF BASIN

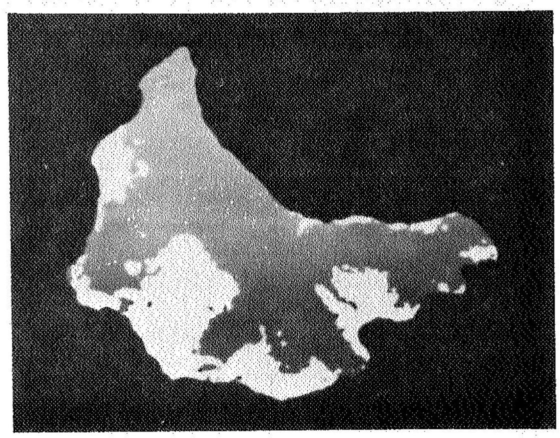

GRAY STEP 6 31.3% OF BASIN

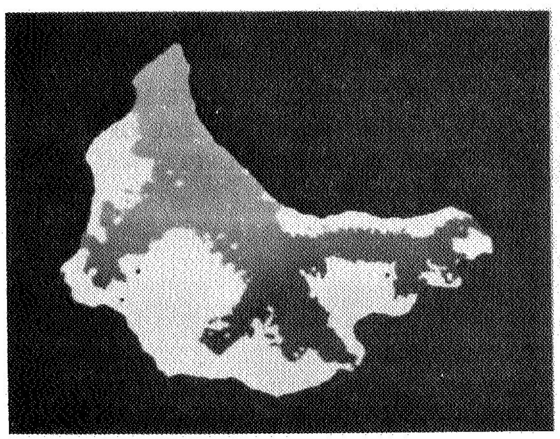

GRAY STEP 4 46.4% OF BASIN

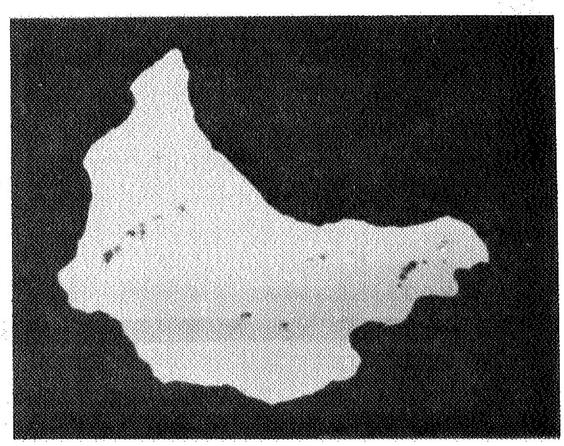

GRAY STEP 2 97.7% OF BASIN

FIG. 7 USE OF BINARY MASKS TO EVALUATE AREAL CHANGES IN SNOW DERIVED FROM THE DATE-TO-DATE DIFFERENCING TECHNIQUE

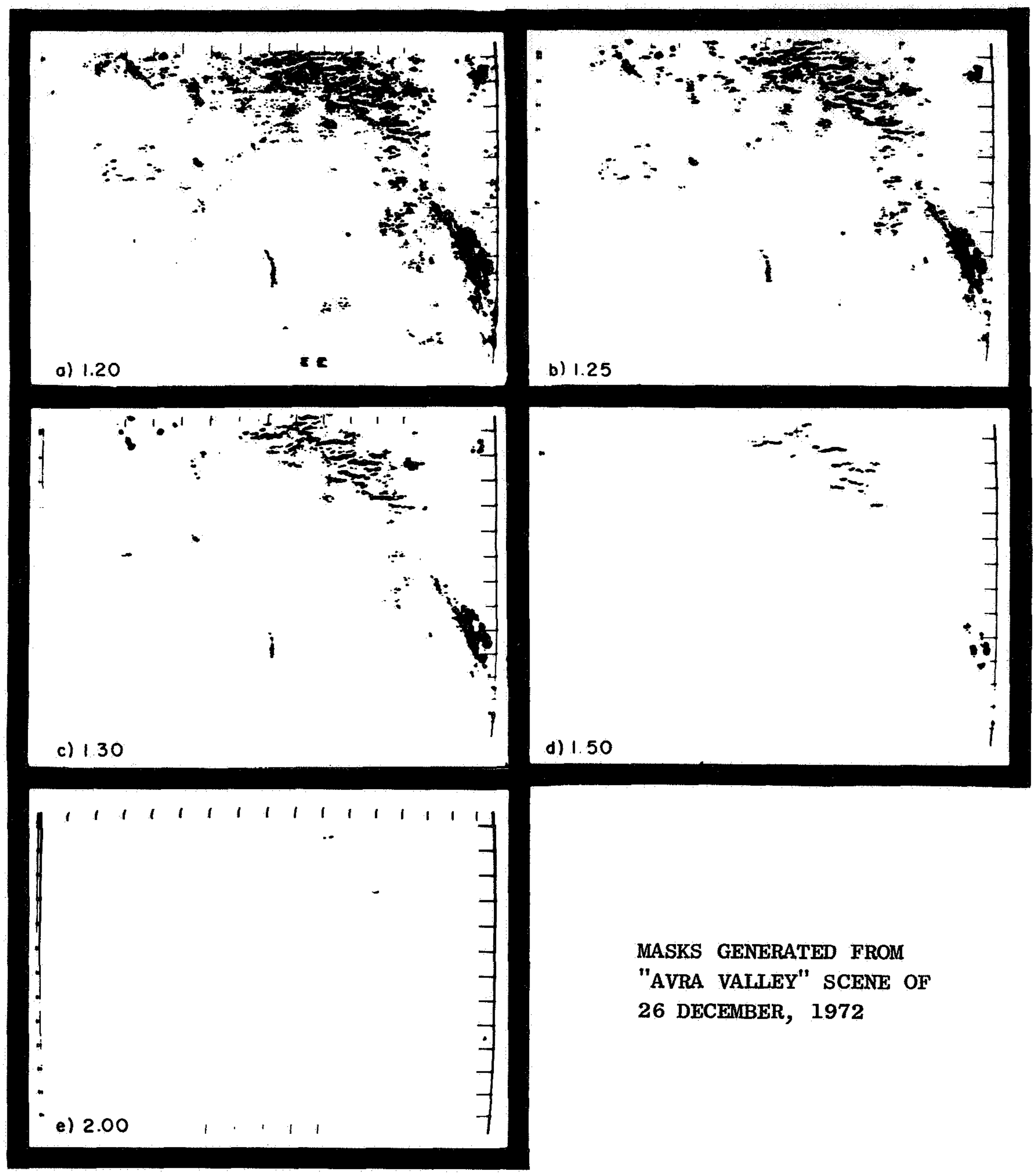

FIG. 8 TEMPORAL CHANGES IN VEGETATIVE COVER USING THEMATIC MASKS GENERATED USING SELECTED RATIOS OF BAND 6 (MSS-6) TO BAND 5 (MSS-5). [Ratio values indicated in each panel]

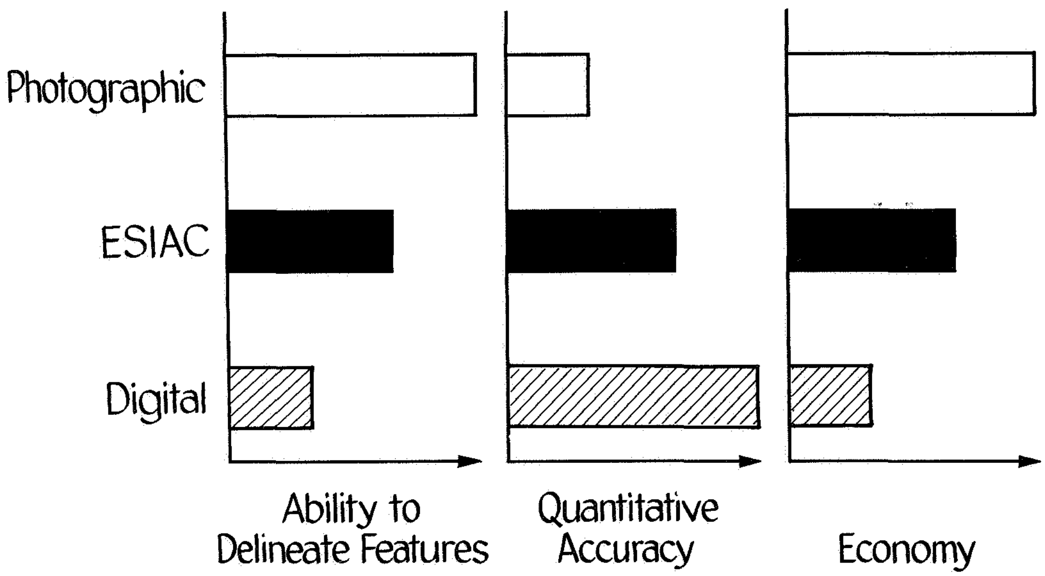

FIG. 9 RELATIVE RANKING OF DATA PROCESSING METHODS

Paper I 5

ADVANCED PROCESSING AND INFORMATION EXTRACTION TECHNIQUES APPLIED TO ERTS-1 MSS DATA

William A. Malila and Richard F. Nalepka, *Environmental Research Institute of Michigan, Ann Arbor, Michigan*

ABSTRACT

Conventional automatic data processing and information extraction techniques fall short of providing the information required by the user in some applications. For those cases, advanced techniques are needed to permit the extraction of the necessary information. This paper describes advanced techniques we have developed and provides examples of their application to ERTS-1 MSS data.

The techniques described are designed to help overcome problems in location, mensuration, and classification accuracies which result from geometric distortions of the ERTS MSS data, the relatively coarse resolution of the sensor, and variations in atmospheric state over the region to be surveyed. It is shown that each of these factors can seriously degrade one's ability to extract necessary information. Further, it is shown that advanced techniques can alleviate the effects of these factors.

1.0. INTRODUCTION

This paper presents results obtained under ERTS Investigation MMC-136. As a part of this investigation, we have been developing and testing techniques for the extraction of information from ERTS data. The two general objectives of the investigation have been to minimize the effects of large spatial resolution element size and to enhance the extraction of large-area survey data. Two topics under each of these general categories are discussed in the sections that follow.

2.0. TECHNIQUES FOR MINIMIZING THE EFFECTS OF LARGE SPATIAL RESOLUTION ELEMENTS

The first topic in this section is estimation of the fractional composition of individual pixels by use of the spectral information obtained from ERTS. It is followed by a description of a procedure for assigning pixels to specific analysis areas identified on maps or photographs, an important detail for classification processing.

2.1. ESTIMATION OF FRACTIONAL COMPOSITION OF INDIVIDUAL PIXELS (PROPORTION ESTIMATION)

One aspect of this investigation is concerned with testing the applicability of advanced information extraction techniques to ERTS-1 MSS data. (These techniques have been developed at ERIM with funding provided by the Supporting Research and Technology program of NASA-JSC under Contract NAS9-9784.) One technique addresses problems associated with accurately determining areas covered by features in the scene using scanners with limited spatial resolution, like ERTS-1 MSS. Clearly, there is a serious problem for features smaller than the instantaneous field of view of the scanner. In addition, problems exist even for larger features since many of the ERTS MSS pixels overlap the boundaries between these and adjoining features. As a result, the radiation represented in those pixels is a mixture of radiation reflected from two or more materials. Since the signals generated in such pixels are not characteristic of any one material, the pixels will generally be improperly classified. Therefore, the area assigned to each material class could seriously be in error. For example, at least 25% of the pixels covering a square field of 50 acres (20 hectares) will overlap its boundaries.

At ERIM we have developed a data processing technique [1] to estimate the proportions of materials contained within each pixel, by taking advantage of the fact that information is gathered in several spectral bands. This permits a more accurate determination of the area covered by each material; the greater the number of spectral bands used, the more the materials that can be considered. We next describe and evaluate the results of a test of this technique on ERTS-1 MSS data. (Some of these results were included in a paper presented at the March 1973 Symposium on Significant Results [2].)

The goal of this initial test was to determine how accurately we could estimate the surface area of a number of lakes and ponds in a small portion of an ERTS frame. The region selected for processing is shown in Figure 1, a black and white aerial photograph of that region.

Using an enlargement of this photo, the surface area of the water bodies was determined. Two methods were used to determine area, dot grid and planimeter, with the results being calibrated by assuming a one mile separation between the section line roads apparent in the photo.

For purposes of comparison, the data were processed using two approaches in addition to the multi-channel proportion estimation algorithm. One of these was the conventional recognition algorithm in which each pixel was assigned to one and only one class. In the other approach, proportions were estimated using only one ERTS-MSS band.

In processing the data the first step was the establishment of training signatures for the major object classes in the scene. The primary scene components in this case were water, trees, and soil. A number of pixels containing pure samples of each of these classes were located and the mean signal vector and associated covariance matrix was determined for each class. Since there were some data quality problems with ERTS Band 6, only Bands 4, 5, and 7 were used to establish signatures and for the ensuing processing.

Having established the signatures, the three processing algorithms (multi-channel proportion estimation, single channel proportion estimation, and conventional recognition) were applied to the data. In order to meaningfully compare the results generated using these algorithms, it was necessary to identify the thresholds which would be used in each of the algorithms. These threshold or parameter values would affect the trade-off between the detection rate and the false alarm rate. For this comparison, it was decided to utilize those parameter values which eliminate water false alarms in the scene (i.e., no non-water pixels classified as water) while at the same time maximizing the detection rate.

The multi-channel proportion estimation algorithm used for estimating water acreage depends upon the values used for two parameters. One of these parameters, ρ, is called the probability of rejection; the other, τ, is the water proportion threshold.

The purpose of the probability of rejection parameter ρ is to eliminate those signals which represent pixels that contain insignificant coverage by a combination of water, bare soil, and vegetation or, equivalently to eliminate signals which represent pixels that contain significant coverage by combinations of other object classes. The probability of rejection parameter ρ operates as follows. If a signal y is not within a probability contour that contains $(1-\rho)$ of the samples for a signature of some mixture of water, bare soil and vegetation, then the proportion of water estimated for the pixel represented by the signal y is taken to be zero.

The objective of the other parameter, the water proportion threshold τ, is to eliminate small proportion estimates of water for pixels which, in reality, contain no water. This parameter operates as follows. A tentative proportion estimate $\hat{p}$ of water is made for the pixel in question. If $\hat{p}$ is less than τ, then the estimated proportion of water is taken to be zero. If $\hat{p}$ is greater than or equal to τ, then $\hat{p}$ is taken as the estimated proportion of water.

Figure 2 gives the operating characteristics of the proportion estimation algorithm for this data set as functions of the probability of rejection and the water proportion threshold. The plots shown in this figure were determined as follows. All the pixels in the scene were classified by photo interpretation into two classes, W and G. A pixel

was put in class W if it contained some water; it was put in class G if it contained no water. The total amount of water surface area estimated for the pixels in class G, divided by the area of the pixels in class G, was taken as the false alarm rate. The total amount of water surface area estimated for pixels in class W divided by the actual (as determined by photo-interpretation) surface area of water in class W was taken as the detection rate.

From the figure we see that for $\tau = 0.4$ or greater, the false alarm rate becomes zero, regardless of the probability of rejection ρ. For a specific value of ρ, we may increase the detection rate by decreasing τ, but the penalty is increased false alarm rate. Examination of the operating characteristics indicates that the combination of parameter settings with $\rho = 0$ and $\tau = 0.4$ yields near optimum results: detection rate = 90.24% and false alarm rate = 0. This detection rate is based upon assigning to each pixel an area equal to 79m x 57m.

The single-channel proportion estimation algorithm operates similarly to the multichannel proportion estimation algorithm, with probability of rejection parameter ρ and water proportion threshold parameter τ. In single-channel proportion estimation, the ρ parameter was used to eliminate those signals which represented pixels containing insignificant coverage by a combination of water and vegetation (proportions may be estimated for only two classes when using a single channel). Because the water signal level in ERTS Band 7 was lower than all others in the scene, a value of zero could be used for the parameter ρ without causing false alarms. Therefore, the results given in Figure 3 are for $\rho = 0$ and varying values for the parameter τ. We see that as τ decreases the detection rate increases, with a penalty of increased false alarm rate. A false alarm rate of zero is achieved for τ values of 0.6 or greater.

For conventional recognition the parameter τ does not enter in, since each pixel is classified as either containing water (100%) or not (0%). The value of ρ, however, did need to be determined. It was found that the occurrence of false alarms was independent of the value of ρ; therefore, the value of ρ which maximized the detection rate was selected.

Before describing the test results, we present here a brief discussion of the areas which were assigned to each pixel. The instantaneous field of view of the ERTS MSS is 79 m X 79 m but, since the data are oversampled along the scan direction, there is overlap in the ground patch covered by successive samples. Therefore, in order that calculations of the total area of an ERTS frame not exceed the actual area viewed in that frame, a smaller effective size has been used in the scan direction. However, for the problem being addressed here, where the area for only one class in the scene is being estimated, one needs to consider the actual ground area viewed by each pixel. In other words, if a pond smaller than 79 m X 79 m is contained within one pixel and that pixel is estimated to contain 50% water, the estimated area of the pond is 50% of 79 m X 79 m and not 50% of

some smaller effective area. Now if this same pond was seen in the overlap area of two successive pixels it would be inaccurate to use the 79 m X 79 m area for each pixel since some portion of the pond would be counted twice.

In order to account for problems of this sort three separate pixel sizes were used in computing estimated area. If the pixel identified as containing some portion of water in excess of the threshold value fell between two pixels on the same scan line which also were identified as containing water, the pixel size for area estimates was assumed to be 79 m X 57 m (the 57 m size was computed based on the 100 nautical mile frame size and number of samples per scan line). "Water" pixels with one "water" neighbor along the scan line were assumed to be 79 m X 68 m and "water" pixels with no "water" neighbors were assumed to be 79 m X 79 m.

Test Results: Using the three processing algorithms described earlier, three water classification maps were generated. These are shown in Figures 4, 5, and 6 for the multichannel proportion estimation, single channel proportion estimation, and conventional recognition algorithms, respectively. The first two maps are printed with symbols whose density is related to the proportion of water estimated in each pixel while the conventional recognition map includes only a single symbol where water was detected implying that the entire ground area viewed in those pixels is covered with water.

Upon comparing Figures 4 through 6 with the aerial photograph in Figure 1 it is clear that the shape of the water bodies was more accurately reproduced on the multichannel proportion estimation map and that more of the small bodies of water are detected on this map. In fact only one of the bodies of water was totally undetected.

In order to compare the area estimation results achieved on individual water bodies using the three algorithms, we present Figure 7. Here we plot on the vertical axis the ratio of area as measured from the photograph to the area determined by automatic processing. On the horizontal axis we plot the shape factor which we define as a constant times the area divided by the perimeter of the water body. Shape factor is used rather than area since water bodies with small shape factors (because of large perimeters or small size) can be expected to be less accurately estimated than those with large shape factors. This expectation is borne out on examining Figure 7 which shows that the spread in accuracy for the three methods is small for water bodies having large shape factors (relatively fewer boundary pixels) and generally increases for smaller shape factors.

The area estimate accuracies are better using the multichannel proportion estimate algorithm in almost every case. There are a small number of cases in which the area is slightly overestimated however it is possible that the areas measured from the aerial photograph were on the low side. In general, the results using the conventional recognition algorithm were much inferior, especially for the smaller shape factor water bodies.

A summary of the results for the entire test site is shown in Table 1. Here we see that 97% of water measured from the photograph was detected using the multichannel proportion estimation algorithm while only about 85% was detected using the other two algorithms. This difference would have been larger if fewer large lakes existed in the scene.

TABLE 1

SUMMARY OF WATER AREA ESTIMATION RESULTS

	Photointerpretation	Fractional Pixel Procedures		Whole Pixel Procedure
		3-Channel Proportion Estimation	1-Channel Proportion Estimation	Conventional Recognition
Number of Water Bodies Detected	19	18	17	13
Total Water Area (Meters^2)	1,041,958	1,006,739	892,118	879,120
Percentage of Photointerpreted Area	100%	97%	86%	84%

We have shown that, for this example, more accurate water surface area estimates are achieved by using multichannel proportion estimation. An example of the successful application of this same technique to a problem in agriculture is described in Reference 3. The problem described there is one of better estimating the area of rice fields in California's Sacramento Valley. Our plans for the coming future are to continue to test the multichannel proportion estimation algorithm on other applications so as to better define its practical utility.

2.2. ASSIGNMENT OF PIXELS TO SPECIFIC ANALYSIS AREAS

It is desirable to evaluate the accuracy of large-area resource surveys made by computer processing of ERTS, or other remote sensor, data. Such evaluations require the checking of recognition results for areas whose identities are known from field observations or other "ground truth" information sources. Even before recognition processing, the training of the classifiers usually involves the use of other areas of known identity that can be located in the remote sensor data.

The location of specific areas and assignment of pixels to individual fields and plots is more of a problem in ERTS data than in airborne scanner data which have finer spatial resolution. For instance, there are less than 600 ERTS pixels per square mile and a maximum of 18* wholly within the boundaries of a 20-acre field. Section and field boundaries are frequently indistinct on ERTS data displays; consequently, errors are made in the visual location of fields and the subsequent assignments of pixels. Pixel misassignments potentially can cause errors in classification results and lead to incorrect conclusions. Even if detected, additional resources are required to correct errors.

Unlike ERTS photographic products, the bulk digital computer-compatible tape (CCT) data are not corrected for any distortions introduced by spacecraft orientation, sensor characteristics, and Earth's rotation. (Bulk data are preferred to precision CCT data for recognition processing because, in the latter, the radiometric accuracy of the data is degraded by re-scanning.) Therefore, when displayed on a line-printer gray-tone map or CRT, substantial distortions are evident in bulk CCT data. Square sections are displayed as parallelograms, and other distortions are present. These distortions increase the difficulty of assigning pixels to specific ground areas, but the major cause of difficulty is the relatively large instantaneous field of view of the MSS scanner.

The problem of correctly assigning ERTS pixels to specific areas is somewhat different from two related problems which are under investigation elsewhere [Refs. 4-9]. Some investigators are studying the cartographic aspects of ERTS data, e.g., image quality and techniques to digitally correct ERTS data to match an Earth coordinate system, using spacecraft attitude information and/or ground control points spread throughout a frame. Others are studying the spatial registration of data from two or more frames that cover the same scene, using ground control points and/or image correlation techniques. The cartographic studies will simplify pixel assignments for areas that are readily identified by their latitude and longitude coordinates, but do not directly address procedures for assigning pixels for areas that are only identifiable on aerial photographs. The spatial registration studies will expedite the transfer of field coordinates from one frame to the next, but again do not consider the problem of initially assigning pixels to fields and test plots.

Techniques for both cartographic correction and spatial registration of ERTS data move data values from their original positions to an overlying grid by nearest-neighbor or interpolation rules. Then, the assignment of pixels to specific fields and test plots can take place; operations on a nearest-neighbor basis increase the uncertainty of true field boundary locations, while interpolation degrades radiometric fidelity. The procedure described here warps Earth coordinates to match ERTS coordinates, effectively computing the location of each pixel, and makes pixel assignments without any movement or interpolation of ERTS data.

---

*Even this number is optimistic because the ERTS scan lines do not generally follow field boundaries. Further the oversampling along ERTS scan lines means that there is overlap between the areas viewed by the scanner for adjacent pixels and thus one must move away from boundaries to eliminate their effects.

2.2.1. PROCEDURE

The ERIM procedure [10, 11] for the computer-aided assignment of ERTS pixels relies on an empirical map transformation derived by least squares calculations from a local network of control points in and around the area of interest, e.g., a 20 x 25-km area on a 15' quadrangle map. These control points can be located on topographic maps and/or on aerial photographs. Differing scales can be handled, and the locations of control points and analysis areas on the maps and/or photographs can be obtained on a relative basis.

The empirical transformation produces rotations to account for the non-polar orbit of ERTS and the difference in orientation between Earth and ERTS-data coordinates, and also corrects for effects of the Earth's rotation and other sources of distortion and error, in a least-squares manner.

The computer-aided procedure was developed because it is often difficult to distinguish "by eye" the corners of sections, fields, and plots of interest on digital displays of ERTS data, and more difficult to locate them accurately. Lack of contrast between materials and any banding or striping in the ERTS data can complicate matters. On the other hand, there generally are some road intersections and other features in the scene around and within the areas of interest that can be distinguished readily in digital displays.

In the procedure, we typically select fifteen to twenty distinguishable points as control points and estimate their ERTS line and point numbers as well as possible by inspection. Earth coordinates for the same points are determined* from a topographic map or an aerial photograph. A least-squares fit of Earth to ERTS coordinates reduces the error in the estimated location of each control point and produces a map transformation

$$\begin{bmatrix} P \\ L \end{bmatrix} = \begin{bmatrix} a_{11} & a_{12} \\ a_{21} & a_{22} \end{bmatrix} \begin{bmatrix} X \\ Y \end{bmatrix} + \begin{bmatrix} b_1 \\ b_2 \end{bmatrix}$$

where P and L are the ERTS data coordinates for points along scan lines and for scan lines, respectively,

$\{a_{ij}\}$ are the empirical transformation coefficients,

X and Y are the Earth coordinates to be transformed,

and b_1 and b_2 are the offset parameters to account for different origins.

*Digitization is facilitated by the use of an x-y digitizing machine.

(A polynomial transformation has been computed but, thusfar, we have found that terms of higher than first order are not significant.)

The above transformation then is used to transfer Earth coordinates of other points, fields, or plots in the vicinity to their corresponding ERTS coordinates. For several purposes, it has been found convenient to place pixel designation information in a fifth channel added to ERTS data.

A companion computer program allows us to define each training or test area by a polygon with an arbitrary number (≤ 63) of vertices and to compute which ERTS pixel centers lie within the polygon. Further, there is a capability to move the polygon sides in or out by specified distances so as to include or exclude pixels whose signal values include effects of boundaries between scene features, for example, to avoid training on pixels that represent more than one material. An illustration of the effect of this procedure is presented in Figure 8. A section (1 mile square) in actual ERTS data was arbitrarily divided into 16 40-acre "fields". Part(a) of Figure 8 displays as blanks the pixels selected for these fields when the acceptance polygon was inset by one-half a resolution element on all sides.* An average of 22 pixels was selected for each 40-acre field. For Part(b), the inset was increased to three-quarters of a resolution element, and the smaller number of acceptable pixels (an average of 16) in each field is apparent. Parts(c) and (d) show the further reduction in the average number of acceptable pixels to 12 and 5 when the inset is increased to 1 and 1.5 resolution elements, respectively. Figure 9 presents other sets of "fields" delineated by the 0.5 resolution element criterion; field sizes of 640, 160, 80, and 10 acres are shown.

As noted above, the inset of one-half a resolution element is the theoretical minimum needed to exclude pixels whose radiometric signals contain boundary effects. A greater inset probably should be used in practice because of possible errors in the location of the control points in both the ERTS and Earth coordinates and in the location of test plot vertices in the maps or photographs. There also are known displacements inherent in the ERTS data which we presently do not explicitly take into account, e.g., the multiplexer delay in the spacecraft which introduces a displacement between the six scan lines in each mirror sweep.

2.2.2. APPLICATION

A relatively large number of training and test fields were identified manually for use in recognition processing of ERTS-1 data for an agricultural problem, before the computer-aided procedure was developed. Errors in the assignment of pixels to a few fields were identified during the course of the processing. One particular example is presented in Figure 10.

---

*Note that the inset must be greater than one-half a pixel dimension along the scan line since the actual resolution element size is 79 x 79 m even though the sampling rate along the scan lines gives an effective pixel width of approximately 57 m.

Section roads were not always clearly discernible and were not present along all sides of every section, so several section lines were placed on line printer maps by simple interpolation between more distinct roads. The section in question is located on a boundary between two townships and happens to be less than one mile long in the N-S direction. Partly because of the smaller size, the lower section boundary was initially placed below the true boundary. Figure 10a presents the original manual assignment of pixels for four fields; the correct section lines are shown on the line printer map (of ERTS Band 5) and the actual field boundaries, as obtained from an aerial photograph, are mapped on the right. Fields 21, 22, and 23 were originally mis-assigned by the analyst. After poor agreement was observed between recognition results and the assigned crop types, these field delineations were checked and revised manually.

After the computer-aided pixel assignment procedure was developed, it was used to assign pixels to these same fields with a 0.5 resolution element inset. The resulting pixel assignments are presented in Figure 10b. Note the apparent good agreement between the selected pixels and the field boundaries, for example, around the notch in the upper right-hand corner of Field 21 and middle of Field 22. In this example, a USGS topographical map served as the standard coordinate reference for several road intersections that were readily identified in the ERTS data. The derived transformation then was applied to the standard coordinates of the section corners to locate them accurately within the ERTS data. Field vertices were determined relative to these section corners in an aerial photograph taken at the time of the ERTS pass. These relative locations of field vertices then were transformed to ERTS coordinates and pixels were selected.

It is difficult to make a quantitative assessment of the accuracy of our procedure, because of the lack of an absolute knowledge of pixel locations. One attempt was made using a large, distinctively shaped lake because there generally is a large contrast between land and water in ERTS Band 7, so that the accuracy of boundary locations could be assessed. Our goals were (1) to select only those pixels that were completely within the lake and (2) to determine whether map-based coordinates of the shoreline features could be accurately placed in the ERTS data. The results showed that a good job was done in selecting only water pixels and that shoreline features were accurately placed around the lake. The average accuracy of positioning was clearly better than one pixel, but we have not quantitatively determined how much better. The results encourage use of the procedure for processing of ERTS data.

3.0. TECHNIQUES FOR ENHANCING THE EXTRACTION OF LARGE-AREA SURVEY INFORMATION

In this section we discuss two topics which are of importance when considering the monitoring and/or surveying of large areas.

3.1. EXTENSION OF CLASSIFIER SIGNATURES

When large areas are surveyed from space, there exists a high probability that environmental and observational conditions will change from

day to day, frame to frame, and/or within a frame. Resulting changes in signal levels received from each class of surface cover can result in degraded machine classification performance and reduced quality of other extracted information. One way to combat such changes is to have available substantial amounts of ground-truth information throughout the survey area; however, this can be expensive. Another way is to adjust the classifier signatures and/or data to counteract the effects of the changes; we call techniques that implement such changes "signature extension" techniques.

In this section, we discuss the improved results obtained with signature extension techniques when signatures extracted from one day were applied to data from the preceding day over the same area. Different amounts of atmospheric haze were present on the two days and the ERTS-1 scan angles were toward opposite sides of the frame. Both an empirical procedure and a theoretical procedure, utilizing calculations of atmospheric effects with a radiative transfer model, were used to adjust Day 1 signatures before they were applied to Day 2 data, and both improved classification accuracy.

The results presented here are from an initial exercise of our signature extension techniques on ERTS-1 data. Only recently did we obtain access to ERTS-1 data sets suited for evaluation of the procedures. We need data on two different days over the same well ground-truthed site, with different amounts of haze present on the two days. A data set, being used in a study in which we are participating under the NASA SR&T program of the Johnson Space Center, met these criteria.

Classifier signatures were obtained for trees and crops on one day and applied directly in processing data from the preceding day. Classification performance was degraded because the different amount of haze present and different observation geometries changed the magnitude and spectrum of the signals received by ERTS-1. By applying certain signature extension procedures, we were able to adjust the signatures used, improve the classification performance, and, thereby, extend the original signatures to the second day.

To help describe the signature extension techniques employed, the following example of tree recognition is given. First, an area that was 100% classified as trees on the first day was found and outlined on a recognition map. When the Day 1 signatures were applied to the Day 2 data, only 67% of the picture elements (pixels) were correctly classified as trees (symbol θ on Figure 11a). Then the signatures were adjusted by an amount determined by subtracting the mean level of signals over a larger nearby area on Day 1 from the mean levels computed for the same area on Day 2. A different adjustment was made for each channel. The adjusted signatures were used in the classifier and the classification percentage increased to 77% (Figure 11b).

Photometer readings had been made on the two days at the time of the ERTS passes. These readings were used to calculate an optical depth at each wavelength for each day. Dr. Robert Turner of ERIM used his radiative transfer model [12] to compute total radiance and path radiance quantities for those optical depths and observation geometries. We then computed signature adjustments based on the model calculations and applied them to the Day 2 data. The result, shown in Figure 11c, is that 88% of the pixels in the area were classified as trees.

The above example is one of the more dramatic cases observed but, nevertheless, is indicative of the trend. The centers of a total of 27 wooded areas were delineated and tested. As shown in Table 2, the average classification accuracy fell from 96% to 88% for no adjustment of the signatures. The two signature extension techniques increased the correct classification accuracies to 92% and 91%, respectively.

TABLE 2

SUMMARY OF CLASSIFICATION RESULTS FOR ONE AREA VIEWED ON TWO SUCCESSIVE DAYS

SIGNATURES	DATA SET	WHEAT % CORRECT	TREES % CORRECT
DAY 1	DAY 1	87%	96%
DAY 1	DAY 2	65%	88%
DAY 1*	DAY 2	71%	92%
DAY 1**	DAY 2	78%	91%
NO. TEST AREAS		10	27

*EMPIRICAL MEAN LEVEL ADJUSTMENT

**THEORETICAL LEVEL ADJUSTMENT
(Photometer Plus Model)

Results for field-center pixels of ten wheat fields also are presented in Table 2. Here, again, the accuracy fell from 87% to 65% with no adjustment, and rose to 71% and 78% for the two types of signature extension procedures.

These preliminary results, in our opinion, demonstrate that the atmosphere poses a problem for accurate machine classification with ERTS data over large areas and indicate that steps can be taken to alleviate the degrading effects of the atmosphere. However, more analysis is required to obtain a better understanding of the sensitivity of classification results to signature adjustments and other signature extension procedures and to develop efficient and accurate procedures for determining and implementing corrections. The next section discusses some of the insights gained to date regarding the atmospheric effects.

3.2. ANALYSIS OF ATMOSPHERIC EFFECTS

The atmosphere significantly affects the amount of energy received at the ERTS satellite, both with an additive path radiance term and an attenuating effect on signals from the Earth's surface. As seen in Figure 12, path radiance constitutes over 50% of the signal from an 8% reflector in ERTS Band 4 (i.e., at 0.55 μm) and, proportionately, it is even greater in signals from darker surfaces. Although atmospheric effects are reduced at the longer wavelengths of ERTS Bands 6 and 7, they still are significant. Some indications of the relative magnitudes were presented in our earlier paper at the ERTS Symposium in March, 1973 [2].

Figure 12 also was presented in the March paper, but is repeated here because it exhibits some of the major dependencies of path radiance and total radiance that are pertinent to a discussion of signature extension over large areas. It represents calculations made with the radiative transfer model. First, we see that the path radiance depends upon the amount of atmospheric haze present, here denoted by horizontal visual range. The effect of haze on total radiance at the satellite is less than on path radiance, because of the compensating effects of atmospheric transmittance which decreases as the amount of haze increases.

The other important effect in Figure 12 is the scan angle effect. There is a tendency to dismiss scan angle as being an unimportant consideration in ERTS data, because the scan is only $\pm 5.5^{\circ}$ from nadir and frequently only fractions of frames are analyzed. However, the theoretical calculations shown here have a noticeable scan angle dependence from one side of a frame to the other, an effect which is intensified by an increase of haze.

For the data set described in Section 3.1, the scene was viewed approximately 4° to the East of nadir on Day 1 and 3° to the West of nadir on Day 2. Photometer readings were used to establish optical depth vs. wavelength profiles for the two days. These profiles differed from our standard atmospheres which are labeled by horizontal visual ranges. Visibility readings of 19 km and 24 km were recorded at airports in the vicinity. Theoretical radiative transfer model calculations for an assumed average background albedo distribution resulted in a signature adjustment vector that includes effects for the differences in both optical depth

and scan angle, and its application resulted in the improved classification accuracy already noted, even though its magnitude is only a few percent (or less) of the average signal value in each band.

Another important factor in path radiance is the average background surface albedo that applies for any given observation. Figure 13 illustrates how surface albedo affects the variations in received signals at 0.55 μm (Band 4). It is very interesting that, for low albedo, an increase in haze (shorter visual range) can decrease the signal in space, while the opposite effect is true for high albedos.

We intend to examine in more detail the sensitivity of classification performance to adjustments of signatures, in an effort to improve procedures. While the signature adjustment procedure effectively applies the same correction to all signals, independent of their magnitudes, a more general procedure would apply to each observation a preprocessing transformation that could depend on the signal magnitude.

Another preprocessing transformation that we have applied to aircraft multispectral scanner data for several years [13], and more recently to ERTS data [14], is ratio preprocessing, i.e., the computation of ratios of signals in different channels for use as classifier inputs and/or for image enhancement. Ratios of signals are more closely related to ratios of spectral reflectances of scene objects if path radiance contributions are subtracted before the ratios are computed. One method developed at ERIM for approximating path radiance is the use of the lowest bonifide signal level in each band. In Bands 6 and 7, water signals are usually the lowest received. Figure 14 presents a manual contour of water signals extracted for Band 6 from approximately 30 water bodies throughout one frame. The dots indicate the sample points and the contour numbers are ERTS data values. The contour pattern agrees with the pattern of airport visibility readings from the five cities noted on the frame.

4.0. CONCLUSIONS

In conclusion, we have discussed several techniques which potentially can improve the quality and quantity of information extracted from ERTS data. We believe that the continued development of interpretive techniques and their incorporation into applications efforts in many disciplines is important to the success of operational Earth Observation systems.

ACKNOWLEDGEMENTS

The authors wish to acknowledge the assistance provided by numerous personnel of the ERIM Multispectral Analysis Section and the ERIM Publications Department.

REFERENCES

1. Horwitz, H., Nalepka, R. F., and Morgenstern, J., "Estimating the Proportions Within a Single Resolution Element of a Multispectral Scanner", Proceedings of the 7th International Symposium on Remote Sensing of Environment, May 1971, Ann Arbor, Michigan.

2. Malila, W. A., and Nalepka, R. F., "Atmospheric Effects in ERTS-1 Data and Advanced Information Extraction Techniques", Presented at the Symposium on Significant Results Obtained from ERTS-1, March 5-9, 1973, New Carrollton, Maryland.

3. Thomson, F. J., "Crop Species Recognition and Mensuration in the Sacramento Valley", Presented at the Symposium on Significant Results Obtained from ERTS-1, March 5-9, 1973, New Carrollton, Maryland.

4. McEwen, R. B., "Geometric Quality of ERTS-1 Images", Presented at the Symposium on Significant Results Obtained from ERTS-1, March 5-9, 1973, New Carrollton, Maryland.

5. Rifman, S. S., "Digital Rectification of ERTS Multispectral Imagery", Presented at the Symposium on Significant Results Obtained from ERTS-1, March 5-9, 1973, New Carrollton, Maryland.

6. Bernstein, R., "Results of Precision Processing (Scene Correction) of ERTS-1 Images Using Digital Image Processing Techniques", Presented at the Symposium on Significant Results Obtained from ERTS-1, March 5-9, 1973, New Carrollton, Maryland.

7. Bauer, M. E., "Identification of Agricultural Crops by Computer Processing of ERTS MSS Data", Presented at the Symposium on Significant Results Obtained from ERTS-1, March 5-9, 1973, New Carrollton, Maryland.

8. Billingsley, F. C. and A. F. H. Goetz, "Computer Techniques Used for Some Enhancement of ERTS Images", Presented at the Symposium on Significant Results Obtained from ERTS-1, March 5-9, 1973, New Carrollton, Maryland.

9. Bizzell, R., L. Wade, H. Prior, and B. Spiers, "The Results of an Agricultural Analysis of ERTS-1 MSS Data at the Johnson Space Center", Presented at the Symposium on Significant Results Obtained from ERTS-1, March 5-9, 1973, New Carrollton, Maryland.

10. Thomson, F. J., et al., "ERIM Progress Report on Use of ERTS-1 Data", Type II Progress Report 1 January through 30 June 1973, Environmental Research Institute of Michigan, Report No. 193300-16-P, July 1973.

11. Malila, W. A., Hieber, R. H., and McCleer, A. P., "Correlation of ERTS MSS Data and Earth Coordinate Systems", Presented at the Conference on Machine Processing of Remotely Sensed Data, October 1973, Lafayette, Indiana.

12. Malila, W. A., Crane, R. B., Turner, R. E., "Information Extraction Techniques for Multispectral Scanner Data", Willow Run Laboratories, Institute of Science and Technology, The University of Michigan, Report No. 31650-74-T, June 1972.

13. Kriegler, F. J., Malila, W. A., Nalepka, R. F., and Richardson, W., "Preprocessing Transformations and Their Effects on Multispectral Recognition", Proceedings of the 6th International Symposium on Remote Sensing of Environment, October 1969.

14. Wagner, T. W., and Polcyn, F. C., "Progress of an ERTS-1 Program for Lake Ontario and Its Basin", Presented at the Symposium on Significant Results Obtained from ERTS-1, March 5-9, 1973, New Carrollton, Maryland.

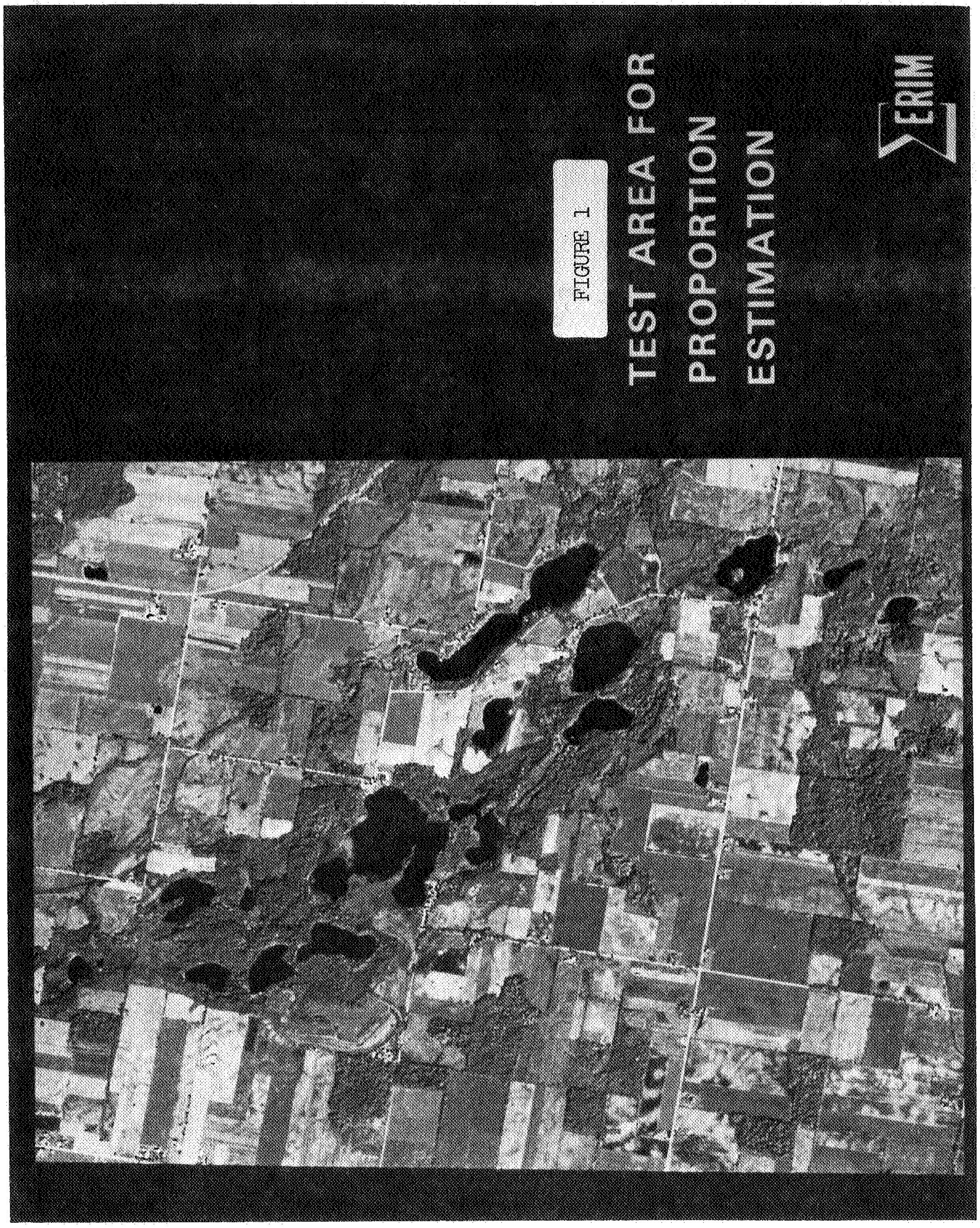
FIGURE 1
TEST AREA FOR
PROPORTION
ESTIMATION
ERIM

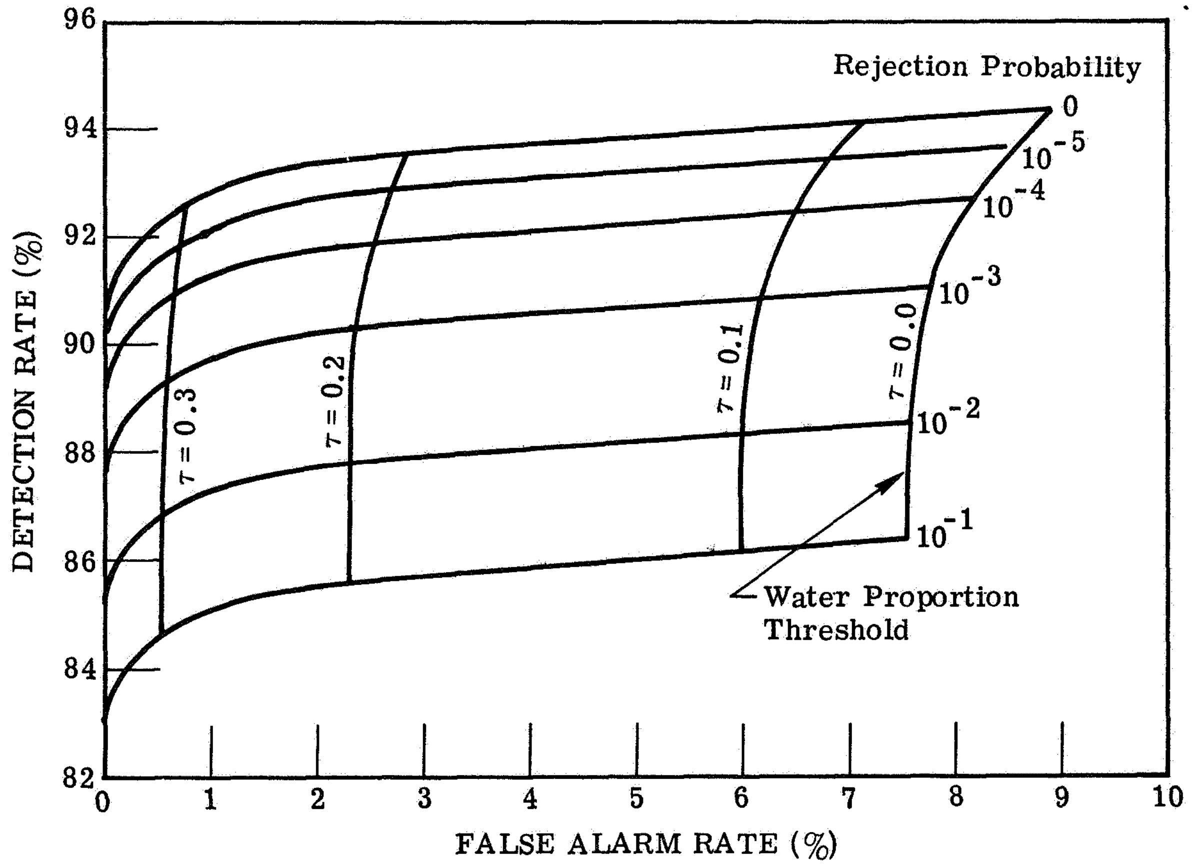

OPERATING CHARACTERISTICS OF PROPORTION ESTIMATION (3 channel)

FIGURE 2

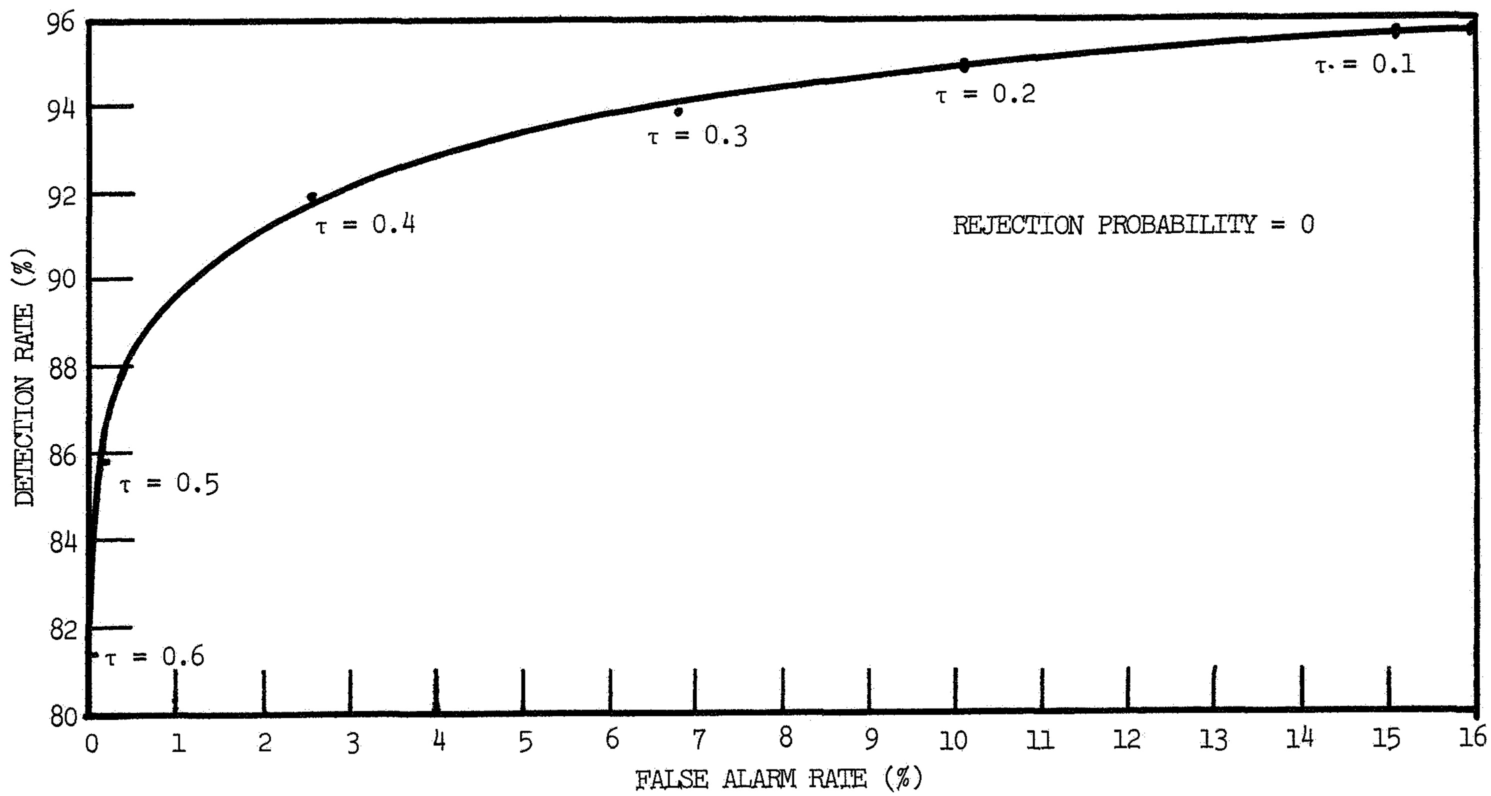

OPERATING CHARACTERISTICS OF PROPORTION ESTIMATION (1 CHANNEL - ERTS BAND 7)

FIGURE 3

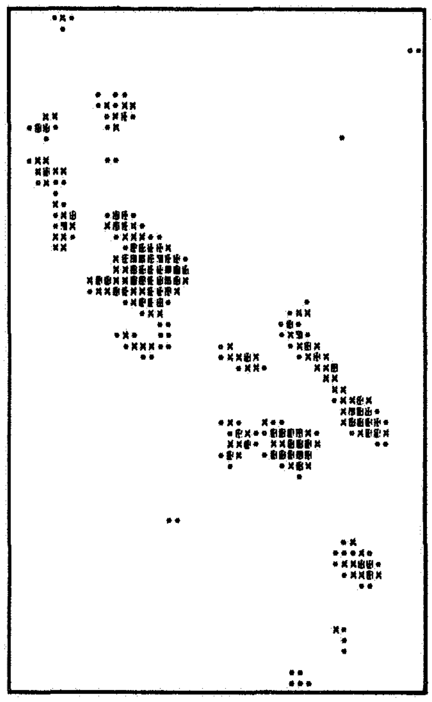

FIGURE 4

PROPORTION ESTIMATE
WATER RECOGNITION MAP
(with ERTS Bands
4, 5, and 7)

ERIM

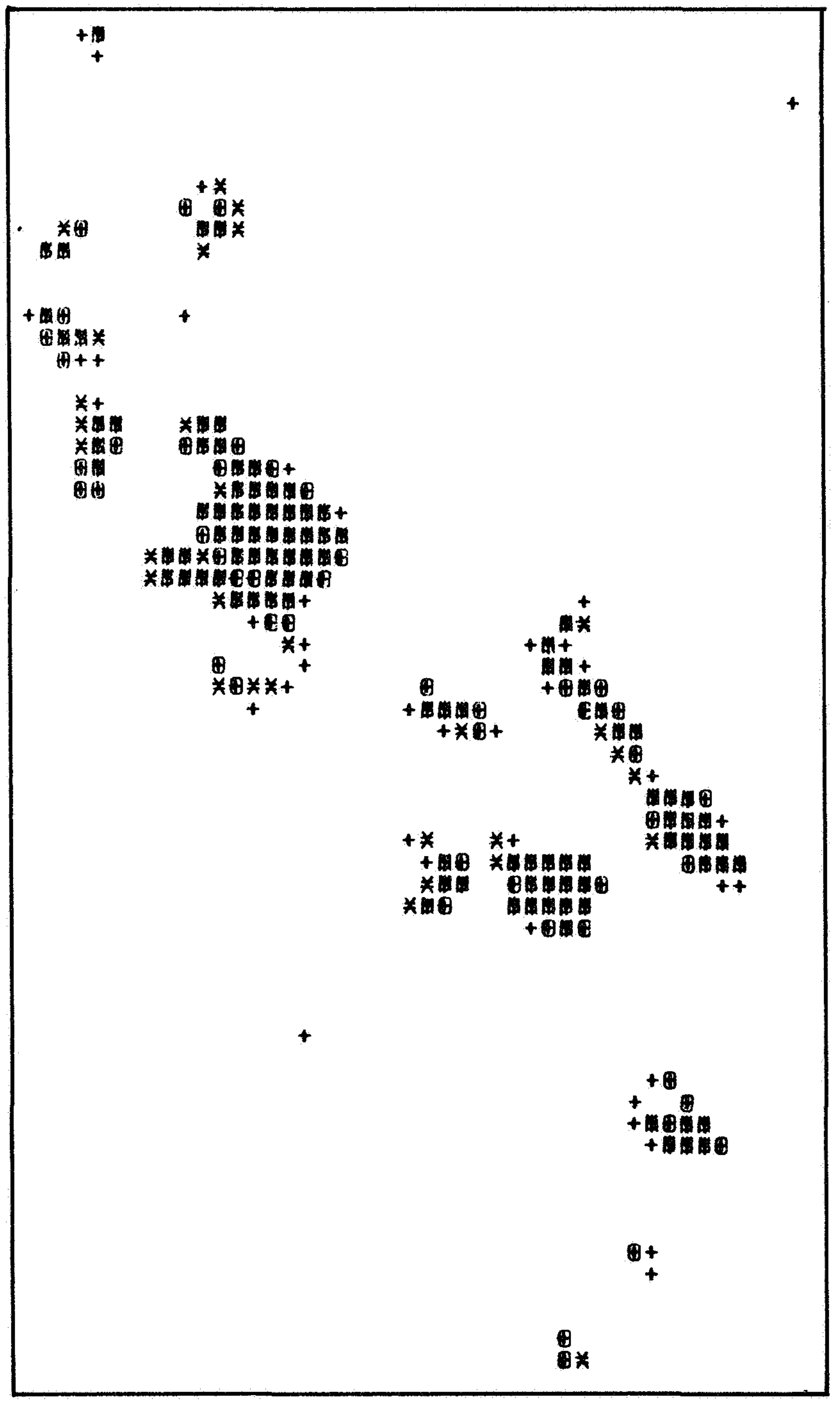

PROPORTION ESTIMATE
WATER RECOGNITION MAP
(With ERTS Band 7 Only)

FIGURE 5

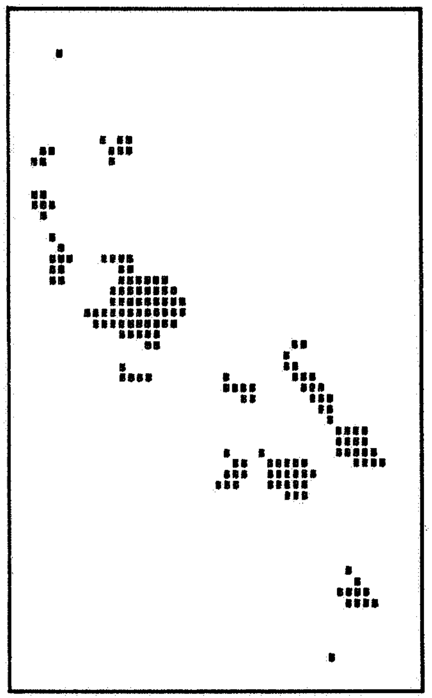

FIGURE 6

CONVENTIONAL
WATER RECOGNITION MAP
(with ERTS Bands
4, 5, and 7)

ERIM

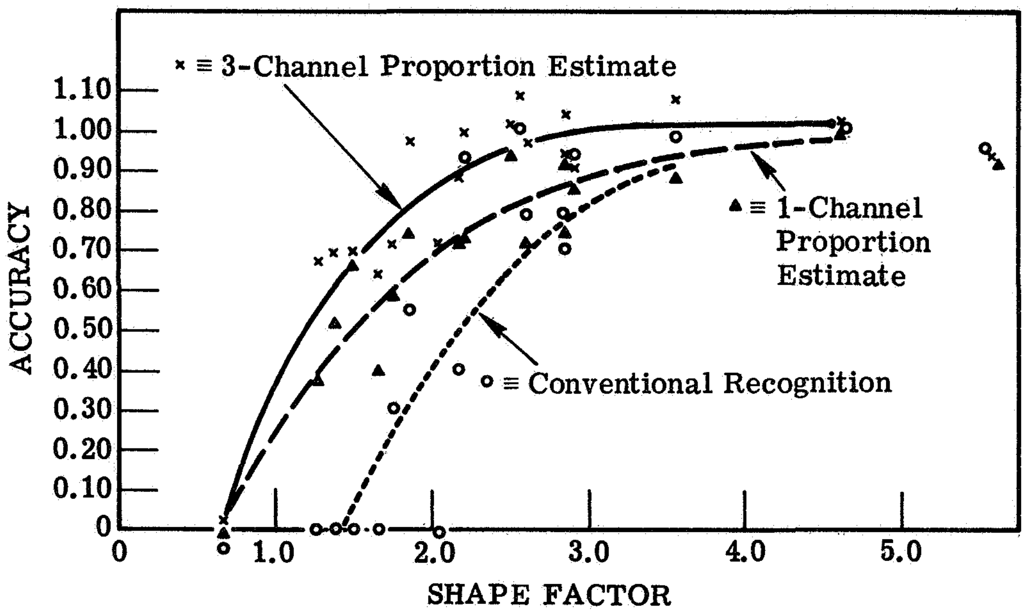

COMPARISON OF EFFECT OF SHAPE FACTOR ON
AREA ESTIMATION OF WATER BODIES

FIGURE 7

ERIM

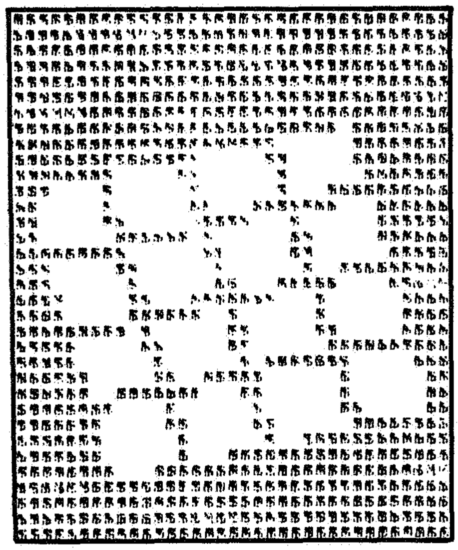

Part (a) 0.5 INSET

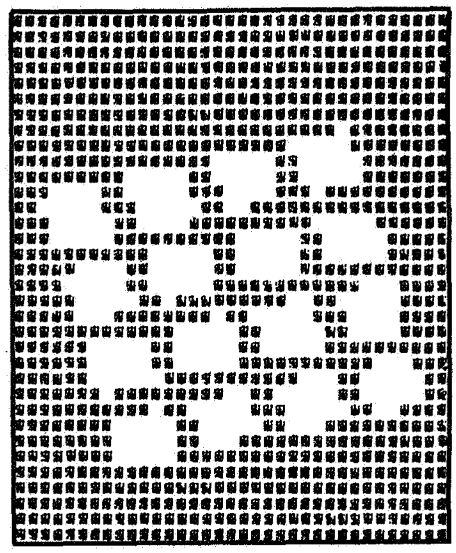

Part (b) 0.75 INSET

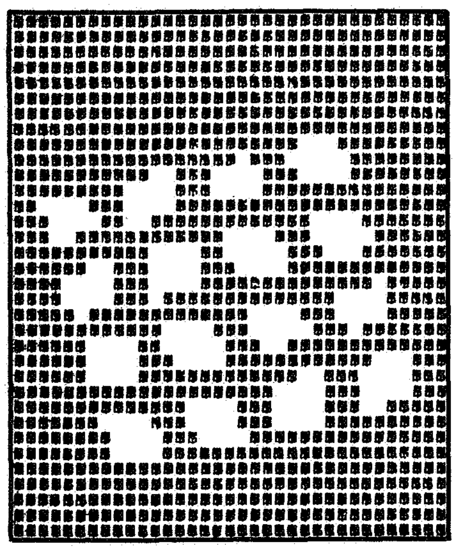

Part (c) 1.0 INSET

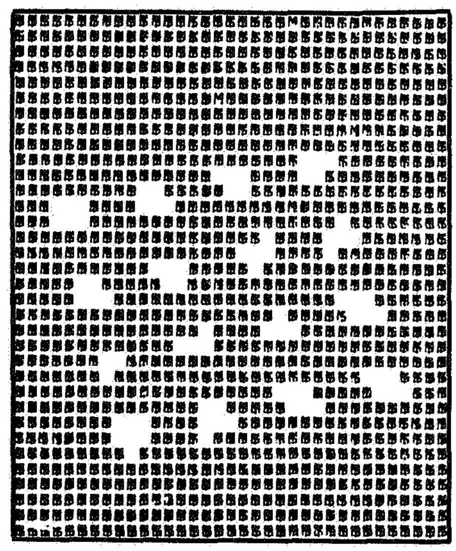

Part (d) 1.5 INSET

EFFECT OF INSET PARAMETER ON PIXEL SELECTION FOR 40-ACRE FIELDS

(Inset Parameter is Measured in MSS Resolution Elements)

FIGURE 8

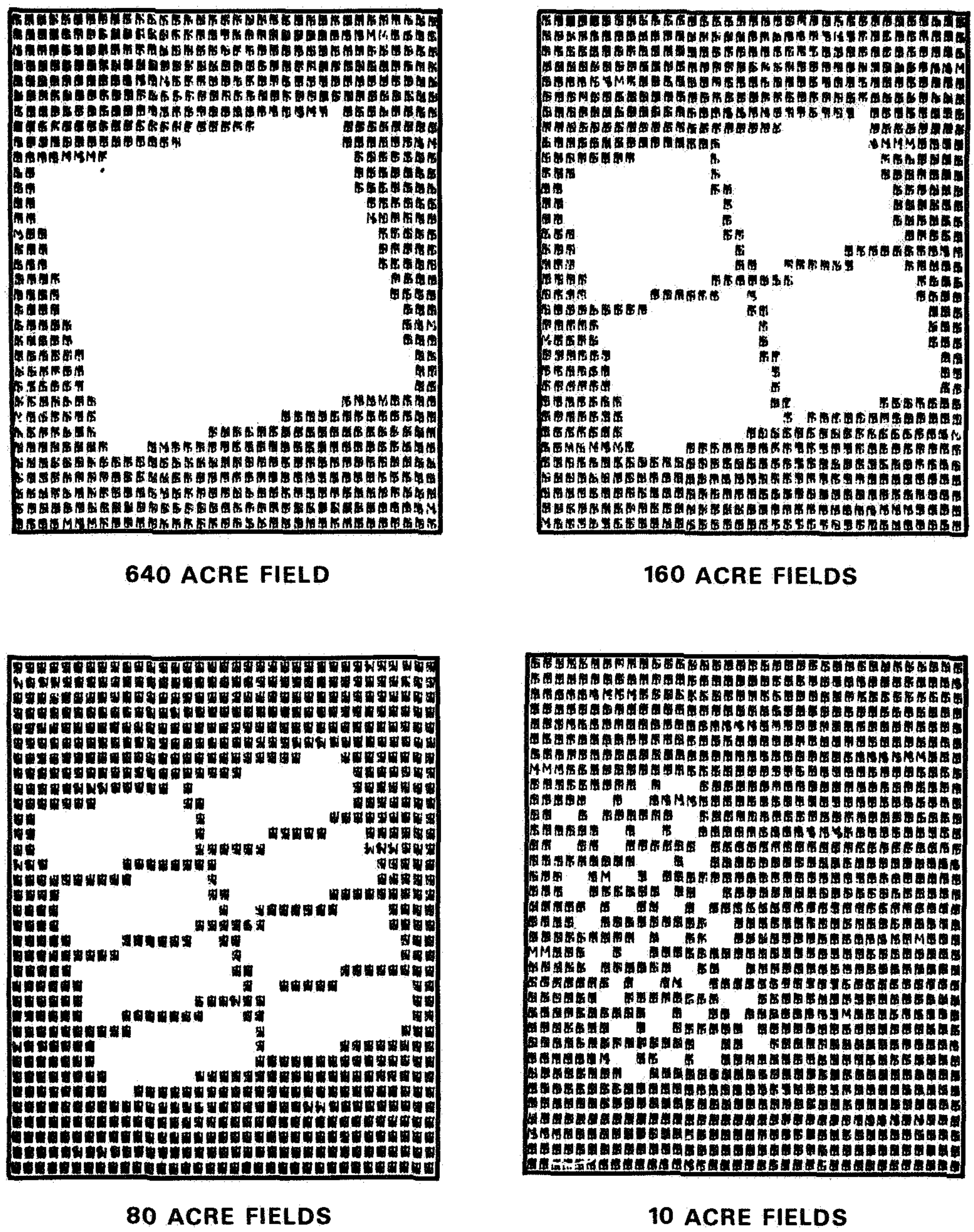

EFFECT OF FIELD SIZE ON PIXEL SELECTION FOR 0.5-RESOLUTION-ELEMENT INSET

ERIM

FIGURE 9

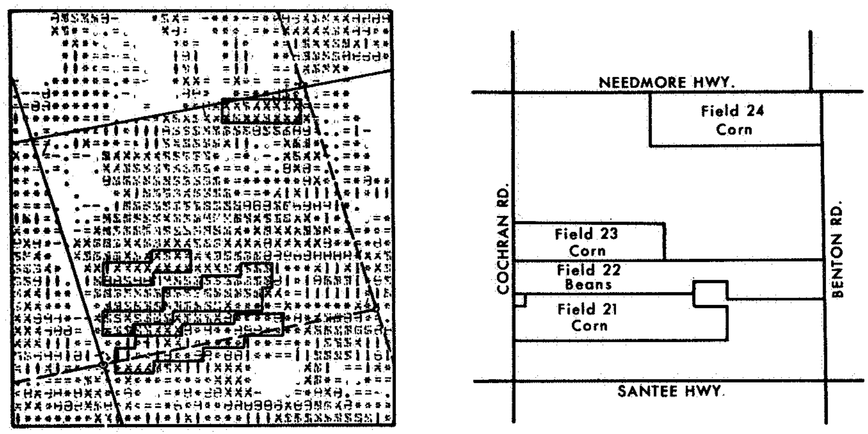

ORIGINAL MANUAL ASSIGNMENT

MAP OF FIELD BOUNDARIES

EXAMPLE OF FIELD LOCATION IN ERTS DATA

FIGURE 10a

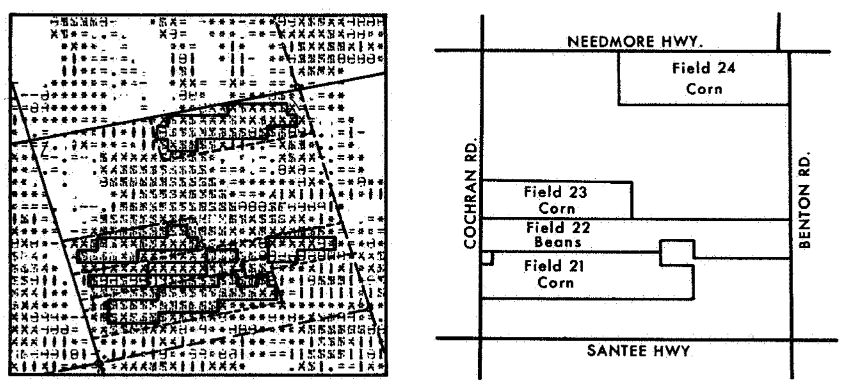

COMPUTER-AIDED ASSIGNMENT

MAP OF FIELD BOUNDARIES

EXAMPLE OF FIELD LOCATION IN ERTS DATA

FIGURE 10b

ERIM

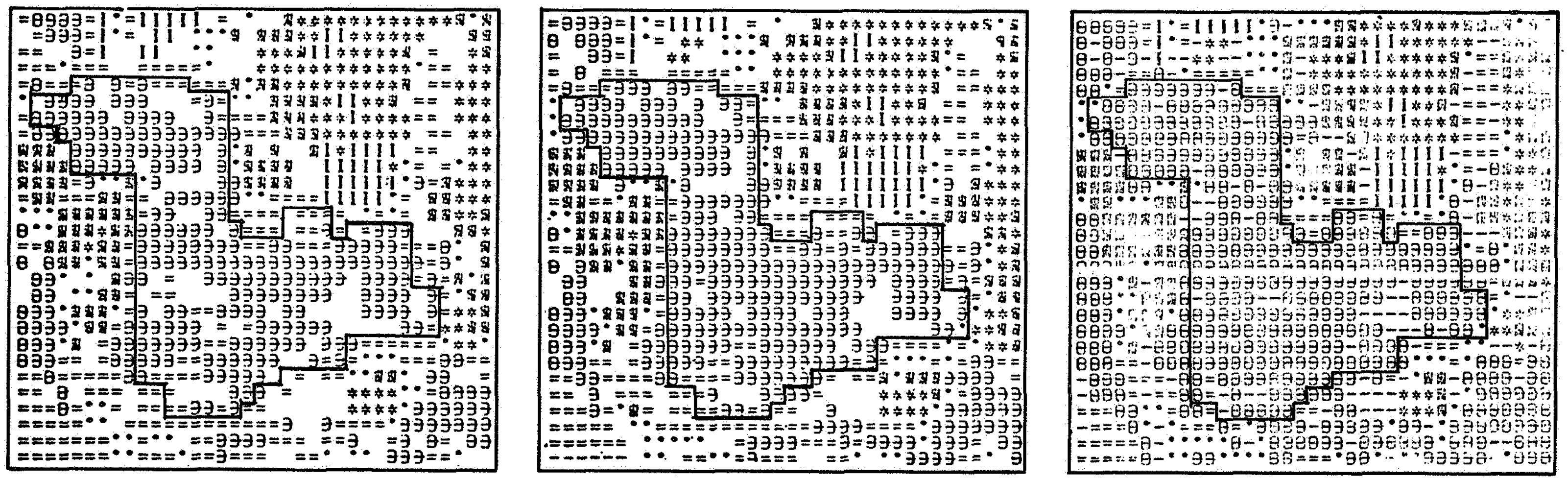

NO ADJUSTMENT OF SIGNATURES

(67% Called Trees)
(a)

EMPIRICAL MEAN LEVEL ADJUSTMENT

(77% Called Trees)
(b)

THEORETICAL MEAN LEVEL ADJUSTMENT

(88% Called Trees)
(c)

Outlined Area Completely Recognized as Trees for Same Day as Signatures.

EXAMPLE OF APPLYING SIGNATURES FROM ONE DAY TO ERTS DATA FROM PRECEDING DAY OVER SAME AREA

FIGURE 11

FIGURE 12

COMBINED SCAN-ANGLE AND VISUAL-RANGE EFFECTS ON RADIANCE AT SATELLITE, 0.55 μm

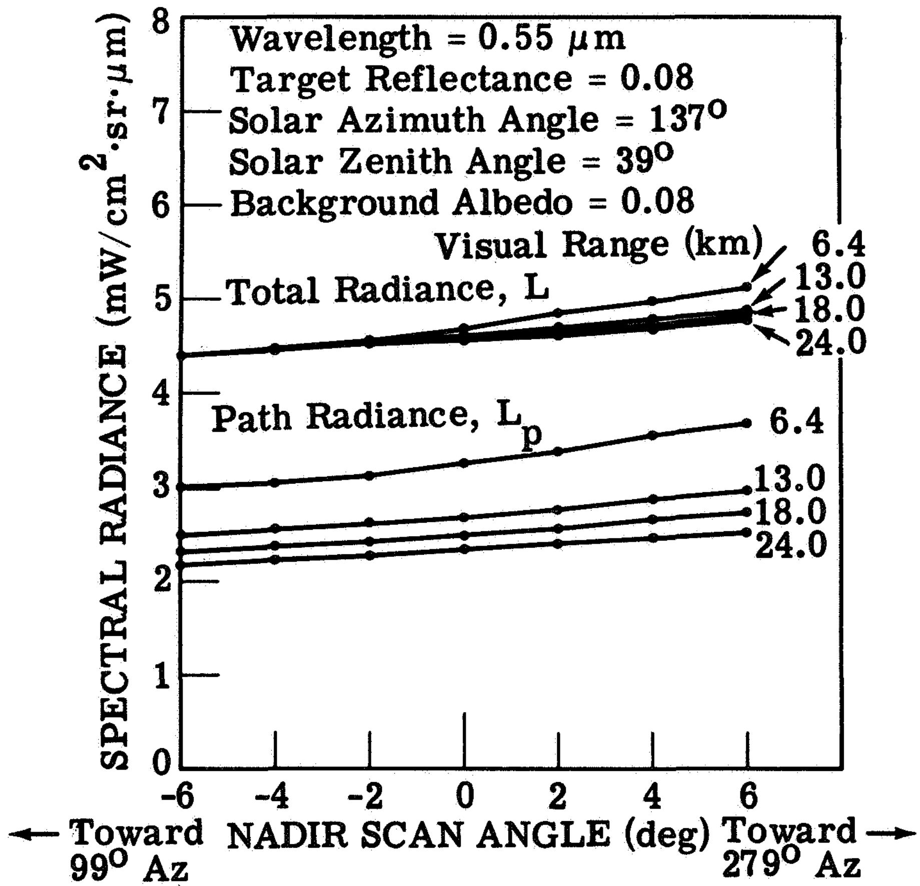

ERIM

FIGURE 13

DEPENDENCE OF RADIATION AT SATELLITE ON VISUAL RANGE, 0.55 μm

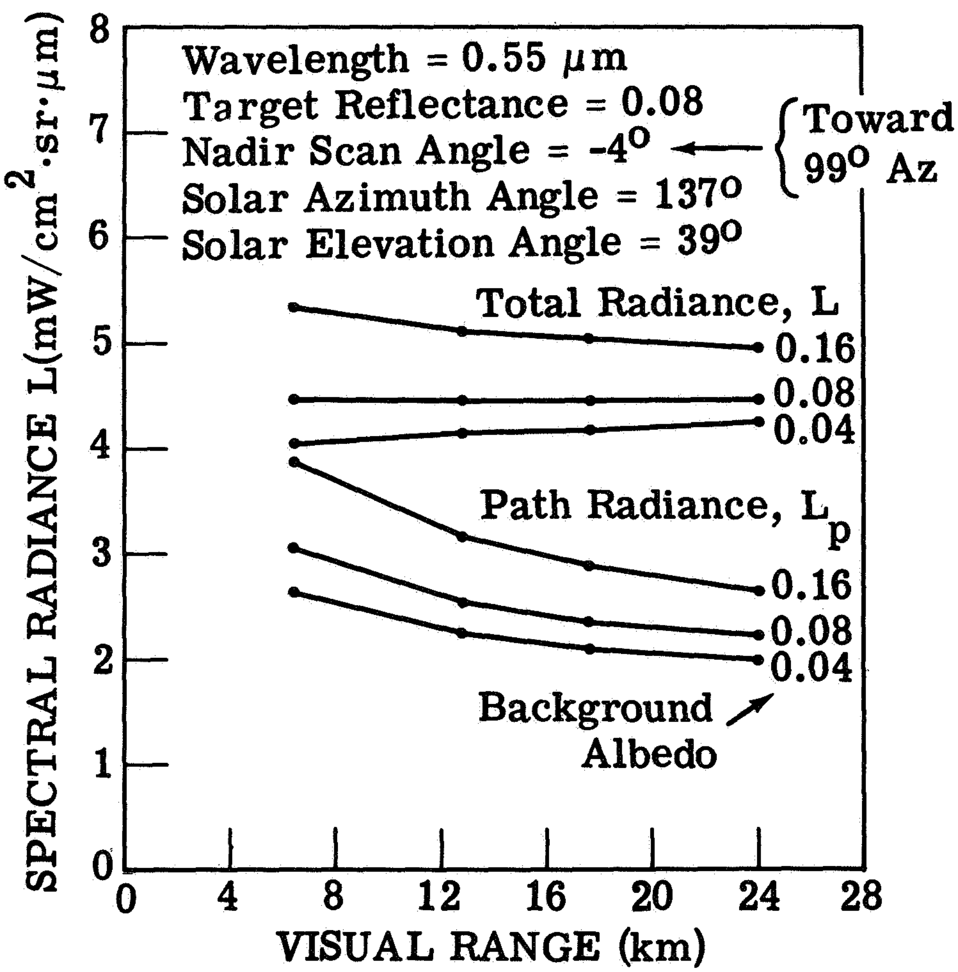

ERIM

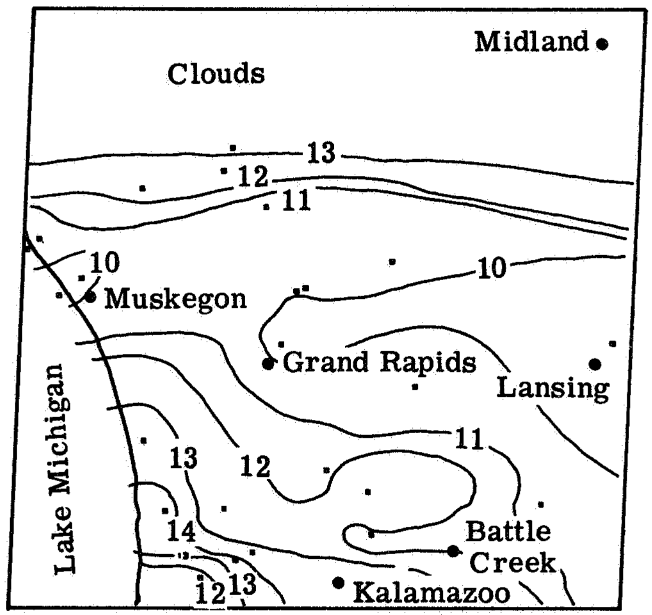

WATER SIGNAL CONTOURS, ERTS Band 6
(Frame 1033-15580)

FIGURE 14

Paper I 6

INTERPRETATION OF ERTS-1 IMAGERY AIDED BY PHOTOGRAPHIC ENHANCEMENT

U. Nielsen, *Research Scientist, Forest Management Institute, Canadian Forestry Service, Department of the Environment, Ottawa, Canada*

ABSTRACT

Agfacontour film can be used to produce relatively economical enhancements of density differences recorded on film. Image interpreters often ask whether enhancement really increases the information content of the original images. Examples of ERTS-1 imagery enhancements show that it is possible to separate density levels which are not discernible by the human eye. It is stressed that these techniques do not replace the photo interpreter, but rather they aid him in the interpretation process. Subtle density variations are made to stand out and an objective classification of the densities forming the image is produced.

INTRODUCTION

Agfacontour Professional is a two-emulsion black-and-white copying film which can be used in photographic enhancement to separate or extract selected density levels from negative or positive images recorded on film. The principles of the technique were described by Ranz and Schneider (1971), Nielsen (1972) and others. The main advantages of the Agfacontour technique and, of most photographic enhancement techniques are:

- simplicity (no other equipment than that found in conventional photographic darkroom is required);
- high resolution (similar to standard photographic reproductions);
- accuracy and repeatability.

Photographic techniques are slower than electronic techniques in producing enhancements, but this disadvantage is offset if hard copies are required.

A key question in the justification for production of enhancements by any method is whether the colour reproductions are just more impressive representations of readily discernible density variations within an image, or whether these colours really represent variations which are not easily identified on the original. I shall try to answer this question with some examples of ERTS-1 imagery (at a scale of 1:1,000,000) and respective Agfacontour enhancements.

INTERPRETATION AND DISCUSSION

In Figure 1 is band 6 of the first ERTS-1 image received in Canada.

Figure 2 is an enhancement of this image. The difference between the deep and shallow lakes on the western and eastern parts respectively are immediately apparent on the enhancement. I do not know whether water depth is the only cause for this difference. Measured on the original image, this difference in density amounted to 0.05 units in the density scale ranging from about 0 to 3. A recent burn, which might be mistaken for a lake on the original, also stands out distinctly on the enhancement.

In Figure 3 the sediment-loaded water of the Mackenzie River delta is discernible of the original image. The enhancement (Figure 4) suggests the possibility of a relative quantification of these sediments. The green colour of the sediment flowing into the larger lake (upper right) can be related to the green colour of the river on the upper left corner. In general, blue represents clear water.

Figure 5 is a copy of band 4 of an ERTS-1 frame covering the area between Ottawa and Montreal. The Ottawa River is imaged in two distinct grey tones. The boundary between these tones is the Carillon dam slightly to the right of the image center. The exact reason for this difference is not known, but can probably be attributed to different amounts of suspended materials. The stretch of the river west of the dam is subjected to the greatest pollution pressures from municipal and industrial (pulp and paper) waste disposal. The enhancement (Figure 6) does not add to this finding although it more dramatically and colourfully separates the different grey levels. But a distinct boundary in the forest cover north of the river is apparent. A change in species composition occurs toward the east in the transition from the Middle Ottawa to the Laurentian Forest Sections. The average difference in density between the western and eastern part (blue and green) on the original is about 0.07 density units. Also, a difference in the woodlots south of the Ottawa River is apparent. On the western half, forests and woodlots are reproduced in a higher density than in the south-eastern half (green and yellow respectively on the enhancement). This could be explained by a reduction of conifers towards the southeast.

These enhancements are also good examples of the danger of generalized statements such as "blue is water" and "green is forest". This type of interpretation or description can be very misleading. One colour can represent several features or conditions, or a particular condition or feature can be represented by several colours. Good examples, on Figure 6, are blue (water and forest), green (water and forest), yellow (water, forest and fields) and red (water, fields, and urban Montreal).

Figure 7 is a copy of band 5 of the same scene shown in Figure 5. The differentiation in the Ottawa River water is not evident. On the enhancement (Figure 8), this difference again becomes obvious. The density difference measured on the original was 0.04 density units. Also the transition of one Forest Section to the other is apparent, as is the

difference between the woodlots south of the Ottawa River.

Figure 9 is a reproduction of band 6 of the same scene as that shown in Figures 5 and 7. Most of the information on forest-cover differences is not evident. Water also has an apparently even density. But in the enhancement (Figure 10) there is a density difference in water. Densitometer measurements revealed that the difference between the areas reproduced in light and dark blue on the enhancement have a density difference of 0.03 density units on the original. Also apparent on the enhancement is an halation effect from the rivers. This was probably due to the reproduction technique used to obtain the original image (overshooting of the autododging system).

Figure 11 is the same enhancement as shown in Figure 10, except that one density slice was replaced with one density slice of the enhancement of the band-5 image. This introduces the southwest-to-northeast-running strips of woodlots into the composite.

CONCLUSIONS

It is evident, that photographic enhancements increase the information content of black-and-white images. But enhancements do not replace the photo interpreter. By making an objective classification of the densities forming the image, enhancements can aid the photo interpreter who, by conventional interpretation of the original image, still has to decide what features and conditions on the ground correspond to the individual densities reproduced in the enhancement.

Figure 1. Section of ERTS-1 image covering parts of Labrador (about latitude 55°N, longitude 63°W).

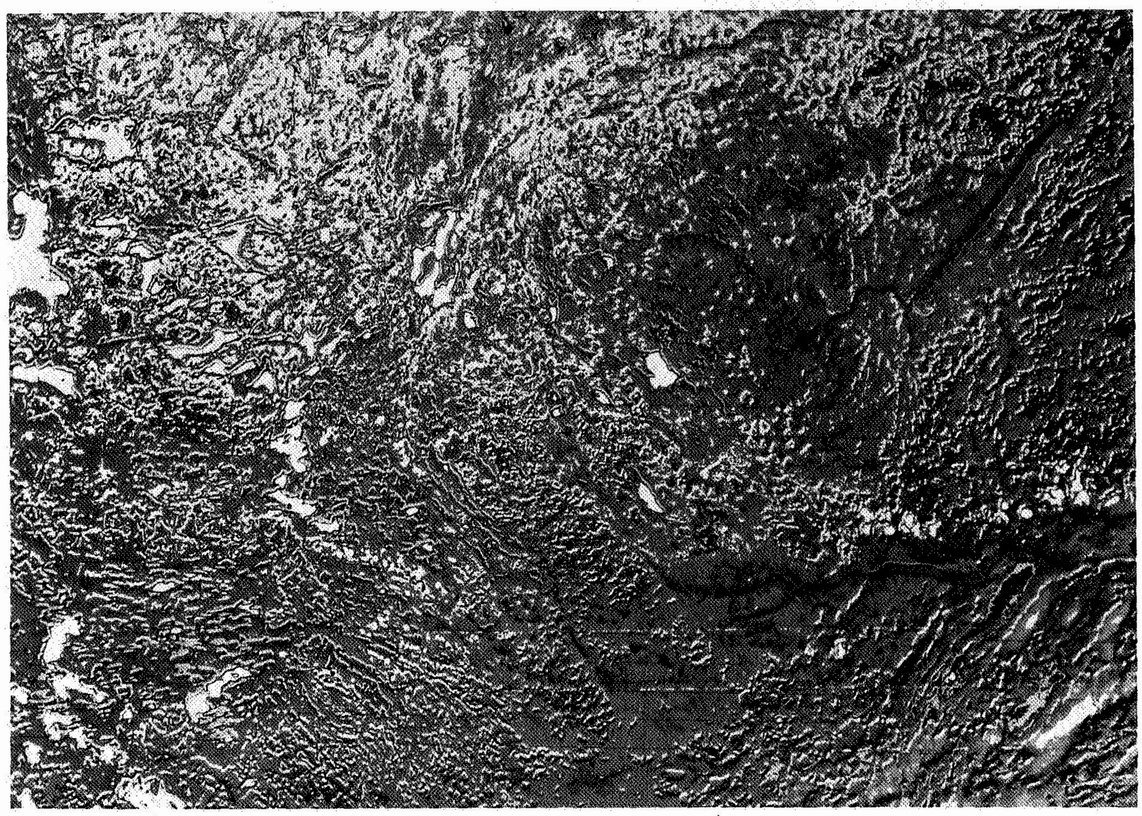

Figure 2. Photographic enhancement of the Labrador image in Figure 1.

Figure 3. ERTS-1 image covering a section of the Mackenzie River delta.

Figure 4. Photographic enhancement of the Mackenzie image in Figure 3.

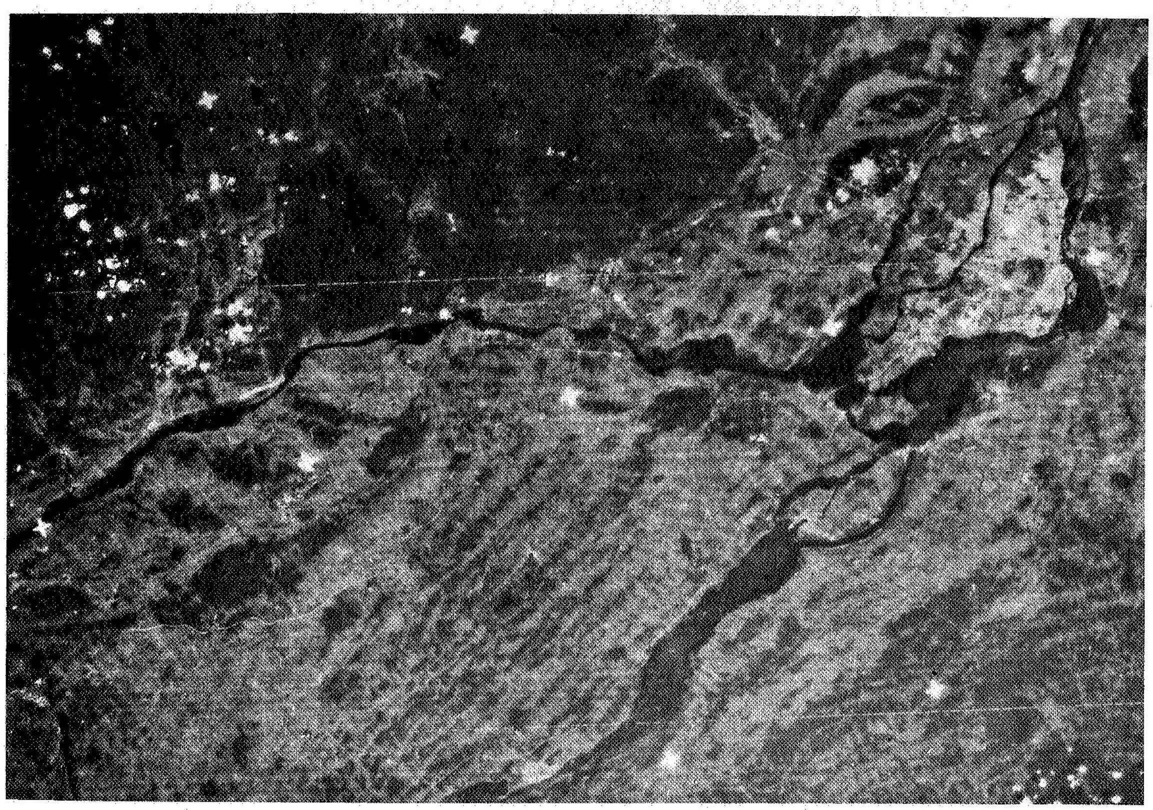

Figure 5. ERTS-1 image, band 4, of the Ottawa-Montreal area.

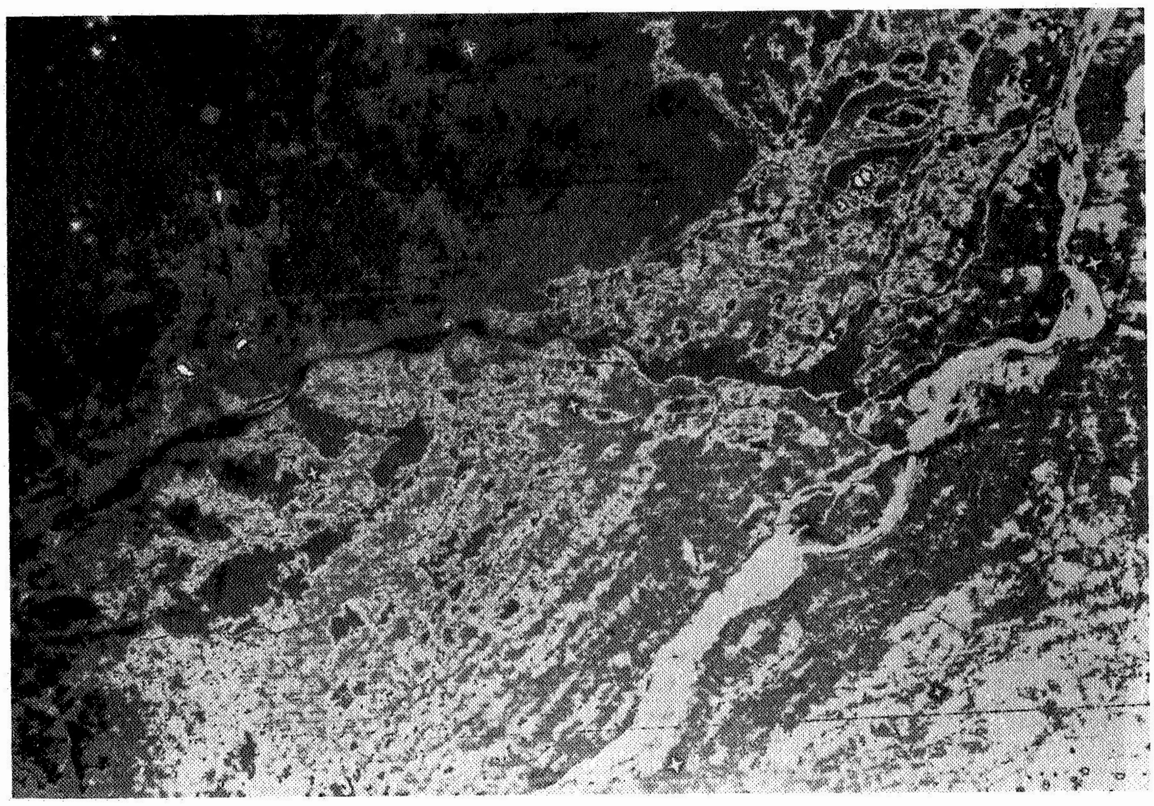

Figure 6. Photographic enhancement of the Ottawa-Montreal, band-4 image in Figure 5.

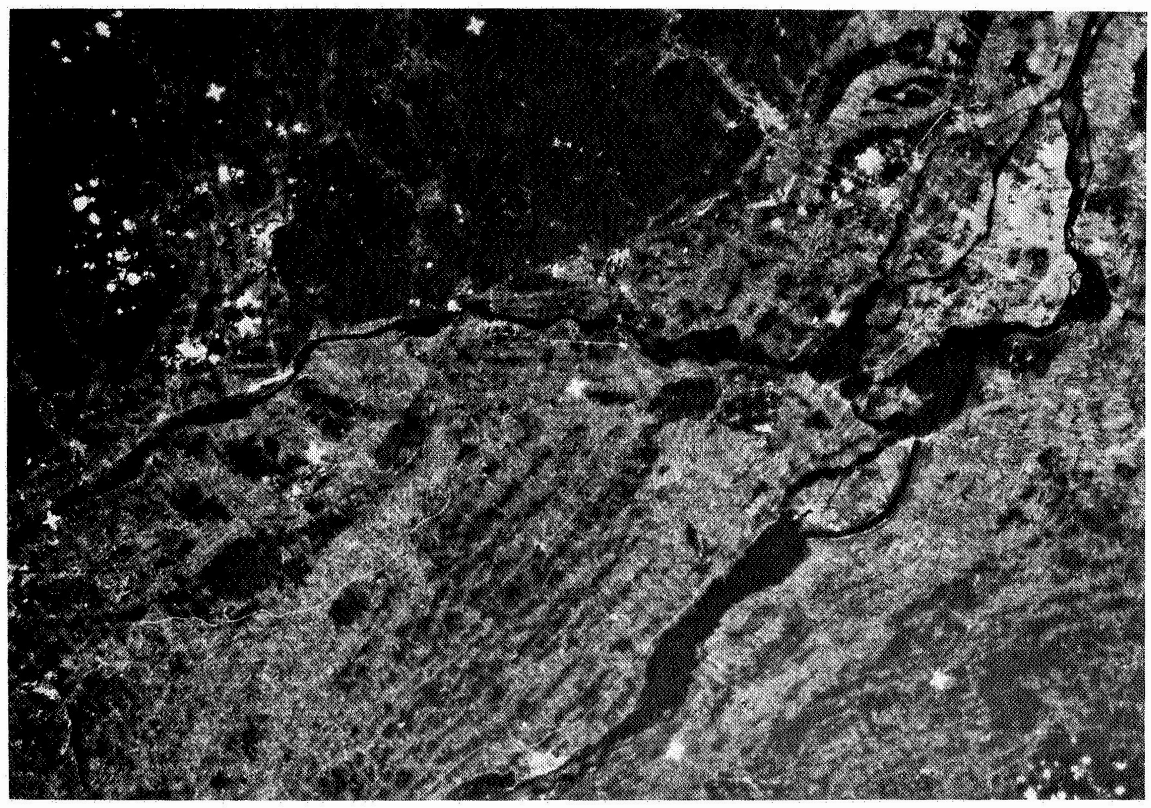

Figure 7. ERTS-1 image, band 5, of the Ottawa-Montreal area.

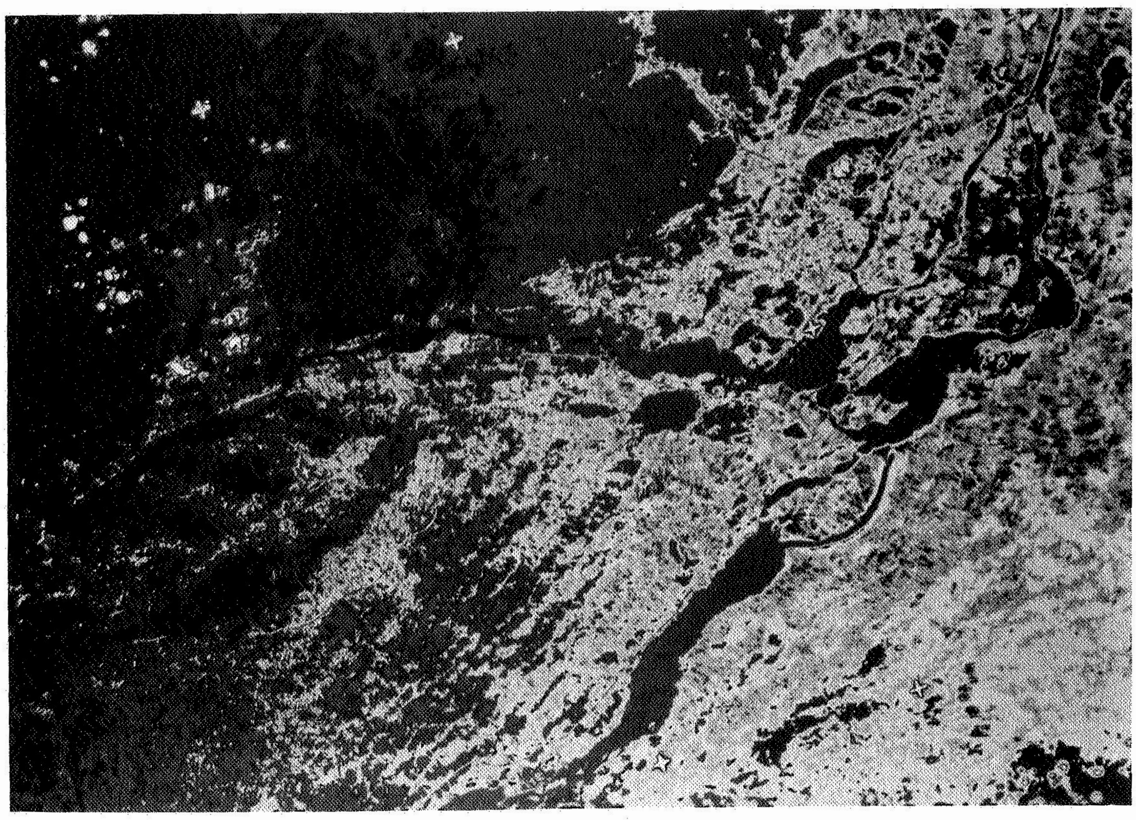

Figure 8. Photographic enhancement of the Ottawa-Montreal, band-5 image in Figure 7.

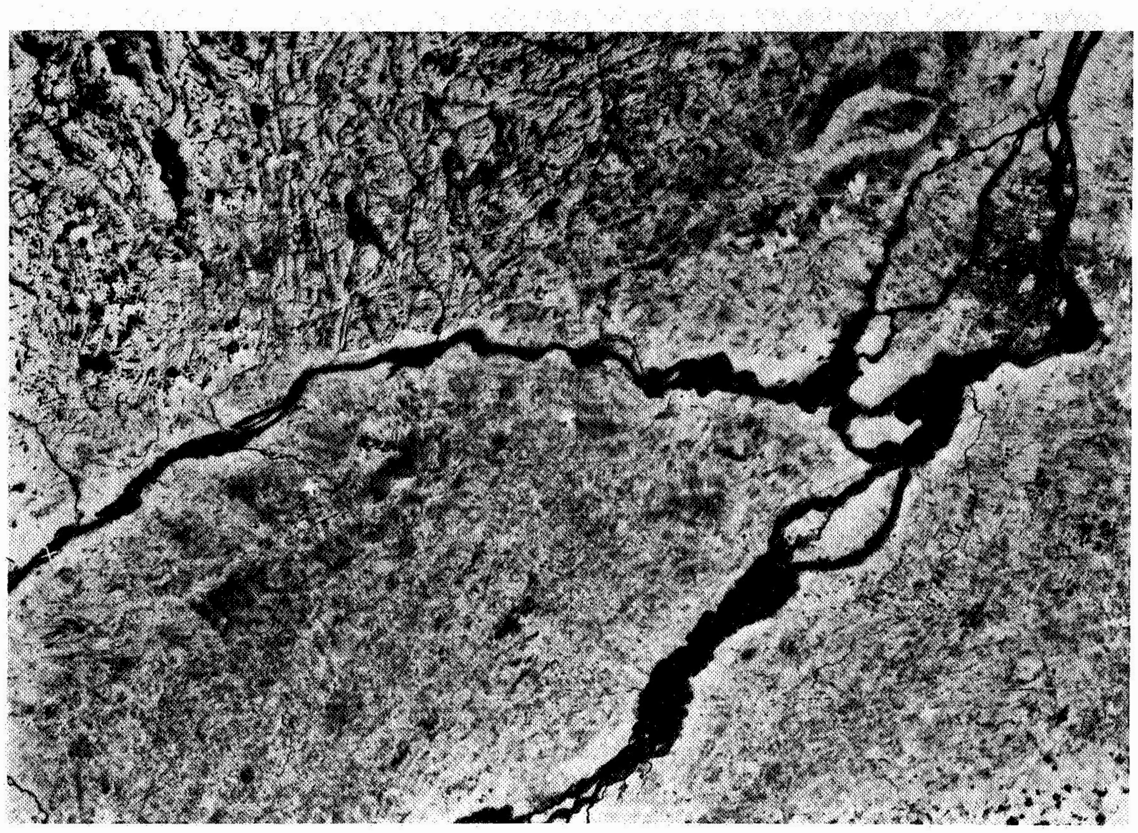

Figure 9. ERTS-1 image, band 6, of the Ottawa-Montreal area.

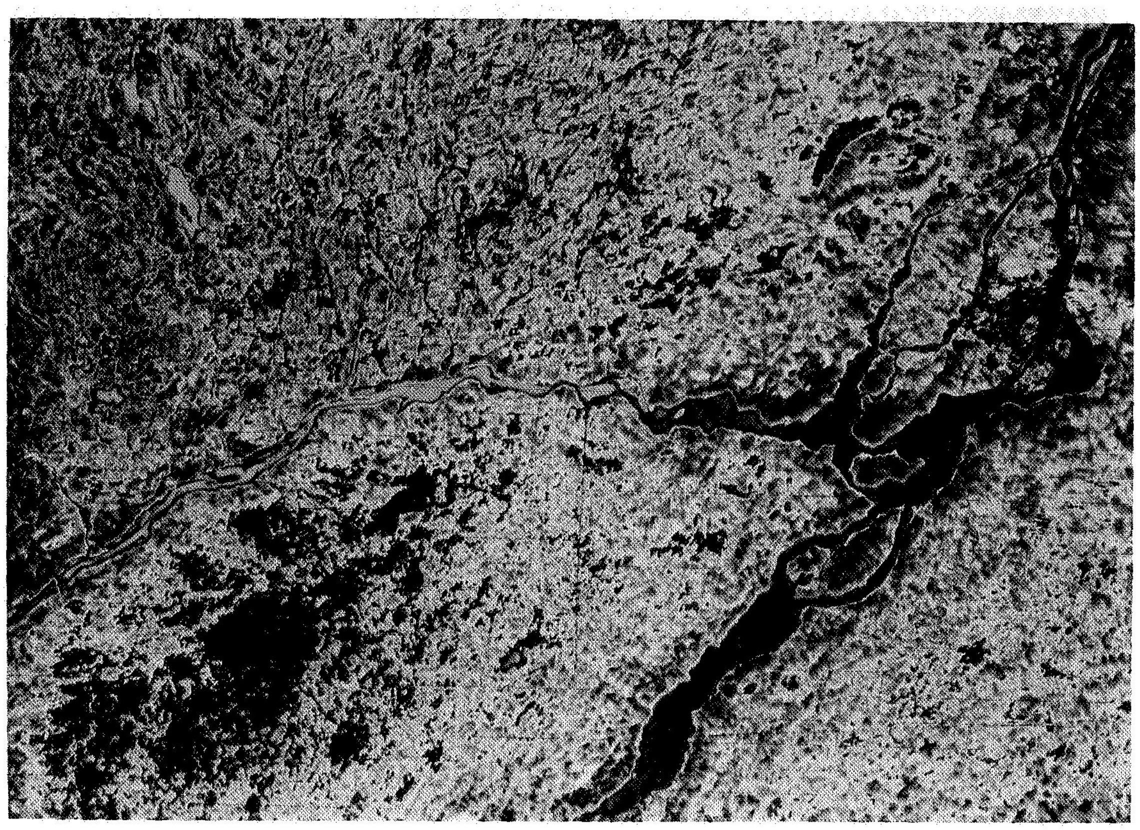

Figure 10. Photographic enhancement of the Ottawa-Montreal, band-6 image in Figure 9.

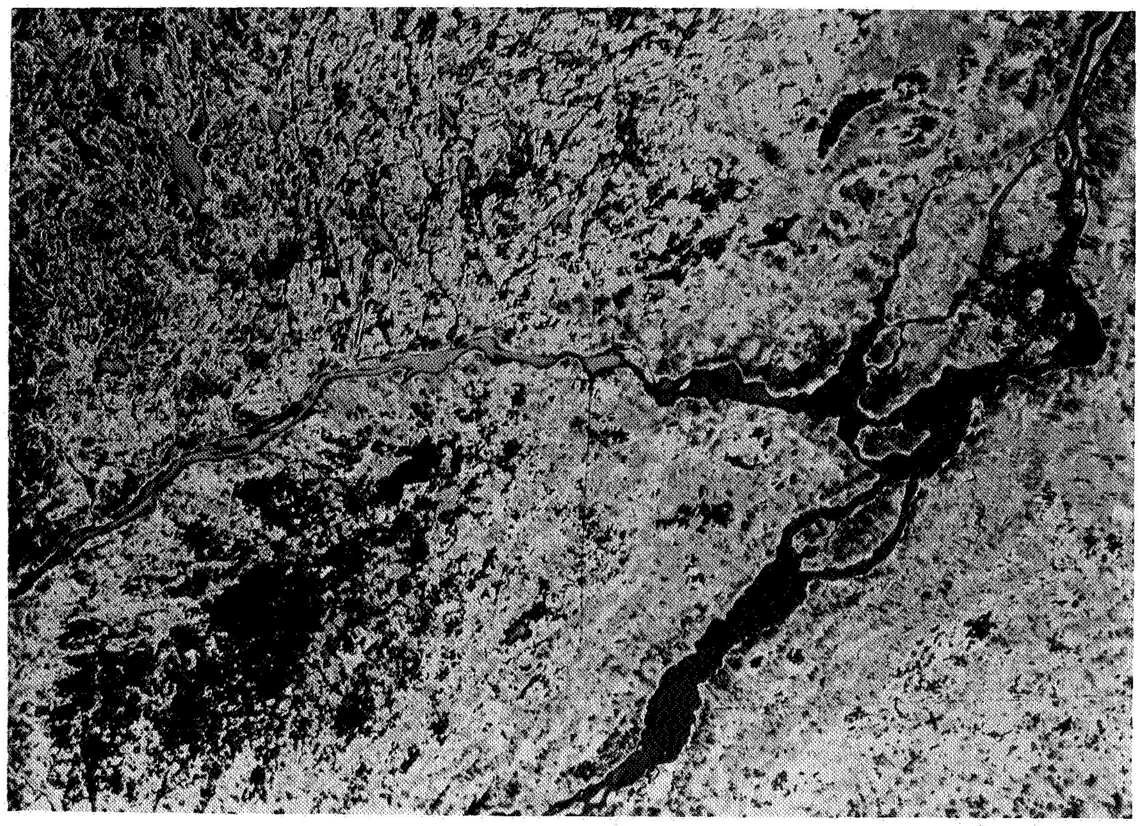

Figure 11. Photographic enhancement of the Ottawa-Montreal, band-6 image in Figure 10 with one density slice replaced by a density slice of band-5 image in Figure 8.

Paper I 7

A TECHNIQUE FOR CORRECTING ERTS DATA FOR SOLAR AND ATMOSPHERIC EFFECTS

Robert H. Rogers, Keith Peacock, and Navinchandra J. Shah, *Bendix Aerospace Systems Division, Ann Arbor, Michigan*

ABSTRACT

A technique is described by which ERTS investigators can obtain and utilize solar and atmospheric parameters to transform spacecraft radiance measurements to absolute target reflectance signatures. A radiant power measuring instrument (RPMI) and its use in determining atmospheric paramaters needed for ground truth are discussed. The procedures used and results achieved in processing ERTS CCTs to correct for atmospheric parameters to obtain imagery are reviewed. Examples are given which demonstrate the nature and magnitude of atmospheric effects on computer classification programs.

INTRODUCTION

The need for target reflectance signatures evolves from the needs of individual Principal Investigators, NASA's requirements to correlate results of a large number of investigators, and the pre-conditions of wide-area extrapolations of ground truth data for automatic data processing techniques. Target reflectance data are needed by all man and machine systems to obtain the unambiguous interpretation of ERTS data. In response to the need for absolute target reflectance signatures, this Experiment MMC 655 is evaluating the capabilities of a wide range of techniques for determining and removing solar and atmospheric parameters and effects from ERTS data. Techniques being evaluated include (1) transferring known ground reflectance to spacecraft measurements, (2) using the ground-based Radiant Power Measuring Instrument (RPMI) to measure, directly, the needed solar and atmospheric parameters, (3) using spacecraft data alone (with little or no auxiliary inputs), and (4) using radiation transfer models employing inputs such as surface pressure, ground visibility, temperature, and relative humidity. This paper evaluates the RPMI technique.

ATMOSPHERIC PARAMETERS

The desired reflectance information is difficult to obtain directly from the ERTS sensor radiance measurements because these measurements are a function of unknown solar and atmospheric parameters caused by the intervening atmosphere, and these parameters vary significantly. The radiance, L, sensed by the spacecraft sensor from a given target, depends not only upon the reflectance, ρ, of the target, but also upon the target irradiance, H, and upon the spectral absorption and scattering of the atmosphere between the target and the spacecraft. This atmosphere attenuates the radiance reflected from the target to the spacecraft and adds to the foreground radiance by backscatter of sunlight from the atmosphere, L_A. The composite radiance, L, recorded within an ERTS band for a spacecraft looking vertically is, therefore, related to the desired target reflectance, ρ, and to the solar and atmospheric parameters; H, τ, and L_A; by:

$$L = \frac{\rho}{\pi} H \tau + L_A \tag{1}$$

where τ is the beam transmittance for one air mass.

The target irradiance, H, has two components; one caused by the direct sun, denoted $H_{SUN} \cos Z$ (in which H_{SUN} is the irradiance on a surface normal to the sun's rays and Z is the solar zenith angle) and a component caused by the sky, denoted H_{SKY}. Expanding H of Equation 1 in terms of the direct sun and sky components and solving the equation for ρ results in

$$\rho = \frac{(L - L_A) \cdot \pi}{\tau \; (H_{SUN} \cos Z + H_{SKY})} \tag{2}$$

For a remote sensing system looking vertically downward, τ is the atmospheric transmission of one air mass. If m is the number of air masses referenced to the zenith air mass (for which m = 1), the atmospheric transmission through some other value of m is given by τ^m. The direct sun component of target irradiance, H_{SUN}, in Equation 2 can be subdivided as

$$H_{SUN} = H_o \, \tau^m, \tag{3}$$

in terms of the solar irradiance normal to the sun's rays outside the atmosphere, H_o. Combining Equations 2 and 3, the desired target reflectance, ρ, in terms of ERTS radiance, L, measurements is

$$\rho = \frac{(L - L_A) \cdot \pi}{\tau \; (H_o \, \tau^m \cos Z + H_{SKY})}, \tag{4}$$

where L_A, τ, H_o, m, cos Z, and H_{SKY} are the solar and atmospheric parameters that must be known to accurately compute target reflectance.

Parameters Readily Determined

In the machine processing of ERTS computer compatible tapes (CCTs), the parameters L, H_o, m, and Z of Equation 4 are easily and quickly determined. Target counts, c_i, recorded on ERTS CCTs are transformed to the target radiance, L of Equation 4 by

$$L_i = c_i \, K_i \;\; mw/cm^2 - sr, \tag{5}$$

where i indicates MSS band number and constants K_i are determined as described on Page 6-14 of the ERTS Data User Handbook (K_4 = 0.0195, K_5 = 0.0157, K_6 = 0.0138, K_7 = 0.0730). The sun zenith angle, Z, is computed from Z = 90 - θ_E, in which the sun elevation angle, θ_E, is also extracted from the ERTS CCT. For sun zenith angles less than 60 degrees, the air mass, m of Equation 4, is given to an accuracy better than 0.25% by m = sec Z. For larger sun angles, a more accurate value is given by Bemporad's formula

$$M = \sec Z - 0.001867 \, (\sec Z - 1) - 0.002875 \, (\sec Z - 1)^2 - 0.0008083 \, (\sec Z - 1)^3. \tag{6}$$

The solar irradiance, H_o, outside the earth's atmosphere is well known and changes less than 6% over a 12-month period. H_o can be determined from NASA-published data (Thekaekara, 1971) or derived from RPMI measurements. Values obtained from RPMI and Dr. Thekaekara's published data for a mean earth-sun distance of 1 astronomical unit (AU), are shown in Table 1.*

If desired, the values specified (for 1 AU) can be corrected for the precise earth-sun distance at the time of ERTS overflight by factors also given in Dr. Thekaekara's report.

The remaining solar and atmospheric parameters needed for Equation 4; L_A, τ, and H_{SKY}; depend on the specific atmosphere within the scene and must be determined by the Principal Investigator at the time of ERTS overflight.

---

*Please refer to back of report for tables, figures, and references.

RADIANT POWER MEASURING INSTRUMENT (RPMI)

One technique for obtaining the remaining atmospheric parameters is to deploy the RPMI shown in Figure 1. This instrument was developed specifically to provide an ERTS investigator with the capability of obtaining the complete set of solar and atmospheric measurements.

The RPMI is a rugged, hand-carried, portable instrument, calibrated to measure both down-welling and reflected radiation within each ERTS MSS band. A foldover handle permits a quick change from wide-angle global or sky irradiance measurements to narrow angle (7.0° circular) radiance measurements from sky and ground targets.

The RPMI's wide dynamic range (1 to 10^6) is tailored to permit measurements to be made over the full range of atmospheric parameters encountered by ERTS. These extremes have been found to include direct beam solar irradiance up to 25 mw/cm^2 in Band 7, sky radiance as low as 0.077 mw/cm^2 - sr in Band 6, and radiance reflected from water surfaces in Bands 6 and 7 as low as 0.02 mw/cm^2 - sr. The RPMI measurements are traceable to an NBS source to an accuracy of 5% absolute and 2% relative from band-to-band. The RPMI calibration is also checked, from time to time, against the NASA Goddard calibration source to ensure uniformity between RPMI and ERTS MSS measurements.

DETERMINATION OF ATMOSPHERIC PARAMETERS

The RPMI is deployed in concert with ERTS overflights to obtain direct measurements, within the four ERTS MSS bands, of (1) global irradiance, H, (2) sky irradiance H_{SKY}, (3) radiance from a narrow solid angle of sky, L_{MEAS} (ϕ), and (4) direct beam-solar irradiance $H_{SUN}(m)$. From these measurements, additional solar and atmospheric parameters, such as beam transmittance, τ; path radiance, L_A; and direct beam-solar irradiance above the atmosphere, H_o, are determined. With these parameters, Equation 4 is applied to transform the ERTS radiance measurements, L, into absolute target reflectance units.

DIRECT BEAM SOLAR IRRADIANCE (H_{SUN})

Direct beam solar irradiance, H_{SUN}, is measured, as shown in Figure 1C, by pointing the instrument directly at the sun with the telescope in place and recording the irradiance at each wavelength.

GLOBAL AND SKY IRRADIANCE

Global irradiance, H, is measured directly in each band as shown in Figure 1B. Additional accuracy in H can be obtained using H_{SUN} (m) and sky irradiance, H_{SKY}, by shadowing the sun and reading global minus direct beam-solar irradiance, and then computing the total target irradiance, using

$$H = H_{SUN} \cos Z + H_{SKY} \tag{7}$$

The sun angle, Z, may be read from the sun dial on the side of the RPMI after leveling the instrument with its bubble level.

BEAM TRANSMITTANCE (τ)

Beam transmittance, τ, per unit air mass is determined directly from

$$\tau = \left(\frac{H_{SUN}}{H_o}\right)^{\frac{1}{m}} \tag{8}$$

when the solar irradiance outside the atmosphere, H_o, is known, as in Table 1. The air mass is calculated from the solar zenith angle, using Equation 6.

If solar irradiance outside the atmosphere, H_o, is not known, τ per unit air mass can be determined by making at least two H_{SUN} measurements, denoted $H_{SUN}(m_1)$ and $H_{SUN}(m_2)$, at air masses m_1 and m_2 and computing

$$\tau = \left(\frac{H_{SUN}(m_1)}{H_{SUN}(m_2)}\right)^{\frac{1}{m_1 - m_2}} \tag{9}$$

If a series of $H_{SUN}(m)$ measurements are made and then plotted on a log scale as a function of air mass, an atmospheric extinction curve similar to that shown in Figure 2 results. By performing a least squares curve fit to the H_{SUN} measurements, greater accuracy in the H_{SUN} values needed for Equation 9 may be derived.

The intercepts of the H_{SUN} lines of Figure 2 with the vertical axis (i.e., m = 0) yields H_o in each ERTS band. These values of H_o can be used in succeeding computations of τ by Equation 8 and as calibration constants to test and recalibrate the RPMI, if necessary, using the sun as a source, at any location in the world.

Beam transmittance, τ, derived from 10 sets of field measurements covering the period January through June of 1973 (Table 2) shows this parameter to range from 70 to 85% in Band 4, from 77 to 90% in Band 5, from 81 to 94% in Band 6, and from 84 to 97% in Band 7.

PATH RADIANCE

The only remaining atmospheric parameter needed to transform ERTS radiance into reflectance is the radiance, L_A, reaching the spacecraft from Rayleigh and aerosol scattering by the atmosphere. As path radiance cannot be measured directly, it must be derived from ground-based sky radiance measurements of the backscatter. The simplest technique is to use the RPMI to measure the sky radiance, L_{MEAS} (ϕ), scattered at angle ϕ, as shown in Figure 3, such that ϕ is identical to ϕ, the angle through which radiation is scattered to the spacecraft, and then to correct this measurement for the difference in air masses between the direction of observation and the direction of the spacecraft. This technique provides a straightforward measurement procedure when $Z > 45°$. When L_{MEAS} is recorded at an angle equal to the scattering angle to the ERTS, the path radiance, L_A, seen by ERTS is

$$L_A = L_{MEAS} \left(\frac{1 - \tau}{1 - \tau^{m_o}} \right), \tag{10}$$

in which m_o is the air mass in the direction of observation (in this case $m_o = \frac{1}{\cos \beta}$) and τ, as previously defined, is the atmospheric transmission per unit air mass. The validity of this formula has been demonstrated by Rogers and Peacock (April 1973) and discussed by Gorden, Harris, and Duntley (1973). Equation 10 is adequate when the atmospheric measurements are made concurrent with the ERTS overflight; (i.e., at a sun angle close to the one at the time of the ERTS flyover).

However, if $Z < 45°$, it is easy to see that $\beta > 90°$ and a simple determination of L_A is not possible. During the summer months, this is frequently the condition at the time of the ERTS overpass. It becomes necessary to make the sky radiance measurements at a time when $Z > 45°$ and to correct for the greater attenuation of the incident sunlight.

A correction factor, T_{ERTS}/T_Z, must be multiplied by Equation 10 to derive the path radiance, L_A, viewed by the spacecraft if the time between the ERTS overpass of the test site and the time of the sky radiance observations is significantly different. An approach for determining this correction factor was reported by Rogers and Peacock (October 1973) and is shown in Figure 3.

Sunlight entering the atmosphere at an angle Z, as shown in Figure 3, is scattered at altitude h in the direction of the observer at point 0. The energy available for scattering depends on the atmospheric extinction coefficient, $\tau_{\infty h}$, measured from outside the atmosphere to altitude h. The attenuation is given by $\exp(-\tau_{\infty h} \cdot m)$. The energy scattered is a function of the scattering coefficient, α_h, at altitude h. Thus, the energy scattered in the direction of the observer from altitude h is proportional to

$$\exp(-\tau_{h\infty} \cdot m) \cdot \alpha_h. \tag{11}$$

The average attenuation, for all altitudes, before the energy is scattered to the observer is given by

$$T = \frac{\sum_N \exp(-\tau_{h\infty,} \cdot m) \cdot \alpha_h}{N \sum_N \alpha_h}, \tag{12}$$

in which N defines each atmospheric altitude used in the summation. Use of the value α_h in the equation expresses the importance of each altitude, h, in contributing energy at the observer location point, 0. A normalizing factor is included in the denominator. Values of $\tau_{h\infty}$ and α_h have been tabulated (Valley, 1965). To adjust $\tau_{\infty h}$ from a standard atmosphere to the actual atmospheric conditions at the observer's location, $\tau_{\infty h}$ is multiplied by $\exp(-\tau_{\infty o})/\tau$, in which τ is the measured atmospheric transmission and $\tau_{\infty o}$ is the extinction coefficient for a beam traversing one atmospheric air mass of a standard atmosphere. This is also given by Valley (1965). Variations in T are small, so the error in using a corrected standard rather than a real atmosphere is small.

Thus, a complete formula which gives the sky radiance, L_A, at the time of the ERTS overpass from L_{MEAS} made at another solar zenith angle and air mass is:

$$L_A = L_{MEAS}(\phi) \left[\frac{1 - \tau}{1 - \tau^{m_o}}\right] \frac{T_{ERTS}}{T_Z}, \tag{13}$$

in which ϕ, the scattering angle to the observer, equals the scattering angle to ERTS, and T_{ERTS} and T_Z are given by Equation 12 for the zenith angles at the time of the ERTS overpass and the time of the L_{MEAS} readings.

The validity of this equation is demonstrated in Figures 4 and 5. Figure 4 shows ground-based sky radiance measurements as a function of the scattering angle for a range of solar air masses. Each of the curves was obtained by pointing the RPMI at the sun and then sweeping it in azimuth and in elevation, taking sky radiance readings at 10° intervals. Alongside each curve, the solar air mass at the time of the observations is given. The curve defined by the open squares, which falls steeply, is for a range of solar air masses, and was produced by recording the zenith sky radiance over a period of several hours. Application of Equation 13 to these data in Figure 4, assuming $T_{ERTS} = 1$, gives the results shown in Figure 5. Except for about ± 5% of scatter, all the points now follow the same line. By selecting L_A from the curve at the scattering angle which exists at the time of ERTS overpass and multiplying this value by T_{ERTS}, the desired value of L_A at the time of the ERTS overpass is determined.

For March, the path radiance was found to be equivalent to that produced by a target having a reflectance of 11% in Band 4, 5% in Band 5, 3% in Band 6, and 1% in Band 7. This radiance error, which varies as shown in Figure 5, is a function of scattering angle (sun angle), to some degree beam transmittance, and average surface reflectance.

GENERATION OF IMAGERY AND DATA CORRECTED FOR ATMOSPHERE

Different approaches for deriving target reflectance from ERTS data are being investigated. The approach that leads to the most accurate reflectance values is the application of Equation 4 and the full set of solar and atmospheric parameters (L_A, H_o, τ, and H_{SKY}). The 27 March 1973 ERTS tape was processed in this manner to produce the color-coded imagery and gray-scaled computer printout of a portion of the ERTS scene shown in Figures 6 and 7. In this case, the color on the TV monitor and the symbol on the computer print-out is directly related to target reflectance. The scenes shown are those of Orchard Lake. The lake is approximately 4.8 km (three miles) on a side and the scene is approximately 9.7 km (six miles) on a side.

To obtain average reflectance and other statistical information (i.e., average counts, average radiance, standard deviations, etc.) on specific target areas, such as the deep water in Orchard Lake, etc., the gray-scale printout is used as a map to establish the coordinates of the target, using scan-line count and resolution element numbers. These coordinates, input to the computer, define data areas (edits) where the desired statistical computations are performed. Results of computations of average reflectance on deep water areas of six lakes established lake reflectance to be from 3 to 5.5% in Band 4, 0 to 2.3% in Band 5, 0 to 0.5% in Band 6, and 0 to 0.37% in Band 7. Spot reflectance measurements on the same lakes with the RPMI showed similar results.

EFFECTS OF ATMOSPHERE ON COMPUTER CLASSIFICATION TECHNIQUES

The ability of computer techniques to classify targets under various atmospheric conditions was studied. Training sets were defined for the eight land use categories shown in the tabulation of Figure 8 for 14 April 1973 ERTS tape acquired over Oakland County, Michigan. Data within the training areas were then used to generate a set of canonical coefficients (R. Dye 1970), one set for each land use category. In the target classification mode, these coefficients were used to form a linear combination of the ERTS measurement to produce a "canonical variable" whose amplitude is associated with the probability of an ERTS measurement being sought. The probability of each land use category being present within each ERTS element of the Oakland County scene is determined and a classified land use map is generated.

To determine how the atmosphere affected these classifications, the canonical coefficients generated from the April tape were first applied to classify the data from the known training areas also contained within this tape. This classification performance, recorded in the tabulation of Figure 8, then served as the basis from which to evaluate performance achieved when the same coefficients are used to process ERTS measurements on the identical targets observed under other atmospheric conditions. To accomplish this, the April observations from the training areas were modified to replace April atmospheric parameters with parameters derived from RPMI measurements for February, March, and May. These parameters are listed in Table 3. Also, the April atmospheric parameters were modified by incremental amounts to generate parametric curves of Figures 8A and 8B.

Figures 8A through 8E show the results of applying the processing coefficient derived for the 14 April atmosphere, denoted A_3, to ERTS measurements acquired under other atmospheric conditions. Figure 8A shows how the classification performance degrades as the ratio of the April $H\tau$ to the new condition $H\tau$ increases when L_A is held constant. This is a parametric curve generated by modifying the April $H\tau$'s in each ERTS band by an equal amount. Figure 8B, also a parametric curve, shows the effect of increasing the differences between April path radiance values and new condition values, while holding $H\tau$ unchanged.

In Figure 8C and 8D, the February, March, April, and May atmospheres; denoted A_1, A_2, A_3, and A_4, respectively in Table 3; are used to evaluate the classification performance. In Figure 8C, as in Figure 8A, only $H\tau$ is permitted to vary but, in this case, the April $H\tau$'s are modified by the $H\tau$'s measured in February, March, and May. In Figure 8D, the effects of deviating the April path radiance by amounts equal to the difference in radiance between April and the other dates is shown.

Figure 8E shows classification accuracy achieved when April training (canonical coefficients) is used to process February, March, April, and May scenes in which the full atmospheres of those conditions prevail.

In Figure 8A through 8E, it is significant to note that the classification performance on some target categories (i. e., bare soil, tended grass, etc.) hold up even under the most severe atmospheres encountered, while the performance on other targets (trees, urban, untended grass, and deep water) degrades rapidly when atmospheric conditions change by the smallest amount from the reference condition (i. e., the condition in which the processing coefficients are generated).

Figure 9 shows the classified data of the April scene with February, March, April, and May atmospheres.

A set of canonical coefficients and target means derived from training areas within one ERTS scene, as shown, cannot be applied to process data from another ERTS scene with any degree of confidence unless the atmospheres within the two scenes are known to be essentially the same. N. J. Shah (1973) has established that the atmospheric parameters for both scenes can be used to modify the canonical coefficients and target means generated from one scene to process the data from the second scene.

Let H_1, τ_1, and L_{A1} be the atmospheric parameters applicable for an ERTS scene containing atmosphere I, for which training sets were previously selected and from which a canonical coefficients matrix C_1 and target means matrix X_1 were generated. Let H_2, τ_2, and L_{A2} be the atmospheric parameters for an ERTS scene with atmosphere II, in which additional processing is desired. The new canonical coefficient matrix, C_2, for processing scene 2, is computed from the matrix C_1 by

$$C_2 = C_1\left(\frac{H_2\tau_2}{H_1\tau_1}\right) \tag{14}$$

The new target means, denoted X_2 for scene 2, are related to means X_1 for scene 1 by

$$X_2 = X_1\left(\frac{H_2\tau_2}{H_1\tau_1}\right) + L_{A2} - L_{A1}\left(\frac{H_2\tau_2}{H_1\tau_1}\right) \tag{15}$$

To illustrate the application of Equation 14 and 15, training and processing coefficients generated for the April scene together with the April and March atmosphere parameters were used to generate the new canonical coefficients and means needed to process the March tape. The results of this processing are shown in Figure 10A, an accurate classification of the original scene. Figure 10B shows the results of processing the same March tape, but using the April training and

coefficients without corrections for atmosphere. In this case, some lakes have been completely misclassified.

SUMMARY

Feasibility of the techniques for obtaining and using atmosphere parameters to transform spacecraft data into absolute target reflectance characterisitcs has been established. The RPMI's wide dynamic range (1×10^6) was found to be essential for obtaining the full set of measurments needed to derive atmospheric parameters.

The field measurements from January through June of 1973 determined the magnitude and range of variations in the beam transmittance, τ, and path radiance, L_A, within the ERTS bands. By generating coefficients needed to develop a land use map and, then, applying these coefficients to process ERTS scenes with new atmospheric conditions, the manner in which the atmospheric variations degrade classification performance was established. A simple technique for correcting these processing coefficients for atmospheric variations was shown.

REFERENCES

S. Q. Duntley, J. I. Gordon, and J. L. Harris; Applied Optics; June 1973; "Measuring Earth-to-Space Contrast Transmittance from Ground Stations"; pgs 1317-1324.

ERTS Data User Handbook; NASA Document 71SD4249; Revised Sept 1972; pg G-14.

R. H. Rogers and K. Peacock; "Investigation of Techniques for Correcting ERTS Data for Solar and Atmospheric Effects"; NASA-CR-131258, E73-10458; April 1973.

M. P. Thekaekara et al.; NASA Document SP-8005; Revised May 1971.

S. L. Valley, Editor; Handbook of Geophysics and Space Environments; AFCRL; 1965; pgs 7-14 to 7-35.

R. Rogers and K. Peacock; "Machine Processing of ERTS and Ground Truth Data"; Proceedings of Purdue LARS Conference on Machine Processing of Remotely Sensed Data; IEEE Catalog No. 73 CHO 834-26E; pgs 4a-14; Oct 1973.

R. H. Dye and D. S. Hanson; "Spectral Signature Recognition"; Bendix Technical Journal, Vol 3, No. 2, Summer/Autumn 1970.

N. J. Shah; "Using Reflectance in Producing Decision Imagery"; Bendix Memo 73-158-R and 0-635, 30 July 1973.

Table 1. Solar Irradiance Outside Atmosphere, H_o (1AU)

MSS Band	RPMI mW/cm^2	Thekaekara mW/cm^2
4	18.65	17.7
5	15.11	15.15
6	12.33	12.37
7	25.17	24.88

Table 2. Beam Transmittance, τ

MSS Band	Average	Minimum	Maximum	Standard Deviation
4	0.799	0.697	0.856	0.051
5	0.852	0.770	0.901	0.048
6	0.885	0.812	0.940	0.051
7	0.899	0.843	0.975	0.052

Table 3. Atmospheric Parameters

Atmosphere	Date	Air Mass, M	Beam Transmittance, τ				Path Radiance L_A mw/cm^2-sr			
			4	5	6	7	4	5	6	7
A1	9 Feb 1973	2.5	0.856	0.901	0.940	0.975	0.27	0.146	0.093	0.1185
A2	27 Mar 1973	1.49	0.796	0.854	0.884	0.888	0.268	0.127	0.081	0.103
A3	14 Apr 1973	1.33	0.74	0.815	0.875	0.889	0.26	0.165	0.108	0.059
A4	21 May 1973	1.18	0.697	0.770	0.812	0.843	0.4	0.189	0.121	0.154

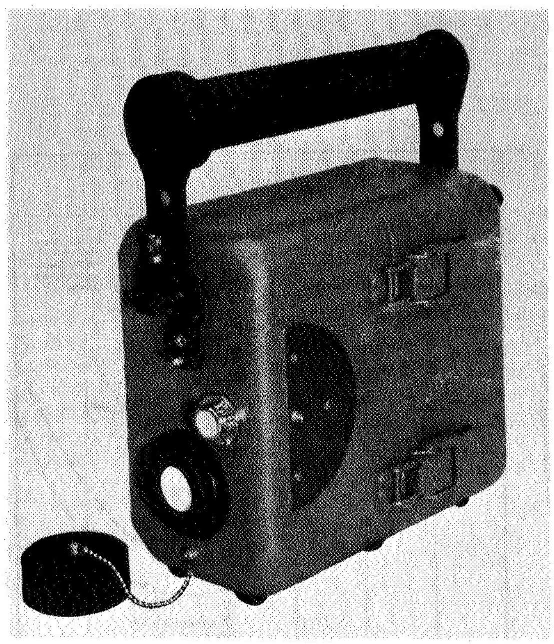

A. RPMI assembled.

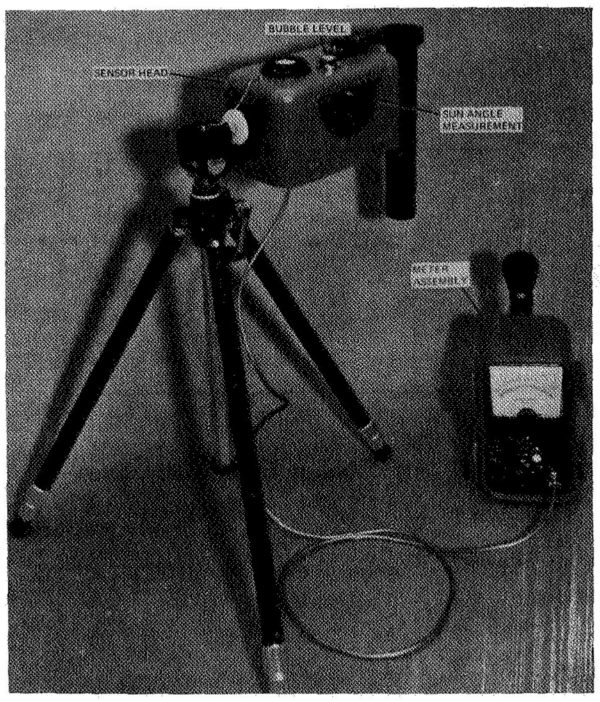

B. Global Irradiance (H) – 2π steradian field of view for measuring downwelling (incident) radiation ERTS MSS bands. Bubble level aids this measurement.

Sky Irradiance (H_{SKY}) – Block sun to measure global irradiance minus direct sun component, in every ERTS MSS band. Angle from zenith to sun is also measured in this mode by reading sun's shadow cast on sun dial.

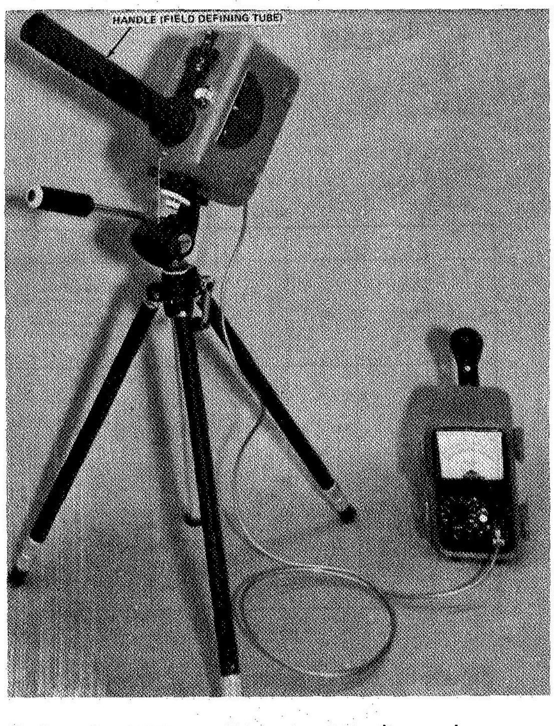

C. Radiance from Narrow Solid Angles of Sky (L_{MEAS}) – Handle serving as field stop permits direct measurements through a 7.0° circular field of view. This mode is also used to measure direct beam solar irradiance, H_{SUN}.

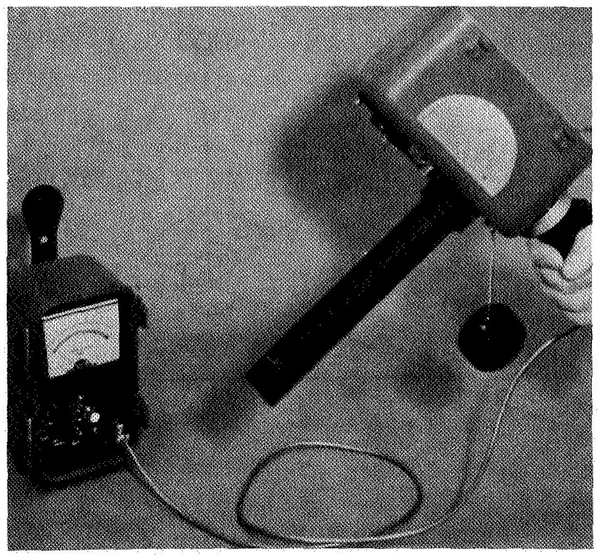

D. Reflected Radiation – Used with small calibration panels and cards to obtain direct measurement of truth site reflectance. Reflectance also immediately derived from ratio of reflected radiance and global irradiance.

Figure 1. Radiant Power Measuring Instrument

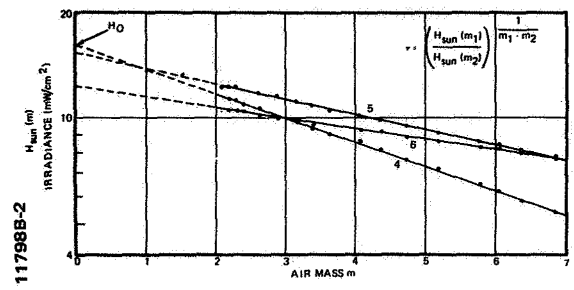

Figure 2. Atmospheric Extinction Curves

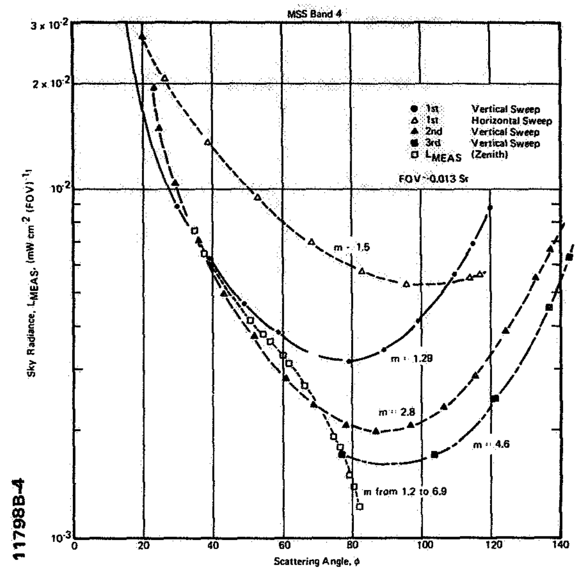

Figure 4. RPMI Sky Radiance Measurements, L_{MEAS}

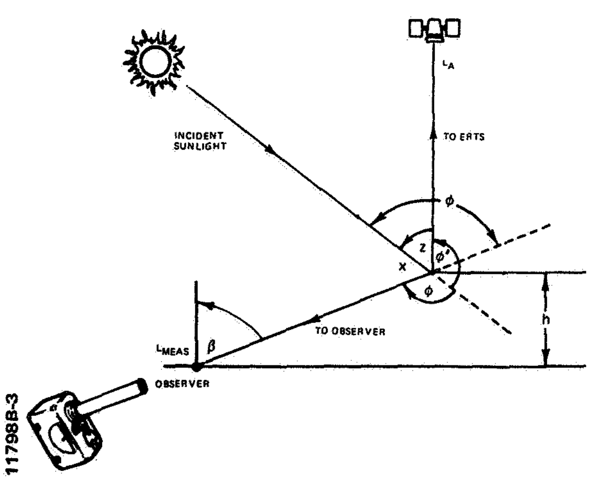

Figure 3. Sky Radiance, L_{MEAS}

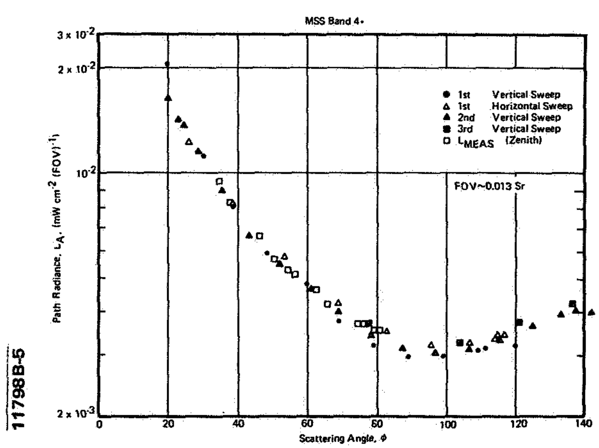

Figure 5. Path Radiance, L_A, from Sky Radiance, L_{MEAS}

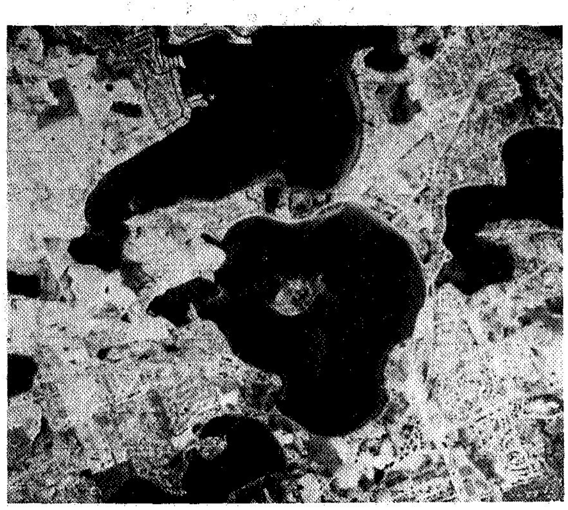

Aerial Photograph

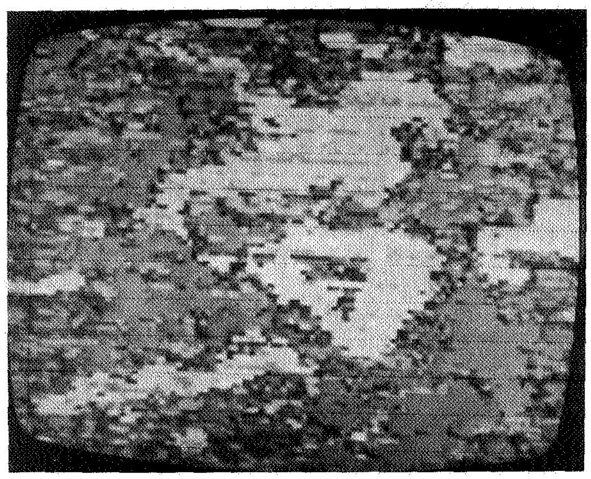

ERTS Band 4 Display

Figure 6. Comparison of Aerial Photograph and Color-Coded TV Reflectance Display

Character	Reflectance Range
	0.000 - 0.006
•	0.010 - 0.014
/	0.018 - 0.027
C	0.031 - 0.035
O	0.039 - 0.047
Q	0.051 - 0.055
@	0.059 - 0.067
Θ	0.071 - 0.075
B	0.079 - 0.087
Ø	0.091 - 0.095
●	0.099 - 0.100

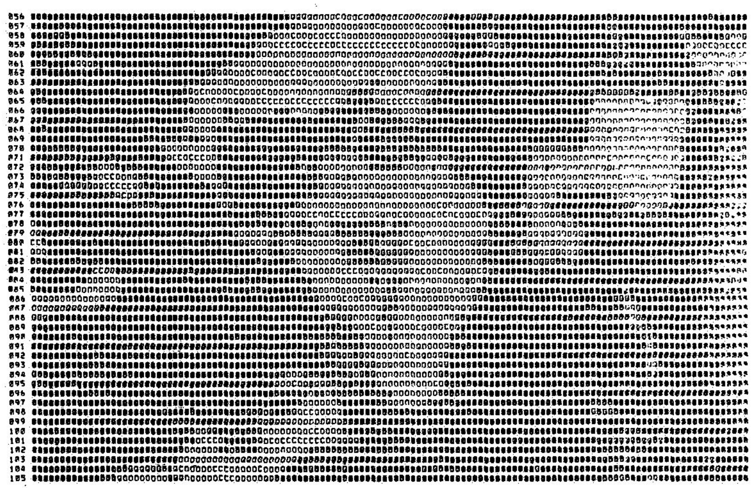

Reflectance Grav Scale Printout
(Band 4)

Figure 7. Reflectance Gray-Scale Printout

11798B-8

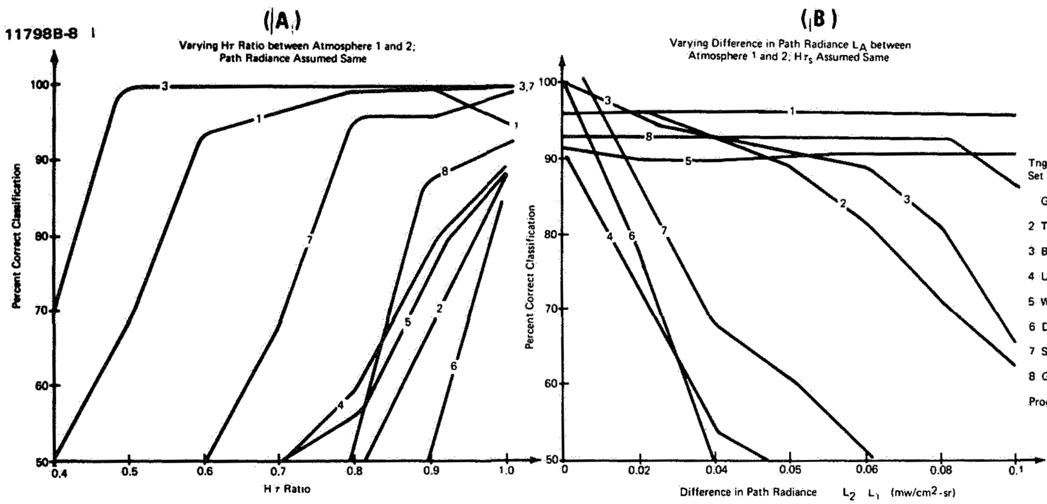

Classification Accuracy Table Results Achieved Under 14 April Atmosphere Denoted A3

Tng Set	Percent Classified as Group	2	3	4	5	6	7	8
Grass (tended)	96.552	0.000	0.000	0.000	0.000	0.000	0.000	3.448
2 Trees	0.000	96.552	0.000	0.000	3.448	0.000	0.000	0.000
3 Barren earth/concrete	0.000	0.000	100.000	0.000	0.000	0.000	0.000	0.000
4 Urban	0.769	0.000	0.769	90.000	5.385	0.000	0.000	3.077
5 Wetlands	0.000	4.706	0.000	1.176	91.765	0.000	0.000	2.353
6 Deep water	0.000	0.000	0.000	0.000	0.000	98.182	1.818	0.000
7 Shallow water	0.000	0.000	0.000	0.000	0.000	0.000	100.000	0.000
8 Grass (untended)	.562	1.562	0.000	0.000	3.125	0.000	0.000	93.750

Program Run Time : 00:00:36

Results of Applying Training Derived from Atmosphere A3 to Data Acquired under Various Atmospheres

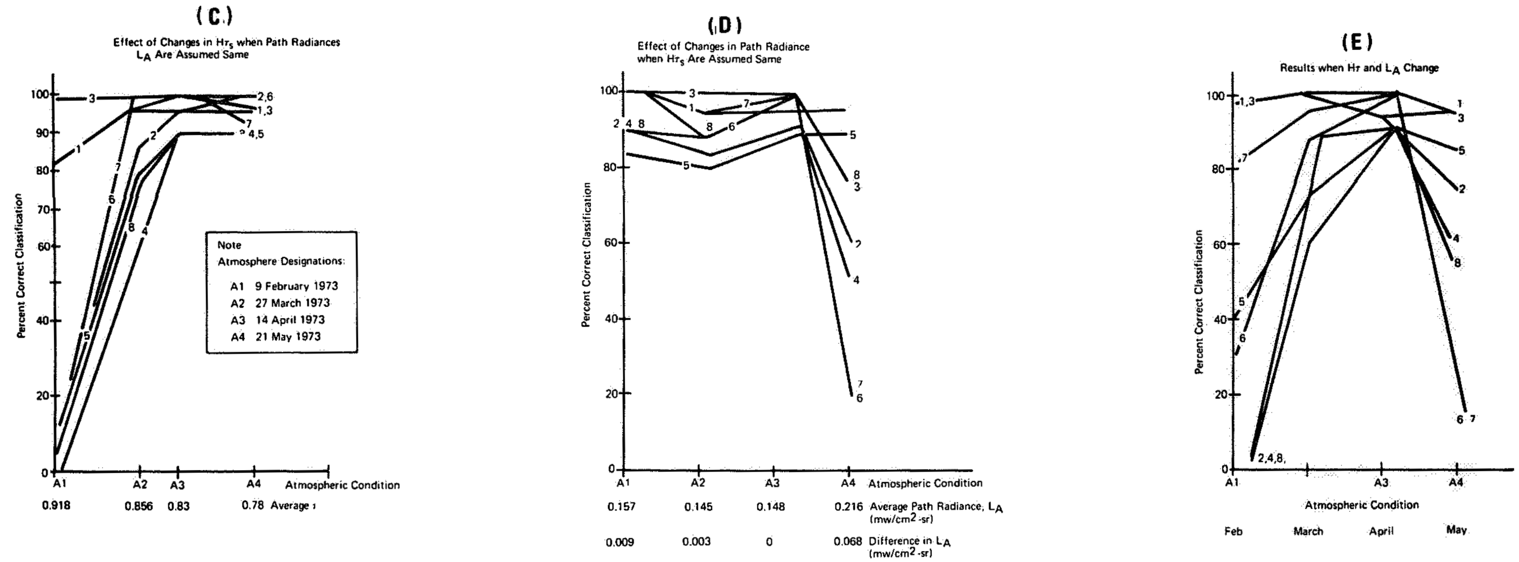

Figure 8. Data Processing Performance under Various Atmospheric Conditions

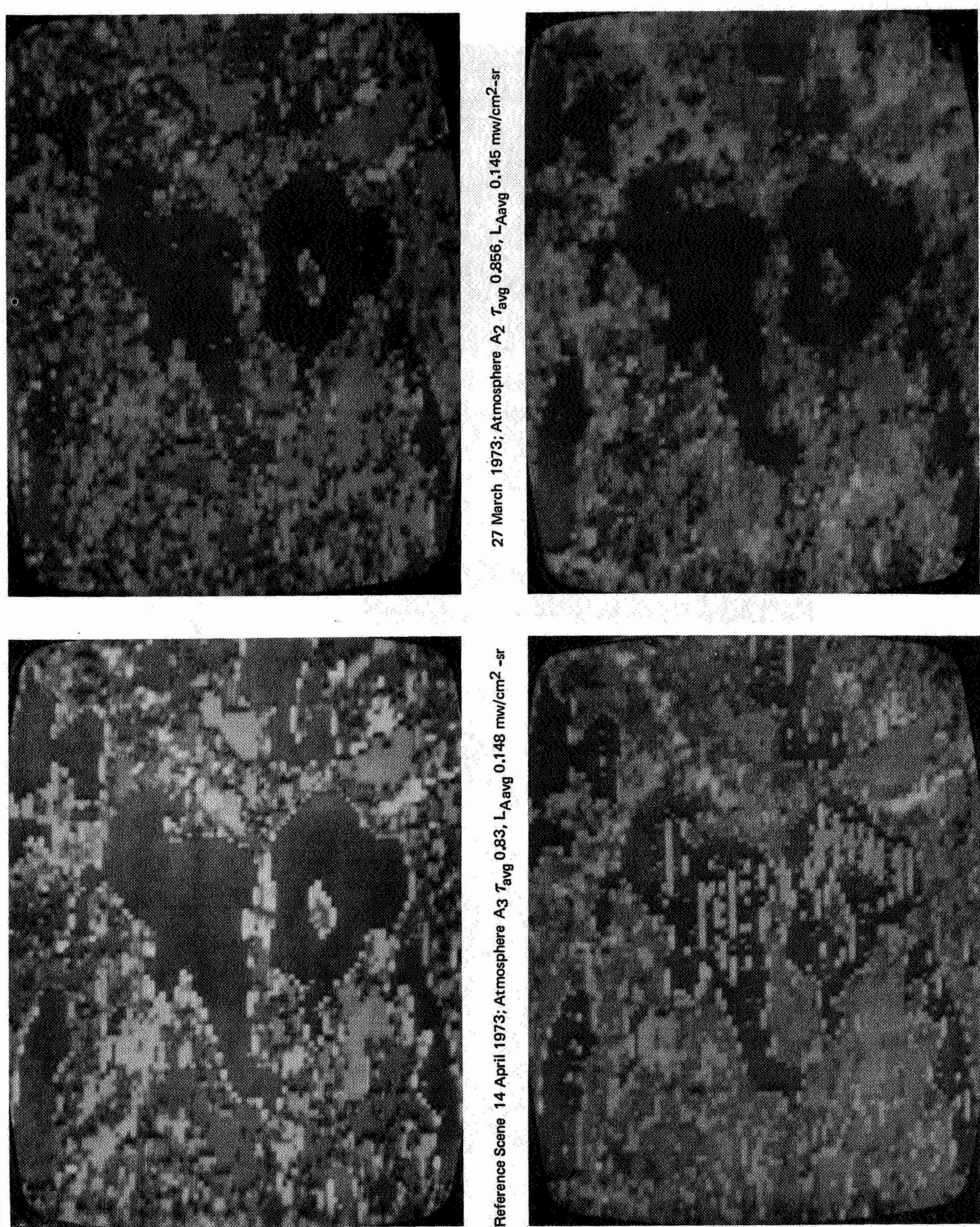

Figure 9. Decision Processed Data Showing Atmospheric Effects on Decision Processing

11798B-10

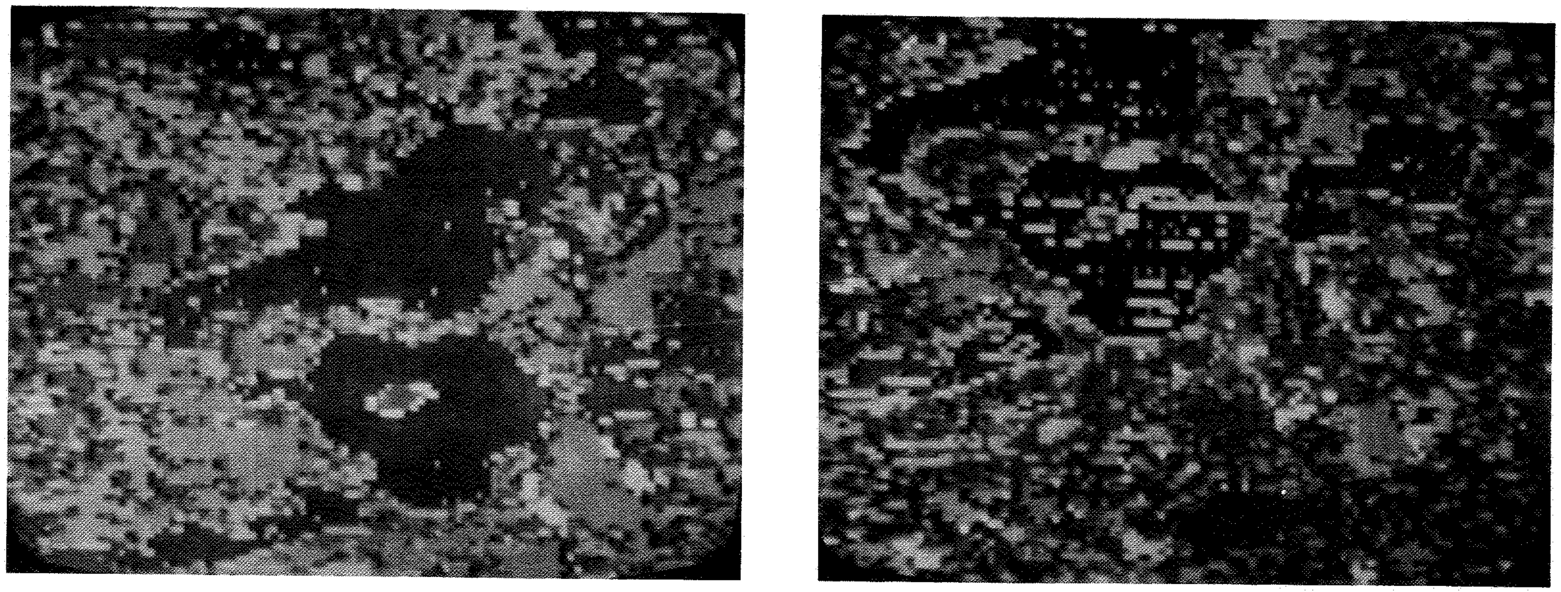

Coefficients Corrected for Atmosphere

Coefficients Not Corrected for Atmosphere

Figure 10. March Scene Classified with April Processing Coefficients

Paper I 8

THE PENN STATE ORSER SYSTEM FOR PROCESSING AND ANALYZING ERTS DATA

G. J. McMurtry, F. Y Borden, H. A. Weeden and G. W. Petersen, *Office for Remote Sensing of Earth Resources (ORSER), The Pennsylvania State University*

ABSTRACT

The Office for Remote Sensing of Earth Resources (ORSER) of the Space Science and Engineering Laboratory (SSEL) at The Pennsylvania State University has developed an extensive operational system for processing and analyzing ERTS-1 and similar multispectral data. The ORSER system was developed for use by a wide variety of researchers working in remote sensing. Both photointerpretive techniques and automatic computer processing methods have been developed and used, separately and in a combined approach. A Remote Job Entry (RJE) system permits use of an IBM 370/165 computer from any compatible remote terminal, including equipment tied in by long-distance telephone connections. Detector errors occuring in two channels of every sixth line of ERTS digital data were examined, and a statistical recalibration method was developed. Errors were eliminated after recalibration. Furthermore, after recalibration of data from two ERTS scenes, classification of a forested area yielded excellent results using spectral signatures developed in another area approximately 150 miles away and from an ERTS scene taken 17 days earlier. Thus, transference of signatures in both time and space appears feasible. Specific results obtained by using this system include a study of land use, discrimination between types of forest resources and vegetation, detection of previously unknown geologic faults and correlation of these with known mineral deposits and ground water, mapping of mine spoils in the anthracite region of eastern Pennsylvania, mapping of strip mines and acid mine drainage in Central Pennsylvania, agricultural land use mapping, and detection of gypsy moth infestation.

THE ORSER SYSTEM

The Office for Remote Sensing of Earth Resources (ORSER) of the Space Science and Engineering Laboratory (SSEL) at The Pennsylvania State University has developed an extensive operational system for processing and analyzing ERTS-1 and similar multispectral data. The ORSER system was developed for use by a wide variety of researchers working in remote sensing. These users represent many disciplines and have a wide range of experience and skill in photointerpretation and computer usage.

Interpretive techniques which are used in the system include computer processing, visual image interpretation, and a hybrid technique which closely integrates photointerpretive techniques with computer analytic procedures.

Computer Processing Facilities

Automatic data processing equipment utilized in the ORSER system is primarily located at The Pennsylvania State University Computation Center. The principal computer is the IBM System 370 Model 165, consisting of a main frame and attached devices for input and on-line storage. Users may have access to the computer in any of three ways: central and remote high speed dispatch points operated by the Computation Center; slow speed Remote Job Entry (RJE) terminals using IBM 2741, Tektronix 4010, or similar remote terminals supported by the user or by the Computation Center; and intermediate speed remote batch terminals, such as the IBM 2780, supported by the user or the Computation Center. The ORSER processing system for MSS data was developed for use with any of these entry points. ORSER investigators use RJE terminals for most developmental work. Bulk output for final runs is directed from an RJE terminal to any of the high speed terminal sites. No program card decks need to be input, as the MSS data processing programs are kept in library files. Files for building control information or for storing output are available to the user. MSS data is input from magnetic tapes which, along with user-owned working tapes, are managed by the Computation Center.

The Digital Data Processing System

A standard digital tape format was designed within which all known MSS sources can conveniently be placed. More than one file per tape is allowed as well as a continuation of a file to another tape. Within the file, four kinds of records exist: (1) identification records, (2) table of contents records, (3) MSS response records, and (4) history records. Each MSS response record consists of a complete scan line. Each scan line is numbered and scan lines are always in ascending order in a file. A working file will usually contain one or more small parts of the whole data set. The table of contents is particularly useful in such cases in avoiding costly searching for data which are not present in the file.

The system is couched in a multivariate framework. Each observation, identifiable by scan line and element number, consists of a vector with as many components as there are channels. At present, each vector is composed of just MSS response values. It is anticipated, however, that the vectors will be augmented by transformed scanner data, or by additional (nonscanner) data such as topographic information.

Although the system is not in a conversational mode, where the user and the system dynamically interact during processing, the preparation of the control specifications by a user operating from an RJE terminal is conversational. Each program accepts input control specifications, processes the MSS data according to the specifications, and outputs the results. For non-RJE operation, control specifications are made and entered into the system by punched cards. All control specifications on the RJE are identical in format to the corresponding punched cards.

The programs discussed here are all operational and are documented at the user's level. Although many other programs are used, those discussed here illustrate the general approach to the processing of MSS tapes. Detailed descriptions of ORSER programs currently available may be found in ORSER/SSEL Technical Report 10-73.

The digital tape processing system for MSS data described here is regularly run for production and has been extended to meet the needs of various related projects. The system was designed to be easily augmented, typified by the addition of a number of supervised and unsupervised analysis and classification algorithms. The general procedure to be employed for a previously unstudied area or type of target will be presented and illustrated here.

The first step is to select the particular targets and areas of interest, primarily using maps. Consultation of the catalogues of imagery and digital tapes will indicate what data are available and their quality. Tapes corresponding to the selected scenes are chosen and the areas of useful data are specified. Subsets are then produced on separate tapes, using the SUBSET program. These subsets are prepared to gain rapid processing and short turn around time. It is likely that this step has already been done in the process of cataloguing and storing ERTS tapes by ORSER, in which case the appropriate library subset tapes would be selected directly.

A run is then made with the NMAP program to show the overall pattern of the data. This program is written to map element brightness, using all channels or any subset of channels. The norm of each multivariate vector is taken as the measure of brightness. The norm is then converted to a percentage of the maximum possible value. This value is translated to the mapping symbol for the percentage range within which it falls. The process is repeated for every element in every scan line in the data blocks specified by the user. Output from the NMAP program consists, then, of a brightness map.

The UMAP program is run next, to map areas of local spectral uniformity. Each element is compared with its near neighbors using the euclidean distance between spectral signatures as the measure of similarity or dissimilarity. If the largest distance is smaller than a value specified by the user, then the symbol for uniformity is assigned to that element. One or more categories of uniformity can be mapped according to distances specified by the user. All elements with distances from their neighbors greater than those specified are mapped as contrasts. The map output shows the pattern of uniformity and contrasts from which the user can designate coordinates for training areas for the targets of interest and determine high contrast boundaries between uniform areas.

Signatures and associated statistics are next obtained by the use of the STATS program, which computes the multivariate statistics for one or more training areas obtained from UMAP or similar output. The user designates a training area by line and element coordinates and the program computes the statistics for all of the data which fall within the boundaries. The mean and standard deviation vectors are found, and

the correlation and variance-covariance matrices are computed as well as the eigenvalues and eigenvectors of these matrices. Frequency histograms for selected channels are also computed.

When most of the targets have been identified by training areas, a classification run is made using the classifier or classifiers deemed most appropriate for the mix of targets under consideration. A variety of supervised classification programs are available, including parametric and non-parametric classifiers with either linear or quadratic discriminant functions. Preprocessing before classification is also possible, using programs for normalization, principal components, canonical analysis, etc. The output of these programs is in the form of a character (or digital) map, with each category of classification represented by a unique symbol.

Digital character maps are useful primarily as working maps for the user in the analysis of MSS data. They are inherently distorted in the length-to-width relationship because of the fixed number of lines and characters per inch of high-speed printer output. The LMAP program, yielding output on the CalComp plotter or the RJE terminals with graphic displays, is intended for the production of distortion-free, finished copy, line maps. There are three main advantages to line maps when compared to character maps: (1) orthographic maps to a selected scale can be made, (2) photographic overlays can be prepared for these maps (this is quite important in the comparison of classification results with corresponding imagery), and (3) legible maps for publication purposes can be prepared.

An example of the use of the programs described above is given in Figures 1 through 8. The MSS data used for this analysis came from ERTS-1 scene 1028-15295, scanned on August 20, 1973. This is an area northeast of Clearfield, Pennsylvania, on which U.S. Route 80 and the West Branch of the Susquehanna River cross. The location of the test site is shown in Figure 1, which was taken from two 7 1/2 minute USGS quadrangle maps. The right hand side of this figure is from a map printed in 1959, before Route 80 was constructed, while the left hand side is from a 1971 map. Figures 2 and 3 show map output for NMAP and UMAP, respectively. The strip of low brightness in Figure 2 follows the river, as does the blank (non-uniform) area shown in Figure 3. Basic statistics for the "stripmine" category, obtained by the STATS program are shown in Figure 4. Statistics for the desired categories, as obtained from a series of sample sites, are input to a classification program. Figure 5 shows the output from the DCLASS program which classifies according to a minimum euclidean distance algorithm. In this case, only two general categories are represented by symbols; unclassified elements are left blank. LMAP output using data from the DCLASS program is shown in Figure 6.

It frequently happens that a sample target is not of sufficient size or area to lend itself to categorization using the STATS program. Such targets may be linear features such as streams, or a series of small scattered features which are not large enough to be represented as uniform areas by UMAP. In such cases, these areas are defined for analysis by an unsupervised classifier which develops its own set of

Figure 1: Test site northeast of Clearfield, Pennsylvania. (Taken from USGS 7 1/2 minute quadrangle maps, "Clearfield" and "Lecontes Mills," both printed in 1971 and 1959, respectively.)

```
BLOCK SPECIFICATIONS
--------------------

   BEGINNING LINE 1030
      ENDING LINE 1059
BEGINNING ELEMENT 2470
   ENDING ELEMENT 2525
   LINE INCREMENT    1
ELEMENT INCREMENT    1

   2470|2475|2480|2485|2490|2495|2500|2505|2510|2515|2520|2525|
       |    |    |    |    |    |    |    |    |    |    |    |
1030 |XXXXXXXXXXXXX- -XXXX-XXXXXXXXXX--XXXXXXXXXXX----XXXXXXXX|
1031 |XXXXXXX--XXX-X-  XXXXXXXXXXXXXX--XXXXXXXXXX----XXXXXXXXX|
1032 |XXXXXXX--XXXXXX-   -XXXXXXXXXXX---XXXXXXXX-----XXXXXXXXX|
1033 |XXXXXXX----XXXXX---    -XXXXXXXXX  -XXXXXXX-----XXXXXXXX|
1034 |XXXXXXX---XXXXXXX-----   --XXXXXX-  --X----------XX---XX|
1035 |XXXXXXXXXXXXXXX-XXXXX-----    --X----------------X---XXX|
1036 |-X---XXXXXXXXXXXXXXXXXX-------   --------------XX---XXXX|
1037 |X----XXXXXXXXXXXXXXXXXXXXXX-XXX-  ----XXXXXX-XX-X---XX-X|
1038 |X--XXXXX---- --XXXXXXXXXXXXXXX--X-- --XXXXXXXXXX-------X|
1039 |XX---XX--XXXXXX---XXXXXXXXXXXXXXXXXX- ---XXXXXXXXXX----X|
1040 |XXXXXXX-XXXXXX-X-----XXXXXXXXXXXXXXXX- -----XXXXXXX-----|
1041 |XXXXXX--X--XXXXXXX-    ---XXXXXXXXXXX- --XXX---XXXXXXXX-|
1042 |XXXXXX--XXXXXX--XXXX-       ----XXX-   --XXXXXXXXXXXXXX-|
1043 |XXXXXX--XXXXXXXXXXXX-------    -   -------XXXXXXXXXXX-XX|
1044 |XXXXXX- XXX-XXXXXXXXXXX------------------XXXXXXXXXXXXX--|
1045 |XXXXXXX-  -X-XXXXXXXXXXXXXXXXXXX--------XXXXXX-XXXXXXXXX|
1046 |XXXXXXXX-    -XXXXXXXXXXXXXXXXXXX------XXXXXXXX----XXXXX|
1047 |XXXXXXX-XXX--   ------XXXXXXXXXXX--XXXXXXXXXXXXX--------|
1048 |XXXXXX--XXXX--XXXXXX-  -XXXXXXXXX--XXXXXXXXXXXXX----XX--|
1049 |--------XXXXXXXXXXXXXX  XXXXXXXXX-XXXXXXXXXXXXXXXX-XXXXX|
1050 |-------XXXXXXXXXXXXXXX- -XXXXXXXXXXXXXXXXX--------XXXXXX|
1051 |XXXXX----XXXXXXXXXXXXXX- -XXXX-XXXXXXXXXXX----XXXXXXXXXX|
1052 |XXXXX-----XXXXXXXXXXXXX- -X--X--XXXXXXXXX----XXXXXXXXXXX|
1053 |XXX-------XXXXXXXXXXXXX  -XXXX-X-XXXXXX--XXXXXXXXXXXXXXX|
1054 |XXXXX-----XXXXXXXXXXXXX  -XXXXXX-XXXXXXXX-XX-XXXXXXXXXXX|
1055 |XXXXX-----XXX-XXXXXXXXX  -XXXXXX-XXXXXXXX--XXXXXXXXXXXXX|
1056 |XX-XX---XXXXXX-XXXXXXXX- -XXXXXX-XXXXXXXXXXXXXXXXXXXXXXX|
1057 |XXXXXXX-XXXXXXXX-XXXXXXX-  XXX---XXXXXXXX-XXXXXXXXXXXXXX|
1058 |XXXXXXXXXXXXXXXXXXXXXXXXX- -XXX---XXXXXXXX-XXXXXX-----XX|
1059 |XXXXXXXXXXXXXXXXX-XXXXXXXX- -XXXXXXXXXXXXX-XXXXXX-XX-XXX|
       |    |    |    |    |    |    |    |    |    |    |    |
   2470|2475|2480|2485|2490|2495|2500|2505|2510|2515|2520|2525|

CLASS   : 14.0      CLASS - : 20.0      CLASS X : 100.0
```

Figure 2 : Brightness map (NMAP).

```
BLOCK SPECIFICATIONS
--------------------

   BEGINNING LINE 1030
      ENDING LINE 1059
BEGINNING ELEMENT 2470
   ENDING ELEMENT 2525
   · LINE INCREMENT    1
ELEMENT INCREMENT    1

 2470|2475|2480|2485|2490|2495|2500|2505|2510|2515|2520|2525|
     |    |    |    |    |    |    |    |    |    |    |    |
1030 |UUUUUU--UUUUU    UUUUUUUUUUUUUUUUUUUUUUUUUUUUUUUUUUUUUUU|
1031 |UUUUUU-U-UUUUU     -UUUUUUUUUUUUUUUUUUUUUUUUUUUUUUUUUUU-|
1032 |UUUUU--U---UUUU   --   -UUUUUUUUU- UUUUUUUUUUUUUUUUUUU-U|
1033 |UUUUU--UUU-UUUUUUU-  --   -UUUUU U -UUUUUUUUUU-         |
1034 |UU--------UUUUUUUUUU--   U-   ---- UUUUUUUUUUU--UUUUUU-|
1035 |UUU--UUUUUUUUUUUUUUUUUUUUU-- -UU  UUUUUUUUUUU---UUUUUUUU|
1036 |UUUUUUUUUUUUUUUUUUUUUUUUUUUUU-- -- UUUUUUUUU--UUUUUUUUUU|
1037 |UUUU--U       -UUUUUUUUUUUUUUU--  U-UUUUUU---------UUUU|
1038 |--UU-U -      -  UUUUUUUUUUUUUUUU-  ---UUUUUU- ----UUUU|
1039 |UUUUUU - UU-- - -  UUUUUUUUUUUUUUUUU U--UUUUUUU-UU-UUUU|
1040 |UUUUU-  -  UUUU-- U-   --UUUUUUUUUUU UUUUUUUUUUUUU-U---|
1041 |  --- UU-UUUUUUUUU   U-   *  - -UU-  UUUUUUUUUUUUUU--UU|
1042 |-  -- UUUUUU------UU-     -UU --   U -UUU-  U-UUUUUU-UU|
1043 |UUUUU U-UUU------UU--UUUUU--   -U--UUUU--UU  -UUUUUUUUU|
1044 |UUUUU     UUUUUUUUU-UUU-U-U------UUUUUU-UUUU-  -UUUUUU-|
1045 |UUUUUUU  -   -UUUUUUUUUUUU-UUUUUUUUUUU--UUU  ---  -UUUU|
1046 |UUUUU----   U-     --UUUUU-UUUUUUUUUUU-UUU  UUUUUU-- --|
1047 |UUU---U-UUU-U        -  UUUUUUUUUUUUUUU- --  UUUUUUUUUU-U|
1048 |- ----U UUUUUUUUUU-    -UU-UUUUUUUUUUU-  -UUUUUUUUUUUU |
1049 |UUUUUU- UUUUUUUUUUUUU U UUU--U--UUUUUUUUUU--    -U-UU---|
1050 |-  UUU-  U-UUUUUUUUUU- --UUUU--- -UUUUUUUUUUUU-UUUUU-U |
1051 |UU-UUUUU -UUUUUUUUUUUU U UUUUU---U--UUUUUUUU-U-    -- - |
1052 |UUUU-UUU- UUUUUUUUUUUU U UUUUUUU---U--UUUUUUU-UUUU-UUUU|
1053 |UUUUUUUU- UUUUUUUUUUUU U UUUUUUUUUU--UUUUU-UU--UUU-UU--|
1054 |UUUU-UUUU UUUUUU-UUUUU U UUUUUUUUUU--UU-UUU-UUU--UUUUU|
1055 |UUUUUUU---UUUUUUUUUUUU - -UUUUUUUUUUUUUU---UUUU----UUUU|
1056 | U-  --UUUUUUU--UUUUUU-    UUUUUUUUUUUU---UUUUUUUUU--UU|
1057 |UUUUUU--UUUUUUU--UUUUUUU - UUUUUUUUUUUUUUUUUUUUUU------|
1058 |UUUUUU-UUUUUUU- --UUUUUU-  -UUUUUUUUUUUUUUUUUUUUUUUUUUU|
1059 |UUUU-  UUU--UU-  -UUUUUUU----UUUUUUUUUUUUUUUUUUUUU--UUU|
     |    |    |    |    |    |    |    |    |    |    |    |
 2470|2475|2480|2485|2490|2495|2500|2505|2510|2515|2520|2525|

CLASS U : 5.0                         CLASS - : 8.0
CLASS   : 15.0                        CLASS * : 100.0
```

Figure 3: Uniformity map (UMAP).

CHANNELS USED : 1 2 3 4

MEANS AND STANDARD DEVIATIONS FOR GIVEN CHANNELS

29.55	26.86	30.78	13.83
3.29	4.80	5.21	3.79

VARIANCE-COVARIANCE MATRIX

10.82			
14.91	23.09		
0.78	0.23	27.16	
-3.27	-5.68	18.00	14.33

CORRELATION MATRIX FOR GIVEN CHANNELS

1.00			
0.94	1.00		
0.05	0.01	1.00	
-0.26	-0.31	0.91	1.00

EIGENVALUES COMPUTED FROM CORRELATION MATRIX.

EIGENVALUES WITH THEIR ASSOCIATED PERCENTAGES:

2.21	1.70	0.06	0.03
55.4	42.4	1.4	0.8

EIGENVECTORS:

0.5227	-0.4645	-0.7059	-0.1129
0.5416	-0.4368	0.6347	0.3362
-0.3800	-0.6257	0.2327	-0.6402
-0.5376	-0.4493	-0.2115	0.6814

DET.= 0.705D-02

SAMPLE CATEGORY : STRIPMINE

Figure 4: Statistics of sample areas for a category obtained by STATS.

```
BLOCK SPECIFICATIONS
--------------------

   BEGINNING LINE 1030
      ENDING LINE 1059
BEGINNING ELEMENT 2470
   ENDING ELEMENT 2525
   LINE INCREMENT    1
ELEMENT INCREMENT    1
```

```
  2470|2475|2480|2485|2490|2495|2500|2505|2510|2515|2520|2525|
      |    |    |    |    |    |    |    |    |    |    |    |
1030 |-------------   --------- ----- -----  ------  -------  |
1031 |--    -  - ---   --------------------   ----   -------  |
1032 |-  --    - ----     ------------ -----------   ------   |
1033 |- -        -------      ---------   -------     ------  |
1034 |          ----------       ------    ----       MM   MM |
1035 |---     ---- ----------         -    - -       MMMMMMMM |
1036 |       ---------------------     -------- -- MMMMMMMMMMM|
1037 |     --  - --------------------      ------ MMMMMMMMMMMM|
1038 |   --  -       ------- -----------    ------       MMM M|
1039 | ------          --------------------  ------- ---  MMMM|
1040 |  -----     ----    -----------------    ---------  MMMM|
1041 |  ----    --------       ------------    ------- --     |
1042 |          ----------            ---      --------    ---|
1043 | -----  -         ----                    M        -----|
1044 |------  ----------   ---  -             MMMMM   ------  |
1045 | -------  -----------     ---- --  ---- MMMMMM  --------|
1046 |---------     --------     ---- -  --- MM M        -----|
1047 |  ----  ---          ---     -- -  --- M      --  MMM   |
1048 |        ---- ----   -    --  -- -------        -- MMMMMM|
1049 |    M   --------------   ---  -------      -  --  MMMM  |
1050 |       -- ------------   ----   ------  ---       MMM   |
1051 |   MMMM  - -  -  ------  ------    --------             |
1052 |   MMM      -    ------  -------     ------ --          |
1053 |MMMMMM     ----  ------  ----------   -----  -          |
1054 | M MMM    ---     -----  ------------   ---   --        |
1055 | MMMMM      -----------   ------------    - ----        |
1056 | MMMMM    -------------   -------------          -      |
1057 |           ---  --------   ----------- ---              |
1058 |        - ----   --------   -------------------   ------|
1059 |        ------ --  -- ----  ------------------------ ---|
      |    |    |    |    |    |    |    |    |    |    |    |
  2470|2475|2480|2485|2490|2495|2500|2505|2510|2515|2520|2525|

       SYMBOL  M : STRIPMINE       SYMBOL - : VEGETATION
```

Figure 5: Classification map using signatures obtained by STATS.

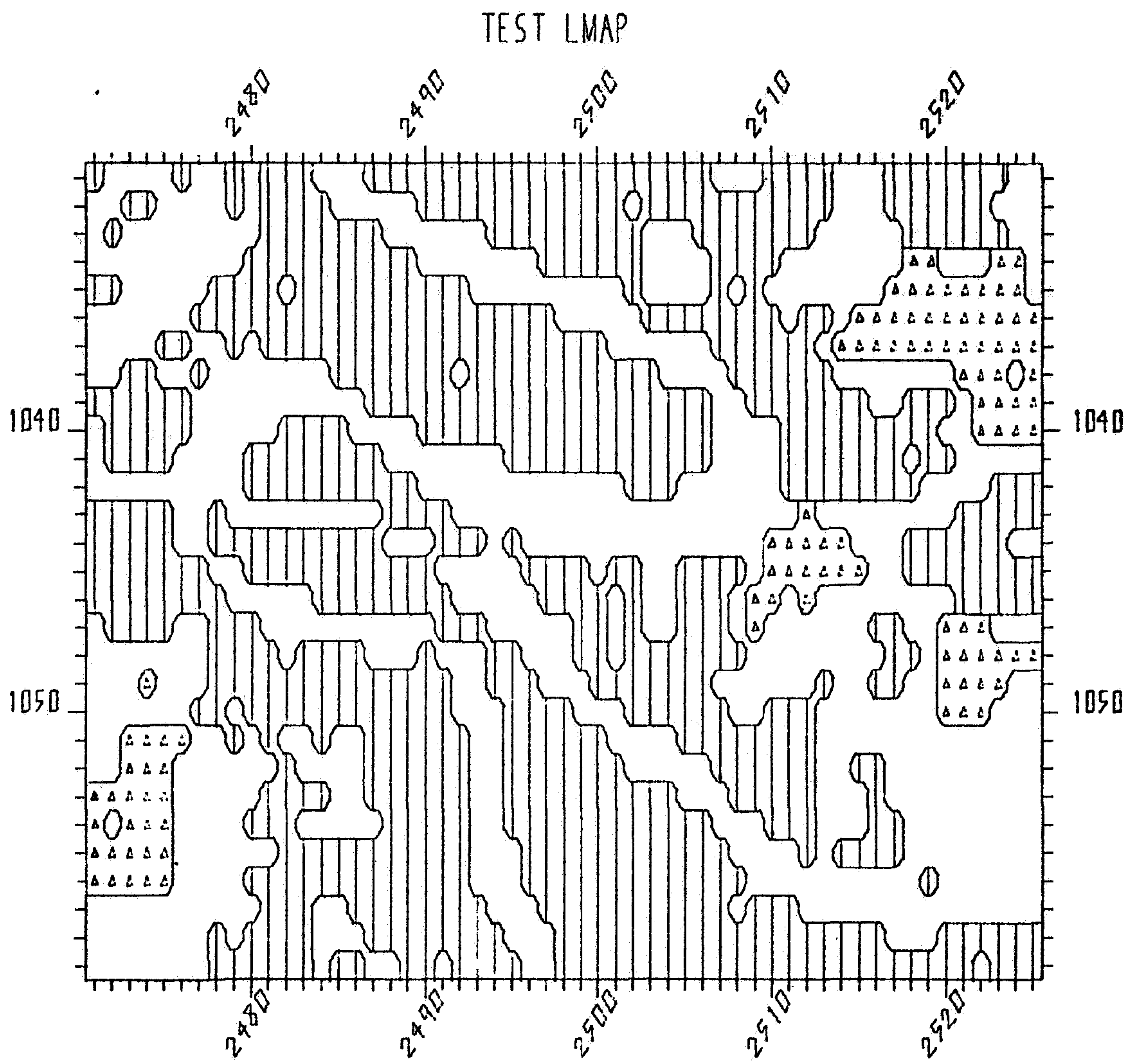

Δ: STRIPMINE
|: VEGETATION
BLANK: Other

Figure 6 : Preliminary classification map of the Clearfield area (LMAP).

spectral signatures and statistics using a clustering algorithm. The map output of one such program, DCLUS, is shown in Figure 7. A comparison of Figure 7, with the DCLASS output of Figure 5 reveals that DCLUS was able to map some features which could not be mapped by DCLASS with STATS signatures. Map output from DCLASS, using signatures from the DCLUS statistics, is shown in Figure 8 in LMAP form.

The approach employed for change detection or where a temporal dimension is involved is similar to the approach for non-temporal analyses in many respects. The major difference is in the establishment of permanent training areas for supervised analysis and classification and permanent analysis areas for unsupervised analysis and classification. These areas must be selected and specified more carefully and with more refinement than when the temporal dimension is not of interest.

HYBRID ANALYSIS

After separate analyses of ERTS-1 data by photointerpretation alone and by computer processing of MSS digital data without the assistance of photointerpretation, it became apparent that each method had shortcomings which might be overcome if the methods were combined. When applying photointerpretation techniques to ERTS imagery, in only a few cases could a feature be uniquely determined by this method alone. The use of U2, C130 and C54 imagery has been found to improve these interpretation results, but photointerpretive techniques have not been completely satisfactory as a single means of analysis. Computer differentiation of areas from scanner data is far superior to that done by the human eye. Computation of areas from the digital data makes delineation of these areas unncesssary and is far more accurate than planemetric methods at the scale of ERTS MSS imagery. Since the end result of processing ERTS-1 data is a map, the automated processes of thematic mapping by computer is the efficient way to go. However, "ground truth" is the key to correct signatures for this mapping. Underflight data and photointerpretation of underflight photography, as well as of ERTS imagery, are vital links leading to valid signatures for the thematic map. A marriage of these two disciplines, photointerpretation and computer processing, is essential for maximum utilization of ERTS-1 data. Thus ORSER investigators evolved a method of ERTS MSS data analysis referred to as the "hybrid approach" and shown in Figure 9. This method involves intimate interaction of the computer analyst and the photointerpreter, using aircraft photography for comparison with the computer output. A Bausch and Lomb Zoom Transferscope is frequently used for this comparison.

CORRECTION OF BANDING IN MSS DIGITAL DATA

In the ERTS-1 instrument configuration, six banks of the four channel sensors record data for six scan lines simultaneously. MSS digital data have been received in which data for every sixth scan line was found to be inconsistent. The effect was first recognized as banding with a modulo of six in computer output maps. To investigate the

```
BLOCK SPECIFICATIONS
--------------------

   BEGINNING LINE 1030
      ENDING LINE 1059
BEGINNING ELEMENT 2470
   ENDING ELEMENT 2525
   LINE INCREMENT    1
ELEMENT INCREMENT    1

  2470|2475|2480|2485|2490|2495|2500|2505|2510|2515|2520|2525|
      |    |    |    |    |    |    |    |    |    |    |    |
1030 |---XXXX------.*.---------XXX----.----XXXXXX---..--------+ |
1031 |--X++X-..XXX--.**---------XXXX-------XXXXXX--...--------++|
1032 |XXXXXX+..-XX---.* *.------------.---XXXX----...---XX-X   |
1033 |-XXXXXX....-XX----.*   *.----------**.-------.....--------X|
1034 |+XX  X+...-XXX------.** **.--------***.----.......===.*==+|
1035 |---+++++----X-----------..*****..-....- -   ...-.=======M |
1036 |.+.  ++---------------------..***---------.--.=========MM|
1037 |  ....-XXXXXX----------X---------.**...------+============|
1038 |-..--XX-******.------XXXXX---------.**.--------+++...=====|
1039 | X----X.  SSSS+=*------XXXXXX---------*.-------XX---.====|
1040 |XXX----* S++----.**.----X-XX--X------.*..--------------=====|
1041 |XX---X*=+.---------.* **..-----X-X-----**..--------XX-++++.|
1042 |MM+++++.+-----------.*      *....---***...--X----XXXXX---|
1043 | ------*.-++++++++++----....*** *****......== XXXXXXXX----|
1044 |--XXX-**-----------+++---.-...........  ..===M=+XXXX----.-|
1045 |+--------**------------+++-+-XX-X--..----.=======+XX------|
1046 |-----X---* **.---------+++++---XX-..---.==MM+X++....-----|
1047 |XX----  .---..******..---++++++-XX-.----+=MM+XXX--.====...|
1048 |+++++++= ----.----+++=**.--+ +--XX-------+++XXXXX--.======|
1049 |=========-X--------------**---+++-X----XXXXXXXXXXX-++==MMMM|
1050 |*=    ==-XX--XXX----XX-.*.----+++XX---XXXX--..======= S S|
1051 |=MM======XXXXXXXXX------.*------ M++---X----.=.++++ M SXX|
1052 |MMMMM=== .XXXXXXXX----X**---------+ +++--------..--XXXX+++M+|
1053 |MM===== =.XX--XX+-------**-------------+++------ = -XXXX ++ +|
1054 |MMMMM= ===-X-++X++---X-* ------------X+++----+=+-XXX  ++++|
1055 |M===== ==.XX--------XX--*  X--X-----X-X+++.-----XX++X SXX|
1056 |M=====*.++X---------XX--. .-----------XXX++++++++++-+XX+ +|
1057 |+++++++==+++----++-----XXX-.**-----------XXXX--+++++++++++++|
1058 |++++++S+-XX---+M+----X---.*.----------X------------..------|
1059 |+++++SSX--------+--=--XX----**-----------XXX-------------.---|
      |    |    |    |    |    |    |    |    |    |    |    |
  2470|2475|2480|2485|2490|2495|2500|2505|2510|2515|2520|2525|

CHANNELS USED  :  1  2  3  4
INITIAL CRITICAL DISTANCE  : 8.5
```

Figure 7: Signature map by DCLUS.

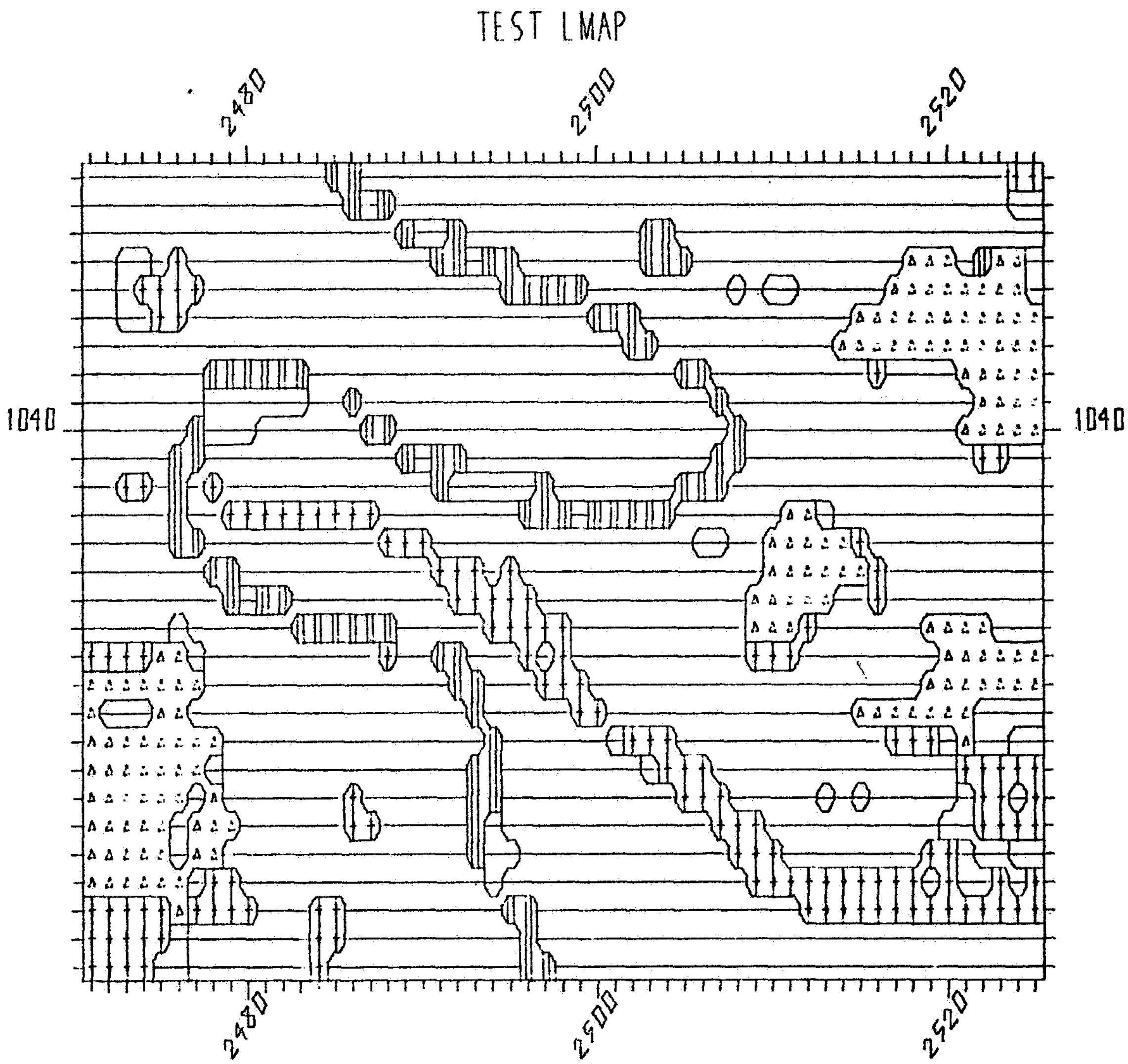

Δ: STRIPMINE
+: HIGHWAY
||: RIVER
—: VEGETATION

Figure 8 : Classification map of the Clearfield area (LMAP).

Explanation of the steps shown in Figure 9 .

PRELIMINARY PROCEDURES

A.[1] Determine scan line and element limits.
B. This becomes the working tape.
C. Identify clouds.
D. Review scene for definable boundaries.

FIRST LEVEL MAPPING

A. Collaboration of the photointerpreter and computer mapper. Select easiest targets first. Choose spectrally homogeneous items with positive geographic locations. Select replications in widely separated areas.
B. Identify some targets (training areas) on NMAP or UMAP.
C. Check for uniformity on UMAP. Attempt to find a large number of like elements. Loop A, B, and C until a sufficient number of training areas are identified.
D. Review statistical characteristics of defined targets.
E. Make first run on classification map.
F. This is a verification step. Project U2 image onto computer map. Identify satisfactory classifications. If some areas lack definition, redefine training areas.

SECOND LEVEL MAPPING

A. Attempt to identify items outside training areas.
B. Define items not subject to definition by training areas. These might be linear features or stream channels. Add these to the list of signatures and continue.
C. This a recycle, with smaller training areas and more weight placed on cluster analysis.

THIRD LEVEL MAPPING

A. Review the classification categories originally defined as desirable. If present map output is unnecessarily refined, combine some groups.
B. Some categories will require broadened spectral parameters. A series of successive approximations will be required to define these units. The resulting training areas will be less spectrally homogeneous.
C. Requires collaboration of the photointerpreter and the computer mapper.
D. Establish limiting goal.

---

[1] The letters correspond directly to those shown in the diagram.

TABLE 1

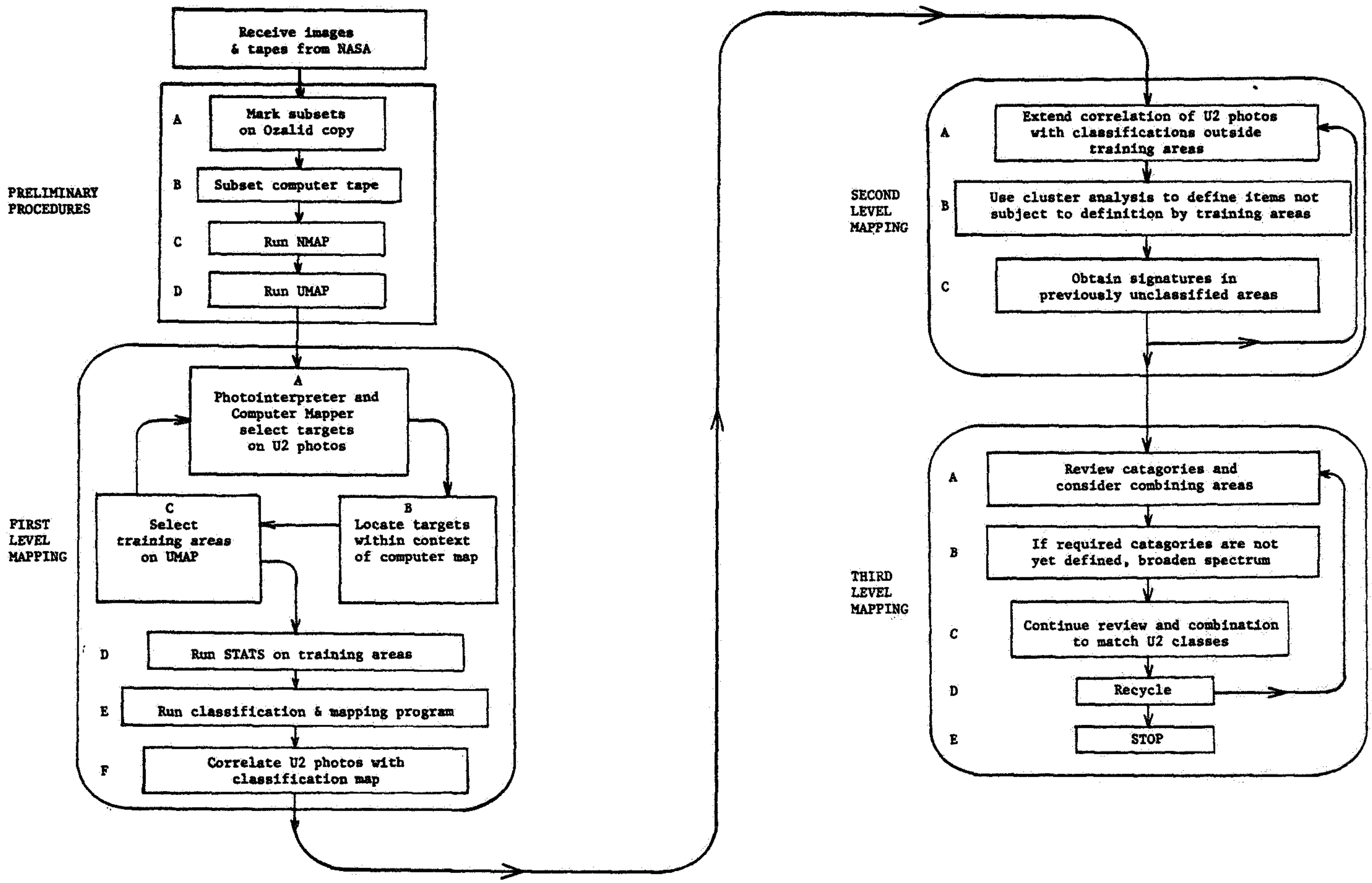

Figure 9: Flow diagram for the hybrid approach to ERTS data processing.

problem, the NMAP program was extended to compute the mean and variance for each channel for each line modulo six. In some cases it was determined that the mean value of every sixth line was less than one-tenth the value for each of the other five lines for the third MSS channel. (The other three channels were consistent for the first five scan lines.) Similarly, the standard deviation of the sixth line in the fourth MSS channel was found to be about six times larger than corresponding values for the other five lines.

It was apparent that the data could be recalibrated, at least in an approximate way, by use of the MSS data alone. Output from the NMAP program indicates which sensors in which of the six banks of sensors are involved. The SUBSET program has been extended to allow input of recalibration parameters for the offending sensor data. The following correction is then applied:

$$\hat{X}_{ijk} = [(X_{ijk} - \overline{X}_{k\ell})/S_{kl}] * s'_{k\ell} + \overline{X}'_{k\ell}$$

where

$\hat{X}_{ijk}$ is the recalibrated value for scan line i, element j, and channel k;

X_{ijk} is the corresponding original value;

$\overline{X}_{k\ell}$ is the computed mean for channel k and for line ℓ = modulo (j,6) + 1 taken from NMAP output;

$s_{k\ell}$ is the corresponding standard deviation;

$s'_{k\ell}$ is the recalibration standard deviation computed as the average of unaffected standard deviations for channel k based on NMAP output; and

$\overline{X}'_{k\ell}$ is the corresponding recalibration mean.

This correction has eliminated the banding problem in all data to which it has been applied.

RESULTS

The applications objectives of the ORSER interdisciplinary investigation are grouped into three major categories: (1) geology and hydrology; (2) inventory of natural resources and land use; and (3) environmental quality.

Applications

Specific results obtained to date include a study of land use, discrimination between types of forest resources and vegetation, detection of previously unknown geologic faults and correlation of these with known

mineral deposits and ground water, mapping of mine spoils in the anthracite region of eastern Pennsylvania, mapping of strip mines and detection of acid mine drainage effects in Central Pennsylvania, agricultural land use mapping, and detection of gypsy moth infestation.

Temporal and Spatial Transference of ERTS Spectral Signatures

Spectral signatures were developed for various vegetative and water targets in a forested area near the East Branch Reservoir in north-central Pennsylvania, using data from ERTS scene 1028-15295 for August 20, 1972. These signatures were then used to classify targets in the Stone Valley Experimental Forest for scene 1045-15243 of September 6, 1972. These signatures were initially used without success. The data for the two scenes were then recalibrated to match means and variances by channel and modulo line number in accordance with the recalibration algorithm given above. After this recalibration, excellent classification of the Stone Valley area was achieved using data from the East Branch area. Since the signatures used for classification were developed from ERTS data collected 17 days earlier and in an area approximately 150 miles away from Stone Valley, it appears that transference of spectral signatures in both time and space is feasible.

COST ANALYSIS

Two major components of the cost for analyzing and interpreting ERTS-1 digital data are computing cost and personnel cost. Computing cost can be partitioned into the cost for spectral signature identification and the cost for processing bulk data after signatures have been identified. The major personnel cost is associated with the development of signatures, since remote sensing analysts and interpreters are required for this phase. In the processing of bulk data, much less personnel time is required, although analysts and interpreters remain closely involved in evaluating the products.

In the Susquehanna River Basin test site in Pennsylvania, two characteristics dominate the analysis and interpretation of ERTS-1 data. These are the diversity of targets and the areal smallness of target units. Compared with other areas where these characteristics are less pronounced, signature identification presents a greater challenge and is therefore likely to be more costly. In addition, the cost for signature identification is contingent upon the nature of the particular problem to be solved and therefore it is difficult to categorically specify this cost.

In the computation cost evaluations provided here, the computer run costs are based on the standard rates charged at the Computation Center of The Pennsylvania State University. The ORSER MSS computer analysis methods emphasize the minimization of computation costs by being designed for signature identification based on short computer runs on small subsets of ERTS-1 data.

Data for personnel and computation cost were obtained for a typical ERTS scene analysis. For the identification of 22 signatures judged necessary

to meet the analysis objectives, the personnel cost was \$400 and the computation cost was \$600, a total of \$1000. Using the 22 signatures, mapping of a full ERTS-1 scene cost \$560, based on a cost of \$0.043 per square mile. Considering signature identification cost plus full-scene processing cost, the cost per square mile was \$0.12. For subsequent scenes of the same area, signature identification cost would be expected to be substantially less because, in the first time through, a great deal of personnel time and computer cost are spent in familiarization and learning for the specific area and targets. Much of this work does not have to be repeated in subsequent analyses of the same area.

Data have been accumulated for the computation costs of running different programs. For subsetting a complete ERTS-1 digital tape, the cost has averaged \$0.032/square mile. The cost of running mapping and classification programs has been found to be dependent on the number of signatures as well as the area to be mapped. The dollar cost per square mile (C) as a function of the number of signatures (S) has been found to adhere to the following formula:

$$C = S\ (2.56)\ 10^{-3}$$

For 15, 30, and 60 signatures, this cost is \$0.038, \$0.075 and \$0.154, respectively.

The computer time required for running mapping and classification programs is also dependent on the number of signatures and the area to be mapped. Typically, one complete ERTS scene can be classified using eight categories in approximately one hour.

The above calculations of analysis and processing costs have not taken into account the cost of developing the digital computer processing system. The system was developed so that it could be easily used for processing ERTS-1 as well as any other satellite or airborne platform MSS digital data. The system development has not been financially supported by the ERTS-1 project, although it has received partial NASA support through a sustaining University grant. Extension and modification of the system has been partially supported in the ERTS-1 project.

Paper I 9

ERTS IMAGE DATA COMPRESSION TECHNIQUE EVALUATION

Curtis L. May, *TRW Systems, One Space Park, Redondo Beach, California*

ABSTRACT

This paper presents the background and results of an investigation concerning the use of multispectral data compression in the ERTS program. An average compression of greater than 2:1 has been achieved under the constraint of zero distortion in the reconstructed image, and four MSS tapes can be compressed to fill less than one reel of magnetic tape. A preliminary study of the hardware implementation of this processor proves the feasability of compression at input bit rates of over 100Mbs.

INTRODUCTION

The objective of this investigation is the determination of the degree of data compression which can be obtained for ERTS multispectral imagery using a set of algorithms which inherently produce zero distortion in the reconstructed data. The results obtained can be used for determining the feasibility of data compression as an integral part of future ERTS programs, either for spacecraft or ground processing applications.

Due to the large volume of data generated by the ERTS system, data handling problems arise in communication links, in ground data processing, and in ground data storage and archiving. In the future, as the data load increases, the feasibility of including an experiment may be threatened by the data rates and processing required. Efficient source encoding (data compression) can yield significant benefits and alleviate such problems by exploiting spectral and spatial redundancies in the data.

The sucess of the earth resources programs is largely dependent on the satisfaction provided users of the data. This satisfaction depends on how well the data, as formatted and processed, helps the individual accomplish tasks relative to his goals. Any processing performed on the data must be accomplished without sacrificing the information fidelity required by the user.

TRW developed a class of low complexity data compression techniques tailored to the characteristics of multispectral data. These techniques are based on the Spectral-Spatial-Delta-Interleave (SSDI) algorithm which is inherently strictly information preserving (s.i.p.), providing reconstructed data identical to the digital sensor data input to the compressor unit. Such compression preserves the data and cannot be criticized by any user as invalidating his data requirements.

The ERTS investigation involved six major tasks:

1. Modification of the TRW developed master data compression computer programs to appropriately reformat the input MSS tapes and generated the required output products.

2. Select 30 subscenes and 4 full scenes from available NASA tapes for processing.

3. Measurement of pertinent MSS data statistics for scenes processed.

4. Measurement of desired global and time-varying compressed data statistics.

5. Generation of reconstructed imagery for selected full scenes, including a scene processed by a low distortion algorithm and a scene subjected to simulated channel errors.

6. Evaluation and interpretation of study results.

Description of Algorithms Used

The Spectral-Spatial-Delta-Interleave (SSDI) algorithm is a method of data compression for multispectral data which removes a maximum amount of redundancy subject to the constraints of moderate complexity and maximal processing speed. The algorithm first operates on the spatial redundancy in each spectral band and then uses the information obtained to reduce spectral redundancies between adjacent bands.

In order to provide a conceptual description of the basic SSDI algorithm, Figure 1 is provided. For simplicity, only three spectral bands are shown and each ground picture element (pixel) I consists of three quantized spectral components, I_α, I_β, I_γ. The algorithm proceeds in the following fashion. First, within each spectial band, each pixel intensity is subtracted from the intensity preceding it along the scan line. To each pixel there can then be assigned a triple of DPCM differences, denoted $(\Delta_\alpha, \Delta_\beta, \Delta_\gamma)$.

These deltas are subsequently differenced to obtain second differences between adjacent spectral bands; viz $d_A = \Delta_\beta - \Delta_\alpha$ and $d_B = \Delta_\gamma - \Delta_\beta$. Each original pixel may now be assigned the triple $(\Delta_\alpha, d_A, d_B)$. Due to spectral correlation, it should be true that on the average, $|d_A| + |d_B| < |\Delta_\beta| + |\Delta_\gamma|$. The triple of interleaved first and second differences allow the unambiguous reconstruction of a pixel given the reconstruction of the intensity of the previous pixel. For the four channel ERTS data, one spatial difference and three spectral differences are transmitted per pixel.

The final step in the SSDI algorithm involves source coding of these SSDI difference symbols. Three methods of coding were investigated; Global Huffman[1], adaptive Huffman, and the universal Rice algorithm[2]. These source encoding techniques use the statistics of the source symbols to generate a compressed bit stream having a bit rate close to the first order entropy of the symbols.

An extension of the SSDI, the SSDIA, uses a block of contiguous pixels to generate the first difference symbols. A higher average compression is obtained with the SSDIA because two dimensional spatial correlation is exploited and sensor and sampling noises are smoothed through averaging. The SSDIA is also strictly information preserving. Another modification allows the mapping of the original pixel intensities within controlled limits before the first differences are formed. This algorithm, the SSDIAM, allows a small degree of distortion in the

reconstructed data but yields a significantly higher compression than either the SSDI or SSDIAM algorithms. The SSDIAM produces minimal visual degradation in the reconstructed imagery and has little or no effect on classification algorithms.

Results of the Investigation

Thirty 5x5 nmi subscenes and four 25x25 nmi scenes were processed. The subscenes were drawn eleven "object classes" such that each subscene contained a single class. These classes, listed in the first column of table 1, were based on coverage of the predominant objects encountered on earth survey missions and the classes span the range of source data activities to be expected. The results of subscene processing serve to roughly bound the expected compressed data rates which could occur.

The performance of the SSDI algorithms is highly dependent on the source data statistics. For this reason, several key statistics relating to compression performance were measured for each scene processed. These statistics are:

- Mean and variance per spectral band and over all bands.
- Cross spectral-spatial correlation.
- Spectral correlation (joint probability distribution of first differences).

The statistics measured on each scene correlated well with the compressed bit rates achieved. In addition, a sensor anomaly occurring every sixth scan line of spectral band five was evident from these statistical measurements. The inherent sensor and quantization noise energy was estimated for each spectral band.

For each scene, several key statistics and global measures of the data compression performance were obtained. These measurements serve as an indicator of the compression to be expected on similar subscenes containing the same object class and permit a comparison of the efficacy of each compression technique for similar data. The following measures were obtained for each scene:

- Probability distribution of the SSDI, SSIDA, and SSDIAM symbols.
- Average compression achieved by the global Huffman coding of the scene using the SSDI, SSDIA, and SSDIAM modes.
- First-order entropy of the symbol distributions.
- Line-by-line time-varying and overall compressed bit rates using the global Huffman, adaptive Huffman, and Rice algorithm on the source symbols.
- Buffer statistics for Rice-encoded data.
- Global Huffman codes associated with the various compression modes.

The overall compressed bit rates achieved for the various object classes are summarized in Table 1. The compressed bit rates generally reflect the level of data activity in the object class and the entries serve as a guide for determining the expected performance of the algorithms for another scene containing the same object class. The compressed bit rate for a scene containing multiple object classes can be estimated by weighing the bit rate of each object class by its percentage of occurrence in the scene.

A typical global Huffman code is shown in Figure 2. Since the code is generally synmetric about the zero level symbol, only one half of the symbol codes are shown. A graph of buffer statistics is shown in Figure 3 for the SSDIA/Rice mode with an output buffer rate of 3 bits/pixel. The scene contains ocean over scan lines 1 through 24 and lines 120 through 160. Catalina Island covers scan lines 25 through 119. Over the ocean, a compressed bit rate of about 1.5 bits/pixel produces buffer underflow. A bit rate higher than 3 bits/pixel occurs over the island to produce a buffer fill.

Compressed data is far more vulnerable to the effects of channel errors than the original PCM data due to the removal of redundancy. The effect and propogation of bit errors during transmission was evaluated and photographs of the reconstructed images were made. Using a one percent memory update rate, error effects were minimal for channel (or tape) bit error rates of 10^{-5} or less.

The low distortion SSDIAM algorithm was studied for two controlled mapping levels. A mapping level of m constrains all reconstructed pixel intensities to lie within $|m|$ levels of the original intensities. For example, with an input intensity of 108 and a mapping level of 1, the reconstructed intensity would be 107, 108, or 109.

The first mapping used was m=1, resulting in a mean square error of .0112 percent and no visual degradation of the reconstructed image. A mapping level of 1 apparently smooths sensor, quantization, and ground processing noises. A second run with m=3 produced a mean square error of .103 percent. Areas of high data activity were well reproduced due to the absence of overshoot and slope overload but some visual degradation occurs in areas of very low data activity due to contouring effects. An improved adaptive SSDIAM would eliminate contouring by varying m dependent on data activity.

To complement the computer simulation of the data compression algorithms. a concurrent investigation of an implementation of the SSDI/Rice data compressor was performed. An overall block diagram of the unit is shown in Figure 4. Using standard SSI and MSI Shottky TTL and bi-polar RAM's, the compressor can handle an input data rate over 100 Mbps with a corresponding weight of 3.7 lbs., and 30.7 watts of power. Large scale integration could improve these figures.

Conclusions and Applications of Investigation

The investigation yielded a significant amount of data regarding source statistics, compression statistics, algorithm performance and tradeoffs, and preliminary hardware considerations.

- Compressed bit rates, averaged over the scene, vary from a minimum of 1.22 bits/sample to a maximum of 3.747 bits/sample for the strictly information preserving algorithms.

- The compressed bit rates obtained, averaged over all scenes processed, are:

  2.99 bits/sample for SHELL/global Huffman
  2.98 bits/sample for SSDI/global Huffman
  2.92 bits/sample for SSDIA/global Huffman
  2.50 bits/sample for SSDIAM/global Huffman
  2.67 bits/sample for SSDI/adaptive Huffman
  2.70 bits/sample for SSDI/Rice

- For well-behaved data, the SSDIA technique gives a lower compressed bit rate than the SSDI algorithm. For anomalous data such as that produced by a defective sensor, this is not always true.

- The essentially information preserving SSDIAM produces a significantly lower compressed bit rate than the strictly information preserving SSDIA algorithm. The effects of such distortion appears minimal when properly performed and areas of high detail are well preserved with no slope overload or overshoot.

- The strictly information preserving algorithms can compress four full 100x100 nmi scenes to occupy the same number of magnetic tapes currently required to store one full scene. An even greater reduction is possible with the essentially information preserving algorithms.

- The effect of channel errors is minimal if the channel bit error rate is less than 10^{-5}. Channels with higher error rates can be used if frequent memory updates are included.

- While not conclusive, the compression obtained on spacecraft data seems to be comparable or higher than that obtained for ground-processed data.

- An implementation of the SSDI/Rice algorithm was developed to illustrate the feasibility of operation at rates above 100 Megabits/second with moderate complexity. Parallel data compressor units operating on blocks of data permit operation at several hundred Megabits/second.

- The SSDI/Rice algorithm is well suited for spacecraft data compression applications. The SSDI/Huffman algorithm provides an efficient data compression and reconstruction technique suitable for use in ground applications.

A considerable wealth of new source and compressed data statistical measurements resulted from this study due to the volume of ERTS data processed and the correlation of these measurements with a standard set of object classes.

Application of this Investigation to ERTS Program

This study concentrated on the low complexity SSDI algorithms combined with source encoding as a technique applicable to either the spacecraft or ground-based data compression of ERTS digitized imagery. The results are quite encouraging regarding the suitability of these techniques for applications in the ERTS program.

The SSDI/Huffman algorithm forms the basis of an efficient technique for ground-based data compression and reconstruction that can be performed with a modest amount of computer processing. Results indicate that the average 100x100 nmi scene can be compressed to a single reel of magnetic tape and reconstructed with no loss of information. This reduction in storage from four reels of tape to a single reel yields economic benefits through a reduction in tape costs and in the tape storage facilities required while permitting a simplified archival procedure to be employed.

The essentially information preserving SSDIM or SSDIAM algorithms can yield reconstructed data which has a fidelity acceptable for many users of ERTS data and allows an even greater compaction of data. An improved adaptive form of this algorithm may allow storage of two 100x100 nmi scenes on a single reel of tape. The distortion induced at present in the data by the ground decompression algorithms is comparable in degree to that produced by the SSDIM with $|m| = 1$. Proposed techniques for the geometric correction of ERTS imagery involve prediction on interpolation of corrected data intensities, a process which is also essentially information preserving. Instead of cascading the operations of decompression, geometric correction, and data compression the three techniques could be combined into a composite algorithm which would increase processing efficiency while minimizing the data stored.

The SSDI/Rice technique is a viable candidate for spacecraft applications permitting a doubling of the data transmitted to ground. The reconstructed data is of high quality provided the channel bit error rate is 10^{-5} or less. To further decrease the effects of channel errors and allow the use of downlinks having a higher bit error rate, error correction coding can be applied to the compressed data.

In conclusion, the results of this study indicate that the use of data compression on ERTS data yields both economic and operational benefits. The tradeoff between strictly and essentially information preserving forms of the algorithms depends on the effect of slight distortion on the various uses of ERTS data.

REFERENCES

1. Huffman, D.A., "A Method for the Construction of Minimum Redundancy Codes", Proc. IRE, Vol. 40, No. 10, pp. 1098-1101, Sept. 1952.

2. Rice, R.F., "The Rice Machine: Television Data Compression", GTD 900-408, JPL, Pasadena, California, Sept. 1, 1970.

			GLOBAL HUFFMAN			
OBJECT CLASS	AD. HUFF.	RICE	SHELL	SSDI	SSDIA	SSDIAM
CLOUDS	1.42	1.31	1.697	1.508	1.491	1.427
WATER	1.51	1.40	1.956	1.921	1.635	1.550
SNOW	1.78	1.79	2.014	2.135	1.890	1.453
PLAINS	2.55	2.67	2.827	2.790	3.251	2.724
DESERT	2.74	2.84	3.081	2.964	2.983	2.484
MOUNTAINS	3.23	3.24	3.403	3.500	3.362	2.798
CITY	3.06	3.09	3.379	3.373	3.343	2.731
FOREST	3.10	3.11	3.339	3.370	3.368	2.891
GRASSLAND	3.32	3.35	3.581	3.536	3.487	2.981
AGRICULTURE	3.41	3.42	3.640	3.566	3.593	3.042

Table 1: Average Compressed Bit Rates for Uniform Object Classes (based on scenes processed)

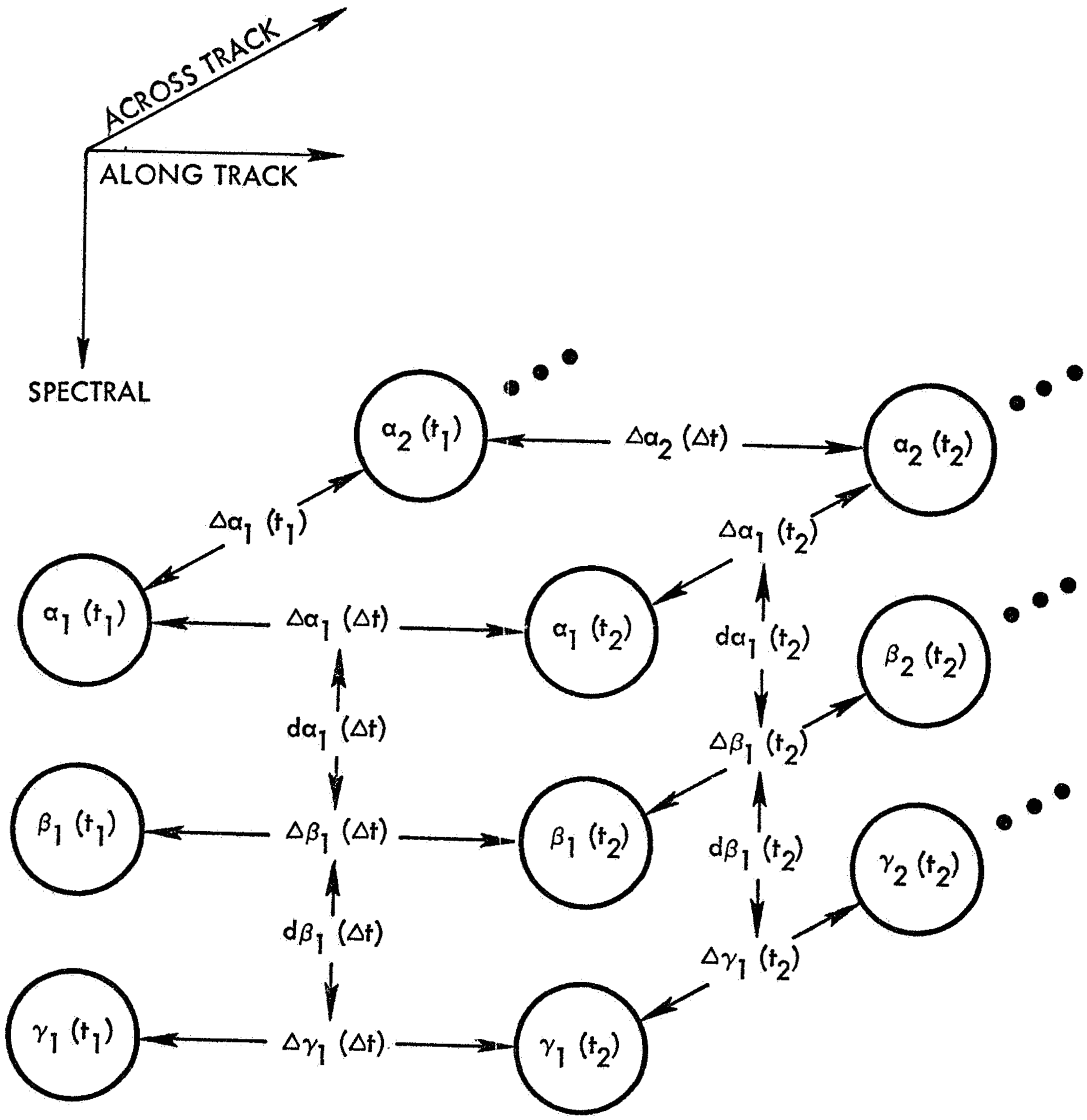

Figure 1. Definition of First and Second Order Differences in SSDI

Figure 2. Typical Huffman Code

SYMBOL LEVEL	PROBABILITY	CODEWORD
-20	.001	1100
-19	.001	1100
-18	.001	1100
-17	.001	1100
-16	.002	1100
-15	.002	1100
-14	.001	1100
-13	.002	1100
-12	.002	1100
-11	.003	1100
-10	.003	1100
-9	.003	11111111
-8	.005	11111110
-7	.006	1111001
-6	.007	1111000
-5	.010	1111101
-4	.012	111000
-3	.018	111011
-2	.046	11010
-1	.144	100

Figure 3: **Buffer Statistics of Scene 15 (Catalina Island)**
Compression Technique Used - SSDIA/Rice
Average Compressed Data Rate - 2.89 bits/pixel
Buffer Output Rate - 3.0 bits/pixel

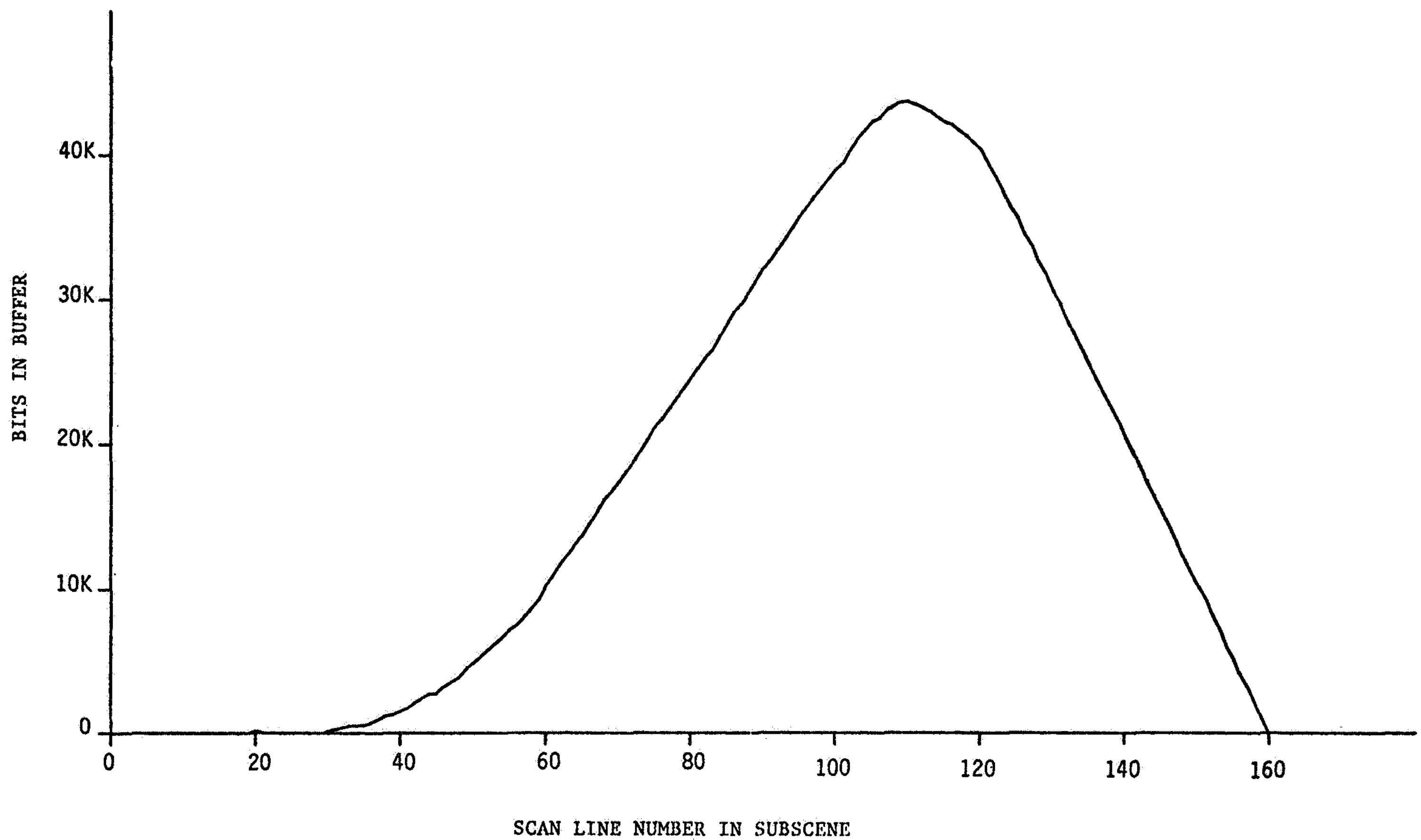

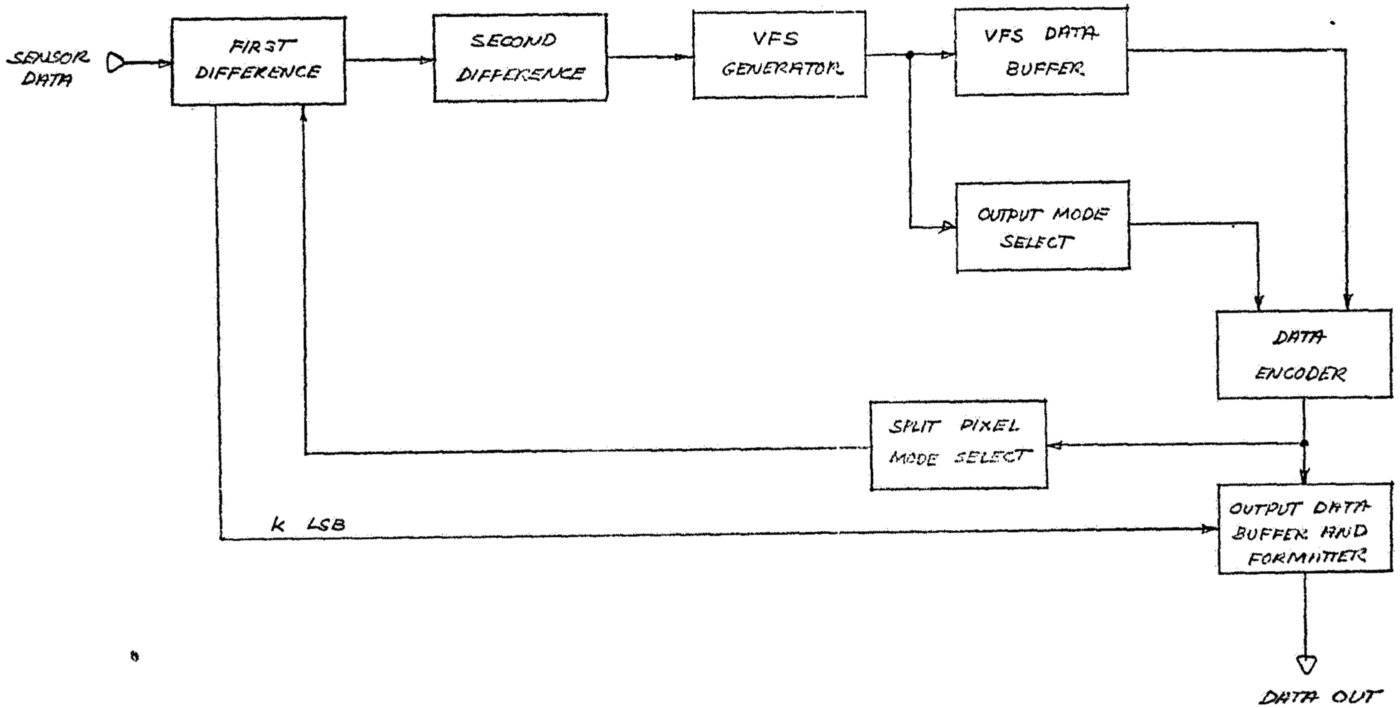

Figure 4: Overall Block Diagram of SSDI/RICE Data Compressor Unit

Paper I 10

EVALUATION OF DIGITALLY CORRECTED ERTS IMAGES

John E. Taber, *TRW Systems Group, One Space Park, Redondo Beach, California 90278*

A view of almost any uncorrected photograph constructed from ERTS MSS data provides a striking example of a small section of the earth as seen from space. Such images, beautiful as they are to the eye, however, contain errors that limit their usefulness where mensuration, precise location and/or temporal registration are required. Figure 1 shows a sequence of steps each of which affected the quality of the data received and the reconstructed image resulting therefrom. When quantitative knowledge of specific errors exists it is usually possible to compensate for them but a valid question concerns the introduction of new degradations in the process.

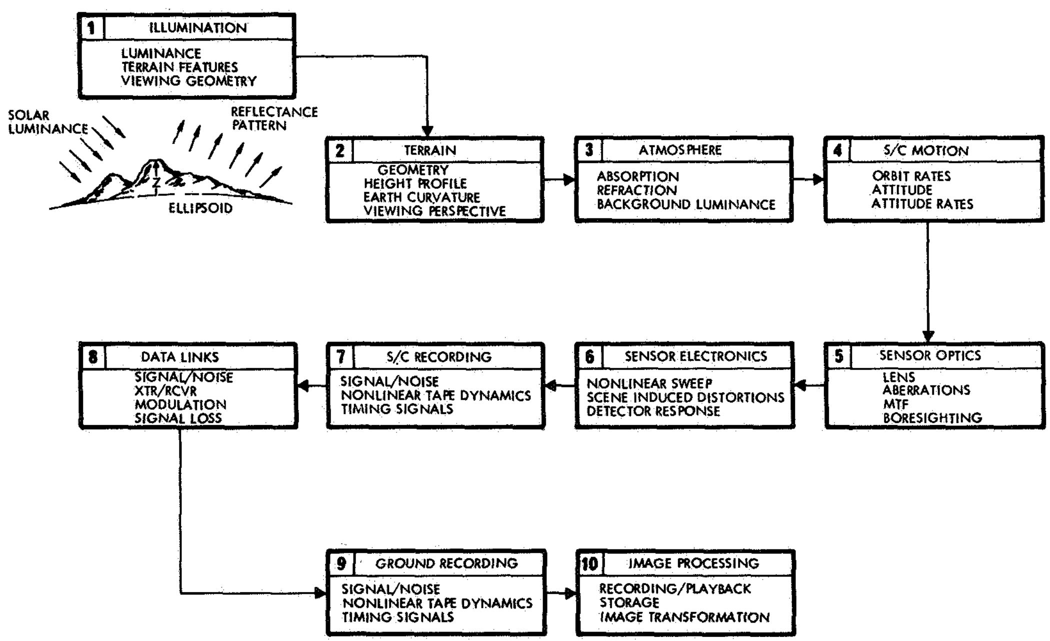

Figure 1. Image Error Source Sequence

While TRW's ERTS-data investigation has been concerned with the entire aspect of image correction, the discussion here is limited to processes by which a set of data samples collected on a geometrically distorted grid can be converted to samples on a different precisely specified grid. It is assumed that a mathematical expression for the desired transformation already exists, though deriving this transformation from spacecraft ephemeris and attitude data, terrain data, and ground control points located within the scene is a subject for discussion by itself. Our concern here will be the effects on image quality (specifically loss of resolution, photometric accuracy, and miscellaneous aberations) that result from various techniques used in accomplishing the resampling.

The resampling techniques evaluated have included nearest neighbor, bilinear, cubic convolution, and various truncated versions of sinc (x). Our conclusion is that cubic convolution yields substantially higher quality output data for scenes typically encountered and can, in some instances, substantially enhance one's ability to abstract information.

To establish the quality of a particular resampling technique one would like to compare the end-product with the original terrestrial scene. But this is not available to us; only the samples collected on an incorrect grid are. By falling back on the sampling theorem, however, we can determine the most likely band-limited replica of the original scene and then use this as a reference for comparison. This is done by summing a series of two-dimensional sinc functions each weighted by the amplitude of the corresponding sample. We call the resulting replica the reference image and verify its uniqueness by deriving a new set of samples at the mid-points of the original set, synthesizing a new replica and verifying that it is no different than the first. For practical reasons, including roundoff of the new samples and failure to include in the new representation samples from outside the desired scene, this reversibility can only be approached; but as further discussion will show, it can be approached quite closely.

The implementation of the above theoretical possibility is impractical for many reasons and therefore more easily implementable techniques, which are close approximations are sought. The nearest neighbor approach consists of defining the value at each point between samples to equal that of the sample closest to it. Similarly, the bilinear approach consists of fitting the region between any four samples with a bilinear function. Figure 2 illustrates a one-dimensional example of a synthesized curve using a nearest neighbor and a bilinear approach. The dark solid curve is the reference curve synthesized from sinc functions, the dotted curve is the nearest neighbor and the light solid curve is the bilinear. Values at any set of new grid points can now be established by taking the height on the corresponding curve at the desired sample position. One can quickly see the intensity errors introduced in the correction process.

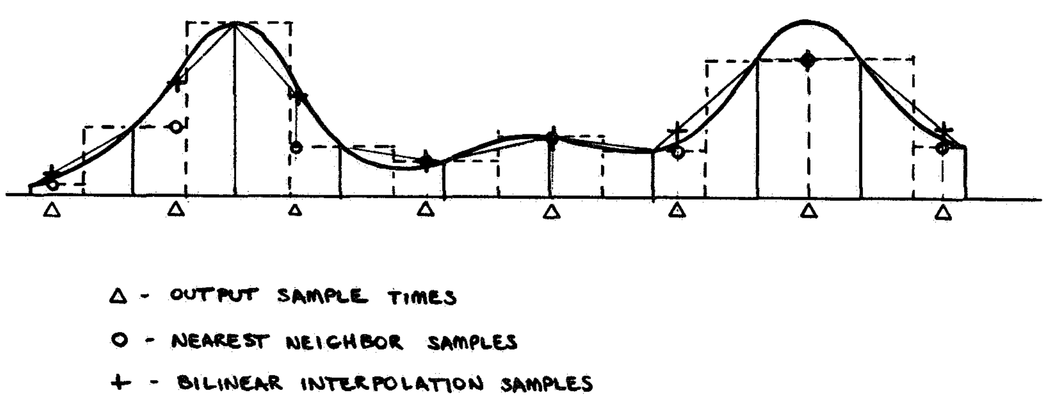

Figure 2. One-Dimensional Synthesized Interpolation Curves for Nearest Neighbor and Bilinear Approaches

We know that the unique band-limited function derived from the sampling theorem is smooth because it is continuous in value and all derivatives. Therefore, in seeking a better interpolation we seek functions with more smoothness than the nearest neighbor (which has no continuity) and the bilinear function which is continuous in value but not continuous in any derivative. A cubic spline permits continuity in value and slope and can be chosen to minimize discontinuity in the second derivative. It has not been plotted in Figure 2 because it lies so close to the reference curve as to be indistinguishable from it. Analysis, however, shows peak errors of two to three percent are possible. The technique used for implementing the cubic spline leads to its name, cubic convolution. Establishing this function in the interval between two samples requires the values of four samples; two on each side of the interval. (In two-dimensions this is 16 points.)

Synthesis of an interpolation function can alternately be obtained by summing a set of impulse responses, one corresponding to each sample. The unit impulse response for the nearest neighbor, the bilinear, and cubic convolution are shown in Figure 3. The impulse response for the band-limited unique interpolation function is of course the sinc function.

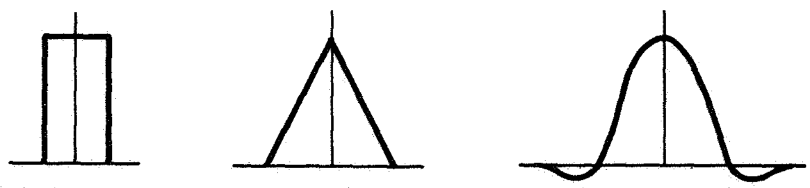

Figure 3. Impulse Responses for Three Interpolation Functions

To indicate the quality of images resampled by these three approaches, refer to Figure 4 which illustrates uncorrected bulk imagery, nearest neighbor, bilinear, and cubic convolution resampling. Reproduction of these images has been accomplished using a line printer where each pixel corresponds to a 3 X 3 dot square and ten grey levels are conveyed by the number of dots in the square which are black or white. One can notice the great detail that exists in the bulk images, the somewhat blocky appearance of the nearest neighbor scene, the degraded resolution of the bilinear scene, and the relatively high quality of the cubic convolution scene.

To evaluate more quantitatively the errors that are introduced during interpolation, TRW has synthesized a smooth curve through a set of received sample points using a sinc impulse function truncated at 30 terms. That the above procedure yields a relatively accurate information-lossless respresentation was verified by resampling the image at mid-original sample points and then inverting the procedure. Comparison of the double interpolated samples with the original samples indicated few differences other than zero and that these were small enough to have been caused by roundoff.

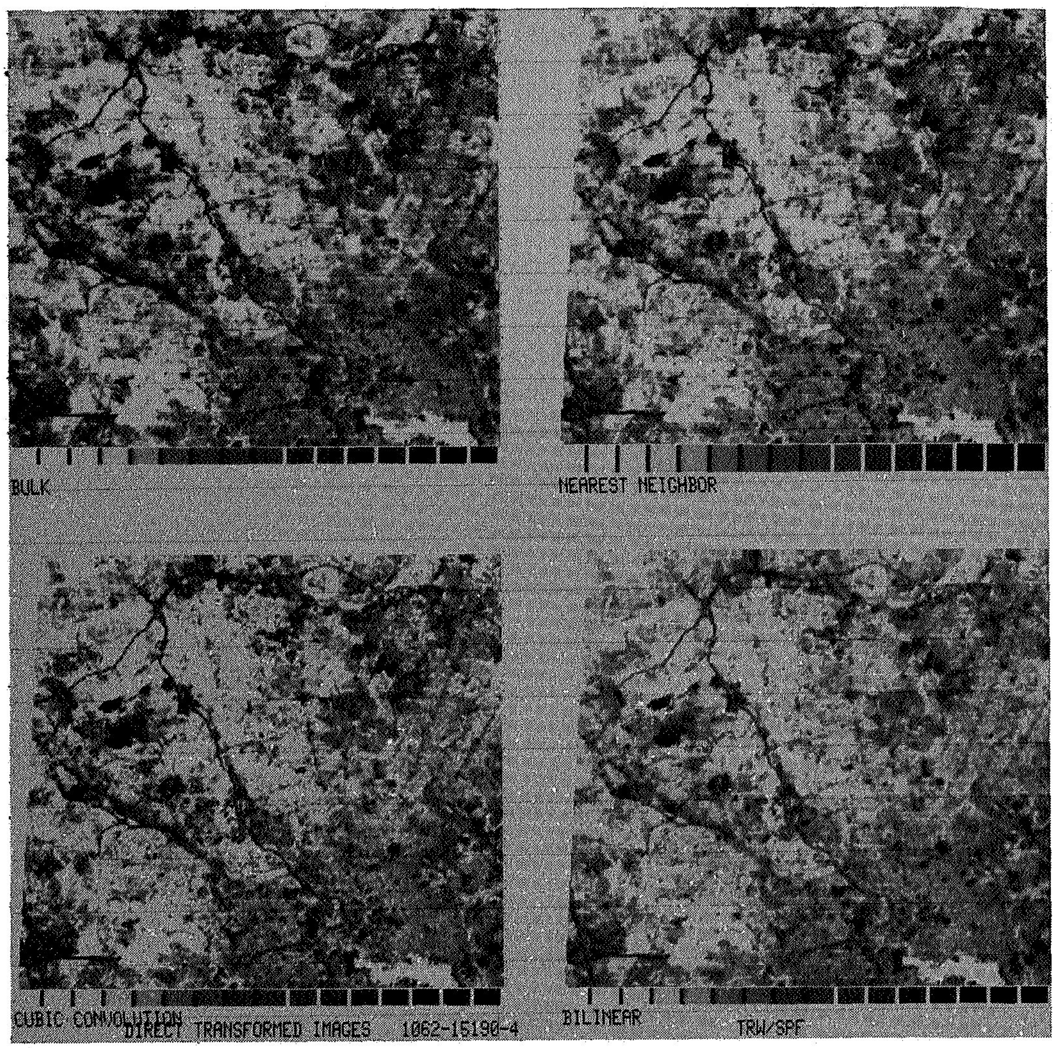

Figure 4. Images Generated from Unprocessed Data and Data Processed by Three Interpolation Techniques

Now assuming this ideally synthesized function is the actual (band-limited) scene profile which led to the initial samples, we are in a position to compare the results of three practical interpolation procedures with the values that would have been obtained had they been collected at the proper location initially. Graphs of the difference between the actual interpolated images (all interpolations are at the mid-point between initial samples) and the synthesized replica of the true scene are shown in Figure 5. Referring back to Figure 2, it is easy to see why nearest neighbor and bilinear interpolation at the mid-point between two substantially different samples lead to much greater errors than the cubic convolution.

Where the scene intensity is changing fairly slowly (and consequently high resolution adds little to the information content) or where the interpolated value lies quite close to an initial grid point, little error is

introduced in any of the three procedures so the examples given above are admittedly extreme cases. Additionally, it can be argued that the errors in the nearest neighbor approach should, in fact, be considered as residual geometric errors rather than intensity errors. In one sense this is true except where a point must be deleted or added due to scale change. In another sense when change detection is the object of geometrically manipulating one image to make it agree with another, fractional pixel displacements in regions of rapid intensity change will introduce errors typical of the graphs shown in Figure 5.

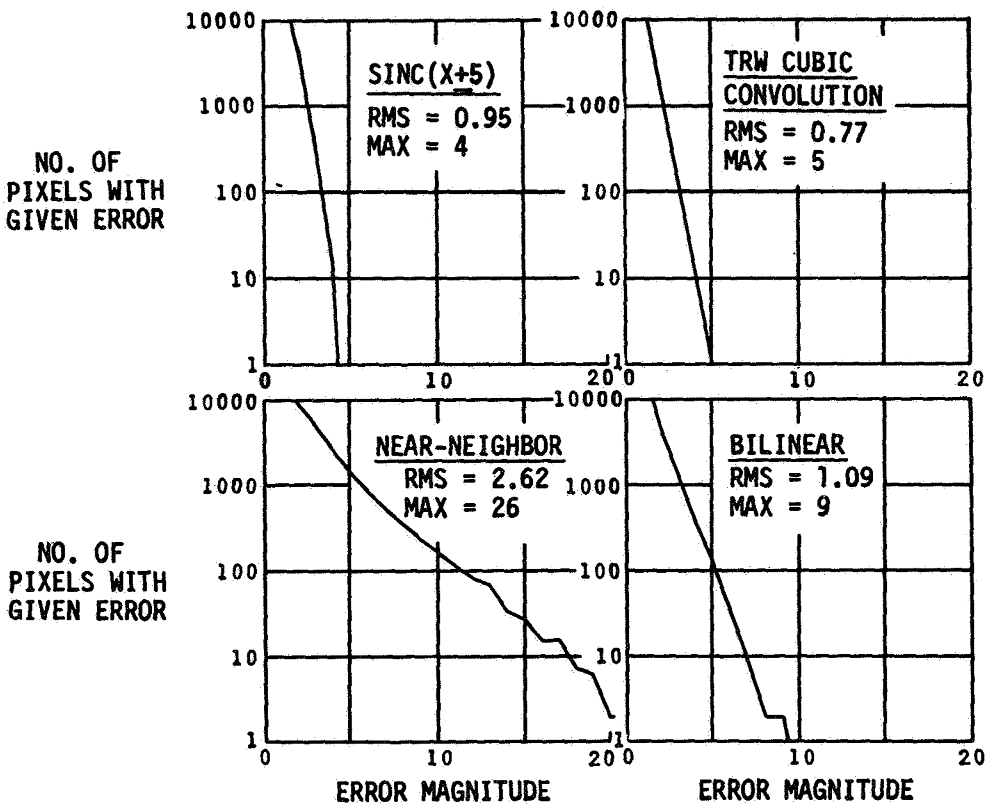

Figure 5. Error Between Registered Images Due to Resampling

A more dramatic demonstration of the impact of nearest neighbor interpolation arises in actual ERTS bulk processed digital tapes. In these tapes scanner line length variations are corrected by the insertion or deletion of a pixel at appropriate intervals. Data collected from the same scene at two times 18 days apart were registered using a smooth transformation and differenced. The result is displayed in Figure 6. Clouds appearing in one scene and not the other are apparent as very black regions. The more interesting aspect of this scene is the band of errors running vertically down the center of the image. This corresponds to the point in each line of one scene where a nearest neighbor line length correction was made. The geometric error is thus only about 1/2 pixel but pronounced intensity errors result.

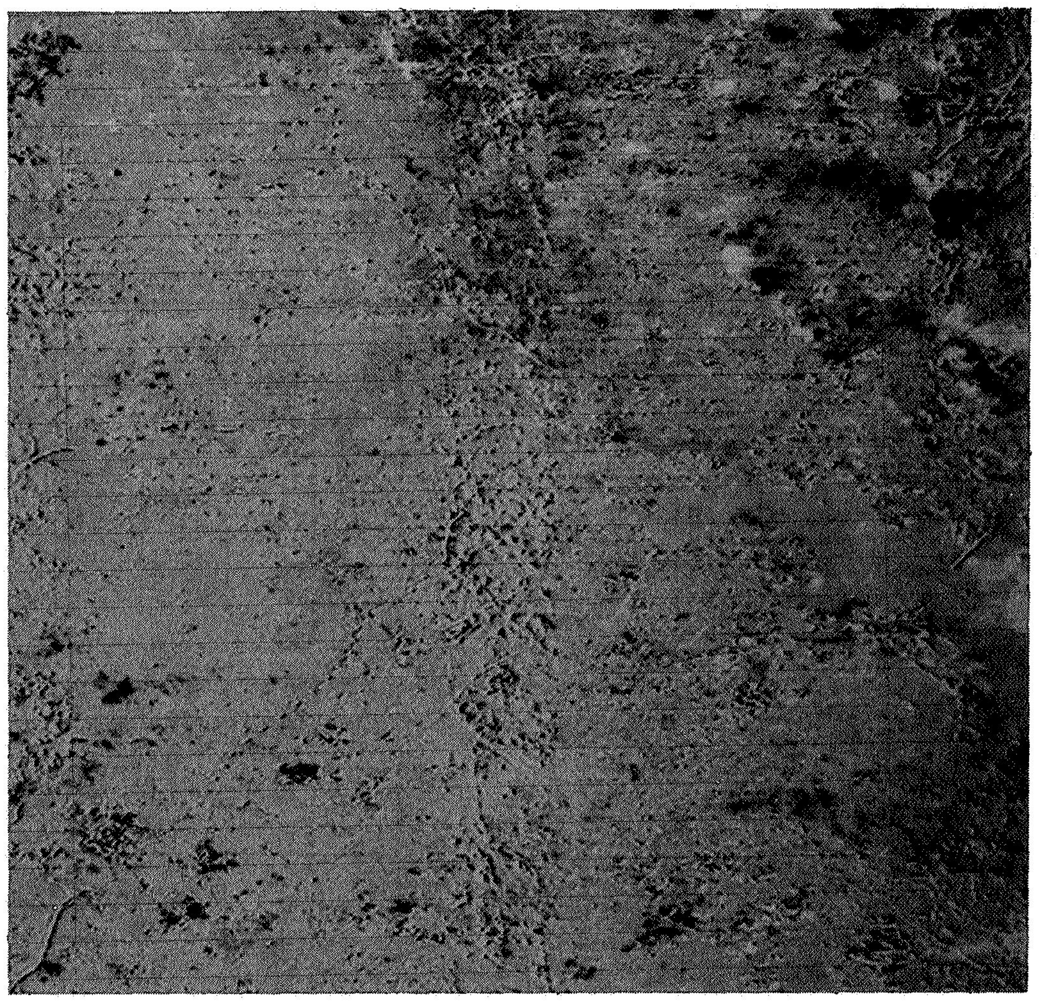

Figure 6. Image of Difference Between a Scene Imaged Twice 18 Days Apart. The Vertical Band in the Center Corresponds to a Nearest Neighbor Line Length Correction in One Original Image But Not the Other

As a last point worthy of mention, application of the cubic convolution to zoomed images permits abstraction of information that might otherwise be missed. Zooming in essence, involves creating artifical pixels between those already existing. Straight replication, as done using the nearest neighbor, clearly fails to add anything and is quite distracting to the eye (see Figure 7). Cubic convolution on the other hand, appears to help the eye find details that might otherwise be missed (see Figure 8). Both represent a four to one zoom.

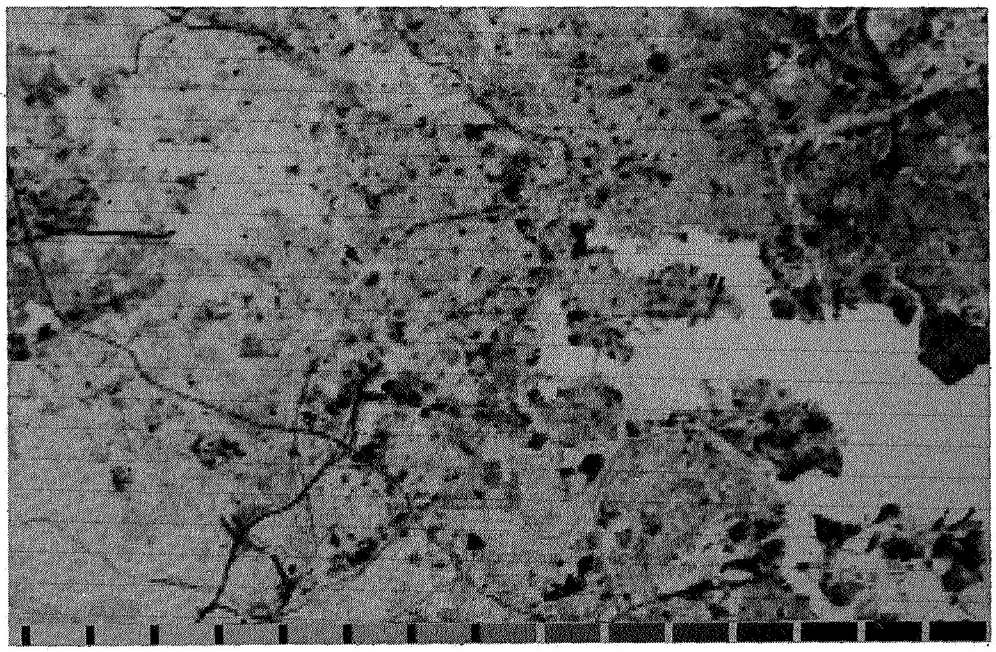

Figure 7. Four-to-One Zoomed Image Using Nearest Neighbor Replication of Additional Sample Points

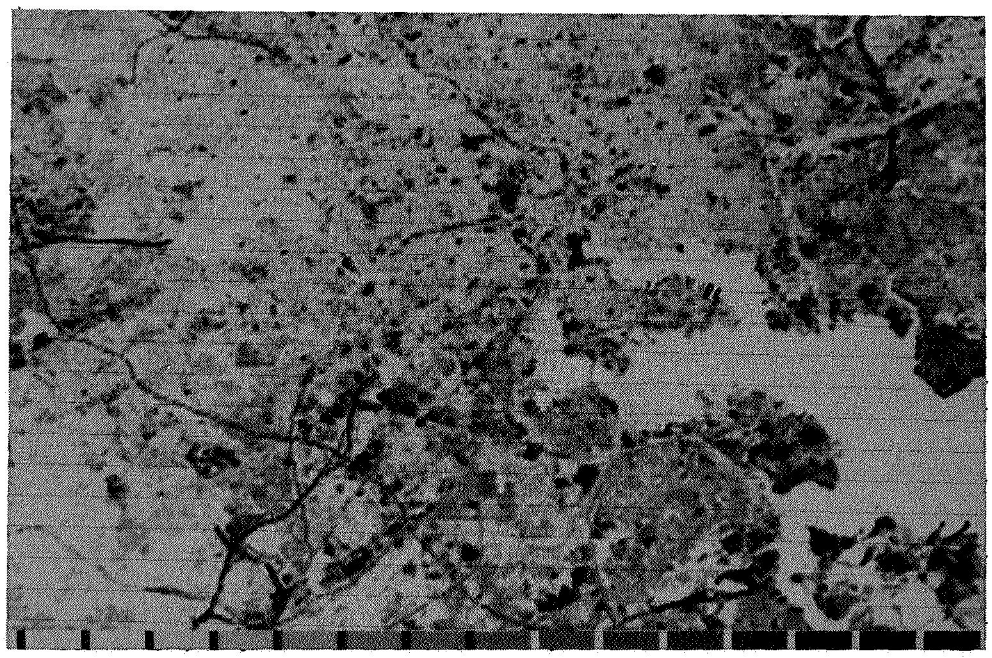

Figure 8. Four-to-One Zoomed Image Using Cubic Convolution to Determine Additional Sample Points

Paper I 11

AUTOMATED THEMATIC MAPPING AND CHANGE DETECTION OF ERTS-1 IMAGES

Nicholas Gramenopoulos, *Manager, Earth Resources Data Processing**

ABSTRACT

Results of an automated thematic mapping investigation using ERTS-1 MSS images are presented. A diffraction pattern analysis of MSS images led to the development of spatial signatures for farm land, urban areas, and mountains. Four spatial features are employed to describe the spatial characteristics of image cells in the digital data.

Three spectral features are combined with the spatial features to form a seven dimensional vector describing each cell. Then, the classification of the feature vectors is accomplished by using the maximum likelihood criterion.

Three ERTS-1 images from the Phoenix, Arizona area were processed, and recognition rates between 85% and 100% were obtained for the terrain classes of desert, farms, mountains and urban areas.

To eliminate the need for training data, a new clustering algorithm has also been developed.

There are several conclusions from this investigation:

a. Through the developed algorithms, it is possible to automatically recognize terrain types.

b. The clustering algorithm eliminates the need for training data and has been combined with the maximum likelihood criterion.

c. The spatial features selected contain the spatial information necessary to recognize terrain types.

d. Combining the spectral data with the spatial features increased the accuracy of the machine recognition.

e. The class statistics vary appreciably between seasons.

f. The results of this investigation are applicable to the production of land-use maps.

*Optical Systems Division, Itek Corporation, Lexington, Massachusetts.

INTRODUCTION

The management of the nation's resources requires that all resources be inventoried at regular intervals. The resources must be monitored to determine changes resulting from weather conditions, urban expansion, industrialization, air and water pollution, changes in farming practices, as well as changes resulting from management decisions. The inventory of the resources requires also that they be precisely located in terms of geographical coordinates. ERTS offers the advantages of countrywide coverage at intervals (18 days) short enough to monitor the fastest changing resources (crops). It also offers a stable platform from which the resources could be mapped.

The conversion of ERTS images and digital tapes to thematic maps that show the distribution of specific resources is the first step in the data reduction process. The production of thematic maps by photointerpretation is an established technique which, however, is time consuming and slow. In order to be useful, thematic maps must be produced economically and machine interpretation of the earth resources imagery offers the potential of low-cost thematic map production. In the meantime, the automatic interpretation techniques must be developed sufficiently so that the functions of the interpretation hardware can be defined. This paper describes an investigation which is devoted to developing automatic interpretation techniques.

The information in the earth resources imagery consists of spatial information (the information conveyed to a human observer by a black and white image) and multispectral information (or color) contained in the changes of transmission between spectral images.

In the ERTS-1 images the basic unit which conveys information is the picture element. Each picture element corresponds to an area increment on the surface of the earth equal to the instantaneous field of view squared (about 80 meters square). Each area increment is characterized by a brightness value in each spectral band. These brightness values are the multispectral information conveyed by the picture elements.

The first level of automatic interpretation is the classification of individual picture elements based on multispectral information. This level appears to be well developed as evidenced by the wide use of multispectral recognition software based primarily on the maximum likelihood criterion.

Most of the information in the ERTS images is spatial and is contained in the distribution of the picture elements over the image area. This spatial information may be conveniently divided into the information carried by small localized areas defined as cells, as well as the information carried by the distribution of the cells over the image.

It has become evident that combining multispectral and spatial pattern recognition techniques can lead to very substantial improvements in the recognition process: (1) the accuracy in resource recognition increases, and (2) the recognition process can be made more efficient.

At first, an analysis of spatial signatures which characterize the terrain types in the ERTS-1 imagery was conducted. The results were utilized in developing significant spatial features which are extracted from the digital data in the computer compatible tapes. Then, the spatial features were combined with three spectral features to form a seven dimensional vector describing an area on the ground about 2.5 kilometers square. Feature vectors from the Phoenix, Arizona area and three different acquisition dates were classified using an heuristic algorithm and the maximum likelihood criterion. An analysis was made of classification errors of the maximum likelihood criterion when the feature vectors of terrain classes are not gaussianly distributed. Non-linear transformations of the feature vectors were developed so that the classification errors were minimized.

To eliminate the need for training data, a new clustering algorithm was developed. Several ERTS-1 images were processed through this algorithm and the classification results are described in this paper.

TERRAIN SPATIAL SIGNATURES

The cell size that has been employed in this investigation is 32 x 32 picture elements which corresponds to about 2.5 x 2.5 kilometers on the surface of the earth. Each cell is, therefore, characterized by 1,024 numbers. Two questions then arise about each cell: (1) what objects on the surface of the earth it might represent, and (2) how could these objects be identified by manipulating these 1,024 numbers.

The first question is answered by the IFOV (80 meters) of the MSS scanner. The objects that are faithfully reproduced by this system are expected to be in the order of one kilometer. Examination of the ERTS photography shows that the objects that can be identified are various geographical features and terrain types, such as bays, lakes, rivers, mountains, urban areas, cultivated land, desert, forest, etc.

The second question is more difficult to answer. It is desirable to develop signatures which uniquely characterize the terrain categories. A signature is defined as a specific pattern of numbers. It is also desirable that each terrain class be characterized by a signature containing less than ten numbers. Assume that such signatures were known. Then, to assign a cell to one of the terrain types, the 1,024 numbers describing the cell are combined to produce a vector with less than ten components which is known as a spatial feature vector. This vector is compared to the spatial signatures, and the cell is assigned to the terrain category whose signature most closely resembles the vector of the cell. Conceptually, the assignment of cells to terrain categories is simple, but there are some difficult practical problems in accomplishing it, such as:

1. The 1,024 numbers of the cell are quite redundant. Their replacement by a feature vector with less than ten components is a data reduction operation which may actually destroy information.

2. There is no theoretical treatment that allows one to select optimal terrain signatures.

3. Comparison of a feature vector to the spatial signatures requires the use of a criterion of "closeness". If the cell is to be assigned to the most probable terrain class, the statistics of each class must be known.

As far as is known, there have been two approaches for the determination of spatial signatures. One of these is to employ well known mathematical functions as components of the feature vector, such as the variance of the cell numbers, and decide later by the results of the recognition whether these mathematical functions are reliable indicators of terrain type. The results of this approach have not been very satisfactory.

The other approach consists of examining the Fourier transforms of cells and identifying patterns which are unique to each terrain type. This is the approach followed in this investigation.

DIFFRACTION PATTERN ANALYSIS

In the ERTS-1 images, the terrain types that one would like to recognize consist of:

Mountains	Clouds	Rivers
Desert or range	Urban areas	Bodies of water
Cultivated land	Hills	Transportation networks

The Fourier transform of an image is a convenient means to isolate and extract spatial signatures. Terrain signatures in the ERTS images can be efficiently analyzed using the Fourier transforming properties of lenses.

The red band (MSS 5) images were selected because they carry more spatial information than the images in the other bands.

The Fraunhofer diffraction pattern of an image is related to its Fourier transform. It is well known that[1], if a transparency is introduced into the front focal plane of a lens and illuminated by a coherent plane parallel beam, the lens will form an image at its back focal plane which is the diffraction pattern of the image. The diffraction pattern has been employed[2] because it is easy to form and has the same general structure as the Fourier transform.

---

[1] Goodman, J. W., Introduction to Fourier Optics, McGraw-Hill Book Co., Inc., New York (1968), p. 86.

[2] Gramenopoulos, N. and Corbett, F., "Diffraction Pattern Analysis of ERTS-1 Images," Technical Report of ERTS-1 investigation.

To obtain diffraction patterns of small portions of ERTS-1 images, a special optical bench is employed. For large size diffraction patterns, a long focal length lens (48 inches long) is being used. The 9-1/2 inch transparencies supplied by NDPF were reduced to a scale of 1:3,000,000 and developed to a gamma of two. The image area whose diffraction was obtained was limited by a circular aperture 2 mm in diameter. (See Figure 1.)

The diffraction patterns have some artifacts not related to the terrain images. To eliminate or suppress artifacts in the diffraction patterns, a mask is employed when photographing the diffraction patterns. The mask is itself the photograph of the diffraction pattern of an image area (from ERTS images) with no detail, such as areas of water from lakes or the ocean. The masks have been used with very good results. They have suppressed artifacts and eliminated overexposure of low spatial frequency components by the central order (See Figure 2.).

Figures 3 and 4 contain sample diffraction patterns from selected areas of ERTS images. The rings in the diffraction patterns are due to the circular aperture employed to limit the image area being transformed. Analysis of the diffraction patterns of the various terrain types has produced the following results:

1. The diffraction patterns of mountains show clusters of intensity at low spatial frequencies and diffracted light spreading in wedge-shaped patterns (fans) away from the center.

2. For cultivated land, a signature consisting of orthogonal rows of frequency spots has been identified. For some images, the signature may be weak in relation to other components of the diffraction pattern.

3. For urban areas, a signature consisting of orthogonal rows of frequency spots has been identified. This signature becomes evident only in the IR-2 image and cannot be confused with the signature for cultivated land, which is detected in the red band (0.6 to 0.7 micrometer).

4. Bodies of water have diffraction patterns with very low energy at frequencies other than the central lobe. Water can be identified by low reflectances in nearly all spectral bands and, therefore, the use of a spatial signature is usually redundant.

5. Deserts also have diffraction patterns with low energy levels of light diffracted at most frequencies other than the central lobe and very low frequencies.

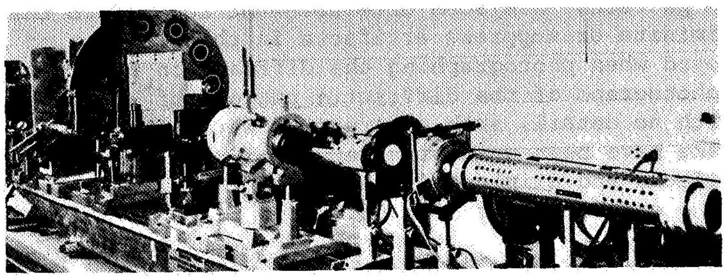

Power spectrum optical bench

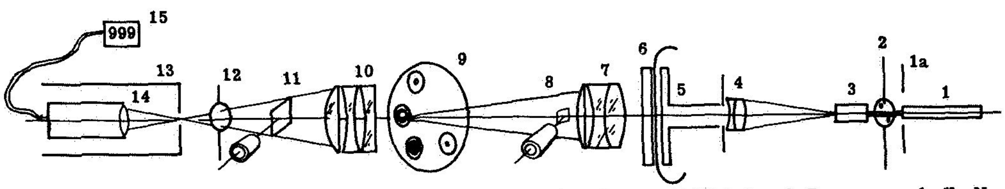

15 Digital readout

13 PM tube casing
14 PM tube

11 Alignment microscope
12 Aperture and baffle

9 Fourier plane filter assembly
10 Collecting lens

7 Transform lens
8 Alignment microscope

5 Pinhole
6 Target plane (film holder)

3 Beam diverger and spatial filter
4 Collimator

1 He-Ne laser
2 ND filter wheel
1a Electronic shutter

Diagram of power spectrum apparatus

Figure 1. Coherent optical bench

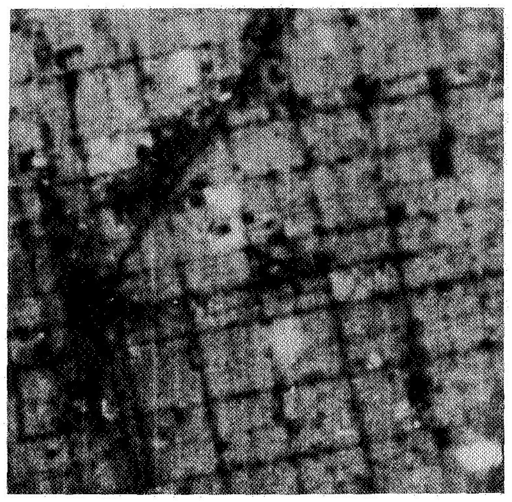

Phoenix, Arizona

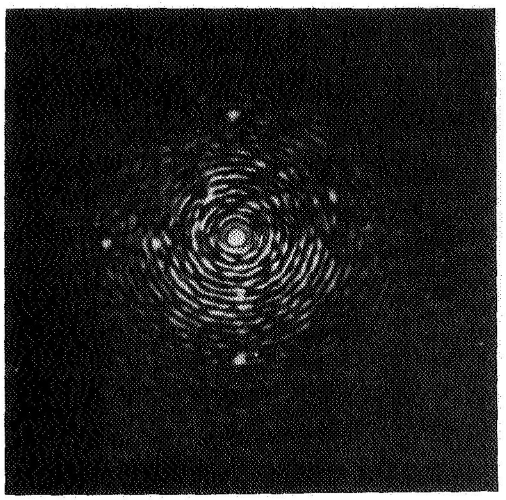

Diffraction pattern with mask

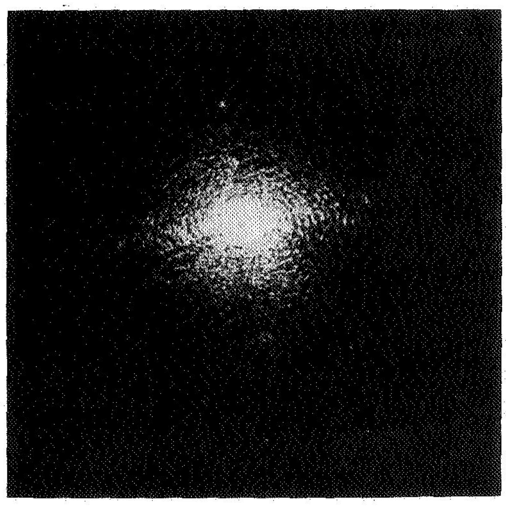

Diffraction pattern without mask

Figure 2. Phoenix, Arizona.
Two diffraction patterns from same area:
one with a spatial filter, one without

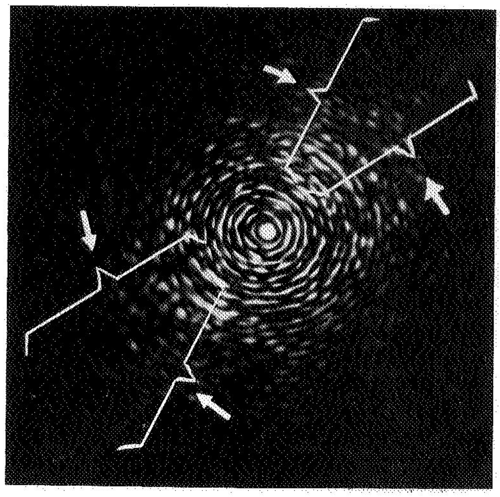

Mountainous

Urban

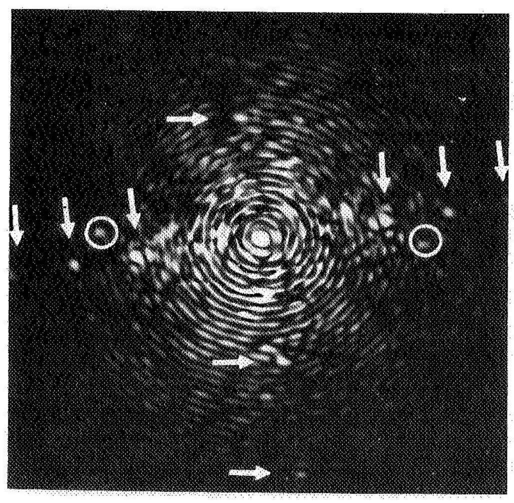

Cultivated

Spots due to fields

Spots due to scan lines

Figure 3. Salton Sea, California.
Diffraction patterns from ERTS-1, image 1070-17495-5

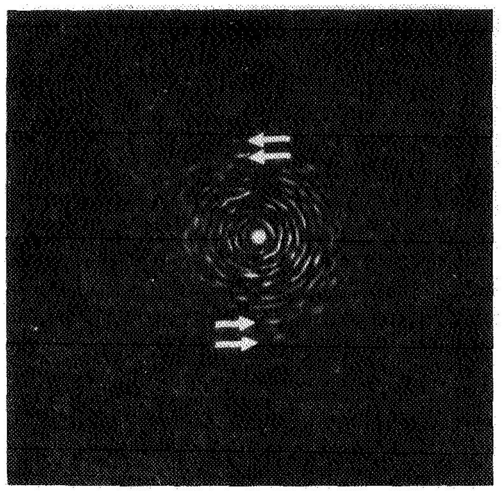

Urban

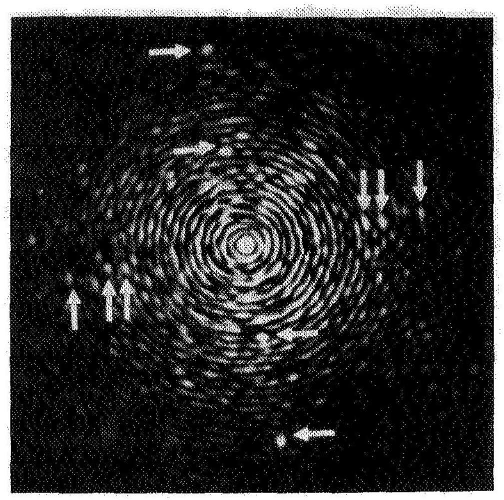

Urban

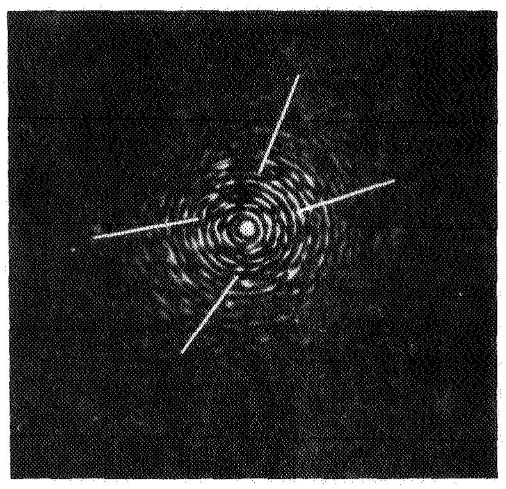

Mountainous

Figure 4. Great Salt Lake, Utah.
Diffraction patterns from ERTS-1, image 1015-17415-7

DIGITAL SPATIAL FEATURES

The digital Fourier transforms of cells representing four types of terrain were computed and are shown in Figure 5. These transforms resemble closely the diffraction patterns of the previous section.

The horizontal direction coincides with the scanning direction of the multispectral scanner. The frequencies represented by the squares vary from 0.39 to 5.9 cycles per kilometer.

Extensive analysis of the Fourier transforms has produced the following results:

1. It appears that frequencies larger than 3.5 cycles/km contain the information needed to discriminate between the terrain types. Frequencies less than 3.5 cycles/km carry significantly less information.
2. Regardless of terrain type, there is significant energy along the vertical frequency ($f_x = 0$, f_y) where x is the horizontal direction and y the vertical. In addition, this column has local peaks at the frequencies $f_y = 2.1$, 4.2 and 6.3 cycles/km. These appear to be due to detector noise from the multispectral scanner. It is necessary to filter out this vertical column to prevent the occurrence of errors in the measurements of spatial feature components.

Four spatial feature components are obtained by measuring the Fourier transform energy in four sectors defined as follows:

1. All frequencies less than 3.5 cycles/km and larger than 5.9 cycles/km are eliminated.
2. In the remaining Fourier transform, the largest peak (or maximum) is determined.
3. The energy in a sector which is $\pi/8$ radians wide and centered on the largest peak is determined. The energy within this sector (S_1) is one of the features.
4. The energies in similar size sectors which are displaced from the first one by $\pi/4$, $\pi/2$ and $3\pi/4$ radians in a clockwise direction are also determined and constitute the features S_2, S_3 and S_4, respectively. (See Figure 6.)

Other spatial features that have been employed are a number representing a count of high derivative values within the cell and numbers obtained from the histogram of the cell pixels.

TERRAIN TYPE RECOGNITION

An algorithm was developed by examining the feature vectors of cells of the same class. Then, the vector space was divided by thresholds forming hyperplanes. The algorithm was then employed to classify the cells from

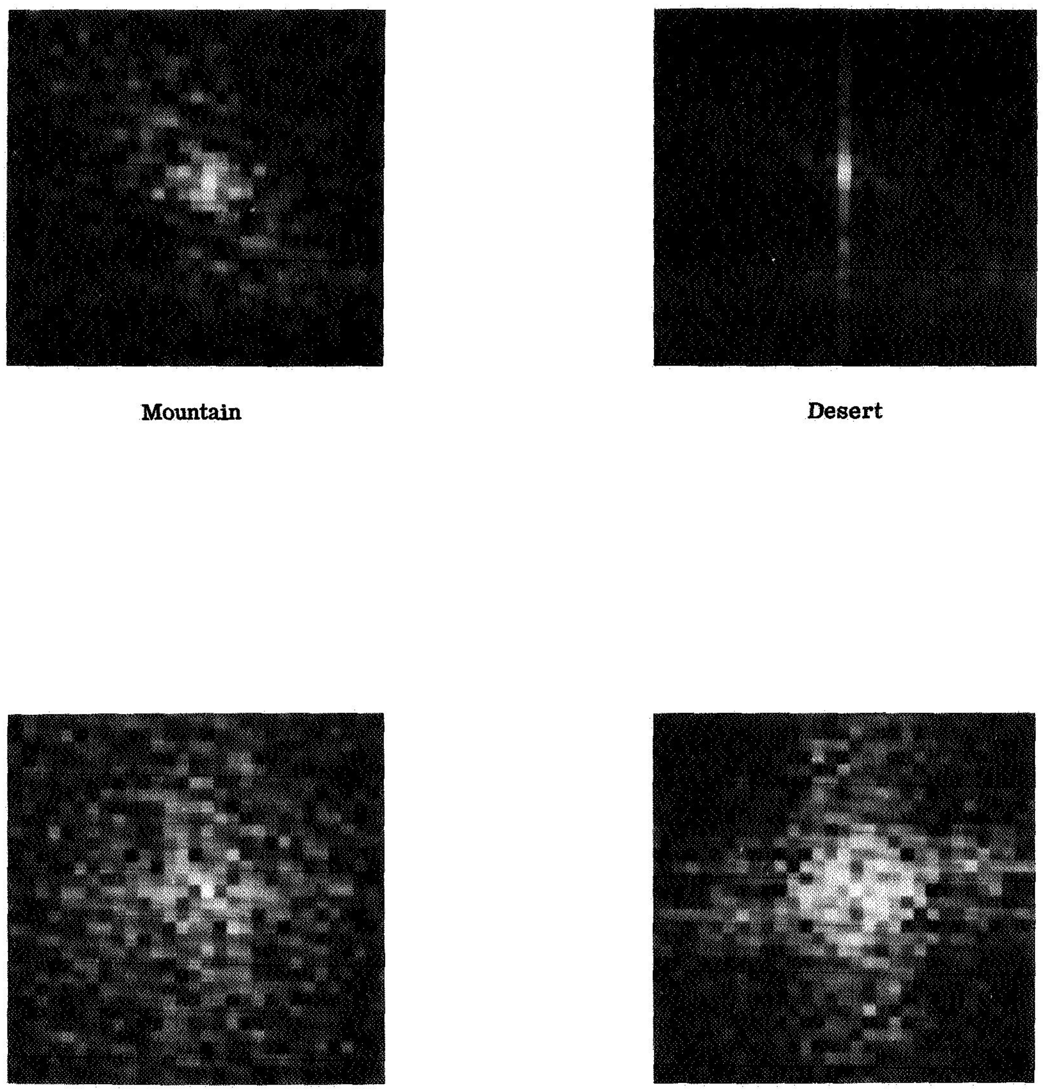

Mountain Desert

City Farms

Figure 5. Digital Fourier transforms of cells

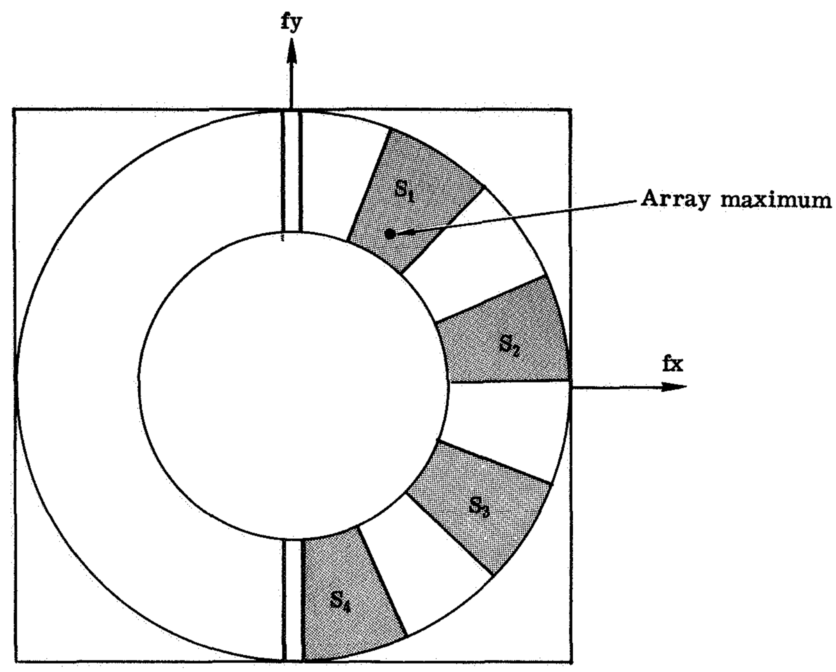

Figure 6. Fourier Transform Integration Regions

a portion of ERTS-1 image no. 1049-17324-5 containing Phoenix, Arizona and the surrounding area in southern Arizona (about 8,000 square km). The thresholds in the algorithm were then adjusted until the recognition results were optimized.

In order to determine the accuracy of the heuristic algorithm, two assignment matrices of cells were developed by photointerpretation. One matrix represents assignments using only the ERTS-1 red band image 1049-17324-5. The other matrix represents assignments using all available information (maps, aerial photography, and a land-use map*). Comparing these two matrices, one finds that the first one has about 2.5% errors, which indicates the error rate of a photointerpreter if he were to use only the red band ERTS-1 image. Most of the errors are due to isolated urban areas near cultivated land, mountains, or desert.

The computer classification matrix was compared to the most accurate photointerpreter matrix. The results are tabulated in Table 1.

The recognition results of most terrain types were very good: 97% for desert, 89% for farms, 80% for mountains, 74% for urban areas, 98% for clouds, 100% for water, 81% for cloud shadows. Only river flood plains which are peculiar geographic features of southern Arizona were recognized poorly (11%).[3] The accuracy of recognition was determined by comparison to existing maps, high altitude (U-2 missions in September and December 1971) and low-altitude aerial photography (mission 212 of the Earth Resources Aircraft Program, from the Johnson Spacecraft Center in Houston, Texas). The accuracy of the cloud recognition was determined by photointerpretation of the ERTS image since the aerial photography was obtained on different dates.

INTEGRATION OF SPECTRAL AND SPATIAL FEATURES

Integration of spectral and spatial features is required in order to exploit the information available in the ERTS-1 imagery. It is also desirable to employ a general recognition algorithm which is independent of the data characteristics. The maximum likelihood criterion[4] which has produced good results with multispectral data has been selected. This criterion requires training data and is optimum only when the terrain

---

*Poulton, C.E., Schrumpf, B.J., Johnson, J.R., "Ecological Resource Analysis from High-Flight Photography for Land Use Planning", Applied Remote Sensing of Earth Resources in Arizona, Proceedings 2nd ARETS Symposium, University of Arizona, November 2-4, 1971.

[3]Gramenopoulos, N., "Terrain Type Recognition Using ERTS-1 MSS Images", NASA SP-327 Symposium on Significant Results Obtained from Earth Resources Technology Satellite-1, March 5-9, 1973.

[4]Marill, T., Green, D.M., "Statistical Recognition Functions and the Design of Pattern Recognizers, IRE Transactions of Electronic Computers, December 1969, p. 472.

TABLE 1. COMPARISON OF CLASSIFICATION RESULTS*

PHOTOINTERPRETER'S ASSIGNMENT

	CLASS	1	2	3	4	5	6	7	8	TOTAL
COMPUTER ASSIGNMENT	0	0	0	3	15	22	6	14	0	60
	1	61	0	0	0	0	0	0	1	62
	2	0	2	0	1	0	0	0	1	4
	3	1	0	417	6	7	8	5	0	444
	4	0	0	3	248	1	9	2	1	264
	5	0	0	5	3	131	2	4	0	145
	6	0	0	1	5	3	71	8	0	88
	7	0	0	1	0	0	0	4	0	5
	8	0	0	0	0	0	0	0	13	13
TOTAL		62	2	430	278	164	96	37	16	1085

Class Identification

0 = Unidentified   4 = Farms
1 = Clouds   5 = Mountains
2 = Water   6 = Urban
3 = Desert   7 = Riverbed
8 = Cloud Shadows

*Heuristic algorithm using spatial features only.

classes form multivariate Gaussian distributions in feature space. In addition, no class is allowed to have a feature vector component which is always zero.

The four spatial features described above were combined with three spectral features to form a seven dimensional vector describing each cell. Using image 1049-17324 as training data, the statistics (co-variance matrices) for desert, farm, mountains and urban areas were computed. Then, using the statistics, the same input data and the maximum likelihood criterion, the cells were reclassified in one of the four categories. The recognition accuracy was 54% for desert, 92% for farms, 97% for mountains, and 92% for cities. Desert was poorly recognized (many desert cells were assigned to the mountain category), and it was suspected that the statistics for the classes were not Gaussian. Analysis of histograms of the classes showed that no component of any class was even approximately Gaussian. All components were positive with small means and large standard deviations. (See Figures 7 and 8.)

NON-LINEAR TRANSFORMATIONS OF THE FEATURE SPACE

Non-linear transformations applied to the feature space change the statistics of the classes. A different transformation is required for each feature component. The transformations must be such that large component values are reduced while small values remain unchanged. (See Figure 9.) Known transformations of this type are the logarithms on various bases such as the natural logarithm or powers less than unity such as the square or third roots. If a logarithmic transformation is selected, the base of the logarithm is adjusted for each feature component so that the class distributions in this component become symmetrical about their means. Similarly, if a power transformation is employed, the power is adjusted for each component so that the class distributions in this component become symmetrical about their means. For example, if the power is 0.5 for all components, then each component of every feature vector is replaced by its square root.

Both logarithmic and power transformations were extensively analyzed. The logarithmic transformations gave good results, but the resultant distributions were sensitive to amplitude variations in the data. In other words, if the logarithm on a certain base is used for one component (for example, the MSS 7 band) the distribution for each class may or may not approximate the Gaussian depending on solar illumination which changes the range of values obtained in this band.

Finally, the non-linear transformations selected are all powers less than 1. For image 1049-17324, the powers for the various components range from 0.8 to 0.025 and have been optimized to produce excellent recognition results in all four classes: desert 89%, farms 97%, mountains, 96%, and cities 95%. In arriving at an optimum transformation for each component, Gaussian distributions cannot be achieved for all classes. In other words, as one adjusts the transformation of say the MSS 5 band, the desert distribution may become more Gaussian while the city distribution may become less Gaussian. There is no reason to believe that all distributions can always be made Gaussian in all components by appropriate transformations. To reduce the possibility of such problems and maintain high recognition rates, the number of different classes should be kept small. (See Figures 10 and 11.)

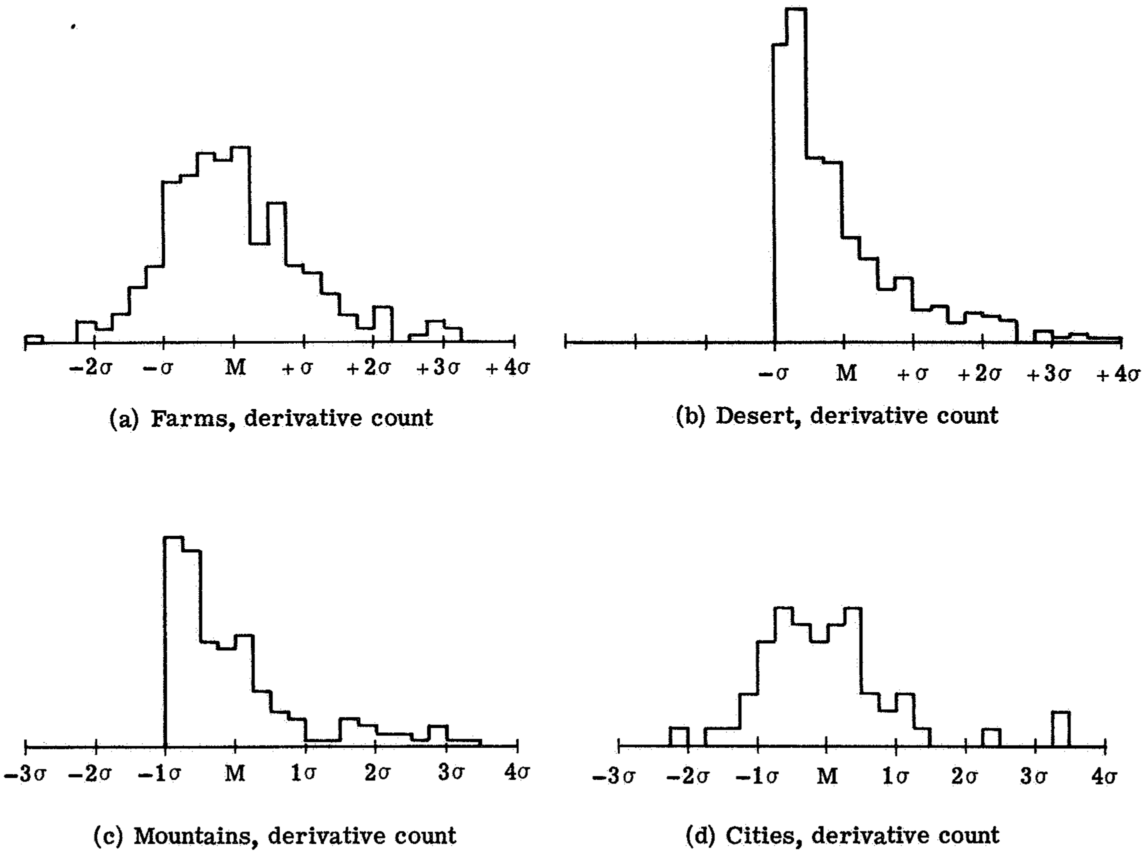

Figure 7. Histograms of Terrain Classes in One Component (in units of standard deviations about the means)

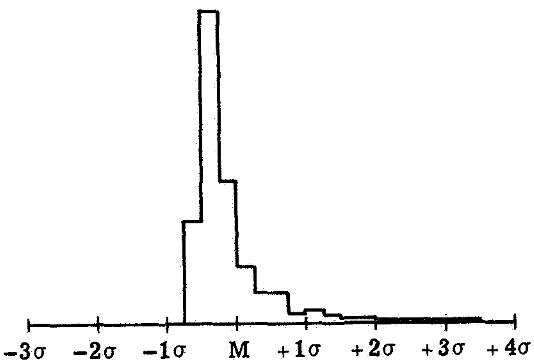

(a) Desert, Y_1 spatial component

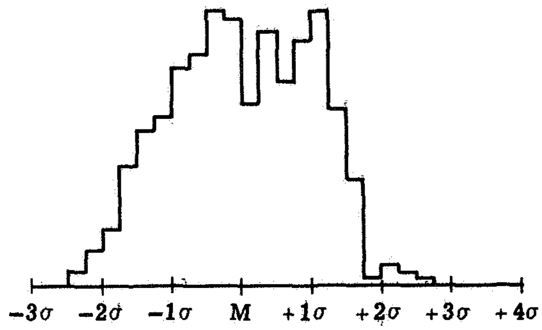

(b) Desert, MSS 7

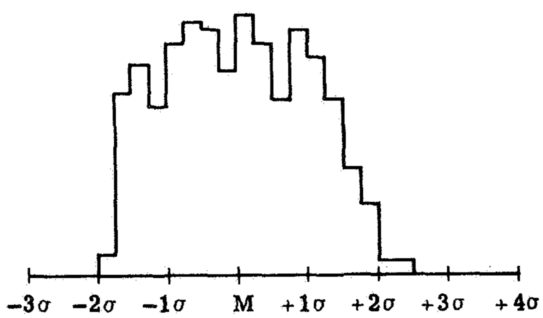

(c) Desert, MSS 5

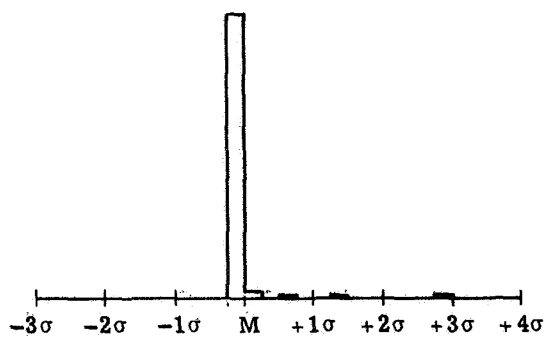

(d) Desert, Y_2 spatial component

Figure 8. Histograms of Desert Distributions in Four Components (in units of standard deviations about the means)

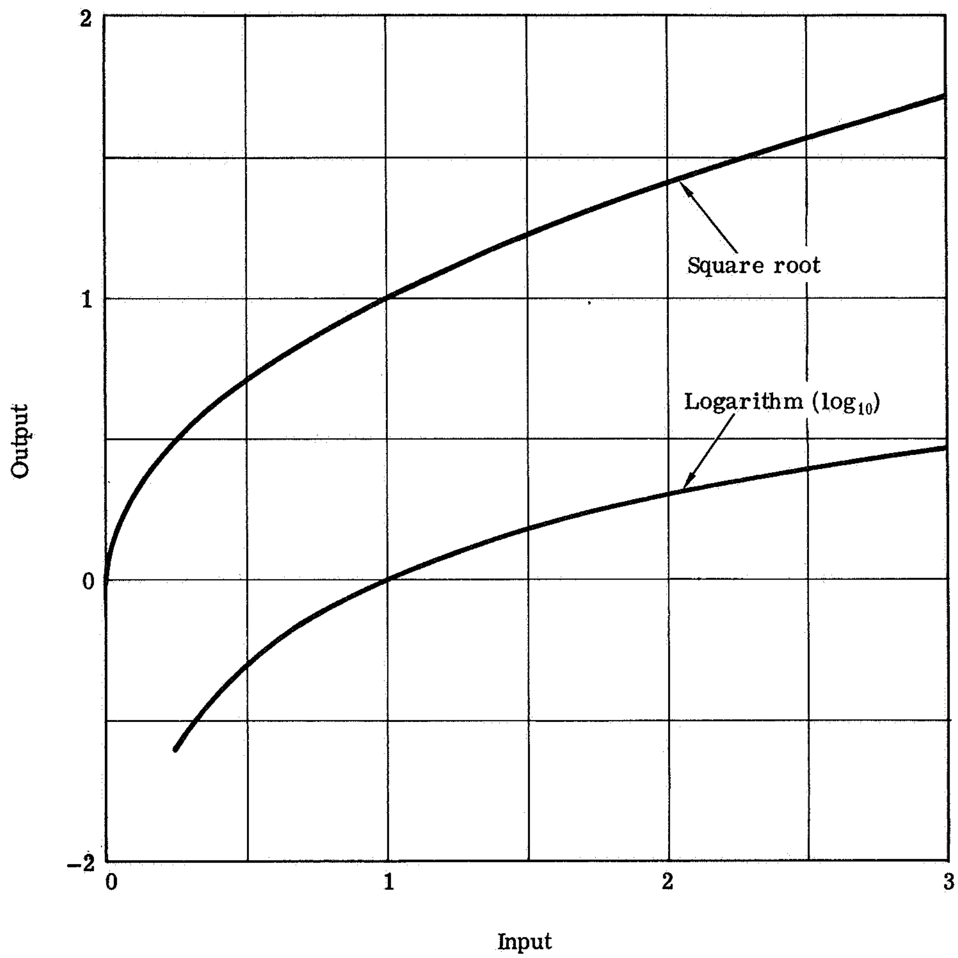

Figure 9. Typical Non-Linear Transformations

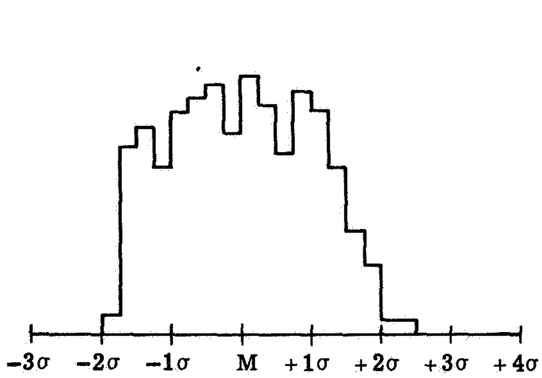

(a) Desert, MSS 5′

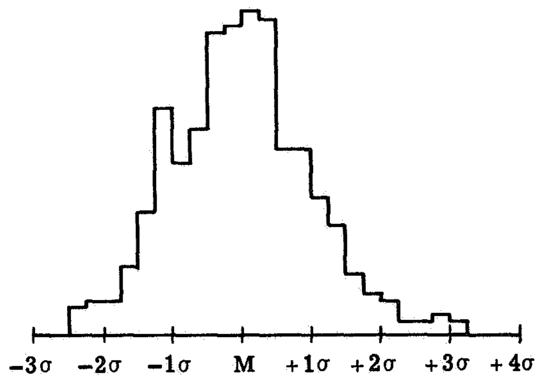

(b) Desert, Y_1'

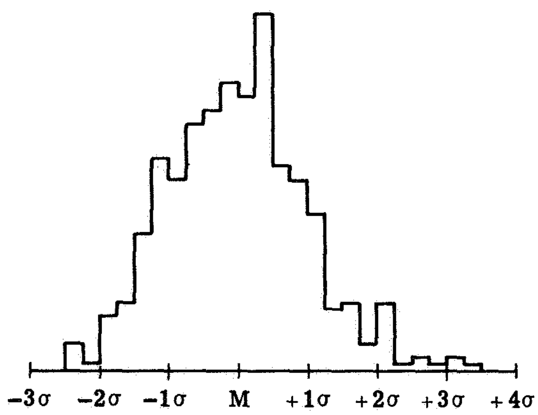

(c) Desert, Y_2'

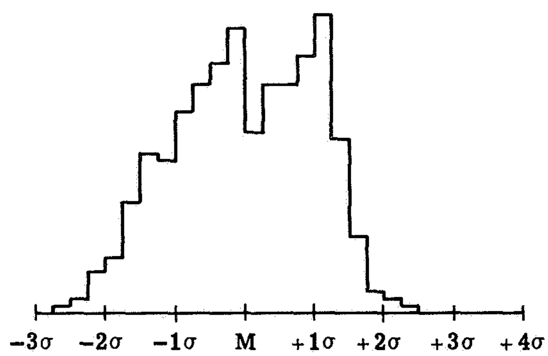

(d) Desert, MSS 7′

Figure 10. Histograms of Desert Distributions
After Non-Linear Transformations, Compare to Figure 8.

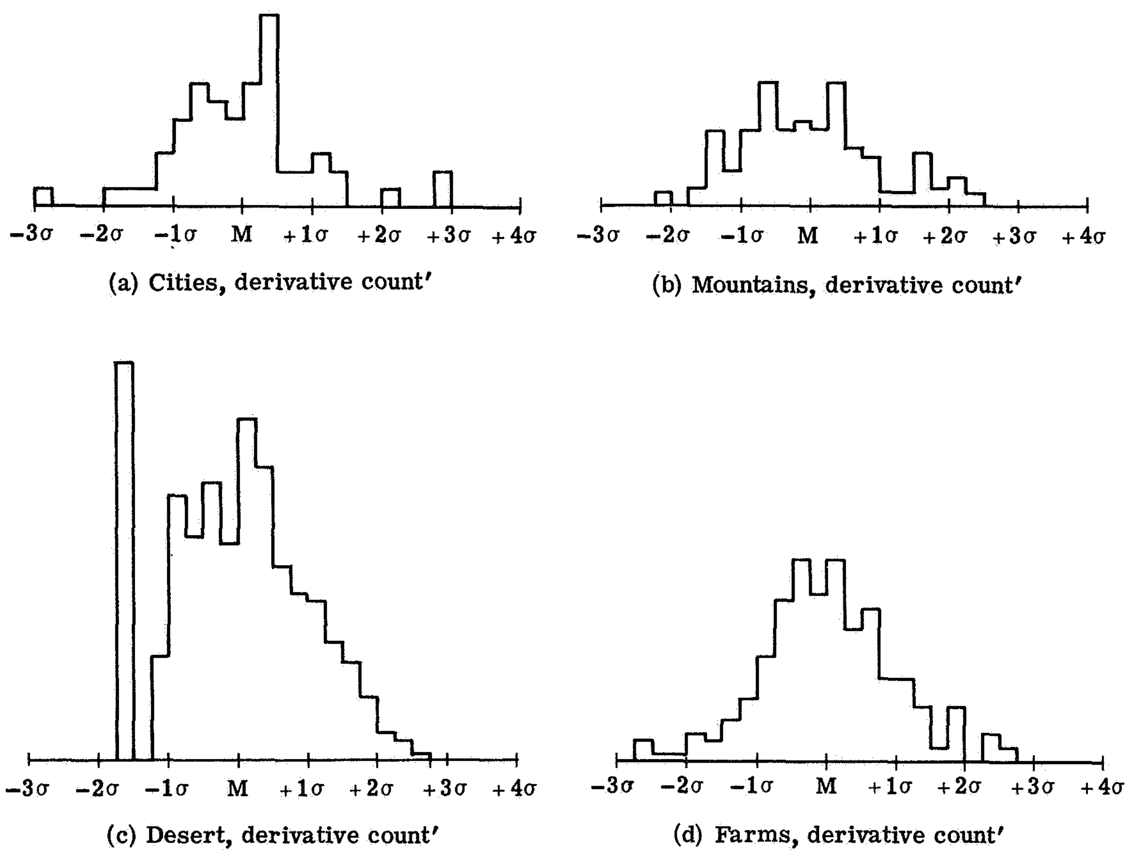

Figure 11. Histograms of Class Distributions
After Non-Linear Transformations, Compare to Figure 7.

Also, the importance of each component in the recognition of each class is not the same. A component may be essential for recognizing one class and relatively unimportant for recognizing other classes. Knowledge of this can be taken advantage of when selecting a transformation for a component. The transformation is adjusted so that a symmetrical distribution is obtained for the class that the component is most important. The effectiveness of each transformation can be judged from the recognition rates achieved.

VARIATIONS IN CLASS STATISTICS

An important question that arises is the variability of the terrain class statistics with time of year and geographic location. If the statistics vary substantially, one must have statistics for each image to be processed. On the other hand, it would be desirable to have one set of statistics stored that would be applicable to a large geographic area for imagery acquired at any time of the year.

To explore this possibility, data from ERTS-1 images 1031-17325 and 1103-17332 were subjected to terrain classification using the statistics developed from training data of ERTS-1 image 1049-17324. The data from all three images cover the same general area around Phoenix, Arizona. The dates of acquisition are August 23, 1972, November 3, 1972, and September 10, 1972, respectively.

The data of image 1031-17325 was first subjected to the non-linear transformations described in the previous section and was then classified using the statistics from image 1049-17324. The recognition results are shown in Table 2. The detection rates for the four classes were: 93% for desert, 93% for mountains, 100% for farms, and 85% for urban areas. The accuracy of recognition of urban areas was not above 90% because many urban cells containing parks or golf courses were assigned to the farm category.

For image 1103-17332, it was noted that the average brightness in all bands was substantially reduced due to lower solar elevations during the month of November. It was felt that the data should be compensated for the change in solar elevation. The average feature space vectors were determined for images 1049-17324 and 1103-17332. Then, the vectors of image 1103-17332 were linearly scaled so that the average vectors for both images would be the same. This compensation assumes that the change in statistics between September and November is simply a change in scale of the feature space. The compensation applied was only an approximation. Then, the compensated data was subjected to the non-linear transformations described in the previous section and was afterwards classified using the statistics from image 1049-17324. The recognition results are shown in Table 3. The detection rates were as follows: 95% for desert, 100% for farms, 78% for mountains, and 49% for urban areas. It is obvious that the statistics employed were not optimum for image 1103-17332 despite the simple compensation applied to the feature space. Some mountain and urban areas were assigned to the desert and farm categories. Figure 12 shows the ERTS image number 1103-17332 with the recognition results superimposed as annotation.

Table 4 summarizes the recognition results for the maximum likelihood criterion and the heuristic algorithm. This table provides a comparison of detection rates for various sets of data and features being employed:

Table 2. Comparison of Classification Results - ERTS-1 Image 1031-17325

Photointerpreter

	CLASS	1	2	3	4	5
Computer	1	429	0	6	0	6
	2	1	407	0	10	7
	3	31	0	114	0	1
	4	1	1	3	57	11
	TOTAL	462	408	123	67	25

Table 3. Comparison of Classification Results - ERTS-1 Image 1103-17332

Photointerpreter

	CLASS	1	2	3	4	5
Computer	1	448	1	14	13	2
	2	17	443	7	6	31
	3	6	0	74	2	1
	4	0	0	0	20	0
	TOTAL	471	444	95	41	34

1 = Desert
2 = Farms
3 = Mountains
4 = Urban
5 = Riverbeds

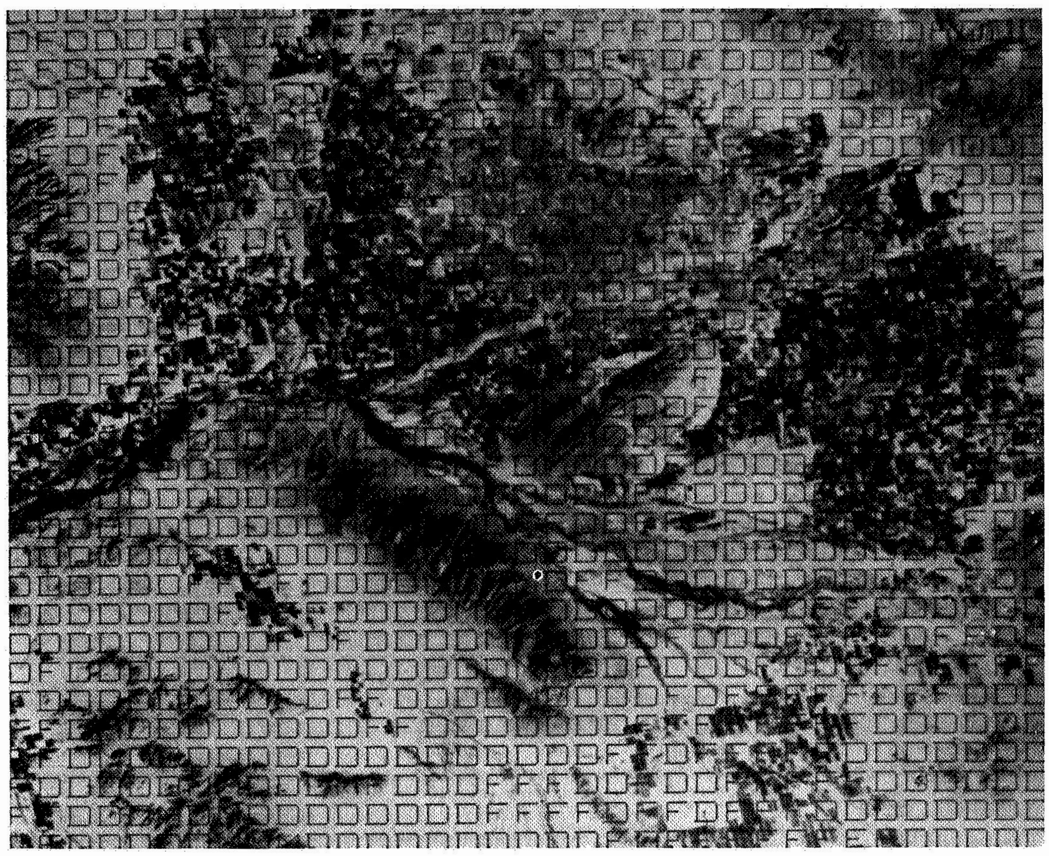

Figure 12. ERTS-1 Image No. 1103-17332-5
Annotated with Terrain Classification Results

D = Desert M = Mountains
F = Farms U = Urban

Table 4. Comparison of Detection Rates (%) with the Maximum Likelihood Criterion

Processing Conditions	Desert	Farms	Mountains	Urban Areas
1049-17324: 3 spectral features only	87	93	96	86
1049-17324: 4 spatial features only	8	83	97	70
1049-17324: Combined 7-dimensional feature vectors	54	92	97	92
1049-17324: Transformed 7-dimensional feature vectors	89	97	96	95
1031-17325: Transformed, 1049 statistics	93	100	93	85
1103-17332: Compensated to solar elevation and transformed 1049 statistics	95	100	78	49
1049-17324: Spatial features only, heuristic algorithm	97	89	80	74

a. Data from ERTS-1 image 1049-17324 was used. The feature vectors were three-dimensional, and the features were the average cell brightness in the MSS 4, 5 and 7 spectral bands. The same vectors were used as training data to compute the class statistics and were then classified by the maximum likelihood criterion. The recognition results are what one could expect when using the maximum likelihood criterion in multispectral recognition.

b. Data from ERTS-1 image 1049-17324 was used. The feature vectors were four-dimensional with spatial features only. All other conditions were as in case a., above.

c. The spatial and spectral features of cases b. and a., respectively, were combined to form seven-dimensional vectors. All other conditions were as in case a., above.

d. The vectors of case c. were non-linearly transformed. Then, the class statistics were computed from them, and they were subsequently classified by the maximum likelihood criterion.

e. The data was seven-dimensional vectors from ERTS-1 image 1031-17325. The vectors had been non-linearly transformed as in case d. The class statistics employed were from case d. (ERTS-1 image 1049-17324.)

f. The data was seven-dimensional vectors from ERTS-1 image 1103-17332. The vectors were scaled so that the average vectors for images 1049-17324 and 1103-17332 were equal. This was an approximate scheme for compensating the lower solar elevation for image 1103. All other processing operations were the same as in case e.

g. The data was from ERTS-1 image 1049-17324 processed using only spatial features and the heuristic algorithms.

Case b. shows that the maximum likelihood criterion gives poor results with spatial features for the desert class. This has been attributed to the wide deviation of the spatial features from Gaussian statistics. (See Figure 8.) This conclusion is supported by case g. which shows very good results when the spatial features are used with the heuristic algorithm rather than the maximum likelihood criterion.

Case a. shows good results using the spectral features with the maximum likelihood criterion. The reason is that the class distributions for these features, though not Gaussian, do not deviate as sharply as the class distributions for the spatial features. This is fortuitous because there has been very extensive use of the maximum likelihood criterion with multispectral data.

Cases c. and d. show that by combining the spectral with the spatial features, the recognition rates for urban areas have improved substantially. Comparing case d. to cases b. and c. shows the importance of the non-linear

transformations in achieving high recognition rates. Also, comparing case d. to cases a. and g. further indicates that combining the spectral and spatial features improves the recognition rate of the urban areas significantly.

For cases e. and f., the recognition rates for desert and farms has improved over the corresponding recognition rates of case d. However, for mountains and urban areas, the recognition rates have progressively deteriorated. It appears, therefore, that the statistics of some classes in a given geographic area vary substantially with the seasons.

From the results of cases a. through g., it appears that the spatial features have not increased the number of classes that are recognized over what can be achieved with multispectral data only. However, the addition of the spatial features has increased the accuracy of recognition significantly for the urban class.

There seems to be redundancy between the spectral and spatial features, particularly for the desert and farm classes. This, of course, is a characteristic of the geographic area and the ground resolved distance of the ERTS-1 data. For example, the spectral features are actually identifying live, dense vegetation rather than farms. In this part of sourthern Arizona, such vegetation is associated with irrigated farmland. In another part of the country, it may be associated with deciduous forests, grassland, etc. On the other hand, the spatial features are identifying farms, whether the farms have live vegetation (growing crops) or are fallow.

Furthermore, the ground resolved distance of the ERTS-1 data is large and only large geographic features (bays, lakes, mountains, farmland, desert, forests, large urban areas, etc.) can be identified. These tend to be highly correlated spectrally and spatially.

CLUSTERING ALGORITHM

Figure 13 shows a block diagram of the clustering algorithm that has been developed. In the first subroutine (Distance Computation) the Euclidean distances between vectors are computed and vectors whose relative distances are smaller than a threshold, are retained and introduced into the next subroutine (Selection of Cluster Centers). Initial cluster centers are formed from the set of selected vectors and are required to satisfy certain criteria. In the next subroutine (Combine Clusters by Divergence), initial cluster centers are compared to each other for statistical separability by applying the divergence criterion. Diffuse cluster centers whose divergences from other clusters do not exceed a set limit are usually mixed clusters and are eliminated. In the following subroutine, a decision is made on whether to recycle the cluster center generation. The decision is based on the number of vectors clustered and the number of separable cluster centers that have been produced already.

When the cluster center generation is terminated, the remaining vectors (non-clustered) are assigned to the cluster centers by the maximum likelihood criterion. As the assignment continues, the clusters grow and their statistics change. Therefore, the assignment is done in several stages by first assigning vectors located close to the cluster centers.

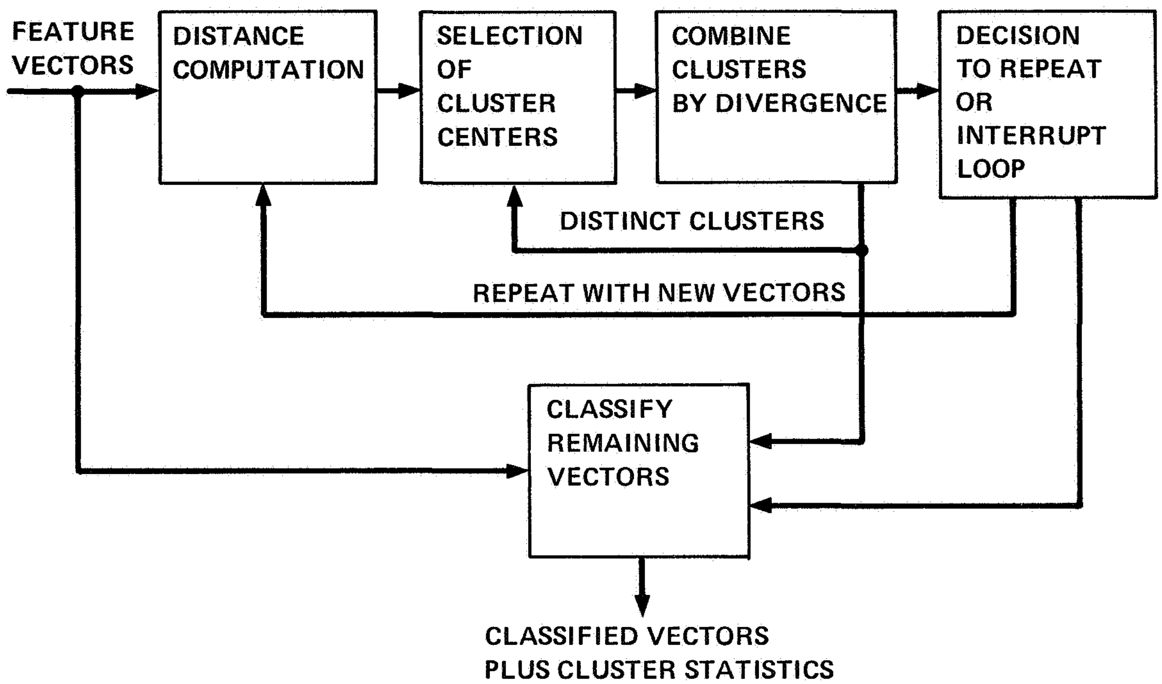

Figure 13. Block Diagram of Clustering Algorithm

The clustering algorithm operates on the basis of a number of assumptions which have been reduced to a minimum, but cannot be eliminated. These assumptions are:

a. An assumption must be made about the cluster statistics. In this case, it has been assumed that the cluster statistics are Gaussian, and therefore, non-linear transformations of the feature vectors are required.

b. Initially, the algorithm assumes that cluster centers are spherical and applies the Euclidean distance criterion.

c. The algorithm finds cluster centers on the basis of local vector densities. Therefore, it is important that equal numbers (approximately) of vectors from each class are being clustered.

The clustering algorithm has been applied to vectors from several ERTS-1 images. We have found that the formation of the cluster centers is the crucial part of the algorithm and it is affected by the relative amplitudes of the vector components (due to the Euclidean distance criterion). It is also very important to introduce about equal numbers of vectors for each terrain class. This is being accomplished by selecting the vectors which are employed by the algorithms to form the cluster centers. A human looks at an ERTS color composite and selects equal size (as far as possible) areas that appear homogeneous. The vectors from these areas form the subset from which the algorithm develops the cluster centers. Consider an image consisting of 70% mountains, 20% farmland and 10% urban. If all the vectors are used for the cluster center formation, then it is quite likely that the urban area would be absorbed in the mountain class. If, however, the vectors used for cluster center formation represent 25% mountains, 20% farmland and 10% urban areas, then the cluster centers will probably be formed correctly. No training data or a priori knowledge of the geographical region is required. The human interacts with the algorithm, but does not bias the algorithm's decisions.

Tables 5 and 6 summarize the results of the clustering algorithm operating on images 1103-17332 from Phoenix, Arizona and 1070-17495 from the Imperial Valley, California. For either image, the clusters are identified by non-zero numbers in the sequence of their formation. Some vectors could not be assigned to any cluster with a high degree of confidence and were left in the zero category. Most of these vectors represented cells containing boundaries between terrain classes. The detection rates for the various terrain classes are also shown in Tables 5 and 6. For image 1103-17332, the detection rates should be compared to the appropriate entry in Table 4.

For image 1070-17495, the clustering algorithm had some surprising results. It produced two water classes and three desert classes. Photointerpretation of ERTS-1 color composites suggests only one water and one desert class.

Table 5. Comparison of Clustering Results - ERTS-1 Image 1103-17332

Photointerpreter

Computer	B	U	D	F	M	R
0	84	10	3	1	20	41
1	3	72	2	3	9	21
2	0	0	339	0	1	1
3	1	0	0	279	3	3
4	3	9	0	0	168	4

Detection Rates, %

Urban	79
Desert	99
Farms	99
Mountains	84

B = Boundaries
U = Urban
D = Desert
F = Farms
M = Mountains and Hills
R = Riverbeds

Table 6. Comparison of Clustering Results - ERTS-1 Image 1070-17495

Photointerpreter

Computer	B	W1	D1	F1	M	D2	W2	D3	F2	U
0	53	0	0	25	5	1	3	0	14	5
1	0	26	0	0	0	0	0	0	0	0
2	0	0	89	0	0	0	0	0	0	0
3	15	0	0	129	4	0	0	0	0	6
4	2	0	0	0	116	0	0	0	0	0
5	0	0	0	0	0	220	0	0	0	0
6	0	0	0	0	0	0	33	0	0	0
7	0	0	0	0	0	0	0	25	0	0
8	4	0	0	5	0	0	0	0	252	0

Detection Rates, %

W1	100
W2	92
D1	100
D2	100
D3	100
M	93
F1	81
F2	95

B = Boundaries
W1 = Clear Water
W2 = Turpid Water
D1 = Bright Smooth Desert
D2 = Bright Rough Desert
D3 = Dark Desert
M = Hills and Mountains
U = Urban
F1 = Irregular Farms
F2 = Rectangular Farms

CONCLUSIONS

Through the developed algorithms, it is possible to automatically recognize terrain types. By using the maximum likelihood criterion, it is possible to achieve high accuracy in the recognition process.

When the correct statistics are employed, the machine recognition appears to be more accurate than a human photointerpreter who has been constrained to use ERTS-1 color composites only. Stated another way, machine recognition appears to be more sensitive and can operate much closer to the resolution limit of the ERTS-1 imagery than the human photointerpreter.

The experimental results show that the accuracy of terrain recognition is affected by the statistics employed. The accuracy is best when the statistics are approximately Gaussian, and it is necessary to apply non-linear transformations to the feature vectors to achieve approximately Gaussian distributions. The class statistics vary appreciably between seasons, such as summer and fall.

The experimental results also showed that combining the spectral data with the spatial features increased the accuracy of the machine recognition.

The clustering algorithm has produced excellent results and forms statistically separable clusters which reflect the scale and resolution of the ERTS-1 data. In some cases, it will produce more classes than photointerpretation of ERTS-1 color composites would suggest.

POTENTIAL APPLICATIONS

The results of this investigation are directly applicable to the automatic production of thematic maps, and in particular, of land-use maps. Anderson et al[5] have described three levels of land-use classification. The terrain classes recognized in this investigation using training data fall in the first classification level. The use of the clustering algorithm with combined spectral and spatial features can increase the number of classes recognized beyond the first level.

[5] Anderson, J.R., Hardy, E.E., Roach, J.T., "A Land-Use Classification System for Use with Remote-Sensor Data", Geological Survey Circular 671, 1972, Washington.

PRINCIPAL COMPONENTS COLOUR DISPLAY OF ERTS IMAGERY

M. M. Taylor, *Defense and Civil Institute of Environmental Medicine**, 1133 Sheppard Avenue West, P.O. Box 2000, Downsview, Ontario M3M 3B9*

ABSTRACT

Combinations of data from the four ERTS bands into colour images are usually made by selecting three bands and displaying each in a different primary colour (red, green, and blue). Because the data from the different bands are correlated, there is a tendency for the derived pictures to occupy only a small portion of the available colour space. In the most common combination, MSS bands 1 and 2, which are highly correlated, are displayed as blue and green respectively, and band 3 as red. This results in a picture which for most regions might as well have been printed in red and blue-green.

In the technique to be presented, colours are not derived from single bands, but rather from independent linear combinations of the bands. Using a simple model of the processing done by the visual system, three informationally independent linear combinations of the four ERTS bands are mapped onto the three visual colour dimensions of "brightness", "redness-greenness" and "blueness-yellowness". The technique permits user-specific transformations which enhance particular features, but this is not usually needed, since a single transformation provides a picture which conveys much of the information implicit in the ERTS data. Examples of experimental vector images with matched individual band images are shown.

INTRODUCTION

The four bands of the ERTS multispectral scanner system provide correlated images. The level of a given picture element (pixel) on one band can to some extent be predicted from the level of that same pixel on another band. The object of this note is to describe a technique of colour display which takes advantage of these correlations to present in a single colour picture essentially all the information sensed by the satellite.

The standard general-purpose colour display of ERTS imagery simulates infrared colour film. Three of the four sensor bands are selected and each presented as a different primary colour to provide a full-colour picture. Band 4 (green) is displayed in blue, Band 5 (red) in green, and Band 6 (nearest infra-red) in red. This ordinarily results in a

picture in which vegetation is represented as shades of red and brown, rock as grey, and water as bluish green. Few other colours appear to any great extent. In particular, few ERTS frames contain both a strong blue and a strong green region. The reason for this is that the data from Bands 4 and 5 are highly correlated. If they were perfectly correlated, there would be no point in printing them in different colours. A single image in the mixture colour, blue-green, would have the same effect. The small differences that do exist between bands 4 and 5 show up as minor variations from bluer to greener blue-green.

The present paper describes a quite different approach to the colour display of multi-spectral imagery. It is not restricted to ERTS data or to four-band imagery, but can be extended to airborne multi-band sensor systems. Rather than attempting to combine pictorially the information from the different bands, the information contained in the various bands is extracted in terms of several statistically uncorrelated images. These extracted images are then used as the basis of a colour display. The human visual system encodes spectral data into a three-dimensional structure, the dimensions being crudely described as "brightness", "red/green" and "blue/yellow". Three of the four independent images derived from the multi-spectral sensor data may be mapped onto these three visual dimensions to provide a colour picture which takes maximal advantage of the colour processing done by the eye.

There are four main stages in the construction of a colour picture by this technique. Firstly, the sensor data are calibrated and transformed to logarithmic values. Secondly, the eigenvectors and eigenvalues of an inter-sensor covariance matrix based on appropriate scenes are derived. Thirdly, a linear transformation to a basis derived from the scaled eigenvectors is applied to the data. At this stage different linear transformations may optionally be applied to bring out different features of the data, but these extra transformations should not ordinarily be required. Fourthly, three of the four dimensions of the transformed space are mapped onto the three dimensions of colour vision and an algorithm applied to determine the appropriate values for the primary colours (red, green, and blue) of which any display must be composed. Not all aspects of the system have yet been implemented in final form, and the examples to be shown result from early experimental versions.

METHODS

Simplified model of the visual system

The discussion which follows is based largely on Jameson (1972) and Vos and Walraven (1972).

The eye has three types of cone receptor, in addition to the rod receptors which are responsible for vision at low light levels. Rods participate very little in the perception of colour at higher light levels and will be ignored in the following. Each of the three types of cone has a fairly broad spectral response. While we may, for convenience, label these types as "blue", "green" and "red" respectively, these labels do not correctly indicate the peaks of their absorption characteristics or the fact that they are quite broadband absorbers. The 3-dB band for the "blue" receptor is approximately 400-490 nm, for the "green" 470-580 nm, and for the "red" 500-630 nm. The "green" and "red" absorption curves have an overlap of approximately 80%. The images given by those two types of cone therefore must usually be very similar, since the cones will be responding largely to the same spectral range.

The cone outputs are probably not linearly proportional to the energies they absorb. For one thing, the cones adapt to the prevailing light level, so that a particular output may correspond to very different energies depending on the recent history of that cone and of its neighbours. More particularly, though, at any particular state of adaptation, the output after initial processing is probably more nearly proportional to the logarithm of the energy impinging on the receptor, and this logarithmic output is the basic data for further processing operations.

A simplified model of the subsequent processing is shown in Fig. 1. The "red" and "green" outputs are summed and differenced, and their sum is summed and differenced with the "blue" output. The red-green sum the major component of the overall brightness signal. There are relatively few blue receptors, possible as few as 2% of the total, and their contribution to perceived brightness is commensurately small. The red-green difference determines the balance of long as opposed to medium wavelengths in the spectrum, since these are the wavelengths where the responses of the red receptors and the green receptors differ most strongly. When the red-green difference is zero, the signal is "yellow" and the percept is yellow or blue. This "yellow" signal must then be balanced against the signal from the blue receptors to determine the overall long vs. short wavelength balance. The blue signal, scaled appropriately, balances the "yellow" signal if the light is white. The result is that there are three essentially independent data channels, one indicating overall brightness, one indicating the red-green balance, and one indicating the blue-yellow balance. Because they are based on logarithms, these balance indicators are affected by the ratios of the energies in the different spectral bands, and hence do not respond to changes in overall illumination level. The three channels, "brightness", "red-green", and "blue-yellow" contain all the information available to the human perceiver about the colour of the world, and are essentially independent.

There have been many attempts to put a Euclidean or other metric onto these three basic colour dimensions. None have been entirely successful, but there are several useful approximations in the literature. If one is to use the three dimensional structure of colour vision effectively, one must be able to specify locations within some Euclidean approximation to the colour space in terms of the primary colours available. No satisfactory algorithm for the full three-dimensional Euclidean colour space as related to both the available primaries and the ERTS statistics has yet been produced, but one based on the space of MacAdam (1971) is being studied.

ERTS data processing

The four ERTS bands produce correlated imagery, just as do the three spectral bands of human vision. If the information contained in the four ERTS images could be conveyed in a space of three dimensions, it could be displayed in a single colour picture, without loss. The standard procedure, shown in Fig. 2, does not do this. The procedure we follow is (1) Compute the covariance matrix that relates the logarithms of the sensor outputs; (2) Find the eigenvectors of the covariance matrix and use them as a basis set for a new description of the data. In this basis, the data are uncorrelated in the four new dimensions, and the amount of data variance contributed by each dimension is given by the associated eigenvalue; (3) Scale the basis by dividing each dimension by the square root of the associated eigenvalue. This forces the variance on each dimension to be unity, and permits arbitrary rotation of the space without introducing covariance between the rotated basis dimensions; (4) Rotate the space in any arbitrary way, to suit particular needs; (5) Choose three dimensions of the resulting four-space for display and map them onto the three dimensions of colour space. This procedure is diagrammed in Fig. 3.

1. Computation of the covariance matrix presents an element of choice. The data that enter into this calculation determine the entire subsequent course of the procedure. In particular, it is desirable that the selection of pixels should be representative of the object types which must be discriminated in the final display. In a completely general purpose system, pixels should be selected at random from everything that the satellite sees. This would result in very good discrimination of clouds and ocean, since most of the earth's surface is covered by one or the other. Very little attention would be paid to urban areas. A slightly more special purpose system would be to sample randomly from frames which are largely cloud-free land. The system used here is still more specialized. Pixels are sampled randomly from frames that other users have requested because they were interested in something in the frame. This weighting technique is still quite general purpose, but what specialization there is follows the interests of the ERTS users. It would be quite feasible to start with the proposition that a display is to be made for foresters or for prairie farmers or for glaciologists, and select the data pixels from scenes of interest to the selected users. Different basis vectors would be derived from different choices.

A different kind of choice is involved in the decision to base the computation on the logarithms of the sensor values. The intent here is to go some way to removing the effect of changes in illumination on the relative spectral values. One alternative possibility would have been to scale all the values so that the sum of the four sensor elements was the same for each pixel. This approach would indeed remove the effects of changing illumination from the differences in the sensor values. It would also enforce a particular primary direction onto the derived space. While such a basic direction (brightness) might be useful, it is probably preferable to be able to leave the choice to a later stage of processing. Flexibility should be retained where possible. Hence the idea of removing the brightness component for separate processing is rejected, and the logarithmic data values are used.

The use of the logarithms of the data values poses a severe restriction on the allowable calibration error. If there is a small relative sensor offset, say 1 unit, it will make a large difference to the ratio between two sensors which read, say, 4 units. Such a small offset will not make much difference to the ratio if the sensors are reading 40 units. Hence the derived colours will change with overall level if there is an appreciable sensor offset. On the other hand, gain variation between sensors will result in a simple additive constant on the logarithm and have no change, independent of overall level.

2. The eigenvectors of the covariance matrix form a basis for a description space within which the covariance matrix is diagonal, having values which are the eigenvalues of the original covariance matrix. In other words, when the eigenvectors are used to describe the data, the resulting values are uncorrelated. This transformation is shown schematically in Fig. 4a-b in a two-dimensional reduction. Each transformed dimension may be treated independently of the others, and the information it carries is independent of the information carried by the others. Assuming that any noise or uncertainty in the measurement is distributed evenly and in an uncorrelated manner over the four sensors, then the information conveyed by a transformed dimension is proportional to half the log of the data variance on that dimension. The eigenvalues of the covariance matrix are these variances, and indicate the relative importance of the new basis dimensions.

3. When the eigenvector basis is scaled (Fig. 4b-c) by dividing each coordinate by the square root of the respective eigenvalue, the distribution that results has unit variance on each dimension. However, the noise distributions are no longer hyperspherical, but are ellipsoidal with axes proportional to the inverses of the associated eigenvalues. This may or may not be relevant for later processing. In either case, the data distribution no longer has any preferred direction.

4. The data distribution in the scaled eigenvector space may be rotated freely by an orthonormal transformation (Fig. 4c-d).

5. The last stage, and probably the most difficult to perform optimally, is the mapping of three of the derived dimensions onto the colour space. There is no clear agreement on the metric of colour space. A symposium volume devoted to the topic (Vos, Friele & Walraven, 1972) indicates the current lack of consensus. It is clear, however, that for any selection of primary colours there is only a finite and well defined set of attainable colours. The colour space is some kind of a skew three-faced pyramid. The data distribution, on the other hand, is a more or less Gaussian sphere, which will not fit conveniently into the colour pyramid. Either outlying points will be plotted in an unattainable region of "colour" space, or most of the data distribution will be clustered into a very small range of colours. Either the clear primary colours (including black) will be effectively unused or many pixels will be represented by supersaturated, impossible colours. Accordingly, the data distribution must be distorted before it is fitted into the colour space. This must be done in such a way that the orthogonal relationships among the dimensions are disturbed as little as possible. The problem is not solved, and colour displays produced to date have utilized a much simpler approach. They have simply tolerated a certain number of supersaturated pixels in order to accomodate a moderate linear expansion of the main cluster of data. In addition, the rectilinear space has been distorted into triangular form in order to bypass the problem of the interaction of dimensions in determining the permissible bounds of the colour space. Instead of the preferred uniform chromaticity space, then, a space is used in which the dimensions are Blue vs Green and Red vs Blue-Green. These dimensions were chosen rather than Red vs Green and Blue vs Yellow in order to minimize the distortion of the uniform chromaticity space when using the NTSC standard colour TV phosphors.

RESULTS

Covariance data were obtained from 14 frames, largely of summer scenes in Southern Canada, which had been requested by other users for their own purposes. Eigenvectors and eigenvalues were determined from the total data sample. 10,000 pixels were used in each frame. The scaled eigenvector matrix derived from the averaged data was then used to describe the data from three frames, one a scene of almost bare rock and an ice-filled fjord on Ellesmere Island (78°W, 80°N approximately) very different from most of the scenes used to generate the covariance matrix; one a prairie scene centred on the city of Winnipeg, Manitoba, and one scene centred on Vancouver, B.C., which had not been included in the averaged data and which contained the silt-laden water of the Fraser River. The first two scenes were imaged in August 1973, the third in Spetember 1972.

Initial processing of the data in each case was done by correcting the sensor data according to tables constructed by Vishnubhalta (Strome and Vishnubhalta, 1973) for mid-August 1973. The output of the tables was the logarithm of the calibrated sensor values, scaled so that as the data ranged from 0-63 so also did the table output. The calibration is not exact for very low readings and sensor drift between September 1972 and August 1973 rendered the calibration poorer for the Vancouver scene than for the other two.

Scattergrams of the data taken pairs of bands at a time from the Winnipeg scene are shown in Fig. 6 and from the Ellesmere scene in Fig. 7. The Winnipeg scene shows high correlation between bands 4 and 5, and between bands 6 and 7, but when one of the visible bands is considered together with one of the infrared bands, the data assume a fan shape. The four-dimensional shape is of a fan thin in two dimensions and fat in the other two -- a conical fan, so as to speak. Such a shape is probably typical of other prairie and farming scenes, though scattergrams have not been made to test this assertion.

The Ellesmere scene shows an entirely different pattern of inter-sensor correlation (Fig. 7). The data in any pair of comparisons fall into well defined branches, converging at the very bright end of the data range. The upper branch in each panel represents the rock and what sparse vegetation may have been included in the sample. The lower branch represents the ice and snow, much of which was probably melting in the summer sun. Melting snow has very low reflectance in the longer wavelengths, but remains bright in the shorter wavelengths.

Scattergrams were not obtained for the Vancouver scene, but one may assume that they would be not much different from those for the Winnipeg scene with the exception that the large amount of water in the scene would emphasis the lower ranges for the infrared bands. Samples would occur which had higher values in band 4 and low values in band 6 and 7. Such points would plot along the bases of the three left panels in Figs. 6 and 7.

Portions of the three scenes are shown in Figs. 8, 9 and 10, in the conventional 4-band picture. Like the other pictures in this report, these figures were taken directly from the screen of the Bendix Multispectral Analyser Display (MAD) at the Canada Centre for Remote Sensing (CCRS), in Ottawa. In Figs. 8, 9, and 10, the left strip is band 4, the right band 7. In each case, but particularly in the Ellesmere scene, it is evident that much of the variation is progressive from one band to the next. Vegetation, of course, shows up lighter in bands 6 and 7. The horizontal bars on the Winnipeg scene represent data errors.

The three scenes were transformed according to the eigenvectors of the same averaged covariance matrix. Scattergrams of the resulting distributions are shown for the Winnipeg and the Ellesmere scenes in Figs. 11 and 12. If all the data that entered the averaging had been transformed into distributions such as these, each panel for the combined data would have shown a circular distribution of unit standard deviation. But since neither of these scenes is representative of the totality of the data, their resulting distributions are not perfect unit circles. The Winnipeg scene shows fairly strong correlation between the second and third dimension in the vector space, and the original fan shape shows up (as it must in at least one projection) in the scattergrams both of the first against the second and of the first against the third dimension (upper left two panels).

The Ellesmere scene involves data which do not even overlap those of the Winnipeg scene, and its bifurcated distribution could never be transformed into a unit hypersphere by any linear transformation. Nevertheless, the averaged data provide vectors which do a fairly good job of rationalizing the strange distribution. Most of the bifurcation appears in the projection of the distribution on the first versus second dimension. (In a space based on the covariance distribution of this particular scene alone, all the bifurcation appears in the single panel of vector 1 vs vector 2, the other panels showing fairly good unit circular distributions). As with the Winnipeg scene, the second and third dimensions are correlated, but this time the correlation is negative. In the colour pictures derived from this eigenspace, the Ellesmere scene is totally in the orange and red area, whereas the Winnipeg scene tends from purple to green.

Images derived from the four vectors of a rotated eigenspace for each of the three scenes are shown in Figs. 13, 14 and 15. These images were obtained by applying individually to each vector an offset to avoid negative numbers, and a scale change, and then treating the data thus transformed as grey scale values. While the resulting vector images look superficially like the individual sensor images shown in Figs. 6 and 7, they are devoid of obvious correlations among themselves. For example, consider the land, the ice at the edge of the fjord, and the large floe at the upper left of the Ellesmere scene. In the sensor images of Fig. 7, this floe gets darker from band 4 to band 7, while the edge stays bright and the land remains mid-grey. In the vector images, no such trends can be seen.

Fig. 16 shows enlarged rotated vector images of a portion of the Winnipeg scene SW of the city. Note that separations are clearly visible in vector 2 between some fields that merge into a single area in vector 3, and vice versa. Neither vector suffices to show all the inter-field discriminations. Vector 1 and 4 show the effects of poor low-level calibration. Both are heavily weighted by bands 6 and 7 in this particular rotation of the eigenspace (vector 1 actually corresponds to a direction in 4-space near the original vector 3), and these bands seem in this image to have the worst low-level calibration correction. Despite the noise in vectors 1 and 4, they may be used to make some discriminations not possible using the other two vectors. In general, each vector makes an independent contribution to the interpretation of the scene.

Let us now consider the amount of information potentially available in each dimension. Since, overall, the data in the various dimensions are uncorrelated, we can treat each separately. The noise which limits the precision of observation includes quantization noise; the signal can vary $\pm$ 0.5 units without altering the reported datum. After logarithmic transformation, the size of the quantum depends on the signal level, being large for small signals but small for large signals. On average, it probably is near 1 unit, since the log scale is stretched to cover the same range, 0-63 units, as the original sensor data. On this assumption, the equivalent noise is 0.08 unit^2. At lower signal levels if the quantum is about 3 1/2 units, the noise may go as high as 1 unit^2. Such levels are found in water regions and shadows. To ease further discussion, let us settle on an estimated quantization and calibration noise of about 0.1 unit^2, probably an optimistic estimate for most scenes.

The effects of quantization and calibration errors at low levels can be seen in the rotated vector images for Winnipeg and Vancouver, particularly in rotated vectors 1 and 4. Strong weighting of these vectors on the low level band 7 is responsible. Such effects do not show on the Ellesmere scene, since most of the sensor data were at high levels where quantization effects are minimal.

The eigenvalues of the covariance matrix determine the variance due to that dimension. When each of the 14 scenes which were averaged is treated individually so as to concentrate the variance in the first dimension for each scene separately, the first dimension accounts for, on average, 96% of the total variance, the second for 79% of the rest, and the third for 74% of the remainder. What is left for the fourth vector has a variance of .37 unit^2, barely above the estimate of quantization variance. Compared to the quantization variance estimate, the signal-to-noise ratio of the four dimensions is about 31 dB, 17 dB, 10 dB and 6 dB respectively.

These figures are obtained when each scene is viewed in its own optimum vector space. When the gross average data are viewed as a group, two things happen. Firstly, there is more overall variance because of the differences among scenes. Secondly, the scenes differ in various ways, so that the overall dimensionality becomes larger. In terms of the last paragraph, the first dimension in the overall data now accounts for only 84% of the variance, the second for 84% of what is left, and the third for 77% of the remainder. The signal-to-noise ratios are 32 dB, 23 dB, 15 dB and 9 dB. These figures show that whereas three dimensions probably give an acceptably complete description of the information available if a scene is described in terms of its own eigenvector space, the fourth dimension may supply some useful information when the scene is described in a space derived from the entire data set. This fact supplies the rationale for rotating the four-dimensional space in various ways to permit different three-dimensional projections which can be viewed in colour space.

We cannot allow the presentation of each scene in its own eigenspace, since this would present the interpreter with intolerable variation in the relation of colour with ground truth. However, one could admit a small set of rotations; one rotation, for example, which would optimally display forests, another which would give best discrimination in agricultural lands, and another for glaciologists. Each interpreter within a discipline would then have to deal with only a single transformation, whose three-dimensional structure would contain essentially all the information relevant to his purposes. Investigation of possible specialized display spaces is intended as an early stage of the continuing investigation. It should be noted that Haralick (1969) found that a three-dimensional space represented well the data from a small forested and mountainous region in Yellowstone Park scanned by a 12-band system operating from the near ultraviolet across the part of the spectrum covered by ERTS. It therefore seems reasonable that three dimensions will adequately deal with most problems of ERTS data display. For those cases where three dimensions are inadequate, either a grey-scale display of the fourth vector or a colour display made up of the second, third and fourth dimensions should supplement the primary colour display.

The actual colour presentation of the three-dimensional display remains an optimization problem. Pleasing displays have been made by several "artistic" techniques, all of which have their faults. The display used for most of the slides which accompanied the verbal presentation of this paper allowed the second eigenvector to control the ratio of red to the average of blue and green, and the third to control the blue/green ratio. The values obtained for red, green and blue were multiplied by a number determined by the first eigenvector, as representing brightness. This choice has two major faults. Firstly, perceived brightness is not wholly independent of colour under this algorithm, and secondly, if the second eigenvector weights the colour strongly into the red, the value of the third will have very little effect on the colour. All objects will appear red when the second vector is strongly negative. An improved technique would distribute data uniformly within the colour space, in such a way that a constant value on one vector would be represented by a perceptually constant effect. A uniform chromaticity space described by MacAdam (1971) seems to provide a promising approach to fulfilling these requirements and an algorithm to use it for display is currently being programmed.

SUMMARY

The correlated data from the ERTS sensors has been transformed into a space in which the four dimensions are uncorrelated and of equal variance. This was accomplished by determining the eigenvectors of the covariance matrix, and dividing the data projections on the eigenvectors by the square roots of the associated eigenvalues. Data thus transformed may be treated in a variety of ways, primarily by rotating the space. Space rotation in this scaled eigenvector space may be performed freely without introducing correlation among the rotated dimensions. In the rotated space, three dimensions are chosen for display as the dimensions of colour space. The resulting colour pictures show discriminations rather better than do displays based on band selection. The amount of information carried by the first dimension is considerably greater than by the second, which is in its turn much more informative than the third. The information carried by the fourth dimension is ordinarily very small, but could be important in particular applications. In such cases a display including the fourth dimension could supplement a standard display. For particular applications special displays may well be made either from a specially derived eigenvector set or from a rotation of the basic eigenvector space to emphasis discriminations of interest for the particular application.

FOOTNOTES

*This is DCIEM Research Paper 73-RP-987

**Much of this work was done using the display systems at the Canada Centre for Remote Sensing, Ottawa, as a cooperative project between The Defence and Civil Institute of Environmental Medicine and the Canada Centre for Remote Sensing. I thank particularly Mr. Gordon Wayne for the long hours of programming he has spent on the project,

and Drs. S.S. Vishnubhalta and S. Schlien for their assistance in providing routines and tables for matrix manipulations and for their stimulating discussions of the principles involved in the work.

REFERENCES

Haralick, R.M. Multi-image pattern recognition: ideas and results. CRES Tech. Rep. 133-11. University of Kansas, Center for Research Inc. 1969.

Jameson, D. Theoretical issues of color vision. In Handbook of Sensory Physiology, Vol. VII/4, Visual Psychophysics. (Eds. Jameson, D. and Hurvich, L.M.) Berlin: Springer-Verlag, 1972.

MacAdam, D.L. Color-difference evaluation. Advances in Chemistry Series, 107, "Industrial Color Technology". American Chemical Society, 1971.

Strome, W.M. and Vishnubhalta, S.S. A system for improving the radiometric corrections for ERTS-1 MSS data. Presented at the XXIV Astronautical Congress, Baku, USSR. October 1973.

Vos, J.J., Friele, L.F.C., and Walraven, P.L. (Eds.) Color Metrics, Soesterberg: AIC/Holland, 1972.

Vos, J.J., and Walraven, P.L. A Zone-fluctuation line element describing colour discrimination. In Vos, Friele and Walraven, 1972.

TABLE I

The scaled eigenvector space derived from the averaged covariance matrix. Entries are the weights of the various bands in the various vectors.

	Band 4	Band 5	Band 6	Band 7
Vector 1	.03	.04	.05	.06
Vector 2	-.14	-.13	.03	.12
Vector 3	.42	.41	.01	.04
Vector 4	.13	.12	-.89	.58

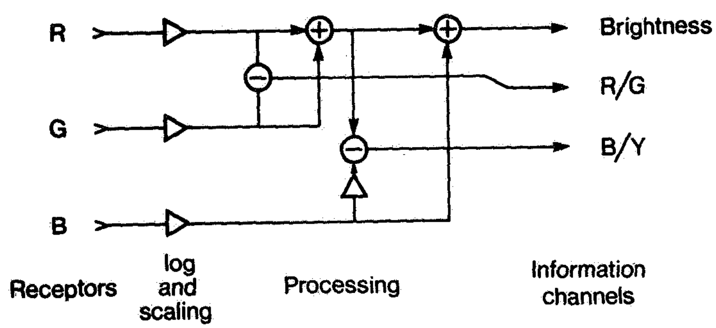

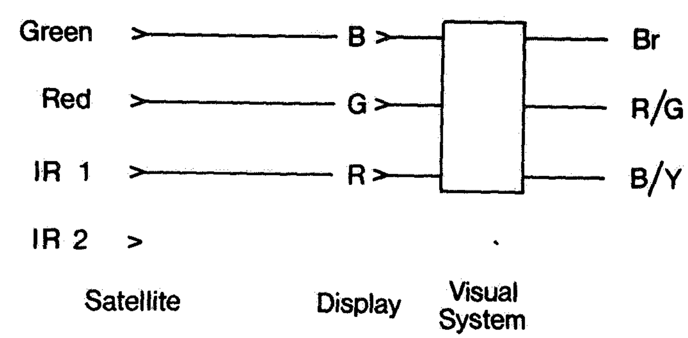

Fig. 1 Simplified flow diagram of colour processing in the visual system.

Fig. 2 ERTS colour display simulating infrared colour film. Three bands are presented individually in three different primary colours, which the visual system then converts to three dimensions of colour space.

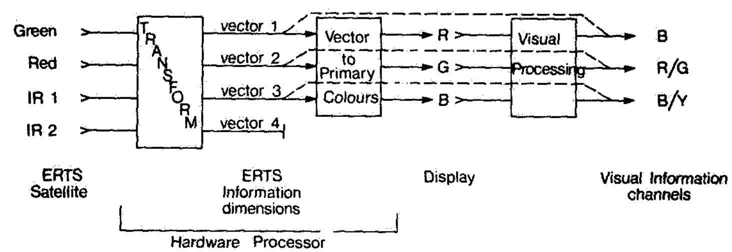

Fig. 3 Schematic description of the principal components colour display. The four data streams are transformed into four streams of uncorrelated data (vector 1-4), three of which are to be mapped onto the three dimensions of colour space. The algorithm to convert from the vector representation to colour primaries is supposed to be the inverse of the processing applied by the visual system to produce the three dimensions from the sensed primaries of the display.

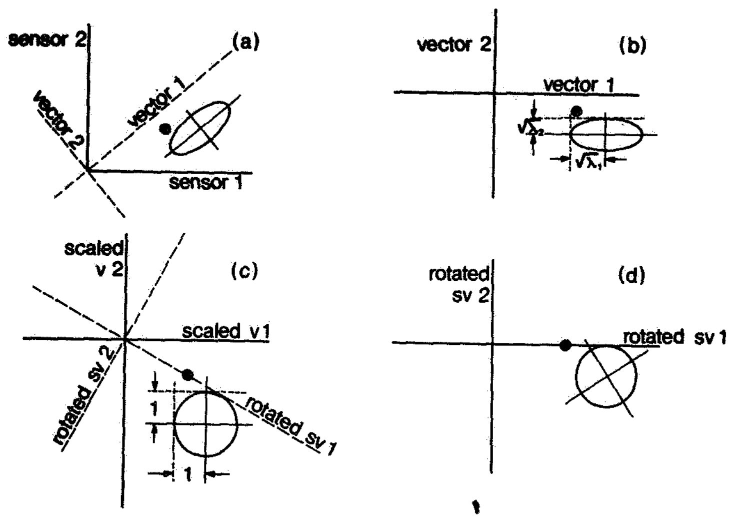

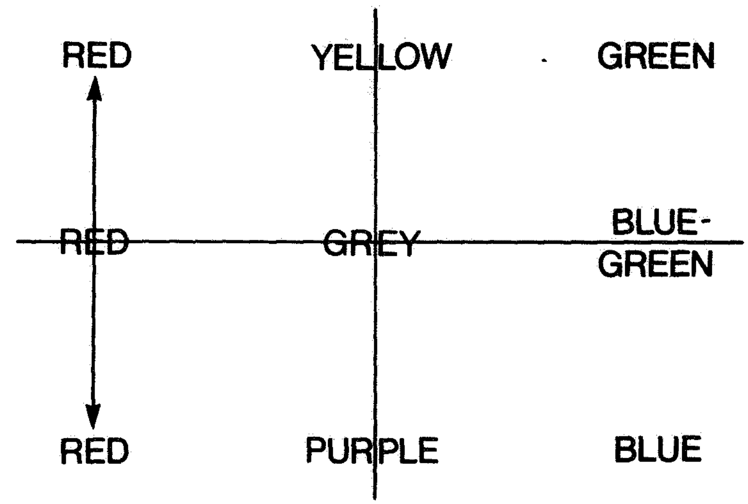

Fig. 4 Stages in the construction of the linear transformation from sensor data to independent vector form. (a) The data from two sensors is correlated, and therefore is distributed in a roughly elliptical form with the main axes diagonal. A single isolated data point is also shown. The eigenvector solution of the covariance matrix determines vectors parallel to the main axes of the ellipse.
(b) The data distribution rotated into the eigenvector representation. The description in this space is not correlated, as is shown by the fact that the axes of the ellipse are parallel to the coordinate axes. The standard deviations are unequal, being the square roots of the eigenvalues. (c) Each dimension is scaled by the square roots of the eigenvalues, so that the standard deviation of the distribution is now unity in every direction. There are no longer any main axes to the data distribution, and the space can be rotated freely without introducing correlation into the description.
(d) An arbitrary rotation which places the isolated data point along an axis. Its representation in this space is now (k,0).

Fig. 5 The simple "triangular" colour space used in the colour slides.

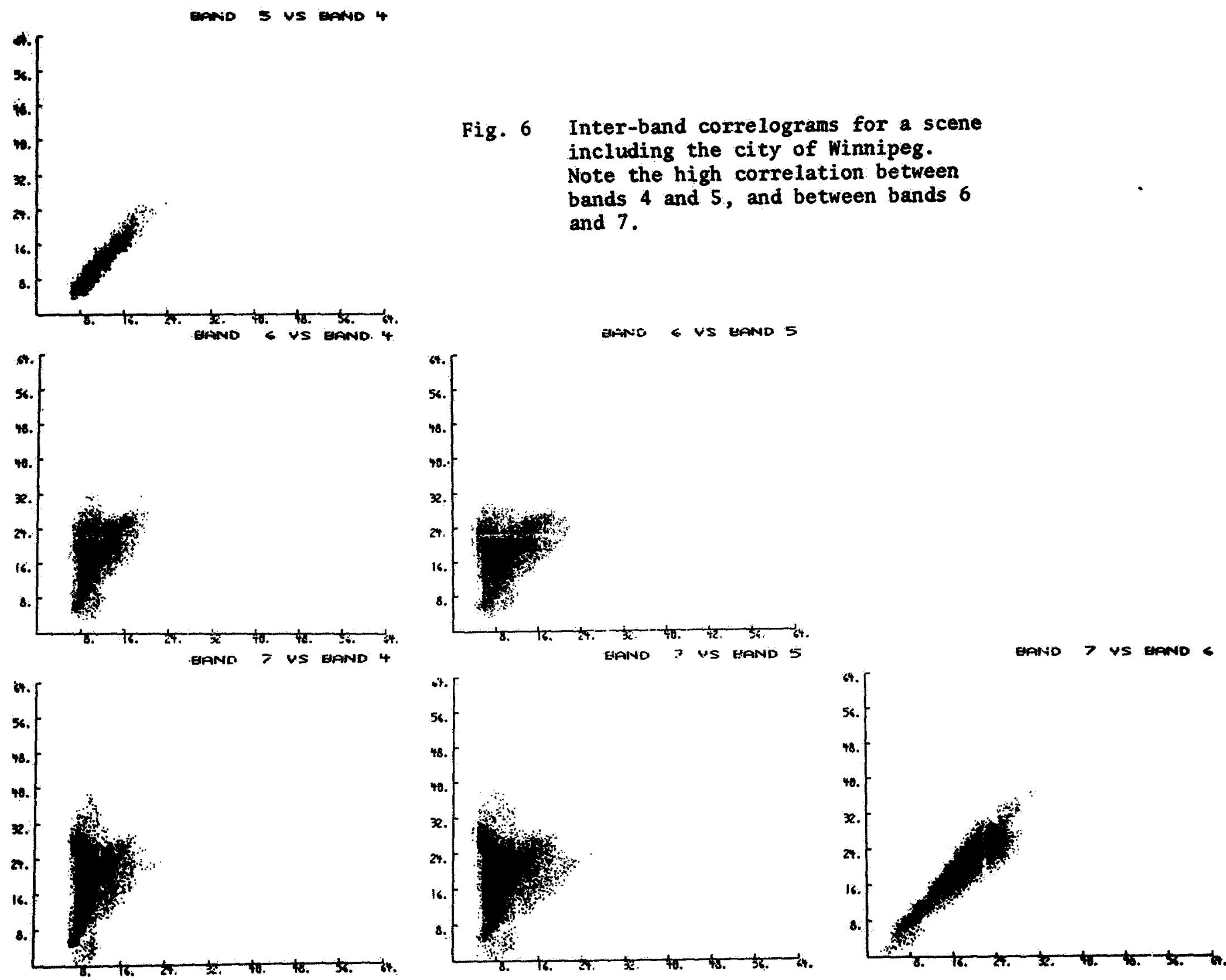

Fig. 6 Inter-band correlograms for a scene including the city of Winnipeg. Note the high correlation between bands 4 and 5, and between bands 6 and 7.

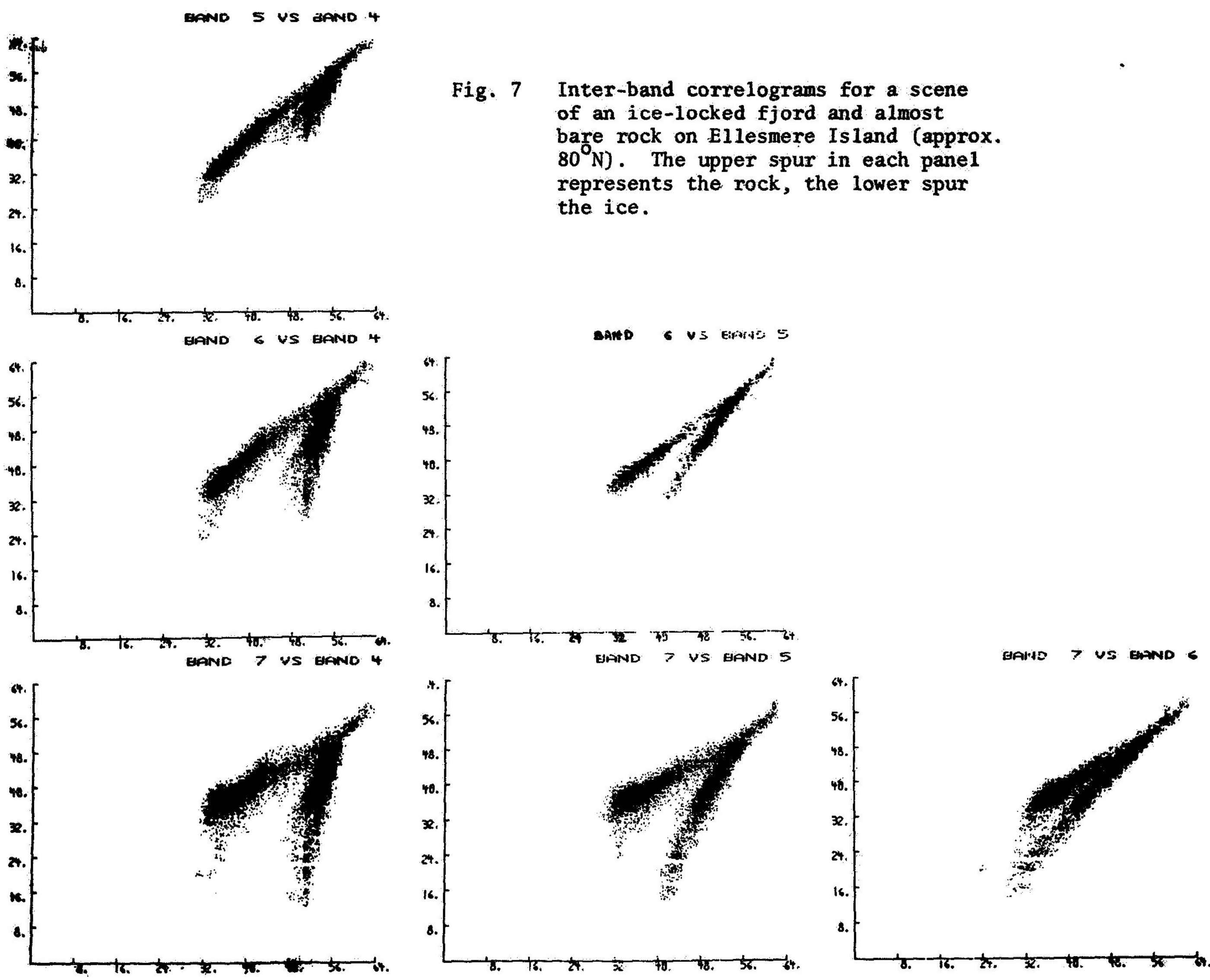

Fig. 7 Inter-band correlograms for a scene of an ice-locked fjord and almost bare rock on Ellesmere Island (approx. 80°N). The upper spur in each panel represents the rock, the lower spur the ice.

Fig. 8 Images from each of the four bands for part of the Winnipeg scene.

Fig. 9 Images from each of the four bands for part of the Ellesmere Island scene.

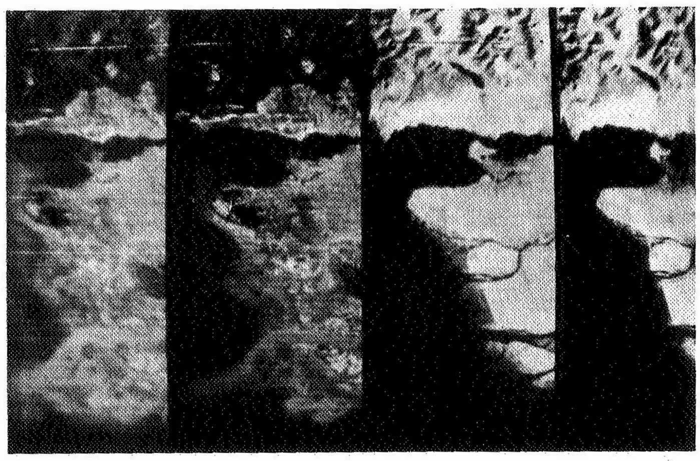

Fig. 10 Images from each of the four bands for a scene including Vancouver city and the mouth of the Fraser River.

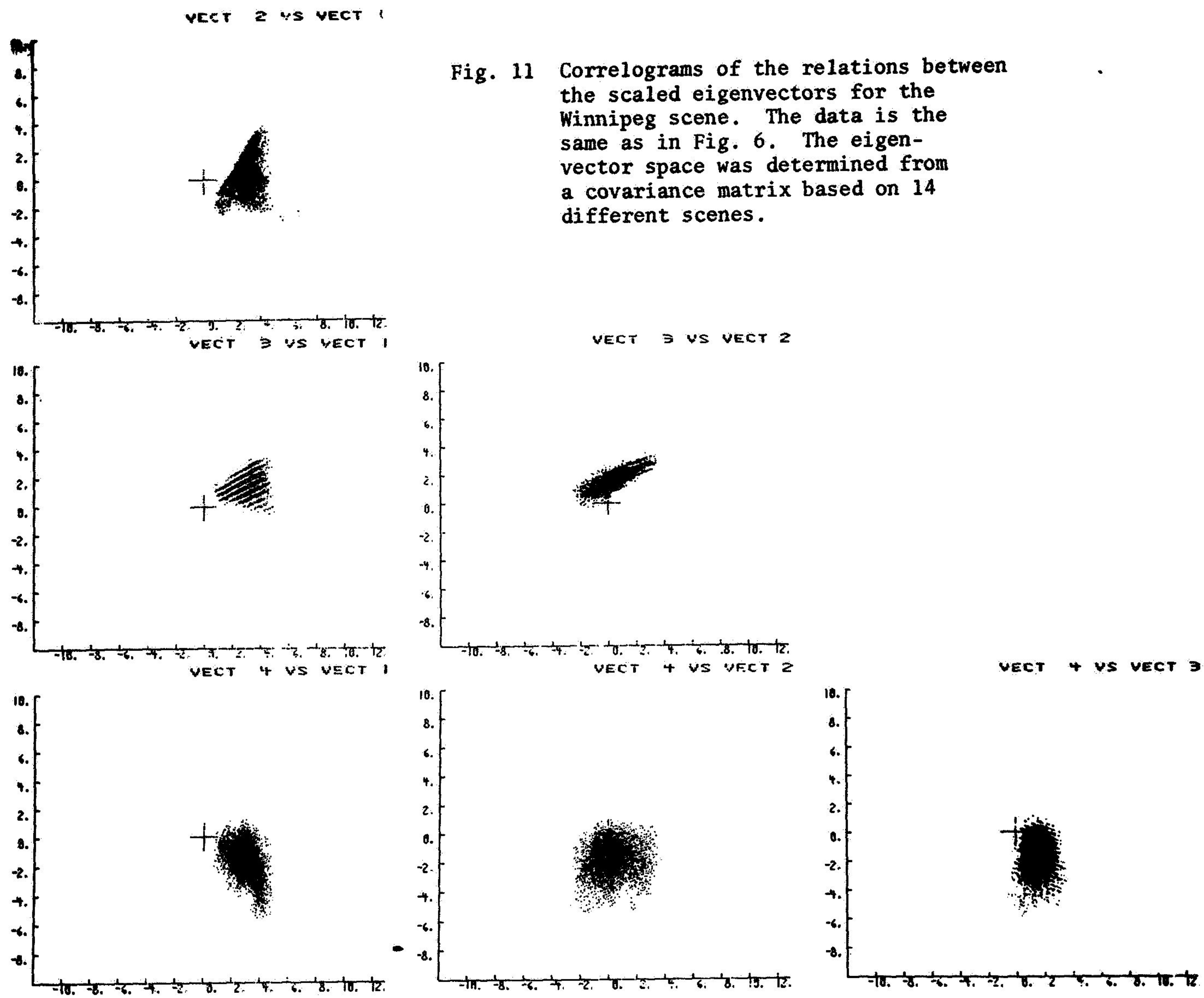

Fig. 11 Correlograms of the relations between the scaled eigenvectors for the Winnipeg scene. The data is the same as in Fig. 6. The eigenvector space was determined from a covariance matrix based on 14 different scenes.

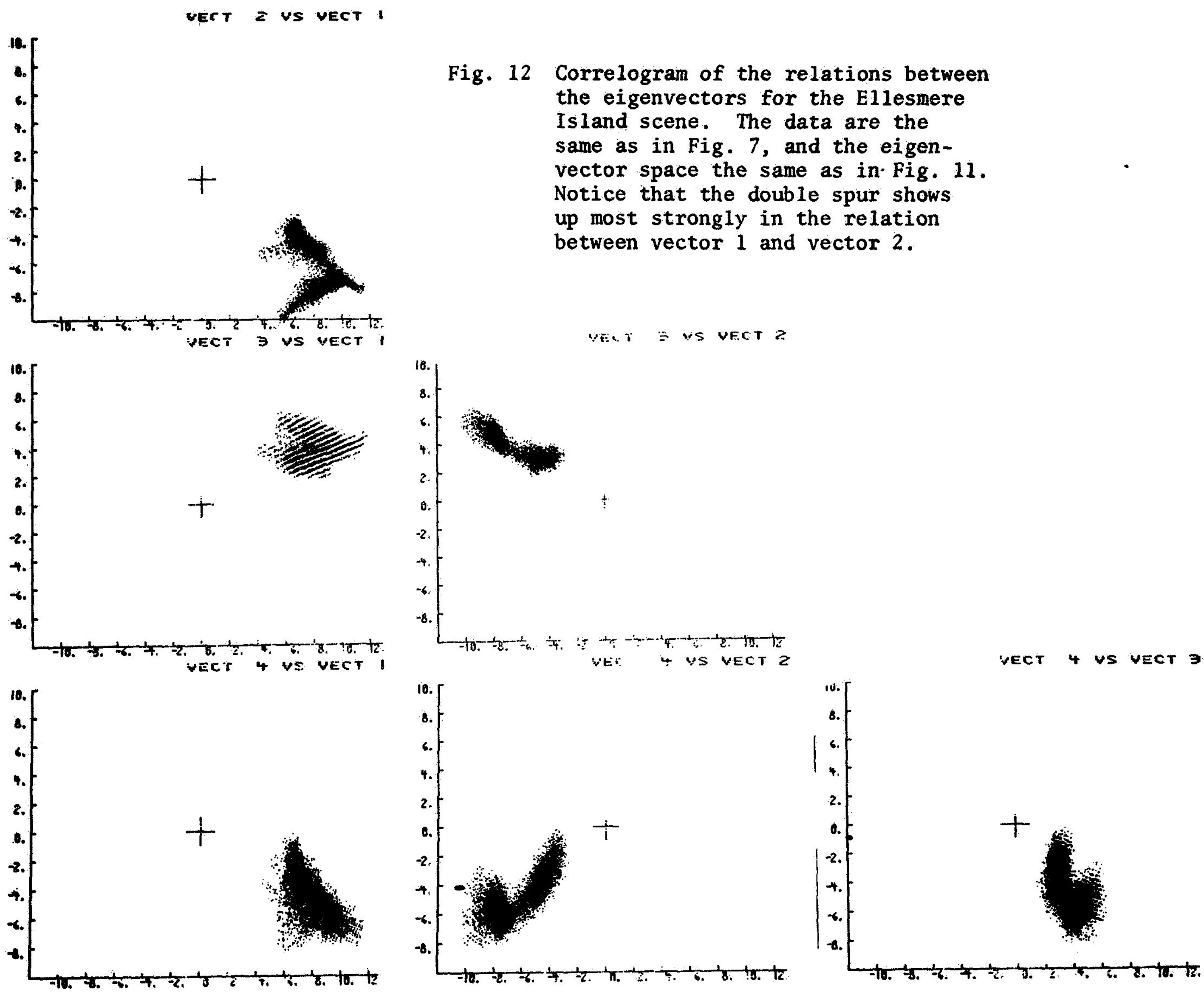

Fig. 12 Correlogram of the relations between the eigenvectors for the Ellesmere Island scene. The data are the same as in Fig. 7, and the eigenvector space the same as in Fig. 11. Notice that the double spur shows up most strongly in the relation between vector 1 and vector 2.

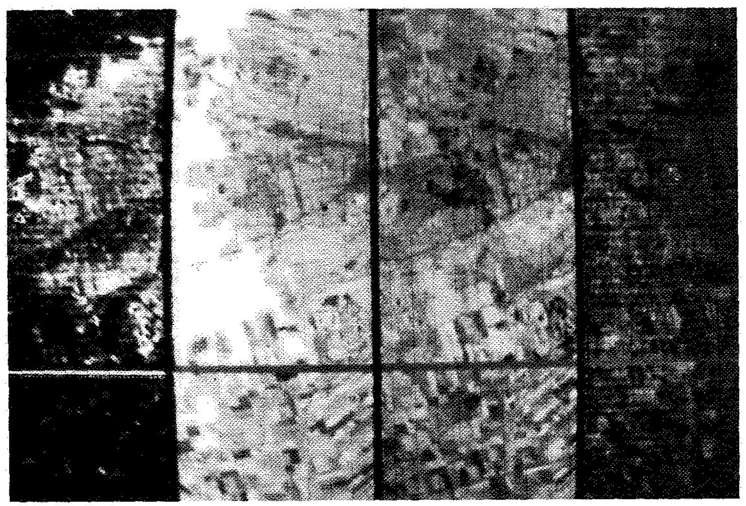

Fig. 13 Images based on the four vectors of a rotated scaled eigenvector space for the Winnipeg scene. The data are the images of Fig. 8. The four vectors are not eigenvectors but are independent linear combinations of the original scaled eigenvectors. Vectors 1 and 4 lie near the noisy (3,4) plane of the original eigenspace.

Fig. 14 Images based on the four vectors of a rotated scaled eigenvector space for the Ellesmere Island scene. The data are the images of Fig. 9.

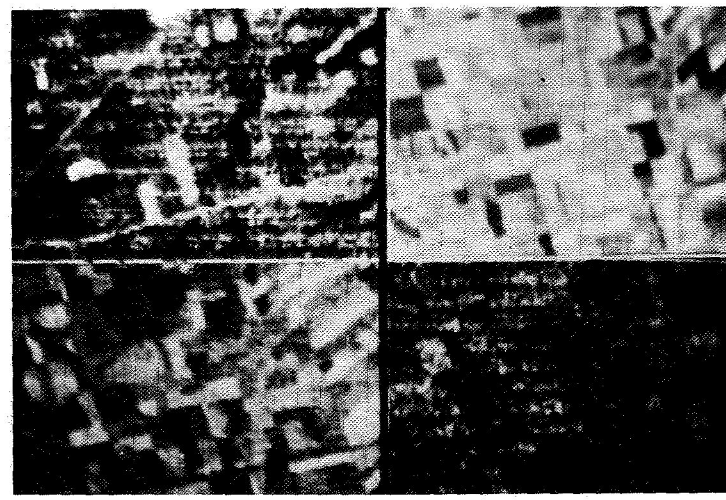

Fig. 15 Images based on a rotated scaled eigenvector space for Vancouver scene. The data are the images of Fig. 10.

Fig. 16 A magnified section of the vector images from Fig. 13, showing fields Southwest of Winnipeg. Vectors 2 and 3 each show discriminations not visible in the other band. Note that these vectors are not eigenvectors, but are derived from a scaled rotated eigenvector space. Vectors 1 and 4 are noisy, due to high loadings on low-level bands (see text). They are both near the (3,4) plane of the original eigenvector space.

Paper I 13

APPLICATIONS OF ERTS DATA TO RESOURCE SURVEYS OF ALASKA

Albert E. Belon and John M. Miller

ABSTRACT

ERTS data, with its demonstrated capability for economical surveys of large areas, affords a unique opportunity to perform urgently needed resource surveys and land-use planning at a critical juncture in the history of Alaska's social and economic development. A facility for retrieval, processing and interpreting ERTS data and aircraft remote sensing data has been established at the University of Alaska. This facility is widely utilized by twelve University ERTS projects and many agencies, public and private, to produce the needed environmental surveys in strategic regions of Alaska. The available facilities for photographic, optical and digital processing of ERTS data are described, along with the interpretive techniques which have been developed. Examples of the applications of these facilities and techniques are given for three environmental disciplines: vegetation mapping for potential archeological sites; marine and sea-ice surveys on the Alaskan continental shelf for the determination of surface circulation and sedimentation patterns and their effects on navigation, pollution assessment, fisheries, location of harbors and construction of off-shore structures; snow surveys for inventories of water resources and flood potential in Alaska watersheds.

INTRODUCTION

ERTS data, with its demonstrated capability for economical surveys of large areas, affords a unique opportunity to perform urgently needed resource surveys and land-use planning at a critical juncture in the history of Alaska's social and economic development. With NASA support the University of Alaska has established the capability to retrieve, process, analyze and interpret ERTS data which is unmatched in Alaska and in many other areas.

This facility, which handles both spacecraft and aircraft remote sensing data, is now available and is being utilized by twelve University ERTS projects and most of the government agencies in Alaska concerned with environmental analyses, resource surveys and planning, as well as other private organizations.

FACILITY FUNCTIONS

The overall coordination and management structure for the effective dissemination and use of ERTS data in Alaska is shown in Figure 1. The organization of the University ERTS program is versatile and utilitarian in order to best serve many investigators and government agency users of Alaskan data.

The methods for coupling new remote sensing technology through cooperative activities with government agencies are outlined by five basic steps detailed in Figure 2. The first function is that of observation in which both the University and outside agencies familiarize themselves with the activities and requirements of the other. The next appropriate event is an exchange of data to ensure that all data that are available can be brought to bear in problem solving. The third function is data analysis in which interpretive services are applied to earth resources data. Frequently such analysis requires facilities of new technologies which are provided by the technical services of the University ERTS program. A very important function is that of joint participation in projects by agencies and the University which aims at avoiding duplication of effort and enhancing operational applications of existing work. Most of the University ERTS projects sponsored by NASA fall in the latter category.

Centralized Facilities

Both basic and reasonably advanced techniques for data processing, enhancement, analysis and interpretation are provided to all Alaska-based users of remotely sensed imagery by the centralized facilities at the University of Alaska in Fairbanks. Figure 3 outlines the scope and detail of the major laboratories, library, shops, and computer center.

The ERTS data library has archived some 30,000 products and serves as a user-oriented browse facility. Specialized outputs of the library include an Alaskan ERTS coverage map, illustrated in Figure 4, which locates geometrically and by scene ID number the principal point of every available ERTS scene with low cloud cover. These are prepared on a seasonal basis to avoid undue map clutter and also because many applications require data from specific seasons only.

Another useful item is the Alaskan ERTS data catalog which lists all low cloud cover scenes of Alaska chronologically along with the usual reference information. Two important features enhance the utility of this ERTS catalog relative to the more comprehensive NASA catalog. The Alaska catalog by being restricted only to Alaska scenes eliminates coverage of the rest of the world and thereby is more convenient for Alaskan users. Secondly, each scene is assigned a principal place name which saves time in searching for specific coverage.

An optical image enhancement and interpretation laboratory contains four major viewing systems. A color additive projector was designed and built in-house to produce 1:500,000 false color composite images from 70mm ERTS chips. A Bausch & Lomb zoom transfer scope is available for transferring satellite and aircraft data onto a map base up to a scale conversion factor of 14:1. The VP-8 image analyzer is shown in Figure 5 and provides a rather powerful tool for electronically analyzing photographic images. Although the VP-8 is basically a color coded density-slicing display device, it contains several novel features which are described later. Our most recent acquisition is a model MS-970-1 multiformat photo interpretation station for enhanced viewing of aerial photography. This unit includes a widespan zoom stereoscope and is capable of handling 70mm, 5 inch, and 9 inch film.

A special feature of the photo laboratory is the LogEtronics Mark III printer used for electronically dodging color and black and white prints. Other standard photo facilities include black and white and color printers and enlargers, a MacBeth Quantalog densitometer, and an array of copy and process equipment.

The heart of our digital data processing laboratory for remote sensing data applications is the CDU-200 color display unit shown in Figure 6. The CDU-200 is an off-line interactive display terminal of an IBM 360/40 located in the University computer center. The color display unit is used for digital manipulation and display of NASA computer compatible tapes. It generates and displays color coded thematic maps from multispectral analysis of ERTS data.

Interpretation Techniques

We have adapted or developed data interpretation techniques at a deliberate pace to match the rather modest resources available. While foregoing the power of the brute force computer systems, we have relied upon man-aided automatic data processing techniques to minimize hardware requirements and still meet investigator requirements and outside agency needs. Emphasizing medium power interpretation techniques was an appropriate expedient because the current pressing need in Alaska is for broad regional, rather than local and intensive, environmental and resource surveys.

Conventional analog interpretation techniques include the following:

- Customized color and black & white printing of enhanced ERTS images for applications such as snow surveys, marine surveys, identification of geologic structures, and vegetative mapping.
- Reconstitution of false color ERTS images using Ektacolor and diazo processes, optical techniques of the color additive projector, and digital techniques with the analog encoder of the CDU-200 color display unit.
- Manual preparation of thematic maps and overlays using photographic and zoom transfer scope techniques.

The currently implemented optical and photographic processing techniques and digital data processing techniques and their interrelationships are shown schematically in Figures 7 and 8.

Digital Image Processing

The CDU-200 color display unit represents the major development of interpretation techniques by the University facility, and reflects our need for digital interpretation of multispectral data without access to a large, dedicated computer system. Figure 9 shows a block diagram of the color display system. A 25 inch color TV monitor is utilized as the output display device. A PDP-11 minicomputer controls the tape drive and three disk refresh memories, each of which stores a portion of an ERTS scene 512 by 512 pixels in size from any three of the four ERTS multispectral bands.

The heart of the color display system is the CD-16 digital color encoder and the AP-3 analog color encoder, which together form the main user interface to the system. By interacting with the display, the investigator manipulates the three dimensional data stream to create man-aided machine classification decisions which have useful correlations with the object space in the real world.

The logical design principle is based upon simple hyperplane decision rules which imply that the data are normally distributed. This simplication underscores the importance of working with well-behaved data and of not insisting upon intensive classification programs for clusters of multispectral data which at best are difficult to discriminate. Trade-offs between machine sophistication and statistical classification power were necessary, but these trade-offs were compromised toward man-aided machine interpretation. Some of the power lost in foregoing the capability for unsupervised classification was regained by coupling into the system the creative elements of human interpretive skills. This has resulted in a system with a favorable cost-benefit ratio: we can perform perhaps 60% of the tasks of the larger systems at about 25% of the initial hardware cost, and the results are satisfactory for broad regional resource surveys which are Alaska's prime need.

There are several ways to use the color display unit. The AP-3 analog encoder provides two system functions. In the first function it linearly transforms up to seven video inputs into three-dimensional color space. Each input can be separately biased, inverted and scaled in the transform. By combining three spectral inputs with blue, green and red coding, one can reconstitute the familiar simulated color-infrared display at a fixed display scale of 1:41,000 at full ERTS resolution. No provision has been made, however, to provide geometrical corrections for skew, rotational and aspect distortions inherent in ERTS digital data. Numerous other intermediate color additive and subtractive displays also can be generated, supporting an almost endless variety of possible color combinations with automatic pixel registration to meet any need for specific feature enhancement. The second system function compares

two video signals by addition, subtraction, or by flicker, which rapidly alternates the two images on the display. The variable flicker rate aids radiometric calibration, when necessary, and enhances spectral or spatial differences between images.

Data interpretation in its truest sense involves the use of the CD-16 digital encoder rather than the analog encoder. The digital encoder translates up to an 8-bit pattern to a field display combination of 16 color and color-accents. For reference purposes, it also generates a 16 level sequence at the bottom of the TV display (see Figure 10) which expresses the bit-color-accent combinations that are selected. This forms a valuable visual reference for the operator as well as documentation of classification signature values when the monitor display is recorded photographically.

The CDU-200 digital display system performs as an off-line terminal of a non-dedicated IBM 360/40 computer with a 128K core memory. The general purpose display capabilities of the CDU-200 and its interface to the IBM 360 allow virtually any image processing and interpretation technique to be tested, and if successful, to be applied on a larger scale. A disadvantage of the more sophisticated pattern recognition techniques (besides swamping our computer capability) is that geophysical data are less easily expressed in a form suited for mathematical optimization than are, for example, agricultural data. One of the powerful features of the CDU-200 is its ability to provide real-time display of the results of the investigator's processing instructions. The investigator who cannot express his classifications, judgments, and results mathematically sometimes can converge to useful results by interacting with the parameters of his multispectral data in a number of stepped processing techniques. When good results are achieved, the capabilities of the IBM 360/40 or other more powerful data processing facilities can be utilized to apply the results to broad regional surveys.

Analog Image Processing

The previously described digital processing and display system is limited to the analysis of ERTS digital tapes. The analog image processing system, the VP-8 image analyzer, when fully integrated to the CDU-200 will extend the full capabilities of the digital system to photographic images as well. The VP-8 also provides a means for generating computer graphics for electronic superposition on the ERTS and aircraft images displayed on the color monitor.

At present, the primary function of the VP-8 image analyzer is color coded density slicing of photographs or transparencies. The output is a conventional color TV monitor, and has the special feature, as with the CD-16 digital encoder, of displaying a narrow band at the bottom of the display providing a visual reference of all level settings, intensities, and colors.

There are eight intensity slicing levels which can be adjusted separately or collectively. The base level adjustment can span the entire density range of the image, and setting six aperture bands determines additional slicing levels above the base level. The aperture bandwidths are adjusted by individual controls, or can be adjusted collectively by a 200:1 multiplier. This permits the choice of linear, logarithmic or other aperture relationships. Any number of level slices above eight is possible by repetitively adjusting the bottom of the next set of slices to the top level of the preceding set. Setting density slicing levels with reference to the built-in digital readout provides the precision which makes feasible such repetitive level slicing.

A novel capability of the VP-8 is that of isometric projection of the image intensities on an XYZ monitor. This presents a pseudo three-dimensional display with image position information on the X and Y axes and with density information on the Z axis, as shown in Figure 11. The isometric image can be manipulated in 3-D space by individual adjustment of rotation, inclination, and relief controls. The effect of the isometric image resembles viewing a relief model where terrain elevation represents image density rather than elevation contours.

Horizontal and vertical cursors are provided and can be adjusted to any position on the image. The horizontal cursor selects any single horizontal scan line for display on the XYZ monitor, as shown in Figure 12, and thus produces an electronic densitometer display. Adjusting the vertical crosshair along the scan line defines point-by-point resolution elements, and the crosshair point is highlighted on the single scan display for visual reference. The digital readout can display the XY coordinates and the image density at the point designated by the crosshairs. The digital readout also can function as a planimeter and measure the areas comprised in any density aperture in engineering units or percent of total area.

APPLICATIONS RESULTS

The goal of our data retrieval, processing, and interpretive facility is to provide the means to analyze ERTS and aircraft remote sensing data to all users , including University investigators, government agencies, and private organizations. We have not attempted to advance the state of the art as such. Four of many possible examples of the applications of this facility are given below to illustrate the results obtainable from these interpretive techniques in terms of Alaskan resource inventories. Other applications of ERTS data to environmental and resource surveys of Alaska are described in other presentations at this symposium.

One of the more unusual projects of the University of Alaska is an archeological study of the lower Yukon River described in Figure 13. The goal of the project is to evaluate the feasibility of identifying old native village sites on ERTS imagery.

Ground based studies have shown that such sites often are along river banks and are associated with areas of lush grass interspersed with vigorous growths of willows. The area near Kaltag on the lower Yukon is the study area, and it is a wilderness region covered by combinations of vegetation types rather than by homogeneous stands of single species. We generated multispectral signatures with the CDU-200 and the IBM 360 for associations of vegetative types in order to produce the classification printout shown in figure 13. The color display unit generated a general classification map of these major vegetation types, as well as a thematic map showing only two types of water (for positional reference) and the potential archeological sites. Verification that ERTS data located an abandoned village site without prior knowledge of its position awaits verification by field work.

Another important application of ERTS data is the study of circulation patterns in Cook Inlet which is an important transportation corridor to half of the state's population and includes both major petroleum production and commercial fishing activities. Figure 14 is a pre-ERTS model of the circulation pattern of the inlet. Because of a five hour difference in tides between the upper and lower inlet, the clear sea water flows north along the eastern shore, while the heavily silt-laden water from the upper inlet come down along the western shore. Figure 15 is a density-sliced display of the lower inlet with an overlay of sea truth sedimentation data acquired coincidentally with the satellite pass. The ERTS data verifies the circulation model quite well. There is a good correlation between sediment load and reflected radiation, so we can assign a value of milligrams per liter to a given radiation intensity displayed as color contours.

As shown by ERTS in Figure 16, sometimes the circulation patterns of the model are incorrect. On 3 November 1972, the highly sedimented water appears on the east side of the inlet with the crossover above the forelands rather than below as the model indicates. This suggests the possibility that the clear marine water flows under the sedimented water and then upwells again to the north. Because of this crossover, this region presents difficult navigation problems at certain phases of the tide. There also are important implications for the fishing industry because salmon tend to congregate at the marine and fresh water boundaries before proceeding to their river spawning grounds.

Another application of ERTS data deals with the snow and breakup survey of the North Slope. Figure 17 shows mid-winter, mid-melting, and post-melting conditions of an area stretching from the Brooks Range to Prudhoe Bay on the Arctic coast. Early in the melt season, thin or non-existant snow appears in the foothills and along river drainages where the snow first begins to disappear. Near the end of the melt season the snow remains only in gullies. This suggests a model of the snow breakup in which the breakup proceeds from the higher elevations where the snow cover has been depleted by wind erosion, to melting in the north-south facing valleys, which starts the run-off process down the river drainages. Then the breakup spreads to the snow cover adjacent to rivers and finally to the plains where the snow disappears last from gullies and lakes.

Image enhancement highlights the impact of man's activities on the snow melt model for the arctic. By 27 May the Sagavanirktok River has open running water, and the Prudhoe Bay road is visible on the original ERTS imagery. On the color enhanced and density-sliced view of Figure 18, this area shows melt plumes which extend to the southwest indicating the direction of prevailing winds. Figure 19 is an aerial view of this road and shows how the wind picks up dust and déposits it downwind thereby accelerating the melting process in the affected areas. This winter there is not much activity on the North Slope, but as oil production activities grow they may have a significant influence on snow breakup characteristics in the arctic. Hydrological modelling of the Alaskan North Slope is an imperative need because clean water at certain seasons is a scarce commodity which will become more precious as man's activities increase.

CONCLUSION

The concept of a remote sensing data retrieval, processing, and interpreting facility located in Alaska for regional users has been implemented and is being benefically applied to a wide segment of ERTS projects in the state. By archiving complete coverage of clear scenes of Alaska, the necessary data products are immediately available for any application. Provision for enhancement and interpretive techniques of moderate sophistication enables much work to be done quickly and at relatively lower cost than would be the case if such work had to be farmed out to overtaxed facilities elsewhere. Investigators have the advantages of working intensively within the geographic region of their interest rather than resorting to occasional field work while doing the analysis in an unrelated environment. The centralized facility established to serve the data users of ERTS-1 should grow in its significant benefits as ERTS-B and other operational remote sensing programs are implemented.

ACKNOWLEDGEMENTS

The authors recognize the contributions of many persons who have worked with one or another phase of the University of Alaska ERTS facility. Especially helpful information for this paper was provided by Dr. William Stringer, Dr. Bjorn Holmgren and Mr. Robert Porter of the Geophysical Institute; by Dr. G. D. Sharma and Mr. Dave Burbank of the Institute of Marine Science; and by Dr. F. F. Wright of the Marine Advisory Program, all affiliated with the University of Alaska. Dr. George Dalke and Mr. Stephen Smith of Interpretation Systems, Inc. were responsible for the technical aspects of the CDU-200 system design and construction under a subcontract with the University of Alaska.

This work was supported by the National Aeronautics and Space Administration under contract NAS5-21833, Task #1.

LIST OF ILLUSTRATIONS

Paper I 14

SCENE CORRECTION (PRECISION PROCESSING) OF ERTS SENSOR DATA USING DIGITAL IMAGE PROCESSING TECHNIQUES

Ralph Bernstein, *Federal Systems Division, IBM Corporation, Gaithersburg, Maryland, USA*

ABSTRACT

Techniques have been developed, implemented, and evaluated to process ERTS Return Beam Vidicon (RBV) and Multispectral Scanner (MSS) sensor data using digital image processing techniques. The RBV radiometry has been corrected to remove shading effects, and the MSS geometry and radiometry have been corrected to remove internal and external radiometric and geometric errors. General purpose and special purpose computer configurations to process this data in a production mode have been defined and their throughputs investigated.

The results achieved to date show that geometric mapping accuracy of about one picture element RMS and two picture elements (maximum) can be achieved by the use of nine ground control points. Radiometric correction of MSS and RBV sensor data has been performed to eliminate striping and shading effects to about one count accuracy. Image processing times on general purpose computers of the IBM 370/145 to 168 class are in the range of 29 to 3.2 minutes per MSS scene (4 bands). Photographic images of the fully corrected and annotated scenes have been generated from the processed data and have demonstrated excellent quality and information extraction potential.

INTRODUCTION

Recent parallel advances in sensors, information extraction techniques, and digital computers have stimulated the investigation of digital processing of earth observation sensor data. For example, the National Aeronautics and Space Administration (NASA) unmanned Earth Resources Technology Satellite (ERTS) uses a solid state multispectral sensor whose output is digitized, transmitted to ground, and stored in a digital form prior to processing [1]. A number of earth resources and land use investigations use digital computers to extract the desired information from the sensor data [2,3]. However, the sensor data suffers from a number of geometric and radiometric errors which, if not removed, will affect the information extraction potential of the data. Thus, it appears logical to investigate the concept of digital processing of the sensor data to remove these errors prior to the information extraction operation.

In the past, the use of digital computers to process sensor data has been limited by processing speed and cost. Recent advances in digital technology have resulted in significantly reducing computer costs, while at the same time increasing computer capacity and speed.

This paper will provide the results of a recent investigation dealing with the geometric and radiometric correction of ERTS sensor data using digital processing techniques.

SENSOR DATA CHARACTERISTICS

Multispectral Scanner. A schematic of the ERTS Multispectral Scanner (MSS) is shown in Fig. 1 [1]. An oscillating mirror and optical system reflect and direct the scene radiance energy into a solid-state detector array sensitive to four spectral bands (0.5-0.6, 0.6-0.7, 0.7-0.8, and 0.8-1.1 micrometers). Six scan lines in each spectral band are simultaneously swept with one mirror sweep. The detectors subtend an instantaneous field of view (IFOV) of 79 meters and their outputs are digitized and transmitted to ground or temporarily stored for later transmission. The sensor provides data of excellent quality and dynamic range, but the data contains geometric errors due to spacecraft roll, pitch, yaw, and altitude deviations as well as other effects such as earth rotation and curvature. It is frequently desired that the data be transformed to a desired map projection (e.g., Universal Transverse Mercator) [1,4].

In addition, the sensor detectors each have their own response characteristics (bias and gain) and if left uncorrected will cause "banding" or "striping" of the resultant image. Table 1 identifies the significant geometric and radiometric sensor corrections that must be considered.

Return Beam Vidicon. The Return Beam Vidicon (RBV) is a three camera system (see Fig. 2) using conventional lenses and shutters, and vidicons for image storage and scanning [1]. The cameras are sensitive to scene radiance energy in the spectral range of 0.48 to 0.83 micrometers. The RBV sensors also have internal and external geometric and radiometric errors which are summarized in Table 2.

CONVENTIONAL ELECTRO-OPTICAL IMAGE PROCESSING

Conventionally, electro-optical image processing has been used to correct the geometry and radiometry of the sensor data and to annotate the data with mission information and latitude/longitude tic marks.

Figure 3 summarizes the NASA Data Processing Facility (NDPF) Image Processing System. The System Correction (Bulk Processing) subsystem provides partial geometric correction to all film data, and provides the capability for high density digital tape (HDDT) generation from which computer compatible tapes (CCT) are generated in the Special Processing subsystem. However, the bulk

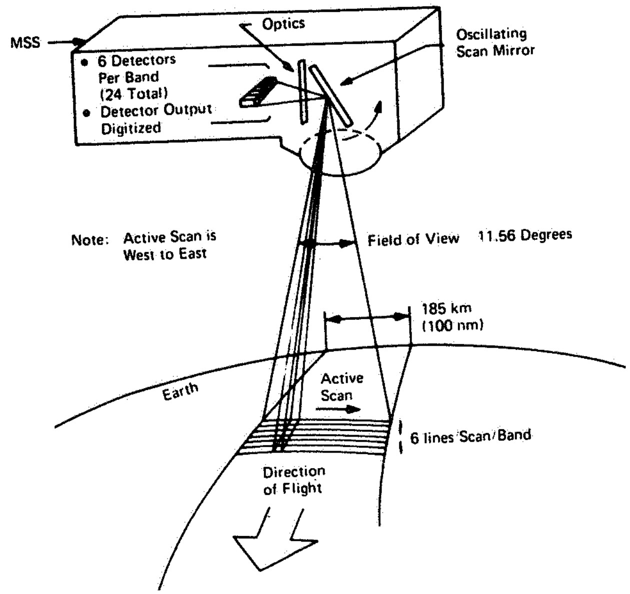

Figure 1. Multispectral Scanner Sensor

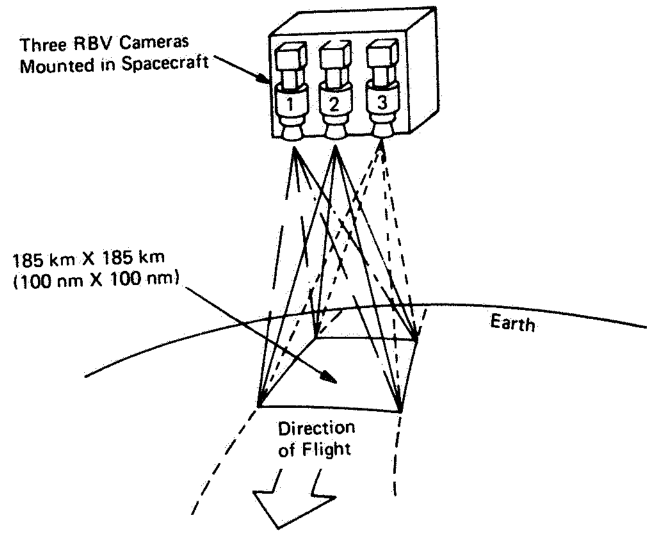

Figure 2. Return Beam Vidicon Camera

Table 1

Multispectral Scanner Sensor Data Compensation

Geometric Correction	
Internal	Mirror Scan Velocity Profile
	Detector Sampling Delay
External	Panoramic Distortion
	Scan Skew
	Earth Rotation
	Spacecraft Velocity
	Perspective Geometry
	Attitude (roll, pitch, yaw)
	Altitude
	Desired Projection (e.g. UTM)
Radiometric Correction	
Internal	Detector Response (Bias & Gain)
External	Atmospheric Attenuation
	Film Recorder Gamma

Table 2

Return Beam Vidicon Sensor Data Compensation

Geometric Correction	
Internal	Lens Distortion
	Scanning Raster Distortion
External	Perspective Projection
	Attitude (roll, pitch, yaw)
	Altitude
	Desired Projection (e.g. UTM)
Radiometric Correction	
Internal	Shading
External	Atmospheric Attenuation
	Film Recorder Gamma

CCT's have no geometric corrections applied. The Scene Correction (Precision Processing) subsystem scans the bulk 70mm films and generates film and CCT products with high geometric accuracy. However, due to the conversion from digital to film to analog and then to film and digital form, some radiometric (intensity) loss occurs. The bulk processing provides excellent radiometry and resolution, and the precision processing excellent geometry. It would be desirable to generate film and tape products that provide the best radiometry and geometry. This can be achieved with digital image processing techniques.

DIGITAL IMAGE PROCESSING CONCEPTS

Digital Image Processing Approach. The MSS and RBV data can be geometrically and radiometrically corrected digitally, using the NDPF CCT data. Figure 4 shows the processing steps involved in digital image correction, and the recording of CCT and film products. It is noted that the sensor data does not go through any unnecessary conversions in the correction process, and the film product is a second generation black and white or color print or transparency. However, in order to geometrically correct the sensor data, the internal and external errors must be determined. The internal errors are due to sensor effects such as non-linear mirror scan profile, and can be precisely determined from pre-launch calibration measurements. The external errors are due to sensor platform and scene characteristics (attitude, altitude, etc.), are variable in nature, and must be determined from ground control data or precise attitude/altitude measurements. Once this information is known, a mapping function can be developed which allows a geometric correction of the sensor data to be made (see Figure 5).

Internal Geometry Determination. The MSS sensor internal geometry distortion is due primarily to mirror scan non-linearity and is determined from pre-launch measurements. It is noted that cross-track distortion is induced into the scene data due to this effect and can cause as much as a seven picture element (pixel) error if left uncorrected.

The RBV sensors have a reseau pattern in the faceplate of each camera [1,4]. Prelaunch calibration determines the reseau positions precisely. Postlaunch location of the reseau marks in the images provide precise information for determining the internal distortion of the RBV. An algorithm has been developed to automatically locate the reseau marks and precisely locate them [4,5].

External Geometry Determination. The external geometry can be determined from either precise attitude measurements, or by the use of scene information. The attitude variation of the ERTS spacecraft is about 0.7^{o} in each axis, and the attitude measurement error is about 0.07^{o} in roll and pitch and about 0.6^{o} in yaw [1]. The attitude uncertainty is not sufficiently accurate for precise external geometry determination and correction. Ground control points (GCP) can be used to provide accurate external geometry information (see Figure 6).

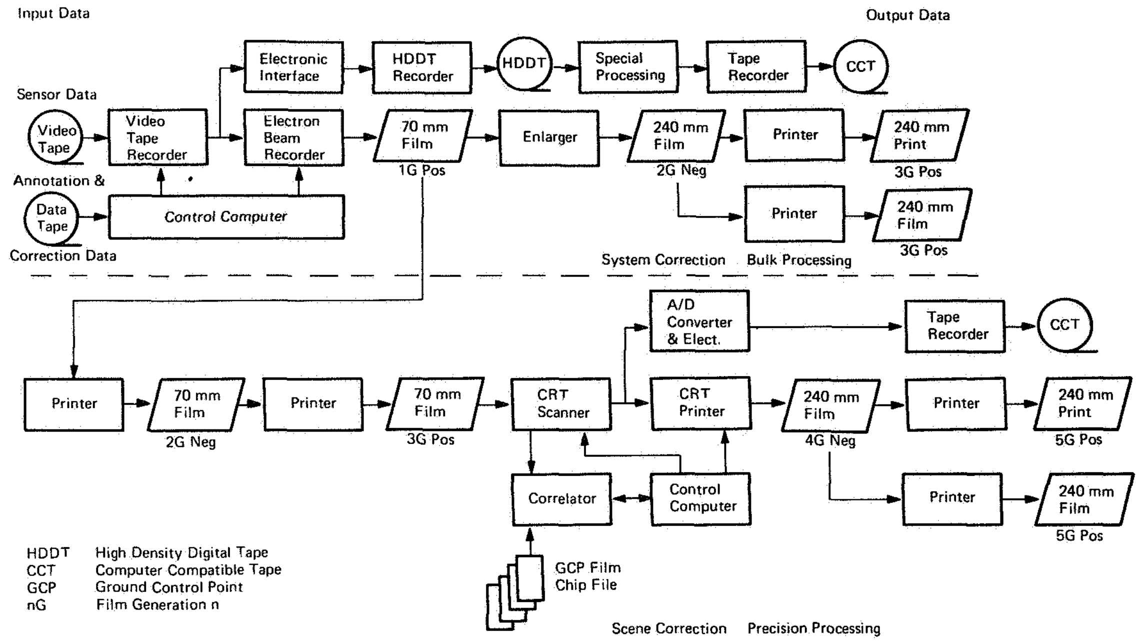

Figure 3. NASA Data Processing Facility Image Processing Subsystem

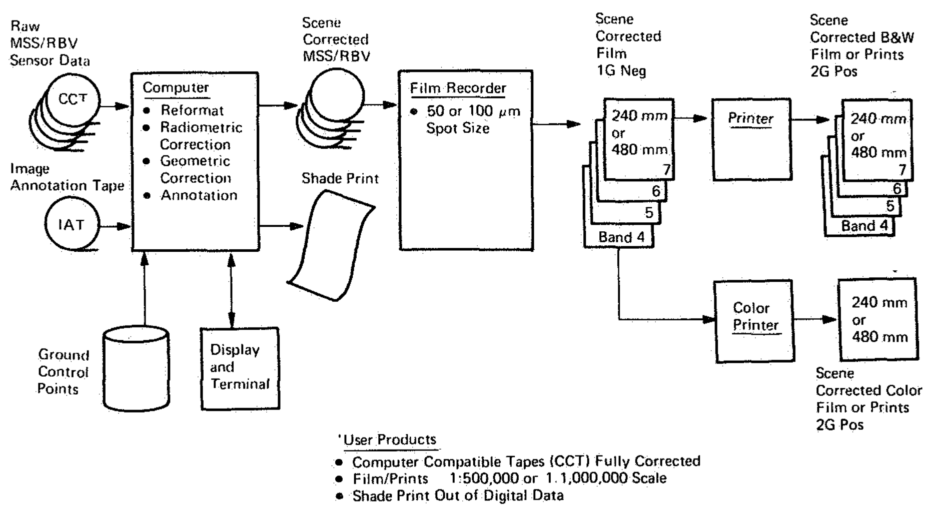

Figure 4. Digital Image Processing Flow and Output Products

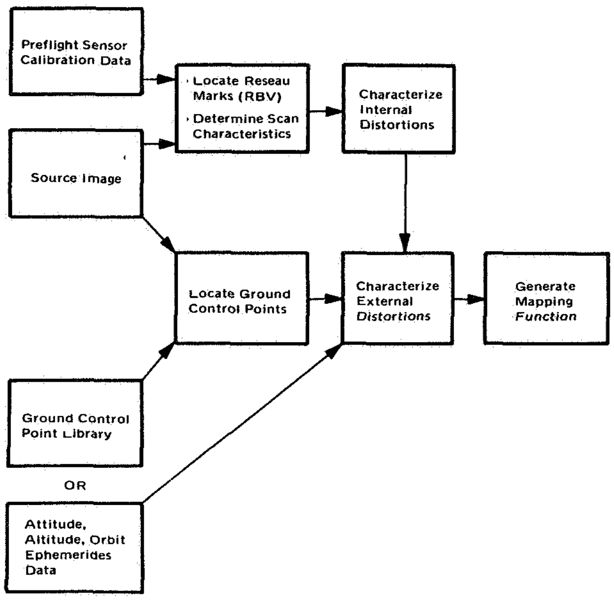

Figure 5. Mapping Function Generation Summary

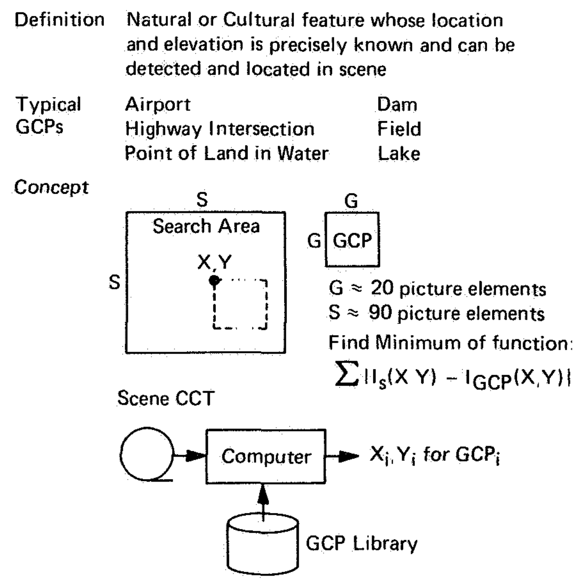

Figure 6. Ground Control Points

A GCP is a detectable natural or cultural feature in the scene whose location and elevation are precisely known. Locating and measuring the positions of a sufficient number of GCP's in the scene provides a measure of the external geometry. Computationally efficient techniques have been developed to locate GCP's in digital data arrays. These techniques are called Sequential Similarity Detection Algorithms (SSDA) [4,6]. Their principal of operation basically involves differencing a random and intensity normalized sample of conjugate points in the GCP and search areas, and summing the differences. When the sum exceeds a selected threshold value, the subimages are considered to be dissimilar, the GCP area is displaced relative to the search area, and another comparison is made. This is continued until a minimum sum function is found. The minimum sum function corresponds to the GCP X, Y coordinates of a "best" match between the GCP and search subimage area. The advantage of this technique relative to conventional correlation or the Fast Fourier Transform (FFT) is that few computations are performed when no similarity exists, resulting in a decrease of registration times of about two orders of magnitude. About nine GCP's are necessary to determine MSS sensor external geometry.

Geometric Correction Concepts. The image spaces and transformations used in the geometric correction of MSS data are shown in Figure 7. The input image is an array of digital data which represents a geometrically distorted one-dimensional perspective projection of some portion of the earth's surface. The output image is a geometrically correct UTM projection of the same ground area.

GCP's are located in the input image and are mapped into the tangent plane using models based on all those errors which can be predicted or determined from tracking data. The nominal GCP locations are mapped from the UTM space to the tangent plane through the equations that relate points in UTM or tangent plane space to points on the earth's surface. The nominal and observed GCP locations in the tangent plane are then used to evaluate the coefficients of the attitude and altitude models.

A network of anchor points spanning the output image is then mapped into the tangent plane and from there (using all the error models) into the input image. Two bivariate polynomials are fit to the two sets of anchor point locations to provide a composite, global mapping from output image to input image.

Typically, for the ERTS MSS geometric correction application, polynomials of degree 3 to 5 have been used. The fifth degree polynomial has the form

$$u = a_{00} + a_{01}Y + \quad a_{23}X^2Y^3 + a_{30}X^3 + \quad + a_{41}X^4Y + a_{50}X^5 \tag{1}$$

$$v = b_{00} + b_{01}Y + \quad + b_{41}X^4Y + b_{50}X^5 \tag{2}$$

Rather than apply the mapping polynomials to all points of the output image, an interpolation grid is established on the output image. This grid is constructed such that, if the four corner points of any grid mesh are mapped with the mapping polynomials, all points interior to the mesh can be located in the input image with sufficient accuracy by bilinear interpolation on the corner points. An output to input mapping operation can be implemented as shown in Figure 8.

Once an individual output image point has been located in the input image, an intensity data value for each point must be derived from the input intensity. A method currently being implemented is nearest neighbor assignment; i.e., the value of the closest data point is assigned. Bilinear interpolation or a higher order intensity computation can be performed based upon neighborhood values to generate a new data value, but will be more expensive computationally.

Radiometric Correction Concepts. The MSS has a total of 24 detectors, six for each band. Each detector output is digitized and quantized into 128 steps for Bands 4, 5, and 6 and 64 steps for Band 7. If the relationship between the correct value and the received value is known, a radiometric or intensity correction can be accomplished by a simple table look-up operation. A typical radiometric correction table is shown in Table 3. Detector #1 response indicates no error, while Detector #2 shows a bias error

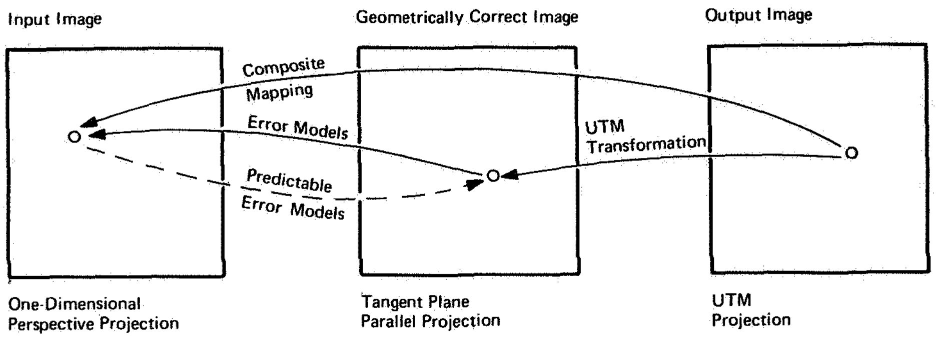

Figure 7. MSS Image Spaces an Transformations

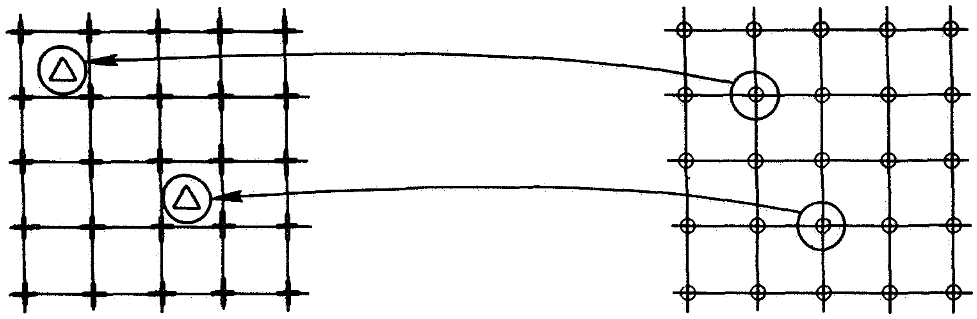

Figure 8. Output to Input Mapping Concept

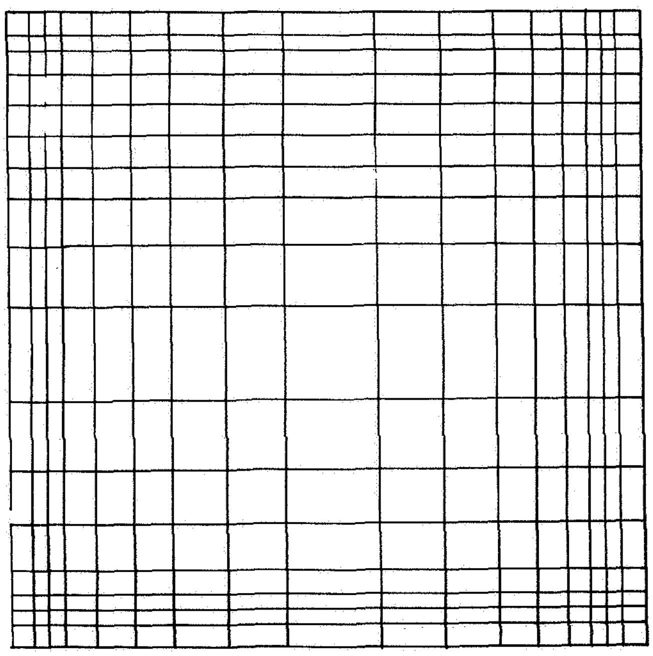

Figure 9. RBV Radiometric Correction Zones

compensation and Detector #24 a gain error compensation. The Received Input Counts are used as an address or pointer to the correct value in the table, and the table value is then used to replace the detector output.

Table 3

Typical MSS Detector Response Correction Table

Detector Output (Counts)	Correct Output			
	Detector #1	Detector #2	...	Detector #24
0	0	1		0
1	1	2		2
2	2	3		4
3	3	4		6
4	4	5		8
.	.	.		.
.	.	.		.
.	.	.		.

The RBV sensor data has significant shading error. This spatially variable intensity error can be determined from prelaunch calibration data by imaging a uniform radiance target. The image can then be subdivided into spatial zones, each having its own intensity correction table, such that the true, spatially-varying correction function is reproduced with an error of no more than one count (see Figure 9).

IMPLEMENTATION OF ALGORITHMS

The concepts discussed in Section 4 have been reduced to practice and individual program modules developed. Figure 10 is a simplified math/logic flow showing the major program modules and how they would be linked in an operational system.

<u>ERTS MSS Control Program</u>. The control program reads user requests and input CCT ID records. It reads into main storage from disk digital images of those GCP's which are contained in the scene and builds a GCP search area definition table for later use by the reformat program. It then controls processing and generates a summary report when scene processing is complete.

<u>Reformat and Radiometric Correction</u>. The reformat program reads the input CCT's, de-multiplexes the band data, combines the 46km (25 nautical mile) data from each of four tapes, and radiometrically corrects the sensor data to produce internally formatted image data on disk files. Concurrently it

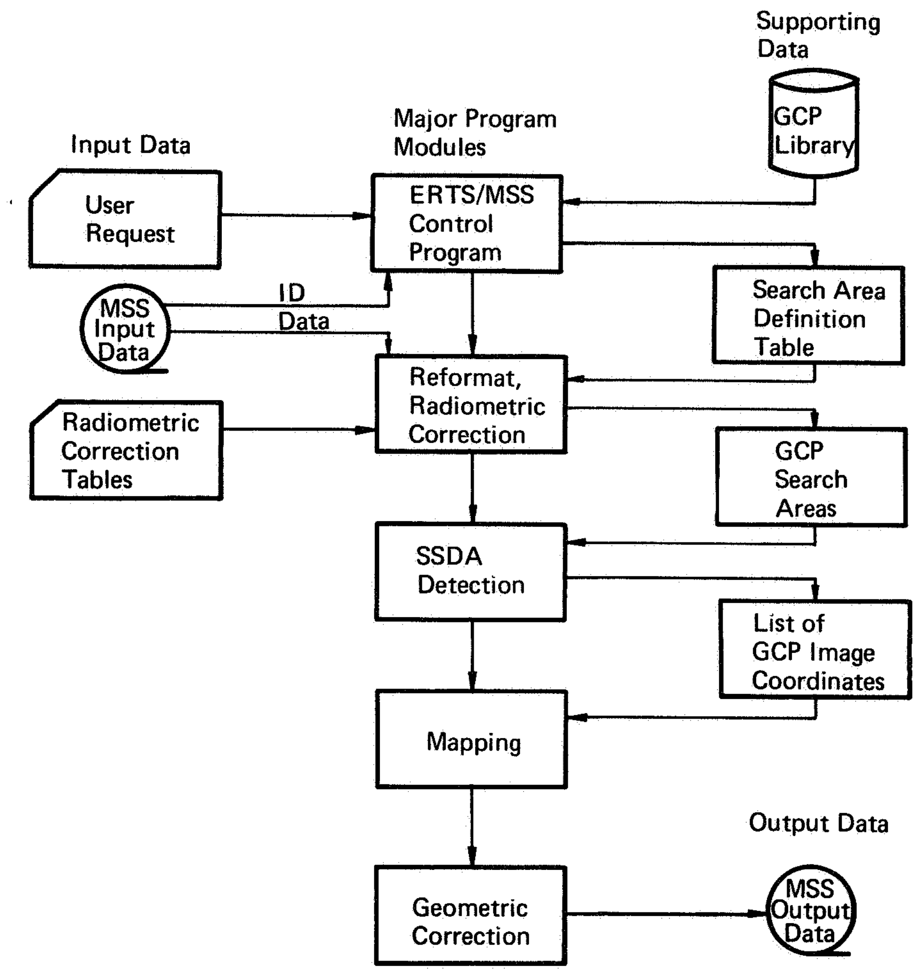

Figure 10. MSS Digital Precision Processing Functional Flow

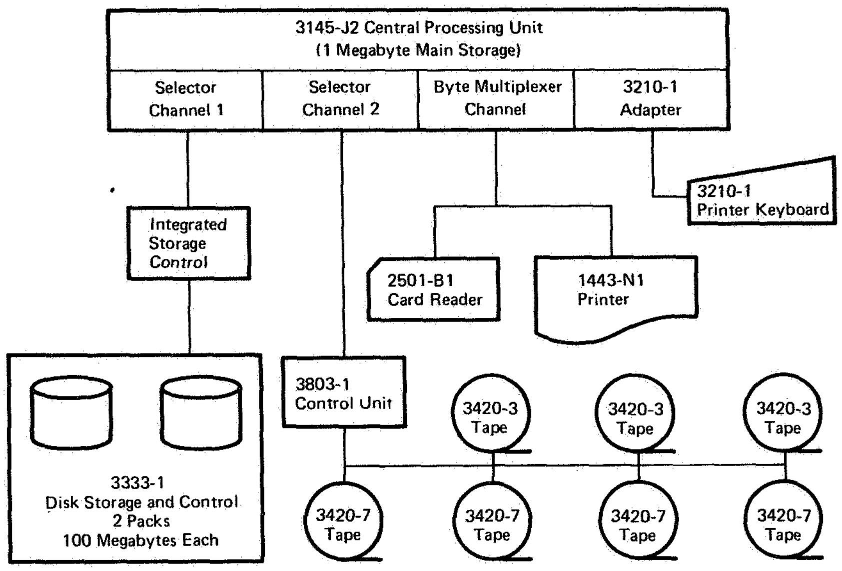

Figure 11. 370/145 Configuration

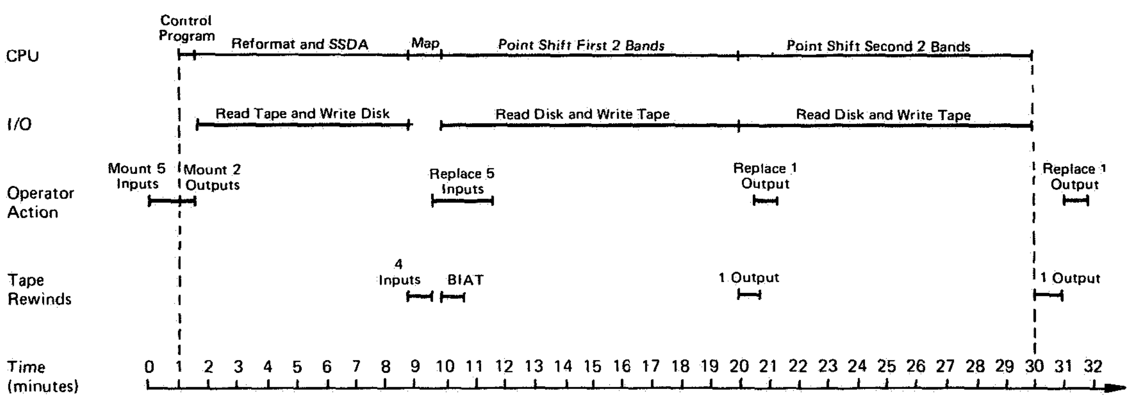

Figure 12. MSS Precision Processing Timeline for the IBM System/370 Model 145

builds GCP search areas by moving subimage areas in specific bands as designated by the input search area definition table to an area in main storage for later use by the SSDA program.

SSDA Detection. The SSDA detection program accesses the GCP search areas and the GCP digital images using pointers contained in the common area. It applies the SSDA and stores registration results in a list in main storage for use by the map program.

Map. The map program computes the mapping function required to geometrically correct the image. It also computes grid point coordinates for the interpolation grid and maps these points into the input image. Finally it computes geographic "tick mark" locations on the image for later use by the geometric correction program.

Geometric Correction. The geometric correction program reads image data from disk (two bands at a time) and accesses parameters (stored by the SSDA and map programs) in main storage via pointers in the common area. It then builds output lines by interpolating between mapped grid points to find the location of the output image pixels in the input image grid network and assigning the nearest neighbor or digitally filtered intensity value to each output pixel. It adds mission, geographic coordinate, scale, and calibration annotation to the images and writes the image and annotation data onto tape.

COMPUTER CONFIGURATIONS AND ANALYSIS

Several general purpose computer configurations and a special purpose computer configuration were developed to implement the image processing algorithms. The design concept was to overlap the CPU time and I/O time to the maximum extent to minimize total elapsed time. The general purpose computers studied were the IBM 370/145, 158, and 168, and the special purpose computer a Microprogrammed Signal Processor (MSP).

IBM 370/145 Configuration and Timeline. The IBM 370/145 is a medium size general purpose computer. The configuration required to process MSS data in a production environment is shown in Figure 11. This configuration uses a one megabyte CPU memory and two packs of disk memory (200M Byte). The sensor data I/O is tape.

The timeline for this configuration is shown in Figure 12. This timeline shows CPU and I/O fully overlapped and elapsed scene processing time of about 29 minutes after tape mounting.

Special Purpose Computer Configuration and Timeline. Figure 13 shows a digital hybrid image processing configuration. The general purpose computer performs the support processing functions such as reformatting the data, locating the GCP's, and computing the mapping function. The special purpose processor implements the geometric and radiometric corrections. The special purpose processor, a Microprogrammed Signal Processor (MSP)

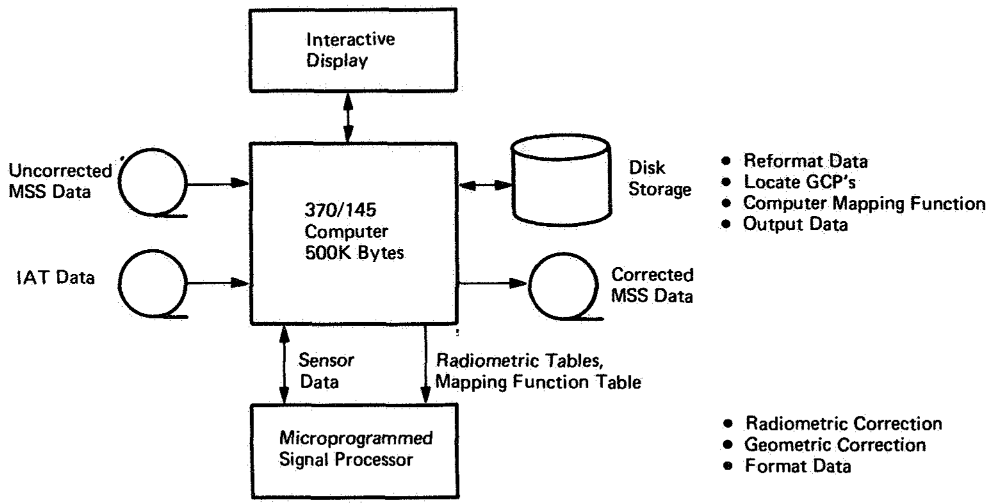

Figure 13. Special Purpose Computer Configuration

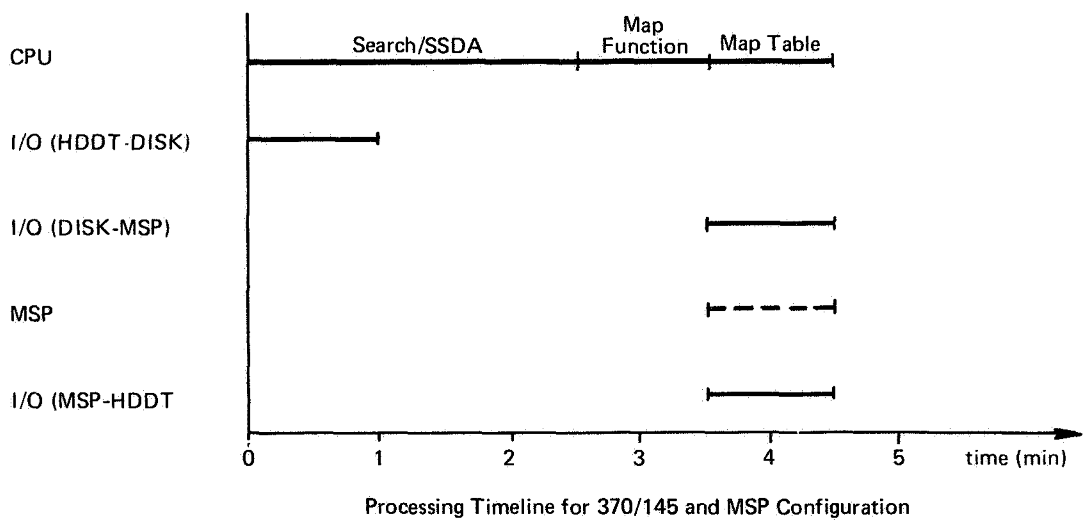

Figure 14. Timeline for Special Purpose Computer Configuration

uses a microprogrammed control storage and is able to implement both the geometric correction and radiometric corrections in less than one μsec per pixel. The timeline for this configuration is shown in Figure 14 and shows that an ERTS MSS scene can be processed in about 4.5 minutes.

Summary of Configuration Analyses. Similar configurations were developed for the other machines, and the processing times are summarized in Table 4. It is noted that the 370/145 processing time is comparable to the NASA Data Processing Facility (NDPF) electro-optical precision processor. It should be further noted that the general purpose processing times are conservative and based upon outputting the sensor data with a 1:1 aspect ratio and at a particular scale to be compatible with an available drum recorder. These times may be reduced by up to a factor of two by the use of a different aspect ratio and the original input data array, as is possible with an electron beam or laser beam film recorder.

GEOMETRIC ACCURACY

A mapping accuracy analysis of the digitally processed image data was performed on both CCT data and on film data. The results are summarized in Table 5. It is significant to note that images with a geometric accuracy of about a picture element can be recorded on CCT allowing accurate temporal change detection and multispectral classification to be performed. Further, maps meeting the National Map Accuracy Standard of 1:125,000 to 1:250,000 scale can be produced from the digital data. Film data with a geometric accuracy of 1-2 picture elements can be produced allowing the recorded ERTS image data to be combined or compared with 1:250,000 to 1:500,000 cartographic or land use maps.

GROUND CONTROL POINT DETECTION AND LOCATION

A number of scenes were processed to determine the accuracy and reliability of the SSDA algorithm for GCP detection and location. GCP and search areas with a temporal separation of up to 180 days were used in this investigation. Table 6 is a summary of the preliminary results. It is noted that by proper selection of bands, good probability of detection and fast processing times can be achieved. However, temporal separations of greater than 90 days for some GCP types may not be desirable. Although the results obtained to date are very encouraging, further investigation in this area is required.

PROCESSED IMAGES

Figures 15 and 16 are MSS images of the Washington, D.C./Chesapeake area that have been digitally processed and recorded on film. Figure 16 is a color composite made from bands 4, 5, and 7. These images demonstrate the excellent quality and resolution that can be obtained from digital image processing techniques.

Table 4

Image Processing Times and Scene Throughput

	370/145	370/158	370/168	NDPF Prec Proc	370/145 & MSP
Processing Times (min)	29	9.0	3.2	30-40	4.5
Scene Throughput/16 hours	33	107	300	28	213
Scenes/Month	990	3210	9000	840	6400

Note: 1 MSS Scene = 4 Spectral Bands

Table 5

Digital Processing Geometric Accuracy - ERTS MSS Data[3]

	RMS Vector Error-Absolute (Meters)	Max Error of 90% of GCP's (Meters)	National Map Accuracy Standard
Digital Data[1] (39 GCP's)	60.6	103	1:125K-1:250K
Film Data[2] (21 GCP's)	135	175	1:250K-1:500K

Notes:

1 Measured Using Computer Shade Prints from Corrected CCT's
2 Measured by USGS from Film Data Recorded from CCT's, Nov. 1973
3 Scene Processed, Chesapeake - 23 Sept. 1972, E-1062-15190

Table 6 Initial SSDA Results

Target Type	Band 4 No. Found/ Tried	Band 4 Average Time (Sec)	Band 5 No. Found/ Tried	Band 5 Average Time (Sec)	Band 6 No. Found/ Tried	Band 6 Average Time (Sec)	Band 7 No. Found/ Tried	Band 7 Average Time (Sec)	Temporal Separation/ Location
Large Land- Water Interfaces	5/5	46	5/5	29	5/5	4	5/5	15	17 Days
Interstate--Grade Highways	1/1	51	1/1	47	1/1	40	1/1	45	Chesapeake
Airports	2/2	12	2/2	4	2/2	8	2/2	22	Search: E-1062-15190
									Window: E-1079-15140
Large Land--Water Interfaces	4/8	50	7/21	27	15/21	5	17/21	14	18 Days
Airports	0/0		1/2	9	2/2	11	2/2	27	Chesapeake
Small Land--Water Interfaces	1/1	49	1/1	30	1/1	8	1/1	29	Search: E-1080-15192
Non-Interstate Highways	0/0		16/16	9	15/16	27	14/16	50	Window: E-1062-15190
Large Land--Water Interfaces	4/6	4	6/6	3	5/6	3	5/6	7	36 Days
Interstate--Grade Highways	2/8	5	6/8	12	6/8	37	6/8	20	Phoenix
Airports	0/2		0/2	-	1/2	48	1/2	7	Search: E-1049-17324
Small Land--Water Interfaces	2/3	12	3/3	12	3/3	49	3/3	6	Window: E-1085-17334
Hills	1/2	6	2/2	6	1/2	5	2/2	52	
Fields	1/1	4	1/1	3	0/1		0/1	-	
Large Land--Water Interfaces	1/2	5	2/2	4	2/2	3	2/2	6	72 Days
									Phoenix
									Search: E-1049-17324
									Window: E-1121-17330
Large Land--Water Interfaces	2/4	3	1/4	2	2/4	2	4/4	7	90 Days
Interstate--Grade Highways	4/8	39	4/8	7	2/8	3	4/8	60	Phoenix
Airports	2/2	49	2/2	8	1/2	6	2/2	71	Search: E-1121-17333
Small Land--Water Interfaces	2/2	64	2/2	8	1/2	3	2/2	62	Window: E-1031-17325
Hills	2/2	52	2/2	16	0/2		2/2	63	
Fields	0/1		0/1	-	0/1	-	0/1	-	
Large Land--Water Interfaces	3/4	5	4/4	3	2/4	2	4/4	5	180 Days
Interstate--Grade Highways	3/5	11	3/5	4	0/5		2/5	54	Phoenix
Airports	0/2		0/2		0/2		2/2	61	Search: E-1211-17334
Small Land--Water Interfaces	1/2	63	1/2	9	0/2		1/2	59	Window: E-1031-17325
Hills	2/2	50	2/2	15	1/2	8	2/2	59	
Fields	0/1		0/1	-	0/1		0/1		

Note: Times are for 360/65 FORTRAN Program.

Figures 15 & 16

(Digitally Processed ERTS Images)

Before Shading Compensation

After Shading Compensation

Figure 17. Before and After RBV Shading Compensation

Figure 17 shows an RBV image before and after digital shading compensation has been implemented. It is noted that near perfect shading compensation has been implemented and regions that were almost completely lacking information due to shading have been recovered.

The MSS raw (bulk) CCT data will show discontinuities as can be seen from Figure 18a. These discontinuities are due to detector sampling delays and other effects causing a spatial data shift which is manifested as a sawtooth-like structure in linear scene features. An experiment was conducted to resample the raw data with the objective of removing this error. Two digital filters were used. A linear intensity assignment filter and a sin x/x approximation. The results of these resampling operations are shown in Figures 18b and 18c. It is noted that both filters will remove the discontinuities, and the resulbs are nearly identical. More experimentation is necessary to fully evaluate the need for and type of MSS resampling required.

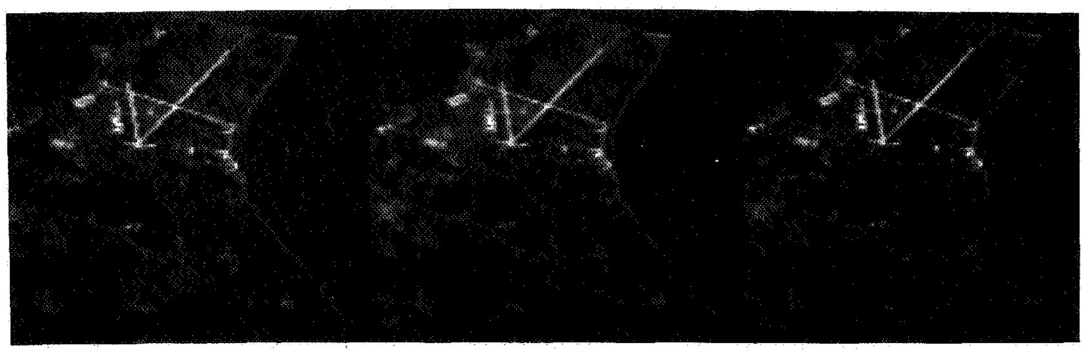

a. Original Image with Detector Sampling Delay Effects

b. Linear Resamplingto Eliminate Detector Sampling Relay

c. Sinx/x Resampling to Eliminate Detector Sampling Delay

Figure 18. Results of Resampling Experiments
(Patuxent Naval Air Station, October 72 Chesapeake Image)

CONCLUSIONS

The following conclusions can be made, based upon the work performed to date:

Geometric Accuracy. A corrected MSS scene can be generated with a one to two picture element mapping accuracy using a bivariate mapping polynomial and nine ground control points.

Radiometric Accuracy. No sensor radiometric degradation is introduced with digital processing. High quality first generation film products and second generation print products can be obtained. Computer compatible tape data with full sensor dynamic range can be generated with no loss of radiometry or resolution.

Processing Times. Medium size general purpose computers can be used to production process ERTS data. Scene processing times (4 bands) in the range of 29 minutes to 3.2 minutes can be obtained with computers in the class of IBM 370/145 to 370/168. Special purpose hardware may be a cost effective alternative.

Processing Automation. Digital image processing automates, to a large extent, the processing of ERTS type data. Multiple film generation stages, with their attendant manual operations and quality control inspections, are eliminated.

ACKNOWLEDGEMENTS

The work reported in this paper was performed by a number of capable and dedicated people. These include D. Ferneyhough, M. Cain, S. Murphrey, C. Colby, R. Depew, W. Niblack, H. Silverman, T. Smith, N. Rossi, T. Gaidelis, H. Markarian, J. Przybocki, and S. Forrer of IBM. Constructive suggestions and support were provided by P. Mooney and S. Shapiro, also of IBM. P. Heffner of NASA Goddard Space Flight Center provided necessary data and encouragement, and Dr. Robert McEwen of the U. S. Geological Survey performed a mapping accuracy assessment of the digitally processed images.

REFERENCES

1. "ERTS Data Users Handbook," NASA Document #715D4249 (Rev. 17 Nov. 1972).

2. "Machine Processing of Remotely Sensed Data," Conference Proceedings, Purdue University, IEEE Catalog No. 73CH0834-2GE, 16-18 October 1973.

3. "Management and Utilization of Remote Sensing Data," Proceedings of Symposium on Remote Sensing, Library of Congress Catalog Card No. 73-88858, 29 October - 1 November 1973.

4. Ralph Bernstein and Harvey Silverman, Digital Techniques for Earth Resource Image Data Processing, presented at AIAA 8th Annual Meeting, FSC 71-6017, 30 September 1971.

5. Ralph Bernstein, Results of Precision Processing (Scene Correction) of ERTS-1 Images Using Digital Image Processing Techniques, Symposium on Significant Results Obtained from the Earth Resources Technology Satellite-1, Vol. II, NASA Document #SP-327.

6. David T. Barnea and Harvey Silverman, A Class of Algorithms for Fast Digital Image Registration, IEEE Transactions on Computers, February 1972.

Paper I 15

SPECTRAL AND TEXTURAL PROCESSING OF ERTS IMAGERY

R. M. Haralick and R. Bosley, *The University of Kansas Center for Research, Inc., Lawrence, Kansas 66044*

ABSTRACT

A procedure is developed to simultaneously extract textural features from all bands of ERTS multi-spectral scanner imagery for automatic analysis. Multi-images lead to excessively large grey tone N-tuple co-occurrence matrices; therefore, neighboring grey tone N-tuple differences are measured and an ellipsoidally symmetric functional form is assumed for the co-occurrence distribution of multi-image greytone N-tuple differences. On the basis of past data the ellipsoidally symmetric approximation is shown to be reasonable. Initial evaluation of the procedure is encouraging.

I. INTRODUCTION

A procedure is being developed to extract textural features for automatic analysis of ERTS multi-spectral scanner imagery. Previous work (Haralick, 1973; Haralick, 1972) indicates that useful textural features can be computed from co-occurrence matrices for grey tones in specific spatial relationships on an image. The performance of the land use classification algorithm using these textural features from only one band is encouraging; up to 75 per cent of the images were correctly classified (Haralick, 1973). Since texture features and spectral features of ERTS multi-images provide different kinds of information, a significant increase in identification accuracy will occur when both features are used together.

Multi-images lead to excessive amounts of storage for the grey tone N-tuple co-occurrence matrices. Therefore, to solve the storage problem we measure grey tone N-tuple differences instead of grey tone N-tuples and assume an ellipsoidally symmetric function form for the co-occurrence distribution of multi-image grey tone N-tuple differences. We expect that the estimated parameters of the ellipsoidally symmetric distribution will lead to textural features which will distinguish between texturally distinct categories on ERTS MSS images over Kansas.

II. TEXTURE

Texture and tone are two fundamental pattern elements used in the interpretation of image data. The concept of tone is concerned with the whiteness, greyness, or blackness of resolution cells of the image. The concept of texture is concerned with the spatial distribution of the grey tones. Tone is based upon the varying shades of grey of the resolution cells in the image, while texture is based upon the spatial distribution of grey tones. However, texture and tone are not independent concepts but are intrinsically related to one another. Although either property can dominate the other depending upon the image context, texture and tone are always present.

When one attempts to objectively use tone and texture pattern elements, the texture-tone concept must be explicitly defined. This can be visualized as follows. When a small area patch of an image has little variation of features of discrete grey tone, then that area is dominated by tonal properties. As the number of distinguishable features of discrete grey tone increases within the patch, then the texture properties will dominate. The size of the small area patch, the relative sizes of the discrete features and the number of distinguishable discrete features are all crucial in this distinction. When the size of the small area patch is reduced to one resolution cell, the only property present is tone. When there is no spatial pattern in the tonal features and the grey tone variation between features is wide, a fine texture results. And as the spatial pattern becomes more defined using more and more resolution cells, then a coarser texture results.

Texture can be termed as being fine, coarse, smooth, rippled, molled, irregular, or lineated. Texture is a property of nearly all surfaces, the grain of wood, the weave of fabric, the pattern of crops in a field, etc. Although texture is quite easy for humans to recognize and describe, it is quite subjective by its nature and is extremely difficult to precisely define and analyze by digital computers. Since the texture of images contains important information for discrimination purposes, textural features could be very useful.

III. REVIEW OF PAST WORK ON TEXTURE

To date there has been at least six different approaches to the problems of measuring and characterizing texture of images: autocorrelation functions, optical transforms, digital transforms, edgeness, structural elements, and spatial grey tone co-occurrence probabilities. The first three approaches all measure spatial frequency either directly or indirectly. Spatial frequency is related to texture because fine textures are rich in high frequencies while coarse textures are rich in low frequencies.

One alternative approach to viewing texture as spatial frequency distribution is to view texture as the amount of edgeness per unit area. Fine textures have a high number of edges per unit area whereas coarse textures have a small number of edges per unit area.

The structural element approach uses a matching procedure to detect the spatial regularity of shapes called structural elements in a binary image. When the structural elements themselves are single resolution cells, the information provided by this approach is the autocorrelation function of the binary image. By using larger and more complex shapes, a more generalized autocorrelation can be computed.

The grey tone spatial dependence approach characterizes texture by the spatial distribution of its grey tones. In coarse textures the distribution changes only slightly with distance, but for fine textures it changes rapidly with distance.

Because of our familiarity with the concepts of spatial frequency and edgeness, these approaches to texture characterizations are readily employed. However, an inherent problem exists with these approaches in regard to grey tone calibration of the image and they are not invariant under even a linear grey tone translation. And the price paid for invariance by compensating with quantization is a loss of grey tone precision in the quantized image.

The power of the structural element approach is that is emphasizes the shape aspects of the discrete tonal features. Weakness of this approach lies in that it can only do so for binary images.

The power of the spatial grey tone co-occurrence approach lies in characterizing the spatial inter-relationships of the grey tones in a texture pattern in such a way that is invariant under monotonic grey tone transformations. Weakness of the approach lies in failure to capture the shape aspects of the discrete tonal features.

IV. TEXTURAL FEATURES

The above description of texture is an idealization of what actually occurs, a gross simplification. Discrete tonal features are actually quite subjective in that they do not necessarily stand out as entities by themselves. Therefore, the texture analysis presented here is concerned with more general or macroscopic concepts rather than discrete tonal features. The procedure developed by Haralick (Haralick, 1972) for obtaining the textural features of an image is based on the assumption that the texture information on an image I is contained in the overall spatial relationship which the greytones in the image I have to one another. More specifically, we assume that this texture information is adequately specified by a set of spatial grey tone dependence matrices, which are computed for various angular relationships and distances between neighboring resolution cell pairs on the image. All of the textural features are then derived from these angular nearest neighbor spatial grey tone dependence matrices.

IV.1 Spatial Grey Tone Dependence Matrices

Let $G = \{0, 1, \ldots, Ng\}$ be the set of possible grey tones that each resolution cell can take on after image normalization by equal probability quantizing to Ng levels. It can be shown that this quantization quarantees that images which are a monotonic transformation of one another, such as lighter or darker images due to variations in film, lighting, or development, will produce the same results. Let Nx be the number of resolution cells in the horizontal direction and Ny the number of resolution cells in the vertical direction in the image to be analyzed so that $Lx = \{1, 2, \ldots, Nx\}$ and $Ly = \{1, 2, \ldots, Ny\}$ are the horizontal and vertical spatial domains. Then $Ly \times Lx$ will be the set of resolution cells of the image. And the image I can be represented as a function which assigns some grey tone in G to each resolution cell or pair of coordinates in $Ly \times Lx$; $I: Ly \times Lx \rightarrow G$.

Essential to our conceptual framework of texture are four closely related measures called angular nearest neighbor grey tone spatial dependence matrices. The concept of angular nearest neighbor for a resolution cell is the adjacent resolution cell for a given angle, as shown in Figure 1.

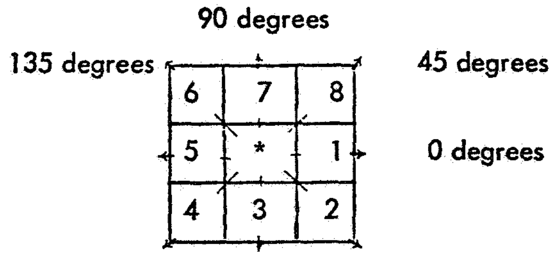

FIGURE 1. Eight nearest neighbor resolution cells of cell '*'. Resolution cells 1 and 5 are the 0-degree nearest neighbors to resolution cell '*', resolution cells 2 and and 6 are the 135-degree nearest neighbors, etc. Note that this information is purely spatial, having nothing to do with grey tone values.

We assume that the texture information in our image I is contained in the overall or "average" spatial relationship which the grey tones in image I have to one another. Specifically, we shall assume that this information is adequately specified by the matrix of relative frequencies Pij with which two neighboring resolution cells separated by distance d occur on the image, one with grey tone i and the other with grey tone j. These matrices of spatial grey tone dependence frequencies are a function of the angular relationship between the neighboring resolution cells as well as a function of the distance between them. Figure 2 illustrates the set of all horizontal neighboring resolution cells separated by distance 1. This set along with the image grey tones would be used to calculate a distance i horizontal spatial grey tone dependence matrix. Formally, for angles quantized to 45° intervals the unnormalized frequencies are defined by:

$$P(i,j,d,0^{\circ}) = \#\{((k,l),(m,n)) \in (L_y \times L_x) \times (L_y \times L_x) \mid k-m=0,\ |l-n|=d,\ I(k,l)=i,\ I(m,n)=j\}$$

$$P(i,j,d,45^{\circ}) = \#\{((k,l),(m,n)) \in (L_y \times L_x) \times (L_y \times L_x) \mid (k-m=d,\ l-n=-d) \text{ or } (k-m=-d,\ l-n=d),\ I(k,l)=i,\ I(m,n)=j\}$$

$$P(i,j,d,90^{\circ}) = \#\{((k,l),(m,n)) \in (L_y \times L_x) \times (L_y \times L_x) \mid |k-m|=d,\ l-n=0,\ I(k,l)=i,\ I(m,n)=j\}$$

$$P(i,j,d,135^{\circ}) = \#\{((k,l),(m,n)) \in (L_y \times L_x) \times (L_y \times L_x) \mid (k-m=d,\ l-n=d) \text{ or } (k-m=-d,\ l-n=-d),\ I(k,l)=i,\ I(m,n)=j\}$$

Note that these matrices are symmetric; $P(i, j; d, a) = P(j, i; d, a)$. The distance metric ρ implicit in the above equations can be explicitly defined by $\rho((k, l), (m, n)) = \max\{|k-m|, |l-n|\}$.

(1,1)	(1,2)	(1,3)	(1,4)
(2,1)	(2,2)	(2,3)	(2,4)
(3,1)	(3,2)	(3,3)	(3,4)
(4,1)	(4,2)	(4,3)	(4,4)

$$L_y = \{1,2,3,4\}$$
$$L_x = \{1,2,3,4\}$$

$$\begin{aligned}
R_H = & \Big\{\big((k,l),(m,n)\big) \in (L_y \times L_x) \times (L_y \times L_x) \,\big|\, k-m=0,\ |l-n|=1\Big\} \\
= & \Big\{\big((1,1),(1,2)\big), \big((1,2),(1,1)\big), \big((1,2),(1,3)\big), \big((1,3),(1,2)\big), \\
& \big((1,3),(1,4)\big), \big((1,4),(1,3)\big), \big((2,1),(2,2)\big), \big((2,2),(2,1)\big), \\
& \big((2,2),(2,3)\big), \big((2,3),(2,2)\big), \big((2,3),(2,4)\big), \big((2,4),(2,3)\big), \\
& \big((3,1),(3,2)\big), \big((3,2),(3,1)\big), \big((3,2),(3,3)\big), \big((3,3),(3,2)\big), \\
& \big((3,3),(3,4)\big), \big((3,4),(3,3)\big), \big((4.1),(4,2)\big), \big((4,2),(4,1)\big), \\
& \big((4,2),(4,3)\big), \big((4,3),(4,2)\big), \big((4,3),(4,4)\big), \big((4,4),(4,3)\big)\Big\}
\end{aligned}$$

FIGURE 2. Illustrates the set of all Distance I Horizontal Neighboring Resolution Cells on a 4 x 4 Image.

For an example of the four distance 1 grey tone spatial dependence matricies, consider Figure 3. Figure 3-a represents a 4x4 image with four grey tones, ranging from 0 to 3. Figure 3-b shows the general form for any grey tone spatial dependence matrix. For example, the element in the (2, 1)-st position of the distance 1 horizontal P_H matrix is the total number of times two grey tones of value 2 and 1 occurred horizontally adjacent to each other. To determine this number, we count the number of pairs of resolution cells in R_H such that the first resolution cell of the pair has grey tone 2 and the second resolution cell of the pair has grey tone 1. Figure 3-c through 3-f shows all four distance 1 grey tone spatial dependence matrices.

IV.2 Textural Features for Multi-Images

Results of previous work in texture using the spatial grey tone dependence matrices as the basis from which all textural features are extracted has been very encouraging (Haralick, 1973). The computational aspects of the procedure are also notable. The number of operations required to process an image using the spatial grey tone dependence matrices is directly proportional to the number of resolution cells, N, present in an image. In comparison, the number of operations needed to use Fourier or Hadamard transforms to extract texture information are of the order of N log N. And, to compute the entries in the spatial grey tone dependence matrices, one needs to keep only two lines of image data in core at a time, keeping storage requirements to a minimum.

Even with these advantages, however, the extraction of texture information from multiimages, as in the case of ERTS MSS data, forces a new approach to the measurement of grey tone N-tuple co-occurrences. The use of the spatial dependence matrices requires that they be stored in the computer. For multi-images containing grey tone N-tuples, we have many more possible combinations of neighboring N-tuples to count and as a result, the dependence matrices will be very large. For example, for four MSS bands in which each grey tone can range through 64 levels, each matrix would have $64^4 \times 64^4$ elements. Even using the symmetry of the matrices to reduce the number of entries does not help since there would be on the order of 10^{15} entries.

The spatial dependence matrices, however, provide a way of escape. In using these matrices, it was observed that they are heavily weighted along the diagonal with decreasing entries farther from the diagonal. Figure 4 gives an

0	0	1	1
0	0	1	1
0	2	2	2
2	2	3	3

FIGURE 3-a.

		Grey Tone 0	1	2	3
	0	#(0,0)	#(0,1)	#(0,2)	#(0,3)
	1	#(1,0)	#(1,1)	#(1,2)	#(1,3)
Grey Tone	2	#(2,0)	#(2,1)	#(2,2)	#(2,3)
	3	#(3,0)	#(3,1)	#(3,2)	#(3,3)

FIGURE 3-b. The general form of any grey tone spatial dependence matrix for an image with integer grey tone values 0 to 3. #(i,j) stands for number of times grey tones i and j are neighbors.

0°

$$P_H = \begin{pmatrix} 4 & 2 & 1 & 0 \\ 2 & 4 & 0 & 0 \\ 1 & 0 & 6 & 1 \\ 0 & 0 & 1 & 2 \end{pmatrix}$$

FIGURE 3-c.

90°

$$P_V = \begin{pmatrix} 6 & 0 & 2 & 0 \\ 0 & 4 & 2 & 0 \\ 2 & 2 & 2 & 2 \\ 0 & 0 & 2 & 0 \end{pmatrix}$$

FIGURE 3-d.

135°

$$P_{LD} = \begin{pmatrix} 2 & 1 & 3 & 0 \\ 1 & 2 & 1 & 0 \\ 3 & 1 & 0 & 2 \\ 0 & 0 & 2 & 0 \end{pmatrix}$$

FIGURE 3-e.

45°

$$P_{RD} = \begin{pmatrix} 4 & 1 & 0 & 0 \\ 1 & 2 & 2 & 0 \\ 0 & 2 & 4 & 1 \\ 0 & 0 & 1 & 0 \end{pmatrix}$$

FIGURE 3-f.

90 DEGREES

30																															
24	26																														
15	23	28																													
6	16	19	8																												
15	7	11	11	8																											
5	6	7	7	6	6																										
1	3	6	6	3	7	3																									
2	5	8	2	8	2	3	8																								
1	6	4	1	4	2	3	4	2																							
1	1	5	4	2	3	4	3	1	2																						
3	1	6	5	1	6	5	1	1	1	2																					
2	3	5	3	2	2	0	2	3	2	0	0																				
0	1	4	6	4	5	5	2	3	0	4	2	0																			
0	2	1	6	2	4	2	2	3	3	2	2	3	0																		
1	2	6	3	5	1	3	4	0	0	5	1	2	1	0																	
0	2	3	5	2	4	2	2	5	1	1	2	6	1	0	2																
0	1	0	3	3	1	2	2	1	2	4	3	1	1	1	4	4															
2	0	3	4	2	2	1	6	1	1	2	0	2	2	2	2	0	6														
0	1	1	1	2	1	0	0	3	1	0	0	3	2	0	4	0	0	0													
0	0	1	0	3	1	1	1	0	0	1	4	1	1	0	0	1	3	0	0												
0	0	1	0	2	0	3	0	2	2	0	2	3	2	1	0	1	0	0	2	2											
0	0	0	0	1	0	4	1	1	2	1	1	2	3	0	3	1	1	2	2	2	2										
0	0	0	1	0	0	0	1	1	0	2	3	2	2	0	1	3	0	1	0	0	1	2									
0	0	1	0	1	0	0	0	1	1	0	4	1	0	2	1	4	2	1	0	0	1	0	0								
0	1	0	0	1	3	0	0	2	1	2	4	0	2	4	7	4	0	2	2	2	0	1	1	2							
0	0	0	0	2	1	0	3	1	1	1	2	1	1	1	1	1	3	1	1	1	0	2	2	2	2						
0	0	0	0	1	0	0	1	0	1	2	2	1	1	2	3	0	3	1	0	1	1	1	1	3	1	2					
0	0	0	0	1	1	1	0	0	0	1	1	2	2	1	3	1	6	3	0	0	1	4	0	2	3	1	0				
0	0	0	1	0	0	0	0	1	0	0	0	2	1	2	2	0	4	0	2	1	8	2	2	8	3	3	0	6			
0	0	0	0	0	0	0	0	0	0	1	0	1	1	0	1	3	2	2	2	0	0	0	1	7	3	4	4	3	8		
0	0	0	0	0	0	0	0	0	0	1	0	1	0	0	1	0	0	1	1	1	0	0	1	1	1	0	3	8	4	2	
0	0	0	0	0	0	0	0	0	0	0	0	0	0	0	0	0	0	0	0	0	0	0	0	0	1	0	1	1	7	6	10

FIGURE 4. Example of Nearest Neighbor Grey Tone Dependence Matrices, Taken from Processing ERTS Data.

example of these matrices. Note that in each case the number of entries decreases as we move away from the diagonal. This suggests that neighboring resolution cells are similar. Choosing any resolution cell in an image at random, we are very likely to find nearly identical neighbors to the cell in all directions and less likely to find dissimilar neighbors. Clearly, a measure which indicates how similar the neighboring N-tuples are and how fast the similarity drops off with distance must contain textural information about the object imaged.

It is therefore reasonable to measure the difference between neighboring grey tone N-tuples and observe this distribution instead of computing the number of times each N-tuple neighbors every other N-tuple. In both cases we measure the co-occurrence of nearest neighbor grey tone N-tuples.

Since the textural features are based on the spatial dependence of grey tone N-tuples, our first step must be to define a binary relation between neighboring resolution cells on which the co-occurrence of grey tones N-tuples can be counted. As above, let $Lx = \{1, 2, \ldots, Nx\}$ and $Ly = \{1, 2, \ldots, Ny\}$ be the set of column and row indexes, respectively, so that $Ly \times Lx$ is the set of resolution cells in the image. Let $G = \{0, 1, \ldots, Ng\}$ be the set of possible grey tones that each component of every grey tone N-tuple can be assigned. Then, the image I can be defined by $I{:}Ly \times Lx \to G \times G \times \ldots \times G$.

Let R be the set of all pairs of resolution cells in a specified spatial relation. Then R is a binary relation on the set $Ly \times Lx$; $R \subseteq (Ly \times Lx) \times (Ly \times Lx)$. For example, the set of all distance 1 horizontally neighboring pairs of neighboring resolution cells would be defined by:

$$R = \Big\{\big((k, l), (m, n)\big) \in (Ly \times Lx) \times (Ly \times Lx) \mid k-m=0, \ |l-n|=1\Big\}.$$

The co-occurrence frequency of grey tone N-tuples $(i_1, i_2, \ldots, i_N)$ and $(j_1, j_2, \ldots, j_N)$ in spatial relation defined by R is

$$P\big((i_1, \ldots, i_N), (j_1, \ldots, j_N)\big) = \frac{\#\Big\{\big((k, l), (m, n)\big) \in R \mid I(k, l) = (i_1, \ldots, i_N), I(m,n) = (j_1, \ldots, j_N)\Big\}}{\#R}$$

where # denotes the number of elements in the set.

Note that this R is symmetric. Assume that $\big((k, l), (m, n)\big)$ is in R. Then $k-m=0$, and $|l-n|=1$ from the definitions of R. But $|l-n|=1$ when $|n-l|=1$.

And if $|n-l| = 1$ and $k-m = 0$, then $\big((m, n), (k, l)\big)$ is in R. Thus, R is symmetric. In fact, by the symmetry of any distance function, R, in general, must be symmetric. And since R is symmetric, P is also symmetric.

IV.3 Textural Feature Extraction Procedure

Let R be a symmetric binary relation pairing nearby neighboring resolution cells. We define the frequency of grey tone N-tuple differences co-occurring in the spatial configuration defined by R as

$$P(x_1, x_2, \ldots, x_N) = \frac{\# \left\{ \big((i, j), (m, n)\big) \in R \mid I(i, j) - I(m, n) = \begin{pmatrix} x_1 \\ \vdots \\ x_N \end{pmatrix} \right\}}{\# R}.$$

Note that P is an even function since

$$\begin{aligned} P(x_1, x_2, \ldots, x_N) &= \# \left\{ \big((i, j), (m, n)\big) \in R \mid I(i, j) - I(m, n) = \begin{pmatrix} x_1 \\ \vdots \\ x_N \end{pmatrix} \right\} / \# R \\ &= \# \left\{ \big((i, j), (m, n)\big) \in R^{-1} \mid I(i, j) - I(m, n) = \begin{pmatrix} x_1 \\ \vdots \\ x_N \end{pmatrix} \right\} / \# R \\ &= \# \left\{ \big((m, n), (i, j)\big) \in R \mid I(i, j) - I(m, n) = \begin{pmatrix} x_1 \\ \vdots \\ x_N \end{pmatrix} \right\} / \# R \\ &= \# \left\{ \big((m, n), (i, j)\big) \in R \mid I(m, n) - I(i, j) = \begin{pmatrix} -x_1 \\ \vdots \\ -x_N \end{pmatrix} \right\} / \# R \\ &= P(-x_1, -x_2, \ldots, -x_N). \end{aligned}$$

Referring to the monotonic behavior of nearly every column in the matrices of Figure 4, and assuming that this behavior occurs on every band of the ERTS multi-images, it is reasonable to assume that the even frequency distribution $P(x_1, \ldots, x_N)$ of the nearby grey tone N-tuple differences can be adequately approximated using an ellipsoidally symmetric distribution; thus we may write

$$P(x_1, x_2, \ldots, x_N) = f(x' A x)$$

for some monotonically decreasing function f.

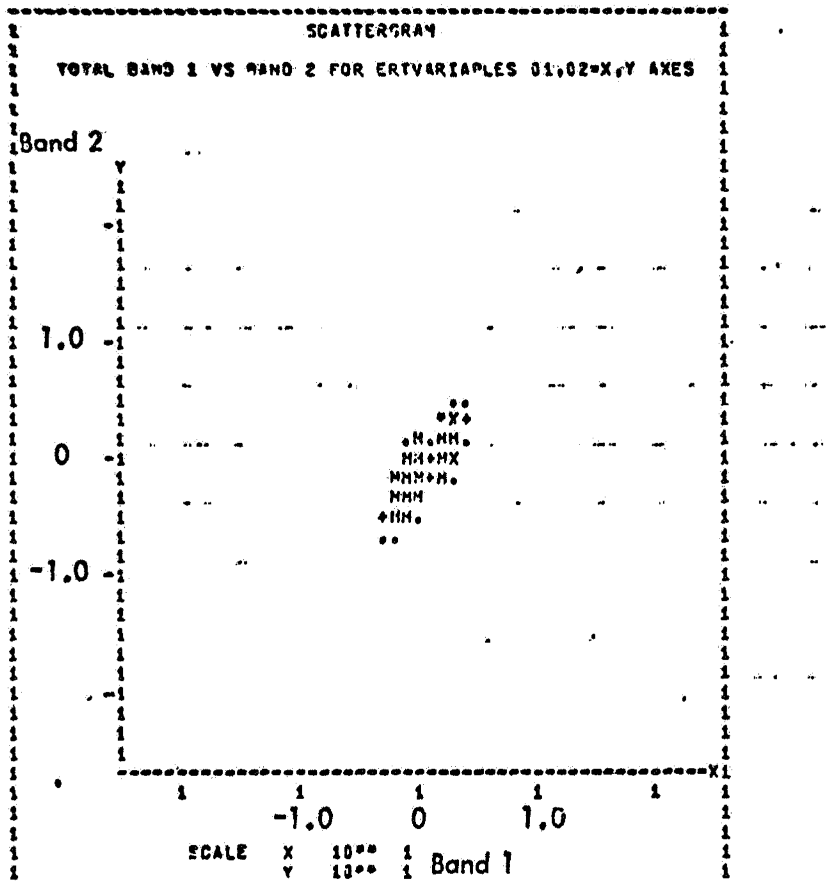

FIGURE 5. Scattergram showing ellipsoidally symmetric distribution of differences for Bands 1 and 2 over a sample 64 x 64 ERTS image.

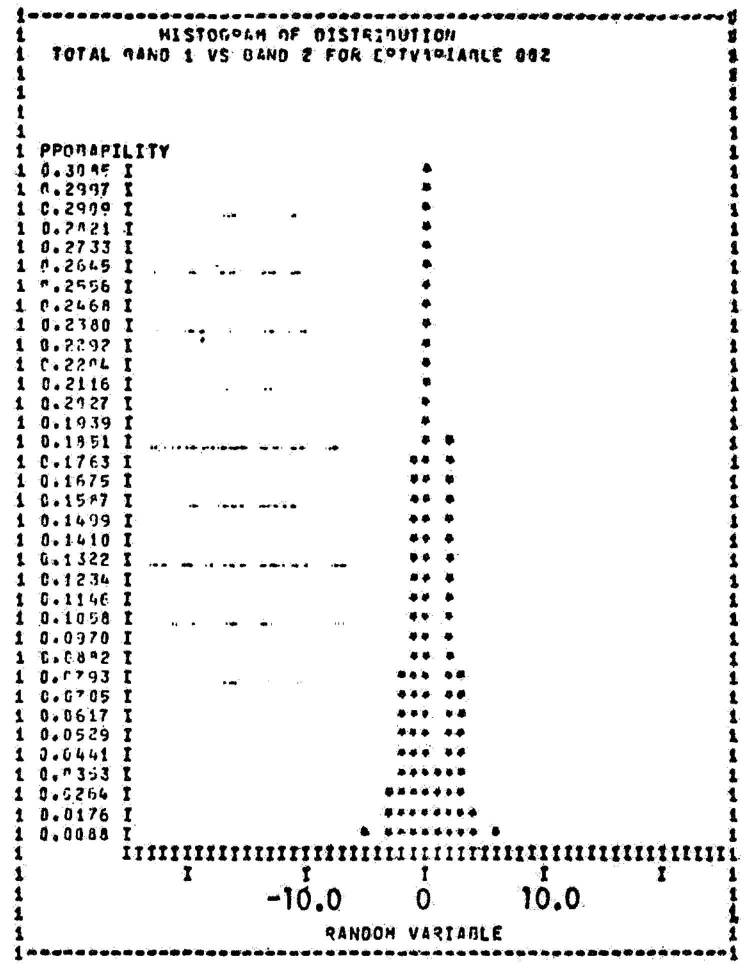

FIGURE 6. Histogram of the distribution of differences on Band 2 for distance 1 horizontally neighboring resolution cells.

This implies that only the function f and the matrix A need to be determined. We take f to be one of the two forms $e^{-1/2\,\mu^2}$, $(1+\mu^2)^{-m}$. Figure 5 is a scattergram of the differences for the first two bands of distance 1 horizontally neighboring resolution cells of a 64x64 sample image. Figures 5 and 6 clearly show the ellipsoidally symmetric functional form of the distribution of neighboring differences. In Appendix I N-dimensional spherical coordinate systems and ellipsoidally symmetric distributions are discussed and it is shown that the matrix A is proportional to the inverse covariance matrix of the N-tuple differences. Thus, we estimate A by a matrix proportional to the inverse of the estimate for the covariance matrix.

Therefore, if the image is blocked into subimages of small area so that each subimage is essentially of one category, we can expect the distribution of grey tone N-tuple differences over each subimage to be a function only of the assumed form of the function f and the covariance matrix of the difference vectors for grey tone N-tuples in a specified spatial relationship within the subimage. This leads us to consider textural features for multi-images based upon the elements of this spatial-spectral covariance matrix.

Consider each covariance matrix as a vector. Consider the distribution of the set of covariance matrices from the blocked image. Since the entries of the covariance matrix are the parameters of the distribution, we would like to have these entries invariant with respect to scale changes on the grey tone N-tuple differences. In order to do this, we scale the grey tone N-tuple differences so that all components have variance 1. The covariance matrix of these normalized differences is equivalent to the correlation matrix. Appendix II shows that this normalization procedure makes the covariance matrix invariant with respect to translating and scaling transformations on the grey tone N-tuples. The normalized covariance matrix can be considered as an extracted texture feature vector in an N(N-1)/2 dimensional hyperspace.

V. RESULTS OF CLASSIFICATION EXPERIMENTS ON ERTS MULTI-IMAGES

In order to obtain an initial estimate of performance of the multi-image texture features an experiment was performed on ERTS satellite imagery over Monterey Bay, California, image ID number 1002-18134. Using a small set of 64 sampled 32x32 subimages and training on 34 of these, 80 per cent of the remaining 30 test samples were correctly classified according to four land-use categories: coastal forest, annual grassland, urban area, and water, as shown in Table I. This is encouraging since previous accuracy using spatial dependence matrices on band 5 over the same general area was only 70.5 per cent as shown in Table II.

The ability to obtain good ground truth and several distinct categories in the California data was not the case for an ERTS image over Finney County, Kansas, which was used in the final experiments. Approximately a 40 mile by 60 mile section near Garden City, Kansas, on image (ID number) 1330-16512 was processed with initially four categories; grassland, large fields, small fields, and water. Both texture procedures, using spectral multi-image features and the single band 5 spatial dependence matrix, were used on the image. Tables III and IV show the results of classification for distance 1 resolution cells while Tables V and VI show distance 8 results. In both cases the single image classification is higher. However, when both distances 1 and 8 are used together, classification accuracy for both procedures is nearly identical, as shown in Tables VII and VIII, about 70 per cent.

This implies that much more information is contained in the Kansas data texturally than spectrally. In hope of adding more texture information, a measure of entropy relating to the correlation matrix was added to the spectral features. The effect of this new feature upon classification accuracy is presently being evaluated. We are also adding higher order components to the grey tone N-tuples in an attempt to gain more textural information from the data.

VI. CONCLUSION

The procedure developed here for the extraction of textural information from ERTS multi-images gives encouraging results. The procedure is quite simple to employ and is a natural evolution of the previous texture extraction technique based upon angular nearest neighbor grey tone dependence matrices. It retains the power of the previous approach to texture by characterizing the spatial interrelationships, or co-occurrences, of the grey tone N-tuples present in a texture pattern in multi-images in such a way as to be invariant under monotonic grey tone transformations.

KANSAS DATA :

IMAGE NO. : 1330-16515 18 JUN 73

AREA PROCESSED : 40MI. BY 60MI (APPROX.)

GARDEN CITY, KANSAS

SPECTRAL-TEXTURAL SUBIMAGE :

32 POINTS PER LINE

32 LINES

TEXTURAL SUBIMAGE :

64 POINTS PER LINE

64 LINES

MSS BAND 5

CALIFORNIA DATA:

IMAGE NO. : 1002-18134 25 JUL 72

AREA PROCESSED : 40 MI BY 100 MI (APPROX.)

MONTEREY BAY, CALIFORNIA

SPECTRAL-TEXTURAL SUBIMAGE :

32 POINTS PER LINE

32 LINES

TEXTURAL SUBIMAGE :

64 POINTS PER LINE

64 LINES

MSS BAND 5

		ASSIGNED CATEGORY				
		COASTAL FOREST	ANNUAL GRASSLAND	URBAN AREA	WATER	TOTAL
TRUE CATEGORY	COASTAL FOREST	5	0	5	0	10
	ANNUAL GRASSLANDS	0	7	0	0	7
	URBAN AREA	0	1	7	0	8
	WATER	0	0	0	5	5
	TOTAL	5	8	12	5	30

Table I. Contingency Table for Land Use Classification of ERTS-1 Satellite Imagery of Monterey Bay, California Using Spectral-Textural Features. Classification Accuracy on Test Set =80%.

FEATURES	NO. OF SAMPLES IN TRAINING SET	NO. OF SAMPLES IN TEST SET	OVERALL ACCURACY OF TEST SET
SPECTRAL-TEXTURAL	34	30	80%
TEXTURAL	260	172	70.5%

Table II. Results of Land Use Classification Experiments from Satellite Imagery of Monterey Bay, California.

		ASSIGNED CATEGORY				
		GRASSLAND	LARGE FIELDS	SMALL FIELDS	WATER	TOTAL
TRUE CATEGORY	GRASSLAND	47	11	5	0	63
	LARGE FIELDS	3	142	32	1	178
	SMALL FIELDS	17	46	52	0	115
	WATER	0	1	6	1	8
	TOTAL	67	200	95	2	364

TABLE III. Contingency Table for Land Use Classification of Satellite Imagery over Kansas Using Spectral-Textural Features, Distance 1, Four Categories. Classification Accuracy on Test Set =67%.

FEATURES	NO. OF SAMPLES IN TRAINING SET	NO. OF SAMPLES IN TEST SET	OVERALL ACCURACY OF TEST SET
SPECTRAL-TEXTURAL	548	364	67%
TEXTURAL	140	88	76%

TABLE IV. Results of Land Use Classification Experiments from Satellite Imagery of Kansas, Distance 1, Four Categories.

TRUE CATEGORY	ASSIGNED CATEGORY: GRASSLAND	LARGE FIELDS	SMALL FIELDS	WATER	TOTAL
GRASSLAND	32	9	22	0	63
LARGE FIELDS	7	147	24	0	178
SMALL FIELDS	18	44	53	0	115
WATER	0	4	4	0	8
TOTAL	57	204	103	0	364

TABLE V. Contingency Table for Land Use Classification of Satellite Imagery over Kansas Using Spectral-Textural Features, Distance 8, Four Categories. Classification Accuracy on Test Set =64%.

FEATURES	NO. OF SAMPLES IN TRAINING SET	NO. OF SAMPLES IN TEST SET	OVERALL ACCURACY OF TEST SET
SPECTRAL-TEXTURAL	548	364	64%
TEXTURAL	140	88	76%

TABLE VI. Results of Land Use Classification Experiments from Satellite Imagery of Kansas, Distance 8, Four Categories.

		ASSIGNED CATEGORY				
		GRASSLAND	LARGE FIELDS	SMALL FIELDS	WATER	TOTAL
TRUE CATEGORY	GRASSLAND	52	7	4	0	63
	LARGE FIELDS	2	145	31	0	178
	SMALL FIELDS	12	42	61	0	115
	WATER	0	1	6	1	8
	TOTAL	66	195	102	1	364

TABLE VII. Contingency Table for Land Use Classification of Satellite Imagery over Kansas Using Spectral-Textural Features, Distances 1 and 8, Four Categories. Classification Accuracy on Test Set= 71%.

FEATURES	NO. OF SAMPLES IN TRAINING SET	NO. OF SAMPLES IN TEST SET	OVERALL ACCURACY OF TEST SET
SPECTRAL-TEXTURAL	548	364	71%
TEXTURAL (17)	140	88	73%

TABLE VIII. Results of Land Use Classification Experiments from Satellite Imagery of Kansas, using both Distances 1 and 8 of the Spectral-Textural Features and all 17 Textural Features.

		ASSIGNED CATEGORY				
		GRASSLAND	LARGE FIELDS	SMALL FIELDS	WATER	TOTAL
TRUE CATEGORY	GRASSLAND	49	4	6	1	60
	LARGE FIELDS	6	150	27	1	184
	SMALL FIELDS	10	34	67	2	113
	WATER	0	4	0	4	8
	TOTAL	65	192	100	8	365

Table IX. Contingency Table for Land Use Classification of Satellite Imagery over Kansas using Spectral-Textural Features with the Bayes Classifier, Distance 1. Classification Accuracy of Test Set =69%.

		ASSIGNED CATEGORY				
		GRASSLAND	LARGE FIELDS	SMALL FIELDS	WATER	TOTAL
TRUE CATEGORY	GRASSLAND	31	10	19	0	60
	LARGE FIELDS	5	140	38	1	184
	SMALL FIELDS	12	46	51	4	113
	WATER	1	4	2	1	8
	TOTAL	49	200	110	6	365

Table X. Contingency Table for Land Use Classification of Satellite Imagery over Kansas using Spectral-Textural Features with the Bayes Classifier, Distance 8. Classification Accuracy of Test Set =61%.

APPENDIX I

N-DIMENSIONAL SPHERICAL COORDINATE SYSTEMS AND ELLIPSOIDALLY SYMMETRIC DISTRIBUTIONS

We illustrate the N-dimensional spherical coordinate system in the calculation of the volume of the N-dimensional hypersphere. Next we show how suitable functions can be used to define ellipsoidally symmetric density functions and we determine the normalizing constant for any function. Finally, we show that for any ellipsoidally symmetric density f $(\sqrt{x^T A x})$, the matrix A is proportional to the inverse covariance matrix of x and we determine the constant of proportionality.

I.1 Volume of an N-dimensional Hypersphere

Let V be the volume of a N-dimensional hypersphere of radius r_o. By definition

$$v = \underset{\sqrt{\sum_{i=1}^{N} x_i^2} \leq r_o}{\int \int \cdots \int} dx_1\, dx_2 \ldots dx_N$$

To evaluate this N-fold integral, we transform to spherical coordinates.

$$x_1 = r \cos \theta_1 \cos \theta_2 \ldots \cos \theta_{N-3} \cos \theta_{N-2} \cos \theta_{N-1}$$

$$x_2 = r \cos \theta_1 \cos \theta_2 \ldots \cos \theta_{N-3} \cos \theta_{N-2} \sin \theta_{N-1}$$

$$x_3 = r \cos \theta_1 \cos \theta_2 \ldots \cos \theta_{N-3} \sin \theta_{N-2}$$

$$\vdots$$

$$x_j = r \cos \theta_1 \cos \theta_2 \ldots \cos \theta_{N-j} \sin \theta_{N-j}$$

$$\vdots$$

$$x_N = r \sin \theta_1$$

Figure 7 illustrates the geometry of the spherical coordinate system we use for a 3-dimensional system.

Three-Dimensional Spherical Coordinate System

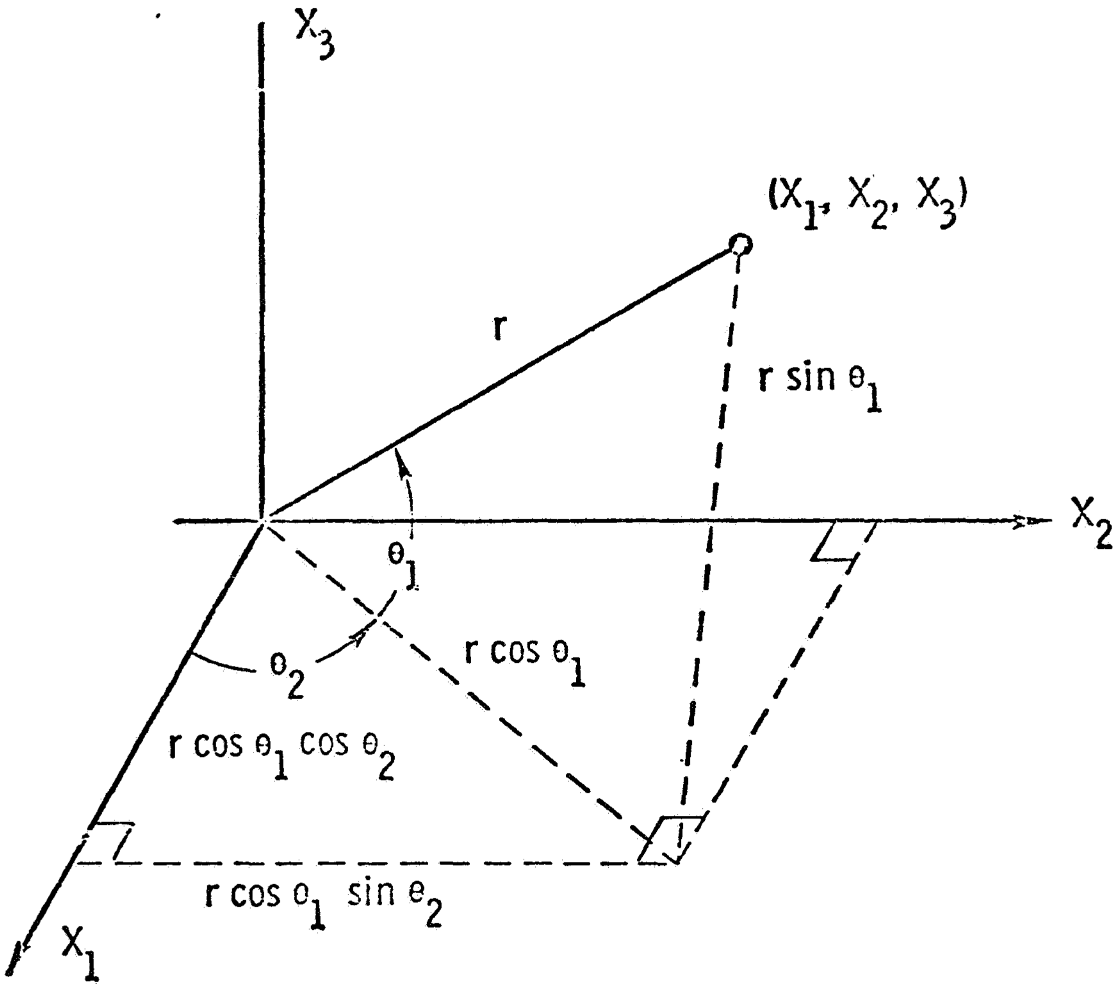

$$\left.\begin{aligned} x_1 &= r \cos \theta_1 \cos \theta_2 \\ x_2 &= r \cos \theta_1 \sin \theta_2 \\ x_3 &= r \sin \theta_1 \end{aligned}\right\}$$

Transformation between rectangular coordinate system and spherical coordinate system.

FIGURE 7. Three-Dimensional Spherical Coordinate System.

The Jacobian J of this transformation is defined by the determinant J.

$$J = \begin{vmatrix} \frac{\partial x_1}{\partial r} & \frac{\partial x_2}{\partial r} & \cdots & \frac{\partial x_N}{\partial r} \\ \frac{\partial x_1}{\partial \theta_1} & \frac{\partial x_2}{\partial \theta_1} & \cdots & \frac{\partial x_N}{\partial \theta_1} \\ \vdots & & & \\ \frac{\partial x_1}{\partial \theta_{N-1}} & \frac{\partial x_2}{\partial \theta_{N-1}} & \cdots & \frac{\partial x_N}{\partial \theta_{N-1}} \end{vmatrix}$$

$$\begin{vmatrix} \cos\theta_1 \cos\theta_2 \cdots \cos\theta_{N-1} & \cos\theta_1 \cos\theta_2 \cdots \cos\theta_{N-2} \sin\theta_{N-1} & \cdots & \sin\theta_1 \\ -r\sin\theta_1 \cos\theta_2 \cdots \cos\theta_{N-1} & -r\sin\theta_1 \cos\theta_2 \cdots \cos\theta_{N-2} \sin\theta_{N-1} & \cdots & r\cos\theta_1 \\ -r\cos\theta_1 \sin\theta_1 \cdots \cos\theta_{N-1} & -r\cos\theta_1 \sin\theta_2 \cdots \cos\theta_{N-2} \sin\theta_{N-1} & \cdots & 0 \\ \vdots & \vdots & & \vdots \\ -r\cos\theta_1 \cos\theta_2 \cdots \sin\theta_{N-1} & r\cos\theta_1 \cos\theta_2 \cdots \cos\theta_{N-2} \cos\theta_{N-1} & \cdots & 0 \end{vmatrix}$$

To find the value of the Jacobian, factor r out of the last (N−1) rows and from each column factor out its first entry.

$$J = r^{N-1} \cos^{N-1} \theta_1 \cos^{N-2} \theta_2 \ldots \cos \theta_{N-1} \sin \theta_1 \sin \theta_2 \ldots \sin \theta_{N-1}$$

$$\begin{vmatrix}
1 & 1 & 1 & \cdots & 0 \\
-\tan \theta_1 & -\tan \theta_1 & -\tan \theta_1 & \cdots & \cot \theta_1 \\
-\tan \theta_2 & -\tan \theta_2 & -\tan \theta_2 & \cdots & 0 \\
\vdots & \vdots & \vdots & \cdots & \vdots \\
\vdots & \vdots & -\tan \theta_{N-3} & \cdots & 0 \\
 & -\tan \theta_{N-2} & \cot \theta_{N-2} & \cdots & 0 \\
-\tan \theta_{N-1} & \cot \theta_{N-1} & 0 & \cdots & 0
\end{vmatrix}$$

Subtracting column 2 from column 1, column 3 from column 2, ... column N from column N-1 there results

$$\begin{vmatrix}
0 & 0 & 0 & \cdots & 0 & & 1 \\
0 & 0 & 0 & \cdots & -\tan \theta_1 & -\cot \theta_1 & \cot \theta_1 \\
\vdots & \vdots & \vdots & & & \cot \theta_2 & 0 \\
\vdots & \vdots & \vdots & & & 0 & \vdots \\
 & \vdots & -\tan \theta_{N-3} & -\cot \theta_{N-3} & & \vdots & \vdots \\
 & -\tan \theta_{N-2} & -\cot \theta_{N-2} & \cot \theta_{N-2} & & \vdots & \vdots \\
-\tan \theta_{N-1} & -\cot \theta_{N-1} & \cot \theta_{N-1} & 0 & \cdots & 0 & 0
\end{vmatrix}$$

Since all entries in the upper left triangle are zero, the value of the determinant is easily found as minus one times the product of entries on the lower left to upper right diagonal.

$$J = r^{N-1}\cos^{N-1}\theta_1 \cos^{N-2}\theta_2 \ldots \cos\theta_{N-1} \sin\theta_1 \sin\theta_2 \ldots \sin\theta_{N-1}(-1) \prod_{N=1}^{N-1} (-\tan\theta_N - \cot\theta_N)$$

Notice that $\tan\theta + \cot\theta = \frac{1}{\sin\theta \cos\theta}$. Now upon simplifying we obtain

$$J = (-1)^N r^{N-1} \cos^{N-2}\theta_1 \cos^{N-3}\theta_2 \ldots \cos\theta_{N-2}$$

and $|J| = r^{N-1} \cos^{N-2}\theta_1 \cos^{N-3}\theta_2 \ldots \cos\theta_{N-2}$ since

$\cos\theta_i > 0$ for $-\Pi/2 \le \theta_i \le \Pi/2$, $i=1, 2, \ldots N-2$.

In spherical coordinates the volume V of the N-dimensional hypersphere of radius r_o is readily evaluated.

$$V = \int_{r \le r_o} \int_{\theta_1=-\frac{\Pi}{2}}^{\Pi/2} \ldots \int_{\theta_{N-2}=-\frac{\Pi}{2}}^{\Pi/2} \int_{\theta_{N-1}=0}^{2\Pi} r^{N-1}\cos^{N-2}\theta_1 \cos^{N-3}\theta_2 \ldots \cos\theta_{N-2}\, dr\, d\theta_1 \ldots d\theta_{N-1}$$

Separating the integrations,

$$V = \int_{r=0}^{r_o} r^{N-1} dr \int_{\theta_1=-\frac{\Pi}{2}}^{\Pi/2} \cos^{N-2}\theta_1\, d\theta_1 \ldots \int_{\theta_{N-2}=-\frac{\Pi}{2}}^{\Pi/2} \cos\theta_{N-2}\, d\theta_{N-2} \int_{\theta_{N-1}=0}^{2\Pi} d\theta_{N-1}$$

$$\text{Since } \int_{\theta=-\frac{\Pi}{2}}^{\Pi/2} \cos^N\theta\, d\theta = \frac{\Gamma\left(\frac{N+1}{2}\right)\Gamma\left(\frac{1}{2}\right)}{\Gamma\left(\frac{N+2}{2}\right)},$$

C-11

$$V = \frac{r_1^N}{} \left[\frac{\Gamma\left(\frac{N-1}{2}\right) \Gamma\left(\frac{1}{2}\right)}{\Gamma\left(\frac{N}{2}\right)} \right] \left[\frac{\Gamma\left(\frac{N-2}{2}\right) \Gamma\left(\frac{1}{2}\right)}{\Gamma\left(\frac{N-1}{2}\right)} \right] \cdots\cdots \left[\frac{\Gamma\left(\frac{2}{2}\right) \Gamma\left(\frac{1}{2}\right)}{\Gamma\left(\frac{3}{2}\right)} \right] 2\pi$$

$$= \frac{r_o^N}{N} \, 2\pi \frac{\Gamma\left(\frac{1}{2}\right)^{N-2} \Gamma\left(1\right)}{\Gamma\left(\frac{N}{2}\right)}$$

But $\Gamma\left(\frac{1}{2}\right) = \pi^{1/2}$ and $\Gamma(1) = 1$

$$V = \frac{r_o^N}{N} \frac{2\pi \pi^{\frac{N-2}{2}}}{\Gamma\left(\frac{N}{2}\right)} = \frac{2 r_o^N}{N} \frac{\pi^{\frac{N}{2}}}{\Gamma\left(\frac{N}{2}\right)} .$$

I.2 Suitable functions for Ellipsoidally Symmetric Distribution.

Suppose f is a real function, defined on domain R, a subset of $[0,\infty]$, and satisfying $f(\mu) \geq 0$ for all μ in R and $\mu^k f(\mu)d$ is finite for $k \leq N+1$. We show that f is suitable for defining a ellipsoidally symmetric density function and we determine the constant c so that of $(\sqrt{x' Ax})$ is an ellipsoidally symmetric density.

Let A be a NXN symmetric positive definite matrix and X an NX1 vector. Consider the ellipsoidally symmetric function $f(\sqrt{x' Ax})$. We wish to determine a constant C such that of $(\sqrt{x' Ax})$ is a density function.

It is clear that $C = \dfrac{1}{\displaystyle\int \cdots \int_{\sqrt{x' Ax} \; R} f\sqrt{x' Ax} \; dx_1 \ldots dx_N}$.

To determine the value of the integral, we will make a transformation which rotates ans scales. Let T be an orthonormal matrix such that $T'AT = D$, where D is a diagonal matrix. Make the change of variables

$$X = TD^{\frac{-1}{2}} z.$$

The Jacobian J of this transformation is

$$J = \begin{vmatrix} \frac{\partial x_1}{\partial z_1} & \frac{\partial x_2}{\partial z_1} & \cdots & \frac{\partial x_N}{\partial z_1} \\ \frac{\partial x_1}{\partial z_2} & \frac{\partial x_2}{\partial z_2} & \cdots & \frac{\partial x_N}{\partial z_2} \\ \vdots & & & \\ \frac{\partial x_1}{\partial z_N} & \frac{\partial x_2}{\partial z_N} & & \frac{\partial x_N}{\partial z_N} \end{vmatrix} = |TD^{-1/2}| = |T| \; |D|^{-1/2}$$

Since T is an orthornormal matrix, $|T| = 1$ and

$$|D| = |T'AT| = |T'|\ |A|\ |T| = |A|.$$

So the Jacobian is the determinant $|A|^{-1/2}$ which is positive since A is positive definite.

$$I = \int \cdots \int_{\sqrt{x'Ax} \in R} f\left(\sqrt{x'Ax}\right)\ dx_1 \ldots dx_N$$

$$= |A|^{-1/2} \int \cdots \int_{\sqrt{z'D^{-1/2}T'ATD^{-1/2}z} \in R} f\left(\sqrt{z'D^{-1/2}T'ATD^{-1/2}z}\right) dz_1 \ldots dz_N$$

$$= |A|^{-1/2} \int \cdots \int_{\sqrt{z'z} \in R} f(z'z)\ dz_1 \ldots dz_N$$

Now change to spherical coordinates.

$$z_1 = r \cos\theta_1 \cos\theta_2 \cdots \cos\theta_{N-1}$$

$$z_2 = r \cos\theta_1 \cos\theta_2 \cdots \cos\theta_{N-2} \sin\theta_{N-1}$$

$$\vdots$$

$$z_j = r \cos\theta_1 \cdots \cos\theta_{N-j} \sin\theta_{N-j+1}$$

$$\vdots$$

$$z_N = r \sin\theta_1$$

The Jacobian of this transformation is $(-1)^{N-1} r^{N-1} \cos^{N-2}\theta_1 \cos^{N-2}\theta_2 \ldots \cos\theta_{N-2}$.

$$I = |A|^{-1/2} \int_{r\varepsilon R} \int_{\theta_1=-\Pi/2}^{\Pi/2} \cdots \int_{\theta_{N-2}=-\Pi/2}^{\Pi/2} \int_{\theta_{N-1}=0}^{2\Pi} f(r) r^{N-1} \cos^{N-2}\theta_1 \cos^{N-3}\theta_2 \ldots \cos\theta_{N-2}\, dr\, d\theta_1 \ldots d\theta_{N-1}$$

$$= |A|^{-1/2} \int_{r\varepsilon R} r^{N-1} f(r)\, dr \int_{\theta_1=-\Pi/2}^{\Pi/2} \cos^{N-2}\theta_1\, d\theta_1 \int_{\theta_2=-\Pi/2}^{\Pi/2} \cos^{N-3}\theta_2\, d\theta_2 \ldots$$

$$\int_{\theta_{N-2}=-\Pi/2}^{\Pi/2} \cos\theta_{N-2} \int_{\theta_{N-1}=0}^{2\Pi} d\theta_{N-1}$$

Since $\int_{\theta=-\Pi/2}^{\Pi/2} \cos^N\theta\, d\theta = \dfrac{\Gamma\left(\frac{N+1}{2}\right) \Gamma\left(\frac{1}{2}\right)}{\Gamma\left(\frac{N+2}{2}\right)}$, the integrals are readily evaluated.

$$I = |A|^{-1/2} \int_{r \epsilon R} r^{N-1} f(r)dr \left[\frac{\Gamma\left(\frac{N-1}{2}\right) \Gamma\left(\frac{1}{2}\right)}{\Gamma\left(\frac{N}{2}\right)} \; \frac{\Gamma\left(\frac{N-2}{2}\right)\Gamma\left(\frac{1}{2}\right)}{\Gamma\left(\frac{N-1}{2}\right)} \cdots \frac{\Gamma\left(\frac{2}{2}\right)\Gamma\left(\frac{1}{2}\right)}{\Gamma\left(\frac{3}{2}\right)} \right] 2\pi$$

$$= |A|^{-1/2} \int_{r \epsilon R} r^{N-1} f(r)dr \quad \frac{\Gamma\left(\frac{1}{2}\right)^{N-2}}{\Gamma\left(\frac{n}{2}\right)} \; 2\pi$$

$$= \frac{2(\pi)^{N/2}}{|A|^{1/2}\,\Gamma\left(\frac{N}{2}\right)} \int_{r \epsilon R} r^{N-1} f(r)dr$$

Therefore, the constant c is

$$c = \frac{|A|^{+1/2}\,\Gamma\left(\frac{N}{2}\right)}{2\,(\pi)^{N/2} \int_{r \epsilon R} r^{N-1} f(r)dr} \;.$$

Next we determine the normalizing constant c for the forms $e^{-\frac{1}{2}u^2}$ and $(1+u^2)^{-m}$.

Case 1. Multivariate Normal

The density function for the multivariate normal distribution is of the form

$$f(\sqrt{x'Ax}) = e^{-\frac{1}{2}x'Ax}, \quad o \leq x'Ax \leq \infty$$

$$\text{or,} \quad f(r) = e^{-\frac{1}{2}r^2}, \quad o \leq r \leq \infty .$$

Since $\int_{r \in R} r^{N-1} f(r)dr = \int_o^\infty r^{N-1} e^{-\frac{1}{2}r^2} dr = \int_o^\infty (2u)^{\frac{N-2}{2}} e^{-u} du = 2^{\frac{N-2}{2}} \Gamma\left(\frac{N}{2}\right)$

then the normalizing constant is

$$c = \frac{\Gamma\left(\frac{N}{2}\right)}{2\pi^{\frac{N}{2}} |A|^{-\frac{1}{2}} \int_{r \in R} r^{N-1} f(r)dr} = \frac{\Gamma\left(\frac{N}{2}\right)}{2\pi^{\frac{N}{2}} |A|^{-\frac{1}{2}} 2^{\frac{N}{2}-1} \Gamma\left(\frac{N}{2}\right)}$$

$$= \frac{1}{(2\pi)^{\frac{N}{2}} |A|^{-\frac{1}{2}}}$$

and, $$f(\sqrt{x'Ax}) = \frac{1}{(2\pi)^{\frac{N}{2}} |A|^{-\frac{1}{2}}} \cdot e^{-\frac{1}{2}x'Ax}, \quad o \leq x'Ax \leq \infty .$$

Case 2. Multivariate Pearson Type VII.

Let $$f(\sqrt{x'Ax}) = (1 + x'Ax)^{-m}, \quad o \leq x'Ax \leq \infty ,$$

then,

$$\int_{r \in R} r^{N-1} f(r)dr = \int_o^\infty r^{N-1}(1+r^2)^{-m} dr = \int_o^1 \left(\frac{1-u}{u}\right)^{\frac{N-2}{2}} u^m \frac{du}{2u^2}$$

$$= \frac{1}{2} \frac{\Gamma\left(\frac{N}{2}\right)\Gamma\left(m-\frac{N}{2}\right)}{\Gamma(m)}, \quad m > \frac{N}{2} .$$

And the normalizing constant is

$$c = \frac{\Gamma\left(\frac{N}{2}\right) \Gamma(m)}{2\pi^{\frac{N}{2}} |A|^{-\frac{1}{2}} \frac{1}{2}\Gamma\left(\frac{N}{2}\right)\Gamma\left(m-\frac{N}{2}\right)} = \frac{\Gamma(m)}{\pi^{\frac{N}{2}} |A|^{-\frac{1}{2}} \Gamma\left(m-\frac{N}{2}\right)}$$

and, $$f(\sqrt{x'Ax}) = \frac{\Gamma(m) |A|^{\frac{1}{2}}}{\pi^{\frac{N}{2}} \Gamma\left(m-\frac{N}{2}\right)} (1 + x'Ax)^{-m}, \quad m > \frac{N}{2}, \quad o \leq x'Ax \leq \infty .$$

1.3 Covariance Matrix For Multivariate Distributions.

Given the density function $f(\sqrt{x'Ax})$ we want to find the covariance matrix Σ,

$$\Sigma = E(xx') = c \int \cdots \int_{\sqrt{x'Ax} \in R} xx' f(\sqrt{x'Ax}) dx_1 \ldots dx_N$$

where c is a normalizing constant and N is the dimension of x. Using the orthonormal transformation $T'AT = D$, where D is a diagonal matrix, and scaling with $x = TD^{-\frac{1}{2}}z$, we have

$$\Sigma = c \int \cdots \int_{\sqrt{z'z} \in R} (TD^{-\frac{1}{2}}z)(z'D^{-\frac{1}{2}}T')\, f(\sqrt{z'z})\, |A|^{-\frac{1}{2}} dz_1 \ldots dz_N$$

since

$$x'AX = z'D^{-\frac{1}{2}}T'ATD^{-\frac{1}{2}}z = z'D^{-\frac{1}{2}}DD^{\frac{1}{2}}z = z'z$$

and

$$J = \begin{vmatrix} \frac{\partial x_1}{\partial z_1} & \cdots & \frac{\partial x_N}{\partial z_1} \\ \vdots & & \\ \frac{\partial x_1}{\partial z_N} & \cdots & \frac{\partial x_N}{\partial z_N} \end{vmatrix} = |TD^{-\frac{1}{2}}| = |T|\,|D|^{-\frac{1}{2}} = |D|^{-\frac{1}{2}} = |T'AT|^{-\frac{1}{2}} = |A|^{-\frac{1}{2}} \; .$$

Rearranging,

$$\Sigma = c\,|A|^{-\frac{1}{2}}\, T D^{-\frac{1}{2}} \int \cdots \int_{\sqrt{z'z} \in R} z z'\, f(\sqrt{z'z})\, dz_1 \ldots dz_N \; D^{-\frac{1}{2}} T',$$

where $z'z$ is an N x N matrix. Looking at the off diagonal terms, for $i \neq j$,

$$\int \cdots \int_{\sqrt{z'z} \in R} z_i z_j\, f(\sqrt{z_i z_j})\, dz_1 \ldots dz_N = 0$$ since we are integrating an odd function over even limits.

For terms of Σ along the diagonal, for $i=j$,

$$\int \cdots \int_{\sqrt{z'z} \in R} z_i^2\, f(\sqrt{z'z})\, dz_1 \ldots dz_N = \int \cdots \int_{\sqrt{z'z} \in R} z_1^2\, f(\sqrt{z'z})\, dz_1 \ldots dz_N$$

and changing to spherical coordinates,

$$= \int_{r \in R} \int_{\theta_1 = -\pi/2}^{\pi/2} \cdots \int_{\theta_{N-2} = -\pi/2}^{\pi/2} \int_{\theta_{N-1} = 0}^{2\pi} r^2 \cos^2\theta_1 \ldots \cos^2\theta_{N-1} f(r) r^{N-1} \cos^{N-2}\theta_1 \ldots \cos\theta_{N-2}\, dr\, d\theta_1 \ldots d\theta$$

$$= \int_{r \in R} r^{N+1} f(r)\, dr \int_{\theta_1 = -\pi/2}^{\pi/2} \cos^N\theta_1\, d\theta_1 \cdots \int_{\theta_{N-2} = -\pi/2}^{\pi/2} \cos^3\theta_{N-2}\, d\theta_{N-2} \; 2\int_{\theta_{N-1} = -\pi/2}^{\pi/2} \cos^2\theta_{N-1}\, d\theta_{N-1}.$$

Since $\int_{-\pi/2}^{\pi/2} \cos^k \theta\, d\theta = \dfrac{\Gamma\left(\frac{k+1}{2}\right)\Gamma\left(\frac{1}{2}\right)}{\Gamma\left(\frac{k+2}{2}\right)}$

then

$$\underset{\sqrt{z'z}\in R}{\int\cdots\int} z_i^2 f(\sqrt{z'z})\,dz_1\ldots dz_N = \underset{r\in R}{\int} r^{N+1} f(r)dr \; \frac{\Gamma\left(\frac{N+1}{2}\right)\Gamma\left(\frac{1}{2}\right)}{\Gamma\left(\frac{k+2}{2}\right)} \frac{\Gamma\left(\frac{N}{2}\right)\Gamma\left(\frac{1}{2}\right)}{\Gamma\left(\frac{N+1}{2}\right)} \cdots \frac{\Gamma\left(\frac{4}{2}\right)\Gamma\left(\frac{1}{2}\right)}{\Gamma\left(\frac{5}{2}\right)} \; 2\,\frac{\Gamma\left(\frac{3}{2}\right)\Gamma\left(\frac{1}{2}\right)}{\Gamma\left(\frac{4}{2}\right)}$$

$$= \frac{2\pi^{\frac{N}{2}}}{N\Gamma\left(\frac{N}{2}\right)} \underset{r\in R}{\int} r^{N+1} f(r)dr.$$

From I.2,

$$c = \frac{\Gamma\left(\frac{N}{2}\right)|A|^{\frac{1}{2}}}{2\pi^{\frac{N}{2}} \underset{r\in R}{\int} r^{N-1} f(r)\,dr}$$

so that

$$\Sigma = \frac{\Gamma\left(\frac{N}{2}\right)|A|^{\frac{1}{2}}}{2\pi^{\frac{N}{2}} \underset{r\in R}{\int} r^{N-1} f(r)\,dr} |A|^{-\frac{1}{2}} \, TD^{-\frac{1}{2}} \; \frac{2\pi^{\frac{N}{2}}}{N\Gamma\left(\frac{N}{2}\right)} \underset{r\in R}{\int} r^{N+1} f(r)\,dr \; D^{-\frac{1}{2}} T'$$

and, $\Sigma = T D^{-1} T' \quad \dfrac{\int r^{N+1} f(r)\,dr}{N\int r^{N-1} f(r)\,dr}$

where $T'AT = D$, or $D^{-1} = T'A^{-1}T$.

So that

$$\Sigma = A^{-1} \quad \frac{\int r^{N+1} f(r)\,dr}{N\int r^{N-1} f(r)\,dr}$$

Since the integrals are constants for any f, the covariance matrix is directly proportional to A^{-1}. We determine the constant of proportionality for the multivariate normal and Pearson Type VII distributions.

Case 1. Multivariate Normal

For the multivariate normal, the density is of the form $f(r) = ce^{-\frac{1}{2}r^2}$ where $r^2 = x'Ax$, $0 \leq r \leq \infty$.

Since $\int_0^\infty r^k e^{-\frac{1}{2}r^2} dr = 2^{\frac{k-1}{2}} \Gamma\left(\frac{k+1}{2}\right)$

then $\int_0^\infty r^{N+1} f(r)\, dr = c\, 2^{\frac{N}{2}} \Gamma\left(\frac{N+2}{2}\right)$

and $\int_0^\infty r^{N-1} f(r)\, dr = c 2^{\frac{N-2}{2}} \Gamma\left(\frac{N}{2}\right)$

so that $\Sigma = A^{-1} \dfrac{2^{\frac{N}{2}} \frac{N}{2} \Gamma\left(\frac{N}{2}\right)}{N_2 \frac{N}{2}^{-1} \Gamma\left(\frac{N}{2}\right)}$

and thus, $\Sigma = A^{-1}$

or, $A = \Sigma^{-1}$.

Case 2 Multivariate Pearson Type VII.

$$f(r) = c\,(1 + r^2)^{-m}\ ,\quad o \leq r \leq \infty .$$

Since $\displaystyle\int r^{N+1} f(r)\,dr = \frac{c}{2}\ \frac{\Gamma\left(\frac{N}{2}+1\right)\Gamma\left(m-\frac{N}{2}-1\right)}{\Gamma(m)}$

and $\displaystyle\int r^{N-1} f(r)\,dr = \frac{c}{2}\ \frac{\Gamma\left(\frac{N}{2}\right)\ \Gamma\left(M-\frac{N}{2}\right)}{\Gamma(m)}$

then, $\displaystyle \ddagger = A^{-1}\ \frac{\frac{cN}{2}\ \Gamma\left(\frac{N}{2}\right)\Gamma\left(m-\frac{N}{2}-1\right)}{2N\,c\,\Gamma(m)} \cdot \frac{2\,\Gamma(m)}{c\Gamma\left(\frac{N}{2}\right)\left(m-\frac{N}{2}-1\right)\Gamma\left(m-\frac{N}{2}-1\right)}$

$$= A^{-1}\ \frac{1}{2\left(m-\frac{N}{2}-1\right)} \qquad \text{Hence,}\quad A = \frac{1}{2\left(m-\frac{N}{2}-1\right)}\ \ddagger^{-1}.$$

APPENDIX II

NORMALIZATION PROCEDURE TO MAKE COVARIANCE MATRIX INVARIANT UNDER TRANSLATING AND SCALING TRANSFORMATIONS

Let Σ_x be a covariance matrix for the difference vectors of grey tone N-tuples in a specified spatial relationship within a subimage. We transform the covariance matrix to obtain the normalized covariance matrix Σ_y using $y = Dx$, where x is the difference vector and D is diagonal. Thus, assuming zero mean,

$$\begin{aligned}\Sigma_y &= E(yy') = E\,(Dxx'D') \\ &= D\,E\,(xx')\,D' \\ &= D\,\Sigma_x\,D \quad \text{since } D' = D.\end{aligned}$$

For normalization, we have

$$d_{ii} = \frac{1}{\sqrt{\sigma_{ii}}}$$

where σ_{ii} is the ii^{th} element of Σ_x and is the variance σ_i^2 of the i^{th} component of x.

Assume that all grey tone N-tuples have a scale factor a and an additive factor c so that for N-tuples $ax_1 + c$ and $ax_2 + c$, the difference becomes

$$y = (ax_1 + c) - (ax_2 + c)$$

$$y = a(x_1 - x_2).$$

Hence, translational effects due to bias terms are cancelled but scaling effects are marked by the diagonal transformation $y = Ax$ so that the elements of the covariance matrix become

$$\Sigma = E\,(yy1) = E\,(Axx'A')$$

$$\Sigma = A\,\Sigma_x\,A$$

where A is a diagonal matrix. We must show that $\ddagger_N$, the normalized covariance matrix of $\ddagger$, is identical to $\ddagger_y$. Normalizing $\ddagger$ we have

$$\ddagger_N = D\ddagger D$$

$$= D\,(A\ \ddagger_x A)\,D$$

where D is again diagonal but in this case,

$$d_{ii} = \frac{1}{\sqrt{\sigma_{ii}\ a_{ii}^2}}$$

with a_{ii} the ii^{th} element of diagonal matrix A. For the ij^{th} element of $\ddagger_N$ we have

$$\sigma_{Nij} = d_{ii}\ a_{ii}\ \sigma_{ij}\ a_{jj}\ d_{jj}$$

$$= \frac{a_{ii}\ \sigma_{ij}\ \ a_{jj}}{\sqrt{\sigma_{ii}\ \ a_{ii}^2}\ \sqrt{\sigma_{jj}\ \ a_{jj}^2}}$$

$$= \sigma_{ij},$$

Thus, this procedure of normalization makes the entries of the normalized covariance matrix invariant with respect to translating and scaling transformations on the grey tone N-tuples.

REFERENCES

Anderson, J. R., E. E. Hardy, and J. T. Roach, "A Land-Use Classification System for Use with Remote-Sensor Data," Geological Survey Circular 671, U. S. Geological Survey, Washington, D. C., 1973.

Cutrona, L. J., E. N. Leith, C. J. Palermo, and L. J. Porcello, "Optical Data Processing and Filtering Systems," IRE Transactions on Information Theory, vol. , no. , pp. 336-400, June, 1960.

Darling, E. M., and R. D. Joseph, "Pattern Recognition from Satellite Altitudes," IEEE Transactions on Systems, Man, and Cybernetics, vol. SSC-4, pp. 38-47, March, 1968.

Egbert, D., J. McCauley, and J. McNaughton, "Ground Pattern Analysis in the Great Plains," Semi-Annual ERTS A Investigation Report, Remote Sensing Laboratory, The University of Kansas Center for Research, Inc., Lawrence, Kansas, August, 1973.

Fu, K. S., and J. M. Mendel, "Adaptive Learning and Pattern Recognition Systems," Academic Press, New York, 1972.

Fukunaga, K., "Introduction to Statistical Pattern Recognition," Academic Press, New York, 1972.

Goodman, J. W., "Introduction to Fourier Optics, McGraw-Hill Book Co., New York, 1968.

Gramenopoulos, Nicholas, "Terrain Type Recognition Using ERTS-1 MSS Images," Symposium on Significant Results Obtained From the Earth Resources Technology Satellite, NASA SP-327, pp. 1229-1241, March, 1973.

Haralick, R. M., et al, "Preliminary Report on Land Use Classification Using Texture Information in ERTS-A MSS Imagery," Report No. 2262-1, NASA Goddard Space Flight Center Contract NAS 5-21822, The University of Kansas Center for Research, Inc., Lawrence, Kansas January, 1973.

Haralick, R. M., et al, "Texture-Tone Study with Application to Digitized Imagery," U. S. Army Engineer Topographic Laboratories Contract DAAK02-70-C-0388, CRES Technical Reports 182-2, and 182-3, The University of Kansas Center for Research, Inc., Lawrence, Kansas 1971, 1972.

Haralick, R. M., "A Texture-Context Feature Extraction Algorithm for Remotely Sensed Imagery," Proceedings 1971 IEEE Decision and Control Conference, Gainesville, Florica, pp. 650-657, December, 15-17, 1971.

Haralick, R. M., and D. E. Anderson, "Texture-Tone Study with Application to Digitized Imagery," CRES Technical Report 182-2, The University of Kansas Center for Research, Inc., Lawrence, Kansas, November, 1971.

Haralick, R. M., K. Shanmugam, and I. Dinstein, "Texture Features for Image Classification," IEEE Transactions on Systems, Man, and Cybernetics, to be published 1974.

Hardy, E. E., and J. R. Anderson, "A Land Use Classification System for Use with Remote-Sensor Data," Machine Processing of Remotely Sensed Data, (Conference Proceedings), Lafayette, Indiana, October, 1973.

Horning, R. J., and J. A. Smith, "Application of Fourier Analysis to Multispectral/ Spatial Recognition," Management and Utilization of Remote Sensing Data ASP Symposium, Sioux Falls, South Dakota, October, 1973.

Kaizer, H., "A Quantification of Textures on Aerial Photographs," Boston University Research Laboratories, Technical Note 121, 1965, AD 69484.

Kirvida, L., and G. Johnson, "Automatic Interpretation of ERTS Data for Forest Management," Symposium on Significant Results Obtained from the Earth Resources Technology Satellite, NASA SP-327, pp. 1076-1082, March, 1973.

Lendaris, G. G., and G. L. Stanley, "Diffraction-Pattern Sampling for Automatic Pattern Recognition," Proceedings of the IEEE, vol. 58, no. 2, pp. 198-216, February, 1970.

Lewis, A. J., "Geomorphic Evaluation of Radar Imagery of Southeastern Panama and Northwestern Columbia," CRES Technical Report 133-18, The University of Kansas Center for Research, Inc., Lawrence, Kansas, February, 1971.

MacDonald, H. C., "Geologic Evaluation of Radar Imagery from Darien Province, Panama," CRES Technical Report 133-6, The University of Kansas Center for Research, Inc., Lawrence, Kansas, July, 1969.

Matherson, G., "Elements Pour Une Theorie des Milieux Poreaux, Masson, Paris, 1967.

Miesel, W., "Computer Oriented Approaches to Pattern Recognition," Academic Press, New York, 1972.

O'Neill, E., "Spatial Filtering in Optics," IRE Transactions on Information Theory, vol. , no. , pp. 56-65, June, 1956.

Preston, K., "Coherent Optical Computers, McGraw-Hill Book Co., New York, 1972.

Read, J. S., and S. N. Jayaramamurthy, "Aytomatic Generation of Texture Feature Detectors," IEEE Transactions on Computers, vol. , no. , pp. 803-812, July, 1972.

Rosenfeld, A., and M. Thurston, "Edge and Curve Detection for Visual Scene Analysis," IEEE Transactions on Computers, vol. C-20, no. 5, pp. 562-569, May, 1971.

Rosenfeld, A., and E. Troy, "Visual Textural Analysis," University of Maryland Computer Science Center, TR-70-116, June, 1970.

Serra, J., and G. Verchery, "Mathematical Morphology Applied to Fibre Composite Materials," Film Science and Technology, vol. 6, pp. 141-158, 1973.

Shulman, A. R., Optical Data Processing, John Wiley & Sons, Inc., New York, 1970.

Sutton, R., and E. Hall, "Texture Measures for Automatic Classification of Pulmonary Disease," IEEE Transactions on Computers, vol. C-21, no. 7, pp. 667-676, July, 1972.

Swanlund, G., "Honeywell's Automatic Tree Species Classifier," Honeywell Systems and Research Division, Report 9D-G-24, December 31, 1969.

Yaglom, A. M., Theory of Stationary Random Functions, Prentice-Hall, Inc., New Jersey, 1962.

DIGITAL IMAGE ENHANCEMENT TECHNIQUES USED IN SOME ERTS APPLICATION PROBLEMS

Alexander F H. Goetz and Fred C. Billingsley, *(Jet Propulsion Laboratory, California Institute of Technology, Pasadena, California)*

ABSTRACT

Enhancement and classification are not competing methods for machine image analysis. In fact enhanced images can be used alone or as inputs to classification routines. However, in some problems the spatial relationships are equal in importance to the classification results and enhancements can be designed to provide both types of information in one image.

Enhancements discussed include contrast stretching, multiratio color displays, Fourier plane operations to remove striping and boosting MTF response to enhance high spatial frequency content. The use of each technique in a specific application in the fields of geology, geomorphology and oceanography is demonstrated.

INTRODUCTION

Digital processing of ERTS images is the only means of fully utilizing the quantitative data contained in them. Two general classes of digital data manipulation have emerged which can be defined loosely as classification and enhancement.

Classification is understood as the identification of subsets of (typically) multispectral data based on several decision criteria. The classification can be "supervised," in which training areas are established, or "unsupervised," in which boundaries are drawn among sets of data which naturally cluster. The results, in the form of spatially-arranged decisions

* Jet Propulsion Laboratory, California Institute of Technology, Pasadena, California

This paper presents the results of one phase of research carried out at the Jet Propulsion Laboratory, California Institute of Technology, under Contract No. NAS 7-100 sponsored by the National Aeronautics and Space Administration.

substituted for the data, are normally displayed on line printer sheets with appropriate symbols.

Enhancements, on the other hand, are in general manipulations of image data directly, and the result is displayed as an image. This technique allows the photo-interpreter to make decisions, based on a useful subset of the image data, which otherwise may be beyond the capability of computer pattern recognition techniques or prohibitively costly. Types of enhancements, such as the combined color ratio display discussed below, can also be considered to be preludes to classifications in which the interpreter draws the boundaries. However, the retention of the spatial relationships in the manipulated image adds a dimension particularly useful to a human interpreter.

Enhancement techniques should not be regarded as competing with classification techniques. Each has its own specific application to which it is best suited. Enhancements can very well be used as "preprocessed" data for classification schemes. For instance, coherent noise suppression methods described below can be used to remove the six-line striping found on almost all ERTS images which blurs division boundaries in classification schemes. In the following discussion several techniques for enhancement will be outlined and their application to specific problems using ERTS data will be presented.

TECHNIQUES AND APPLICATIONS

Contrast Stretching

The ERTS MSS was designed with a sufficient dynamic range to make images at low sun angles in arctic regions as well as at high sun angles in low-latitude, high albedo desert regions. Consequently most images occupy only a

fraction of the available dynamic range and, therefore, have relatively low contrast. The result is most apparent in the "false color IR" reproductions of three MSS bands. In general only shades of red are apparent because the highest contrast in the image is between bands 4 or 5 and bands 6 and 7. Increasing the contrast of the individual bands before color composites are made is strikingly effective, as shown in Figure 1.

Although contrast can be increased by photographic means, manipulating digital data directly in the computer has the advantage that the stretching or increase in contrast is absolutely controlled and no data are lost due to non-linearities and base fog increase. In addition data remains in a quantitatively retrievable form.

Contrast stretching to form images of higher color contrast with a neutral average color balance begins with the formation of a histogram of the number of picture elements (pixels) versus the brightness or digital number (DN). The maximum of the histogram is shifted to the center of the output picture gray level distribution. The brightness range of interest, which may be all or part of the data displayed in the histogram, is then expanded to fill the entire black-white range of the output film. The stretch may be linear or non-linear, depending on which portion of the brightness range requires the greatest contrast enhancement. Stretching is discussed in more detail by Billingsley and Goetz (1973) and Rowan et al (1974).

Precise geologic mapping was not possible on the unstretched images. However, the stretched false color IR composite shown in Figure 1 provided enough detail to map all the major geologic units (Goetz et al, 1973). Automatic classification schemes were not required and subsequently, expensive computer processing was unnecessary.

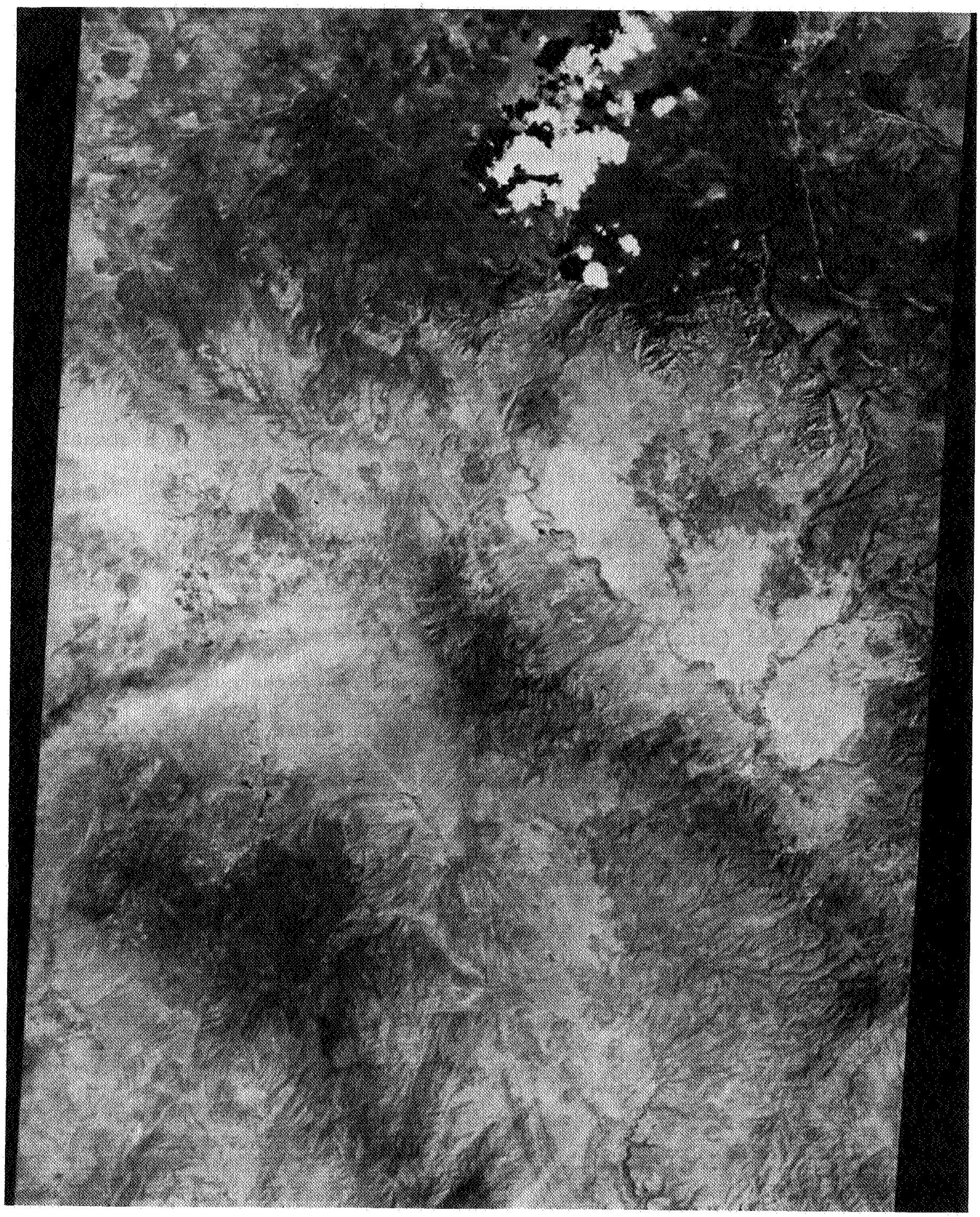

Figure Ia. Color composite of MSS bands 4, 5, and 7 provided by NDPF. EIOI4-I7375.

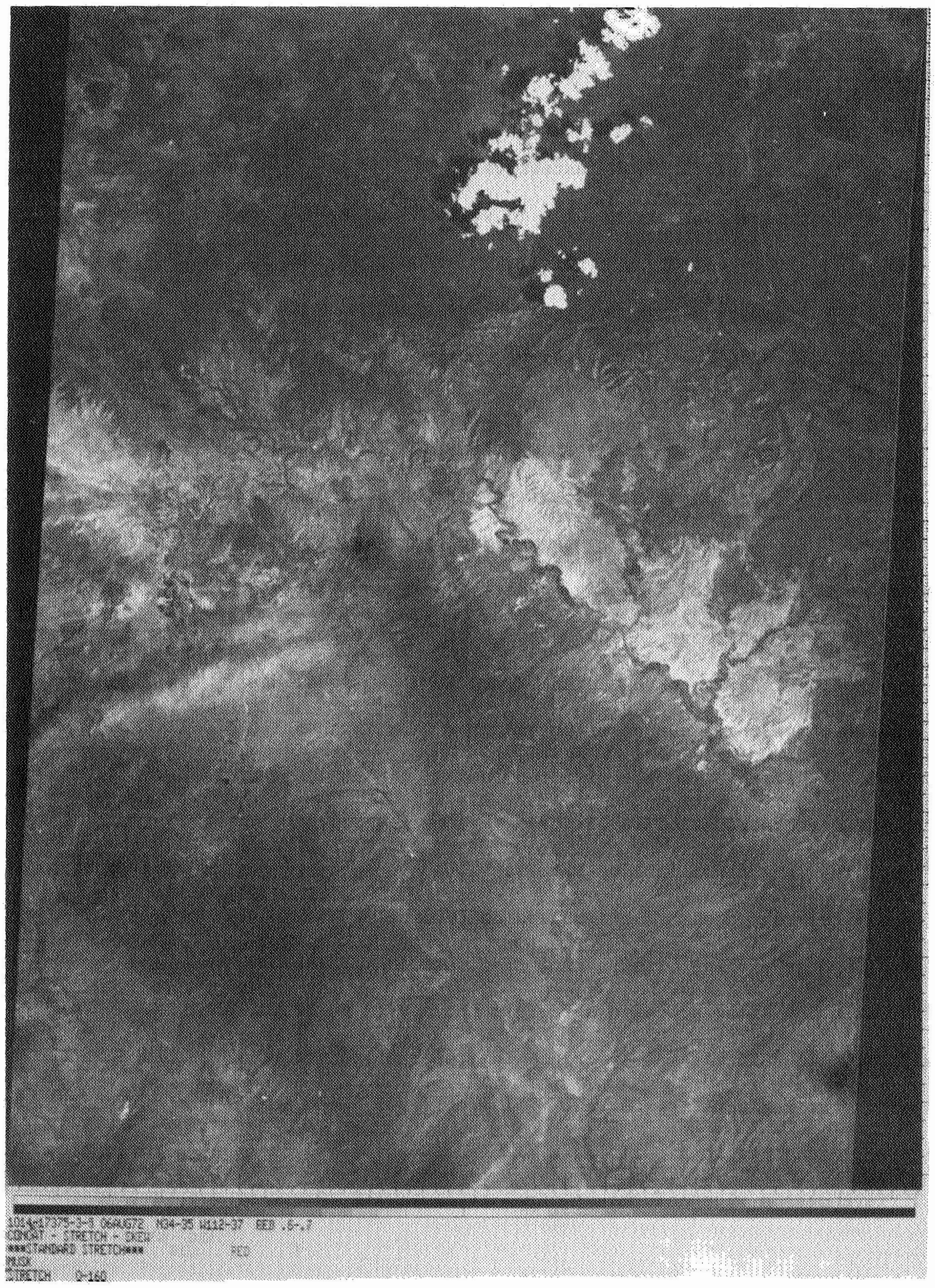

Figure Ib. Same scene as Figure Ia, but produced from digital tape. Each band was contrast stretched by a factor of I.5 before compositing.

Ratioing

The method of ratioing multispectral images can be viewed as another form of contrast enhancement. Its greatest value is in the enhancement of images which have very low contrast or ones in which there is high terrain relief. Smedes et al (1971) and Crane (1971) have used ratioing as a preprocessing step for further analysis by automatic classification techniques.

The advantage of the color combined ratio technique to be discussed is that, with a minimum of computer manipulation, an image can be produced in which maximum contrast among targets of interest is achieved with concomitant preservation of spatial detail necessary for photo interpretation.

Twelve ratios, of which only three are independent, can be produced from the four MSS bands. The ratioing process itself consists of dividing the brightness DN of an image in one spectral band by the DN of another, point by point. Corrections for path radiance must be made, particularly for low albedo objects, because the presence of an additive term in the signal will cause errors in the ratio. The use of cloud shadows in the image for determining the path radiance contribution is discussed by Goetz (1973).

Ratioing is a normalization process which clusters regions of like spectral reflectivity, regardless of brightness differences brought about by geometric factors such as surface orientation. The ratioing process is important for differentiating among geologic materials because there are no sharp diagnostic absorption lines in mineral spectra. The separability of types is based on the slopes of the reflectivity curves. Whitaker (1965) made one of the earliest successful attempts to discriminate among rock units on the moon on the basis of differences in slope of the spectral reflectivity curves at two wavelengths.

Photographic masking techniques were used. Billingsley _et al_ (1970) demonstrated a similar capability using digital techniques.

The present technique makes use of three ratios. Each ratio is individually stretched to the maximum without appreciable loss of data. Since terrain effects are minimized by ratioing, the brightness distribution in the ratio image is much narrower than in either original picture, making possible a much greater contrast enhancement. An increase in contrast by a factor of 10 is often possible. Non-linear stretches also can be applied. Typically, individual ratios are converted to black and white film transparencies. Color additive prints are made from combinations of three such transparencies. Figures 2 and 3 show the result of the ratio process for an area near Goldfield, Nevada. Figure 2 shows the contrast stretched color additive composite of MSS bands 4, 5, and 7. Figure 3 is the ratio of bands 4/5, 5/6, and 6/7 produced as red, blue, and green, respectively. Several photographic methods, including masking, were tried but were not successful in separating out areas containing limonite. Rowan _et al_ (1973) discuss the results of a study using the ratio image in Fig. 3. Areas of hydrothermal alteration, with associated gold and silver mineralization, were uniquely detected in the mining districts in the Goldfield area. The separation of the altered areas is based on the fact that limonite and hydrothermally altered clays have a characteristic dip in their reflectance spectra near 0.9 μm. However, the spectra are similar to those of the clays filling the surrounding playas. Only ratioing, severe contrast stretching, and the use of color compositing made possible the separation. This application has promise for detecting hydrothermally altered areas and possible associated mineralization in arid regions world-wide. The time required to produce the three ratios for the 1/3 ERTS frame was 4½ minutes on the JPL 360/44, considerably less than required for a full classification procedure.

Figure 2. Stretched color additive composite of bands 4, 5 and 7 of frame EI072-I800I showing the region surrounding Goldfield, Nevada.

Figure 3. Ratio color composite of the frame shown in Figure 2. The alteration zone surrounding Goldfield is shown in green above center near the left hand edge of the frame.

Krinsley (1973) used color ratio combinations in the study of large playas in central Iran. With prior ground control bearing strengths can be inferred from the changing hydrologic conditions through the seasons. On the basis of this work a new route has been selected across the Great Kavir which would shorten the present distance between northern and central Iran by 760 km. Figure 4 shows a CCT playback of band 7 with a contrast stretch designed to preserve most of the image data. Detail in the playa is absent. A stretch applied to the playa alone is shown in Fig. 5. Although detail is shown well in the black and white stretched image, the color combined ratio image in Fig. 6 is much more useful because the entire surrounding area is visible while the moist areas are greatly enhanced. The ratio pictures also show subtle variations in salt crust morphology and in moisture content (Krinsley, 1973).

Spatial Frequency Enhancement

Filtering in both the frequency and spatial domains has applications in enhancing geologic structures and in increasing apparent resolution in ERTS frames. Figure 7 shows an area on the Coconino Plateau discussed by Goetz et al (1973). A 1 x 35 element horizontal spatial filter was applied to increase local contrast sharply and make visible linear structures, joints and faults not otherwise discernible on the unenhanced image. An additional result of the application of the horizontal filter is the removal of striping effects.

Enhancement of high frequency spatial information in ERTS images is necessary when the ultimate resolution is required. Morrison and Cooley (1973) are studying rapid arroyo cutting in southern Arizona. The ERTS MSS resolution is not quite sufficient for some aspects of the study. Figure 8 documents an attempt to boost the modulation transfer function (MTF) by operations in the

Figure 4. Portion of frame EI06I-0638I-5 showing a large Iranian playa. Contrast stretch has subdued playa detail.

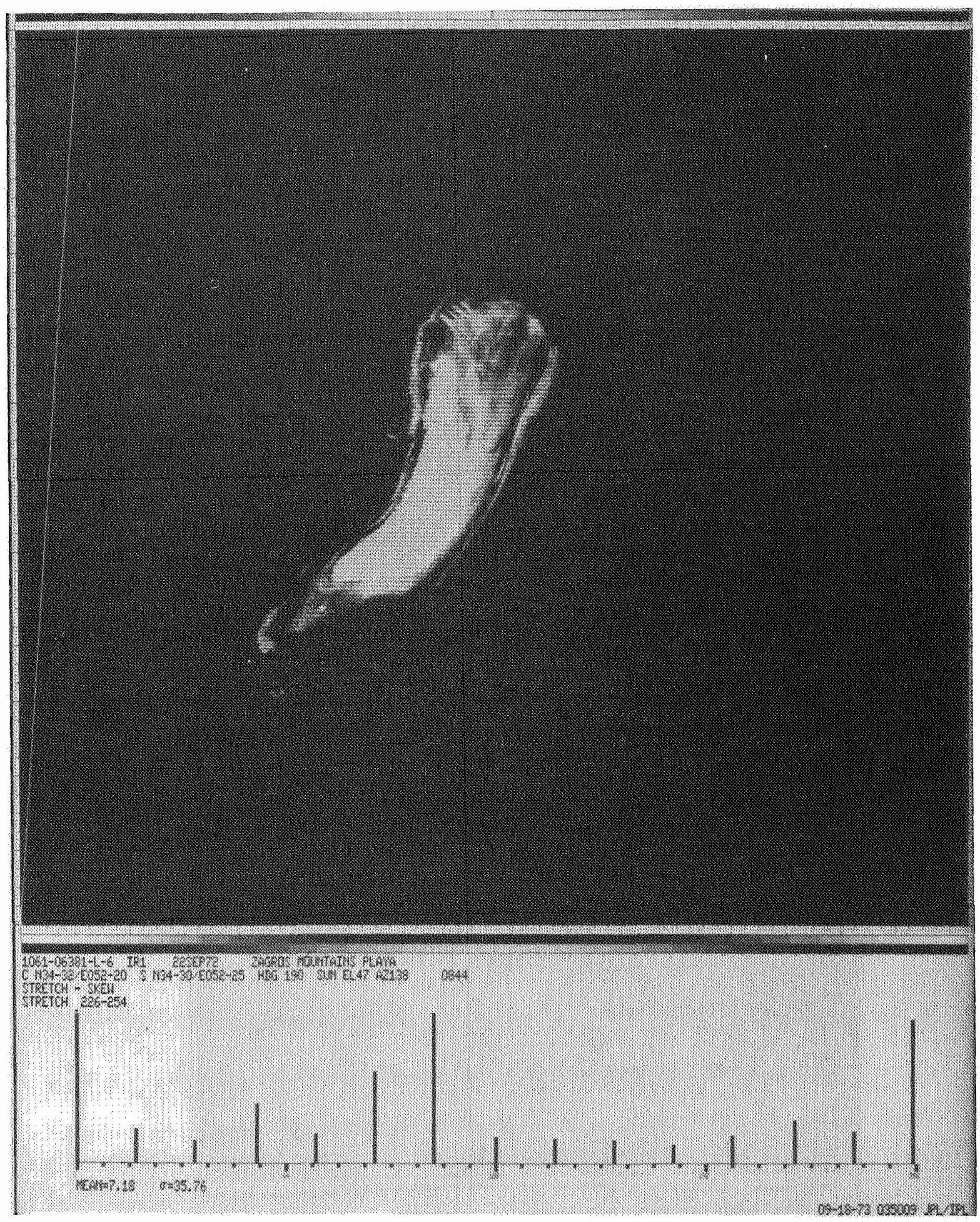

Figure 5. Playa region in band 6 has been contrast enhanced approximately by a factor of I5. Only I5 gray levels are displayed.

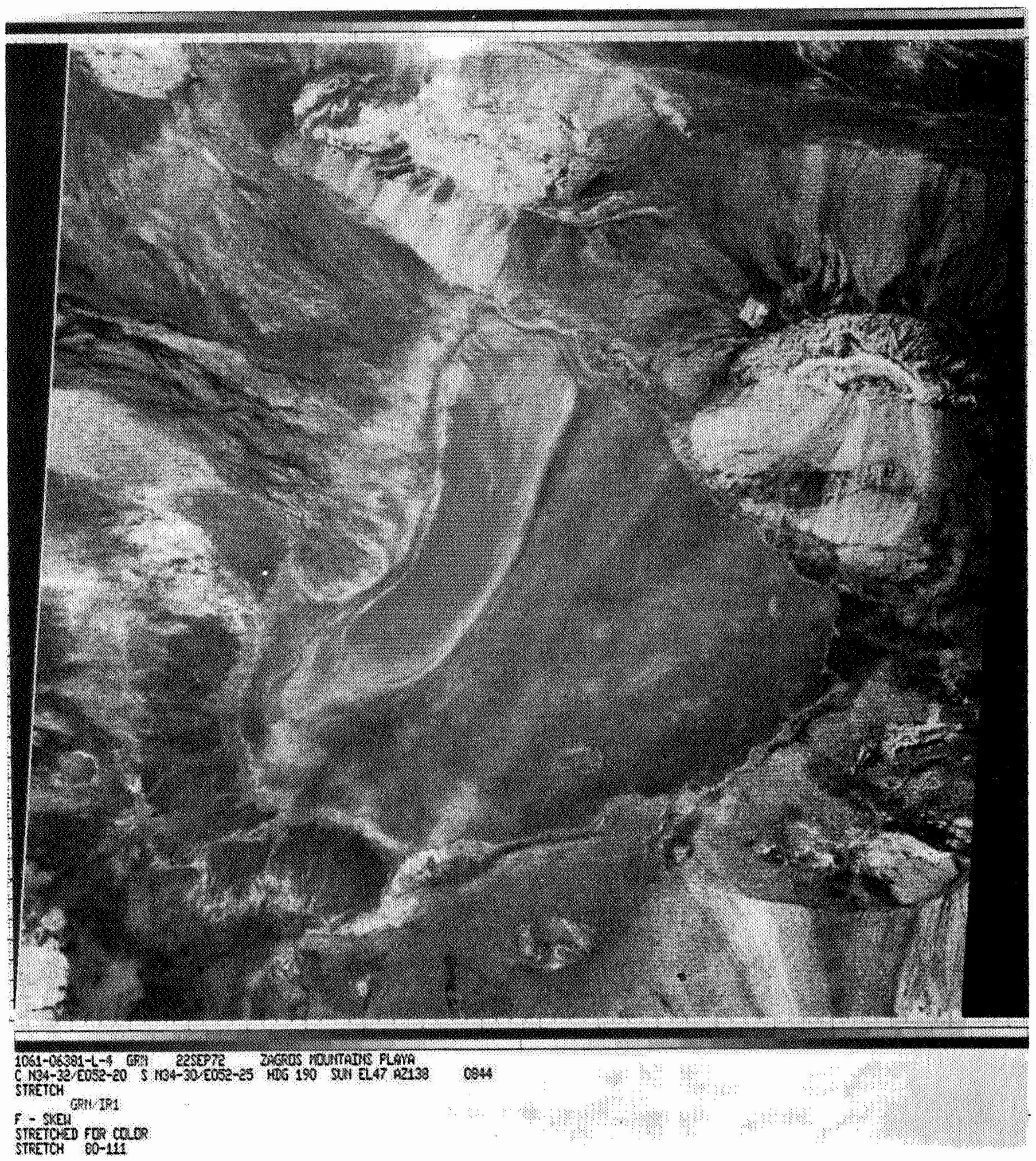

Figure 6. Ratio color composite of band ratios 4/7, 5/6, 5/7.

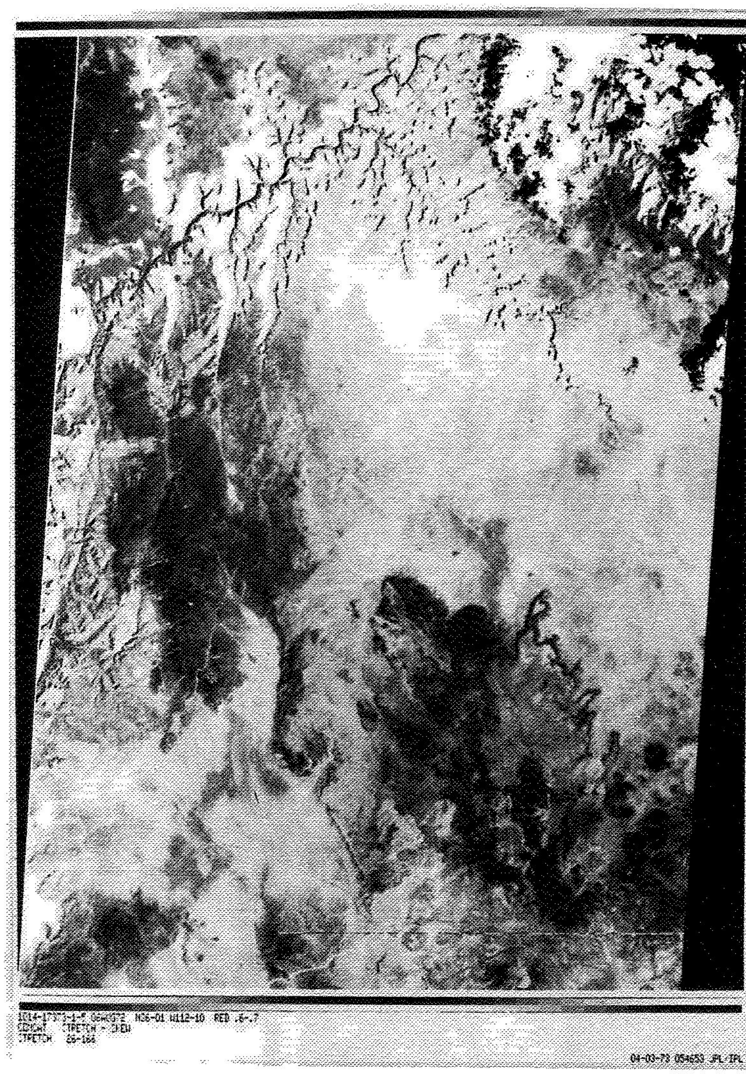

Figure 7a. Portion of frame EIOI4-I7373-5 showing Coconino Plateau.
Figure 7b. Figure 7a after application of a I x 35 element spatial filter to enhance linear features.

frequency domain as discussed by Nathan (1971). This type of filtering raises the modulation of high spatial frequency components (fine detail) in relation to the low frequency components (gross changes). Since to date there is no precise calibration of the MTF of the MSS, a correction function has been chosen which produces a graceful correction without ringing. Figure 8a is taken from a 9-inch positive transparency as received from Goddard Space Flight Center. Figure 8b is the image taken from the CCT and magnified by introducing pixels at each intersection which have the average value of their neighbors. This procedure minimizes high frequency losses otherwise introduced in the display by the film recorder. A significant difference is noted between Figures 8a and b, since the former is a 5th generation print and the latter can be considered to be second generation. Figure 8c represents 8b after MTF correction. Notice the increased sharpness of the field boundaries and visibility of the roads. In particular, the drainage detail has been significantly increased over that seen in the GSFC print.

Multiple Operations

Figure 9 is an example of the application of a number of methods discussed above applied to a specific problem in physical oceanography. Figure 9 is a small portion of a frame covering the New York Bight. Of particular interest is the large group of apparent internal waves (Apel and Charnell, 1973) seen for the first time in this image. Figure 9a is a 256 x 256 pixel portion of Frame E 1024 - 15071 and an average of bands 5 and 6 to which a cube root stretch has been applied. A two-dimensional Fourier transform was computed and those coefficients associated with the six-line striping, shown by the bright points in the right half of Fig. 9a, were removed. Fig. 9b shows the noise image which

Figure 8a. I5 x I5 km. segment of EII02-I7274-5 made from NDPF 9 inch transparency showing region surrounding Wilcox Playa, Arizona.

Figure 8b. Same area as Figure 8a, produced from digital tape and magnified by doubling the numbers of lines and samples by adding interpolated pixel values.

Figure 8c. Same as Figure 8b with an added MTF correction to boost high spatial frequency information.

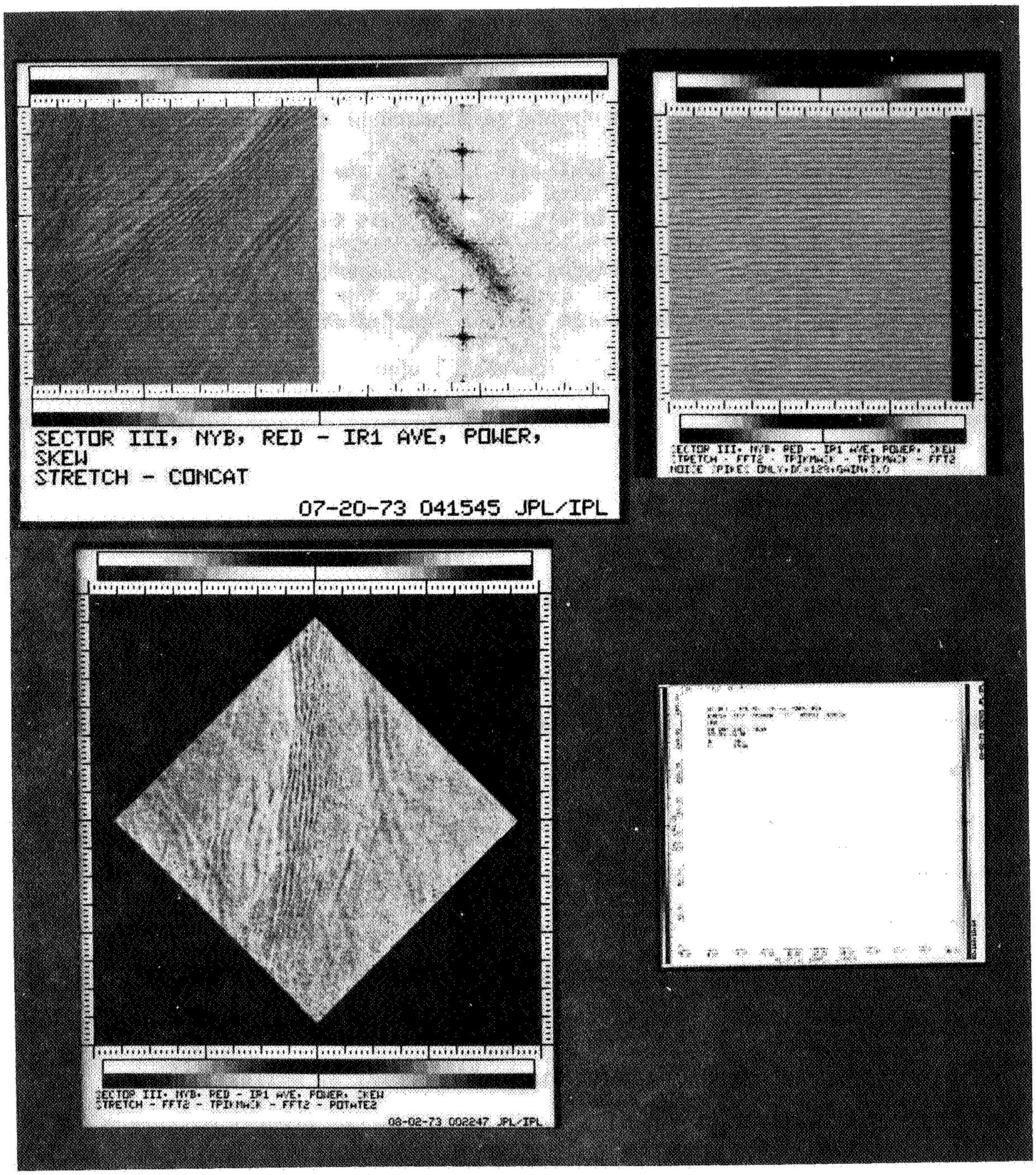

Figure 9a. Upper left image pair. 256 x 256 segment of EI024-I5071, bands 5 and 6 averaged. 2 dimensional Fourier transform of the image showing noise spikes from 6 line striping as black points. 9b) Noise image removed from 9a to produce 9c. 9c) Enhanced wave image rotated 45°. 9d) Line average plot of pixel values.

was removed to produce Fig. 9c. The inverse transform was computed and a gain factor of 1.5 applied to increase contrast. The resulting image was rotated 45° to position the wave fronts perpendicular to the scan lines and this image is shown in Fig. 9c. Selected lines in the upper portion of the image were averaged and plotted in Fig. 9d. In this figure the extraordinary nature of the waves, with wavelengths of over ½ kilometer, can be seen. The alternating light and dark bands are surface manifestations of low amplitude internal waves in the mixed layer, interacting with the boundary of the continental shelf. The locally induced surface currents collect hydrophobic materials in stripes and smooth the capillary waves causing a change in apparent reflectance.

SUMMARY

A number of applications problems in the fields of geology, geomorphology, and oceanography have been attacked by use of computer enhanced ERTS images. Displaying a useful subset of image information in a proper spatial context is the key to successful man-machine interaction. A number of problems can be solved with simple and relatively inexpensive techniques in the computer which are cumbersome if not impossible to perform photographically. Enhancement methods complement classification techniques and, in some cases, enhancements can provide preprocessing inputs to classification routines for superior results.

ACKNOWLEDGMENTS

The authors wish to thank J. Addington, R. Blackwell, A. Gillespie, and P. Paluzzi for their unstinting labors in producing the enhancements shown in this paper.

REFERENCES

Apel, J. R. and R. L. Charnell 1973, Oceanic Internal Waves of North America and Africa as Observed from ERTS. Proc. of 3rd ERTS Symposium, Dec. 10-14, Washington, D. C.

Billingsley, F. C. and A. F. H. Goetz 1973, Computer Techniques used for Some Enhancements of ERTS Images, Proc. of the Symp. on Significant Results Obtained from ERTS-I, NASA SP-327, p. 1159.

Billingsley, F. C., A. F. H. Goetz and J. N. Lindsley 1970, Color Differentiation by Computer Image Processing, Photographic Science and Engineering, 14, 28.

Crane, R. B. 1971, Pre-processing Techniques to Reduce Atmospheric and Sensor Variability in Multispectral Scanner Data, Proc. 7th Symp. on Remote Sensing of Environment, Univ. Michigan, p. 1345.

Goetz, A.F. H., F. C. Billingsley, D. P. Elston, I. Lucchitta, and E. M. Shoemaker 1973, Application of ERTS to Geologic Problems on the Colorado Plateau, Arizona, Proc. of 3rd ERTS Symposium, Dec. 10-14, Washington, D.C.

Goetz, A. F. H. 1973, Quality and Use of ERTS Information in Geologic Applications. Proc. of the 4th Annual Conf. on Application of Remote Sensing of Arid Land Resources and Environment, Nov. 14-16, Tucson, Ariz.

Krinsley, D. G., 1973, Preliminary Road Alignment Through the Great Kavir in Iran by Repetitive ERTS-I Coverage, Proc. of ERTS-1 Symp. Dec. 10-13, Washington, D. C.

Morrison, R. B. and M. E. Cooley 1973, Application of ERTS-1 Multispectral

Imaging to Monitoring the Present Episode of Accelerated Erosion in Southern Arizona, Proc. of the Symp. on Significant Results Obtained from ERTS-I, NASA SP 327, p. 283.

Nathan, R. 1971, Image Processing for Electron Microscopy: I Enhancement Procedures, Advances in Opitcal and Electron Microscopy, Barer and Cosslett Eds., Vol. IV, Academic Press 424 pp.

Rowan, L. C., P. H. Wetlaufer, A. F. H. Goetz, F. C. Billingsley and J. H. Stewart 1974, Discrimination of Hydrothermally Altered Areas and of Rock Types using Computer Enhanced ERTS Images, U.S.G.S. Professional Paper in press.

Smedes, H., M. M. Spench and F. J. Thompson 1971, Preprocessing of Multispectral Data and Simulation of ERTS Data Channels, Proc. 7th Symp. on Remote Sensing of Environment, Univ. of Michigan.

Whitaker, E. A. 1965, Interpretation of Ranger VII Records, JPL Technical Report TR 32-700, Part II, Experimenters Analysis and Interpretation.

AUTHOR INDEX

"The aeronautical and space activities of the United States shall be conducted so as to contribute to the expansion of human knowledge of phenomena in the atmosphere and space. The Administration shall provide for the widest practicable and appropriate dissemination of information concerning its activities and the results thereof."

—NATIONAL AERONAUTICS AND SPACE ACT OF 1958

NASA SCIENTIFIC AND TECHNICAL PUBLICATIONS

TECHNICAL REPORTS: Scientific and technical information considered important, complete, and a lasting contribution to existing knowledge.

TECHNICAL NOTES: Information less broad in scope but nevertheless of importance as a contribution to existing knowledge.

TECHNICAL MEMORANDUMS: Information receiving limited distribution because of preliminary data, security classification, or other reasons. Also includes conference proceedings with either limited or unlimited distribution.

CONTRACTOR REPORTS: Scientific and technical information generated under a NASA contract or grant and considered an important contribution to existing knowledge.

TECHNICAL TRANSLATIONS: Information published in a foreign language considered to merit NASA distribution in English.

SPECIAL PUBLICATIONS: Information derived from or of value to NASA activities. Publications include final reports of major projects, monographs, data compilations, handbooks, sourcebooks, and special bibliographies.

TECHNOLOGY UTILIZATION PUBLICATIONS: Information on technology used by NASA that may be of particular interest in commercial and other non-aerospace applications. Publications include Tech Briefs, Technology Utilization Reports and Technology Surveys.

Details on the availability of these publications may be obtained from:

SCIENTIFIC AND TECHNICAL INFORMATION OFFICE

NATIONAL AERONAUTICS AND SPACE ADMINISTRATION

Washington, D.C. 20546